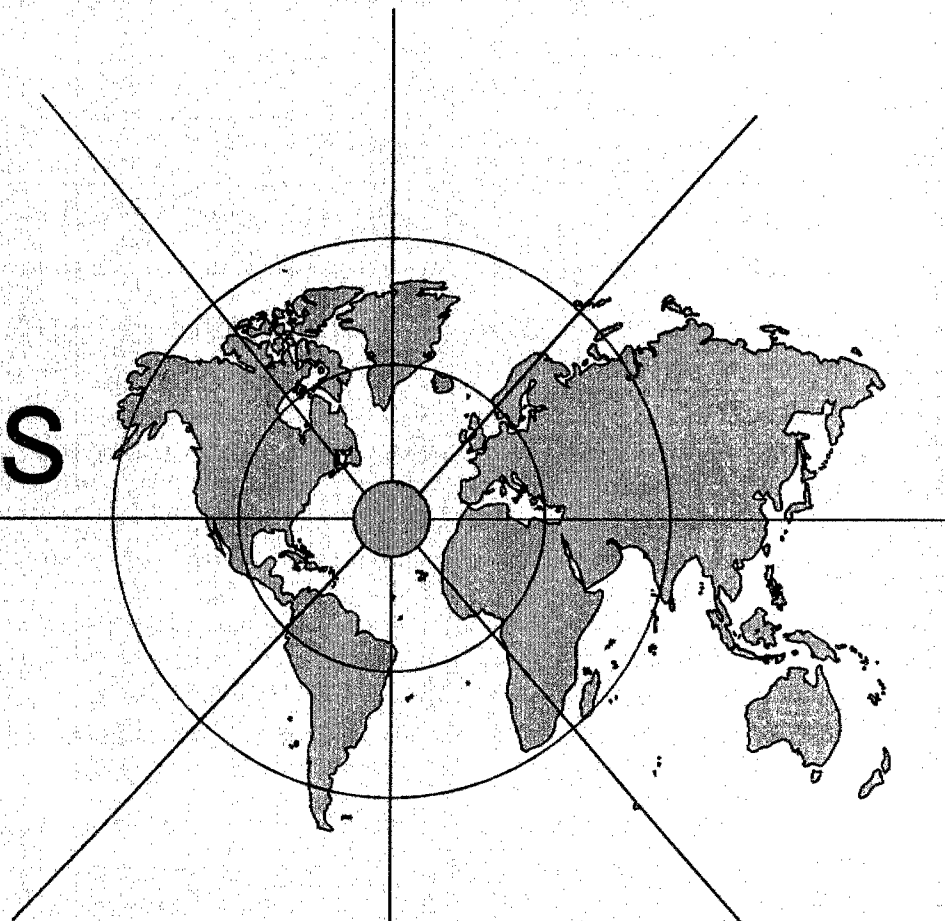


Proceedings of the Forty-Sixth IWCS



Approved for public release
Distribution Unlimited

INTERNATIONAL WIRE AND CABLE SYMPOSIUM

NOVEMBER 17 THRU 20, 1997

DTIC QUALITY INSPECTED 8

19980303 026

Sponsored by
International Wire and Cable Symposium, Inc. (IWCS)
Eatontown, New Jersey
<http://www.iwcs.org/iwcs/>

With Participation by
US Army Communications-Electronics Command (CECOM)
Fort Monmouth, New Jersey

PROCEEDINGS OF 46TH INTERNATIONAL WIRE AND CABLE SYMPOSIUM

Sponsored by
International Wire and Cable Symposium, Inc. (IWCS)
Eatontown, New Jersey
<http://www.iwcs.org/iwcs/>

With Participation by
US Army Communications-Electronics Command (CECOM)
Fort Monmouth, New Jersey

**PHILADELPHIA MARRIOTT HOTEL
PHILADELPHIA, PENNSYLVANIA
NOVEMBER 17, 18, 19 AND 20, 1997**

DTIC QUALITY INSPECTED 3

APPROVED FOR PUBLIC RELEASE: DISTRIBUTION UNLIMITED

MISSION

The International Wire and Cable Symposium provides a forum for the exchange of technical information amongst suppliers, manufacturers, and users on technological advancements in materials, processes, and products used for voice, data and video signal transmission systems.

TECHNICAL PAPERS

Tuesday, November 18

9:00 am	PLENARY SESSION	Broadband Access <i>Track 1-- Fiber</i>
1:00 pm	SESSION 1	Aerial I
1:00 pm	SESSION 2	Fiber Optic Connectors/Components <i>Track 2 -- Copper</i>
1:00 pm	SESSION 3	Copper Wire and Cable I <i>Track 3 -- Materials</i>
1:00 pm	SESSION 4	Polymeric Materials

Wednesday, November 19

Track 1 -- Fiber

9:00 am	SESSION 5	Aerial II
9:00 am	SESSION 6	Fiber Splicing
		<i>Track 2 -- Copper</i>
9:00 am	SESSION 7	Copper Wire and Cable II <i>Track 3 -- Materials</i>
		<i>Track 3 -- Materials</i>
9:00 am	SESSION 8	Fiber Ribbons <i>Track 1 -- Fiber</i>
		<i>Track 1 -- Fiber</i>
2:15 pm	SESSION 9	Submarine
2:15 pm	SESSION 10	Cable Installation <i>Track 2 -- Copper</i>
		<i>Track 2 -- Copper</i>
2:15 pm	SESSION 11	Broadband/Outside Plant <i>Track 3 -- Materials</i>
		<i>Track 3 -- Materials</i>
2:15 pm	SESSION 12	Fiber Coating & Environment
4:00 pm	SESSION 13	Poster Papers

Thursday, November 20

Track 1 -- Fiber

8:30 am	SESSION 14	Fiber and Cable Design I
8:30 am	SESSION 15	Testing/Field Evaluation
		<i>Track 2 -- Copper</i>
8:30 am	SESSION 16	Copper Wire and Cable III <i>Track 3 -- Materials</i>
		<i>Track 3 -- Materials</i>
8:30 am	SESSION 17	Fire and Flame <i>Track 1 -- Fiber</i>
		<i>Track 1 -- Fiber</i>
1:00 pm	SESSION 18	Fiber and Cable Design II
1:00 pm	SESSION 19	Fiber in the Loop <i>Track 3 -- Materials</i>
		<i>Track 3 -- Materials</i>
1:00 pm	SESSION 20	Fiber Reliability

PAPERS

The papers in this volume were printed directly from unedited reproducible copies prepared by the authors. Responsibility for contents rests upon the authors and not the symposium committee or its members. All rights reserved by the International Wire and Cable Symposium, Inc., 174 Main Street, Eatontown, New Jersey 07724.

PROCEEDINGS/PUBLICATIONS INTERNATIONAL WIRE AND CABLE SYMPOSIUM (IWCS)

Proceedings - Bound - Available from IWCS

39th IWCS Proceedings - 1990 - \$15.00

40th IWCS Proceedings - 1991 - \$15.00

44th IWCS Proceedings - 1995 - \$40.00

46th IWCS Proceedings - 1997 - \$50.00

Copies of original proceedings not listed above can be reproduced for \$75.00 per copy plus shipping.

Publications - Bound - Available from IWCS

Index of IWCS Papers (1983-1990); PUB #1001RP-1991 - \$15.00

PIC Insulation Testing Field Experience; PUB #1003RP-1992 - \$25.00

Fiber Optic Cables; PUB #1004RP-1992 - \$25.00

Extra Copies of the 1997 Proceedings can be obtained for: 1 - \$50; 2 - \$100; 3 - \$150; 4 - \$190; 5 - \$230; 6 - \$270; 7 - \$310; 8 - \$350; 9 - \$390; 10 - \$430; 11 and above - \$430 plus \$30 for each additional copy.

Shipping/Handling:

Proceedings

\$ 7.50 per copy USA only

\$20.00 per copy Surface Mail
(overseas - 4 to 6 weeks)

\$35.00 per copy Airmail (Europe)

\$40.00 per copy Airmail (Asia)

Publications

\$ 4.00 per copy USA Only

\$10.00 per copy Surface Mail
(overseas - 4 to 6 weeks)

\$15.00 per copy Airmail
(Europe and Asia)

Payment: Make a check or bank draft payable in U.S. Dollars drawn on a U.S. Bank, to the INTERNATIONAL WIRE & CABLE SYMPOSIUM, INC. or use your VISA/MC/AMEX by providing number and expiration date and forward request to: International Wire and Cable Symposium, Inc., 174 Main Street, Eatontown, NJ 07724. Telephone inquiries may be directed to Ms. Pat Hudak (732) 389-0990. Prices are subject to change.

Photocopies are available for complete sets of papers for 1964 through 1996. Information on prices and shipping charges should be requested from the:

US Department of Commerce

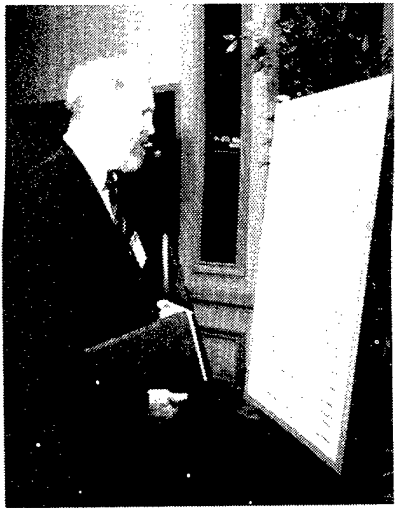
National Technical Information Service (NTIS)

Springfield, Virginia 22161

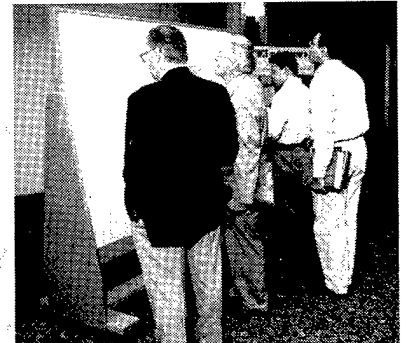
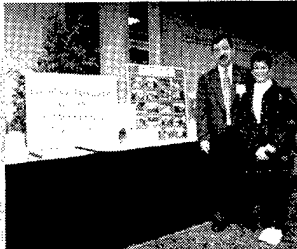
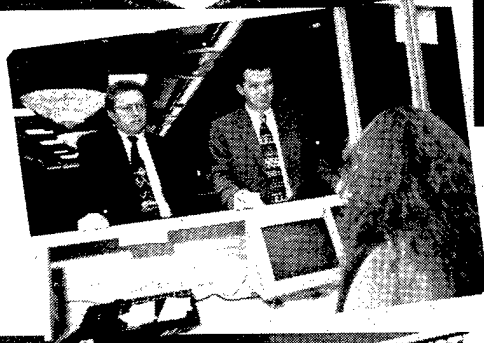
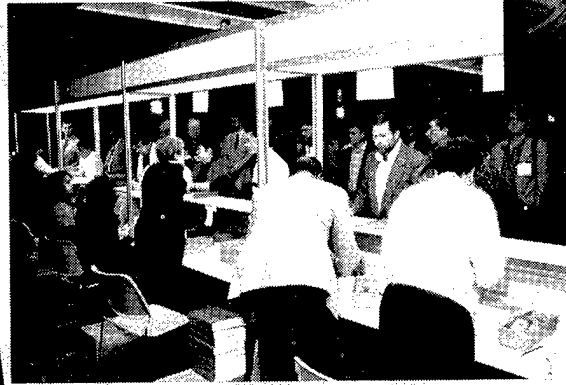
Telephone: (703) 487-4650

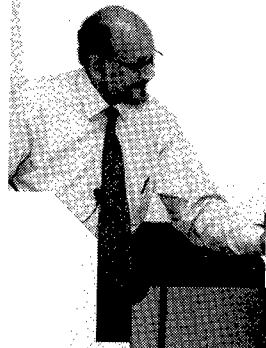
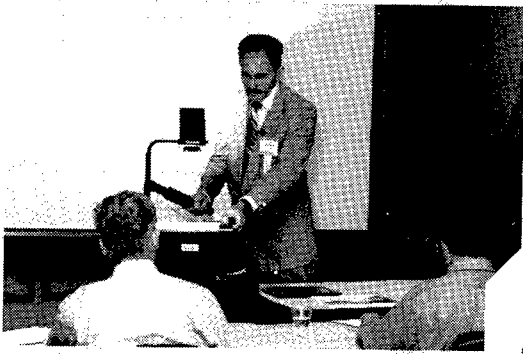
Include Title, Year and "AD" Number

13th Annual Wire Cable Symposium (1964)	- AD 787164
15th Annual Wire Cable Symposium (1966)	- AD A006601
16th International Wire Cable Symposium (1967)	- AD 787165
17th International Wire Cable Symposium (1968)	- AD 787166
18th International Wire Cable Symposium (1969)	- AD 787167
19th International Wire Cable Symposium Proceedings 1970	- AD 714985
20th International Wire Cable Symposium Proceedings 1971	- AD 733399
21st International Wire Cable Symposium Proceedings 1972	- AD 752908
22nd International Wire Cable Symposium Proceedings 1973	- AD 772914
23rd International Wire Cable Symposium Proceedings 1974	- AD A003251
24th International Wire Cable Symposium Proceedings 1975	- AD A017787
25th International Wire Cable Symposium Proceedings 1976	- AD A032801
26th International Wire Cable Symposium Proceedings 1977	- AD A047609
27th International Wire Cable Symposium Proceedings 1978	- AD A062322
28th International Wire Cable Symposium Proceedings 1979	- AD A081428
29th International Wire Cable Symposium Proceedings 1980	- AD A096308
30th International Wire Cable Symposium Proceedings 1981	- AD A110859
31st International Wire Cable Symposium Proceedings 1982	- AD A125662
32nd International Wire Cable Symposium Proceedings 1983	- AD A136749
33rd International Wire Cable Symposium Proceedings 1984	- AD A152119
34th International Wire Cable Symposium Proceedings 1985	- AD A164384
35th International Wire Cable Symposium Proceedings 1986	- AD A180828
36th International Wire Cable Symposium Proceedings 1987	- AD A189610
37th International Wire Cable Symposium Proceedings 1988	- AD A200903
38th International Wire Cable Symposium Proceedings 1989	- AD A216023
39th International Wire Cable Symposium Proceedings 1990	- AD A233634
40th International Wire Cable Symposium Proceedings 1991	- AD A244038
41st International Wire Cable Symposium Proceedings 1992	- AD A259235
42nd International Wire Cable Symposium Proceedings 1993	- AD A279242
43rd International Wire Cable Symposium Proceedings 1994	- AD A293473
44th International Wire Cable Symposium Proceedings 1995	- AD A303506
45th International Wire Cable Symposium Proceedings 1996	- AD A324572
Kwic Index of Technical Papers, International Wire Cable Symposium (1952-1982)	- AD A027588

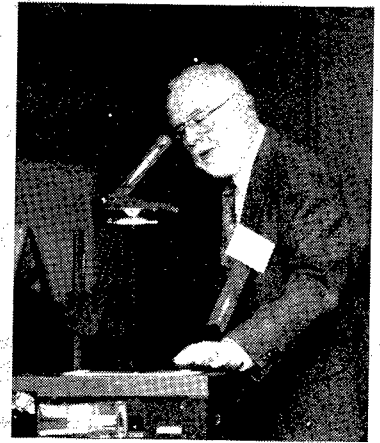
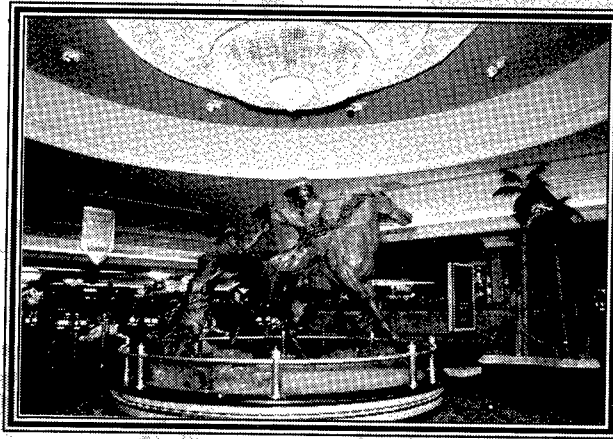


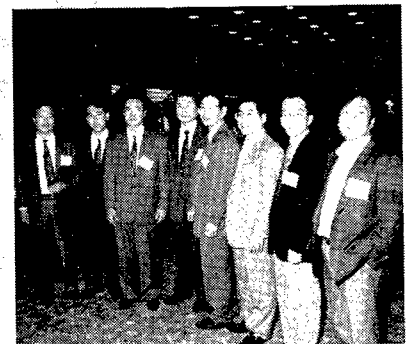
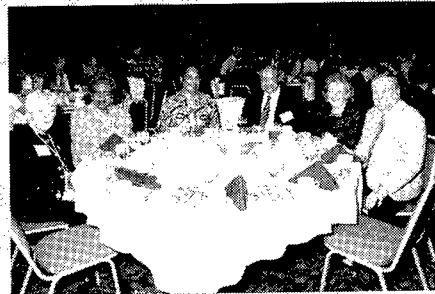
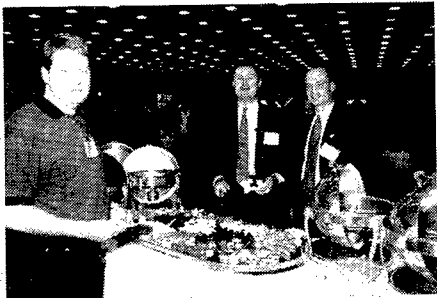
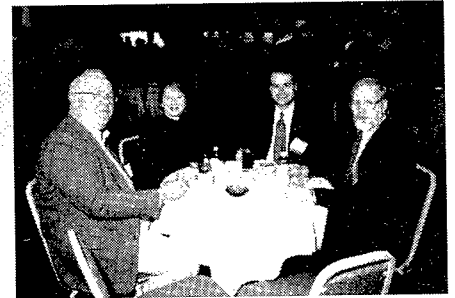
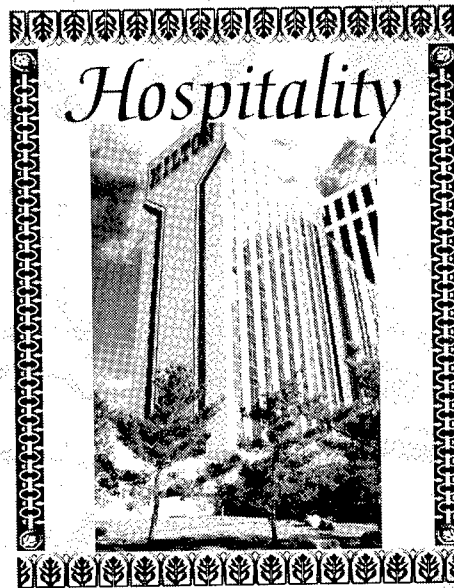
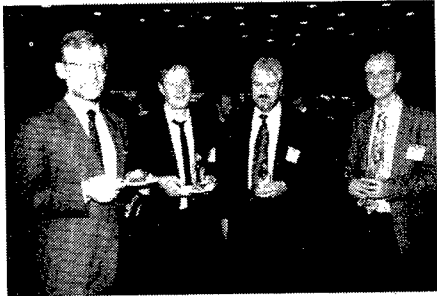
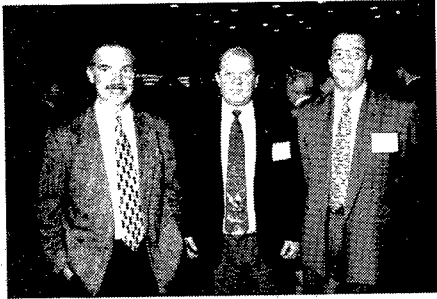
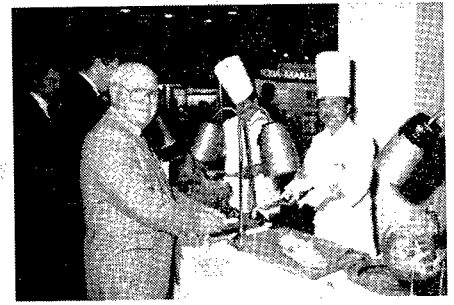
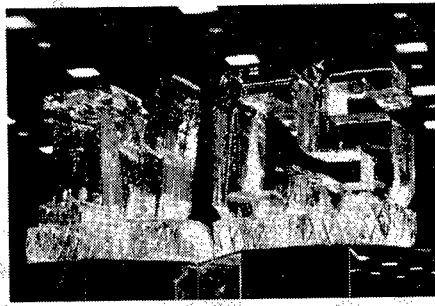
Registration

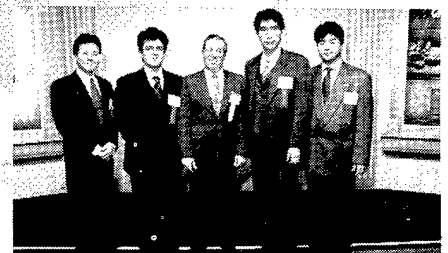
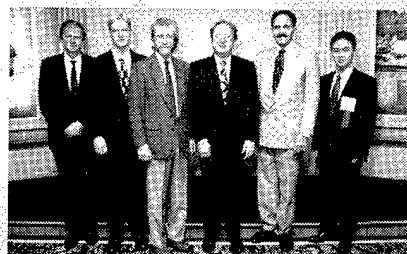
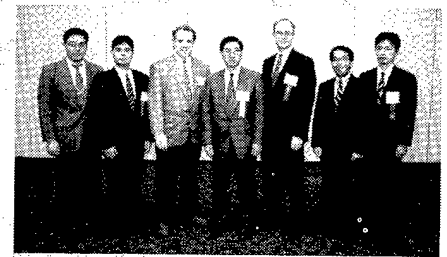
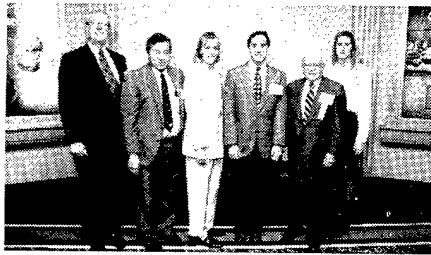
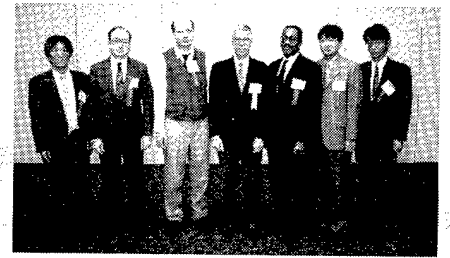
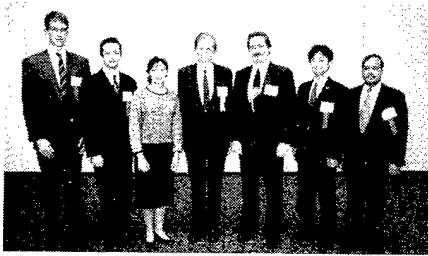


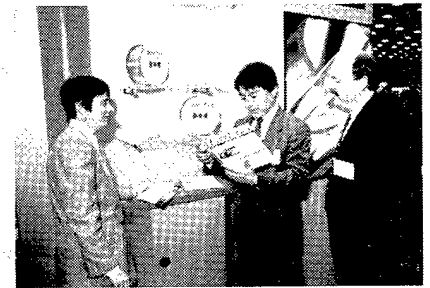
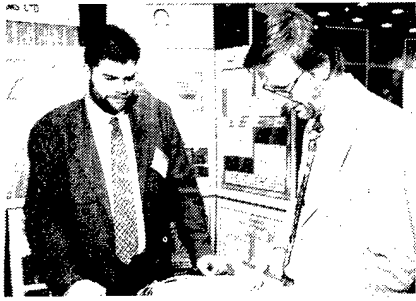


Educational









AWARDS

Outstanding Technical Paper

- H. Lubars and J. A. Olszewski, General Cable Corp. — 1968
"Analysis of Structural Return Loss in CATV Coaxial Cable"
- J. P. McCann, R. Sabia and B. Wargotz, Bell Laboratories — 1969
"Characterization of Filler and Insulation in Waterproof Cable"
- D. E. Setzer and A. S. Windeler, Bell Laboratories — 1970
"A Low Capacitance Cable for the T2 Digital Transmission Line"
- R. Lyenger, R. McClean and T. McManus, Bell Northern Research — 1971
"An Advanced Multi-Unit Coaxial Cable for Toll PCM Systems"
- J. B. Howard, Bell Laboratories — 1972
"Stabilization Problems with Low Density Polyethylene Insulations"
- Dr. H. Martin, Kabelmetal — 1973
"High Power Radio Frequency Coaxial Cables, Their Design and Rating"
- D. Doty, AMP Inc. — 1974
"Mass Wire Insulation Displacing Termination of Flat Cable"
- T. S. Choo, Dow Chemical U.S.A. — 1975
"Corrosion Studies on Shielding Materials for Underground Telephone Cables"
- N. J. Cogelia, Bell Telephone Laboratories and G. K. Lavoie and J. F. Glahn, US Department of Interior — 1976
"Rodent Biting Pressure and Chemical Action and Their Effects on Wire and Cable Sheath"
- T. K. McManus, Northern Telecom Canada Ltd. and R. Beveridge, Saskatchewan Telecommunications, Canada — 1977
"A New Generation of Filled Core Cable"
- F. Suzuki, S. Sato, A. Mori and Y. Suzuki, Sumitomo Electric Industries, Ltd., Japan — 1978
"Microcoaxial Cables Insulated with Highly Expanded Polyethylene By Chemical Blowing Method"
- S. Masaki, Y. Yamazaki and T. Ideguchi, Nippon Telegraph and Telephone Public Corporation, Japan — 1979
"New Aluminum Sheath Cable Used for Electromagnetic Shielding"
- P. Kish and Y. BeBorgne, Northern Telecom Canada Limited, Montreal, Canada — 1980
"General Crosstalk Model for Paired Communication Cables"
- C. J. Arroyo, N. J. Cogelia, Bell Laboratories, and B. J. Darsey, Western Electric — 1981
"Thermal Behavior of Experimental Plenum Cable Sheaths Determined in a Radiant Heat Chamber"
- R. H. Whiteley, Raychem Ltd. — 1982
"A Comprehensive Small Scale Smoke Test"
- V. A. Fentress, Raychem Corp. and D. V. Nelson, Stanford University — 1983
"Fracture Mechanics Evaluation of the Static Fatigue Life of Optical Fibers in Bending"
- M. Fujise and Y. Iwamoto, KDD Research & Development Laboratories, Tokyo, Japan — 1984
"Self-Core-Alignment Arc-Fusion Splicer Based on a Simple Local Monitoring Method"
- James A. Krabec and John W. Kincaid, Jr., Belden Technical Research Center — 1985
"Advances in the Optimization of Multi-Layer Shield Design"
- Simon D. Dadakarides and Bruce B. Lusignam, Stanford University — 1986
"Magnetically Loaded Cables"

Best Presentation

- N. Dean, B.I.C.C.—"The Development of Fully Filled Cables for Distribution Network"
- J. D. Kirk, Alberta Government Telephones—"Progress and Pitfalls of Rural Buried Cable"
- Dr. O. Leuchs, Kable and Metalwerke—"A New Self-Extinguishing Hydrogen Chloride Binding PVC Jacketing Compound for Cables"
- S. Nordblad, Telefonaktiebolaget L. M. Ericsson—"Multi-Paired Cable of Nonlayer Design for Low Capacitance Unbalance Telecommunications Network"
- N. Kojima, Nippon Telegraph and Telephone—"New Type Paired Cable for High Speed PCM Transmission"
- S. Kaufman, Bell Laboratories—"Reclamation of Water-Logged Buried PIC Telephone Cable"
- R. J. Oakley, Northern Electric Co., Ltd.—"A Study Into Paired Cable Crosstalk"
- G. H. Webster, Bell Laboratories—"Material Savings by Design in Exchange and Trunk Telephone Cable"
- J. E. Wimsey, United States Air Force—"The Bare Base Electrical Systems"
- Michael DeLucia, Naval Ship Research and Development—"Highly Fire-Retardant Navy Shipboard Cable"
- William L. Schmacher, AMP Inc.—"Design Considerations for Single Fiber Connector"
- Richard C. Mondello, Bell Labs—"Design and Manufacture of an Experimental Lightguide Cable for Undersea Transmission Systems"
- I. Wadehra, IBM Corporation—"Performance of Polyvinyl Chloride Communication Cables in Modified Steiner Tunnel Test"
- J. J. Refi, Bell Laboratories—"Mean Power Sum Far-End Crosstalk of PIC Cables as a Function of Average Twist Helix Angle"
- G. S. Anderson, Belden Corporation—"Installation of Fiber Optic Cable on 457 Meter Tower"
- A. Yoshizawa, The Furukawa Electric Co., Ltd.—"Structure and Characteristics of Cables for Robots"
- J. R. Bury, Standard Telecommunication Laboratories, Ltd., Hailow, England—"Development of Flame Retardant, Low Aggressivity Cables"
- William E. Dennis, Dow Corning Corporation, Midland, Michigan—"Hydrogen Evolving Tendencies of Cable Fillers and Optical Fiber Coatings"
- Stephen Hornung, British Telecom Research Laboratories—"Manufacture and Performance of Fibre Units for Installation by The Viscous Drag of Air"
- Dave Fischer, Superior Cable Corp.—"Progress Towards the Development of Lighting Test for Telecommunication Cables"
- John C. Chamberlain, Siecor Corp.—"Zero Halogen Fire Retardant Fiber Optic Shipboard Cable"

Outstanding Technical Paper

1987

Stephen B. Pierce — Conel Laboratories — "Digital Transmission on Customer Premises Wiring"

1988

Martin C. Light Jr., James A. Moses, Mark A. Sigmon and Christopher A. Story — Siecor Corp. — "Design and Performance of Telecommunication Cable Optimized for Low Fiber Count"

1989

Michel Plasse, Lise Desroches and Paul-Andre Guilbert — Northern Telecom Canada Limited — "High Performance Twisted-Pair Cable for LAN Systems"

1990

Trevor N. Bowmer, Russell J. Miner, Irene M. Plitz, Joseph N. D'Amico and Lal M. Hore — Bellcore — "Thermal Stability Tests for Polyolefin Insulations"

1991

Shigeru Tomita, Michito Matsumoto, Tetsuro Yabuta and Takuya Uenoya — NTT — "Preliminary Research into Ultra High Density and High Count Optical Fiber Cables"

1992

Nathan E. Hardwick III and Kris Kathiresan — AT&T Bell Laboratories and J. G. Hartley — Georgia Institute of Technology — "Analysis of Fiber Optic Cable Design Conditions in Vicinity of Steam Lines — Ruptured and Pristine"

1993

Dr. Yoshinori Namihira and Toshio Kawazawa — KDD R&D Laboratories; and Naoki Norimatsu — KDD Company, Limited — "PMD Reduction of Optical Fiber Cables for Transoceanic Optical Amplifier Submarine Cable Systems"

1994

Toshio Kurashima, Kazuo Hogari, Satoshi Matsuhashi, Dr. Tsuneo Horiguchi, Dr. Yahei Koyamada and Yutaka Wakui — NTT Access Network Systems Laboratories; and Hiroshi Hirano — NTT Technical Assistance & Support Center — "Measurement of Distributed Strain in Frozen Cables and Its Potential for Use in Predicting Cable Failure"

1995

Jean Luc Lang and Jean-Francois Libert — Alcatel Submarine Network; David I. Curtis and Peter Worthington — STC Submarine Systems Ltd. — "Optical Performance of Submarine Cables in Optically Amplified High Bit Rate Systems"

1996

Mitsuru Kamikatano and Matsuhiro Miyamoto — Fujikura Limited; and Osamu Ogawa — Tokyo Electric Power Company — "A Time-Varying Optical Fiber Strain Measurement by Using Brillouin Ring Amplifying System"

Outstanding Poster Paper

William Wood — Bell Communication Research — "Performance Analysis of Optic Fiber Cleavers"

Dr. R. Raman — Conel Laboratories — "Loss at Dissimilar Fiber Splices"

Werner Bernard and Susan C. Grant — Siecor Corporation — "Fiber Optic Drop Cables in the Subscriber Loop"

Steve Lischynsky, Helmut Lukas, Robin McIntyre and Grant Pacey — Bell-Northern Research Ltd. — "New Technology for a Single Mode Mechanical Splice"

G. Scott Glaesemann — Corning Inc. — "The Effect of Proof Testing on the Minimum Strength of Optical Fiber"

Svend Hopland and Albert Klykken — Norwegian Telecom — "Installation of Submarine Fiberoptic Cables in Rugged Coastal Terrain"

Willem Griffioen — PTT Research — "Mechanical Lifetime of Optical Fibers"

Dr. Sverker Forsberg — Swedish University of Agricultural Sciences; and Jan Björkman — Telia AB — "Release of Lead from Lead-Sheathed Telecom Cables in Soil"

Richard S. Wagman, Gregory A. Lochkovic and Kevin T. White — Siecor Corporation — "Component Optimization for Slotted Core Cables Using 8-Fiber Ribbons"

Jan Björkman — Telia Network Services; and Dr. Torbjörn Svensson — Telia Research AB — "Ageing of Fibres and Ribbon in Water and Filling Compound"

Best Presentation

Richard Rossi — General Cable Company — "Cable Sheathing Design and Performance Criteria"

Janice B. Haber — AT&T Laboratories — "Single-Mode Media and Apparatus for Fiber to the Home"

Michel de Vecchis — Les Cables de Lyon — "Results on a Large Scale Installation of a Fibre Optic Distribution Network"

Harold W. Friesen — AT&T Bell Laboratories — "An Improved Characteristic Impedance Measurement Technique"

Sue V. Wolfe — STC Submarine Systems — "Structure and High Voltage DC Behaviour of Submarine Cable Mouldings"

Peter Latoszynski — Telecom Australia — "Development of Co-Extruded Polyethylene/Polyamide 12 Insect Resistant Telecommunications Cable"

Timothy S. Dougherty — AT&T Network Cable Systems — "The Temperature of Aerial Plant and Its Effect Upon Foam-Skin Insulation Life" and Wolfgang Wenski — Kabelmetal Electro GmbH — "First Large Scale FITL Installation: Experience From Opal '93"

Barry J. Keon — Telstra — "The Effects of Optical Fiber Coating and Ink Materials on the Corrosion of the Glass Surface"

Dr. Dan L. Philen — AT&T Bell Laboratories — "Optical Fiber for Amplified Undersea Systems"

Dr. Priya L. Tabaddor — Lucent Technologies Incorporated, Bell Laboratories — "An Evaluation of Protective Polymer Coatings for Optical Fiber Applications"

ELMER F. "ACE" GODWIN SCHOLARSHIP

1994

Sara Ransom, Massachusetts Institute of Technology,
Freshman — Materials Science Engineering Major

Jurron Bradley, Vanderbilt University, Senior —
Chemical Engineering Major

1995

Jason Chang, Princeton University, Freshman —
Chemistry Major

Fionna Murray, Virginia Tech, Junior — Mechanical
Engineering Major

1996

Anthony Tindall, Cornell University, Freshman —
Mechanical Engineering Major

John Belle, North Carolina State University,
Sophomore — Electrical Engineering Major

GOLD SUSTAINING CONTRIBUTORS

A F A Industries

20 Jewell Street
Garfield, NJ 07026

Akzo Nobel Aramid Products

801-F Blacklawn Road
Conyers, GA 30207

Alcatel Cable

30 Rue P. Bérégovoy
92111 Clichy Cedex
France

AlphaGary Corporation

170 Pioneer Drive
Leominster, MA 01453

Breen Color Concentrates, Inc.

11 Kari Drive
Lambertville, NJ 08530-3411

Chase & Sons

19 Highland Ave.
Randolph, MA 02368

Corning Inc.

35 West Market St.
MP-R0-03
Corning, NY 14831

DSM Desotech Inc.

1122 Saint Charles St.
Elgin, IL 60120

DuPont Company

5401 Jefferson Davis Highway
Richmond, VA 23234

Essex Group, Inc.

1710 Wall Street
PO Box 1750
Ft. Wayne, IN 46801-1750

Facile Holdings, Inc.

185 6th Avenue
Paterson, NJ 07509

Fujikura Ltd.

1-5-1, Koto-ku, Kiba
Tokyo, 135
Japan

The Furukawa Electric Co., Ltd.

6, Yawata-Kaigandori
Ichihara, Chiba, 290, Japan

Fusion UV Systems, Inc.

910 Clopper Road
Gaithersburg, MD 20878

Hitachi Cable, Ltd.

5-1-1 Hitaka-Cho
Hitachi-shi, Ibaraki-ken 319-14
Japan

Lucent Technologies

Bell Labs Innovations
2000 Northeast Expressway
Norcross, GA 30071

Millennium Petrochemicals Inc.

11500 Northlake Drive
Cincinnati, OH 45249

Neptco Incorporated

PO Box 2323
Pawtucket, RI 02861

Nippon Telegraph and Telephone Corp.

1-7-1 Hanabatake
Tsukuba, Ibaraki, 305
Japan

Nokia-Maillefer, Inc.

1856 Corporate Drive, Suite 135
Norcross, GA 30093

Olex Cables

207 Sunshine Road
Tottenham, VIC 3012
Australia

Optical Fibres

Second Avenue
Deeside Industrial Park
Deeside, Flintshire CH5 2NX
United Kingdom

Owens Corning

One Owens Corning Parkway
Toledo, OH 43659

Penreco

4401 Park Ave.
Dickinson, TX 77539

Plasma Optical Fibre

PO Box 1136
5602 BC Eindhoven
The Netherlands

Siecor Corporation

PO Box 489
Hickory, NC 28603

**SpecTran Communication Fiber
Technologies**

50 Hall Road
Sturbridge, MA 01566

The Stewart Group Inc.

259 Steelcase Road West
Markham, Ontario
Canada L3R 2P6

GOLD SUSTAINING CONTRIBUTORS

Sumitomo Electric U.S.A., Inc.
21221 S. Western Ave., Ste. 200
Torrance, CA 90501

Teknor Apex Company
505 Central Avenue
Pawtucket, RI 02861

UBE Industries (America), Inc.
666 Fifth Avenue
New York, NY 10103

Union Carbide Corporation
39 Old Ridgebury Road
Danbury, CT 06817-0001

WaterGuard Cable Products, Inc.
14135 I-10 East Freeway
Houston, TX 77015

Witco Corporation
One American Lane
Greenwich, CT 06831-2559

SILVER SUSTAINING CONTRIBUTORS

ACOME of France
Mortain, France

Air Logistics Corporation
Pasadena, CA

Alcatel Kabel AG & Company
Mönchengladbach, Germany

Barcel Wire and Cable Corporation
Irvine, CA

BICC Cables Limited
Cheshire, United Kingdom

Kromberg & Schubert GmbH u. Co.
Rhede, Germany

LaserMike
Dayton, OH

Siemens AG
Neustadt, Germany

Weber & Scher Mfg. Co., Inc.
Lebanon, NJ

TABLE OF CONTENTS

TUESDAY MORNING—9:00 AM—11:00 AM

Grand Ballroom (Salons G/H), Fifth Floor

Announcement/Greetings

Elmer F. Godwin, President/Director, IWCS, Inc., Eatontown, NJ

James R. Leech, Chairman, IWCS, Union Carbide Corp., Somerset, NJ

Dr. Marek Kapuscinski, Chairman, Plenary Session, NORDX/CDT, Quebec, Canada

PLENARY SESSION: BOARDBAND ACCESS

Speaker: Dr. Robert W. Lucky, Corporate Vice President, Applied Research, Bellcore, Red Bank, NJ

TUESDAY AFTERNOON—1:00 PM—4:30 PM

Salon E

TRACK 1—FIBER

SESSION 1: AERIAL I

Chairperson: Dieter S. Nordmann, Alcatel Cable, Hannover, Germany

Design of Aerial Optical Fiber Cable System Suitable for Easy Branching—*H. Iwata, M. Okada, S. Tomita, N. Kashima, T. Hoshijima, M. Kama*, NTT Access Network Systems Laboratories; *K. Nishizawa*, NTT Technology and Development Support Center, Ibaraki, Japan..... 4

Development of Aerial Optical Fiber Cable with Greater Length of Cable Compared to Supporting Wire—*Y. Ishibashi, A. Watanabe, O. Arai, K. Ishii, Y. Kurosawa, H. Yamazaki*, Hitachi Cable, Ltd., Ibaraki, Japan..... 12

Development of Optical Drop Wire and Drop Wire Stranded Cable—*K. Watanabe, M. Kusakari, O. Koyasu, A. Mogi, M. Miyamoto*, Fujikura, Ltd., Chiba, Japan..... 17

Continued Investigations of ADSS Designs and Reliability Considerations with Respect to Field Voltage Tracking, and Cable Installation Practices—*D. A. Keller, J. P. Bonicel, C. Bastide, F. Davidson*, Alcatel Cable-OFCCC, Claremont, NC; *D. J. Benzel*, Alcatel Cable, Calais, France..... 24

The Development of Test Methods to Optimise ADSS Cable Clamping Systems—*M. Davies, R. Sutehall*, Pirelli Cables, UK; *M. Collins, M. Murphy*, Dulmison, UK..... 32

A Study on Behavior of Fiber Ribbons in SZ-Grooved Spacer and Its Application to Aerial Cable—*H. Ishikawa, Y. Suetsugu, T. Saito, M. Watanabe, A. Makiyama, J. Ohta, S. Tanaka*, Sumitomo Electric Industries, Ltd., Yokohama, Japan..... 42

TUESDAY AFTERNOON—1:00 PM—4:30 PM

Salon F

TRACK 1—FIBER

SESSION 2: FIBER OPTIC CONNECTORS/COMPONENTS

Chairperson: Dr. John Mellis, British Telecom Laboratories, Suffolk, U.K.

2 × 800 Optical Switch Using Fiber Butting Method—*M. Okuda, S. Naraoka, S. Yamaguchi, K. Kamiko*, Furukawa Electric Co., Ltd., Chiba, Japan .. 51

Development of Mini-MPO Connector—*K. Takizawa, T. Arikawa, Y. Tamaki, H. Yokosuka*, Fujikura Ltd., Chiba, Japan..... 57

Fabrication of High-Temperature Resistant Bragg Gratings in Optical Fibers—*M. A. Fokine*, Institute of Optical Research, Stockholm, Sweden 64

Wideband Rejection Fiber Grating in SC-Type Connector—*K. Kohmoto, K. Asano, H. Hosoya, H. Yokosuka*, Fujikura Ltd., Chiba, Japan 68

Pigtail-Type Optical Attenuator Using Metal-Doped Optical Fiber—*M. Saijo, Y. Morishita, Y. Ariga, K. Sugi, K. Muta*, Showa Electric Wire & Cable Co., Ltd., Kanagawa, Japan 74

UV-Transparent Coatings for Optical Fiber—*Å. Claesson, B. Sahlgren, M. Fokine, R. Stubbe*, Institute of Optical Research, Stockholm, Sweden.... 82

Coatings Having Enhanced UV Transparency for the Fabrication of Optical Fiber Gratings—*D. A. Simoff, M. A. Paczkowski, D. Inniss, T. A. Strasser, J. M. Borick, J. R. Pedrazzani, R. P. Espindola, R. M. Atkins, K. T. Nelson, J. Aspell, V. J. Kuck*, Lucent Technologies, Murray Hill, NJ; *R. Ragan*, California Institute of Technology, Pasadena, CA 86

TUESDAY AFTERNOON—1:00 PM—4:30 PM

Salons A/B

TRACK 2—COPPER

SESSION 3: COPPER WIRE AND CABLE I

Chairperson: Dr. Marek Kapuscinski, NORDX/CDT, Quebec, Canada

Forty Years of Electrical Cable Testing and Fault Location—*R. D. Macey*, Rutherford Cable Repairs, Rutherford, New South Wales, Australia 94

Impact of Power Variation on 3rd Order Passive Intermodulation of Coaxial RF-Cables and Their Connectors—*H. Gohdes*, RFS Kabelmetal, Hannover, Germany 97

Impedance Regularity of Copper Data Cables: How to Be Sure—*D. Prudhon, M. French*, Alcatel, Paris, France..... 102

EMC Compliance Testing of Link Termination in Local Area Networks—*D. Prudhon, M. French*, Alcatel, Paris, France..... 107

Relating Coupling Attenuation to Shield Transfer Impedance and Pair Balance in Data Communications Cables—*E. J. Lawrence*, Berk-Tek, New Holland, PA; *D. C. Hess*, Alcatel Cabling Systems, New Holland, PA; *M. Pelt*, Alcatel Cabling Systems, Brussels, Belgium 111

TUESDAY AFTERNOON—1:00 PM—4:30 PM

Salons C/D

TRACK 3—MATERIALS

SESSION 4: POLYMERIC MATERIALS

Chairperson: James A. Caballero, Synergistics Industries (NJ), Inc., Farmingdale, NJ

Determination of the Real Lifetime of Polymeric Cable Materials— <i>D. R. Parris, Z. Gao, Siemens AG, Neustadt, Germany</i>	122
A New Generation Polyethylene Resins for Cable Jacketing Applications— <i>L. Rogestedt, H.-B. Martinsson, Borealis AB, Stenungsund, Sweden</i>	126
Non-Halogenated, Non-Braided, Easy-To-Install Central Office Power Wire— <i>K. E. Cope, Pirelli Cables North America, Columbia, SC</i>	132
Die Drool in Chemically Crosslinkable Polyolefin Compounds— <i>S. W. Horwatt, G. A. Hatrich, Millennium Petrochemicals, Inc., Cincinnati, OH</i>	138
Physical Property and Toxicological Improvements in Premise Cable Insulations— <i>J. S. Borke, Millennium Petrochemicals Inc., Cincinnati, OH</i>	146
Silicone Crosslinking Methods— <i>S. K. Crawford, Essex Group Inc., Lafayette, IN</i>	151
The Effect of Viscoelastic Material Properties on Optical Fiber Cable— <i>S. Hassett, A. Parsons, R. Wagman, Siecor Corp., Hickory, NC</i>	156

TUESDAY EVENING

Exhibit Hall, Fourth Floor

Hospitality Hour—6:30 PM–8:00 PM

Suppliers Forum—6:30 PM–8:30 PM

Admission by badges issued to all registrants

WEDNESDAY MORNING—9:00 AM–11:35 AM

Salon E

TRACK 1—FIBER

SESSION 5: AERIAL II	
<i>Chairperson:</i> John R. Sicotte, Corning Inc., Corning, NY	
Development of New Aerial Distribution Cables with 4-Fiber Ribbons— <i>I. Kobayashi, D. Iwakura, R. Takaoka, E. Konda, R. Matuoka, Y. Sekii, H. Izukura, Y. Ohkawa, Y. Kamikura, Furukawa Electric Co., Ltd., Chiba, Japan</i>	166
Development of Aerial Cluster-Type Optical Drop Cable— <i>F. Hosoi, M. Hara, Y. Kamikura, Furukawa Electric Co., Ltd., Chiba, Japan</i>	176
OPGW: Do They Creep Differently?— <i>J. P. Bonicel, O. Tatat, Alcatel Telecommunications Cable, Claremont, NC; R. Girbig, G. Hog, Alcatel Kabel, Monchengladbach, Germany</i>	181
Materials, Design, and Performance of the Next Generation of All Dielectric Self-Supporting Aerial Loose Tube Fiber Optic Cable— <i>R. G. Gravely, III, J. W. Thornton, Fitel Lucent Technologies, Carrollton, GA</i>	191
New Effective Method to Calculate Temperature Increase During Short-Current Test on OPGW Cables— <i>C. Bastide, O. Tatat, Alcatel Telecommunications, Claremont, NC; T. Verhaege, Alcatel Alsthom Recherche, Marcoussis, France</i>	198

WEDNESDAY MORNING—9:00 AM–11:35 AM

Salon F

TRACK 1—FIBER

SESSION 6: FIBER SPLICING	
<i>Chairperson:</i> Dr. Peter R. Bark, Siecor Corp., Hickory, NC	
Flexible Connectorless Single Fibre Organisation in Exchange Cross Connects and Customer Access Applications— <i>R. Hailes, Telecom New Zealand Ltd., Wellington, New Zealand; S. Maguire, Fibernet New Zealand, Wellington, New Zealand</i>	205
A New Mechanical Splice for Optical Fiber— <i>K. Murakami, Y. Nakatani, K. Urata, H. Kunugiyama, T. Teraoka, H. Nakai, Hitachi Cable, Ltd., Ibaraki, Japan</i>	212
A New Concept in Splicing: FOCS— <i>B. Joly, A. Vincent, M. Reslinger, G. Godard, P. Laurency, Alcatel Cable Interface, Bezons, France; H. Aoustin, France Telecom/CNET-DTD/CAI, Lannion, France; M. Boitel, T. Mahe, France Telecom/CNET-DTD/RCV, Lannion, France</i>	218
Single-Fiber Mechanical Splice for Single-Mode Optical Fiber— <i>T. Nakano, J. Yamakawa, T. Shigematsu, Furukawa Electric Co., Ltd., Chiba, Japan</i>	225

WEDNESDAY MORNING—9:00 AM–11:35 AM

Salons A/B

TRACK 2—COPPER

SESSION 7: COPPER WIRE AND CABLE II	
<i>Chairperson:</i> Hans A. Mayer, Olex Cables, Melbourne, Australia	
Management for Renewal of the Metallic Access Network— <i>D. Tomizu, H. Harada, M. Inoue, NTT Access Network Systems Laboratories, Ibaraki, Japan</i>	231
Crosstalk Model for Pair-Shielded Data Cables— <i>M. Backmann, C. Pfeiler, A. Wassmuth, Nokia Kabel GmbH, Nuremberg, Germany</i>	238
Relating Total Reflected Energy to Input Impedance in Balanced Pair Transmission Lines— <i>T. M. Hayes, Lucent Technologies, Norcross, GA</i>	244
Investigation of Ingress on Bi-Directional CATV System— <i>H. Omura, M. Katoh, Furukawa Electric Co., Ltd., Kanagawa, Japan</i>	253

WEDNESDAY MORNING—9:00 AM–11:35 AM

Salons C/D

TRACK 3—MATERIALS

SESSION 8: FIBER RIBBONS	
<i>Chairperson:</i> Nils Artlöve, Telia AB, Farsta, Sweden	
An Overview of Key Ribbon Handleability Attributes— <i>G. A. Lochkovic, S. K. Moorjani, N. I. Patel, R. J. Speights, B. L. Stephens, Siecor Corp., Hickory, NC</i>	260

UV Color Coatings and Matrix Material Design for Enhanced Fiber Optic Ribbon Products— <i>K. Konstadinidis, N. W. Sollenberger, S. Siddiqui, K. W. Jackson, J. M. Turnipseed, T. W. Au, R. P. DeFabritis, C. R. Taylor</i> , Lucent Technologies, Norcross, GA	274
The Effect of the Mechanical Properties of UV-Curable Resins on the Strippability of Optical Fiber Ribbons— <i>A. Murata, K. Mitsuhashi, K. Oohashi</i> , Fujikura Ltd., Chiba, Japan	281
Contact Mechanics of a Fiber Optic Ribbon— <i>M. Tabaddor, K. W. Jackson, R. Travieso</i> , Lucent Technologies, Norcross, GA	289

WEDNESDAY—11:45 AM–2:15 PM

Grand Ballroom, Salons G/H, Fifth Floor

AWARDS LUNCHEON

Speaker: Yvonne Kaye, Ph.D., Philadelphia, PA

Admission by badges issued to all registrants

WEDNESDAY AFTERNOON—2:15 PM–4:50 PM

Salon E

TRACK 1—FIBER

SESSION 9: SUBMARINE

Chairperson: Michel Rousseau, Alcatel Cable, Clichy, France

The Selective Use of Marinized Terrestrial Cable for Underwater Applications— <i>S. O'Bow-Hove</i> , Alcatel Submarine Networks, London, England; <i>T. Kutt</i> , Tyco Submarine Systems, NJ	298
---	-----

A New High Bit Rate Submarine Product Range: The OALC 4 Cable— <i>Y. Charles, J.-F. Libert, P. Worthington, J.-L. Lang</i> , Alcatel Submarine Networks, Calais, France	306
---	-----

Long Term Behaviour of Hydrogen Induced Losses in Installed Fiberoptic Submarine and Underwater Cables— <i>S. Hopland</i> , Telenor Nett AS, Oslo, Norway	316
---	-----

Assessment of Hydrogen Ingress in Submarine Cables at Joints and Terminations— <i>J.-F. Libert, F. Ruelle, P. Worthington</i> , Alcatel Submarine Networks, Calais, France	326
--	-----

WEDNESDAY AFTERNOON—2:15 PM–4:50 PM

Salon F

TRACK 1—FIBER

SESSION 10: CABLE INSTALLATION

Chairperson: Dr. Howard Wichansky, U.S. Army Communications-Electronics Command (CECOM), Fort Monmouth, NJ

A Study of Air Blown Fiber for a Long Distance Tube— <i>I. Sakabe, W. Katsurashima, H. Sano, S. Tanaka</i> , Yokohama, Japan	341
--	-----

Blown Fibre—A Reference Test Blowing Route— <i>K. Cockrill, J. Nixey, R. Studd</i> , BT Laboratories, UK; <i>M. Davies, R. Sutehall</i> , Pirelli Cables, UK	348
--	-----

Study on Additional Fiber Blowing Technique— <i>W. Katsurashima, H. Ishikawa, H. Sano, S. Tanaka</i> , Sumitomo Electric Industries, Ltd., Yokohama, Japan	354
Current Developments in Cable-in-Duct Blowing Techniques— <i>W. Griffioen</i> , KPN Research, Leidschendam, The Netherlands; <i>G. Plumettaz</i> , Plumettaz SA, Bex, Switzerland	363
Characteristics of a Ribbon Type 16-Fiber Pass Unit— <i>K. Ishida, K. Kobayashi, A. Mogi, K. Oohashi, M. Miyamoto</i> , Fujikura Ltd., Chiba, Japan	368

WEDNESDAY AFTERNOON—2:15 PM–4:50 PM

Salons A/B

TRACK 2—COPPER

SESSION 11: BROADBAND/OUTSIDE PLANT

Chairperson: Fred Narayan, Phelps International Corp., Coral Gables, FL

New Copper Cabling Systems for Residential Home Network— <i>M. Lissillour, O. Bouffant, H. Le Cozic, P. Guillas</i> , France Telecom, BD/CNET/DTT, Lannion, France	374
--	-----

Field Test of Telephony Service by Utilizing a Cable Television Network— <i>Y. Sato, H. Ishida, M. Kato</i> , Furukawa Electric Co., Ltd., Hiratsuka, Japan; <i>S. Zenimura, K. Yoshikawa</i> , Tokyo Electric Power Co., Inc., Tokyo, Japan; <i>T. Anada, S. Masumitsu</i> , Tokyo Telecommunication Network Co., Inc., Tokyo, Japan	381
---	-----

Building Italian HFC Broadband Distribution Network: Field Experiences and Special Installation Solutions— <i>M. Bottanelli, E. Cottino</i> , SIRT S.p.A., Cassina de' Pecchi, Italy	391
--	-----

New CATV-Coaxial Cables and Components for Hybrid Fiber/Coax (HFC) Networks with High-Speed Data Transmission— <i>P. E. Zamzow</i> , Alcatel Cable, Monchengladbach, Germany; <i>H. Schürmann</i> , Alcatel Cable Benelux, Seneffe, Belgium; <i>A. Ludl</i> , Consultant to Alcatel, Monchengladbach, Germany ..	396
--	-----

WEDNESDAY AFTERNOON—2:15 PM–4:50 PM

Salons C/D

TRACK 3—MATERIALS

SESSION 12: FIBER COATING & ENVIRONMENT

Chairperson: Dr. Raymond E. Jaeger, SpecTran Corp., Sturbridge, MA

New Coatings Developments and Characterizations and Multi-Uses Cables Materials for FTTH— <i>A. Morgand, D. Boscher, B. Cadier, A. C. Reau, Y. Ruello</i> , France Telecom, Lannion, France	409
---	-----

Applicability of UV Curable Urethane Acrylate Coating at High Drawing Speed— <i>M. Sugimoto, Y. Naito, H. Uchida, Z. Komiya, T. Ukachi</i> , Japan Synthetic Rubber Co. Ltd., Tsukuba, Japan	418
--	-----

Environmentally Friendly Strategies for Telecommunications Providers— <i>T. N. Bowmer</i> , Bellcore—Network Integrity Solutions, Morristown, NJ	426
--	-----

Life-Cycle Assessment of Cables— <i>R. Färlin, K. Nygård-Skalman</i> , Ericsson Cables AB, Hudiksvall, Sweden	436
Recycling of Plastic Scrap from Outside Plant in NTT— <i>T. Konaka, S. Murai, S. Nishi</i> , Nippon Telegraph and Telephone Corp., Ibaraki, Japan	443

WEDNESDAY AFTERNOON—4:00 PM–6:30 PM

Exhibit Hall, Fourth Floor

SESSION 13: POSTER PAPERS

<i>Chairpersons:</i> Dr. Reiner J. Gerdes, TransTel Group, Inc., Atlanta, GA, and Dieter S. Nordmann, Alcatel Cable, Hannover, Germany	
Optical Fibre Colouring: Gravity Feed vs. Pressurized Inking— <i>B. E. Buluschek, M. Blarrik</i> , Swisscab E. Kertscher S.A., Yvonand, Switzerland ..	452
Study of the Relationship Between Optical Fiber Strength after Splicing and the Method of Optical Fiber Cleaning Prior to Splicing— <i>J. Suzuki, S. Yaguchi, M. Yoshinuma</i> , Fujikura Ltd., Chiba, Japan	457
Evaluation of Color Stability of Optical Fiber Coatings— <i>S.-H. Chou, J.-C. Lin, C.-M. Hsiao, H.-F. Lin, H.-P. Hsu, Y.-c. Lin, Y.-K. Tu</i> , Chunghwa Telecom, Taiwan, R.O.C.	462
Numerical Simulation of Optical Fiber Coating Process— <i>K. J. Lyytikäinen</i> , Nokia-Maillefer, Vantaa, Finland	468
Installation Advantages with Ribbon Technology— <i>H. Serrander, H. Olofsson</i> , Ericsson Business Networks AB, Sundbyberg, Sweden.....	473
New Closure System with Single Fiber Access for Continuous Network Operation— <i>W. Stieb, F. Grajewski</i> , Alcatel Kabel, Germany	478
Development of Compact Fusion Splicer for Aerial Optical Fiber Cable— <i>H. Hongu, T. Sano, Y. Hishikawa, H. Takayanagi, K. Osaka</i> , Sumitomo Electric Industries, Ltd., Yokohama, Japan	483
Development of Small Size and High Performance Flat Intra-Office Optical Fiber Cable using Fiber Cord and Fiber Ribbon Cord— <i>Y. Nagase, H. Tamura, M. Yoshida</i> , Toyokuni Electric Cable Co., Ltd., Saitama, Japan.....	488
Design of Compact Optical Fiber Identification (ID) Tester and Talk Set for Optical Subscriber Loops— <i>Y. Enomoto, N. Tomita, H. Terui, Y. Yamada, N. Uchida</i> , NTT Access Network Systems Laboratories, and NTT Opto-electronics Laboratories, Ibaraki, Japan	493
Design and Development of Optical Fiber Jointing Techniques for Efficient Construction of Aerial Distribution Cable Systems— <i>M. Takaya, T. Katagiri, S. Nagasawa, N. Kashima</i> , NTT Access Network Systems Laboratories, Ibaraki, Japan	500
New Connector Block Mechanism Applied to Cable Connection— <i>S.-h. Kim, K.-h. Chin, S.-k. Kang, C.-h. Kim</i> , Korea Telecom, Teajon, Korea	506
Mini-MPO Connector— <i>N. Shimoji, J. Yamakawa</i> , Furukawa Electric Co., Ltd., Chiba, Japan	510
Development of 72-Channel Optical Fiber Connector— <i>K. Kanai</i> , Furukawa Electric Co., Ltd.; <i>O. Suzuki, T. Watanabe, S. Toda</i> , Fujitsu Ltd., Kanagawa, Japan	516

Radiation Aging and Degradation Mechanism of Polymer Insulation for Electric Cables— <i>M. Sugiyama, M. Nitta, T. Tani</i> , Yazaki Electric Wire Co., Ltd., Shizuoka, Japan; <i>T. Seguchi, T. Yagi</i> , Japan Atomic Energy Research Institute, Gunma, Japan	521
Novel Conduit Inspecting System— <i>R.-S. Kuo, W.-L. Lin, M.-S. Lu, C.-H. Chen, L.-J. Huang, S.-T. Chang, S.-W. Lai, H.-P. Hsu, Y.-C. Lin, Y.-K. Tu</i> , Chunghwa Telecom Co., Ltd., Taiwan, R.O.C.	526
A New Approach on Optical Fiber Cable Network Supervision System— <i>H. Silvino de Almeida Prata</i> , Telebrás, Campinas, São Paulo, Brasil	530
Measurement of Coupled Noise Attenuation— <i>D. Wilhelm</i> , GHMT, Bexbach/Saar, Germany	534
Review on the Correlation Between Residual Strain of Fibers in Ribbon and Ribbon Property— <i>G. W. Seo, Y. H. Jeon, S. H. Kim</i> , Daewoo Telecom Ltd., Incheon, Korea	539
Development of New Mechanical Splice— <i>T. Tanaka, Y. Fujiwara, Y. Tamaki, H. Yokosuka</i> , Fujikura Ltd., Chiba, Japan.....	547
Cable Reference Measuring Clamp KRMZ 1200— <i>F. Streibert</i> , GHMT, Bexbach/Saar, Germany	552
Investigation of a Dual Purpose Cable Component: A Water-Blocking Tensile Glass Fiber Strand— <i>T. P. Hager</i> , Owens Corning, Granville, OH; <i>A. G. Bringuier</i> , Siecor Corp., Hickory, NC	556
Fiber Grating Based Chromatic Dispersion Compensators: Packaging and System Performances— <i>P. Peretta, F. Pozzi, M. Signorelli</i> , SIRT A S.p.A. Cables and Optical Technologies, Milano, Italy.....	563
Typhoon Toughened ADSS Cables— <i>S. G. Kipp, A. Peng, K. Tsai</i> , Baycom Opto-Electronics Technology Co. Ltd., Taiwan, R.O.C.	568

THURSDAY MORNING—8:30 AM–12:00 NOON

Salon E

TRACK 1—FIBER

SESSION 14: FIBER AND CABLE DESIGN I	
<i>Chairperson:</i> Manuel R. Santana, Lucent Technologies, Bell Laboratories, Norcross, GA	
A Mechanical Model for Studying Stress and Strain Caused by Temperature Variations in Fibre Optic Cables— <i>J. L. Rodríguez, V. Latorre, V. Abadía</i> , BICC Cables de Comunicaciones, S.A., Zaragoza, Spain.....	573
Manufacturing and Characterization of Multicore Fibers— <i>J.-F. Bourhis, R. Meilleur, P. Nouchi, A. Tardy, G. Orcel</i> , Alcatel, Conflans-Sainte-Honorine, France.....	584
Design Strategies for High Fiber Count Plenum Cables— <i>J. T. Chapin, M. F. Marx, P. A. Moss, W. M. Newton, M. Viriyayuthakorn, C. G. Wilson</i> , Lucent Technologies, Norcross, GA	590
Development and Actual Environment Testing of Optical Fiber Cables with Small Diameter Stainless Pipe— <i>Y. Sudo, T. Ohsako, K. Nemoto, H. Ishizaki</i> , Ocean Cable Co., Ltd., Kita-Kyushu, Japan	602

Development and Design for Optimizing High-Count OPGW— <i>C. H. Jung, S. C. Park, Y. I. Lee, H. J. Kang</i> , Taihan Electric Wire Co., Ltd., Kyungki-Do, Korea	609
Low PMD Fibers by an On-Line Spinning Apparatus— <i>M. Caiata, F. Cocchini, A. Mazzotti, A. Monetti, A. Schiaffo</i> , FOS Fibre Ottiche Sud, Battipaglia, Italy	617

THURSDAY MORNING—8:30 AM–12:00 NOON

Salon F

TRACK 1—FIBER

SESSION 15: TESTING/FIELD EVALUATION

Chairperson: James R. Leech, Union Carbide Corp., Somerset, NJ

Applicability of All-Dielectric Self-Supporting Cable Systems to Very High Voltage Overhead Power Lines— <i>C. N. Carter, J. Deas</i> , National Grid Company plc, Leatherhead, UK; <i>N. R. Haigh, S. M. Rowland</i> , BICC Cables Ltd., Helsby, UK	622
An Approach to Increasing Multiplexed Optical Signals on the Optical Multi-Coupler System— <i>H. Nasu, H. Omura</i> , Furukawa Electric Co., Ltd., Kanagawa, Japan; <i>Y. Shinoda, Y. Kuze</i> , Tokyo Electric Power Co., Tokyo, Japan	632
Testing of Expendable Optical Fibers for Unmanned Ground Vehicles Applications— <i>D. K. Anderson, S. J. Burgett, T. B. McAlpin</i> , Redstone Arsenal, AL; <i>J. R. McMinn</i> , Morgan Research Corp., Huntsville, AL	642
An Optical-Cable Identification System Using Optical Interference between Two Optical Fibers— <i>Y. Azuma</i> , NTT Maintenance and Service Operations Dept., <i>K. Matsuno, K. Arakawa, K. Yoshida</i> , NTT Technical Assistance and Support Center, Tokyo, Japan	650
A Novel Surveillance System for Installed Fiber Optics Cables Using Stimulated Brillouin Interaction— <i>M. Niklès, L. Thévenaz, A. Fellay, M. Facchini, P. A. Robert</i> , Swiss Federal Institute of Technology of Lausanne, Switzerland; <i>P. Salina</i> , Swiss Telecom PTT, Bern, Switzerland	658
Reflective Influence Consideration for Sub-Carrier Multiplexing System— <i>T. Kato, H. Omura, S. Takashima</i> , Furukawa Electric Co., Ltd., Kanagawa, Japan	666
Automatic Optical Cables Sheath Monitoring System— <i>E. Cottino, A. Damiano, I. Piffari</i> , SIRT S.p.A., Cassina de'Pecchi, Italy; <i>A. Regini</i> , Radiodetection Ltd., Bristol, UK	675

THURSDAY MORNING—8:30 AM–12:00 NOON

Salons A/B

TRACK 2—COPPER

SESSION 16: COPPER WIRE AND CABLE III

Chairperson: Leo Chatter, DCM Industries, Inc., Union City, CA

Assessment of the Uniformity of Twists— <i>J.-H. Walling, J.-F. Richard</i> , NORDX/CDT, Montreal, Canada; <i>V. LeNir</i> , V.P.S. Enterprises, Montreal, Canada	681
Termination of a Screen in Practice: Earthing Versus Grounding— <i>M. Pelt, P. De Win</i> , Alcatel Cabling Systems Competence Center, Brussels, Belgium	692
Performance Assessment of Baluns— <i>J.-H. Walling, M. Belanger</i> , NORDX/CDT, Montreal, Canada; <i>J. Scharf</i> , Analog-Elektronik, Metzingen, Germany	698
About the Influence of Residual Elongation and Thermal Expansion on the Sagging Performance of Glass Fiber Reinforced Aerial Service Wires— <i>J.-H. Walling</i> , NORDX/CDT, Montreal, Canada	708
Development of Cross-Inductive Cable for Train Location Detection in the Superconducting Maglev Train Control System— <i>M. Ono</i> , Central Japan Railway Co., Tokyo, Japan; <i>Y. Sakai</i> , Railway Technical Research Institute, Tokyo, Japan; <i>M. Ohta</i> , Japan Railway Construction Public Corp., Tokyo, Japan; <i>O. Koyasu</i> , Fujikura Ltd., Chiba, Japan; <i>K. Tazumi</i> , Hitachi Cable Ltd., Tokyo, Japan; <i>K. Mita</i> , Sumitomo Electric Industries Ltd., Osaka, Japan	720

THURSDAY MORNING—8:30 AM–12:00 NOON

Salons C/D

TRACK 3—MATERIALS

SESSION 17: FIRE AND FLAME

Chairperson: Inge B. Kovacs, Consultant for Polycheck Limited, Hackettstown, NJ

Trends and Developments in Flame Retardants for Cables— <i>S. C. Brown</i> , Alcan Chemicals Ltd., Banbury, England	727
The Long Term Behaviour of Halogen Free, Flame Retardant Material Under Diverse Conditions— <i>M. Nilsson, K. Nygård-Skalman, M.-C. Ljung</i> , Ericsson Cables AB, Hudiksvall, Sweden	736
Highly Stabilized Flame Retarded Polyolefin Insulation Compounds— <i>L. Y. Lee</i> , Millennium Petrochemicals Inc., Cincinnati, OH	744
Testing of Cables Designed for Fire Resistance: A Comparison of U.S. and European Standards— <i>S. Richter</i> , Consulting Engineer, Eckental, Germany; <i>R. Schmidt</i> , Martinswerk GmbH, Bergheim, Germany	752
Nanocomposites: Radiative Gasification and Vinyl Polymer Flammability— <i>J. W. Gilman, T. Kashiwagi, S. Lomakin</i> , National Institute of Standards and Technology, Gaithersburg, MD; <i>J. D. Lichtenhan, P. Jones</i> , Edwards Air Force Base, CA; <i>E. P. Giannelis, E. Manias</i> , Cornell University, Ithaca, NY	761
Comparison of Fire Behavior of Copper and Fiber Optic Cables in Large and Full Scale Fire Test Facilities— <i>J. T. Chapin</i> , Lucent Technologies, Norcross, GA; <i>L. Caudill, J. R. Hoover</i> , DuPont, Wilmington, DE	775

PLENARY SESSION
"BROADBAND ACCESS"



DR. ROBERT W. LUCKY
Corporate Vice President, Applied Research
Bellcore, Red Bank, NJ

Robert W. Lucky was born in Pittsburgh, PA, and attended Purdue University, where he received a B.S. degree in electrical engineering in 1957, and M.S. and Ph.D. – degrees in 1959 and 1961. After graduation he joined AT&T Bell Laboratories in Holmdel, NJ, where he was initially involved in studying ways of sending digital information over telephone lines. The best known outcome of this work was his invention of the adaptive equalizer – a technique for correcting distortion in telephone signals which is used in all high speed data transmission today. The textbook on data communications which he co-authored became the most cited reference in the communications field over the period of a decade.

At Bell Labs he moved through a number of levels to become Executive Director of the Communications Sciences Research Division in 1982, where he was responsible for research on the methods and technologies for future communication systems. In 1992 he left Bell Labs to assume his present position at Bellcore.

He has been active in professional activities, and has served as President of the Communications Society of the IEEE (Institute of Electrical and Electronics Engineers), and as Vice President and Executive Vice President of the parent IEEE itself. He has been editor of several technical journals, including the Proceedings of the IEEE, and since 1982 he has written the bimonthly "Reflections" column of personalized observations about the engineering profession in Spectrum magazine. In

1993 these "Reflections" columns were collected in the IEEE Press book Lucky Strikes...Again.

Dr. Lucky is a Fellow of the IEEE and a member of the National Academy of Engineering. He is also a consulting editor for a series of books on communications through Plenum Press. He has been on the advisory boards or committees of many universities and government organizations, and was Chairman of the Scientific Advisory Board of the United States Air Force from 1986-1989. He was the 1987 recipient of the prestigious Marconi Prize for his contributions to data communications, and has been awarded honorary doctorates from Purdue University and the New Jersey Institute of Technology. He has also been awarded the Edison Medal of the IEEE and the Exceptional Civilian Contributions Medal of the U.S. Air Force.

Dr. Lucky is a frequent speaker before both scientific and general audiences. He has been an invited lecturer at about one hundred different universities, and has been the guest on a number of network television shows, including Bill Moyers' "A World of Ideas," where he has discussed the impacts of future technological advances. He is the author of the popular book Silicon Dreams, which is a semi-technical and philosophical discussion of the ways in which both humans and computers deal with information.

Dr. Lucky and his wife, Joan, currently reside in Fair Haven, NJ.

LUNCHEON SPEAKER



YVONNE KAYE PH.D.
Philadelphia, Pennsylvania

Yvonne Kaye Ph.D. has been in the field of Human Services since 1951. Her expertise has been in the area of addictions, thanatology and relationship challenges. On the publication of her book, "Credit, Cash and Codependency – the Money Connection", in both English and Spanish, Dr. Kaye has become widely known as a specialist in financial and spiritual bankruptcy. Her book "366 Encouragements for Prosperity" published in English and Chinese, established her as an International Motivator.

Motivational Speaker, Humorist, Talk Show Host, Author, Columnist, Businesswoman, Dr. Kay is still on her own exciting journey of enlightenment, human growth and change. Believing that we can make decisions about the way we feel and what we do, she encourages people to use their imagination to their greatest good. Positive thinker and perennial student of life and humour, Dr. Kaye motivates people to improve their lifestyle and embrace their individual journeys of transition. Her mission is teaching people how to alleviate their stress increasing their mental, physical, spiritual, emotional and financial

well-being, using those experiences as lessons in living...and laughing more.

She is especially effective as a Banquet, Conference and Seminar Speaker and has presented at the United Nations. Recently presentations have been made at as diverse organizations as The National Association of Demolition contractors in Las Vegas, The Veterans Administration in Johnson City, TN, Cafeteria aides, school bus drivers, secretaries and teachers' aides. Her approach is eclectic and very appropriate for Educational & Religious Institutions, Medical Professionals, Human Services, Business, Industry, Holistic and Spiritual Associations and the Entertainment Industry. Her presentations reach all walks of life, all employees as well as administration. Dr. Kaye is an equal opportunity presenter!

Dr. Kaye has been affectionately referred to as Mental Health's answer to Erma Bombeck! She is featured in Marquis' Who's Who of American Women, 1997/1998.

Design of Aerial Optical Fiber Cable System Suitable for Easy Branching

Hideyuki Iwata, Masaru Okada, Shigeru Tomita, Norio Kashima,
Tetsuya Hoshijima, Mitsuo Kama, *Kaoru Nishizawa

NTT Access Network Systems Laboratories
*NTT Technology and Development Support Center

1-7-1, Hanabatake, Tsukuba, Ibaraki, 305 JAPAN

ABSTRACT

In this paper, we describe the design and performance of new self supporting (SS) optical cable which employs 4-fiber ribbon and a closure for aerial distribution networks. This cable with SZ-slotted rod is suitable for use with the mid span access technique which allows easy branching. This is because fiber ribbon can be extracted easily from a slotted rod without cutting it. We also describe a new less expensive closure for aerial optical fiber cable which reduces the required joining time. This cable and the closure will be useful in relation to constructing optical distribution networks economically for fiber to the home (FTTH).

INTRODUCTION

The demand for multimedia communication services has been growing and optical fibers are being introduced into the distribution networks of access networks to help meet this need. Figure 1 shows the access network configuration. ⁽¹⁾ This network consists of feeder and distribution cables. The feeder cable is installed in a duct and joined to the distribution cable to provide subscriber access. Cable branching by midspan access technologies allows the economic construction of efficient access networks for uncertain levels of demand.

In Japan, most of the distribution network consists of aerial cables except in metropolitan areas. Recently, the amount of installed self-supporting (SS) optical fiber cable has been increasing every year. Several years ago, SS optical fiber cables were used for trunk lines where there were either no under ground facilities or where they would have been difficult to construct. At that time, there

was no need for branch distribution cables or drop cables, therefore these cables are not suitable for such applications. However, it is necessary to decide when to install SS cables in distribution network and cost is also an important factor.

Focusing on those issues, we developed new SS optical cables for distribution networks. These cables will be useful in terms of developing optical distribution networks toward fiber to the home (FTTH).

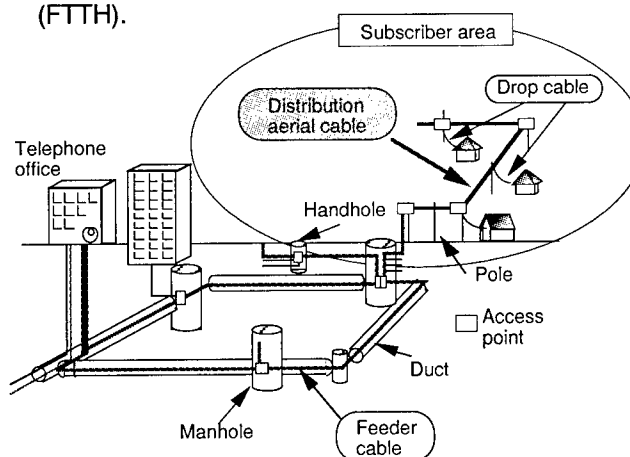
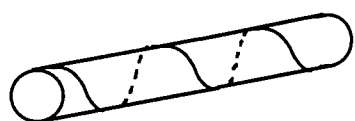


Figure 1. Access Network Configuration

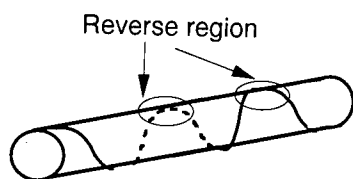
CABLE DESIGN

Slotted rod design

We designed the slotted rod for the new SS optical fiber cable with a view to achieving easy branching and sufficient friction force. Easy branching requires a certain excess length of ribbon fiber for identification and joining work. Our cable with an SZ-slotted rod is suitable for easy branching. This is because a fiber ribbon can be drawn easily from a slotted rod without cutting it. In addition, the friction force between the rod and the fiber ribbon is slightly larger than with conventional cable in order to prevent fiber the moving during such work.



(a) S-stranding



(b) SZ-stranding

Figure 2 Slotted rod structure

Unidirectional (S) and SZ-slotted rod

There are two major slotted rod structures as shown in Fig.2. Type (a) is called the S-slotted rod structure, and here a slot is cut around the center of the rod unidirectionally. Type (b) is called the SZ-slotted rod structure, and in this case a slot is cut around the center of the rod and the direction alternates with a certain frequency. With type (a), the ribbons are stranded around the center of the rod in the same way as the slots. This makes it hard to extract ribbons without cutting the rod. However, with type (b), the ribbons are placed in meandering slots and the ribbons can be extracted from the slotted rod easily. The ease with which they can be extracted and the fact that it is unnecessary to cut the rod means that type (b) SZ-slotted rods are suitable for easy branching with the mid span access technique.

Calculation of Sag

For case of easy branching, a certain excess length of ribbon fiber is needed for identification and joining work. The use of a conventional identification tool requires a 20 mm space, between the slotted rod and the ribbon fiber. The sag length is determined by the reverse angle, the distance between the center of the rod and the ribbon in the slots, and the reverse pitch. Figure 3 shows the calculation model for sag S which is the distance between a slotted rod and an extracted the ribbon fiber.⁽²⁾ a is the distance between the center of the rod and the ribbon when the ribbon is

in the slots. P is the reverse pitch of the SZ-slotted slot, Φ is the reverse angle of the slot through the cross-section of the rod, and L is the removed length of cable jacket. When the center of the removed length of sheath is the reverse pitch point, the sag S_1 is expressed as

$$S_1 = \sqrt{\left(\frac{A}{2}\right)^2 + \left(\frac{L}{2}\right)^2} \quad \text{[1]}$$

$$A = 2 \int_0^{\theta} \sqrt{1 + (f_1'(\theta))^2} d\theta \quad \text{[2]}$$

$$f_1(\theta) = \frac{a\Phi}{2} \sin \theta \quad \text{[3]}$$

$$\theta = \frac{L\pi}{2P} \quad \text{[4]}$$

Conversely, when the center of the removed length of sheath is between the reverse points, the sag S_2 is expressed as

$$S_2 = \sqrt{\left(\frac{A}{2}\right)^2 + \left(\frac{B}{2}\right)^2} \quad \text{[5]}$$

$$A = 2 \int_0^{\theta} \sqrt{1 + (f_2'(\theta))^2} d\theta \quad \text{[6]}$$

$$B = 2 \sqrt{\left(\frac{L}{2}\right)^2 + f_2(\theta)^2} \quad \text{[7]}$$

$$f_2(\theta) = \frac{a\Phi}{2} \cos \theta \quad \text{[8]}$$

Figure 4 shows the relationship between the sag length and the ratio of removed length to reverse pitch for different distances between the center of a rod and a ribbon. The filled circles and squares indicate distance of 2 mm and 4 mm, respectively, between the center of the rod and the fiber ribbon. The solid line shows the sag length for a given length of removed cable jacket at the center of the reverse pitch. The dotted line is the sag length at the mid-point between reverse regions. Based on

these results, we should select a short reverse pitch or remove a long length of cable jacket to obtain sufficient sag for a small count cable with a small outer diameter. But we select a short reverse pitch, we must consider the fact that a reduction in reverse pitch increases the strains and bending in the fiber ribbon. To prove this equation, we used several SZ-slotted rod cables and compared the measured and calculated values as shown in Fig 5. The solid line with open circles and error bars shows measured values, the dotted line with filled circles shows calculated values. There is no big difference between the two values.

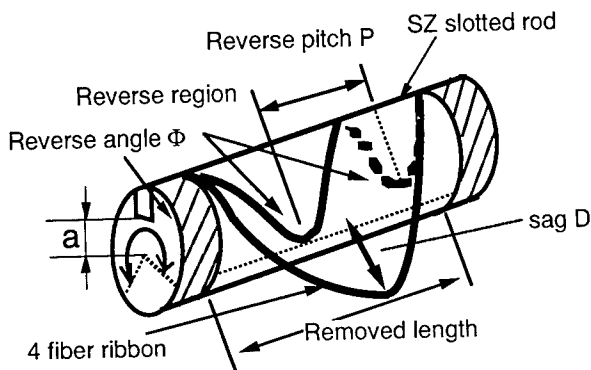


Figure 3 Calculation model for an SZ slotted rod with the cable jacket removed.

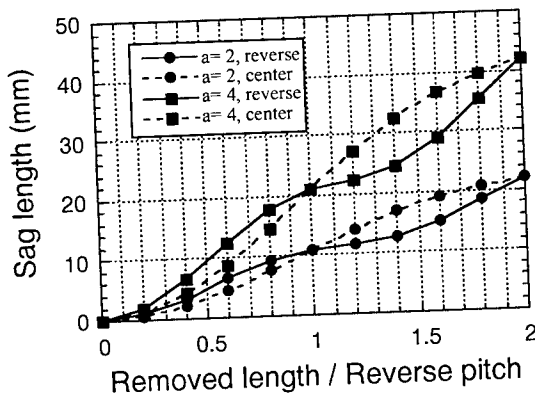


Figure 4 Relationship between sag length and removed length / reverse pitch

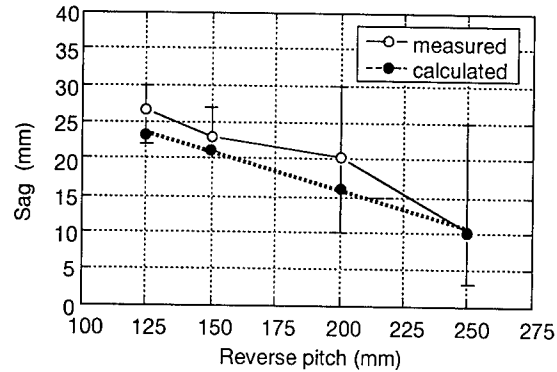


Figure 5 Relationship between reverse pitch and sag

Friction force F

When the mid span access technique is employed, a cable is branched at short distances along the cable route. The minimum distance is probably that between adjacent poles, because branching work is usually undertaken near a pole. If there is no friction force between the slotted rod and a ribbon fiber, the fiber can be moved easily. This affects the nearest jointing point because the length of the fiber in a closure is reduced by moving the fiber and this may cause bending or a large elongation in joined fibers. The slot locus of the SZ-slotted rod can be expanded into a plane as shown in Fig. 6.⁽³⁾ The friction force T_1 between a fiber ribbon and a slotted core at sections (A) and (D) are expressed as

$$T_1 = T_2 \exp(-\mu\theta) + \frac{WR}{1-\mu^2} \{ (1-\mu^2) \cos\theta - 2WR \sin\theta \} \quad [9]$$

Also those at sections (B) and (C) are expressed as

$$T_1 = T_2 \exp(\mu\theta) + \frac{WR}{1-\mu^2} \{ (1-\mu^2) \cos\theta + 2WR \sin\theta \} \quad [10]$$

$$\theta = \frac{L\pi}{P} \quad [11]$$

where T_2 is the pulling force on the fiber ribbon, a is the distance between the center of the rod and the ribbon when the ribbon is located in the slots, P is the reverse pitch of the SZ-stranded slot, W is the weight of the fiber ribbon, L is the cable length, μ is the friction coefficient between a fiber ribbon and a slotted core and R is bending radius of the fiber ribbon.

We measured the friction force of a cable with a reverse pitch of 125 mm and a distance of 2.1 mm

between the center of the rod and the ribbon which was in the slots. Figure 7 shows the measured and calculated friction force. The error bars with open triangles show measured values and the dotted line shows calculated values. There is no big difference between the values and the friction force is sufficient for a fiber which moves by accident during branching work.

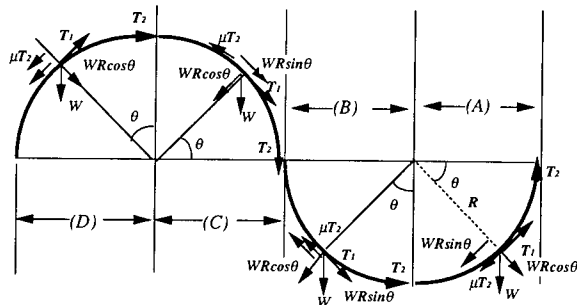


Figure 6 Slot locus of the SZ-slotted rod expanded into a plane

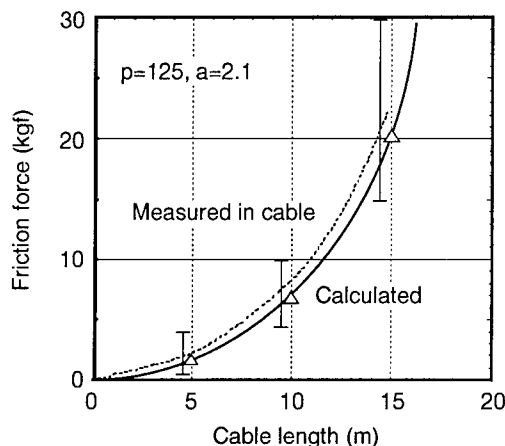


Figure 7 Comparison between calculated and measured values

Self supporting structure Elongation characteristics

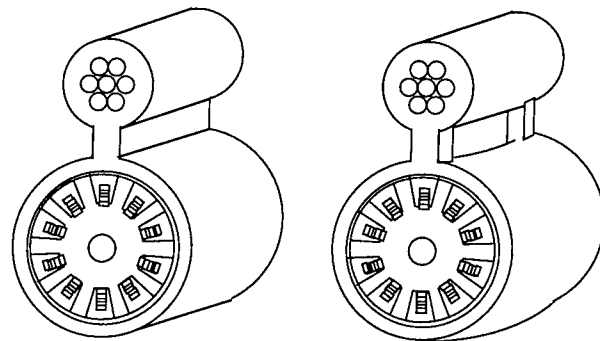
Two type of SS structure are shown in Fig.8. The basic SS structure consists of a messenger wire and a cable core sheath together with polyethylene.

Type (a) is called figure 8, and here the messenger wire and cable core are combined with the cable jacket along whole length of the cable. Type (b) is called with window. The cable core is longer than the messenger wire to avoid

excessive fiber elongation. The long term reliability of the optical fiber must be ensured and so it should not suffer the same elongation as the messenger wire.

The cable core may expand because of the difference between the linear expansion coefficients of the cable core and the messenger wire, and huge elongation caused by high speed winds. This elongation value is critical in terms of optical fiber reliability.

Figure 9 shows the relationship between temperature and cable core expansion force. The open squares show the characteristics of type (a) cable with a 40 m/s wind. The open circles show those of type (b) cable without wind. The filled circles indicate those of type (b) cable with or without. These results show that cable core expansion can be suppressed because the cable has excess length and elongation in the messenger wire does not induce elongation in the fiber in the cable.



(a) Figure 8

(b) With windows

Figure 8 Self-supporting structure

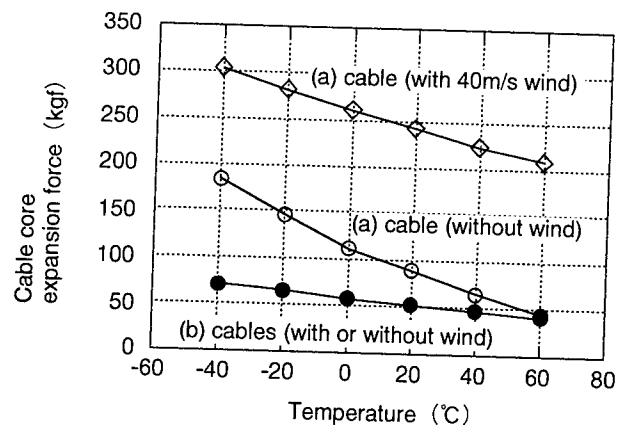


Figure 9 Relationship between temperature and cable core expansion force

Window characteristics

Windows are placed at certain intervals along the cable to improve its wind characteristics. Figure 10 shows the relationship between cable angle and wind force coefficient for type (a) and (b) cable. The dotted line with open circles show the characteristics of type (a) cable as regards lift force and the dotted line with the filled squares shows those of type (b) cable. A small lift force is suitable for suppressing wind induced oscillation. These results show that type (b) cable is better at avoiding such oscillation.

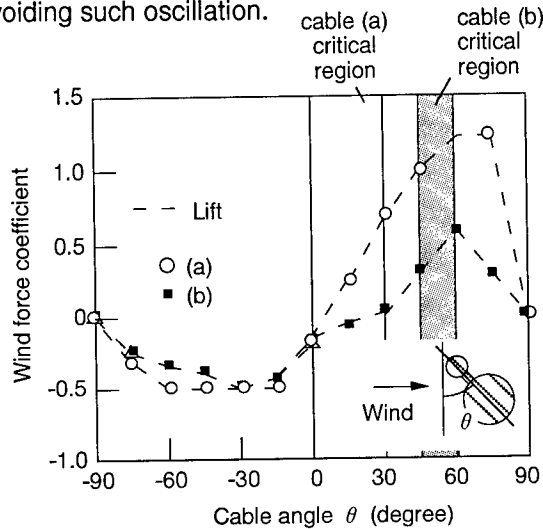


Figure 10 Relationship between cable angle and wind force coefficient

CABLE PERFORMANCE

A cross-sectional view of the newly designed prototype aerial optical fiber cable is shown in Fig.11. Five 4-fiber ribbons are assembled in an SZ stranded slotted rod. The SS structure consists of a messenger wire and a cable which are combined together with polyethylene and the cable core is longer than the messenger wire to avoid excessive fiber elongation.

Table 1 shows measured the transmission, mechanical and temperature characteristics of our prototype cable. We measured the fiber attenuation by using optical time domain reflectometry (OTDR) at 1550 nm. We also used an LED and a n optical power meter to evaluated aspects of mechanical performance such as bending, lateral force and wind force and elongation and we also undertook a temperature

cycle test between -30 and 70 °C. We found all the values to be as good as those of currently used cable.

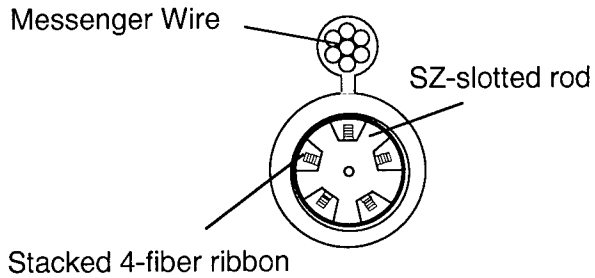


Figure 11 Prototype 100 fiber cable structure

Table 1 Prototype cable performance

Test item	Result
Attenuation at 1550 nm	<0.25 dB/km
Temperature cycle at 1550 nm: -30~+70°C	<0.05 dB/km increase at +70°C
Bending: 200 mmR	No loss increase
Lateral Force: 40 N/mm	No loss increase
Tension: 10000 N	No loss increase

CABLE RELIABILITY

We are undertaking long term field tests on the performance of these cables at facilities in Okinawa (high wind and high temperature) and Hokkaido (high wind and low temperature).

We measured such environmental parameters such as temperature, humidity and wind force. The influence of strong wind measured in terms of its pulling force on the messenger wire indicated by the displacement of the X and Y axis. We measured long term changes in attenuation using OTDR and the strain distribution of fibers in the cable by Brillouin optical fiber time domain reflectometer (BOTDR).

The fiber strain in the prototype cable installed in Okinawa shown in Fig 12. The top line and bottom line show the strain distribution of the center fibers after installation and after 4 months, respectively and it can be seen that, there was no changes.

We will continue to measure the distribution of the fiber to obtain the long term reliability of the developed aerial cable in a hard environment.

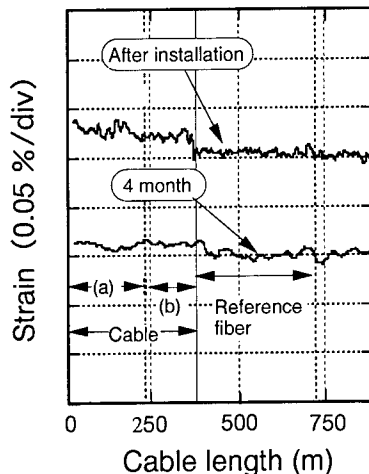


Figure 12 Fiber strain distribution in the cable

CLOSURE FOR AERIAL OPTICAL FIBER CABLE

Closure structure

The closure for aerial optical fiber cable should be in expensive and work on it should be completed quickly. Figure 13 is a schematic view of our newly developed closure for aerial optical fiber cable. The closure consists of a sleeve, and cable adjusting, accommodation, sealing parts. Table 1 compares the currently used and newly developed closures.

The newly developed sleeve is compact and one parts. 4-fiber ribbons are stored by turning them back on themselves and four multi transferable (MT) connectors or splicing sleeves are then accommodated in a tray. The structure for sealing and holding the slotted rod is simple and provides easier workability than the currently used closure.

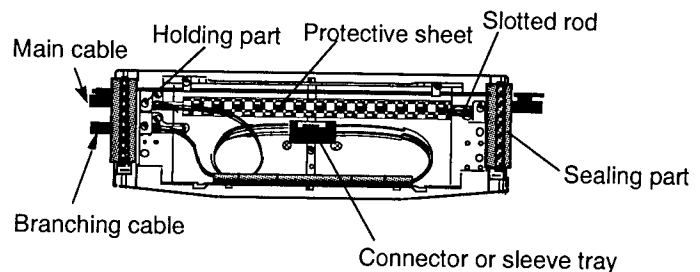


Figure 13 Schematic view of new closure

Closure performance

Figure 14 compares the mid span access time for 100 fiber cable for branching 40 fibers using the current method and our new method. The procedure is divided into four stages, removing the cable jacket, holding the slotted rod, ground, accommodating the fiber ribbons, and sealing the closure. The total mid span access time is less than that half required with the conventional method.

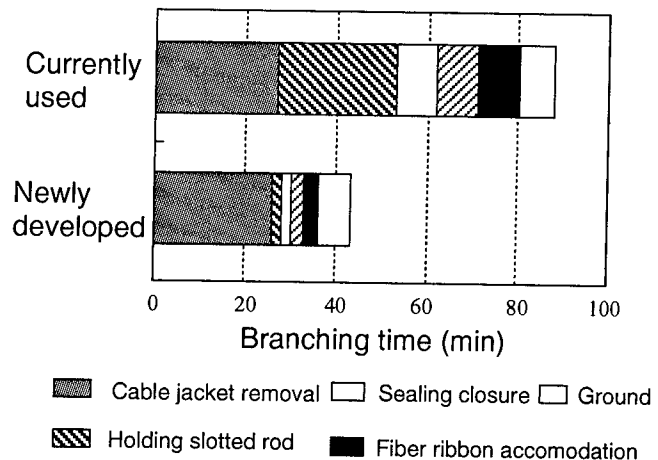


Figure 14 Branching time by midspan access

CONCLUSION

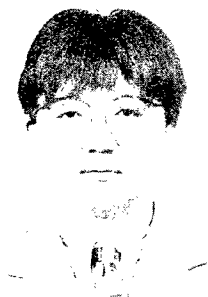
We developed a new SS cable can avoid the problems of elongation and wind induced oscillation, by having windows between the cable core and the messenger wire. By using SZ-slotted rod for the cable core and the newly developed closure, the required branching time for 40 fibers from 100 fiber cables can be reduced by about 50%.

ACKNOWLEDGMENTS

The authors wish to thank K.Nishimura, T.Yabuta and H.Akimoto for continuous encouragement.

References

- [1] H.Iwata, M.Tsutsumi, E.Nakamura, N.Matsumoto, S.Hayami, S.Nagasawa and T.Tanifuji, "Pre-connectorized 1000-fiber single slotted core cable" 44th IWCS, pp. 627-634 (1995).
- [2] M.Okada et al., "Study on slotted rod structure for mid span access" IEICE'96, September (1996).
- [3] H.Akimoto et al., "Study on optical cable technology for construction of optical distribution networks" IEICE'96, September (1996).



Hideyuki Iwata
NTT
Access Network
Systems Laboratories
Tsukuba, Ibaraki,
305, JAPAN

Hideyuki Iwata is a research engineer. He was born in 1965 and received B.E. and M.E. degrees in electronic engineering from Yamagata University in 1989 and 1991, respectively.

He joined NTT in 1991. Since 1993 he has been engaged in research on high-density and pre-connectorized optical fiber cable. Mr. Iwata is a member of IEICE of Japan.



Masaru Okada
NTT
Access Network
Systems Laboratories
Tsukuba, Ibaraki,
305, JAPAN

Masaru Okada is an engineer. He was born in 1970 and graduated from Kisarazu National College of Technology in 1991. He joined NTT in 1991. Since 1995 he has been engaged in research on aerial optical fiber cable.



Shigeru Tomita
NTT
Access Network
Systems Laboratories
Tsukuba, Ibaraki,
305, JAPAN

Shigeru Tomita was born in 1960 and received B.E. and Ph.D. degrees in electrical engineering from Nihon University in 1983 and 1992, respectively.

In 1983 he joined NTT Laboratories, where he has been engaged in research on optical fiber cable. He is currently a senior research engineer at NTT.

Dr. Tomita is a member of the Institute of Electronics, Information and Communication Engineers of Japan.



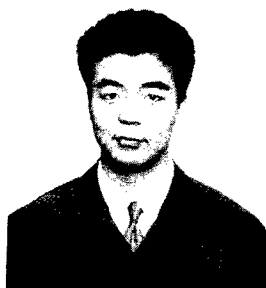
Norio Kashima
NTT
Access Network
Systems Laboratories
Tokai, Ibaraki,
319-11, JAPAN

Norio Kashima is the leader of the optical fiber cable research group. He was born in 1950 and received B.E. and M.E. degrees from Yokohama National University, Japan, in 1973 and 1975, respectively and a Ph.D. degree from the Tokyo Institute of Technology, Japan, in 1984. He joined NTT in 1975. He has been engaged in the research and development of fiber design, fusion splicing, optical connectors, transmission systems, access network operation systems, and optical cables. Dr. Kashima is a member of IEEE and IEICE of Japan.



Mitsuo Kama
NTT
Technology
Department
Shinjiku, Tokyo,
163-14, JAPAN

Mitsuo Kama was born in Tokyo, Japan, on May 26, 1960. He received a B.E. degree in electrical engineering from Tokyo Metropolitan University, Japan, in 1984. He joined NTT in 1984. He has been engaged in development work on outside plant technology for optical-fiber cable systems. He is now manager of the Technology Department at NTT head office. He is a member of the Institute of Electronics, Information and Communication Engineers of Japan.



Tetsuya Hoshijima
NTT
Technology and
Development
Support center
Chiba, Chiba,
261, JAPAN

Tetsuya Hoshijima was born in Okayama on February 14, 1964. He received a B.E. degree in electrical engineering from Hiroshima University in 1986. He joined NTT in 1986. He has been engaged in developing optical fiber cable closure for subscriber lines. He is presently engaged in planning the promotion of technology transfer. He is now an engineer in NTT Technology and Development Support Center. He is a member of the Institute of Electronics, Information and Communication Engineers of Japan.



Kaoru Nishizawa
NTT
Tomakomai
Branch
Tomakomai,
Hokkaido,
053, JAPAN

Kaoru Nishizawa was born in 1964. He joined NTT in 1988 after graduation from the Science University of Tokyo. Since 1995 he has been engaged in the development of aerial optical fiber cable in NTT Technology and Development Support Center.

He is now an engineer and chief management planner at NTT's Tomakomai Branch.

DEVELOPMENT OF AERIAL OPTICAL FIBER CABLE WITH GREATER LENGTH OF CABLE COMPARED TO SUPPORTING WIRE

Yoshio Ishibashi, Akira Watanabe, Osamu Arai, Kenji Ishii, Yoshinori Kurosawa
and Hideo Yamazaki

Hitachi Cable, Ltd.

5-1-1, Hitaka-cho, Hitachi-shi, Ibaraki-ken, 319-14, Japan

ABSTRACT

A new aerial optical cable for distributing fibers to subscribers, has been developed. The cable has so-called Figure-8 construction, and consists of 4-fiber ribbons, SZ-slotted core for easy taking out of fiber ribbons and splicing at any point along the cable length[1]. For aerial installation the cable is designed to have a cable portion length that is greater than the supporting wire portion. Trial cable was manufactured, and its optical and mechanical performance was examined.

1.0 INTRODUCTION

Digital network systems employing optical fiber transmission are spreading in large cities. However, digital network systems are also necessary in suburban and rural areas to realize FTTH(Fiber To The Home). In suburban and rural areas, an aerial cable is preferable because the cable installation can be performed without difficulty. Conventional aerial optical fiber cable exists but is not suitable for this usage because the cable is not designed for subscriber network use. Therefore a new aerial optical fiber cable which can be used for distributing fibers to users is urgently required.

A new aerial optical fiber cable was designed to attain (1)more compact size using 0.3 mm thick ribbons, (2)SZ-slotted core structure for easy taking out of ribbons, (3)Figure-8 construction with greater length compared to the supporting wire length to reduce strain which would be applied during installation work and in strong winds.

2.0 CABLE CORE STRUCTURE

The cable is designed so as to accommodate 100 single mode fibers (twenty five 4-fiber

ribbons) in slots of an SZ-slotted core. Currently in Japan, low fiber count(not more than 300 fibers) underground cables consist of a stack of five 0.3mm thick 4-fiber ribbons in each slot instead of 0.4mm thick ribbons[2]. Therefore aerial cable must have the same scheme of thin ribbon stacking to minimize the cable core diameter. SZ-slotted core is adopted to make it easy to pull ribbons out from it for the purpose of branching. Dimensions of the slots should be large enough to allow a fiber ribbon stack to move freely in the slot. Available length for removing of the cable jacket is a maximum of 500mm, which is restricted by the length of the splicing box for branching. When pulling ribbons out from a 500mm length of the slotted core, the distance between ribbons and the surface of the slotted core must exceed the 20mm which is required to insert the ID tester(identifier to confirm objective fiber ribbon detecting evanescent power leaked out from bent ribbon). The distance is determined by three parameters which are oscillating pitch, angle and pitch circle radius as shown Figure 1.

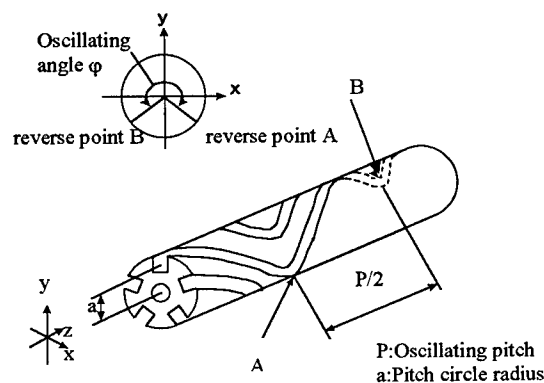


Fig.1 parameters of slotted core

Length L (mm) of ribbon accommodated in the slotted core stripped of jacket by l (mm) is approximately calculated by following equation.

$$L \approx \left[1 + \left(\frac{\pi a \phi}{2P} \right)^2 \right] \cdot l \dots \dots \dots (1)$$

where,

- L :Length of ribbon pulled out from slotted core (mm)
- a :pitch circle radius (mm)
- ϕ :Oscillating angle (rad.)
- P : Oscillating pitch (mm)
- l :Length of slotted core without jacket (mm)

The distance d (mm) between the pulled out ribbon and the slotted core is obtained from the equation below, assuming that d, L and l make a right triangle.

$$d = \sqrt{\left(\frac{L}{2} \right)^2 - \left(\frac{l}{2} \right)^2} \dots \dots \dots (2)$$

Assuming that the diameter of the slotted core lies between 9mm and 12mm and the oscillating angle lies between 250 and 300 degrees, from our manufacturing experience, the required pitch circle radius comes between 2.5mm and 4.0mm. An oscillating pitch of not more than 300mm is found from this relationship, as shown in Figure 2. The ease of pulling out of ribbons is increased when the slotted core has a curvature which is induced by winding of the cable as stated later.

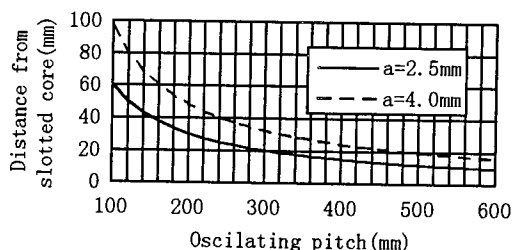


Fig. 2 Relationship between oscillating pitch and the distance between the pulled out ribbon and the slotted core

3. SELF-SUPPORTING CONSTRUCTION

The slotted core is applied with suitable tapes. The cable core and supporting wire are jacketed together with black polyethylene into a Figure-8 construction. In the jacketing process, the greater length of cable core compared to the supporting wire is added and the web of the

Figure-8 cable is separated by inserting pins at regular intervals to maintain the excess length. Consequently, the fiber cable portion snack back and forth along the cable length. The value of added excess length lies in the range of 0.2% to 0.35%. This configuration of cable can be manufactured in a single jacketing process. The construction of trial cable is shown in Figure3.

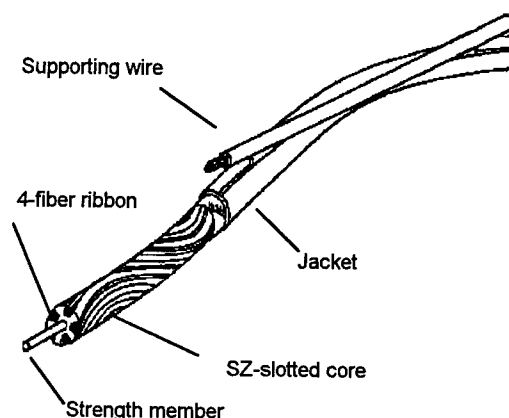


Fig. 3 Construction of self-supporting cable

The maximum value is determined from the outside appearance of strung cable. The cross-sectional area of supporting wire is designed to have sufficient strength for the lump load which will occur if a maintenance person climbs the ladder leaning against the cable, and also against distributed load which will occur if the strong wind pressure is applied.

$$T_1^3 + \left[\left\{ \frac{W^2 S^2}{24 T_0^2} + \frac{P m (W S + P) (S - m)}{2 S^2 T_0^2} + \alpha (t_1 - t_0) \right\} E A - T_0 \right] T_1^2 = \left\{ \frac{W_1^2 S^2}{24} + \frac{P_1 m (W_1 S + P_1) (S - m)}{2 S^2} \right\} E A \dots \dots \dots (3)$$

where,

- T_1 :Tension when load P_1 is applied (N)
- t_1 :Temperature when load P_1 is applied(K)
- T_0 :Tension at stringing (N)
- t_0 :Temperature at stringing (K)
- W :Cable weight per unit length (N/m)
- W_1 :Effective cable weight per unit length at wind blowing (N/m)
- S :Span length (m)
- m :Distance from supporting pole (m)
- α :Thermal expansion co-efficient (1/K)

P :Weight of branching box (N)
 P_1 :Load applied by wind blowing (N)
 E :Young's modulus (N/mm²)
 A :Cross-sectional area of supporting wire (mm²)

W_1 is obtained from equation (4)

$$W_1 = \sqrt{W^2 + (kpD_c / 1000)^2} \dots\dots\dots(4)$$

Where,

k :Drag co-efficient for Cable
 D_c : Height of Cable (mm)
 p :Wind pressure (N/m²)

P_1 is obtained from equation (5)

$$P_1 = \sqrt{P^2 + (k_b p A_b)^2} \dots\dots\dots(5)$$

Where,

K_b :Drag co-efficient for branching box
 A_b :Area of branching box (m²)

The tension T_0 (N) at the initial stage is given by following equation,if the lump load is applied near the center of the span.

$$T_0 = \frac{m}{2d_0} (S - m) \left(W + \frac{2P}{S} \right) \dots\dots\dots(6)$$

where,

d_0 : Sag at the initial stage (m)

Calculations are made assuming that the lump load is applied at the center of span for worst case.

In the case of applying a ladder, the calculation can be done by replacing $P_1 = P + W_L$ (W_L : Weight of ladder with a maintenance person) for equation (5) and $W_1 = W$ for equation (4).

Thus the size of wire strand is selected considering tensile strength, with a safety factor of two or more.

For example with conditions described in Table1 the size of the wire strand comes to not less than 18mm².

Figure 4 shows the relationship between tensile force and elongation for manufactured aerial cable. When the elongation exceeds 0.24% the winding of cable is not observed any more.

Table1 Conditions for calculation

Item	Value
Cable weight	3.43N/m
Cable height	23mm
Weight of branching box	147N
Area of branching box	0.12m ²
Span	60m
Maximum initial sag	0.85m
Wind pressure	980N/m ²
Temperature at installation	35°C
Temperature at time of wind blowing	-30°C
Thermal expansion co-efficient of wire strand	1.1x10 ⁻⁵ /K
Young's Modulus of wire strand	171.5kN/mm ²

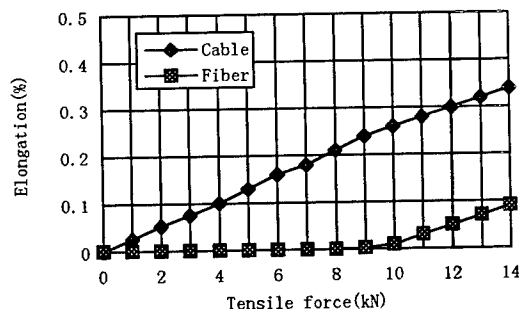


Fig. 4 Relation between cable elongation and fiber elongation

4. CHARACTERISTICS OF AERIAL OPTICAL FIBER CABLE

The characteristics of the newly developed aerial cable were investigated through a temperature cycling test and mechanical performance tests.

Table2 shows results of the tests carried out on the manufactured cable .In each test, attenuation was measured at 1.55 μ m. Initial attenuation of the cable was a maximum of 0.22dB/km, average of 0.20dB/km and minimum of 0.18dB/km.The attenuation increase observed during the temperature cycling test carried out over the range of -30 °C to 70 °C was less than 0.05dB/km.

Results of mechanical tests such as the tensile test, bending test, lateral force test etc. are also

shown in Table2. Attenuation changes were not observed during any test described in the Table.

5. CONCLUSION

The newly developed 100-fiber aerial cable for subscriber networks provides for easy branching and gives low strain characteristics even if predicted tensile loads are applied. This type of cable can be manufactured in a single jacketing process. For this reason the newly developed cable leads to cost saving. The manufactured trial cable shows good performance in temperature cycling and mechanical tests.

REFERENCES

- [1] N.Okada, A.Mogi,N.Misono , et al., "A SZ Slot Ribbon Fiber Cable For Subscriber Network",Proc. 38th IWCS,1989,pp.155-161
- [2] F.Hosoi, M.hara and E.Konda, "Development of Downsized Slotted Rod Optical Fiber Cables",Proc. 45th IWCS, 1996,pp.506-510

Table 2 Result of temperature cycling test and mechanical test (@1.55 μ m)

Item	Condition	Attenuation increase
Temperature Cycling	-30 °C to +70°C	less than 0.05dB/km
Tensile force	12740N	No increase
Bending	Bending radius 160mm ± 180 deg. 5times	No increase
Bending at Low temperature	-30°C Bending radius 160mm ± 180 deg 5times	No increase
Lateral Force	1960N/10cm for 1 min.	No increase
Squeezing	Tensile force 1960N Radius 250mm Squeezing angle 90deg. 4 times	No increase
Torsion	± 90 deg./1m	No increase
Impact	9.8N-1m	No increase



Yoshio Ishibashi

Hitaka works,
Hitachi Cable ,Ltd

5-1-1,Hitaka-cho,
Hitachi-shi,
Ibaraki-ken,
319-14,Japan

Yoshio Ishibashi was born in 1950. He graduated from Tohoku University with a M.E.degree of electronics engineering in 1975. He joined Hitachi Cable,Ltd in 1975 and has been engaged in design and development of metallic cables and optical fiber cables. He is now a senior engineer of telecommunication design department.



Akira Watanabe

Hitaka works,
Hitachi Cable ,Ltd

5-1-1,Hitaka-cho,
Hitachi-shi,
Ibaraki-ken,
319-14,Japan

Akira Watanabe was born in 1950. He graduated from Hitachi Ibaraki Technical College with electrical engineering in 1972. He has been engaged in design and development of metallic cables and optical fiber cables. He is now a senior engineer of telecommunication design department.

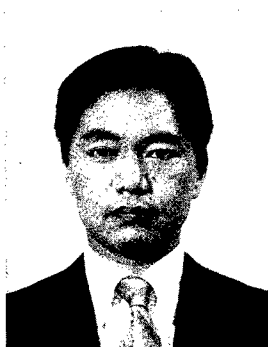


Osamu Arai

Hitaka works,
Hitachi Cable ,Ltd

5-1-1,Hitaka-cho,
Hitachi-shi,
Ibaraki-ken,
319-14,Japan

Osamu Arai was born in 1960. He graduated from Ibaraki University with a B.E. degree of mechanical engineering in 1983. He joined Hitachi Cable, Ltd in 1983 and has been engaged in manufacturing and development of optical fiber cables. He is now an assistant manager of optical fiber cable section of optical fiber & communication cable department.



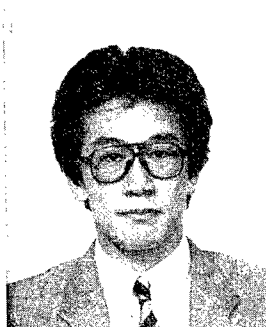
Kenji Ishii

Hitaka works,
Hitachi Cable ,Ltd

5-1-1,Hitaka-cho,
Hitachi-shi,
Ibaraki-ken,
319-14,Japan

Kenji Ishii was born in 1959. He graduated from the Musashi institute of technology with a B.E.degree of electrical engineering in 1983. He joined Hitachi Cable,Ltd in 1983 and has been

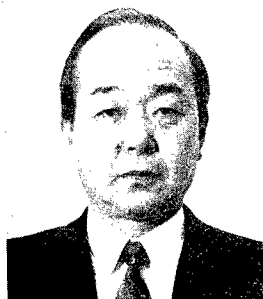
engaged in manufacturing and development of metallic cables and optical fiber cables. He is an assistant manager of tecomunication section of optical fiber & communication cable department.



Yoshinori Kurosawa

Optoelectronic System
Laboratory,
Hitachi Cable ,Ltd
5-1-1,Hitaka-cho
Hitachi-shi,
Ibaraki-ken,
319-14,Japan

Yoshinori Kurosawa was born in 1962. He joined Hitachi cable,Ltd after graduation from Waseda University with a B.E. degree of mechanical engineering in 1985 and has been engaged in research and development of optical fiber and optical fiber cable. He is a member of IEICE of Japan.



Hideo Yamazaki

Head office,
Hitachi Cable,Ltd

2-1-2,Marunouchi,
chiyoda-ku,Tokyo
100,Japan

Hideo Yamazaki was born in 1940. He graduated from Keio gijyuku University with a B.E.degree of electrical engineering in 1964. He joined Hitachi Cable,Ltd in 1964,and has been engaged in development ,design and also manufacturing of metallic cables and optical fiber cables. He is now a general manager of telecommunication division.

DEVELOPMENT OF OPTICAL DROP WIRE AND DROP WIRE STRANDED CABLE

Koichiro Watanabe, Masahiro Kusakari, Osamu Koyasu,
Akio Mogi, Matsuhiko Miyamoto

Fujikura. Ltd., Telecommunication cable department, Opt-electronics laboratory
1440, Mutsuzaki, Sakura-shi, Chiba, Japan

Abstract

The structure of the newly developed optical drop wire for the aerial and the drop wire stranded cable for the aerial and there performance are reported in this paper.

As for the optical drop wire, the structure that a messenger wire and two steel wires for the fiber protection were arranged in parallel was investigated because of the cost decrease. This is the structure which can be manufactured in 1 process. We manufactured a trial wire, and evaluated the loss characteristics, the temperature characteristics, the mechanical characteristics, then it was confirmed that it had good performance.

The structure of the drop wire stranded cable stored plural optical drop wires in the pipe-shaped accommodation body. Furthermore, a messenger wire is added to this cable. We manufactured a trial cable, then it was confirmed that an optical drop wire could be pulled out easily. And, we evaluated the loss characteristics, the temperature characteristics, the mechanical characteristics. Then, it was confirmed that it had the good performance.

Introduction

It is expected to provide the multimedia service of handling the high-speed data and the image for each home, and the research and development is advanced to build the access network by using the optical cables. Because an article to use for wiring, and the execution become necessary for each subscriber, the part of optical wiring for the residence in the access optical network is a high cost territory

comparatively of the distance. Therefore, to realize the access optical network in low cost, it is important, to decrease the price of the optical drop wire. The article fee such as a closure and the execution cost can be reduced by summarizing the access point.

It is important to reduce the number of the manufacture processes to manufacture the optical drop wire in the low cost. Though three manufacture processes were necessary for the usual optical drop wire, it can be manufactured with the structure which we investigated this time in one process.

Requirement

The main requirement item of the optical drop wire is shown in the table 1. And, the main requirement item of the drop wire stranded cable is shown in the table 2.

Table 1. The main requirement to the optical drop wire

The maximum tension	700 N
The number of the fibers	1 or 2
Bending radius	30 mm
Temperature range	-30~70°C
Others	·Easy to separate the messenger wire ·Easy to take out the fiber

Table 2. The main requirement to the drop wire stranded cable

The maximum tension	8000 N
The number of the optical drop wires	maximum 12
Temperature range	-30° 70°C
Others	• Easy to pull out of the optical drop wire

Cable structure

Optical drop wire

The structure of the optical drop wire is shown in the fig. 1. As for this cable, the steel wire of a diameter 1.2 mm for self supporting, the steel wire of a diameter 0.4 mm for the fiber protection and the optical fiber are arranged in parallel. Both of 0.25 mm and 0.5 mm can be used as an outside diameter of the fiber. The sheath is polyvinyl chloride (PVC). The notch in the part which connects the optical fiber storage part with the part of the messenger wire is the thing to make the disjunction of the part of the messenger wire and the optical fiber storage part easy. The notch in the center of the optical fiber storage part is effective in taking out the fiber easily.

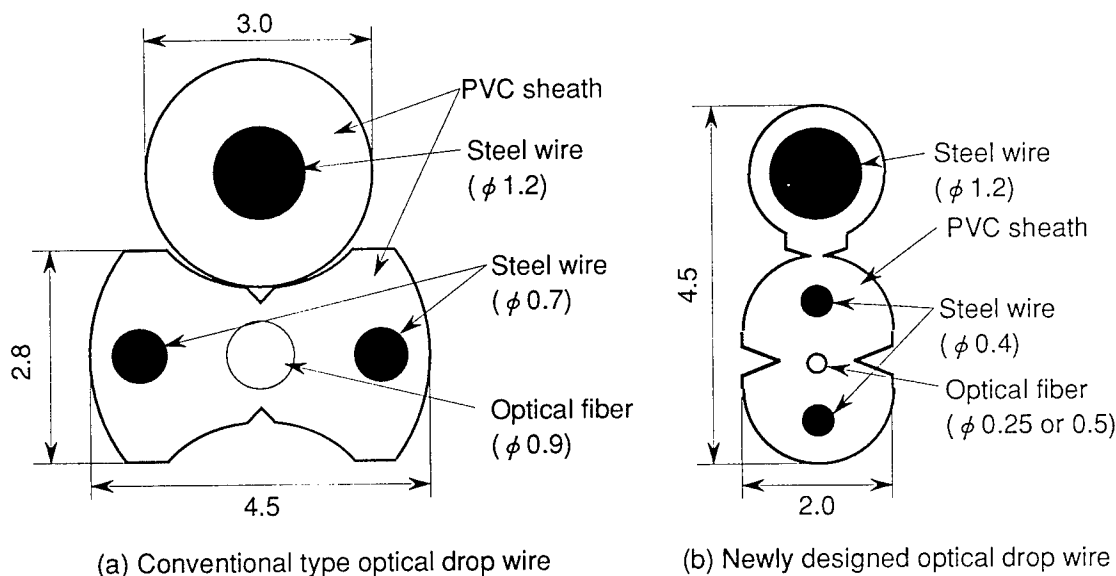


Fig 1. The structure of the optical drop wires

Drop wire stranded cable

The structure of the drop wire stranded cable is shown in the fig. 2. It is the structure that the optical drop wire of 12 maximums was stored in the pipe-shaped accommodation body. The subscriber of the number of the stored optical drop wire can be backed up in one access point by this structure. The length which is necessary to drop must be pulled out with this cable. Therefore, the cross section area of the optical drop wire to occupy is being made about 30%. And, the PVC which added the lubrication material to the sheath is being used to make the frictional coefficient of the optical drop wires low.

The evaluation result

Optical drop wire

The trial production wire was made to confirm the characteristic of the optical drop wire that is consist of the fiber of the outside diameter 0.25 mm. Then, the temperature characteristic and the mechanical characteristic were evaluated. As for the temperature characteristic, the thermal cycling from -30 degrees to 70 degrees was done, and the loss change was measured. The result is shown in the fig. 3. The loss change is very little, and it is a good characteristic.

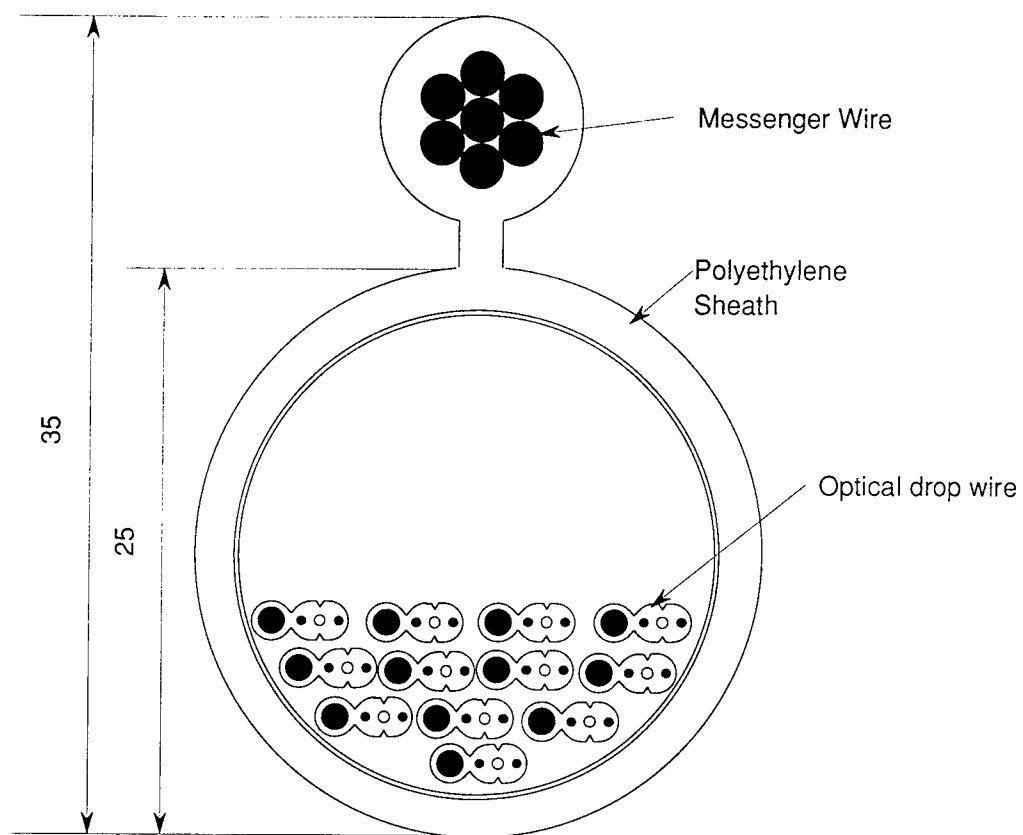


Fig 2. The structure of the drop wire stranded cable

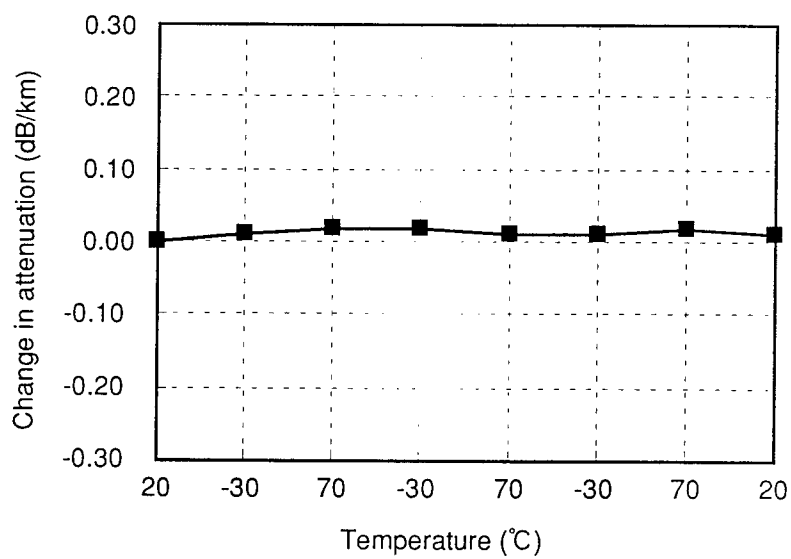


Fig 3. Thermal cycling of the optical drop wire

As for the mechanical characteristic, the lateral pressure test, the bending test, the bending test in low temperature, the tensile test were carried out. The test conditions are shown in the table 3. There is no loss increase in all the tests. And, as for the bending test in low temperature, the crack on the surface of the sheath wasn't observed.

Drop wire stranded cable

As for the drop wire stranded cable, the trial production cable which mounted 12 optical drop wires was manufactured. Then, the temperature characteristic, the mechanical characteristic were evaluated. And, the frictional coefficient of the optical drop wires and the pulling out force of the optical drop wire from the drop wire stranded cable were investigated.

As for the temperature characteristic, the thermal cycling from -30 degrees to 70 degrees was enforced, and the loss change was measured. The result is shown in the fig. 4. The loss change is very small, and it is a good performance.

As for the mechanical characteristic, the lateral pressure test, the elongation test, the squeezing test, the bending test, the torsion test and the impact test were carried out. The test conditions are shown in the table 4. There is no loss increase in all the tests.

Table 3. Mechanical test condition for the optical drop wire

Items	Test condition
Lateral pressure	1200 N/25 mm
Bending	R=30 mm, 10 cycle
Bending in low temperature	R=30 mm, -30°C
Elongation	700 N

Table 4. Mechanical test condition for the drop wire stranded cable

Items	Test condition
Lateral pressure	2000 N/100 mm
Elongation	8000 N
Squeezing	4000 N, R=250 mm
Bending	R=150×5 times
Torsion	sample length = 1 m angle = $\pm 90^\circ$ ×5 times
Impact	R=10 mm, 1 kg×1 m

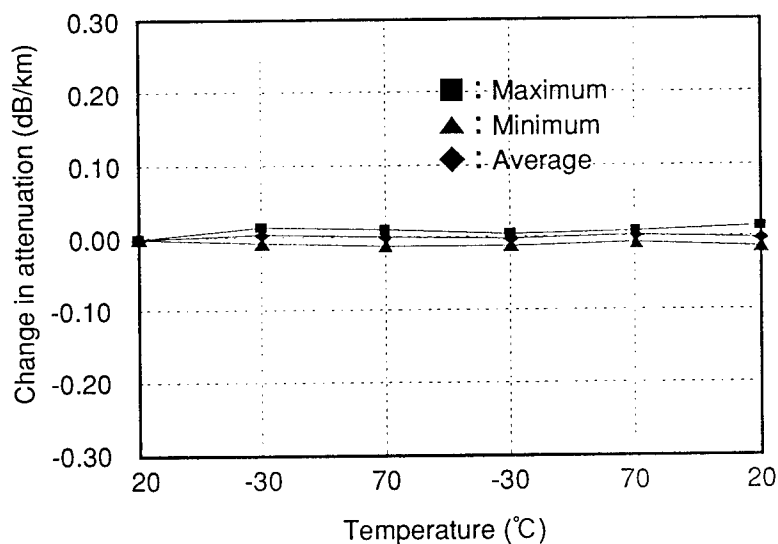


Fig 4. Thermal cycling of the drop wire stranded cable

The method of measuring the frictional coefficient of the optical drop wires is shown in the fig. 5. And, the measurement result is shown in the table 5. The frictional coefficient of developed PVC is smaller than half of the frictional coefficients of usual PVC.

About 3 times of the interval of the telephone pole was presumed, and the evaluation of the pulling out force of the drop wire from the drop wire stranded cable was enforced by using the sample of 110 m. It was evaluated about 2 ways as a condition when it was laid straight and when the bend of $R=250 \times 90$ degrees was put in 2 places. The measurement method is shown in the fig. 6.

And the measured pulling out force is shown in the fig. 7. Even when the bend is inserted, the pulling out force is about a maximum 140 N. We can pull out easily even when we work on the telephone pole.

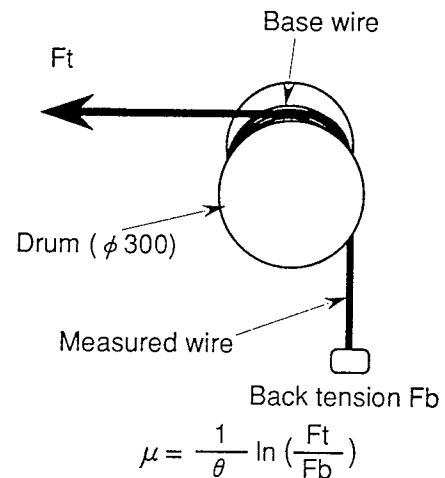


Fig 5. The method of measuring the frictional coefficient

Table 5. Frictional coefficient

PVC	Frictional coefficient (relative value)
Usual	1.0
Newly developed	0.46

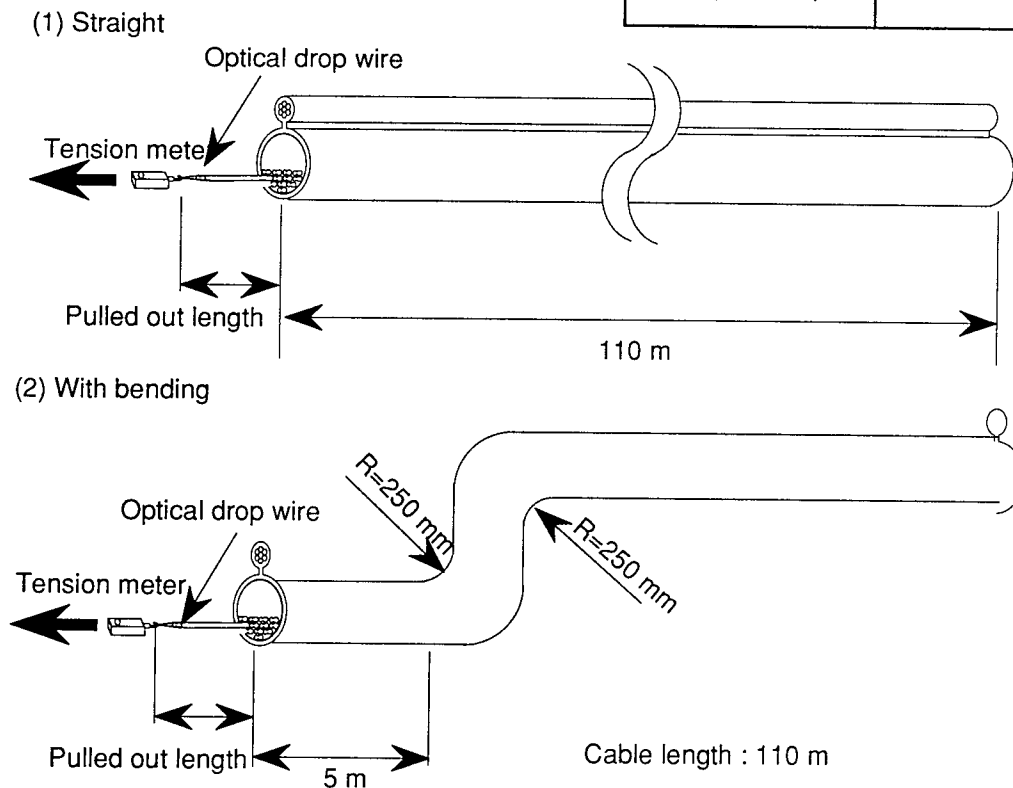


Fig 6. Measurement method of pulling out force

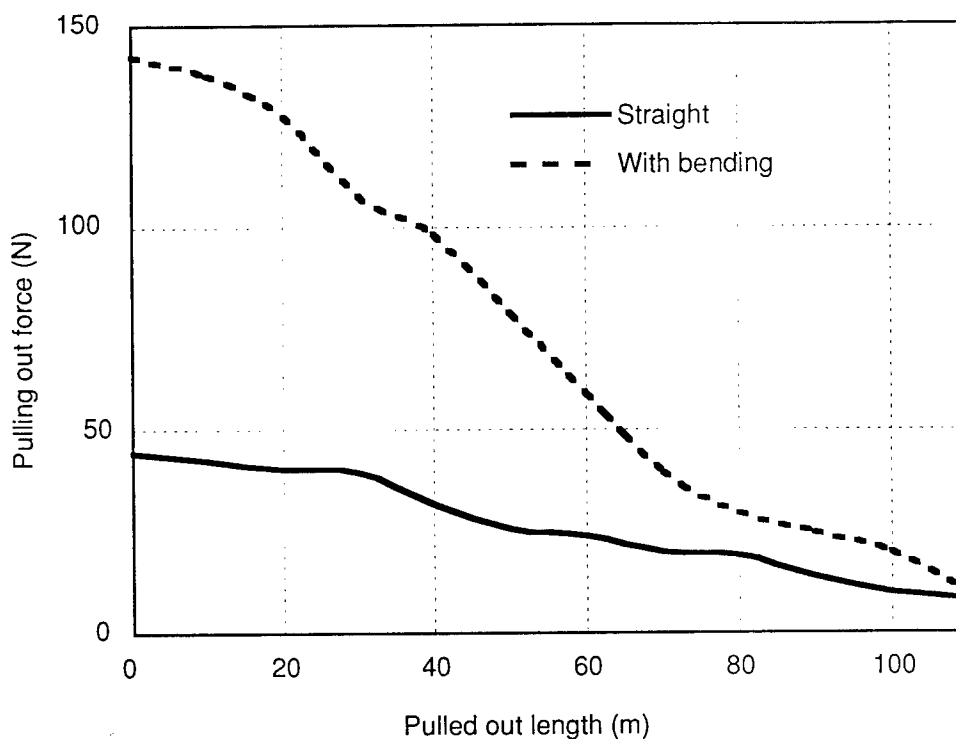


Fig 7. Pulling out force

Conclusion

We investigated the optical drop wire which could be manufactured in 1 process. Then, we confirmed that the performance of the optical drop wire developed newly was good.

And, we investigated the drop wire stranded cable of the structure that the plural drop wires were stored in the pipe. It was confirmed that there was a problem in neither the pulling out performance nor the cable performance.

References

1. K. Tomiyama, Y. Nakatsuji, K. Hogari, S. Furukawa, "Studies on Aerial Optical Drop Cable To Residential Premises", 1996 Communications Society Conference of IEICE of Japan
2. Y. Nakatsuji, K. Hogari, S. Furukawa, S. Koshio, K. Nishizawa, "Studies on Optical Cable for Residential Premises and Office Buildings", 1997 IEICE of Japan General Conference
3. K. Watanabe, M. Kusakari, M. Miyamoto, K. Suzuki, "Development of Optical Drop Wire Stranded Cable for Aerial", 1997 IEICE of Japan General Conference
4. S. Furukawa, K. Hogari, I. Sankawa, M.

Terasawa, M. Kama, N. Kasihma, "Optical Fiber Distribution System for Residential Premises", Technical Report of IEICE of Japan, CS97-40 (1997-06)

Koichiro Watanabe

Opto-Electronics
Laboratory
Fujikura Ltd.

1440, Mutsuzaki,
Sakura-shi, Chiba,
285, Japan

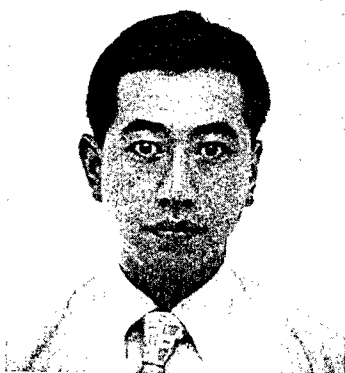


Koichiro Watanabe was born in 1959. He received a B.E. degree in electrical engineering from Tohoku University in 1982. Since joining Fujikura Ltd. in 1988, he has worked on the development of optical fiber cables. He is now an engineer of the Telecommunication Cable Department of the Opto-electronics Laboratory and a member of IEICE of Japan.

Masahiro Kusakari

Opto-Electronics
Laboratory
Fujikura Ltd.

1440, Mutsuzaki,
Sakura-shi, Chiba,
285, Japan



Masahiro Kusakari was born in 1965. He received a B.E. degree from Nagasaki University in 1990. Since joining Fujikura Ltd., he has worked on the development of optical fiber cables. He is now an engineer of the Telecommunication Cable Department of the Opto-electronics Laboratory and a member of IEICE of Japan.

Akio Mogi

Opto-Electronics
Laboratory
Fujikura Ltd.

1440, Mutsuzaki,
Sakura-shi, Chiba,
285, Japan



Akio Mogi was born in 1946. He joined Fujikura Ltd. from Haneda Institute High School in 1967 and has been engaged in research and development of metallic and optical cable. He is now the manager of the Telecommunication Cable Department of the Opto-electronics Laboratory and a member of IEICE of Japan.

Osamu Koyasu

Opto-Electronics
Laboratory
Fujikura Ltd.

1440, Mutsuzaki,
Sakura-shi, Chiba,
285, Japan



Osamu Koyasu was born in 1953. He joined Fujikura Ltd. from Kisarazu Technical College in 1973 and has been engaged in research and development of cable. He is now an engineer of the Telecommunication Cable Department of the Opto-electronics Laboratory and a member of IEICE of Japan.

Matsuhiro
Miyamoto

Opto-Electronics
Laboratory
Fujikura Ltd.

1440, Mutsuzaki,
Sakura-shi, Chiba,
285, Japan



Matsuhiro Miyamoto was born in 1953. He received a M.S. degree from Tokyo Institute of Technology in 1978. Since joining Fujikura Ltd., he has worked on the development of optical fibers and cables. He is now the chief manager of the Telecommunication Cable Department of the Opto-electronics Laboratory and a member of IEICE of Japan.

CONTINUED INVESTIGATIONS OF ADSS DESIGNS AND RELIABILITY CONSIDERATIONS WITH RESPECT TO FIELD VOLTAGE TRACKING, AND CABLE INSTALLATION PRACTICES.

D.A. Keller¹, D.J. Benzel², J.P. Bonicel³, C. Bastide⁴, F. Davidson⁵.

^{1,3,4,5} Alcatel Cable-OFCCC Claremont, NC. ² Alcatel Cable, Calais, France

ABSTRACT

New field and test findings have revised ADSS design and reliability considerations.

Dry band arcing field failures of ADSS cables in the past two years have generated the need to re-examine the 12 kV field voltage limit for an HDPE jacket. Failed field cables were examined and field voltage tests performed which may confirm a need to re-evaluate or change the 12 kV allowance for HDPE jackets. Previous research is compared with the new findings to clarify the technical challenges that remain in an effort to insure a 20 year life expectancy for ADSS cable in a field voltage environment.

A new thermoplastic anti-tracking material is subjected to 3,000 hours of salt fog testing and its performance is compared to a cross-linked material's performance during 3,000 hours of salt fog testing.

In a 400 km heavy ice loading installation in North America, significant increase in sag was observed due to the ice load greatly exceeding expectations. Hyperbolic equations are presented as they are currently used in a simplified but accurate sag and tension spreadsheet. This spreadsheet could be used in the field on a portable PC to educate and demonstrate the expected sags for heavier loading, determine the limits of the cable, and to adjust tensions as necessary.

Throughout this paper a continued link is established from Alcatel's 1995 ADSS paper "Design and Reliability Considerations for Long Span, High Voltage, ADSS Cables" IWCS Proc. 1995, to provide an improved and continued understanding of the issues in 1995 and the current design considerations, given the new findings.

BACKGROUND

Design and reliability considerations for ADSS cables are revised due to new field and test findings over the past two years.

Several dry band arcing or tracking field failures of tracking and non-tracking jacketed ADSS cables from several manufacturers in the past two years

have generated the need to re-examine the 12 kV field voltage limit for an HDPE jacket with respect to ADSS cables and installation.

In the previous 1995 IWCS paper it was stated "The field voltage potential, not the line voltage, at the specific ADSS cable location on the tower, with respect to the conductor location, directly relates to the degradation resulting from tracking and dry band arcing. If the field voltage is less than 12 kV, then ordinary PE compounds can be used". [1]

Several cable failures from various manufacturers, have been brought to our attention, whereby the cable had been located in < 12 kV field voltage zone. Apparently the cable had been initially placed in a "safe" zone, however deterioration of the PE jacket occurred and the cables had failed.

These failures generated the need to reexamine this 12 kV field voltage limit for PE sheaths.

It is difficult to simulate an expected leakage current for an environment of <12 kV field voltage in laboratory tests. "From experience of testing and trials it is considered that if this latter current is less than 1mA, then damage will not occur as a result of arcing activity".[2,3,4] The salt fog test generally provides a typical 1 mA to 10 mA current which usually exceeds what one would expect in a ≤ 12 kV field voltage.[1] The salt fog test also exceeds the 1.7 mA as recorded in a current "coastal with severe marine pollution" trial. [2]

Salt Fog Testing Results

Knowing the best exploratory option would be to generate a worst case scenario, a 1000 hr salt-fog test which insured dry-band arcing was chosen. Employing the IEEE P1222 [10] as a guide, GEC ALSTHOM's procedure listed below was utilized.

"The cable sheath was subjected to ultra-violet weatherometer followed by a 1,000 hour salt fog test under conditions of mechanical and electrical stress. A sample of ADSS cable from a production run is cut to a length of approximately 3.5 m and sealed at each end by a suitable technique, such as an adhesive-lined heatshrink end cap. It is then supported in an ultra-violet aging assembly which combined temperature control and moisture

condensation periods, as described in ASTM Standard G53-84, and conditioned for 2,000 hours.

After the conditioning phase the sealed termination may be removed and the sample given a 24 hour drying period.

Suitable profiled electrodes are then fitted to the cable sample to include the UV exposed length at a separation of at least 1 m and less than 1.5 m. The electrodes should have internal and external radius of curvature of ≥ 3 mm.

The cable sample shall be held horizontally under mechanical tension in a fog chamber with a clearance of at least 0.5 m from the floor, ceiling, walls and other test equipment.

The tension device shall have an insulated support at the high voltage end of the cable. Attached to it is a threaded rod to enable tension to be applied to the cable. An attempt should be made to avoid an electrical stress concentration appearing near the high voltage (HV) end of the cable because this would be unrepresentative of service conditions. Generally the stress relieving device is applied at or near the termination.

The ground end of the cable shall be held by the same design of spiral grip and liner used in service. The mechanical tension is conveniently applied to the cable through this grip by attaching it to the plate which acts on a helical spring in contact with the frame supporting the cable. A typical spring design has a cord diameter of 10 mm and an uncompressed length of 100 mm. The spring constant is typically 6 mm compression for each 10 kN of tensile load.

The sample is wiped with de-ionized water before starting the test. The test conditions shall be for a conducting mist of saline fog to be supplied to the chamber at a rate equal to $0.4 \pm 0.1/h$ for each cubic meter of chamber volume and at a temperature of $20^\circ \pm 5^\circ$ C. The NaCl content of the water shall be 10 ± 0.5 kg/m³. The mist shall be produced by atomizing a jet of salt water using a cross jet of air, per the example described in IEC Standard 60-1. An aperture of not more than 80 cm shall be provided for the natural exhaust of air.

The duration of the test shall be 1,000 hr, but the test should be interrupted at intervals of approximately 100 hr to examine the samples for signs of damage and to check the mechanical tension.

Preferably, the 50 Hz power supply shall be capable of 1 amp at the test voltage and the protection level shall be set at this value.

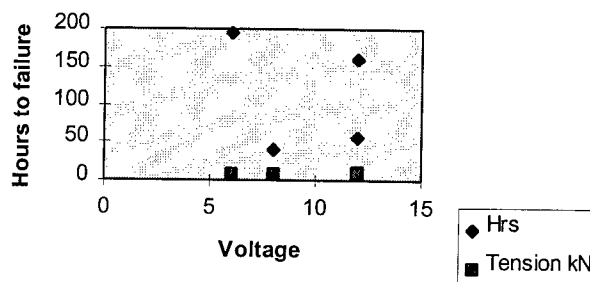
Meeting the test requirements shall be considered successful if there are no signs of tracking on the sample and if erosion damage does not reduce the wall thickness by more than 50%. No flash-overs

shall occur nor shall breakdown take place inside the cable.[5]

Salt Fog Testing Results

Two cable samples were subjected to 12 kV and 8/10 kN and failed in 56 and 160 hours respectively. At 56 hours the first sample had sheath punctures and was considered a failure. The second sample burned at 160 hrs. A third sample subjected to 8 kV and 8 kN was considered a failure with a sheath puncture occurring in 40 hours. A fourth sample was subjected to 6 kV and 8 kN, failed in 195 hours with some arcing damage to the jacket. A fifth sample is currently undergoing a 4 kV test. The results are graphed below.

PE Jacket Failures: Salt Fog Tests



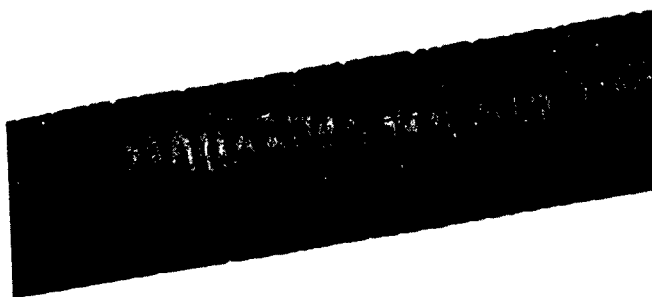
The variability of the performance is generated from the objectivity variance of failure mode and the actual variability of the environment inside the chamber. If there is a puncture in the jacket then the performance is considered a failure early on in the test, while a sample which avoids a puncture may reach the burning stage before it is considered a failure. Also one must consider that for a particular sample, once the arcing activity makes a foothold or accomplishes an initial breakdown of the molecular bonds in the jacket, the deterioration is then quite rapid.

Overall, these salt fog -voltage test failures indicate a need to re-evaluate or change the 12 kV allowance for non-AT HDPE jackets.

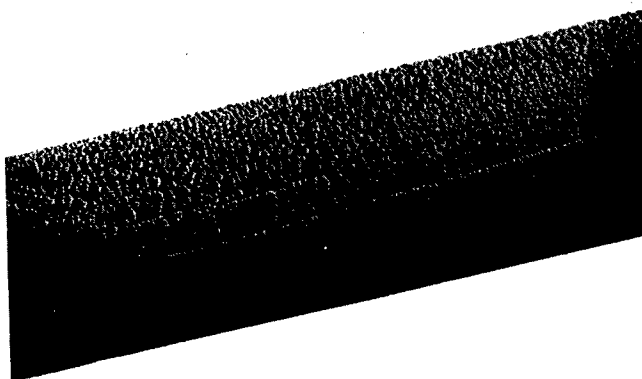
Cross-linked materials typically perform better in dry arc or salt fog testing [1,5], however, a thermoplastic material which performs well in the 1,000 hr test would have some benefits.

A thermoplastic AT material has been developed (ATM2) which has withstood 5 and 20 kV environments for four years on a 380 kV installation on a NECKARWERKE line in ESSLINGEN, GERMANY, with no evidence of cable degradation. [1] The ATM2 was then subjected to 3,000 hrs of a 30 kV and 15 kN salt fog test.

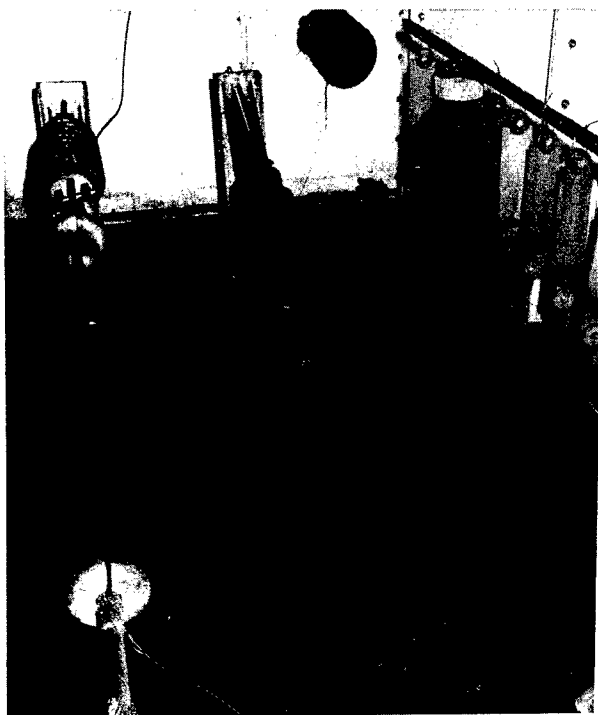
A photograph of the earthed end of the cross-linked ATM1 material after 3,000 hours is shown on the next page.



A photograph of the earthed end of the thermoplastic ATM2 material after 3000 hours is shown below:

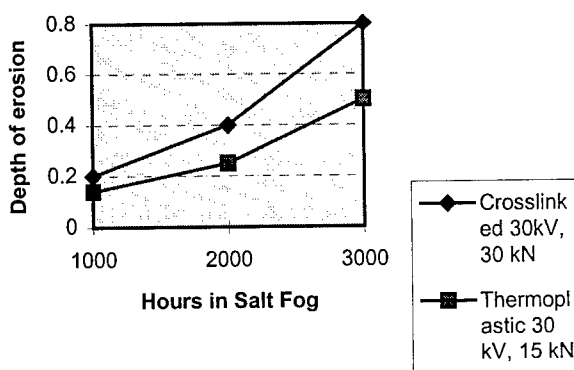


A photograph of the salt-fog test set-up is shown below; ATM2 left, standard HDPE Failed cable on right:



Previous research with a cross-linked material (ATM1) [1] is compared with the ATM2 thermoplastic cable material in the salt fog test. ATM1 was subjected to 30 kV and 30kN while the ATM2 cable was subjected to 30kV and 15 kN. The new material performed sufficiently well as an excellent replacement for PE jackets in field voltage environments.

AT Jacket Erosion; Salt Fog Tests



The above results show that ATM2 is a very capable material which may one day replace the cross-linked ATM1. We need to confirm the performance at a 30 kN tension in order to continue to consider ATM2 as a full replacement for ATM1.

Field Voltage Summary Conclusions

These new findings indicate that the <12 field voltage range continues to contain technical challenges in an effort to insure a 20 year life for the ADSS cable in the field voltage environment.

From the current data our recommendation is that ATM2 (or similar) anti-tracking material be used for 4-12kV, and the ATM1(or similar) anti-tracking material be used for the 12-20 kV field voltage range.

FIELD TESTING UPDATE

Minervois, France

An Electricite de France (EdF) test facility, as sited in Alcatel's 1995 ADSS paper, is the location of two ADSS cables which span a 500 meter valley, labeled span C and F, which are being monitored for vibration. Testing to date has resulted in no vibration damage.

Neckarwerke, Germany

A continued monitoring 380 kV installation on a Neckarwerke line in Esslingen, Germany has completed four years duration with no evidence of any cable degradation. The ADSS cable has been installed in 5 and 20 kV field locations on the tower

to demonstrate the effect of different levels field potential in less severe environments having less than 54 hours dry band arcing per year. No damage has been observed to date.

Quebec, Canada

Approximately 400km of ADSS cable was installed in a harsh environment with temperature extremes of -50 to +35 C, high wind and heavy ice load conditions. The average span length 80 meters, initial cable sag of 1% and a geographical region ranging from coastal to approximately 300km inland. Cable installations were performed prior to the onset of winter weather conditions. After installation completion, the optical fibers were tested and OTDR traces were recorded.

During winter months, significant accumulation of ice and snow buildup on the cable resulted in excess sag exceeding desired clearances. The ice / snow load was estimated at 2.5 cm during the time of maximum sag. The cable sag under this load ranged from 1 to 2 meters and in some spans, 3 meters. Due to accessibility to the facilities being limited, the fibers were not tested during this heavy load period. After the ice / snow load was removed (melted), cable sag ranged from 1 to 1.5 meters in most spans and occasionally 2 meters. The initial sag at installation was 0.8 meters.

With the cable ice load gone, OTDR testing was performed and indicated no increases in fiber attenuation. Cable tensions were checked after being removed and it was determined the initial stringing tensions were lower than originally specified. Consecutive spans of 30 or more existed without dead ends which allowed additional "slack" to accumulate in the maximum sag locations. The cable was retensioned to initial specifications and fibers were tested to ensure original performance values. Cable and hardware performed as designed even under severe conditions that exceed installation specifications.

Field Experience with Heavy Ice Loading

In the above 400 km heavy ice loading installation in Quebec, observations were made of unexpected increases in sag.

In working with the end user, it was found to be beneficial to provide sag and tension tables to the user which demonstrates all the possibilities of loading, tension and sag. Ordinarily these tables can be great in number due to all of the possibilities.

We needed a simple method to demonstrate the physics of the loading, tension and sag relationship which could be fully disclosed to the user. Implementing sag and tension calculations in a spread sheet in which all of the equations were available to the user as well as formatted inputs and outputs were the answer. Use of a spreadsheet capable of demonstrating the possibilities quickly

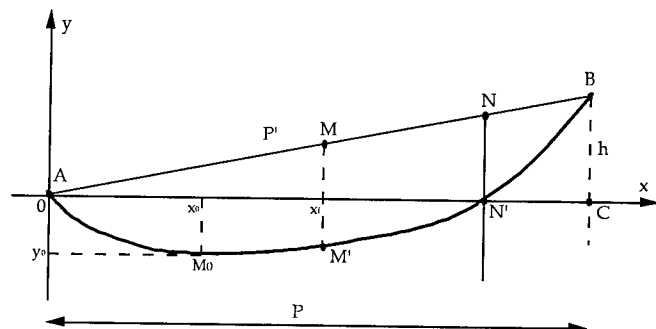
could help educate the user and develop a sort of "common sense" of what to expect.

Hyperbolic equations are presented as they are currently used in a simplified but accurate sag and tension spreadsheet. This spreadsheet could easily be used in the field on portable PC to educate and demonstrate the expected sags for heavier loading. The spreadsheet could also be used in the field for the user to be able to determine the limits of the cable and to adjust sags as needed. The spreadsheet format also allows working with multiple sheets in a "book", allowing the user to reference different cable information, or use the multitasking of windows to run other software such as word processing.

First an exercise was performed to determine the significance of parabolic approximation versus hyperbolic equations given a height difference of zero for the span:

Span (m)	500	800	1000	1500
Sag (m)				
$fn=P^2/8a$	14.21	36.36	56.82	127.84
$fn=a(ch(P/2a)-1)$	14.22	36.46	57.06	129.08
Cable length (m)				
$l=P+(P^3/24a^2)$	501.1	804.4	1008.6	1529.1
$l=2a \operatorname{sh}(P/2a)$	501.1	804.4	1008.6	1529.2

Some small differences do exist, however either parabolic approximations or hyperbolic equations would be suitable. It was found that Excel could easily handle the hyperbolic equations, even for height differences, thus the more difficult equations were used. [6,7,8,9] A brief summary of derived equations is provided as follows:



Some other variables:

C_x coefficient of surface, typically 1.1, range (1.0-1.2)

S_0 (m^2) surface area

v (m/s) wind speed

ρ_a (kg/m³) air pressure (1,226 kg/m³)

$\rho_a v^2/2$ Dynamic wind pressure

Ice load:

$$p_g = \rho_g g (S_0 - S)$$

ρ_g (kg/m³) Ice density (generally 917 kg/m³)

S (m²) surface area of cable

E KN/mm² cable modulus

h_3 (m) difference of level

ρ m span

sh hyperbolic sine

ch hyperbolic cosine

($x \sigma y \sigma$) coordination of the lowest point

Wind force:

$$F = C_x S_0 \rho_a \frac{v^2}{2}$$

Equation of the cable shape:

$$y = a \operatorname{ch}\left(\frac{x - x_0}{a}\right) - a \operatorname{ch}\left(\frac{x_0}{a}\right) = 2a \operatorname{sh}\left(\frac{x - 2x_0}{2a}\right) \operatorname{sh}\left(\frac{x}{2a}\right)$$

Where a is the catenary parameter.

Lowest point:

$$x_0 = \frac{P}{2} - a \ln \left[\frac{h}{2a} \frac{1}{\operatorname{sh}\left(\frac{P}{2a}\right)} + \sqrt{\left(\frac{h}{2a} \frac{1}{\operatorname{sh}\left(\frac{P}{2a}\right)} \right)^2 + 1} \right]$$

$$y_0 = -2a \operatorname{sh}^2\left(\frac{x_0}{2a}\right)$$

$h = 0 \implies x_0 = P/2$

$h > 0 \implies x_0 < P/2$

To find a , we have to solve the following equation:

$$h = 2a \operatorname{sh}\left(\frac{P}{2a}\right) \operatorname{sh}\left[-\frac{P}{2a} + \ln \left(\frac{\sigma}{p_0 a} + \sqrt{\left(\frac{\sigma}{p_0 a} \right)^2 - 1} \right) \right]$$

Where σ is cable tension

Abscissa of the point where sag is maximum:

$$x_{f_{\max}} = x_0 + a \ln \left(\frac{h}{P} + \sqrt{\left(\frac{h}{P} \right)^2 + 1} \right)$$

Maximum sag:

$$f_{\max} = 2a \operatorname{sh}\left(\frac{x_{f_{\max}}}{2a}\right) \operatorname{sh}\left(\frac{2x_0 - x_{f_{\max}}}{2a}\right) + \frac{hx_{f_{\max}}}{P}$$

$h = 0$ and sag is maximum for $x = x_0 = P/2$

$$f = 2a \operatorname{sh}^2\left(\frac{P}{4a}\right)$$

Cable length:

$$l = 2a \operatorname{ch}\left(\frac{P - 2x_0}{2a}\right) \operatorname{sh}\left(\frac{P}{2a}\right)$$

Equation of state:

$$(A) - (A)x[B + C + \frac{1}{ES}(D - D) + 1] = 0$$

$A =$

$$a_2 \sqrt{\operatorname{sh}^2\left(\frac{P}{2a_2}\right) + \left(\frac{h}{2a_2}\right)^2}$$

Where B is:

$$\alpha (T_2 - T_1)$$

Where C is:

$$\frac{h(p_2 - p_1)}{ES}$$

Where D_1 is:

$$a_2 p_2 \operatorname{ch} \left[\frac{P}{2a_2} - \ln \left[\frac{h}{2a_2} \frac{1}{\operatorname{sh} \left(\frac{P}{2a_2} \right)} + \sqrt{\left(\frac{h}{2a_2} \frac{1}{\operatorname{sh} \left(\frac{P}{2a_2} \right)} \right)^2 + 1} \right] \right]$$

Where D_2 is:

$$a_1 p_1 \operatorname{ch} \left[\frac{P}{2a_1} - \ln \left[\frac{h}{2a_1} \frac{1}{\operatorname{sh} \left(\frac{P}{2a_1} \right)} + \sqrt{\left(\frac{h}{2a_1} \frac{1}{\operatorname{sh} \left(\frac{P}{2a_1} \right)} \right)^2 + 1} \right] \right]$$

Where T_1, T_2 are representative of the two states,
Where a_1, a_2 are catenary parameters of the two states

Suspension angle A and B:

$$\phi_A = \frac{\pi}{2} - \operatorname{Arctg} \left[\operatorname{sh} \left(\frac{x_0}{a} \right) \right]$$

$$\phi_B = \frac{\pi}{2} - \operatorname{Arctg} \left[\operatorname{sh} \left(\frac{P - x_0}{a} \right) \right]$$

Mechanical tension at A and B:

$$\sigma_{tA} = p_0 a \operatorname{ch} \left(\frac{x_0}{a} \right)$$

$$\sigma_{tB} = p_0 a \operatorname{ch} \left(\frac{P - x_0}{a} \right)$$

SUMMARY

Several dry band arcing or tracking field failures of tracking and non-tracking jacketed ADSS cables from various manufacturers in the past two years have generated the need to re-examine the 12 kV field voltage limit for HDPE. Previous research with a cross-linked material (ATM1) [1] was compared with the ATM2 thermoplastic cable material in the salt fog test. The new ATM2 material passed 3,000 hours at 30 kV and 15 kN which indicated that ATM2 is an excellent replacement for PE jackets in field voltage environments. From the result of our

tests, our recommendation is that ATM2 thermoplastic anti-tracking material be used for 4-12kV, and the ATM1 anti-tracking material be used for the 12-25 kV field voltage range.

In a 400 km heavy ice loading installation in North America, we have observed increases in sag due to 25 mm ice thickness on the ADSS cable. Hyperbolic equations were derived to work well in a spreadsheet in order to facilitate the quick field demonstration of all the possibilities of loading, tension and sag. This field tool should assist the end user in understanding and correcting sagging issues.

ACKNOWLEDGEMENTS

The authors would like to thank Mike Marklove of GEC ALSTHOM, Stafford, UK, for his cooperation and support in the salt-fog cable testing.

REFERENCES

- [1] D.A. Keller, O. Tatat, R. Girbig, M. Adams, R. Bohme, C. Larsson, "DESIGN AND RELIABILITY CONSIDERATIONS FOR LONG SPAN, HIGH VOLTAGE, ADSS CABLES", International Wire and Cable Symposium Proceedings, 1995, pp
- [2] N.R. Haigh, S. M. Roland, A.J. Taha, and Chris N. Carter, "A FULLY INSTRUMENTED INSTALLATION AND TRIAL OF A NOVEL ALL-DIELECTRIC SELF-SUPPORTING CABLE SYSTEM FOR VERY HIGH VOLTAGE OVERHEAD POWER LINES." International Wire and Cable Symposium Proceedings, 1996, pp 60-67.
- [3] S. M Roland and IV Nichols "The effects of dry-band arc current on aging of self-supporting dielectric cables in high fields", IEE Proc.- Sci. Meas. Technol. 143 (1996) pp 10-14.
- [4] G. Carlton, C.N. Carter, A.J. Peacock, R. Sutehall, "Monitoring on all-dielectric, self-supporting optical cable for power line use" 41st IWCS Reno, November 1992, 59-63.
- [5] J.C.G Wheller, M.L. Lissenburg, J.D.S Winchcliffe, M.E. Slevin, "The Development and Testing of a Track Resistant Sheathing Material for Aerial Optical Fibre Cables" 5th International Conference on Dielectric Materials, Measurements and Applications, Canterbury, June 88.
- [6] Yves Porcheron, "Lines aeriennes, Contraintes de conception, Centre d'Equipement du Reseau de Transport d'Electricite de France. 4421-6, 1992.

[7] E. Maurer, "Die Berechnung der Freileitungen mit Rücksicht auf die mechanischen Verhältnisse der Leiter", SEV Bulletin Nr. 2, 1936, pp 41-53, SEV Bulletin Nr. 3, 1936, pp 65-73.

[8] P.F. Winkelmann, "Sag-Tension Computations and Field Measurements of Bonneville Power Administration", AIEE Transactions, Vol 78, February 1960, pp 1532-1548.

[9] V.W. Kelsey, "Practical Solutions of Catenaries", 1984 14000 E. Linvale Pl#210, Aurora, CO 80014.

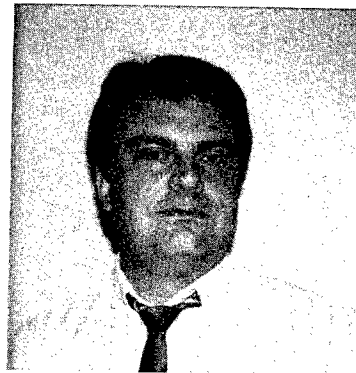
[10] "IEEE Standard for All Dielectric Self-supporting Fiber Optic Cable (ADSS) for Use On Overhead Utility Lines" IEEE P1222 Draft, September 1995.

AUTHORS



David A. Keller -
ALCATEL CABLE,
2512 Penny Rd.
Claremont NC.
USA David A.
Keller born in
Harrodsburg, Ky,
USA in 1960,
received his B.S
degree in Mechanical Engineering
from the University
of Kentucky in
1983. He has held

several positions in both Optical Fiber Process Engineering and Product Development before and after joining Alcatel in 1987. Since May of 1996 he has held the position of Senior Cable Development Engineer at the Alcatel Optical Fiber Cable Competence Center in Claremont, NC.



Christian Bastide
ALCATEL CABLE,
2512 Penny Rd.,
Claremont, NC,
28610, USA

Christian was born in 1957. He joined Alcatel Cable after his graduation from the Grenoble University with the DEA (physics) degree and with a thesis

(microbending in optical fiber) in

1985 and he has been engaged in research and development of optical fiber cables. He is the Group Leader for Computer Modeling.



Dave J. Benzel -
ALCATEL CABLE,
Calais, France,
Dave J. Benzel
born in Buffalo, NY,
USA in 1965,
received his B.S
degree in Electrical Engineering from
Clarkson University
in 1987. He has
held several

positions in Field Eng, Plant Eng. and Product Dev. after joining Alcatel in 1991. Since May of 1997 he has held the position of Technical Manager for the manufacturing facility in Calais, France.

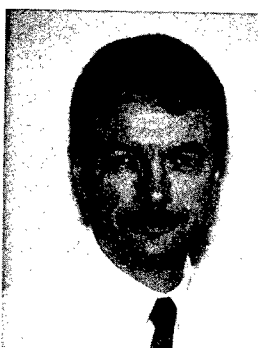


Frank E. Davidson
ALCATEL CABLE
2512 Penny Rd.,
Claremont, NC,
28610, USA Frank
received his B.S. in
Electrical

Engineering from the University of North Carolina at Charlotte in 1988.

He has held several

positions in Optical Cable Product Development, Applications and Field Engineering before and after joining Alcatel in 1992. Since October 1994, he has held the position of Product Manager in Alcatel Telecommunications Cable, Claremont, NC.



Jean-Pierre Bonicel
Alcatel Telecom.
Cable
2512 Penny Road,
Claremont NC.
28610, USA.

Jean-Pierre Bonicel was born in 1952. He received his engineering degree from the Institut des Sciences de l'ingenier de Montpellier (ISIM) in 1976. He joined

Les Cables de Lyon, now Alcatel Cable, in 1977 where he was in charge of material and mechanical problems for telecommunications cables. Now he is the Alcatel Optical Fiber Cable Competence Center Manager.

THE DEVELOPMENT OF TEST METHODS TO OPTIMISE ADSS CABLE CLAMPING SYSTEMS

M. Davies, R. Sutehall, Pirelli Cables UK
M. Collins, M. Murphy, Dulmison, UK

ABSTRACT

A range of reference test methods have been developed to approve tension and suspension clamps for use with All Dielectric self-supporting (ADSS) optical fibre cables. These methods have been used to develop and optimise the design rules for the clamping system.

BACKGROUND

The demand for all dielectric self-supporting (ADSS) optical fibre cables has increased rapidly over the last decade. Applications have ranged from very short span drop cables into business premises, short and medium span cables in rural locations and alongside railway lines, through to longspan cables strung along overhead power lines. The growth in demand has been spurred more recently by the liberalisation of network provision, encouraging transport and power utilities to further exploit their existing infrastructures by providing communication services for third parties.

The growth in ADSS demand has lead to the generation of new cable standards, but there has been little formal activity on defining test methods and functional requirements for the cable clamping system where the stress exerted on the cable is at its highest. Historically, the tension and suspension clamps used have been designed through knowledge gained by clamp manufacturers' experience with stranded metallic conductors. However, all dielectric cables inevitably perform mechanically and environmentally in a different manner to metallic cables. Further, the responsibilities of the cable supplier, clamp supplier and installer may not always be clear, particularly where well established standards are not readily available.

An holistic approach to an integrated cable clamping system has therefore been undertaken, in order to clearly define relevant test methods, and to investigate the optimisation of the system thereby ensuring the long-term system reliability.

DEFINITION OF TESTS

The tests were selected by considering overall system performance. Due account was taken of established methods used for metallic cables, with particular reference to the properties of all-dielectric optical fibre cables that might have the most significant impact on installation reliability.

The areas to consider were clamping at the tension towers or poles (where the system loads are at their highest), clamping at suspension points, and the effects of wind-induced vibration on the system, as illustrated in figure 1.

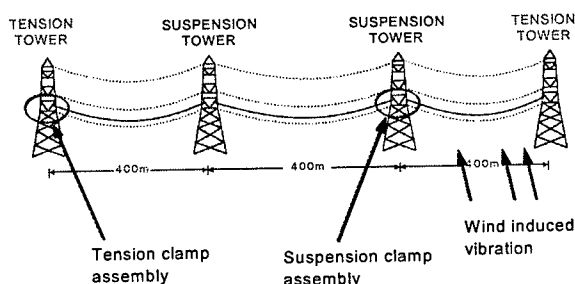


Fig. 1. Span Diagram

In addition, it was necessary to consider environmental conditions and the impact of temperature extremes on clamping performance, since high and low temperatures combined with high loadings are more likely to influence all dielectric designs than traditional metallic ones.

TENSION CLAMPING

The highest loads in an aerial installation act on the clamps at the tension points (figure 2). These loads may be as high as a cable's maximum working tension (MWT) at sub-zero to zero temperatures, due to the effect of ice loading, or combined ice and wind loading. For tropical climates, the MWT may be at ambient temperatures when high wind speeds are experienced. Higher temperatures may occur when background temperatures are raised at a cable's surface due to solar radiation. Loading

at the high temperature is likely to be low to moderate (for example at the installed or everyday stress (EDS), since additional wind loading would cool a cable to lower temperatures. For the purposes of this paper, EDS is defined to be one third of the MWT.

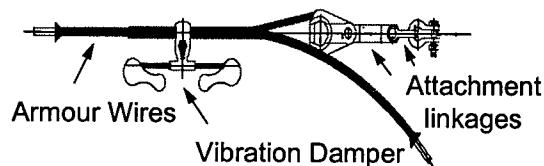


Fig. 2. Typical Tension Clamp

In addition to EDS, the combined effects of increased loadings and temperature extremes may be experienced for extremely short (minutes), medium (hours) or long (days or weeks) periods of time and these all need to be addressed within the testing regime.

Ultimate Tensile Failure (UTF)

Whilst cable clamp systems must work up to a maximum working tension, many customers require safety factors for system operation of between two and three times this figure, particularly for mechanical properties and sometimes for optical properties. There may also be a maximum limit for health and safety reasons when a cable is required to act as the fuse within the clamping system. As will be discussed later, many factors determine the ability of an ADSS cable to be successfully clamped to withstand loading across a wide temperature range. It is not sufficient merely to calculate a cable's breaking strength from its component parts, or to test to break only at ambient temperatures, since the cable has an associated temperature range, typically quoted to reflect its ability to function when cycled to the test method quoted in IEC794-1⁽¹⁾. The test should be conducted across the same temperature range when fitted with the appropriate clamps for ultimate tensile failure (UTF).

The distinction between UTF and UTS (Ultimate Tensile Strength) or RTS (Rated Tensile Strength) is made at this stage to distinguish the fact that the UTF may vary with temperature and that the failure may not be related purely to the tensile strength of the cable, but could depend on clamp design, cable design or cable materials. Failure mechanisms may include

clamp slippage, sheath rucking and sheath neckdown as well as cable break. Additionally, the relationship between cable UTS and clamp UTS is not fixed. Both need to be sufficiently strong to comply with customers' required safety factors. Typically, the clamp UTS will exceed the cable UTS, but in certain designs, such as central tube cables, the cable modulus may need to be high in order to limit the fibre strain margin. The UTF test method is illustrated in Figure 3.

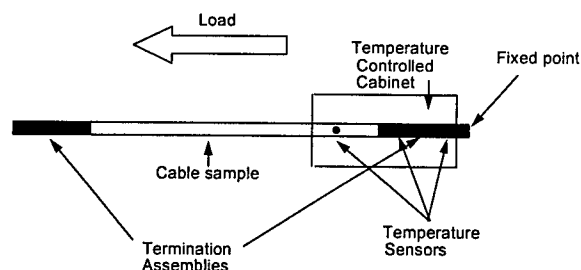


Fig. 3. Ultimate Tensile Failure Test Method

The cable test length (approximately 10 m) is loaded onto the test bed with fittings and the cable tensioned to a nominal initial tension (10% MWT) and the cable/clamp interface marked. A thermocouple is fitted at the midpoint of the tension clamp, which is located within a 2 m long temperature cabinet. The temperature in the cabinet is then increased (or decreased) at 1° C/minute until the test temperature is attained and the system is then allowed to stabilise for thirty minutes. The load is then steadily increased until a system failure occurs.

It is important to stress that the cable temperature should be closely controlled to within $\pm 2^\circ \text{C}$, to ensure test accuracy and reproducibility.

This test, in addition to proving system loading limits, may be used during the initial development phase of a cable/clamp system; it allows a "fingerprint" of system performance to be established for UTF versus temperature, which may be compared to previous fingerprints. Extreme points (for example the maximum temperature) may be used for statistical process control (SPC) and worst-case points may be used to simplify the number of loading/temperature tests performed.

The agreed limits of load and temperature combinations depend on the application. However, with an appropriate cable clamping system design, it is possible to achieve two to

three times the maximum working tension across the whole temperature range. An "ideal" performance would be for UTF to be equivalent to the cable's UTS.

Sheath Grip

Having established the instantaneous UTF load, it is then necessary to consider the extreme loads that the system may experience for sustained periods. Whilst the system must operate to MWT, it is possible that this load will be exceeded, perhaps to twice MWT, in extreme conditions. Whilst the system may not be required to perform optically at such extremes, optical performance should recover on the removal of the high load. Additionally, many customers will require a safety factor for the cable's sustained sheath grip performance over and above MWT.

The sheath grip test uses the same test equipment as the UTF test with similar clamping and heating arrangements and the loading conditions are based on an existing British Standard, BS3288⁽²⁾. Once the temperature has stabilised, the load is increased to 105% of MWT, then decreased to 100%, which is then held for the test period (one hour). The load is then increased to 210% of MWT, reduced to 200% and held for the same period of time. The overloading (105% and 210%) is to overcome initial bedding-in of system components.

Due to the possible reaction to compressive radial forces of ADSS cables compared to metallic cables, it is important to monitor a selection of fibres to ensure that the optical performance is not degraded by the operation of the clamp at load and temperature extremes. During the first loading period there should be no change in the fibre's optical performance. Additionally, there shall be no relative movement between the cable and the clamp during both loading periods. In addition to being an adaptation of BS3288, this test can be combined with the tensile test of IEC794-1-E1 and fibre strain monitored during loading.

Creep

The duration of the sheath grip test is short relative to a cable's required lifetime. A test that included sustained loading was therefore required. Creep tests already exist, for example in IEEE P1222⁽³⁾, but do not address creep

performance at temperature extremes (which may be more critical for ADSS cables, especially at high temperature) and do not explicitly consider testing the cable clamping system. The duration and magnitude of loads across the operating temperature window will vary by application and with daily temperature variation. However, sustaining loads at a reasonable fraction of MWT (such as at EDS) for the test period (1000 hours) and at temperature extremes allows an accelerated lifetime test to be performed. Again, the UTF "fingerprint" will assist in the choice of suitable loading/temperature combinations, with an "ideal" fingerprint (UTF = cable UTS) being a predictor of good, stable creep performance

For ease of carrying out the test and to enable better control of the test variables, a horizontal test bed was used in preference to a vertical one. This also provides easier access to the fibres if optical monitoring is to be carried out for research purposes.

The test apparatus is similar to that used for UTF and sheath grip testing. The cable is loaded into the test apparatus with the specific clamps, a pre-load equivalent to MWT is applied and then released back to the test load. Pre-loading is important because bedding-in of the cable elements might otherwise dominate the apparent creep length measurements. Using the specified clamps is an important part of the test, since this ensures the creep performance of the system. As with the other clamp tests, the cable is heated, or cooled, to the required temperature which is maintained for the test duration.

Two loading conditions may be distinguished. First, a constant load (MWT to reflect worst case sustained loading) is applied and maintained throughout the test in order to monitor extension over time, as is normal with creep testing.

Second, a decaying load test may be carried out, whereby an initial load (EDS) is applied (after an MWT pre-load) and the decay of load is measured as the cable creeps. This second case most closely reflects the reality of a cable installation, which is loaded between two fixed points, and illustrates the time to stability of the installed system. Once the initial load has been applied and the initial cable extension recorded, the cable may extend (creep) further during the test (1000 hours). This extension, which causes the load to decrease by an amount "Y" (see

figure 4), is due to additional bedding-in of the elements, if this has not been fully achieved during the pre-load, and due to material creep. Y should be sufficiently small so that the additional cable sag resulting does not cause infringement of ground clearance or cable clashing restrictions.

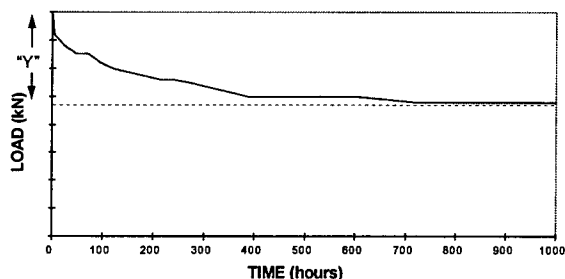


Fig 4. - Decaying Load Creep Test

Achieving an asymptotic load is indicative of a stable system that will not continue to creep to failure over time. In an ideal system, the load decrease Y will be small and the asymptotic load achieved very early within the 1000 hour test, with the application of high loads at temperature extremes.

TENSION CLAMP OPTIMISATION

Once the test methods were determined, it was necessary to define the cable clamping system variables in order to investigate the sensitivity of the system to variations in its parts, and hence to allow performance optimisation criteria to be established. Whilst there are many variables, it was decided to initially focus on the prime parameters inherent within the cable design, the cable materials and the clamp design.

Cable Design Variables

There are a wide number of ADSS cable designs, some of which are illustrated below (figures 5-8).

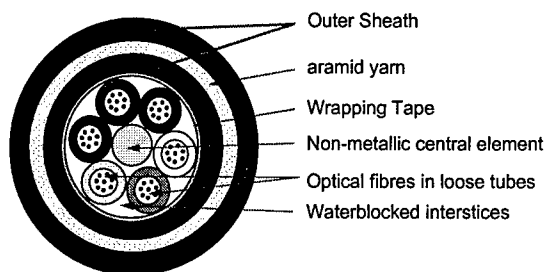


Fig. 5. Multi-loose tube, aramid strength member cable

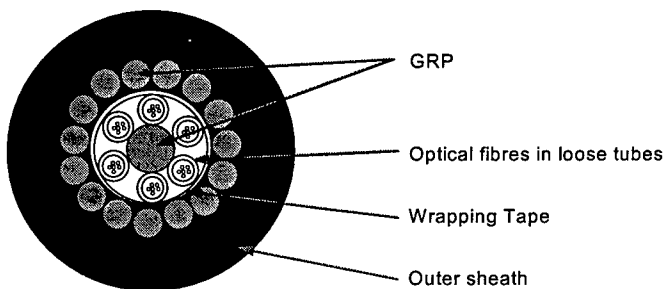


Fig. 6. Multi-loose tube, grp strength member design

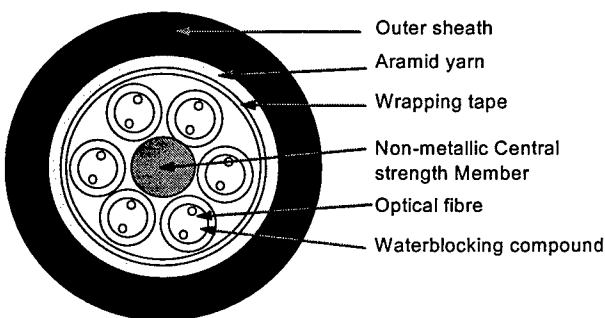


Fig. 7. Single sheath, multi-loose tube, aramid strength member design

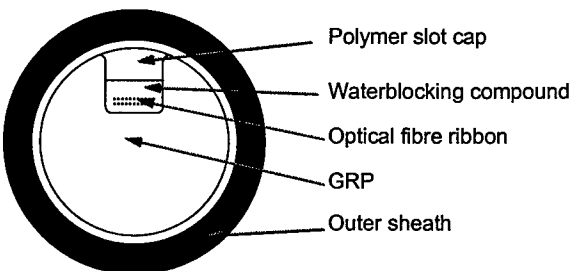


Fig. 8. Fibrespan

These designs vary widely in terms of tensile strength and radial compression resistance, which both critically influence cable clamping and can be very different to metallic cable values. The cables may have a single or double sheath, be central or stranded loose tube, and have different sheath radial thicknesses and outer diameters.

Cable Material Variables

A major material departure from metallic cables is the composition and influence of the sheath material. This may be a thermoplastic or cross-linked material and there are a wide range of candidate materials with varying modulus and hardness values, which vary further under the influence of heat. This variation is important for ADSS cables, where high background temperatures may be increased by the effects of solar radiation. Moduli and hardness values for typical ADSS materials are given below in figures 9 and 10.

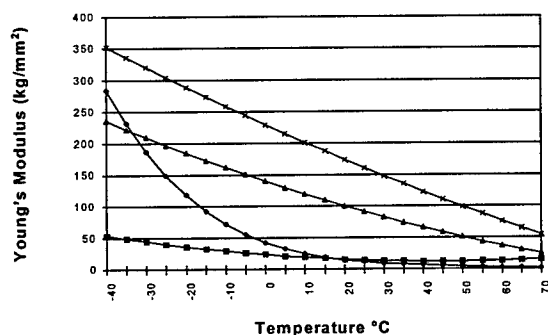


Fig. 9. Sheath Material Young's Modulus versus Temperature

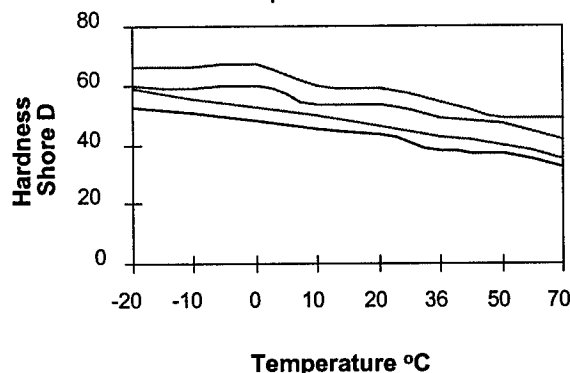


Fig. 10. Sheath Hardness versus Temperature.

Other material factors include the composition of the strength member (aramid, GRP, water-blocking) and processing conditions.

Tension Clamp Variables

There are a wide number of tension clamp variables. These include the use of a single-piece or two-piece dead-end, clamp material, number and diameter of wires, length of the assembly, radial compression exerted on the cable and helix angle of the wires. An additional consideration is the ease of fitting the clamps correctly, since the clamping ability may be compromised by poorly fitted clamps.

Optimising the Variables

In order to investigate the influence of all the variables, a Design of Experiment (DoE) approach was used to reduce the number of experiments and tests required with a "change only one variable at a time" approach. This led to a rapid selection of optimum and non-optimum conditions, which were then verified with specific experiments using these conditions.

Figure 11 shows the UTF for an optimised and a non-optimised system. The difference in performance is significant, particularly at high temperatures. The optimised system achieved UTS throughout the temperature range.

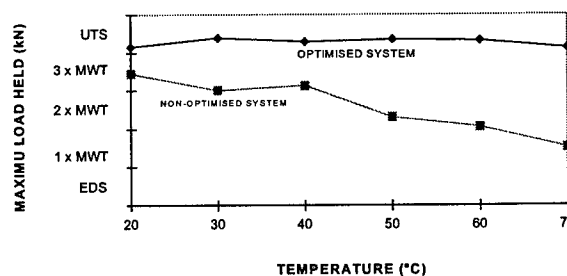


Fig. 11. UTF for Optimised and Non-optimised Cable Clamp Systems

The optical performance was monitored during the optimised test to verify suitability of the clamp system, as shown in figure 12. No significant optical change was observed at 70° C until the load was well in excess of 2 x MWT.

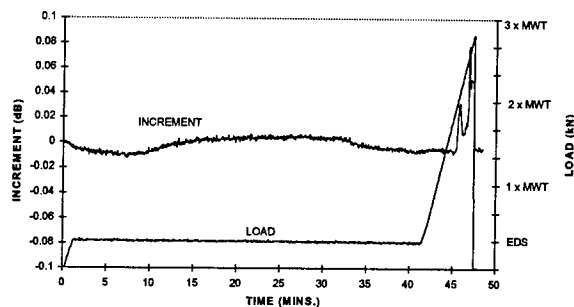


Fig. 12. Optical Monitoring During UTF Test at 70° C.

A comparison between single piece and two piece tension clamps was carried out (figure 13). Although it is possible to optimise the single piece system for short span applications, the performance of the two piece system is significantly better.

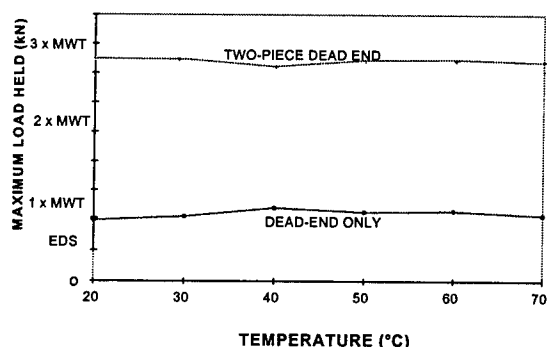


Fig.13. UTF Test for Single Piece and Two Piece Assemblies

The difference in creep performance between non-optimised and optimised systems can be even more dramatic than for the UTF test, where the former may degrade to failure within hours and the latter is able to sustain very high loads and temperatures for over 1000 hours. These are graphically illustrated in figure 14. It should be noted that this example is at MWT, not at the recommended load of EDS.

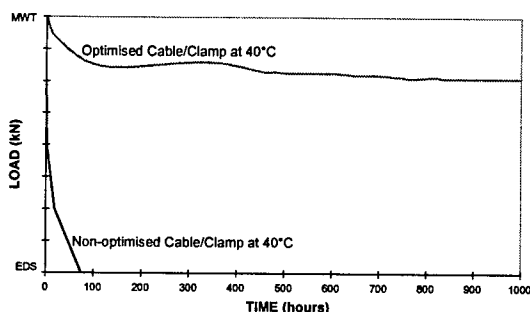


Fig. 14. Creep Performance.

Low temperature testing to -50° C, was also investigated. Whilst no significant difference in performance was observed between low temperature and 20° C, it is possible that as the material's modulus and hardness increase, particularly if the sheath has a large radial thickness, then the load transfer from the clamps through to the strength member may be compromised.

SUSPENSION CLAMPS

Suspension clamps (figure 15) are applied at intermediate poles or towers between the tension points. Their function is to hold the cables on the poles or towers that are not designed to withstand maximum tensile loads. This is more cost effective than using heavier structures, or pole stays, that are used at tension towers or poles.

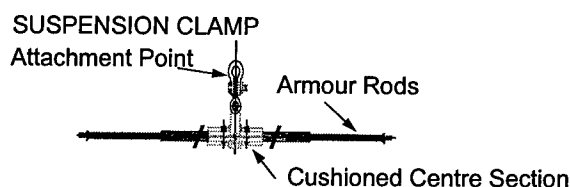


Fig 15. Typical Suspension Clamp

The suspension points may well not be in a straight line, due to undulating terrain and slight route deviations, and thus the clamps need to be tested for their ability to accommodate a line deviation angle of up to ten degrees. The clamps also need to protect the installation from unbalanced loads that may occur from structure-to-structure due to differences in cable loading, and hence need to allow cable to slip through between specified minimum and maximum loads.

For short-span, low-load applications, pulleys may also be used instead of conventional suspension fittings. The main advantage is that during unbalanced loading conditions the load applied to the structure is minimal. An assessment of a cable's ability to withstand wear, caused by friction with the pulley, needs to be undertaken.

Line Deviation Angle

The cable is loaded into the test apparatus and clamped at the end points with suitable tension clamps (figure 16). Test fibres are spliced together to form a continuous loop and the cable loaded to EDS.

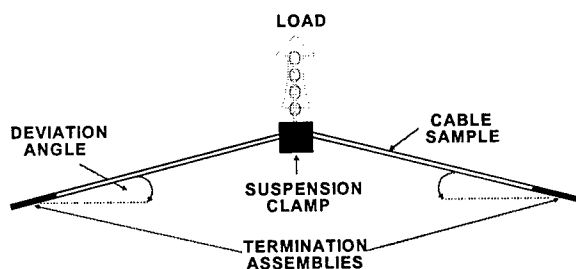


Fig. 16. Line Deviation Angle Test Apparatus

A suspension clamp is then fitted at the mid-point and raised until the required deviation angle is achieved, whilst maintaining the MWT load (which could be experienced during ice-loading). A typical deviation angle for ADSS might be 5°, so a worst case figure of 10° is recommended. The fibres are monitored continuously and the load is maintained for one hour. During the test there shall be no change of optical power and after the test there shall be no visual damage to the cable. For safety reasons, the test should be repeated at twice MWT and no visual damage confirmed.

Differential Load Withstand Test

This test is undertaken to ensure protection of the cable system and the support structures from uneven loading in adjacent spans. The cable is loaded into the test apparatus (figure 17) and tension and suspension clamps fitted.

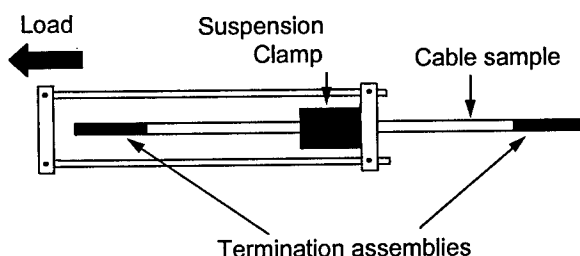


Fig. 17. Differential Load Withstand Test Apparatus.

A load is then applied to one side of the suspension clamp and increased until the clamp

slips. The maximum slip load calculation is based on two adjacent iced spans at MWT. One span is then assumed to shed its ice load and reduce in tension to EDS. The slip load is therefore MWT minus EDS, or two thirds MWT (assuming $EDS = \frac{1}{3} MWT$), which represents the difference in tension between the spans. The minimum load is taken as half this value (EDS) and is required to ensure some stability in the system for low uneven loads. If slip was allowed at too low a value, then frequent suspension clamp realignment of the line would be required.

Optimising Suspension Clamping

The suspension clamp design itself dominates system performance in both the line deviation and differential load withstand tests. Provided that the cable is protected from sharp point bending by the clamp, and that any plastic materials used as cushioning within the clamp have a wide temperature window, then no special cable design considerations are necessary.

VIBRATION

The cable and clamps (both tension and suspension) will be subjected to vibration effects induced by wind flow, with stress at the clamps causing potential damage to the clamped cable. Test methods have already been defined (for example EN187000⁽⁴⁾), but as with clamp design, these are very much derived from metallic conductors and thus have limitations when applied to ADSS designs.

Aeolian Vibration

Aeolian vibration is a high frequency low amplitude vibration induced by laminar air flow (2.5 to 7 m/s). It is recommended that vibration tests be conducted at a load equivalent to the cable EDS as this represents the day-to-day value of loading. Use of a higher load is unrealistic; such an increased load is most commonly associated with ice accretion and consequently there are two competing effects: an *increase* vibrational frequency due to the increased load; a *decrease* in vibrational frequency due to the increased effective cable diameter (Strouhal formula⁽⁵⁾, figure 19). Use of EDS to define test load therefore constitutes a known, realistic and effective compromise. The test methods already defined^(3,4) may be used,

but there are a wide number of variables that should be investigated further for their effects on ADSS cables, as discussed below

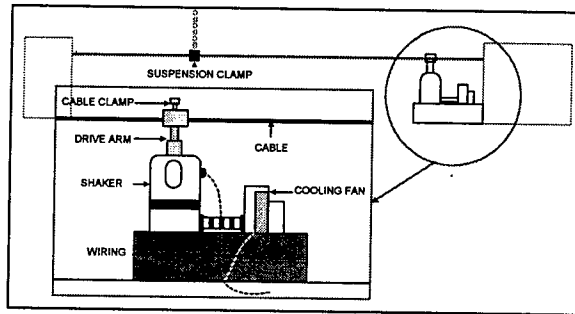


Fig. 18. Aeolian Vibration Test Apparatus.

30 m of cable is loaded into the test span and the tension clamps fitted. Suspension clamps are fitted at the mid-point of the test span and then the test load (EDS) is applied. The nearest resonant frequency to that calculated from the Strouhal formula⁽⁵⁾ (figure 19) is selected for the test and the power of the shaker is adjusted to achieve the required amplitude. The test is carried out for 10^8 cycles and no change of fibre attenuation during or after the test permitted.

$$\text{Frequency} = \frac{185 \cdot V}{d} \quad \text{Hz}$$

where: V = wind velocity (m/s)
 d = cable diameter (mm)
 185 = Strouhal number

Fig. 19 . Strouhal formula.

The test may be carried out with or without suitable vibration dampers, but since their field use may vary, it would be advisable to test the cables without such devices and hence simulate worst case conditions.

An additional test parameter, not covered by the test method, is the change of cable modulus, or UTS retention, which may be significant if self-damping occurs, due to interstrand friction in the strength member. This test involves subjecting the cable, plus tension clamps, to a tensile test without removing the clamps and comparing the result to unvibrated cable results.

One of the parameters for further investigation is the test frequency. Sweeping the frequency between certain minimum and maximum figures would more readily simulate the real-life conditions where wind speed is varying. The

use of frequency sweeping, or the gathering of actual field vibration data, has indicated that the amplitudes of displacement and the frequencies at which these act, often differ from the Strouhal formula⁽⁵⁾. Again, some of these differences may be attributed to the differences between metallic and non-metallic designs, and in particular, the self damping properties may vary significantly. Other parameters for further study include the applied load, the application of constant or decaying loads, cable amplitude, test endurance (10^8 cycles or greater) and temperature.

Galloping

Cable galloping is a low frequency, high amplitude vibration caused primarily when ice forms on the cable. The cable profile then causes lift which promotes galloping. This galloping may continue for hours or even days.

As with aeolian vibration testing, test methods have been defined^(3,4) and are based on similar equipment to that shown in figure 18. 30 m of cable is loaded into the test span and a load equivalent to EDS is applied. 100,000 cycles are carried out at the calculated frequency⁽⁴⁾. The cable is monitored to ensure no optical degradation during or after the test and, as for aeolian vibration, is tensile tested to confirm that the strength has not degraded.

There are a number of variables with this test method that need to be investigated further. These include cable load, fibre anchoring methods, load pre-conditioning effects and the high back strains induced in the test equipment that are not simulated in the field and test temperature. The difference in weight and construction between ADSS and metallic designs suggests that the direct transfer of a metallic cable test may lead to variations in test reproducibility for non-metallic designs.

Optimising Vibration Performance

The vibration performance of the cable/clamp system can be optimised by considering tension clamp design (preventing cable to clamp wear), cable sheath material and ensuring suspension clamp articulation (movement restriction could cause wear in the system). Also to be considered are cable sag (which may be optimised to reduce incidence of vibration), strength member composition (to minimise

interstrand friction in the strength member) and vibration damper performance.

SUMMARY

A number of test methods have been proposed to test tension clamps, suspension clamps and vibration as part of an ADSS cable/clamp system. The inter-relationship of the cable and the clamp has been shown to be important, with load and temperature being critical. Optimised system designs have been achieved using these test methods which will maximise system reliability.

REFERENCES

1. IEC 794-1: "Optical Fibre Cables - Part 1: Generic Specification".
2. BS 3288: "Insulator and Conductor Fittings for Overhead Power Lines. Part 1: Performance and General Requirements".
3. IEEE P1222: "Standard for All Dielectric Self-Supporting Fiber Optic Cables (ADSS) for Use on Overhead Utility Lines".
4. EN 187000: "Generic Specification for Optical Fibre Cables".
5. Transmission Line Reference Book (EPRI 1979), Chapter 1, Section 4.

AUTHORS



Martin Davies
Pirelli Communication
Cables Limited
Wednesbury Street
Newport, S. Wales
UK. NP9 0WS

Martin Davies is Chief Engineer with the Communications Cables Division of Pirelli Cables UK, where he is responsible for research and development of new cables, materials and access network plant. He has been an active member of a number of standardisation bodies, including BSI, ETSI and IEC. Currently, he is a member of the CENELEC joint working group, developing standards for optical cables to be used along electrical power lines.



Ralph Sutehall
Pirelli Communication
Cables Limited
Wednesbury Street
Newport, S. Wales
UK. NP9 0WS

Ralph Sutehall is a Senior Engineer with the Communications Division of Pirelli Cables in the UK, where he is responsible for installation development. He has been working with fibre optic cables for 24 years and is an active member of the CIGRE working group on fibre optics.

Maurice Murphy
Dulmison UK Limited
Macadam Road
Earlstrees Ind. Estate
Corby, Northants
UK. NN17 4JN

Maurice Murphy is a graduate Civil Engineer from Queen's University in Canada. He worked for several years as a Transmission Design Engineer and then a Research Engineer for B.C. Hydro in Canada. In 1988 he became the Chief Engineer of Dulmison Inc. USA. In 1995 he became General manager of Dulmison UK. He is an active member of the IEEE in both the Fibre Optic and Conductor Dynamics Task Forces and with the CIGRE Working Group on Fibre Optics



Mike Collins
Dulmison UK Limited
Mcadam Road
Earlstrees Ind. Estate
Corby, Northants
UK. NN17 4JN

Mike Collins is employed as Sales Manager for Dulmison UK Limited. Following an apprenticeship he obtained a bachelor of science degree. He has been employed by Dulmison for the past 7 years, 5 of those being the Senior Engineer specialising in helical fittings and vibration control systems for power conductors and ADSS cables.

A STUDY ON BEHAVIOR OF FIBER RIBBONS IN SZ-GROOVED SPACER AND ITS APPLICATION TO AERIAL CABLE

Hiroki Ishikawa, Yoshiyuki Suetsugu, Takashi Saito, Masakazu Watanabe,
Akihito Makiyama, Jun-ichi Ohta and Shigeru Tanaka

Sumitomo Electric Industries, Ltd. ,Yokohama Japan

ABSTRACT

In order to adequately design SZ-grooved spacer especially for fiber ribbons, we have made theoretical and experimental analysis on SZ-grooved spacer cable. The analysis included the calculation of curvature radius and bending vector direction distribution. Also included was the calculation of a fundamental ribbon behavior based on an energy minimum principle in ribbon strain energy as a function of SZ-parameters. From the results of these analysis, we have clarified the SZ-groove design theory from the aspects of transmission property and mid-span accessibility.

Application of the above key studies to self-supporting structure enabled 100-fiber SZ-grooved spacer aerial cable consisting of 4-fiber ribbons to be successfully manufactured and tested.

INTRODUCTION

Recently fiber optic network has been spreading into residential subscriber area. In order to construct the subscriber network with lower cost, a demand for aerial optical cable with SZ-grooved spacer is increasing, because of its easiness in mid-span access and drop operation. ¹ In addition, the cable is desired to consist of fiber ribbons in order to achieve high density and high count aerial cable.

However, it has not been studied on design theory of SZ-grooved spacer for fiber

ribbons. Thus we have conducted theoretical and experimental analysis in order to clarify the adequate groove design theory from the aspects of optical loss and mid-span accessibility.

In this paper, we present the study to clarify the SZ-groove design standard and cable testing results of manufactured cable, adequately design with the developed design standard and newly developed highly reliable self-supporting structure.

RIBBON BEHAVIOR ANALYSIS

General Description of SZ- locus

In this section, we define and explain the SZ-locus description and derive the curvature radius and principle normal vector distribution of the locus along cable longitudinal direction. The curvature radius is calculated on both straight and bent cable.

Maximum and minimum curvature radius was reported in reference [2]. But in our report, the curvature radius and principle normal vector direction are calculated at any point along the SZ-locus in longitudinal direction for the preparation of ribbon behavior analysis.

SZ- locus Formula.

SZ-locus is characterized by three parameters; a reversing pitch, P , a path radius, a and a reversing angle, ϕ , as shown in Figure 1. In our study, the reversing angle ϕ was fixed to 275° because it is necessary to adopt this value in order to equalize fiber length in any groove when cable is bent. ³

Position vector of SZ-locus is described by equations (1). In equations (1), k is a phase angle corresponding to the cable length normalized by the reversing pitch, P . When the cable is bent, the locus is as equations (2) in which R means a cable bending radius and x , y and z axis are set as shown by figure 2.

$$\begin{aligned} x &= -a \sin\left(\alpha + \frac{\phi}{2} \sin k\right) \\ y &= a \cos\left(\alpha + \frac{\phi}{2} \sin k\right) \\ z &= \frac{P}{2\pi} k \quad \left(k = \frac{2\pi}{P} l\right) \end{aligned}$$

(l means cable longitudinal coordinate) (1)

$$\begin{aligned} x &= -a \sin\left(\alpha + \frac{\phi}{2} \sin k\right) \\ y &= R - \left\{ R + a \cos\left(\alpha + \frac{\phi}{2} \sin k\right) \right\} \cos \theta \\ z &= \left\{ R + a \cos\left(\alpha + \frac{\phi}{2} \sin k\right) \right\} \sin \theta \end{aligned}$$

($\theta = l/R$) (2)

Curvature Radius distribution.

Curvature radius, ρ of any locus is obtained by equation (3).

$$\frac{1}{\rho} = \sqrt{\left(\frac{dx}{ds}\right)^2 + \left(\frac{dy}{ds}\right)^2 + \left(\frac{dz}{ds}\right)^2}$$

(s means SZ-locus length) (3)

Substituting equations (2) for (3), curvature radius can be derived as a function of l which means length along cable longitudinal direction.

Using these equations, curvature radius distribution along a cable was calculated for both a straight and a bent cable as described by figure 3 in which the SZ-parameters are assumed as $P=500\text{mm}$, $a=2.5\text{mm}$ and

$R=500\text{mm}$. For bent cable, two different groove positions were considered. One is that the locus is on outside of the cable bent (inset A), and the other is that the locus is on inside (inset B).

As shown in figure 3, the minimum curvature radius appears at the middle point in between reverse points in groove bent as inset (A).

Normal Vector of SZ-locus. Principle normal vector of any locus can be obtained as second derivative of position vector with respect to s .

We calculated the principle normal vector of SZ-locus using equations (1). The calculation result is shown schematically in figure 4 by arrows. The direction and the magnitude; the reciprocal of curvature radius, varies along cable length direction. As shown in figure 4, principle normal vector directs to cable center at middle point in between neighboring reverse points, and rotate in opposite direction of locus rotation. At reverse point, the vector is tangent to the cylinder involves the SZ-locus, and has almost minimum magnitude.

Fundamental Ribbon Behavior Analysis

In this section, fiber strain energy calculation is carried out in order to comprehend fundamental ribbon behavior, and derive the relationship between SZ-parameters and the ribbon behavior.

Strain Energy Calculation. In order to comprehend the ribbon behavior in SZ-groove, we assumed two types of model behavior as shown in figure 5 (a) and (b). In the model (a), ribbon is not twisted at any longitudinal point in the groove. On the other hand in the model (b), ribbon is twisted along longitudinal direction and ribbon surface is always parallel to groove bottom. Using these two models, we calculated strain energy of glass fibers in a ribbon but ignored a contribution of fiber coating resin and ribbon matrix resin because of their smaller Young's modulus and for convenience of calculation. On the model (a), only bending strain energy

was calculated because ribbon was not twisted. On the model (b), bending and torsion strain energy was calculated. In the strain energy calculation, we used the results of curvature radius and principle normal vector calculation.

An example of strain energy calculation result is shown by figure 6 in which SZ-parameters are assumed as $P=500\text{mm}$, $a=2.5\text{mm}$ and $\phi=275^\circ$. As for the ribbon structure, 4-fiber ribbon of 1.1mm width and 0.4mm thickness was assumed. Horizontal axis of figure 6 means phase angle k and vertical axis means the sum of strain energy generated in four fibers per unit length. As seen in figure 6, we have done the calculation for a quarter of reversing pitch.

It is expected that one of the models (a) or (b) with smaller strain energy is likely as the fundamental ribbon behavior. The strain energy is the integration of bending and torsion strain energy with respect to cable length for a pitch.

SZ-Parameters and Ribbon Behavior.

We calculated the fiber strain energy for various SZ-parameters and compared the strain energy integrated with respect to cable length for a reversing pitch of the model (a) with (b). The comparison was done for 4-fiber ribbon and 8-fiber ribbon whose result is shown in figure 7 (A) and (B), respectively. The figures 7 describe the relationship between total strain energy and the parameters of SZ-grooved spacer structure, a pitch and a path diameter, 2a.

In the SZ-spacer which have parameters in unhatched area of figures 7, the integrated strain energy of fiber behave as model (a) is smaller than that of model (b), so a ribbon would behave as untwisted model. From this figure, the groove design standard can be drawn as that for an SZ-spacer whose parameters are in the unhatched area, grooves must be designed to permit rotation of a ribbon or ribbon stack, and for an SZ-spacer in the hatched area, grooves can be designed just to suit for the size of the ribbon stack.

Experimental Verification. In order to verify the fundamental ribbon behavior rule, we manufactured two test cables and observed the ribbon behavior. One of the cables was consisted with 4-fiber ribbons and had SZ-grooved spacer of which parameters were in untwisted area; the reversing pitch was 300mm and path diameter of ribbon was 6.3mm. The other test cable was consisted with 8-fiber ribbons and with SZ-spacer in twisted area; the pitch was 700mm and path diameter was 10.4mm. Their SZ-parameters are indicated by circles in figures 7.

For the test cables, we fixed the ribbons in the groove with epoxy resin and cut at interval of 20mm for 4-fiber ribbon cable and of 30mm for 8-fiber ribbon cable. On the cut sample, we measured ribbon angle which is defined as shown in figure 8. The measurement results are demonstrated in figures 9 with designed groove angle variation. From the figure 9 (A), it can be seen that 4-fiber ribbon in SZ-groove which has parameters in untwisted area scarcely changes its angle, that means it is not twisted. On the other hand, in figure 9 (B), 8-fiber ribbon in SZ-groove which has parameters in twisted area changes its angle following the groove angle, so the 8-fiber ribbon is twisted.

From this result, it can be said that theoretically drawn ribbon fundamental behavior rule is verified experimentally.

Summary of Analysis

From these analysis, SZ-groove design standard was clarified. It is that there are two different SZ parameters combination area. In the untwisted area, grooves must be designed to permit ribbon stack rotation, and in the twisted area, grooves can be designed just to suit for the size of the ribbon stack.

DEVELOPMENT OF SELF-SUPPORTING AERIAL CABLE

The newly developed design standard for the ribbon SZ cable was applied to 100-

fiber self-supporting cable with 4-fiber ribbons which is in demand for subscriber network in Japan. ⁵ In this section, we describe SZ-groove design concept, newly developed self-supporting structure and the performance of manufactured cable.

SZ-Grooved Spacer Design Concept

Minimum Slack Length Estimation.

One of the most important points in SZ-grooved spacer design is ribbon slack length estimation, because it limits mid-span accessibility. Here the ribbon slack length is defined as the distance between spacer surface and ribbons took out from groove without being cut for finite sheath removal length.

If sheath removal length is equal to n times reversing pitch P , slack length d can be estimated easily by equation (4), in which L means sheath removal length.

$$d = L \sqrt{\frac{\lambda}{2}}$$

$$\lambda = \frac{(\text{Ribbon length Laid in a Pitch})}{P} - 1 \quad (4)$$

We considered the case, in general form, that the sheath removal length is not equal to n times P , where the slack length is effectively reduced from what is given by equation (4). The minimum slack length can be estimated by choosing removal position as shown by figure 10. Figure 11 shows an example of minimum slack length estimation. Here, sheath removal length is 500mm, and path radius is 2 to 6.

Using this technique, we designed the SZ-grooved spacer to get at least 20mm for 500mm sheath removal.

Ribbon behavior. From the result of slack length design and to reduce cable diameter, the SZ-parameters of developed cable was set to be as $P=300\text{mm}$, and $a=6.3\sim 8.9\text{mm}$. As seen in figure 7 (A), this spacer is almost in untwisted area. Thus we designed the groove cross-section as to permit ribbons stack rotation.

Self-Supporting Structure

In order to achieve low cost and highly reliable aerial cable, we have developed new self-supporting structure which is demonstrated schematically in figure 12 and described in reference [6]. In the developed cable, supporting wire and cable are linked intermittently and cable has excess length to supporting wire in order to avoid cable elongation caused even by wind pressure. And the linkage is made up with the same material with sheath and is made up in jacketting process to reduce manufacturing cost.

Manufactured Cables Design

Figure 13 shows manufactured cable cross-section. The cable dimension is summarized in Table 1. The cable has a five SZ-grooved spacer and each groove contains five 4-fiber ribbons. Cable diameter is 14mm and supporting wire is 7/2.0 steel wire. Cable has 0.3% excess length against supporting wire.

Test Results on manufactured Cable

Transmission Characteristics. We measured optical loss on the manufactured 1km cable and the measurement result is summarized in Table 2. Excellent properties was confirmed by the obtained average loss of 0.19dB/km at 1.55 μm .

Mechanical Properties. Mechanical tests were carried out on the manufactured cable under conditions shown in Table 3 in which test results are also described. There were no optical loss increase during and after test for every test item.

Mid-Span Accessibility. On the manufactured cable, we measured ribbon slack length for 500mm sheath removal. Figure 14 shows the measurement result. The minimum slack length in any groove was above 20mm, designed minimum slack length. Therefore, test result supports the validity of our minimum slack length estimation method.

SUMMARY

Through the analysis of ribbon behavior in SZ-grooved spacer by fiber strain energy calculation, we have clarified the fundamental ribbon behavior rule and confirmed its validity by experimental observation. And from the ribbon behavior rule, we derived a standard for designing the groove dimension. Using these results, we have manufactured 100-fiber self-supporting SZ-cable, and confirmed its excellent performance.

In addition, we have employed a newly developed single process self-supporting sheath technique, and realized low cost self-supporting aerial cable.

References

- [1] M. Okada et al., in Proc. of the 1996 Comm. Society of IEICE, B-940, p425 (1996)
- [2] T. S. Swiecicki et al., in Proc. of IWCS, p404 (1978)
- [3] K. Niikura et al., Sumitomo Electric Tech. Review, No.29, p70 (1990)
- [4] G. W. Seo et al., in Proc. of IWCS, p449 (1995)
- [5] N. Kashima et al., in Tech. Digest of the 2nd OECC, 10E1-1, p516 (1997)
- [6] H. Ishikawa et al., in Tech. Digest of the 2nd OECC, 10E1-3, p520 (1997)

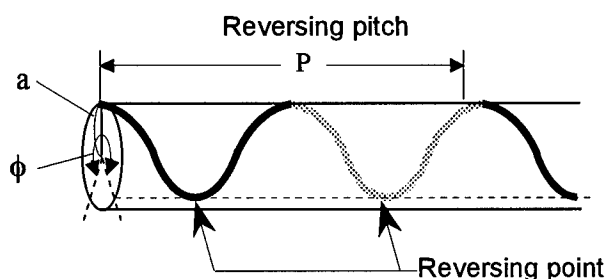


Fig. 1 SZ-locus parameters

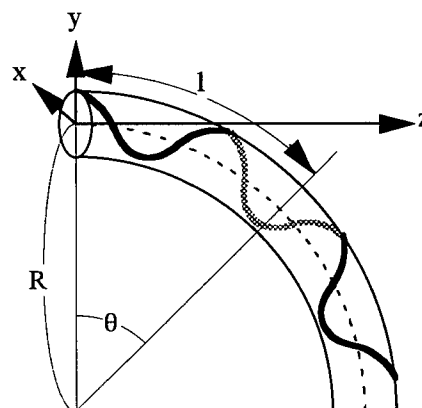


Fig. 2 Axis direction on bent cable

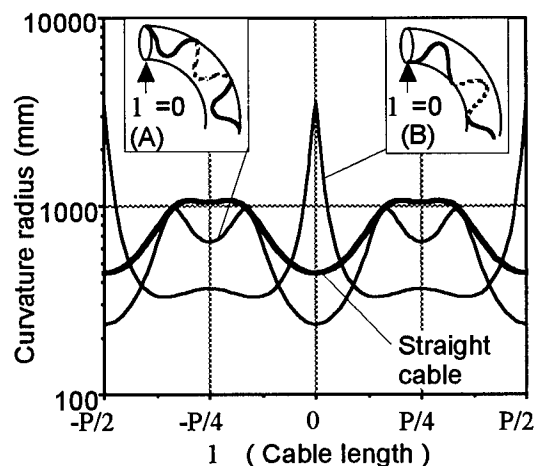


Fig. 3 Curvature radius distribution of straight and bent SZ-locus
($P=500\text{mm}$, $\phi=275^\circ$, $a=2.5\text{mm}$, $R=500\text{mm}$)

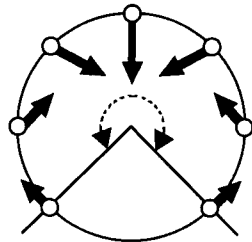


Fig. 4 Principle normal vector direction and curvature magnitude

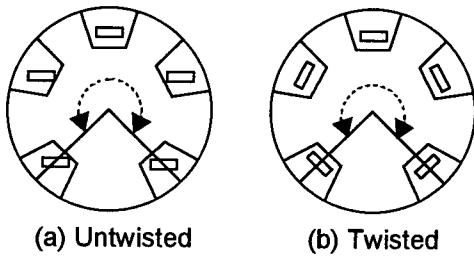


Fig. 5 Fundamental ribbon behavior model

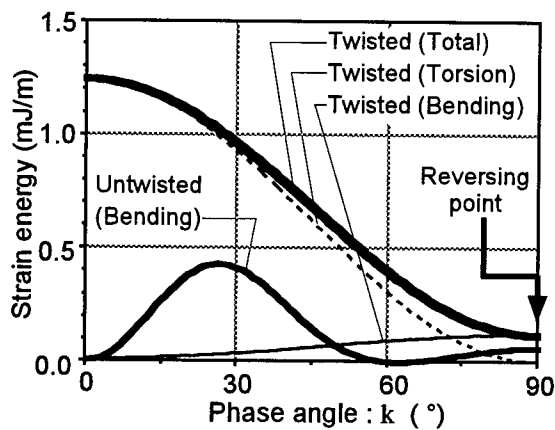
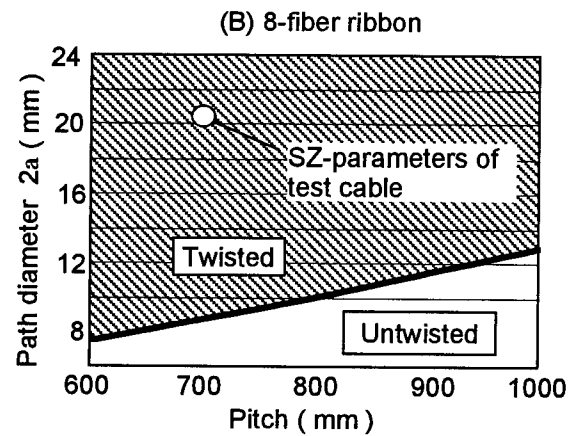
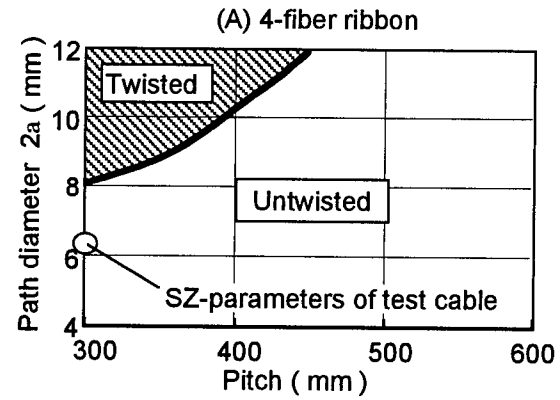


Fig. 6 Strain energy distribution of glass fiber in 4-fiber ribbon
($P=500\text{mm}$, $\phi=275^\circ$, $a=2.5\text{mm}$, $R=500\text{mm}$)



Figs. 7 Relationship between fundamental ribbon behavior and SZ-parameters

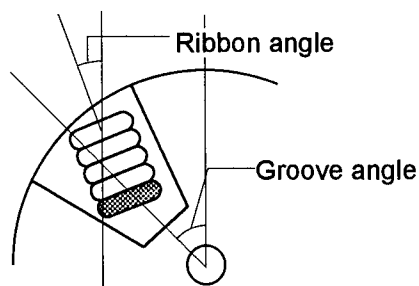


Fig. 8 Ribbon angle and groove angle definition

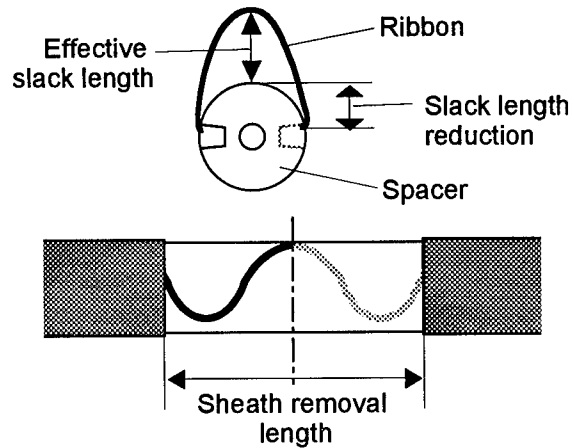
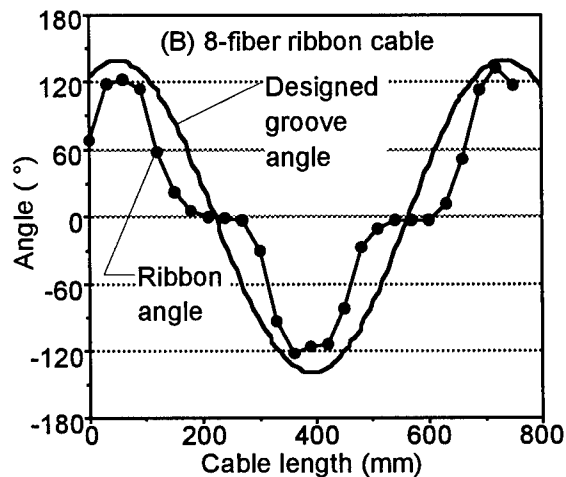
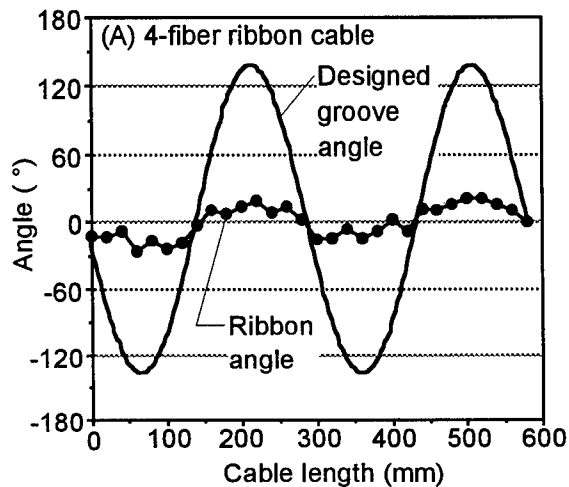


Fig. 10 Worst sheath removal position



Figs. 9 Ribbon and groove angle variation in test cable

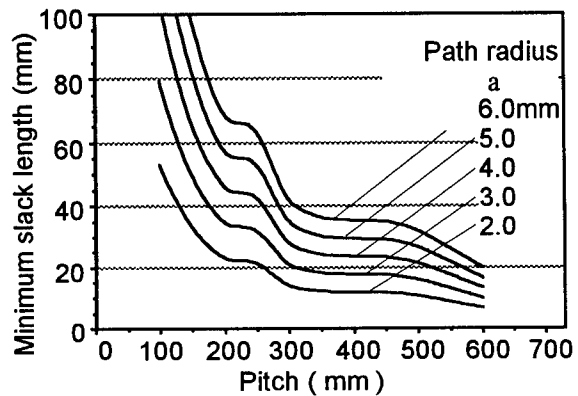


Fig. 11 Estimated minimum ribbon slack length (Sheath removal length = 500mm)

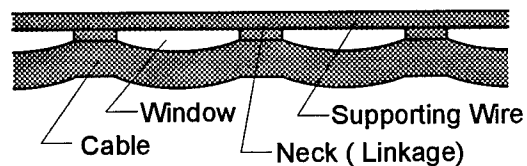


Fig. 12 Newly developed self-supporting structure

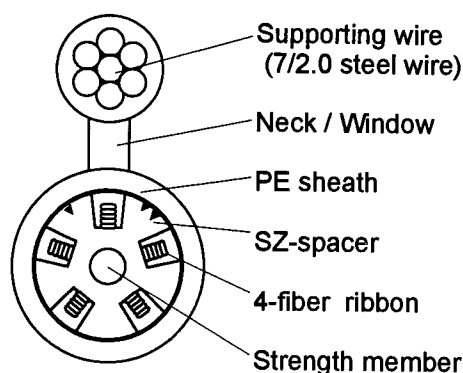


Fig. 13 Manufactured cable cross-section

Table 1 Dimension of manufactured cable

Fiber count	100
Supporting wire	7/2.0 Steel Wire
Fiber ribbon	4-fiber ribbon
Ribbon number	5/Groove
SZ-pitch	300mm
Cable diameter	14mm

Table 2 Transmission characteristic

Item		Result
Initial loss (1.55mm)	Avg.	0.19
	Max.	0.22
Heat cycling -30~+70°C (1.55μm)		<0.1 dB/km

Table 3 Mechanical test condition and results

Item	Condition	Result
Tension	9,800N	<0.1dB Loss increase
Bending	R=10D	
Crush	1,960N/100mm	
Twist	±90°/1m*10 times	no residual loss increase (@1.55μm)
Impact	1kg Weight*1m	
Squeeze	R=250mm tension=1960N 4 times	

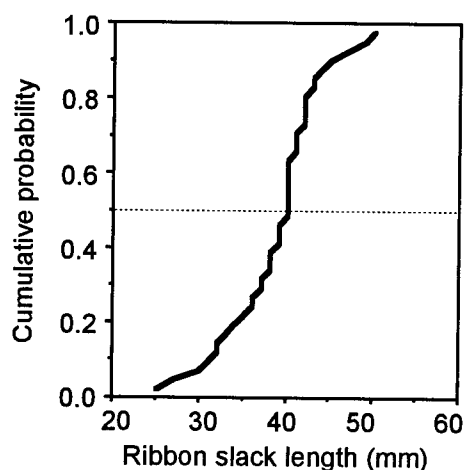


Fig. 14 Measured ribbon slack length distribution
(Sheath removal length =500mm)



Hiroki Ishikawa

Sumitomo Electric
Industries, Ltd.
1, Taya-cho, Sakae-ku,
244, Yokohama, Japan

Hiroki Ishikawa received his M. E. degree in applied physics from Tohoku University in 1990.

He joined Sumitomo Electric Ind., Ltd. in 1990 and he has been engaged in research and development of fiber-optic cables. Mr. Ishikawa is a member of Communications R&D Department in Yokohama Research Labs.



Yoshiyuki Suetsugu

Sumitomo Electric
Industries, Ltd.
1, Taya-cho, Sakae-ku,
244, Yokohama, Japan

Yoshiyuki Suetsugu received his B. S. degree in physics and Ph. D. degree in applied physics from Tsukuba University in 1984 and 1996 respectively.

He joined Sumitomo Electric Ind., Ltd. in 1984 and he has been engaged in the research and development of optical fibers and fiber-optic cables. Dr. Suetsugu is a senior engineer of Communications R&D Department in Yokohama

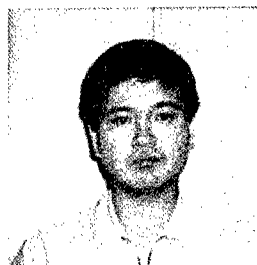


Takashi Saito

Sumitomo Electric
Industries, Ltd.
1, Taya-cho, Sakae-ku,
244, Yokohama, Japan

Takashi Saito received his B.E. degree in electronics engineering from Sendai Radio College of Technology in 1992.

He joined Sumitomo Electric Ind., Ltd. in 1992 and he has been engaged in process development of communication cable. He is now an engineer of Communication Cable Division.



Jun-ichi Ohta

Sumitomo Electric
Industries, Ltd.
1, Taya-cho, Sakae-ku,
244, Yokohama, Japan

Jun-ichi Ohta received his M. S. degree from Tokyo Institute of Technologies in 1987.

He joined Sumitomo Electric Ind., Ltd. in 1987 and he has been engaged in research and development of optical fibers. He is now a senior engineer of Communication Cable Division.



Masakazu Watanabe

Sumitomo Electric
Industries, Ltd.
1, Taya-cho, Sakae-ku,
244, Yokohama, Japan

Masakazu Watanabe received his B.E. degree in communication engineering from Osaka University in 1985.

He joined Sumitomo Electric Ind., Ltd. in 1985 and he has been engaged in process development of communication cable. He is now a senior engineer of Communication Cable Division.

Shigeru Tanaka

Sumitomo Electric
Industries, Ltd.
1, Taya-cho, Sakae-ku,
244, Yokohama, Japan

Shigeru Tanaka received his M. E. degree in 1976 and Ph. D. degree in 1989 from Tokyo University.

He joined Sumitomo Electric Ind., Ltd. in 1976 and he has been engaged in design and characterization of optical fibers and fiber-optic cables. Dr. Tanaka is now a manager of Communications R&D Department in Yokohama Research Labs.



Akihito Makiyama

Sumitomo Electric
Industries, Ltd.
1, Taya-cho, Sakae-ku,
244, Yokohama, Japan

Akihito Makiyama received his B. E. degree from Kyushu Tech. University in 1994.

He joined Sumitomo Electric Ind., Ltd. in 1994 and he is now an engineer of Communication Cable Division

2 × 800 Optical Switch Using Fiber Butting Method

Makoto Okuda, Seiichi Naraoka, Shizuka Yamaguchi, Kazuo Kamiko

The Furukawa Electric Co., Ltd.
6, Yawata-kaigandori, Ichihara, Chiba 290, Japan

ABSTRACT

A compact high-density 2 × 800 optical switch has been developed by employing a new fiber arrangement method named fiber butting. This method realizes optical axial alignment by putting 800 optical fibers with interval of 127 μm on a plate with V grooves and placing two optical fibers on the opposite side in a way to face them. A prototype of 2 × 800 optical switch features outer dimension of 270 mm × 104 mm × 55 mm. The 2 × 800 optical switch features insertion loss of 0.27 dB on average for mobile optical fiber 1, insertion loss of 0.30 dB on average for mobile optical fiber 2, return loss of 46.8 dB on average, durability of 1.0 million times or more, and repeatability of 0.1 dB or less.

1. INTRODUCTION

Along with increasing use of optical fiber cable for access networks, optical fiber monitoring systems have been introduced. Figure 1 shows configuration of the monitoring system.^{[1][2][3][4][5][6][7]} The monitoring system has a instrument to select an optical fiber out of hundreds of them and to perform switch-over and monitor optical fiber cable. As optical fiber cable increases, the monitoring system is required to handle more fibers. In order to address this requirement, it is important to develop a compact optical switch with high density. We have developed a new optical switch which satisfies the performance requirements listed in Table1.

Table 1 The performance requirements

Item	Performance
Insertion loss	< 0.4 dB
Return loss	> 40 dB
Switching time (adjacent port)	< 1.5 sec
Switching time (maximum)	< 3 sec
Durability	> 1 million times
Repeatability	< 0.3 dB

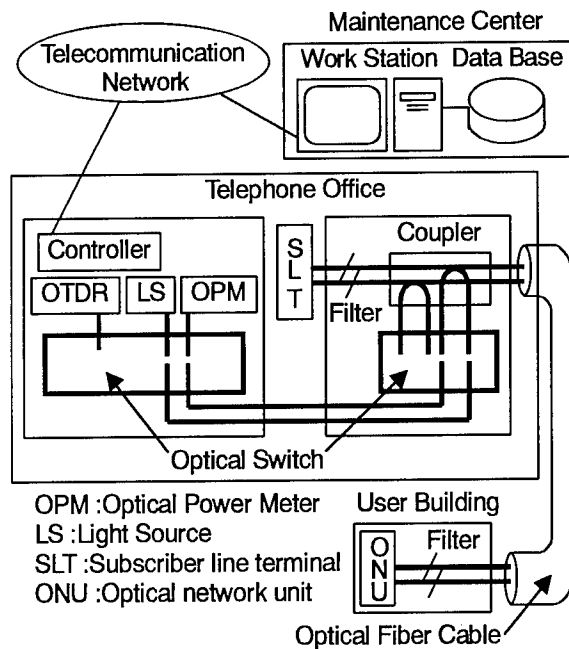


Figure 1 Monitoring System

2. STRUCTURE

2.1 Principle of switch

Figure 2 shows basic configuration of the newly-developed optical switch. In order to reduce size of the optical switch, the optical fiber butting method is employed to directly move mobile fibers of $125\mu\text{m}$ in diameter and perform switch-over by aligning optical axis on V grooves.^{[4][8]} Interval between fixed fibers is reduced from $250\mu\text{m}$ to $127\mu\text{m}$ to raise density. As shown in Figure 2, one eight-fiber ribbon is piled on top of another eight-fiber ribbon, and the pair is placed on the V-groove plate. Then each optical fiber is adjusted so as for an optical fiber of the upper ribbon to be placed between two optical fibers of the lower ribbon, i.e., optical fibers of the upper and lower ribbons are arranged alternately. Finally the pair of eight-fiber ribbons are fixed altogether on the plate.^{[6][7]}

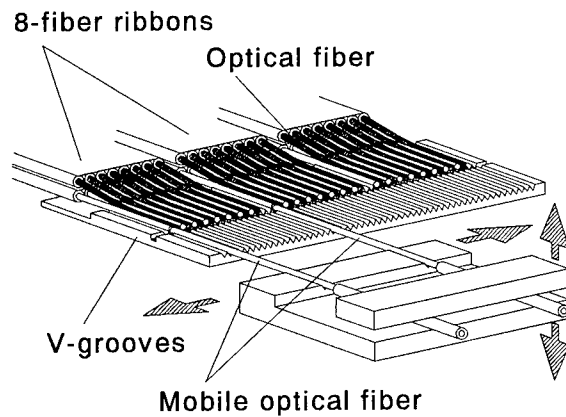


Figure 2 Basic configuration

2.2 Arrangement of optical fibers

Figure 3 shows how to arrange optical fibers to achieve the configuration illustrated in Figure 2.

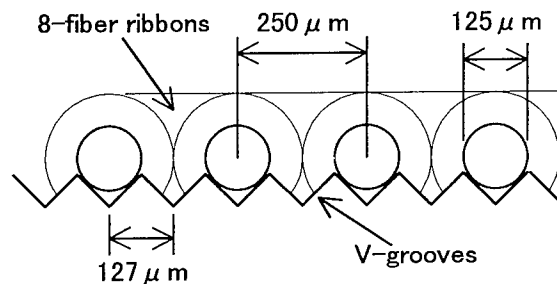


Figure 3 The lower 8-fiber ribbon

First the lower eight-fiber ribbon is placed on the V-groove plate. Location of each optical fiber is adjusted so that it can fit in every other V groove on the plate. Interval between optical fibers is $250\mu\text{m}$ as V grooves are arranged with interval of $127\mu\text{m}$. Figure 4 shows how to mount the upper eight-fiber ribbon.

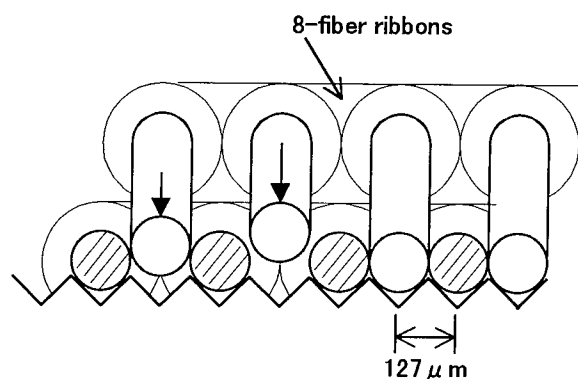


Figure 4 The upper 8-fiber ribbon

As the lower eight-fiber ribbon is already placed, it functions as a guide to help the upper ribbon be correctly piled on. Consequently fiber-positioning errors hardly occur such as fiber crossing, and every V groove is properly filled with optical fiber. This optical fiber arrangement method enables us to realize high-density optical switch arranging optical fibers with interval of $127\ \mu\text{m}$ while using two conventional eight-fiber ribbons with fiber interval of $250\ \mu\text{m}$. This method has made it possible to double the number of optical fibers mounted on the V-groove plate, i.e., from 400 fibers to 800 fibers.

2.3 Structure of the new optical switch

Figure 5 shows appearance of the new optical switch. Outer dimension of this optical switch is 270 mm in width, 104 mm in depth, and 55 mm in height. It is able to handle twice as many optical fibers as the conventional 2×400 optical switch while keeping its size unchanged.^[8] The new optical switch is composed of fiber moving unit and fiber holding unit as well as mobile optical fibers, V-groove plate, and 800 fixed fibers shown in Figure 2. The

fiber moving unit is to move mobile optical fibers while the fiber holding unit is to hold mobile optical fibers on the V-groove plate so as to press them into V grooves. These units and optical fibers are sealed in housing with matching oil. Out of the housing, 800 fibers and two optical fibers come out from the same side. Pulse motor is employed as a drive for fiber moving unit and fiber holding unit.

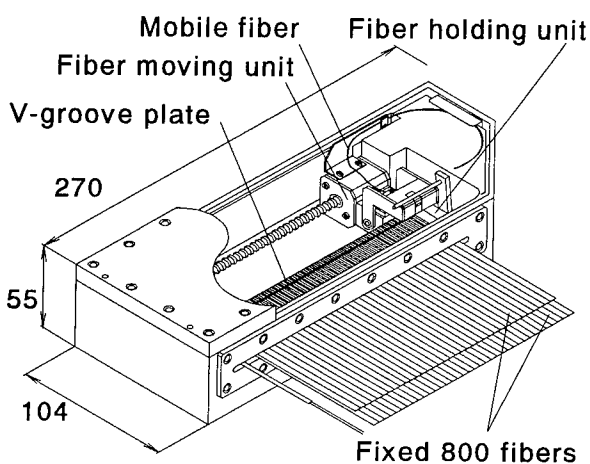


Figure 5 Switch structure

3. POSITIONING METHOD

A prototype of the new optical switch developed a problem, i.e., insertion loss occasionally exceeded 1 dB, depending on ambient temperature. The cause of this problem was found that the new optical switch employed the same fiber moving and driving units as the conventional one. In the new optical switch, interval of fixed optical fibers was reduced to almost half, accuracy of positioning mobile optical fibers must have been raised by two times. When positioning accuracy of fiber moving unit is doubled and resolution of driving unit is raised, however, the optical switch will get bigger in size and its price

will get higher. Instead of changing hardware design, therefore, we decided to modify software to control fiber moving unit in a way to cope with fluctuation of ambient temperature. This software modification has realized optimal driving operation for any ambient temperature, and insertion loss has been improved to the same level as that of the conventional optical switch.

4.Characteristics of the optical switch

4.1 Insertion loss

Figure 6 shows histogram of insertion loss. LED with wavelength of $1.31\ \mu\text{m}$ is used as a light source. Insertion loss here includes that of the optical switch and that of inlet connector. Mobile optical fiber 1 and mobile optical fiber 2 are mobile optical fibers. Insertion loss is 0.27 dB on average, 0.57 dB at maximum, and 0.18 dB at minimum for mobile optical fiber 1. Insertion loss is 0.30 dB on average, 0.61 dB at maximum, and 0.19 dB at minimum for mobile optical fiber 2.

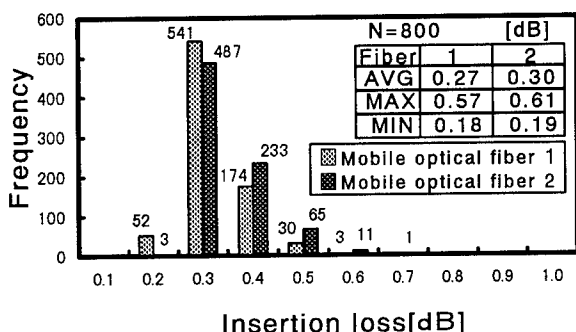


Figure 6 Insertion loss histogram

4.2 Return loss

Figure 7 shows histogram of return loss. Wavelength of light source is $1.31\ \mu\text{m}$. Return loss is 46.8 dB on average and 42.3 dB at minimum.

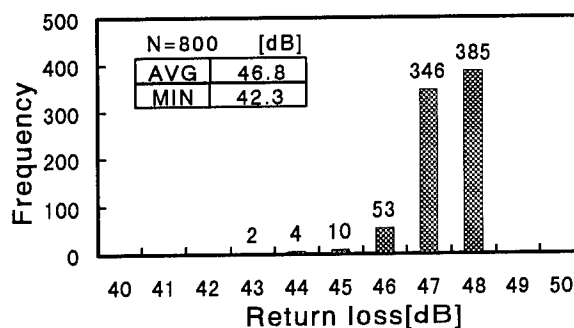


Figure 7 Return loss histogram

4.3 Temperature cycling test

Figure 8 shows fluctuation of insertion loss detected in temperature cycling test (0-50 deg C, 6 hour cycle). Fluctuation of insertion loss is found less than 0.1 dB.

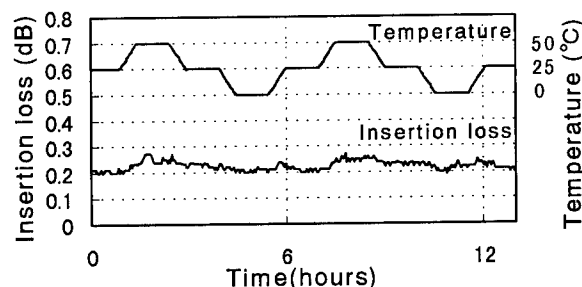


Figure 8 Temperature cycling test

4.4 Switching time

Maximum switching time and switching time between adjacent ports were evaluated. Maximum switching time is defined as time required to switch from an optical fiber at one end of 800-fiber block to another fiber at the other end. It is found to be 3 seconds. Switching time between adjacent ports is found to be 1.1 seconds.

4.5 Long-term durability

Long-term durability of the optical switch was evaluated by connecting mobile optical fibers to two of the 800 fixed fibers alternately. Insertion loss was measured once every 500-time turn. Figure 9 shows evaluation result. Fluctuation of insertion loss is 0.1 dB or less. Insertion loss is found stable throughout 1.0 million times, and long-term durability is demonstrated.

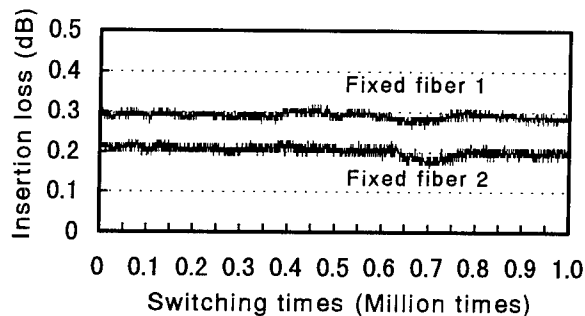


Figure 9 Repeatability of insertion loss

5. CONCLUSION

The 2×800 optical switch has been developed, featuring the same size as the conventional 2×400 optical switch with outer dimension of $270 \text{ mm} \times 104 \text{ mm} \times 55 \text{ mm}$.^[8] It is able to handle two times as many optical fibers as the conventional one. The new optical switch features insertion loss of 0.27 dB on average for mobile optical fiber 1, insertion loss of 0.30 dB on average for mobile optical fiber 2, return loss of 46.8 dB on average, durability of 1.0 million times or more, and repeatability of 0.1 dB or less.

REFERENCES

- (1) N. Tomita, et al., "Future prospects of automatic fiber testing system for fiber-optic subscriber loops", OECC'96 Tech. Dig., July 1996
- (2) N. Tomita, et al., "Optical fiber line support system", NTT Rev., vol.3 no.1 pp-97-104, 1991.
- (3) N. Tomita, et al., "Design and performance of a novel automatic fiber line testing system with OTDR for optical subscriber loops", IEEE J. Light wave Technol., vol. 12, no. 5, pp. 717-726, May, 1994.
- (4) I. Nakanishi, et al., "Optical fiber selector with a fiber moving head and multi-fiber array", in Nat. Conv. Rec. IEICE, Sep 1995, B-651
- (5) N. Tomita, et al., "Automatic and optimum sensing of Fresnel reflections in optical fiber system with connectors using OTDR", SPIE proc. vol.2594, pp. 31-40, Oct. 1995.
- (6) Y. Enomoto, et al., "High density technologies of FTM and IFTM for access network systems.", in Nat. Conv. Rec. IEICE, April 1997, SB-8-7
- (7) Y. Enomoto, et al., "High density fiber termination module (FTM) for AURORA", OECC'97, Technical Digest, pp536-537, July 1997
- (8) S. Naraoka, " 2×400 SMF optical switch using axial alignment with counterpart fibers in a V groove", IWCS'96, pp894-899, 1996



Makoto Okuda
The Furukawa Electric Co., Ltd.
6, Yawata-kaigandori Ichihara, Chiba,290,
Japan

Makoto Okuda was born in Osaka, Japan, in 1965. He received the B.E. degree in electronics engineering from Mie University in 1989. He joined The Furukawa Electric Co., Ltd., in 1989 and has been engaged in research and development of optical fiber switches.



Sizuka Yamaguchi
The Furukawa Electric Co., Ltd.
6, Yawata-kaigandori Ichihara, Chiba,290,
Japan

Sizuka Yamaguchi was born in Fukui, Japan, in 1954. He joined The Furukawa Electric Co., Ltd., in 1975 and has been engaged in research and development of mechanical apparatus for automated assembly system.



Seiichi Naraoka
The Furukawa Electric Co., Ltd.
6, Yawata-kaigandori Ichihara, Chiba,290,
Japan

Seiichi Naraoka was born in Tokyo, Japan, in 1961. He received the B.E. degree in mechanical engineering from Tohoku University in 1985. He joined The Furukawa Electric Co., Ltd., in 1985 and has been engaged in research and development of joining technology and optical switches.



Kazuo Kamiko
The Furukawa Electric Co., Ltd.
6, Yawata-kaigandori Ichihara, Chiba,290,
Japan

Kazuo Kamiko was born in Chiba, Japan, in 1960. He received the B.E. degree in mechanical engineering from Chiba University in 1984. He joined The Furukawa Electric Co., Ltd., in 1984 and has been engaged in research and development of optical connectors and optical switches.

Development of Mini-MPO Connector

Kazuhiro Takizawa, Toru Arikawa, Yasuhiro Tamaki and Hiroshi Yokosuka

Fujikura Ltd. Opto-Electronics Laboratory
Sakura-shi, Chiba, JAPAN

ABSTRACT

We have successfully developed the 2- and 4-fiber mini-MPO connector which has a higher packaging density than conventional 2-fiber MPO connector or 2-fiber connector which uses zirconia ferrule. The basic structure of the mini-MPO connector is similar to that of the conventional MPO connector. Miniaturization of the connector was achieved with the same miniaturization technology employed in the MT ferrule.

The connector, which is used for single-mode fiber, has a mean connection loss of 0.17 dB and a return loss of higher than 50 dB without index matching materials. The various performance tests and the reliability tests were conducted on this newly developed connector and its consistency was verified. The test results confirmed that the connector could be successfully employed in the field.

1. Introduction

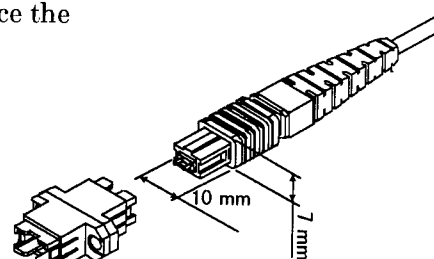
In order to realize effective fiber optic subscriber networks and optical computer networks, it is necessary to connect high density fibers and equipments easily¹⁾²⁾. The MPO (Multi-fiber Push-On / Pull-Off) connector, which is an application of the multi-fiber MT (Mechanically Transferable) connector, is effective for the fiber counts ranging from 2- to 12-fiber and is used widely³⁾⁴⁾⁵⁾.

However, more compact type of the MPO connector is urgently required for the cases where 2- to 4-fiber are connected like interfaces of the fiber channels or the equipments used in fiber optic networks. This paper describes the newly developed mini-MPO connector which is used for the fiber counts ranging from 2- to 4-fiber connection.

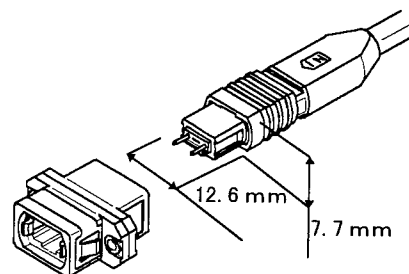
2. Design and Structure

2.1 Structure

Fig. 1 shows the structure of the mini-MPO connector and the conventional MPO connector. The principle structure of the mini-MPO connector is same as that of MPO connector. MT ferrule is used in the MPO connector. The connection principle lies in the structure obtained by polishing the MT ferrule end face diagonally or perpendicularly so as to make the fiber tips protrude out. The fibers can therefore be connected directly (Physical Contact : PC) resulting in a low return loss. The effects of Fresnel reflection can be eliminated when the end face is polished at an angle of 8 degree. Since the



(a) Mini-MPO connector



(b) MPO connector

Fig. 1 Structures of mini-MPO connector and MPO connector

fiber tips protrude from the ferrule end face, the fluctuation in return loss which may be caused by receding of the fibers can be minimized⁶⁾.

The connector can be connected in a dry state without the use of index matching material. This contributes to easy installation and subsequent reconnection. Fibers are positioned precisely and accurately by means of alignment holes and guide pins provided on the ferrules.

The housing is designed to apply pressure on the ferrule from behind by means of a coil spring. It however allows the ferrule a certain degree of movement during insertion and extraction. This structure enables the ferrule end faces to be connected securely with a low insertion loss. As the end faces are constantly kept under a certain pressure by the spring, the connector is stable against harsh environment. The plug and adapter are engaged by fitting a pair of elastic hooks into the corresponding grooves, and the plug housing has the guiding projection to prevent the reverse connection. These mechanisms enable the easy connection and disconnection of the connector. Newly developed mini-MPO connector is also designed by taking these suitable design of MPO-connector into consideration.

Table 1 shows the comparison of the dimensions and the fiber counts between the mini-MPO connector, conventional MPO connector and the SC connector. The cross section of the mini-MPO connector is approximately 70 % compared to the conventional MPO connector. The mini-MPO connector is also more suitable for higher fiber density connection than SC connector.

Fig. 2 shows the structure of the mini-MT ferrule, which is used in the mini-MPO connector, and the conventional MT ferrule. The end face of the mini-MT ferrule is shown in Fig. 3. The size, which is $4.4 \times 2.5 \text{ mm}^2$, is

the same as conventional 1-fiber MT ferrule and it is available for 2- to 4-fiber connection. The development of this new mini-MT ferrule was one of the most important technology to realize the miniaturization of the MPO connector.

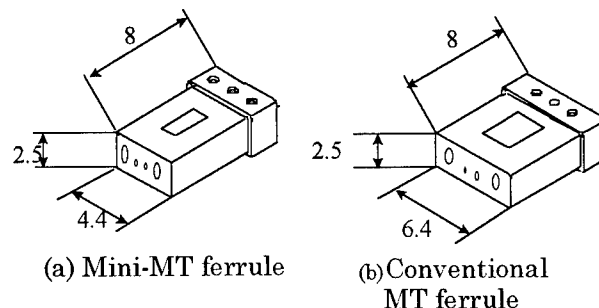


Fig. 2 Structure of the mini-MT ferrule and the conventional MT ferrule

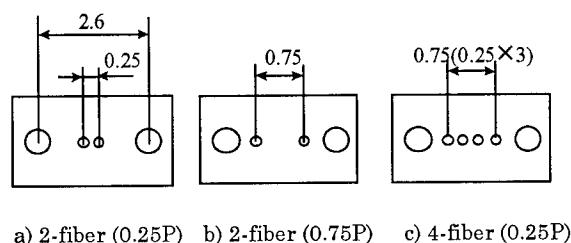


Fig. 3 The end face of the mini-MT ferrule

2.2 Low-loss Connection Design

We now examine the low loss connection technology which is one of the most important requirements for optical connector.

We examine the stabilization of PC finish by polishing technology advancement. As ferrule end faces are abutted against each other, they must have high degree of flatness and angular preciseness. In order to minimize fluctuation in insertion loss caused by attachment / detachment as well as

Table 1 Comparison of dimensions and fiber counts

	Mini-MPO connector	MPO connector	SC connector
Fiber counts	1~4	2~12	1
Cross section (mm)	W10×H7	W12.6×H7.7	W9×H8.3
Area	70mm ²	97mm ²	75mm ²

Table2 Typical data of mini-MPO end faces

Item	Result
Nominal oblique angle	8°
Angular precision accuracy	<0.1°
Roughness of mating face	<1 μm
Nominal fiber protrusion	0.5 μm

environmental factors, the fibers should be abutted too. It is known that the insertion loss increases due to Fresnel reflection as the adhesive applied between ferrules contracts at high temperatures leading fibers being pulled back to widen the interstice between the fiber end faces of a ferrule. To eliminate this, we refined a novel polishing technique to make the fibers project from the ferrule end face by 1 mm. A new high precision polishing machine was developed and is capable of achieving an end face flatness of $1\ \mu\text{m}$ with an angular preciseness of $\pm 0.1^\circ$. Typical performance of the end face evaluation is summarized in Table 2. Fig. 4 shows the insertion loss relation between the case with index matching material and the case without index matching material for the mini-MPO connector terminated by the condition in Table 2. Since both results, the case with and without the matching material, are almost the same, it is confirmed that the condition shown in Table 2 is enough to achieve the stable PC contact.

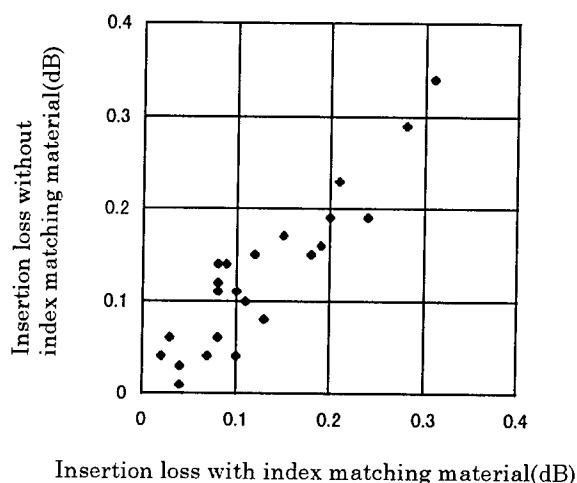


Fig.4 Insertion loss relation ship between the case with index matching material and the case without index matching materia

3.Performance

3.1 Optical Performance

3.1.1 Insertion Loss

Fig. 5 and Fig. 6 show the results of the insertion losses of 2-fiber mini-MPO connectors. Fig.5 shows the result of multi-

mode fiber (62.5/125 μm :Graded Index) and Fig. 6 shows the result of single-mode fiber. The measurement was conducted at a wavelength of $1.31\ \mu\text{m}$ without the use of refractive index matching materials. The average insertion loss of multi-mode fiber was 0.08 dB and of single-mode fiber was 0.17 dB. The results confirmed that the mini-MPO connector was excellent for low-loss connection.

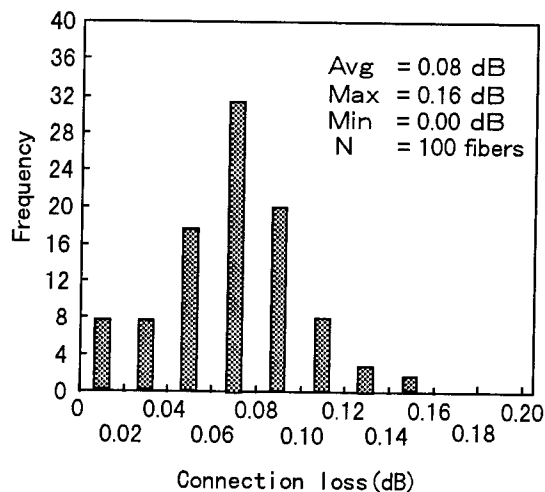


Fig.5 Connection loss of Mini-MPO connector(GI)

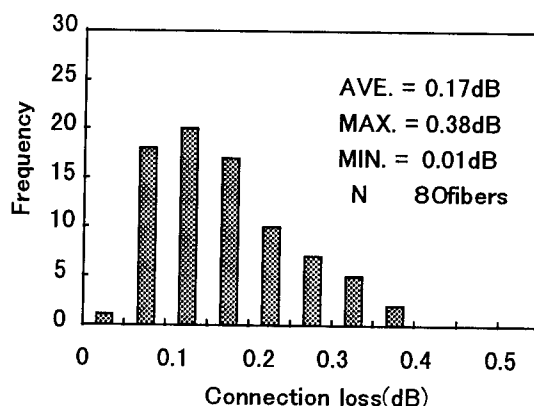


Fig.6 Connection loss of Mini-MPO connector(SM)

3.1.2 Return Loss

The return loss of the single-mode 2-fiber mini-MPO connector was measured when mated with a reference connector. The histogram of the test results is shown in Fig. 7. The return loss was higher than 50 dB for the mini-MPO connector.

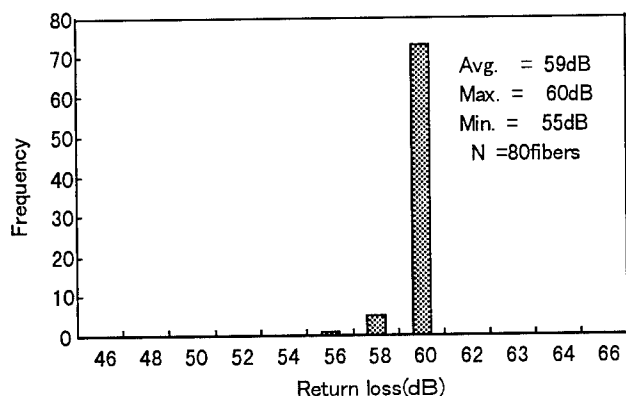


Fig.7 Return loss of Mini-MPO connector(SM)

3.2 Reliability

In order to ascertain the field worthiness of the connector, various reliability tests including those for mechanical performance and resistance to environmental factors were conducted for 2-fiber mini-MPO connector. All tests were conducted at an optical wavelength of 1.31 μm used with single-mode fibers. The results of these tests are shown in the section below.

3.2.1 Side-pull Test

The insertion loss fluctuation and return loss of the connector was measured under the condition that the 20N load was loaded at 90° for the 8 directions. Fig. 8 shows the directions of side loaded. The results of the measurement are shown in Table 3. The insertion loss fluctuations are within 0.3 dB and the return losses are higher than 50 dB.

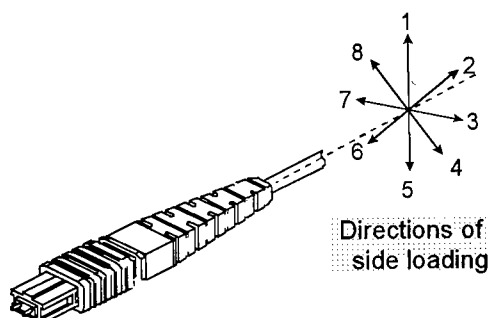


Fig.8 Directions of side loading

Table 3 Result of side-pull test

Direction	Insertion loss fluctuation(dB)	Return loss (dB)
1	0.06	56
2	0.13	59
3	0.01	59
4	0.06	58
5	0.12	60
6	0.08	58
7	0.04	56
8	0.01	58

3.2.2 Temperature Cycling

The insertion loss fluctuation of the connector was measured repeating a 6-hour cycle of -40°C to 70°C every ten times. The results of the measurement are shown in Fig. 9. The loss fluctuation during the test were within 0.1 dB.

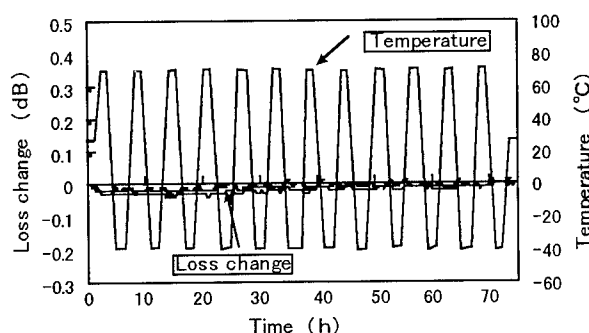


Fig.9 Result of temperature cycling

3.2.3 Condensation Test

As connectors are often exposed to harsh environments, good performance over a broad temperature and humidity range is important. The insertion loss fluctuation during the cycle of -10°C to 65°C with 93% RH at 65°C was measured. Fig. 10 shows the test result. The maximum loss change was less than 0.2 dB.

3.2.4 High Temperature Endurance

The insertion loss fluctuation was measured at high temperature in a constant. The test was conducted continuously for 240 hours at 70°C. The results are shown in Fig. 11. The loss fluctuation were less than 0.1dB.

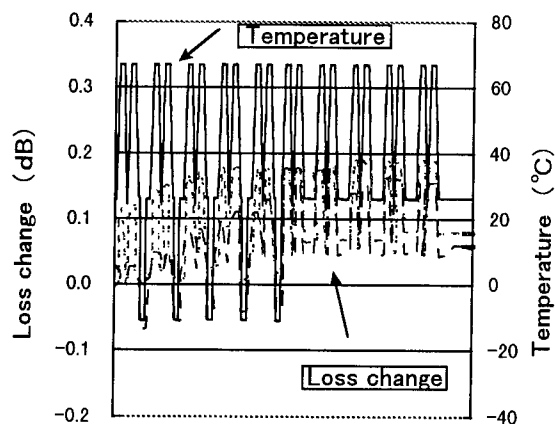


Fig. 10 Result of condensation test

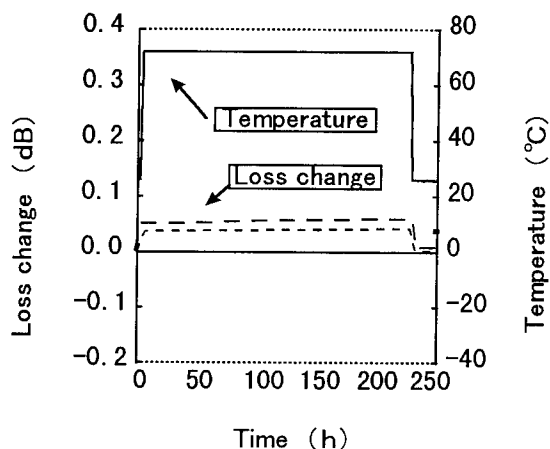


Fig. 11 Result of high temperature test

3.2.5 Low Temperature Endurance

The low temperature endurance was also examined. The test was conducted at -30°C . The results are shown in Fig. 12. The loss fluctuation were less than 0.1 dB.

3.2.6 Durability

Since a primary advantage of connectors is the flexibility to reconfigure fiber optic joints, connector durability over repeated matings is critical. Fig. 13 shows the results of the durability test. The insertion loss was measured every 10 matings with a total of 500 matings. The insertion loss changes after repeated matings were less than 0.3 dB. On the basis of these tests, we have verified that the mini-MPO connector has stable connection performance and low insertion loss.

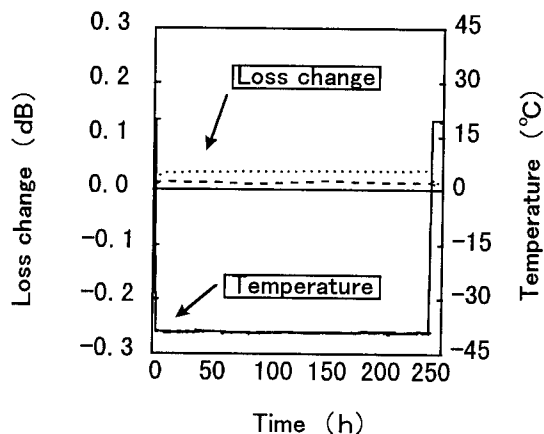


Fig. 12 Result of low temperature test

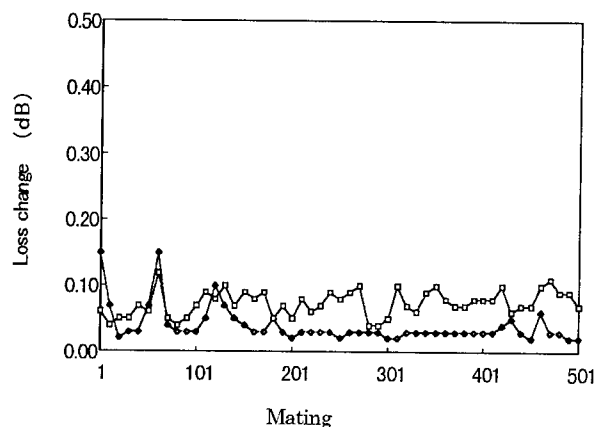


Fig. 13 Result of Durability test

3.2.7 Vibration Test

To evaluate the mechanical stability of the connector, a vibration test was conducted under the conditions listed below. The insertion loss of the connector which was connected via an adapter was measured continuously.

Frequency	:10-55 Hz
Amplitude	:1.5 mm
Direction	:Three axes
Duration	:2 hours per axis

Fig. 14 shows the test results. The insertion loss fluctuation were less than 0.02 dB.

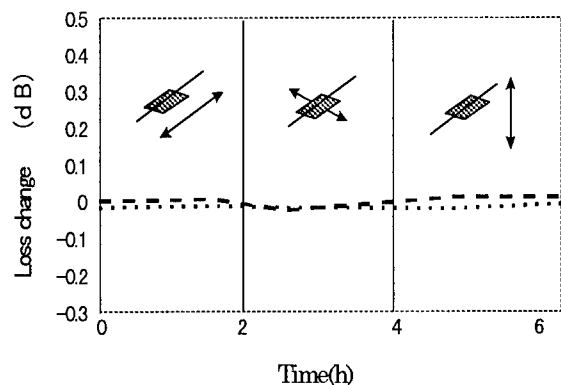


Fig.14 Result of vibration test

4. Conclusion

The mini-MPO connector, which has a higher packaging density than conventional connectors, has been developed. As the cross section is 70% of the conventional MPO connector, it is very high in connection density per fiber. It has an average connection loss of 0.17 dB and return loss of higher than 50 dB for single-mode fiber. The insertion loss changes due to side-pull test were less than 0.3dB. The insertion loss changes due to temperature and humidity concerned environmental tests were less than 0.2 dB. The insertion loss changes after repeated matings were less than 0.3 dB, and the loss changes due to mechanical vibration were less than 0.02 dB.

Overall, performance of the mini-MPO connector is excellent. Test results compare favorably with many other fiber connector technologies, indicating this connector is suitable for high density connections for fiber-optic communication applications.

References

- 1) H. Yokosuka et al. : "Multifiber Optical Components for Subscriber Networks", ECTC '96, pp487-493,1996
- 2) H. Yokosuka : "Recent Progress in Fiber Splicing and Connector Technology", IOOC-95 Technical Digest Vol.1, TuA2-2, 20-21, 1995.
- 3) S. Nagasawa et al. : "A High-Performance Single-mode Multifiber Connector Using Oblique and Direct Endface Contact

Between

Multiple Fibers Arranged in a Plastic Ferrule", J. Lightwave Technol., vol.13, no.6, pp.987-994,1995

- 4) S. Nagasawa et al. : "Single-Mode Multifiber Connectors for Future Large Scale Subscriber Networks", ECOC'93, MoP1.5, pp.29-32, 1993.
- 5) Y. Kikuchi et al. : "High Fiber Count Push-on Pull-off Connector", 43th IWCS Proceedings, pp.627-632, 1994.
- 6) T. Satake et al. : "Single Mode Multifiber Connector Performance", ECTC '96, pp494-499, 1996



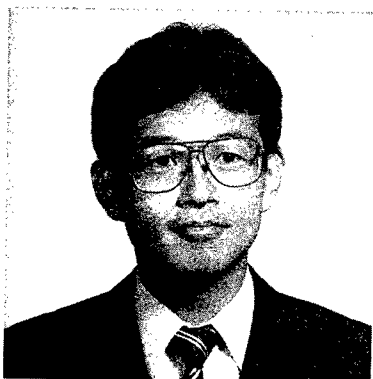
Kazuhiro Takizawa
Fujikura Ltd.
1440 Mutsuzaki Sakura, Chiba, 285, Japan

Kazuhiro Takizawa was born in 1968. He graduated from Yokohama National University with an M.E. degree in 1993. He joined Fujikura Ltd., and has been engaged in the research and development in the Fiber and Cable Accessory Department of the Opto-Electronics Laboratory. He is a member of the IEICE of Japan.



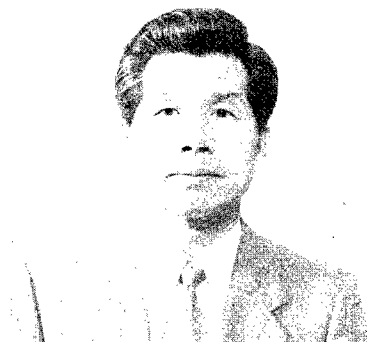
Yasuhiro Tamaki
Fujikura Ltd.
1440 Mutsuzaki Sakura, Chiba, 285, Japan

Yasuhiro Tamaki was born in 1955. He received a B.E. degree in mechanical engineering in 1977 from Saitama University. He joined Fujikura Ltd. in 1982. He is now a manager in Fiber and Cable Accessory Department of the Opto-Electronics Laboratory and a member of the IEICE of Japan.



Toru Arikawa
Fujikura Ltd.
1440 Mutsuzaki Sakura, Chiba, 285, Japan

Toru Arikawa is an assistant manager of Fiber and Cable Accessory Department in Opto-Electronics Laboratory. He received B.E. and M.E. degrees in image science engineering from Chiba University in 1982 and 1984, respectively. He joined Fujikura Ltd. after his graduation, and has been engaged in the research and development of optical fibers, components and accessories.



Hiroshi Yokosuka
Fujikura Ltd.
1440 Mutsuzaki Sakura, Chiba, 285, Japan

Hiroshi Yokosuka graduated in mechanical engineering from Tokyo Metropolitan Technical Junior College in 1967. He has been engaged in development of telecommunication cables and accessories. He is now a deputy general manager of Opto-Electronics Laboratory and a general manager of the Fiber and Cable Accessory Department of the laboratory. He is a member of IEICE of Japan.

FABRICATION OF HIGH-TEMPERATURE RESISTANT BRAGG GRATINGS IN OPTICAL FIBERS

Michael A. Fokine

Institute of Optical Research, Stockholm, Sweden

ABSTRACT

A method of manufacturing fiber Bragg gratings with stable high-temperature characteristics is presented and demonstrated. The fiber Bragg gratings are manufactured by a combination of hydrogen treatment and a high-temperature annealing process. Theory and initial tests indicate that these gratings result from a redistribution of fluorine in the core of the fiber.

INTRODUCTION

Fiber Bragg grating technology has progressed rapidly since the discovery of photosensitivity in germanium doped silica fibers by Hill et al¹. in 1978. Fiber Bragg gratings are utilized in a wide range of applications such as sensors, fiber lasers, and as components in optical communication systems with dispersion compensating gratings or wavelength selective filters as examples.

There are two main mechanisms suggested to be responsible for the change in refractive index in optical fibers when exposed to UV-radiation. The first is based on color-center changes induced by UV-radiation while the second is based on local structural changes in the glass matrix by UV-radiation².

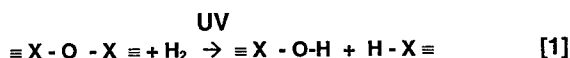
Long-term reliability of fiber Bragg gratings has been a concern in field applications due to the characteristic decay behavior of gratings at elevated temperatures. Although the stability of gratings has been improved significantly, a decay behavior can often still be observed.

THEORY OF FORMATION OF CHEMICAL GRATINGS

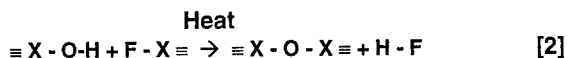
To increase the temperature stability of Bragg gratings, we have developed fibers for the

purpose of producing chemical gratings. The fibers were designed by doping the core of silica based fibers with germanium and fluorine using modified chemical vapor deposition (MCVD) technique.

Germanium is used to increase the refractive index of the core but also as a promoter for hydroxyl formation when exposed to UV-radiation^{3,4}. The chemical reaction can be described by equation 1, where X represents either Si or Ge, H and F represent hydrogen and fluorine respectively. Chemical bonds are represented as straight lines.



The fluorine is used due to its chemical interactions with hydroxyls producing hydrogen-fluoride^{5,6} as shown by equation 2.



The fibers are placed in an high-pressure hydrogen chamber at low temperature to allow in-diffusion of molecular hydrogen. After the fiber has been prepared in this way, a standard grating is written in the core of the fiber. Due to the presence of hydrogen during grating writing, the UV-radiation induces a photochemical reaction resulting in a periodic formation of hydroxyl-groups with the same period as the inscribed grating. Following this procedure, the grating is heated to temperatures in the range of 900-1000 °C. The hydroxyl groups in the core of the fiber are believed to chemically react with the fluorine, as shown in equation 2, producing hydrogen-fluoride which can diffuse within the glass network. Due to the periodic hydroxyl formation when exposed to holographic UV-

radiation the result will be a periodic depletion of fluorine in the core resulting in a periodic variation of the refractive index.

EXPERIMENT

Set-up and preparation

The two fibers used in the experiments were doped with estimated ~10 mol% and ~12 mol% germanium and ~2 % and ~3 mol% fluorine respectively. The fibers were hydrogen loaded at 10 MPa for a duration of approximately 2 weeks. The fibers were then exposed to UV-radiation of a wavelength of 242 nm by transverse holographic method⁷ to produce 10 mm long gratings with a reflectivity of near 100%.

The gratings were then placed, without applied tension, in the center of a tube furnace. The temperature of the furnace was measured at the location of the gratings. The grating reflectivity and transmission spectra were monitored by using a white-light source and a spectrum analyzer.

Developing the grating

The temperature of the furnace was increased from room-temperature to 900 °C at a rate of 25 °C/min and then held constant at 900 °C. As can be seen in figure 1, the initial grating decreases as the temperature is increased and is completely erased after a few minutes at 900 °C showing a typical grating degradation behavior. A few minutes later however, a new grating evolves and saturates.

Accelerated aging

To further examine the stability and behavior of the gratings, the temperature was increased to 1007 °C and 1106 °C while the change in grating reflectivity was monitored. The resulting normalized decrease in reflectivity for the two different fibers at 1007 °C and 1106 °C are shown in figure 2 and 3 respectively.

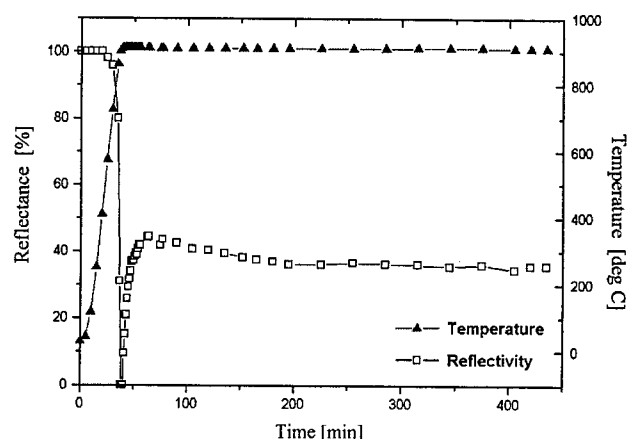


Figure 1: Reflection spectra of grating during heating process showing the degradation of initial grating reflectivity and the growth and saturation of new temperature stable grating.

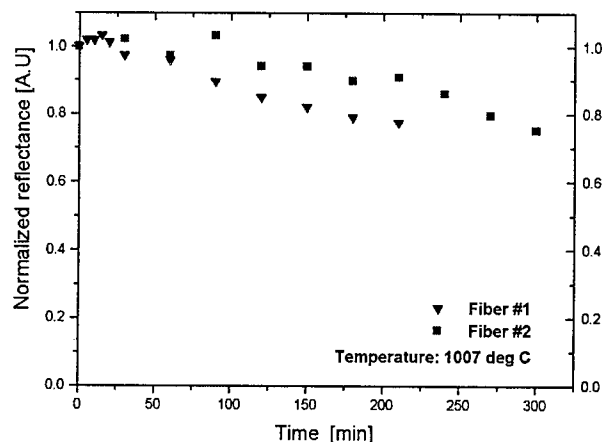


Figure 2: Normalized decrease in reflectivity of gratings at 1007 °C over a time period of 300 minutes.

To study the long-term stability of the gratings, the temperature was set to 810 °C and the reflectivity was measured over a time period of ~550 hours. The results from the experiment, shown in figure 4, do not show any significant degradation.

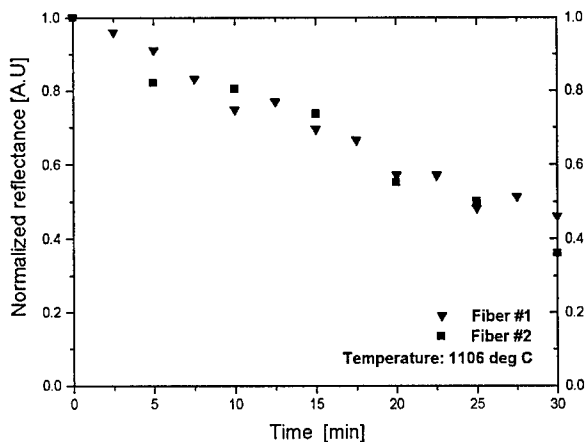


Figure 3: Normalized decrease in reflectivity of gratings at 1106 °C over a time period of 30 minutes.

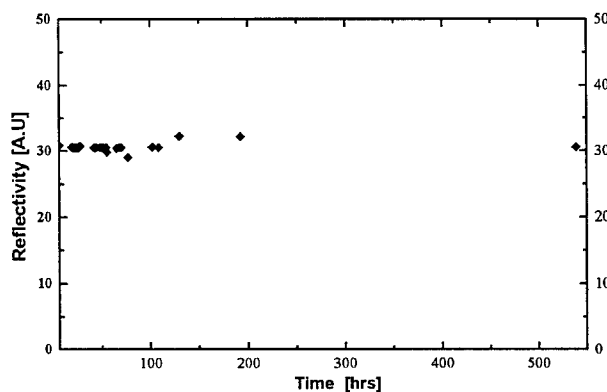


Figure 4: Reflectivity of developed grating at a temperature of 810 °C over a time period of approximately 550 hrs.

Discussion

To evaluate the degradation behavior of the gratings, the experimental results shown in figure 2 and figure 3 were compared to the diffusion behavior of a structure with a periodic dopant concentration variation with a period equal to that of the grating period. The attained diffusion coefficient and behavior at 1007 °C and 1106 °C agrees well with the value of the diffusion coefficient of fluorine derived by Kirchhof et al⁵. Using these values at 810 °C, the

degradation would then be expected to be less than 2% over a time period of 550 hours.

Although the mechanism for the index change in these types of gratings has not definitely been confirmed, the growth behavior and degradation behavior at 1007 °C and 1106 °C of these gratings clearly support the proposed theory.

During the growth of the developed grating there is an initial decay of the reflectivity (figure 1), before reaching a more stable level, which implies that there may be several mechanisms responsible for the change in refractive index.

Other types of fibers have also been tested including a standard germanium doped single-mode (SM) fiber and a boron-germanium doped fiber both manufactured using MCVD technique. In both cases, gratings have evolved in a similar manner as shown in figure 1, when subject to hydrogen loading prior to writing the gratings. The reflectivity however, of the gratings in these fibers have been very low compared to those in fluorine core-doped fibers. A possible explanation of grating formation in standard germanium and boron-germanium doped fibers is that there is fluorine deposited in the cladding layers of the fiber.

Experiments have also been performed where the hydrogen loading procedure has been omitted. Although the gratings have been subject to the same temperature treatment as previous experiments no grating growth was detected in any type of fiber after erasure of the initial grating. These results clearly indicate that hydroxyls are required for the grating formation process to take place.

Hydrogen was used in these experiments, but may be replaced with deuterium to reduce absorption effects in the 1.5 μm telecommunication window. The use of deuterium in the formation of chemical gratings has not been confirmed at this time.

APPLICATIONS

Due to the high-temperature resistivity of these new gratings they are well suited for a range of sensing applications which involve high-temperatures or applications with high-demands on life-time expectancy and reliability e.g. fiber components in rugged environments which are

temporarily or continuously subjected to high temperature. These gratings can also be used in production of fiber grating based components which require high temperature treatment/curing.

CONCLUSION

A method for fabricating high-temperature resistant fiber Bragg gratings has been demonstrated and a theory for the origin of the change in refractive index has been presented. The experiments performed so far do not definitely confirm the suggested theory to be responsible for the change in refractive index, if it is caused by modulation of the fluorine concentration or if other dopants or other mechanisms such as structural relaxation/densification are involved. However, the related observations found in literature and the behavior from the accelerated aging tests do support the proposed theory.

High-temperature resistant gratings have been fabricated in standard SM-fiber and boron-germanium co-doped fibers although resulting in a lower reflectivity compared to the fluorine doped fiber designed for these experiments. Gratings in these types of fibers need yet to be explained, as do the initial decay behavior of the developed grating.

ACKNOWLEDGEMENTS

The author wishes to thank M. Granberg at Ericsson Components and K. Kleveby, F. deBrito, at the Institute of Optical Research, FiberLab, for fabricating the fibers used in the experiments and B. E. Sahlgren, R. Stubbe and U. Persson at the Institute of Optical Research for advice and valuable discussions concerning fiber Bragg gratings.

REFERENCES

(1) K. O. Hill, Y. Fujii, D. C. Johnson, B. S. Kawasaki, "Photosensitivity in optical fibre

waveguides: applications to reflection filter fabrication", Appl. Phys. Lett. 32(1978) pp.642

(2) B. Poumellec, F. Kherbouche, "The Photorefractive Bragg Gratings in the Fibers for Telecommunications", J. Phys. III France, 6, (1996), pp.1595-1624,

(3) P. J. Lemaire, R. M. Atkins, V. Mizrahi, W. A. Reed, "High pressure H₂ loading as a technique for achieving ultrahigh UV photosensitivity and thermal sensitivity in GeO₂ doped optical fibers", Electron. Lett., 29, (1993), 1191.

(4) K. Awazu, H. Hosono, H. Kawazoe, "Chemical reactions of Ge-related species in SiO₂:GeO₂ optical fibers", in Proc. SPIE, 2044, (1993), 78.

(5) J. Kirchhof, S. Unger, K.-F. Klein, B. Knappe, "Diffusion behaviour of fluorine in silica glass", J. of Non Cryst. Solids, 181, (1995), pp. 266-273.

(6) J. Kirchhof, S. Unger, H.-J. Pißler, and B. Knappe, "Hydrogen induced hydroxyl profiles in doped silica layers", in OFC'95 Vol. 8, 1995 OSA Tech. Dig. Series, paper WP9.

(7) G. Meltz, W. W. Morey, and W. H. Glenn, "Formation of Bragg gratings in optical fibers by transverse holographic method", Opt. Lett., 14, (1989), pp. 823.

Michael A Fokine
Institute of Optical Research,
S-100 44 Stockholm
Sweden



Michael A Fokine graduated from the University of Linköping, Sweden in 1995 with a MS in physics. In 1995 he joined the Institute of Optical Research, Sweden, as a researcher in optical fibers and fiber Bragg gratings.

WIDEBAND REJECTION FIBER GRATING IN SC-TYPE CONNECTOR

Katsutoshi Kohmoto, Kenichiro Asano, Hideyuki Hosoya,
and Hiroshi Yokosuka

Fujikura Ltd., Sakura, Chiba, Japan

ABSTRACT

The chirped fiber grating that rejects two widebands (1.55 μ m band and 1.65 μ m band) has been developed, and is assembled in SC-type connector. Generally, the length of chirped fiber grating is longer when the rejection bandwidth is wider, and it is difficult to assemble the grating in connector. We propose a novel low cost assembly method through the use of a process similar to that of ordinary assembly of connector. With this method, the optical and mechanical characteristics and reliability were measured and excellent results were obtained.

1. INTRODUCTION

At the terminating end of the remote fiber test system(RFTS)¹⁾²⁾, a filter is assembled in the connector of the termination cable to filter off the test light. Usually, dielectric multilayer thin film is used as the filter. But in this case, it is difficult to fabricate the filter inserted connector at low cost, because of the need of special components and high precision slit machining for inserting the thin film. To explore new technology, as a substitute for the thin film, the use of fiber grating is examined³⁾. Ordinary, fiber grating rejects light at very narrow band wavelength. But since the test light used in RFTS is wideband in nature, the fiber grating has to reject the light for wideband wavelength at terminating end of RFTS. It is possible to widen the rejection bandwidth by using the chirped fiber grating.

Fiber grating has many advantages. For example, it has very low transmission loss at transmission band, and there is no necessity for slit machining because grating is directly fabricated in fiber. Improvement of optical characteristics is expected, together with low cost realization. On the other hand, fiber grating also has some disadvantages, as follows. Firstly, the length of fiber grating has to be long to reject wideband. Secondly, the strength of fiber at the section of the grating could be deteriorated. Therefore it is difficult to assemble fiber grating in connector. We propose a novel assembling method that could overcome the above problems, together with low cost realization.

2. FABRICATION

2.1 Fiber Grating

Fiber grating was fabricated⁴⁾ in a single mode fiber using two chirped phase mask. A KrF excimer laser($\lambda=248$ nm) was used as UV light source. UV coating of the fiber was stripped before exposure to the UV light. There are two chirped gratings separately for rejecting the two wavebands at 1.55 μ m band (1550nm \pm 20nm) and 1.65 μ m band(1650nm \pm 5nm), as shown in Fig.1. The length of the grating is 25mm for 1.55 μ m band and 10mm for 1.65 μ m band. These are the designed length for rejecting each waveband sufficiently even if a wavelength shift is occurred as described later. We assume the 1.31 μ m band(1310nm \pm 20nm) as transmission band.

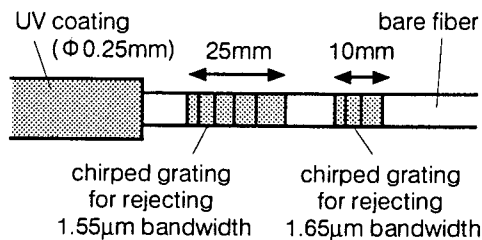


Fig.1. Fiber grating

The fiber grating can be damaged easily because the UV coating is stripped. Therefore a proof test (9.8N, 1s) was performed on it after UV radiation, and only the sample that pass the test was to be assembled in the connector to meet the strength requirement. The failure strength of each samples was measured. The result was shown in Fig.2. The Weibull modulus, m , of 3 was obtained. The result is similar for the samples in which UV coating is stripped and without the grating fabricated. Therefore we can see that there is no deterioration in the strength of the fiber at the grating section when the grating is fabricated.

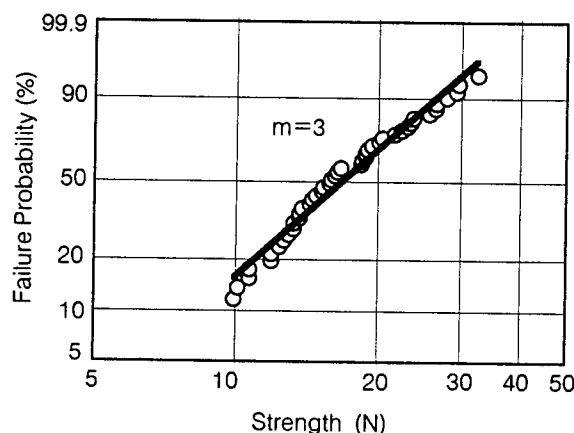


Fig.2. Weibull distribution of fiber grating

2.2 Assembly

The fiber grating is assembled in SC-type connector. The photograph of the connector with the grating assembled section is shown in Fig.3. The structure of the SC-type connector is straight forward and it is shown in Fig.4. The

grating is inserted into the flexible tube, and the tube is filled with resin to reinforce the strength of the fiber grating. Subsequently the housing of SC-type connector is fitted, and a portion of fiber with a diameter of 0.25mm is inserted into a reinforcement cord (PVC sheath with a diameter of 2mm and aramid yarn). The end face of the connector is polished with Physical Contact (PC) finishing. By this method, fibergrating of up to 40mm in length can be assembled. Low cost is also realized, because no expensive components are used and almost the same procedure as assembling a ordinary filterless connector is employed.

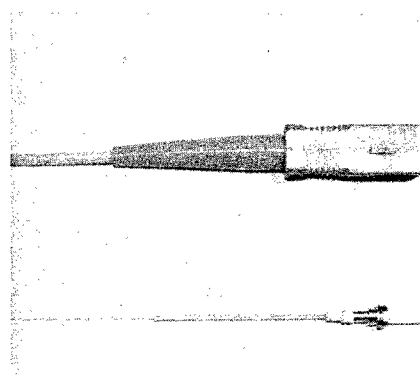


Fig.3. Photograph of SC-type connector with fiber grating

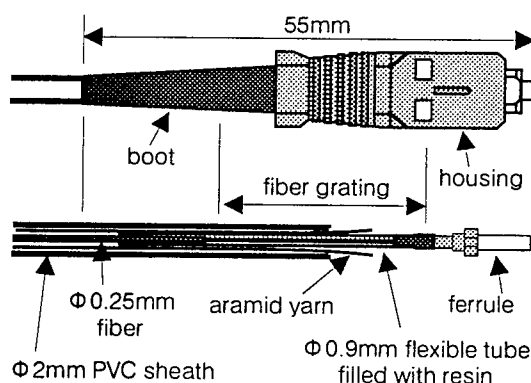


Fig.4. Schematic diagram of SC-type connector with fiber grating

Wavelength shift in rejection band spectrum occurs during assembly procedure. The shift is about 1.6nm toward the shorter wavelength direction. This shift is most probably due to the stress exerted on the grating, which occurs when the resin hardens. To compensate for this shift in waveband, the fiber grating is fabricated with rejection waveband shifted towards the longer wavelength direction from the desired waveband, so that the desired rejection waveband can be obtained eventually.

Using the above method, we fabricated the pigtail with SC-type connector and with fiber grating assembled.

3. EVALUATION

The optical, temperature, and mechanical characteristics of the pigtail were measured.

3.1 Transmission Spectrum

The transmission spectrum of the pigtail was measured by cut-back method. The result is shown in Fig.5. The transmission loss, including a connection loss, is less than 0.7dB at transmission band, greater than 25dB at rejection band.

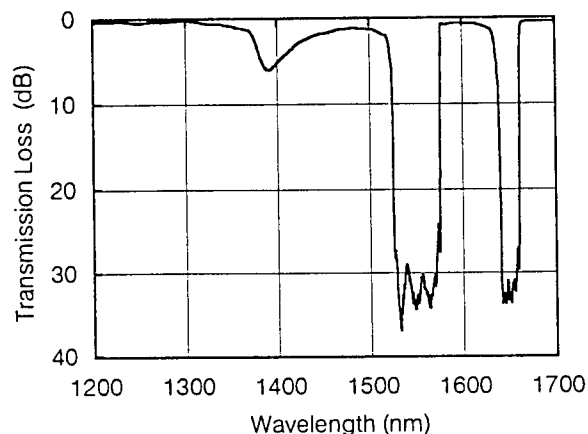


Fig. 5. Transmission spectrum

20 pigtails were fabricated in the same way and the transmission spectrums were measured. The histograms of the transmission loss at transmission band and rejection bands of the 20 pigtails are shown in Fig.6. The value of the transmission loss is the worst case at each bands. The transmission loss is less than 0.7dB at transmission band, between 23dB and 30dB at rejection bands, and the standard deviation, σ , is 0.17dB at transmission band, 2dB at rejection bands.

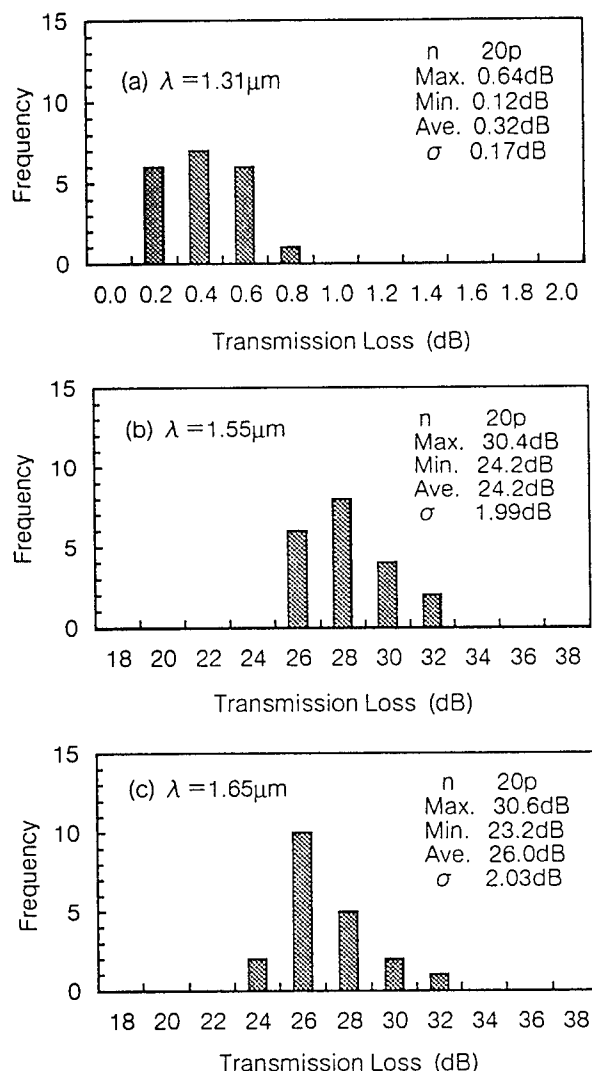


Fig.6. Histogram of transmission loss

3.2 Return Loss Spectrum

The return loss spectrum of the pigtail was measured. The result is shown in Fig.7. The return loss is greater than 30dB at transmission band, and less than 0.5dB at rejection band. There are noises, as shown in Fig.7, in the region of less than 1250nm, and between 1350nm and 1450nm, because of the insufficient power of the light source used.

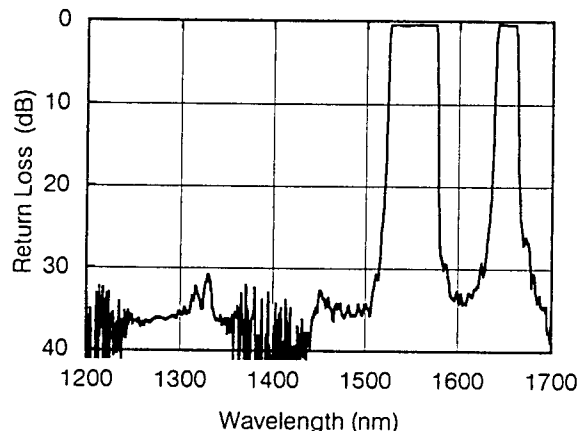


Fig. 7. Return loss spectrum

The wavelength shift in rejection band spectrum occurs when temperature is changed. The shift was measured, and the result is shown in Fig.9. In the temperature range of -20°C to 70°C , the shift is about 5nm and the dependent coefficient is $0.05\text{nm}/^{\circ}\text{C}$. Therefore the rejection bandwidth should be designed to have a wide margin to compensate for this wavelength shift when fiber grating is fabricated.

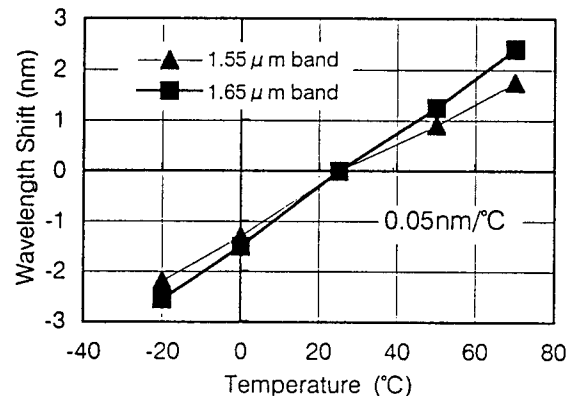


Fig.9. Wavelength Shift vs. Temperature

3.3 Temperature Cycling Test

Temperature cycling test ($-20^{\circ}\text{C} \sim 70^{\circ}\text{C}$, 2 cycles) was performed for the pigtail, and the fluctuation of the transmission loss at transmission band was measured. The result is shown in Fig.8. The fluctuation is small and is less than 0.05dB.

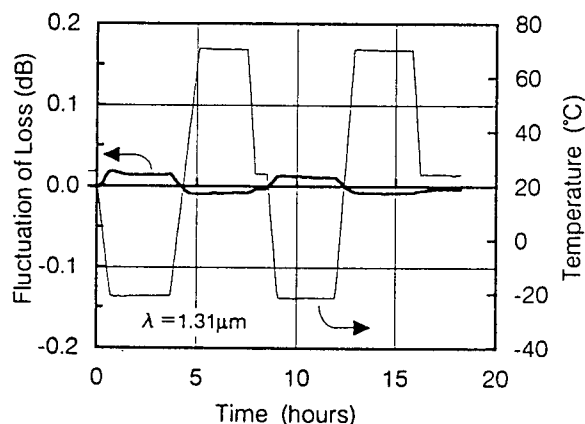


Fig. 8. Temperature cycling characteristics

3.4 High Temperature and High Humidity Test

High temperature and high humidity test (70°C , 90%RH, 240 hours) was performed for the pigtail, and the fluctuation of the transmission loss at transmission band was measured. The result is shown in Fig.10. The fluctuation is small and is less than 0.05dB.

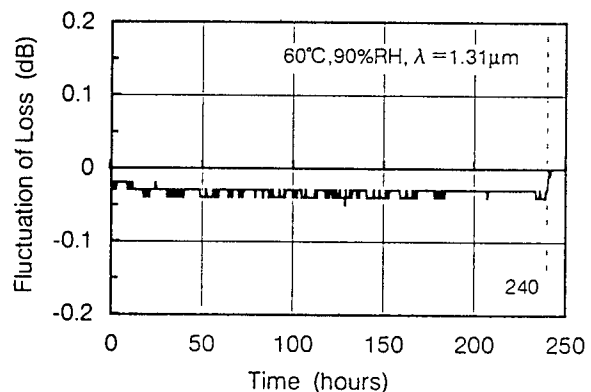


Fig.10. High temperature and high humidity characteristics

3.5 Tensile Test

Tensile test was performed for 5 pigtails, and the fluctuation of the transmission loss at transmission band and the wavelength shift at rejection bands were measured. The portion of the reinforcement cord was tensioned by 68.6N. The result is shown in Table 1. The fluctuation of the loss is small (less than 0.01dB) and the wavelength shift is also small (less than 0.01nm).

Table 1. Result of Tensile Test

		Max.	Min.	Ave.
fluctuation of transmission loss (dB)	1.31 μ m	0.01	0.00	0.001
wavelength shift (nm)	1.55 μ m	0.01	0.00	0.004
	1.65 μ m	0.01	0.00	0.003

The reinforced cord portion of pigtail was tensioned by 68.6N. Number of sample was 5.

3.6 Bending Test

Bending test was performed for 5 pigtails, and the fluctuation of the transmission loss at transmission band and the wavelength shift at rejection bands were measured. The boot section of SC-type connector of the pigtail was bent at right angles. The result is shown in Table 2(a). No significant fluctuation was shown.

As a reference, the same measurement was performed for the grating section, without the housing fitted. The grating section was bent with a radius of 30mm. The result is shown in Table 2(b). The fluctuation of the loss is small (less than 0.02dB) and the wavelength shift is also small (less than 0.3nm).

Table 2. Result of Bending Test

(a) The boot section was bent at right angles.
Number of the sample was 5.

fluctuation of transmission loss (dB)	1.31 μ m	N.A.
wavelength shift (nm)	1.55 μ m	N.A.
	1.65 μ m	N.A.

(b) The grating section without the housing fitted was bent with a radius of 30mm.

Number of the sample was 5.

		Max.	Min.	Ave.
fluctuation of transmission loss (dB)	1.31 μ m	0.02	0.00	0.003
wavelength shift (nm)	1.55 μ m	0.30	0.01	0.10
	1.65 μ m	0.28	0.00	0.09

4. CONCLUSION

The novel method for assembling the wideband rejection fiber grating in SC-type connector was proposed. The optical, temperature, and mechanical characteristics of the pigtail were examined. Excellent results were obtained. This method is most applicable for FC-type, D-type connector.

REFERENCES

- 1) T. Ebihara, N. Nakao, and M. Kuroiwa, ECOC'96, pp.3.39-42(1996).
- 2) N.Tomita, H.Takasugi, N.Atobe, I.Nakamura, F.Takaesu, and S.Takashima, J.Lightwave Technol., Vol.12, pp.717-726(1994).
- 3) K.Hogari, Y.Miyajima, S.Furukawa, N.Tomita, K.Tomiyama, and M.Ohashi, Electron.Lett., Vol.32, pp.1230-1231(1996).
- 4) M.Nakai, K.Kohmoto, T.Kumeno, S.Suzaki, and A.Wada, Proc. 1997 IEICE GENERAL CONFERENCE, C-3-151. (Japanese)

AUTHORS



Katsutoshi Kohmoto

Opto-Electronics Laboratory Fujikura Ltd.

1440, Mutsuzaki, Sakura, Chiba, 285, Japan

Katsutoshi Kohmoto was born in 1968. He received the M.E. degree in electrical and electronics engineering from Okayama University in 1993. He joined the Fujikura Ltd. in 1993 and has been engaged in the research and development of telecommunication cables and accessories since 1996. He is a member of the institute of Electronics, Information and Communication Engineers of Japan.

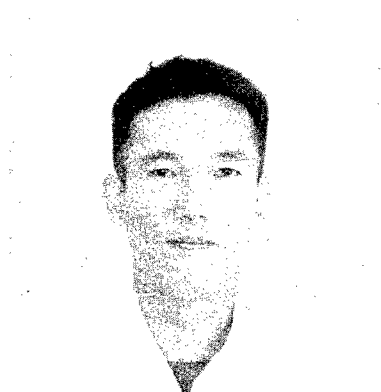


Hideyuki Hosoya

Opto-Electronics Laboratory Fujikura Ltd.

1440, Mutsuzaki, Sakura, Chiba, 285, Japan

Hideyuki Hosoya was born in 1959. He received the M.Sc. degree in Physics from Yamagata University in 1983. He joined the Fujikura Ltd. in 1983 and has been engaged in the research and development of telecommunication cables and accessories. He is presently a manager in the Fiber and Cable Accessory Department of the Opto-Electronics Laboratory and a member of the institute of Electronics, Information and Communication Engineers of Japan.



Kenichiro Asano

Opto-Electronics Laboratory Fujikura Ltd.

1440, Mutsuzaki, Sakura, Chiba, 285, Japan

Kenichiro Asano was born in 1966. He graduated in opto-electronics engineering from Tokyo Kokugakuin College of Technology. He joined Fujikura Ltd. in 1989 and has been engaged in the research and development of telecommunication cables and accessories. He is a member of the institute of Electronics, Information and Communication Engineers of Japan.



Hiroshi Yokosuka

Opto-Electronics Laboratory Fujikura Ltd.

1440, Mutsuzaki, Sakura, Chiba, 285, Japan

Hiroshi Yokosuka graduated in mechanical engineering from Tokyo Metropolitan Technical Junior College in 1967. He has been engaged in the research and development of telecommunication cables and accessories. He is presently a deputy general manager of Opto-Electronics laboratory and a general manager of the Fiber and Cable Accessory Department of the laboratory. Mr. Yokosuka is a member of the institute of Electronics, Information and Communication Engineers of Japan and the Japan Society of Mechanical Engineers, respectively.

Pigtail-type Optical Attenuator using Metal-doped Optical Fiber

Masashi Saijo, Yuichi Morishita, Yumi Ariga, Kazunari Sugi and Ken-ichi Muta

SHOWA ELECTRIC WIRE & CABLE CO.,LTD

4-1-1, Minamihashimoto, Sagamihara, Kanagawa, 229-11, JAPAN

ABSTRACT

Metal-ion doped optical fiber for optical absorption is developed by doping light-absorbing metal in optical fiber core. Pigtail type optical attenuators which allow to achieve desired attenuation levels by adjusting the length of the absorption fiber are prepared and evaluated. Such optical attenuators are characteristic in the following points:

(1) The absorption level is finely adjustable in steps of 0.1dB, and optical attenuators of desired attenuation levels are easily fabricated. (2) The optical attenuator easily endures 100-hour exposure of 100-mW high-power light. (3) The polarization dependent loss is below 0.1dB. (4) The attenuators are highly reliable. (5) The optical attenuator is easily connectable with other fibers by fusing or by using optical connectors. (6) The tensile breaking strength is 58.5 N on the average, indicating the optical attenuator is as strong as ordinary single-mode fibers.

I. INTRODUCTION

Optical signals transmitted at a same level in an optical communication network of optical fiber are different in the power level at receiving ends depending, for example, on the line length. Large differences in power levels of optical signals at receiving ends are unfavorable in building an optical transmission network due to restrictions on the receiving level and the dynamic range. Optical attenuators therefore are used generally in optical communication networks to adjust the receiving

power level.

In addition, it has become possible recently to transmit high-power light in optical fibers by the use of erbium-doped fiber amplifiers (EDFA) and high-power laser diodes. Optical attenuators therefore must be of high reliability and endure high-power light.

Metal-ion doped optical fibers where transition metals are doped in optical fiber core have been developed, and they have been fabricated into connectable fixed optical attenuators to meet such requirements [1-6], shown in Photo.1.

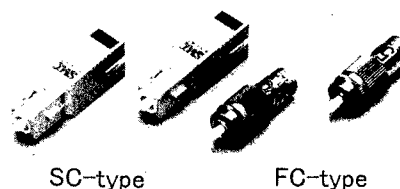


Photo.1 Fixed optical attenuator using metal-ion doped absorption fiber.

Such fixed optical attenuators of metal-ion doped optical fiber had the following merits:

- (1) The fixed optical attenuators adequately endure 100-mW (+20 dBm) high-power light exposure of 100 hours because the light is gradually absorbed and attenuated along the metal-ion doped optical fiber.
- (2) The level of attenuation is similar for both wavelength bands of 1.3 μ m and 1.55 μ m.
- (3) The polarization dependent loss is as small as below 0.1 dB.

- (4) The environmental characteristics are favorable.
- (5) The construction has been simplified improving the reliability.

The connectable fixed optical attenuators, however, had the following shortcomings:

- The attenuation level is not finely adjustable (e.g., in steps of 0.1dB).
- Connector plugs are large and often inconvenient in equipment.

Two types of absorption fibers, 1.6 dB/m (at $\lambda=1.55 \mu\text{m}$) [7] and 14 dB/m (at $\lambda=1.31 \mu\text{m}$) in unit absorption, are developed this time utilizing past experiences in developing fixed optical attenuators of metal-ion doped optical fibers. Pigtail type optical attenuators, which allow to achieve desired attenuation levels by adjusting absorption fiber lengths, are then developed and evaluated.

II. DESIGN

• Design of metal-ion-doped Optical Fiber

Metal-ion doped optical fibers having light-absorbing transition metal ions in the optical fiber core are used as optical attenuators.

Dopant metals can be nickel (Ni), cobalt (Co), chromium (Cr) or others which show absorptions at communication wavelength bands of $1.31 \mu\text{m}$ and $1.55 \mu\text{m}$, but cobalt is used this time for the relative ease of making fibers and stability in silica glass.

The fiber parameters and structure of pigtail type optical attenuators using the absorption fibers are the same as those of single-mode fibers for the assumed connection to such fibers as shown in Table 1 and Fig.1, respectively.

Two types of absorption fibers, Type 1 and Type 2 in Table 1, are prepared in this study. Characteristics of the Type 1 absorption fiber include that the operating wavelength is $1.55 \mu\text{m}$, that the attenuation is on the order of 1 to 2 dB/m, and that the coating is UV-resin coating. Connection to other fibers is made by fusing. Characteristics of the Type 2 absorption fiber, on the other hand, are that the operating wavelength is $1.31 \mu\text{m}$, that the attenuation is on the order of 10 to 20 dB/m, and that it is nylon jacketed. Connection to other fibers is made using connectors.

Type 1

Type 2

Photo.2 Pig-tail type attenuator

Table 1. Design of Absorption Fiber Parameter

Item	Type1.	Type2.
Attenuation	1 to 2 dB/m	10 to 20 dB/m
Operating wavelength	$1.55 \mu\text{m}$	$1.31 \mu\text{m}$
Cut-off wavelength	$<1.45 \mu\text{m}$	$<1.25 \mu\text{m}$
Mode field diameter	$9.5 \pm 1.0 \mu\text{m}$	$9.5 \pm 1.0 \mu\text{m}$
Cladding diameter	$125 \pm 2.0 \mu\text{m}$	$125 \pm 2.0 \mu\text{m}$
Coating	UV-resin coat	Nylon Jacket
Coating Diameter	$250 \mu\text{m}$	$900 \mu\text{m}$
Method of connection	Fusing	Optical connector (or fusing)

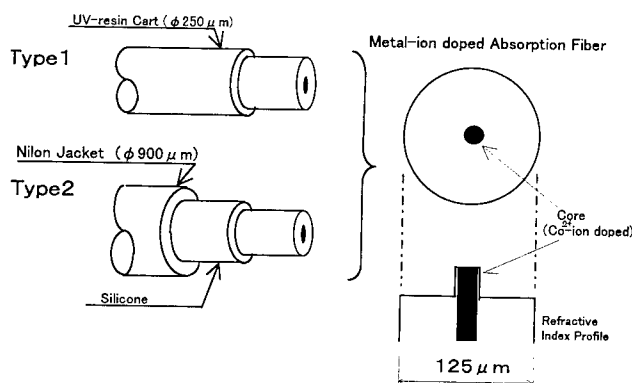


Fig.1 Fiber structure

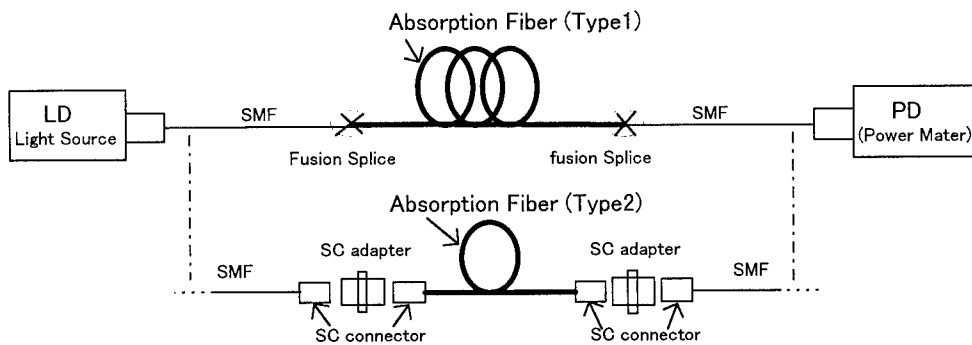


Fig.2 Measurement of Pig-tail type attenuator.

Type 1 and Type 2 absorption fibers are fabricated into pigtail type optical attenuators as follows for subsequent measurements (B through F below):

- Single-mode fibers are connected by fusing to both ends of the Type 1 absorption fiber.
- SC optical connectors are attached to both ends of the Type 2 absorption fiber.

III. CHARACTERISTICS

A. Measurement of Parameters of Metal-ion Doped Optical Fibers

Two types of absorption fibers for pigtail type optical attenuators were prepared and their parameters were measured. Results are shown in Table 2. As seen in the table, parameters measured on prepared absorption fibers agree well with their design parameters given in Table 1.

Table 2. Measured Absorption Fiber Parameters

Item	Type1.	Type2.
Attenuation	1.58dB/m	13.8dB/m
Operating wavelength	1.55 μ m	1.31 μ m
Cut-off wavelength	<1.4 μ m	<1.1 μ m
Mode field diameter	9.6 μ m	8.6 μ m
Cladding diameter	124.3 μ m	124.5 μ m

B. Wavelength Dependence

Wavelength dependence of attenuation was measured on the prepared two types of absorption

fibers at wavelengths around the respective operating wavelengths. Results are shown in Figs. 3 and 4.

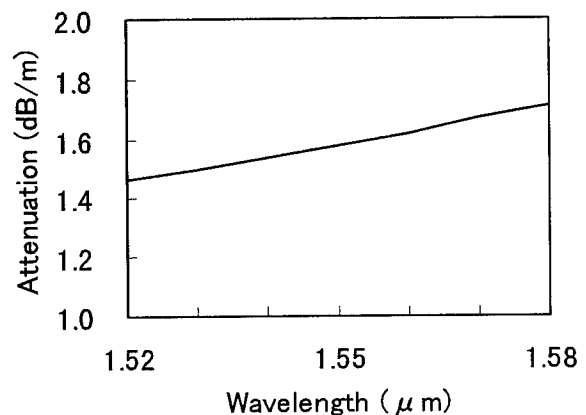


Fig.3 Wavelength dependence (Type 1)

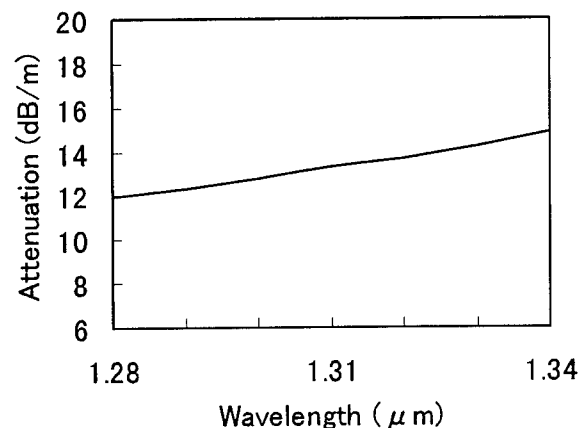


Fig.4 Wavelength dependence (Type 2)

The attenuation of light in absorption fibers is increasing gradually as the wavelength increases. It is judged that this wavelength dependence of attenuation is reflecting the optical absorption characteristics of the cobalt dopant.

C. Attenuation with Fiber Length

The fiber length dependence of attenuation was measured by changing the length of absorption fiber of each pigtail type optical attenuator.

As for the Type 1 absorption fiber, the attenuation was measured by connecting a single-mode fiber for measurement to each end of an absorption fiber. The absorption fiber lengths were 0 to 3 m. Results are shown in Fig. 5. As seen in the figure, the attenuation increases in proportion to the fiber length indicating that cobalt has been doped in the core uniformly in the longitudinal direction. In addition, the figure also indicates that the attenuation can be changed finely in the range of 0 to 5 dB (or more) by adjusting the fiber length. (It is possible, for example, to finely adjust the attenuation in steps of 0.08dB by changing the absorption fiber length in steps of 5 cm.)

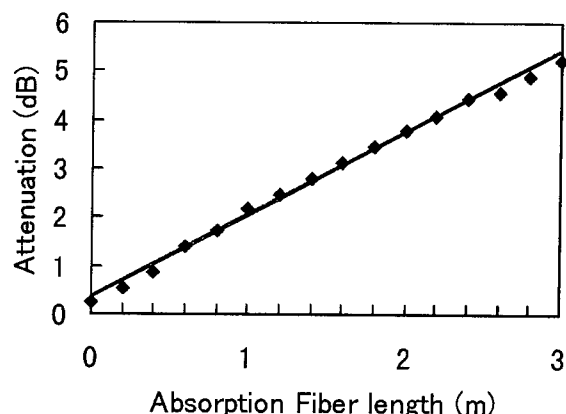


Fig.5 Attenuation with absorption fiber length
(Type 1: $\lambda=1.55 \mu\text{m}$)

As for the Type 2 absorption fiber, pigtail type optical attenuators were fabricated attaching an SC optical connector to each end of the absorption fiber. The fiber lengths were in the range of 10 to 100 cm.

The optical attenuation in such pigtail type optical attenuator was measured by attaching it to master connectors. Results are shown in Fig.6. As seen in the figure, the attenuation also increases in proportion to the fiber length, and it is possible to obtain an attenuator of desired attenuation by adjusting the fiber length.

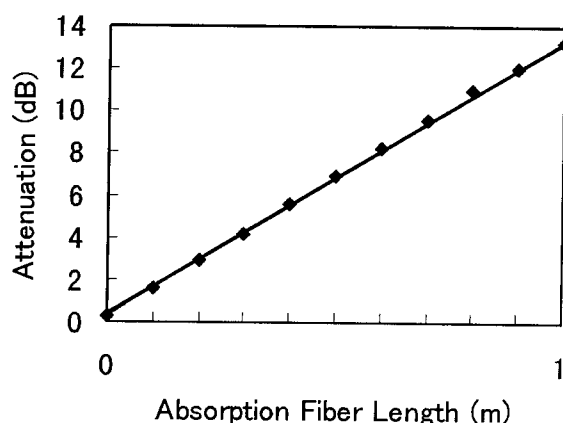


Fig.6 Attenuation with absorption fiber length
(Type 2: $\lambda=1.31 \mu\text{m}$)

D. Fiber Length Dependence of Polarization Dependent Loss

The fiber length dependence of polarization dependent loss (PDL) was measured by changing the absorption fiber length of pigtail type attenuators. It should be noted that the initial value of the measuring instrument was 0.003 dB. Results are shown in Figs. 7 and 8. The figures indicate that the PDL is below 0.04 dB and favorable. It is estimated that such favorable result comes from isotropic distribution of cobalt dopant in the radial direction [3-5].

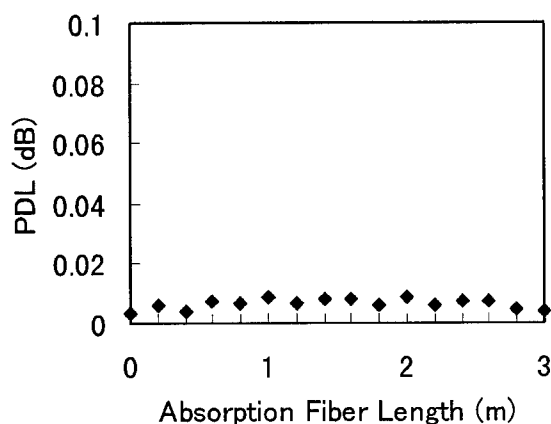


Fig.7 PDL (Type 1: $\lambda = 1.55 \mu\text{m}$)

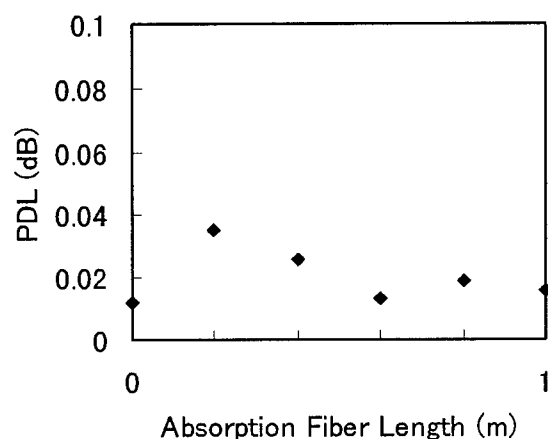


Fig.8 PDL (Type 2: $\lambda = 1.31 \mu\text{m}$)

It is judged therefore that pigtail type optical attenuators show satisfactory power endurance because the heat from light absorption is dispersed also for the case of high-power light input.

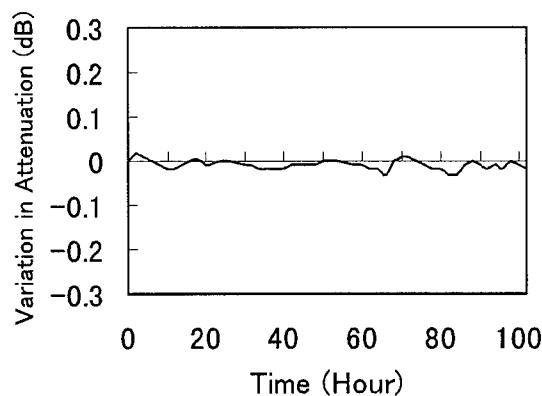


Fig.9 Power endurance (Type 1: $L=3\text{m}$)

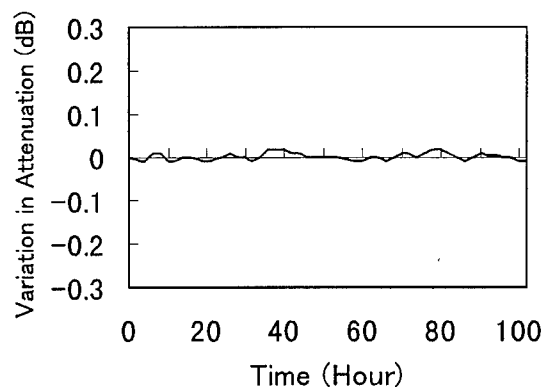


Fig.10 Power endurance (Type 2: $L=0.5\text{m}$)

E. Power Endurance

The endurance of absorption fibers to high-power light input was measured. The test was carried out by measuring variations in attenuation while continuous light of 100 mW ($\lambda = 1.48 \mu\text{m}$) was transmitted for 100 hours. Results are shown in Figs. 9 and 10.

As seen in the figures, the variation in attenuation is within ± 0.1 dB, which is favorable indicating that the power endurance of absorption fibers is satisfactory. The light is absorbed gradually and dispersively in and along the absorption fiber in pigtail type optical attenuators.

F. Temperature Cycling Test

The two types of pigtail type optical attenuators were subjected to heat cycle test between -25 and $+70^\circ\text{C}$ for 100 cycles. The Type 1 sample consisted of an absorption fiber of 3 m long with single-mode fibers fused to both ends of the absorption fiber. The Type 2 sample consisted of an absorption fiber of 0.5 m long and SC optical connectors attached to both ends of the absorption fiber.

Results are shown in Fig. 11. The variation in

attenuation was ± 0.1 dB for the Type 1 sample (3 m) and ± 0.2 dB for the Type 2 sample (0.5 m).

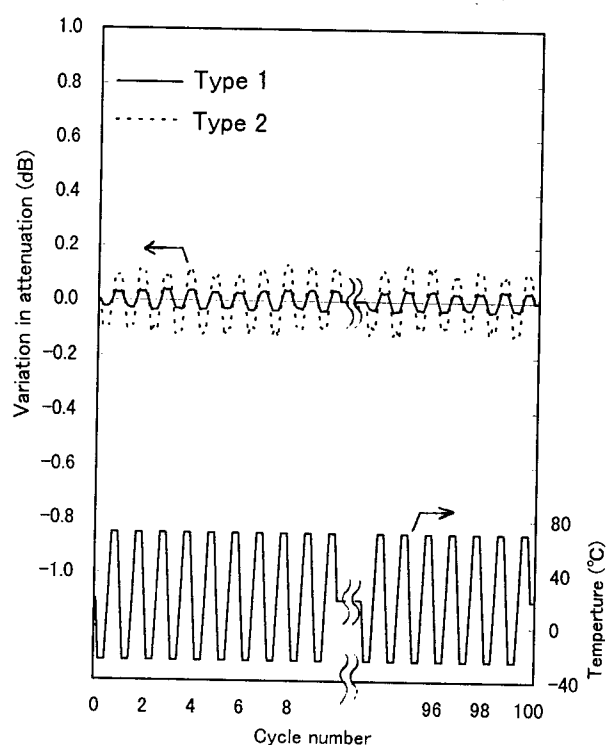


Fig.11 Temperature Cycling Test

G. Tensile Strength Test

The UV-resin coated Type 1 absorption fiber was subjected to the tensile strength test. The tensile force which increased at a rate of 50 cm/min was applied to an absorption fiber sample of 50 cm long, and the strength at which the sample broke was measured. In addition, UV-coated single-mode fiber was also subjected similarly to the tensile strength test for comparison. The number of samples was 30 in each test. Results are shown in Table 3.

Table 3. Tensile Strength Test

Item	Data
Metal-ion doped Fiber	Ave. 58.5 N
Single-mode Fiber	Ave. 56.3 N

The tensile strength of the absorption fiber is comparable with that of the single-mode fiber, indicating that the fiber strength is affected little by doping a transition metal.

H. Return Loss

The return loss was measured on Type 2 pigtail type optical attenuators having SC connectors. The end surfaces of each absorption fiber were polished for connection of SC connector by the advanced physical contact (AdPC) technique [8]. The number of samples subjected to the test is 30 (i.e., 60 end surfaces). Results are shown in Fig. 12

The average return loss was 49.6 dB, which is comparable with that of ordinary AdPC-polished optical connection, confirming that there is no effect of metal-ion doping on return loss.

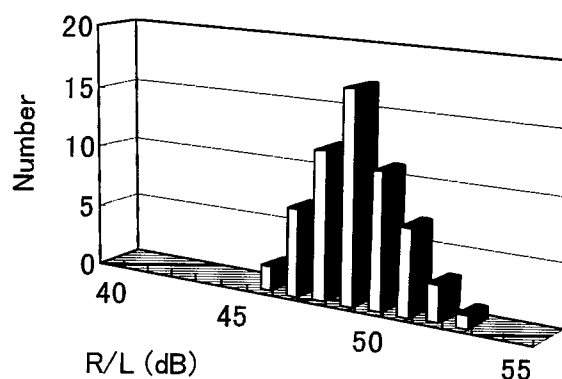


Fig.12 Return Loss

IV. CONCLUSION

Pigtail type optical attenuators using two types of metal-ion doped optical fibers were developed and tested. Their characteristics are as follows:

- The attenuation is finely adjustable in steps of 0.1 dB by changing the fiber length, and it makes possible to make attenuators of desired attenuation.
- The attenuators easily endure high-power light of 100 mW (+20 dBm).
- The polarization dependent loss is as small as below 0.1 dB.
- Environmental characteristics are favorable with attenuation variations on the order of ± 0.2 dB before and after heat cycle tests.

- The attenuators can be connected with other fibers easily by fusing or by using optical connectors.
- The attenuators have strengths (ave. 58.5 N) similar to those of conventional single-mode fibers.

With such favorable characteristics, the pigtail type optical attenuators can be applicable to optical transmission equipment and optical communication networks which require high-reliability and high-precision light level adjustments.

REFERENCES

- [1] K.Kanayama, K.Takada, Y.Takeuchi, K.Kato, "Characteristics of SC Type Optical Attenuator using Metal Doped Fiber," IEICE Japan, General Conference, C-347, 1994.
- [2] R.Nagase, Y.Takeuchi, K.Kanayama, S.Mitachi, K.Kato, "SC-type fixed optical attenuator using metal doped fiber," Technical Report of IEICE Japan, EMD95-4, 1995.
- [3] Y.Takeuchi, R.Nagase, S.Mitachi, "High Performance SC-type Fixed Optical Attenuator Using Co-doped Fiber," Tech Dig of IOOC'95, WA1-2, vol.2, Hong Kong, 1995.
- [4] Y.Takeuchi, R.Nagase, S.Mitachi, "SC-type Fixed Optical Attenuator Using Metal-ion-doped Optical Fiber," NTT R&D, vol.45, No.6, Japan, 1996, pp.595-600.
- [5] M.Saijo, Y.Morishita, A.Kumagai, Y.Ariga, Y.Takahashi, K.Sugi, K.Muta, H.Matuura, "Fixed Optical Attenuator -Development of Metal Doped Optical Fiber-," Showa Electric Wire and Cable Review, vol.45, No.2, Japan, 1995, pp.93-97.
- [6] M.Saijo, Y.Morishita, A.Kumagai, Y.Takahashi, K.Sugi, K.Muta, "Characteristic of Optical Attenuator and Optical Terminator using Metal Doped Optical Fiber," IEICE Japan, General Conference, C-262, 1996.
- [7] Y.Ariga, Y.Morishita, M.Saijo, K.Sugi, K.Muta, "Optical Attenuator of Pig-tail Type using Metal Doped Optical Fiber," IEICE Japan, General Conference, C-3-112, 1997.
- [8] K.Kanayama, Y.Ando, R.Nagase, S.Iwano, "Evaluation Method and Performance of Advanced Low-Reflection Optical Connectors," International Wire & Cable Symposium Proceedings, 1992, pp.785-791.

AUTHORS



Masashi Saijo was born in Tokushima, Japan, on January 1, 1969. He received the B.Eng. degree in Applied Physics and Chemistry from the University of Electro-Communications, Tokyo, Japan, in 1992.

In 1992, he joined Showa Electric Wire & Cable Co., Ltd.(SWCC), Kanagawa, Japan. He has been engaged in development of optical fiber devices.

Mr. Saijo is a member of the Institute of Electronics, Information and Communication Engineers (IEICE) of Japan.



Yuichi Morishita was born in Tokyo, Japan, on March 28, 1965. He received the B.Eng. degree in Applied Physics from Science University of Tokyo, Japan, in 1988.

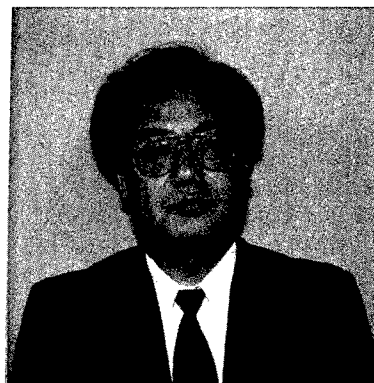
In 1991, he joined Showa Electric Wire & Cable Co., Ltd.(SWCC), Kanagawa, Japan. He has been engaged in development of optical fiber and optical fiber devices.

Mr. Morishita is a member of the Institute of Electronics, Information and Communication Engineers (IEICE) of Japan.



Yumi Ariga was born in Hokkaido, Japan, on February 25, 1969. She received the B.Eng. degree in Applied Electronics from the University of Hokkaido Institute of Technology, Hokkaido, Japan, in 1992.

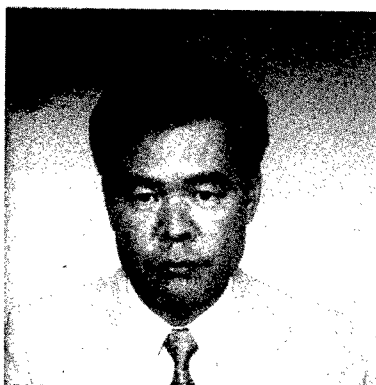
In 1993, she joined Showa Electric Wire & Cable Co., Ltd.(SWCC), Kanagawa, Japan. She has been engaged in development of optical fiber.



Ken-ichi Muta was born in Nagasaki, Japan in 1950. He received B, M and Ph.D. degree in Organic Materials Science from Tokyo Institute of Technology in 1974, 1976 and 1980 respectively.

In 1980, he joined Showa Electric Wire & Cable Co., Ltd.(SWCC), Kanagawa, Japan. He has been engaged in development of optical fiber and optical fiber devices.

Dr. Muta is a member of the Institute of Electronics Information and Communication Engineers (IEICE) of Japan, Applied Physics and Ceramics Society.



Kazunari Sugi was born in Tokyo, Japan, on December 24, 1954. He received the B.Eng. degree in Mechanical Engineering from Waseda University, Tokyo, Japan, in 1976.

In 1985, he joined Showa Electric Wire & Cable Co., Ltd.(SWCC), Kanagawa, Japan. He has been engaged in development of optical fiber devices.

Mr. Sugi is a member of the Institute of Electronics, Information and Communication Engineers (IEICE) of Japan.

ADDRESS

• M.Saijo and K.Sugi

Engineering Sect.1

Optics & Communications Engineering Dept.

Information Communications Div.

SHOWA ELECTRIC WIRE & CABLE CO.,LTD

4-1-1, Minamihashimoto, Sagamihara, Kanagawa, 229-11, JAPAN

• Y.Morishita, Y.Ariga and K.Muta

Optics & Electronics Laboratory.

Information Communications Div.

SHOWA ELECTRIC WIRE & CABLE CO.,LTD

4-1-1, Minamihashimoto, Sagamihara, Kanagawa, 229-11, JAPAN

UV-TRANSPARENT COATINGS FOR OPTICAL FIBER

Åsa Claesson, Bengt Sahlgren, Michael Fokine, and Raoul Stubbe

Institute of Optical Research, Stockholm, Sweden

ABSTRACT

Bragg gratings have been produced in germanosilicate optical fibers by exposing the fiber, through a polymer coating, to an interference pattern in the ultraviolet wavelength region. Two different coatings, Teflon AF[®] 1600 and Kynar[®] 7201, were applied on the fiber by dip coating and their optical properties in the 200-300 nm range were investigated. During the grating fabrication process, Teflon AF showed no sign of degradation at the fluencies required for efficient grating manufacturing. When Kynar 7201 was used, the coating darkened and decomposed.

INTRODUCTION

Bragg gratings in optical fibers¹ are used in a large variety of applications. The simplest grating is a periodic variation of the refractive index in the core of the fiber, which acts as a wavelength-selective reflector. Such gratings are e.g. used as strain sensitive elements in multiplexed fiber sensor systems, external Bragg reflectors to stabilize semiconductor lasers or to perform filter functions in WDM applications. It is also possible to produce gratings with tailored transmission characteristics, eg chirped gratings for dispersion compensation, and tilted gratings for radiation mode taps (side-tap filters). Fiber Bragg gratings are usually fabricated in singlemode GeO₂/SiO₂ optical fibers by exposing the fiber core to a fringe pattern of ultraviolet light in the 240 nm region. The pattern can be accomplished either by using an interferometer² or a phase mask³.

The fiber coatings most commonly used today, such as UV-curable acrylates and thermal curing silicones, are opaque at the wavelengths where germanosilicate optical fibers are photosensitive. Thus, to be able to fabricate fiber Bragg gratings the coating has to be removed, mechanically or chemically, before the gratings can be written. After the grating fabrication procedure, the fiber needs to be recoated, in order to make the component manageable for real applications. This is a tedious process that increases the cost of fiber Bragg grating components.

Recently, Espindola *et. al.*⁴ demonstrated the first Bragg gratings written through a UV-curable coating. The results were encouraging, however, this jacket darkens and the transmittance degrades on exposure, which limits the effective grating writing time. A UV-transparent coating, that is unaffected by UV-exposure, would make stripping of the fiber unnecessary, which in turn would make the grating fabrication procedure easier and faster and make it possible to avoid the degradation that occurs if a bare fiber is exposed to air. In this paper we present an investigation of two fluorinated polymers, one of them showing the necessary UV-tolerance.

EXPERIMENTAL

Two polymers were investigated: Kynar[®] 7201 (VDF/TFE copolymer) and Teflon AF[®] 1600.

Kynar[®] 7201

PVDF is the addition polymer of vinylidene fluoride (1,1-difluoroethylene: CF₂=CH₂). It is a linear fluoropolymer. The carbon-fluorine bond is extremely strong, which leads to the exceptional properties for which fluoropolymers are well known; stability at relatively high temperatures and resistance to aggressive chemicals. The material is known for its piezoelectric and pyroelectric properties, comparable to those of piezoelectric ceramics, and is an important polymer for ferroelectrics.

PVDF is reported stable in harsh chemical, weathering and oxidizing environments, almost approaching the stability of fully fluorinated polymers such as PTFE (Teflon). The material is also stable under ultraviolet or other high-energy radiation, and has low water absorption, of the order 0.02%. It has useful mechanical properties from -60 to 150°C.

PVDF coatings are prepared by melt extrusion or from solutions. A problem is PVDF's limited solubility in organic solvents. This is overcome by introduction of monomers such as TFE (tetrafluoroethylene: CF₂=CF₂) or HFP (hexafluoropropene: CF₂=CF-CF₃). Copolymers with VDF as main constituent are described by

Tournut⁵. These copolymers have lower crystallinity and higher solubility in organic solvents than pure PVDF. VDF/TFE copolymer coatings, applied from solution, were among the early coatings for optical fibers.

PVDF, under the tradename Kynar, was developed in the early 1960's by Pennwalt Co. A VDF/TFE copolymer (80/20 mol%) in pellet/powder form is sold under the name Kynar 7200/7201 by Atochem Elf Aquitaine in France.

Kynar 7201 is easily dissolved in acetone. Thin films can be made by dipcoating. Films thicker than 50 μm tend to develop bubbles during solvent evaporation, and are hard to keep even. The setup used to coat fibers from solution consists of a homemade flexible funnel of silicone, with a small diameter (150-300 μm) nozzle. The die is filled with solution, and a bare fiber pulled downwards, through the nozzle. In the system of manually pulling the fiber, centering is not possible, and upon inspection through a microscope, the coat turned out to be one-sided. By pulling the fiber through the nozzle a second time, immediately following the first, it was possible to cover the whole fiber. All fibers were coated in this way. In conventional drawing towers, where the coating is applied inline, centering devices are used and this problem will be mitigated. Prior to coating, all fibers were chemically stripped of original coating (acrylate) using dichloromethane, and then thoroughly cleaned with ethanol.

A transmission spectrum for a representative Kynar 7201 film, 50 μm thick, is reproduced in figure 1. The films are clear and transparent in the visible region, with a slow decrease of transmission at shorter wavelengths. Absorption at 240 nm is around 30% for this thickness. At wavelengths under 220 nm, the absorbance increases more rapidly. When thin films (20 – 50 μm) of Kynar 7201 were exposed to a pulsed excimer pumped frequency doubled dye-laser at a wavelength of 242 nm, the plastic rapidly degraded, darkened and decomposed. Degradation was observed after single pulses. It is possible that the plastic could withstand the power of a continuous-wave laser without degradation, and that it is the high peak power of the pulsed laser that causes the deterioration. If so, this plastic would still be attractive as a transparent coating for simplified grating fabrication, that uses continuous lasers.

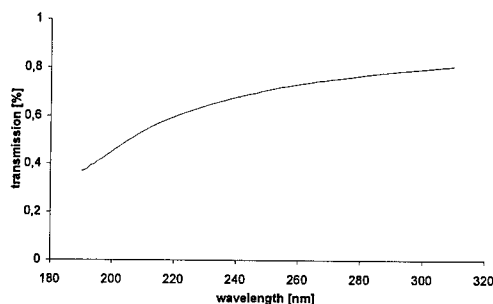


Figure 1 Transmission spectrum from a film of Kynar® 7201, 50 μm thick

Teflon AF® 1600

Crystalline PTFE (polytetrafluoroethylene - Teflon) is the most chemically resistant polymer known and it can be used at high temperatures. It also has a very low coefficient of friction and is electrically insulating. However, it is hard to process, due to low melt viscosity and very low solubility. Teflon also has rather poor mechanical properties. To overcome some of this, PTFE is often used in blends or copolymers with other fluoropolymers, such as fluorinated ethylene propylene (FEP) and perfluoroalkoxy (PFA).

In 1994, Du Pont presented a new product under the tradename Teflon AF, a copolymer of TFE and perfluoro-2,2-diethyldioxole (PDD) as introduced by Korinek⁶. Teflon AF has an amorphous structure, which leads to high transparency, even at short wavelengths. The material retains the excellent chemical inertness of PTFE, but is solvable in selected fluorinated solvents, and complemented with good mechanical and physical properties. Another amorphous fluoroplastic, Cytop®, with properties similar to Teflon AF, is manufactured by Asahi Glass in Japan. Unique to Teflon AF is the exceptionally low refractive index and high gas permeability. The manufacturing costs for both these materials are high, and they are among the most expensive man-made polymers.

Teflon AF1601-18 is an 18% solution of Teflon AF in a fluorinated solvent. Fibers were coated with the die-setup outlined above. All fibers were pulled twice through the die to ensure coating all around of the fiber. By studying crosssections in a microscope, it was confirmed that the coating indeed did cover all sides of the fiber, but also that the coating was uneven. Using devices to properly center the fiber in the nozzle, this unevenness would be very small. In this experiment, however, unevenness was not of major concern. After drying at room

temperature for a few minutes, the solvent was removed in two steps by heating. For improved adhesion, the manufacturer recommends heating to 330°C for 10-15 minutes and the use of a fluorosilane as an adhesion promoter. Neither of these measures was taken in our experiments.

Films of Teflon AF was investigated in a UV-visible spectrophotometer, the transmittance spectrum is reproduced in figure 2. The films are clear and very transparent. At 240 nm, the absorption is less than 5% for a film of 100 μm .

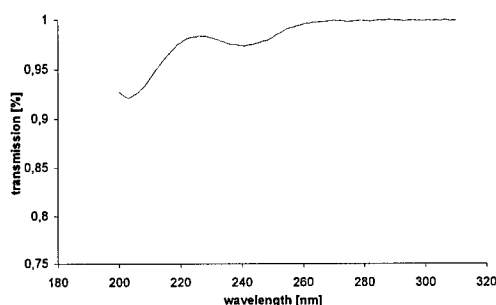


Figure 2 Transmission spectrum from a film of Teflon AF® 1600, 100 μm thick

No signs of degradation could be seen after exposing the Teflon AF films to a pulsed excimer pumped frequency doubled dye-laser at 242 nm, for an extended period of time (minutes). Encouraged by this, boron-codoped fibers were coated with an approximately 6 μm thick jacket of Teflon AF, and 1 cm long Bragg gratings were written through the coating, using an interferometric technique⁷. The estimated fluency in the core per pulse was 1 J/cm², and the accumulated dose for writing this grating was 140 J/cm². A reflection spectrum from the grating is presented in figure 3.

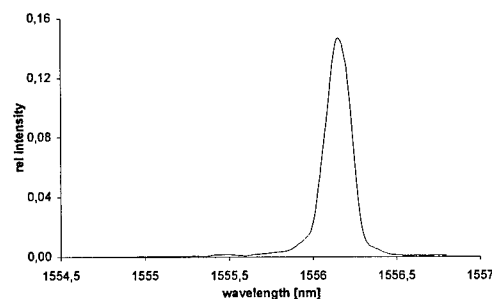


Figure 3 Reflection spectrum from grating written through thin Teflon AF coating.

CONCLUSIONS

Two different coatings, Teflon AF® 1600 and Kynar® 7201, were spun on silica glass and their optical properties in the 200-300 nm range were investigated. Both show good transmission in the 240 nm region but Kynar 7201 degrades when the film is exposed to high fluency. Germanosilicate fibers were dipcoated with Teflon AF 1600 and Bragg gratings were written into these fibers by exposing the fiber, through the coating, to an interference pattern at a wavelength of 242 nm. During the grating fabrication process the Teflon AF coating showed no sign of degradation at the fluencies required for efficient grating manufacturing. Teflon AF 1600 is thus a promising candidate coating for a grating fabrication process where the gratings can be written through the coating, making stripping and recoating unnecessary. However, the low index can pose a problem when Teflon AF is used as a jacket on conventional fibers, since it can lead to guiding of undesired cladding-modes.

REFERENCES

- [1] I. Bennion, J.A.R. Williams, L. Zhang, K. Sugden, N.J. Doran, "UV-written in-fibre Bragg gratings," *Optical-and-Quantum-Electronics*, **28**, 93, (1996)
- [2] G. Meltz, W.W. Morey, and W.H. Glenn, "Formation of Bragg gratings in optical fibers by a transverse holographic method," *Opt. Lett.*, **14**, 823, (1989)
- [3] K. Hill, B. Malo, F. Bilodeau, D.C. Johnson, and J. Albert, "Bragg gratings fabricated in monomode photosensitive optical fiber by UV exposure through a phase mask," *Appl. Phys. Lett.*, **62**, 1035, (1993)
- [4] R.P. Espindola, R.M. Atkins, D.A. Simoff, K.T. Nelson, and M.A. Paczkowski, "Fiber Bragg gratings written through a fiber coating," In Proc. OFC'97, postdeadline paper PD4, (1997)
- [5] C. Tournut, "New copolymers of vinylidene fluoride," *Macromol. Symp.*, **82**, 99, (1994)
- [6] P.M. Korinek, "Amorphous fluoropolymers - a new generation of products," *Macromol. Symp.*, **82**, 61, (1994)
- [7] A. Asseh, H. Storøy, B.E. Sahlgren, S. Sandgren, and R.A.H. Stubbe, "A writing technique for long fiber Bragg gratings with complex reflectivity profiles," *J. of Lightwave Technol.*, **15**, 1419, (1997)

ABOUT THE AUTHORS

Åsa Claesson received the MSc degree in Materials Engineering in 1997, from Uppsala University, Sweden. She is currently employed as research engineer at the Institute of Optical Research in Stockholm.

(Asa.Claesson@optics.kth.se)

Mailing address: Åsa Claesson, Institute of Optical Research, S-100 44 Stockholm, Sweden)

Bengt E Sahlgren, born in Stockholm, 1960, MSc in Mechanical Engineering -87 from the Royal Institute of Technology, Stockholm. He is currently employed as research scientist at the Institute of Optical Research in Stockholm. Bengt Sahlgren has 8 years of scientific experience in the field of fiber-optics. His main interest is manufacturing techniques of fiber Bragg gratings and fiber-optic sensor systems. (Bengt.Sahlgren@optics.kth.se)

Michael A Fokine graduated from the University of Linköping, Sweden in 1995 with a MS in physics. In 1995 he joined the Institute of Optical Research, Sweden, as a researcher in optical fibers and fiber Bragg gratings. (Michael.Fokine@optics.kth.se)

Raoul A H Stubbe was born in Norrköping 1961. He received the MSc and PhD degrees in Engineering Physics in 1985 and 1991, respectively, both from the Royal Institute of Technology, Stockholm. He is currently employed as research scientist and project manager for several fiber optics related research projects at the Institute of Optical Research in Stockholm. Raoul Stubbe has more than 10 years of scientific experience of fiber-optics and holds several patents in the field. His main interest is applications of fiber Bragg gratings for fiber-optic sensor systems and telecommunication. Raoul Stubbe is a member of the European Optical Society (Raoul.Stubbe@optics.kth.se)

COATINGS HAVING ENHANCED UV TRANSPARENCY FOR THE FABRICATION OF OPTICAL FIBER GRATINGS

Debra A. Simoff, Mark A. Paczkowski, Regina Ragan*, Daryl Inniss, Thomas A. Strasser, John M. Borick, J. Renee Pedrazzani, Rolando P. Espindola, Robert M. Atkins, Katherine T. Nelson, Jennifer Aspell**, Valerie J. Kuck**

Bell Laboratories, Lucent Technologies, Murray Hill, NJ

***Dept. of Applied Physics, California Institute of Technology, Pasadena, CA**

****Specialty Fiber Devices, Lucent Technologies, Murray Hill, NJ**

ABSTRACT

Optical fiber gratings are typically manufactured by side-irradiation of the fiber core through a mask with a UV laser after the coating has been removed. In the current process, the most time-consuming and labor-intensive steps are stripping and reapplying the polymer coating. We propose that grating manufacture can be simplified by the development and use of UV transparent fiber coatings, so that gratings can be made by UV irradiation of the fiber core *through* the polymer coating. This could enable rapid spool-to-spool processing and also improve reliability, since the handling associated with the removal and reapplication of the coating increases the chances of damaging the glass fiber. We demonstrate the principle by writing a 76% reflectivity fiber grating through a ~12 μm thick, thermally cured poly(methyl silsesquioxane) coating, with no apparent damage to the coating. We also report gratings written through UV cured acrylate coatings developed for this application using a novel low UV absorbing photoinitiator.

BACKGROUND

Holographic gratings formed in the core of optical fibers are finding increasing use in a variety of optical device applications.¹ These include fiber lasers, semiconductor laser stabilizers, pump reflectors, dispersion compensators, filters, demultiplexers, and gain equalizers. Such gratings may also be used as strain sensors in architectural applications. Projected market volumes for gratings in certain of these applications are thousands or tens of thousands per year. This burgeoning market

has stimulated development of manufacturing methods for grating mass production.

An optical fiber comprises an inner core of relatively high refractive index, an outer cladding, and a polymer coating. The core is made of ultraviolet (UV) photosensitive glass, such as a germanosilicate, so that a grating can be induced by UV irradiation. The dominant method for photo-inducing gratings in optical fibers is by side-writing into a stripped fiber with UV light through the fiber cladding. The fiber is exposed to UV light having an intensity that varies periodically along the length of the fiber. This, in turn, creates periodic refractive index variations in the fiber core. The periodically varying intensity pattern is typically achieved by applying a UV beam through an optical phase mask.² Alternately, the intensity pattern can be provided by an amplitude mask or by interference of a pair of coherent UV beams.³ In each of these techniques, the source of UV light is usually a high intensity UV laser.

Before writing a grating, the fiber is frequently first photosensitized for writing by treating it with hydrogen or deuterium under elevated temperature and pressure. The hydrogen or deuterium diffuses into the core through the polymer coating and the glass cladding. Typical treatment conditions are 3500 psi, 50-70°C for 3 days. Such treatment enhances the sensitivity of the UV photosensitive core so that the grating can be written at lower intensity.

Presently, a time-consuming step in grating fabrication is removing and subsequently reapplying the protective polymer coating that was applied to the fiber at the time of drawing. The coating is needed to protect the sensitive

fiber from contamination and mechanical damage, but typical coatings are highly UV absorbent and inhibit grating formation. This is largely because most commercial fiber coatings are UV curable and incorporate highly absorbing photoinitiators in order to initiate the curing reaction. Such coatings are damaged by UV laser beams. Upon exposure to UV, the coatings block the light via absorption, converting the energy to heat. They discolor and will eventually ablate, given sufficient exposure. Thus, an initial step in conventional grating writing is stripping the polymer coating, as by soaking the fiber in hot sulfuric acid.

Gratings have been written prior to the application of the coating,⁴ but these typically have low reflectivities due to the single pulse exposure.

Here, we demonstrate that with the proper combination of low UV-absorbing polymer, photosensitized glass, and controlled intensity radiation that UV-induced gratings can be side-written into polymer coated fibers without removing the polymer, thus permitting higher fabrication throughput of fiber gratings.

RESULTS AND DISCUSSION

In order to demonstrate the principle of writing a grating through a polymer coating, we needed an optical fiber having a suitable UV transparent coating. As mentioned above, most commercial optical fibers are coated with UV curable polymers that contain highly UV absorbing photoinitiators. They may also contain other UV absorbing species, e.g., antioxidants or moieties in the polymeric resin itself. At the standard coating thickness of 62.5 μm , these coatings are essentially opaque at the wavelengths typically used for grating writing (240-260 nm).

The strongest UV absorbers in polymers are usually conjugated double bonds, e.g., $-\text{C}=\text{C}-$, especially in aromatic rings. Most conventional photoinitiators contain such groups. Before curing, acrylates themselves are UV absorbant due to conjugation of double bonds within the acrylate group, $\text{H}_2\text{C}=\text{CH}-\text{C}(=\text{O})$. Fortunately, upon cure the acrylate $\text{C}=\text{C}$ bonds convert to single bonds, $-\text{C}-\text{C}-$, so that UV absorption is diminished. Preferred coatings for grating fabrication should

be substantially devoid of aromatic moieties or other conjugated unsaturation, as well as metal ions. Crystallites, separated phases, and other heterogeneities should also be avoided since they can cause scattering if their size is large relative to the period of the grating. Chemical species commonly used in polymers which do *not* significantly absorb UV light at $\lambda > 240$ nm include the following single bonds: C-H, C-O, C-Si, O-H, Si-O, Si-H, C-F, and C-Cl. Thus, various aliphatic hydrocarbons, silicone polymers, fluorocarbons, and certain chlorocarbons can be expected to have at least partial transparency.

Selection of Silsesquioxane Coating. An available specialty optical fiber was identified with a non-UV-cured coating that was expected to be reasonably UV transparent. The coating was a thermally cured poly(methyl silsesquioxane), a polymer that is sometimes referred to as a ladder siloxane or "glass resin." Its structure (Figure 1) bears some resemblance to silica, in that each Si atom is bonded in three directions to other O-Si groups. Because of its similarity to silica, this polymer was expected to have low UV absorbance at wavelengths >240 nm. The coating was thin (~ 12 μm), which contributed to its transparency. The coated fiber was sensitized by treating with D_2 under pressure, and was used to write both long period and short period (Bragg) gratings with two different laser setups.⁵

Long-Period Fiber Gratings Written Through

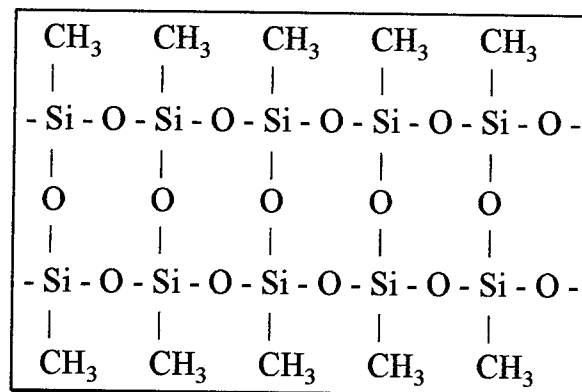


Figure 1. Idealized chemical structure of poly(methyl silsesquioxane).

Silsesquioxane Coating. In the first experiments, attempts were made to write long-period gratings⁶ using an amplitude mask and a KrF pulsed UV laser at 248 nm. The fiber was held taut next to the mask and was exposed to radiation intensities of 100-130 mJ/cm². At 130 mJ/cm², 1 dB loss developed at the selected wavelength after exposure for approximately 5 minutes. Examination of the fiber surface showed some physical damage to the polymer with periodicity comparable to that of the amplitude mask, but the coating remained intact and the damage appeared to be superficial. Decreasing the power to 100 mJ/cm² resulted in 0.5 dB loss, and minor damage to the surface of the polymer.

Fiber Bragg Gratings Written Through Silsesquioxane Coating. To write short period gratings, an interference mask was used with a defocused 242 nm frequency-doubled dye laser that was pumped with a XeF excimer laser pulsed at 30 Hz. The radiation was defocused to decrease the fluence. In the first attempt, the focal point was moved to 2 inches behind the fiber. After ~3 minutes of exposure at 20 mW there was no evidence of a grating impressed in the fiber core. The focal point was then moved to within 1 inch of the fiber. A weak reflector (~3%) was observed. In subsequent attempts a 10% reflector was grown in less than 1.5 minutes and a 76% reflector was grown after 6 minutes of exposure (Figure 2). In none of these cases was damage to the polymer coating detected.

Experiments with the silsesquioxane coated

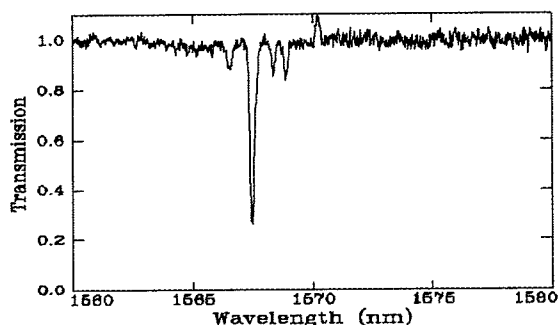


Figure 2. Normalized transmission spectrum of a 76% reflectivity optical fiber Bragg grating written through a 12 μ m thick poly(methyl silsesquioxane) coating.

fiber demonstrate the principle of forming gratings by writing through a polymer coating. The silsesquioxane, however, is not an ideal coating candidate for various reasons. On the plus side, it has high UV transparency and excellent thermal and chemical stability. But unlike conventional fiber coatings, it is thermally cured, not UV cured, and thus is not compatible with conventional fiber draw processes. To date, the silsesquioxane has only been applied in thin layers, and cannot easily be applied without cracking at a standard 62.5 μ m thickness. As a further drawback, it cannot readily be stripped for splicing using conventional chemical or mechanical techniques.

Development of Acrylate Coatings Using Novel Low UV Absorbing Photoinitiator.

Ideally, we would prefer to use a coating which could be UV cured, and whose chemistry and mechanical properties were similar to those routinely used on optical fiber. Fortunately, many current commercial fiber coatings have been developed to be substantially non-yellowing, and as a result their base resins (oligomers plus monomers) have relatively low UV absorbance. We obtained the base resin for one such coating from a supplier where the photoinitiator and any other potentially absorbing additives were omitted at our request. We next identified a novel low-absorbing free radical photoinitiator capable of curing this coating. The UV spectrum for the new initiator is compared with that of a commonly used commercial photoinitiator in Figure 3. Spectra were collected by diluting the photoinitiators in hexane and scanning in a quartz cuvette having a 50 μ m path length. The novel initiator is much less UV absorbant at 240-260 nm than the commercial photoinitiator, despite being 25 times more concentrated.

Although the novel initiator has relatively low UV absorption, it dissociates readily upon UV irradiation to form free radicals and initiate the acrylate curing process. Incorporation of 3-10 phr* of the initiator into the low UV absorbing commercial acrylate base resin gave a UV curable material whose mechanical properties after cure were similar to those of a commercial

* phr = parts per hundred parts of resin

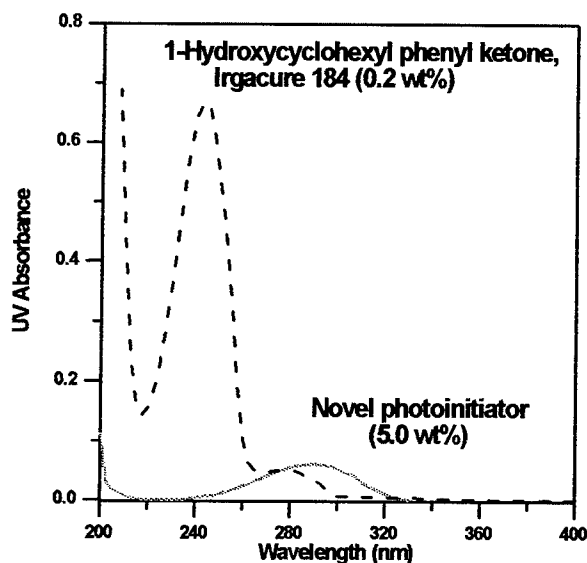


Figure 3. UV spectra of a commercial photoinitiator and the novel photoinitiator in hexane (50 μm path length).

secondary coating. UV spectra of cured films predicted that 25% transmission at 250 nm should be achievable for a 62.5 μm coating of the modified acrylate versus ~0% transmission for commercial acrylate fiber coatings at this wavelength.

The efficiency of the novel photoinitiator is lower than that of most commercial photoinitiators, which can result in poor surface cure and tackiness of the coatings due to oxygen inhibition. In order to improve cure speed, we typically added small amounts (< 0.5 phr) of a non-aromatic thiol.

Fibers were drawn and coated with this modified acrylate coating on conventional draw towers. Coatings were applied and UV cured at various thicknesses from 20-65 μm . A high degree of cure was achieved at a draw speed of 1 m/s using a single 30" UV lamp. While this draw speed would be slow for manufacturing standard telecommunications fibers, it is considered to be acceptable for the relatively short lengths needed for specialty fiber markets.

Acrylate Coating Degradation Upon UV Laser Exposure. Besides enhancing the initial, as-cured UV transparency of the acrylate coating, it is important that the coating maintain

a certain level of UV transparency during the grating writing process. To assess the UV stability of the acrylate coating when exposed to a UV laser, cured films of the resin were irradiated with a laser while percent transmission was monitored (Figure 4). These measurements were made using a CW frequency-doubled Ar-ion laser operating at 257 nm. The initial UV transmittance at 257 nm for a 22 μm film was ~60%. The UV transmittance decayed gradually with exposure, after an apparent induction time. The rate of decay decreased with a decrease in the incident power level, and was slower at 257 nm than at 248 nm. The initial decrease in UV transparency occurred without visible yellowing. The decrease in UV transparency limits the effective writing time for creating fiber gratings.

Gratings Written Through Modified Acrylate Coating.

Bragg gratings were successfully written through the modified acrylate coating in fibers having various coating thicknesses and with several different laser/mask configurations. Both long-period and short-period (Bragg) gratings were written, and both pulsed and continuous wave (CW) lasers have been used. Figure 5 displays the spectrum for a 20%

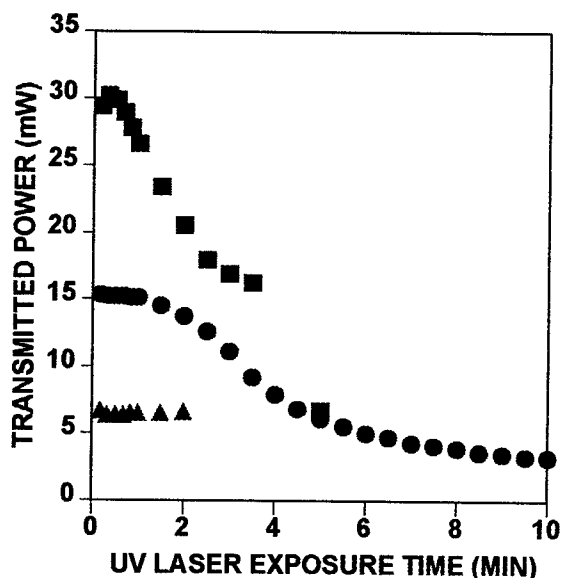


Figure 4. Figure 4 UV transmission decay of acrylate coating films exposed to 257 nm laser radiation: (■) 22 μm film between quartz plates, 50 mW incident beam; (●) ~15 μm film in air, 20 mW incident beam; (▲) 22 μm film between quartz plates, 10 mW incident beam.

reflectivity Bragg grating written through a 29 μm UV cured modified acrylate coating using a 242 nm frequency doubled dye laser pumped by a XeF excimer laser. The beam was partially defocused, so that the power was only ~25% of that typically used to write gratings in stripped fiber. The writing speed and ultimate strength of these gratings are less than that achievable with a stripped fiber, since the writing process competes with eventual UV darkening of the coating. The writing process stops before visible yellowing of the coating can be observed.

Use of High Photosensitivity Glass Fiber.

One way to overcome the stability limitation of the modified acrylate coating is to use a more photosensitive fiber that allows writing of a stronger grating in a shorter amount of time.⁷ We achieved enhanced photosensitivity by increasing the concentration of germanium-oxygen deficiency centers (GODCs) in the fiber core.^{8,9} Using such a high GODC fiber with the modified acrylate coating, together with H_2 sensitization of the core, we wrote a 33% reflectivity grating through a 40 μm thick coating and a 50% reflectivity grating through a 25 μm coating. These gratings were written using a CW frequency-doubled Ar-ion laser operating at 257 nm.

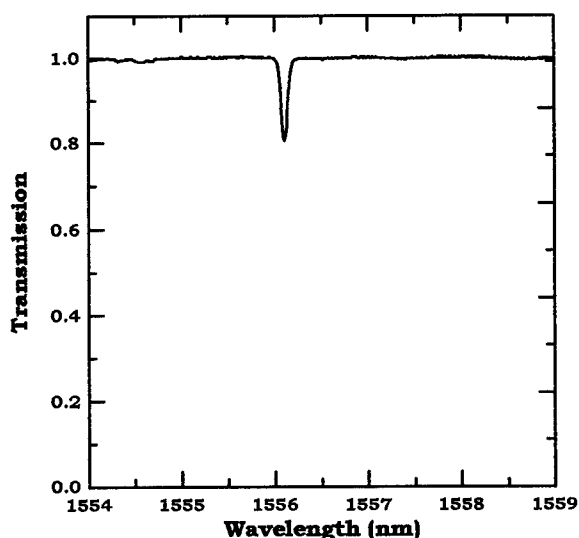


Figure 5. Normalized transmission spectrum of a 20% reflectivity optical fiber Bragg grating written through a 29 μm UV cured acrylate coating.

SUMMARY

We have demonstrated a new, simplified method for fabricating optical fiber gratings wherein the fiber is irradiated through a relatively UV transparent polymer coating. Demonstrations were made using both a thermally cured silsesquioxane coating, and a UV cured urethane acrylate modified to have enhanced UV transparency by incorporation of a novel low UV absorbing photoinitiator. The writing speed and resultant grating strength can be increased by using special high photosensitivity glass. This process avoids the laborious steps of stripping and reapplying the polymer coating. It should also improve yields and long term reliability by avoiding handling and damage of bare glass. Such a process has positive implications for mass production of gratings in high volume markets.

ACKNOWLEDGMENTS

We appreciate the contributions of E. A. Chandross, J. R. Bautista, F. V. DiMarcello, A. C. Hart, K. S. Kranz, R. G. Huff, D. J. DiGiovanni, N. Conti, and S. Cabot in the preparation of fibers for this work.

REFERENCES

- ¹ A. E. White and S. G. Grubb "Optical Fiber Components and Devices," Ch. 7 in *Optical Fiber Telecommunications*, Vol. IIIB, T. L. Koch and I. P. Kaminow, ed., Academic Press, pp 267-318 (New York, 1997).
- ² D. Z. Anderson, T. Erdogan, V. Mizrahi, "Method for forming a Bragg grating in an optical medium," US Patent 5,327,515.
- ³ W. H. Glenn, G. Meltz, E. Snitzer, "Method for impressing gratings within fiber optics," US Patent 4,725,110.
- ⁴ L. Dong, J.-L. Archambault, L. Reekie, P. St. J. Russell, D. N. Payne "Single Pulse Bragg Gratings Written During Fibre Drawing," *Elect. Lett.*, **29**(17), 1577 (1993).
- ⁵ J. Aspell, D. Inniss, V. J. Kuck, M. A. Paczkowski, D. A. Simoff, "Formation of gratings in polymer-coated optical fibers," US Patent 5620495.
- ⁶ For references on long period gratings, see: A. M. Vengsarkar, "Long Period Fiber Gratings Shape Optical Spectra," *Laser Focus World*, June, 1996; A. M. Vengsarkar, J. R. Pedrazzani, J. B. Judkins, P. J. Lemaire, "Long-period Fiber-grating-based Gain Equalizers," *Optics Letters*, **21**(5), 336-338 (1996);

V. Bhatia, A. M. Vengsarkar, "Optical Fiber Long-Period Grating Sensors," *Optics Letters*, **21**(9) 692-694 (1996); A. M. Vengsarkar, P. J. Lemaire, V. Bhatia, T. Erdogan, J. E. Sipe, "Long-period Fiber Gratings as Band-rejection Filters," *Journal of Lightwave Technology*, **14**(1), 58-65 (1996).

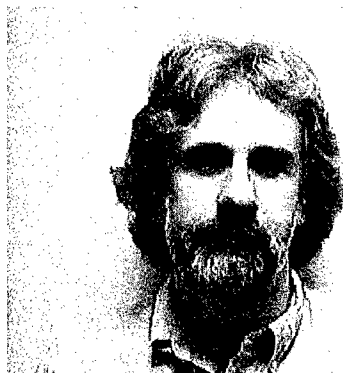
⁷R. P. Espindola, R. M. Atkins, D. A. Simoff, K. T. Nelson, M. A. Paczkowski, "Fiber Bragg Gratings Written Through a Fiber Coating," *Post-Deadline Paper*, Optical Fiber Conference, Dallas, TX, April, 1997.

⁸ R. M. Atkins, K. T. Nelson, K. L. Walker, "Photorefractive Optical Fiber," US Patent 5157747.

⁹ P. J. Lemaire, R. M. Atkins, V. Mizrahi, W. A. Reed, *Elect. Lett.* **29**, 1191-1193 (1993).



Jennifer Aspell received her B.S. in electrical engineering from Rensselaer Polytechnic Institute in 1985, her M.S. in electrical engineering from the University of California, Berkeley, in 1986, and her M.S. in management from Purdue University in 1997. Ms. Aspell began her career at Lucent Technologies in 1985 and is currently the director of Lucent's Specialty Fiber Devices business.



Robert Atkins is a member of technical staff in the Optical Fiber Research Department at Bell Labs in Murray Hill, NJ, where he studies defects in silica and silica-based glasses. He has acquired a Ph.D. in Chemistry from the University of Bristol (UK).



John Borick is a member of technical staff in the Specialty Fiber Devices Division of Lucent Technologies in Murray Hill, NJ. He conducts process engineering and manufacturing of optical fiber Bragg gratings and holds a BS in Electrical Engineering from Fairleigh Dickinson University.



Rolando Espindola is a member of technical staff in the Optical Fiber Research Department at Bell Labs in Murray Hill, NJ. He is currently engaged in research of fiber gratings, fiber lasers and amplifiers. Rolando recently earned a Ph.D. in Electrical Engineering from Northwestern University.



Daryl Inniss is a member of technical staff in the Optical Fiber Research Department at Bell Labs in Murray Hill, NJ. He began his career studying the mechanism which leads to fracture of silica optical fibers, and is currently developing high power fiber lasers and amplifiers. Dr. Inniss received a Ph.D. in Chemistry from UCLA.



Valerie Kuck is a member of technical staff in the Polymer and Chemical Engineering Dept. at Bell Labs in Murray Hill, NJ. She has conducted materials development in a variety of areas, including stabilization and aging of polyethylene insulation, glass resins, tin/lead solders and liquid crystal displays. She holds an MS in Chemistry from Purdue University.



Katherine Nelson is a member of technical staff in the Optical Fiber Research Department at Bell Labs in Murray Hill, NJ. Her research is focused on the fabrication of optical fiber preforms by MCVD, including optimization of the manufacturing process, production of specialty fiber, and fundamental studies of glass chemistry. She holds an MS in Materials Science & Engineering from Stevens Institute of Technology.



Mark Paczkowski is a member of technical staff in the Polymer and Chemical Engineering Dept. at Bell Labs in Murray Hill, NJ where he does polymer materials and process research. Dr. Paczkowski received a Ph.D. in Chemistry from the University of Pennsylvania.



Renee Pedrazzani is a member of technical staff in the Optical Fiber Research Department at Bell Labs in Murray Hill, NJ. She is currently working in the field of fiber optic gratings, concentrating on fabrication of the next generation of Bragg gratings. She has received an MS in Electrical Engineering from Virginia Tech.

Regina Ragan is pursuing a Ph.D. in Applied Physics at CalTech in Pasadena, CA, with an emphasis on electronic materials. She holds a BS in Materials Science and Engineering from UCLA.



Debra Simoff is a member of technical staff in the Polymer and Chemical Engineering Dept. at Bell Labs in Murray Hill, NJ. She conducts research on optical fiber coatings and other polymers used for telecommunications, and has earned an MS in Polymer Science and Engineering from UMASS Amherst.



Thomas Strasser graduated with a Ph.D. in Material Science and Engineering from Cornell University in 1993. He has been at Bell Labs, Murray Hill, NJ since then investigating UV-induced effects in fibers and waveguides.

FORTY YEARS OF ELECTRICAL CABLE TESTING AND FAULT LOCATION

Richard D Macey

Rutherford Cable Repairs, Rutherford New South Wales, Australia

ELECTRICAL CABLES OF VARIOUS TYPES AND USES EVER SINCE CONCEPTION HAVE BEEN REMARKABLY RELIABLE BUT EVEN DURING CONSTRUCTION, FAULTS SUCH AS POOR INSULATION, PARTIALLY AND FULLY BROKEN CONDUCTORS HAVE OCCURRED AND DURING THE EARLY PART OF THIS CENTURY, HAS CAUSED MANY PROBLEMS TO OVERCOME AND ELIMINATE.

LOCATING THESE FAULTS WAS A NIGHTMARE FOR MOST AS NO ATTEMPT TO ANALYSE THE FAULT WAS MADE AND THE CONCEPT OF DIAGNOSIS AND PRELOCATION WAS NOT CONSIDERED. IT WASN'T TILL THE 1950'S THAT ECONOMICS BECAME IMPORTANT WHEN ENSURING RELIABILITY AND SPEED OF FAULT LOCATION AND REPAIR.

UNSAFE METHODS WERE USED, IE REPLACE THE FUSE WITH AN EVEN BIGGER ONE, OR CONNECT THE FAULTED CABLE TO A LARGE TRANSFORMER IN ORDER TO DESTROY THE CABLE AT THE FAULTED POINT. OR EVEN CUT THE CABLE INTO SMALLER LENGTHS TO LOCATION. ALL VERY DANGEROUS AND OBVIOUSLY TIME CONSUMING.

DURING THE 1960'S, ENGINEERS AT LONG LAST FINALLY BEGAN TO DEVELOP A SYSTEMATIC APPROACH.

Evaluation or diagnosis is still done by time honoured methods of comparison using ohm metres and insulation test sets and more recently, symmetrical load testers particularly for flexible cables as used in the mining industry.

Many factors can confuse the operator when using these basic instruments:

- Dirty connectors
- Various lengths of cable
- Induced voltages
- Partially broken conductors
- Splits in insulation

Continuity instruments are only suitable for basic continuity checks, phase rotation in the case of A.C. cable and polarity when dealing with D.C. cable. Partial break apparatus is essential to guarantee the integrity of the conductors, particularly if the cable is flexible.

Insulation testers are similarly misleading as most operators lack the technical ability to apply them correctly, particularly when testing higher voltage cables. ie 6600 Volts and above. The application of 5kVDC phase to earth on a 6.6kV phase to phase cable would mostly indicate adequate

insulation with readings of 100 Meg Ohms, or greater suggesting that there was no deficiency in the integrity of the insulation.

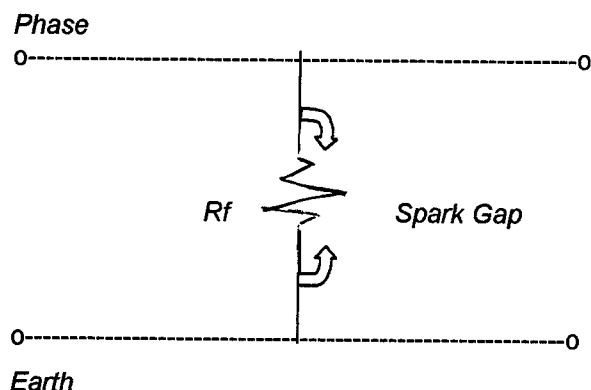
Due to normal operating cable movement however, the cable if re-energised would prematurely fail, as the spark gap in parallel with the fault would ionise, allowing the earth leakage mechanism to trip.

In these cases, experience has shown that voltages of 10kVDC phase to earth are required to reliably indicate incipient faulty areas. This highlights the need of the operator to understand the characteristics and limitations being tested before any diagnostic or proof testing is carried out.

The use of ohmmeters and insulation test sets can only perhaps suggest that there is a problem with a cable or associated apparatus as there is no guarantee of achieving a reliable result.

Pre Conditioning was an engineer's soul destroying method of by passing the technical niceties of prelocation by liberally destroying the cable at the faulted area. Preconditioning was and in some cases perhaps still is done by using crude, unsafe methods such as larger fuses and bigger burn out devices, completely ignoring the characteristics of a fault which can be gainfully used.

Simply described, a cable fault is a fault resistance with a spark gap in parallel and is inherently non-linear because of the varying ionisation times of the spark gap.



The engineers' original interest in preconditioning a fault was to change the characteristics of the fault so those available instruments could be used to pin point faults by literally destroying the insulation and or conductor.

Preconditioning of faults became exercises in futility with the introduction of modern cables. For example, XLPE insulated (cross-linked polyethylene), oil pressure cooling and conductors of aluminium material. This caused consternation to the fault burning people, as each of these types of cable have peculiarities of their own.

XLPE, with its memory and long time constants associated with the effects of absorption, resist any change. However, oil filled cables with the ability to dissipate, by convection, any carbon/conductive forming process when heat/voltage is applied, therefore making them very difficult to burn whilst application of heat to cables with aluminium conductors do not do any more than vaporise the conductor.

Pre Determining the position of a fault is essential if the cable is buried, or more than 100 metres in length, buried in a noisy environment, or worse still, a submersible cable. The procedure to accurately pre locate a fault has changed significantly over the years as new techniques became available. Initially, cable faults were located ranging from methods described as resistive, capacitive, low and high resistance bridges, to pulse echoes, (if you resided in Australia). If you resided in the United Kingdom, Time Domain Reflectometer (TDR's) were used, if you happen to be American, Radar Test Sets were used – all very confusing. This followed by Impulse Current Equipment (ICE), Impulse Voltage

and now in the 1990's, a return to the previously abandoned classical compromise of reflection techniques.

Some of the inherent difficulties when considering the use of bridges are, (although when circumstances are correct, they can be as accurate as 0.2% of the cable route length).

- Know the exact cable length
- Not allowing the bridge to be confused by two faults
- Attempting to pre locate a fault of similar resistance to the inherent resistance of the cable

The use of Radar Test Sets for pre locating anything other than an open or short circuit in a cable can be difficult if not impossible as it is essential that the cable fault represents a significant discontinuity on the surge impedance profile of the cable. In the case of shunt faults, this means that the fault resistance must be comparable with the cable surge impedance profile of the cable. As typical values of surge impedance lies between 10 and 100 ohms, it becomes necessary to apply "fault burning" techniques to lower the fault resistance so that the fault point can be realistically observed on the instrument screen.

Radar Test Sets propagating a wave of short duration and known frequency. In travelling the conductor length, part or all of the energy is reflected at points where there are irregularities. Knowing the velocity of propagation, it is then possible to deduce the distance to the said irregularity. This method does need a sound conductor, as it is a comparative procedure and in some cases can detect electrically unsymmetrical cables and can be used for cable length measurement.

The need to pre locate all types of faults on all types of cables both accurately and economically, saw the development of the Impulse Current Methods (ICM) in the 1970's. This instrument is a highly developed Radar Test Set but instead of exhibiting a signal to be applied to the cable, it makes use of current transients that occur when a surge generator or capacitor discharge unit is "fired" into a cable.

Current transients are safely recorded via a linear coupler and recorded easily as the surge generator has inherently low output impedance at high frequencies. When a surge generator is discharged into a cable with a high resistance fault, the voltage wave passes beyond the cable fault before the spark gap breaks down and ionisation occurs. (This is known as Ionisation Delay).

When the fault does not conduct, a new wave front travels back to the surge generator, where it is reflected once again, and back towards the fault because of the gross mismatch that the surge generator represents.

The difficulty with all this is that the operator needs to be skilled and familiar in order to interpret the various traces as different types of faults produce varying wave displays that are then in turn recorded via a digital interface.

The 1980's have seen the wheel re-invented. High voltage from a surge generator ionises the spark gap where upon a stabilising unit capable of maintaining a low voltage - high current, produces a low resistance fault (previously high), hence making pre location by a pulse echo not only possible, but unbelievably easy - even under very wet conditions.

Pin Pointing exact location of faults saves time, effort and money, by being able to Pin Point the correct position at which to excavate and repair the damaged cable. After pre locating a fault, isolation

Richard D Macey
3 Kyle Street
Rutherford New South Wales 2320
AUSTRALIA

Richard Macey has been involved in testing, fault locating and repair of electrical cables since 1965. Firstly as an electrician in heavy industry, then generation followed by mining and since 1969, is a self employed engineer. Richard employs some 200 people in several locations throughout Australia, South Africa and India. In doing so, is responsible as the Group Managing Director for the repair of average 400 cables per week up and including 66kV. The service aspect of repairing cable is complimented with turnkey packages involving design, supply of switchgear and transformers, as well as development of a 100% waterproof coupler system.

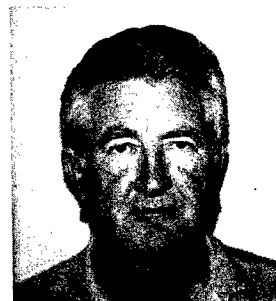
Richard's interests include a Harley Davidson Motor Cycle and flying a 2 x 4 meter wingspan radio controlled B24 Liberator - and he isn't even American !

of the fault by investigating as small as 0.2% of the cable length should now be quickly achievable and is normally done using a surge generator or capacitor discharge unit that will develop a acoustic discharge across the spark gap.

The acoustic level is typically determined by the resistance and spark gap stability as well as the amount of energy being delivered to the fault - that energy being measured in joules (watts per second). The typical energy level of capacitor discharge units is 400 joules and when discharged, in an average time of 0.01 seconds, an acoustic signal develops as a result of some 40kVA being discharged.

However, as most fault paths are unstable, various acoustic results are achieved and it may well be necessary to use a scismophone (acoustic detector) when dealing with a buried cable to amplify the result.

In **Conclusion**, the 1990's have seen the abandonment of preconditioning and introduction of faster methods of pre locating. Although only some of the many possible methods of locating have been described, the basic principals remain the same and the final choice of equipment is often a compromise as to the skill of the operator and what is practically available. The ultimate success depends very much upon the attention to detail by the responsible person and there is no magic crystal ball!



IMPACT OF POWER VARIATION ON 3RD ORDER PASSIVE INTERMODULATION OF COAXIAL RF-CABLES AND THEIR CONNECTORS

Hartmut Gohdes

RFS kabelmetal, Division of kabelmetal electro GmbH, D-30179 Hannover, Germany

Abstract

Aim of the work was to find out the relationship between the 3rd order intermodulation-signal generated by cable assemblies and the stimulating power level. The theoretical relationship will be described, and statistically evaluated results of measurements of different types of cable assemblies will be presented and discussed. Possible reasons and proposals for further investigations will be given.

Introduction

During the last years, wireless telecommunication has increased significantly. Therefore the available frequency-spectrum has to be used efficiently. Beside the increase of information rate by using digital information transfer and multiplex-modulation, smaller band- and channel-spacings are possibilities to reach this aim. This bears problems to solve.

One of those problems is distortion caused by 3rd order intermodulation products of passive devices (IM3-products).

For that reason, 3rd order intermodulation is a topic of growing interest. Manufacturers and customers are discussing IM3 values, which are determined by different test-methods, at different frequencies, and at different power levels of the stimulating signals.

Generation of passive intermodulation

IM-products are generated in non-linear devices at all possible sum- and difference-frequencies of two or more signals. They are disturbing, if they fall into the band of operation. Often this is the case with IM-products of odd order. 3rd-order IM-products are generated at the frequencies $f_{im3} = 2 \cdot f_1 \pm f_2$, and are generally of higher level than those of 5th and higher orders.

If f_{im3} falls into a receiving-channel, this signal is disturbing transfer of information.

IM-products can be generated by active components (amplifiers etc.) and passive components like filters, duplexer, RF-cables, waveguides and antennas.

Sensitivity to unwanted signals is very high in passive components, if they are used for transmission and reception at the same time. Unwanted signals caused by the high power transmitters can disturb low level received signals.

If we assume two signals:

$$u(t) = U_1 * \cos(\omega_1 t) + U_2 * \cos(\omega_2 * t + \varphi) \quad (1)$$

and a characteristic of the device:

$$i(t) = a_1 * u(t) + a_2 * u^2(t) + a_3 * u^3(t) \quad (2)$$

intermodulation of 3rd order is generated among signals of other frequencies:

$$i_3(t) = c_{12} * U_1 * U_2^2 * \cos(2\omega_2 - \omega_1)t + 2\varphi) + c_{21} * U_2 * U_1^2 * \cos(2\omega_1 - \omega_2)t - 2\varphi) \quad (3)$$

If the power series is expanded to powers higher than 3, it can be observed, that coefficients of higher power also contribute to the 3rd order IM-level, because they also produce signals of $2\omega_2 - \omega_1$ and $2\omega_1 - \omega_2$ [1].

The amplitude of the IM3-signal is depending on the amplitudes of the input signals. If c_{12} and c_{21} are considered as constants and contribution of coefficients of higher power is neglected, equal variation of the signal-power of both signals causes three times the power variation of the IM3-signal. This relationship can be displayed as a straight line with a constant gradient of 3 in logarithmic scale. If there is any contribution of IM from higher power coefficients, the gradient will deviate from this value.

Sources of intermodulation are considered as point sources inside the device under test. Hence, the IM3-signal is propagating in both directions of a two-port device.

Measurement

Measurement of passive IM3 is a comparatively new challenge to the industry, so standardization of techniques and procedures is in process actually in IEC TC 46 WG 6. RFS kabelmetal is contributing to these international standardization efforts.

IM3-products of passive components are usually of much smaller level than those of active components. IM3 products of cable assemblies are typically in the range of -150 dBc to -160 dBc. Hardware for the test set-up must be selected carefully or built by oneself to achieve lowest self-intermodulation.

The measurements were performed with two different set-ups. One for the 900 MHz range (GSM) and one for the 1800 MHz range (DCS 1800). In both cases reflected intermodulation was measured. To prevent high intermodulation generation, like it is the case with lumped terminations, the DUT was terminated by approximately 120 m of 1/4" cable with a soldered connector. The filters and duplexers are selected from standard GSM- and DCS 1800 hardware. The block-diagrams are shown in figure 1 and 2.

Synthesizer-sources are locked to the frequency reference of the spectrum-analyzer to perform accurate zero-span measurements. Each signal is amplified by a 100 W power-amplifier to the desired level. Combination of the two signals is done in the 900 MHz-set-up by two filters and tuned lines, in the 1800 MHz set-up by a 3 dB-hybrid. Therefore the 900 MHz-set-up works only with a particular pair of frequencies, while the 1800 MHz-set-up can be run with different pairs. The task of the duplexer is to separate the low-level IM3-signal from the high-level stimulating signals. It is one of the most critical parts of the set-up. It must provide only the lowest and the most stable IM3-products. The duplexer is supplying the stimulating signals to the DUT, which is connected to the other critical component, the cable-load. It must also be of very low intermodulation. The portion of the IM3-signal, which is travelling back into the duplexer, is separated, filtered and amplified before it is displayed on the screen of the spectrum-analyzer. The IM3-frequency is 914 MHz, or 1760 MHz, respectively. The LNA allows a fast and low noise signal detection. Spikes of a short risetime can still be detected with those set-ups.

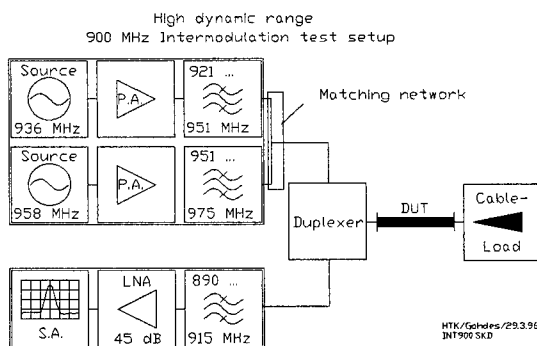


Figure 1: 900-MHz IM3-set-up

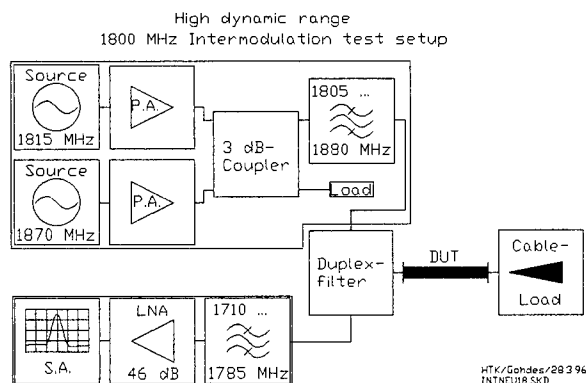


Figure 2: 1800 MHz IM3-set-up

Calibration of the set-up is done in two steps: The gain of the IM3-path is measured with a calibrated source connected to the testport, and the level of the stimulating signals is adjusted with a calibrated powermeter connected to the testport.

Once the set-up is calibrated, IM3-level of the system itself without a DUT must be measured. The self-intermodulation limits the dynamic range of the measurement system. In table 1, the level of self-intermodulation for every input-level is noted.

900 MHz [dBm]	37	40	43	46	48
System IM3 [dBm]:	-134	-128	-123	-113	-107
1800 MHz [dBm]	37	40	43	46	-
System IM3 [dBm]:	-136	-134	-128	-122	-

Table 1: power level of each signal and level of system-IM3

Self-intermodulation and measurement error introduce measurement uncertainties into the measurement. In this case, measuring intermodulation of 10 dB more than the system-intermodulation at 43 dBm input levels causes a measurement error of approximately $\pm 5,5$ dB. If relative measurements are done, the measurement error is reduced to about ± 2 dB, because system IM3-level is subtracted nearly completely from the results. Noise of the spectrum-analyzer and level uncertainty of the sources remain.

To minimize the influence of measurement error and piece-to-piece deviation, a number of 20 - 30 assemblies of each type was tested. It was noted, that intermodulation-level changed by some dB, if the same DUT was connected and measured several times. For that reason, all power levels were adjusted and stored into the memory of the synthesizers, before the measurements were started. Measurements were done by connecting the DUT to the set-up once and measure it at every stored power-level.

First measurements were taken with 0,5 dB steps. Due to the measurement uncertainty, the changes of intermodulation were too small to give reliable results. Since 0,5 dB steps gave no further information, 3 dB-steps respectively 2 dB steps were used instead. The power levels are shown in table 1.

The different types of assemblies are shown in table 2.

Only devices with 7-16 connectors were tested, because IM3-performance of this connector-type is substantially better than of other connector types. For low-intermodulation applications, this connector will be chosen in most cases.

	Type	Length	I.C. material	O.C. material	I.C. contact	O.C. contact
1	High flexible jumper 1/2"	2 m	copper clad aluminium wire	Copper	Soldered	Soldered
2	High flexible jumper 1/2"	2 m	silver coated copper strand	Copper	Soldered	Soldered
3	jumper 1/2"	2 m	copper wire	Copper	Soldered	Soldered
4	High flexible jumper 1/2"	1,5 m	copper clad aluminium wire	Copper	Spring Finger	Flared
5	jumper 1/2"	1,5 m	copper wire	Copper	Spring Finger	Collet
6	cable 7/8"	1,5 m	copper tube	Copper	Spring Finger	Collet

Table 2: Tested cable assemblies

Measurement results and evaluation

The evaluation procedure for assembly type 1 will be described in great detail. The results of the other types were evaluated similarly.

Thirty samples were tested. Mean value and standard deviation were calculated for each power-

level. Figure 3 shows the results of the 900 MHz measurements in a diagram, figure 4 those of the 1800 MHz measurements. Mean values and standard deviation of the measurements are presented by the triangles and the whiskers. A linear regression line is calculated from all the mean values. It is plotted as "linear (Assembly Type 1)". This allows a visual check of the correspondence between measured values and regression line. Assuming that the relationship between change of stimulating levels and change of IM3-level is constant, this relationship is characterized by the gradient of the regression line.

R^2 is a measure of certainty, which also gives information about the correspondence between data and regression line.

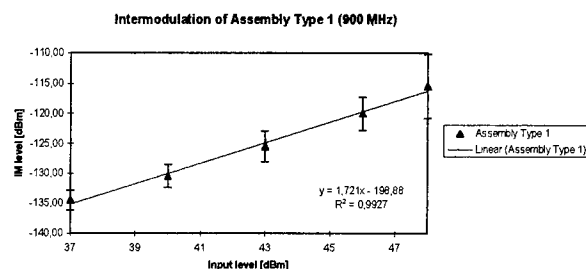


Figure 3: Intermodulation 900 MHz of Assembly type 1

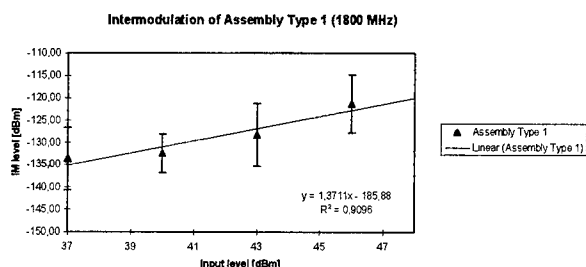


Figure 4: Intermodulation 1800 MHz of Assembly type 1

Because assembly 1 is a specially IM3-optimized product, IM-values appear very low and stable. They are very close to the system dynamic. Standard deviation of the measurements with one power level is higher at 1800 MHz than at 900 MHz.

Assembly 4 is made of the same cable-type as Assembly 1, but with non-soldered connectors. The contact zone of the helically corrugated outer conductor is not so well defined as it is for the soldered assembly type 1. Also the inner conductor spring finger contact causes more IM3 as its soldered counterpart. This type of assembly shows the highest level of IM3 and the maximum standard deviation of all tested types. For that reason, we can achieve the best measurement accuracy with this type.

Like for assembly type 1, standard deviation for 1800 MHz is higher than for 900 MHz.

Figure 5 and Figure 6 show the results of the measurements and the regression line.

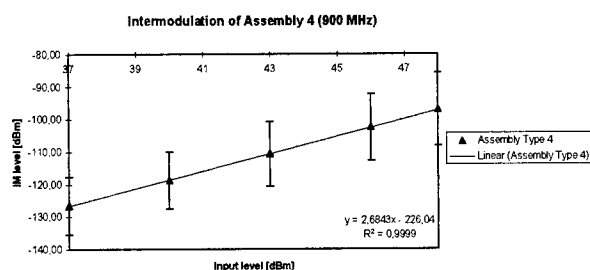


Figure 5: Intermodulation 900 MHz of Assembly type 4

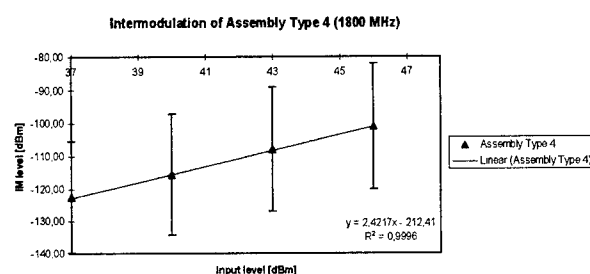


Figure 6: Intermodulation 1800 MHz of Assembly type 4

Table 3 and Table 4 show the number n of tested devices, the gradient of the regression-line and R^2 for all tested types of assemblies:

Type	n	lin. reg.	R^2
Type 1	30	1,72	0,99
Type 2	20	2,0	1,0
Type 3	20	1,48	0,99
Type 4	20	2,68	1,0
Type 5	20	2,17	1,0
Type 6	20	1,79	1,0

Table 3: Regression gradient 900 MHz

Type	n	lin. reg.	R^2
Type 1	30	1,37	0,91
Type 2	20	2,27	1,0
Type 3	20	1,36	1,0
Type 4	20	2,42	1,0
Type 5	20	1,96	0,98
Type 6	20	0,83	0,94

Table 4: Regression gradient 1800 MHz

Discussion

The quality of approximation of the regression-line is indicated by the measure of certainty (R^2).

For most types, R^2 is very good and near to 1. Assembly type 1 has a worse R^2 of 0,91 at 1800 MHz, and R^2 of assembly type 6 at 1800 MHz is 0,94.

In both cases, the measured IM3 is very close to the noise-floor. Thus the measurement uncertainty for 37 dBm stimulating power is very high. If the IM3-values of 37 dBm are excluded from the data of these two data sets, R^2 is increasing.

Table 5 shows the results of the corrected 1800 MHz measurements.

Type	n	lin. reg.	R^2
Type 1	30	1,86	0,98
Type 2	20	2,27	1,0
Type 3	20	1,36	1,0
Type 4	20	2,42	1,0
Type 5	20	1,96	0,98
Type 6	20	1,08	0,99

Table 5: Corrected Regression gradients at 1800 MHz

Now the linear regression-line-model seems to describe the examined behaviour sufficiently well, but still the calculated gradient is not constant.

Neglecting the contribution of coefficients of higher power than 3 at the frequency of the 3rd order, the expected gradient is 3.0

Among the different types of assemblies and even between the two frequency-ranges, remarkable differences can be observed. The gradient of the regression line varies from 1,08 up to 2,68.

There are several possible reasons:

1. The factors c_{12} and c_{21} are not constant and depending on the applied power of the stimulating signals.

In [2] a variety of mechanisms are given, which can be responsible for the generation of IM3-products. These effects are different in their characteristic dependency on the stimulating power. It is most likely, that for every stimulating power-level a different combination of those effects are dominant. Hence, c_{12} and c_{21} are a result of the actual combination of effects.

2. Contribution of the higher power terms at third order frequencies is not negligible.

Expansion of the power series to an odd power higher than 3 shows, that the terms of higher odd power also produce mixing signals at third order IM-frequencies. The IM3-signal will be influenced by each of the different contributors of the higher powers. Figure 5 shows an example for the superposition of a positive 3rd power coefficient (Pout1) and a negative 5th power coefficient (Pout2). The result is plotted as 'Poutges'. An extreme value can be observed at the point of intersection of 'Pout1' and 'Pout2'. Left of it the gradient is less, and right of it more than 3.

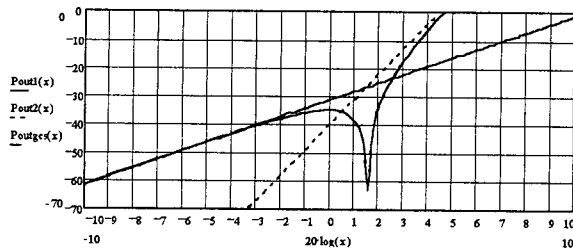


Figure 7: Influence of negative higher order coefficient

3. IM3-level is depending on the duration of RF-penetration.

The devices were tested with consecutively increased power-levels. It might be possible, that the IM3-level changes during the test due to heating- or 'burn in'-effects. However, this is most unlikely, because some tests with consecutively decreased power-levels gave the same results as with increased power-levels.

CONCLUSION

6 Types of cable assemblies of different construction and IM3-behaviour were selected. 20 to 30 samples of each type were measured. The relation between IM3-level and stimulating power-level was characterized. Statistical evaluation of the result shows an individual behaviour of each type at each frequency-range. Some possible reasons were given.

The conclusion of the experiment is, that only those IM3-values of similar stimulating signal-level can be compared.

It is not allowed, to calculate IM3-levels for other stimulating signal-levels, in order to make measurements at different power levels comparable.

It is highly recommended, to adjust the level of the stimulating signals very accurately for any measurement.

Some possible explanations have been given. To prove those theoretical considerations, further examinations are necessary. Especially test-set-ups with higher dynamic ranges and higher power-levels promise to give deeper understanding.

ACKNOWLEDGEMENTS

The author would like to thank Dr. Nagel and Mr. Fischer of RFS kabelmetal for encouragement to write this paper and for the fruitful discussions.

Also Mr. Schumacher and Mr. Bernasch have to be mentioned, who made innumerable IM3-measurements.

REFERENCES

- [1]: "A Study Of Multipaction in Multicarrier RF Components", J.S. Petit, A.D. Rawlins, p. 41 ff.
- [2]: "A Study Of Passive Intermodulation Interference in Space RF Hardware", A.P. Foord, A.D. Rawlins, p. 60 ff.

Author

Hartmut Gohdes
RFS kabelmetal
Kabelkamp 20
D-30173 Hannover
Germany



Hartmut Gohdes was born in 1963. He studied electronics at the Fachhochschule Hannover and obtained his Dipl.-Ing. (FH) degree in 1991. In the same year he joined RFS kabelmetal as a development engineer, where he is responsible for the design of transmission lines. He is engaged in the field of RF-measurement, especially the measurement of passive intermodulation.

IMPEDANCE REGULARITY OF COPPER DATA CABLES: HOW TO BE SURE

Daniel Prudhon and Martin French
ALCATEL (Data Cable), Paris, France

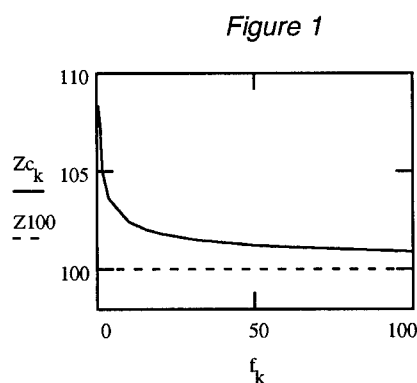
ABSTRACT

Analysis of work leads us to believe that the random aspect of an input diagram vs. frequency of a balanced pair can mask some periodic defects. The main consequence being that certain cables, after installation, can show abnormalities with Return Loss and attenuation. An analysis rule of the impedance trace has been established to avoid on-site problems

IMPEDANCE MEASUREMENT

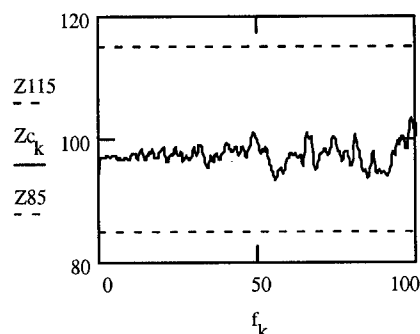
With data cables, the characteristic impedance is generally obtained from the input impedance measurement at different frequencies. This test is commonly made with an S-parameter test. This is in fact a reflection measurement and the results will therefore fluctuate with the frequency.

The theoretical variation of the characteristic impedance of a pair is a curve tending toward an asymptote, as shown in fig.1,



However, in reality the result of the measurement seems to present some random variations around the theoretical line (fig.2).

Figure 2



An examination of such a diagram leads us to believe that the fluctuations of the characteristic impedance with frequency may actually be random. The conclusion therefore is that the cable does not present any periodic structural irregularities.

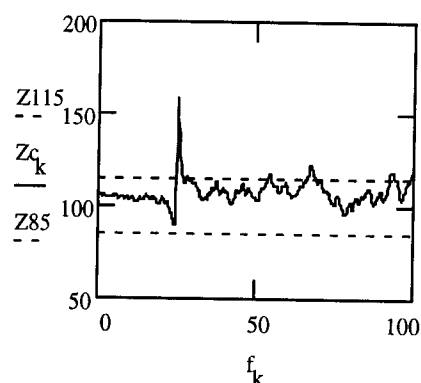
However, we may have to be more cautious, as some of these periodic defects could actually be hidden amongst this "random noise".

THE PERIODIC DEFECT

A physical periodic irregularity on the pair, like a variation of the distance between two wires, will generate a peak on the impedance diagram. This corresponds to local variations of the impedance of the pair.

Periodic fluctuations will generate reflection on the pair. These reflected signals will be in phase for frequencies corresponding to the distance between irregularities. Such a defect gives an impedance diagram as shown on Fig. 3.

Figure 3

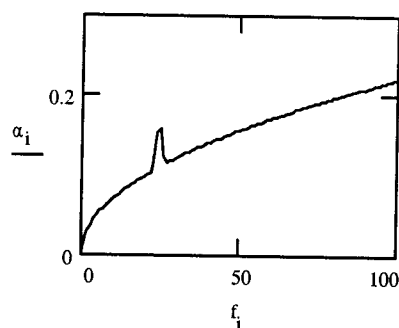


The height of the peak depends on the type of the physical defects, their number, the distance to the first one, the distance between two adjacent defects and the size.

THE HIDDEN PERIODIC DEFECT

When the defect is as shown in Fig. 4, it is very simple to see. However sometimes it could be far less obvious to detect, particularly during the manufacture of the cable.

Figure 4



If the irregularity is apparent over the entire length of the pair, a simple measurement from one extremity will show it. Unfortunately, the defects are generally periodic only on a part of the length. For example we could have 30 to 100m of pair without any problem and 10 or 20 irregularities over the next 50 m. In this case the reflected signal by the local impedance variations will be too weak to be seen from the origin of the cable.

It gives much smaller variations on the impedance diagram, that could be concealed amongst the noise generated by all of the random irregularities of the pair. With this type of defect, even if it is hidden amongst the noise of the impedance diagram it could in fact create a peak of attenuation

as seen in Fig. 4. This could give a diagram with an absorption peak at one specific frequency.

If the period of the irregularities is very precise, then as a consequence the width of the peak will be very narrow and the height will be high. If the period varies slightly, then the peak will be broader but smaller. Its actual frequency depends on the periodicity of the physical defect of the pair.

REQUIREMENTS OF THE STANDARDS

The usual nominal impedance for data cables is 100 Ohms with the tolerance given by the major Standards being $\pm 15\Omega$. However some of the Standards recommend the use of a smoothing function to plot the Impedance trace. Within the Standardisation committees today they are now moving towards specifying a Return Loss measurement to characterise the fluctuation of the input impedance of the pair.

We will not get into the discussion on whether the test should be a simple Return Loss or a Structural Return Loss. We will only discuss if it is logical or not to ask whether there is a worsening impedance regularity with an increasing frequency.

Table 1

	1 to 20 MHz	20 to 100 MHz
Return Loss (dB)	23	$23 - 10 \log (f/20)$

Values of " structural return loss" proposed in ISO/IEC 11801 and TIA/EIA 568A

Table 2

Frequency in MHz	1	10	20	31,25	62.5	100
Return Loss (dB)	23	23	23	21	18	16

Calculated values of structural return loss

A lower value of Return Loss means more reflected power and therefore a worse quality of the trace. At 100 MHz, the trace can be rougher than at 1 MHz.

The transmission media can actually be worse and have to carry higher bit rates.

At the very least the impedance should have the same smoothness all over the bandwidth of the channel and as the cable is the longest part of the physical link between active equipment we have to

require the same impedance regularity from 1 up to 100MHz.

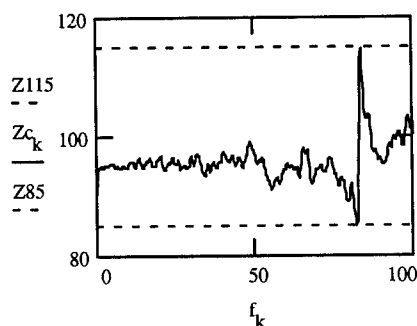
THE SEARCH FOR THE PERIODIC DEFECT

We have seen previously, that the safest way to detect a periodic defect is to verify there are not any obvious abnormalities in the attenuation trace. Unfortunately, it is difficult to measure the attenuation of a pair up to 100 MHz on a length longer than 300 metres. Therefore there is a real problem with cables over this limit.

The only remaining possibility is to analyse the diagram of Input Impedance vs Frequency. When the diagram is like Fig. 3, the defect is also obvious.

However, an impedance trace, as seen in Fig. 5, can be moved into a very large peak, just by cutting a few cm's off the cable.

Figure 5



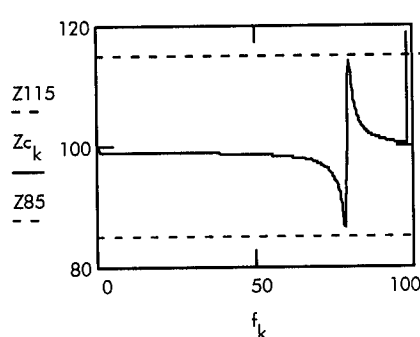
This phenomena is well known by the manufacturing teams within our production units. A pair with a poor impedance peak can be rectified by just cutting a few metres off. A new test is performed and the results become good!

To explain this, we will take a very simple case :

We have a pair with one parameter - for example, the outer diameter of one wire - that varies in a sinusoidal way. The other parameters are constant and the period of the variation is 1.2 m

This case is simplified to avoid the noise due to the other moving parameters. Depending on the amplitude of the periodic variation we obtain a diagram as shown in Fig. 6.

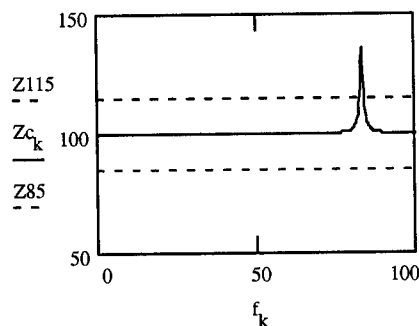
Figure 6



Even with a small perturbation at around 83 MHz, the result stays inside of the tolerance of $\pm 15\Omega$. (between -14 and +14 Ω)

But if the measurement is taken a little bit further down the pair then the impedance regularity becomes out of the limits, with a peak of 134 Ω .

Figure 7



So the question is obvious - is the pair good or is it bad?

The actual standards do not give really the answer.

THE VIRTUAL PAIR

To go further in this analysis, we decided to create a mathematical model representing the fluctuation of the input impedance of a pair with structural local variations. To keep in fashion, we called this project "the virtual pair".

Our first idea was to calculate the dimension of the local irregularities of the pair and to be able to see them on the wires, because obviously, it seems easier to look after something when you know the size.

The first model we made considered two types of irregularities: the periodic and the random. The

study of the input impedance based on a single point of reflection has been presented previously by Harold W. Friesen, so the model for random defects was established.

Regarding the periodic irregularities, we used a Fast Fourier Transform (FFT), to go from the time domain (corresponding to the physical location of defects on the pair) to the frequency domain (giving a reflection coefficient vs frequency).

Another difficulty was to include the attenuation of the reflected wave in the calculation.

This mathematical representation gave very good results, the shape of the obtained diagram was close to the reality. But unfortunately we have physically seen only few periodic defects, and the correlation between the rough estimate of the size of the irregularity and the measured peak of impedance was not perfect.

Further investigations conducted on a new model based on strange attractor. This new representation based on the theory of chaos seems to fit better with the reality. This let us think that there is some organisation behind this apparently random diagram of an impedance versus frequency.

THE IMPACT OF A LOCAL DEFECT

Using this new model, we have calculated the impact of a local defect on the pair in two different cases:

- one single defect
- a periodic defect

Case of a single defect :

In the table below, we give the influence of a single local irregularity of impedance.

Table 3

Distance to the defect	1 m	10 m	30 m
size of the defect i.e. variation on the insulation diameter	+/- 0.3mm	+/- 0.3mm	+/- 0.3mm
size of defect in local impedance variation	10 Ω	10 Ω	10 Ω
Amplitude of Zc variation input impedance	+/- 9 Ω	+/- 8 Ω	+/- 7 Ω

Case of a periodic defect:

In the chart here below, we give the impact of a very small variation of the diameter of insulation on an insulated wire of a UTP of 100 Ω of impedance.

Table 4

Periodicity of the defect	10 m	1.2 m	10 m	1.2 m
size of the defect i.e. variation on the insulation diameter	+/- 0.85 μ m	+/- 0.85 μ m	+/- 0.5 μ m	+/- 0.5 μ m
size of defect in local impedance variation	1.5 Ω	1.5 Ω	1 Ω	1 Ω
frequency of the impedance irregularity	10 MHz	83 MHz	10MHz	83MHz
minimum amplitude of the input impedance	86 - 114 Ω	60 - 140 Ω	91 - 109 Ω	73 - 127 Ω
maximum amplitude of the input impedance	134 Ω	240 Ω	122 Ω	176 Ω

A tiny irregularity may create a very high peak on the impedance diagram. A perfectly periodic variation of ± 0.5 mm on the insulation of a wire may create an abnormality of impedance up to $\pm 60\Omega$.

At the other extreme, a local single irregularity has a very limited influence on the impedance regularity of a pair.

THE OTHER PERIODIC DEFECT

Our mathematical model led us to believe that the main origin of impedance irregularities are periodic. In our manufacturing machines there are a lot of revolving parts able to create different frequencies, by their different sizes and speeds and by composition of different sources to create resonance frequencies for example. The cause of an impedance peak could actually be a composition between different frequencies and this certainly doesn't simplify the analysis of the problem.

The search of these frequency generators is very difficult, but a careful study may be conducted to find out the main sources of problems. Generally the identification of less than 10 critical points is enough to stabilize the impedance regularity of the cable. Different construction of cable may improve the stability of the impedance, and in this case the number of factors to control could be less.

THE SOLUTIONS

The first problem to solve, is to identify on the impedance diagram, the "hidden periodic defects". They have a special shape on the curve (Fig. 6). A careful analysis permits us to find it, and afterward, a very simple calculation will give the worst predictable case.

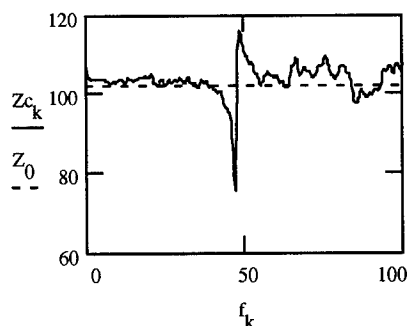
Here is a typical input impedance diagram given by a periodic defect. To calculate the worst impedance peak (Z_{worst}), we have to know the maximum (Z_{max}) and the minimum (Z_{min}) of the impedance abnormality, as shown in the Fig. 8.

The formula here below gives Z_{worst} .

Equation 1

$$Z_{\text{worst}} = Z_0 \cdot \frac{1 + \delta}{1 - \delta} \quad \text{with} \quad \delta = \frac{Z_{\text{max}} - Z_{\text{min}}}{Z_{\text{max}} + Z_{\text{min}}}$$

Figure 8



This calculation permits us to be sure that the cable contains no periodic defects able to have an negative influence on the transmission of data

CONCLUSION

The model of the input impedance of a balanced pair is a chaotic system rather than a truly random distribution. Therefore a careful examination may actually help to forecast potential problems. Traces such as those shown in figures 3, 5 and 8 are an indication of such latent problems but an easy calculation will predict the worst peak of impedance on a length post installation.

AUTHORS

Daniel Prudhon, was born in France in 1943 and received his Engineering degree from the University of Lyon in 1965. From 1966 to 1967 he taught Mathematics and in 1968 became a member of a technical committee working on the jointing of long distance voice cables. He has worked for Alcatel Cable for over 8 years now and is heavily involved in cable design, the development of processes and materials and cable measurement techniques. Daniel holds nine patents in his field of expertise. He is now responsible for R&D within Alcatel (Data Cable).



Martin French has been in cable manufacturing for over 11 years, five having been spent within Alcatel Cable. His degree, from the University of North London, was in Polymer Science, specialising in Low Smoke Zero Halogen materials. He is the European Product Marketing Manager for Alcatel (Data Cable)



EMC COMPLIANCE TESTING OF LINK TERMINATION IN LOCAL AREA NETWORKS.

Daniel Prudhon and Martin French
ALCATEL (Data Cable), Paris, France

ABSTRACT

The screening efficiency of the cable and of the connector can be measured individually. Technical groups are now working in different standard committees to define EMC tests on Links or Channels. Such tests are being made in a laboratory environment. Up to now realistic there has been no way to verify the efficiency of the interface between the cable and the connector. This is especially true after the cabling has been installed. A tester has now been developed to measure the quality of the screen boundaries.

TEST ON CABLES AND CONNECTORS

The quality of the screen of a cable is generally given by a measurement of its Transfer Impedance. The principle of the test is to inject a current outside of the shield of the cable and to measure the induced voltage inside of the cable along the conductors. The Transfer Impedance is calculated as the ratio between the voltage and the current. As a 'rule of thumb', the smaller the Transfer Impedance, the better is the shielding of the cable. The actual test method is defined in IEC96-1.

The measurement of Transfer Impedance is made on a very short length of cable and can be tested at a maximum frequency of roughly up to 100 MHz. For higher frequencies the cable to be measured is so short that the precision of the measurement becomes insufficient.

As has been stated before, Transfer Impedance is a very good way to characterise the quality of a screen, but only really between 30 to 100 MHz.

The Standards dictate values at 1 and 10 MHz and the requirement for 100MHz is still for further study.

As with the cable, the same type of measurement can be made on a shielded connecting hardware,

with similar remarks on accuracy and frequencies as above.

Transfer impedance is a good way to qualify the theoretical efficiency of a screen on a short length of cable, with two main disadvantages:

- measurement limited to 100 MHz
- only on a very short length.

TEST WITH AN ABSORBING PROBE

To understand and possibly avoid these problems, in the beginning of 1995, we began a study on measurements with an absorbing clamp. Another goal was to have a tool to measure the EMC behaviour of shielded and unshielded cables in a wider range of frequencies. A presentation on this subject will be made by Mr Eric Lawrence of Berk-Tek.

The test to measure EMC behaviour is easy to conduct, and the obtained results on shielded cables fit with transfer impedance measurements. It could also be used to measure the bonding of the screen of the cable to the connecting hardware. Another advantage of this type of test is that it could be conducted up to 1GHz in differential mode and higher in common mode.

However it is difficult to use this type of method to measure the termination after installation as the clamp is cumbersome and may be disturbed by ambient electromagnetic noise.

THE TEST ON THE LINK

Currently manufacturers of active equipment are carrying out their EMC tests with cabling that has the most favourable configuration, to ensure full compliance with all of the different regulations. However this is not a realistic and practical approach. To provide better confidence to the end user, a standardization committee is now working on a configuration of a basic link for EMC testing of active equipment. (ISO/IEC, JTC1, SC25, WG3).

The test set up contains 90 metres of horizontal cable coiled and laid up on different planes with differing bend radius. It is designed to represent the worst possible configuration of a cable installation with regard to EMC performance. It has to be installed on a turn-table inside of an anechoic chamber.

This is a typical test set up that is performance in a laboratory environment, to qualify active devices for data transmission. It should be possible to use it to qualify the performances of cables and connectors together. However, only a few labs will construct such a test set up.

BONDING THE SCREEN TO THE CONNECTOR

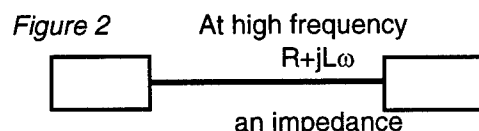
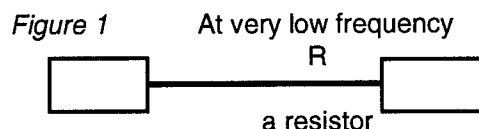
Today it is easy to find on the general market screened cables and connectors that have very good shielding efficiencies. Assuming this then the only remaining problem is to be sure that the mounting of the connecting hardware will be properly done. Transmission performance may be measured and controlled with an hand held tester, and many excellent devices are available, but with regard to the EMC behaviour of the Link, you have only to hope that the connection is good. Up to now there has been no way to control this after installation.

Consequently this is why we decided to launch a study on a EMC field tester.

THE PRINCIPLE OF CONNECTION AT HIGH FREQUENCIES:

To bond together two points, we generally use a copper wire. The electrical parameter we take in account is the resistance of this wire.

At high frequencies we have to consider an additional parameter: the inductance of the wire. In this case, we have an impedance of connection, which will increase with the frequency.



Resistance & impedance of 10mm of drain wire
In the table below we give the resistance and the equivalent impedance of a 10mm length of copper drain wire of 0.5mm. The resistance in direct current is 0.87 m Ω /10mm

Table 1

frequency (MHz)	resistance m Ω /10mm	impedance m Ω /10mm
1	1,9	56
10	5,5	177
100	16,8	560

If we compare the impedance of a 10mm long drain wire with the transfer impedance of a FTP cable it corresponds to approximately 1 metre of cable.

ACCEPTABLE LENGTH FOR A DRAIN WIRE UP TO 100 MHZ

If a drain wire is too long it will act like an antenna and radiate onto the shield of the cable.

Some people will state that the length of inefficiency of a connection is $\lambda/30$. A drain wire longer than 100mm is not efficient at frequencies higher than 100 Mhz.

To divide a disturbance by a factor of 10 is generally sufficient to solve a lot of EMC problems. To obtain this level the drain wire should be shorter than $\lambda/150$.

This means only 20mm at 100 MHz.

ON SITE CONTROL

To keep the efficiency of the shielding high, the quality of its connection should be controlled. The first point to check is the continuity and this is possible with the existing testers. The second point is the quality of the connection at high frequencies and this is much more difficult. One solution could be, for example, to check that the drain wire is short enough. However this is tedious, time consuming and expensive to take off each outlet. A careless dismantling of the outlet could also damage the link.

This control remains the weak point of the EMC compliance of an installed link.

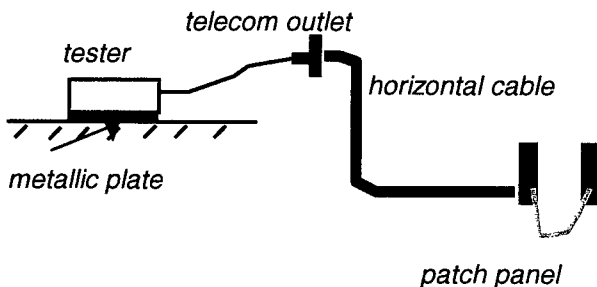
THE FIELD TESTER

A tester as been developed to check the efficiency of the shield bonding to the connector.

If a signal is injected externally onto the shield, then the received level on the conductors inside of the cable corresponds to the quality of the shielding. This is the principle of a transfer impedance measurement.

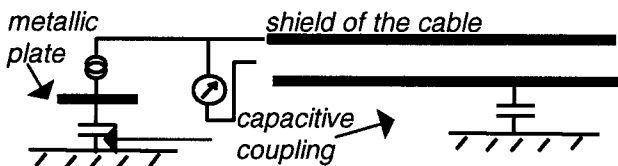
Practically, the tester is laid on the floor, and is capacitively coupled to the structure of the building through a metallic plate. A pulse is applied between the plate and the ninth pin of the connector (the point to bond the shield). The system measures the received level between all the conductors bonded together and the shield. This test corresponds to a measurement in common mode of the shielding effectiveness.

Figure 3



The main problem to solve, was that the capacitance of coupling to the structure of the building as this depends on the type of floor. A wooden floor gives a worst coupling than a concrete floor.

Figure 4



The initial prototype measured the capacitance between the plate and the ground, and then adapted the size of the pulse to this value. To solve this problem in the actual prototype, the system is working in a constant current; this make the electronics of the tester easier to produce and more reliable.

The width of the pulse is chosen to limit the measurement at the connection point.

RESULTS

Tests have been made to compare the results obtained with the tester and shielding efficiency measured with an absorbing probe.

The actual version of hand held tester has only indicating light-emitting diodes (LED). Each step corresponds to 3 dB.

Table 2 gives the results of a test made with a four pair cable with an overall shield made with a wrapped aluminium foil (FTP) and a 0.5mm drain wire . The connector is a classical 8 pin RJ 45 with a ninth pin to connect the drain wire. There is no shielding around the connector.

Table 2

Length of the drain wire (mm)	31	22	10
screening efficiency (dB)	13	20	27
number of segments (corresponding dB)	3 (15)	4 (20)	5 (25)

correspondence between screening efficiency measured with an absorbing clamp, and values obtained with the hand held tester.

This first series of test has been conducted in our laboratory with the tester laid on a cement floor. The results fit together, and seem to be precise enough for on site control.

Tests on a wooden floor:

To validate the principle of operation in a constant current, measurements with the same configuration have been made inside of an old building with wooden floors, where the coupling to the structure of the premise is very weak.

The obtained results are slightly less precise, and between measurements we can sometimes have one segment (3dB) of difference.

CONCLUSION

The requirement for the design of the hand held tester is:

- low cost
- usable on site
- ability to detect misconnecting of the shielding
- immunity to outside disturbances.
- robustness

The target price of the equipment has been reached and the precision of the test is accurate enough to detect a bad shielding bond.

This tester will permit the verification on site that the bonding of shielding has been properly done. This is an excellent and safe way to warranty to the end user that the cabling system will be in compliance with the EMC rules.

AUTHORS

Daniel Prudhon, was born in France in 1943 and received his Engineering degree from the University of Lyon in 1965. From 1966 to 1967 he taught Mathematics and in 1968 became a member of a technical committee working on the jointing of long distance voice cables. He has worked for Alcatel Cable for over 8 years now and is heavily involved in cable design, the development of processes and materials and cable measurement techniques. Daniel holds nine patents in his field of expertise. He is now responsible for R&D within Alcatel (Data Cable).



Martin French has been in cable manufacturing for over 11 years, five having been spent within Alcatel Cable. His degree, from the University of North London, was in Polymer Science, specialising in Low Smoke Zero Halogen materials. He is the European Product Marketing Manager for Alcatel (Data Cable)



RELATING COUPLING ATTENUATION TO SHIELD TRANSFER IMPEDANCE AND PAIR BALANCE IN DATA COMMUNICATIONS CABLES

Eric J. Lawrence¹, David C. Hess², Michiel Pelt³

¹Berk-Tek, New Holland, Pennsylvania; ²Alcatel Cabling Systems, New Holland, Pennsylvania; ³Alcatel Cabling Systems, Brussels, Belgium

ABSTRACT

This paper explores the relation of coupling attenuation to surface transfer impedance, a measurement of shielding effectiveness and demonstrates that pair balance is independent of shielding effectiveness. It also shows that both shielding effectiveness and pair balance contribute to coupling attenuation of a paired cable. Examples are presented of cables having independently varying degrees of pair balance and similar surface transfer impedance. The coupling attenuation of these cables have been measured and show the effect of pair balance on coupling attenuation as it is independent of changes in shielding effectiveness. Examples are also presented of cables having different levels of shielding effectiveness, measured by transfer impedance, but which have similar pair balance. The coupling attenuation results from these cables are also presented and show the effect of shielding effectiveness on coupling attenuation as it is independent of changes in pair balance.

INTRODUCTION

Coupling attenuation is gaining popularity as a method of characterizing the resistance to electromagnetic interference (EMI) of shielded and unshielded data communications cables.

A number of standards and draft standards refer to coupling attenuation and surface transfer impedance. Each method is pertinent and useful in certain situations. Coupling attenuation is valid for field-testing and is also a relatively quick method to evaluate the performance of the cable. Surface transfer impedance and pair

balance are more suited to cable parameter specification, development and qualification. Establishing a relationship between these parameters is useful for identifying cable with particular degrees of performance for specific system applications and provides additional information that will be useful in predicting system EMC (electromagnetic compatibility) performance.

PROTOTYPE CONSTRUCTION

In order to effectively demonstrate the theorized relationships between coupling attenuation, longitudinal balance and surface transfer impedance, cable prototypes needed to be constructed with differing degrees of balance and with differing degrees of shielding effectiveness.

Five types of samples were constructed for use in making measurements for presentation in this paper. The five types of samples consist of four twisted pairs manufactured using bare, annealed copper wires covered with a thermoplastic insulation material. The diameter of the conductors ranged from 0.51 mm to 0.57 mm depending on the prototype. The wide range of conductor sizes was the result of design decisions made to achieve the different balance characteristics. Table 1 describes the five types of samples.

Table1: Sample Types

Type	Description
A	Overall Shield, Shield Type 1, Typical Balance
B	Overall Shield, Shield Type 2, Typical Balance
C	Overall Shield, Shield Type 2, Worse Balance
D	Unshielded, Worse Balance
E	Unshielded , Typical Balance

Sample types "A", "B" and "C" employ an overall aluminum/polyester laminate shielding foil applied longitudinally over the twisted pairs. The foil tape is isolated from the four pairs by a thermoplastic tape. A stranded, tinned copper drain wire is located between the two tapes and is in constant contact with the aluminum side of the aluminum/polyester laminate tape. The samples were constructed such that type "A" and type "B" samples have similar balance characteristics, but exhibit different transfer impedance characteristics due to a difference in shield construction of the aluminum/polyester shielding tape. Similarly, type "B" and type "C" samples should have similar transfer impedance characteristics since they have the same shield construction, but they are expected to exhibit different balance characteristics.

The samples that were constructed to have typical balance are designed and manufactured such that they comply with ANSI/TIA/EIA-568-A requirements for category 5 cables. The samples that were constructed to have poor balance are similar to their corresponding samples with typical balance, except that the electrical performance parameters are not expected to comply with category 5 requirements. This is due to the intentionally poor balance of the individual pairs, which will adversely affect key electrical parameters. The effect of balance on near-end crosstalk, for example, has been previously explored. [1]

Sample type "D" and type "E" do not employ shields like types "A", "B" and "C" so transfer impedance, which is a measurement of a shield's performance, was not measured and is not applicable. These samples were constructed to have different degrees of pair balance as measured by longitudinal conversion loss.

Sample type "D" and sample type "C" were constructed to have poor balance as compared to their counterparts, sample type "E" and sample type "B", respectively. The poor balance is achieved by introducing differences between the two insulated conductors, which form each twisted pair. The design differences introduced into sample type "C" and sample type "D", in order to achieve degraded balance, were necessarily different from each other since sample type "C" employs an overall shield whereas sample type "D" is unshielded.

RESULTS

The purpose of this paper is to demonstrate that pair balance and shielding effectiveness of paired cables are independently related to coupling attenuation for data communication cables. Standardization work of these types of performance tests is currently in progress in standards committees. Therefore, it is necessary to document the conditions used by the authors to evaluate these parameters for use within this paper.

Longitudinal Conversion Loss

To quantify the balance of a twisted pair, the definitions and methods found in ITU-T recommendation G.117: Transmission Aspects of Unbalance about Earth (Definitions and Methods) [2] and recommendation O.9: Measuring Arrangements to Assess the Degree of Unbalance about Earth [3] were used. Within these documents, there are a variety of different methods, which are applicable for one or two port networks. This paper uses the longitudinal conversion loss (LCL) parameter, which is defined in ITU G.117 as the ratio of the longitudinal voltage to the transverse voltage expressed as a decibel for a one port network [2]. The longitudinal voltage (common mode) is applied to the same cable end as the transverse (or differential) voltage is measured.

This section of the paper presents the results obtained from the LCL testing on the various cable prototype samples. For each cable type, the longitudinal conversion loss was measured from 1 MHz to 100 MHz using 801 frequency points equally spaced on a logarithmic frequency scale. North Hills 0322BF-A BALUNs were used to measure the transverse signal and convert this signal to a longitudinal signal, which was measured using a Hewlett-Packard 8751A Network Analyzer.

Three samples for each of the five prototypes were prepared and measured. The samples were each one hundred-meters in length and were suspended in the air by plastic sheaves, which kept the sample isolated physically from itself as well as any metallic or conductive elements.

Each of the three samples from each cable type was measured for LCL on each of the four pairs. The values of the four pairs for each sample were averaged together in the voltage domain and then converted into decibels. The worst case balance was determined by using the minimum value of the three samples at every frequency point, which had been measured. The average or nominal balance for the sample type was determined by averaging the three samples together in the voltage domain at every measured frequency and converting the resultant average voltage ratio into decibels. The individual values had to be transformed into the voltage domain.

The results for sample type "A" are shown in the following two figures. The first of the two graphs shows the worst case data as described previously and is seen in figure 1.

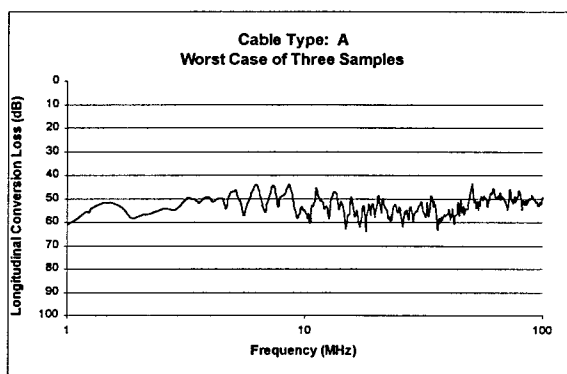


Figure 1

The second graph, shown in figure 2, represents the nominal LCL as a function of frequency based on three samples.

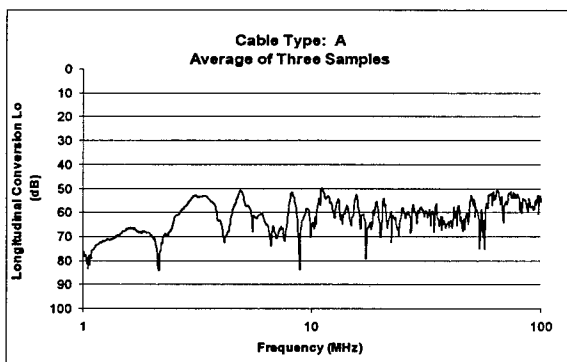


Figure 2

The trace in figure 2 is about five decibels better than the worst case graph when the peaks are

considered. This prototype has a nominal LCL of about 50 dB and a worst case LCL of slightly worse than 45 dB.

The results for sample type "B" are shown figure 3 and figure 4. Again, the first graph represents the worst case LCL of the three samples and is shown in figure 3.

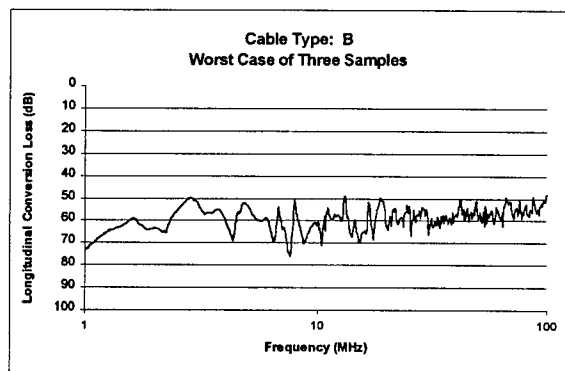


Figure 3

The nominal LCL as a function of frequency is shown in the figure 4 and is also based on three samples measured.

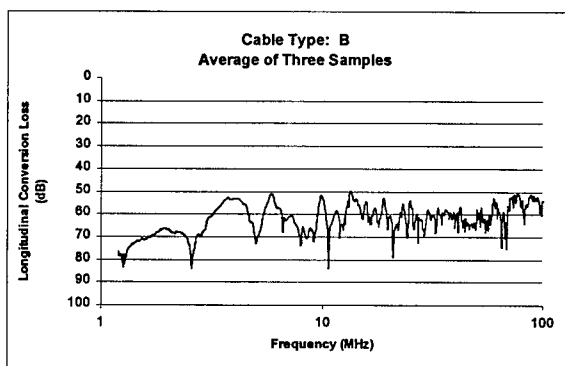


Figure 4

The nominal LCL of sample type "B" is about 50 dB when considering the peaks, which is very close to the measured nominal for sample type "A". The worst case LCL graph is just slightly worse than 50 dB and is about 5 dB better than sample type "A". This difference may be due to differences in sample preparation or due to insufficient number of samples.

The results for sample type "C" are shown in the following two graphs. Figure 5 represents the worst case LCL of the three samples although the individual pairs of each sample were combined as discussed previously.

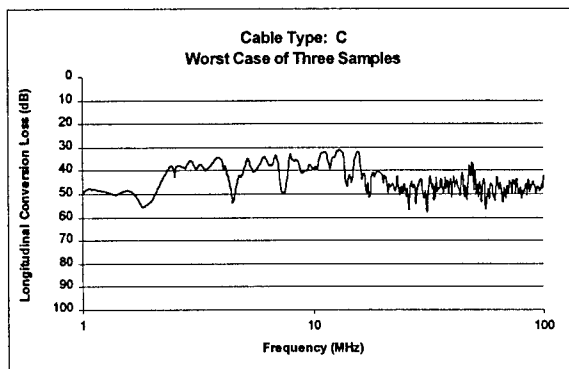


Figure 5

The nominal longitudinal conversion loss of sample type "C", as a function of frequency, is shown in figure 6. The nominal balance is slightly worse than 40 dB with one peak approaching 35 dB. The worst case shown in figure 5 has peaks, which are in the 30 to 35 dB range. The LCL performance of sample type "C" is approximately 12 to 14 dB worse on average than either sample type "A" or sample type "B". This is as expected since the sample was constructed to have poor balance characteristics.

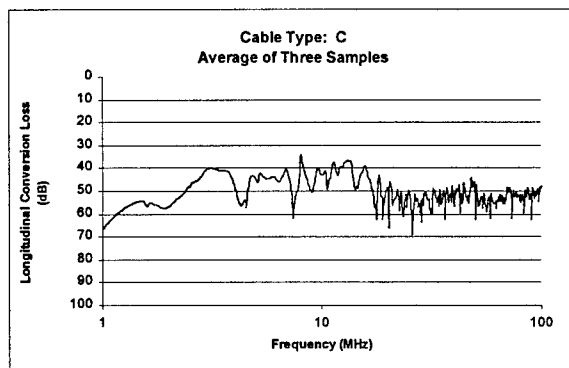


Figure 6

The results for sample type "D" are shown in the following two figures. Unlike the three previous types, this sample type is an unshielded twisted-pair cable (UTP) although it also possesses four pairs. Figure 7 displays the worst case LCL data for this cable type based on three measured samples.

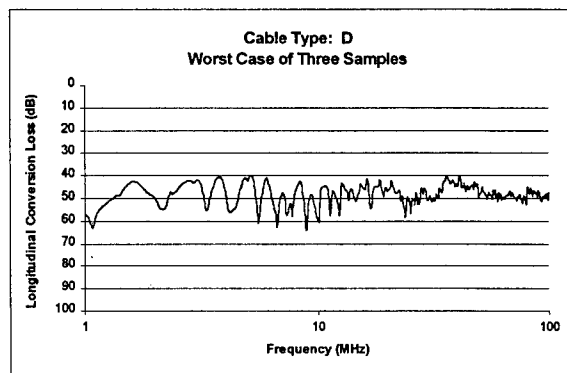


Figure 7

Figure 8 shows the nominal LCL as a function of frequency for cable type "D". As is seen, the nominal LCL is slightly better than 40 dB whereas the worst case LCL performance is about 40 dB. Again, the measured trace signatures are evaluated by looking at the peak values. Cable type "D" was constructed to have poor balance, similar to cable type "C". The difference between the two is that cable type "C" has an overall shield, but cable type "D" is unshielded. There is about a five decibel difference between the two cable types, on average.

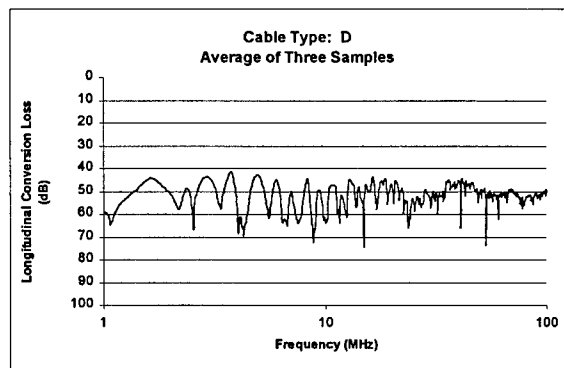


Figure 8

The results for sample type "E" are shown in figures 9 and 10. Cable type "E" is also unshielded, like cable type "D", but it was constructed to have typical balance characteristics. As with the other cable types, the worst case graph is presented first and is shown in figure 9.

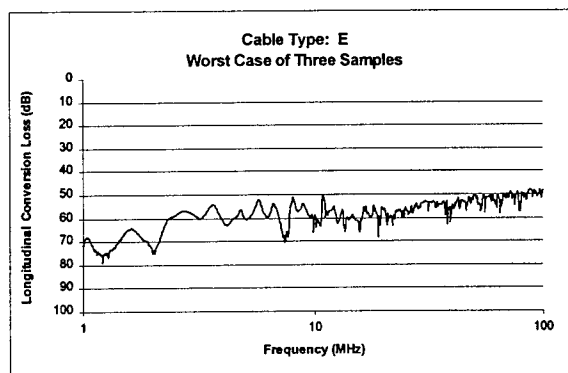


Figure 9

Figure 10 is the nominal LCL for cable type "E" and is shown as a function of frequency. As is demonstrated graphically, the nominal balance of cable type "E" is between 50 and 55 dB whereas the worst case LCL was measured to be about 50 dB when considering the peaks.

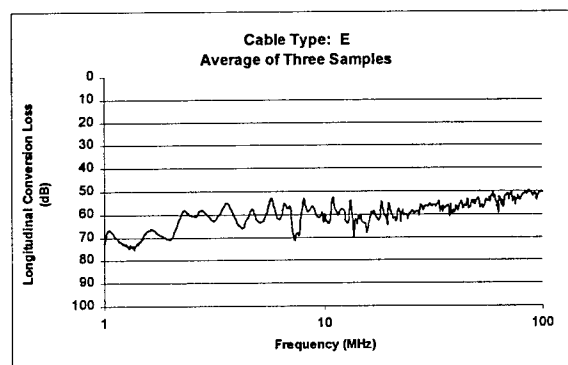


Figure 10

The average LCL performance of cable type "E" is almost eleven decibels better than cable type "D". This is similar to, but one to three decibels less than, the difference between the typical and poorly balanced shielded samples.

For both the shielded (FTP) and unshielded (UTP) examples shown above, the results show that the poorly balanced cable types have a greater difference in balance at lower frequencies (less than 20 MHz) than at higher frequencies (between 20 and 100 MHz). This is illustrated in table 2.

Table 2: Frequency Dependency of Balance

Cable Type Difference	Average 1 - 20 MHz	Average 20-100 MHz	Average 1 - 100 MHz
B - C (FTP)	16 dB	10 dB	14 dB
A - C (FTP)	15 dB	7 dB	12 dB
E - D (UTP)	13 dB	6 dB	11 dB

It is also evident that the difference between UTP types (typical and poorly balanced) is less for all three categories (columns) than the two cases of FTP differences by 1 to 4 dB. Conclusions concerning differences between FTP and UTP cannot be made based on these results. The physical means of constructing the unshielded prototypes to have poor balance was quite different than the means of constructing the shielded samples. Any similarity or difference in the absolute level of difference is coincidental.

Longitudinal conversion loss data was presented for frequencies up to 100 MHz only. This was the frequency limitation of the test BALUNs used in order to have acceptable balance. The authors considered using modal decomposition to extend the measurements from 100 MHz to 500 MHz, but opted to present the data obtained through more conventional measurement methods using a BALUN. It has been demonstrated, however, that LCL measurements are both possible up to 500 MHz using modal decomposition techniques and capable of good agreement with a BALUN [4].

Surface Transfer Impedance

Screening effectiveness was determined through measurement of the surface transfer impedance of the cable sample's shield. Surface Transfer Impedance is one method of determining the screening effectiveness of a cable.

For the purposes of this paper, the surface transfer impedance was measured using the line injection method as described in IEC 1196-1 [5]. The line injection method presented in IEC 1196-1 is intended for coaxial cable. The can be adapted for use with twisted-pair cable although the results may not be as good as is shown by Hoefft [6]. This is accomplished by connecting both conductors of all pairs together at both ends to form one common conductor. Similarly, all shields are connected together at both ends to form a common shield. The paired cable is then tested in a similar manner as a coaxial cable. The common mode impedance between these conductors and the shield is measured, by a time domain reflectometer, and used to load the ends of the cable in a resistor network. By adjusting the velocity of propagation of the injection line, so it matches the sample being tested, the upper test frequency is extended to

above 1000 MHz. Data has been presented at frequencies in excess of 20 GHz using line injection methods and has been found to be accurate and reliable [7].

The surface transfer impedance is presented in this section for the three sample types that employ shields. These are cable types "A", "B" and "C". Three, one meter (1 m) samples were prepared and measured for each of the sample types. The three measurements for each type were averaged together at all measured frequencies in order to reduce the amount of data and make comparisons more accurate. A Hewlett-Packard 8751A Network Analyzer was used to make the measurements. The transfer impedance fixture used to perform the line injection was custom built.

The transfer impedance of sample type "A" is presented in figure 11.

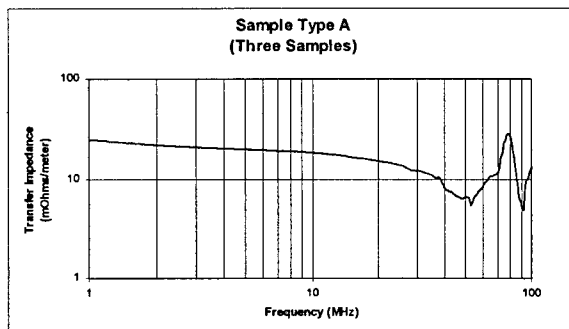


Figure 11

The transfer impedance at low frequencies (1 MHz and below) is close to the DC resistance of the shield. At very low frequencies (less than 10 kHz), comparing the measured transfer impedance to the DC resistance of the shield is one common practice to ensure that the measurement results are as expected. As frequencies get higher, the transfer impedance gets lower. This is due to the fact that the shield appears thicker as frequencies go up due to the skin effect. Lower transfer impedance values indicate a higher level of shielding effectiveness.

The data for cable type "A" shows a resonance at about 80 MHz. Similar resonances are found in cable type "B" and cable type "C". This resonance indicates a problem in the line injection test fixture and is not indicative of the actual performance. It is expected that the

transfer impedance would continue to lower until inductive coupling became prominent. At that point, the transfer impedance is expected to increase at about 20 dB per frequency decade. Based on this, the values measured above 90 MHz can be considered to be accurate.

The transfer impedance for cable type "B" is shown in figure 12 as a function of frequency from 1 MHz to 100 MHz.

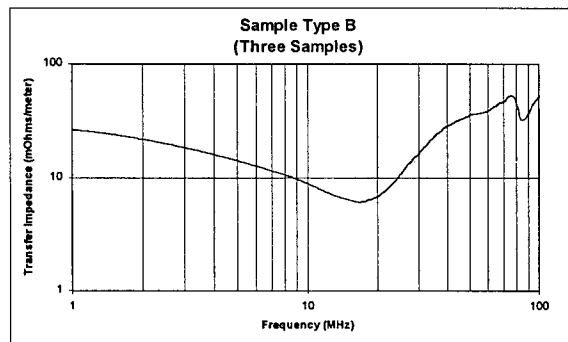


Figure 12

The resonance around 80 MHz is evident, but it does not affect the trace signature as drastically as it did in sample type "A". This could be due to the higher magnitude of transfer impedance of sample type "B" as compared to sample type "A". The elbow in the transfer impedance trace, where inductive coupling becomes predominant, is evident in this sample at slightly below 20 MHz. This is much lower in frequency than cable type "A" and indicates that the shield of cable type "B" is less effective at higher frequencies than the shield employed with cable type "A".

The transfer impedance results of cable type "C" is presented in figure 13.

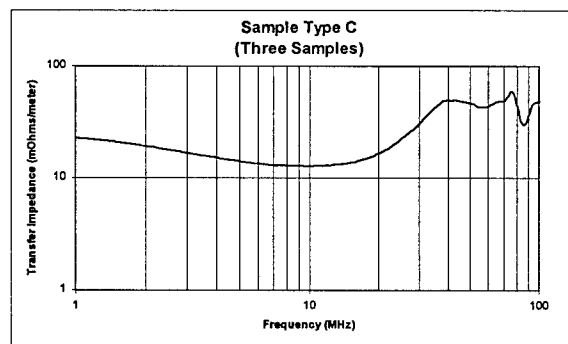


Figure 13

Although the transfer impedance of cable type "C" at low frequencies (less than 2 MHz) and at high frequencies (greater than 70 MHz) is very similar to cable type "B", the middle portion is worse. This indicates that there may be a problem in the contact resistance of the connections and, like the resonance problem, is probably not an true indication of the shield's performance in this frequency region.

Cable type "A" was constructed to have different shielding effectiveness than both cable types "B" and "C". To quantify this difference, the transfer impedances for cable type "B" and cable type "C" were independently compared with the transfer impedance of cable type "A". The resultant ratio can be expressed as a decibel and is shown in figure 14.

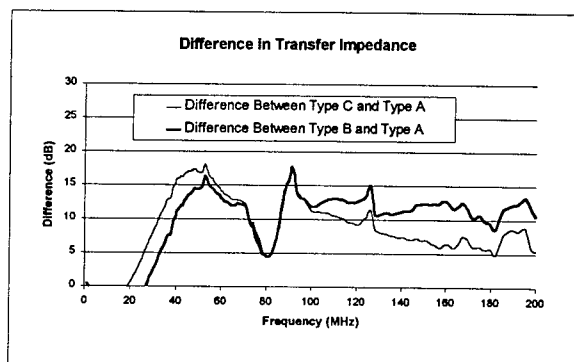


Figure 14

At low frequencies, both cable type "B" and cable type "C" have similar performance to cable type "A". This is because at very low frequencies, the DC resistances of the shields are similar and they are acting like a solid cylindrical shield as explained in Vance [8]. At higher frequencies (greater than 50 MHz), there is a greater difference although the data is somewhat distorted around 80 MHz again due to resonances.

The average difference between the shield types is summarized in table 3. Table 3 shows that below 50 MHz, there is little average difference between the shield types. At frequencies between 50 MHz and 200 MHz, there is an average improvement of 9 to 11 dB in the shielding effectiveness of cable type "A" as compared to cable type "B" or cable type "C". The actual difference may be greater, but cannot be seen due to resonance problem at 80 MHz.

Table 3
Performance Differences in Shield Constructions

Difference	1 – 50 MHz	50 – 200 MHz
Type A – Type B	1.0 dB	11.6 dB
Type A – Type C	-1.0 dB	9.2 dB

It is also evident that there is about a 2 dB improvement in surface transfer impedance in sample type "C" as compared to sample type "B" even though these sample types have the same shield construction. This offset is evident even at low frequencies and suggests that the aluminum thickness on sample type "C" may be slightly thicker than on sample type "B".

Coupling Attenuation

Coupling attenuation was measured in accordance with prEN BASIC 5-4-6 [9] using an absorbing clamp to measure the power coupled from the cable sample, which is energized in a differential mode through a BALUN transformer. This section of the paper presents the coupling attenuation results, which were measured on all three samples from each of the five cable types.

Coupling attenuation measurements were performed on an electrically long cable sample from 30 MHz to 1000 MHz on 801 linearly spaced frequency points using a Rohde and Schwarz MDS-21 Absorbing Clamp. A second Rohde and Schwarz MDS-21 Absorbing Clamp was used as the absorber at the far end. The distance between the two absorbers was ten meters, which is the cable length tested although the physical length of the samples was 350 meters. The remaining portion of the cable, which was not between the two absorbers, was left on the reel and this served as the perfect termination [10]. The data for each cable type is presented in the following series of graphs.

The coupling attenuation for cable type "A" is presented in figure 15 on the next page.

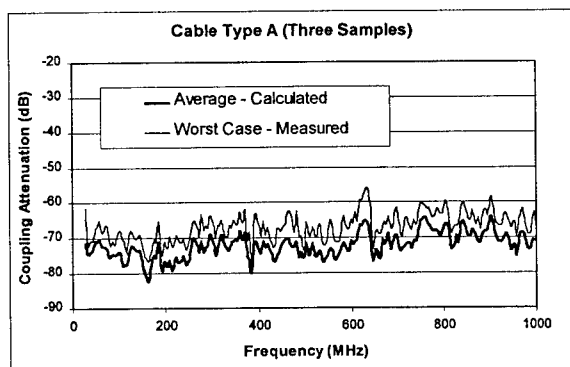


Figure 15

The graph consists of two traces. The darker trace is the average of all pairs in all three samples calculated in the power domain. The lighter of the two traces is the worst case coupling attenuation of all pairs in all three samples. The average of the three samples is better than -70 dB for most frequencies below 600 MHz.

The coupling attenuation results for sample type "B" is presented in figure 16 as a function of frequency from 30 MHz to 1000 MHz. Again, there are two traces, one each for average and worst case. The darker trace is the average trace. The average trace is worse than -70 dB for most frequencies above 400 MHz.

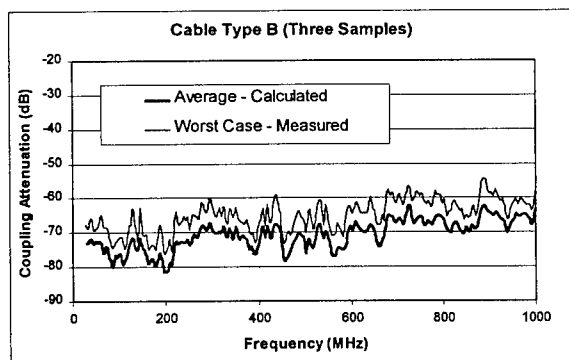


Figure 16

Comparing the graphs for cable type "B" to the graphs for cable type "A", it appears that there is not a great difference between average magnitudes at frequencies below 600 MHz. Above 600 MHz, the differences in coupling attenuation performance become apparent.

The coupling attenuation results for sample type "C" is presented in figure 17 from 30 MHz to 1000 MHz. Above 800 MHz, a severe

degradation in coupling attenuation is observed where the trace changes by about 10 dB on average.

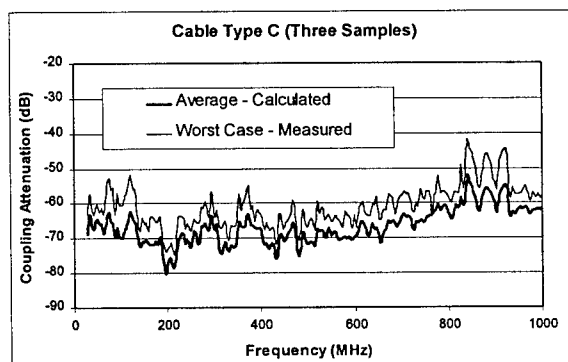


Figure 17

The coupling attenuation results for sample type "D" is presented in figure 18 from 30 MHz to 1000 MHz. The average coupling attenuation is above (worse than) -50 dB for frequencies above 500 MHz.

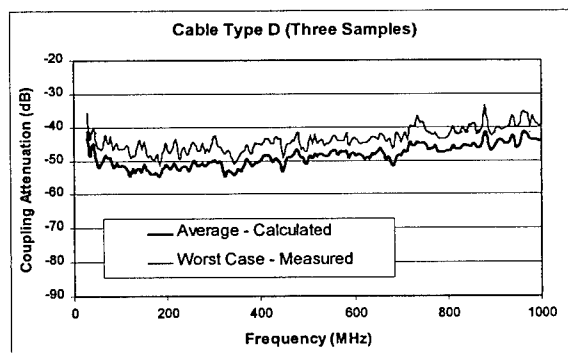


Figure 18

The coupling attenuation results for sample type "E" is presented in figure 19 from 30 MHz to 1000 MHz.

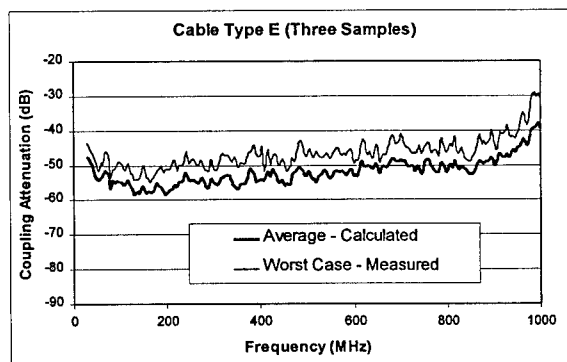


Figure 19

The coupling attenuation performance of cable type "E" shows an upward trend above 800 MHz. This degrades the apparent average performance of this cable type although the performance below 200 MHz is quite good. This is evident in figure 20, which shows the portion of figure 19 from 30 MHz to 200 MHz.

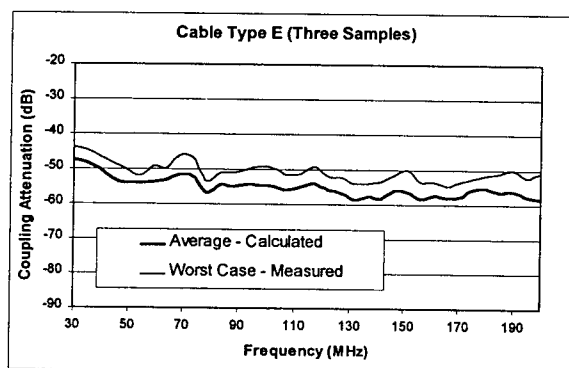


Figure 20

The data is summarized in table 4 which represents the average value from 30 MHz to 1000 MHz for both the worst case trace and average trace from the previous graphs. The average was calculated using linearly spaced frequency samples calculated in the power domain. The resultant averages were converted in decibels for inclusion in the table.

Table 4
Average Coupling Attenuation, 30 –1000 MHz

Sample Type	Average Trace	Worst Case Trace
A	-71	-65
B	-69	-63
C	-64	-56
D	-48	-42
E	-50	-43

There is about a 2-dB average difference between cable type "A" and cable type "B". Cable type "A", which was constructed to have better shielding effectiveness, has the better coupling attenuation. The difference in coupling attenuation between these two cable types is not as much as the difference between shielding effectiveness, which was measured to be almost 10 dB on average. These two cables exhibited approximately a 9-dB difference in shielding effectiveness as is seen in table 3. Cable type "A" has a lower balance by about 2 dB on average, which may contribute to the difference between coupling attenuation and transfer impedance. Limitations on realized noise floors

in the coupling attenuation measurement procedure may also be a factor. This is an area of continued research and development.

Cable type "C" exhibits about a 5 dB lower coupling attenuation than cable type "C". This difference is not as great as the 10-dB difference in Balance as measured at high frequencies between these types as seen in table 2. Measurements of transfer impedance show that there is about a 2-dB improvement in shielding effectiveness of type "C" over cable type "B" which may account for part of this difference. The average balance difference between the two types at frequencies above 100 MHz also needs to be measured perhaps using modal decomposition.

Similarly, there is only an average measured difference in coupling attenuation between cable type "D" and cable type "E" of about 2 dB. The drastic upward swing of the cable type "E" performance adversely affected the average value for this cable type. If the performance at frequencies below 200 MHz is compared, the difference in coupling attenuation increases to about 4 dB. The 4 dB difference between the unshielded sample types is less than the 11 dB difference in balance which was measured at frequencies below 100 MHz using LCL and even less than the 6 dB difference seen at frequencies above 20 MHz using LCL. The 4-dB difference is proportionally the same difference to the measured balance results as was observed in the FTP differences between cable type "C" and cable type "B".

CONCLUSION

Results are presented showing shielded cable samples, which have similar transfer impedance performance, but which have different balance characteristics. A corresponding difference in coupling attenuation is observed. Similar results are also presented showing unshielded samples with different balance characteristics and a corresponding change in coupling attenuation. Results from measurements on shielded cable samples which have similar balance characteristics, but which have different transfer impedance performance, are presented along with a corresponding change in coupling attenuation.

The magnitude of difference in the coupling attenuation results between the sample types with the two shield types was not as great as expected and may be due to current limitations in the test procedure used such as the noise floor of the measurement set-up.

It was also anticipated to see a greater difference in coupling attenuation between the two unshielded cable types. Although a difference was measured, it was not as great in magnitude as the change in longitudinal conversion loss. This may indicate that the absorbers have drastically attenuated the common mode signals in the unbalanced samples. The common mode signals are created by differential to common mode conversion. This makes the coupling attenuation appear abnormally good. These absorbers both precede the current probe and are located at the end of the tested length (10 meters away) during the coupling attenuation testing. This will need to be explored through additional experimentation and research.

The unbalanced samples appeared to degrade the LCL performance more at lower frequencies than at higher frequencies as compared to their balanced counterparts. The balance of cables above 100 MHz needs to be more fully investigated to gain additional insight into the frequency dependencies of balance and the relation between pair balance and coupling attenuation. Modal decomposition techniques may be applicable for this purpose.

ACKNOWLEDGMENT

The authors wish to thank Mr. Ken Wenrich for the many hours he spent in the characterization of samples for Longitudinal Conversion Loss and Surface Transfer Impedance.

REFERENCES

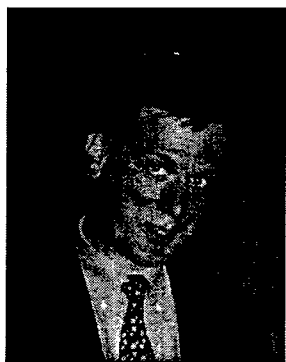
- [1] J. Walling et al: "Crosstalk Measurements as a Means to Characterize the Balance of Data Grade Wires", Proceedings from the 45th International Wire and Cable Symposium, pp751-760, 1996.
- [2] ITU Recommendation: "Transmission Aspects of Unbalance About Earth (Definitions and Methods)", Fascicle III.1 – Recommendation G.117.
- [3] ITU Recommendation O.9: "Measuring Arrangements to Assess the Degree of Unbalance about Earth", Fascicle IV.4 – Recommendation O.9.
- [4] K. Yanagawa et al: "Modal Decomposition (Non-BALUN) Measurement Technique: Error Analysis and Application to UTP/STP Characterization to 500 MHz", Proceedings from the 44th International Wire and Cable Symposium, pp126-133, 1995.
- [5] "Surface Transfer Impedance: Line Injection Method (Frequency Domain)", Paragraph 12.2, CEI/IEC 1196-1:1995, First Edition, pp177-199.
- [6] L. Hoeft et al: "Measurement of Surface Transfer Impedance of Multi-Wire Cables, Connectors and Cable Assemblies", Symposium Record of the 1992 IEEE International EMC Symposium, pp308-314.
- [7] B. Eicher et al: "Very Low Frequency to 40 GHz Screening Measurements on Cables and Connectors; Line Injection Method and Mode Stirred Chamber", Symposium Record of the 1992 IEEE International EMC Symposium, pp302-307.
- [8] E. Vance: "Coupling to Shielded Cables", New York, Wiley Interscience, 1978.
- [9] prEN BASIC 5-4-6: "Generic specification for electrical test methods for cables used in analogue and digital communication and control systems", part D: "Coupling Attenuation, Absorbing Clamp Method", CLC/TC 46X/WG3
- [10] B. Szentkuti, A. Peurala: "New Views on the Absorbing Clamp in the Testing of Cable Screening effectiveness", Proceedings of EMC Conference in Zurich, 1983.

AUTHORS



Eric Lawrence
Berk-Tek
132 White Oak Road
New Holland, PA
17557

Eric Lawrence received his BS in Electrical Engineering from Widener University in May 1987. Since then he has worked in the Wire and Cable Industry developing coaxial and paired cables for electronic and data communications applications. Eric has been employed at Berk-Tek for the past four years and is currently the Manager, Design and Development Engineering. Eric is an active member of TIA TR41.8.1 working group and US expert on IEC SC 46C / WG7 and SC 46A / WG2 working groups. Eric is a member of BICSI and a Registered Communications Distribution Designer (RCDD).



David Hess
Alcatel Cabling Systems
7 Great Valley Parkway
Malvern, PA
19355

David Hess has worked for more than twenty-one years in product design and development in the fields of electronic and optical data communication cabling. He is currently employed as a Vice President of Product Marketing with Alcatel and participates on various data communication and interface standards committees in TIA/EIA, ANSI and ISO/IEC. Dave has been active on the TIA TR 41.8.1 Premises Cabling Committee, since 1989, and has been active on the ISO/IEC JTC1 SC25

WG3 Premises Cabling Committee since 1994. Dave has a B.S. degree in Mathematics from Pennsylvania State University and is a member of IEEE and BICSI.

Michiel Pelt
Alcatel Cabling Systems
Bd. Paepsemiaan 16
B-1070 Brussels
Belgium

Michiel Pelt received his degree in Electrical Engineering (Applied Physics) in 1992 from the free University of Brussels. He is currently responsible for EMC research on generic cabling systems within Alcatel Cabling Systems. Michiel is an active member on various standardization committees within CENELEC including TC 215 / WG 2 and TC 46X / WG 3 where he also serves as the Secretary.

DETERMINATION OF THE REAL LIFETIME OF POLYMERIC CABLE MATERIALS

Donald R. Parris and Zhan Gao

Siemens AG, Public Communication Networks, Neustadt, Germany

ABSTRACT

In this paper, four temperature as a function of the time models have been mathematically set up for places where cables can be installed. According to these temperature models the real lifetimes of several potential polymeric cable materials have been predicted using the Arrhenius theory. It was shown that the lifetime of the material in the cable depends strongly on where the cable is installed.

Otherwise, for any temperature as a function of time model, an associated 'equivalent' constant temperature was calculated. This 'equivalent' constant temperature for any model is different from the average temperature, especially for the cold temperature model.

INTRODUCTION

One criteria in selection of materials for use in any application is the lifetime of the material. The lifetime of materials used in the cable industry is an important criteria because such long lifetimes are expected. Lifetimes of materials are typically predicted by accelerated heat aging in relevant environments and then extrapolating these results to lower temperatures via Arrhenius. This method has its conditions and limitations, but remains to be the state of the art method for lifetime predictions. The resulting Arrhenius curve or equation gives the rate of reaction or lifetime as a function of temperature.

In this paper Arrhenius determined lifetime as a function of temperature equations have been combined with temperature as a function of time models to predict a more accurate (real) lifetime. Several temperature as a function of time models are shown and the associated lifetimes of several materials are calculated.

PROCEDURE

Lifetime Prediction via Arrhenius

The lifetime of polymeric materials is often predicted by using the Arrhenius law:

$$k = A \cdot \exp(-E/RT) \quad (1)$$

where k is the rate of reaction (degradation) of the polymer, A is a constant, E is the activation energy, R is the gas constant and T is absolute temperature in Kelvin.

Integrating Eq(1) with time, we get

$$\int_0^t k \cdot dt = \int_0^t A \cdot \exp(-E/RT) \cdot dt \quad (2)$$

The left side of Eq(2) represents a quantity of reactions occurred or of molecules degraded during the time, t . If the amount of the degraded molecules reaches the critical value, M_c , the polymer will fail. The time, t_c , that it takes for reaching the critical value, M_c , can be defined as the lifetime of polymer (t_c).

$$M_c = \int_0^{t_c} A \cdot \exp(-E/RT) \cdot dt \quad (3)$$

If the temperature in Eq(3) does not depend on time ($T=\text{constant}$), the lifetime t_c can be described by:

$$\begin{aligned} t_c(T) &= (M_c/A) \cdot \exp(E/RT) \\ &= B \cdot \exp(E/RT) \end{aligned} \quad (4)$$

with

$$B = M_c/A$$

Eq(4) indicates that the lifetime decreases with increasing temperature. The activation energy E and constant B can be determined by

conducting experiments at various constant temperatures.

In practical cable applications, the temperature of the environment where the cable is installed often changes with time, ($T=T(t)$). Replacing T with $T(t)$ in Eq (3), we have

$$\int_0^{t_c} \exp(-E/RT(t)) \cdot dt = M_c/A = B \quad (5)$$

If the temperature as a function of time for an installed cable is known, the lifetime of the cable in this place can be numerically calculated from Eq (5).

In our experiment, the lifetimes of various polymeric cable materials were analyzed. From each material, a strip was first extruded using standard manufacturing temperatures and cooled in a water trough. Standard 'dumbbell' samples for tensile testing were cut from the extruded strips. The samples were divided into four groups that were aged at four different 'elevated' temperatures. Three samples of each material were removed on a regular basis from each temperature environment. The frequency of sample removal was based on the aging temperature and the expected lifetime at that temperature. The elongation to break for each sample was measured with a crosshead speed of 50 mm/min. A material was considered to be at the end of its life when the elongation to break for two of the three samples decreased to 10%.

So, in this way for each polymeric cable material, four lifetimes at four different aging temperatures were determined. From the measured values, the activation energies, E , and the constants, B , were calculated and are shown in Table 1.

	Activation Energy (E) [J]	Constant (B) [years]
Polymer A	93404	2.004e-14
Polymer B	78903	1.723e-12
Polymer C	88236	6.481e-15
Polymer D	79626	1.289e-13
Polymer E	83491	4.040e-14
Polymer F	81305	9.814e-13

Table 1: Activation Energies (E) and constants (B) of several potential polymeric cable materials.

A typical Arrhenius diagram is shown in Figure 1, where the logarithm of the lifetime is plotted

versus the inverse of the temperature in degrees Kelvin. It is obvious that the slope of the line in this figure indicates the ratio between the activation energy, E , and the gas constant, R , and the point where $1/T$ approaches to zero represents the constant B .

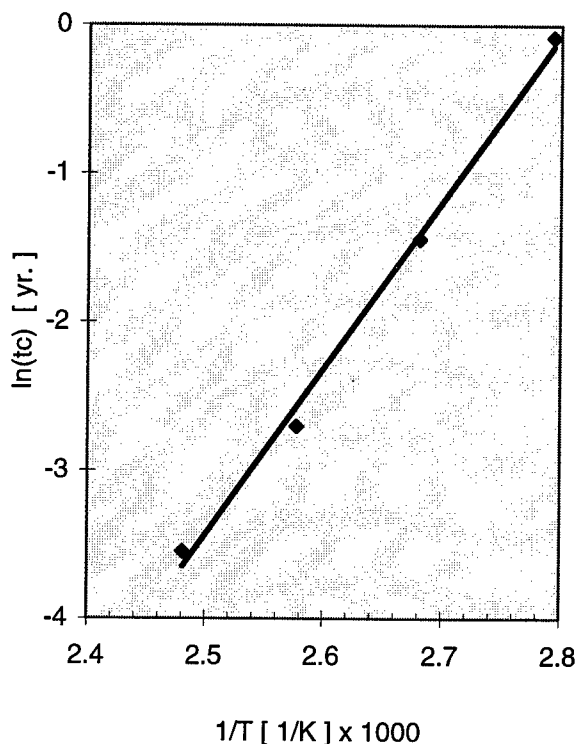


Figure 1: Lifetime of a polymeric cable material as a function of temperature.

Temperature Models

Temperature as a function of time has been modelled assuming a sinusoidal temperature variation over each day and over each year. It is assumed that temperature varies 10°C each day with the low temperature occurring at midnight and the high temperature at noon. The yearly variation, as well as the yearly absolute high and low temperatures, depends on the climate zone¹ in our model. Over a year, December 31 is the coldest day of the year and June 30 the warmest day. The high and low temperatures for the year are listed in Table 2.

Aerial cables in the sunshine have been shown to reach a peak daily temperature of about 10°C higher than the air temperature² and this has been included in the first three models. Buried cables may be a concern depending on where they come out of the ground. The fourth model

represents a hypothetical pedestal in a tropical environment.

A typical temperature model equation looks like:

$$T = a + b \cdot \sin\left(\frac{3\pi}{2} + \frac{\pi}{12}t\right) + c \cdot \sin\left(\frac{3\pi}{2} + \frac{\pi}{4380}t\right) \quad (6)$$

where t is time in hours and T is temperature in degrees Celcius. The daily and yearly temperature variations for these four models are graphically shown in Figure 2.

Climate	low (°C)	high (°C)
cold	- 50	40
moderate	- 20	45
hot	- 5	50
extremely hot	20	60

Table 2: High and low temperatures of the four temperature models.

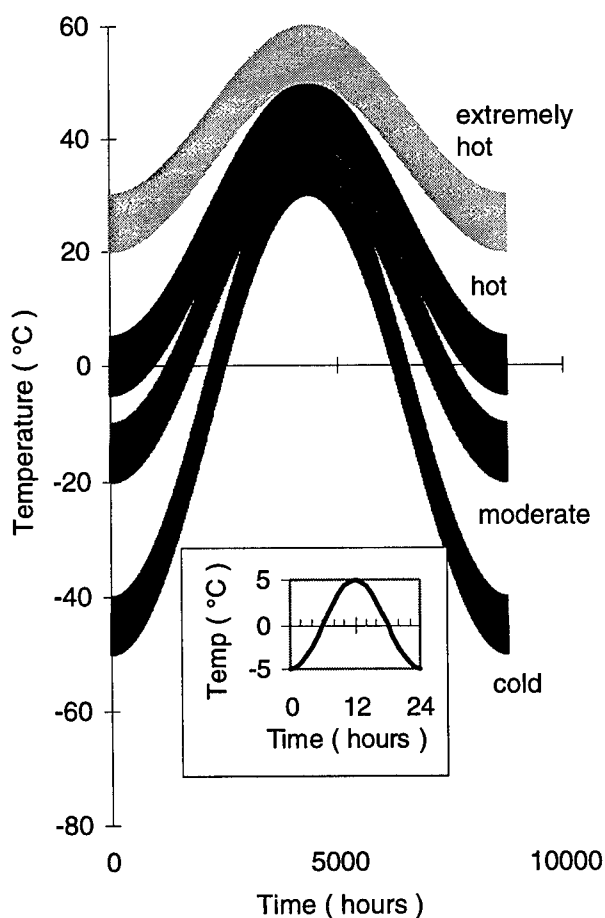


Figure 2: Four Temperature Models.

RESULTS AND DISCUSSION

Calculations

According to Eq(5) and Eq(6), the lifetimes of the cable materials have been numerically calculated and are shown in Table 3.

Material	Lifetime (years)			
	cold	moderate	hot	extremely hot
A	704	317	159	41
B	197	96	52	16
C	30	14	7.3	1.8
D	20	10	5.4	1.5
E	28	14	7.4	2.3
F	289	140	75	22

Table 3: Lifetimes of the potential cable materials installed in four climate zones.

It is shown that the lifetime of the polymeric cable materials strongly depends on where they will be used. For example, the lifetime of the material A will be reduced by more than seventeen times, when it is moved from the cold climate to the extremely hot climate. The dependence of the lifetime on the climate is different for the materials as it shown in Table 3. This is determined by the activation energy of the material.

	cold	moderate	hot	extremely hot
high temp (°C)	40	45	50	60
low temp (°C)	-50	-20	-5	20
average temp (°C)	-5	12.5	22.5	40
equivalent temp (°C)	22	28	33	45

Table 4: High, Low, Average and Equivalent Temperatures.

For each temperature model, an 'equivalent' constant temperature can be calculated from Eqs. 4 & 5. This 'equivalent' temperature is dependent on the environment and on the material as well. For the material A, the equivalent temperature for these four models is calculated and is shown in Table 4. The equivalent temperature is different from the average temperature for each temperature model in Table 4 and is always higher. The difference between them is very large (about 27 °C) for the cold temperature model and

decreases, as the model moves to the extremely hot temperature model. It is shown that the lifetime of the polymeric material is essentially determined by the upper temperature range in each temperature model, especially in the cold temperature model.

SUMMARY

From this work one can see that:

A method has been developed to calculate a practical lifetime of materials in a variable temperature (real life) environment.

The lifetime of materials can be more accurately predicted based on detailed knowledge of the application environment.

For any temperature as a function of time model, an associated 'equivalent' constant temperature can be calculated.

The 'equivalent' constant temperature value for any model is not the same as the average temperature.

REFERENCES

1. DIN IEC 721 Standard, Teil 2-1, Sept. 1986, "Klassifizierung von Umweltbedingungen"
2. W.M.H. Schulze, Telefunken-Zeitung, Jg. 35. (June 1962), Heft 136, P143-147, "Temperaturverhältnisse bei Fernmeldekabeln im Erdboden und in der Luft."

BIOGRAPHIES



Donald R. Parris is the Manager of Materials Technology at Siemens AG, Telecommunications Cable Division in Neustadt,

Germany. He has B.S. and M.S. degrees in Materials Engineering from Virginia Polytechnic Institute and State University. He has been an employee of Siecor Corp., USA since 1986 and is currently on his second assignment at Siemens in Germany. He has previously authored 2 IWCS papers and holds 2 patents.

Mailing address:

Siemens AG, OEN NK E K5
Austrasse 101, 96465 Neustadt, Germany



Zhan Gao was born in Shanghai, China in 1963. He received his B.S. and M.S. degrees in Material Science and Engineering at the University Tongji, Shanghai, in 1985 and 1988, respectively. In 1991, he joined Siemens AG in Neustadt, Germany where his key task was to finish a corporate research project between Siemens AG and the University Erlangen-Nuremberg. Since receiving his Ph.D. from the University Erlangen-Nuremberg in 1994, he has worked in the areas of cable and materials testing and theoretical modeling at the Siemens AG, Telecommunication Cable Research and Development Department.

Mailing address:

Siemens AG, OEN NK E K5
Austrasse 101, 96465 Neustadt, Germany

A NEW GENERATION POLYETHYLENE RESINS FOR CABLE JACKETING APPLICATIONS

Laila Rogestedt and Hans-Bertil Martinsson

Borealis AB, Stenungsund, Sweden

ABSTRACT

Polyethylene resins, intended for jacketing applications, must meet a wide range of requirements. In applications where high toughness, good barrier properties and hard surface are required, e.g. in power and fiber optical cables, high density polyethylene (HDPE) is often recommended. However, HDPE suffers often from high shrinkage, particularly disadvantageous in fiber optical cables, and low environmental stress crack resistance (ESCR). In a new type of materials, described in this paper, a good balance between all properties of importance in jacketing applications has been obtained. By choosing a proper catalyst and process technology system, based on bimodal technology, optimal molecular weight as well as comonomer distribution have been obtained. The new materials can be easily processed, with a good surface smoothness, over a wide range of cable line conditions. The materials are further characterised by a low shrinkage level as well as excellent ESCR. Since the new type of materials have high density, the water permeability is low and the abrasion resistance as well as the mechanical properties are very good.

INTRODUCTION

Polyethylene resins have, due to the good barrier and mechanical performance, been used for a long time in different cable jacketing applications. Conventional high pressure material, LDPE (low density polyethylene), was earlier the most important material in telecommunication cables. During recent years there has been a clear trend towards linear material, with LDPE being replaced by linear low density polyethylene, LLDPE. In power cables, linear material is the predominant material. Due to requirements for high temperature resistance

in these applications, high or medium density polyethylene, HDPE or MDPE, is generally used.

In fiber optical cables, simpler constructions with less strength members are often seen today, which implies high toughness of the jacket material. A HDPE material provides high mechanical strength, good barrier properties and hard surface. As a consequence, HDPE is often specified as jacket material in fiber optical cables today. However, high density polyethylene has some inherent drawbacks when used in jacketing applications. The environmental stress crack resistance, ESCR, decreases when the density is raised (1). One of the main drawbacks with HDPE materials is the high shrinkage. High shrinkage in polyethylene jackets is a long known problem, especially in fiber optical cables (2-5). A high shrinkage of the jacket material creates stresses in the fibers, which in turn gives attenuation (transmission loss) in the cable. Low shrink materials, commercially available today, usually suffers from bad processability.

In this paper a new type of polyethylene resins is presented. By choosing proper catalyst and process technologies a new type of jacketing compounds has been designed. The aim of this work has been to develop materials with a good balance in all properties of importance in jacketing applications. The materials must be optimised to give the best performance during the production and the installation of the cable as well as during the final end use of the product. To be able to fulfil all requirements, new technology has been applied. The new materials, presented in this paper, are based on the new technology for bimodal polyethylene, Borstar™, developed by Borealis (Borstar is a trademark of Borealis A/S, Denmark). A bimodal process provides unique possibilities to tailor-make materials due to its multi reactor system. In each reactor an optimised molecular weight

distribution as well as comonomer distribution can be obtained.

Two new HDPE materials, at two different melt flow rate (MFR) levels, have been designed and studied in this work. The high MFR material, which will be focused on in this paper, is designed to give the lowest shrinkage possible and hence very suitable for fiber optical applications. The low MFR material is, due to its higher melt strength, more suitable for bigger cable constructions, like in power cables. Two commercial references have been included in the study for comparison.

EXPERIMENTAL

Materials

Data on the materials used in the study is found in table 1. All materials contain 2,5% carbon black (nominally) and are stabilised against thermal degradation. In some cases an LLDPE and an LDPE jacketing grade (commercial grades) have been included for comparison. The first reference, REF-1, is designed to give the lowest possible shrink and consequently used mainly in fiber optical cables. The other reference, REF-2 is a "standard" HDPE jacketing grade used in various applications.

Table 1. Data on materials used

MATERIAL	NEW-1	NEW-2	REF-1	REF-2
MFR ₂ (g/10 min.)	1,5	0,3	1,7	0,25
Density- base resin (kg/m ³)	942	942	942	941
Density compound (kg/m ³)	954	954	954	953
Main application	Fiber optical	Power	Fiber optical	Power/ fiber optical

Methods

A pilot cable line with a 60 mm/ 24D extruder has been used in the cable experiments. A model cable has been used to study the processability and the shrinkage of the materials. A jacket of one mm thickness has been put directly on a 3 mm single aluminium conductor, using a semi tube die (cable OD 5 mm). The shrinkage has been measured after temperature cycling, 500 mm cable samples, between room temperature and 80°C, five times (VDE 0472, teil 630). It has further been studied on 400 mm samples after

room temperature ageing and oven ageing at 100°C (24 hours).

Mechanical properties have been measured in a tensile test at 50 mm/minute according to ISO 527/5A. Samples were taken from compression moulded plaques. The moulding was performed according to ISO 1872-2-B at 200°C. The same sample types were also used in the abrasion resistance test (ASTM D 4060 / Taber). ESCR was measured in accordance with ASTM D 1693/A in 10% Igepal. Water vapour permeability were studied at 38°C/ 90% RH in 100 micron films (ASTM E 398). A Bohlin plate/plate rheometer was used for rheological characterisation of the materials.

RESULTS

Processability

To study the process window, the materials were run over a wide range of line speed as well as extrusion temperatures. The surface smoothness of the cables were visually examined and the results from extrusion trials at 180°C are presented in table 2. Both new materials have very good processability with smooth surfaces over a wide range of line speeds. The low shrink material, NEW-1, can be run at an extrusion temperature as low as 150°C with a smooth surface remained. This was not possible with any of the other materials, due to high extruder pressure. In comparison with the low shrink reference material, REF-1, the improvement in processability is dramatic. The other reference, REF-2, is a standard jacketing grade requiring a wide process window. The good processability of this grade was confirmed in this test.

Table 2. Surface appearance of cable samples run at different line speeds at an extrusion temperature of 180°C

CABLE LINE SPEED	NEW-1	NEW-2	REF-1	REF-2
15	smooth	smooth	smooth	smooth
35	smooth	smooth	smooth	smooth
75	smooth	smooth	slightly rough	smooth
140	smooth	smooth	severe sharkskin	smooth

The extrusion performance was further evaluated by following the extruder pressure during the trial. In figure 1 the output is plotted against the extruder pressure. The new material creates a

much lower extruder pressure than both references.

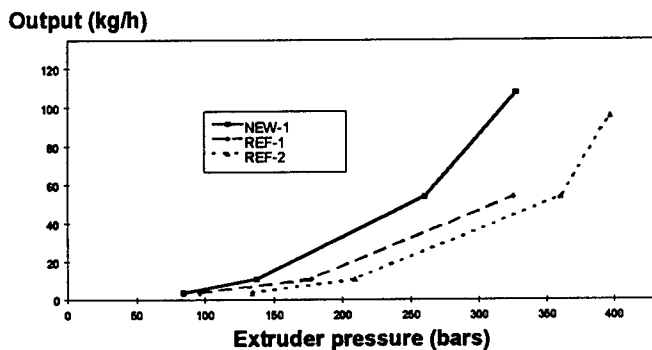


Figure 1. Output versus extruder pressure at an extrusion temperature of 180°C.

Shrinkage

Low shrinkage is a key parameter for a jacket material intended for fiber optical applications. Results from temperature cycling of cable samples is found in figure 2. In this cable construction, the shrinkage is more or less independent of the line speed. There is however a big difference in shrinkage level between the different materials. The both materials, designed for fiber optical applications, NEW-1 and REF-1, have both a very low shrinkage level compared to the standard jacketing grade, REF-2. The low shrinkage level is further confirmed after conditioning at higher temperature, 100°C for 24 hours, figure 3. Low shrinkage in room temperature is important for example during storage and installation of the cable. When the cables are left in room temperature after cutting, the jackets made of NEW-1, NEW-2 or REF-1 do not contract at all. In contrary, the jacket of REF-2 contracts up to 1% already after 24 hours.

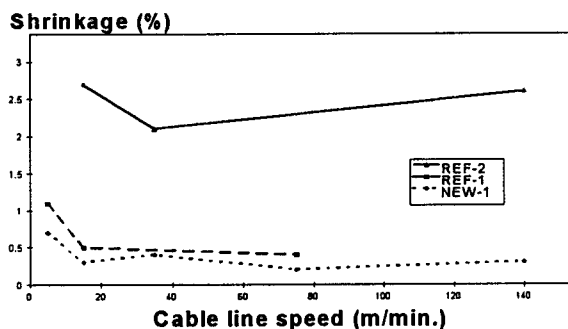


Figure 2. Shrinkage in cable samples after temperature cycling (80°C/5 hours, 5 cycles)

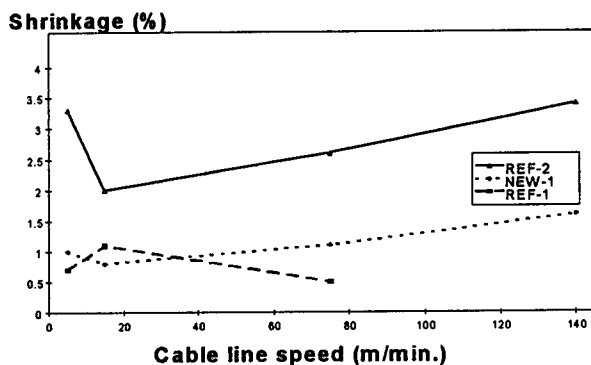


Figure 3. Shrinkage in cable samples after ageing: 24 hours at 23°C followed by 24 hours in 100°C.

ESCR

The superior ESCR performance of the new materials is shown in table 3. No cracks were found in any of the materials after 2000 hours in the Igepal solution.

Table 3. ESCR measurements

MATERIAL	ESCR
NEW-1	No cracks / 2000 hours
NEW-2	No cracks / 2000 hours
REF-1	F ₂₀ ⁽¹⁾ 200 hours
REF-2	F ₂₀ ⁽¹⁾ 500 hours

1) 20% cracks

Other properties

Properties like surface hardness, mechanical strength, abrasion resistance and water permeability are important both during installation and during the final use of the cable. Since a high density level was chosen for the new materials the barrier properties as well as the abrasion resistance is expected to be good. In figure 4 the abrasion resistance of the materials used in this study, NEW-1, NEW-2 and REF-2, is compared with materials of lower density. The abrasion resistance increases with increased density of the material.

The LLDPE grade has however a markedly better resistance than the LDPE grade, even though the densities are on a similar level. The same pattern can be seen for the barrier properties. The water vapour transmission rate through the materials decreases with increasing density, figure 5. Also in this case there is a dramatic difference between the LDPE and the LLDPE grades. The good mechanical strength of the HDPE materials is shown in figure 6.

Abrasion index (mg/1000 cycles)

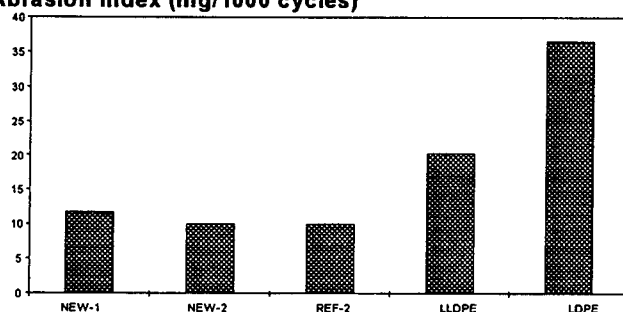


Figure 4. Abrasion resistance - ASTM D 4060 (Taber) HDPE compounds, LLDPE and LDPE.

WVTR (g/m/24 hours)

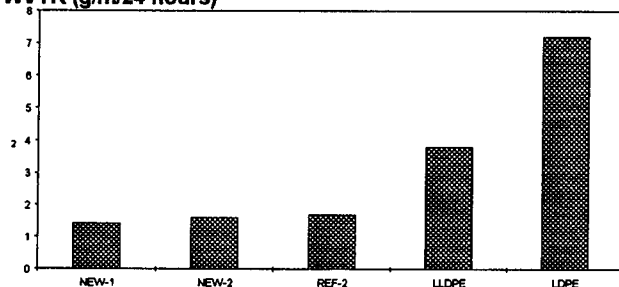


Figure 5. Water vapour trans. rate, 38°C/90% RH (100 micron films) HDPE compounds, LLDPE and LDPE.

Tensile strength at break (MPa)

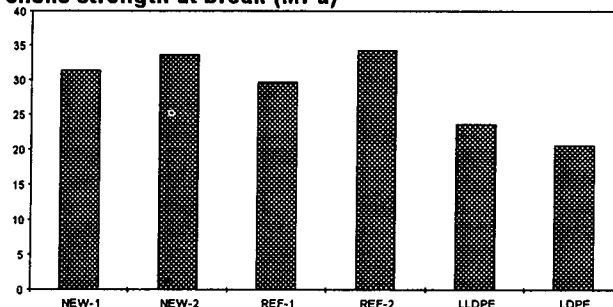


Figure 6. Tensile strength at break HDPE compounds, LLDPE and LDPE.

DISCUSSION

To explain the different extrudability of the two low shrink materials, NEW-1 and REF-1, the rheology of the materials was studied. Viscosity curves of the materials are shown in figure 7. The higher shear thinning ability of the new material is indicated by the steeper slope of the viscosity curve. A gel permeation chromatography analysis (GPC) of the materials gives valuable information of the molecular structure of the materials. The molecular weight distributions (MWD) of the materials are presented in the GPC curves in figure 8. The good processability of the new material can be explained by the higher frequency of short molecules, which act as lubricants in the material.

Complex viscosity (kPas)

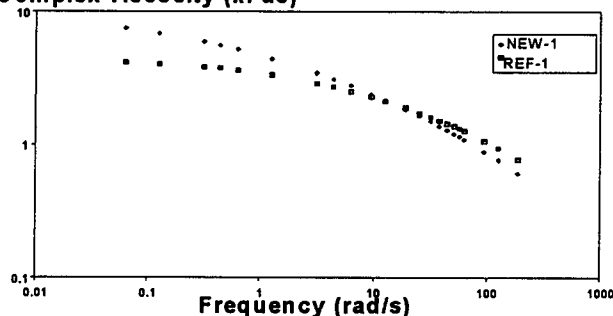


Figure 7. Oscillation study at 200 °C in a plate/plate rheometer.

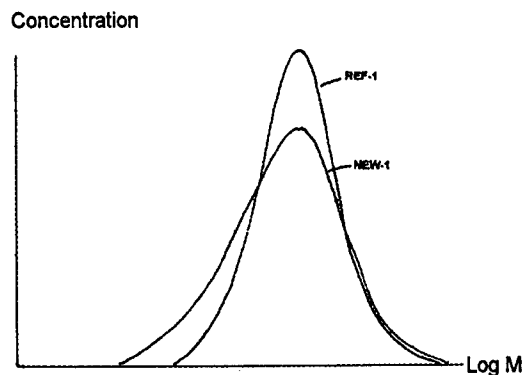


Figure 8. GPC curves of the HDPE compounds, NEW-1 and REF-1

During manufacturing of a plastic product, stresses will be introduced in the material which cause dimensional instability of the final product (6). Factors influencing the dimensional instability are e.g. rapid and/or uneven cooling and shaping stresses that brings the material into the desired form. In the case of cable extrusion, orientation of the molecules plays an important role. After the plastic melt leaves the die, the reorientation or relaxation of the molecules starts. The faster the relaxation of the molecules is, the more material will relax before it solidifies, and the less stresses will be built in the jacket (7). The built in stresses in the material will later release, especially when the cable is exposed to higher temperatures, causing shrinkage of the jacket. In addition, secondary crystallisation can take place, causing further volume decrease of the material.

Longer molecules have longer relaxation times. Higher MFR materials (lower molecular weight), e.g. NEW-1 and REF-1, will consequently have lower tendency to shrinkage. It is however not only the average molecular weight of the resin that determines the shrinkage level, but also the molecular weight distribution (MWD). A proper choice of catalyst system will prevent the formation of very long molecules during the polymerisation. In the GPC curves of figure 8 the two low shrink grades have similar appearance on the long chains side of the curve.

The superior ESCR of the new materials can not be explained by the MWD but by the unique comonomer distribution. The comonomer is preferentially incorporated into the long molecular chains, which then become so called

tie molecules in the material. These tie molecules link the crystallites of the materials, creating a very strong material. The effect of these tie molecules is particularly evident when the amorphous regions are swelled during the ESCR test. This optimised comonomer distribution is obtained by the use of bimodal technology.

Some material parameters are mainly controlled by the density level of the polyethylene resin. Examples of such properties of importance in jacketing are water permeability, abrasion resistance, filling compound resistance and surface hardness. A high density material is preferable when these properties are considered. The slightly lower abrasion resistance of NEW-1 compared to NEW-2 and REF-2 can probably be explained by the higher MFR level (lower molecular weight) of the material. The difference regarding barrier and abrasion properties between the LLDPE and the LDPE grades, is probably an effect of the slight copolymer content of the LDPE grade, which is added to improve the ESCR performance.

CONCLUSIONS

A new generation of polyethylene jacketing resins has been designed and studied in this work. By combining a high density level of the polyethylene resin with bimodal technology, materials with very good balance in all jacketing properties have been obtained. The wide process window, the low shrinkage and the excellent ESCR in combination with the toughness achieved by a HDPE, make this type of new materials ideal for fiber optical as well as power cable applications. With this new generation polyethylene resins a great step has been taken to meet the future requirements for jacketing materials in telecommunications as well as power cables.

ACKNOWLEDGEMENTS

The authors would like to express their sincere appreciation to the other team members of this project within Borealis; Markku Asumalahti, Tarja Korvenoja, Jari Äärilä, Ari Palmroos and Siegfried Wegener. Thanks go also to Mrs Eva Hopstadius for experimental assistance and to all other colleagues at the Wire and Cable Skills Centre, Borealis for fruitful discussions and good co-operations.

REFERENCES

1. Elias, H.G., "Macromolecules, Structures and Properties" Vol. 1, Plenum Press, p. 463 (1984)
2. Stöger, H., Stubbe, R., Ulrich, M., CIRED 1985 8th International Conference on Electricity Distribution, p. 225-230 (1985)
3. Barnes, S.R., Hill, O.C.A., Vyas, M.K.R., Sutehall, R., Fourth International Conference on Plastics in Telecommunications, p. 10/1-10/10 (1986)
4. Richardson, C.G., Proceedings of the 35th International Wire and Cable Symposium, p. 40-42 (1986)
5. Robinson, M., Dye, D., America's NETWORK, Sept. 1, p. 42-43 (1994)
6. Struik, L.C.E., "Internal stresses, Dimensional Instabilities and Molecular Orientations in Plastics", John Wiley, p. 1-3 (1990)
7. Aldhouse S.T.E., McMahon, D., Robinson, J.E., Fourth International Conference on Plastics in Telecommunications, p. 32.1-32.12 (1986)

AUTHORS



Laila Rogestedt received the M.Sc. degree in Chemical Engineering from Chalmers University of Technology, Göteborg, Sweden in 1986. After research work at the Department of Polymer Technology, Chalmers University and at the Department of Macromolecular Science, Case Western Reserve University, Cleveland, Ohio, USA she received a licentiate of Engineering degree from Chalmers University of Technology, 1989. She joined Borealis (Neste at that time) in 1991 and has since then mainly been involved in the development of cable materials for telecommunication and jacketing applications.



Hans-Bertil Martinsson joined the company (former Unifos) 1972 and has since 1988 been responsible for development of communication and jacketing grades for wire and cable.

Author's address:
Borealis AB
444 86 Stenungsund
Sweden

NON-HALOGENATED, NON-BRAIDED, EASY TO INSTALL CENTRAL OFFICE POWER WIRE

Kyle E. Cope

Pirelli Cables North America, Columbia, South Carolina

ABSTRACT

Unbraided low-smoke halogen-free cables for use in cable trays in the central office environment can be difficult to install. This problem arises due to congested cable trays. In order to solve this installation problem, a unique material and process solution has been found. The system reduces the static coefficient of friction by 35-55%. The cable meets UL-44 for RHH/RHW insulation and CSA 105°C appliance wire requirements. In addition, the cable complies with major industry central office power wire specifications such as Bellcore GR-347-CORE.

INTRODUCTION

Many cable users are moving in the direction of specifying low-smoke halogen-free (LSHF) materials for cable insulations. This has been seen in the telecommunications industry, particularly the telephone central office environment. When a device such as a telephone, fax machine or computer modem sends information to another end user on the network, the signal is first sent to the local central office. From there, it can be directed, by switches, through a number of different routes, either directly to the end user, or to another central office. The equipment used in the switch system is DC powered and uses voltages ranging from 24 to 140 volts DC.¹ It is imperative that this equipment run uninterrupted. To ensure this, the switches are powered by batteries which are in turn continuously charged by rectifiers. It is this power wiring between batteries and equipment which calls for LSHF materials.

In the past, the primary insulation material used in this cable was chlorosulphonated polyethylene. This material had excellent flame resistance properties and flexibility, but when burned, produced large amounts of smoke and toxic, corrosive gas. Electrical fires in telecommunication and other environments have resulted in fatalities and destruction of equipment. The smoke emission and halogenated nature of the insulated cable was deemed partly responsible for the severity of the damage.²

This has resulted in the need for a wire insulated with a non-halogenated low-smoke material which would have acceptable performance to power the equipment in central offices.

The power wire is generally installed in cable trays run along the ceiling of the basement in a central office. These wires are in very close proximity to both fluorescent lighting and sprinkler systems. They are also very often installed close to sensitive electrical equipment. This environment requires specific performance of the wire insulation. Wet ratings are needed because of the sprinkler systems and resistance to UV is needed because the cable may be stored outdoors or run outside for a brief segment. Resistance to fluorescent lighting is needed as well¹. The cable needs to be flexible to pull around cable tray bends and must be rugged to withstand sharp tray edges. Toxicity, corrosion and smoke should be minimized for public safety and also for protection of the sensitive electronic equipment. These properties have been summarized in UL-44³, CSA C22.2 No. 210.2⁴, Bellcore GR-347-CORE⁵, and specific user specifications.

DESIGN OF DUAL LAYER CABLE VS. SINGLE LAYER EVA

Dual Layer Approach

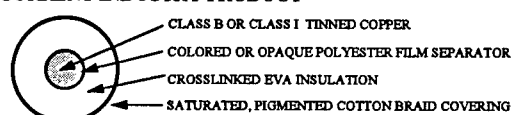
The common current design available for LSHF Central Office applications consists of a single layer of EVA (Ethylene Vinyl Acetate) covered with a cotton braid. EVA provides a good level of flexibility to the insulation and has the benefit of easily mixing with other compounding ingredients. However, it can fall short in areas of strength and ruggedness.

The proposed design consists of two coextruded layers. This allows the designer to combine properties into a singular insulation. This is commonly seen in ruggedized utility distribution cable; a flexible inner layer, possibly linear low density polyethylene (LLDPE), is covered by a tougher material such as high density polyethylene (HDPE). The HDPE provides the ruggedized properties, while the LLDPE inner layer prevents the cable from being too stiff for installation.

Dual Layer Design Breakdown

The proposed design utilizes an inner layer and outer layer of defined ratio. The layers are designed to provide flexibility, physical properties, ruggedness, and various resistances to UV and oil.

CURRENT INDUSTRY PRODUCT



PROPOSED DESIGN

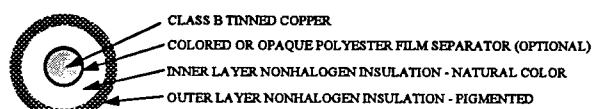


Figure 1 - Design Breakdown

ADVANTAGES OF NON-BRAIDED DESIGN OVER BRAIDED DESIGN

Flexibility

The use of a braid has been seen to reduce the flexibility of the cable. This can have an impact when trying to install around corners or when the cable is coming off cable trays to an installation panel. If the flexibility is high enough, the need for Class I (braided) strand may be eliminated in some sections of the installation.

The cable flexibility can be measured by performing a 3-point bend test such as a modified ASTM D 740 test method. Using a mechanical testing machine, the maximum load to bend a cable around a prescribed bend radius was measured. In this case, the higher the force, the more difficult the cable is to bend.

During installation, retention of shape after permanent training is desirable. A cable with a high degree of springback can be difficult to work with and possibly dangerous if the cable rapidly snaps back.

When bent around similar mandrels, the proposed non-braided design provided better flexibility over the braided design as well as approximately 15° less springback.

Table 1: Flexibility and Physical Properties of
750 KCM Power Cable with Separator Tape

	Braided Design	Proposed Non-Braided Design
Flexibility, kN	0.89	0.74
Springback, angle°	30	15
Tensile Strength, MPa	9.41	12.6
Elongation, %	191	178

Low Smoke Properties

The description "low-smoke halogen-free" implies certain properties. However, all low smoke materials are not the same. Two materials can both pass the "LS" rating per UL-1685⁶, but produce different smoke levels. Any cable with the "LS" listing has passed UL requirements and is considered low smoke. However, test data in Table 2 shows that the braid component can add up to 169 points to the smoke density. The braid is required to be saturated with a flame retardant per Bellcore GR-347-CORE, but results in a smoke producing component. The ICEA values shown in Table 2 are applicable to LSHF jackets. ICEA insulation requirements at similar levels are currently awaiting publication.

Table 2: NBS Smoke Chamber Data for Low Smoke Insulation Systems, Flaming-Mode

	Braid /Insulation	Proposed Non-Braided Design	ICEA Jacket Reqt.
D _s , 4 min.	126	11	50 max.
D _{max}	375	206	250 max.

Removal of the braid is a natural progression for the product. Bellcore has suggested in Section 1.2 of GR-347-CORE that the braid be removed from the design.

Ruggedness Retention

A natural concern with removing the braid is that the cable is now less protected from damage than it was before. This is true in the case of some abuse tests, but not the tests which are most applicable to cable installation in cable trays and performance. These tests are summarized in Tables 3 and 4.

The most important tests for the central office application are scoring and abrasion tests. When cables are installed in a cable tray, they may rub against the edge of the tray or run against some sharp edges. The outer layer improves the overall ruggedness of the cable compared to a braided EVA cable.

Table 3: Ruggedized Properties for Cable Tray Installations

	Braided Design	Proposed Non-Braided Design
Abrasion, # cycles	67	113
Scoring, # cycles	5	8

Two other applicable tests, used for ruggedized cable, are blunt and sharp impact. Cable may be hit with rubber mallets to bend around corners or other obstacles. In this case, the protection offered by the braid is apparent. However, cable produced using the proposed two layer design, when struck with a rubber mallet showed only minor scuffing.

Table 4: Ruggedized Properties Simulating Cable-Forming Abuse

	Braided Design	Proposed Non-Braided Design
Blunt Impact, J	9.73	7.35
Sharp Impact, J	3.08	1.99

Crush and puncture properties, as tested per UL and ICEA are rarely seen in cable tray applications. These tests were initially developed by the military to ensure the robustness of cables which may be run over by military vehicles. Cables for installation in cable trays are not subject to these types of loads. Occasionally, a cable reel may run over a cable end at the end of the reel, but this results only in minor scuffing of the insulation surface. All ruggedized testing was performed using the methods described in ICEA S-81-570⁷.

INSTALLATION PROPERTIES AND LOW COEFFICIENT OF FRICTION

One of the major benefits that the braid provides is a low friction surface for installation. The smooth surface of the braid, compared to the rubbery feel of the EVA insulation is readily apparent. Typical non-braided, material systems show poor results in terms of manpower needed, scrapped cable and overall inefficiency. The problem lies in the high coefficient of friction associated with a non-braided surface. Table 5 shows the force needed to pull a cable with various coefficients of friction. As more cable enters the tray, more weight has to be moved. Over long pulling lengths, these forces can quickly become unmanageable.

Table 5: Pulling Force to Overcome Static Friction

Weight of Cable in Tray	Proposed Non-Braid Design	Braided Design	Common Non-Braided Design
	$\mu_s = 0.73$	$\mu_s = 1.00$	$\mu_s = 1.50$
0.5 kN	0.37 kN	0.50 kN	0.75 kN
1.0 kN	0.73 kN	1.00 kN	1.50 kN
1.5 kN	1.10 kN	1.50 kN	2.25 kN

2.0 kN	1.46 kN	2.00 kN	3.00 kN
2.5 kN	1.83 kN	2.50 kN	3.75 kN

ADVANTAGES OF THE PROPOSED SHEATH SYSTEM

The proposed design solves the friction problem by providing a cable which has a very low friction insulation surface.

Friction Laws

During installation, as the pulling force is slowly increased, an opposing force of equal magnitude appears. This opposing force is associated with the interlocking microscopic irregularities between the cable and the pulling surface. When the applied force reaches a critical value, the opposing force is overcome and the cable begins to move. This opposing force (f) is related to the static coefficient of friction (μ_s) which is:

$$f < \mu_s N \quad (1)$$

Where N is the normal force between the cable and the pulling surface.

Once the cable is in motion, the force necessary to keep it in motion with a constant velocity is usually less than the force needed to get motion started. This kinetic coefficient of friction (μ_k) is:

$$f = \mu_k N \quad (2)$$

COF Data

The decrease in friction seen in versions of the proposed design has been 35-55%.

The cable is tested using a modified ASTM D 1894 setup. A track is constructed of the material over which the cable will be pulled. This may be aluminum or steel based on an empty tray, or it may be the test cable itself if the tray is filled with similar cable.

The test cable is then placed horizontally over the test track and the cable end is attached to a load cell of a mechanical tester. The cable is pulled via a cord which moves over a pulley to change the direction of the force. As the cable is pulled, the load cell measures the load exerted on the cable. Only the insulation surface and the track are in contact.

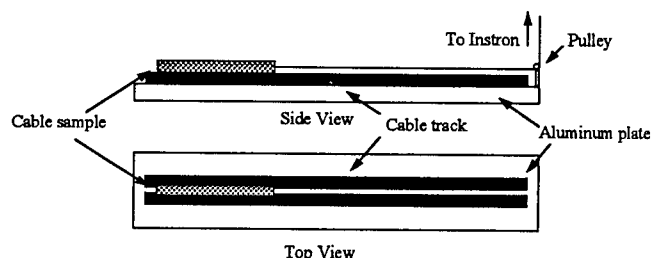


Figure 2 - Friction Testing Layout

With the initial load, average load and the cable weight known, the static and kinetic friction factor can be calculated as above. Tests are repeated 10 times and an average factor is obtained. Table 6 shows results for braided and the proposed non-braided cable pulled over itself.

Table 6: Coefficient of Friction - Cable Pulled Over Itself

	μ_s - static	μ_k - kinetic
Proposed Non-Braid Design	0.73	0.59
Braided Design	1.00	0.72
Current Non-Braid Design	1.50	1.23

Stability of Sheath System

Any material system used for reducing friction should remain a part of the cable system and not easily deteriorate. Cable may be exposed to water, sunlight, extreme cold, or other environments. If these conditions adversely effect the sheath system, when the time comes to install the cable or another cable over the existing one, the cable may have lost it's properties of low coefficient of friction.

To test the sheath system stability, a cable of the proposed two layer design was subjected to a variety of conditioning tests. Tests included: submersion in water, exposure to heat and exposure to cold. The sheath system stability was also tested after the cable was energized and after scraping the cable over a blunt edge of a typical cable tray.

None of the conditions adversely affected the performance of the sheath system. Testing showed that use of the sheath system reduced

the static coefficient of friction from 35 - 55% of the original value.

Each condition shown in Table 7 was tested on a different cable sample. Therefore, the COF data in column 1 is not the same for each condition. The friction behavior of each sample was baselined without conditioning and without the new material system as part of the cable.

FUTURE WORK

Currently, there are limited specifications covering low smoke halogen free materials. ICEA has a guide, ICEA T-33-655 for Low-Smoke, Halogen-Free (LSHF) Polymeric Cable Jackets. ICEA standard S-73-532/NEMA WC 55 includes insulation requirements. This standard has been approved by NEMA codes and standards and is awaiting publication. While these and other specifications begin to appear, cable manufacturers and users will have to agree on the property requirements of the application so that the ultimate expectations of LSHF products are met.

CONCLUSIONS

To recap the benefits of the new sheath system, versus a braided design, several special factors associated with the application of these cables in cable trays must be noted. The non-braided design is more flexible than the braided design aiding in installation, particularly around corners and entering and exiting cable trays.

The non-braided design produces less smoke than the braided design. The braid, while offering a degree of insulation protection and a smooth outer surface for installing, is a smoke producing component of the cable design.

As seen in the test data, the design has not only solved the friction problem associated with unbraided designs by providing the outer cable surface with a lower coefficient of friction than that seen on cables using a braid, but improves all other mechanical and fire related properties.

Table 7: Sheath System Stability of Proposed Design

Baselined Friction Behavior, Without New Sheath System and Unconditioned	Condition	Friction Behavior of New Sheath System after Conditioning
μ_s		μ_s (% change)
1.10	None	0.73 (-34)
0.95	Cold (-35°C/4 hours)	0.55 (-42)
1.21	Humidity (95%, 100°C/3 days)	0.69 (-43)
1.15	Moisture (23°C tap water/1 hour)	0.71 (-38)
0.96	Long Term Heat (121°C/7 days)	0.57 (-41)
1.27	Abrasion	0.69 (-46)
1.19	Energized (hot) track	0.49 (-59)

REFERENCES

- ¹ F. Makan "Non-Halogen, Low-Smoke Insulation for Low Voltage Telecommunications Power Wire Applications" IWCS, p780, 1993.
- ² G. Waag "Improving Fire Safety with Wire and Cable Compounds" Wire Technology International, p20, May 1993
- ³ UL-44 Underwriters Laboratories Inc. Standard for Thermoset-Insulated Wires and Cables. January 27, 1997.
- ⁴ CSA C22.2 No. 210.2 Canadian Standards Association Standard for Appliance Wiring Material Products, October 1992.
- ⁵ Bellcore GR-347-CORE, Generic Requirements for Central Office Power Wire, November 1996.
- ⁶ UL-1685 Underwriters Laboratories Inc. Standard for Vertical-Tray Fire-Propagation and Smoke-Release Test for Electrical and Optical-Fiber Cables. February 25, 1997.
- ⁷ ICEA S-81-570 Standard for 600 Volt Direct Burial Cable Single Electrical Conductors and Assemblies with Ruggedized Extruded Insulation. March 5, 1996.

AUTHOR

Kyle Cope received a B.S. in Materials Science and Engineering from Drexel University in 1993. He is an Engineer for Materials Development in the RD&E Center of Pirelli Cables North America headquartered in Columbia, South Carolina. His main focus is on the engineering of materials for use in energy and fiber optic cables.



Kyle Cope
Pirelli Cables North America
710 Industrial Drive
Lexington, SC 29072

DIE DROOL IN CHEMICALLY CROSSLINKABLE POLYOLEFIN COMPOUNDS

Steven W. Horwatt and George A. Hattrich

Millennium Petrochemicals, Inc.
Cincinnati, Ohio

ABSTRACT

Die drool is a commonplace, sometimes chronic, processing problem which can have serious effects on the final quality and appearance of extruded products, including wire and cable constructions. A laboratory scale test for assessing the severity of die drool for a given compound has been developed. In this study, the effects of several extrusion parameters on the die drool generation of an automotive wire insulation compound were examined. It was found that die condition, particularly the presence of damage and defects in the die surface, strongly influenced the rate of die drool. In addition, the rate of die drool was found to increase at higher extrusion rates and temperatures. Die cooling was found to be effective in reducing the rate at which compounds generated die drool.

INTRODUCTION

The undesirable accumulation of material around the exit of an extrusion die is commonly referred to as die buildup or die drool, and it is observed in a wide variety of polymer systems and extrusion processes. Die buildup can be particularly problematic in processes employing the continuous vulcanization (CV) technique, such as the insulation of automotive primary wiring. Problems arise in the CV technique because the die is enclosed by a tube filled with high pressure steam and, thus, is inaccessible during the wirecoating operation, preventing removal of the accumulating material by the operator of the line.

Eventually, die buildup releases from the die face in one of two ways. The buildup can attach to the wire insulation in the form of a complete or partial ring of material (as shown in Figure 1), commonly referred to in the wire and cable industry as a die ring, horsecollar, donut, or fuzzball. In addition to causing tears or other flaws in the wire insulation, these rings can create problems in the automated

harnessing operation, causing wire breaks and downtime. Die buildup which does not adhere to the insulation eventually falls into the CV tube and is washed down the tube by steam condensate. If the die drool is only partially crosslinked when it detaches from the die face, numerous particles can adhere to one another, forming large pieces which can clog steam traps, screens and water seals and result in unscheduled shutdowns.

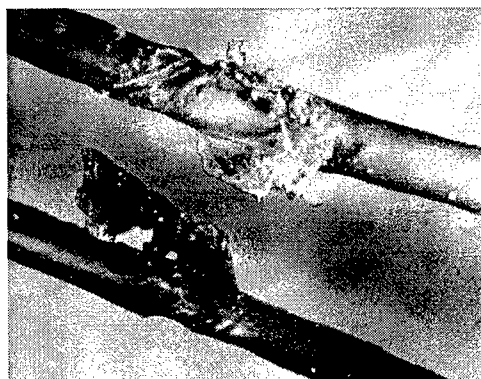


Figure 1. Two automotive wires having processing defects resulting from die buildup.

In general, die buildup is a widely experienced, seldom studied phenomenon. While a wide variety of causes and aggravating factors for die buildup have been proposed, the basic mechanism is still not understood. A number of factors which have been proposed as sources of die buildup are ¹:

1. Low molecular weight polymer species.
2. Volatiles, including moisture.
3. Presence of a filler material.
4. Poor dispersion of pigments.
5. Draw down and take off rates.
6. Amount and rate of die swell.
7. Atmospheric conditions including humidity.
8. Die exit angles, land length, and land entrance size.
9. Dissimilar component viscosities.
10. Die condition (including cleanliness, presence of damage, defects, etc.)

11. Pressure fluctuations in screw channel.
12. Improper melt temperature.

Although many of these factors appear to aggravate die buildup, it appears that none of them is the actual root cause.

While it is true that unfilled polymers will produce die buildup under certain circumstances, highly filled compounds generally produce die buildup at a substantially higher rate and at much lower temperatures than the unfilled base resins. The level of filler in the compound appears to have a strong influence on the rate at which the compound generates die drool, probably due to interactions between the filler and the polymer. Whether these filler-polymer interactions are physical or chemical in nature is unknown. The high filler levels present in automotive primary wire insulation compounds make these compounds highly prone to die buildup problems.

The base resin of the compound being extruded also influences the rate at which the compound generates die buildup. Even similar polymers produced on different reactor types sometimes generate die buildup at different rates. This difference in die buildup rate may be due to different levels of low molecular weight species in polymers produced on different reactors.

One of the few attempts in the literature to address the causes of die buildup is a brief article by Klein ², in which die buildup is attributed to extrudate swell. Klein hypothesized that die buildup occurs when the extrudate swells so severely that molten polymer scrapes against and adheres to the surface of the die. The logical extension of this reasoning is that die buildup can be minimized by minimizing the tendency of the resin or compound to exhibit extrudate swell.

There are some contradictions to the theory that die swell and die buildup are directly related, however. The incorporation of a rigid filler into a polymer melt reduces the normal stresses during extrusion ^{3,4}. The result of the reduction of normal stresses is that polymers exhibit less extrudate swell when filled, whereas filled polymers typically exhibit more severe die buildup than the corresponding base polymers.

Some techniques for alleviating die buildup are known in the patent literature. For example, the

addition of fluoropolymer processing aids to a resin or compound can sometimes reduce or even entirely eliminate die buildup ⁵. Unfortunately, the function of the fluoropolymers can be inhibited by some other additives, especially in highly filled compounds ^{6,7}. There appear to be no general principles known for designing compounds which are resistant to the formation of die buildup.

Coating the die surface and in the interior of the die with lubricious materials such as fluoropolymers or polysiloxanes has also been found to reduce die buildup for some systems, although the useful life of such coatings can be quite short when highly filled compounds are extruded ^{8,9}. Manufacturers have devised dies utilizing mechanical means (such as pins) of breaking up the material accumulating at the die exit ¹⁰. It is also known that cooling of the die helps reduce or even eliminate die buildup in wirecoating operations ¹¹.

A serious obstacle to a deeper understanding of the variables controlling die buildup is the lack of a reliable laboratory scale test method which can predict the tendency of a compound to exhibit die buildup. Experiments performed on commercial scale equipment are typically narrow in scope, due to expense. Die buildup is often an intermittent phenomenon, varying not only day to day, but also from lot to lot of compound, and from extruder to extruder (or even between various constructions on the same extruder). Most published studies of die buildup are qualitative rather than quantitative in nature.

Two quantitative techniques for assessing the rate of die buildup are found in the literature. Kurtz, et. al. scribed circles on the face of the die, designating 25 percent increments of die face cross sectional area ⁶. The times required to cover various fractions of the die surface were used as a measure of die buildup rate. Since die buildup does not always advance across the die face in a uniform front, the time to cover a designated area can be somewhat variable, and this technique was not considered in this study.

In the second method of die buildup measurement described in the literature, Chan collected and weighed the amount of die buildup which attached to the extrudate as a function of time ¹². This method was not an actual measure of die buildup rate, however, as the amount of material remaining

on the die surface was not quantified. This technique was adapted for the current study, but it was found to have deficiencies and was discarded.

This paper presents a description of a laboratory scale test to assess the level of die buildup as a function of compound and process variables.

EXPERIMENTAL PROCEDURES

Melt Index Die Swell (MIDS) Test

Extrudate swell was measured using an extrusion plastometer (ASTM D1238) fitted with a short-landed die. The plastometer temperature was 125 °C. The die used had a diameter of 0.0824 inches and a length of 0.028 inches. Samples weighing five grams were preheated under a 2000 g load for 6 minutes before initiation of the test. Testing load was 5000, 10,000 or 20,000 grams. Six inches of extrudate were obtained and discarded, then another six inch length of extrudate was collected, cooled for one hour and measured at the center and one inch from each end. Three specimens for each compound were tested in this way and all measurements averaged to obtain extrudate diameter. The swell ratio is the ratio of extrudate diameter to the die diameter.

Accumulation Rate Measurements

Compound was extruded through a 3/4-inch laboratory extruder (hereafter referred to as Extruder 1) equipped with a screw having an L/D of 20/1 and a compression ratio of 1:1. The die used had a diameter of 0.075 inches and was a crosshead wirecoating die in which the guider tip was blind (i.e., the end of the guider tip was blocked to prevent backflow of material into the guider).

The measurements were performed by extruding compound at 100 RPM for 10 minutes, then shutting off the extruder and carefully collecting the accumulated material from the face of the die. The extrudate and die buildup were weighed and a ratio of the weights calculated. The extruder was purged for 10 minutes between shutdown for sample collection and the initiation of a new test. Thirty minute purges were conducted when changing compounds.

DIE BUILDUP TEST DEVELOPMENT

Elevated Die Face Temperature Experiments

The technique employed by Chan required some modification to implement, as die buildup does not attach to the extrudate during thermoplastic extrusion of commercial automotive wire insulation compounds. For this reason, a shield was placed around the strand die mounted on Extruder 1, and a heat gun was directed past the die to raise the air at the die face to a temperature of 350-400 °F. In this configuration, die buildup occurred at a much faster rate than during thermoplastic extrusion, and the material accumulating at the die exit periodically broke free and attached to the extrudate in a process illustrated in Figure 2.

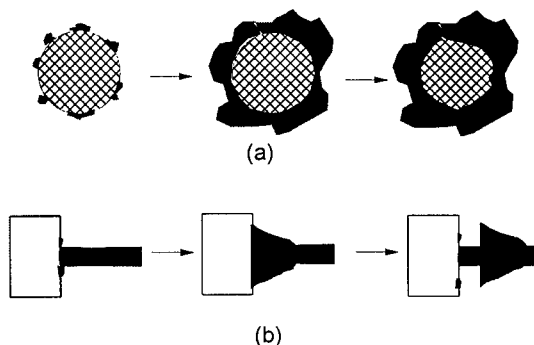


Figure 2. Illustration of the die ring formation process, shown from two perspectives: (a) front view of die exit, (b) side view of die face. Material accumulates at die exit, forming a coherent ring, which eventually crosslinks and attaches to the extrudate.

Unfortunately, the time required for detachment of the die buildup was excessive (one hour or more for each event) and very irreproducible. Therefore, this technique was also abandoned. However, several qualitative observations were made in the course of these experiments. In thermoplastic extrusion, the material accumulating at the die exit is continuously pushed aside by fresh material, causing the buildup to spread out in a thin layer across the entire die face. When the die face temperature is sufficient to quickly crosslink the die buildup, the fresh drool builds a conical deposit projecting off the die face along the length of the extrudate. Eventually, the deposit begins to occlude the opening of the die, placing enough stress on the die ring to force it off the face of the die.

Extrudate Swell Measurements

In order to investigate Klein's theory of the relationship between die buildup and extrudate swell, the MIDS test was performed on three commercial automotive wire insulation compounds: A, B and C. From evaluations on industrial scale equipment, the compounds were known to have different tendencies to exhibit die buildup: Compound A showed a moderate level of die buildup, Compound B showed a slight level of die buildup and Compound C showed virtually no die buildup.

The swell ratio as a function of melt flow rate for each of the three commercial compounds is shown in Figure 3.

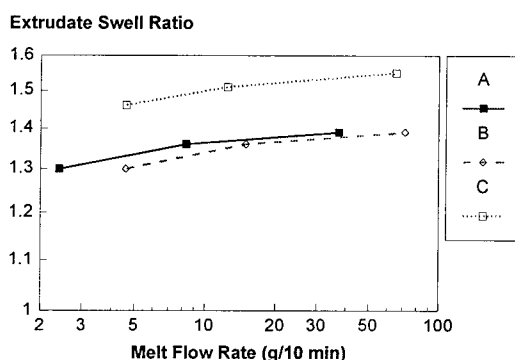


Figure 3. Extrudate swell ratio as a function of melt flow rate for three commercial automotive wire insulation compounds. The melt flow rate was varied by imposing three different loads (5000, 10000 and 20000 grams).

Compound C, which in practice exhibits the lowest level of die buildup, shows the most severe extrudate swell behavior. There is little difference in the extrudate swell behavior of Compounds A and B, even though their tendencies to exhibit die buildup are quite different. These results indicate that extrudate swell is not correlated to the die buildup behavior of these compounds.

Accumulation Rate Measurements

Die buildup rate was assessed through direct collection and weighing of the material accumulating on the die face. Since the amount of die buildup would clearly increase with the amount of compound extruded, the die buildup rate was expressed as the ratio of the weight of accumulated material to the weight of compound extruded.

The accumulation rate method has some distinct advantages over the measurement of the time to cover the surface of the die. The direct measurement of the quantity of material deposited on the die face is more objective than the judgment of coverage time and also accounts for the three-dimensional nature of the deposit. However, the weights obtained are very small (typically in the range of 5-25 mg for a 10 minute run), so the detachment of the die ring must be painstakingly performed and a reliable analytical balance is essential.

A series of three such measurements using Compound A is shown in Figure 4. Following the standard procedure, die buildup rate was measured for a 10 minute period with the extruder being purged for 10 minutes between runs. A series of measurements was also carried out in which the extruder was shut down and allowed to sit idle for 10 minutes between runs without purging. There was a slight increase in the rate of die buildup when the compound was allowed to sit in the extruder, indicating that residence time has an effect on the rate of die buildup. This effect may be due to thermal degradation of the polymer or some other component of the compound at the processing temperature.

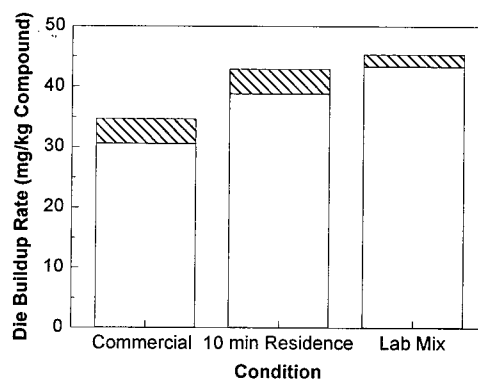


Figure 4. Mass accumulation rate as a measure of die buildup rate, showing the effects of residence time in the extruder and laboratory versus commercial scale mixing equipment. The stack bars indicate the 95% confidence limit.

In the third set of measurements, it was seen that material compounded on a small laboratory mixer showed a higher rate of die buildup than material produced on a commercial scale mixer. This comparison indicates that mixing has an effect on the die buildup behavior of the compound. Whether

this effect is due to differences in the quality of mixing or due simply to differences in shear or thermal history between the lab and commercial equipment is not known.

Figure 5 shows the die buildup rate as a function of output rate for two different 3/4-inch laboratory scale extruders (designated Extruder 1 and 2). The temperature profile for both extruders was set to a flat 250 ° F. For both extruders, the die buildup rate increased with increasing output rate, even though the die buildup rate is normalized on the mass of extrudate. This increase could translate into a larger number of defects on a given quantity of wire as production rates are increased.

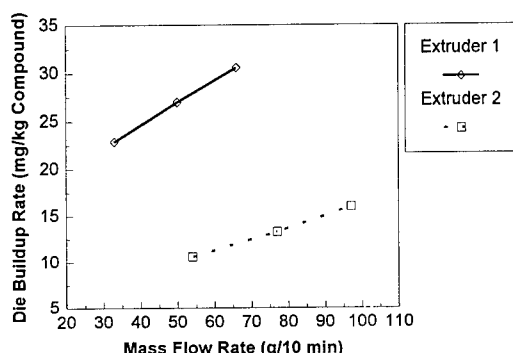


Figure 5. Die buildup rate of compound A as a function of extruder output for two different 3/4-inch laboratory extruders. The same die and head were used on each extruder.

The die buildup rate was significantly higher on Extruder 1 than Extruder 2 at comparable output rates. The same die and head were used on each extruder for these experiments, but the two extruders are quite different in several respects. Extruder 1 has an oil heated barrel with a single control zone and no cooling, while Extruder 2 has an electrically heated, 3-zone barrel with air cooling. The thermal history of the compound within each extruder is thus different, and this difference could account for the difference in die buildup rate. The screw of Extruder 1 has an L/D of 20/1 and a compression ratio of 1:1, while the screw of Extruder 2 has an L/D of 26/1 and a compression ratio of 4:1.

It is likely that the higher die buildup rate on Extruder 1 is due to the lack of barrel cooling on that extruder. This situation is observed frequently in industrial practice, where die buildup tends to occur to varying degrees on different lines, even when running the same compounds and

constructions. It also indicates that general application of this method of assessing die buildup requires that control compounds be used when comparing data obtained on different extruders.

Since neither of the extruders were equipped with die cooling, that variable could not be examined in depth. However, a simple arrangement was constructed in which plastic tubing connected to an in-house air supply was set to blow across the face of the die for cooling. This experiment was carried out on both extruders running at a screw speed of 100 RPM. Instead of generating die rings of approximately 20 mg in 10 minutes, Extruder 1 generated so little die buildup after 1 hour that the buildup could not be accurately detached for weighing. A similar reduction was observed for Extruder 2. This experiment illustrates the dramatic reduction in die buildup which can be obtained with die cooling.

In order to ascertain the relationship between die buildup generated on a small laboratory extruder and to the rate of die buildup on a commercial line, three compounds with differing levels of die buildup generation were formulated. Die buildup rate measurements were made in the laboratory, and similar measurements were carried out on a 3 1/2-inch commercial wire line with the CV pulled away and the wire removed to provide the same test geometry as the laboratory extruder. Figure 6 shows the laboratory-measured die buildup rate as a function of the die buildup rate measured on the commercial line.

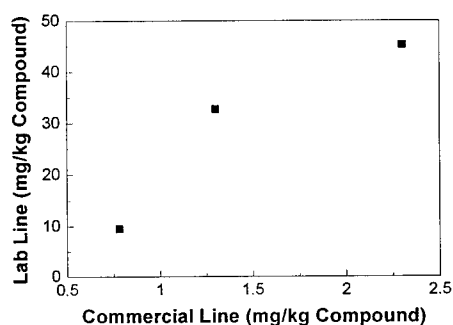


Figure 6. A comparison of the rates of die buildup measured on a 3 1/2 -inch commercial wirecoating line to those measured on a 3/4-inch laboratory extruder.

The commercial line shows a dramatically lower die buildup rate, one order of magnitude less, than that determined on the laboratory extruder. However, the same trend is shown on both extruders. This

trend indicates that the laboratory scale test could be useful in ranking the relative tendencies of compounds to generate die buildup in commercial processes.

Die buildup rate measurements conducted with various dies is shown in Figure 7. All four dies had identical entry angles and land lengths. Die 1 was a die which had seen significant use and had numerous scratches and imperfections. Die 2 was an identical die from the same fabricator, but it had never been used. The die buildup rate observed for Die 2 was substantially lower than that of Die 1, highlighting the importance of handling and cleaning wirecoating dies with care.

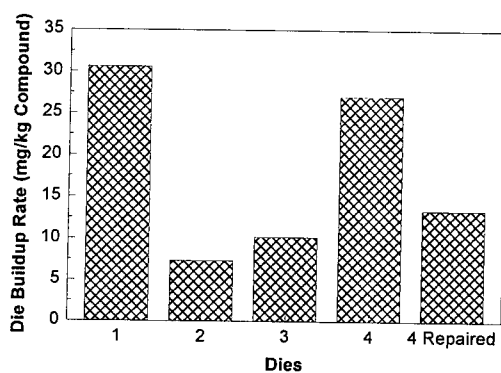


Figure 7. Comparison of die buildup rate measured on four dies of identical design. The dies were: (1) a heavily used die, (2) a previously unused die from the same manufacturer, (3) an unused die from a different manufacturer, (4) a defective die with a burred exit.

Dies 3 and 4 were produced by a different fabricator from the same materials as the first two dies. Die 3 was properly fabricated, but the hole in Die 4 was not drilled completely through the die, leaving a ridge of burred material approximately 0.05 inches wide which partially occluded the die exit. The die buildup rate for the defective die was substantially higher than that of the normal die. Die 4 was then repaired by completing the course of the die opening, which resulted in a die buildup rate similar to that obtained with Die 3.

The final variable examined in this study is the effect of die construction material and surface treatment on die buildup. As mentioned previously, certain types of die surface treatments (e.g., teflon coating) have been shown to decrease die buildup. However, such treatments are expensive and short-lived, making them commercially unattractive. There are other surface treatment techniques which

decrease surface roughness, improve the corrosion resistance of the metal and actually increase the service life of the die. The effects of these treatments on die buildup have never been reported in the open literature.

For this experiment, a set of identical dies were fabricated from untreated 600 and 420 stainless steel. The 420 SS dies were subjected to nitride, chrome plating and cryogenic surface treatments. The nitride and chrome plating treatments provide smooth, hard surfaces, while the cryogenic treatment provides a very hard but slightly rough surface. The 420 stainless steel was selected because it is one typically used in the construction of automotive wirecoating dies. The 600 stainless steel was selected because it is a harder, more corrosion-resistant material than the 400 series steels.

All of the fabricated dies were placed in an ashing furnace for 2 hours at 700 °F and 25 in Hg vacuum and then cleaned in an ultrasonic bath before use. This cleaning was to remove any residual oils and debris remaining on the die surfaces from the fabrication process. It was observed that such residues can increase the die buildup rate initially observed when extruding with a given die, resulting in a time dependent die buildup rate. This phenomenon is shown in Figure 8 for one of the untreated 420 SS dies, where the die buildup rate varied over time, eventually reaching a plateau when the residue on the die had been purged away.

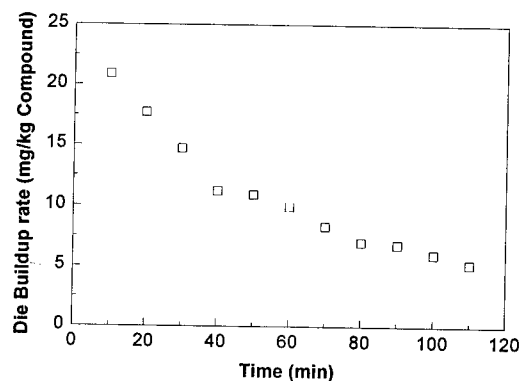


Figure 8. Die buildup rate as a function of time for an untreated 420 stainless steel die as received from the manufacturer. The time dependency of the die buildup rate is an artifact of residues from the die fabrication process.

The die buildup rates for the various dies after cleaning are shown in Figure 9. There are some apparent differences between the various surface treatments, but the two untreated dies showed the lowest rate of die buildup. This experiment seems to indicate that die buildup cannot be eliminated through the use of standard metal surface treatments, although more sophisticated coating techniques are known to be effective in reducing die buildup.

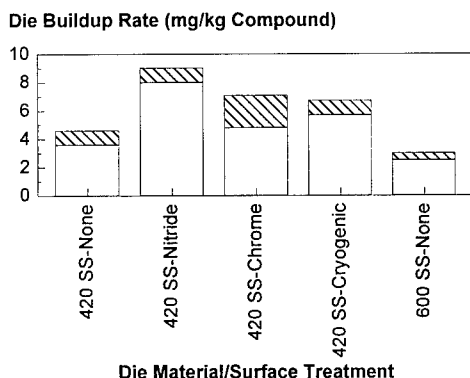


Figure 9. Die buildup rate for Compound A extruded through dies having various surface treatments. The stack bars indicate the 95% confidence limit.

CONCLUSIONS

A laboratory scale test for assessing the relative tendency of a compound to produce die buildup in commercial scale wirecoating operations has been developed. Applying this test, the following conclusions have been reached:

1. The rate of die buildup is increased by the presence of defects, scratches and gouges at the die exit.
2. Various extruders can exhibit very different die buildup rates, even when identical extrusion heads and dies are used.
3. Die construction materials and surface treatment appear to have an effect on the die buildup rate of extruded compounds. However, the lowest rate of die buildup seemed to be obtained with dies having no surface treatment.
4. Die cooling can dramatically reduce the rate of die buildup during extrusion.

REFERENCES

1. Gander, J.D. and Giacomini, A.J., "Review of Die Lip Build-Up in Plastics Extrusion," ANTEC 96, Toronto (May, 1996), pp.1113-1117.
2. Klein, I., "Die Drool: What Causes It, How to Avoid It", Plastics World, May, 1981.
3. Dealy, J.M. and Wissbrun, K.F., Melt Rheology and Its Role in Plastics Processing, Van Nostrand Reinhold, New York, (1989).
4. White, J.L., Czarnikci, L., and Tanaka, H., Rubber Chemistry and Technology, 53:823, (1980).
5. Priester, D.E. and Chapman, G.R., "Reducing Die Build-Up in Extrusion Applications," Polyolefins IX, SPE RETEC, Houston (February, 1995).
6. U.S. Patent 5,008,056 (1991).
7. Priester, D.E. and Stewart, C.W., "New Processing Additives for Polyolefins Minimize Formulation Interactions," SPE ANTEC, Detroit (May, 1992), pp. 2024-2028.
8. U.S. Patent 3,942,937 (1976).
9. U.S. Patent 2,403,476 (1946).
10. U.S. Patent 5,162,120 (1992).
11. Wooddell, G.L. and Itzkoff, M.L., "Crosslinkable Polyethylene for Wire and Cable: An Update," Wire Journal International (May, 1982), p. 62.
12. Chan, C.-M., "Viscosity and the Formation of Die Drool at the Polymer-Metal Interface: Effects of Surface Coatings," International Polymer Processing, X:3, pp200-203, (1995).

AUTHORS



Steven W. Horwatt
Allen Research Center
11530 Northlake Drive
Cincinnati, OH 45249

Steve Horwatt received his B.S. (1986) and M.Eng. (1987) in Chemical Engineering from the University of Louisville. He received his Ph.D. in Polymer Science from Case Western Reserve University in 1991. Since 1991, he has been employed by Millennium Petrochemicals (formerly Quantum Chemical), in the Wire and Cable research and development group, principally in the Automotive and Appliance wire area.



George A. Hattrich
Allen Research Center
11530 Northlake Drive
Cincinnati, OH 45249

George Hattrich has a B. S. Degree in chemical engineering from the New Jersey Institute of Technology. He has 34 years experience in the polymer industry with 24 years specifically associated with the wire and cable industry. George started his career with Monsanto Chemical Co. where he held a variety of positions in the Quality Control and Technical departments. He joined Reichold Chemicals Inc. in 1973 which became BP Performance Polymers Inc. in 1985. At RCI and BPPPI, George was responsible for the development and customer technical service of XLPE compounds for wire and cable. In 1993, George joined Quantum Chemical Co. (now Millennium Petrochemicals, Inc.) as a Development Associate responsible for customer technical service of XLPE compounds for the Automotive and Appliance wire markets.

PHYSICAL PROPERTY AND TOXICOLOGICAL IMPROVEMENTS IN PREMISE CABLE INSULATIONS

Jeff S. Borke

Millennium Petrochemicals Inc.
Cincinnati, Ohio

Abstract

Specifications for premise cable are constantly changing to compensate for faster networks and broader bandwidths, as well as the demand for more environmentally friendly cable materials. To address these issues, a new halogenated, non-diphenyl oxide flame retarded polypropylene compound has been formulated for use in premise wire applications. The new compound shows improved electrical, physical and toxicological properties.

Background

In the local area network (LAN) market there is a continual demand for premise cables that have faster data transfer rates and broader bandwidths. These demands have forced manufacturers to optimize current premise cable constructions as well as to develop new constructions for the future.

In the past, PVC had been the standard insulation material for premise cables. In recent years, increasingly stringent flame, smoke and signal transmission speed requirements have opened the market for flame retardant polyolefin and fluoropolymer materials (FEP). With the high cost of FEP and the advances in jacketing materials and flame retardant systems, polyolefins have become commonplace in the premise cable industry. Advances in electrical, toxicological and flame properties of polyolefin based systems are the key to their continued use in the premise cable market.

The quality foci for all premise cables start with the insulated copper conductor. Insulation type and dimensional stability of the insulated copper conductor dictate electrical, toxicological and flame

properties of the final premise cable¹. Electrical properties such as attenuation, impedance and capacitance are directly influenced by insulation dimensions, eccentricity of the conductor to the insulation, twisted pair configurations and other construction based variables².

Flame and toxicological properties depend upon what types of raw materials and flame retardants are used to construct the premise cable. One of the most common flame retardant systems used in polyolefins is based on the efficient and inexpensive brominated compound, decabromodiphenyl oxide (DBDPO). However, debates have been occurring for years as to whether diphenyl oxide (DPO) based flame retardants produce trace quantities of toxic dioxins and furans when burned. Initial studies³ in 1986 showed that incomplete combustion of DBDPO at 510°C-630°C produced dibenzofurans (PBDFs) and dibenzo-p-dioxins (PBDDs) with total yields of 10 percent. Further studies by several companies and laboratories confirmed the production of PBDFs and PBDDs at burning conditions between 400°C and 800°C but at much lower quantities⁴.

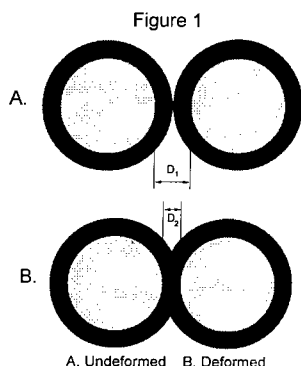
In response to these studies, the European Economic Community proposed a directive to ban the use of brominated DPOs. Though the directive was never implemented, several European companies require signed documentation that no components of a cable contain brominated DPOs.

Objectives

Many polyolefin premise wire insulations are based on high density polyethylene (HDPE) because of its

excellent dielectric, toughness and mechanical properties. After insulating the conductor, processes such as twinning (process of twisting two conductors together) and jacketing would routinely damage or deform the insulation causing inferior electrical properties in the final cable.

As manufacturers developed Category 5 cables that required 100 MHz signal ratings, twisting of the conductor pairs became tighter and even HDPE lacked the toughness to withstand the deformation or cut-in that occurs during the twinning process (Figure 1). Greater insulation wall thickness helped compensate for the insulation deformation but at a higher cost.



Another approach would be to use a tougher material which could reduce wall thickness, and in turn, cost. One method to address the above would be to replace HDPE with polypropylene (PP) insulation compounds. This replacement would improve electrical and physical properties of the premise wire. These improvements would result from PP's inherently superior thermal resistance, dielectric constant and toughness when compared to HDPE.

In the following report, formulations based on HDPE and PP were evaluated for electrical and mechanical improvements. Also addressed is the replacement of the commonly used DBDPO flame retardant system with a new halogenated system that does not form dioxins or furans but maintains equivalent flame retardancy and physical properties.

Experimental Test Methods

All insulation compounds were extruded using a 2-1/2" 20:1 Davis Standard extruder equipped with a Maddock screw to apply a 10 mil wall onto 22 AWG solid copper conductor.

Crush Resistance (UL1581)

Crush resistance is a test method used to correlate the ability of insulation to resist deformation under an applied load. The crush test uses an Instron Universal Testing Machine to apply an increasing load at a constant rate. The test is complete when the insulation crushes, allowing contact with the conductor, completing an electrical circuit. The maximum load is then recorded as the crush resistance value.

Dielectric Testing (ASTM D150)

Dielectric properties were acquired using a HP4342A Q-Meter. In accordance with ASTM D1928 two 50 mil compression molded plaques of each insulation compound were used for Q-Meter testing.

Limiting Oxygen Index (LOI) (ASTM D2863)

This test method describes a procedure for measuring the minimum concentration of oxygen that will support flaming combustion. In accordance with ASTM D1928, 125 mil compression molded plaques were used.

Tensile Properties (ASTM D638)

Tensile properties were measured using insulated wire with the conductor removed.

Results & Discussion

Electrical and Mechanical Enhancements

Figure 2 compares the dielectric constant of PP and HDPE based insulation compounds used for CMR (riser specification) rated constructions. Compared to HDPE, PP has a lower dielectric constant even after formulation.

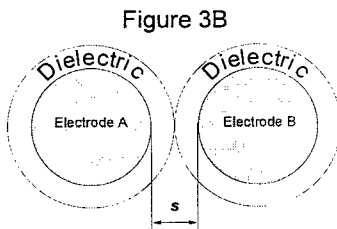
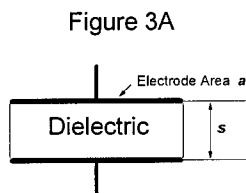
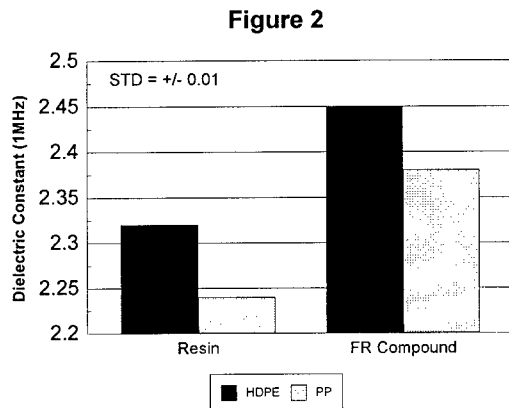
The dielectric constant is important whenever capacitance effects can deteriorate electric properties of the final cable⁵. The capacitance of a parallel plate capacitor (Figure 3A) is given as:

$$C = \frac{Da}{4\pi s}$$

Where **C** is capacitance, **D** is the dielectric constant, **a** is the electrode area, and **s** is the distance between electrodes.

In Figure 3B the electrodes have been replaced by a twisted pair, with the insulation as the dielectric. In this configuration there are two possible ways to reduce the capacitance effects.

- 1) Reducing the dielectric constant **D** of the insulation and
- 2) Increasing the distance between conductors **s** by increasing insulation thickness.



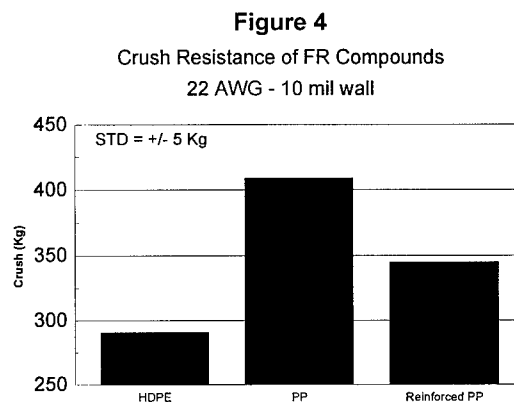
The most desired resolution is to reduce the dielectric constant of the insulation compound which allows manufacturers to reduce the wall

thickness of the insulation as well as saving raw material costs.

As previously stated, when using insulation materials that deform during the twinning process the capacitance is adversely effected. Figure 4 shows crush resistance data of three insulation compounds used for CMR rated constructions. Due to PP's inherently better hardness and higher yield strength, the PP based compounds outperformed the HDPE based compounds in crush resistance by 40%.

Flame Retardancy Issue

The reinforced PP compound in Figure 4 addresses a flame retardancy issue inherent to polypropylene. Unlike polyethylene, polypropylene has an abundance of tertiary hydrogens on the polymer chain. When burned, these tertiary hydrogens induce an unzipping reaction that breaks the polymer chain into smaller chains more rapidly than polyethylene. During combustion, the polymer chains decrease in size, causing the polymer viscosity to decrease to a point where dripping readily occurs.



Dripping can have both positive and negative effects during large scale flame tests. The positive effect of dripping is that dripping material takes with it the heat required to maintain combustion, causing the flame to extinguish. The negative effect of dripping occurs in flame tests that include a smoke specification. In the case where dripping material accumulates in the bottom of the testing apparatus,

smoldering develops resulting in high smoke density levels. mechanical, and electrical properties.

To prevent dripping, manufacturers sometimes use specific jacketing materials that help encapsulate the insulation materials during the burn test. These jacketing materials help keep the insulations from being exposed to the flame. The reinforced PP compound addresses the dripping issue by the addition of a reinforcing filler that prevents dripping during the burning process.

Once this reinforcing filler has been added, an improvement of 20% in crush resistance over polyethylene is still seen in the PP formulations. These improvements in crush resistance will help manufacturers reduce wall thickness of the insulation that had been previously increased to compensate for insulation deformation and inferior capacitance values.

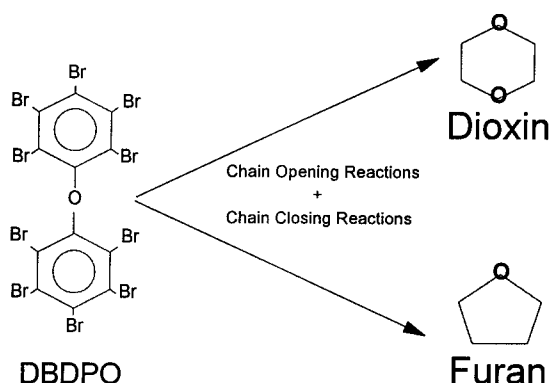
Toxicological Enhancements

Table 1

Physical Property	Compound 1 DBDPO Based	Compound 2 NDFF Flame Retardant
Limiting Oxygen Index %LOI (ASTM D2863)	25%	25 %
Tensile Strength (ASTM D638)	22.7 MPa	22.7 MPa
% Elongation (ASTM D638)	650%	650%
Crush Resistance (UL1581)	410 Kg	410 Kg
Dielectric Constant (ASTM D150)	2.39	2.39
Dissipation Factor (ASTM D150)	0.0005	0.0005

Table 1 shows the physical properties of insulation compounds when a non-dioxin and furan forming (NDFF) flame retardant is used as a replacement for DBDPO. Compound 1 uses DBDPO as the brominated flame retardant. Compound 2 uses a brominated NDFF based flame retardant. Without the DPO type molecule, the ring opening and closing reactions that form brominated dioxins and furans cannot occur (Figure 5). As seen in Table 1, using the NDFF flame retardant as a direct substitution to DBDPO does not degrade the flame,

Figure 5



Conclusions

By replacing the traditionally used HDPE based insulation compounds with polypropylene, the superior dielectric and mechanical properties inherent to polypropylene are retained even after flame retardant incorporation. Dielectric constant and crush resistance enhancements found in polypropylene allow manufacturers to reduce costs by reducing insulation thicknesses.

The replacement of DBDPO with another non-DPO base flame retardant showed no properties deficiencies. Other observed benefits included enhanced processability and bloom reduction. This compound will allow manufacturers to sell premise cables into applications where the manufacturer restricts the use of DPO based compounds.

References

- (1) Optimization of High Performance Unshielded Twisted Pair Media, Paul Z. Vanderlaan, 1994 IWCS Proceedings, pp.320-327
- (2) Parameters Affecting Near-End Crosstalk in Screened Cables, J.P. Savage, T.G.Hardin, 1977 IWCS Proceedings, pp.420-427
- (3) Buser, Environmental Science Technology, 1986, 20, pp.404-408
- (4) The Issue of Decabromodiphenyl Oxide and Brominated Dioxins and Furans, Paul F. Ranken, Ethyl Corporation, 1993
- (5) Engineering Properties and Applications of Plastics, Gilbert F. Kenney, John Wiley & Sons, Inc., 1957, P 229



Jeff S. Borke

Research Engineer
Millennium Petrochemicals Inc.
11530 Northlake Drive
Cincinnati, OH 45249

Jeff Borke received his B.S. degree in Chemical Engineering from the University of Cincinnati in 1993. He joined Millennium Petrochemicals Inc. (formerly Quantum Chemical Co.) in 1993 and has worked in the Wire & Cable research and development group.

Silicone Crosslinking Methods

Shannon K. Crawford

Essex Group Inc., Lafayette, Indiana

ABSTRACT

Numerous crosslinking methods are employed to transform a silicone based compound into a structured polymeric network. Traditional curing methods involve thermal and room temperature vulcanization. Silicone elastomers also respond well to radiation curing, though uncured silicone compounds having inadequate green strength can experience processing problems in wire production operations. Reported approaches to increasing green strength have been based on selective compounding and "crosslinking" prior to irradiation.

This paper will present a survey of established silicone crosslinking reaction mechanisms, along with details on novel silicone cure methods which have been described in the literature.

INTRODUCTION

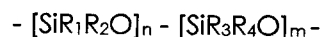
Silicone polymers are an important class of materials as they provide a unique balance of properties and can bridge the gap between fluoropolymers and crosslinked polyethylene and other elastomers. The silicon-oxygen linkages of the polymeric backbone are key to its thermal, oxidative, ozone, corona, UV and chemical resistance, as well its excellent flexibility, low compression set, flame retardancy, tensile strength at elevated temperatures and electrical properties.

Silicone compounds have found use in various wire and cable applications, including ignition, fixture and appliance wire, along with power and control cables. A typical silicone rubber formulation will contain a silicone polymer, reinforcing and/or extending fillers, curing agent and additives, such as a process aid and color concentrate.

SILICONE POLYMERS

Chemistry

The basic repeating unit of the most commonly used silicone polymers is:



where R = -CH₃, -C₆H₅, -CH=CH₂, or -CH₂CH₂CF₃.

Polymers can be custom made to suit a particular application by altering the type and level of alkyl substituents. For example, the low temperature property of dimethyl silicone can be improved by substituting some methyl groups with phenyl groups. The incorporation of vinyl groups increases free radical crosslinking efficiency, while the presence of trifluoropropyl groups improves chemical resistance. A number of side group combinations are possible. The silicone polymer classifications listed in Table 1 are designated in ASTM D-1418.

Table I. ATSM Designations

Classification	Description
MQ	Dimethyl Silicone
PMQ	Methyl Phenyl Silicone
VMQ	Methyl Vinyl Silicone
PVMQ	Methyl Vinyl Phenyl Silicone
FVMQ	Methyl Vinyl Fluoro Silicone

The molecular weight of conventional thermally crosslinked silicone rubber is typically 300,000 to 800,000. The end groups are predominately methyl or vinyl. In comparison, room temperature vulcanizing silicones are < 100,000 molecular weight with hydroxyl or vinyl terminal functional groups.

Crosslinking

Organic peroxides are commonly used to crosslink silicone rubber. Peroxides decompose at elevated temperatures, producing free radicals, which in turn react with substituents on the polymer chains. Peroxides are categorized into two types, those that react specifically with vinyl groups and those which crosslink through both vinyl and methyl groups. Reaction mechanisms are shown in Figure 1 and Figure 2.¹ The curing of the dimethyl polymer is straight forward. The proposed methylvinyl siloxane mechanism was based on experimental observations.

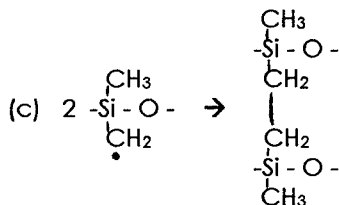
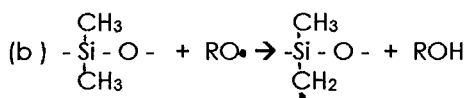


Figure 1. Peroxide Cure Mechanism for MQ

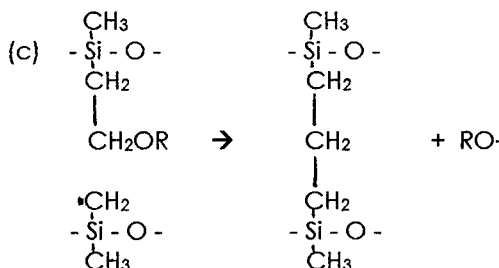
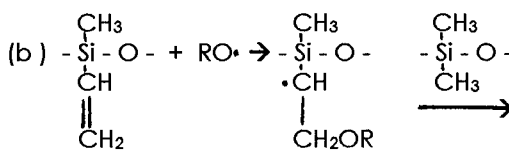


Figure 2. Peroxide Cure Mechanism for MVQ

The temperature required to initiate cure depends of the peroxide used. Upon extrusion, silicone compounds used for wire and cable applications can be cured via hot air vulcanization (HAV) or continuous steam vulcanization (CV).

Silicones which undergo room temperature crosslinking are often divided into two categories: addition and condensation cure. Those materials crosslinking via condensation may be packaged as a one or two component system. A one package addition system is possible with an inhibited catalyst but heat is then required to initiate crosslinking.

Addition crosslinking reactions occur between the vinyl groups of silicone polymers and polyfunctional silicon hydride crosslinkers, and are usually catalyzed by a platinum complex. Figure 3 shows the reaction mechanism.¹

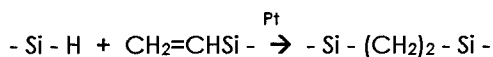
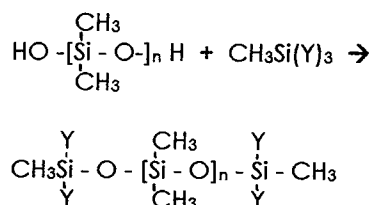


Figure 3. Addition Cure Mechanism

Silanol terminated polymers are employed in compounds cure by a condensation mechanism. In a one component system an excess of crosslinker is added to the base to react with the terminal silanol groups on the polymer to "block" them from reacting. During cure, moisture from the air reacts with the blocked silanol end groups, regenerating the silanol groups from which subsequent condensation reactions can take place. Two component systems do not employ blocked functional groups so the crosslinker (alkoxy silane) and catalyst (metallic salt) are not added to the silicone base until the material is be used. Postulated condensation reactions mechanisms are proposed in Figures 4 and 5.¹

(a) Reactions during compounding:



(b) Reactions during cure:

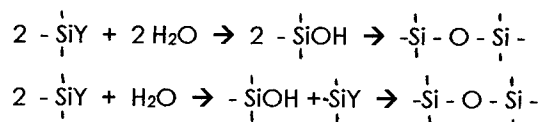


Figure 4. One Component Mechanism

and

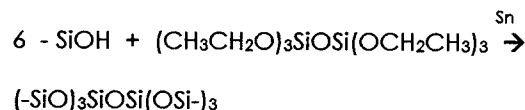


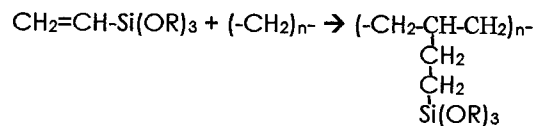
Figure 5. Two Component Mechanism

The condensation reactions described above are found in products such as silicone sealants, adhesives, coatings and encapsulants. Condensation cure mechanisms for wire and cable products are the basis of moisture cure compounds. Rather than the formation of -Si-O-Si- bonds, moisture cure hinges on the creation of -C-Si-O-Si-C- bonds.

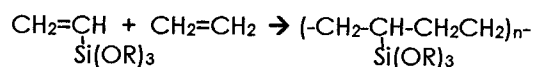
Moisture curable polymers are prepared either by grafting a vinyl silane monomer onto polyolefins or copolymerizing a vinyl silane with an alkene. The grafted product can be used in two manners. One process is to premix a grafted polymer and catalyst masterbatch for subsequent extrusion onto wire. The other method is to meter the polyolefin, silane monomer and catalyst directly into the extruder. For both cases, post curing with steam, hot water or open air storage is necessary to complete the crosslinking reactions. Crosslinking takes place in two steps. First, hydrolysis of the alkoxy substituents occurs, then condensation between of the resulting hydroxyl groups transpires.

The moisture curable copolymer system has a longer shelf life than the grafted polymer. This has its advantages. As with the grafted material, a copolymer and catalyst masterbatch are fed into an extruder for processing onto wire. Post curing is again essential. Figure 6 summarizes the moisture cure reactions.

(a) Preparation of Grafted Polymer



(b) Preparation of Copolymer



(c) Silane Crosslinking Mechanism

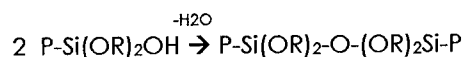
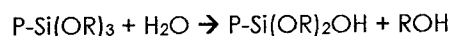


Figure 6. Moisture Cure Crosslink Reactions

Silicone polymers respond well to curing via ultraviolet, electron beam and gamma radiation. Radiation curable organopolysiloxane compositions are found in release coatings, inks, composites, adhesives, sealants and surface modifiers. Radiation curable silicones have also been noted in a few wire applications; as a coating for glass optical fibres² and in a microsphere filled insulation characterized by a low dielectric constant.³

UV curing can progress via free radical, cationic or hybrid systems, depending on the photoinitiator. Electron beam polymerization follows a free radical mechanism. High energy electrons strike polymers and abstract hydrogens from carbon atoms and/or attack sites of unsaturation. Resulting polymeric free radicals combine to form crosslinks which bridge neighboring polymer chains together (Figure 7).

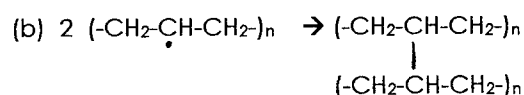
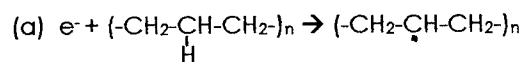


Figure 7. Electron Beam Crosslink Reactions

It is known that insulations and jacketing compounds crosslinked by high energy electrons have improved thermal stability compared to their chemically cured counterparts. Silicone elastomers; however, are not often used in

compounds cured by electron beam. The problem lies in that uncured silicone rubber is very soft and can be easily deformed by handling equipment once extruded onto wire. One patented technique tried to circumvent this problem by "precuring" the silicone once it was formed into the desired shape.^{4,5} A green strength improvement was achieved through compounding.

It was known that the pendant hydroxyl groups on fumed silica fillers hydrogen bond with oxygen atoms contained within the backbone of a silicone polymer. This hydrogen bonding reinforced the silicone and increased its tensile strength significantly. In addition, it was claimed that exposure of the silicone compound to vapors and solutions of ammonia and other volatile amines induced a transient cure which improved physical properties to the extent that the compound could withstand the stresses created by the handling equipment and that irradiation was possible. Electron beam irradiation with two to ten Mrd was sufficient to promote physical properties similar to a peroxide cured material.

Other interesting polysiloxane curing methods have been documented. One study described the substitution of amine based epoxy curing agents for the organotin catalyst used in the room temperature vulcanization of a polymethylvinylsiloxane-polystyrene graft copolymer.⁶ The objective was to increase the shelf life of the catalyzed compound. The mechanism was similar to that of the one component condensation reactions previously described. In this case, the reaction products of an alkoxy silane crosslinker and various amines were used to block the silanol end groups on the polymer chain. Vulcanization then proceeded as the alkoxy groups were hydrolyzed by moisture contained in the system.

In another study, photochlorinated polydimethylsiloxanes were crosslinked with thiol and amine compounds.⁷ It was known that halogen containing polymers (polyvinylchloride, neoprene, fluoro rubbers) had been crosslinked with thiols and amines in the presence of acid acceptors, and that crosslinking was based on nucleophilic substitution reactions on the carbon-halogen bonds. The authors suggested this was a new silicone vulcanization method and the study was to be expanded to investigate the crosslinking of polyvinylchloride and chlorinated polydimethylsiloxane blends.

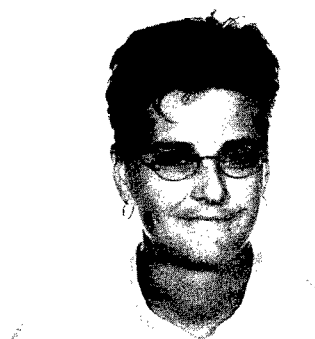
Further more, other unique silicone crosslinking methods have been patented. Compounds with elastomeric properties have been prepared by reacting lower molecular weight carboxyalkyl terminated dimethylsilicone with diglycidyl ethers of di- and bis-phenol.⁸ Also, boron compounds have been reacted with dimethylsiloxane to create polydimethylborosiloxane.⁹ Polyorganoborosiloxanes have been referenced in patents which describe a unique "putty" which can both flow and bounce.¹⁰

SUMMARY

This paper described traditional silicone cure mechanisms and highlighted other novel approaches to crosslinking silicones. Many of these curing methods have not been commercialized and are still in the experimental stages, they are, none-the-less, interesting chemistries which should not be discounted as having potential for use in wire and cable applications.

REFERENCES

1. M. Morton, *Rubber Technology*, 3 Ed., Chapman & Hall, London, 1995, Pg. 381-382
2. F. Hockemeyer, US Patent 4,571,349 (18 Feb. 1986)
3. T. Yamanishi, US Patent 5,115,103 (19 May 1992)
4. J.G. DuPont, US Patent 4,362,674 (07 Dec, 1982)
5. J.G. DuPont, US Patent 4,490,314 (25 Dec, 1984)
6. S.I. Antonenko, *International Polymer Science and Technology*, 1990, Vol. 17, No. 2, pg. 8-9
7. H. Inoue, *Journal of Applied Polymer Science*, 1992, Vol. 46, Iss. 5, pg. 931-935
8. J. Keil, US Patent 4,623,694 (18 Nov. 1986)
9. M. Aisman, *Sci. Papers ICT. C*, 1976, 24, pg. 85-92
10. A.H. Frazer, *High Temperature Resistant Polymers*, Wiley & Sons, 1968



Shannon K. Crawford
Essex Group Inc.
3400 Union Street
Lafayette, IN 47905

Shannon joined Essex as Polymer Chemist III in 1995. She has been involved in the development of wires and cables, primarily for industrial and automotive applications. Her areas of interest and responsibility are radiation curing and supervision of the analytical lab. Shannon graduated from Mayville State College in 1985 with a B.S. in Chemistry and Mathematics.

THE EFFECT OF VISCOELASTIC MATERIAL PROPERTIES ON OPTICAL FIBER CABLE

Stephen Hassett, Alan Parsons and Richard Wagman

Siecor Corporation, Hickory, North Carolina

ABSTRACT

Evidence suggested that the optical attenuation of a fiber optic cable may decrease with time. To determine if the attenuation is not constant, a slotted core cable was tested mechanically and a stranded loose tube cable was tested environmentally. In both cases the attenuation decreased with time in a log-log manner.

It is hypothesized that the decrease in attenuation with time is due to the viscoelastic properties of some of the cable materials. Viscoelasticity describes the dual nature of plastics which are the predominant cable materials. Plastic behavior is a combination of viscous and elastic behavior, and is modeled with a combination of springs and dashpots.

Stress relaxation testing was performed to investigate the viscoelastic nature of four common cable materials at two different temperatures. All of these results show the same log-log behavior as seen in the cable attenuation tests. This empirical testing supports the hypothesis.

INTRODUCTION

In the fiber optic cabling industry, optical attenuation is often treated as an absolute. For example, attenuation performance is typically presented without any reference to the time at which the measurement was made. However, some industry specifications and procedures recognize a time dependency as their attenuation performance limits are based on a defined time period.

Cable attenuation values have been observed to decrease over time. This was noticed particularly when there were large attenuation increases in experimental cables and when cables experienced extended periods under stress. Because this data was not collected with the intent of studying time related behavior, only limited modeling was possible.

The importance of time as a variable can be seen by looking at the tensile-bend test based on the FOTP-33¹ test procedure. It is a static load test used to determine the combined tensile and bend performance of a cable in the field. For this test some specifications require attenuation measurements at specific times after the peak load is attained. The specific times are used to determine if there are attenuation increases caused by a cable increasing in length with time. However, if a cable does not significantly increase in length with time and the attenuation decreases with time, the specified times may allow for lower measured attenuations. The cable which increases in length with time and the cable that does not are examples that show the danger of applying attenuation limits to simulated field tests.

Understanding the effect of time on attenuation has implications for test specifications, interpreting test data and the design of fiber optic cable.

This paper describes an investigation into the time related behavior of optical fiber cable attenuation. The study of this behavior is reported in the Cable Testing section. A hypothesis relating material properties to the observed attenuation decreases is detailed in the Attenuation Mechanisms section. The theoretical foundation of the applicable material properties is reviewed in Plastic Materials Theory section, and finally, applicable testing on cable materials is reported in the Materials Testing section.

CABLE TESTING

To better understand the impact of time on attenuation, two experimental cables were manufactured and tested. The intent was to manufacture designs that explored the limits of cable performance so that time effects could be easily observed. One cable was a slotted core cable with 16 fiber ribbons in slots that were

intentionally too small. The other cable was a stranded loose tube cable with a central member that was intentionally too small.

Ribbon Cable Attenuation Change

While they must meet similar mechanical and environmental requirements, slotted core ribbon (SCR) cables differ from stranded loose tube in some of their design aspects. For one, the fibers in a ribbon do not act like individual fibers suspended in a filling compound. The fibers are captured in a ribbon matrix that protects the fibers from mechanical damage, and also arranges the fibers into a package that is convenient for splicing and connectorization. However, in certain situations fibers in a ribbon experience additional strains because the fibers are mechanically coupled together within the ribbon structure.

In ribbon cables, ribbon stack integrity (how well ribbons stay together in a stack) is a performance concern along with fiber strains from stranding. The choice of the cable pitch parameter is a compromise between temperature performance and cable bend performance. For slotted core designs, the central member acts as both the tensile element and the cold temperature anti-buckling element. This allows for a compact design with a very high fiber packing density for fiber counts greater than 100.

In an SCR cable, the slot size needs to be large enough to allow ribbon movement during cable bending. The ribbons attempt to move to minimize tensile and compressive strains from bending. When their movement is restricted, the fibers press against the slot walls through the

ribbon matrix, and the resultant pressure causes attenuation increases. The entire pressure of the ribbon stack is typically transferred through the fibers at the four corners of the rectangular ribbon stack (corner fibers) so these fibers usually experience higher attenuations. The fibers not on the perimeter of the ribbon stack (interior fibers) only press against other fibers and ribbons, and typically have lower attenuations.

The experimental ribbon cable was manufactured with undersized slots to sensitize the cable design to bending stresses. The cable was wound onto a wooden reel with a 1.3 m drum diameter. Attenuation measurements at 1550 nm were made on specific fibers in the ribbon stack at 1 hour, 41 hours and at 114.5 hours after winding. The same cable was then wound onto a 1.7 m drum. Again, attenuation measurements at 1550 nm were made on the same fibers at 1 hour, 17 hours, 41 hours and at 166.5 hours after winding.

The data is shown in Figure 1 where each line represents the average of four fibers. The graph shows that there is a definite time dependence to the measured attenuation coefficients. It is apparent that bend radius, time and position in the ribbon stack are factors in the attenuation change, and that the attenuation decreased with time in a manner that is best fitted by a log-log relationship. The slopes shown in Figure 1 indicate that the rate of attenuation decrease with time, and the R^2 indicates how well the curve is fit by linear regression. R^2 is a statistical measure of how well a linear regression describes the data with one indicating perfect correlation and zero indicating no correlation. The R^2 was highest when the

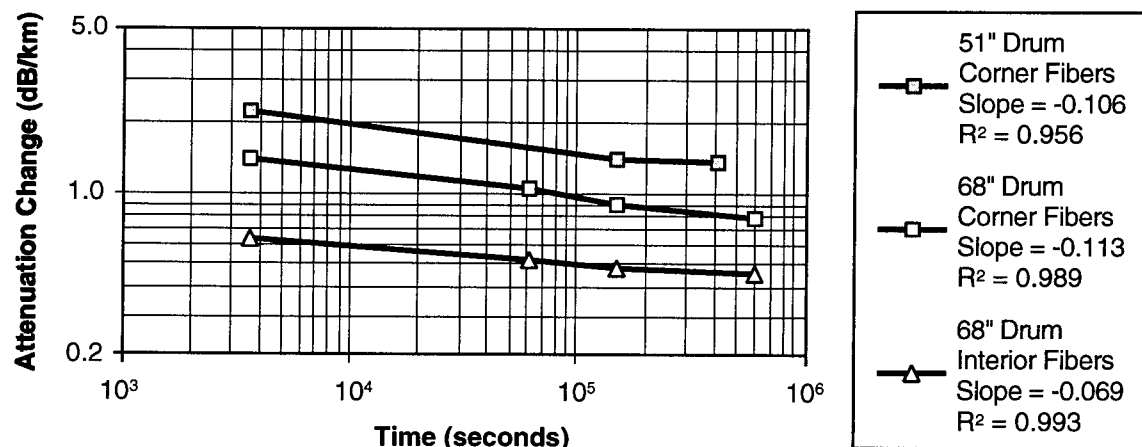


Fig. 1. Log of Attenuation Change at 1550 nm Versus Log of Time for SCR Cable Bending

logarithm was taken of both the change in attenuation and the time.

Loose Tube Cable Attenuation Change

While the SCR cable was designed to be overly sensitive to mechanical bending forces, the loose tube cable was designed to be overly sensitive to environmental forces by using an undersized central member.

The tensile design of a loose tube cable is different than an SCR cable. In the case of the SCR cable, the tensile strength comes primarily from the central member. However, in many commercially available loose tube cables, the tensile strength comes primarily from yarns or rovings which are wrapped around the loose tubes. The central member size for a loose tube cable is determined by the amount of low temperature cable shrinkage to be allowed. The central member resists the low temperature cable shrinkage caused by the plastics in the cable, or in other words the central member provides anti-buckling. Undersizing the central member raises the low temperature where significant attenuation increases occur during temperature cycling.

An all-dielectric stranded loose tube cable with 10 buffer tubes was manufactured. A total of 18 fibers were monitored for change in attenuation at 1310 nm and 1550 nm. The cable was spliced to an automated test system integrating a computer controlled chamber, an optical switch and an OTDR. A two cycle time-temperature profile was programmed from -40°C to +70°C using a 24 hour transition

between temperatures and a 96 hour soak at temperature. Attenuation measurements were made every six hours. The attenuation data for two typical fibers, along with the time-temperature profile, is shown in Figure 2. The tick marks on the time scale are spaced six hours apart.

At the extremes, especially at the cold temperatures, it is evident that there are peak attenuations in the middle of the soak period. Before the soak is over, a downward slope is seen at both the 1310 and 1550 nm values. As with the slotted core cable in bending, the initial increases in attenuation decrease over time and follow a log-log relationship. By looking at the second cold temperature soak, and picking a time zero of six hours before the peak attenuation, the results shown in Figure 3 were developed. For clarity in Figure 3, only nine of the measured fibers are shown. These fibers represent the entire range of observed increases in attenuation.

The slopes were calculated by linear regressions, and they are listed in the same order as the curves. Note that the four lower curves have a higher slope than the upper five which may indicate the mechanisms for the decrease in attenuation are different for the two sets of curves.

Cable Testing Summary

Attenuation decreases in both bending and temperature cycling using two very different cable designs show a log-log time dependence. This suggests that other attenuation changes

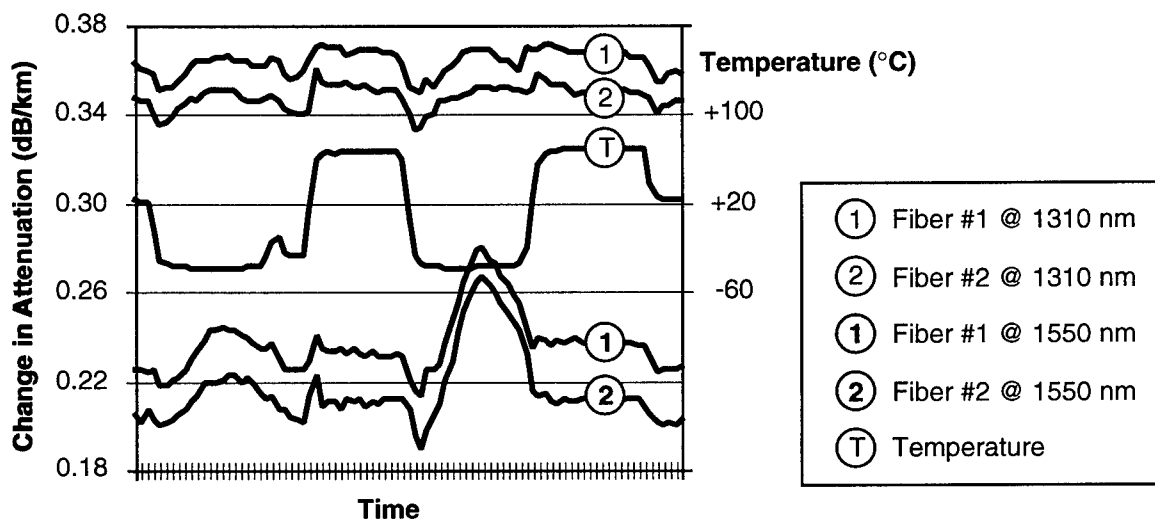


Fig. 2. Typical Attenuation Change Versus Time for Temperature Cycling

will show the same time dependency, and that the attenuation decreases will have different slopes. The source of the attenuation and time relationships is examined below.

ATTENUATION MECHANISMS

It is hypothesized that the decrease in attenuation with time is largely due to the viscoelastic properties of the cable materials. The applicable viscoelastic properties are the properties where a material is dimensionally changed by a force over time. There are a number of potential mechanisms for material deformation that could lead to decreases in attenuation.

One potential mechanism for decreases in attenuation involves microbending attenuation. Microbending attenuation is typically caused by non-uniform forces that lead to irregular small radius bends in an optical fiber². Non-uniform forces can be caused by uniform forces being concentrated at the high points of microscopically rough surfaces. However, if materials with rough surfaces deform with time, the forces are spread out over a larger area which would lead to less irregular bending of an optical fiber.

A second potential mechanism for attenuation decreases involves cable shrinkage due to temperature. The plastic materials of a cable shrink more than an optical fiber which can cause attenuation increases. Materials with low coefficients of thermal expansion such as fiberglass or steel are added to cables to reduce the amount of low temperature cable shrinkage due to the plastics. In this case, the plastics are

held in tension while the fiberglass is held in compression. If the plastics are deformed with time such that their length is increased, the amount of cable shrinkage will decrease along with any attenuation increases.

The attenuation behavior versus time for a set of test results is probably a combination of mechanisms. In addition, these mechanisms involve a number of materials that have different properties, and these properties are time and temperature dependent.

Before investigating material test results to test the hypothesis, the concept of viscoelasticity and the basic theory underlying plastic behavior is reviewed.

PLASTIC MATERIALS THEORY

Many of the materials in a fiber optic cable are polymers, and their ability to deform with time is related to their structure. Polymers are made up of long chained molecules. These chains may either form crystalline or amorphous regions. Crystalline regions are areas where the chains form a tightly packed structure while amorphous regions are areas where the chains are loosely packed with a random structure. Polymers are either amorphous or semi-crystalline (a mix of crystalline regions and amorphous regions). An example of an amorphous polymer used in cables is polycarbonate (PC). Examples of semi crystalline polymers used in cables are polyethylene (PE) and polypropylene (PP). Polymers may also be crosslinked where there are physical links between chains at various points along the chains. An example of crosslinked polymers are the urethane acrylates

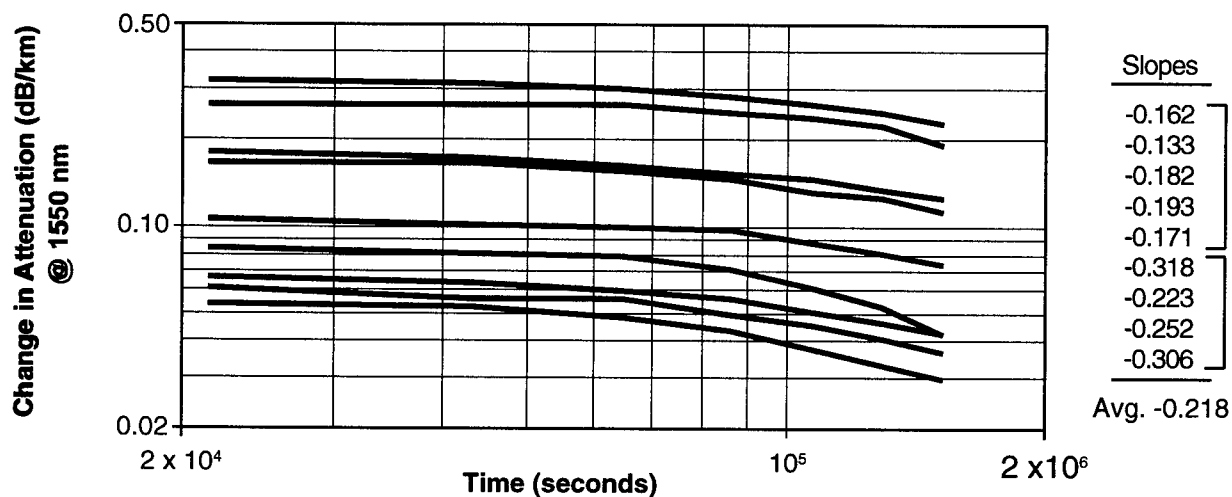


Fig. 3. 1550 nm Attenuation Change Versus Time After Peak Attenuation at 2nd -40°C Cycle

(UA) used as fiber coatings, inks, and ribbon matrix materials.

One aspect of polymers is that they have a T_g (Glass Transition Temperature) which describes the temperature at which the polymer's amorphous regions transition from brittle (glassy) behavior to rubbery behavior. Above T_g , large sections of polymer chains (eg. a 50 atom length of chain) have room to move, whereas below T_g , only small sections (eg. 1 to 4 atom segments) of the polymer chains are mobile.

Materials are commonly selected due to the location of their T_g in relationship to the product's temperature operating range. For instance, cable jackets have glass transition temperatures below -60°C and exhibit rubbery behavior in typical cable operating ranges. This rubbery behavior is required for a jacket to be able to withstand strains and compressions that can be as high as 3%, when for example a cable is bent at 15 times its diameter. Other times it is beneficial to have glassy behavior from a plastic. Such a plastic would have a T_g that is high relative to the cable operating temperatures. It is desirable for outer fiber coatings and rigid structural elements to behave in a glassy manner.

Effects of T_g and Crosslinking

Modulus is one physical property that is affected by the glass transition temperature. Figure 4 demonstrates how modulus changes as a plastic transitions across temperature. Upon warming from low temperatures, the first drop in modulus is in the region of the T_g . A second drop in modulus occurs as viscous flow begins. This second drop in modulus does not occur for

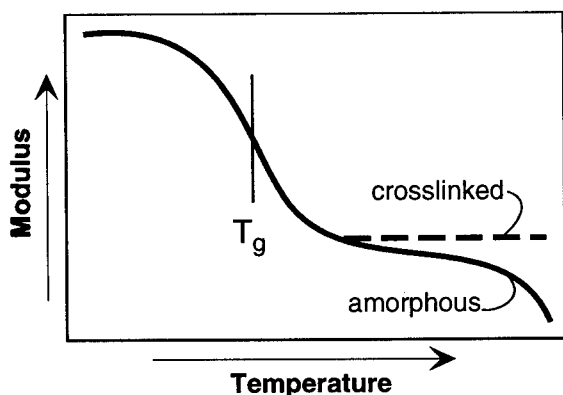


Fig. 4. Modulus Versus Temperature for a Typical Polymer

crosslinked materials. Above T_g , the crosslinked materials are bound by the physical crosslinks, and therefore, modulus measured above T_g is representative of the amount of crosslinking present.

Effects of Time

Based on the Time-Temperature Superposition Principle, it can be shown that polymers behave the same way versus time that they do versus temperature³. A relationship between modulus and time is shown in Figure 5.

This behavior of polymers occurs because of the relationship that a chain has with its surrounding environment. A chain, in an amorphous region, is locked in place by entanglements with other chains along the length of the chain as well as by the proximity of nearby chains. As temperature increases, molecular motion and the space between the chains increases allowing the chain to slip out of entanglements. Similarly, as a strain is applied for a longer period of time (lower strain rate), the chains are allowed more time to slip past each other and out of entanglements. Therefore at low temperatures or fast strain rates the material behaves in a brittle manner since chain movement is restricted. At high temperatures or low strain rates the material flows more easily because chain movement is easier.

The term viscoelasticity is used to describe a material such as a polymer that exhibits a combination of an elastic response (predominant response at fast strain rates) and a viscous response (predominant response at slow strain rates). Each individual polymer will have a different viscoelastic behavior based on percent crystallinity, degree of crosslinking, and chain

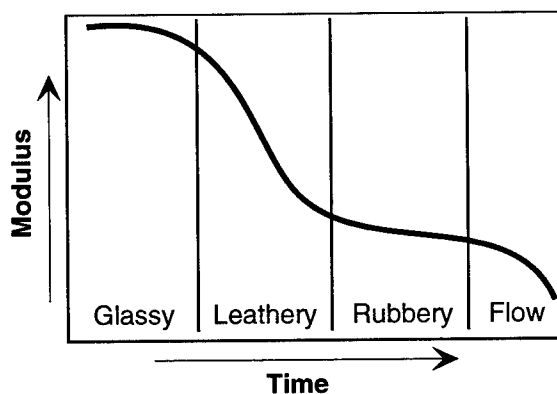


Fig. 5. Modulus Versus Time for a Typical Polymer

stiffness. Polymer scientists model this behavior to better visualize the responses of a polymer to stresses and strain.

Viscoelastic Models

Early models for viscoelastic behavior are the Maxwell model and the Voigt-Kelvin model both of which utilize spring and dashpot elements⁴. The spring is representative of an elastic deformation in that once a load is removed from a sample, it returns to its original length. The dashpot is representative of viscous flow where the reaction to a load is time dependent and permanent. A dashpot represents chains as they move past one another producing permanent deformation.

The Maxwell model is represented by a spring and a dashpot in series. This model produces an immediate elastic and recoverable deformation to a tensile stress; however, if given enough time, the model will produce an additional deformation as the dashpot is pulled apart. As the stress is released the spring will return to its original size, but the deformation of the dashpot will be permanent.

The Voigt-Kelvin model is represented by a spring and dashpot in parallel. In this model the dashpot behavior initially dominates the response to stress because it takes time for the dashpot to pull apart. After a long period of time the spring behavior dominates the response. As the stress is released, the spring dominates and pulls the dashpot back to its original position.

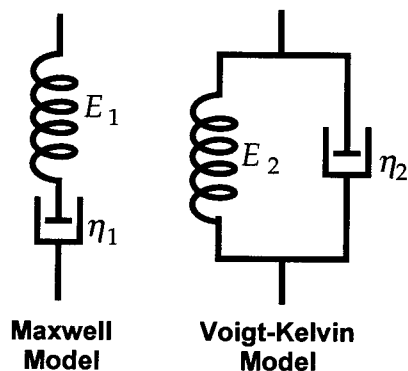


Fig. 6. Common Viscoelastic Models

Both the Maxwell and the Voigt-Kelvin models are too simplistic to adequately describe the viscoelastic behavior of plastics. A combination of these two models, the four element model, more closely describes polymer behavior, but still remains simple enough to visualize plastic

behavior. When stress is applied, the four element model shown in Figure 7 exhibits an initial elastic response followed by plastic flow.

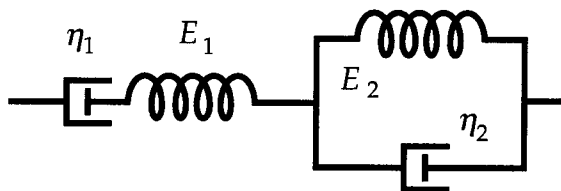


Fig. 7. The Four Element Model

Upon removal of the stress, there is an immediate complete recovery due to the elastic response followed by a slow plastic recovery which does not ever fully recover. It is theorized that the four element responses are as follows: 1) dashpot η_1 represents molecular slippage, 2) spring E_1 represents elastic straining of atom to atom bond angles and lengths, 3) dashpot η_2 represents slippage of entanglements, and 4) spring E_2 represents the restoring force brought about by thermal agitation of chain segments. The four element model is the simplest model that allows one to properly visualize the plastic behavior seen in materials testing⁴.

MATERIALS TESTING

Representative polymer cable materials were tested to determine if the viscoelastic properties of the cable materials cause decreases in attenuation with time. To the extent that viscoelasticity is the cause, it is expected that the time dependent behavior of cable materials will be similar to the attenuation versus time behavior disclosed in this paper.

The Materials Chosen

A medium density polyethylene, a polypropylene, a polycarbonate and a urethane acrylate material were chosen for testing. These materials represent both thermoplastic and crosslinked plastics with glass transition temperatures (T_g) both above and below room temperature.

The medium density polyethylene, which has a T_g below -60°C , was tested at room temperature and at -30°C . The polypropylene, which has a T_g around -20°C , was tested at room temperature. The polycarbonate, which has a T_g around 150°C , was tested at room temperature. The urethane acrylate, which has a T_g of 40°C and is crosslinked, was tested at room temperature and at -30°C . At room temperature,

the urethane acrylate is transitioning from a glassy material to a rubbery material.

The Type of Test

Creep test and stress relaxation test are the two commonly used tests to determine the strength of a material versus time. In the creep test, the force is held constant while the increase in elongation is monitored. In the stress relaxation test, the elongation is held constant while the decrease in force is monitored. In the fiber optic cable application, the stress relaxation test best fits the expected mechanisms for attenuation decreases.

In each of the mechanisms listed previously, the forces deforming the plastic decrease as the material deforms so the creep test is not appropriate. For example, in the cable shrinkage mechanism as the plastics under tension are deformed, the difference in length between the plastics and the glass or steel is reduced. The reduced length difference leads to a lower force on the plastics.

Stress Relaxation Testing

Each of the materials was stretched to 1% elongation and held there for at least one hour. The testing on the thermoplastic materials – polyethylene (PE), polypropylene (PP) and polycarbonate (PC) – was performed on a load frame with a load cell while the urethane acrylate was tested on a DMA (Dynamic Mechanical Analysis) test apparatus.

Typical results are shown in Figure 8 and Figure 9. The results in Figure 8 show the

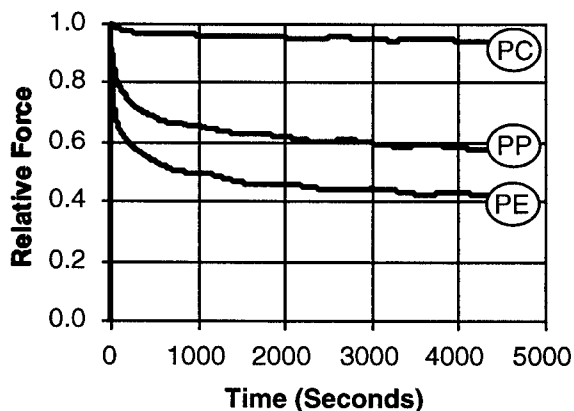


Fig. 8. Relative Force Versus Time for the Thermoplastics at Room Temperature

results for the thermoplastic materials at room temperature (RT) while Figure 9 shows the results of the urethane acrylate at room temperature and -30°C.

To put the data in a form to be analyzed, several treatments were used. First, to determine the length of time a sample was at 1% elongation, a modified time was used. In the stress relaxation tests, it took between thirty and sixty seconds to reach 1% elongation. Because a sample will begin stress relaxing before the sample reaches 1%, the time zero for a sample at 1% elongation was assumed to be the time at 0.5% elongation.

For the load frame testing, temperature changes due to the air conditioning caused variations in the data. The residuals from the curve fitting contained a constant height sine wave consistent with a $\pm 0.5^{\circ}\text{C}$ temperature change. A best fit sine wave was subtracted from the initial data to obtain better curve fitting results by removing the temperature fluctuations from the data.

Most of the material samples were taken from actual cables, and some of the samples had irregular cross-sections. Rather than using an approximate cross-sectional area to calculate stress, the force was normalized so that the maximum stress during a test had a value of one.

Analysis of Data

The stress relaxation data was analyzed to determine the best fitting function, to compare the different test conditions, and to compare the different materials. A summary of the analysis is

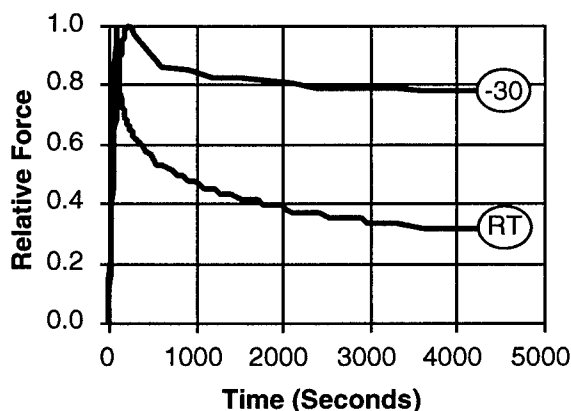


Fig. 9. Relative Force Versus Time for the Urethane Acrylate

shown in Tables 1 and 2. Each row of the tables shows the setup and duration of the testing and the results of linear regression. The measure of the rate of stress relaxation is the slope shown in column (8). This indicates how fast the force is decreasing with time. In an equation for these log-log plots, the slope would be the exponent of time.

Column (9) shows the values of R^2 from the linear regression of $\log(\text{force})$ by $\log(\text{time})$. Overall the values of R^2 were highest when the logarithms of both the change in force and time were taken. In a number of individual cases, using only the logarithm of time led to similar values of R^2 , but in other cases they were lower.

Analysis of Data - Testing Differences

Potential end effects in the testing due to the clamps used to hold the samples were investigated. For example, one may compare rows (A) and (B) of Table 1. Since there is little difference in the slopes for a 35 mm and a 280 mm gage length, end effects are evidently not an issue.

The time the samples were held at particular elongations does not have a major effect on the measured slope. This can be seen in the urethane acrylate data in Table 1. While data sets (G) and (I) include the results for the entire duration of the testing, data sets (H) and (J) show the results excluding the first hour of testing. The slopes of (G) and (H), as well as (I) and (J) are not significantly different.

Data Set	(1) Material	(2) Gage	(3) Temp	(4) Elong	(5) Time	(6) Range	(7) n	(8) Slope	(9) R^2
(A)	PE	35	23	1.0%	1.2	All	499	-0.105	0.994
(B)	PE	280	23	1.0%	1.2	All	331	-0.097	0.993
(C)	PE	50	23	1.0%	1.7	All	11	-0.137	0.988
(D)	PE	50	-30	1.0%	1.7	All	11	-0.122	0.977
(E)	PP	100	23	1.0%	1.8	All	499	-0.081	0.997
(F)	PC	100	23	1.0%	2.1	All	498	-0.010	0.963
(G)	UA	9.6	23	1.3%	11.7	All	105	-0.324	0.984
(H)	UA	9.6	23	1.3%	11.7	> 1 hr	81	-0.379	0.994
(I)	UA	8.1	-30	1.0%	6.4	All	81	-0.043	0.964
(J)	UA	8.1	-30	1.0%	6.4	> 1 hr	45	-0.037	0.935

Table 1. Average Stress Relaxation Results for Various Cable Materials

Test Data	(1) Material	(2) Gage	(3) Temp	(4) Elong	(5) Time	(6) Range	(7) n	(8) Slope	(9) R^2
(a)	UA	9.0	23	0.8%	6.1	> 1 hr	43	-0.425	0.977
(b)	UA	7.1	23	1.0%	13.3	> 1 hr	95	-0.383	0.991
(c)	UA	12.6	23	2.0%	15.8	> 1 hr	106	-0.329	0.984

Table 2. Stress Relaxation Results for Various Elongations

- (1) PE = polyethylene, PP = polypropylene, PC = polycarbonate, UA = urethane acrylate
 (2) Gage length of sample in mm (3) Test Temperature in °C (4) Elongation of sample during test
 (5) Time in hours that sample was held at elongation (6) Portion of the time used to calculate the slope
 (7) Number of data points (8) Slope of the linear regression of $\log(\text{force})$ by $\log(\text{time})$
 (9) R^2 of the linear regression

Key for Tables 1 and 2

The slope or rate of stress relaxation may depend on the elongation at which the samples are tested. Table 2 shows the data for three tests on the urethane acrylate with three different elongations. These tests show a tendency for the rate of stress relaxation to increase at lower elongations.

Analysis of Data - Material Differences

The two materials tested below their glass transition temperatures, polycarbonate and the urethane acrylate at -30°C , had the lowest slopes or the slowest rate of stress relaxation. Of the materials tested around or above their glass transition temperature, the urethane acrylate had the highest slope followed in order by polyethylene and polypropylene.

The rate of stress relaxation for the polyethylene is relatively constant over a broad temperature range. Rows (C) and (D) of Table 1 show limited data comparing 23°C and -30°C for polyethylene and the slopes are similar.

Materials Testing Summary

All of the material test results which represent four different materials show a log-log relationship between force and time. In these results, temperature fluctuations have been accounted for, the effect of grips was found to be negligible, the time a material was under test did not significantly change the results; and although the test elongation changed the slope, it did not change the log-log relationship.

The results also follow polymer theory. For example, the materials tested below their T_g had the slowest rate of stress relaxation; and a polyethylene had similar results when tested at two different temperatures above its T_g .

CONCLUSION

The work reported here supports the hypothesis that at least a large part of the decrease in attenuation with time is due to the viscoelastic properties of some of the cable materials. Additionally, the attenuation measurements show that this effect can be significant. Using empirical data, the time based attenuation and stress relaxation results are both fit best by log-log relationships with slopes of the same order of magnitude. These relationships hold even though there were many variables in the testing. The attenuations were measured on two different cable designs, one in a mechanical test

and the other in an environmental test. The forces were measured on four different materials, at two different temperatures and for different lengths of time.

Of course, there are differences between the slopes for the cable attenuation results and the stress relaxation results of the various materials. To accurately predict attenuation versus time would require cable models that combine the different viscoelastic properties of the various polymers, and that potentially combine various mechanisms for decreases in attenuation.

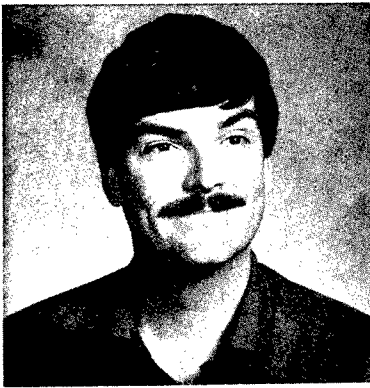
ACKNOWLEDGMENTS

This paper would not have been possible without the assistance of many people; however, the authors would like to especially recognize Eric Caldwell, Hilde Hagemester and Chris Eoll.

REFERENCES

- 1 EIA 455-33A, "FOTP-33 Fiber Optic Cable Tensile Loading and Bending Test", 1988, Electronic Industries Association.
- 2 "Single-Mode Fibers: Fundamentals", E.G. Neumann, 1988, p. 134, Springer-Verlag.
- 3 "Introduction to Physical Polymer Science", L.H. Sperling, 1986, pp. 384 -386, Wiley-Interscience.
- 4 "Fundamental Principles of Polymeric Materials", Stephen L. Rosen, 1982, pp. 245-246, Wiley-Interscience.

AUTHORS



Stephen L. Hassett was born in MontClair, NJ, in 1960. He received his B.S. degree in Engineering Science and Mechanics in 1981, a B.S. degree in Mechanical Engineering in 1982 and a Masters in Mechanical Engineering in 1984 all from the Georgia Institute of Technology. He joined Siecor in 1984. At Siecor he has worked at the Telecommunications Cable Plant in process development, connector development, product evaluation and product engineering. He is currently employed in Siecor's Canadian Cable Plant as the Quality Manager.



Richard S. Wagman was born in Dallastown, PA, in 1956. He received his B.S. degree in the Engineering Science honors program at Pennsylvania State University in 1978 and his B.S. in Electrical Engineering from Johns Hopkins University in 1984. He joined Siecor in 1985, where he has worked with cable, materials and test design. He is currently employed in the Research, Development and Engineering Department as a Subject Matter Expert in Cable Design.



Alan Parsons was born in Pittsfield, MA, in 1964. He has both a Bachelor's and a Master's of Science degrees in Materials Engineering specializing in Polymers from North Carolina State University. He joined Siecor in 1989 as a Materials Engineer and has also worked as Supervisor of the Materials Lab in Siecor's Research, Development, and Engineering Department. He is currently Manager of Materials Development at Siecor's RD&E Facility.

Development of new aerial distribution cables with 4-fiber ribbons

**Ichiro Kobayashi Daisuke Iwakura Ryuji Takaoka Eiji Konda Ryuichi Matuoka
Yuichi Sekii Hideyuki Izukura Yoshiyuki Ohkawa Yasuhiro Kamikura**

The Furukawa Electric Co., Ltd. Ichihara, Chiba, Japan

ABSTRACT

We have developed new aerial distribution cables which are indispensable for realizing the FTTH. Three types have been designed and manufactured: straight slotted rod cable, SZ-slotted rod cable and encapsulation cable. Trial cables of three types showed excellent transmission and mechanical characteristics. The SZ-slotted rod cable structure, which possesses outstanding mid-span access characteristic, is very well suited to the optical distribution cable.

1.Introduction

As communication services using personal computers such as the Internet become increasingly popular, an infrastructure which can provide broad-band service of high speed data, picture and so on with low cost is in greater demand. To satisfy this requirement, the development of the FTTH using optical fiber cables for the entire route from the central office to the customers is being promoted. [1] In Japan, for wiring in business areas or to distant locations, the CT/RT system combining metallic cables and optical fiber cables has been employed. In this system, the underground feeder cable portion is composed of optical fiber cables, and the distribution cable portion uses metallic cables. Hitherto, to realize the FTTH, it was necessary to develop a new optical fiber cable which is suited as a distribution cable.

2.Required conditions of aerial distribution cable

In the distribution networks, cables containing from several tens up to about 200 fibers will spread over wide areas and are usually installed on poles. In the distribution cable, as compared with the feeder cable, branching of cables and dropping to the customers occur very frequently. [2]

The required conditions of aerial distribution cable may be summarized as follows.

Cable structure using 4-fiber ribbons

The cable structure should be composed of 4-fiber ribbons considering not only easy jointing with feeder cables or other distribution cables, but also switching the wiring route in case of trouble.

Self-supporting type cable structure

The cable structure should be of self-supporting type in order to minimize working time and to enhance safety in the cable installation.

Considerations for aerial installation environment

An aerial cable is suspended between poles, and a suspending tension is applied to the cable. When the temperature rises after installation, the cable becomes elongated due to the thermal expansion of the members composing the cable. In windy conditions, elongation strain is applied to the cable between poles due to the wind pressure. Accordingly, it is necessary to design a cable structure whose life is not shortened due to the strain on the optical fibers resulting from such

factors. It is also essential that the fiber ribbons in the cable do not move as a result of the vibration or the like.

mid-span access

It must be possible to access to the fiber ribbons easily at any arbitrary position along the cable in order to drop to the customers.

3. Cable design

The aerial distribution cable was designed in order to satisfy the requirements mentioned in Section 2. We aimed at developing a cost-effective low fiber count cable of about 20 fibers.

The design features as an aerial distribution cable using 4-fiber ribbons are the self-supporting cable structure with cable excess length, prevention of the movement of the fiber ribbon, and simplification of the manufacturing process.

3.1 Self-supporting cable with cable excess length

The aerial cable is suspended between poles, and the suspending tension applied to the cable increases high temperature and windy condition. The maximum strain applied to the cable is expressed in the formulas (1) and (2). [3]

$$d_1^3 + \left\{ 1350 \times \left(\frac{5104.16W_c}{EA} + 65\alpha \right) - 0.746 \right\} d_1 = \frac{595300W}{EA} \dots (1)$$

$$T_{\max} = \frac{4410W}{d_1} \dots (2)$$

d_1 ; Dip (temp:-30°C, wind pressure:980N/m², span:60m)

W_c ; Cable weight

W ; Cable effective weight

$$W = \sqrt{W_c^2 + 1000D^2}$$

D ; the total outside diameter of the supporting wire and cable

EA ; Stiffness of the cable

α ; Equivalent liner expansion coefficient of the

cable

T_{\max} ; Maximum allowable tension on the cable

We calculated the maximum tension and maximum strain from these formulas, and designed the cable with the following criteria.

(1) Breakdown strength of the suspension member should be more than twice the maximum tension.

(2) In order to prevent strain from being applied to the cable core even if the maximum strain is applied to the entire cable, the cable core should have an excess length of more than 0.3% against the suspension member (Fig. 1).

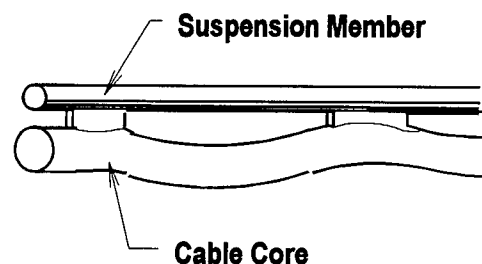


Fig.1 Self-supporting Cable With Cable Excess Length

3.2 Prevention of movement of fiber ribbon

Even in the case of self-supporting cable structure with an excess cable length, the cable core is not free from the elongation due to the temperature change and the vibration from the wind. Accordingly, evaluation was made of the moving characteristic of the fiber ribbon when the elongation strain corresponding to the thermal expansion of the cable and the vibration are applied simultaneously. The ease of movement of the fiber ribbon in the slot was evaluated by the pulling force of the fiber ribbon from the slot. The relation between the fiber ribbon pulling force and the moving characteristic is shown in Fig. 2. By securing the enough pulling force of the fiber ribbon from

the slot, the amount of movement of the fiber ribbon can be kept small.

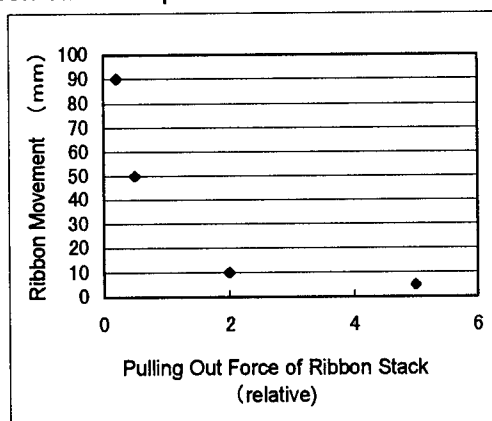


Fig.2 Vibration Test Result

3.3 Simplification of the manufacturing process

To produce an economical distribution cable, a structure capable of simplifying the manufacturing process was studied. The first point is the reduction of the manufacturing processes of self-supporting cable. Conventional pre-hanger cables require three sheath processes, which are cable sheath, supporting wire sheath, and the molding process. This time, we developed a method of providing the excess cable length in the cable sheathing process, and thus simplified the manufacturing process.

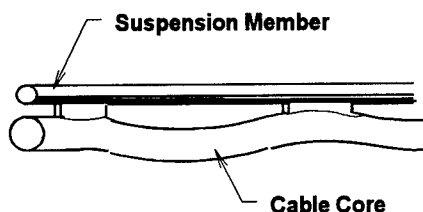
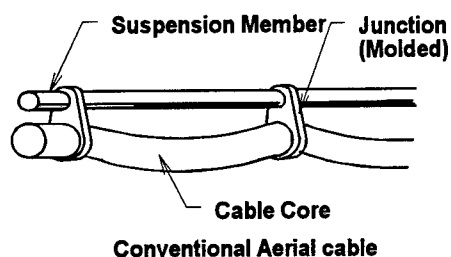


Fig.3 Structure of Self-supporting Cable

The second point is the tandem operation of the fiber assembling process and sheath process. We studied the cable structures that is most suitable to manufacture in tandem line.

4. Cable structure

In order to determine the most optimal cable structure as the aerial distribution cable using 4-fiber ribbons, we investigated three different types of cable cores.

4.1 straight slotted rod type

The straight slotted rod structure has been long studied as a structure capable of manufacturing in one process instead of the conventional two-process manufacture. [4] The sectional structure of the straight slotted rod type cable is shown in Fig. 4.

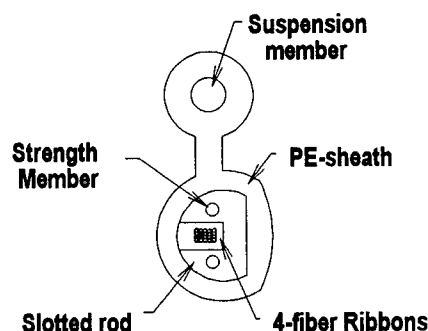


Fig.4 Cross-section of The Straight Slotted Rod Type Cable

4-fiber ribbons are stacked in five layers and inserted into a slotted rod having a linear slot. The slot size was designed so that the ribbon stack could rotate freely in the slot. The slot width and depth were determined so that the circle having the diameter over the diagonal line of the ribbon stack could be drawn as an inscribed circle. The slotted rod has two strength members on both sides of the slot, and the thickness of the slot bottom and rib were determined so that that cable size becomes minimum and yet satisfies the mechanical characteristics. The slotted rod is 7 mm in width and 5 mm in height in overall dimensions.

In the consideration of the easy access to the fiber ribbon at the mid-span access, the slot is a dry structure and not filled with jelly. Furthermore, to prevent the fiber ribbon from

moving, the ribbon stack and the slot are intermittently fixed with a solid resin.

The outside diameter of the cable not including the suspension member portion was 9.7 mm, and the mass was 71 g/m.

4.2 SZ slotted rod type

The SZ slotted rod is a structure having excellent mid-span access performance. The structure of the SZ slotted rod is shown in Fig. 5.

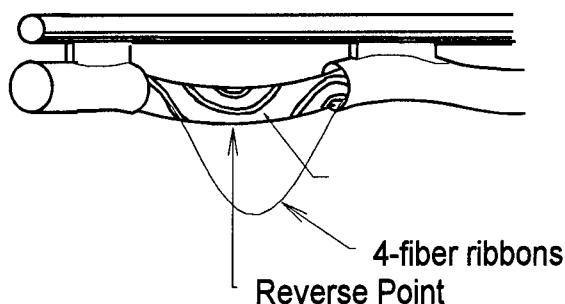


Fig. 5 SZ-reverse stranded Cable

Since each slot changes its direction periodically, it has a hill-like locus near the reverse point. Therefore, if the sheath near the reverse point is removed, the fiber ribbons can be easily taken out from the slotted rod. The locus of the slot is determined by the reverse angle, SZ reverse pitch, and cable outside diameter.

The reverse angle was determined so as to minimize the difference of the length of the slots when the SZ slotted rod is bent. In the present development, special consideration was given to reducing the cable diameter in order to realize low price, and also to optimizing of the SZ reverse pitch to achieve a good accessibility to the fiber ribbons.

(1) Reduction of the diameter of the SZ slotted rod

The sectional structure of the SZ slotted rod type cable is shown in Fig. 6.

The 4-fiber ribbons are stacked and accommodated in each slots. The slot size was designed to enable the ribbon stack to rotate freely in the slot. The slot width and depth were determined so that the circle having the diameter over diagonal line of ribbon stack could be drawn as an inscribed circle.

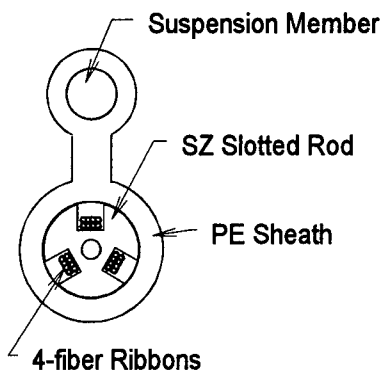


Fig. 6 Cross-section of The SZ Slotted Rod Type Cable

The rib thickness was determined from the results of the past studies so as to satisfy the mechanical tests such as lateral pressure.

Next, the number of slots was optimized so as to accommodate six fiber ribbons. The relation between the number of slots and slotted rod outside diameter is shown in Fig. 7. Fig. 7 shows that the slotted rod outside diameter would be minimum in the three-slots structure.

From these studies, the outside diameter of the slotted rod could be reduced to about 5 mm.

2 slots	3 slots	6 slots
5.3mm	4.9mm	6.4mm

Fig. 7 Result of Review of outside diameter SZ Slotted Rod

(2) Optimization of the SZ reverse pitch

To determine the SZ reverse pitch, studies were made of the ease of the fiber access, pull-out force of fiber ribbon, and manufacturing efficiency.

Excess length of the fiber ribbon in mid-span access is determined by the sheath removing length, slotted rod outside diameter, reverse angle, and SZ reverse pitch. The slotted rod outside diameter and the reverse angle have

already been optimized, as mentioned above. Therefore, in order to obtain more fiber ribbon length in a shorter length of sheath removal, the SZ reverse pitch needs to be shortened.

The relation between the SZ reverse pitch and excess length of the fiber ribbon is shown in Fig. 8. To keep the excess length necessary for fiber jointing, the SZ reverse pitch must be kept under 150 mm.

The relation between the SZ reverse pitch and the pulling-out force of fiber ribbon is shown in Fig. 9. To retain a sufficient pulling-out force to ensure that the fiber ribbon does not move, the SZ reverse pitch must be less than 150 mm.

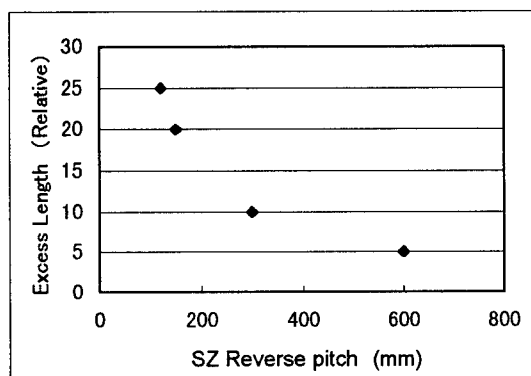


Fig. 8 Excess Length of Fiber Ribbon
(Sheath removed length is 500mm)

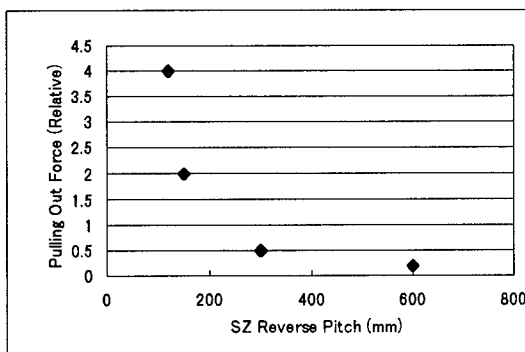


Fig. 9 Pulling Out Force of Fiber Ribbon

4.3 Encapsulation type

The encapsulation type is a structure in which the stack of fiber ribbons is integrated by a plastic material instead of a slotted rod. Since no slotted rod is used, the diameter can

be reduced, and an economical structure is realized. The cable structure of encapsulation type of the trial cable is shown in Fig. 10.

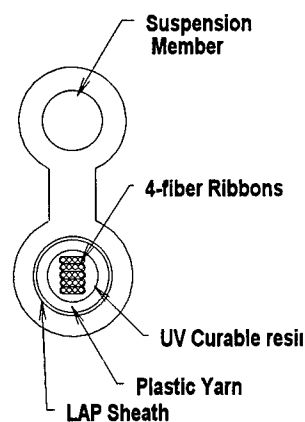


Fig. 10 Cross-section of Encapsulation Type Cable

After stacking 4-fiber ribbons in five layers, a unit was fabricated by using an ultraviolet curable resin. To enable the unit to be picked out easily from the cable when the sheath is removed, plastic yarn was set up around the unit as a buffer layer, and a LAP sheath is applied to form the cable.

The cable outside diameter not including the suspension member portion was 5.5 mm, and the mass was 31 g/m.

5. Cable characteristic

The results of the evaluation of the three types of cables are summarized below.

5.1 Transmission loss in manufacturing process

The transmission loss characteristics of the trial cable were investigated in the manufacturing processes. The results are shown in Fig. 11. No significant loss change was observed in the manufacturing process. It was confirmed that the manufacturing properties were excellent.

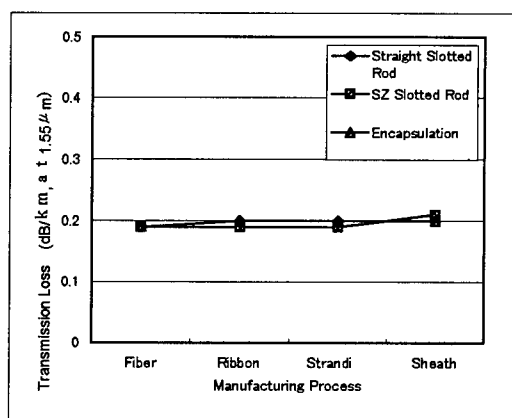


Fig.11 Transmission Loss Change In Manufacturing Process

5.2 Temperature characteristics

Changes in transmission loss were investigated when the temperature was changed from -30 to +70°C. The results are given in Fig. 12. There was almost no significant loss change in any of the cables in the above temperature range.

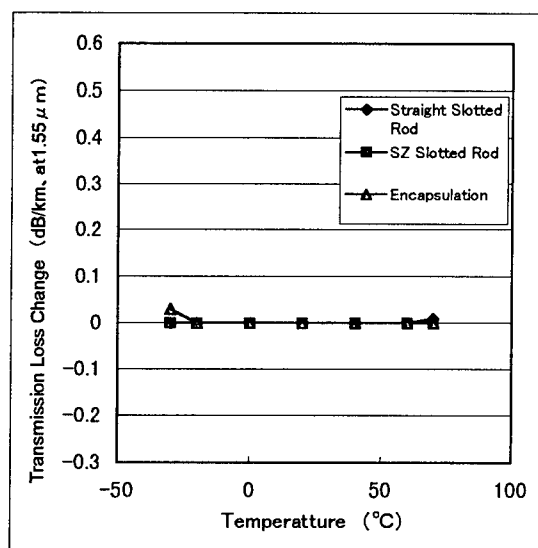


Fig.12 Transmission Loss Change In Temperature Cycling

5.3 Tensile characteristics

An elongation strain equivalent to the maximum elongation (0.3%) assumed in the aerial environments was applied to the cable,

and transmission loss changes and the strain of the fiber were measured. There was no increase in transmission loss in any of the cables. The results of the measurement of the strain changes of the fibers are shown in Fig. 13. In each cable, the elongation strain on the fiber only occurred when the elongation of the suspension member exceeded 0.3%. It was confirmed that the cable core has sufficient excess length against the suspension member.

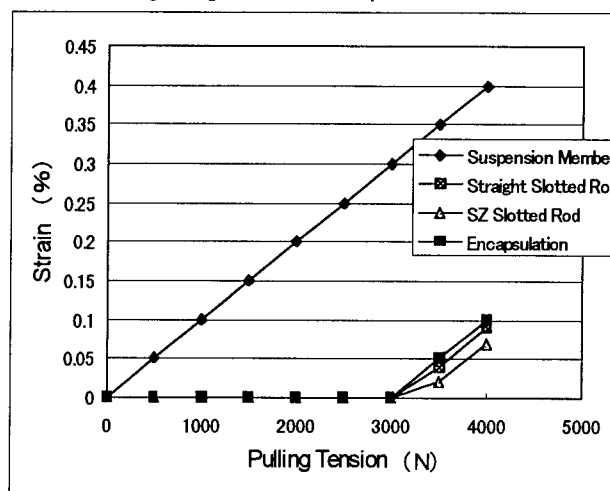


Fig.13 Tensile Test (Fiber Strain)

5.4 mid-span access

After the removal of the sheath in a length of 500 mm, the excess length of the fiber ribbon when picked out from the slotted rod was measured. The results are shown in Table 1. Each cable was confirmed to have sufficient excess length as required for fiber jointing.

Table 1 Excess Fiber Length of Trial Cable

Type of Cable	Straight Slotted Rod	SZ Slotted Rod	Encapsulation
Excess Length (mm)	43	33	-

We then evaluated the working efficiency of the ribbon extraction. In the straight slotted rod structure, since the resin is present intermittently in order to prevent the ribbon movement, it is necessary to remove the resin

and thus deteriorates the mid-span access efficiency.

The SZ slotted rod structure was confirmed to be optimal for the fiber ribbon access because there is no resin around the fiber ribbon.

The encapsulation type requires removal of UV curable resin around the fiber, so the mid-span fiber ribbon access was difficult.

5.5 Other mechanical characteristics

The cables were evaluated for bending test, lateral pressure test, impact test, and twist test. The results are shown in Table 2. Each cable presented excellent characteristics.

Table2 Result of Mechanical Test

Item	Condition	Result
Bending	6D	<0.05 dB (at1.55 μ m)
Lateral Pressure	1960N/100mm	<0.05 dB (at1.55 μ m)
Impact	1kg \times 1m	<0.05 dB (at1.55 μ m)
Twist	$\pm 180^\circ$ /1m	<0.05 dB (at1.55 μ m)

5.6 Vibration test

SZ slotted rod type cable which was best in mid-span access performance was evaluated further. With the cable installed between poles, vibration was imposed on the cable and the transmission loss change, the movement of the fiber ribbon, and the strength of the self-supporting cable structure with excess cable length were investigated. Results of transmission loss are shown in Fig. 14. There was almost no significant change in loss, and no movement of the fiber ribbon was observed. There was no structural damage to the cable after the test.

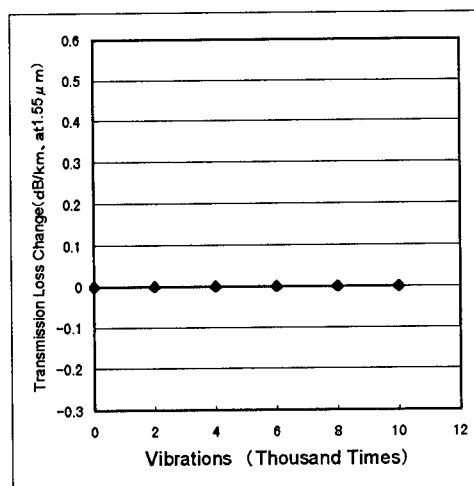


Fig.14 Transmission Loss Change In Vibration

5.7 Installation test

With the cable installed between poles, transmission loss change and the fiber ribbon movement were observed in the long term. Results are given in Fig. 15. Herein, there was almost no significant loss change and no movement of fiber ribbon.

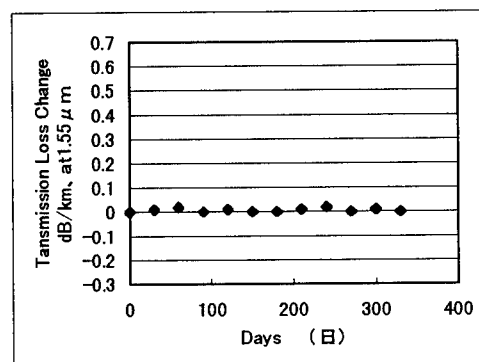


Fig.15 Transmission Loss Change of SZ slotted lot type cable

6. Comparison of cable structures

The features and the evaluation results of the three trial cables are summarized in Table 3.

Table3 Comparison of Characteristics

	Straight Slotted Rod	SZ Slotted Rod	Encapsulation
Diameter (mm)	9.7	8.2	5.5
Weight (g/m)	71	47	31
Transmission Loss	Very Good	Very Good	Very Good
Temperature	Very Good	Very Good	Very Good
Tensile	Very Good	Very Good	Very Good
Mid-span Access	Good	Very Good	Negative
Mechanical	Very Good	Very Good	Very Good
Vibration	-	Very Good	-
Installation	-	Very Good	-

The transmission and the mechanical characteristics were excellent in all types. The cable outside diameter and mass were minimum in the encapsulation structure, and maximum in the straight slotted rod structure.

In the mid-span access performance, which is one of the most important characteristics of the distribution cable, the SZ slotted rod structure presented excellent results. The straight slotted rod structure and encapsulation structure were not superior in working efficiency because of the presence of resins around the fiber ribbon.

Accordingly, it was concluded that the SZ slotted rod structure was the most suitable as the aerial distribution cable for FTTH.

Since the encapsulation structure is minimum in diameter in the three types, it will be possible to realize a lower price in the future.

7. Conclusion

In order to realize the FTTH, we have developed optical fiber cables for aerial distribution network. In consideration of the aerial installation environment, the cable was designed on the basis of the excess length of

optical fiber and moving behavior of the fiber ribbon. In addition, a structure which enables tandem manufacturing process was also investigated to realize low price.

Three trial types were manufactured: straight slotted rod structure, SZ slotted rod structure, and encapsulation structure.

All three types of trial cables showed excellent transmission characteristics and mechanical characteristics. The SZ slotted rod structure, which is outstanding in the mid-span access performance that is required in the distribution cable, is considered to be best suited to the aerial distribution cable. Furthermore, as the encapsulation structure can be minimized in diameter among three types, it will be possible to realize a lower price in the future. Henceforth, we will study ways to enhance the fiber ribbon extracting property in the encapsulation structure.

References

- [1] Bessho, Y. et al.: Deployment of research and development of FTTH, NTT Technical Journal, Vol. 9, No. 4, 1997.
- [2] Hirooka, A. et al.: Optical fiber related technology and its installation technology realizing a radical cost reduction, NTT Technical Journal, Vol. 9, No. 4, 1997.
- [3] NTT, PROCURMENT DOCUMENTATION " Optical Fiber Cables and Fiber Jointing for Aerial Access Distribution Network " December 6, 1995
- [4] A. Gouronnec et al., "MULTIPULLING AND CABLING IN LINE: A NEW PROCESS", 33th IWCS, 1984

AUTHORS



Ichiro Kobayashi

The Furukawa Electric co., Ltd.
6,YawataKaigandori Ichihara, Chiba
290,Japan

Ichiro Kobayashi received his B.S. degree in Physics from Chuou university in 1986. He joined The Furukawa Electric Co., LTD. in 1986 and has been engaged in the development of the optical fiber and cables. He is now a senior research engineer of Opto-Technology Laboratory. He is a member of the Institute of Electronics ,Information and communication Engineers of Japan.



Disuke Iwakura

The Furukawa Electric co., Ltd.
6,Yawata Kaigandori Ichihara, Chiba
290,Japan

Daisuke Iwakura received his M.E. degree in Engineering from Electro-Communications University in 1993.He joined The Furukawa Electric co., Ltd. in 1993 and has been engaged in research and development of optical fiber cables. He is now a research engineer of Opto-technology laboratory

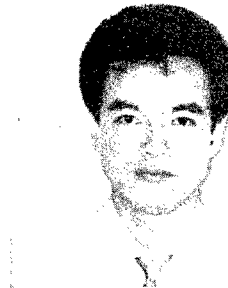


Ryuji Takaoka

The Furukawa
Electric co. ,Ltd.

6,Yawata Kaigandori
Ichihara, Chiba
290,Japan

Ryuji Takaoka received his M.E .degree in Mechanical Engineering from Keio University in 1996.He joined The Furukawa Electric co., Ltd. in 1996 and has been engaged in research and development of optical fiber cables. He is now a research engineer of Opto-technology laboratory.

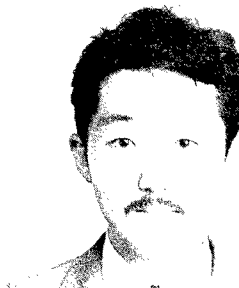


Eiji Konda

The Furukawa
Electric co., Ltd.

6,Yawata Kaigandori
Ichihara, Chiba
290,Japan

Eiji Konda joined The Furukawa Electric co., Ltd. in 1977 and has been engaged in research and development of materials and optical fiber cables. He is now a engineer of Opto-technology laboratory.



Ryuichi Matsuoka

The Furukawa
Electric co.,Ltd.

6,Yawata Kaigandori
Ichihara, Chiba
290,Japan

Ryuichi Matsuoka received his M.E. degree in Electronics Engineering from Osaka University in 1991. He joined The Furukawa Electric co., Ltd. in 1991 and has been engaged in the development of optical fiber and cables. He is now a production engineer of Transmission Systems division.



Yuichi Sekii

The Furukawa
Electric co., Ltd.

6, Yawata Kaigandori
Ichihara, Chiba
290, Japan

Yuichi Sekii received his B.E. degree in Applied Physics from Nihon University in 1990. He joined The Furukawa Electric co., Ltd. in 1990 and has been engaged in the development of optical fiber cables. He is now a production engineer of Transmission Systems division.



Yasuhiro Kamikura

The Furukawa Electric co., Ltd.
6, Yawata Kaigandori Ichihara, Chiba
290, Japan

Yasuhiro Kamikura received his B.E. degree in Electronic Engineering from Tokyo University in 1975. He joined The Furukawa Electric co., Ltd. in 1975 and has been engaged in the development of optical fiber and cables. He is now a general manager of Opto-technology laboratory. He is a member of the Institute of Electronics, Information and communication Engineers of Japan.



Hideyuki Izukura

The Furukawa
Electric co., Ltd.

6, Yawata Kaigandori
Ichihara, Chiba
290, Japan

Hideyuki Izukura received his B.E. degree in Electronic Engineering from Chiba Institute of Technology in 1990. He joined The Furukawa Electric co., Ltd. in 1990 and has been engaged in the development of optical fiber cables. He is now a equipment engineer of Transmission Systems division.



Yoshiyuki Ohkawa

The Furukawa
Electric co., Ltd.

6, Yawata Kaigandori
Ichihara, Chiba
290, Japan

Yoshiyuki Ohkawa received his B.E. degree in Metallurgy and Materials Engineering from Tokyo University in 1987. He joined The Furukawa Electric co., Ltd. in 1987 and has been engaged in the development of optical fiber cables. He is now a production engineer of Transmission Systems division.

Development of Aerial Cluster-type Optical Drop Cable

F. Hosoi, M. Hara, and Y. Kamikura

The Furukawa Electric Co., Ltd. Ichihara, Chiba, Japan

1. Abstract

We have designed and test-manufactured aerial cluster-type optical drop cable for use in the concentrated dropping of multiple drop cables to residential homes. We evaluated the mechanical properties of this cable and assessed its suitability in terms of dropping work (installation). In addition, we also designed, test-manufactured, and evaluated a new type of drop cable for use within aerial cluster-type optical drop cable.

2. Introduction

In recent years we have witnessed the rapid expansion of optical fiber networks to residential homes. On account of this expansion, it has become increasingly important to devise methods to efficiently and inexpensively drop optical fibers to these homes.^{1,2)}

When using a single-fiber drop cable to drop a fiber from an optical cable containing fiber ribbons, only one or two optical fibers within a particular ribbon are actually used at the drop point -- the remaining fibers are left unused. This presents a problem in terms of fiber utilization efficiency. Another problem is that, during the dropping work, there exists a risk of increasing the transmission loss of other optical fibers in use. The following method presents one approach for resolving these problems. That is, during construction, access points, from where fibers from several to several tens in number will be dropped, are designed at suitable locations beforehand. From there, aerial cluster-type optical drop cables, each of which is comprised of multiple single-fiber drop cables, are strung on poles. When the need for a drop arises, a drop cable is taken from the cluster at the pole nearest to the subscriber and led to the home.³⁾ In this paper, the authors report on the design, test-manufacture, and evaluation of such aerial cluster-type optical drop cable.

3. Cable design

Fig.1 shows the structure of aerial cluster-type optical drop cable. When dropping a drop cable to a subscriber's residence, a drop cable is taken from a previously strung cluster and led directly to the residence^{4,5)}. Here, in relation to aerial cluster-type optical drop cable, we first designed a single-fiber drop cable to be mounted within the aerial cluster-type optical drop cable and next designed the overall aerial cluster-type optical drop cable. The procedure is explained below.

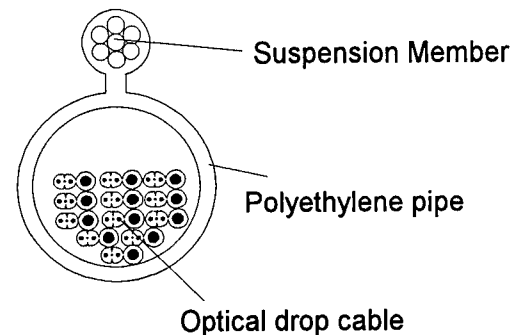


Fig. 1 Aerial cluster-type optical drop cable

3.1 Design of a new drop cable for use in aerial cluster-type optical drop cable

Shown in Fig. 2 (b) is the structure of a new drop cable designed by us for use with the aerial cluster-type optical drop cables of Fig. 1.

With the conventional drop cable (Fig. 2(a)), a flat cable is wrapped around a strength member.

In our design, in contrast, the strength member and the cable are combined as an integral unit. This makes it possible to manufacture the cable in one process, thereby keeping down cable costs.

Furthermore, through a reappraisal of cable installation tension and fiber screening level, we were able to reduce the diameter of the strength members from 0.7 mm to 0.4 mm, thus cutting down the overall cable size and reducing the material costs.

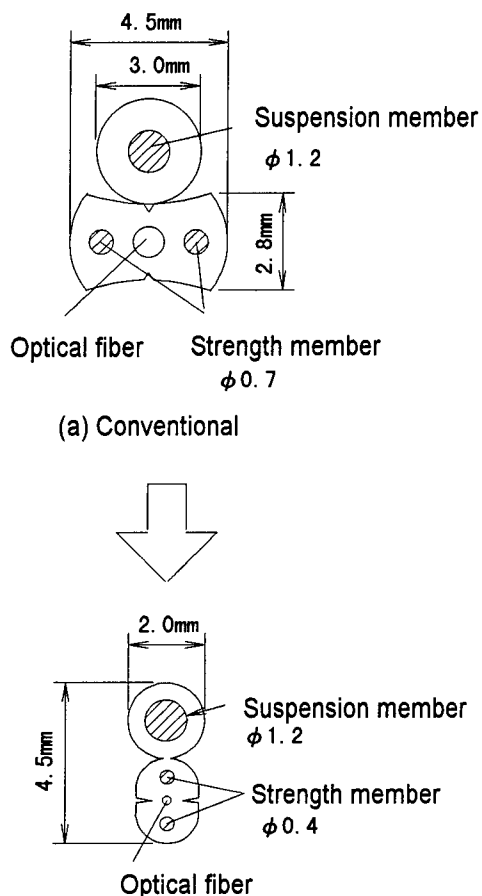


Fig. 2 Aerial drop cables

3.2 Design of the aerial cluster-type optical drop cable

As shown in Fig. 1, this cable is comprised of (a) a polyethylene pipe integrated with a suspension member and (b) aerial drop cables. Because the drop cables are contained loosely within the pipe, it is possible to, wherever a drop is necessary, simply cut a hole in the pipe, draw out the required length of drop cable, and directly connect it to the subscriber's residence. Because the connection is direct, joint work is unnecessary.

The pull-out characteristics of the drop cable as it is drawn from the pipe are an important consideration for aerial cluster-type drop cable. That is, because the drop cable is to be physically pulled out by installation personnel, the force required to draw out the cable must be small or, in other words, the cable must have little pull-out resistance. Here, we investigated the pull-out resistance characteristics of the drop cable.

3.2.1 Relation between drop cable surface type and drop cable pull-out resistance

First, we studied the effects of the surface condition of the drop cable. Two types of drop cables which are made of different sheath materials (both PVC) with different coefficients of friction were made and their pull-out resistance from the piped cable was measured. Then we applied a Teflon lubricant to the surface of these drop cables, and again measured the pull-out resistance. Twelve drop cables are placed in the pipe and the pull-out resistance was measured when one of the drop cables was pulled out from the pipe while the pipe was kept straight. The result in terms of the value is shown in Table 1. We note that the lubricant had a beneficial effect on both the Type A and Type B PVC sheath. Also, despite the fact that, without any lubricant, the pull-out resistance of the Type B cables was 2.2 times that of the Type A cables, the application of the lubricant reduced the pull-out resistance of the two to very nearly the same value. The use of a lubricant not only lowers the pull-out resistance, but also, because the pull-out resistance does not depend on the underlying material when lubricated, significantly expands the range of the material selection options.

Table 1 Relation between lubrication and drop cable pull-out resistance

	Type A sheath	Type B sheath
Drop cable pull-out resistance without lubricant	37.6 N	83.2 N
Drop cable pull-out resistance with lubricant	15.3N	17.4N

3.2.2 Relation between drop cable occupation ratio and drop cable pull out resistance

We next measured the change in pull-out resistance with a change in the pipe internal diameter. We selected Type A PVC as the drop cable sheath and applied lubricant over the surface of the drop cables. The pipe cables, each 60 m in length, were then laid straight. The measurement results are shown in Fig.3. The horizontal axis in the figure indicates the occupation ratio of the cables within the pipe (i.e., the cross-sectional area of the drop cables divided by that of the pipe). Here, we note that the pull-out resistance of the drop cables does depend on the occupation ratio. Considering that the drop cables are to be physically pulled out by installation personnel on site, the pull-out resistance must be limited to about 100 to 150 N; if we take the maximum pull-out length to be 60 m, then we find that the pipe must have an occupation ratio of about 35 to 39% or less.

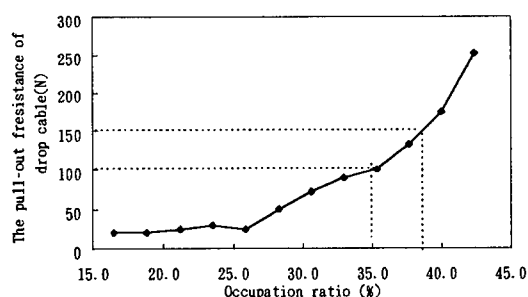


Fig. 3 Relation between drop cable pull-out resistance and occupation ratio

4. Cable evaluation

4.1 Evaluation of drop cable for mounting in aerial cluster-type optical drop cable

We evaluated the aerial drop cable of Fig. 2 (b) by conducting a variety of tests with cables containing either 0.25 or 0.5 mm fiber. The results are shown in Table 2. From the table, we note that there are no problems with the characteristics of cables containing either type of fiber. From the aspect of downsizing,

we decided to use the 0.25 mm optical fiber cables for mounting in the aerial cluster-type optical drop cable.

Table 2 Mechanical and temperature characteristics of newly designed aerial drop cable

Wavelength: 1.55 μ m

Item	Condition	Loss change	
		0.25mm fiber	0.5mm fiber
Transmission loss (Average)	OTDR	0.19 dB/km	0.19 dB/km
Temperature cycling	-30°C to +70°C	≤ 0.01 dB/km	≤ 0.01 dB/km
Bend	r=30mm ±180° Bending	≤ 0.01 dB	≤ 0.01 dB
Lateral pressure	1200N/25mm	≤ 0.01 dB	≤ 0.01 dB
Impact	Cylinder 1kg 20mm ϕ dropped on cable from 1m height	≤ 0.01 dB	≤ 0.01 dB
Tensile	0.3% extending	≤ 0.01 dB	≤ 0.01 dB

4.2 Evaluation of aerial cluster-type optical drop cable

4.2.1 Evaluation of pull-out resistance

We used a cluster having a 28% occupation ratio for our evaluation of pull-out resistance. Measurements were made not only with the pipe laid straight, but also, in consideration of actual installation in the field, with two bends as illustrated in Fig. 4. The results are shown in Table 3. The pull out resistance was 50 N or less for the straight pipe, and 120 N or less with the bends. These results shows that there is no problem in the practical environment.

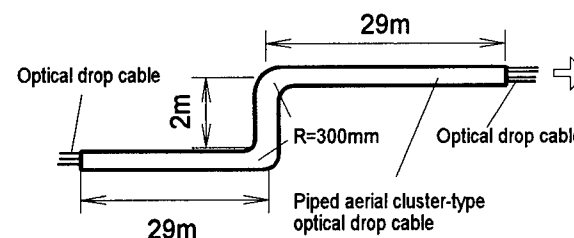


Fig. 4 Evaluation of pull-out resistance when aerial cluster-type optical drop cable was bent

Table 3 Results of drop cable pull-out resistance measurements

Cable condition	Pull-out resistance (N)	
	Max.	Ave.
Straight	50N	43N
Bent at 2 locations	120N	90N

4.2.2 Mechanical and temperature characteristics

Measurement results of the mechanical and temperature characteristics of the aerial cluster-type optical drop cable are shown in Table 4. We note here that there are no problems in terms of cable characteristics.

Table 4 Mechanical and temperature characteristics of the aerial cluster type optical drop cable

Wavelength: 1.55 μ m

Item	Condition	Loss change
Transmission loss (Average)	OTDR	0.19 dB/km
Temperature cycling	-30°C to +70°C	≤ 0.01 dB/km
Bend	$r=6D$ (D is cable diameter) $\pm 180^\circ$ Bending	≤ 0.01 dB
Lateral pressure	4000N/100mm	≤ 0.01 dB
Torsion	$\pm 180^\circ$ /1m	≤ 0.01 dB
Squeeze	Cable 125m Tension 10000N R=250 mm	≤ 0.01 dB
Impact	Cylinder 1kg 20mm ϕ dropped on cable from 1m height	≤ 0.01 dB
Tensile	10000N	≤ 0.01 dB

5. Conclusion

We designed and evaluated aerial cluster-type optical drop cable to facilitate the efficient and concentrated dropping of optical fiber cables to residential homes.

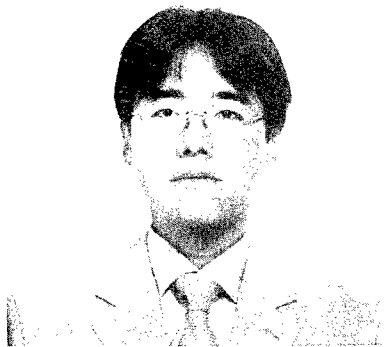
The pull-out resistance of a drop cable over a 60 m length was 50 N or less for the straight pipe, and 120 N or less with the bends, thereby allowing installation personnel to easily draw out a drop cable from the cluster

on site.

We examined the mechanical and temperature characteristics of this cable. Good results were obtained.

6. References

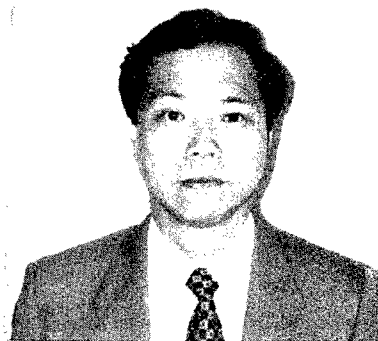
- (1) H. Ishikawa, K. Hogari, N. Yasuhara, M. Terasawa, M. Kama, and M. Hirahara, "Cost Reduction Technologies of Optical Drop Cable and Indoor Cable," Proceedings of EC 97, pp. 179-185.
- (2) Y. Nakatsuji, K. Hogari, S. Furukawa, S. Koshio, and K. Nishizawa, "Studies on Optical Cable for Residential Premises and Office Buildings," IEICE B-10-20, p. 529, 1997.
- (3) K. Hogari, K. Tomiyama, and O. Kawata, "A Proposal of Optical Fiber Dropping Method for the Residential Home," IEICE SB-7-9, pp. 696-697, 1995.
- (4) K. Tomiyama, Y. Nakatsuji, K. Hogari, and S. Furukawa, "Studies on Aerial Optical Drop Cable to Residential Premises," IEICE B-957, p. 442, 1996.
- (5) F. Hosoi, M. Hara, and Y. Kamikura, "Development of Aerial Cluster-type Optical Drop Cable," IEICE B-10-24, p. 553, 1997.



Fumiki HOSOI

The Furukawa Electric Co.,Ltd
6,Yawata Kaigandori,Ichihara, Chiba,290,
Japan

Mr. Hosoi received his M.E. degree in Physics engineering from Tokyo University in 1995. He joined The Furukawa Electric Co., Ltd and has been engaged in research and development of optical fiber cable. He is now a research engineer of optical fiber transmission research department, opto-technology laboratory.



Yasuhiro KAMIKURA

The Furukawa Electric Co.,Ltd
6,Yawata Kaigandori, Ichihara, Chiba, 290,
Japan

Mr. Kamikura received his B.E. degree in Electronic Engineering from Tokyo University in 1975. He joined the Furukawa Electric co., ltd. in 1975 and has been engaged in the development of the optical fiber and cables. He is now a general manager of Opt-Technology Laboratory. He is a member of the Institute of Electronics, Information and communication Engineers of Japan.



Masami HARA

The Furukawa Electric Co.,Ltd
6,Yawata Kaigandori, Ichihara, Chiba, 290,
Japan

Mr. Hara received his M.E. degree in Physics from Osaka University in 1987. He joined The Furukawa Electric Co., Ltd and has been engaged in research and development of optical fiber cable. He is now a research engineer of optical fiber transmission research department, opto-technology laboratory.

OPGW : DO THEY CREEP DIFFERENTLY?

J.P. Bonicel ¹, O. Tatat ¹, R. Girbig ², G. Hog ²

¹ Alcatel Telecommunications Cable, Claremont, North Carolina

² Alcatel Kabel, Monchengladbach, Germany

ABSTRACT

We have performed creep tests on the two basic OPGW designs that we are proposing to the market : the aluminum slotted core and the steel tube designs. The tests have been performed at different levels of tensile stress. The conditions for the tests are the ones recommended by the IEC and so is the calculation method used to fit the creep versus time equation in order to get long time extrapolations. The results of the tests will be presented, compared to typical data from the literature, and discussed. Fitting of the results with the theoretical time and stress dependence equation of creep is presented. Starting from results obtained on a limited sampling of cables, typical and maximum creep at 10 years are proposed as calculation inputs for circumstances where a very accurate value is not needed. This should generally be the case for OPGW as they are quite often installed with a reduced sag compared to the conductors they are overhanging, so that creep occurring on both conductors and OPGW must not lead to a dramatic reduction of their safety distance. Illustration of the long term creep impact are given in the form of calculated initial and final sags.

INTRODUCTION

The elongation of stranded conductors has been described (2) as resulting from :

- a)elastic elongation,
- b)thermal elongation,
- c)creep,
- d)elongation due to the slack in the wires during stranding,
- e)radial compression and local indentation of conductor layers at wire contacts.

Elongation resulting from a) and b) is reversible. Elongation resulting from c), d), e) is permanent and responsible for increasing the sag of the conductor along its life.

This is why attention must be paid to the permanent elongation factors. Additionally, one may be concerned with the reduction of the optical fiber strain margin of Optical Ground Wires (OPGW) due to the permanent elongation.

A good description of the permanent elongation of overhead electrical line conductors has already been given and prediction equations have been presented (1).

Typical creep figures for stranded conductors have also been proposed (2), as a function of the nature of the armoring wires.

Most of the new high voltage lines are now incorporating an OPGW instead of a conventional earth wire. Information about the creep behavior of such OPGW is required by the line designers in order to computerize sag and tension calculations.

CREEP

The so called conductor creep can be considered as the addition of the metallurgical creep e_c of the materials and the geometrical settlement e_s of the different components of the cable.

According to Cigre (2) :

e_s depends on the mechanical tension and e_c depends on the mechanical tension but also on the temperature and the time.

$$e_c = K f(T) s^a t^m(s) \quad \text{and} \quad e_s = H s g$$

in which :

K = constant depending on the material.
 f(T) = function increasing with temperature.
 T = temperature of the conductor.
 s = conductor stress.
 t = time.
 a, m(s) = experimentally determined coefficients.
 H = coefficient depending on the conductor.
 g = coefficient depending on internal factors.

The IEC 1597 proposes as the total creep of the conductor (metallurgical creep plus wires settlement):

$$e = K_c e^{fT} s^y t^m \quad \text{where :}$$

K_c = creep coefficient mainly depending on number of wires in the conductor.
 f = coefficient for the temperature dependence.
 y = coefficient for the stress dependence.
 m = coefficient for the time dependence.

Usually a creep test is performed at constant temperature and stress so that the previous equation can be simplified :

$$e = A t^m$$

or $\ln e = \ln A + m \ln t$

A graph of the strain against time plotted on a log scale should be a straight line. Actually, as shown in fig.1, there is a time t_s where the data deviates from the straight line law. The main reason for this deviation is the permanent elongation due to the wires settlement, which is not time dependent and takes place at the beginning of the test. A linear regression law shall be fitted to all points in which the time exceeds t_s .

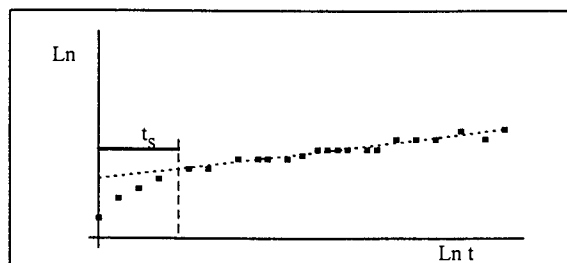


Fig.1 : creep vs. time, typical dependence

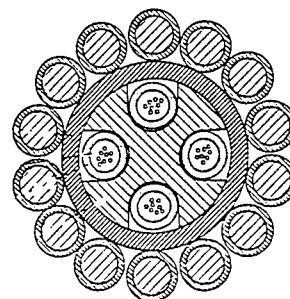
Recently, the IEC has proposed a test procedure for the measurement of the creep of overhead conductors (5). The test is performed preferably at 20 %UTS and for a 1000 h duration. The linear regression has to be established from all data collected after 1 hour from the start of the test. Some of the tests whose results are given have been performed and results were analyzed according to this document. Other tests, performed earlier have been analyzed from data collected after 24 hours from the start of the test.

CABLES TESTED

Two main designs of Optical Ground Wires were developed within ALCATEL : the Aluminum Slotted Core and the Steel Tube designs. They have been described in previous papers (3;4) and their performances were presented.

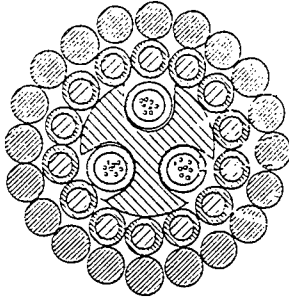
Some representatives of both designs have been tested for creep according to the test procedure recommended by the International Electrical Commission (5). The test duration was either 1000 or 4000 hours and the main purpose of the test was to extrapolate the creep at 10 years from the actual results.

Figure 2 presents the construction and main characteristics of the cables selected for the test.



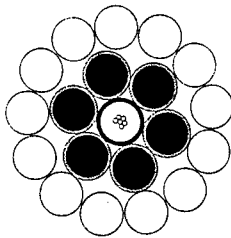
OPGW 87T87

Diameter : 15.6 mm	UTS : 10550 daN
Weight : 750 kg/km	DC resistance : 0.36 Ω/km
Supporting section : 87.4 mm ²	



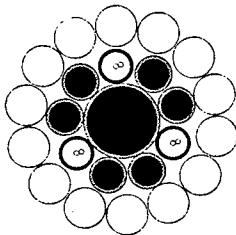
OPGW 107/44

Diameter : 15.3 mm	UTS : 7350 daN
Weight : 550 kg/km	DC resistance : 0.32 Ω/km
Supporting section : 106.8 mm ²	



ASLH-D(S)bb 1x6E9/125 (52/29-5.5)

Diameter : 12.0 mm	UTS : 5150 daN
Weight : 365 kg/km	DC resistance : 0.53 Ω/km
Supporting section : 81.1 mm ²	



ASLH-D(S)bb 3x2E9/125 (44/26-4.7)

Diameter : 11.3 mm	UTS : 4400 daN
Weight : 327 kg/km	DC resistance : 0.62 Ω/km
Supporting section : 70.0 mm ²	

Fig.2 : description and characteristics of cables tested

The IEC test procedure does not specify the creep load to be applied to the cable. It only recommends 20 % UTS if not specified in other documents.

We have decided to use a worst case Every Day Stress as creep load. The EDS is actually the load that will endure an aerial cable during most of its service time. Although for short term periods (a few hours up to a few days)

and because of harsh climatic conditions of ice and wind it may endure much higher tensile load that should, however, never be higher than the maximum allowed tension for the cable. Typically high wind induces tensile load in the range of 40 % UTS and heavy ice or combination of both may lead to 60 to 70 % UTS.

An overhead aerial conductor which is exposed to such very high load, even for a very short time, will get a permanent elongation rapidly because it has been stressed into the plastic deformation zone of the tensile/elongation diagram. This permanent elongation has the same magnitude as the elongation induced by long term creep at EDS.

Additional creep testing has been performed at up to 60% UTS but these results should not be extrapolated for periods as long as several years.

TEST RESULTS

All the creep curves are shown in the appendix.

Test 1 : OPGW 87T87

Once the test is performed and the curves drawn, a difficulty is to select the range of data to be used for extrapolating the results at longer time.

Creep due to structural effects happens rapidly because it does not take a long time for the armoring wires to get their final position one to each other once the cable is loaded.

This structural effect is responsible for the rather high creep observed during the first few hours of test. Then the creep curve is closer to a straight line and this is representative of the long term material creep.

We did two extrapolations : worst case is obtained from all the data from 1 to 1000 hours (according to IEC procedure) and best case is got from all the data from 10 to 1000 hours. Respective extrapolated equations are:

$$\text{worst case} : e = 0.0324 \cdot t^{0.229}$$

$$\text{best case} : e = 0.0393 \cdot t^{0.191}$$

And the creep at 10 years is :

worst case : 0.44 mm /m

best case : 0.35 mm/m

Test 2 : OPGW 107/44

The same considerations lead to the following extrapolations :

worst case : $e = 0.0357 t^{0.247}$

best case : $e = 0.0422 t^{0.214}$

And the creep at 10 years is :

worst case : 0.59 mm /m

best case : 0.48 mm /m

Note : differences with OPGW 87T87 : 2 armor layers instead of 1

creep load is 25 % UTS instead of 20 %

Test 3 : OPGW ASLH-D(S)bb 1x6 E9/125 (52/29-5.5)

This test was performed prior to the recommendations for test from the IEC. Consequently, the test duration was 4000h and the regression was performed from all the data got later than 24 h after the starting of the test

equation : $e = 0.0073 t^{0.266}$

creep at 10 years : 0.15 mm /m

Note : differences with OPGW 87T87 and 107/44 : this is a central steel tube design
creep load is 16 % UTS

Test 4 : OPGW ASLH-D(S)bb 3x2 E9/125 (44/26-4.7)

This test was also performed prior to the recommendations for test from the IEC. Consequently, the test duration was 4000h and the regression was performed from all the data got later than 24 h after the starting of the test

equation : $e = 0.0276 t^{0.228}$

creep at 10 years : 0.37 mm /m

Note : differences with OPGW 87T87 and 107/44 : this is a stranded steel tube design
creep load is 17 % UTS

Conclusion from tests 1, 2, 3 and 4 :

The basic conclusion of these tests is that a typical creep at 10 years to be considered for OPGW is in the range 0.4-0.6 mm/m. This is in very good accordance with the figures given by the IEC for overhead conductors.

Such result may be used by high voltage line designers to calculate initial and final sags.

The main purpose of such test results is to consider the long term cable creep when sagging a cable on a high voltage line. Consequently, the starting point of the curve to be considered shall be representative of the cable loading history at the sagging time.

It is unrealistic to consider that a cable is sagged within an hour after having been laid out.

It is also a good installation practice to allow the cable a recovery time after lay out in order to release torsion or other laying induced stresses before sagging and clamping. If the cable has been allowed to recover, and so to creep, during 10 hours at the installation tension before sagging, we can deduct the creep at 10 hours from the creep at 10 years.

Cable ref.	Creep at 10 years	Creep at 10 hours	(Creep 10y - creep 10h)	Load (%UTS)
OPGW 107/44	0.59/0.48	0.06/0.07	0.53/0.41	25
OPGW 87T87	0.44/0.35	0.05/0.06	0.39/0.29	20
OPGW ASLH-D(S)bb 1x6 E9/125 (52/29-5.5)	0.15	0.01	0.14	16
OPGW ASLH-D(S)bb 3x2 E9/125 (44/26-4.7)	0.37	0.05	0.32	17

For typical sagging tension (usually close to 15 % UTS), and when the cable is allowed to recover for a few hours before sagging, the

typical creep to be considered for final sag determination is less than 0.5 mm/m

High load testing : creep/load dependence

OPGW 87T87, 107/44, ASLH-D(S)bb 1x6 E9/125 (52/29-5.5) and OPGW ASLH-D(S)bb 3x2 E9/125 (44/26-4.7) have been tested at several load levels.

For each load level, the creep at 10 years was extrapolated. The results are summarized in fig.3, where a general trend of linear relationship between $\ln(\text{creep})$ and $\ln(\text{load})$ can be seen.

Actually, such a curve may only be used to get a rough idea of the creep at 10 years for load level lower than 20 to 25%UTS. As already mentioned, it is unrealistic to consider a creep at 10 years for load levels much higher than the EDS. It makes more sense to use such high loading test results for short term extrapolations (a few hours to a few month).

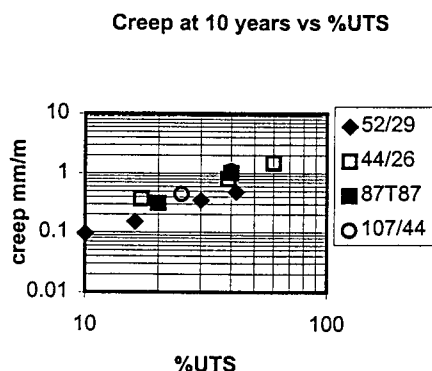


fig.3

OPGW CREEP AS AN OVERHEAD LINE DESIGN PARAMETER

The main function of an earth wire, and so of an OPGW is to protect the current carrying conductors from lightning shot. In that respect the earth wire hangs above the conductors. When designing a line, the engineer considers the clearance to be respected between the lowest conductor and the ground or other obstacles such as crossing another line. He determines a maximum sag for the lowest

conductor. This sag must not be overcome, even after long term creep.

The other conductors are laid parallel to this lowest conductor so that their clearance is respected. Then the earth wire or the OPGW is sagged similarly. Being the highest conductor of the line, the OPGW may not have other clearance concerns than with the other conductors it is overhanging. Consequently, its final sag shall not exceed the final sag of the other conductors. Very often, OPGW are strung higher than conductors (reduced sag) and they always contain steel (reduced creep compared to conductors), therefore the risk for the OPGW to have its sag increase more than the conductor's is very low. This is why it is assumed that in most cases, an OPGW's typical creep value is enough for the engineer to design the line. On the other side, ice load may be higher on OPGW than on conductor, so that permanent elongation of OPGW can be higher than for conductors, but this is not a long term creep induced phenomenon and it should be estimated from other data than creep at 10 years.

The typical values given in this paper were determined from a sampling of cables of 2 different designs. We assume that these figures may not apply to quite different designs such as plastic core.

Creep Related Sag Increase

A few examples of how long term creep impacts the sag are given hereafter.

In the following calculation we have considered an OPGW 87T87, an installation tension of 20%UTS at 15°C (parameter = 2290 m) and we have calculated the final sag after 10 years for spans ranging from 100 to 850 m and assumed a typical creep at 10 years equal to 0.5mm/m.

The sag increase after ten years is plotted against the span length (fig.4). The sag increase is about 12 % for a typical span of 400m. By sagging the cable at 23%UTS, the final sag would be similar to the initial sag when a tension of 20%UTS is applied. This means that such a small long term creep may be easily compensated with a slightly higher initial tension.

Creep induced sag increase
(creep = 0.5 mm/m)

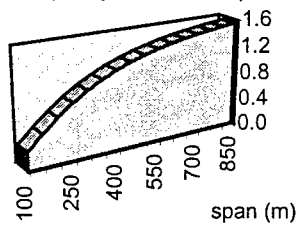


fig.4

Fig.5 presents the calculated sag increase assuming creep value of 0.4, 0.6, 0.8, 1.0, and 1.2 mm/m. In case of a 1.2 mm/m creep, the same calculation as above demonstrate that a 28 %UTS initial tension must be necessary for creep compensation. This is a lot and would add more creep to the cable. However, we anticipate that 1.2 mm/m creep is not possible on an OPGW with a composite armoring (steel + aluminum) in normal environment. Such creep may only result from exceptional climatic events such as thick ice sleeve or ice combined with a high speed wind.

Creep impact to the sag increase

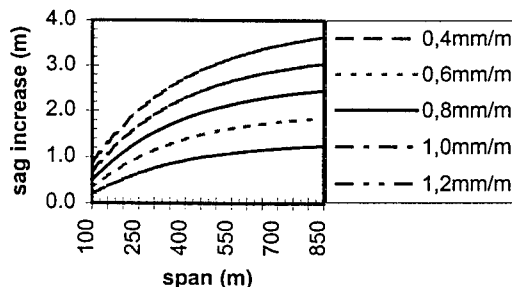


fig.5

CONCLUSION

According to the tests results that are presented, we can conclude that :

As any other metallic armored cable, OPGW creeps.

OPGW do not creep differently from a conductor of approximate construction and made of the same materials. Basic overhead

conductors creep estimation given in international documents such as IEC 1597 are very close to what has been determined when testing our aluminum slotted core and steel tube OPGW. For rough calculation, typical creep at 10 years figure is 0.4 to 0.5 mm/m and a worst case, pessimistic figure is 1 mm/m for both our OPGW designs.

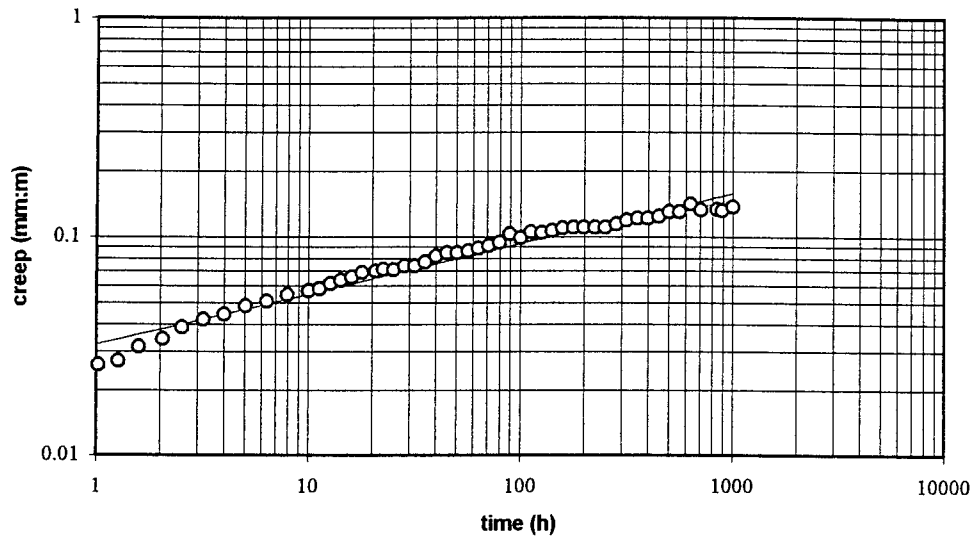
Creep values under every day stress are very small compared to the fiber strain margin (10 times lower) for both our cable designs. The fiber strain margin is negligibly reduced.

Creep is a function of time but also stress. Tests have also been performed at much higher tension than the EDS, and some results were given, but the results must not be extrapolated to a longer time period than a few weeks because such a high tension is only withstood for short time periods by the conductor during exceptional climatic events.

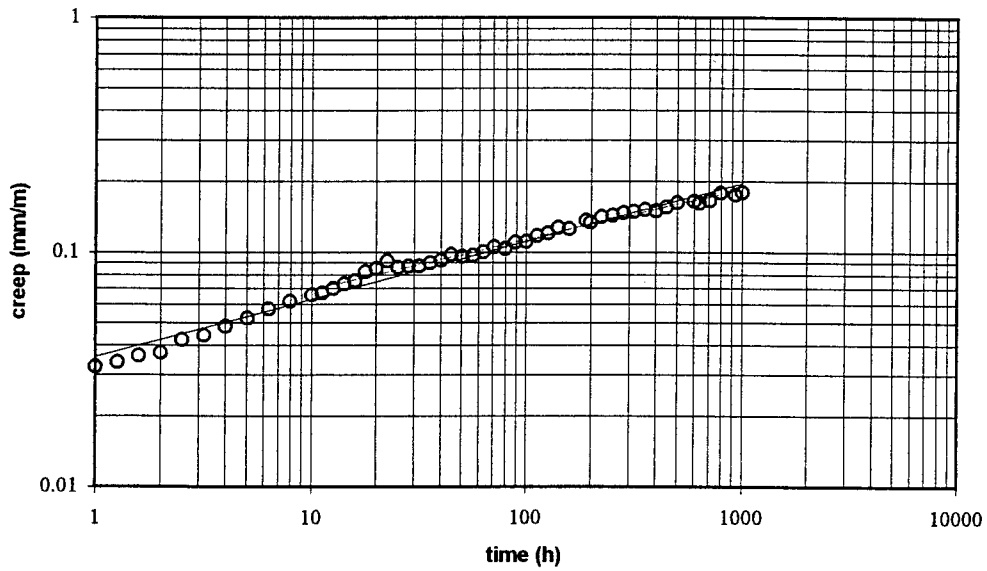
REFERENCES

- (1)-CIGRE Electra n7, pp 63-75, Working Group 22.05, "Permanent elongation of conductors. Predictor equation and evaluation methods"
- (2)-International Electrical Commission, Committee 7, "Technical Report IEC 1597"
- (3)-J.P. Bonicel, C.G. Cortines, J.C. Delomel, G. Hog, S. Pouilly, O.Tatat, P.E. Zamzow, "Optical Ground Wire - A Worldwide Technical Survey and Comparison", Proc. 42nd IWCS (1993).
- (4)-J.P. Bonicel, G. Couvrie, O.Tatat, "Lightning Strike Resistance of OPGW", Proc. 44th IWCS (1995).
- (5)- International Electrical Commission, Technical Committee 7, "7/489/CDV-Draft IEC 1395 Ed.1-Overhead Electrical Conductors. Creep test".

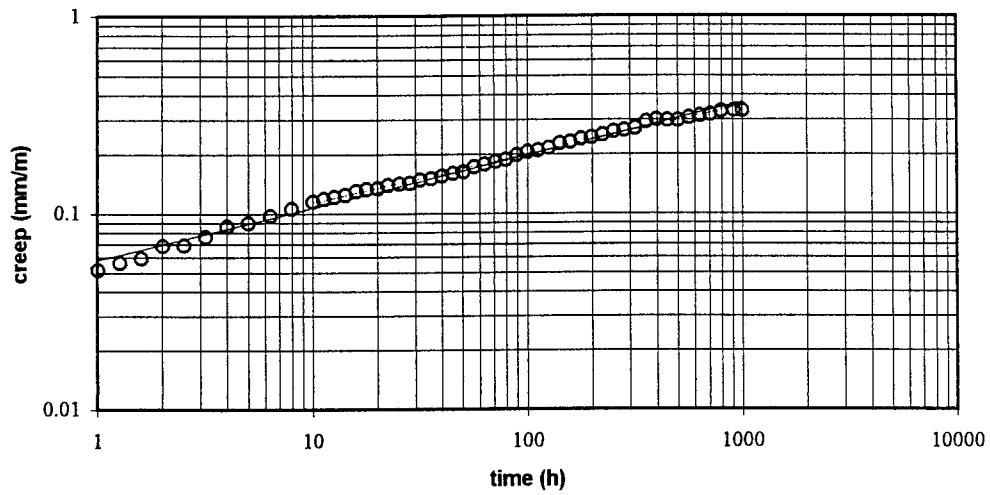
OPGW 87T87 - 20% UTS



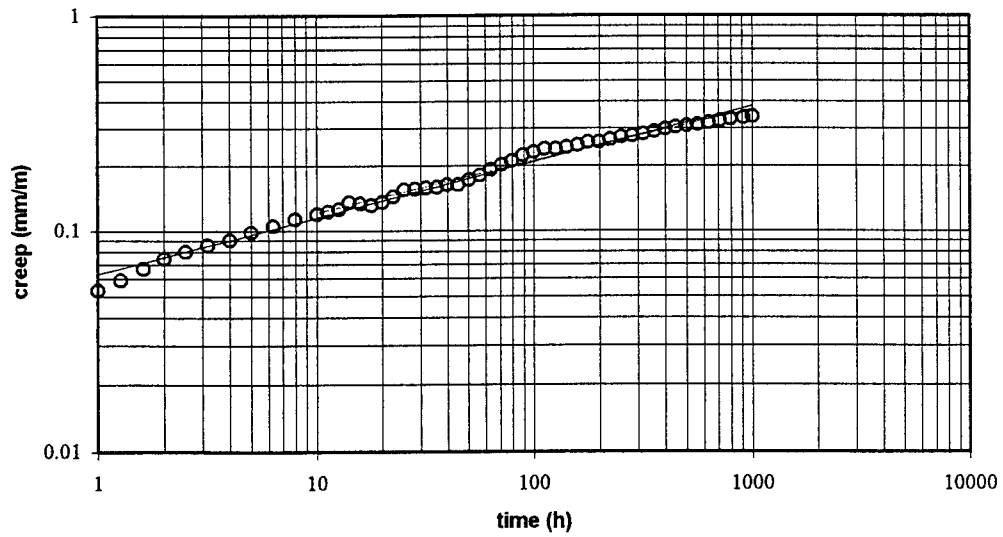
OPGW 107/44 - 25 %UTS



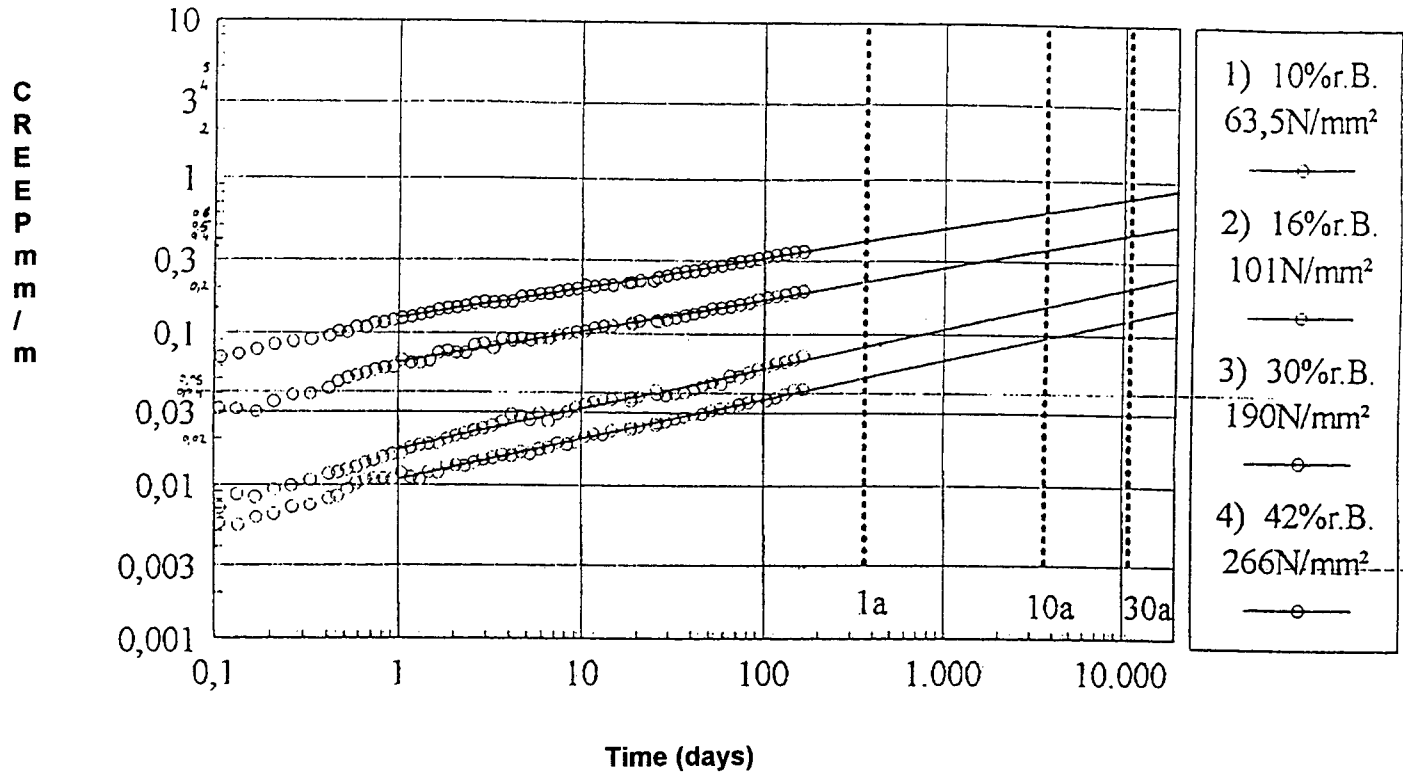
OPGW 107/44 - Creep at 40 %UTS



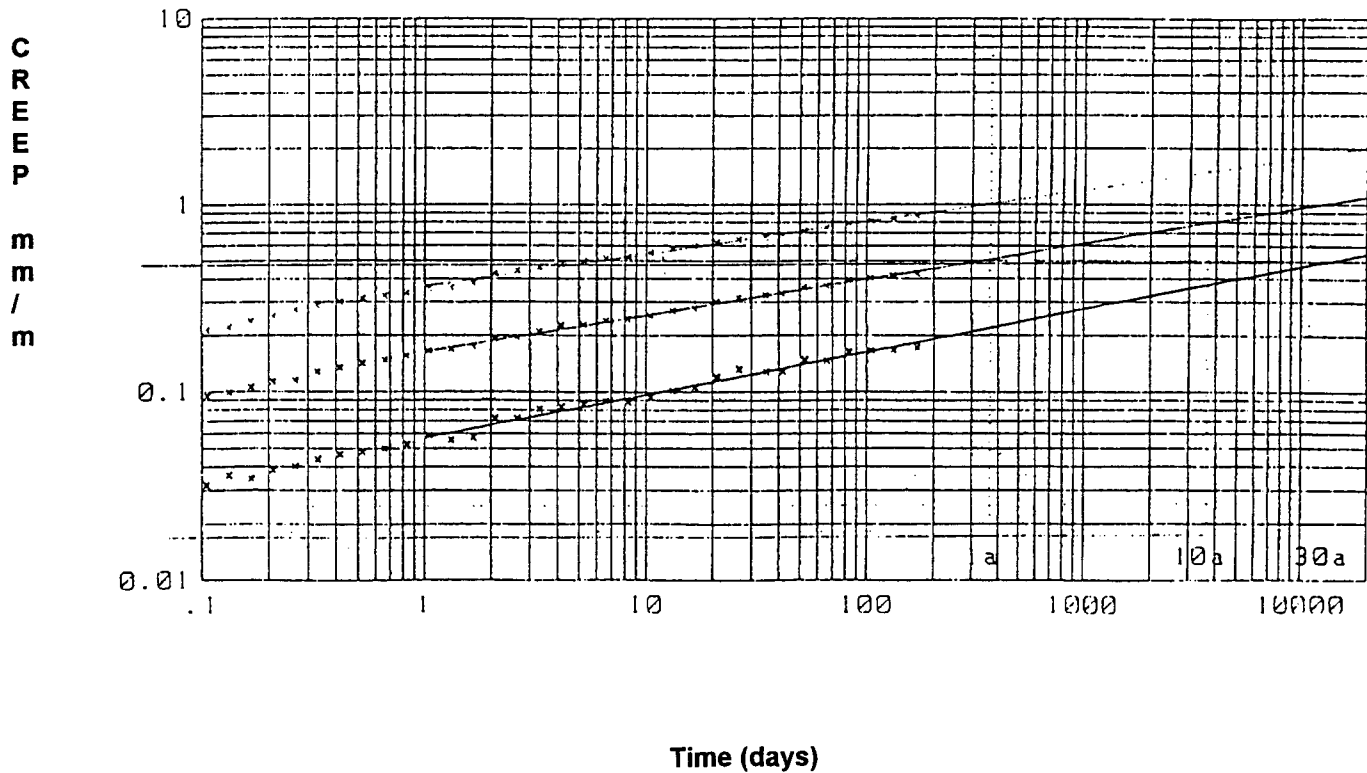
OPGW 87T87 - 40%UTS



OPGW ASLH_D (S) 1 x 6 EG / 125 (52 / 29-5.5)



OPGW ASLH_D (S) bb 3x2 EGU25 (44/26-4.7)





AUTHORS

Jean Pierre Bonicel
Alcatel Telecommunication
Cable
2512, Penny Road Claremont
NC, 28610, USA

Jean Pierre BONICEL was born in 1942. He received his engineering degree from the Institut des Sciences de l'Ingenieur de Montpellier (ISIM) in 1976. He joined Les Cables de Lyon, now Alcatel Cable in 1977 where he was in charge of material and mechanical problems for telecommunication cables. Now he is the Alcatel Optical Fiber Cable Competence Center manager.



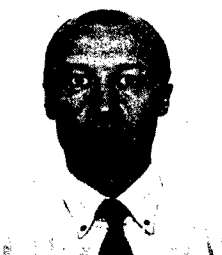
Reinhard Girbig
Alcatel Kabel Bonnenbroicher
Str. 2-14 41238
Monchengladbach,
GERMANY

Reinhard GIRBIG (43) received his Dipl.-Ing. Degree from the Rhur University Bochum in 1982 and joined AEG Kabel in 1987 as a development engineer in the fiber optics area, responsible for the technical aspects of OTDR measurement. In 1991 he became head of the Optical Fibre Cable Installation Technique Group. Between May 93 and April 1996 he was working as a project engineer and responsible for the Transmission and Characterization Group in the Alcatel Optical Fiber Cable Competence Center in Bezons, France. He is now responsible for the engineering department in the Product Group Optical aerial Cables within Alcatel Cable.



Georg Hog
Alcatel Kabel
Bonnenbroicher Str. 2-14
41238 Monchengladbach,
GERMANY

Georg HOG (46) obtained his Dipl.-Ing. Degree from the University of Aachen and joined AEG Kabel in 1977. After being engaged in the development of symmetrical telecommunications cables he became responsible for this group in 1980. In 1985 he became head of the Development Group for Optical Fiber Cables. He is now responsible for the Product Group Optical aerial Cables within Alcatel Cable.



Olivier Tatat
Alcatel Telecommunication
Cable
2512, Penny Road Claremont
NC, 28610, USA

Olivier TATAT, born in 1959, received his engineering degree from the Institut des Sciences de l'Ingenieur de Montpellier (ISIM) in 1982 and joined Les Cables de Lyon, now Alcatel Cable in 1985. He has been working in the Alcatel Optical Fiber Cable Competence Center in Bezons, France for 5 years as a project engineer involved in the development of aerial cables. He is now the Material Technology Group leader of the OFCCC relocated in Claremont, USA.

MATERIALS, DESIGN, AND PERFORMANCE OF THE NEXT GENERATION OF ALL DIELECTRIC SELF-SUPPORTING AERIAL LOOSE TUBE FIBER OPTIC CABLE

Richard G. Gravely, III
James W. Thornton

Fitel Lucent Technologies, Carrollton Georgia

ABSTRACT

Deployment of self supporting aerial cables is expected to show continued growth, especially in light of the deregulation laws opening up a wealth of new opportunities in the communications field. All-Dielectric Self-Supporting (ADSS) cable designs are popular. These cables can be placed in various locations to accommodate space considerations without the need for power interruption. Although ADSS designs in loose tube construction have been in existence for many years, there have been recent developments in design, increased fiber counts, and improvements in raw materials. In this paper we discuss new raw materials for improved handling, the application of dry water blocking materials and a 288 fiber count design.

INTRODUCTION

ADSS optical cables are deployed when aerial cables provide the most cost effective solution to fiber deployment. There are also situations where aerial cables are virtually the only solution; as over river crossings, mountain slopes, or across a highway. Existing rights of ways (ROW) make aerial cable deployment attractive and cost effective. There is no need for costly expenses incurred during underground cable deployment which can account for up to 30% of total project costs. Therefore, ADSS cable is an excellent choice for a variety of applications.

Since ADSS cables are expected to address many applications, the cable manufacturer must develop different designs. High fiber count cables which allow tremendous amounts of information to be transmitted or dropped where dedicated fibers are required must be available to the consumer. To meet these applications in a loose tube construction, buffer tubes have to be stranded in the cable's core. One approach to this design is a single layer of many buffer tubes stranded about a very large central member. Although this design meets the high fiber count objective, it is impractical in real world applications where cable diameters and span length capabilities are of primary interest.

A dual layer construction has been developed to significantly reduce cable outer diameters and drastically improve span length capabilities. On the other end of the spectrum is the need for lower fiber count cable designs with an outer diameter that can meet the requirements of a customer's existing attachment hardware.

For those applications where the ADSS cable might be directly entering the indoor facility, an outdoor/indoor ADSS riser rated product has been developed. This product employs Low Smoke and Zero Halogen (LSZH) flame retardant jacketing materials that ensure that the cable will meet the riser rating requirements of the NEC via the UL1666 burn testing guidelines.

And finally, consistent with the market place, DryBlock™ water blocking capabilities have been incorporated into the ADSS cable design as an option. This product uses "dry" water blocking materials to improve cable handling and reduce core access time.

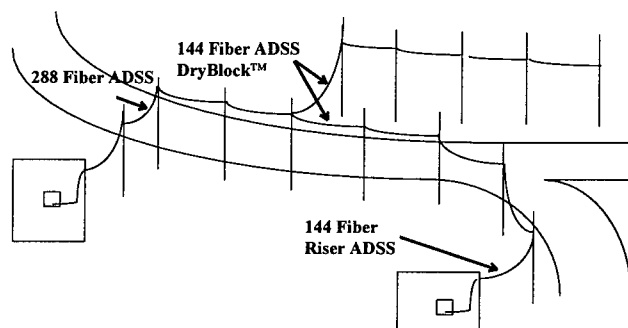


Figure 1:
Hypothetical Application of Different ADSS Designs

DESIGN

There are several design aspects inherent to loose tube cable that make them a popular choice. Optical fibers are loosely placed within buffer tubes that are stranded about a central strength element via the Reverse Oscillating Lay (ROL) technique.

This construction provides excellent mid-span accessibility and zero fiber strain even at operational or installation loads, two sought after attributes by end users. Inner and outer jackets separate the cable's yarn strength elements. Aramid yarns are counter-helically applied about the inner jacket. The number and denier (kg/9000m) is carefully chosen per application to ensure that the cable can support expected loading conditions. The ADSS design is capable of supporting up to 288 fibers in a dual buffer tube layer construction, with either standard MDPE jacket or special anti-tracking jacket, to optimize span and performance criteria. Additionally, the application of newest technology in advanced buffer tube materials and DryBlock™ water-blocking materials can be applied to afford a high performance craft friendly design.

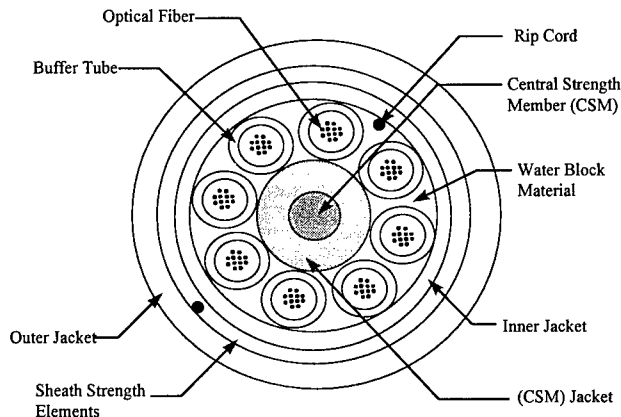


Figure 2: Single Layer ADSS

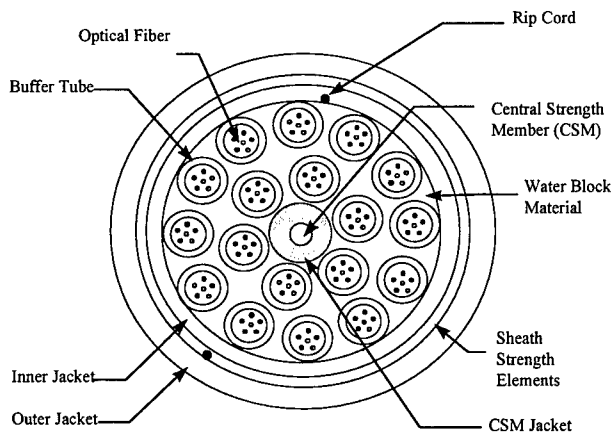


Figure 3: Dual Layer ADSS

High Fiber Count ADSS Design

Traditionally, ADSS designs have consisted of a single layer of buffer tubes. This design has inherent restrictions on cable performance when fiber counts exceed 144. A dual layer buffer tube ADSS cable design has been developed to address the short comings of a single layer buffer tube construction.

The dual layer construction, available in fiber counts up to 288, significantly improves important cable parameters including cable outer diameter (20% reduction), cable weight (35% reduction), and cable span lengths (70% increase) per figure 4.

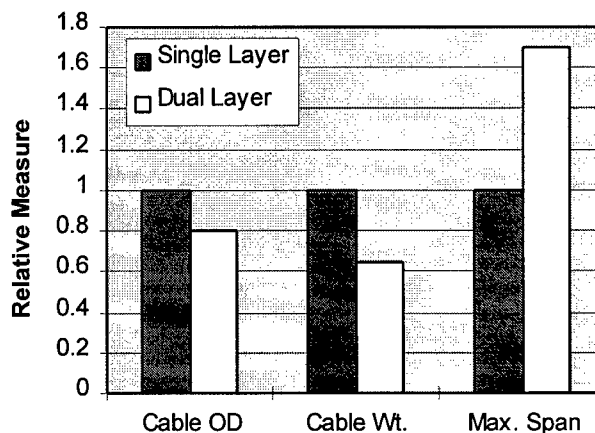


Figure 4: Dual vs. Single Layer ADSS

These enhancements to existing designs offers product that is easier to handle in the field (smaller & lighter) as well as a product that supports long span capabilities in a high fiber count construction.

CABLE PERFORMANCE

Since ADSS cable is required to have a high tensile strength, the cable components need to operate as a single unit. Coupling between the sheaths, aramid, and core is necessary to carry the load properly. All three new ADSS cable designs, low count (≤ 36 fibers) ADSS, high count (> 144 fibers) ADSS, and DryBlock™ ADSS, were tested to verify good cable performance. The following tests were performed:

- Ultimate Tensile Test
- Elevated Temperature Test
- Galloping Test
- Mechanical Testing
- Riser (UL1666) Testing

Ultimate Tensile Test

A representative sample of cable from each design was tested per FOTP-33. During the first tensile test, attenuation and fiber strain measurements were taken at 50 lbs increments up to the maximum rated tension. None of the cables exhibited any fiber strain or change in attenuation up to the maximum rated tension.

Then the cables were tested with attached dead-ends to evaluate slippage and cable structure integrity at the maximum rated tension. None of the cables exhibited any fiber strain, increase attenuation change, cable slippage, and/or cable damage after 15 minutes at the maximum rated tension.

Finally, the cables were tensile tested with attached dead-ends until failure was observed. All of the cables broke at nearly twice their maximum rated tension and outside of the attached dead-ends.

Elevated Temperature Test

All three cable designs were tested for elevated temperature tensile performance. Each cable was terminated at each end with dead-ends. One cable end was placed in a solar heat box, while the other end was kept at ambient temperature. Tension was increased to the maximum installed load while simultaneously raising the temperature in the box to 50°C. After one hour, no slippage occurred on any of the cables. The dead-ends were removed after the test to verify mechanical integrity of the jacket. No jacket damage was present on any of the cables after the dead-ends were removed.

Galloping Testing

The galloping test was conducted in accordance with Institute of Electrical and Electronics Engineers (IEEE) P1222 (draft) to assess the performance of cable and hardware under typical galloping motions. These large amplitude vibrations can cause severe wear on the cable jacket and hardware. The galloping condition occurs when the single loop frequency (fundamental frequency) of the span is reached during cable vibration.

Because a vibrating cable normally contains a large number of standing wave loops, the product of frequency (f) and wavelength (λ) or loop length (l) is the traveling wave velocity (V)⁴.

$$V_t = \lambda f = 2fl \quad (1.1)$$

This is the velocity with which an impulse moves from one end of the span to the other. It is a function of cable tension and weight per unit length.

$$V_t = \sqrt{\frac{H}{m}} \quad (1.2)$$

H = tension in newtons ($\text{kg}\cdot\text{m}/\text{s}^2$)

m = mass per unit length (kg/m)

The number of standing wave loops on a span is the span length (S) divided by loop length (l).

$$n = S / l \quad (1.3)$$

Combining equations (1.1) and (1.3), we can express the equation in terms of frequency f and arrive at the following equation:

$$f = \frac{nV_t}{2S} \quad (1.4)$$

If we set $n=1$, then the equation is solved for the fundamental frequency of the span. This frequency is typically reached under galloping conditions, but not aeolian.

If a cable is installed at a set sag (γ), then the cable tension H can be expressed as follows:

$$H = \frac{mS^2}{8\gamma} \quad (1.5)$$

Combining equations (1.2), (1.4), and (1.5), we can express the fundamental frequency of the span f as the following:

$$f = \sqrt{\frac{1}{8\gamma}} \quad (1.6)$$

The solution expresses the fundamental frequency as a function of only the set cable sag γ . Therefore, the fundamental frequency for a light or heavy cable is the same if both cables are installed with the same initial sag.

The galloping testing was performed on all three cable designs tensioned to a minimum of 50% of the maximum installation tension or a maximum of 500

kg (1100 lbs). A shaker is placed on the active span of cable to induce the galloping conditions. The observed conditions for all three cable designs is displayed in the following table.

Cable Design	Amplitude (in)	Frequency (Hz)
Low Count ADSS (≤ 36 fibers)	20	3.5
High Count ADSS (> 144 fibers)	20	3.2
DryBlock™ ADSS	20	3.5

Table 1: Galloping Comparisons

The galloping and tension were maintained for 100,000 cycles. No increase attenuation change was observed during the tests. At the end of testing, the cables and hardware exhibited no wear. The test setup is shown in figure 5.

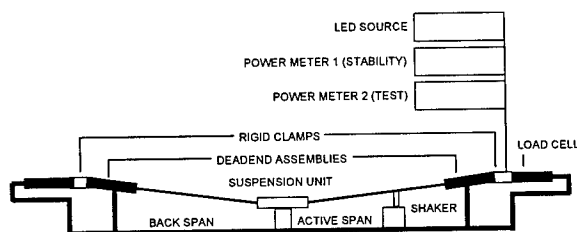


Figure 5: Galloping Test Setup

Mechanical Testing

The cables were tested for mechanical performance per EIA/TIA test standards. The following table shows the performance of the test cables.

Test Performed	Results	Test Procedure
Impact	max. $\Delta = -0.03$ dB	FOTP-25
Crush	max. $\Delta = -0.03$ dB	FOTP-41
Twist	max. $\Delta = -0.01$ dB	FOTP-85
Flex	max. $\Delta = -0.02$ dB	FOTP-104
Tensile	no attenuation Δ	FOTP-33

Table 2: High Fiber Count ADSS

Test Performed	Results	Test Procedure
Impact	no attenuation Δ	FOTP-25
Crush	max. $\Delta = -0.02$ dB	FOTP-41
Twist	max. $\Delta = -0.01$ dB	FOTP-85
Flex	max. $\Delta = -0.02$ dB	FOTP-104
Tensile	max. $\Delta = -0.04$ dB	FOTP-33

Table 3: Low Fiber Count ADSS

Riser (UL1666) Testing

A flame resistant polyolefin jacket material is applied for both the inner and outer jackets. This material also provides cable with a Low Smoke and Zero Halogen rating (LSZH). The testing is conducted by Underwriters Laboratories per UL1666 to verify riser compliance with NEC fire codes. The cable testing has resulted in a full UL listing of this product up to 144 fibers. For the outside plant environment, the product meets all mechanical and environmental requirements per Bellcore GR-20, Issue 1.

MATERIALS

Material advancements allow the ADSS cable to meet increasing needs of the fiber optic industry. These include more flexible buffer tube material for better handling and a fire resistant jacket material for riser rated outdoor/indoor ADSS. Also, dry water-blocking materials will enhance cost savings during cable installation.

Flexible Buffer Tubes

Recently, customers have voiced the need for more flexibility in the buffer tubes for better handling. Many design and performance questions arise when the decision is made to completely change a material that is a significant makeup of the cable design. The primary considerations for the buffer tube material are:

- Tube compression resistance
- Flexibility & kink resistance, Score & Snap
- Material compatibility

Tube Compression Resistance. The primary function of a buffer tube is to provide protection to the fiber. The buffer tube cannot collapse under mechanical and environmental stresses in the field.

The following table summarizes mechanical performance, per Bellcore GR-20, for cable containing new buffer tube material.

Test	Parameters	Results
Tensile & Bend	600 lb load	Avg. Change: 0.01 dB Max. Change: 0.02 dB
Water Pen.	1 meter, 24 hr.	Pass
Cyclic Flex	100 cycles, 6.5kg wt.	Avg. Change: 0.00 dB Max. Change: 0.02 dB No Damage
Test	Parameters	Results
Twist	10 cycles, +/- 360°	Avg. Change: 0.01 dB Max. Change: 0.02 dB No Damage
Impact	25 cycles, 2kg wt. 150mm drop Ht.	Avg. Change: 0.01 dB Max. Change: 0.01 dB No Damage
Compression	220 N/cm 10 minutes	Avg. Change: 0.01 dB Max. Change: 0.08 dB No Damage

Table 4: Mechanical Results

Flexibility, Kink Resistance, Score & Snap.

Perhaps the most important aspect of the buffer tubes for the end user is its flexibility. The new buffer tube material was compared to PBT which is commonly used in the industry. The kink resistance of each tube material was determined using a modified Tube Kinking test from draft IEC 794-1-2, method G7. A 750 mm tube sample was taken from each material and was marked 125 mm from each end. The tube sample was mounted in the test device, shown in figure 6, with the movable and fixed clamps separated by a distance h . This was adjusted until the two tube marks coincided and a loop of 500 mm circumference was formed. The movable clamp was moved between positions 1 and 2 over a distance L at a speed approximately 10 mm/s.

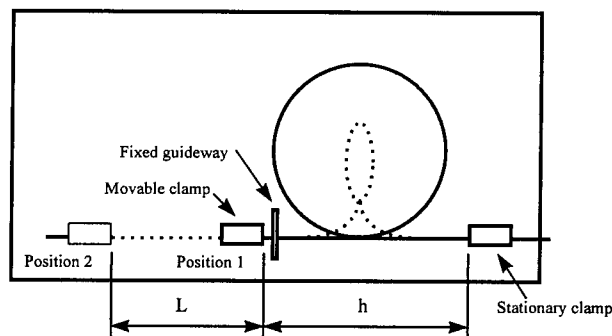


Figure 6: Tube Kinking Setup

Position 2 and length L was recorded when a kink was visible on the buffer tube samples. The bending circumference of the buffer tube was then determined by the following equation:

$$\text{Bending Cir. (mm)} = 500 \text{ mm} - L \text{ (mm)}$$

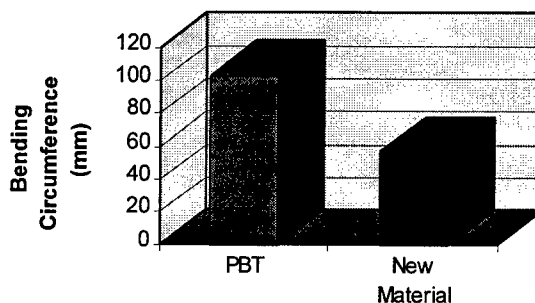


Figure 7: Tube Kinking Results

The new buffer tube material showed better flexibility while maintaining good kink resistance. The following table demonstrates the higher tube resistance to kinking for the new buffer tube material as compared to PBT.

Additionally, the buffer tube should be easily entered providing quick access to fibers. Tubes can be accessed in different ways such as a tube slitting or scoring and snapping. The latter method is usual accomplished when terminating a cable. To score and snap, the technician should nicking the tube and then press firmly on the opposite side of the mark to snap the tube. The new material exhibited easy tube entry when employing both methods.

Material Compatibility. The new tube material was tested in both the filling and flooding compounds for 45 days at 85°C per Bellcore GR-20, Issue 1, section 6.3.4. The new buffer tube material

did not exhibit any splitting, cracking, or delamination when inspected under 5x magnification. The samples were tensile tested and demonstrated a greater than 10% elongation-at-break.

Riser Rated Outdoor/Indoor ADSS

Although limited in application, the offering of an Outdoor/Indoor Riser Rated ADSS cable design is significant. For an application where fiber is being routed from an indoor environment to different location(s), a cost analysis can be made to determine which design option is best. The cost considerations are as follows:

1. Added cost of Outdoor/Indoor Riser Rated ADSS (vs. conventional ADSS)
2. Cost savings based on splicing (\$/splice x # of splices)
3. Cost savings based on elimination of splice housing or transition area
4. Cost impact on link loss budget (splice elimination reduces link loss)

A specially engineered polyolefin material is used as the inner and outer jacket of this cable to ensure flame resistance. The material is also a Low Smoke and Zero Halogen product which minimizes safety concerns to personnel and equipment in the event of a fire. Not only is this material resistant to flame, the material is completely stable in UV light; a must for outside aerial cable. The result is an ADSS cable designed for the outdoor environment per Bellcore and the indoor environment per UL1666.

DryBlock™ ADSS Design

Much has been documented about the attributes and performance of dry water blocking materials^{1,2,3}. Their obvious succession into aerial cable designs is not a novel one with regards to water blocking performance. However, the greatly improved coupling coefficients seen between cable components is advantageous in an ADSS cable. This allows all of the cable components to contribute to the overall modulus of the cable instead of being limiting to the strength elements alone. Also, improved coupling of cable components to the central strength member is advantageous in low temperature conditions where the plastics exhibit the propensity to shrink. The shrink-back characteristic of the plastics (buffer tubes and

jacket) is inhibited when highly coupled to the central strength element.

Additionally, a reduction in cable weight is realized when removing conventional flooding compounds in favor of "dry" water blocking materials. An increase in span length on the order of 5% and a weight reduction of up to 10% has been calculated for a dual layer 288 fiber count ADSS cable in NESC Light Loading conditions. The significance of the DryBlock™ construction is a cable design that can address some applications where a flooded design counterpart can not.

	DryBlock™ % Change (Depends upon cable design)
Weight	10% Decrease
Span	5% Increase

Table 5: DryBlock™ Attributes

CONCLUSIONS

Worldwide usage and applications of ADSS cables continues to increase. Improvements to cable design and response to customer requirements is essential to compete in the fiber optic cable market. Improved buffer tube material is available to address issues regarding flexibility and handling for the user. DryBlock™ constructions are available to reduce installation time/costs and improve handling. Dual layer, high fiber count capable designs are available for high density needs while maximizing span length capabilities. Design and material improvements have been developed and applied to produce the next generation of All Dielectric Self-Supporting (ADSS) aerial loose tube cables.

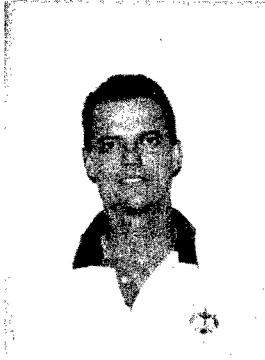
REFERENCES

- ¹ Clyburn III, C. and Bringuier, A., "A Dry Core Loose Tube Cable for Outside Environments", *Proceedings of the International Wire and Cable Symposium*, 1995.
- ² Gravely, R.G., and Stokes, S.R., "An Improved Loose Tube Cable with Dry Water Blocking Components", *Proceeding of the National Fiber Optics Engineering Conference*, 1995.

³ Thornton, J.W., Chastain, S.M., and Motz, S.D., "Materials, Development, and Field Trials of a Dry Core Cable", *Proceeding of the National Fiber Optics Engineering Conference*, 1996.

⁴ Gilbert/Commonwealth, "Transmission Line Reference Book - Wind-Induced Conductor Motion", Electric Power Research Institute, 1979.

BIOGRAPHIES



Richard G. Gravely, III

Richard Gravely is Senior Product Engineer for Fiber Optic Cable & Apparatus at Fitel Lucent Technologies. Mr. Gravely's primary responsibility is new product developments. Prior to joining Fitel Lucent Technologies, he held the position of Cable Design Engineer with Sumitomo Electric from 1992 to 1996. Richard received his BSEE degree in 1991 from North Carolina State University.



James W. Thornton

James Thornton holds the position of Design Engineer in the R&D Department at Fitel Lucent Technologies. He received his BSME degree from the Georgia Institute of Technology. Since joining the company, he has been responsible for the development of Fiber Optic Cable. Mr. Thornton is a member of the American Society of Mechanical Engineers (ASME).

NEW EFFECTIVE METHOD TO CALCULATE TEMPERATURE INCREASE DURING SHORT-CURRENT TEST ON OPGW CABLES

Christian Bastide, Olivier Tatat, Thierry Verhaege *

Alcatel Telecommunications, Claremont, North Carolina

* Alcatel Alsthom Recherche, Marcoussis, France

ABSTRACT

OPGW (Optical Ground Wires) are increasingly being used to provide an optical fiber communication link on high voltage overhead transmission lines. Present trend is to produce smaller and smaller OPGW, with a high fiber count and at a low manufacturing cost. Consequently, their reliability is another very important consideration ; the optical transmission link has to operate successfully during the planned life of the power transmission line.

One of the most severe tests of OPGW is their ability to withstand an electrical fault (short circuit current) and to protect optical fiber inside. Such faults can result in very large temperature rises almost instantaneously.

This paper presents a simple theoretical model to calculate temperature in the different layers of 2 OPGW designs, aluminium slotted core OPGW and steel tube OPGW and shows a good agreement between temperature measurements and calculations.

INTRODUCTION

High voltage power lines are designed to operate successfully for a long service life, usually more than 30 years. Consequently, long term reliability of these cables is of paramount importance. OPGW cables have to provide a ground wire function as well as a reliable transmission line over the service life. Severe and rigorous tests must be carried out to determine this level of confidence.

In service, OPGW are strung on HV pylons and could be subjected to fault currents providing rapid temperature rises up to 160°C or more, depending upon a number of factors such as :

- magnitude of I^2dt (I : current, dt : duration of the electrical pulse)
- construction of the core
- material type (Aluminum, Almelec or Aldrey, steel, polymeric materials, ...)
- number of layers
- ambient temperature

The exposure of optical fiber to high temperature variations can affect the mechanical (decreasing of the RTS), and optical properties (increasing of optical attenuation) and also their aging behavior in the long term. Therefore, information about temperature of optical fibers inside the OPGW core is very important.

To evaluate cable resistance to electrical conditions, some tests are performed in laboratory, in particular, the short-circuit current test : OPGW is subjected to an electrical pulse during a short time (i.e. I=15kA during less than 1second). This test requires specific and costly electrical equipment.

Analysis

OPGW cables are generally composed of several assembled elements, devoted to different functions :

- mechanical reinforcing
- current carrying
- information carrying

Two OPGW designs have been developed : the slotted core design and the steel tube design ; figures 1 and 2 illustrate the 2 structures.

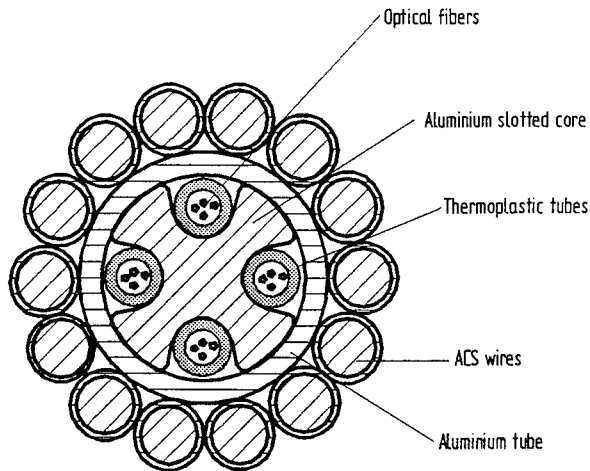


Figure 1 : slotted core design

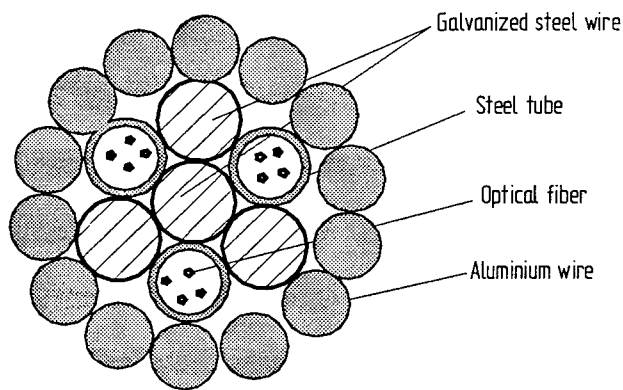


Figure 2 : steel tube design

Cable 1 includes a slotted core of aluminum alloy, which carries a part of the total current ; its 4 helicoidal slots guide 4 optical buffer tubes ; these elements are the most sensitive to hot spots : heated plastic tubes and grease can melt at high temperature. The core is surrounded by a tube of pure aluminum, which is the most conductive element, and therefore the most rapidly heated by Joule effect. Mechanical reinforcing is obtained with an armor of 14 ACS (Aluminum Clad Steel) wires ; these wires also participate to current carrying, due to their aluminum coverage, and to the use of low carbon steel ; their temperature remains moderate, so that they can extract heat from the aluminum tube. Therefore, the thermal excursion

of plastic tubes and optical fibers results of a competition between the heat transfer velocities from the core, the tube, the armor and the external environment.

Cable 2 design is very different, because there is no slotted core, and the hottest part of the cable is its external armor of aluminum alloy, inner galvanized steel wires moderately participate to the current carrying, and present intermediate temperatures ; they are alternated with stainless steel tubes, filled with grease and optical fibers ; the question here is to know how rapidly the heat flows from the armor to the inner wires, and from the armor to the external environment. Because the mechanical properties of aluminum alloy wires are affected above 200°C, it is necessary to keep this temperature as a maximum value.

Theoretical background

The general heat equation to be solved is :

$$\gamma c \frac{\partial \theta}{\partial t} = k \Delta \theta + \frac{E^2}{\rho}$$

$\theta(^{\circ}C)$: local temperature

$\Delta \theta(^{\circ}C / m^2)$: temperature

$$\text{Laplacian } (= \frac{\partial^2 \theta}{\partial x^2} + \frac{\partial^2 \theta}{\partial y^2} + \frac{\partial^2 \theta}{\partial z^2})$$

$\gamma c (J / m^3 .^{\circ}C)$: volume heat capacity

$E(V / m)$: electrical field

$\rho(\Omega . m)$: electrical resistivity

The 50 Hz skin effect is negligible.

Boundary conditions are encountered on the interfaces between two elements :

$$-k \frac{\partial \theta}{\partial n} = h(\theta - \theta_e)$$

$\frac{\partial \theta}{\partial n} (^{\circ}C / m)$: temperature

derivative perpendicularly to the interface

$k(W / m .^{\circ}C)$: thermal conductivity

$\theta_e(^{\circ}C)$: external reference temperature

$h(W / m^2 .^{\circ}C)$: heat exchange coefficient

The h value is relatively low in the case of exchanges with the external ambience, or with another cable element via an air or grease thin strip ; it can be considered infinite in the case of non-separable elements, as the aluminum and steel part of an ACS wire ; the boundary condition becomes then : $\theta = \theta_e$.

Due to the complex cable geometry, the general solution requires a finite element model and a complex set of input data, which makes it less easy to use, to control and to interpret. The comparison of the data orders of magnitude, and preliminary simulations, allow a set of approximations which can lead to a user-friendly model, as developed below.

Temperature evolution inside a cable element

In order to rough out the problem, the temperature evolution inside a cable element has been simulated in a first time, considering simplified boundary conditions.

Figure 3 indicates the results obtained for a very large aluminum coated steel (ACS) wire ; it is composed of a low carbon, ($\Phi = 4.76 \text{ mm}$), steel core, surrounded by an aluminum coating, up to $\Phi = 5.5 \text{ mm}$; the assigned power input is equal to $3 \text{ kA}^2 \cdot \text{s}$, deposited in 1 second.

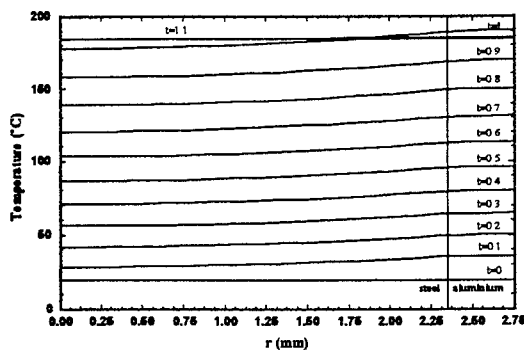


Figure 3 : Thermal evolution of a $\Phi 5.5 \text{ mm}$ ACS 20SA wire ($3 \text{ kA}^2 \cdot \text{s} - 1 \text{ s}$)

Temperature differences inside this wire do not exceed 12°C during the pulse, and vanish less than 0.1 second after this one ; they would be still lower for lower diameter ACS wires, and for homogenous metallic wires, tubes or slotted cores.

Considering each metallic element as isothermal is therefore a valuable approximation, which can greatly simplify the models without any severe incidence on the global results.

There could be a great advantage to accept a similar approximation for non-metallic elements, like a thermoplastic tube, filled with grease and optical fibers ; but thermal diffusivity is here much lower, and significant temperature difference appear, as illustrated by figure 4.

The thermoplastic tube and its grease and fibers content are considered homogenous ; the tube is embedded in an aluminum core, supposed to ramp from 20°C to 220°C in 1 second, after which it remains at this temperature level ; imperfect contacts reduce to 5000 W/m^2 (which is a realistic value) the thermal exchange coefficient between the thermoplastic tube and the core.

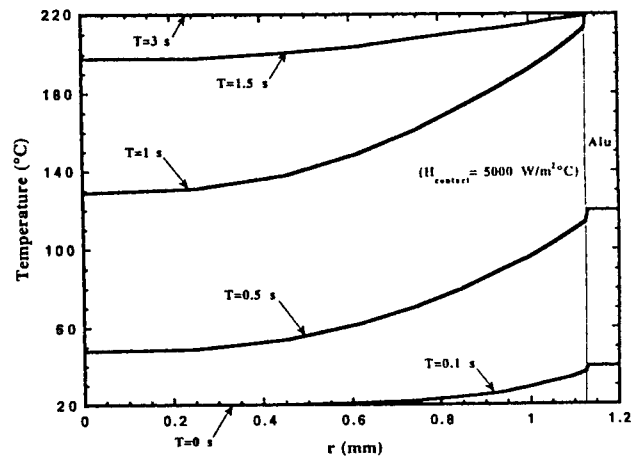


Figure 4 : Thermal evolution of a thermoplastic tube filled with grease and optical fibers

Important temperature differences appear during the current pulse, but they vanish after 1 second. The element mean temperature can be approached in a simple model, where the core/element exchanges are not limited by the contact resistance, but also by the thermal resistance of the element itself ; in practice, it leads to heat exchange coefficients in the range of 500 to $1000 \text{ W/m}^2 \cdot ^\circ\text{C}$.

Based on the previous approximations, the model is now constituted of elements, each of them being characterized by homogenous physical properties, temperature and current density.

Thermal resistance, contact surface

Adjacent elements of different temperatures exchange heat, via contact thermal resistance which are generally difficult to establish, because they largely depend on hidden parameters, as contact geometry and pressure, plastic and elastic deformation, surface roughness and oxidation, possible presence and nature of filling compound.

Typical values, related to a flat contact surface, are $2500 \text{ W/m}^2\cdot^\circ\text{C}$ with air in the gap and $1000 \text{ W/m}^2\cdot^\circ\text{C}$ with filling compound ; they correspond to a mean gap of only $\approx 10 \mu\text{m}$ of air or filling compound to be crossed by the flowing heat ; consequently, only the zones of apparent contact efficiently participate to the thermal exchange ; radiation and convection coefficients in large gaps are only in order of $10 \text{ W/m}^2\cdot^\circ\text{C}$.

The full cylindrical surface can be considered for example in the case of a tube/core contact ; effective contact surfaces are an order of magnitude smaller in the case of an armor/core contact, two orders in the case of an armor/armor contact ; the contact pressures vary conversely, with a positive effect on the heat exchange coefficient.

The heat exchange coefficients compared with heat capacities result in an approximation of a response time, for the thermalization of elements in contact. The orders of magnitude are very different, as illustrated by table 1. In particular, internal exchanges are generally faster than the external ones which means that all the cable elements will be exposed at least to the mean cable temperature.

Table 1 : Typical response times for thermalization of different cable elements

Type of exchange	Core/ fibers	tube/ core	armor/ core	armor/ armor	cable/ exterior
air gaps	1 s	2 s	20 s	1 min	10 min
grease gaps	1 s	0.5 s	4 s	10 s	10 min

Validation of the model

According to the previous analysis, the cable is dissociated in elements, characterized each one by a geometry, a temperature dependent resistivity and a temperature dependent volumic heat capacity ; a matrix defines the thermal exchange coefficients: element/element and element/exterior.

At each time step, the calculation program establishes the cable resistance, the electrical field, the total current and its distribution among the different elements, their thermal balances and resulting temperatures ; synthetic results are also produced, as the maximum reached temperatures and the power input ($\text{kA}^2\cdot\text{s}$).

The tested cable was a steel tube design (ASLH-D(S)bb3x24E9/125, previously defined). A fine temperature sensor (T thermocouple) was stuck on the armor's outer surface, and protected as well as possible against external exchanges ; a second one crossed the armor, and penetrated one of the three steel tubes containing optical fibers in grease (all the attempts failed to measure properly the galvanized steel wires temperatures, without perturbation of the cable characteristics).

Figure 5 indicates the imposed d.c. current, with a main pulse simulating the short-circuit, followed by a long-continued reduced current, allowing the cable resistance measurement, after what the current is nullified.

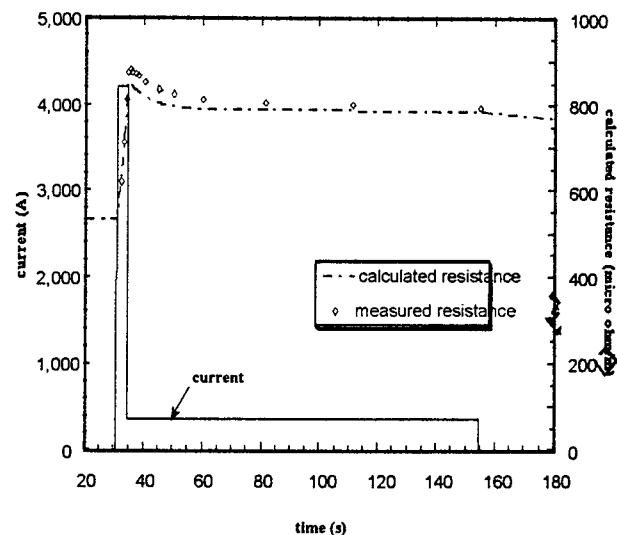


Figure 5 : Validation test : current and resistance

The main difference between experimental results and calculations is the peak armor temperature. Analysis imposes that this peak really exists :

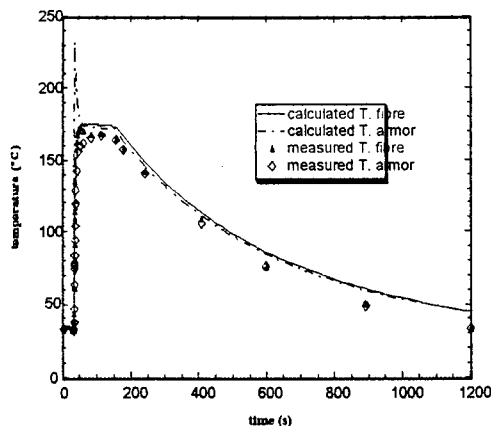


Figure 6 : Validation test : temperatures

- the heat received by the grease and fibers after the short-circuit necessarily comes from the armor, the temperature of which necessary decreases.
- the measured decreasing resistance after the short-circuit attests that the temperature of the low resistivity elements (i.e. the armor) decreases.
- measured temperatures are smoothed by the sensor thermal time response, increased by its unperfected thermal contact with the cable element.

These results suggest that direct temperature measurement is not an adequate method for establishing the peak temperatures, and that a cable resistance measurement and/or a numerical simulation can produce more reliable information.

Cable resistance

Direct temperature measurement is very problematic : sensors modify the cable structure, present problems of thermal inertia and are influenced by the environment and the other cable elements.

In comparison, recording the cable voltage and current is relatively easy, and enables to determine the cable resistance evolution, with a

time response lower (if necessary, less than 1 ms).

The mean cable temperature can be calculated

from $T_c = 20 + \frac{R - R_{20}}{\alpha R_{20}}$, where R_{20} et R are

the resistance of a given cable length at 20°C and in the considered transitory state. T_c relies more precisely to the mean temperature of the most conductive elements, ie generally those which contain pure or aluminum alloy, and reach the highest transitory temperatures ; it does not directly rely to the non metallic or steel elements. It is the reason a peak resistance, and thus a peak value T_p of T_c is generally observed,

precisely at the end of the current pulse ; T_c tends to a limit T_b after the pulse, precisely at the rate at which the temperatures of conductive and non conductive elements tend to a same value T_b , defined by the cable thermal balance.

Figure 7 resumes the synthetic information accessible by the resistance measurement, translated in the form of a cable temperature T_c .

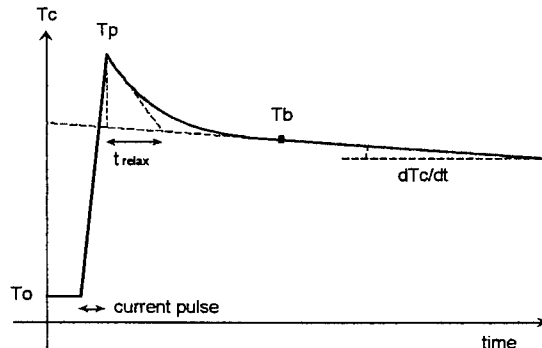


Figure 7 : information accessible by the resistance measurement, translated in the form of a mean cable temperature T_c

T_0 is the cable temperature before the pulse, which can generally be considered as uniform over the cable cross section. If T_0 is known (ambient temperature), the measured resistance is a mean to control and refine the calculated theoretical cable resistance.

T_p is the maximum temperature of the high conductivity elements ; if optical buffer tubes are in direct contact with such elements, T_p is a good approximation of the maximum superficial temperature of these buffer tubes.

T_c decreases exponentially from T_p to a new limit T_b ; the difference $(T_p - T_b)$ is an image of the internal temperature differences created by the current pulse ; it means that low conductivity elements at an initial temperature lower than T_b , receive heat from the high conductivity elements at the initial temperature T_p , until to reach the uniform cable temperature T_b .

The measured relaxation time t_{relax} relies to heat capacities and thermal contact resistance ; comparison of experimental and calculated results enables to roughly identify the contact resistance, which are generally difficult to evaluate.

Without resorting to a numerical model, a rough estimation is still possible. The cable is divided in 2 elements : high (H) and low (L) conductivity, with known heat capacities, respectively C_H and C_L (J^oC.meter of cable) ; the global heat exchange coefficient U (W^oC.meter of cable) between elements H and L can be easily be determined from :

$$U \cdot t_{relax} = \frac{C_H C_L}{C_H + C_L}$$

In the particular case of approximation of

$$C_H = C_L = \frac{C}{2} \quad (C : \text{global cable heat capacity}),$$

$$\text{this relation becomes : } U = \frac{C}{4t_{relax}}$$

A last information given by the resistance measurement is the slow $\frac{dT_c}{dt}$ shift of the cable uniform temperature, due to its thermal exchange with the environment ; it enables to evaluate the external heat exchange coefficient U_e (W^oC.meter of cable), from :

$$U_e \cdot (T_c - T_e) = C \cdot \frac{dT_c}{dt} \quad (T_e ; \text{ ambient temperature})$$

CONCLUSION

A simple theoretical model has been developed, with some assumptions (temperature is uniform in every element of the cable). A simple program (input data : geometry of the cable, nature of element materials, conditions of the short-circuit current) running on a computer, allows to calculate the temperature in the different layers of OPGW cables (slotted core and steel tube designs). It avoids carrying out costly tests that require specific measurement equipment and allows improving the OPGW design and their reliability.

Results provided by this software are more reliable than experimental results carried out directly on cable samples where the position of sensors, the quality and size of the sensor, the thermal inertia of sensors and their contacts with cable components are key parameters that it is very difficult to control.

We strongly recommend using our software to determine the real temperature of OPGW components. Short circuit current performed directly on OPGW samples must be restricted to the control of change in attenuation.

AUTHORS

Christian Bastide
Alcatel Telecommunications
Cable, PO Box 39, 2512 Penny
Road, Claremont, NC 28610

C. Bastide was born in 1957. He joined Alcatel Cable after his graduation from the Grenoble University with the DEA (physics) degree and with a thesis (microbending in optical fiber) in 1985 and he has been engaged in research and development of optical fiber cables. He is an engineer of the cable design Group of the Optical Fiber Cable Competence Center.



Thierry Verhaege
Alcatel Alsthom Recherche,
Route de Nozay, 91460
Maqroussis France

T Verhaege was born in Tourcoing, France, in 1953. He graduated as Ingénieur de l'Ecole Centrale des Arts et Manufactures in 1976, after what he taught thermal and electrical engineering in Afirca for two years. He joined the Laboratoires de Marcoussis (later renamed Alcatel Alsthom Recherche) in 1978, as a research engineer. Working on renewable energies, he developed numerical models for solar houses. He was involved from 1986 in A.C. applications of superconductivity, and developed in 1995 with GEC Alsthom the first 40 kV fault current limiter. He also works with Alcatel Cable, on the design and modeling of classical and superconducting cables.



Olivier Tatat
Alcatel Telecommunications
Cable, PO Box 39, 2512 Penny
Rd., Claremont, NC 28610

Olivier Tatat, born in 1959, received his engineering degree from the Institut des Sciences de l'Ingenieur de Montpellier (ISIM) in 1982 and joined Les Cables de Lyon, now Alcatel Cable in 1985. He has been working in the Alcatel Optical Fiber Cable Competence Center in Bezons, France for 5 years as a project engineer involved in the development of aerial cables. He is now the Material Technology Group leader of the OFCCC relocated in Claremont, NC.

FLEXIBLE CONNECTORLESS SINGLE FIBRE ORGANISATION IN EXCHANGE CROSS CONNECTS AND CUSTOMER ACCESS APPLICATIONS

by Russell Hailes* and Séan Maguire**

***Telecom New Zealand Limited, Wellington, New Zealand**

****Fibernet New Zealand, a division of New Zealand AMP Ltd, Wellington, New Zealand**

ABSTRACT

Single mode fibre optic cable was introduced to New Zealand in 1982. Since 1982 the method of managing and terminating fibres in Telecom New Zealand's exchanges has developed in various directions with differing degrees of success. In 1988 Telecom New Zealand realised that if a haphazard installation approach continued, the fibre network would quickly become inflexible and unmanageable. Fibre is now used for a multitude of different applications with connections often required to different parts of an exchange for a wide variety of services and the foresight in those early years has produced a fully flexible distribution system.

INTRODUCTION

The original use for fibre optic cable by Telecom New Zealand was to transmit long haul telecommunications, with the optical fibre superseding coaxial cable and microwave radio systems.

The coaxial lead-in cable associated with these systems was traditionally terminated directly in the transmission rooms on distribution frames, with short connectorised jumpers from the distribution frame to the transmission equipment. When optical fibre was first installed Telecom followed the same practice.

To date over 145,000 fibre kilometres have been installed by Telecom New Zealand with uses varying from trunk and junction to central business fibre, point to point applications, fibre to customer concentration points, and fibre in the local loop. In addition, the current deployment of a Hybrid Fibre-Coax broadband network brings with it the requirement to efficiently manage even larger numbers of fibres.

For Telecom New Zealand, it became clear that a simple and flexible optical cabling system was required to manage existing and future cables and fibres from the network site manhole to the Optical Fibre Distribution Frames (OFDF) through to the Fibre Optic Transmission System (FOTS) equipment.

As a result, Telecom embarked on a project to solve this fibre management problem and the subsequent research and development lead to the design, manufacture, and deployment of a suite of fibre management hardware that provides a very flexible and tidy solution.

The Ideal Solution:

The criteria for an ideal Optical Fibre Distribution System were listed and these were the terms of reference for all subsequent system developments. These criteria stated that an ideal Optical Fibre Distribution System must:

- Provide the flexibility to connect any optical fibre to any piece of optical equipment or to any other fibre.
- Provide maximum end to end optical fibre integrity.
- Provide good access for operational requirements.
- Provide good optical fibre density.
- Minimise the requirement for cord storage.
- Provide access to individual fibres with no/minimum disturbance to adjacent fibres.
- Provide a clear growth path for network expansion.
- Provide maximum future proofing.
- Minimise optical insertion and return loss.

The Existing Problems:

Some of the problems with the originally deployed systems which contributed to the formation of the ideal criteria included:

- No common fibre termination point within the exchange making it difficult to connect any fibre to any other fibre or to any FOTS terminal and therefore design flexibility was compromised.
- Patchcords of various lengths were required making it difficult to choose a stock of standard lengths to hold on site.
- The storage of excess length of patchcord had become a real issue.
- Optical connectors were expensive to buy and maintain, and to practically verify their operational performance in the field.
- Instances of connector faults were increasing.
- Instances of disturbing adjacent circuits, while technicians were working on the system, were increasingly impacting on customer service.
- The ongoing difficulty and cost of upgrading air gap connectors to PC connectors or future upgrades to the latest connector technologies.
- Haphazard approach to network growth.
- Connectivity of outside plant fibres to connectors.
- The uncertainty of connector return loss (a later driver) of connectors in service and the inability to effectively test on site. This became a factor with the advances in transmission equipment.

THE SOLUTION

As with all good solutions the answer was very simple one and mirrored what Telecom had learnt from copper over the last 100 years. The issues came with developing and implementing this solution.

The Key Element:

The heart of the solution developed is the SFO (Single Fibre Organiser) which allows single fibre management where each splice is stored separately, see Fig 1. To the uninitiated this looks like a plastic envelope, but this envelope has revolutionised the handling of fibre for Telecom New Zealand and allowed Telecom to meet all the requirements of their ideal OFDF. The SFO allows Telecom to manage fibres on an individual basis.

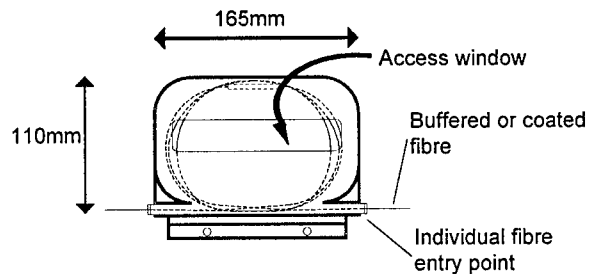


Fig 1. SFO Envelope with a pair of spliced fibres

The SFO envelope allows fibres to be stored (referred to as terminated) until they are required, see Fig 2.

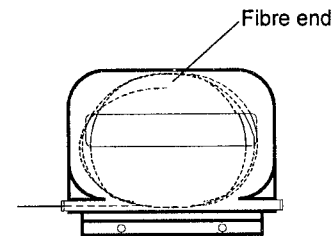


Fig 2. Fibres stored (terminated) in an SFO

While stored in the SFO, fibres can be tested if required using a pigtail and a mechanical splice. When a fibre is required for connection to equipment or to another fibre, the fibres to be spliced are introduced to the SFO envelope through the opposing entry points and fed out through the access window. The fibres are then spliced together and fitted with a splice protector.

The spliced loop can then be coiled up and inserted into the SFO through the access window. See Fig 3. The splice protector can sit at the top or bottom of the SFO giving flexibility for the jointer and for any re-splicing that may be required.

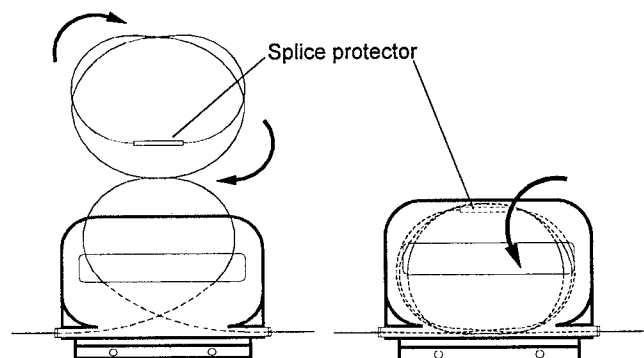


Fig 3. Fibres are spliced & coiled in an SFO

The Module:

Individual SFOs are packaged into assemblies of 24 with suitable mounting hardware, see Fig 4.

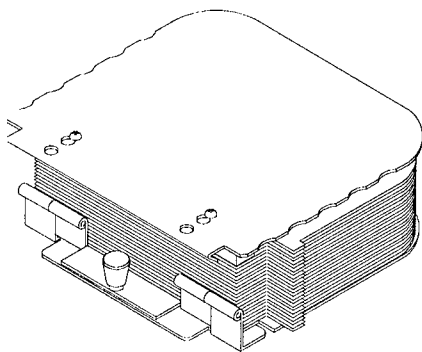


Fig 4. SFO Assembly capable of housing 24 individual splices

Each SFO assembly is mounted into an OFDF module, see Fig 5. This OFDF module is the 'building block' from which the complete Fusion Optical Fibre Distribution System is constructed.

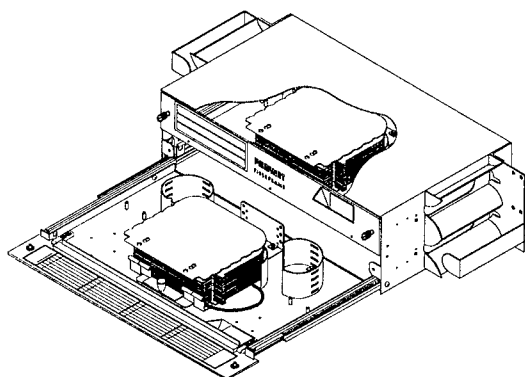


Fig 5. OFDF Module, 2 drawer, each fitted with an SFO assembly

With the building blocks in place a set of design and installation guidelines were developed to cover all possible situations whether it be a large or small site, an existing or a new site or even a customer specific site. These rules allow for consistent and tidy installations and with the building block approach, a common set of practices could be applied whether working in a customer site, remote road side cabinets, or Telecom exchange.

The System:

There are many options to choose from when configuring the OFDF system for a particular site. Fig 7 over leaf shows the complete systems used in an exchange or large customer site. There are options for smaller sites but these are not shown.

The system above can be split into 4 main areas:
The Exchange Cable Well, The Main OFDF, The Intermediate OFDF, and The Emergency Restoration OFDFs.

1) The Exchange Cable Well

The external network cable enters the Exchange Cable Well (or Exchange Manhole) and is spliced onto flame retardant tight buffered building cable in a joint closure which is fixed to the wall or layed in a cable tray. There is no need to re-access this joint and primarily it serves as a sheath change location from the Outside Plant (OSP) cable to the building cable. The flame retardant building cable is then routed to the Main OFDF.

2) The Main OFDF (MOFDF)

At the MOFDF, all the fibres from the building cables, (from the exchange cable well) are terminated (stored) in SFOs in a zone designated as 'Line Side'. The MOFDF is the first OFDF located inside a building and in most cases is a cross connect OFDF where fibres from the outside plant network are cross connected to fibres from the Intermediate OFDFs (IOFDF) in the equipment rooms. Building cables from the IOFDFs in the FOTS equipment areas are terminated on the MOFDF in a zone designated as 'Equipment Side'.

Fibre connection between the 'Line Side' and the 'Equipment Side' on the MOFDF is made by fusion spliced jumpers (single or dual fibre cords). The jumper cord is cut to length as required thus there is no storage of excess cord required.

3) The Intermediate OFDF (IOFDF)

Intermediate OFDFs are located in the transmission room racks in each row which has FOTS equipment to be connected. This allows the easy deployment of pigtails to service the FOTS equipment, see Fig 6. Building cables from the 'Equipment Side' of the MOFDF are terminated in the IOFDFs and connection to FOTS equipment is achieved by fusion spliced pigtails. Couplers, when required are fitted in separate drawers at the IOFDF but otherwise follow the same procedure.

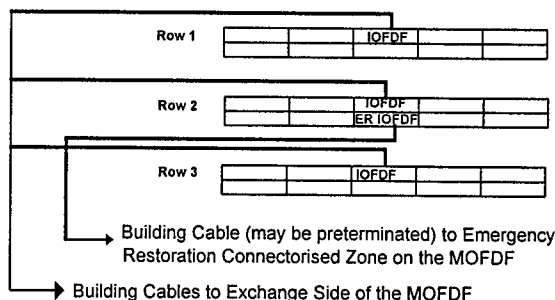


Fig 6. Typical FOTS layout of Transmission Room

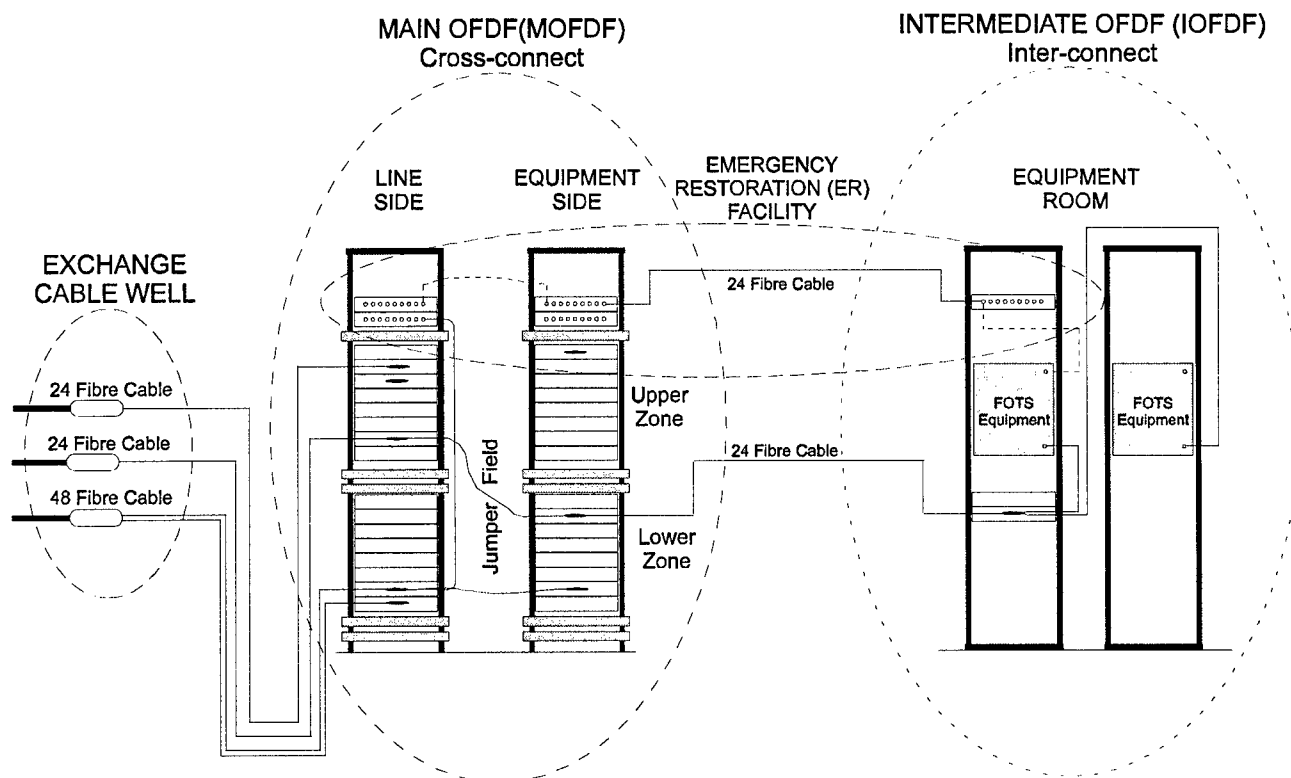


Fig 7. Typical Layout of the developed OFDF System Solution

4) The Emergency Restoration OFDFs

Transmission room operators had been used to using connectorised patchcords to quickly get FOTS onto different fibres if required in an emergency. The requirement to do this with a fusion jumper cord was not well accepted at first. The Emergency Restoration (ER) OFDF part of the system was developed at day one to satisfy the concerns from the operations people who felt they were losing the ability for fast restoration that connectorised OFDFs had traditionally given them.

Emergency restoration of important circuits is provided by jumpering spare fibres from the lower zones of the 'Line Side' to patch panels in a connectorised zone at the top of the MOFDF. One or more building cables are similarly connectorised above the 'Equipment Side' at the MOFDF and routed to centralised Emergency Restoration (ER) patchpanels in the FOTS equipment areas. Restoration of service to spare optical fibres is achieved by placing patchcords between 'Line Side' and 'Equipment Side' patchpanels at the MOFDF and between the FOTS equipment and the ER patchpanel in the equipment areas.

Experience has shown the need to connectorise all long term spares is not warranted and only a small proportion of fibres in any cable are brought to the ER patchpanel on pigtails. This trend is assisted by the increasing use of fault tolerant SDH rings and the availability of fusion splicers for emergency restoration via splicing if required.

The System and System Rules:

Along with the OFDF modules and racks are some components which assist in tying the system together. These include vertical cable guides, horizontal troughs, and the overhead trunking. These components of the OFDF System provide safe and tidy cable and cord transport between modules, racks, rows, and areas. The vertical cable guides assist with the management of cables and fibre cord into each side of the OFDF modules and provide minimum bend radius control. The horizontal troughs provide the transport of fibre cord between vertical racks in the same row and in situations where OFDFs are mounted back to back. The overhead trunking assists with the transport of fibre cord from the IOFDFs to the various FOTS in the equipment room.

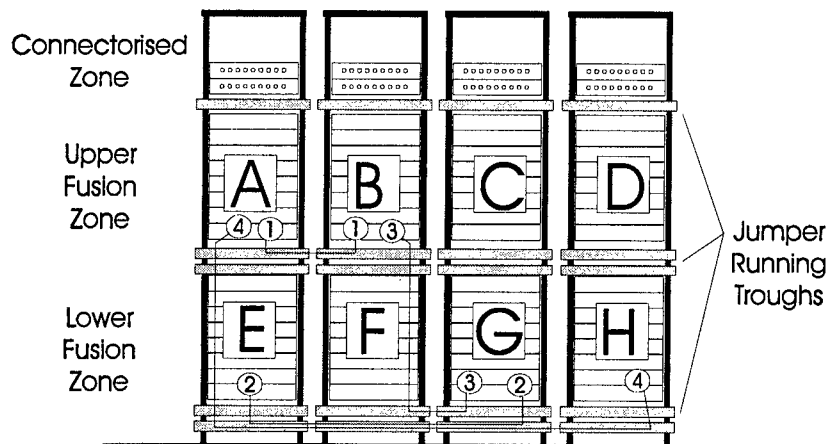


Fig 8. Jumper Routing in Multiple Verticals

Where OFDFs are installed in multiple verticals, a set of rules was developed to allow for the consistent and tidy installation of cables and jumpers. See Fig 8.

Based on some simple rules and the modular building blocks of the OFDF system, a common set of practices can be applied whether working in a customer site, remote road side cabinet, or Telecom exchange. Some of these practices are:

- Fibre must maintain a minimum 30 mm bend radius at all times.
- Fusion splicing modules must not be mounted higher than 1.7 m from the floor.
- All permanent connections on the OFDF's are to be fusion spliced
- Where OSP cables are brought directly into the OFDFs (small sites only), the cable should enter from the bottom of the OFDF vertical.
- Building cable must be used between the main OFDF and intermediate OFDF's.
- The OFDF template, designed for this system, must be used to position components in the MOFDF racks
- At a small site the MOFDF can be an inter-connect type if there is never likely to be more than 48 fibres on the site and everything is within the same room or the pigtail does not exceed 20m in length.
- Outside plant cable can be terminated directly onto the MOFDF if there is no associated exchange cable well or manhole and there is never likely to be more than 48 fibres and the MOFDF is closer than 10m from the point of entry of the cable.
- All jumpers are run on the opposite side of a vertical to the cables thus cables and cord never share the same side.
- All jumpers must run down into the troughs.
- When running jumpers between adjacent racks, route jumpers through the top trough.

- When running jumpers greater distances than one rack, route jumper through the bottom trough.
- Vertical runs should pass behind the troughs

TESTS

The plastic envelope single fibre organiser concept has been working for the last six years without problems. Two series of tests have been performed on the SFOs during that period. Both have been of a practical nature where a system has been operated over the fibres with a low system margin and the systems monitored by Bit Error testing while mistreating the SFO's. The most recent test is described below.

This test was carried out as part of a "proof of concept" procedure for a new ring architecture for customer SDH in the Central Business Districts.

The SDH test set was set up to measure BER (Bit Error Rate). The variable attenuation was set at approximately 0.5 dB below the level which produced constant errors. See Fig 9. Even at this level single errors were being produced at the rate of approximately 3 per hour.

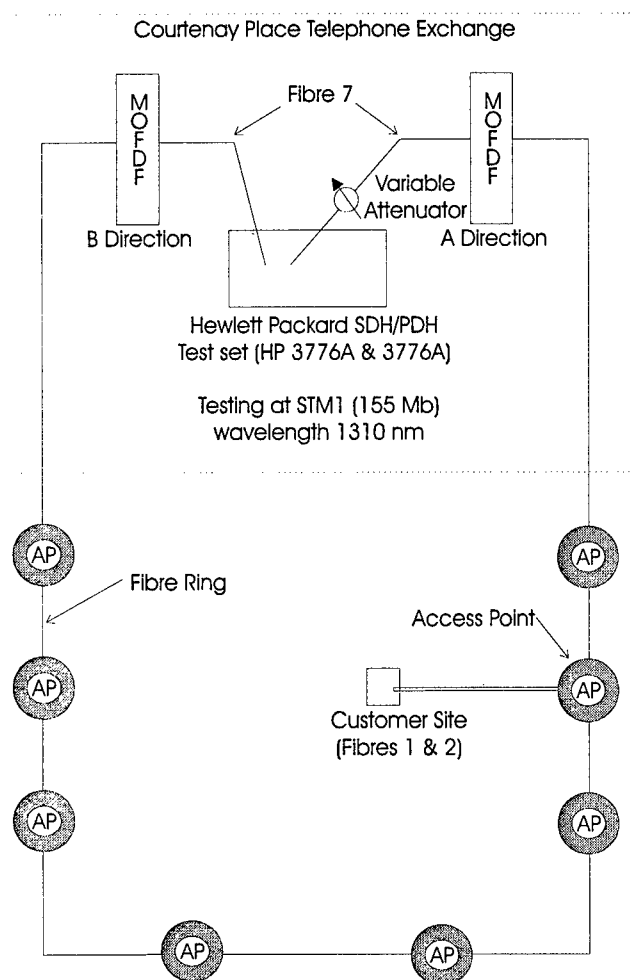


Fig 10. Test Arrangement

The OFDF components were mistreated as to a level far higher than would be expected under normal working conditions, including

- the drawers slammed in and out
- the SFO (Single Fibre Organisers) squeezed together
- cables/fibres were flicked, slapped and shaken
- SFOs scrunched up
- SFO assembly hinged up and down severely
- SFO envelopes flipped vigorously

A burst of errors was detected when the SFOs were actually scrunched up otherwise no errors were produced unless the fibre was bent on purpose to convince yourself the instrument was working.

DISCUSSION

The first OFDF of this type was installed in 1990 by Telecom New Zealand in their New Plymouth exchange terminating 180 fibres. The SFO's were made out of standard plastic zip bags held together with a two hole binder. The bottom two corners were cut away to allow fibre entry. This installation worked well though did highlight difficulties in getting the concept accepted. Technicians had been used to having what they saw was the convenience of connectors and the use of bank bags and binder clips did not look high tech enough for fibre optics. However the installation did prove the benefits of this type of distribution system and the human issues were able to be worked through. We were able to follow the copper model of a cross connect frame to give full flexibility and have interconnect frames close to the equipment for the final 20 metres without suffering losses through poor connectors. Incidences of accidental traffic interruptions fell away to nil.

The majority of Telecom New Zealand's OFDFs are now fusion OFDF modules and a number of projects are currently under way to upgrade the remaining older OFDF system.

The same SFO concept has been successfully applied to cross connection facilities in the external plant environment. In one case the OFDF drawers were mounted in a pressurised cabinet placed in a manhole, and in a second case an underground closure was used to house the SFOs as a cross connection facilities.

The emergency restoration overhead was required for fusion spliced OFDFs to be accepted by Telecom's Network Operations group and all "long term" spares had to be terminated on connectors at the top of the rack. There was a perception that connectors were required for quick restoration. Because of the acceptance of fusion spliced OFDF and self healing rings the need for this overhead is being reviewed and has already been downgraded to only connectorising two spares in any cable.

Without connectors the Fusion OFDF has major cost advantages and good fibre density per vertical. Issues with connector performance, such as insertion and return loss, are related to the equipment suppliers connector only and therefore become a minor issue.

CONCLUSIONS

The new OFDFs have met all the requirements of Telecom New Zealand's ideal optical fibre distribution system by providing a fully flexible system and removing all the issues associated with connectors and the storage of cord. OFDFs are well managed and tidy and therefore promote good work practices by those having to work on them.

One of the major benefits of the new OFDF's has been the acceptance by Telecom's Network Operations to allow work on fusion OFDFs during the working day. Because of accidental disruptions to adjacent circuits while work was being carried out on the older connectorised OFDFs all work had to be carried out after business hours. No system outages have been traced back to persons working on the new OFDFs.

ACKNOWLEDGEMENTS

The authors would like to thank those within both Telecom New Zealand and Fibernet New Zealand who assisted with the development and deployment of the elements and system described and for giving approval for this paper to be published.

Russell Hailes is a Senior Engineering Consultant with Telecom New Zealand. He has worked in outside plant since joining the then New Zealand Post Office in 1965. Russell has been involved with fibre optic and associated practices since the introduction of fibre to New Zealand in 1982.



Séan Maguire is a senior account manager (Telecoms) at Fibernet New Zealand, a division of New Zealand AMP Ltd. He holds a BE in mechanical engineering from Bolton Street University of Dublin, Ireland. He has been involved with fibre optic development since graduating in 1988 and since joining Fibernet in 1991 has held positions in development, product management and account management.



A New Mechanical Splice for Optical Fiber

Kazuya Murakami, Yoshihiro Nakatani, Kohei Urata,
Hiroyuki Kunugiyama, Tatsuo Teraoka, Hisanori Nakai

Hitachi Cable, Ltd.

1-1, Hitaka-cho, 5-chome, Hitachi-shi, Ibaraki-ken, Japan

ABSTRACT

A new mechanical splice for ϕ 0.25mm single optical fiber has been developed which is of very small size and high performance. This technology makes it possible to easily connect fibers in less than 4 minutes without the need of electricity. The average insertion loss is less than 0.1dB at 1.31 μ m wavelength.

1. INTRODUCTION

Efforts have begun to put FTTH (Fiber To The Home) systems into practice.⁽¹⁾ The distribution system to each subscriber requires many fiber connections between a cable and codes for subscribers. Most of those connections are made on the top of telephone poles in Japan.⁽²⁾ Therefore, the mechanical splice is expected to be an easier method rather than an arc fusion splice, because ease of assembly, short splicing time and no need of electricity are anticipated.⁽³⁾

To make a mechanical splice, however, accurate alignment of the two fibers requires a high precision guide groove. Usually, an existing guide groove is made of glass or metal, etc. and is assembled in a plastic housing.⁽⁴⁾ Therefore, it has a complicated structure with many parts, and is not very compact.

Therefore, a new plastic-molded structure has been developed with the integration of a V-shaped groove into its support to reduce the number of parts and the overall size without affecting performance.

2. STRUCTURE

The structure of the mechanical splice is shown in Figure 1. It consists of five parts: the plastic support with a V-shaped groove, three plastic cover plates and a metal clamp spring. Of the three plastic cover plates, one and the other are used for fixing part of bare fibers and coated fibers, respectively.

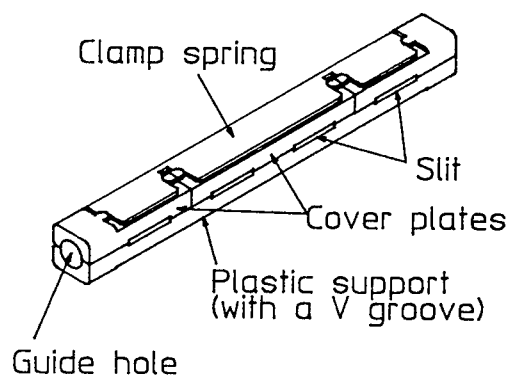


Fig.1. Structure of mechanical splice

3. SPLICING PROCEDURE

Figure 2 shows the splicing procedure with the mechanical splice. In order to make fiber insertion easy, a new scheme of assembly has been adopted using wedges in which splicing fibers are held by the plastic support and the cover plates.

First, a wedge is inserted in the splice to make a small gap between the support and the cover plates. Two fibers, which are stripped and cleaved at designated lengths, are put in the V-groove on the plastic support, with their end faces opposed on the same optical axis. When wedge is pulled out of the slits, the fibers are fixed tightly in the V groove support by the cover plates. Index matching material on the V groove helps to reduce reflections.

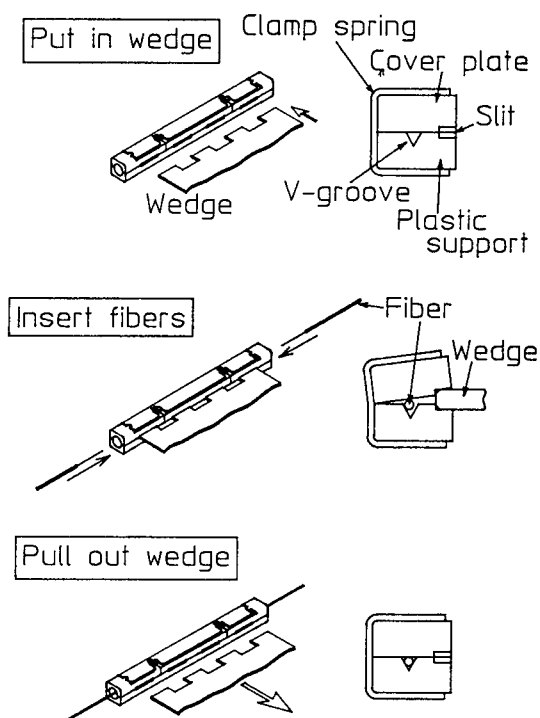


Fig.2. Splicing procedure

4. OPTICAL CHARACTERISTICS

4.1 Insertion loss

Figure 3 shows the insertion loss of the mechanical splice. The parameters of the optical fiber used for measurement are listed in Table 1.

The average insertion losses are 0.06dB and 0.05dB at 1.31 μm and 1.55 μm wavelengths, respectively.

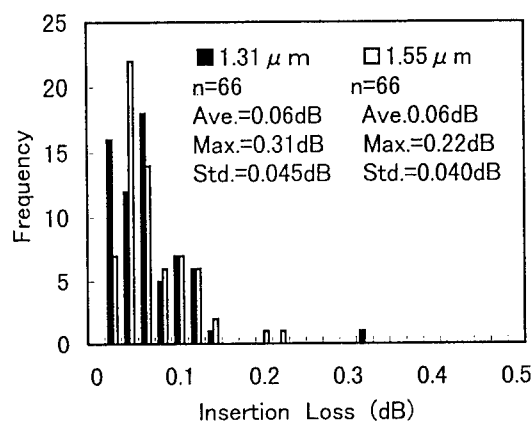


Fig.3. Insertion loss

Table 1. Optical fiber parameters

Type	Single mode
Diameter	0.25mm
Clad diameter	0.125 ± 0.001 mm
Mode field diameter	$9.2 \sim 9.4 \mu\text{m}$
Core eccentricity	$< 1 \mu\text{m}$

4.2 Return loss

Figure 4 shows the return loss of the mechanical splice. Minimum return loss is more than 45dB at $1.31 \mu\text{m}$ and $1.55 \mu\text{m}$ wavelengths.

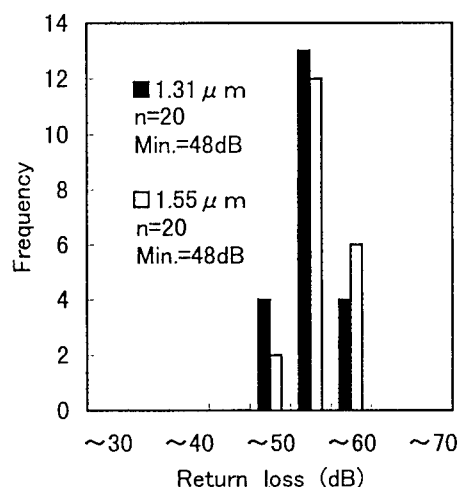


Fig.4. Return loss

5. ENVIRONMENT TEST

5.1 Temperature cycling test

The change in the insertion loss under temperature cycling ($-40 \sim +70^\circ\text{C} / 6\text{h} \times 10\text{cycles}$) is shown in Figure 5. It is less than 0.1dB at $1.31 \mu\text{m}$ and $1.55 \mu\text{m}$ wavelengths

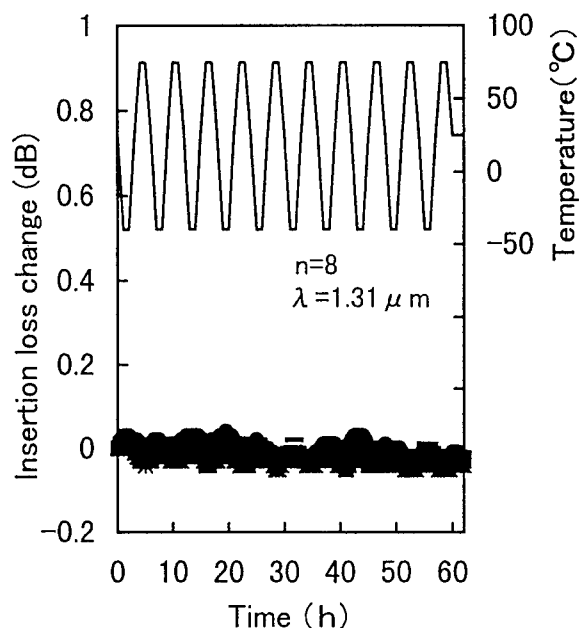


Fig.5. Insertion loss change under temperature cycling

5.2 Thermal aging test

The change in the insertion loss under thermal aging ($+85^\circ\text{C} \times 336\text{h}$) as shown in Fig.6 is less than 0.1dB at $1.31 \mu\text{m}$ and $1.55 \mu\text{m}$ wavelengths

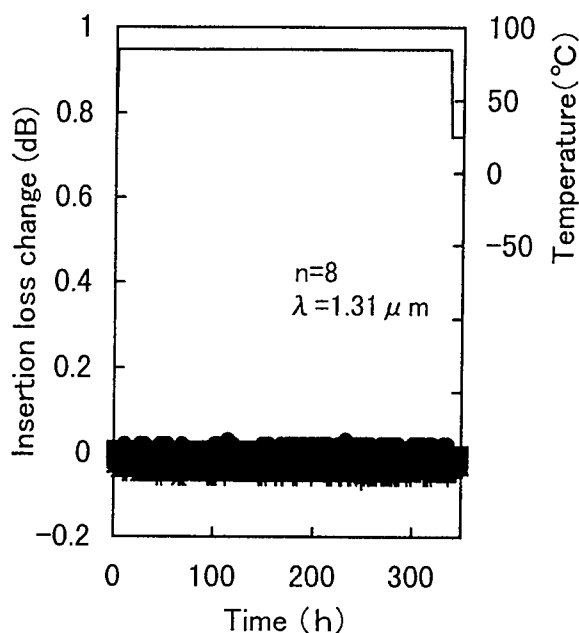


Fig.6. Insertion loss change under thermal aging

5.3 Dump heat cycling test

The change of the insertion loss under dump heat cycling ($-10 \sim +65^{\circ}\text{C}$ 93%RH at $+65^{\circ}\text{C} / 48\text{h} \times 5\text{cycles}$) is shown in Figure 7. It is less than 0.1dB at $1.31 \mu\text{m}$ and $1.55 \mu\text{m}$ wavelengths.

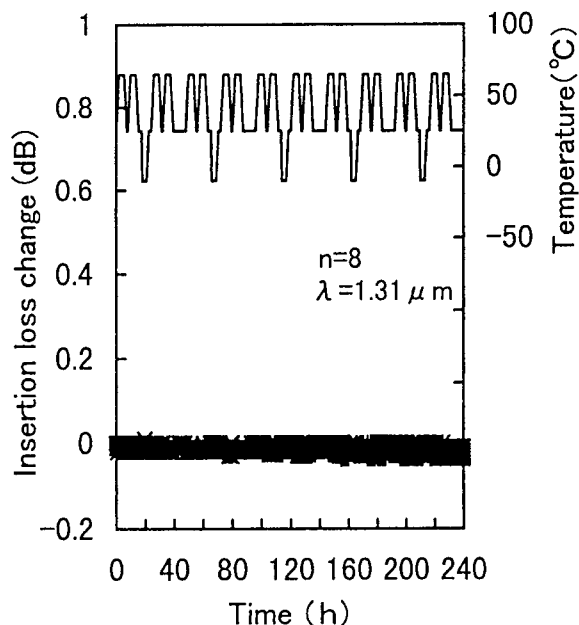


Fig.7. Insertion loss change under dump heat cycling test

6. MECHANICAL CHARACTERISTICS

Vibration and impact tests were conducted. Table 2 shows the test conditions and the results. The change in the insertion loss is less than 0.1dB under both tests.

Table 2. Mechanical characteristics

Test	Condition	Insertion loss change
Vibration	10~55Hz 2 hours/axis for 3 axis	<0.1dB
Impact	100G 3 times/axis for 3 axis	<0.1dB

7. CONCLUSION

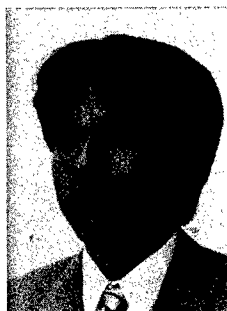
We have developed a new mechanical splice for $\phi 0.25\text{mm}$ single optical fiber. In order to make fiber insertion easy, a new scheme of assembly has been adopted with the use of wedges.

The resulting average insertion loss is less than 0.1dB, and the change in the insertion loss under temperature cycling ($-40 \sim +70^{\circ}\text{C} / 6\text{h} \times 10\text{cycles}$) is less than 0.1dB.

The developed mechanical splice will become indispensable technology for the deployment of FTTH systems.

REFERENCES

- [1] H.Iwata, M.Tsutsumi, E.nakamura,
N.Matsumoto, M.Nozaawa, S.Hayami,
S.Nagasawa and T.Tanifuji "Pre-
connectorized 1000-fiber Single
Slotted core Cable", Proc. of 44th
IWCS, pp627-634, 1995.
- [2] M.Nozaawa, M.Kihara, M.Takaya,
T.Katagiri, S.Nagasawa, N.Kashima,
T.Maruyama, "Field test results of
aerial cable jointing techniques for
access network", 1997,
Natl.Conc.Rec.IEICE, B-10-49, 1997
(in Japanese)
- [3] M.Takaya, M.Kihara, T.Katagiri,
S.Nagasawa, N.Kashima, "Design and
Development of Mechanical Splice for
Aerial Distribution Cables", 1997,
Natl.Conc.Rec.IEICE, B-10-50, 1997
(in Japanese)
- [4] T.Seto, Y.Yamaguti, H.Takeuchi,
K.Inada, T.Iwai, "Field test of
mechanical splice", 1997,
Natl.Conc.Rec.IEICE, C-5-11, 1997
(in Japanese)

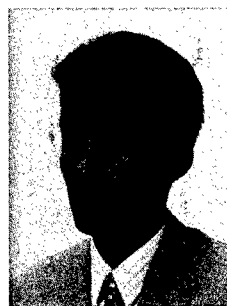


Kazuya Murakami

Hitachi Cable, Ltd.

1-1, Hitaka-cho, 5-
chome, Hitachi-shi,
Ibaraki-ken, 319-14,
Japan

K. Murakami was born in 1962. He joined Hitachi Cable, Ltd. after graduation from Tohoku University in 1985. He is a researcher at the opto-electronic system laboratory. Since 1985, he has been engaged in research and development of optical fibers and optical devices. He is a member of the IEICE of Japan.

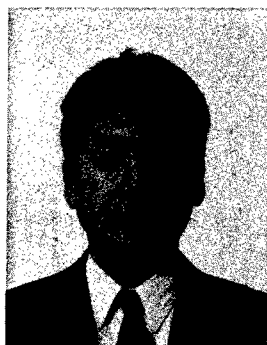


Yoshihiro Nakatani

Hitachi Cable, Ltd.

1-1, Hitaka-cho, 5-
chome, Hitachi-shi,
Ibaraki-ken, 319-14,
Japan

Y. Nakatani was born in 1972. He joined Hitachi Cable, Ltd. after graduation from Tokyo Metropolitan Institute of Technology in 1996. He is a researcher at the opto-electronic system laboratory. Since 1996, he has been engaged in research and development of optical devices.

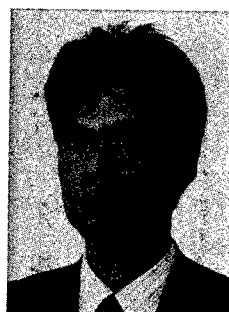


Kohei Urata

Hitachi Cable, Ltd.

1-2, Marunouchi, 2-chome, Chiyoda-ku, Tokyo, 100, Japan

K. Urata was born in 1949. He joined Hitachi Cable, Ltd. after graduation from Musashi Institute of Technology in 1971. He is a manager of the engineering section of the telecommunication division.

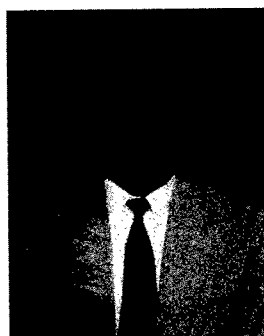


Tatsuo Teraoka

Hitachi Cable, Ltd.

1-1, Hitaka-cho, 5-chome, Hitachi-shi, Ibaraki-ken, 319-14, Japan

T. Teraoka was born in 1955. He joined Hitachi Cable, Ltd. after graduation from Yamagata University in 1980. He is a senior researcher at the opto-electronic system laboratory. Since 1983, he has been engaged in research and development of optical fibers and cable. He is a member of the IEICE of Japan.

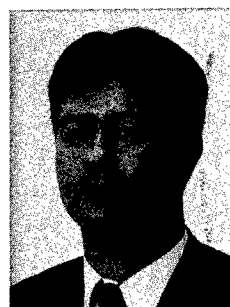


Hiroyuki Kunugiyama

Hitachi Cable, Ltd.

Isagosawa-cho, Hitachi-shi, Ibaraki-ken, 319-14, Japan

H. Kunugiyama was born in 1951. He joined Hitachi Cable, Ltd. after graduation from Kitakata Technical High School in 1969. He is an engineer at the optical device engineering department of Takasago works. Since 1990, he has been engaged in the design of optical devices.



Hisanori Nakai

Hitachi Cable, Ltd.

1-1, Hitaka-cho, 5-chome, Hitachi-shi, Ibaraki-ken, 319-14, Japan

H. Nakai was born in 1954. He joined Hitachi Cable, Ltd. after graduation from Tokyo Institute of Technology in 1979. He is a senior researcher at the opto-electronic system laboratory. Since 1996, he has been engaged in research and development of optical fibers and cable. He is a member of the IEICE of Japan.

A NEW CONCEPT IN OF SPLICING : FOCS

**Bertrand JOLY, Alain VINCENT, Michel RESLINGER,
Gérard GODARD, Philippe LAURENCY**

ALCATEL CABLE INTERFACE ; BEZONS, FRANCE

Hervé Aoustin

FRANCE TELECOM/CNET - DTD/CAI ; LANNION, FRANCE

Michel BOITEL, Thierry MAHE

FRANCE TELECOM/CNET - DTD/RCV ; LANNION, FRANCE

ABSTRACT

In this paper we present an ensemble constituted of a new mechanical splice of very simple design (FOCS/S) and a multifunction tool (FOCS/T) which allows to assemble the splice on the fiber in one operation without energy.

Recent fibre evolutions and in particular their improvements in cylindricity and surface-core concentricity allow to envisage really innovative splicing techniques which would feature good optical performances associated with reliability, easy assembly, small size and low cost.

INTRODUCTION

Fibre splicing today is primarily done using fusion for permanent connection of single mode fibers and optical connectors for permanent connection of multimode fibres.

For transient or temporary connexions users tend to prefer mechanical splices.

The perception of fusion splices is the satisfactory level of optical performances and reliability at the cost of a heavy investment in fusion splicers with their energy requirement and necessary maintenance.

Optical connectors, on the other hand, because of their standardized interface tend to incorporate precision ferrules which have to be manipulated carefully and are usually polished. This together with their size and cost jeopardize their field applicability.

With these inputs in mind, the objectives of our development were to create a complete new splicing system which would offer satisfactory characteristics, small size at low cost using a compact installation tool operable without outside power by personnel with no specific training.

This led to the FOCS (Fibre Optic Connection System).

SYSTEM DESCRIPTION

The FOCS system features :

- a fully thermoplastic mechanical splice..... FOCS/S (applicable to singlemode and multimode fibres)
- a multifunction assembly tool.... FOCS/T

FOCS/S

The main feature of the splice is the alignment of the two fibers in one precision V groove. In order to obtain excellent return loss performance, the fibres are cleaved at an angle and the optical continuity is ensured using an index matching gel.

In order to lower the cost of the mechanical splice, we started from the very beginning with a 2 piece design :

- a base including the fibre introduction compartments, the precision V groove and the index matching gel container
- a cover including the fiber clamp and the splice cover locking mechanism

Insertion loss (monomode fibers)

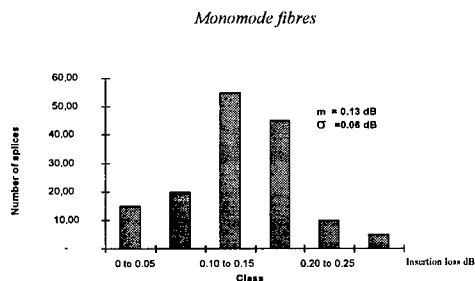
The optical results we obtain with various fibres assembled using FOCS/T tool are the following :

α dB (20°C) λ	Statistical values	Standard deviation
1.3 μ	m = 0.16 dB	σ = 0.12 dB
1.55 μ	m = 0.15 dB	σ = 0.10 dB

These results were obtained from 70 splices made at France Telecom/CNET using fibres of various brands.

At ALCATEL CABLE INTERFACE we have tested FOCS/S with commercially available ALCATEL fibres. We have obtained the statistical distribution shown on fig. 1 ; these results were obtained on 150 splices realized with 3 different tools.

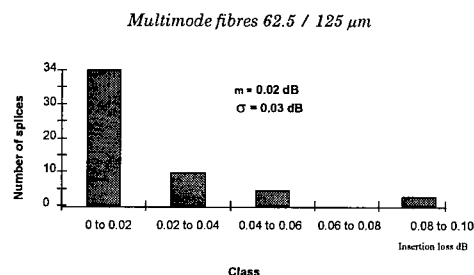
FIG. 1



Insertion loss (multimode fibers)

The typical results we obtain with various 62,5/125 fibres assembled using FOCS/T tool are average m = 0.02 dB, standard deviation σ = 0.03 dB with a maximum value of 0.13 dB. The statistical distribution is shown on fig. 2 ; these results were obtained on 50 splices installed with one tool.

FIG. 2



Working temperature

The objective of our study was FOCS/S to reach a temperature range of -30° C to +80° C. To that aim, we have made complete temperature ageing tests the results of which will be presented at IWCS 97.

Pulling strength resistance : The minimum pulling strength is 4 N.

Return loss : Return loss depends on the use of FOCS/T. The minimum return loss value with typical singlemode fibres cleaved at right angle is 50 dB at room temperature.

Immersion : FOCS/S can stay in water at 20° C for 8 days with an attenuation increase of less than 0.05 dB.

Dimensions : Dimensions of FOCS/S are 25x7x3.6 mm.

A picture of FOCS/S is shown on figure 3.

Simplicity of the design and dimensions of FOCS/S make it a very competitive product which can be used in a very large number of different environments.

FOCS/T

FOCS/T tool is a multifunction robot which accomplishes the following actions :

- stripping of the two 250 μ fibres
- their angle cleave
- introduction of the 2 fibres in the FOCS/S splice
- locking of FOCS/S

It is operated through one manual rotative handle appearing on the right side of the FOCS/T tool shown on fig. 4.

Details of the FOCS/T mechanism can be seen on fig. 5 with the upper cover removed. The right-hand side handle is manually rotated together with the horizontal camshaft located in the back of the tool.

The cams push all the moving parts of FOCS/T i.e. translating and rotating fibre holders, stripping blades, cleaving blades, and FOCS/S splice holder.

Installing the fibres

The two clean 250 μ fibres are inserted in FOCS/T tool as shown on fig. 6. They are installed in a cross-over and butt situation in order to reduce the overall dimension of the tool ; they are held under two levers which attach them on mobile carts.

Then the operator begins to crank the handle as shown on fig. 7.

Stripping the fibres, installing FOCS/S

This operation was subjected to a lot of effort in order to deliver fibres with a very clean surface without the need for any additional fibre cleaning.

It is carried out using 2 blades - fixed and mobile - which are made of high resistance metal of specific shape. As the operator begins to crank the handle, the two blades are applied on the fibres while the mobile fibre holders pull the fibres on both sides. Cleaving of the fibres is achieved using two sliding pads.

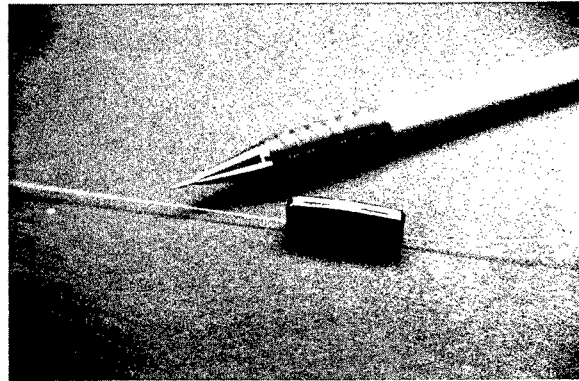


FIG. 3

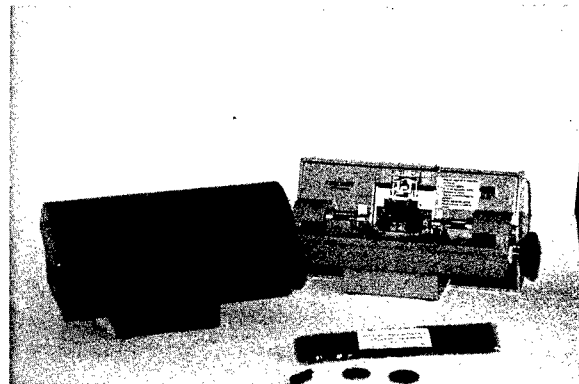


FIG. 4

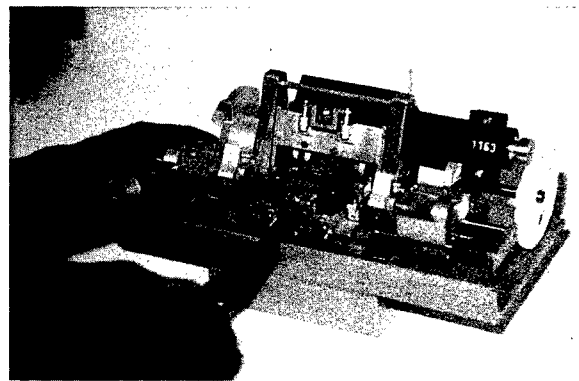


FIG. 5

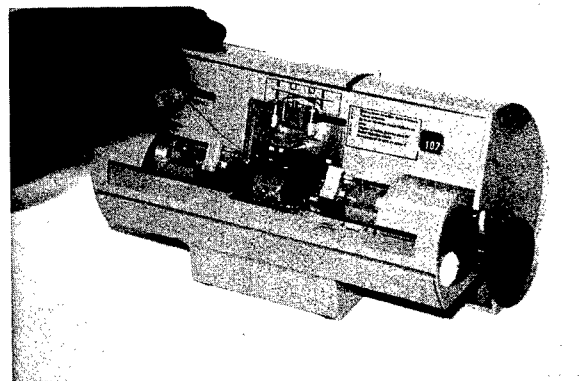


FIG. 6

The coating residues are received in a cartridge located in the tool pedestal.

As shown on fig. 8, the FOCS/S holder is then put into place.

Gripping and twisting the fibres

This operation is needed in order to obtain a calibrated angle cleave of the 2 fibres. As the operator continues to crank the handle, two jaws are gripping the fibres and a torsion is applied as the 2 mobile fibre holders tip down.

Cleaving the fibres

Two diamond blades are applied on the fibres which are cleaved at the prescribed angle. The return loss performance we obtain with FOCS/S installed using FOCS/T is excellent, that is to say better than 60 dB at 1.3 μ and 1.55 μ and in the temperature range -30° C, +80° C.

Fibres introduction in FOCS/S

As the operator keeps on cranking the handle, FOCS/T tips down the central part of the tool and, as the mobile fibre holder carts move forward, the fibres are introduced gently in FOCS/S splice.

Locking of FOCS/S

Locking of FOCS/S is done by two pistons actuated by FOCS/T ; the splice holder is delivered to the operator (see fig. 9) and the 2 fibres are released.

FOCS/T tool has been operationally tested between 0° and +40° and stored between -25° and +80° according to France Telecom requirement (see ref. 1).

FOCS/T incorporates a counter which totals the number of splices ; inscriptions appearing on the tool help to visualize its status and assist the operator.

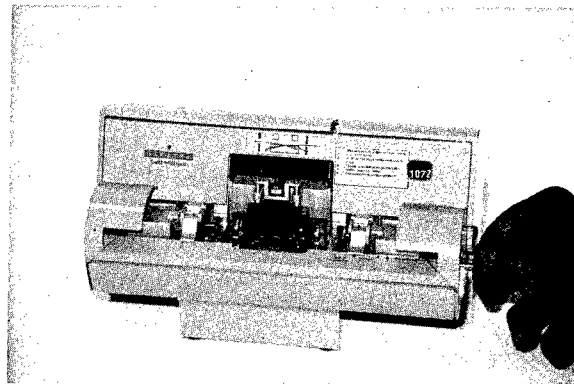


FIG. 7

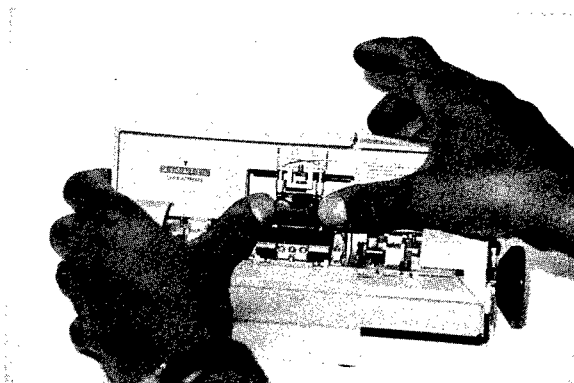


FIG. 8

The operator has nothing else to do than clean the fibres, install them in FOCS/T, crank the handle and watch the operation. The total splice time takes thirty seconds to one minute.

Let us recall that FOCS/T does not call for any outside power and does not require any training from the operator.

With a weight of 1.6 kg and a size of 228 x 120 x 120 mm, FOCS/T carries out an ensemble of operations which are, to our knowledge, unique on the market place.

Acknowledgement

The present work has been carried out with the participation of France Telecom.

CONCLUSION

The performances obtained from FOCS system - that is to say FOCS/S + FOCS/T - together with its ergonomics lead to a massive simplification of optical fibre splicing, both singlemode and multimode. This opens broad new perspectives concerning optical fibre implementation in both access networks and LAN.

REFERENCES

1. « Taux de réflexion des raccords de fibres optiques » : M. BOITEL, JM CAILLEAUX, T. MAKE, Y. RUELLO. Opto Conference, 15-16 May 1990, Proceedings pp 490,493.
2. « Statistical analysis of the incremental increase in insertion loss of angled end face mechanical splices » : S. SHAH, R.E. SPICER, W.C. YOUNG. Bellcore Publication.
3. « Raccordement des fibres optiques multimodes en réseaux de vidéo communications ». Y. RUELLO, JP STEPHAN, C. VERGEZ, FL. MALAVIEILLE. Opto Conference, 17-19 May 1988, Proceedings pp 217, 221.



FIG. 9

AUTHORS



Bertrand JOLY - ALCATEL CABLE INTERFACE
35, rue Jean-Jaurès - 95871 Bezons, France

Bertrand Joly was born in 1941 in France. He received the graduation from the Aeronautics Engineering school in 1964. As a NASA Fellow, he spent two years at the University of Berkeley, California, where he obtained a Masters and Ph.C. degree in electrical engineering. B. Joly has been Deputy General manager of Alcatel Cable Interface since 1991, in charge of business development in the field of telecommunications copper and fiber networks. He was appointed head of the Telecommunications Cables Accessory Competence Center of Alcatel Cable in 1992.



Alain VINCENT - ALCATEL CABLE INTERFACE - 35
rue Jean-Jaurès - 95871 Bezons, France.

Alain Vincent was born in Paris in 1949, he received his engineering degree from the Conservatoire National des Arts et Métiers, Paris, in 1980. After many activities in the telecommunications equipments field within the Alcatel Cable Group, he joined Alcatel Cable Interface in 1991, where he is in charge of the development of copper and optical fiber telecommunication cable accessories.



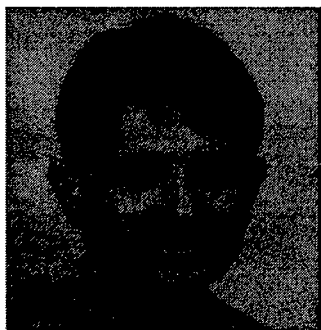
Micher RESLINGER graduated from the University of Technology of Mulhouse (France) in 1978. He has been with Alcatel since 1981 in charge of development of fiber optic accessories in the field of fusion splices and fiber optic cleavers.



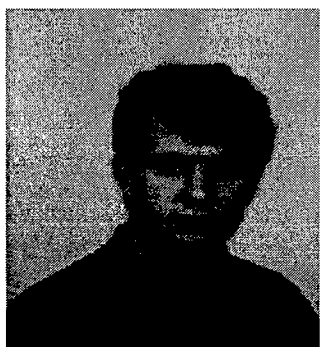
Gérard GODARD was born in 1946. He specialized in micro mechanical engineering and joined **ALCATEL** in 1989. Since then he has been involved in the design of fusion splices and cleaving tools.



Philippe LAURENCY was born in 1957. He graduated with BTS Degree in Mechanical Engineering. Since 1988 he is with **ALCATEL** and has specialized in fibre optic cable splicing for submarine cables and terrestrial applications.



Michel BOITEL Graduated from the Ecole Nationale Supérieure d'Optique in 1969 and he joined the **CNET** in 1970. He has worked on optical fiber R&D until 1996, he his now engaged in video networks developpement.



Hervé AOUSTIN Graduated from the Ecole Nationale Supérieure des Arts et Metiers in 1990. He is engaged in fiber connection R&D since he joined the **CNET** in 1992.

Thierry MAHE has been engaged in fibre connection R&D until 1996, he now deals with video networks developpement.

Takeyuki Nakano , Jun Yamakawa , Takashi Shigematsu

THE FURUKAWA ELECTRIC CO., LTD.

6, Yawata-kaigandori, Ichihara, Chiba 290 JAPAN

ABSTRACT

Along with a rapid move to introduce multimedia to communication technology, building FTTH (Fiber To The Home) network as low as copper cable communication network in cost is strongly required. Joining technology of optical fiber, in particular, faces many challenges to seek for lower insertion loss, higher reliability, and outstanding splicing workability. Authors have developed a mechanical splicer, as one of solutions to overcome these challenges, which mechanically fixes cleaved optical fibers in mirror state. Using the mechanical splicer, the entire process from removal of optical fiber coating through splicing is completed in as short as about three minutes. It is found to feature average insertion loss of 0.135dB.

1.INTRODUCTION

For recent years, optical fiber has been making rapid progress in being introduced into an access network. As a result, a simple but highly efficient splice has been being called on to allow for a lead-in of aerial optical cables, a joining of indoor optical cables in the house of a user with a termination cable, and so on. Aerial splicing points are exposed to more unfavorable environments, either working or operating, than on the ground. As a problem common to both aerial and indoor applications, it is necessary to take several things into due consideration, which does not relate to splicing technology directly, such as ensured power availability, working noise, etc. From these points of view, the splicing-technique in need should not require any power supply but must allow for easy working and high reliability.

As a solution to such requirements, a mechanical splice system has been proposed.⁽¹⁾

This paper will report a mechanical splicer, which makes optical fiber easily splicable by merely inserting it in a pre-assembled part. And its structural design as key to the performance of such splicer will be dealt with while taking up the results of trial, testing and evaluation on the construction of such structural design.

2.STRUCTURE OF MECHANICAL SPLICE

Figure 1 shows structure of the mechanical splice. It is composed of a V-groove plate, one lid to clamp bare fibers, two lids to clamp coated fibers, and three clamp springs. Each of the plate and the lids is held with a single clamp spring in order to properly maintain fiber aligning accuracy and tensile strength.

The center of the V-groove where optical fibers meet each other is filled with index matching gel so as to reduce fresnel reflection which is generated at the gap between optical fiber ends and causes deterioration of optical performances.

Plastic material with thermal expansion coefficient at the order of $1.0 \times 10^{-5}/^{\circ}\text{C}$ is selected for the plate and the lids in order to maintain favorable temperature characteristics.

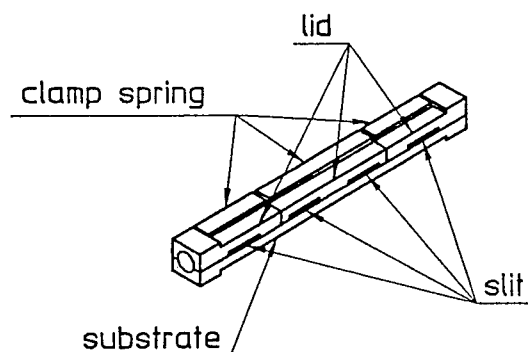


Figure 1 basic structure

On the plate, there are two types of V-grooves : one for coated optical fiber with diameter of $250\ \mu\text{m}$ and the other for bare fiber with diameter of $125\ \mu\text{m}$. Ideally shape of the junction between these two grooves should be smoothly changed both in depth and width, so as to insert optical fibers smoothly. It is very difficult, however, to fabricate a mold for such grooves in the current precision machining technology. Authors succeeded in realizing this shape by employing a special mold fabrication method.

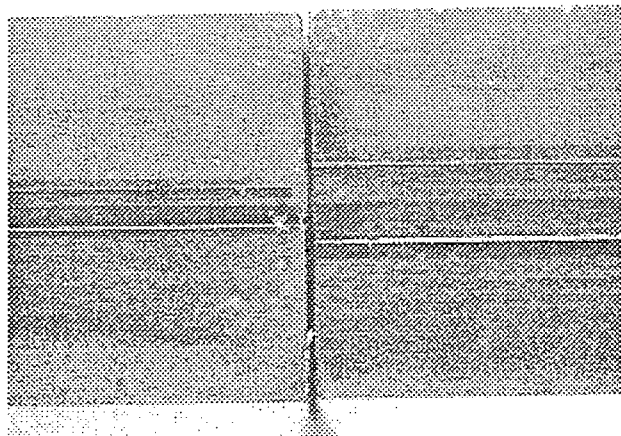


Figure 2 V-groove fabricated by current machining method

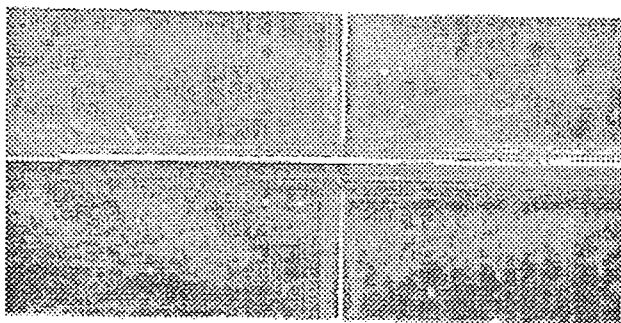


Figure 3 V-groove fabricated by new method

3.DESIGN OF CLAMP SPRING

Dimensions of the mechanical splicer are $4 \times 4 \times 40$ [mm]. The splicer is as big as a reinforcement sleeve for the fusion splice. Thus the mechanical splicer can fit cabinet and closure employing the conventional sleeve. The clamp spring features U shape so as to clamp the lids and the plate and to firmly fix optical fibers. Spring constant of this U-shaped clamp spring is expressed as :

$$P=k\delta, \sigma=PL/Z, k=EI/(\Lambda_A+\Lambda_B+\Lambda_C)$$

$$\Lambda_A=S_1 \cdot I_1^2/3$$

$$\Lambda_B=C_R \cdot R^3 \quad [n=(I_1+I_2/R)]$$

$$C_R=(n^2+0.5)(\theta_1+\theta_2)\pi/180+2n\sin\{(\theta_1+\theta_2)+\pi/180\}+0.25\sin\{2(\theta_1+\theta_2)+\pi/180\}$$

$$\Lambda_C=S_2(I_1+I_2+I_3)^2$$

where :

p = load [N]

k = spring constant [N/mm]

δ = flexure [mm]

E = modulus of longitudinal elasticity [N/mm²]

I = moment of inertia of area = $bt^3/12$ [mm⁴]

Λ = inertia moment of axial spring line against load action line [mm³]

σ = stress [N/mm²]

Z = section modulus = $bt^2/6$ [mm³]

b = plate width [mm]

t = plate thickness [mm]

L = length measured perpendicularly against load action line [mm]

The spring is made from stainless steel so as to feature sufficient resistance to circumstantial ambience. Plate thickness of the spring should be increased to some extent to raise pressing force onto fibers. If the thickness is increased too much and flexure increases, however, spring limit of stainless steel would be topped, which might allow plastic deformation of the spring to take place. If this occurs, the spring will not function properly. Besides as the mechanical splicer is small in size, flexure can not be raised too much. Taking these restricting conditions into account, authors calculated appropriate plate thickness and flexure by means of the equation for spring constant. The mechanical splice reported herein was set to a spring pressure of 19.6N/cm.

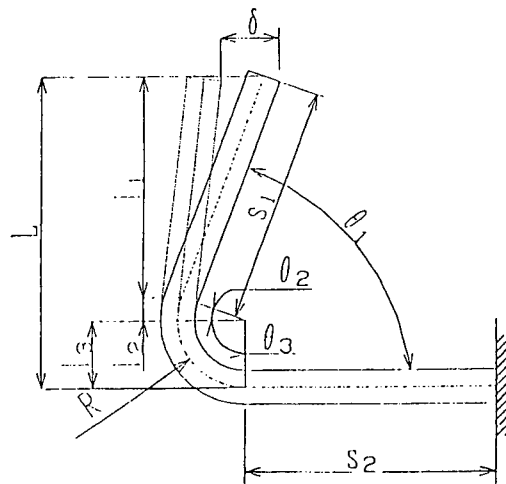


Figure 4 figure of clamp spring

4. CONNECTION PROCEDURE

Figure 5 shows how to insert optical fibers into the mechanical splicer. In a bid to make splicing work easy, the mechanical splicer is pre-assembled, and optical fibers are inserted to the pre-assembled mechanical splicer.

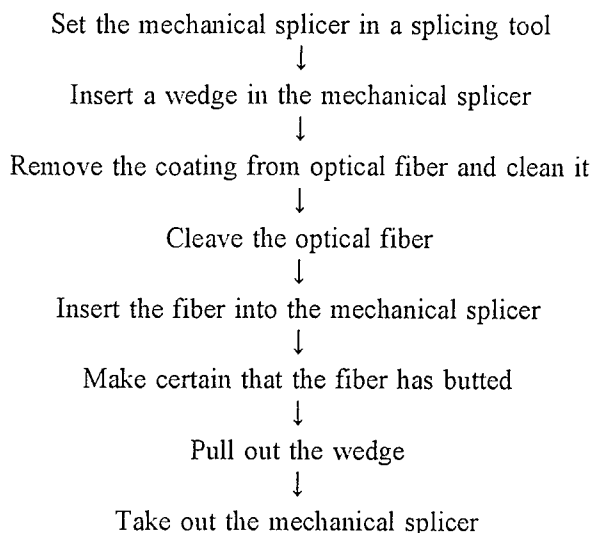


Figure 5 flow chart for splice

Slits are made on one side of the lid. Wedges which are slightly wider than the slits and are installed on a splicing tool are inserted to the slits by the splicing tool in order to secure gap of several tens of micrometers between the V-groove plate and the lid. Optical fibers are inserted to this gap. Using the splicing tool again, optical fibers meet each other at the center of the mechanical splicer. Figure 6 shows a conceptual diagram of wedge insertion.

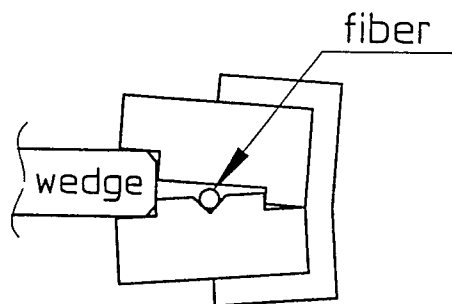


Figure 6 conceptual diagram of wedge insertion

Coating on optical fiber is removed with a mechanical remover, and optical fiber is cleaved with a optical fiber cleaver. Neither of these tools need electric power. The splicing tool is also not electrically driven. It is possible, therefore, to splice

optical fibers with this procedure even when no electric power supply is available.

5. CHARACTERISTICS OF MECHANICAL SPLICE

Prototypes of the mechanical splicer were fabricated based on the above-mentioned design, and they were evaluated in the following aspects :

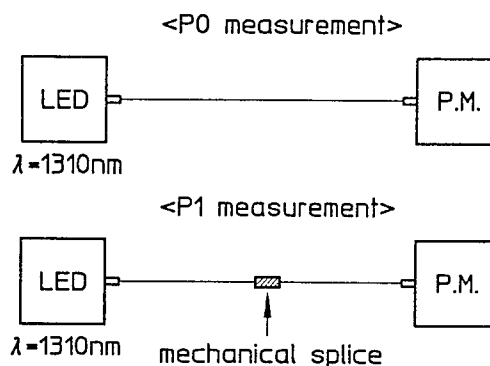
- 1) insertion loss
- 2) return loss
- 3) temperature characteristic
- 4) time requirement for splicing

Outcome of these evaluation are reported below.

5.1 Insertion Loss

Insertion loss was evaluated by using the measurement system shown in Figure 7. A loss of an optical fiber alone (P0) was measured first. Next the same optical fiber measures was cut into two, and they were spliced by means of the mechanical splicer. Then the loss of the spliced fiber (P1) was measured. Insertion loss was defined as $P0 - P1$.

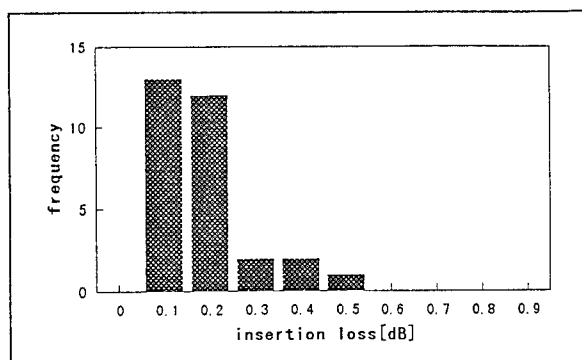
LED with wavelength (λ) of 1310nm was used as a light source. The Number of samples (n) was set at 30.



$$\text{insertion loss} = P0 - P1$$

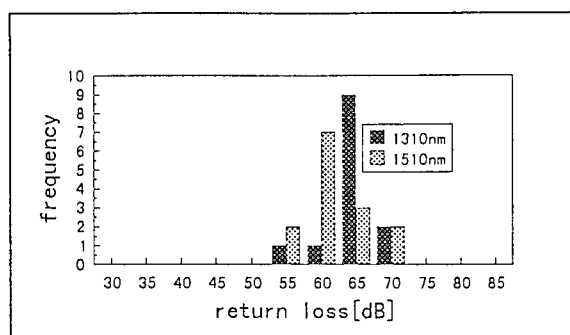
Figure 7 measurement system of insertion loss

Figure 8 shows histogram of insertion loss. Insertion loss is found favorable : its average is 0.135 dB and its maximum is 0.41 dB.



	[dB]
n	30
ave	0.135
max	0.41
min	0.04
std	0.08

Figure 8 histogram of insertion loss



	1310nm	1550nm
n	16	16
ave	62.48	59.24
max	68.10	67.90
min	50.40	54.00
std	4.072	4.108

Figure 10 histogram of return loss

5.2 Return Loss

Return loss was evaluated by using the measurement system shown in Figure 9. LED was used as a light source, and its wavelength was 1310nm and 1550nm. The number of samples (n) was set at 16.

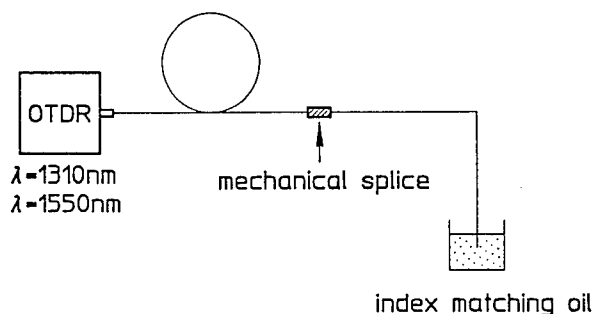


Figure 9 measurement system of return loss

Figure 10 shows histogram of return loss. The minimum return loss is found to be 50.40 dB when wavelength is set at 1310nm. Due to index matching gel injected inside, the mechanical splicer is found to feature sufficient return loss.

5.3 Temperature Characteristic

Temperature characteristic was investigated by using the measurement system shown in Figure 11.

Test conditions were as follows :

temperature cycle : -30 °C to 70 °C

the number of the test runs : 10 cycles (8 hours / cycle)

item measures : to monitor insertion loss continuously

wavelength:1310nm

Figure 12 shows an example of measurement results. Variance of insertion loss is less than 0.1 dB, which demonstrates sufficient temperature characteristic.

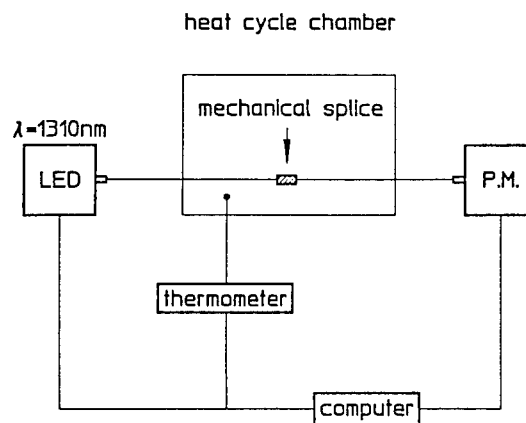


Figure 11 measurement system of temperature characteristic

6. CONCLUSION

- 1) The new optical fiber splicing technology has been developed. This technology requires no electric power supply. It is expected to improve efficiency of optical fiber splicing.
- 2) The newly-developed mechanical splice is small in size : $4 \times 4 \times 40$ [mm]. It can be applied to cabinet and closure using the conventional fusion sleeve.
- 3) The mechanical splice is found to feature outstanding characteristics : average insertion loss of 0.135 dB, temperature variance of 0.1 dB or less, and minimum return loss and 50.40 dB.

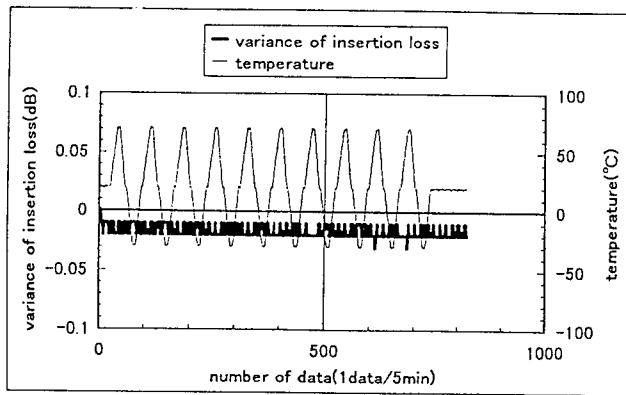
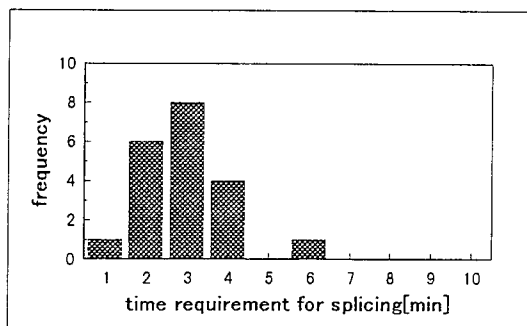


Figure 12 temperature-loss characteristic

5.4 Time Requirement For Splicing

The trial-manufactured mechanical splicer was used to measure the time required for splicing in an aerial splicing environment. The worker rode on a bucket vehicle and really used an aerial optical cables to carry out an operation of splicing. A total of twenty joining were made. The time required from start to end as shown in Figure 5 "flow chart for splicing" was set as the splicing time.



n	20
ave	2.95
max	6.00
min	1.00

Figure 13 histogram of time requirement for splicing

Results involved are shown in Figure 13. The time requirement was 2.95 minutes on the average, and 6.0 minutes at the maximum. From these findings, it could be gathered that using the proposed mechanical splicer herein will allow us to splice the optical fiber in a satisfactorily short time.

7. REFERENCES

- (1) M. Takaya et al. "Design and Development of Mechanical Splice for Areal Distribution Cables", Trans. IEICE, vol. B-10-50, p559, 1997



Takeyuki Nakano

The Furukawa Electric Co., Ltd.

6, Yawata-kaigandori,
Ichihara, Chiba 290
Japan

Takeyuki Nakano was born in Shizuoka, Japan, in 1972. He received the B.E. degree in mechanical engineering from Shizuoka University in 1994. He joined The Furukawa Electric Co., Ltd. in 1994 and has been engaged in development of optical fiber connectors.



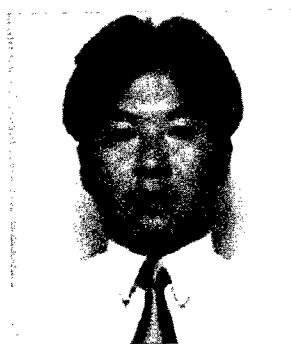
Jun Yamakawa

The Furukawa Electric
Co., Ltd.

6, Yawata-kaigandori,
Ichihara, Chiba 290
Japan

Jun Yamakawa was born in Hokkaido, Japan, in 1965. He received the B.E. degree in applied electronic engineering from University of Electro Communications, Tokyo, Japan, in 1989.

He joined The Furukawa Electric Co., Ltd. in 1989. Since then he has been engaged in R&D on optical component. Mr. Yamakawa is a member of The Institute of Electronics, Information and Communication Engineers of Japan.



Takashi Shigematsu

The Furukawa Electric
Co., Ltd.

6, Yawata-kaigandori,
Ichihara, Chiba 290
Japan

Takashi Shigematsu was born in Shizuoka, Japan, in 1963. He received the B.E. degree in precision engineering from Yamagata University, Yamagata, Japan, in 1986. He joined The Furukawa Electric Co., Ltd. in 1986. Since then he has been engaged in R&D on plant and facilities div.

MANAGEMENT FOR RENEWAL OF THE METALLIC ACCESS NETWORK

Daisuke TOMIZU, Hiroshi Harada, and Masateru Inoue

NTT Access Network Systems Laboratories
Tsukuba-shi, Ibaraki-ken, JAPAN

ABSTRACT

A new method has been established for Management of the metallic access network, especially for planning investment for renewal of CCP cables(Color Coded Polyethylene cables) which occupy the major portion of aerial cables. In addition to decrepitude,we usually use other parameters, such as the defective condition of conductors, failure, demand, service usage, and revenue,as indicators to decide the order of priority for areas to renew. In using this method, the analysis of each area is performed from various viewpoints. So the result is comprehensive and quantitative, and we can easily decide the order of priority for renewal and efficiently make an effective investment plan. This paper describes the management procedure and describes how the method was practically applied at a central office.

1. INTRODUCTION

NTT is going ahead with a plan to provide optical fiber cables to all homes by 2010,but still has many metallic cables that must be maintained to a high quality to cope with the advance of multimedia communication services.[1][2] For example, the rapidly expanding ISDN service and ADSL high speed telecommunications. Many CCP cables have already exceeded their service life, and number of decrepit cables is increasing. It is therefore necessary to renew CCP cables to maintain a high level of customer service and to control maintenance costs. Obviously it would be best to renew all the cables at once; however,this would require an enormous labor input and excessive cost. For efficient and effective renewal, it is important to decide the order of priority of areas to be renewed, (In this case, area refer to Fixed Distribution Area(FDA), which is the

minimum unit for access network management). Conventionally,outside plants were renewed when they became very decrepit or when a disaster or dead end occurred. Such renewal was not strategic but negative. Recently, in this age of keen competition and demand for advanced services. NTT has to investigate each FDA from the viewpoint of not onlydecrepitude but also various factors such as the condition of defective conductors, failures, demand, revenue,and the kinds of services used.

This being the case, a systematic method is required for evaluating each FDA both quantitatively and comprehensively, and for determining priority for renewal.

2.PROCEDURE FOR FORMULATING THE CCP CABLE RENEWAL PLAN

The procedure, shown in Figure1, is as follows: At first, a central office area in which renewal has to be performed is decided upon. Next, each FDA belonging to the central office is analyzed with regard to decrepitude, defective conductors, failure, demand, revenue, and the kinds of services used. Based on the result of each analysis, a score is given to each FDA for each factor,and it is evaluated based on the total score. In addition, amount of CCP cable to be renewed and investment is calculated. (Figure.1)

2.1 Selection of Central Office

NTT has about 7000 central offices. They are classified into six groups depending upon the scale of the city that they belong to. The groups are SA, A, B, C, D, E in descending order of size (Table.1). [3]. In the central office areas belonging to groups SA or A, deployment of optical fiber cables is being promoted because they are big industrial cities, lucrative, and there is a high demand for optical fiber cables. For this particular case, the central

office was selected from group B, which includes some industrial regions. This area is a middle scale city and the priority for deployment of optical fiber cables is not so high. So management of the metallic access network is necessary and it is also important to renew CCP cables.

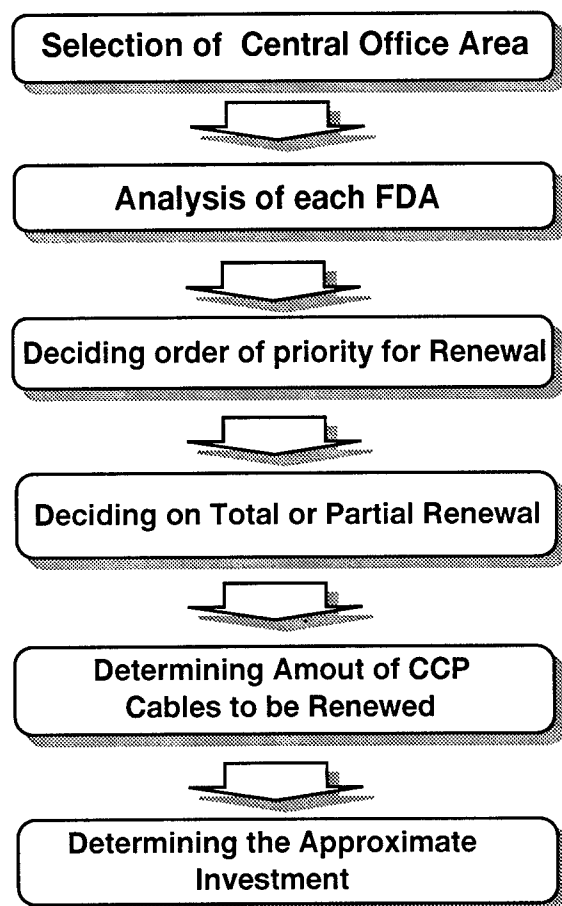


Figure.1 CCP Cable Renewal Management Flow-Chart

2.2 Analysis of Fixed Distribution Area

After selection of the central office, each FDA is analyzed based on the extent of decrepitude, the ratio of defective conductors, the condition of failures, the possibility of dead ends, the level of revenues, and the kind of services customers use. All the indices of factors are obtained numerically. To be more specific, the ratio of decrepit cables is obtained by dividing the sum of the lengths of CCP cables installed more than 17 years ago by the sum of the lengths of all CCP cables. The ratio of defective conductors is obtained by dividing the number of defective conductors by the number of all conductors. Regarding failure, although the

information cannot be found in the plant database used for network management, it is possible to abstract it from the system used in the repair service attendant bureau. Then the plant data and failure data is related by matching the telephone numbers commonly existing in both databases (Figure.2).

Table.1 Central office grouping

Group	Location of Office	Number of Offices
SA	Large Business Areas	13
A	Government-Designated Municipalities	156
B	Cities having Prefectural Office	261
C	Middle Rank Cities	197
D	Small Cities	6525
E	Rural Areas	

Owing to this fusion, the failure condition at every FDA can be determined (Figure.3). The index of failures can be obtained by multiplying the number of failures per unit cable and average down time. Down time refers to the time taken for repair. Due to the long distance from a repair base, considerable time and cost are incurred for repair despite the fact that occurrences are rare. This is the reason that down time is included in this index. The condition of dead ends is used as an index for demand. This index is expressed as the ratio of the number of essential conductors after two years to the number of currently available conductors. If it exceeds one, it is predicted that a dead end will occur two years later. Revenue analysis is based on area ranking allocated to each FDA by clarifying four ranks depending on revenue per circuit. the revenue of rank 1 is over 10,000 yen, the revenue of rank 2 is between 6,000 and 10,000 yen, the revenue of rank 3 is between 5,000 and 6,000 yen, and the revenue of rank 4 is less than 5,000 yen. As for customer services used, the number of circuits for the ISDN64 service is an important parameter because the number of subscribers to the ISDN64 service is increasing remarkably.

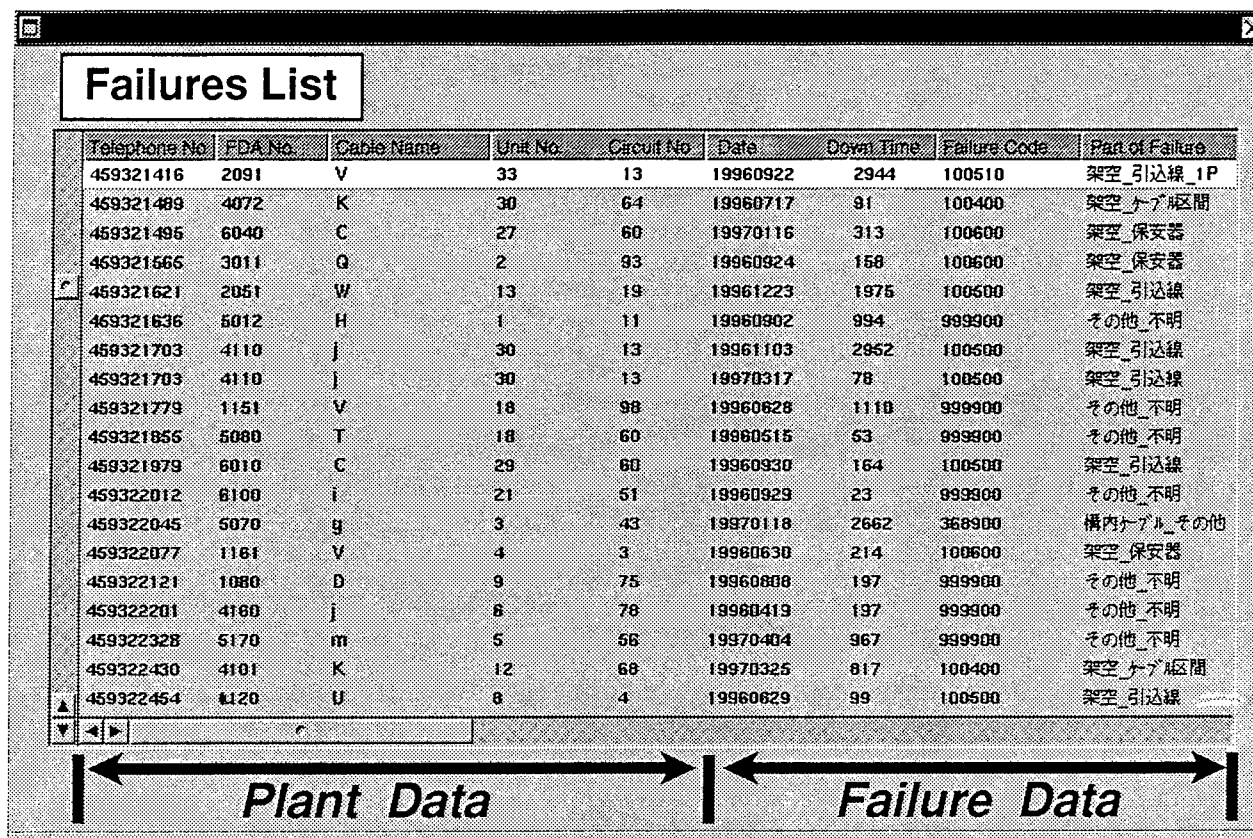


Figure.2 Matching Data of Plants and Failures

2.3 Evaluation of each FDA

The order of priority for renewal is decided according to the results calculated at the previous step. At that time, the standards are set to give a score to each FDA. The standards are shown from Table.2 to 7. The scores are accumulated for every FDA, and the results used as indices for comprehensive evaluation. If the area rank is 1, the FDA is given to 10 points. With regard to other factors, scores are given to each FDA as follows: The results calculated for each factor and total scores for the FDAs are shown in Table.8 and Figure.4. The FDA numbers are arranged in order of size with total scores. The ratio of decrepit cables for FDA No 4160 is 9.82%, so it is given no points. The ratio of defective conductors is 3.11%, so it receives 6 points. The indices of failure and demand are 4410 and 0.78, so it receives 10 points and 2 points respectively. The score for revenue is 6, and the score for ISDN64 is 6. The total points is therefore 30 points. As a result, the order of priority for renewal can easily be determined.

2.4 Deciding on Total or Partial renewal

Next, it has to be decided whether total or partial renewal is necessary depending on the decrepitude which influences the quality of CCP

cables. If the ratio of decrepit cables is over 60%, total renewal is chosen, otherwise partial renewal is chosen.

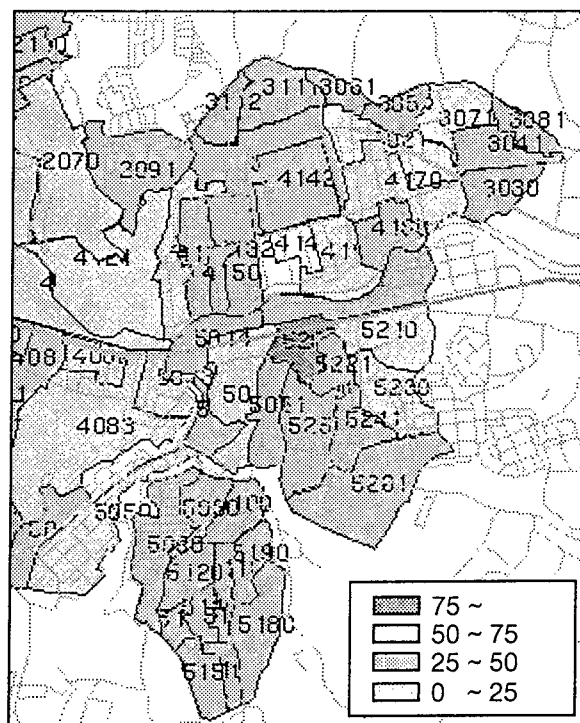


Figure.3 Distribution of Failures

Table.2 Standards for Decrepitude

Percentage of Decrepit Cables	Point
81~100	10
71~80	8
61~70	6
41~60	4
21~40	2
0~21	0

Table.3 Standards for Defective Conductors

Percentage of Defective Conductors	Point
81~100	10
71~80	8
61~70	6
41~60	4
21~40	2
0~21	0

Table.4 Standards for Failure

Failure Parameter	Point
2500~	10
2000~2500	8
1500~2000	6
1000~1500	4
500~1000	2
0~500	0

Table.5 Standards for Demand

Dead End Parameter	Point
1.0~	10
0.8~1.0	6
0.5~0.8	2
0~0.5	0

Table.6 Standards for Revenue

Revenue (Area Rank)	Point
1	10
2	6
3	2
4	0

Table.7 Standards for ISDN64 Service

Number of INS64 Conductors	Point
50~	10
40~50	8
30~40	6
20~30	4
10~20	2
0~10	0

2.5 Calculation of Approximate Product Process and Investment

The sum of the length of all CCP cables is the value taken as the approximate production process for each FDA in which total renewal is to be carried out. For each FDA in which partial renewal is to be performed, it is taken as the sum of the length of cables constructed more than 17 years ago.

Approximate investment is calculated by multiplying the renewal charge per kilometer by the product process. The result of the process and investment is accumulated in the order of priority and is shown on a graph (Figure 5). If the budget is limited, the cumulative process can easily be grasped within the budget. Conversely speaking, we can determine the cost for the cumulative process if it is previously decided.

Table.8 Total Score for each FDA

FDA No	Sum of All CCP	Sum of Old CCP	Ratio of Decreptitude	Score.1	Defective Conductors	Valuable Conductors	Ratio of Defective
4160	4160.00	2872.00	282.00	9.82	0.00	28.00	900.00
3021	3021.00	2927.00	266.00	9.09	0.00	8.00	800.00
4133	4133.00	4269.00	442.00	10.35	0.00	19.00	900.00
2180	2180.00	909.00	185.00	20.35	0.00	11.00	200.00
4143	4143.00	2251.00	468.00	20.79	0.00	23.00	500.00
5050	5050.00	784.00	11.00	0.00	0.00	11.00	268.00

V: Ratio of Defective	Score.2	Number of F	Failures per Unit	Down Time	Failure Index	Score.3	Used Conductors	Demand	D
4160	00	3.11	6.00	30.00	3.33	1323.00	4410.00	10.00	720.00
3021	00	1.00	2.00	59.00	7.38	519.00	3827.63	10.00	648.00
4133	00	2.11	4.00	27.00	3.00	517.00	1551.00	6.00	810.00
2180	00	5.50	10.00	11.00	5.50	520.00	2860.00	10.00	141.00
4143	00	4.60	8.00	22.00	4.40	517.00	2274.80	8.00	409.00
5050	00	5.50	10.00	11.00	5.50	255.00	1858.00	6.00	103.00

Used Conduct	Demand	Developing	Dead End	Score.4	Area Rank	Score.5	INS64 Conductors	Score.6	Total Score
4160	720.00	655.00	44.00	0.78	2.00	2.00	6.00	34.00	6.00
3021	648.00	762.00	271.00	1.29	10.00	2.00	6.00	13.00	2.00
4133	810.00	770.00		0.86	8.00	2.00	6.00	36.00	6.00
2180	141.00	122.00		0.61	2.00	2.00	6.00	3.00	0.00
4143	409.00	356.00		0.71	2.00	2.00	6.00	14.00	2.00
5050	103.00	103.00		0.00	6.00	2.00	6.00	1.00	0.00

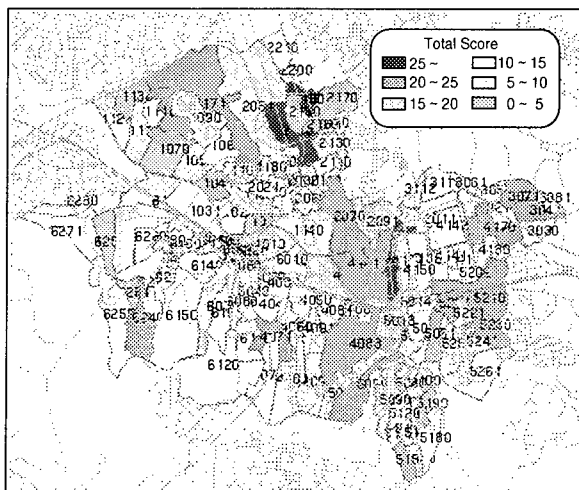


Figure.4 Distribution of Total Score

3. VERIFICATION of THE EFFECT of RENEWAL

After renew all of CCP cables, the effect appears in the form of decreased failures. The distribution of failures before renewal is shown in Figure.6, and the distribution of failures after is shown in Figure.7.

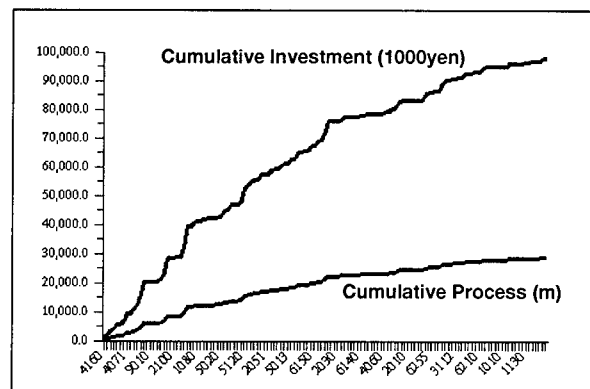


Figure.5 Cumulative Process and Investment

In comparing the two figures, it can be seen that failures in FDA No.5050 have decreased. As this FDA was given high priority, the effects appeared early. The number of failures in the whole of the central office area decreased from 64 to 29. This confirms that effective renewal was achieved using this method.

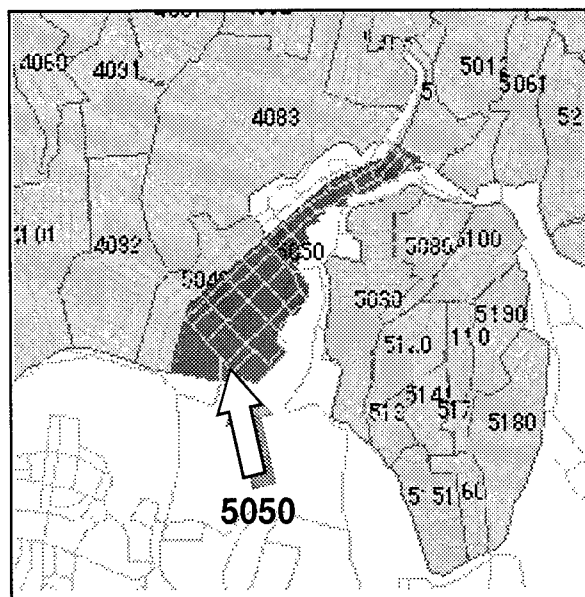


Figure.6 Distribution of Failures before Renewal

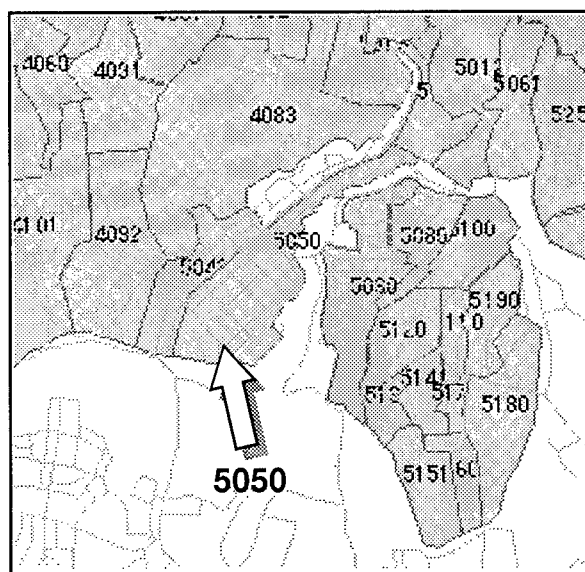


Figure.7 Distribution of Failures after Renewal

4.CONCLUSION

In order to comprehensively evaluate many areas like FDA in management of a metallic access network, it is effective to give a score based on various factors and to accumulate these scores in such a way that the evaluation is objective and unaffected by who performs the analysis. It is then easy to decide the order of priority for renewal based on numerical evaluation. Future, by using

this method, it is possible to determine the approximate product process and investment efficiently, and to flexibly cope with changes of process limits or budget. As this method is systematic, it can be performed on a personal computer, so labor for planning investment is greatly reduced. For this particular case, we used the support system for access network management, developed by our group. Of course, the standards for giving scores are variable, so it is possible to perform various simulation in order that the policy and objectives of any branch office can be reflected in the investment plan.

ACKNOWLEDGEMENTS

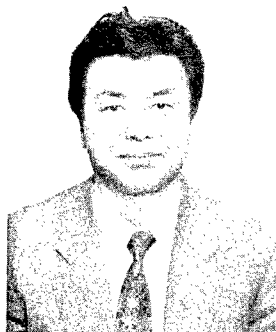
The authors wish to gratefully acknowledge the guidance of Tamaki Ito and Masayuki Suwa. Thanks are also due to Hideki Ueno at Ehime branch office for his cooperation.

REFERENCES

- [1]Y.Wakui "Environment of Optical Access Technology "Proceeding NTT Technical Journal Apr.1994 Vol.6 No.4 in Japanes
- [2]T.Ito, 45th IWCS, "Management for deployment of the optical access network", Nov.1996H.Ishihara"Design for Access Network Facilities" Proceeding Ohm Co. Ltd. in Japanes
- [3]H.Ishihara "Design for Access Network Facilities" Proceeding Ohm Co. Ltd. in Japane



Daisuke Tomizu
NTT Access Network Systems Laboratories
1-7-1 Hanabatake, Tsukuba-shi, Ibaraki, 305
JAPAN
Daisuke Domizu recieved his B.E.and M.E. degrees in civil engineering from Kyoto University in 1992 and 1994. He joined NTT in 1994. He is engaged in the development of access network management system at NTT.

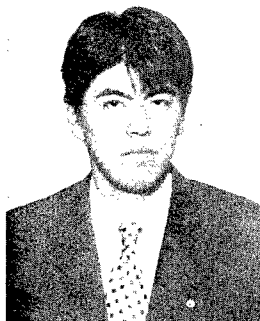


Hiroshi Harada

NTT Access Network Systems Laboratories

**1-7-1 Hanabatake, Tsukuba-shi, Ibaraki, 305
JAPAN**

Hiroshi Harada is Senior Research Supervisor at NTT Access Network Systems Laboratories. He joined NTT in 1965. He is engaged in the development of operation system as a system engineer at NTT Access Network Systems Laboratories, Japan.



Masateru Inoue

NTT Access Network Systems Laboratories

**1-7-1 Hanabatake, Tsukuba-shi, Ibaraki, 305
JAPAN**

Masateru Inoue joined NTT in 1996. He was engaged in the development of access network management system at NTT Access Network Systems Laboratories, Japan.

CROSSTALK MODEL FOR PAIR-SHIELDED DATA CABLES

Martin Backmann, Dr. Christian Pfeiler, Andreas Waßmuth

NOKIA KABEL GMBH, Nuremberg, Germany

ABSTRACT

Due to the increasing demand for higher bandwidth the frequency and dynamic range covered by copper data cables is expanding. Generally well designed and produced cables using the technology of individually shielded pairs (S/STP) are capable to provide a positive attenuation-to-crosstalk-ratio (ACR) even for hundreds of MHz.

During the development phase from 100 MHz (Cat. 5, ISO 11801) /1/ to 600 MHz (Cat. 6, E DIN 44312/5) /2/ especially crosstalk performance has to be improved. The possibilities for improvements in attenuation for given impedance and conductor diameter are limited.

It is found that extremely length dependent effects are visible. Measurements show a length dependent crosstalk maximum which is above the specified limit at frequencies of about some 10 MHz when the length of the cable is 100 m or shorter. For different Cat. 5-cables it is found that for standard delivery length a crosstalk level of 80...90 dB up to 100 MHz is normal and the maximum only occurs when cutting down to shorter length (≤ 100 m).

Therefore the need for a special cable design appears to guarantee Cat. 6-performance for horizontal cables. Before defining design rules a mechanism explaining this effect is described. Computer simulations are compared with measurements to put some evidence in the model. It leads to a deeper understanding for an optimised cable design to avoid crosstalk problems, an essential aspect of future data cable design /3/.

Before the introduction of the crosstalk model the transfer impedance of the individual pair shield is described by the formulas known from literature. The impact of the transfer impedance values on the crosstalk of the S/STP-cables is discussed later.

TRANSFER IMPEDANCE OF SINGLE SHIELDED PAIRS

During the measurement of the transfer impedance of symmetrical cables the even-mode of a pair is considered and can be regarded as a coaxial cable. If the outer conductor of the coax is a metal foil of the width b wrapped around the insulated inner conductor with a radius r , the lay length l , the thickness d and the conductivity κ , the transfer impedance can be calculated as follows /4/

$$Z_k = R_0 \left(\frac{1}{\sin^2(\alpha)} + \frac{jrd}{\delta^2 \tan^2(\alpha)} \right), \quad (1)$$

with the DC-resistance

$$R_0 = \frac{\sqrt{l^2 + (2\pi r)^2}}{lbd\kappa},$$

the angle

$$\alpha = \arctan\left(\frac{l}{2\pi r}\right)$$

and the depth of penetration

$$\delta = \frac{1+j}{\sqrt{j\omega\mu_0\kappa}}.$$

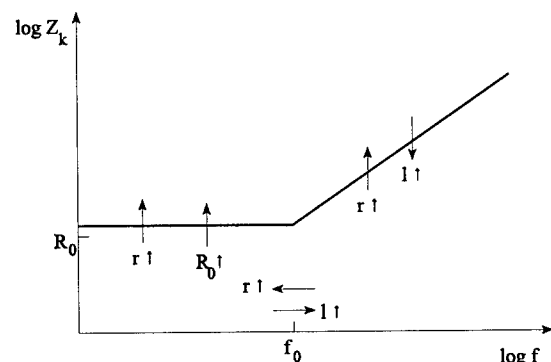


fig. 1 schematic frequency effect of the transfer impedance of a single shielded pair and influence direction of the main parameters

The transfer impedance of a single shielded pair of a standard Cat. 5 quality is up to a frequency of approximately 1 MHz constant. The value is a little bit higher than the DC-resistance. For frequencies higher than 1 MHz the transfer impedance is proportionally rising with the frequency. That is due to the inductivity of the wrapped metal foil. The influence of the variation of the main parameters on the transfer impedance of a single shielded pair is shown in fig. 1.

As the screening effect is high when the transfer impedance is low it is necessary to achieve a minimum relation between the values at the highest and lowest considered frequency. Fig. 1 and eq. (1) show different alternatives. Especially the diameter of the shield has high impact on transfer impedance, but also on other transmission parameters.

NEXT-MODEL FOR S/STP-CABLES

The near end crosstalk between two individually shielded pairs is caused by a multi step mechanism:

- 1) The interfering pair is fed at the near end with a signal in odd-mode. Due to non-ideal symmetry of the pair a part of this signal converts to even-mode. This results in a current in the shields.
- 2) The current causes an even-mode voltage in the interfered pair. The interference mechanism is described by the transfer impedance of the shielded pair; the transfer impedance is per definition the ratio of the even-mode voltage and the current in the shield.
- 3) Due to non-ideal symmetry of the interfered pair a part of the even-mode voltage converts to odd-mode and can be detected as crosstalk.

Besides the frequency effect of the transfer impedance the frequency dependent attenuation is important for the frequency effect of the crosstalk. Furthermore it is to be considered that the even-mode of a shielded pair is in most cases not terminated with the characteristic impedance of the even-mode waves.

The following simplifications are assumed for further modelling:

- The signal amplitude in even-mode and odd-mode are always connected by a constant value of the longitudinal conversion loss α_{LCL} . This is not dependent on the direction of conversion nor of the frequency.
- A current distribution in the shields of the pairs is not taken into consideration.
- The even-mode is not terminated; the magnitude of the reflection coefficient is 1.
- The superposition of partial waves is always constructive; the phases are disregarded.
- The attenuation in even-mode and odd-mode is the same.
- The transmission lines are homogeneous.

The following data are assumed (Cat. 5 S/STP cable):

- even-mode characteristic impedance:

$$Z_g = 30 \, \Omega$$

- velocity of propagation:

$$v = 0.8 \, c_0$$

- longitudinal conversion loss:

$$\alpha_{LCL} = -40 \, \text{dB}$$

- propagation constant:

$$\gamma = 2,4 \frac{\text{mNp}}{\text{m}} \sqrt{\frac{f}{\text{MHz}}} + j \frac{\omega}{v}$$

- transfer impedance:

$$Z_k = \begin{cases} 0.1 \frac{\Omega}{\text{m}}, f \leq 1 \text{MHz} \\ 0.1 \cdot e^{2,65 \log\left(\frac{f}{\text{MHz}}\right)} \frac{\Omega}{\text{m}}, f > 1 \text{MHz} \end{cases}$$

For the crosstalk sum four different signal paths of direct NEXT or caused by reflection are considered (fig.2):

- 1) A part of the transmitted signal in pair 1 converts to even-mode, influences pair 2 via near-end-crosstalk (NEXT), converts back to odd-mode and is received at A2. The NEXT between two coaxial elements is $/4/$:

$$\alpha_n = 20 \log \frac{Z_k}{4Z_g |\gamma|}$$

For the first partial wave the attenuation sum is:

$$\alpha_1 = 2\alpha_{LCL} + \alpha_n$$

- 2) Another partial wave converts to even-mode, propagates to E1, after a total reflection occurs at the open end E1 influences pair 2 via far-end-crosstalk, converts back to odd-mode and is received at A2.
- 3) Same like 2 but: first conversion to even-mode, far-end-crosstalk (FEXT) to E2, total reflection, propagation to A2 and conversion to odd-mode. For FEXT holds $1/4$:

$$\alpha_f = 20 \log \left(\frac{Z_k l}{2Z_g} \right) - 20 \log(e) \operatorname{Re}(\gamma) l$$

The attenuation sum for the paths 2) and 3) is identical:

$$\alpha_{23} = 2\alpha_{LCL} + \alpha_f - 20 \log(e) \operatorname{Re}(\gamma) l$$

- 4) Propagation to E1, conversion to even-mode, near-end-crosstalk to E2 and total reflection at E2 followed by propagation to A2 and conversion to odd-mode. The attenuation for this partial wave is:

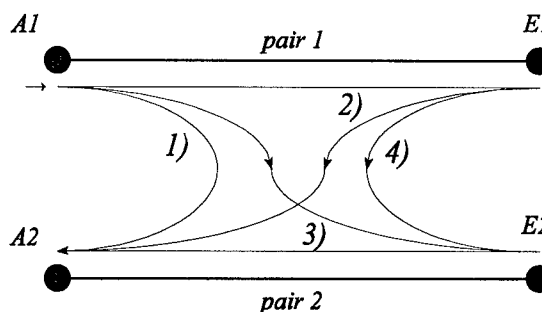


fig. 2 paths of crosstalk and reflection waves taken under consideration for crosstalk calculation

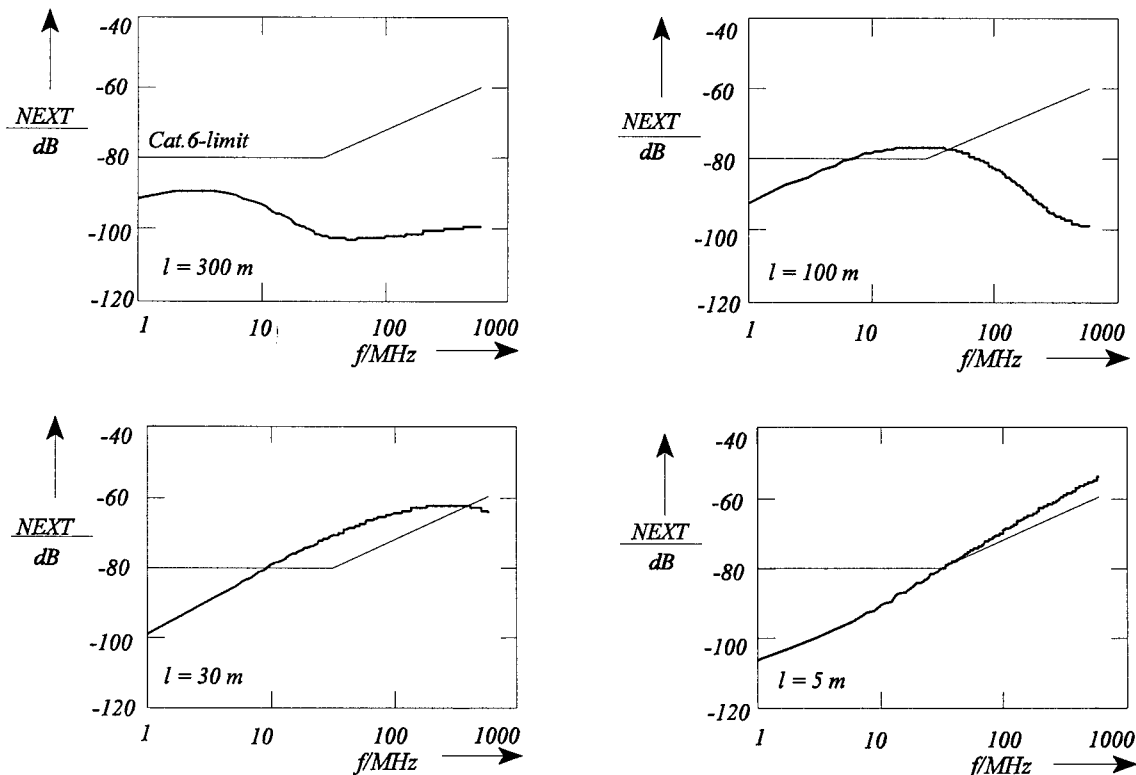


fig. 3 evaluation of the crosstalk model for various cable lengths

$$\alpha_4 = \alpha_n - 2(\alpha_{LCL} - 20 \log(e) \operatorname{Re}(\gamma) l)$$

The amplitudes of the partial wave are added and the resulting NEXT is:

$$\alpha_{res} = 20 \log \left(10^{\left(\frac{\alpha_1}{20}\right)} + 2 \cdot 10^{\left(\frac{\alpha_{23}}{20}\right)} + 10^{\left(\frac{\alpha_4}{20}\right)} \right) \quad (2)$$

The evaluation of eq. 2 for four different cable length is shown in fig. 3. Only for the length of 300m the calculated NEXT is below the specified limit. For the typical length of horizontal wiring (< 100 m) the crosstalk maximum is above the NEXT limit /2/. The frequency range for maximum value decreases with the cable length increasing. For longer cable length the characteristic maximum shifts towards lower frequencies reducing its maximum value at the same time.

The most important parameters are the longitudinal conversion loss (LCL) and the transfer impedance of the single shielded pair. A reduction of 1 dB in LCL leads to a reduction of 2 dB in NEXT. Also by improving the transfer impedance of the single shielded pair the maximum value of the NEXT maximum is reduced. So it is possible to meet the Cat. 6 requirements at a constant LCL level.

COMPARISON OF THE MODELS AND MEASUREMENTS

Fig. 4 presents the measured and calculated values of the transfer impedance for two variations of a single screened pair. The foil of variation 1) has a shorter lay length and a smaller width compared to variation 2).

A helpful characteristic value is the ratio of the transfer impedance at 100 MHz and the DC-resistance of the pair shield. For a Cat. 6-type this ratio should be 10 times smaller than for a Cat. 5 typ.

Fig. 5 presents measurements of the near-end-crosstalk for different length of a Cat. 5 cable. The comparison with fig. 3 shows generally a good fit. Especially the position of the length dependant maximum shows a good correspondence.

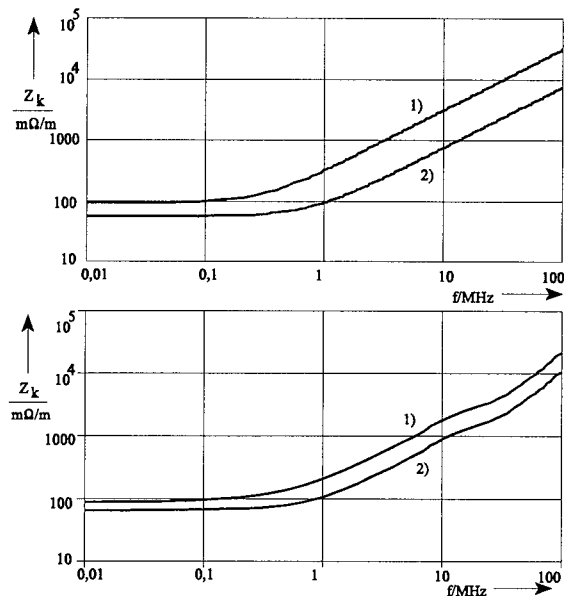


fig. 4 comparison of calculation and measurement of the transfer impedance of two types of single shielded pairs; 1) has shorter length of lay and smaller foil width than 2)

Nevertheless it can be seen from the measurement at longer length that further effects lead to a rising NEXT at higher frequencies. This can possibly be led back to direct coupling by electric or/and magnetic fields.

The measurement for short length shows effects of resonances. This is not taken into account in the presented model but indicates clearly the importance of the termination of even- and odd-mode waves.

CONCLUSION

The presented model enables an improved design of S/STP data cables. The model is based on a coupling theory that takes the conversion between odd-mode and even-mode, transfer impedance of the single shielded pair and the theory for far end and near end crosstalk of coaxial lines into account.

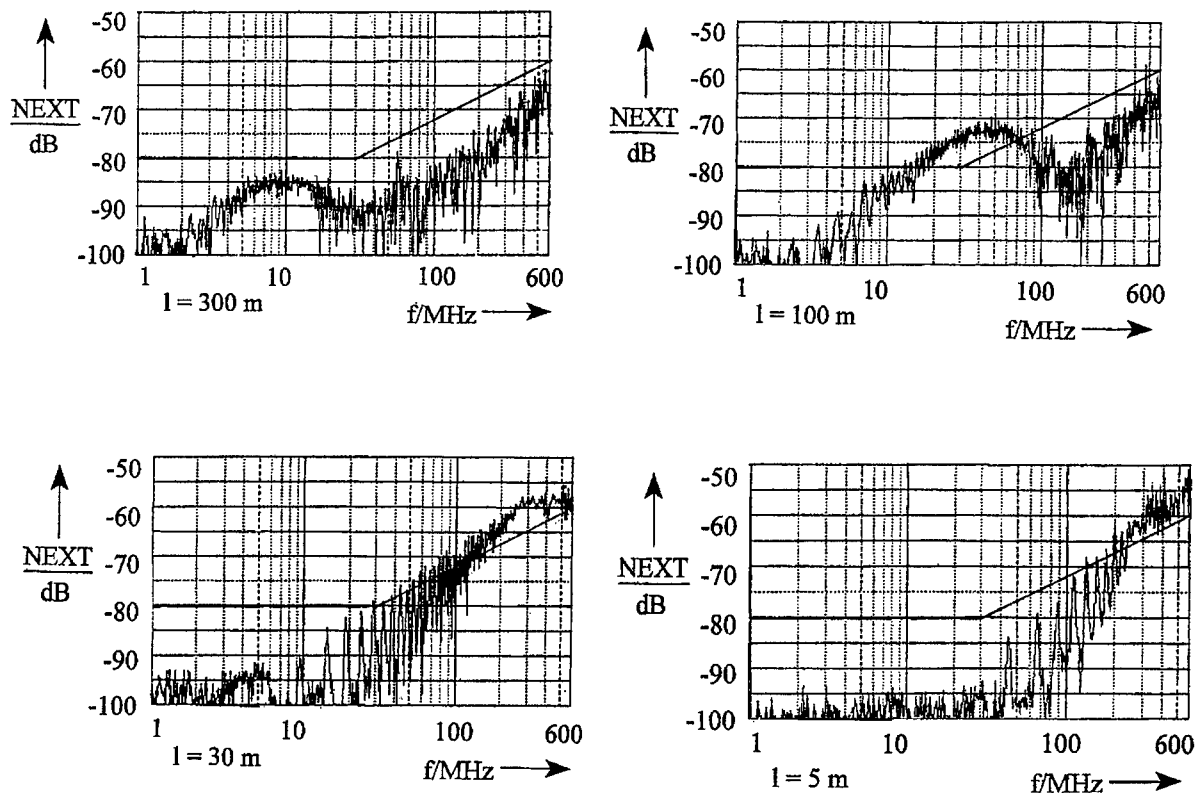


fig. 5 crosstalk measurement of a Cat. 5 S/STP-cabel at various lengths

The crosstalk model also explains the unexpected differences of the measurement results between typical production and installation length. This leads to additional requirement for quality

control and measurement to avoid that special problem.

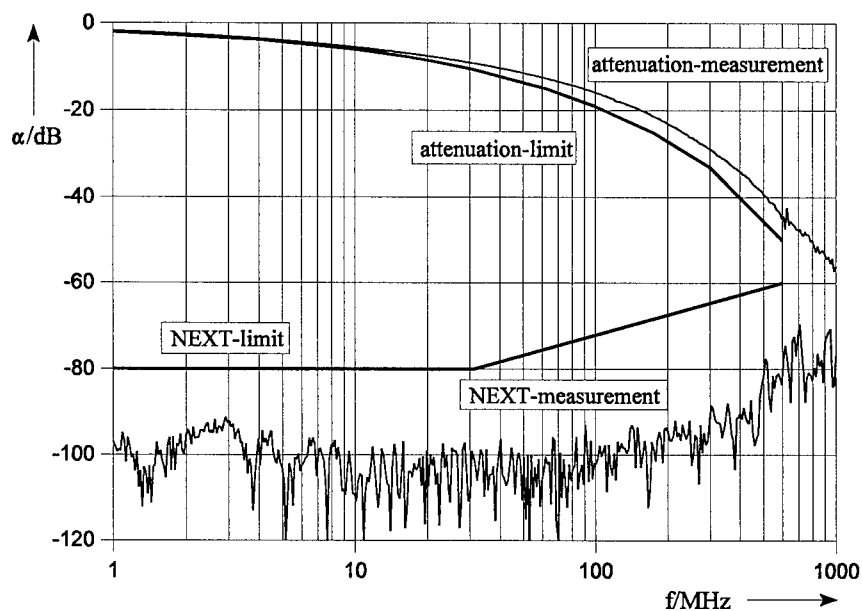


fig. 6 crosstalk and attenuation measurement of a high end Category 6 cable (UC 600 SS 22 4P, NOKIA KABEL GMBH); length of cut $l = 90$ m

Fig. 6 shows as a result a NEXT and attenuation measurement of a high end S/STP cable (100m). Positive crosstalk-to-attenuation-ratio (ACR) up to frequencies high above 600 MHz is achievable with respect to the mentioned design rules.

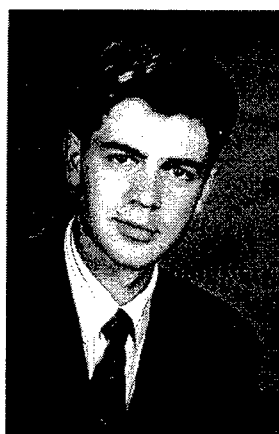
REFERENCES

- /1/ ISO/IEC 11801:1995: Information technology - Generic cabling for customer premises.
- /2/ E DIN 44312-5:1996-08: Anwendungsneutrale Verkabelungssysteme, Teil 5: Verkabelungsstreckenklasse E.
- /3/ *Waßmuth, A.*: Quo vadis Kupferkabel? Zukunft der symmetrischen Datenübertragungskabel. *telekom praxis*, Heft 1/1996, p. 28-32
- /4/ *Kaden, H.*: Wirbelströme und Schirmung in der Nachrichtentechnik. Springer-Verlag, 1959

AUTHORS



Martin Backmann (32) received his diploma in mechanical engineering in 1991 at the RWTH Aachen University. He joined the process development department of NOKIA KABEL GMBH in 1991 and has been involved in various projects for new data cable technology.



Christian Pfeiler (32) received his diploma in electrical engineering in 1990 at the University of Dortmund. In 1995 he obtained a doctor's degree (Dr.-Ing.) at the same university. He joined the product development department of NOKIA KABEL GMBH in 1995.



Andreas Waßmuth (35) joined the company after his studies in electrical engineering at Ruhr Universität Bochum in 1986. After positions in development and support for Local Area Networks he took over responsibility for the R&D-activities of copper telecommunication cables.

Mailing address

NOKIA KABEL GMBH
 Wohlaue Strasse 15
 D-90475 Nuremberg
 Phone: +49 911 8337 176
 Fax: +49 911 8337 206
 Email: christian.pfeiler@x400.nokia.lion.de

Relating Total Reflected Energy to Input Impedance in Balanced Pair Transmission Lines

T. M. Hayes
Bell Laboratories
Lucent Technologies
Norcross, Georgia 30071

Abstract: Structural return loss (SRL) and characteristic impedance (Z_0) have been important parameters within the Categories 3, 4, and 5 industry standards for several years^{1,2}. There is a wealth of contributions within IWCS as well as standards bodies that develop and validate these parameters. Recently there has been a growing departure from these separate metrics in favor of input impedance (Z_{in}). Emerging specifications, marketing information, and popular perception have attempted to position Z_{in} as the preferred method of specifying reflected energy in premises cabling. This paper will investigate the appropriateness and robustness of input impedance as an exclusive limit to total reflected energy (S_{11}).

Introduction:

Before reviewing the relationship between various measures of cable signal reflection, it is important to recognize that the received signal quality is ultimately the only parameter of concern. Reliable reflection parameters such as return loss (RL), Z_0 , and SRL have been specified because they are readily measured³ and can be non-deterministically related to received signal noise⁴. We have seen from previous work that SRL leads to received noise (excess loss and delay jitter) about 10dB weaker than near end cross-talk (NEXT) noise for cables exhibiting Category 5 levels of performance.⁴ Significant improvements in NEXT beyond Cat 5 have warranted modest improvement in SRL in order to maintain the same relative importance in the noise contribution.

This paper will utilize actual cable measurement data to evaluate the volatile nature of Z_{in} . It will be seen that cable pairs that fail a given requirement for return loss will often pass an equivalent input impedance specification by chance of the phase relationship to both random

and periodic structure. Time and frequency domain representations of S_{11} , the actual measured reflection coefficient, will be explored to gain understanding of the observed variation and poor repeatability of Z_{in} . Further, a statistical approach will quantify the mean energy content "missed" or not represented in the input impedance response of a broad selection of standard and premium grade Category 5 cables available on the market today. Finally, mathematical modeling will further support the measurement evidence.

Definitions:

- S_{11} (Reflection Coefficient)^{3,5} \equiv ratio of complex amplitudes of the reflected and incident voltage waves - This is the measured value!
- Impedance \equiv Complex proportionality constant between the voltage and current⁶

$$\text{(Ohms } \Omega\text{): } Z = \frac{V(\text{voltage})}{I(\text{current})}$$

- Return Loss \equiv Total reflected energy (dB): reflection due to impedance mismatch and non-uniform structure:

$$RL = -20 \log |S_{11}| = -20 \log \left| \frac{Z_{in} - 100}{Z_{in} + 100} \right|$$

(ASTM D 4566 eqn 40 referenced to 100 Ω)

- Structural Return Loss \equiv reflected energy (dB) due to non-uniform structure

$$SRL = -20 \log \left| \frac{Z_{in} - Z_0}{Z_{in} + Z_0} \right|$$

(ASTM D 4566 eqn 39)

- Z_0 (ohms) Characteristic Impedance \equiv Impedance that is 'characteristic' or representative of the cable - this value is mainly a function of material and geometry. ASTM D 4566 Characteristic Impedance-METHOD 3 best describes the general case.

- Input Impedance (ohms):

$$Z_{in} = 100 \cdot \frac{1 + S_{11}}{1 - S_{11}} \quad (\text{ASTM D4566 eqn 34})$$

referenced to 100Ω

Notice that RL and Z_{in} are mathematically related. As a complex quantity, Z_{in} represents the total reflected energy. However, apparently in order to maintain simple specifications or facilitate direct measurements on a network analyzer, input impedance specifications only rely on the magnitude of Z_{in} ($|Z_{in}|$) or the real part of Z_{in} . Consequently a portion of the reflected energy is not represented when the imaginary or phase components of Z_{in} are dropped from the response. Equation 34 decreases the relative significance of the imaginary portion by an order of magnitude. Herein lies the impairment of $|Z_{in}|$ to assure that specified reflection performance is realized. If Z_{in} specifications were of the type of an ellipse centered at $100 + j0\Omega$ much of this difficulty would be eliminated.

Conversely, in the computation of RL and SRL the real and imaginary components of S_{11} are equally weighted and thus avoid the impairment which Z_{in} suffers. Additionally, RL can be measured directly without computer processing therefore little rational can be offered to favor $|Z_{in}|$ specifications.

Complex Math Fundamentals:

For our purposes, a complex number is used to express the magnitude and phase of a sinusoidal signal or the relationship of multiple sinusoids.

<u>sinusoidal</u> <u>signal</u>	<u>polar</u> <u>representation</u>	<u>rectangular</u> <u>representation</u>
$\cos(\omega t + 0)$	$1 \angle 0$	$1 + j0$
$0.5 \cos(\omega t + \pi/3)$	$0.5 \angle \pi/3$	$0.25 + j0.433$

where $\omega = 2\pi \cdot \text{frequency}$

$$2\pi \text{ radians} = 360^\circ$$

A complex number has two parts:

- in rectangular form \rightarrow real and imaginary: $C = a + jb$ where
 $j = \sqrt{-1}$
- in polar form \rightarrow magnitude and phase:

$$|C| = \sqrt{a^2 + b^2} \quad \phi = \tan^{-1}\left(\frac{b}{a}\right)$$

$$a = |C| \cos \phi \quad b = |C| \sin \phi$$

Industry Representative Category 5 Cable

Sample 1: A 100m sample was arbitrarily chosen from within a 1000' package for study. The following charts illustrate the measured reflection performance of a cable pair.

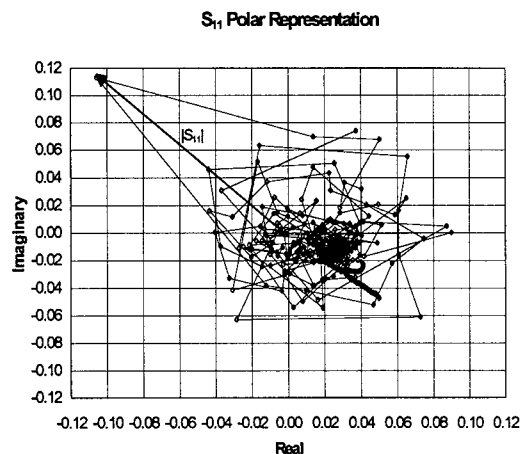


Figure 1: S-Plane Result

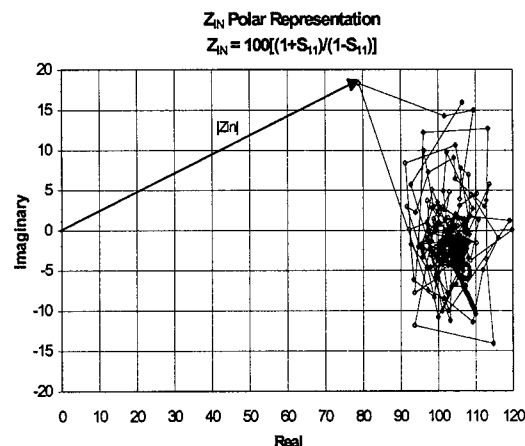


Figure 2: Z-Plane Result

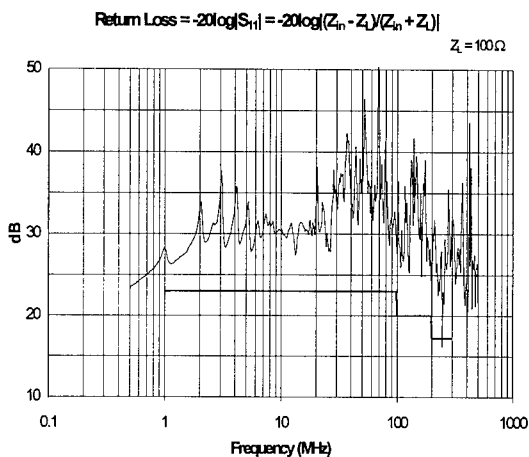


Figure 3: Return Loss Result

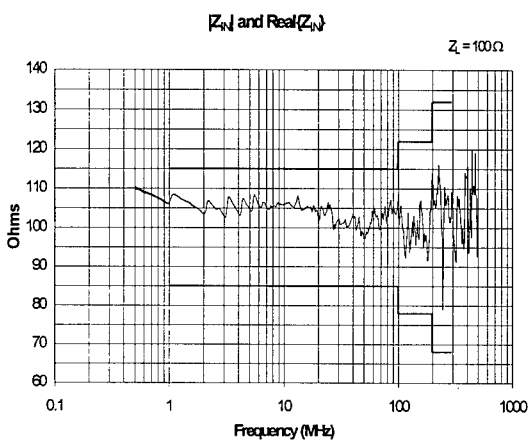


Figure 4: $|Z_{in}|$ and $\text{Real}\{Z_{in}\}$ Results

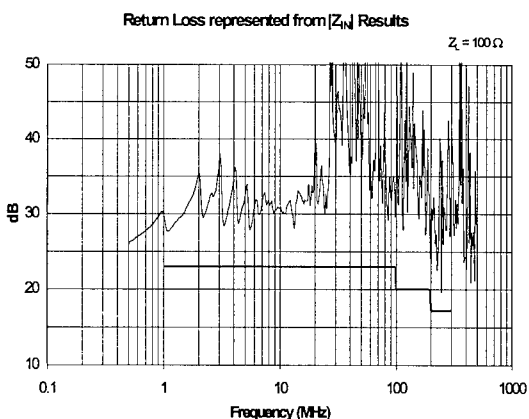


Figure 5: Equivalent Return Loss from $|Z_{in}|$

Figures 1 and 2 show the swept frequency results of S_{11} and Z_{in} in rectangular coordinates (S-plane and Z-plane respectively). Notice that S_{11} is evenly distributed about the origin ($0+j0$) while Z_{in} is centered about $100+j0$. All the

reflection information is conveyed in both charts. Because Z_{in} (complex) is biased about the characteristic impedance (approximately 100Ω), the imaginary axis information is generally de-emphasized more than 10 to 1. The magnitude of the vector from the origin to the worst case reflection is substantially comprised of the real component. This is further illustrated in Figure 4 where the magnitude and real portions of Z_{in} are plotted versus frequency. It is difficult to discern the two traces due to their near equality. Figure 3 shows the true return loss and an equivalent RL specification derived from a popular proposed $|Z_{in}|$ requirement plotted versus frequency. Figure 5 illustrates the RL captured in $|Z_{in}|$ with the above mentioned equivalent spec.

If these specs are used for pass/fail criterion the following conclusions would result:

Figure 3: fail (min margin = -1.0dB)

Figure 4: pass (min margin = $+13.1\Omega$)

Figure 5: pass (min margin = $+2.4\text{dB}$)

Details of the calculations are as follows:

$S_{11} = -0.106 + j0.113$ (actual measured value of reflection coefficient @ 246.3MHz)

$$S_{11} = 0.155 \angle 133.2^\circ$$

$$\begin{aligned} \text{RL} &= -20\log|-0.106 + j0.113| \\ &= -20\log(0.155) = 16.19\text{dB} \end{aligned}$$

$$\begin{aligned} Z_{in} &= 100 \left(\frac{1 + (-0.106 + j0.113)}{1 - (-0.106 + j0.113)} \right) \\ &= 78.964 + j18.285 = 81.053 \angle 13.038^\circ \Omega \end{aligned}$$

$$\text{RL}_{\text{from } |Z_{in}|} = -20 \log \left| \frac{81.05 - 100}{81.05 + 100} \right| = 19.60\text{dB}$$

The results obtained from the $|Z_{in}|$ data understate the total reflected energy at 246.3MHz by 3.4dB . In this case, this error results in the incorrect pass/fail decision. Additionally, this error is not confined to worst case points but rather is a random variable affecting all measured frequencies.

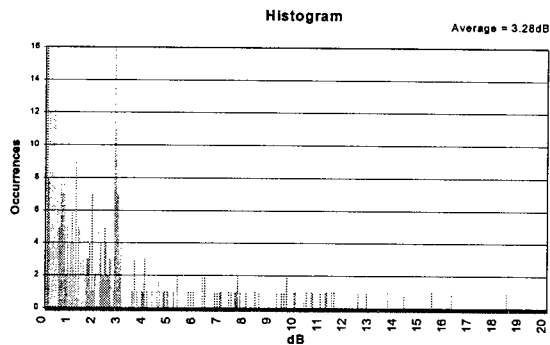


Figure 6: Swept Frequency Error Histogram

Figure 6 illustrates a histogram describing the degree to which $|Z_{in}|$ understates the total reflected energy at all measured frequencies. On a log basis, 3.28dB is the average observed error. The range is approximately 0 - 18dB. Stated in linear terms; $|Z_{in}|$ reports approximately 61.35% of the total reflected energy in this sample. Nearly 40% of the information is lost. These statistics were derived by integrating the RMS power over frequency.

The magnitude of the S_{11} vector illustrated in Figure 1 is independent of the phase. Rotating this vector will not change the return loss reported. However, the magnitude of the Z_{in} vector illustrated in figure 2 is phase dependent. Rotating the Z-Plane data will cause significant changes in the reported input impedance. The next example will explore this phenomenon with results of a cut and test experiment from a given cable pair.

Industry Representative Category 5 Cable

Sample 2: A different 100m sample was arbitrarily chosen from within a 1000' package. The following charts illustrate the measured reflection performance of a cable pair. The measurements were taken initially. Then, while minimally disturbing the test sample, the cable was cut 12" from the near end and measurements were again taken.

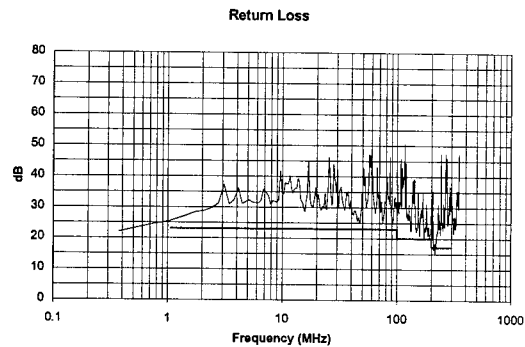


Figure 7: Initial RL Result

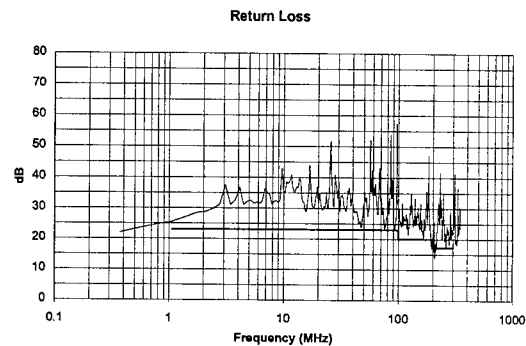


Figure 8: RL Result After Cut

Figures 7 and 8 illustrate the actual return loss computed directly from S_{11} for both before and after cut cable conditions. The two traces show close agreement. Certainly the same pass/fail decision results. Subtle differences are thought to be related to the slight alteration of the cable (removing 12") and the new relative loss (α) weighting of the roughness function.

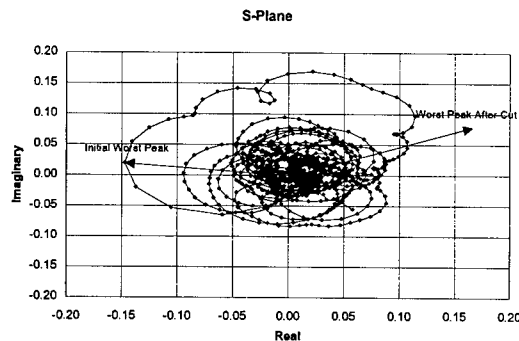


Figure 9: Initial S-plane Result

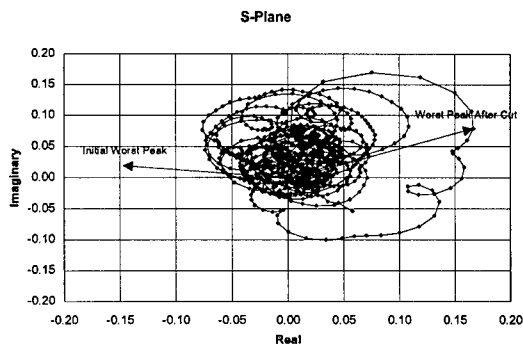


Figure 10: S-plane Result After Cut

Figures 9 and 10 illustrate polar representations of S_{11} . RL is simply $-20 \cdot \log(|S_{11}|)$. The phase dependence at the measurement end is clearly demonstrated. Cutting the sample causes a rotation of points about the origin in the S-plane. Worst case vectors are included to facilitate comparison of the 208.37MHz results before and after cutting. The magnitude differs slightly due to the periodic and random structure interaction and relative attenuation weighting as discussed above.

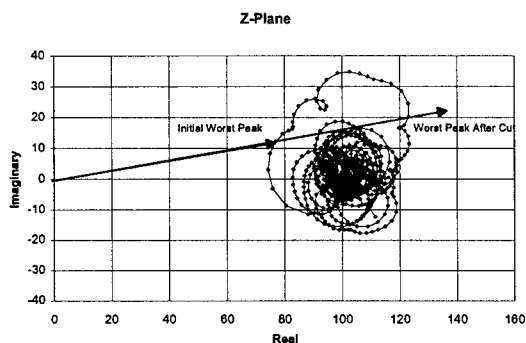


Figure 11: Initial Z-plane Result

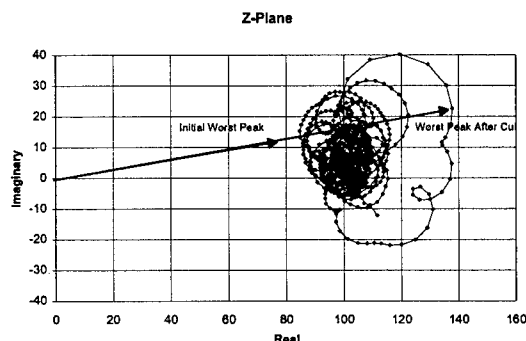


Figure 12: Z-plane Result after Cut

Figures 11 and 12 illustrate polar representations of Z_{in} . Z_{in} is computed from S_{11} as shown in equation 34. All the reflection information is

contained in these figures. If one visualizes upper and lower spec limits at 115Ω and 85Ω it is readily seen that significant energies are permitted in the imaginary direction. Again, this is the case due to the scale of real and imaginary terms. The vector from the origin to each measurement point is almost entirely real. Cutting the sample causes a rotation of points about $Z_0 + j0$ in the Z-plane. Worst case vectors are included to facilitate comparison of the 208.37MHz results before and after cutting.

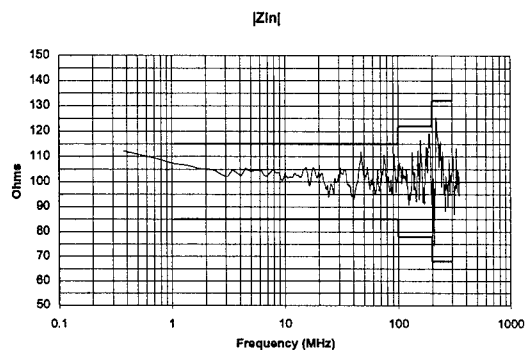


Figure 13: Initial Input Impedance Result

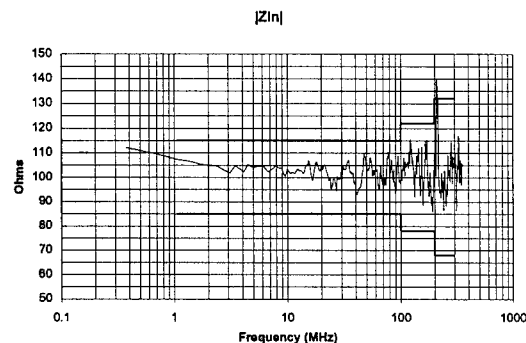


Figure 14: Input Impedance Result After Cut

Figures 13 and 14 illustrate the frequency domain representation of $|Z_{in}|$. Input impedance at individual frequencies can swing wildly because of the effect previously described. Here, a 60Ω change is observed at 208.37MHz as the result of cutting 0.3% of the sample length (12").

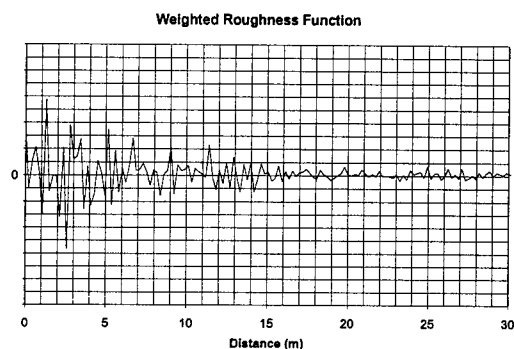


Figure 15: Initial Impedance Time Response

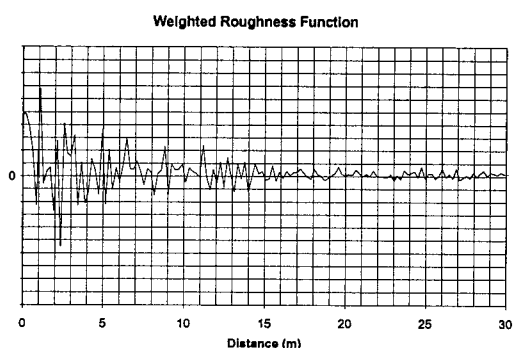


Figure 16: Impedance Time Response After Cut

Figures 15 - 16 illustrate time domain representations of S_{11} on a linear basis. S_{11} frequency domain results were transformed to the time/distance domain⁷ to gain insight into the similarities and differences of the results. Although difficult to resolve in the illustrations, strong features were shifted by -12 inches after cut and retest.

	Initial Result	After Cut
S_{11}	$-0.125+j0.077$	$0.167+j0.079$
RL (dB)	16.65	14.68
$Z_{in} (\Omega)$	$76.92+j12.15$	$137.88+j22.51$
$ Z_{in} (\Omega)$	77.9	139.7

Table 1: 208.37 MHz Results

The phase response is established at the measurement interface. Cutting seemingly insignificant lengths from the cable results in a frequency dependent different phase response. This is illustrated in the S and Z-plane figures 9-12. Cutting just 12" results in a substantial rotation in the S-plane. Consequently, if one assumes that $|Z_{in}|$ = "actual impedance" only chance or luck would prevail regarding the assessment of quality.

In general, Z_{in} will understate the actual reflection to a large extent (a later section will statistically quantify). If the reflection is entirely in the quadrature component, $|Z_{in}|$ would report perfect performance (no reflection) at that select frequency. In reality, there would be a finite reflection. Only when S_{11} is entirely real would $|Z_{in}|$ represent the full reflection. The IEC has recognized this difficulty and only specifies input impedance in transmission lines void of significant structure.²

In the above example, the cable was altered by 0.3% while the input impedance changed 79.4%. It is exceedingly improbable that the actual relationship of voltage and current altered to the same degree. The time domain sequences suggest quite the opposite. The responses are nearly identical except shifted by one foot. The conclusion should be that input impedance is not equal to impedance (Z_0) for pairs with structure. Consequently, it is inaccurate to suggest that input impedance is the "true", "unaveraged", or "actual" impedance.

Theoretical Model:

The following exercise will demonstrate theoretical agreement with observations made on actual cable measurements. The equation below, taken from a previous IWCS publication⁴, relates a pair's roughness function, characteristic impedance, and propagation constant to reflection coefficient.

$$S_{11}(\omega) = \frac{\gamma(\omega)}{Z_0(\omega)} \int_0^l W(x) e^{-2\gamma(\omega)x} dx$$

ω = radian frequency

x = distance

γ = propagation constant

W = roughness function

Z_0 = characteristic impedance

l = length

A superposition of a normally distributed random variable with a periodic sequence was used for the roughness function $W(x)$ to model random and periodic structure in a transmission line. In this case only one periodic was present but in general there could be many each having arbitrary initial phase.

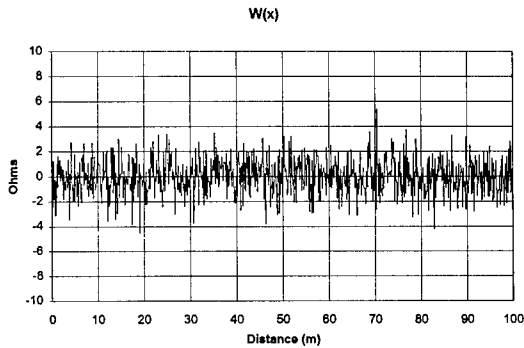


Figure 17: Roughness Function $W(x)$

Iterations of the simulation alter the phase of the periodic without affecting the random structure. This attempts to reproduce the cut and test effect. There is a similar difficulty as with altering a real cable sample. Changing the phase by shifting the $W(x)$ function like cutting the cable results in a different relative weighting on near-by features. Conversely, altering the periodic phase without affecting the random sequence changes the superposition of the two sequences. Each of these approaches yield results similar to observations from actual cable samples.

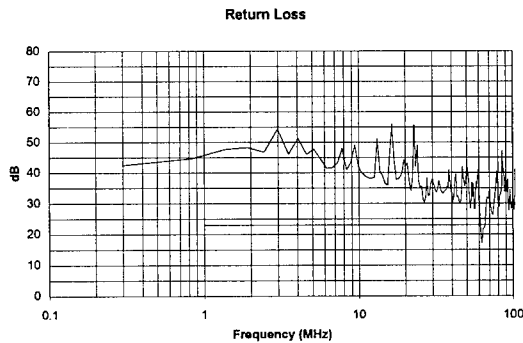


Figure 18: RL from model; phase = 0°

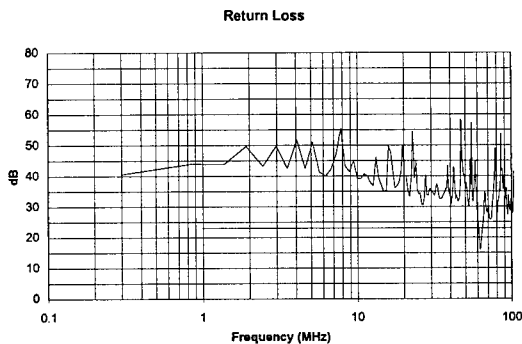


Figure 19: RL from model; phase = 90°

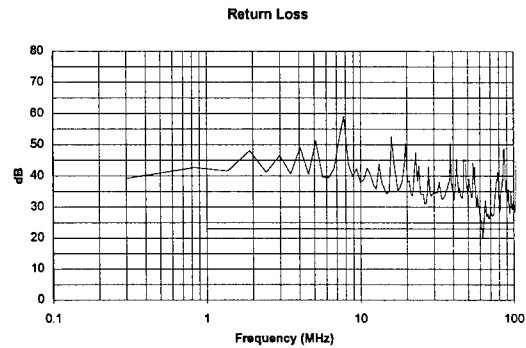


Figure 20: RL from model; phase = 180°

Figures 18-20 illustrate the model RL output for three initial phase relationships. The RL results show close agreement. As in the actual cable sample, subtle differences can be attributed to the weighting and interaction factors. A failure by several dB would be concluded from each condition.

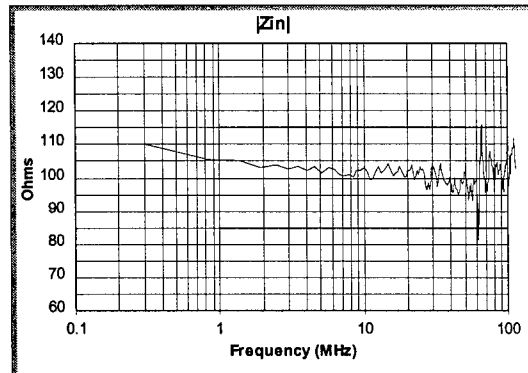


Figure 21: $|Z_{in}|$ from model; phase = 0°

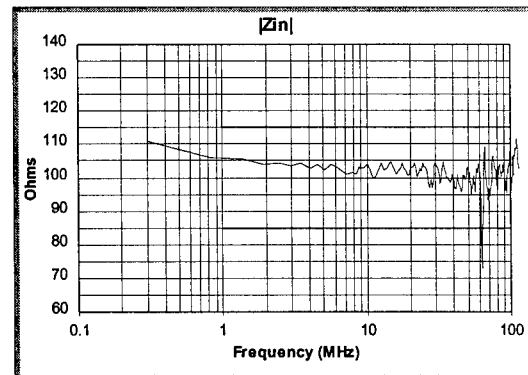


Figure 22: $|Z_{in}|$ from model; phase = 90°

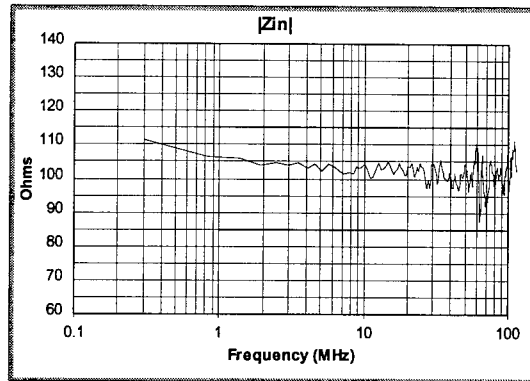


Figure 23: $|Z_{in}|$ from model; phase = 180°

Figures 21-23 illustrate the model $|Z_{in}|$ output for three initial phase relationships. The $|Z_{in}|$ results show average agreement. The random structure is generally similar between all three model iterations. However, at specific frequencies significant variation can result. At 62.5MHz $|Z_{in}|$ varies from 82 Ω , 73 Ω , 110 Ω across the three simulations respectively. Pass/fail determination depends on starting phase. Other frequencies with only random structure can exhibit the same effect to a lesser degree.

Statistical Sampling of Category 5 Cables:

Results from 88 Category 5 cables selected from various manufactures and distribution channels and 272 observations of Lucent data show close agreement. 100m samples were suspended and S_{11} was swept frequency measured and recorded from both ends for each pair of every cable. RMS and dB values were computed from RL and $|Z_{in}|$ for all eight scans from each observation. An average RMS and dB difference statistic was computed for each sample. Finally, statistics from these average differences were computed. The results are illustrated in Figures 24 and 25 and numerated in Table 2.

RL error is defined as the level of energy (in dB) not reported in a $|Z_{in}|$ response. In other words, on average $|Z_{in}|$ reports reflected energy at a level approximately 4.5dB better than the actual level. The RMS approach relates the energies on a linear basis. 5dB equates to approximately 56%.

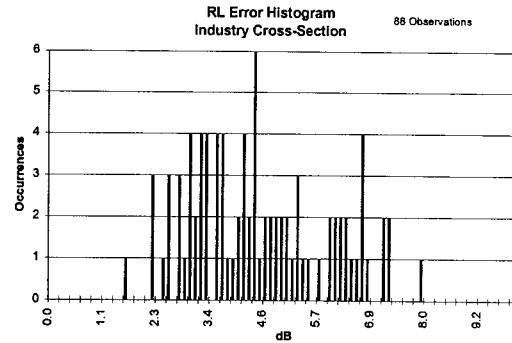


Figure 24: Histogram of Industry Representative Samples

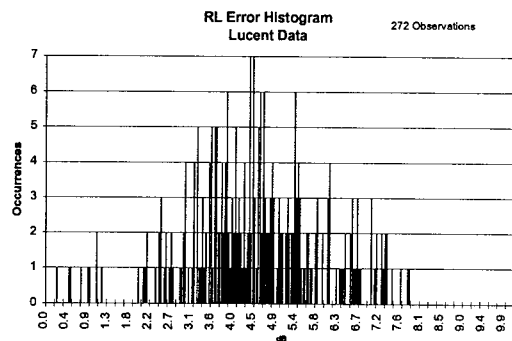


Figure 25: Histogram of Lucent Data

Industry Samples		
	RMS % (represented)	RL error (dB)
avg	53.20	4.41
max	70.10	1.58
min	33.41	7.82
std dev	8.70	1.46
Lucent Data		
avg	52.79	4.51
max	96.45	0.20
min	20.94	10.24
std dev	11.10	1.47

Table 2: Distribution of Average Results

Conclusions:

Input impedance is of value in that it leads to characteristic impedance, however, input impedance can only be described as a non sufficient condition for quality assurance. $|Z_{in}|$ is an unreliable indication of reflected energy and is dependent on random chance. Examples have shown substantial discrepancies in pass/fail decisions against emerging standards. $|Z_{in}|$ is particularly permissive of periodic structure. Close agreement was observed between actual cable data and theoretical prediction. Further, relating thousands of discrete measurements over

dozens of cable samples results in a nearly 4.5dB or 53% RMS understatement of reflected energy.

On the other hand, RL or combined limits of SRL and Z_0 are necessary and sufficient and are readily measurable. These measurements have been standardized⁴ and widely referenced in existing cabling standards.² Input impedance should not be accepted as a reliable or robust metric for product conformance.

References:

1. ANSI/EIA/TIA 568A
2. ISO/IEC 11801
3. ASTM D 4566-94, Standard Test Methods for Electrical Performance Properties of Insulations and Jackets for Telecommunications Wire and Cable
4. Friesen, H. W., "Relating the Structural Return Loss of Cable Pairs to the Associated Attenuation Deviation and Delay Jitter", 44th International Wire & Cable Symposium Proceedings, 1995, pp 261-268
5. S-Parameter Design, Hewlett Packard Application Note 154
6. Su, K. L., *Fundamentals of Circuits, Electronics, and Signal Analysis*, Waveland Press, Inc., Prospect Heights, Illinois, 1986
7. Oppenheim, A. V. and Shafer, R. W., *Discrete-Time Signal Processing*, Prentice Hall, Inc., Englewood Cliffs, New Jersey, 1989



Trent M. Hayes
Bell Laboratories
Lucent Technologies
Norcross, GA 30071

Trent is a Member of Technical Staff in the Electronic Wire and Cable Product and Standards Development Group at Lucent Technologies/Bell Laboratories. He received a BEE degree from the Georgia Institute of Technology in 1990 and a MSEE degree from Clemson University in 1991. Trent has been involved in high performance cable design and cable measurement development for the past six years.

INVESTIGATION OF INGRESS ON BI-DIRECTIONAL CATV SYSTEM

Hideyuki OMURA, Mitsunori KATOH

Information & Electronics Laboratories, THE FURUKAWA ELECTRIC CO.,LTD.

5-1-9, Higashiyawata Hiratsuka, Kanagawa, 254, JAPAN

Telephone:81-463-24-8448 Facsimile:81-463-24-8491

Abstract

In order to understand ingress encountered in an upward link of the bi-directional CATV system, we had observed not only status of ingress but also transmission performance of QPSK-modulated signal on an operating system. Upward-link spectra were analyzed and the frequency characteristics of ingress were made clear. It was made obvious that the error status caused by ingress was burst occurrence. Furthermore, ingress mechanism was analyzed theoretically and experimentally. As the result, the soaking route onto a signal line was made clear.

1.Introduction

The bi-directional CATV systems provide high performance for not only multi-channel video distribution service but also interactive applications such as telecommunication service, video-on-demand service, computer network service, and so on[1]-[2]. These interactive applications have great ability to compete with conventional teleco-service. In order to realize high quality interactive service, some major degradation problems on upward link, ingress, amplifier non-linearity, white noise[3]-[4], have to be understood and overcome.

Particularly, ingress seriously damages signal quality according to soaked level into cables depends on the shield effectiveness of coaxial cables and/or connectors.

In this paper the results of observation of ingress spectra and the affection to QPSK signals on a cable plant are presented and also ingress mechanism into coaxial cables is investigated.

2.Upward link noise characteristics

2.1 Status of ingress

Common ingress sources found in an upward-link are amateur radio operators, citizen's band operators, local AM broadcast, local short-wave and international short-wave.

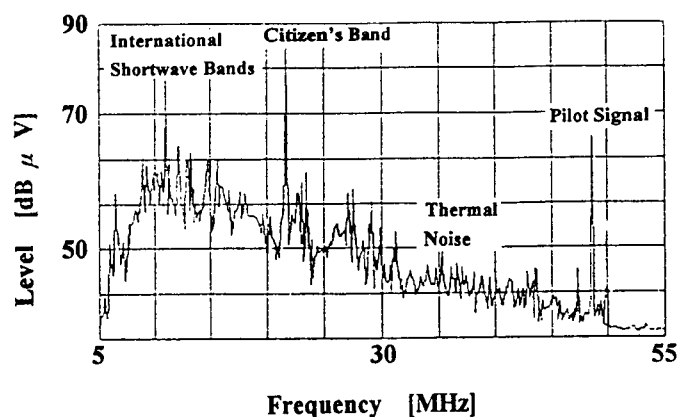


Fig.1 Upward-link spectrum observed at a central station

We observed status of ingress on a cable plant. The plant has 28300 subscribers and 844 amplifiers. Fig.1 shows an example of observed spectrum on a CATV upward-band at 10 to 50 MHz. The citizen's band ingress at 27 MHz might be a result of local operators transmitting near a cable plant in close proximity to bad connectors and/or shielding. The international short-wave bands ingress appeared around 10 MHz as well.

Such status might be varied depending on electromagnetic field intensity around the cable plant.

The intensity of citizen's band is dominated by distance from the signal source. The more the cable plant is close to the signal source, the higher the intensity affects to the plant. The citizen's band signals are mostly generated from truck drivers or amateur operators.

The intensity of international short wave around the cable plant might be determined by status of the ionosphere.

The ionosphere is consist of several layers.

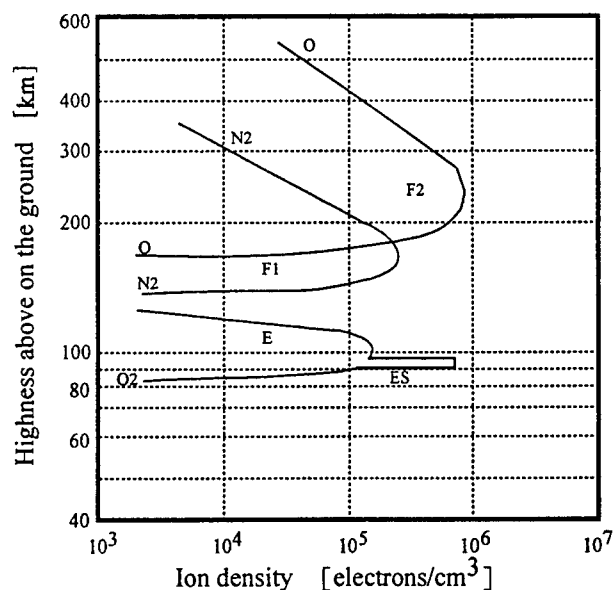


Fig.2 Distribution of ion density in the ionosphere

Distribution of ion density in the ionosphere is shown in Fig 2. The ion density is dominated by atmospheric condition and varies every moment according to temperature, humidity, sun location, terrestrial magnetism and so on. The reflection value on the ionosphere is determined by the ion density in the each layer and transmitted electromagnetic field intensity from foreign countries to Japan must be varied according to the reflection value.

2.2 Status of white noise

The white noise of an upward link is based on the thermal noise of a 75 ohm terminating resistor. This noise is carried through each trunk amplifier adding its own noise and is carried to the headend. Total white noise value can be calculated by equation (1).

$$\text{White noise value} = 4kTBR + NF + 10\log(N) \quad (1)$$

where k is Boltzmann's constant, T is the absolute temperature, B is the transmission band width, R is the resistance, NF is the noise figure, N is the total number of amplifier. The noise is generated by a resistor R at temperature T . The noise figure of an amplifier represents noise contribution and is assuming the same for all amplifiers.

2.3 Whole noise characteristics

Whole noise characteristic is determined by status of ingress and white noise. Fig.3 shows noise level characteristic versus the number of trunk amplifiers. The noise level was measured as a function of the number of trunk amplifiers which could launch signals to the central station. The signal paths of upward-link were opened/cut by the

bridger gate switches. The white noise level increases depending on the number of amplifiers according to equation (1)(for theoretical value see solid line in Fig.3). The measured value at 50MHz indicated by circles are found in good agreement with the theoretical value. On the other hand, the measured value at 10MHz indicated by crosses differ from the theoretical value. This level increasing at 10MHz is caused by the ingress of international short-wave. In usual case, ingress level is mostly higher than white noise floor and ingress worse deteriorates transmission quality than white noise.

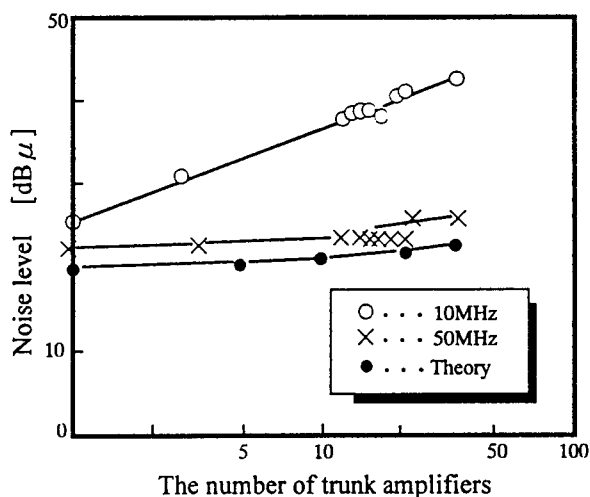


Fig.3 Noise level characteristic versus the number of trunk amplifiers

3.Impact of ingress against the QPSK signals

The QPSK transmission quality at 33MHz, bit error status, was observed on the CATV plant described above, on which the upward-link noise characteristics were observed. Fig.4 shows the experimental set-up used on this field measurement. The upward-signals transmitted from each subscriber were received with a receiver unit at the headend. The upward signals were divided with a

divider and launched from each output-port. The one of divided signals were combined into a QPSK transmission block by an electrical coupler. On this QPSK transmission block a QPSK modulator and a demodulator were connected each other via an electrical coupler. A transmitter and receiver of a transmission analyzer were connected to the modulator or demodulator, respectively. BER was measured at the receiver site.

In this experiment carrier frequency of the QPSK signal was 33 MHz.

Fig.5 shows the %ES characteristic versus BER. The %ES is given by the next equation.

$$\%ES = 100 \{1 - \exp(-NP)\} \quad (2)$$

where N is the transmission velocity of 4.096MHz, P is the BER. The theoretical value of %ES is determined by the ratio between total transmission time and "errored second", that is the second in which one or more errors can be observed. However the theoretical value shows random error occurrence, the measured value is almost different from the theoretical value. Therefore, the error status must be burst occurrence. Such interference is dominated by not white noise but to ingress.

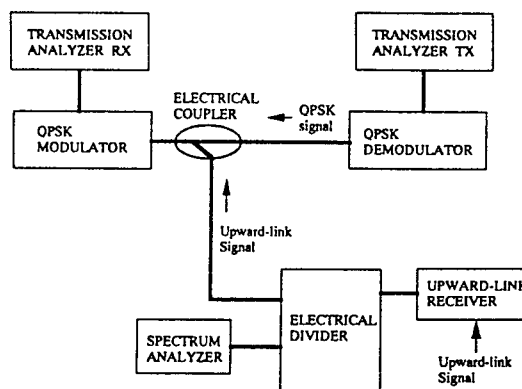


Fig.4 Block diagram of QPSK signal transmission quality

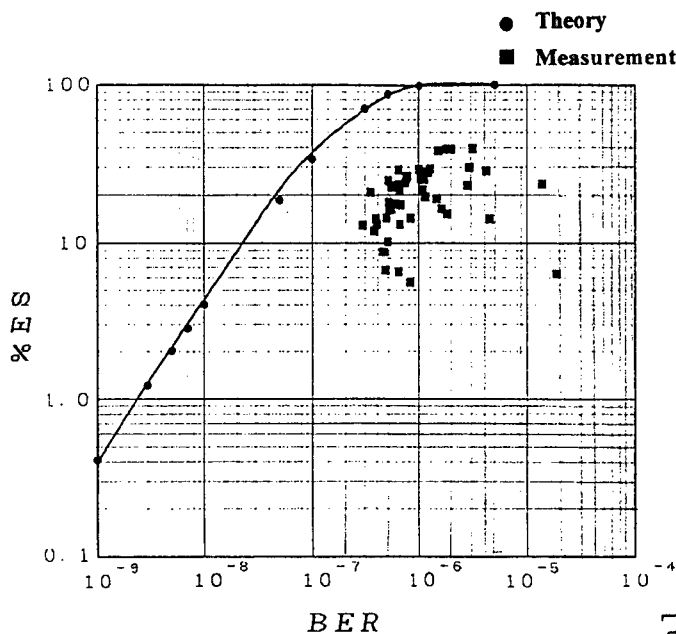


Fig.5 %ES characteristic versus BER

4. Investigation of ingress mechanism

Ingress interferes with upward-link signals and deteriorates transmission quality as described above.

Ingress is defined as unwanted external signals entering a cable plant. These signals enter at weak points in systems such as the faulty shieldings of coaxial cables and/or connectors. We investigated the soaking route of ingress experimentally and theoretically.

4.1 Shield effectiveness of coaxial cables

Firstly, we analyzed the shield effectiveness of coaxial cables according to equation (3). Assuming electromagnetic field intensity of 30dBm/m surrounding cables, soaking voltage into cables was calculated. Fig.6 shows the shield effectiveness of coaxial cables as a function of frequency. It was made clear that completely shielded cables were able to sufficiently eliminate the electromagnetic field

on the CATV upward-band at 10 to 50 MHz.

$$10\log P =$$

$$20\log |Q| + 20\log |qE_v| + 20\log I(1, f) - 20\log \pi |H_0^{(2)}(k_0 r_0)| - m - 10\log R - 10\log 10^{-3} \quad (3)$$

where P is the induced voltage on a signal line, I is the inducing efficient on a signal line, $H_0^{(2)}$ is the 2nd order Hankel function, R is the resistance of termination, and q and m are the constants obtained experimentally.

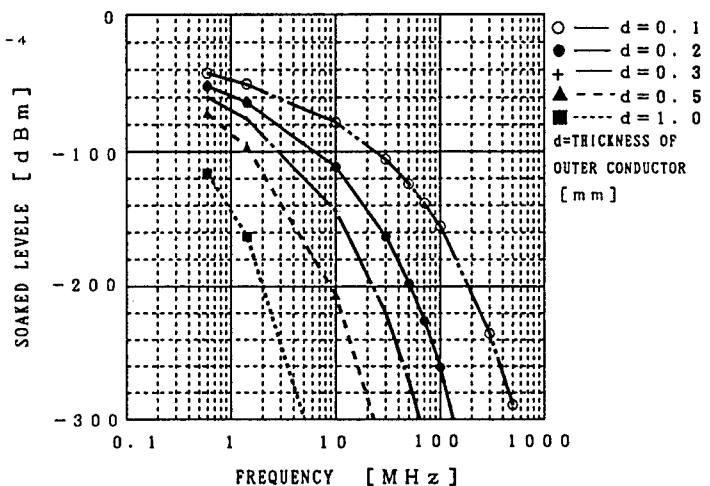


Fig.6 Shield effectiveness of coaxial cables

4.2 Electromagnetic field in the shield gap

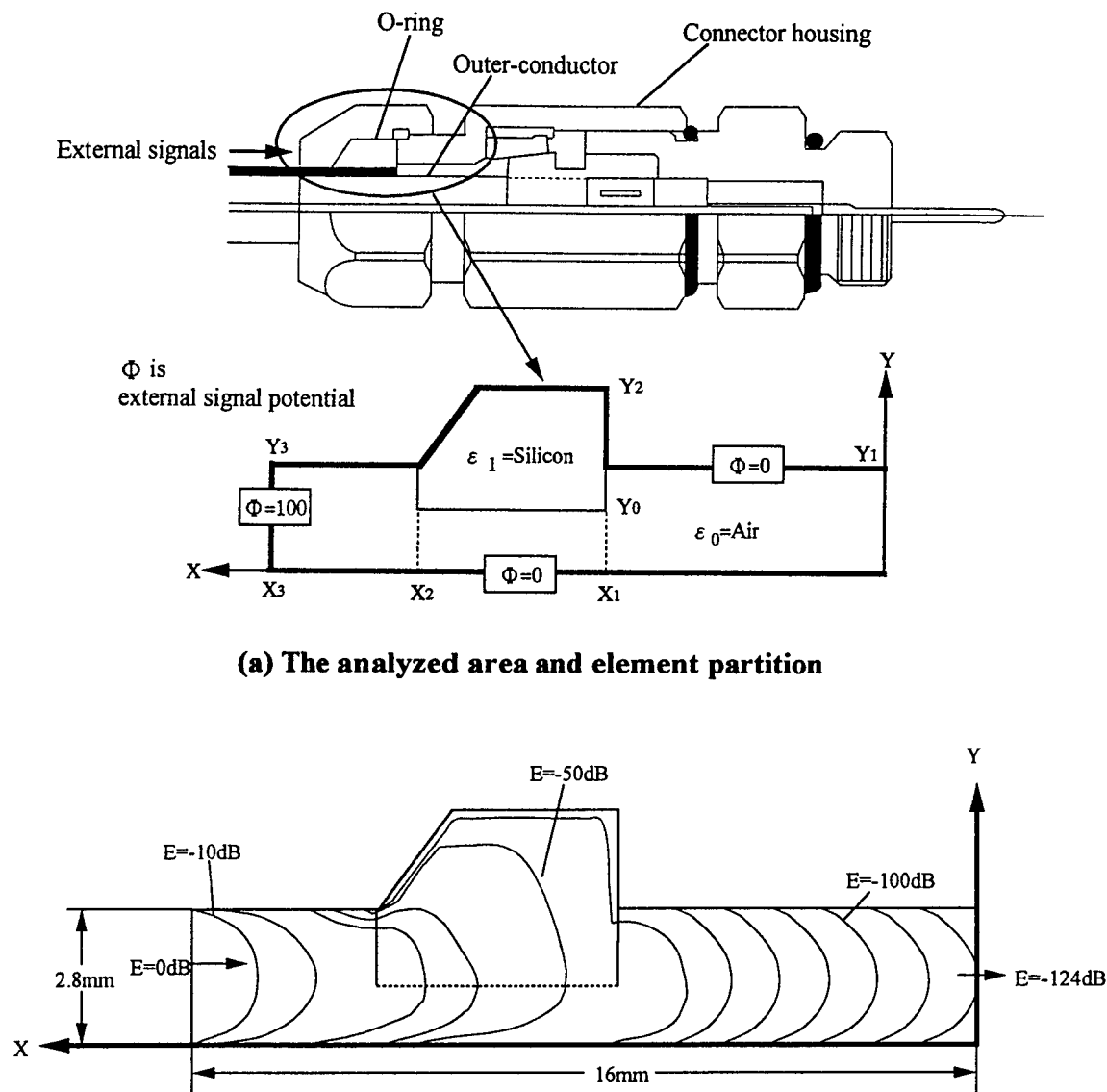
Secondly, we made an analysis with the finite element method in order to solve the electromagnetic field pattern in the cylindrical gap between an outer-conductor and a connector housing such as wave-guide structure.

Fig.7 (a) shows the analyzed area, the cylindrical gap between an outer-conductor and a connector housing, and element partition over the cylindrical gap. The analysis area was parceled 7340 elements and 3843 nodes.

The calculated electromagnetic field intensity

distribution is shown in Fig.7 (b). The results describe the electromagnetic field intensity could be sufficiently suppressed during traveling over the gap.

Namely, the external signals hardly soak into coaxial cables by the wave-guide mode in spite of the presence of some gaps between an outer-conductor and a connector housing.



(b) Calculated electromagnetic field intensity distribution

Fig.7 Electromagnetic field intensity over the cylindrical gap between an outer-conductor and a connector housing

4.3 Soaking contribution of surface current

Thirdly, we had experimental measurements of soaked level into a cable with the scheme which is illustrated in Fig.8.

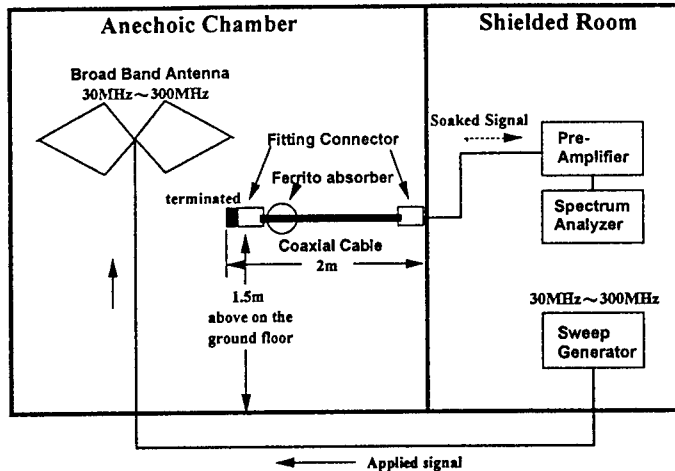


Fig.8 Experimental scheme to measure the soaked level into a coaxial cable

The cable set under test consisted of a coaxial cable and two fitting connectors. Electrical contact condition between the outer-conductor and the connectors intentionally made weak where contact resistance was $3\text{m}\Omega$. Therefore, small gaps were

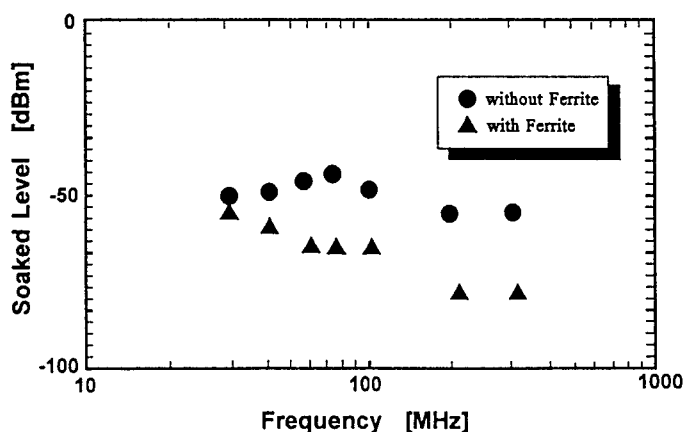


Fig.9 Soaked level characteristics as a function of frequency

presented between the outer-conductor and the connector housings. The electromagnetic field at $30\sim 300\text{MHz}$ applied the cable set with a wide-band antenna. Electromagnetic field intensity around the cable set was about 0dBm/m .

Fig.9 shows soaked level characteristics as a function of frequency. In the case that a ferrite absorber was set on the outer-conductor, as shown in Fig 8, the soaked level was reduced because the surface wave was absorbed by the ferrite absorber.

4.4 Discussion

The results explained above shows some notices as follows:

- Complete shielded cables have sufficient shielding effect against the external electromagnetic field.
- The external electromagnetic field enters into cables due to a total discontinuity of the shield, by not the wave-guide mode but the surface current mode.

A discontinuity of the shielding causes improper handling or installation of connectors and/or coaxial cables. However the connection between a connector and a cable is tight enough to conduct RF signals, the surface current induces onto the shielding can couple to the signal line. In order to reduce ingress level, the ground connection should be kept on being strong, making a good pressure between equipment and an earth plate. Otherwise current absorbers should be set on shield surface to reduce the surface current.

Conclusion

Ingress status was observed and error characteristics were confirmed with a QPSK transmission test on a CATV plant. As the

results common frequencies of ingress was represented and also it was made clear that error status was burst occurrence. Furthermore, in order to make the ingress mechanism clear, we had two analyses and an experimental measurement. As the results it was made obvious that ingress was the entrance into a cable of any surface wave on an outer-conductor caused by the electromagnetic field around cables and the soaked level could be reduced with a ferrite absorber because the surface wave was eliminated.

REFERENCE

[1] M.Maeda, et. al:"An FM-FDM HDTV Optical CATV System employing Demand Access Technique", OEC'90,

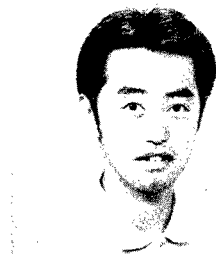
11D1-2, pp36-37, 1990

[2] M.Thapar, et. al:"Architectures of Video Servers", NCTA Technical Papers, pp141-148, 1994

[3]A.Giorgio:"Transmission System Evaluation for Two-Way Cable", IEEE Transactions on CATV, vol. CATV-4, No.3, 1979

[4] C.Rich, et. al:"Performance History in Two-Way Cable Plants Utilizing A PSK Communication System", NCTA

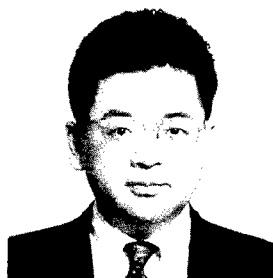
Technical Papers, pp251-260, 1987



Hideyuki Omura

Furukawa Electric Co.Ltd
5-1-9, Higashiyawata
Hiratsuka, Kanagawa, 254,
JAPAN

Hideyuki Omura received a Master's Degree in electrical engineering from Tokai University, Kanagawa, Japan in 1987. He joined Furukawa Electric Co., LTD in 1987 and he has been involved in the development of bi-directional CATV for 4 years. At present he is working in Video transmission system and equipment research section of Information & Electronics Laboratory. Mr. Omura is a member of the institute of Electrical Engineers of Japan.



Mitsunori Katoh

Furukawa Electric Co.Ltd
5-1-9, Higashiyawata
Hiratsuka, Kanagawa, 254,
JAPAN

Mitsunori Katoh received a Bachelor's Degree in instrumentation engineering from Keio University, Kanagawa, Japan in 1981. He joined Furukawa Electric Co., LTD in 1981. At present he is working in multimedia communication systems research section of Information & Electronics Laboratory.

AN OVERVIEW OF KEY RIBBON HANDLEABILITY ATTRIBUTES

Gregory A. Lochkovic, Shail K. Moorjani, Naren I. Patel,
Ron J. Speights, and Barney L. Stephens

Siecor Corporation, Hickory, North Carolina

ABSTRACT

As the use of optical fiber cables penetrates deeper into the telecomm networks, applications requiring high fiber count cables have become more common. As such, optical cables with fiber counts ranging to 1,000 continue to receive serious attention. In these applications it is becoming highly critical to achieve optimum packing density for minimization of overall cable diameters [1]. It has been recognized that ribbonized fibers provide optimum packing efficiency [2], while at the same time provide an organized structure that facilitates rapid splicing and connectorization. For those applications in which labor savings and efficiency are the primary concerns, ribbon cables can be highly desirable.

To date, only token efforts have been made in the literature to address the desirable handleability attributes of a ribbon in an encompassing manner, and have typically been focused on a single feature (for example, thermal ribbon strippability [3]). This paper, on the other hand, discusses several key handleability attributes (as prioritized by customer needs) as well as potential design tradeoffs associated with optimizing for single features. The discussion is limited to 12 fiber ribbon (f/r) designs and includes: definitions, proposed test methods and their associated rating systems, and examination of the interdependence of these properties.

INTRODUCTION

Handleability of ribbons is defined as the handling stages that a ribbon undergoes during installation and potential subsequent fiber access of a cable: beginning with the separation

of a ribbon from the cable and concluding with its final fixation in the fiber optic system.

Multiple ribbon handleability attributes merit discussion; however, we have chosen to focus on a select few based on customer needs and the frequency of need/application by installers.

- Thermal Strip
- Peelability
- Separability
- Furcatability
- Robustness

We have evaluated an array of 12 fiber ribbon designs, competitive and otherwise, which allows us to discuss proposed definitions of the key attributes for future technical reference, proposed test methods with rating systems, and the areas of potential interdependence of these key attributes.

In particular, we have found that manipulation of only the adhesion at the matrix and fiber interface to optimize for peelability can degrade other handleability characteristics such as ribbon separability and robustness. The interdependence of these ribbon handleability characteristics indicates a need for balancing ribbon designs for all key handleability characteristics.

DEFINITIONS

Before embarking on a discussion of the chosen ribbon handleability attributes, it is necessary to establish a common understanding of the proposed terminology. It is hoped that this will serve as baseline terminology for future reference in the literature.

Ribbon Thermal Strip

Thermal strippability implies the ability to remove the fiber and ribbon coatings from a multi-fiber ribbon. Applications in the field typically require the removal of all coatings from the ribbon in order to expose the glass for fusion splicing or mechanical connectorization. Complete removal of all coatings in a cohesive tube-like manner and minimal debris remaining on the glass is highly preferred. Of course, no fiber breakage is acceptable. When the stripped coatings crumble during stripping, residue inevitably remains in the thermal stripping device. If this residue is not well cleaned from the tool on a regular basis, the probability for fiber breakage increases dramatically.

The Fujikura HJS-01 (Hot Jacket Stripper) and the Sumitomo JR4A ribbon thermal strippers have gained wide popularity in the US market for stripping 12 fiber ribbons. All work presented in this paper was performed with the Fujikura tool.

Ribbon Peelability

Peelability implies the potential to remove matrix from a ribbon in a continuous fashion from the fibers of that ribbon, while leaving the individual fiber coatings (including coloring) intact and free from damage, to access specific fibers for further rerouting or repair [4]. There are many modes of access to individual or multiple fibers in a ribbon or ribbon cable. Various solvent paste kits (containing alcohols, acetates, etc.) have been available from the inception of tape-less fiber optic ribbons. However, matrix peelability is a more popular and effective technique of fiber access from a ribbon due to reduced handling, time to access, and number of tools required. A ribbon exhibiting good peelability will allow the complete removal of matrix from each side of the ribbon within the desired fiber access area with minimal potential for the matrix to continue to debond from the fibers outside of the intended access area.

Siecor's TKT-060 (Figure 1) matrix peel kit has been developed specifically for this purpose, and has demonstrated excellent peeling

performance on a wide variety of peelable and semi-peelable ribbon designs.

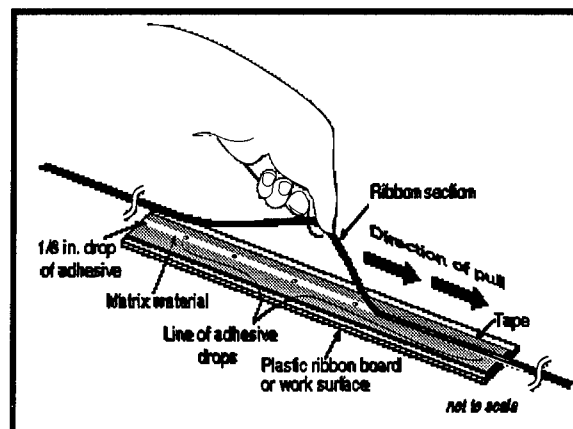


Figure 1: Siecor Matrix Peel Kit

Ribbon Separation

Ribbon separation is the ability to separate sub-units (or groups of one or more coplanar fibers) from a ribbon unit for rerouting or repair. This process is typically performed by hand; however, special tools have previously been developed [3] which provide a higher degree of separation precision with minimal disturbance to live traffic on the affected fibers. A ribbon exhibiting good separation potential will demonstrate good bonding of the newly exposed edge fibers to the remainder of their intended sub-groups ensuring limited risk of straying fibers that could inadvertently be broken as an unbuffered member. Also, it is desirable to minimize stringers [3] to ensure a smooth separation of the sub-units when using a specialized tool. A stringer results from an inconsistent matrix tear plane resulting in a ragged edge on the separated ribbon sub-units. Stringers can fold over or dislodge and become jammed in the tool causing high pulling forces during separation and possible high attenuation and fiber breakage. Additionally, stringers can create difficulty when accessing individual sub-units from splice trays due to the tendency to hook/catch neighbor ribbons as a sub-unit is lifted from the splice tray.

Ribbon separation tools have been considered in Japan [5]. At this time, separation tool designs are under consideration by a few suppliers domestically, but no tools are commercially

available at the time of this writing. A Siecor tool devised for this purpose is shown in Figure 2.

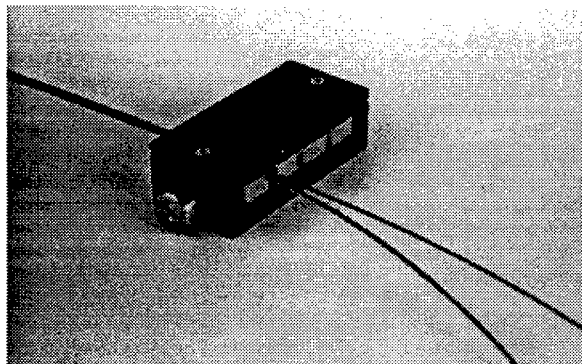


Figure 2: Separated Ribbon Using Siecor Separation Tool

Ribbon Furcatability

Often, in the field or preconstructed in the manufacturing plant, fibers are "broken out" or separated from their individual units, and inserted into furcation tubing (~0.38 mm ID X 0.9 mm OD) for added protection/robustness in applications where fibers will be individually routed to patch panels, etc. This has traditionally been a simple operation for fibers from Loose Tube cable designs; however, ribbonized fibers offer some challenges when the ribbon design has not taken furcatability (mainly a function of ribbon fiber breakout and matrix peelability) into account. Preferred ribbon furcatability character implies a ribbon design wherein the individual fibers from a ribbon can be easily removed from the main structure, and subsequently inserted through 2 or more feet of furcation tubing without damage to the fiber coatings or ink layer, and without intermediate operations to remove excess matrix material from one or several fibers.

The authors are unaware of any special tools or equipment on the market at this time intended specifically for performing ribbon furcation. Currently, this function is typically carried out by hand.

Ribbon Robustness

Once a ribbon has been successfully handled in any of the previously described methods, the ribbons are invariably placed into space minimized housing units; field enclosures, splice trays, and routing cabinets to name a few. The housing units are typically designed for gentle routing of the fibers or ribbons to be enclosed; however, ribbons will often be partially twisted or tangled upon completion of an assembly. Adverse field conditions and lack of familiarity with housing unit designs contribute to this condition.

A weak ribbon or a sub-unit from that ribbon exhibiting poor edge fiber adhesion, when subjected to twisting or tight bending radii, will often result in a fiber or fibers straying from the ribbon array dependent upon the robustness of the ribbon design. This will increase the probability of a pinched or broken fiber either as the housing unit is closed or upon re-entry.

A ribbon exhibiting acceptable levels of installed robustness must be capable of maintaining its coplanar cross-section (no straying fibers, ribbon splitting, or buckling of the ribbon X-section) when subjected to twists or tight bending radii. Further, an adequately designed ribbon should exhibit little to no reduction in composite strength after handling to accommodate future modifications to the deployed ribbon condition.

DESCRIPTION OF TESTED RIBBONS

To focus the discussion, only 3 ribbon designs have been chosen for inclusion in this paper. The 3 designs chosen were selected to represent the range of possibilities typically encountered by the craft. The ribbons will be referred to in this paper as A, B, and C. A brief description of each ribbon design can be found in Table 1.

Table 1: 12 Fiber Ribbon Designs for Discussion

Ribbon	Ribbon Thickness	Matrix Modulus	Ink to Matrix Adhesion	Comments
A	thin ($< 300 \mu\text{m}$)	medium	high	Design could provide basis for high density cable.
B	thick ($> 300 \mu\text{m}$)	medium-high	low	Design provides ease of matrix removal.
C	thick ($> 300 \mu\text{m}$)	medium-high	medium	Design provides good matrix removal and high degree of robustness.

The remainder of this paper will discuss proposed methods for rating the effectiveness (not "pass/no pass" status) of the various ribbon designs against the key ribbon handleability attributes. Further, the test results of each of the above ribbon designs will be reported and discussed.

TEST METHODS AND TESTING

Ribbon Thermal Strip

Ribbon thermal strip is a required test in many customer specifications. Most of these specifications require that 30 mm of ribbon and fiber coatings can be mechanically removed with commercially available stripping tools with no resultant fiber breaks and minimal residue left on the stripped glass. This is a well established test method (see Mills [4]), and will not be readdressed herein; however, the following rating scale has been included to facilitate discussion.

Thermal Strip Fiber Cleanliness Rating Scale

- 1 All fibers clean after strip without subsequent wiping/cleaning required.
- 2 Slight residual debris remains after strip with single alcohol wipe cleaning required.
- 3 Moderate debris remains after strip with 2 alcohol wipes cleaning required.
- 4 Heavy debris remains after strip with > 2 alcohol wipes cleaning required.
- 5 Incomplete strip with some coating not cleanable using the alcohol wipes.

NOTE: Since ribbon thermal strip fiber cleanliness is a major function of fiber design, and only a very minor function of ribbon design, the rating scale has been laid out for

completeness only, and will not be further discussed.

Thermal Strip Tube-off Rating Scale

Note: Tube-off is the ability to remove the ribbon, ink, and fiber coatings intact from the glass (no crumbling or disintegration of the composite coating structure).

- 1 Complete tubing with no composite coating distortion.
- 2 Complete tubing with slight coating distortion/deformation.
- 3 Substantial ($\geq 75\%$ complete) tubing with moderate coating distortion/deformation.
- 4 Incomplete ($\geq 25\%$, but $< 75\%$) tubing with significant coating disintegration.
- 5 No tubing; total coating composite disintegration.

The thermal strip testing results are tabulated below:

Table 2: Ribbon Thermal Strip Tube-off Results

Ribbon	Matrix Tube-off	Comments
A	1	high adhesion of all interfacial layers allows cohesive tube-off of all layers as a unit.
B	1	low adhesion of matrix to ink has an inconsequential effect on tube-off character.
C	1	medium adhesion of matrix to ink has an inconsequential effect on tube-off character.

NOTE: Ribbonized fiber strip force (which forces tubing as opposed to shearing away of

fiber coatings from the glass) has shown the greatest effect on matrix tube-off in our studies.

Intuitively, one would expect that as the adhesion of the matrix to fiber decreases, the thermal strip tube-off character would diminish due to the reduced cohesive character of the composite coating structure. Likewise, one would expect that as the matrix modulus decreases, a reduced structural stability of the composite coating structure would follow yielding poor tube-off as well. However, as indicated above, these have been shown to be only minor effects in our testing with the major contributor to tube-off character lying in the ribbonized fiber strip force.

Ribbon Peelability

Currently, many customer specifications require that ribbon coatings be removable for access to the enclosed fibers without damaging the individual fiber coatings. Traditionally, for mid-span access scenarios, solvent based pastes have been used to soften the ribbon coatings to the extent that they can be wiped away from the fiber (coating) surface. More recently, however, several ribbon suppliers have developed ribbons capable of having the ribbon matrix material removed from each side of the ribbon in a tape-like peel away from the fiber coatings.

In order to discern between levels of peelability, a new test has been developed to grade the ribbon peel performance:

Tools and Materials

- Quick setting adhesive such as a cyanoacrylate (ex., Loctite 495 Superbond).
- Cloth backed tape (ex., Shurtape made by Shuford Mills, Pt# PC690).
NOTE: many cloth backed medical tapes and some vinyl backed tapes are appropriate for this application.
- A rigid or semi-rigid substrate (ex., any table top or elongated stiff surface).

Peel Procedure

- Cut a strip of the cloth backed tape approximately 1 ft. in length (or longer depending on the length of access desired for testing).

- Apply the tape, adhesive side down, to the top of a working surface (the rigid or semi-rigid substrate).
- Place an initial small drop of adhesive at the leading edge of the tape, and then a series of drops in a linear fashion every 2 to 3 inches along the length of the tape (~1 ft for purposes of the testing discussed in this paper).
- Cut a test sample of ribbon approximately 1.5 - 2 times the length of the chosen tape length.
- Place the section of ribbon under testing on top of the small glue drops. Approximately 2 - 4 inches of ribbon should extend behind the location of the initial adhesive drop to provide a pulling tail to initiate the subsequent peel process. Using a spatula or other non-aggressive flat tool, gently press on the ribbon section to ensure that it is in contact with the adhesive at all locations along the tape. The remainder of the ribbon should extend past the end of the tape to allow the potential for continued peel beyond the last adhesive drop.
- Once the adhesive has set, lift the ribbon from the leading edge of the tape to initiate the ribbon matrix rupture from the fiber surface. Then, continue to pull the ribbon along the length of the tape and beyond until the ribbon coating has broken away from the ribbon structure

Peelability Rating Scale

- 1 All ribbon matrix peels cleanly. The entire length of ribbon matrix peels with little effort or tension. No ribbon matrix is left on the fibers or the edges of the ribbon. Once past the end of the tape/adhesive, the ribbon matrix continues to peel without fragmenting.
- 2 The ribbon matrix peels cleanly from the ribbon along the tape/adhesive section; however, once past the tape/adhesive section, the ribbon matrix breaks or begins to fragment.
- 3 The ribbon matrix fragments along the tape/adhesive section of peel resulting in a reduced width peel of ribbon matrix from the ribbon structure. However, continuous strips of ribbon matrix (although reduced in width) form along the entire length of the tape/adhesive section.

- 4 The ribbon matrix fragments along the tape/adhesive section of peel. **NO** continuous strips of ribbon matrix are formed along the entire tape/adhesive section. However, some separation of ribbon matrix from the ribbon structure is evident beyond the adhesive drop on at least a subset of the adhesive drops.
- 5 The ribbon matrix will **NOT** peel from the ribbon. The ribbon matrix breaks or, never separates from the ribbon structure, as the ribbon is lifted from each adhesive drop. **NO** ribbon matrix strip is formed beyond each adhesive drop.

The peelability testing results are tabulated below:

Table 3: Ribbon Peelability Test Results

Ribbon	Peelability	Comments
A	5	matrix removal only in area of adhesive.
B	1	once initiated, matrix removal propagates until craft terminates peel.
C	2	once initiated, matrix removal propagates to the end of the cloth tape.

NOTE: We found advantage in a ribbon exhibiting peel character with termination at the end of the cloth tape. This limits the separation of matrix from ink only to the controlled area of interest, and minimizes the risk of post-handling delamination.

Clearly, a lower level of matrix to fiber adhesion results in an easier peel of the matrix from the ribbon fibers.

Ribbon Separation

Many customer specifications also call out requirements for the ability to separate fibers or sub-units of fibers from the ribbon in either single fiber, mid-span, or end-span scenarios. With the advent of ribbons possessing more readily accessible fibers (peelable), this has now become a critical test given that ribbon coating adhesion to the fibers is generally

diminished in peelable ribbon designs. Obviously, the fibers in a peelable ribbon design will now be much more separable; however, the concern now lies in the ability of the newly exposed edge fibers to maintain their juxtaposition relative to the other fibers in their respective sub-units.

As such, to aid in designing ribbons that are both peelable and resistant to edge fiber wandering after ribbon separation, a test method and rating scheme has been developed to grade the ribbon separation performance. Although the test is readily applicable to end-span testing, the primary focus is on mid-span ribbon separation. Although the test has not been written to investigate attenuation performance during separation, it could readily be incorporated for further characterization [6].

Tools and Materials

- Ribbon separation tool (as specified by the ribbon manufacturer - please see the photograph in Figure 3 for the Siecor tool design used in this testing). Per Bellcore GR-20, as a minimum, the tool should be able to separate the 12 fiber ribbon into 2 6-fiber sub-units.
- 5X magnifying eyepiece or reasonable equivalent.

Separation Procedure

- Obtain a sample of ribbon approximately 0.3 meter in length or longer.
- Place the sample to be tested in the separation tool with approximately 40 cm or more of the sample (short side) available for gripping in a subsequent step.
- Once the sample has been fully loaded in the separation tool, either fix the short side in a clamping device or grasp by hand.
- Next, the separation tool is moved away (pulled) from the short side (generating the ribbon separating action) over a distance of ~0.25 m at an approximate 0.1 m/s rate of pull. The rate of pull is derived from a 0.25 m separation action performed over a 2.5 second interval. The rate of pull is reasonable with respect to the low attenuation generated at this rate (in the event of live traffic ribbon separation), and the expectation that the craft will accept the relatively short associated time duration. The ribbon can be separated into

any sub-group combination. For this testing, the ribbons were separated into sub-groups of 6 fibers each.

- Remove the separated ribbon sample, and inspect using the 5X eyepiece before proceeding to the next step.
- At this point, one is interested in the robustness of the new sub-units. A test demonstrating effectiveness in determining the robustness of the new sub-units is the ribbon transverse flex test. Please see the "Ribbon Installed Robustness: Ribbon Transverse Flex" section of this paper for the test procedure. The test is performed in the same manner with the exception that the ribbon sub-unit is flexed twice; once with the exposed (where new edge fiber resides) side on the inner diameter, and again with the opposite side on the inner diameter.

Separation Rating Scale

It is assumed that no broken fibers are acceptable for any separation process. Therefore, broken fibers have not been recognized in the following rating scale.

- 1 During the separation process, no stringers (longitudinal strips of matrix) form along either sub-unit, no stray fibers are generated, and the ribbon separation force is low. Subsequent transverse flex testing of each sub-unit generates no stray fibers.
- 2 During the separation process, some stringers may be generated along either sub-unit, no stray fibers are generated, and the ribbon separation force is generally low - although some high/low variation may be experienced. Subsequent transverse flex testing of each sub-unit generates no stray fibers.
- 3 During the separation process, some stringers may be generated along either sub-unit, no stray fibers are generated. Some high/low ribbon separation force variation may be experienced. Subsequent transverse flex testing results in partial ($\leq 50\%$ of the length along the sub-unit) edge fiber straying in one or both sub-units.
- 4 During the separation process, some stringers may be generated along either sub-unit, and no edge fiber straying is generated in either sub-unit. High/low ribbon separation force variation may be

experienced. Subsequent transverse flex testing results in $\geq 50\%$ edge fiber straying in one or both sub-units.

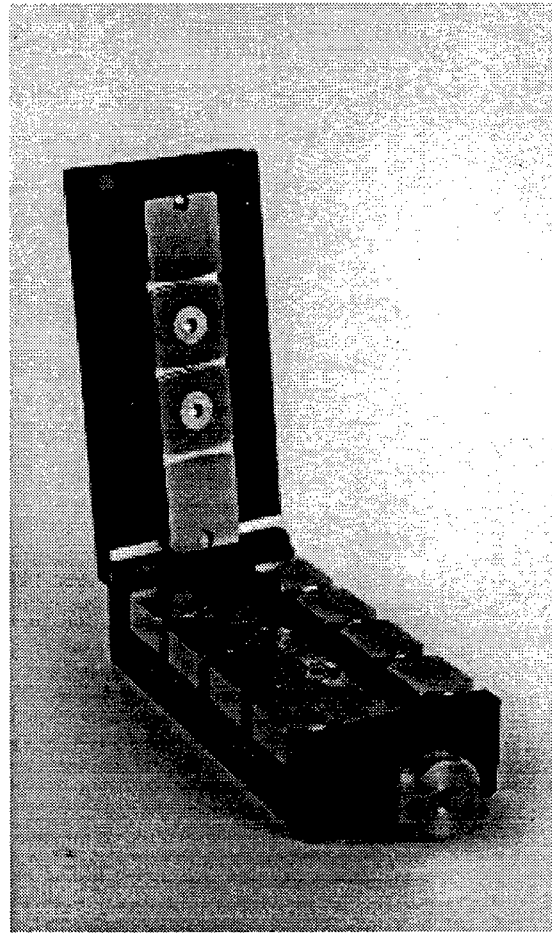


Figure 3: Siecor Ribbon Separation Tool

- 5 During the separation process, some stringers may be generated along either sub-unit, and edge fiber straying is generated in one or both sub-units. High/low ribbon separation force variation may be experienced. No subsequent transverse flex testing is required due to the stray fibers generated during initial separation.

The ribbon separation testing results are summarized in Table 4:

Table 4: Ribbon Separation Test Results

Ribbon	Separation	Comments
A	1	high matrix to fiber adhesion allows good separation and subsequent bending behavior.
B	4	low matrix to fiber adhesion allows newly exposed edge fibers to fall away from sub-units.
C	1	medium matrix to fiber adhesion allows robust separation and subsequent bending behavior.

As expected, lower adhesion of matrix to fiber results in worse separation character. Surprisingly, however, no difference in separation character was noted for the medium matrix to fiber adhesion level "C". Thus, allowing the ribbon designer a wider window of development opportunity.

It should be noted that, in general, the separation method noted in this paper represents a least risk (with respect to stray fibers and fiber breaks) scenario. Hand separation has demonstrated a high likelihood of stray fiber generation. Further, razor blade separation has been shown to induce fiber coating damage resulting in post handling fiber breaks.

Ribbon Furcatability

Furcatability of ribbon fibers is a ribbon property that is not specifically covered in an official specification document. In order for ribbonized fibers to be easily furcated, any residue matrix must be easily removable from the colored fiber surface. Some specifications address this issue indirectly by ensuring that the ribbon design in question maintains a low fiber breakout force, causes no fiber coating and minimal color damage upon removal of a fiber from the ribbon structure, and allows the ability to remove a fiber from a ribbon for lengths greater than 1 meter. No reference is made, however, to the amount of residue matrix remaining on a fiber after breakout from a

ribbon or the ease of removal of the residue matrix from the fiber surface. While not critical to the optical performance of a ribbon or the spliceability of the ribbonized fibers, a highly furcatable ribbon can save significant labor hours particularly in indoor plant applications where the ribbons are often furcated and individual fibers routed to key patch panel points.

A test has been developed to help quantify, during the ribbon development stage, the furcation character of various ribbon designs.

Tools and Materials

- Standard set of scissors
- Alcohol pad (ex., Lym•Tech "Lint Free Cleaning Pad or equivalent)
- Green or blue scrub pad (commonly available in commercial solvent-based mid-span access kits)
- Thermoplastic tubing (0.380 mm ID X 0.90 mm OD X ~610 mm L)

Ribbon Furcation Procedure

- As a minimum, fibers 1, 6, 7, and 12 shall be tested (insertability into the thermoplastic tubing upon removal from the ribbon coating) for each ribbon sample.
- Using scissors, cut the end of an ~ 650 mm ribbon sample at a 45° angle. For consistency, it is suggested that the short portion of the angle be on the aqua side of the ribbon.
- Fan (brush the fiber ends), the end of the ribbon with a protected finger tip to initiate fiber to ribbon coating separation at the end of the ribbon.
- Beginning with the blue fiber, peel each fiber from the composite structure until all 12 fibers are separated.
- Finally, insert the designated fibers fully thru the furcation tubing described above, and rate per the following criteria.

Ribbon Furcation Rating Scale

The response is the weighted average of the 4 tested fibers per ribbon per the following rating scale:

- 1 Fiber removes from the ribbon and inserts thru 610 mm (~2 feet) of tubing on the first try. No additional cleaning required.
- 2 Fiber requires some easy cleaning: ≤ 5 wipes with an alcohol pad.

- 3 Fiber requires more difficult cleaning: ≤ 2 moderate wipes with a scrub pad, but no color removal.
4. Fiber requires difficult cleaning: > 2 moderate wipes with a scrub pad, with some color removal possible.
- 5 Cannot successfully furcate the ribbonized fiber from the sample without excessive force which removes coloring and fiber coating or without causing fiber breaks.

Overall rating (response):

$$\text{Furcatibility} = \frac{F1 + (5 * F6) + (5 * F7) + F12}{12}$$

where: F1 = furcation rating for fiber 1 (blue), etc.

Following are the results of Siecor's ribbon furcatibility testing:

Table 5: Ribbon Furcatibility Test Results

Ribbon	Furcatibility	Comments
A	3.1	high adhesion of matrix to fiber makes cleaning for insertion into furcation tubing difficult.
B	1.6	low adhesion of matrix to fiber allows easy cleaning for insertion into furcation tubing.
C	1.2	low adhesion of matrix to fiber allows easy cleaning for insertion into furcation tubing.

The testing shows that lower adhesion levels of the matrix to the colored fiber surface generates a more readily furcatable ribbon. Interestingly, ribbon C performed in a slightly enhanced mode to ribbon B (with the lowest adhesion). This is explained by the slight ($\leq 5 \mu\text{m}$) increase in matrix thickness of ribbon C relative to ribbon B. The increased matrix thickness (thus, strength) allows a more cohesive peel of the matrix from the fiber once the fiber has been separated from the ribbon. This effect is reduced when peeling matrix from

the ribbon (as opposed to the separated fiber) due to the requirement for the matrix to overcome both cohesion and adhesion.

Ribbon Installed Robustness

Ribbon twist tests, as referenced in many customer specifications, ensure both a base level strength and minimum fatigue character ribbon design. The authors, however, sought to establish a test or tests wherein alternate ribbon designs could be ranked with respect to robustness/strength for development purposes. A robustness rating allows the ribbon developer to optimize (as opposed to merely test against a minimum level of acceptance) a ribbon design for robust character while balancing for other properties such as microbending resistance and general handling characteristics.

Two tests have been developed to rate ribbon robustness: "Ribbon Twist to Failure" and "Ribbon Transverse Flex". We also combined both tests to gain an understanding of the fatigue resistance of the various ribbon designs. This is summarized in the "Flexed, Twist to Failure" column of the test results.

Ribbon Twist to Failure

This is merely an extension of the test referenced above. The test equipment and set-up is identical with the following exceptions:

1. A 1 kg weight replaces the 0.1 kg weight to demonstrably exhibit the point of failure (ribbon typically folds or debonds along the axial plane in the center of the structure).
2. The ribbon is twisted in one direction until the ribbon fails (debonds or folds).
3. The test response is the number of uni-directional twists to failure.

Recognizing that an installed ribbon may be subjected to bending along its axial as well as its transverse planes, a test was devised, "Ribbon Transverse Flex", to evaluate a ribbon structure's behavior when the ribbon is bent against its transverse axis around a mandrel.

Ribbon Transverse Flex

Tools and Materials

- A bending mandrel: for this testing, an aluminum mandrel (see photograph in Figure 4) was designed with an inner bending radius of 80 mm. The depth of the slot was milled to a depth of $\sim 380\text{ }\mu\text{m}$ to allow ribbon insertion while limiting the tendency of the ribbon to relieve strain through twisting during bending. A Plexiglas cover with the same outer radius was attached to the mandrel again to limit the ribbon twist during bending. The Plexiglas cover allows the tester to view the behavior of the ribbon during bending.

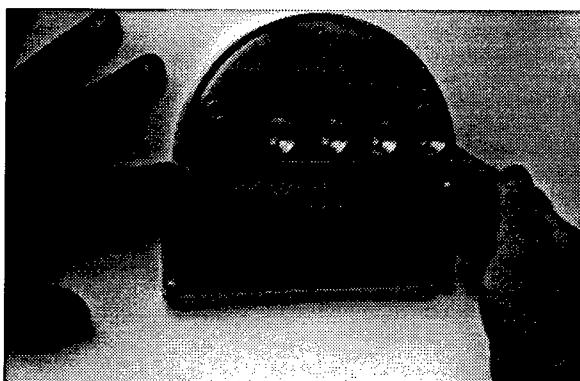


Figure 4: Siecor Ribbon Transverse Flex Mandrel

Ribbon Transverse Flex Procedure

- Obtain an approximately 50 cm sample length of 12 fiber ribbon.
- Place the sample to be tested on the mandrel with ≥ 2 cm of excess extending beyond the mandrel entrance (left hand side as viewed in the photograph).
- Manually or mechanically clamp the excess length in place.
- Slowly ($\sim 60^\circ$ per second), bend the ribbon sample laterally around the full bending radius of the mandrel.
- No holding time was imposed on the flexed ribbon in this testing.
- At approximately the same rate ($\sim 60^\circ$ per second), release pressure on the ribbon, allowing it to egress from the mandrel, until it is fully relieved.
- Observe the ribbon sample and rate it as per the following rating criteria.

Ribbon Transverse Flex Rating Scale

- 1 Upon release from the mandrel, the sample shows no adverse effects from the bending.
- 2 Some minimal delamination of the matrix from the fibers is observed during the bending process. Typically, the delamination is limited along the length of a single fiber, and is noted in ≤ 5 zones. Each delamination is ≤ 1 mm in length.
- 3 Moderate delamination of the matrix from the fibers is observed during the bending process. The delaminations extend across the ribbon (two or more fibers), are > 1 mm, but ≤ 2 mm in length, and appear in multiple zones (> 5). No fiber or group of fibers separate from the ribbon.
- 4 Significant delamination of the matrix from the fibers is observed during the bending process. The delaminations extend across the ribbon (two or more fibers), are > 2 mm in length, and appear regularly along the sample length. Some fiber/s may separate from the ribbon.
- 5 The ribbon debonds or splits between fibers in an axial direction during the bending process resulting in an inability to continue the test. The ribbon cannot be fully bent around the mandrel.

Table 6, on the following page, summarizes the results of Siecor's ribbon robustness testing.

The ribbon robustness testing indicates that a high level of matrix to fiber adhesion can negatively affect the handling (fatigue) robustness of a ribbon structure as evidenced by the "Flexed Twists to Failure" results. Further it indicates that a medium level of adhesion can provide advantage through the ability to minimize general delamination in handling while allowing a low level relative slip between the fiber and matrix toward a less brittle composite structure.

Overall Testing Summary

The property of adhesion plays a major role in the handleability performance of coatings used in fiber optic strands, inks, and ribbon matrix materials. These applications require different levels of uniform adhesion to their substrate materials in order to achieve optimized

Table 6: Ribbon Robustness Test Results

Ribbon	Twists to Failure	Transverse Flex Rating	Flexed Twists to Failure	Comments
A	7.8	5	0 (could not test after flexing)	high matrix to fiber adhesion created a brittle structure that totally degrades during flexing.
B	6.6	2.7	6.3	flexing generated a subtle degradation in ribbon strength.
C	7.4	1	7.4	flexing generated no noticeable degradation to ribbon strength.

optical and mechanical fiber and ribbon performance.

In this paper, it is assumed that the fiber coatings and inks are well adhered to one another providing a high level of composite structural cohesion. The remaining ink/matrix interface is of interest. Controlled adhesion of the matrix to the ink is sought to allow a robust ribbonized unit capable of a high degree of manipulation/handling. However, the ribbon matrix must demonstrate ease of peelability/removal from the ribbon fibers to allow access to the individual fibers. Hence, it is desirable to optimize the adhesive forces between the matrix and ink to the extent that the ribbon maintains its structural integrity until fiber access is desired.

If the adhesion between the matrix and fiber is low, we have demonstrated that ribbon separability suffers greatly as evidenced by the test results of ribbon B. Ribbon B was designed to have very low adhesion between the matrix and the fibers. As such, the ease of peelability for this ribbon was the very best. However, when separating the ribbon into two 6 fiber sub-units, we found that the newly exposed edge fibers were highly susceptible to straying from their intended units. This is an undesired feature in high fiber count environments where unitization brings a certain level of orderliness and sanity to the craft person. Additionally, stray fibers or the likelihood of straying will hamper subsequent mass splicing operations.

On the other hand, if the adhesion between the matrix and fiber is high, good separability was observed as evidenced by the test results of

ribbon A. Obviously, with the high matrix to fiber adhesion, the peelability is very poor. However, we were surprised to find that the robustness (per the combined flex and twist testing) suffered greatly.

Neither ribbons A nor B demonstrate an optimum ribbon design with respect to handleability. Ribbon C, however, was designed with a medium level of matrix to fiber adhesion, and yields an optimized ribbon design with respect to handleability. Table 7, on the following page, is a summary chart of the comparative rankings (1st - best to 3rd - worst) of ribbons A, B, and C, for each handleability characteristic:

Ribbon C possessed a medium matrix to fiber adhesion, medium/high matrix modulus, and thick cross section. It clearly demonstrates the most optimum ribbon configuration, relative to handleability performance, in this testing. Peelability was the only category falling outside a ranking of 1st. Ribbon C's peelability ranking of 2 implies that the fibers were expressly accessible in the zone of interest, but that the matrix did not peel further than the intended zone. The authors propose that this is actually an enhanced feature (due to the controlled adhesion) over a ribbon design allowing the matrix to peel in a continuous tape-like fashion. Peel of a continuous nature may result in undesired post handling peel propagation beyond the intended access zone; thus, compromising fiber protection.

Table 7: Ribbon Comparative Handleability Rankings

Ribbon	Strip	Peel	Separability	Furcatability	Flex/Twist (fatigue)	Average Ranking
A	1st	3rd	1st	3rd	3rd	2.5
B	1st	1st	2nd	2nd	2nd	1.8
C	1st	2nd	1st	1st	1st	1.3

CONCLUSION

Given the increased level of handling in the field to accommodate the explosion in communication and information transfer, it is essential that today's fiber optic cable components withstand frequent manipulation. As such, we have tested 3 ribbon designs with varying levels of adhesion, matrix modulus, and thickness with ribbon handleability as our focus. We chose 5 key handleability attributes and developed test and rating systems for each. Our testing indicates the need for a balanced ribbon design which is optimized for all handleability attributes. We have shown that highly optimizing for one attribute, ribbon peelability for instance, can place other handleability attributes at risk.

ACKNOWLEDGMENTS

The authors thank the many people who contributed to this development program. Special thanks go to Annette Kirby and Ellen Dugger for their vigilant testing, and to Randy Fulbright and Greg Mills for their contributions in development of the test methods and rating systems.

REFERENCES

1. Tomita, S., Matsumoto, M., Yabuta, T., & Uenoya, T., "Preliminary Research into Ultra High Density and High Count Optical Fiber Cables," *40th IWCS Proceedings*, St. Louis, MO, 1991, pp. 8 - 15.
2. Jackson, K.W., Santana, M.R., Sollenberger, N.W., Brown, R.J., Kroupa, K.M., & Webb, S.H., "A Modular Ribbon Design for Increased Packing Density of Fiber Optic Cable," *42nd IWCS Proceedings*, St. Louis, MO, 1993, pp. 20 - 27.
3. Mills, G.A., "Testing of 4- and 8-Fiber Ribbon Strippability," *41st IWCS Proceedings*, Reno, NV, 1992, pp. 472 - 475.
4. Beasley, W.E., Neveux, P., Yamane, Y., "Meeting the Demands of the Local Loop with Improved Ribbon Fiber Midspan Access," *NFOEC Proceedings*, Vol. 2, 1994, pp. 401 - 409.
5. Sawano, H., Kikuchi, Y., Kobayashi, K., Okada, N., Mosono, N., Suzuki, H., Sato, N., "One-Thousand-Fiber Optical Cable Composed of Eight Fiber Ribbons," *38th IWCS Proceedings*, Atlanta, GA, 1989, pp. 240 - 245.
6. Wagman, R.S., Lochkovic, G.A., White, K.T., "Component Optimization for Slotted Core Cables Using 8-Fiber Ribbons," *44th IWCS Proceedings*, Philadelphia, PA, 1995, pp. 472 - 478.

AUTHORS



Gregory A. Lochkovic is the Manager of UV Product Development at Siecor RD&E in Hickory, NC. His responsibilities include the development of UV related products for both domestic as well as Japanese markets. He received a B.S.M.E. in 1985 from Purdue University and an M.S. in Manufacturing Systems from Clarkson University in 1993. He has worked in various areas of fiber optic cable product and process development since graduation in 1985, and has been with Siecor since 1991. He has been awarded 7 patents and has authored/co-authored 5 publications.



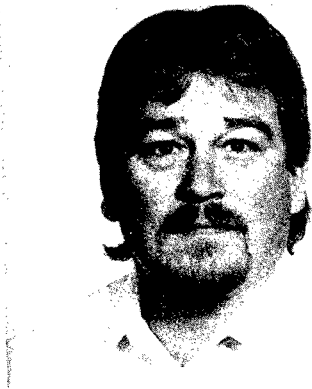
Naren I. Patel joined Siecor Corporation in 1979, and is the Staff Materials Specialist in Research, Development & Engineering. He received his B.S. degree in Chemistry from Gujarat University, India, B.S. (Technology) from the Department of Chemical Technology of Bombay University, and Ph.D. from the University of Leeds, U.K. Prior to joining Siecor, he had served as the Director of Quality Control, and Director of Research and Development in the textile industry.



Shail K. Moorjani is a Materials Engineer at Siecor Research, Development and Engineering in Hickory, North Carolina. He received his B. Tech. in Chemical Engineering from Osmania University, India in 1993 and his M.S. in Chemical Engineering from Michigan State University in 1996. Since he joined Siecor in August 1996, he has been involved in development of UV curables to be used in various optical communication cables.



Ronald J. Speights is a Process Development Technician in the UV Department at Siecor RD&E in Hickory, NC. He has received an Associates degrees in Science - Pre-engineering as well as Arts - English. He also received a B.S. in Business Administration from Gardner-Webb University in 1996. He has been involved with UV product and process development since its earliest beginnings at Siecor. He has been at the RD&E facility since 1993 with daily involvement in the research and development of multiple fiber optic ribbon cable products and processes.



Barney L. Stephens is a Process Development Technician in the UV Department at Siecor RD&E in Hickory, NC. He has been at the RD&E facility since 1991, and has been involved in the development of multiple fiber optic ribbon cable products and processes since 1993.

UV COLOR COATINGS AND MATRIX MATERIAL DESIGN FOR ENHANCED FIBER OPTIC RIBBON PRODUCTS

Kariofilis Konstadinidis, Neil W. Sollenberger, Shahab Siddiqui, Ken W. Jackson, John M. Turnipseed, T. W. Au, Raymond P. DeFabritis, and Carl R. Taylor

Bell Laboratories, Lucent Technologies, Inc., 2000 NE Expressway, Norcross, GA

ABSTRACT

With fiber optic ribbon cable moving closer to the customer, fiber branching becomes more frequent and additional craft-friendly features are desired in a ribbon. In particular, installers need to be able to both divide the ribbon into convenient, integral sub-units and to be able to cleanly access individual fibers from a ribbon in the middle of a cable span or from the end of the ribbon. In this paper we describe the methodology by which we engineered the bulk, surface, and interfacial properties of UV inks and ribbon matrix materials to achieve both integral sub-unit breakout and clean single fiber access while maintaining overall ribbon robustness.

INTRODUCTION

Not only is the demand for fiber optic ribbon continually increasing, but the need for improved performance for a variety of applications is also increasing. Initially, the major applications of fiber optic ribbon were for point to point applications where installation costs were driven primarily by cable packing density and mass splicing productivity. For these applications, a robust ribbon structure and excellent ribbon stripping performance were major requirements. Design of ribbon structures that have excellent stripping characteristics and high long term reliability requires an understanding of the interactions among the materials and processes involved.¹⁻⁶ With fiber optic ribbon cable moving closer to the customer, branching becomes more frequent and additional craft-friendly features are desired. In particular, installers need to be able to both divide the ribbon into convenient, integral sub-units and cleanly access individual fibers from a ribbon in the middle of a cable span as well as at the end of a ribbon. Existing ribbon structures that have

incorporated quick and easy fiber access into their design require re-ribbonizing of the fibers into sub-units after complete fiber separation from the original ribbon.⁷

Achieving integral sub-unit breakout and clean single fiber access requires intrinsically opposing properties of the materials comprising a ribbon. In this paper we describe the methodology by which we engineered the bulk, surface, and interfacial properties of the ribbon material system to achieve both integral sub-unit breakout and clean single fiber access. In particular, the bulk properties of the ribbon matrix and the adhesion at the matrix/ink interface were optimized by selecting materials with the correct range of properties and/or adjusting the processing conditions.

Design of Experiments principles were used to determine the optimum material properties and processing conditions. The resulting ribbon product, while being backward compatible with the alcohol gel/pad entry method, can be entered easily and quickly in midspan using a glue and tape method that leaves no matrix residue on the fibers, and retains 100 % of the ink on the fiber for correct identification.⁷ The same method can be used to access the fibers at the end of the ribbon for quick and clean removal of matrix. Moreover, the ribbon is robust enough to allow for excellent ribbon stripping using commercially available tools over a wide range of tool temperatures from 75°C to 160°C. During stripping the matrix-ink-coating composite comes off in a single piece minimizing the need to clean the blades of the stripping tool every single time. The ribbon is separable into user-determined sub-units that act as individual ribbons in all respects. UV colored fibers and enhanced ribbon samples have been aged at high temperature and humidity, both in air and in cable filling compound for extended periods of time (up to 259 days). The unique features

of the ribbon described above are retained after accelerated aging. Lastly, the retention of the craft friendly access features have been verified for a wide range of environmental conditions.

DESIGN OBJECTIVES

The goal of this work was to develop new UV curable inks and ribbon matrix materials for a ribbon design with the following features:

Quick and easy midspan and end-fiber access

The matrix should be easily removable using the newly-developed glue and tape method.⁷ No matrix residue should be left on the fibers and no ink should be transferred onto the matrix. The ribbon should be backward compatible with the present ribbon access method (alcohol gel/pad).

Robust sub-units

The ribbon should be separable into integral 4- and 6- and, in the case of 24-fiber ribbons, 8- and 12-fiber sub-units. The individual fibers should stay within the sub-unit during normal handling and installation conditions.

Controlled matrix peel

During midspan or end fiber access with the glue and tape method, the matrix peel should stop where the tape stops. This feature is crucial in ensuring the integrity of the ribbon after midspan access.

Robust ribbon stripping

The ribbon should be strippable with commercially available tools over a wide temperature range. The matrix-ink-coating composite should come off in one piece. Any coating residues on the glass should be removable with one alcohol wipe.

Excellent aging and reliability

The ribbon should retain its craft friendly features after heat and humidity aging in air and cable filling compound under simulated field conditions,

Meet Bellcore requirements

The ribbon should meet or exceed all GR-20 requirements and objectives for colored fiber and ribbon products.

The main challenge in achieving these objectives is that some of them require contradicting material properties. For example, high ink-to-matrix adhesion is good for ribbon stripping and sub-unit robustness, but detrimental to fast and easy fiber access. Similarly, a soft matrix material helps sub-unit

separation and robustness, but is adversarial to ribbon stripping. So the goal of this work is to balance the ink-to-matrix adhesion and tune in the mechanical properties of the matrix, in order to arrive at a ribbon product that has the foregoing attributes and can be manufactured in a manageable processing window.

DESIGN OF EXPERIMENTS

Factors

The two main design parameters used in this work are the adhesion of the matrix to the ink and the matrix modulus. The former was adjusted by changing the surface properties of the ink through changes in the ink formulation. The matrix modulus was adjusted by changes in the formulation as well. The general design principle was the following: as the ink-to-matrix adhesion decreases, a higher-modulus matrix material is needed to compensate for the adhesion loss as illustrated schematically on Figure 1.

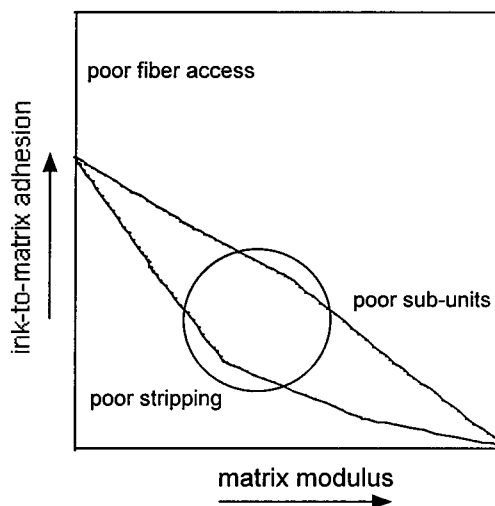


Fig. 1. Schematic representation of the effect of matrix modulus and ink-to-matrix adhesion on ribbon properties

It should be noted, however, that there is a limit where the adhesion becomes so low that it is no longer possible to separate the ribbon into sub-units without the fibers falling out of the matrix. The optimum region has been determined by testing several UV curable matrix materials and several high speed UV curable inks with variable surface properties.

Responses

The following ribbon performance attributes were used to determine the optimum material formulations:

Ribbon stripping. Each sample was stripped using two commercial tools. Tool A was set at 75°C, 105°C, and 135°C, while tool B was set at 120°C, 140°C, and 160°C. Five samples were stripped at each tool temperature setting for a total of 30 samples and the average strip yield was recorded.¹ A successful strip is defined as one where the coatings composite is removed cleanly and any residue can be wiped off the fiber using an alcohol wipe.

Midspan fiber access. Two methods were used to test the ease of fiber accessibility. In the glue and tape method, a drop of glue is placed between the ribbon and a plastic substrate and is used to break the ink/matrix bond. A double sided tape then propagates the matrix/fiber separation initiated by the glue. The procedure is repeated for the other side of the ribbon. In addition to a pass/fail criterion, we have also used a more quantitative way of measuring success rate and identifying entry failure modes. The second midspan fiber access method involves soaking the ribbon in an alcohol gel and wiping the matrix off the fibers with a textured pad. In this method, both the adhesion of the matrix to the colored fibers and the swelling of the matrix in alcohol play an important role. The results were recorded as soaking time to remove the matrix, or effort to remove the matrix for a fixed soaking time. Both methods can be used to access the fibers at the end of a ribbon, however, the easier way for end fiber access is to separate the fibers first and wipe the matrix off with a textured pad.

Sub-unit separation and robustness. A 2 meter ribbon sample was split into either two 6-fiber or three 4-fiber sub-units either by hand or with a dental floss tool. The samples were wound into loose 10 cm diameter coils and observed for fiber separation from the matrix. Sub-unit stripping was also used as a measure of robustness.

Ribbon aging. The ribbon performance attributes were checked after accelerate aging as described in a later section.

Bellcore. The ribbon samples were also tested against all Bellcore GR-20 requirements and objectives.

UV COLORED FIBER PROPERTIES

Adhesion to matrix

The adhesion of a fiber to a ribbon matrix material for inks with different surface properties was measured using a proprietary method. The results

shown on Fig. 2 indicate that the ink/matrix adhesion can be effectively controlled by adjusting the surface properties of the ink through small formulation changes. The ink/matrix adhesion can be changed by more than a factor of two with minimal formulation changes.

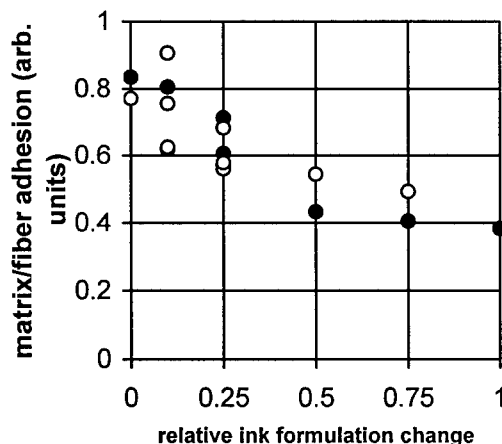


Fig. 2. Effect of ink surface properties on colored fiber adhesion to ribbon matrix

RIBBON PERFORMANCE

The optimum materials for the new ribbon design were selected based not only on meeting the design objectives, but doing so in the widest possible processing window. A complicating factor in materials selection for ribbon is that three major processes are involved in arriving at the final product, namely fiber draw, UV coloring, and ribboning. Each processing step exposes the fiber to additional UV radiation, possibly changing the bulk and interfacial properties of the materials in the final product. All these processing steps had to be taken into account during the materials design process and strict quality control was required. As an example, Figure 3 shows schematically the effect of ink and matrix UV dose on ribbon properties. Very low ink-to-matrix adhesion results in ribbon stripping and sub-unit failure, while high adhesion results in failure to access the fibers.

Fiber access

As set in the objectives, the optimum ribbon design can be accessed quickly and easily using the glue and tape method. No matrix residue is left on the fibers and 100% of the ink is retained for color identification. A built-in feature in the design is the controlled peel of the matrix. When the matrix is removed from a section of the ribbon, the rest of the structure remains intact and retains its robustness. For

matrix to be removed from additional length of ribbon, it has to be placed back on the tape, however, no glue is needed to initiate matrix removal.

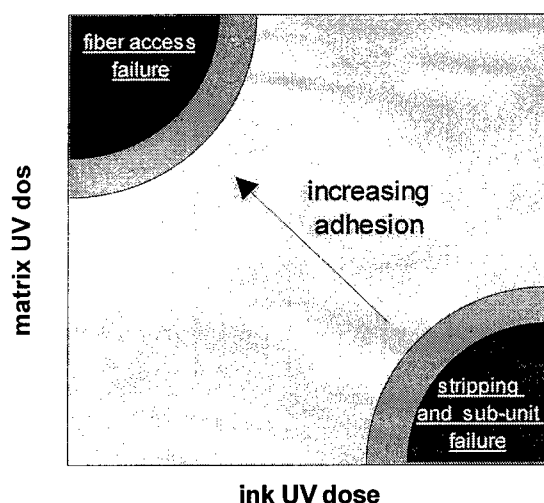


Fig. 3. Effect of matrix and ink cure on ribbon fiber access and stripping properties.

Ribbon stripping

Figure 4 shows the ribbon stripping yield averaged for several ribbon samples within the processing window. Results are shown for as-manufactured ribbon, and after aging for 14 days in room temperature water, 30 days @ 85°C/85% RH in air, and 30 days at 85°C in cable filling compound. In all cases the total stripping yield is higher than 95%.

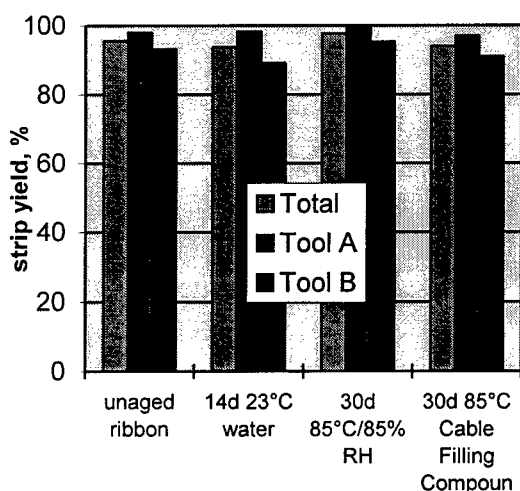


Fig. 4. Strip yield of 12-fiber ribbons as manufactured and after aging in different environments

Table 1. Strip yield of 6-fiber (from 12-fiber ribbon) and 12-fiber subunits (from 24-fiber ribbon)

	Tool A		
	75°C	105°C	135°C
6-fiber unaged	90%	100%	100%
6-fiber aged	90%	100%	100%
12-fiber unaged	100%	100%	100%
12-fiber aged	100%	100%	100%

Sub-unit separation and robustness

The new ribbon can be easily separated into integral sub-units either by hand or a dental floss tool. The easiest way to demonstrate sub-unit robustness is try to strip them using the standard 12-fiber ribbon stripping tools. Table 1 shows the stripping yield for 6-fiber sub-units obtained by splitting a 12-fiber ribbon in half, and 12-fiber sub-units obtained similarly from a 24-fiber ribbon. Although sub-units have one of the edge fibers "exposed" (no matrix protection), and despite the fact that the ink to matrix adhesion is relatively low to allow for easy fiber access, the strip yield of sub-units is high, indicating a very robust structure.

ACCELERATED AGING

Ribbon samples were aged at six temperature/humidity conditions for up to 259 days both in air and in cable filling compound. The exact aging conditions are shown on Table 2. The samples were then selectively tested for ribbon stripping, fiber access, sub-unit robustness, and ink retention. Table 3 shows the results for ribbon stripping after long term aging using tool A. The ribbon retains its excellent stripping characteristics after hydrolytic and oxidative aging. This excellent aging behavior is also seen after aging in cable filling compound. Most importantly, the ribbon retains its easy fiber access properties after long term aging. This is indicative of the stability of the ink to matrix adhesion both in air and in cable filling compound.

Table 2. Long term ribbon aging conditions

condition	medium	maximum duration, days
75°C	air, cable grease	259
95°C	air, cable grease	84
125°C	air, cable grease	40
85°C/85% RH	air, cable grease	196
95°C/95% RH	air, cable grease	84
120°C/100% RH	air, cable grease	23

Table 3. Ribbon strip yield after long term aging in air

days in aging	75°C	95°C	125°C	85°C 85%RH	95°C 95%RH	120°C 100%RH
17						100%
23						100%
28			100%			
49		100%			100%	
84					100%	
112				100%		
119	100%					
154				100%		
196				100%		
203	100%					
231	100%					
259	100%					

CONCLUSIONS

We have demonstrated that by using experimental design methods we have been able to balance the bulk, surface, and interfacial properties of a ribbon structure to manufacture a ribbon product that has quick and easy fiber access features without sacrificing ribbon or sub-unit robustness.

ACKNOWLEDGEMENTS

The authors would like to acknowledge the support and contributions of Manuel Santana, Ruben Travieso, Tim Dougherty, Charles Aloisio, Ken Kroupa, John Szwec, Daniel Harper, Heng Ly, Billy Oates, Tommy Bell, and Peter Kim.

REFERENCES

1. P.K. Kim, N. W. Sollenberger, K.W. Jackson, *Proceedings of the 44th International Wire and Cable Symposium*, 1995, pp. 635-639.
2. K.W. Jackson, T.L. Parker, J.R. Petisce, N.W. Sollenberger, C.R. Taylor, *Proceedings of the 42nd International Wire and Cable Symposium*, 1993, pp. 28-35.
3. K.W. Jackson, R.C. Moore, J. R. Petisce, N.W. Sollenberger, C. R. Taylor, J. M. Turnipseed, *Proceedings of the 10th NFOEC*, 1994, pp. 93-100.
4. J.R. Keesee, G.A. Lochkovic, D. Smith, J.R. Toler, *Proceedings of the 43rd International Wire and Cable Symposium*, 1994, pp. 430-439.

5. J. P. Bonicel, D. Keller, G. Kylen, J. Schulte, G. Paternostro, G.C. Cortines, C. Lasne *Proceedings of the 41st International Wire and Cable Symposium*, 1992, pp.25-31.

6. R.D. Mohen, T.W. Nolan, L.P. Provost, *Wire Journal International*, 25(12), 1992, pp. 63-72.

7. W.E. Beasley, P. Neveaux, Y. Yamane, *Proceedings of the 10th NFOEC*, 1994, pp. 401-409.

BIOGRAPHIES



Kariofilis Konstadinidis

2000 NE Expressway, Norcross, GA 30071

Kariofilis Konstadinidis is a Member of Technical Staff in the Materials Technology and Quality Engineering group at Bell Laboratories of Lucent Technologies Inc., Norcross, GA. He is involved in the development, qualification, and implementation of UV curable materials for optical fiber applications. He received his Diploma in Chemical Engineering from the Aristotle University of Thessaloniki, Greece, in 1987 and his Ph.D. in Chemical Engineering from the University of Minnesota in 1992. He did his post-doctoral work at Bell Laboratories in Murray Hill, NJ prior to joining Lucent in Norcross in 1995.



Neil Sollenberger

2000 NE Expressway, Norcross, GA 30071

Neil W. Sollenberger is a Member of Technical Staff in the Ribbon Technology Group at Lucent

Technologies/Bell Laboratories in Norcross, GA. He is responsible for various aspects in the design and development of fiber optic ribbons. Prior to his current assignment, his responsibilities have included the design and development of fiber optic cables, both copper and fiber optic closures and terminals, as well as cabinets for loop electronics. Neil Sollenberger joined AT&T Bell Laboratories in 1978. He has a B.S. degree in Agricultural Engineering from University of Georgia, and an M.S. degree in Mechanical Engineering from Georgia Institute of Technology.



Shahab Siddiqui

2000 NE Expressway, Norcross, GA 30071

Shahab Siddiqui is a Member of Technical Staff in the Materials Technology and Quality Engineering group at Bell Laboratories of Lucent Technologies Inc., in Norcross, GA. He joined AT&T Bell Laboratories in 1984 and worked in many areas of both fundamental and applied polymer chemistry at Bell Labs in Murray Hill, Princeton and Richmond. Currently he is responsible for the design and development of UV curable inks and other materials for fiber optic applications at Norcross. He received a Ph.D. degree in Physical Organic Chemistry from the University of Kentucky in 1982. His graduate thesis work dealt with photochemistry of carbanions.



Kenneth W. Jackson

2000 NE Expressway, Norcross, GA 30071

Kenneth W. Jackson is a Distinguished Member of Technical Staff in the Fiber Optic Cable and Materials Engineering Department at Lucent

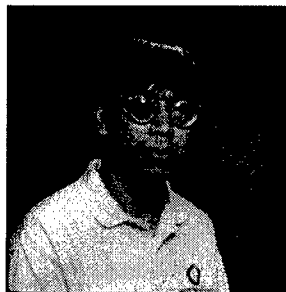
Technologies, Inc., Bell Laboratories, Norcross, GA. He is responsible for the design and development of outside plant cables. He joined the Western Electric Co. in 1970 having received a B.S.M.E. from Auburn University. He joined AT&T Bell Laboratories in 1981 having received an M.S.M.E. and Ph.D. in Mechanical Engineering from the Georgia Institute of Technology. Since 1981 he has worked in the areas of Optical Fiber Fabrication, Fiber Optic Connector Design and Development, Materials' Design and Fiber Optic Cable Design and Development. He has been awarded 8 patents and has 16 publications. He is a registered Professional Engineer in the state of Georgia, a member of ASME and the American Statistical Association.



John M. Turnipseed

2000 NE Expressway, Norcross, GA 30071

John Turnipseed is a Member of Technical Staff in the Materials Technology and Quality Engineering group at Bell Laboratories of Lucent Technologies, where he is engaged in the development and implementation of radiation curable materials intended for use in telecommunications products. He received B.S. and M.S. degrees in Analytical Chemistry from the University of Virginia prior to joining the Western Electric Company in 1972.

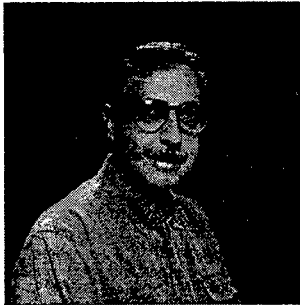


T. W. Au

2000 NE Expressway, Norcross, GA 30071

David T. Au is Member of Technical Staff in the Fiber Optics Engineering Department at the Lucent

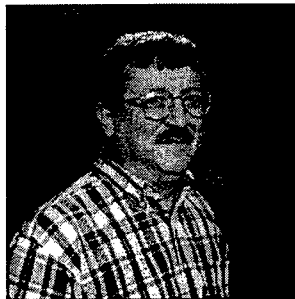
Technologies facility in Norcross, GA. Over the last ten years with Lucent, he has been involved in various research and manufacturing projects in the areas of semiconductor and printed circuit boards. He received the B.S. and M.S. degrees in chemical engineering from Auburn University in Alabama. He is a member of Tau Beta Pi and Omega Chi Epsilon.



Raymond P. DeFabritis

2000 NE Expressway, Norcross, GA 30071

Raymond P. DeFabritis is a Senior Technical Associate in the Materials Technology and Quality Engineering Group at Lucent Technologies inc., Bell Laboratories in Norcross, GA. Starting in 1968 with an AAS degree from the Academy of Aeronautics, his experience has been in microelectronics interconnection circuitry, materials, engineering, and UV color codes for optical fiber/ribbon products. He has been awarded two patents.



Carl R. Taylor

2000 NE Expressway, Norcross, GA 30071

Carl R. Taylor is currently a Bell Laboratories Technical Manager of the Materials Technology and Quality Engineering Group at Lucent Technologies' main Fiber Optic Manufacturing site in Atlanta. The group has responsibility for the design and engineering of materials used in fiber optic cable and apparatus products as well as responsibility for the quality of all incoming materials and components. He has previously been supervisor of the Plastics Engineering and Characterization Group in Atlanta and Supervisor of the Polymers Materials Research,

Engineering, and Applications Group at Bell Laboratories in Murray Hill, NJ. Prior to joining Bell Laboratories in 1977, he earned a B.S. in Chemistry from the College of Wooster in Ohio and a Ph.D. in Physical Chemistry from the University of Wisconsin in Madison. He holds nineteen patents and has authored or co-authored 29 publications.

The Effect of the Mechanical Properties of UV-Curable Resins on the Strippability of Optical Fiber Ribbons

AKIRA MURATA, KEIKO MITSUHASHI, and KEIJI OOHASHI

OPTO-ELECTRONICS LABORATORY, FUJIKURA LTD.
1440, MUTSUZAKI, SAKURA-SHI, CHIBA, 285 JAPAN

ABSTRACT

We have investigated the strippability of four-fiber ribbons using a thermal stripping tool, from the standpoints of the presence of stripping residues and the value of the stripping force. In this paper, we took a notice the adhesive force between the glass and the primary coating, as well as the mechanical properties of primary coatings, and examined the relationship between strippability and those properties. We then examined the effect of the test condition on the strippability of ribbons. Finally, we discussed the factors affecting strippability on the basis of the results of the measurement of strippability and observation of the coatings.

INTRODUCTION

With the increase in requests for high-density optical fiber cable, the use of ribbon fibers is increasing. Ribbon fibers are superior for processability compared to single fibers in loose tubes, as many fibers can be spliced at a time and little time is required to splice. When the coatings of ribbons are stripped with a thermal stripping tool, two primary problems tend to occur. One involves the degree of stripping force, and the other concerns the presence of stripping residue. If particles of the coating adhere to the glass following stripping, they must be wiped off which may result in high labor costs. The higher stripping

force leads to poor processability. Therefore, ribbons with lower stripping force and no stripping residue are optimum. These properties depend not only on the temperature of the stripping tool and the stripping speed¹⁻³⁾, but also on the mechanical properties of the coatings, particularly the primary coatings of the fibers. The stripping process of the coating for single fibers has been reported^{4,5)}, but that for ribbons is not clear. In order to improve the strippability of ribbons, It is important to understand the stripping process and the properties affecting strippability. In this study, we take a notice the properties (mechanical properties and adhesion force) of primary coating, as the primary coating is the origin of stripping residues and we think its properties are the most important factor affecting the strippability. Moreover, we examine the stripping condition dependence of strippability, particularly from the a standpoint of the existence of stripping residue. We do not consider the effect of the design of thermal stripping tool on strippability.

EXPERIMENTS

Fibers and Ribbons

Four-fiber ribbons were prepared using 0.25-SM-fibers consisting of several types of primary coatings and one secondary coating. Primary coatings of varying breakage elongation

Table 1. Properties of the primary coatings of the used fibers in four-fiber-ribbons

	A	B	C	D	E	F	G	H	I	J	K	L
Elongation	110	155	185	115	150	185	225	250	90	125	200	225
Strength	0.13	0.12	0.11	0.14	0.10	0.17	0.30	0.52	0.12	0.11	0.18	0.27
Adhesion	low	low	low	med.	med.	med.	Med.	Med.	High	high	High	High
Pull-out Force ¹⁾	40	45	50	120	110	100	110	125	140	150	150	140

1) Pull-out force are expressed with relative value as F's pull-out is 100

and adhesion force were chosen, as specified in Table 1. Tensile elongation and breakage strength were measured using primary coating sheets 0.20 mm in thickness with a test speed of 50 mm/min at 25 °C. The cure dose was 300 mJ/mm². The level of adhesion between the glass and primary coating is represented by the pull-out force⁶⁾ of the fibers measured at 25 °C prior to color coding. The pull-out force most accurately reflects the adhesion between the glass and primary coatings. Low adhesion indicates that delamination will occur easily if the fibers undergo mechanical perturbation.

The same Ink coating and ribbon matrix were used in all ribbons. The thickness of the ribbons was approximately 0.30 mm.

Stripping method

Stripping tests were performed using a conventional thermal stripping tool HJS-01 manufactured by Fujikura Ltd. The stripper is fixed in Tensilon as shown Figure 1, and the stripping stress is monitored. The temperature of the heated plate of the stripping tool is measured with a contact thermometer. The temperature ranges from 100 °C to 140 °C. The pre-heating time is 30 s and the test speed is at a constant rate, ranging from 3 mm/min to 500 mm/min. The stripped length varied from 5 mm to 30 mm for most experiments performed with 25mm of stripped length. The stripping force was defined as the maximum value of the stress. Evaluation of the amount of stripping residue is performed by counting the remaining particles of the primary coatings on the glass surface following stripping. The radius of the large particles is over 100 µm, while that of the small particles is from 10 µm to 100 µm. Cleanliness is divided in seven levels, from 1 (poor) to 7 (excellent), corresponding to the numbers of the residues. The criteria are listed in Table 2. An excellent level means that there are no particles on the glass. There are 10 test samples, and the stripping force and level of stripping residue are averaged. When one of the fibers was broken, it was not counted and was retested.

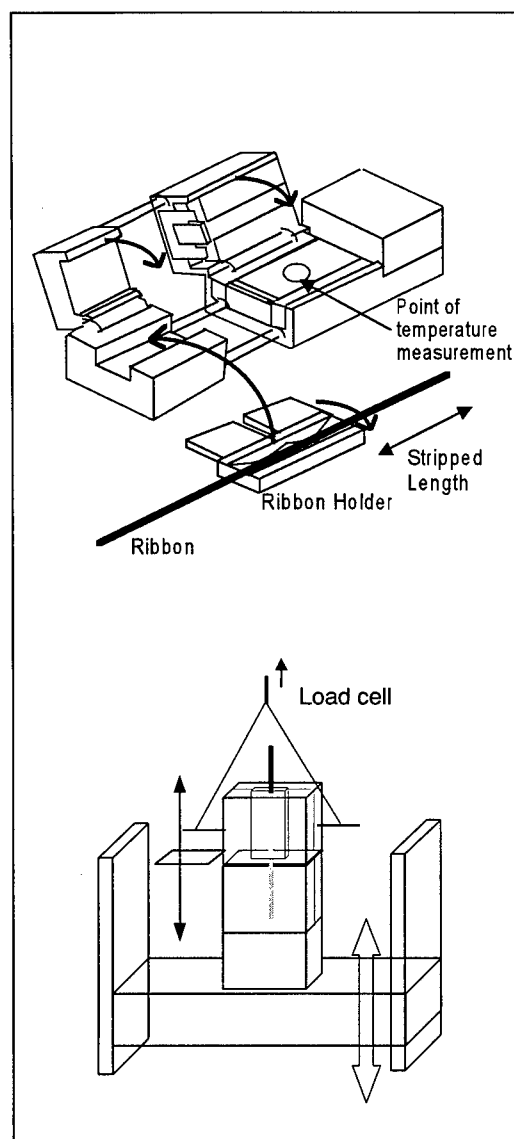


Figure 1. Sketch of experimental procedure

Table 2. The criteria of the level for the existence of the coating residue.

		Big Particle	Small particle
1	Poor ↑	10 <	Any cases
2		3 - 10	Any cases
3		0 - 3	5 <
4		0 - 3	< 5
5		0	5 <
6	↓ Excellent	0	0 - 5
7		0	0

RESULTS AND DISCUSSION

The effect of the properties of primary coatings on strippability

Table 3 shows the summary of the stripping test at 120 °C. The test speed is 100 mm/min. In the case of lower-adhesive primary coatings, only a few particles were observed even in lower-elongation primary coatings. On the other hand, in the case of medium- or higher-adhesive primary coatings, more residue tend to remain for lower-elongation coatings.

Table 3. The summary of the thermal stripping test.

Using low adhesion primary coatings

	A	B	C
Stripping Force	0.72	0.75	0.82
Level of residue	5.5	6.8	7

Using medium adhesion primary coatings

	D	E	F	G	H
Stripping Force	1.14	1.2	1.33	1.07	1.07
Level of residue	1.7	2.4	5.2	5.8	6.1

Using high adhesion primary coatings

	I	J	K	L
Stripping Force	1.15	1.37	1.22	1.65
Level of residue	1.3	1.5	2.8	4.3

Figure 2 shows the relationship between the pull-out forces of the fibers and the stripping forces of the various ribbons. Fibers are divided into three groups based on their pull-out force. Overall, the stripping force generally correlates with the pull-out force, but the fibers with a high or medium pull-out force show little correlation in the divided group. It seems that the other factor except adhesion force affects the value of stripping force. Figure 3 shows the relationship between the pull-out force and the level of stripping residue. In the case of lower-adhesive primary coatings, there are very few residues, but for fibers with a medium or high pull-out force, residues or fragments of primary coatings remain on the glass after stripping. It is clear that the amount of residue does not

correlate to the pull-out force value in the case of fibers with high or medium pull-out force. All cases, all stripping residues could be removed in one wiping with alcohol moistened tissues.

Figures 4 and 5 show the relationship between the elongation of primary coatings and stripping force and the level of stripping residue, respectively. There is no correlation between elongation and stripping force, but the levels of stripping residue on the ribbons using primary coatings with high or medium adhesion shows good correlation with the elongation of primary coatings. Ribbons using high-elongation primary coatings showed less residue. Figure 6 shows the relationship between the breakage strength and level of residue. There is no relationship between the breakage strength and

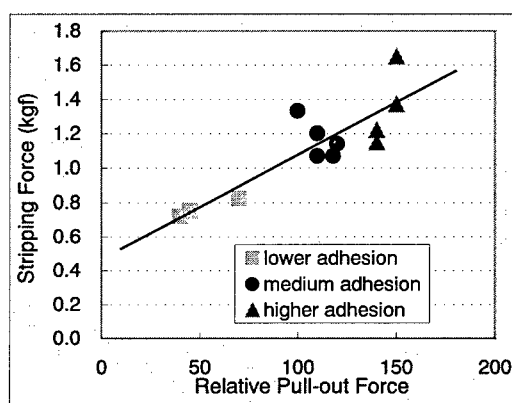


Fig.2 Relationship between the relative pull-out force and stripping force tested at 120 °C.

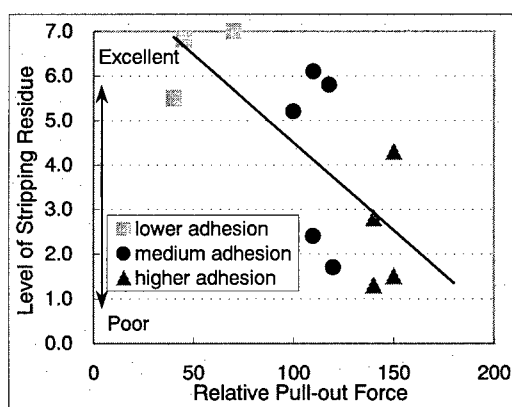


Fig.3 Relationship between the relative pull-out force and the amount of stripping residue tested at 120 °C.

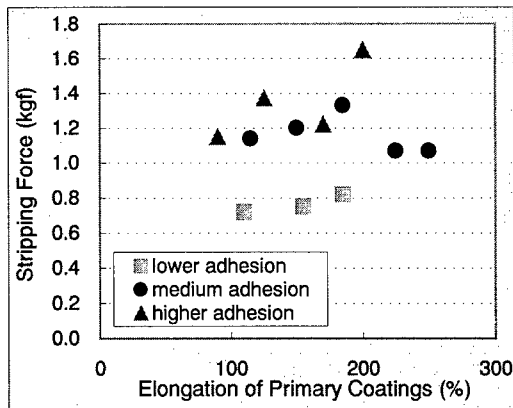


Fig.4 Relationship between the elongation of primary coatings and stripping force tested at 120 °C.

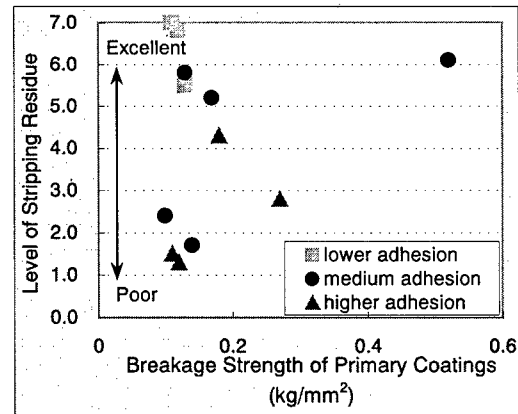


Fig.6 Relationship between the breakage strength of primary coatings and level of residues tested at 120 °C.

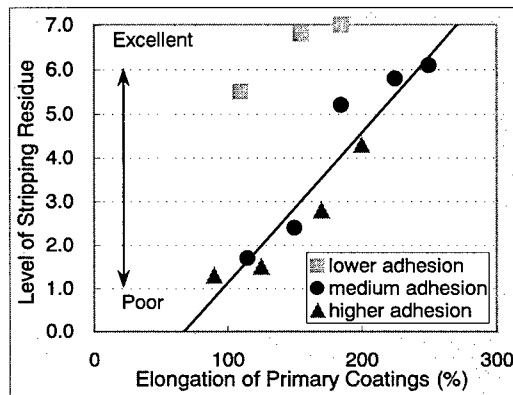


Fig.5 Relationship between the elongation of primary coatings and level of residue tested at 120 °C.

strippability. This seems to be related to the stripping process, as will be discussed in a later section. In this paper, the elongation and the strength of primary coatings are measured at 25 °C in tensile mode. In fact, the stripping tests were performed at 120 °C. The elongation of primary coatings at 25 °C and 120 °C are not identical. However, we believe that there is some correlation between the elongation at those temperatures, as the glass transition temperatures are much higher. As the result that, strippability of ribbons at 120 °C correlates with the elongation of primary coatings at 25 °C.

Temperature- and Test-Speed-Dependence of Strippability

In previous papers it was pointed out that there was an optimum temperature for thermal stripping^{1,3)}. The temperature-dependence of the stripping force and the remaining coating residue for ribbons with high- and medium-adhesion fibers D, E, F, H, J, and K are measured. The test temperatures are 100 °C, 120 °C, and 140 °C.

Figures 7 and 8 show the temperature-dependence of the stripping force and the level of residue, respectively. The stripping forces generally decrease with an increase in the temperature. The stripping force of ribbon E shows minimum value at 120 °C, on the other hand that of F shows the maximum value at 120 °C. The temperature dependence of

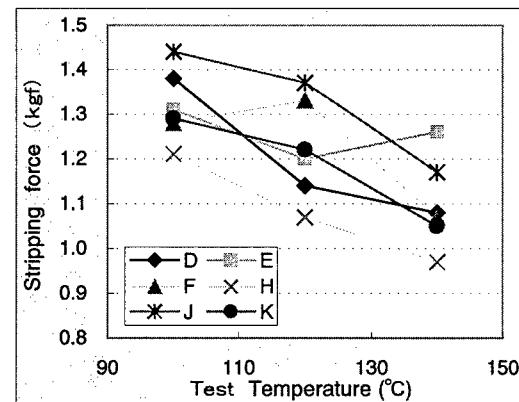


Fig.7 Relationship between the test temperature and stripping force.

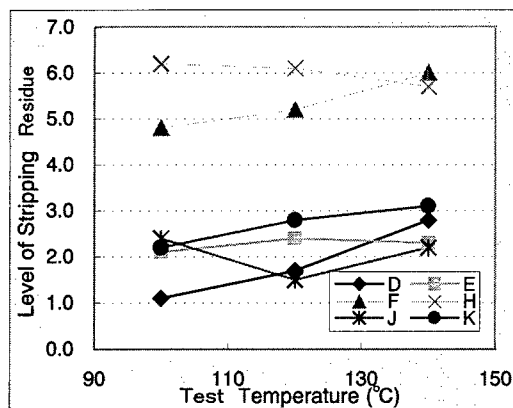


Fig.8 Relationship between the test temperature and level of residue.

stripping force is not uniform and depends on the type of primary coatings. The amounts of residue also change with the test temperature and decrease slightly at higher temperatures. However, a drastic improvement in strippability was not observed in these temperature regions. The formation of residue cannot be prevented even if the stripping temperature is controlled.

In the field, thermal stripping work is normally performed by hand, and therefore the stripping speed is not constant and may be so fast. Strippability may be dependent on the stripping speed. Figure 9 shows the relationship between the stripping force of ribbon J that shows poor strippability and the stripping speed. The stripping speed varied between 3 mm/min and 500 mm/min. The higher the stripping speed, the higher the stripping forces. The level of coating residue worsens slightly with an

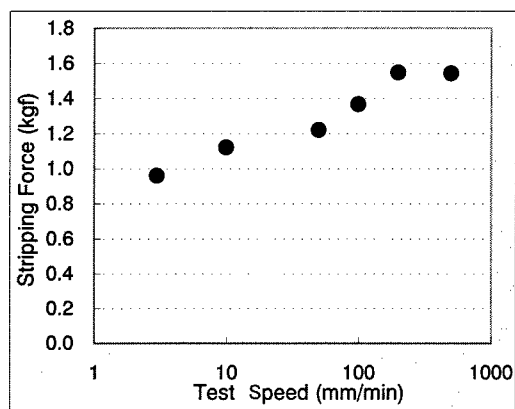


Fig.9 Relationship between the stripping speed and the stripping force tested at 120 °C.

increase in the stripping speed, as indicated in Figure 10. This suggests that the strippability with thermal stripping by hand operating may be poor.

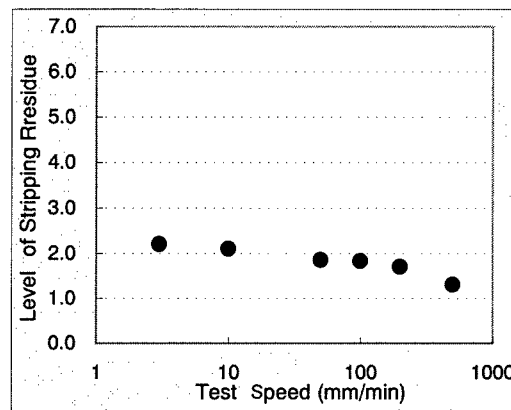


Fig.10 Relationship between the stripping speed and level of residue tested at 120 °C.

Stripping Mechanism

In all ribbons in these experiments, the profiles of the time-stress curve were similar, though the temperature and test speed varied. Figure 11 shows a typical time-stress curve for thermal stripping. Both axes are expressed in arbitrary scales. The stress increases dramatically at the time stripping is begun, decreases drastically following a very sharp peak, and then gradually decreases. When the stress reaches its maximum value, the stripped length is only 0.5 mm to 2 mm, depending on the test speed. To confirm the origin of the

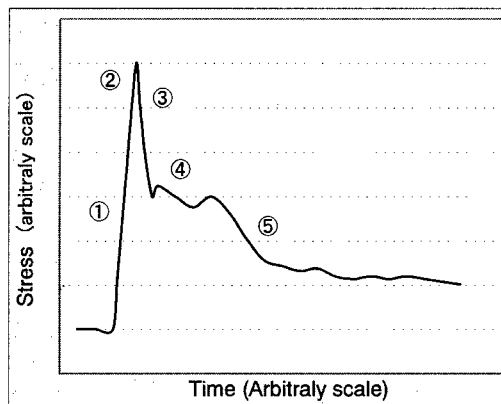


Fig.11 Typical time-stress curve during thermal stripping.

peak, we observed the interface of the glass and the primary coating at the five points indicated in Figure 11. The results are summarized in Table 4. Delamination did not occur immediately before the peak (point No. 2), but the delamination occurred at the interface of the glass and the primary coating of fibers near the blade of the stripping tool immediately after the peak (point No. 3). The delamination spread gradually with the progress of the stripping process. The maximum value of the stripping force is caused by the formation of the initial delamination. As a result, the stripping force is considered to correlate with the pull-out force. Actually, however, correlation between the stripping force and the pull-out force is not good, as shown in Figure 2. We consider the reason for this to be the fact that other properties, such as breakage strength of the primary coatings affect the stripping force.

Table 4. The mode of delamination at various stage of stripping

point	delamination	State of delamination
①	No	-
②	No	-
③	Yes	1mm (near the blade side)
④	Yes	3mm (near the blade side)
⑤	Yes	Several places

In the previous section, we examined stripping properties using a 25 mm length of ribbon. This stripping length is convenient for fusion splicing. In this section, we examined the stripping force of various lengths of ribbons in order to confirm the stripping mechanism. Figure 12 shows the stripping force at various stripped lengths and a stripping speed of 3 mm/min and 100 mm/min. The stripping forces are virtually constant with varying stripped lengths. This supports the results showing that the maximum peak value is caused by the formation of the delamination discussed above.

Stripping residue is made of broken particles of soft primary coatings. The large

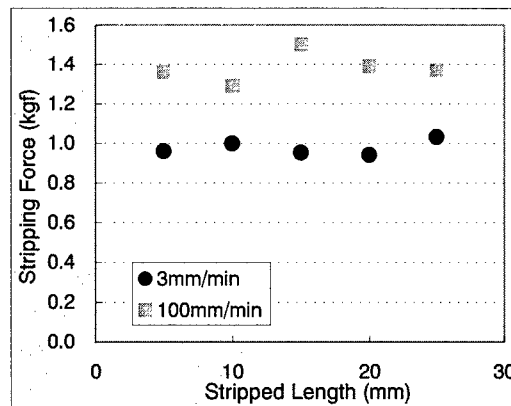


Fig.12 Relationship between the stripped length and stripping force tested at 120 °C.

(approximately 100 μ m) and small (10 or 20 μ m) particles adhere primarily on the middle section of the glass. The sketch is shown in Figure 13. In order to clarify where the particles come from, sectional and side views of the stripped coatings were observed under a microscope. It was found that only 1 mm length of coating near the blade was broken. Sketches of sectional view are illustrated in Figure 13. In the initial stage of stripping, the coating near the blade is compressed, as shown in Figure 13. If the elongation of primary coatings is small, the

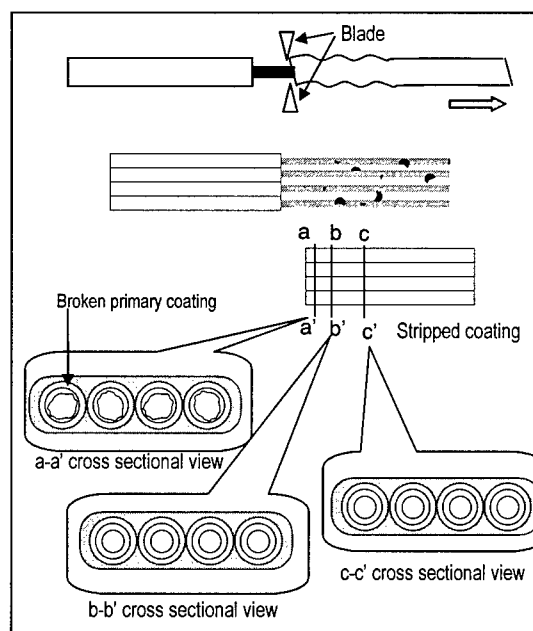


Figure 13. Sketch of the stripping process and the sectional view of stripped coatings

primary coatings will break. The broken primary coatings adhere to the glass and remain on the glass in the subsequent stripping process. If the elongation of the primary coating is large, the primary coatings are able to withstand the compression stress. Therefore, coatings with high elongation show less residue.

CONCLUSION

The strippability of four-fiber ribbons has been investigated through the use of a thermal stripping tool, from the standpoints of the presence of stripping residue and stripping force. The following conclusions can be drawn regarding the relationship between strippability and the properties of UV-curable primary resin:

- 1) The pull-out force of fibers affects the stripping force to some extent, but there is no clear relationship between the pull-out force value and the presence of stripping residue.
- 2) The amount of stripping residue correlate with the elongation of primary coating, ribbons with high-elongation primary coatings show less residue.

Moreover, the following conclusions can be drawn regarding the relationship between strippability and some test conditions:

- 3) The stripping force of ribbons normally decreased along with the temperature. The amount of residue also decreased over the temperature, but no drastic improvement in strippability was observed.
- 4) An increase in the speed causes slightly poor strippability.

Finally, based on examinations of the stripping process, the following conclusion can be drawn:

- 5) The maximum value of the stripping force is correlated to the formation of delamination. The pull-out force of fibers is one of the main factors affecting stripping force.
- 6) The coating residue is produced by the edges of stripped coating pieces near the blade. Ribbons using primary coatings with high elongation show less residue as the coatings are resistant to compression stress that occurs in the initial stage of stripping.

REFERENCES

- 1) K. W. Jackson, T. L. Parker, J. R. Petisce, N. W. Sollenberger, and C. R. Taylor, Proceedings of the 42nd IWCS, 28, 1993.
- 2) P. K. Kim, N. W. Sollenberger, and K. W. Jackson, Proceedings of the 44th IWCS, 635, 1995.
- 3) C.-K. Chien, H.R.Cole, J. R. Toler, Proceedings of the 45th IWCS, 554, 1996
- 4) H. C. Chandan, J. R. Petisce, J. W. Shea, and C. R. Taylor, Proceedings of the 41st IWCS, 239, 1992
- 5) A. Dwivedi and J. L. Smith, Proceedings of the 45th IWCS, 381, 1996
- 6) A. Murata, K. Oohashi, and A. Shinji, Proceedings of the 45th IWCS, 322, 1996

AKIRA MURATA



Opto-Electronics
Laboratory
Fujikura LTD.
1440, Mutuzaki,
Sakura-shi, Chiba,
285, Japan

Akira Murata was born in 1963. He joined Fujikura LTD. in 1992 after receiving his ph. D. in environmental science from Chiba University. He has been engaged in research and development for optical fibers, and is now an engineer in the Telecommunication Cable Material section and a member of the IEICE of Japan.



KEIJI OOHASHI

Opto-Electronics
Laboratory
Fujikura LTD.
1440, Mutuzaki,
Sakura-shi, Chiba,
285, Japan

Keiji Oohashi was born in 1956. He graduated from the Tokyo Institute of Technology in 1980 with a B.E. degree in chemistry. After eight years of work as an engineer in the field of materials for motor vehicles, he joined Fujikura LTD. in 1988. He has been engaged in research and development for optical fibers and optical fiber coatings. He is now chief of the Telecommunication Cable Material section and a member of the IEICE of Japan.

KEIKO MITSUHASHI



Opto-Electronics
Laboratory
Fujikura LTD.
1440, Mutuzaki,
Sakura-shi, Chiba,
285, Japan

Keiko Mitsuhashi joined Fujikura LTD. in 1991 after receiving her B.S. in Industrial chemistry from Chiba University. She has been engaged in research and development for optical fibers and polymers. She is now an engineer in the Telecommunication Cable Material section and a member of the IEICE of Japan.

CONTACT MECHANICS OF A FIBER OPTIC RIBBON

Mahmood Tabaddor, Ken W. Jackson, and Ruben Travieso
Bell Laboratories, Lucent Technologies, Inc., Norcross GA 30071

ABSTRACT

In the design of optical fiber cables, the ability to satisfy the contradictory needs of low optical loss and high optical fiber density is strategic. One design, the fiber optic ribbon, has proven to be a practical and effective means of developing high fiber count cables with low optical losses. However, slightly higher losses can occur in corner optical fibers within a stack of ribbons in a cable. This additional loss is stipulated to be the consequence of the local contact deformations experienced by those corner fibers. In this paper, we apply the finite element method to study the contact deformations of the corner optical fiber pressing against a core tube. The parameters of this study are the core tube radius, core tube modulus, matrix modulus, and fiber position. Results show how values of the aforementioned parameters affect optical fiber deformations and therefore, optical loss.

INTRODUCTION

For fiber optic cables, the ideal design is one that can protect and house a high number of optical fibers within a small volume while ensuring a low level of optical loss. The sources of such loss can be either external (environment, installation, etc.) or internal (loads applied by cable components). For fiber optic ribbon cables, it has been observed that corner optical fibers within a stack of ribbons can experience a relatively higher loss than other fibers within the stack¹.

The optical losses induced by optical fiber axis distortions have been divided into two categories: (i) macrobending and (ii) microbending losses. The characterization of such bending losses, in particular, microbending, has been the subject of extensive research²⁻⁵. These studies point to the very small scale nature of microbends and as Marcuse⁶ notes, 'deviations of the order of nanometers and correlation lengths of fractions of millimeters can cause very serious microdeformation losses.' For a ribbon in a central tube type cable, it is the cumulative effect of the microdeformations of the fibers over the length of the cable that is believed to be the source of the observed losses. These microdeformations of the corner fibers are attributed to the contact induced deformations and stresses as they press against the cable core tube containing the ribbon stack. To achieve lower transmission losses, this contact interaction must be closely examined.

LITERATURE REVIEW

In an attempt to model the mechanics of microbends, some researchers have applied elasticity theory to estimate the effect of various coating parameters on a loss-related parameter for optical fibers. Shuie⁷⁻⁸ and Shuie et al.⁹ have assumed that the microbending losses of a coated optical fiber can be linearly correlated to the internal pressure on the glass induced by an external hydrostatic pressure. The formulation is based on a multi-layer cylindrical model with a rigid glass core. Shuie developed an

analytical formulation for the internal pressure along with parametric plots outlining the regions of low pressure and therefore, low loss. In the same spirit, Suhir¹⁰ and Vangheluwe¹¹ have developed formulas for the effective spring constant of coated optical fibers. Roorda¹² used the formulation of Vangheluwe¹¹ to model the coated optical fiber as a beam on an elastic foundation. He found that the buffering action of a soft primary does not always hold true. The effectiveness of the primary in reducing fiber curvature is related to the distance over which the fiber is bent.

Keese et al.¹³ found that for optical fiber ribbons experimentally-measured loss had a minimum for matrix modulus values between 150-350 MPa for 180-micrometer coated optical fibers. Murase et al.¹⁴ applied a finite element analysis of a ribbon under lateral pressure only. They found that a thicker ribbon and higher matrix modulus decrease the 'stresses propagated to the fiber surface'. Kobayashi et al.¹⁵, using finite element analysis, also found that a higher modulus for the matrix leads to lower microbending losses.

Since the fiber optic ribbon is a composite structure, work done in the area of composite mechanics is worth examining. One common approach to obtaining a closed form analytical model for coated fibers in a matrix is the Concentric Cylinder Model (CCM). Here we cite only a few references regarding the optimization of coatings to achieve certain desirable outcomes such as low strain failure or low residual thermal stresses¹⁶⁻¹⁷.

Finally, research performed on the contact mechanics of multi-layer objects is relevant. Some models include analytical and numerical investigations into the effect of asperities, surface shape, and layer mechanical properties on the contact stresses and

deformations¹⁸⁻²¹.

In this paper, we present the results of a finite element contact model meant to provide insight into the deformations of the end optical fiber in a ribbon pressing against a core tube.

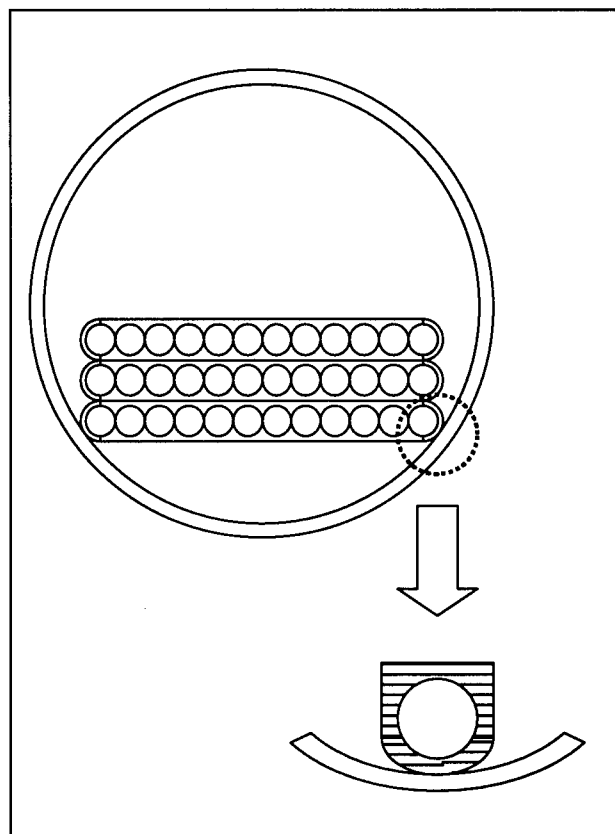


Figure 1 Schematic of Ribbon in a Core Tube

MODEL

The model we examine is based on the simplifications shown in Figure 1. Figure 1 shows a cross section of a stack of ribbons within a core tube. Looking at Figure 1, we see that it is the two lower corner optical fibers in the stack that contact the core tube when the cable is bent under tension. Actually, the two upper corner optical fibers will experience similar contact conditions since the ribbon stack is

helically wound within the cable. To further simplify the analysis, we isolate one of the corner optical fibers and model it as shown in Figs. 1 and 2. For simplicity, the combined effect of any external loading on the cable and that of the ribbon stack is replaced by a uniform displacement (Figure 3a). To solve this model, we rely on finite element analysis. We used a commercial finite element code²² with nonlinear contact analysis capabilities.

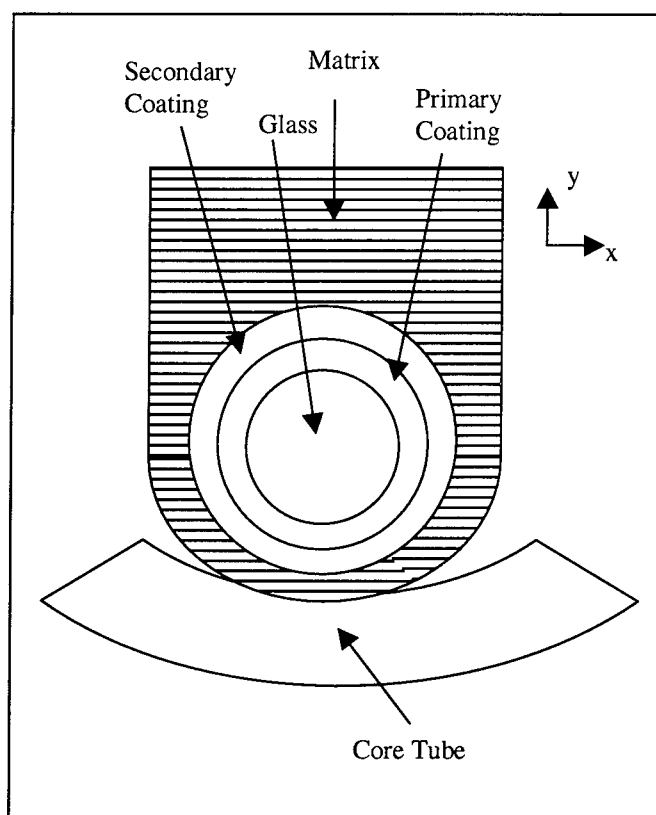


Figure 2 Schematic of Model

Based on our simplifications, we consider only a two-dimensional plane-strain model. With this assumption, we ignore the correlation length aspect of microbending and instead, concentrate on deformations within the glass core. Our measure of microbending is assumed to be a direct relationship between optical loss and the relative deformation of the core center (Figure 3a, point A) and the

glass/primary interface (Figure 3a, point B). Point B is directly below the center point A. The displacements for each point are measured from their initial unloaded configurations. Then the difference between the point displacements is calculated and normalized (the choice of a normalizing factor is discussed in the results section). This choice of relative displacement provides us with some measure of the strain (and stress) imparted to the glass core. Using the normalized displacement calculations, we suppose that a decrease (increase) in the relative displacement under loading of these two points is indicative of attenuation (amplification) in optical loss. As defined, the relative displacements will be positive for an optical fiber in a state of compressive stress along the axis defined by points A and B.

The independent variables in this study are the core-tube radius and modulus, matrix modulus, and optical fiber position within the ribbon. The finite element model of an end optical fiber in a ribbon resting on a core tube is shown in Figure 3a. This finite element model is a half model that allows for improved computational efficiency. However, to investigate the effect of optical fiber position, the symmetry of the model is lost and a full model is necessary. The boundary conditions of the contact model include a uniform downward displacement applied to the upper edge of the model and a fixed support at the lower boundary of the core tube (Figure 3a). For the half-symmetry model, we created over 5600, 2-D structural solid elements along with a range of 40-120 contact elements²². For the full model, we generated a model meshed with over 10000, 2-D structural solid elements and over 100 contact elements. Figure 3b shows an enlargement of the mesh density near the contact region. All contact is assumed frictionless.

RESULTS

For this model, the geometrical and mechanical properties of the optical fiber, primary and secondary coatings were kept constant. These values are listed in Table 1. All materials are assumed to follow a response dictated by a linearly elastic constitutive rule. Since the materials are viscoelastic, the modulus values chosen for each material are the equilibrium modulus values. The applied displacement was set to 5% of the outer diameter of the secondary coating. We chose the following values for each variable: matrix modulus (7, 35, 70, 350, 700 MPa); core tube modulus (7, 70, and 700 MPa); core tube radius (2.5-7.0 mm); and fiber offset (0, 2.54 and 20 micrometers). The Poisson ratio for all materials (except the primary) was set to 0.3. The core-tube radius refers to the inner diameter of the core tube. Arrow C in Figure 3a marks the secondary coating radius and Arrow D marks the thickness of the ribbon. Fiber position describes the x-position shift (Figure 2) of the center of the coated optical fiber within the matrix. The thickness of the core tube is set to 0.0254 cm for all cases. Even though the actual core tube thickness is greater, we found that contact stresses are not affected by core-tube material beyond a certain distance from the contact region. This allowed modeling of a smaller portion of the core tube thereby reducing computational time.

Table 1

Glass Modulus	70.0 GPa
Primary Modulus	0.7 MPa
Secondary Modulus	0.7 GPa
Primary Poisson Ratio	0.4999
Primary OD	180 micrometers
Secondary OD	250 micrometers
Glass OD	125 micrometers

Core-Tube Radius

First we investigate the effect of core-tube radius.

From Hertzian contact theory²³, we infer that the smaller the core-tube radius, the more its influence on the developing contact stresses and deformations. With this in mind, we chose to examine the smallest core-tube radius within our range of concern (with a ribbon thickness of 300 microns). We also selected 7 MPa as the modulus value for both the core tube and the matrix. The choice of the most compliant modulus for the matrix and core tube is dictated by the fact that this combination will produce the largest contact region. The contact region will be a measure of the influence of core-tube radius for all values under consideration.

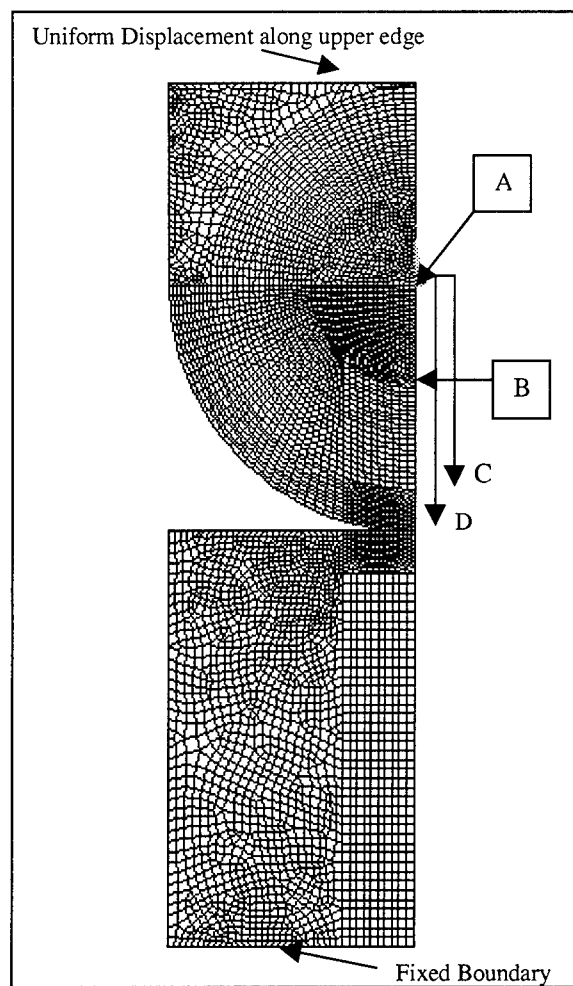


Figure 3a Finite Element Mesh of Half-Model

Table 2 shows the difference between the normalized relative deformations of points A and B for a flat core tube versus a core tube with a small radius. For all displayed results, we use the value of the relative displacements for the flat surface case as the normalizing factor. We see that the error is only that of a few percentage points. With this result, we can confidently use a simplified model of an optical fiber ribbon sitting on a flat surface. Note that these results are valid only for core-tube radii larger than or near 2.54 mm.

influence of the Young's moduli of the matrix and the core tube. Figure 4 shows the results for a ribbon thickness of 300 microns. In Figure 4, E_c denotes the core-tube modulus. Each point represents one run of the finite element code. Sidestepping issues involved in mesh refinement and contact penetration, we observe the following trends:

Table 2

Core Tube Inner Radius	Normalized Displacement
2.54 mm	0.96
Flat surface	1.0

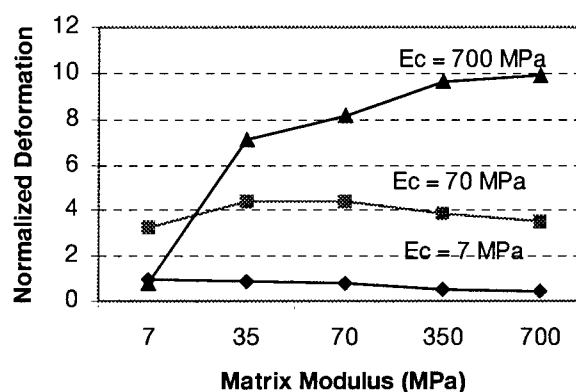


Figure 4 Normalized Deformations for Ribbon Thickness of 300 microns.

Normalized deformations for the hardest core-tube are most sensitive to changes in the matrix modulus compared to the lower core-tube moduli values. Except for a small portion of the low range of matrix moduli values, the normalized deformations are found to be most sensitive to changes in the core-tube modulus as the matrix modulus is decreased. For core-tube moduli of 7 and 70 MPa, the normalized deformations are essentially constant with changes in matrix modulus. As noted previously, for a core-tube

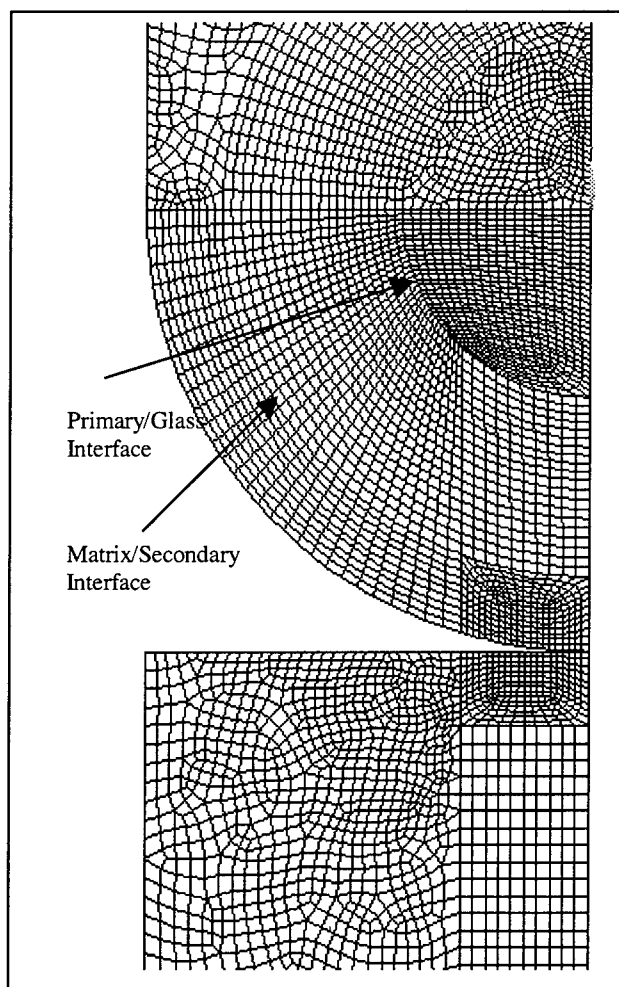


Figure 3b Enlarged View of Contact Area

Matrix and Core-Tube Moduli

This section describes a parametric study of the

modulus of 700 MPa, there is a pronounced drop in the normalized deformations with low-modulus matrix materials. However, it can be stated that the choice of a lower core-tube modulus results in lower normalized deformations. Hence, for the modulus range under consideration, a stiff matrix with a softer core tube may prove to be beneficial in reducing losses.

Fiber Position

Now we consider the effect of the end fiber position on the resulting normalized deformations. This variable provides some insight into the influence of end fiber eccentricity on the resulting contact deformations. Table 3 lists the normalized deformations for the perfectly centered fiber and two offset positions, where the ribbon thickness was set to 300 micrometers and both core-tube and matrix moduli were set to 7 MPa.

We see that the normalized deformations are increased as the offset grows so that a ribbon with low fiber eccentricity will incur reduced deformations.

Table 3

Fiber Offset (micrometers)	Normalized Deformation
0	1.01
2.54	1.93
20.3	3.25

Interfacial Stresses

Another important consequence of the ribbon end pressing against the core tube is the interfacial stresses that develop at the secondary/matrix boundary. If the interfacial radial stresses at the interface are tensile, the probability of delamination

increases. The stresses may not be sufficient to initiate such interfacial separations, however, they may be a mechanism whereby initial interfacial imperfections (due to manufacturing) are further degraded. For this reason, we briefly discuss some of the results on the stress patterns observed for the contacting ribbon model.

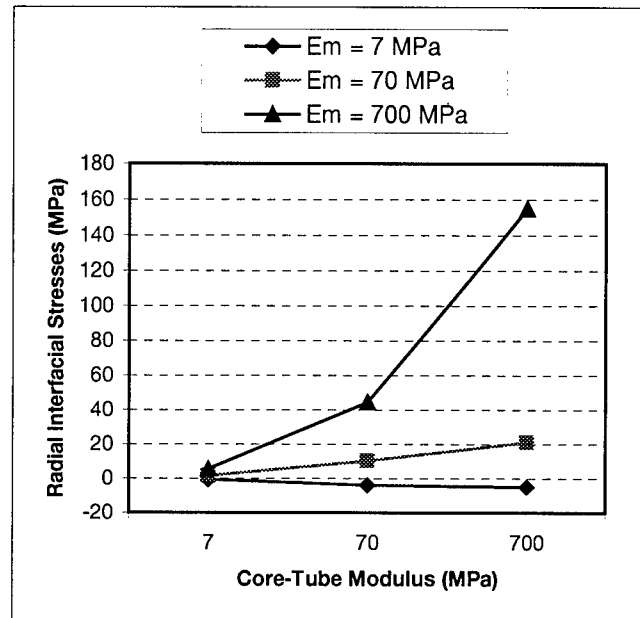


Figure 5 Radial Stresses at Matrix/Secondary Interface

Figure 5 shows the values of the interfacial stresses at a selected node on the secondary/matrix interface. The plot shows that as the values of both moduli increase, the radial interfacial stresses increase, changing from a compressive to a tensile state. We see that in general the trends to satisfy very low tensile radial stresses and normalized deformations are compatible. Whether these particular values of stress are sufficient to initiate debonding would require accurate and reliable measures of interface strength. Nevertheless, the presence of any tensile radial interfacial stresses is undesirable and should be

minimized. Figure 6 shows the resulting stress patterns generated by the finite element model (for a modulus of 70 MPa for both core tube and matrix).

The tensile interfacial stresses were found to occur in the region denoted by A in Figure 6. A secondary region of high tensile radial stresses was also found near the top. However, since this region is near the fixed displacement boundary, and unless this model matches closely the actual loading conditions, then St. Venant's²³ principle tells us that the stress distribution is not reliable near the boundaries.

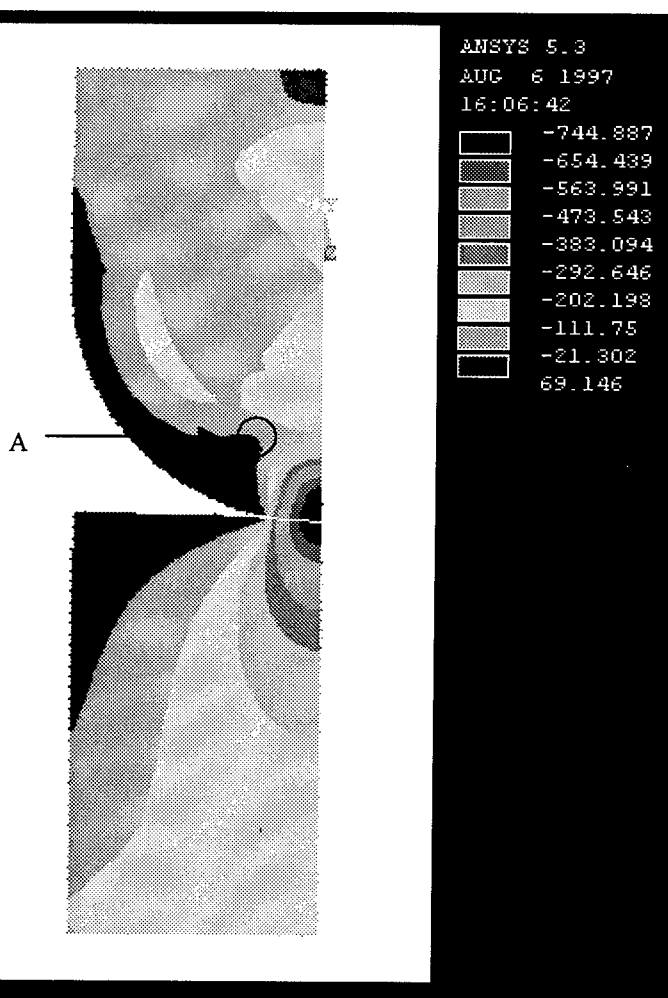


Figure 6 Radial Stress Contours

SUMMARY

We studied the contact deformations of an end optical fiber in a ribbon pressing against a core tube. By using the finite element method, we were able to perform a parametric study of the contact deformations and stresses. We found that any efforts to minimize optical fiber loss should take into account mechanical properties of both contacting surfaces. We chose a differential deformation of two points within the optical fiber as a measure of optical loss. For the range of parameters under consideration, we found that the choice of a hard matrix with a compliant core tube will yield lower contact-induced deformations. Results showed that the influence of the core tube radius is negligible whereas the fiber position is a possible factor influencing loss. Furthermore, numerical results revealed a small region of tensile radial stresses at the matrix/secondary interface. Such stresses, alone or in conjunction with other sources of stress, could destabilize initial interfacial weaknesses due to imperfections in the ribbon.

ACKNOWLEDGMENTS

The authors would like to acknowledge the insightful discussions with John Malluck, Dave Peckham, and Montri Viriyayuthakorn.

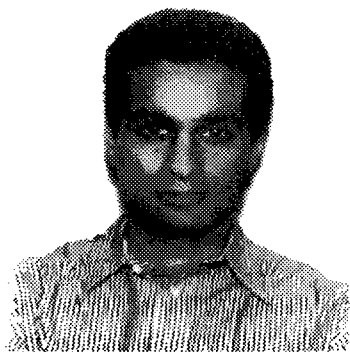
REFERENCES

1. Tomita, S., Matusmoto, M., Nagasawa, S., and Tadatoshi, T., 1993, Ultra High-Density Optical Fiber Cable with Thin Coated Fibers and Multi-Fiber Connectors, in **Proceedings of the 42nd International Wire and Cable Symposium**, Philadelphia, PA.
2. Arya, V., Murphy, K.A., Wang, A., and Claus, R.O., 1995, Microbend Losses in Singlemode Optical Fibers: Theoretical and Experimental

- Investigation, **Journal of Lightwave Technology**, Vol. 13, No. 10, pp.1998-2002.
3. Gloge, D., 1975, Optical-Fiber Packaging and Its Influence on Fiber Straightness and Loss, **The Bell System Technical Journal**, Vol. 54, No. 2, pp. 245-262.
 4. Unger, C. and Stocklein, W., 1994, Investigation of the Microbending Sensitivity of Fibers, **Journal of Lightwave Technology**, Vol. 12, No. 4, pp.591-596.
 5. Renner, H., 1992, Bending Losses of Coated Single-Mode Fibers: A Simple Approach, **Journal of Lightwave Technology**, Vol. 10, No. 5, pp. 541-551.
 6. Marcuse, D., 1984, Microdeformation losses of single-mode fibers, **Applied Optics**, Vol. 23, No. 7, pp. 1082-1091.
 7. Shuie, S.T., 1995, Design of Double-coated Optical Fibers to Minimize Thermally and Mechanically Induced Microbending Losses, **Journal of Optical Communications**, Vol. 16, No. 4, pp. 152-155.
 8. Shuie, S.T., 1994, Hydrostatic Pressure-Induced Microbending Losses in Tightly-jacketed Double-coated Optical Fibers, **Journal of Optical Communications**, Vol. 15, No. 4, pp. 144-149.
 9. Shuie, S.T., Chen, K.Y., and Tseng, S.D., 1997, Axial Strain Induced Microbending Losses in Tightly-jacketed Double-coated Optical Fibers, **Journal of Optical Communications**, Vol. 18, No. 1, pp. 10-14.
 10. Suhir, E., 1988, Spring Constant in the Buckling of Dual-Coated Optical Fibers, **Journal of Lightwave Technology**, Vol. 6, No. 7, pp. 1240-1244.
 11. Vangheluwe, D.C.L., 1984, Exact Calculations of the Spring Constant in the Buckling of Optical Fibers', **Applied Optics**, Vol. 23, No. 13, pp. 2045-2046.
 12. Roorda, J., 1994, Amplified Microbending in Coated Optical Fibers, **Journal of Engineering Mechanics**, Vol. 120, No. 4, pp. 917-921.
 13. Keesee, J.R., Lochkovic, G.A., Smith, D., and Toler, J.R., 1994, A Comprehensive Approach to Ribbon Design with a Focus on Materials, in the **Proceedings of the 43rd International Wire and Cable Symposium**, pp. 430-439.
 14. Murase, T., Shiraishi, K., Kawano, T., Sakai, M., and Shiono, T., 1995, Mechanical Properties of Optical Fiber Ribbon, in **Proceedings of the 44th International Wire and Cable Symposium**, Philadelphia, PA, pp. 485-489.
 15. Kobayashi, K., Okada, N., Mitsuhashi, K., Ishida, K., Miyamoto, M., and Araki, S., 1995, Coating Design of Thin-Coated Ribbons using 250 um Coated Fibers, in **Proceedings of the 44th International Wire and Cable Symposium**, Philadelphia, PA, pp. 607-615.
 16. Hadjiprocopiou, M., Reed, G.T., Hollaway, L., and Thorne, A.M., 1996, Optimization of fibre coating properties for fiber optic smart structures, **Smart Materials and Structures**, Vol. 5, pp. 441-448.
 17. Carman, G.P., Averill, R.C., Reifsnider, K.L., and Reddy, J.N., 1993, Optimization of Fiber Coatings to Minimize Stress Concentrations in Composite Materials, **Journal of Composite Materials**, Vol. 27, No. 6, pp. 589-612.
 18. Rajendrakumar, P.K. and Biswas, S.K., Elastic Contact between a Cylindrical Surface and a Flat Surface: A Non-Hertzian Model of Multi-Asperity Contact, **Mechanics Communication Research**, Vol. 23, No. 4, pp. 367-380.
 19. Djabella, H. and Arnell, R.D., 1994, Finite element analysis of elastic stresses in multilayered systems, **Thin Solid Films**, Vol. 245, pp. 27-33.
 20. Soh, A.K. and Soh, C.K., An Improved Method for Determining Contact Stresses, **Journal of Strain Analysis**, Vol. 31, No. 3, pp. 169-176.
 21. Gao, H., Chiu, C.H., and Lee, J., 1992, Elastic Contact Versus Indentation Modeling of Multi-Layered Materials, **International Journal of Solids and Structures**, Vol. 29, No. 20, pp. 2471-2492.
 22. ANSYS/Mechanical, ANSYS Inc., Houston, PA.
 23. Flugge, W., 1962, **Handbook of Engineering Mechanics**, McGraw-Hill Book Co., New York.

AUTHOR BIOGRAPHIES

Mahmood Tabaddor is a Member of Technical Staff in the Fiber Optic Cable and Materials Development and Engineering Department at Bell Laboratories,



Lucent Technologies. He has his graduate degrees in Mechanical Engineering (M.S.) from University of Michigan and Engineering Mechanics (Ph.D.) from Virginia Polytechnic Institute and State University. He is a member of the American Academy of Mechanics and the American Society of Mechanical Engineers.

2000 NE Expressway, Lucent Technologies, Room 1D36, Norcross GA 30071
mtabaddor@bell-labs.com

Kenneth W. Jackson is a Distinguished Member of Technical Staff in the Fiber Optic Cable and Materials Development and Engineering Department at Lucent Technologies/Bell Laboratories, Norcross, GA. He is responsible for the design and



development of outside plant cables. He joined Western Electric Company in 1970 having received a

B.S.M.E. from Auburn University. He joined AT&T Bell Laboratories in 1981 having received an M.S.M.E. and Ph.D. in Mechanical Engineering from the Georgia Institute of Technology. Since 1981 he has worked in the areas of Optical Fiber Fabrication, Fiber Optic Connector Design and Development, Materials Design and Fiber Optic Cable Design and Development. He has been awarded 9 patents and has 16 publications. He is a registered Professional Engineer in the state of Georgia, and a member of ASME and ASA.

Ruben Travieso is a Bell Laboratories Technical Manager of the Ribbon Technology and Installation Engineering Group at Lucent Technologies, Inc., in Norcross, GA. The group has responsibility for development and manufacturing of Fiber Optic Ribbons used in Outside Plant and Premises Cables. Responsibilities also include the development of



High Fiber Count Cables, Installation Tools and Kits, and the Outside Plant Installation Testing Laboratory in Chester, NJ. Prior to his current assignment, he was Engineering Manager of the Installation Engineering Group and has had responsibility for the design and development of Fiber Optic Connectors. He has been awarded 4 patents. Ruben Travieso joined AT&T Bell Laboratories in 1986. He has a B.S. degree in Mechanical Engineering from the Georgia Institute of Technology and an M.S. degree in Mechanical Engineering from Stanford University.

THE SELECTIVE USE OF MARINIZED TERRESTRIAL CABLE FOR UNDERWATER APPLICATIONS

Sasha O'Bow-Hove

**Alcatel Submarine Networks
London
England**

Tiiu Kutt

**Tyco Submarine Systems
New Jersey
USA**

ABSTRACT

Marinized Terrestrial Cables (MTC) can provide a cost-effective solution in certain select repeaterless applications but the cost advantage decreases rapidly as the scope of application is expanded. The reduction in system cost is a function of a number of factors including: cable design and testing, marine operations, cable protection methodology and maintenance philosophy. Optimal solutions (either submarine or MTC) can only be realised by considering all of these factors together.

INTRODUCTION

In recent years the repeaterless underwater market has become highly competitive in areas such as Scandinavia where national telecommunications markets have been de-regulated [1].

To meet this demand, new low-cost underwater cable designs known as Marinized Terrestrial Cables (MTCs) are being considered in addition to traditional submarine cables, as a means to extend terrestrial systems offshore [2].

Submarine cables are by necessity expensive as they have been specifically designed for installation, operation and maintenance in extreme water depths, environments and weather conditions.

The comprehensive fully-qualified product range provided is therefore favoured for high-capacity high-reliability systems, where the cost of restoration/repair can be significant.

However, for some low-capacity low-risk applications a lower-cost lower-performance product may prove adequate depending on the system importance [3].

This paper considers the typical characteristics of such MTC applications in terms of their potential environments and the generic requirements needed to address them.

TYPICAL MTC ENVIRONMENTS





The driving force behind the emergence of MTC is predominantly economic so typical MTC environments are those that lend themselves to low installation and maintenance costs.

Specifically, any advantage gained by the use of MTC should not be eroded by an increase in route engineering, cable protection or system repair/restoration costs - as intrinsic to high capacity information 'highways'.

The benefits that MTC can provide are therefore best suited to low capacity applications in less aggressive environments - such as lake, river and fjord crossings and some selective island links, as indicated in Table 1 [3].

The key features of such low-risk environments, confirmed in advance through appropriate marine studies, normally include:

- absence of any significant fishing or shipping threat (i.e. no anchorage areas)
- benign sea-bottom, in terms of relatively smooth terrain and very low currents (if any)
- short span lengths, generally less than 20 km
- shallow depths, generally less than 300m

TABLE 1: TYPICAL MTC APPLICATIONS								
Marine Environment		System Characteristics		Sea Bottom State		Main External Threats		Potential Risk
		Length	Depth	Terrain	Currents	Fishing	Anchor Drag	
River		short	shallow	soft sediments	can be high but steady	-----	small	low
Lake		short - medium	shallow - medium	soft sediments	usually benign	local only	-----	minimal
Fjord		short	medium - deep	soft sediments and rocks	small tidal	local only	-----	low
Island Links		short	shallow	can be rough in a few places	small tidal	local only	limited	low

With the risk of cable damage potentially low, any incidental damage is most economically repaired at convenience (e.g. in good weather) or with the cable being simply replaced [3].

In either case, the high design penalty associated with full repair capability is avoided and allows design and cost optimisation with respect to:

- size, weight and flexibility for simple transportation
- strength to lay and recover the cable
- sea-bed stability once laid, i.e. relative density
- environmental robustness over its lifetime, i.e. chemical, mechanical and thermal
- compatibility with marine handling equipment

In some cases design elements can provide multiple functionality, allowing further simplification.

TYPICAL MTC DESIGN FEATURES

Compared to highly engineered submarine cables, the simpler the MTC design the more the cost-benefit for a given application.

Although many designs are possible, generic MTC design features are typically as illustrated in Figure 1 and Table 2 and include:

- similar fibre core to land cable (very high fibre count, low fibre proof-test)
- 'loose' fibre packaging to give additional strain relief
- minimal pressure/water barrier (can be non-metallic if shallow depth)
- strength member (for weight rather than pure strength)
- limited jointing (in-line or factory at most)
- one or two cable designs in product range (only one used in any particular application)

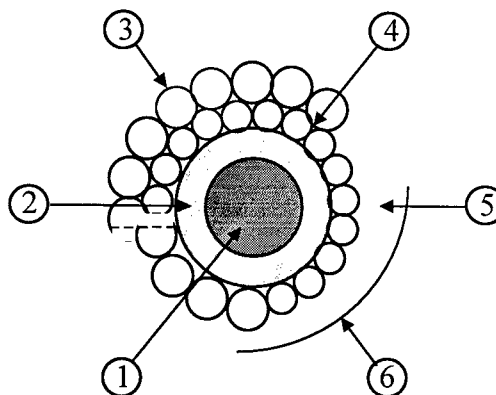


Figure 1: Typical MTC generic design

TABLE 2: TYPICAL MTC DESIGN FEATURES				
	ITEM	FEATURE	MTC	SUBMARINE
1	CORE	design packaging fibre count	terrestrial loose high (≥ 100)	as LW cable loose/tight medium (≤ 48)
2	BARRIER	type hermeticity method	plastic/metallic part/full overlap/extrusion	metallic full weld/contact pressure
3	ARMOUR	size grade treatment	small/medium low/medium galvanised	medium/large medium/high galvanised/preformed
4	COMPOUND	use	water-block	water-block
5	SHEATH	type	plastic/roving	roving
6	CABLE	design development manufacture cables joints/transitions overall cost	simple quick and simple simple one or two types limited/none low	complex long and comprehensive very precise product range product range + UJ relatively high

Cost reductions provided by MTC designs are not simply restricted to material savings. In addition to those indicated in Table 2, other savings can result from a reduction in stock inventories, spares holdings and in the ancillary equipment needed to process them.

The test regime needed to qualify MTC can also be radically simplified compared to submarine cables, resulting in rapid time-to-market.

required for submarine cables, as described in ITU-T Recommendation G.976 [4]. For instance, the required test load/duration can be only one third of that normally applied to submarine cables with joints [3].

The most appropriate test regime for all MTC applications, shown schematically in Figure 2, is still under review within ITU-T SG6. It is likely to be based on elements of Recommendation G.976 and the draft ETSI specification. It must be compatible with proposed marine operations.

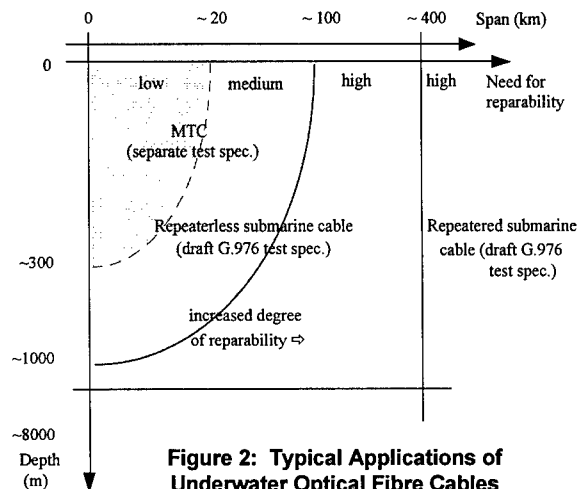


Figure 2: Typical Applications of Underwater Optical Fibre Cables

This test regime is considerably less comprehensive and severe than that normally

MARINE OPERATIONS

Marine operations for underwater applications normally include the following activities:

- route engineering
- transportation and installation
- protection methodology (as applicable)
- maintenance philosophy

In the case of complex routes, as common to submarine cable applications, each inter-related activity can be fairly demanding and expensive because of the variety of depths, terrain and threats to be considered along the route. A wide range of cable types, transitions and external protection schemes needs to be managed.

TABLE 3: TYPICAL MTC TEST REQUIREMENTS

TEST ITEM	TYPICAL REQUIREMENT	MAIN ISSUE(S)
MANUFACTURE		
Optical loss	power budget	design lifetime
Cable Diameter (d)	design limits	storage, sea-bed stability
Weight in air	design limits	drum/pan transportation
Weight in water (w)	design limits	tensile loads, sea-bed stability
HANDLING		
Coilability	yes, if required	barge/ship transportation
Tensile (sheave)	$\geq 2.5 \text{ wh}/0.5\text{m radius}$, 10+ mins	installation and recovery
Crush	10 kN, 100 mm plate/plate	transportation, equipment
Impact	50 J	storage, sea-bed integrity
Flexure	20d-30d radius, 30 times	factory transfer
OPERATION		
Temperature	-10°C/+60°C, 6 hrs	transfer, storage
Pressure	0.11h bar, 24 hrs	sea-bed integrity at design depth (h)
Hydrogen	power budget	design lifetime
Water Ingress	as agreed with user	cable re-use on damage repair
Cable Joints	90% cable test, if required	factory joints, repair if required

Much simpler techniques can and should be considered for identified MTC applications, where a single cable type should be sufficient to meet the necessary system reliability and lifetime requirements.

Route Engineering

Route engineering activities normally comprise a route study and a route survey. However, for MTC applications a route survey is not usually required or cost-effective if the route study has been conducted properly. The route study may form part of an early feasibility exercise if necessary.

The route study is the initial decision-making activity. Its fundamental purpose is to identify all political, economic and practical aspects related to the route [6]. It therefore influences the selection between MTC and submarine cable.

The criteria normally used in this decision, as expanded in Table 4, include:

- system requirements (e.g. importance, cost)
- artificial hazards (e.g. fishing, anchorage)
- natural hazards (e.g. currents, rock outcrops)
- practical issues (e.g. depth, length, access)

The route study should identify the likely cable type involved, the installation equipment required

and any additional external protection needed to ensure field reliability.

Discussions should be held with local authorities and fishing bodies for this purpose, together with inspection of landing sites and access points as necessary. To ensure low costs, a decision process similar to that shown in Figure 3 may be used.

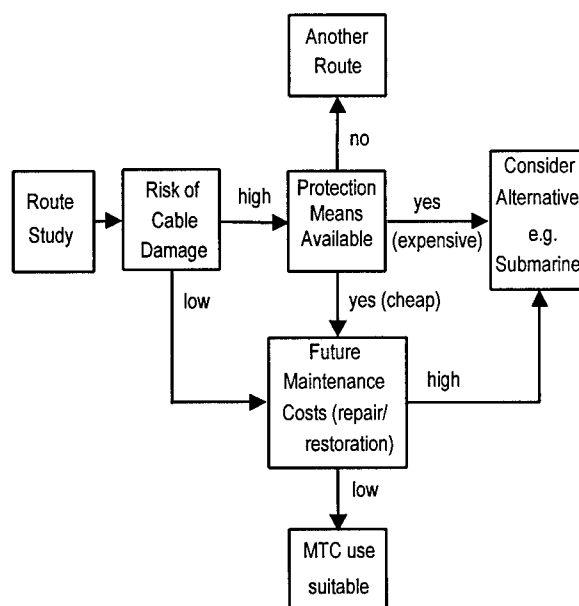


Figure 3: Typical MTC decision process

TABLE 4: TYPICAL ROUTE CONSIDERATIONS AND RELATIVE FIT				
CRITERIA	FEATURES	POTENTIAL ISSUES	MTC FIT	SUB FIT
SYSTEM REQUIREMENTS	importance	customer, preference	low	high
	cost	budget, restoration	low	high
	capacity	low or high	low	high
	upgradability	future requirements	×	✓
	maintenance philosophy	repair/replace, timing	as convenient	any time
ARTIFICIAL HAZARDS	fishing	local, commercial	local	(commercial)
	anchorage	exclusion zones	×	(✓)
	commercial shipping	ships in distress	×	(✓)
	outfalls	sewage, industrial waste	×	×
	pipeline/cable crossings	permits, suspensions	(✓)	✓
	dumping areas	munitions, waste products	×	×
	extraction/dredging areas	gravel, sand etc.	×	×
	offshore oil/gas activity	future re-routing	×	✓
NATURAL	currents	cable/sand movement	✓	✓
	rock outcrops	alter-courses, suspensions	✓	✓
	slopes	suspensions, slack	✓	✓
	water outflows	lochs, dams, valleys etc.	✓	✓
	ice accumulation areas	ice-rafting	×	(✓)
	chemicals	H ₂ S, background radiation	×	✓
	sand waves	movement, de-burial	×	✓
PRACTICAL ISSUES	depth	pressure, tension	<300m/1000m	<6000m
	length	manufacture, transport	<20km/100km	<400km
	access to landing	transport, equipment	✓	✓
	usual traffic to be carried	national/international	national	international
	fault history in area	poor risk assessment	×	(✓)
	networking arrangements	re-routing facility	✓	✓
	social use	resorts, tourism etc.	✓	✓
	LEGEND	✓ : complies to typical requirement, () : normally to be avoided, but can be overcome at cost × : normally cannot be accommodated		

Transportation

The preferred means of transportation will be influenced by the length and type of cable to be used and the location and accessibility of the landing-sites.

For land-locked routes, it is common to transport cable from the factory by road or rail where possible, with transfer to a variety of craft (e.g. small boats, barges, pontoons). This can happen either at site or at some convenient point nearby. The underlying purpose is to reduce the high cost of mobilisation and craft hire, which is normally on a daily rate.

Similar considerations apply to 'open-sea' routes, however transfer can be made nearer to the

factory into appropriate sea-going vessels, including 'vessels-of-opportunity'.

For some short applications, the use of craft may be unnecessary if the cable can be pulled and/or floated across. In such cases it is common to supply cables on drums as this simplifies operations both in the factory and at the landing-site. However, very large or heavy armoured cables may not be readily transportable in sufficient length, due to the excessive size of drum needed or weight to be carried.

Other than dock-side jointing, which impinges on the cable design and increases project cost/complexity, other means of transporting long cable lengths by land include the use of large

pans or containers. In most cases cable coilability is a pre-requisite.

The most cost-effective method to adopt will depend on the specific characteristics of the proposed application. It can however influence the installation methodology.

Installation

Considerably less sophisticated equipment is needed for MTC applications compared to submarine cables because of the shorter, shallower low-risk environments. There is generally little need for precise cable handling/control systems (e.g. slack control) or for exact ship station-keeping - if a ship is in fact used.

Because of the low-risk environment, the installation process can also be rationalised to the simple surface lay of cable, with any additional protection requirement carried out post-lay. The use of divers can be considered if necessary.

Installation equipment may include a small cable engine or cable transporter to move the cable overboard, and a sheave to control its passage. The cable engine can also be used to transfer cable onboard prior to lay.

Cable Protection

Should protection be required conventional armouring is normally sufficient. If armouring proves inappropriate or inadequate, other alternatives that can be considered include articulated pipe and cement-bagging. However there are depth and cost limitations to their effective use.

Cable protection by plough-burial, jetting or rock-dumping is not normally a cost-effective option for MTC applications because of the high costs involved compared to the limited area to be protected.

Maintenance Philosophy

A maintenance philosophy is required for all underwater applications even though various protection schemes can be used to mitigate threats to acceptable levels.

TABLE 5: TYPICAL MAINTENANCE OPTIONS

#	TYPE	FEATURES
1	Not repairable	<ul style="list-style-type: none">• no joint design• full replacement
2	Factory repairable	<ul style="list-style-type: none">• only factory joint• exchange spare for system cable
3	Field rejoinable	<ul style="list-style-type: none">• 'hybrid' field joint• limited repair conditions• limited strength
4	Fully repairable	<ul style="list-style-type: none">• full field joint• robust repair conditions• restores cable strength

In the event of cable damage, a wide range of maintenance options can be typically considered, as shown in Table 5.

As indicated previously, cable replacement (options 1 and 2) and cable repair at convenience (option 3) are most cost-effective for MTC applications, whilst full cable repairability (option 4) is a necessary expensive attribute of submarine cables.

Any necessary spares-holding, cable and/or repair equipment, must be configured into the maintenance philosophy adopted.

PRACTICAL CONSIDERATIONS

Tangible cost advantage can be gained by designing and using MTC in its appropriate application.

However, such advantage can be all too easily eliminated by a desire to expand the capabilities of a design or its range of application in isolation from other aspects of cable design and marine operations.

A variety of configurations, depths and span lengths may be possible, but will need review to ensure that the added complexity and cost still make MTC attractive

Similar considerations apply regarding any desire for branching units or improvement in repair capability. By their nature, such attributes require the highest level of development and therefore

normally fall outside the intent of MTC. After all, such characteristics are already inherent in submarine cables.

The use of MTC must therefore be sufficiently selective for true cost-effectiveness and successful application.

CONCLUSIONS

This paper has attempted to summarise the main considerations relating to the effective use of MTC in low-risk environments, as a low-cost alternative to submarine cable

It has been shown that:

1. Simplified MTC designs can provide cost savings in terms of construction, materials, testing and ancillary equipment.
2. Rationalised marine operations must complement the use of MTC in order to maintain the cost advantage.
3. Less sophisticated marine techniques can be used compared to submarine cable; a route survey may not be needed, and a single cable type may suffice.
4. The transportation, installation and protection options influence the cable design and vice-versa. All aspects need to be considered together.
5. The MTC cost advantage can be easily eroded through added complexity or increased performance requirements.
6. The use of MTC must therefore be sufficiently selective in order to make MTC attractive.

ACKNOWLEDGEMENTS

The authors would like to thank their respective Directors for permission to publish, and to thank

their colleagues and business associates for their helpful information and advice.

REFERENCES

- [1] Opening address of ITU-T SG6 Q11/6 Rapporteur's Experts Group Meeting in Stockholm, Sweden - November 1994.
- [2] Marinized Terrestrial Cable definition, as provided in ITU-T Recommendation G.972, 1977 version.
- [3] R.E.Frantz, S. O'Bow-Hove, 'Submarine Cable - What's in a Name', SubOptic 97, May 1997.
- [4] Single-Mode Optical Fibre Cables to be used as Underwater Cables for Lakes, River Crossings etc., interim ETSI specification prl-ETS 300634, 1996 revision.
- [5] Test Methods Applicable to Optical Fibre Submarine Cable Systems, ITU-T Recommendation G.976 (ex-Goss3), 1997 version.
- [6] M.R. Constable, 'Industry Demands of Marine Planning: Addressing the Deficiencies', SubOptic 97, May 1997.

ACRONYMS

MTC: Marinized Terrestrial Cable
LW: Lightweight
UJ: Universal Joint
ETSI: European Telecommunications Standards Institute
ITU-T: International Telecommunication Union - Telecommunication Standardisation Sector
LCE: Linear Cable Engine

BIOGRAPHIES

Sasha O'Bow-Hove



Alcatel Submarine Networks
Christchurch Way
Greenwich, London SE10 OAG
England

Tiiu Kutt



Tyco Submarine Systems
101 Crawfords Corner Road
P.O.Box 3030
Holmdel, New Jersey, USA

Sasha studied engineering at Cambridge University and then glass technology at Leeds University. He has worked on optical fibres and cable design since 1977 and submarine cables since 1987. As a senior principal engineer, his duties have included bid support, contract issues and the international standardisation of submarine cables. He regularly participates in ITU-T SG15 and SG6, occasionally in ETSI and IEC.

Tiiu received her doctorate in civil engineering and engineering mechanics from Columbia University in 1985. Since then, she has worked in several organisations at AT&T on a broad range of problems involving telecommunications cable and repeater installation and recovery as well as tow cables. She is currently part of Tyco Submarine Systems, a former business unit of AT&T.

A NEW HIGH BIT RATE SUBMARINE PRODUCT RANGE THE OALC 4 CABLE

Yves CHARLES - Jean-François LIBERT - Peter WORTHINGTON - Jean-Luc LANG

**ALCATEL SUBMARINE NETWORKS
536 Quai de la Loire - BP 849 - 62225 CALAIS CEDEX - FRANCE -**

I. - INTRODUCTION

Long-haul optical submarine cable systems have been in service for approximately 10 years.

Early systems operating at a single wavelength and with regenerative repeaters were tolerant of loss changes in the cable.

Present and future systems using optical amplifiers and wavelength-division multiplexing (WDM) require very stable optical transmission characteristics over a wide wavelength range.

Fibre designs optimised for WDM operation present new challenges to the cable designer.

The enormous bandwidth which is provided by WDM systems also means that the cost of outage time is increased, and hence even greater reliability is required of the submerged plant.

For the cable, this requires a high degree of protection of the transmission path for all service conditions.

This paper describes the development of a new cable range for long-haul amplified systems. Qualification of the cable has been completed with a comprehensive series of factory tests and sea trials.

2. - DESIGN OBJECTIVES FOR THE CABLE

The main design objective for the cable is to provide a reliable protection for the transmission path, which is suitable for both present and future fibre designs.

The cable range that has been developed provides a suitable environment for the fibres, with very low stresses on the fibre in all service environments.

The cable can accommodate up to 24 fibres. Although long-haul main trunks normally only require a small number of fibres (typically 4), some branching unit options or unrepeated spurs will require higher fibre counts.

The OALC 4 cable range is based on the same central lightweight cable and provides a versatile carrier for all types of fibre in all service conditions.

3. - WDM FIBRE REQUIREMENTS

The optical bandwidth of an Erbium-doped fibre amplifier (EDFA) is typically greater than 20 nm and allows transmission of many wavelengths with channel spacing of typically 1 nm.

Each channel operates at an output power comparable to single wavelength systems, so that total output power is higher for WDM systems.

The high output power is required to maximise amplifier spacing, but also increases the non-linearities in the fibre :

- ⇒ Brillouin scattering
- ⇒ Raman scattering
- ⇒ Self and cross phase modulation
- ⇒ Four wave mixing

Four wave mixing which create sum and difference frequencies when several wavelengths are present, is a major problem for WDM systems and must be minimised.

One solution is to reduce non linear effects by increasing the effective area of the fibre to reduce the optical power density.

Designs of fibre with a larger effective area generally have increased mode field diameter and are more sensitive to bend-induced loss.

The bend loss is highly wavelength dependent, so it is very important to minimise bend-induced loss increment which could cause loss variation over the operating spectrum of the WDM system.

Figure 1 shows the measured macro bend loss of some representative fibres, including experimented large effective area designs (LEA).

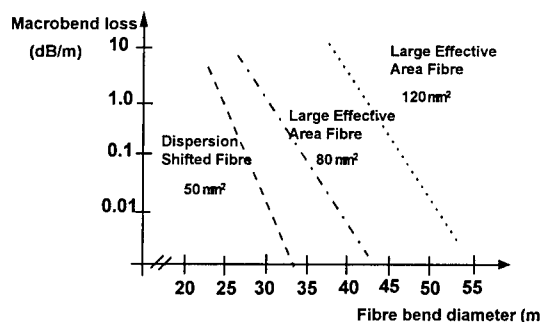


Figure 1
Macro bend sensitivity of fibres

The LEA fibres show much higher bend-induced loss compared to standard DS fibres. For example, at a bend diameter of 50 mm, an LEA fibre with an effective area of $80 \mu\text{m}^2$ may have a bend sensitivity 2 or 3 orders of magnitude higher.

The cable design must ensure that the fibres are accommodated with minimum stress to avoid macro and microbend-induced loss.

4. - CABLE DESIGN

The structure of the deep water lightweight (LW) cable is shown in **Figure 2**.

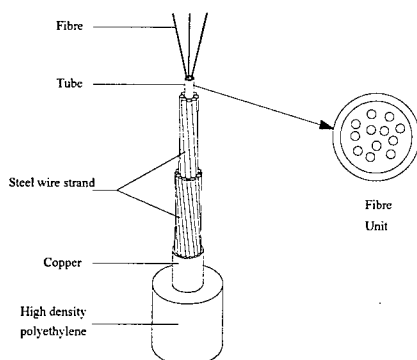


Figure 2
Description of the LW OALC-4 cable

The fibres are contained in a continuously welded stainless steel tube which provides protection from hydrostatic pressure and external stresses.

The tube is filled with a thixotropic gel which buffers the fibres and prevents axial water ingress in the event of a cable cut on the sea bed.

The cable strength member comprises 2 layers of high tensile steel wires providing a stable vault structure around the central steel tube.

The wires are enclosed in a copper tube which is continuously welded and drawn down over the wires. The copper tube provides the main power feed path and also acts as a hermetic barrier to prevent radial ingress of hydrogen. The interstices of the strand are intermittently water-blocked using a 50 % on, 50 % off ratio, which gives the optimum performance in limiting water ingress.

The composite copper/steel centre conductor of the cable is protected and insulated using a high density polyethylene sheath. Overall diameter of the LW cable is 17 mm. The main physical characteristics of the cable are summarised in **table 1**.

	UNITS	VALUE
Weight in air	kg/km	560
Weight in water	kg/km	330
Storage factor	km/m ³	3.5
Cable breaking load	kN	70
Modulus	km	> 21

Table 1

5. - CABLE PERFORMANCE

5.1. - Cable optical performance

The central fibre unit is the most important factor in providing the fibres with a stable and reliable environment.

The fibres are drawn into the continuously welded steel tube in a straight lay. The process is controlled to give a small excess length of fibre (typically 0.1 %), which ensures that there is no tensile stress in the fibres after deployment on the sea bed.

Tensile strains during laying and recovery are also reduced by the excess fibre length.

Note that the cable NTTs rating and fibre proof test are based on the worst case assumption of no excess fibre length. The effect of the excess length is to further improve the fibre reliability in service.

The fibres in the tube are buffered by the thixotropic gel filling which provides some axial restraint to restrict relative movement between the fibres and between the fibres and tube. This ensures stability of the fibre environment in service.

5.1.1. - WDM fibre trials

Since WDM systems require fibres with higher effective areas ($> 50 \mu\text{m}^2$), it was decided to characterise different fibre designs, to evaluate the effects of mode field diameter, and of cut-off wavelength, with regard to bending and microbending.

□ **Macrobending** : the test consists of bending the fibres under a radius covering the range 9 mm - 15 mm, and measuring the attenuation loss at 1550 nm.

Figure 3 shows the effect of the MFD (mode field diameter) for 2 fibres having a low λ_c of 1100 nm (cut-off wavelength). The increase in MFD of around $0.36 \mu\text{m}$ gives an increase in bend sensitivity in a ratio of 6, for a bending radius of 10 mm.

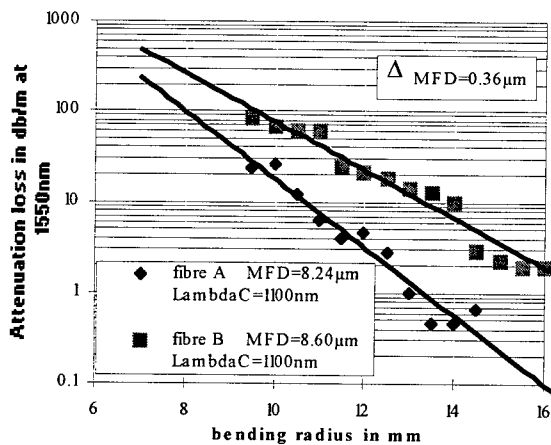


Figure 3
Macrobending sensitivity of WDM fibres
 $\lambda_c = 1100 \text{ nm}$

Figure 4 shows the beneficial effect of the cut-off wavelength, for 2 fibres having an MFD around $8.6 \mu\text{m}$. An increase in λ_c of around 455 nm decreases the bending sensitivity in a ratio of around 6, for a bending radius of 10 mm.

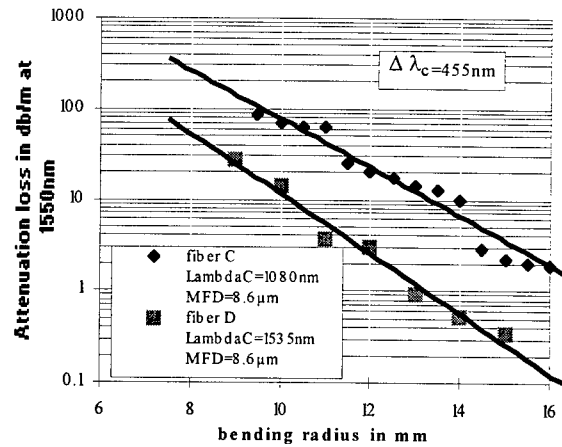


Figure 4
Macrobending sensitivity of WDM fibres
 $\text{MFD} = 8.6 \mu\text{m}$

□ **Microbending** : the test consists of winding under tension approximately 900 m of fibre, in one layer, on a spool having a grid on its bottom. The attenuation loss is recorded at 1550 nm.

Figure 5 shows the effect of the MFD, for 6 fibres having the same λ_c , around 1300 nm. An increase in MFD of around $0.65 \mu\text{m}$ gives an increase in attenuation in a ratio around 6. It is also interesting to see that, for two fibres having the same MFD of $8.60 \mu\text{m}$, a decrease in λ_c (from 1300 nm down to 1200 nm) gives a higher sensitivity (from 0.230 dB/km to 0.275 dB/km). All these evaluations lead to the careful selection of the optical characteristics of the fibres, in order to have uniform behaviour of the fibres, all along the system.

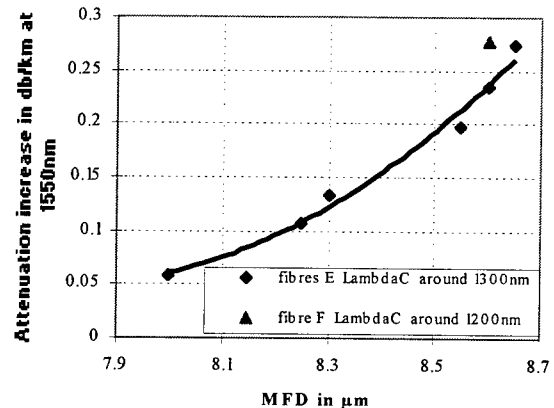


Figure 5 - Microbending sensitivity of WDM fibres

5.1.2. - Optical performance - Factory tests

Table 2 shows the optical performance of a prototype cable during the manufacturing processes, using a WDM fibre selected according to MFD and λ_c criteria.

	Initial	Optical module	Extrusion
Attenuation at 1550 nm (dB/km)	0.206	0.208	0.207
λ_o (nm)	1580.60	1580.70	1580.60
PMD (Ps/\sqrt{km})	0.04	0.06	0.05

Table 2

It can be seen that there is no significant change of the optical parameters during the cabling process.

The stability of optical transmission characteristics of the cable were measured by means of :

- Ageing test
- Temperature cycling test

Ageing test :

A cable prototype of more than 4000 m is put inside an oven. The temperature is maintained at 70° C for 1500 hours, which is representative of an ageing at sea bottom temperature for 25 years. Optical monitoring is performed at 1240 nm and at 1550 nm.

Figures 6 and 7 show the record at these two wavelengths, for a selected WDM fibre, and for a reference fibre.

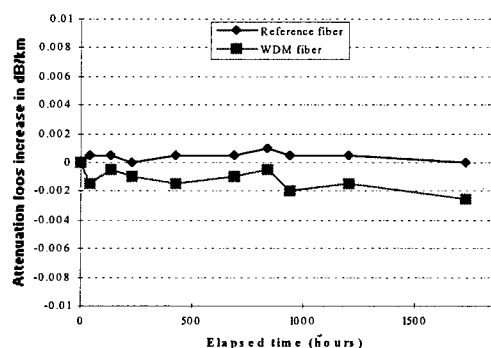


Figure 6

Ageing test 1800hours at 70°C. 1240nm record

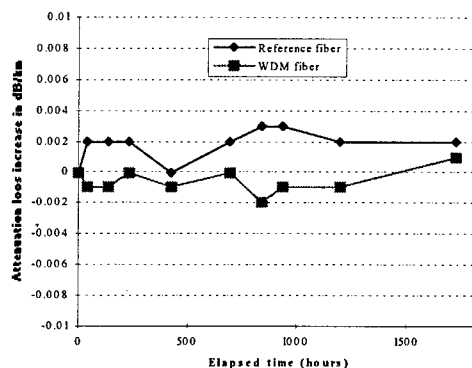


Figure 7

Ageing test 1800hours at 70°C .1550nm record

No significant evolution at 1240 nm, nor at 1550 nm are recorded. No effect due to hydrogen is recorded.

Temperature cycling test :

A cable prototype of more than 4000 m is submitted to 5 cycles [3° C, 20° C, 35° C] to simulate the temperature encountered by the cable during laying operation.

Then it is submitted to 5 cycles [20° C, - 20° C, + 65° C] in order to simulate the temperature encountered during storage.

Figures 8 and 9 show the record of attenuation at 1550 nm for two selected WDM fibres and one reference fibre.

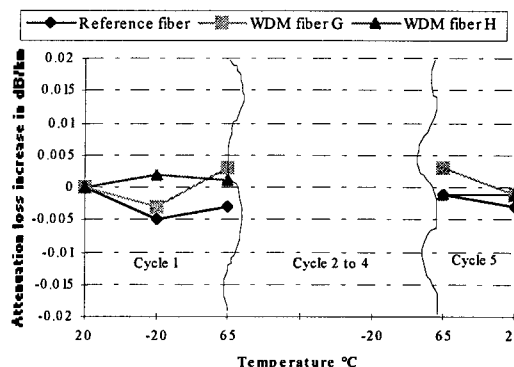


Figure 8
Laying test

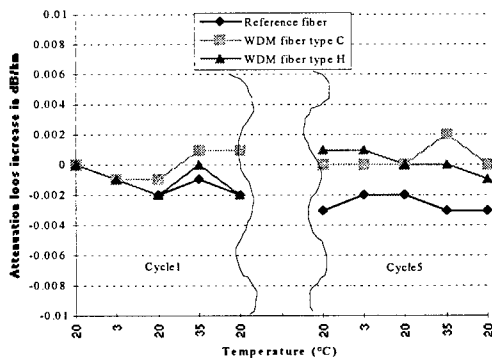


Figure 9 - Storage test

It is noticed that no significant evolution in attenuation is seen during the test simulating the laying and no irreversible effect is seen after the storage test.

5.2. - Cable mechanical performance

The central fibre unit is protected by the close packed steel wire strength member and copper tube.

This provides a structure which is very resistant to crush and pressure.

The strand wires use a very high tensile grade of steel ($> 2100 \text{ N/mm}^2$) which gives a cable UTS of approximately 70 kN and a modulus (ratio of UTS to weight in water) of over 21 km.

The combination of the low cable weight in water and low drag forces which result from the small diameter of the cable means that recovery tensions in deep water are lower than for conventional cables.

Recovery tension (at 8 km depth)	42 kN
NTTS	50 kN
UTS	70 kN

Table 3

The estimated recovery tension at 0.5 knot in a depth of 8 km is approximately 42 kN.

This represents about 60 % of the UTS (ultimate tensile strength) of the cable, which is similar to comparable figures for conventional cable.

Hydrogen

The cable structure contains both radial and axial blocks to hydrogen penetration.

The thixotropic gel inside the steel tube provides the axial block. Penetration is limited by diffusion through the material, which is a very slow process.

The copper tube around the steel wires provides the radial barrier to hydrogen. It prevents hydrogen that is generated externally (for example, on cable armouring) from penetrating the centre of the cable.

The central steel tube acts as a secondary barrier which is not needed in normal services conditions.

However, this tube minimizes penetration by water of hydrogen in the event of cable damage, and thus reduces the length of cable which may need to be replaced during a repair.

5.3. - Cable protection

For deep water LW cable, the polyethylene sheath provides the high voltage insulation for the power feed conductor and an abrasion resistant layer to protect the centre of the cable.

A high density grade of polyethylene (HDPE) was selected for this application to give maximum abrasion resistance.

Abrasion tests carried out on different materials at appropriate stress levels show this material to be superior to previous sheath materials.

Cable	Material	Cycles to failure
OALC4	HDPE	65,000
Previous	LLDPE	15,000

Table 4

For additional protection of deep water cable from fishbite, or abrasion risk, a LWP cable (Lightweight protected) has been developed (See Figure 10).

This uses a longitudinal steel tape plus an additional HDPE outer sheath to improve both penetration and abrasion resistance.

For shallow water protection, a comprehensive range of armoured cables has been developed, all based on the central 17 mm LW cable (See **Figure 10**).

A high tensile grade of armour wire is used for the single armour design and for the first layer of the double armour cables (1400 N/mm^2).

This provides high breaking strength and a linear load/elongation characteristic up to high elongations.

This reduces fibre elongation during deployment, and reduces residual elongation in the event of the cable being subjected to high transient tension.

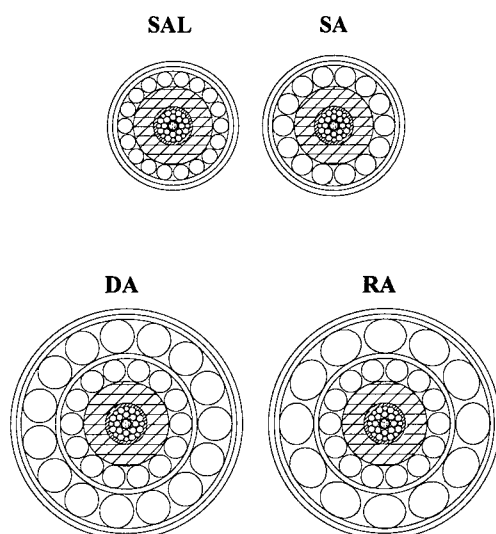


Figure 10
OALC 4 Armoured cable range

6. - CABLE QUALIFICATION

After fibre selection, according to Appendix 5, a comprehensive set of tests were conducted, including factory tests, as well as sea trials, in order to provide full confidence in reliability of the cable design.

6.1. - Factory tests

Factory tests were conducted, according to International Submarine Cable Standard (ITU Recommendations G 976).

This was the opportunity to check each cable functionality under any situation which could be encountered during the cable life (manufacturing, transfer, storage, laying, recovery and in service).

All the mechanical tests were achieved at a level up to the specified values (NOTS, NTTS) or at least under levels of tension greater than the worst expected load encountered during marine operations.

Hereafter is the list of tests performed in the factory :

- Tensile test in free gyration conditions
- Tensile test in blocked gyration
- Tensile fatigue test
- Long length tensile test
- Bending resistance around the sheave
- Thermal test and Hydrogen ageing test
- High voltage test
- Hydrostatic pressure resistance
- Crush and impact tests
- Water ingress test
- Abrasion test
- Inter-layer adhesion test

Thermal test and Hydrogen ageing test are detailed in paragraph 5.1.2.

6.2. - Sea Trials qualification

Two sea trials were conducted during the qualification of the 17 mm product. They gave the opportunity to confirm the good cable behaviour under all installation and maintenance operations.

6.2.1. Sea trial N° 1

The main objectives of this sea trial were to obtain results on the mechanical performance and handling of the 17 mm LW cable.

In order to do that a lightweight cable prototype 20 km long was manufactured and tested at sea as follows :

- a) Lay and recovery from the stern, using the linear cable engine.
- b) Lay from the stern with linear cable engine, then recovery from the bow, using the drum engine.

a) Lay and recovery from the stern

First phase (lay)

- The laying of this cable was successfully performed by the Linear Cable Engine.
- A lightweight repeater was successfully deployed in water depth of 5000 m.
- At the end of the laying, a standby period, during which the cable was in suspension for more than 10 hours. This operation was carried out without any degradation of the optical budget or any slippage of the cable in the linear cable engine.

This first phase showed satisfactory laying of 17 mm LW cable together with a lightweight repeater for deep water installation.

Second phase (recovery)

Instead of doing this operation with the bow sheave and the drum engine, the recovery was completed from the stern and through the Linear Cable Engine.

This unusual way of recovery was selected in order to simulate a cable recovery from deeper depth.

In fact, since the stern did not have a rotating sheave, the inboard tension, due to the cable friction on the stern chute, was increased by a magnification factor of 1.46 (see Figure 11). This recovery in 5000 m depth simulated in practice a recovery from 7000 m depth.

The recovery at high tension through the LCE also validated the good interlayer adherence between all the cable components and the good cable gripping in the LCE engine.

The cable recovery during this second phase was achieved without degradation of the optical or mechanical cable performances.

b) Lay from the stern and recovery from the bow

The 20 km of cable laid and recovered over the stern was then re-used for a second operation.

The cable prototype was completely laid (the two ends in sea water) from the stern, and then recovered from the bow, using the drum engine.

This validated the good cable behaviour around the drum, and confirmed the cable re-usability.

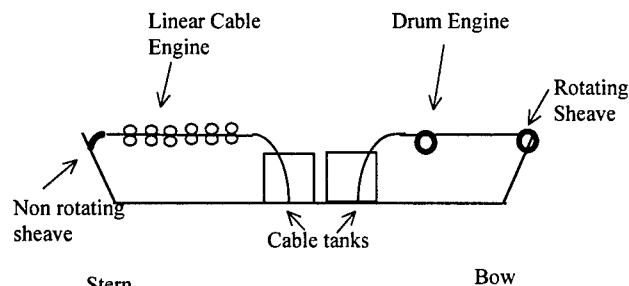


Figure 11
Cablescheme

6.2.2. Sea trial N° 2

The main objectives of this second sea trial were to :

- a) Optically qualify the 17 mm cable design at sea.
- b) Qualify the armoured 17 mm cable types at sea.
- c) Qualify the branching unit.
- d) Qualify cable burial.

a) Optical qualification of the 17 mm cable

A lightweight cable prototype 45 km long, including one repeater and 3 joints, was used (see Figure 12).

The selected fibre, designed for WDM systems, was used for this sea trial.

A large set of optical measurements were performed during the sea trial (Polarisation Mode Dispersion, Chromatic Dispersion, Attenuation) both cut back and OTDR.

Measurements were made before laying, after laying during the standby period and after recovery.

The results obtained can be summarised as follows :

- After laying and after recovery, there was no significant change in the PMD, which remained low (< 0.1 psec/km ¹/₂).
- The chromatic dispersion did not show any significant change. The lambda zero change was less than 0.1 nm which is within the accuracy of the measurement.
- The change in optical attenuation after laying and after recovery was less than 0.001 dB / km.

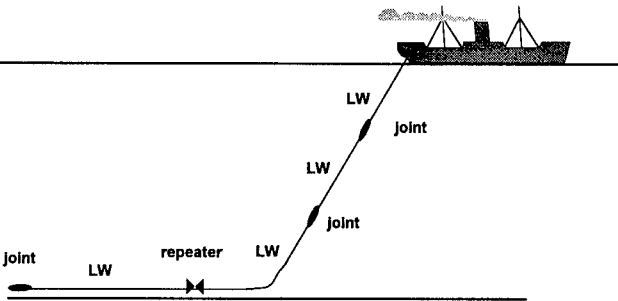


Figure 12
LW System sea trial. Sea depth : 5000 m

	BEFORE LAYING	AFTER LAYING
Attenuation 1550 nm (dB/km)	0.212	0.212
Zero dispersion wavelength (nm)	1586.9	1587
PMD (ps/√km)	0.05	0.05

Table 5 : Optical performance of WDM fibre during deep water sea trial

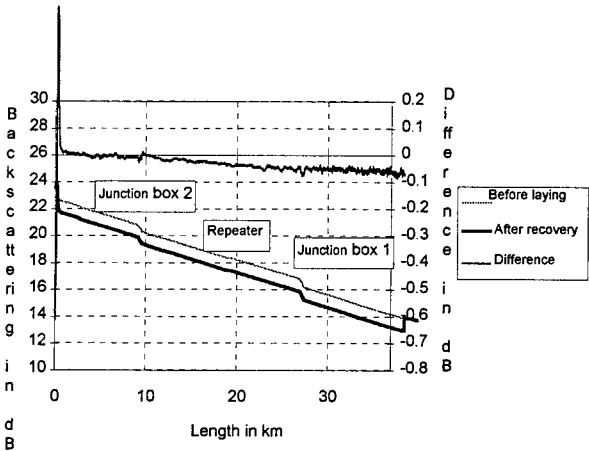


Figure 13
OTDR trace at 1550 nm of WDM fibre during deep depth sea trial

b) Qualification of armoured 17 mm cable types at sea

A cable trial 14 km in length including all armoured types, one armoured repeater and two armoured joints, was successfully laid. The sea trial area was selected for its rough and high slope bottom profiles, allowing the deployment of most of the armoured designs at their maximum deployment.

The achieved depths were respectively :

- Rock armour : 350 m
- Double armour : 470 m
- Single armour : 1100 m
- Single armour light : 2000 m

The cable behaviour during laying and recovery was excellent from both optical and mechanical points of view.

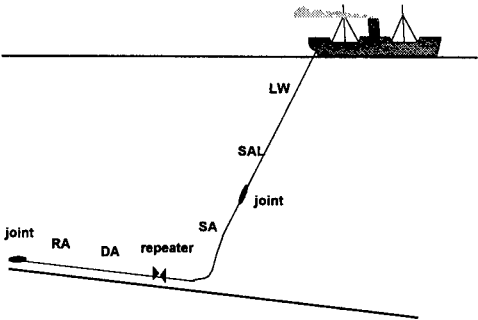


Figure 14
Armoured System Sea Trial

	BEFORE LAYING	AFTER LAYING
Attenuation 1550 nm (dB/km)	0.202	0.202
Zero dispersion wavelength (nm)	1582	1581.9
PMD (ps/ $\sqrt{\text{km}}$)	0.04	0.04

Table 6 : Optical performance of WDM fibre during shallow water sea trial

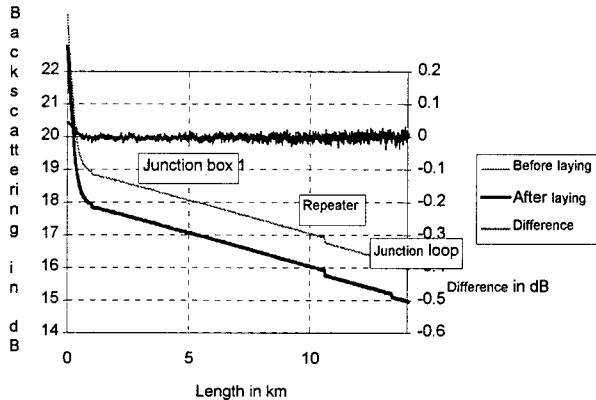


Figure 15
OTDR trace at 1550 nm
during shallow water sea trial

c) Qualification of BU handling and recovery

Handling, deployment and recovery of the branching unit were performed during the sea trial. Weights were connected to the BU legs in order to simulate a recovery from deep water. The BU was then passed around the sheave by the main leg. The load was steadily increased to the NTTS of the cable on the main leg. This exercise did not show any mechanical or optical degradation.

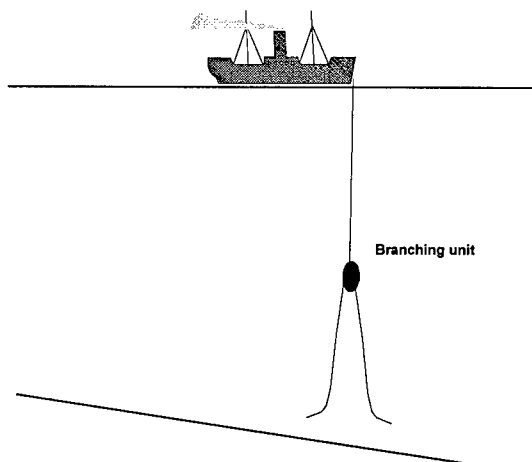


Figure 16
Recovery of the BU over the bow at NTTS load

d) Qualification of cable burial

The armoured length used in sea trial B was then submitted to a burial operation. Optical monitoring was performed throughout the ploughing operation. There was no change in the optical attenuation at any stage of the test.

Burial was achieved in a depth of 1500 m which reinforces the confidence in the good mechanical behaviour of the armoured designs.

7 - CONCLUSION

The OALC-4 cable range has been developed to provide a reliable and cost-effective carrier for present and future high bandwidth fibre optic submarine systems.

The cable structure provides a high degree of protection to the fibres which are maintained in a stable and low stress environment. The combination of the protection provided by the cable design with careful selection of WDM fibre parameters results in minimum loss increments from bending.

Qualification of the cable has been completed with a comprehensive set of factory tests and two extensive sea trials.

These tests have demonstrated the stability of the optical transmission characteristic of the cable under all service conditions.

Authors

Y. CHARLES
Alcatel Submarine Networks
536 Quai de la Loire
62225 Calais Cedex

Yves CHARLES was born in 1967. He is graduated from Ecole Universitaire Des Ingénieurs de Lille (E.U.D.I.L.). He joined Alcatel in 1993 where he is in charge Cable design and product qualification in Calais - France -

J.F LIBERT
Alcatel Submarine Networks
536 Quai de la Loire
62225 Calais Cedex

Jean-François LIBERT received his engineering degree from «Hautes Etudes Industrielles» of Lille (FRANCE). He joined Alcatel in 1984. He is now Technical Manager for Optical Submarine Cable in Calais.

P. WORTHINGTON
Alcatel Submarine Networks
536 Quai de la Loire
62225 Calais Cedex

Peter WORTHINGTON is a development engineer in Alcatel Submarine Networks. He recieved a BSc in Electronics an Electrical Engineering from the University of Birmingham in 1971. Since 1977 he has been involved in the development of optical cables for submarine systems.

JL. LANG
Alcatel Submarine Networks
536 Quai de la Loire
62225 Calais Cedex

Jean-Luc LANG received his degree from «Institut Universitaire de Technologie» of ORSAY (FRANCE). He joined Alcatel in 1975. He is now involved in optical transmission in the technical directorate in Calais.

LONG TERM BEHAVIOUR OF HYDROGEN INDUCED LOSSES IN INSTALLED FIBROPTIC SUBMARINE AND UNDERWATER CABLES

Svend Hopland

Telenor Nett AS, Oslo, NORWAY

ABSTRACT

We present extensive hydrogen data on our installed submarine and underwater cables with no hydrogen barrier through nearly 10 years. The hydrogen induced losses have stabilised at low levels corresponding to loss increases of 0.01-0.04 dB/km at 1550 nm, dependent on cable type. Accelerated tests have shown that the hydrogen in the installed cables originates from the cable production, and will decrease in a time scale of 10-20 years. Measurements on cables with hydrogen absorbing materials and hermetic fibres have shown no traces of hydrogen in the fibres.

INTRODUCTION

Norway has a long coastline and numerous lakes which makes the installation of submarine and underwater fibreoptic cables very attractive. Telenor installed the first fibreoptic submarine cable in 1983 in Sognefjorden on the west coast of Norway, and the first underwater cable was deployed in 1985 in the Mjøsa lake near Lillehammer. Up to now, Telenor has installed in total more than 1.450 km of submarine cable along the Norwegian coast and nearly 800 km of underwater cable in lakes.

During the early installation period we had no hydrogen barrier in the cables to prevent hydrogen ingress in the fibres from corrosion of the armour wires. From early 90's, cost effective solutions with hydrogen barriers such as hermetic fibres and hydrogen absorbing materials were available, and were included as a standard in our cables.

However, Telenor as well as many other cable owners was concerned about hydrogen ingress in their installed cables with no hydrogen barrier. As a consequence, Telenor started in late 1988 an extensive measuring program on installed submarine cables in order to reveal the hydrogen level present in the cables. The initial results indicated low levels of hydrogen during the first few years after installation^{1,2}. However, it was not possible at that time to evaluate the long term development of the hydrogen level.

Telenor has continued to perform hydrogen induced loss measurements on selected installed fibreoptic submarine and underwater cables. In addition, we have performed long term accelerated tests on armoured cables in dry air and in sea water.

Considering the large number of field measurements over nearly 10 years, and the results of the accelerated tests, we are now in a position to give reliable indications of the long term behaviour of the hydrogen induced losses.

SUBMARINE CHARACTER

Cable constructions

Our submarine/underwater cable construction is basically very simple, with a fibre core consisting of fibres in stranded loose tubes or a slotted core element, surrounded by an inner sheath of low density polyethylene. Then follows the armour wire layer(s) with a rubber asphalt/bitumen filling compound, and finally an outer sheath of high density polyethylene, as shown in Figure 1.

Cable routes

The cable network along the coast connects the main populated areas and consists partly of submarine cable and partly of land cable. The overall average submarine route length is 6.9 km, and the maximum sea depths vary typically between 50 and 800 m, with the deepest route of 1300 m. The sea bottom topographies along our submarine cable routes are large mountain formations, sharp and high ridges of several hundred meters, leads and troughs, as well as flat parts. Nearly 100 % of the submarine cables are surface laid due to the high cost of burial.

The average route length for the underwater cables is 6.4 km, and the maximum depths vary typically between 20 and 150 m with the deepest route of 400 m. All cables are surface laid.

FIELD MEASUREMENTS

Measured cables

Due to a great number of installed underwater and submarine cables, we early decided to measure mainly submarine cables, since they are heavier armoured, situated in the harshest environments and also they are prone to mechanical damage due to fishing activities etc. The submarine cables were selected from different part of the coast, with different maximum depths and route topographies. Also, we selected single armoured cables (SA) and double armoured cables (DA) in representative proportions. In total, we have measured 35 cables from the early installation period, which constitute nearly 30 % of all our submarine cables without hydrogen barrier. The selection is therefore in all respects representative for our marine installations. For the underwater cables (SSA) without hydrogen barrier, a smaller selection of 4 cables have been measured.

For these early installed cables, we have measured the hydrogen level with a frequency of 1-2 times a year, during a time period of up to 10 years.

In addition, from the later installation period we have measured 10 cables with hydrogen barriers such as hydrogen absorbing materials and hermetic fibres for comparison. Some of these cables have been regularly measured through a time period of 5 years.

Measurement equipment

For the field measurements we have used two different special OTDR-modules with slightly different centre wavelengths, which both are close to the peak wavelength of the hydrogen induced loss at 1244 nm. With the reference module (OTDR 1), we are able to detect approximately 50% of the 1244 nm peak height, while the other module (OTDR 2), detects approximately 70-80 % of the peak height. They are used simultaneously in order to compare and verify changes in fibre losses. Both modules are checked for stability of centre wavelengths and halfwidths prior to all field measurements. We always measure several fibres in each cable and average values are used to characterise the hydrogen level in the cable.

In all field measurements, the fibres are measured at the wavelengths of our standard OTDR, which are 1306 nm and 1550 nm.

Measurements results

General The majority of the selected measured submarine cables with no hydrogen barrier were installed in the period 1987-89, and thus we can present hydrogen data over a time period of 8-10 years. In addition, we have data from an underwater cable installed in 1985, a 12 year old installation. Unfortunately, our oldest installed submarine cable from 1983, was destroyed by an underwater avalanche some years ago. Recently, parts of it was recovered undamaged and reinstalled, and may provide additional hydrogen data in the future.

Submarine cables with no hydrogen barrier

In Figure 2 is shown the long term fibre losses in SA submarine cables measured with OTDR 1 over a time period of 10 years. The hydrogen induced loss can be calculated as proportional to the difference between the actual fibre loss and the normal fibre loss without hydrogen.

Each SA cable exhibits its own individual time dependent pattern, which may include hydrogen maxima as well as minima. This makes it rather difficult to compare the hydrogen levels among the SA cables. However, we note that after 8-10 years the hydrogen induced losses in the cables are still generally very low. Moreover, at this time the general trend is that the hydrogen induced losses have levelled off and more or less stabilised. A considerable variation in hydrogen level among SA cables can be observed.

In Figure 3 is shown the long term fibre losses in our DA submarine cables. Again, each cable shows an individual time dependent pattern. After 6-7 years the hydrogen induced losses have more or less stabilised at a value which on average is clearly higher than the corresponding 6-7 years level for the SA cables. From Figure 2 and Figure 3 we calculate the ratio between average hydrogen induced losses in SA and DA cables after 6.5 years to be 1: 2.58. This is in good agreement with the ratio of the surface areas of the armour wires for the SA cables and the DA cables, which is calculated to be 1: 2.34.

In Figure 4 is shown the corresponding measured long term losses at 1550 nm for SA cables and DA cables. We observe that the hydrogen induced losses, provided by the hydrogen sensitive OTDR 1 measurements, are mapped into the 1550 nm wavelength. It should be noted, that normal fibre losses in old cables was not always close to 0.20 dB/km and also other minor losses could be present at 1550 nm. However, we can deduce from Figure 3 that the hydrogen induced losses 6-7 years after installation at 1550 nm are in the region 0.01-0.02 dB/km and 0.02-0.04 dB/km for SA cables and DA cables, respectively.

Underwater cables with no hydrogen barrier In Figure 5 is shown the long term fibre losses at the OTDR 1 wavelength for a few underwater cables including our oldest installed cable from 1985. We note that the hydrogen induced losses have levelled off and decreased; a behaviour similar to the submarine cables. Also, we note that the magnitude of the hydrogen levels are close to the levels in the submarine SA cables. This is in agreement with the ratio of the surface areas of the armour wires for the SSA cables and the SA cables, which is calculated to be 0.88: 1.

Submarine cables with hydrogen absorbing materials In our SA and SSA cables, the hydrogen levels are very low, and hydrogen absorbing materials may be used effectively to prevent the hydrogen to reach the fibres. The hydrogen absorbing material is used as part of the cable core filling. Figure 6 shows measurements on installed submarine cables with hydrogen absorbing materials. For comparison, unprotected SA submarine cables as earlier shown in Figure 2, are drawn in as well. We observe no visible traces of hydrogen in the fibres 5-6 years after installation.

Submarine cables with hermetic fibres

Hermetic fibres are considered to be a full proof lifetime protection against hydrogen levels of considerably higher magnitude than measured in our cables. We have since early 90's used hermetic fibres in our DA cables and also in SA and SSA cables. Figure 6 shows fibre losses in DA and SA cables with hermetic fibres. For comparison, DA and SA's without hydrogen protection as earlier shown in Figure 2 and Figure 3, are drawn in as well. Not surprisingly, no traces of hydrogen are visible in the hermetic fibres.

Depth dependence of hydrogen level Our cables has been deployed at sea depths ranging from 30 to 1300 m. In our early measurements, we could not find any depth dependence of the hydrogen level¹. Now, 6 years later, we have re-investigated this feature. In Figure 7 are shown the present measured hydrogen levels versus maximum installation depths for SA as well as DA cables. We note that there is still no evidence of any depth dependence of the hydrogen level. This shows that water depth does not affect the hydrogen levels in the installed cables at any stage of development.

Outer sheath Obviously, the outer sheath of HDPE tightly adhered to the filling compound surrounding the armour wires, plays a very important role in preventing water to reach the armour wires. Other types of outer protection, such as polypropylene yarn/asphalt which are more commonly used on submarine cables, may be prone to be washed out by sea currents during the course of time. This feature is observed on our single SA cable with polypropylene yarn/asphalt, as shown in Figure 8. Here, one part of the cable reaching from one of the landing points down to the deeper part of the route, has gradually developed a much higher hydrogen level than the rest of the cable, probably due to outwashing. Moreover, the overall hydrogen level on the rest of this cable has gradually increased to a higher level than observed on our standard SA cables.

Outer sheath damages If the outer HDPE sheath is damaged, water will have direct access to the armour wires and may also gradually diffuse along some cable length in each direction from the sheath damage. The corrosion and hydrogen level will increase locally and become clearly visible on the OTDR curves.

The total cable length which will be affected by a high hydrogen level is dependent on the nature of the sheath damage. A trawler hit may rip off the sheath in longer lengths, while repair or recovery may only cause a minor local damage to the sheath.

For a minor sheath damage the cable length with a high hydrogen level is typically up to a few hundred meters, which is small compared to the total cable length. Even with a high hydrogen level, the influence on the overall hydrogen level is minor. For a trawler hit, the affected cable length may be longer, and the hydrogen induced losses will be more pronounced. On the other hand, severe sheath damage is often accompanied by significant additional fibre losses and sometimes fibre breaks which by far dominates the total loss picture at 1550 nm.

Since a sheath damage shows characteristic features on the hydrogen sensitive OTDR-curve, it may be easily identified. We have examined all OTDR-curves and may give the following status: We have identified only a few sheath damages on 4 cables out of totally 35 cables; during an installation period of nearly 10 years. On two of the cables the sheath damage were caused by recovery of the cable under repair/changing cable route. On one cable the sheath damage was caused by trawler hits. In the last case the reason for sheath damage has not yet been identified.

Cable burial Due to the high cost of burial, our submarine cables are surface laid. Only in a few cases we have buried shorter cable lengths in sea bed consisting of soft clay or medium coarse/course sands. We have investigated the hydrogen sensitive OTDR-curves in the buried areas and compared them with unburied areas. We have found that only small differences in hydrogen levels can be observed between buried and unburied parts, which may be attributable to inherent length variations of hydrogen level often observed in the cables. We may therefore conclude that burial in these types of seabed does not affect the hydrogen level.

ACCELERATED TESTS

Dry air experiment

We early found evidence that hydrogen was present in the cables shortly after cable production¹. Measurements made on SA cables stored on land at average temperature + 7.1 ° Celsius during 2 years indicated that the

hydrogen level decreased slowly². To further study the behaviour of this production related corrosion reaction in air surroundings, several cable samples were heated to + 60 ° Celsius in dry air for several months. The cable samples were 3-400 m lengths of SA and SSA; taken from leftover lengths of old installed cables, which had been stored dry on land for nearly 5 years. In each sample, the fibres were looped, and the spectral losses of the loops were measured. Hydrogen sensitive OTDR measurements were also performed. It was not possible to keep the temperature continuously high at + 60 ° Celsius due to time sharing of the chamber. In Figure 9 is shown hydrogen peak heights and temperature versus time during the test. The results shows some characteristic features of the production related hydrogen reaction. Firstly, it shows that hydrogen remains in the cables for many years, when cables are stored in air. Secondly, it shows that the hydrogen will eventually be reduced to lower levels. At + 60 ° Celsius, the time needed to reduce the hydrogen level to half of its maximum value is approximately 50 days (average) for the SA cables and approximately 20 days for the SSA cable. It is not straightforward to transfer the time constants at + 60 ° Celsius to lower temperatures. However, our observations indicate that the time constant for reduction of the hydrogen level at + 3-4 ° Celsius will be of the order 2-5 years in dry air surroundings for SA and SSA cables.

Sea water experiment

If cables are deployed in water, the behaviour of the production related hydrogen reaction will be changed. Firstly, in water surroundings, it will be more difficult for the hydrogen generated inside the cable to escape, and the internal hydrogen equilibrium pressure in the cable will increase. Secondly, for the same reason, the time constants for reduction of hydrogen level, will also increase.

In order to study these effects more in detail, and also to reveal any other long term hydrogen effects, a sea water bath was constructed. The cable samples previously used in the dry air experiment were deployed in the sea water bath and subjected to a temperature of + 60 ° Celsius. Also, a recently manufactured SSA cable with hydrogen absorbing material was added in as a reference. Fibres were looped, and the spectral losses of the loops and hydrogen sensitive OTDR measurements were performed regularly. Small problems with the bath temperature was

experienced from time to time. Up to now, the cable samples have been continuously subjected to sea water at a temperature of + 60 ° Celsius for more than 1.5 years. In Figure 10 is shown fibre loss in the samples measured with the hydrogen sensitive OTDR 2, and temperature versus time. Each sample shows a maximum hydrogen level and a subsequent decaying period, which is similar to the dry air test. We note that the maximum hydrogen levels are much higher than in dry air surroundings. This is expected; and in fairly good agreement with other observations made in water bath at similar temperatures ³, considering that the samples have been pre-dried. Also in agreement with this, the "fresh" SSA reference cable, shows a higher maximum value although containing hydrogen absorbing material. From Figure 10, we register that the time constant for the decay of hydrogen is significantly longer than in dry air surroundings. The time needed to reduce the hydrogen level to half of its maximum value is approximately 300 days (average) for the SA cables and approximately 100 days (average) for the SSA cables.

Some very important features are evident from the accelerated test results:

- In the sea water experiment, there are no evidence of any other hydrogen generating mechanism than the production related hydrogen reaction.
- At + 60 ° Celsius, the time constants for the decay of hydrogen in sea water are 5-6 times the time constant for the decay of hydrogen in air.
- We may assume that these results are valid also at sea water temperatures. Since evidence has shown that the time constants for the decay of hydrogen in air at + 3-4 ° Celsius are in the order 2-5 years (for SA and SSA cables), the corresponding time constants in sea water will be approximately 5-6 times longer i.e. in the order 10-20 years and more. For DA cables, even longer time constants can be expected.
- The sea water experiment results are in agreement with the field measurements, which have shown generally stabilised hydrogen levels after 8-10 years. In view of the test results, stable and decreasing hydrogen levels are expected for the installed cables during the next 10-20 years. The time constant for the hydrogen decay will increase with heavier armouring.

CONCLUSIONS

We have presented extensive field measurements of hydrogen levels in our submarine and underwater cables with no hydrogen barrier over a time period of 8-10 years. The measurements have shown that hydrogen levels have generally stabilised after 8-10 years at a magnitude which corresponds to hydrogen induced losses at 1550 nm of 0.01-0.02 dB/km for SA and SSA cables, and 0.02-0.04 dB/km for DA cables. Measurements on cables with hydrogen barriers such as hydrogen absorbing materials and hermetic fibres have shown no traces of hydrogen induced losses in the fibres. In unprotected cables, our standard armour wire protection consisting of bitumen/rubber asphalt compound tightly covered by an outer sheath of HDPE have proven effective in keeping the hydrogen at low levels, except in small cable lengths where the sheath has been damaged. However, very few sheath damages have occurred during our measurements through nearly 10 years. A cable with armour wire protection of polypropylene yarn/asphalt have after 8-10 years developed a clearly higher hydrogen level than our standard cables, probably due to outwashing of the wire protection. We have found no dependence of hydrogen level on water depth or burial in soft clay/sand. Accelerated tests on SA and SSA samples in dry air and sea water have shown that the hydrogen induced losses in the installed cables are caused by a cable production related hydrogen reaction, which will show a decaying behaviour in the long time term. The test results are in agreement with the field measurements, and for the next 10-20 years we expect the hydrogen levels to further stabilise and slowly decay, dependent on cable type.

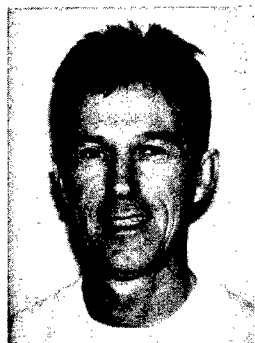
ACKNOWLEDGEMENT

The author greatly appreciates the assistance of Idar Gangsø, Telenor, who has performed the measurements in the field and in the laboratory.

REFERENCES

1. S. Hopland: "Investigation of total and distributed hydrogen levels in installed fiberoptic submarine cables": Proceedings IWCS 1989, pp. 684-688.

2. S. Hopland: "Measurements of low hydrogen levels in installed open fiberoptic submarine cables": Proceedings IWCS 1991, pp. 742-748.
3. Alcatel Cable, Norway: Private Communication.



Svend Hopland

Telenor Nett AS ,
P. Box 6701 , St. Olavs Plass
0130 Oslo, NORWAY.

Svend Hopland graduated from the Norwegian Institute of Technology in 1985 with a PhD. on optical fibres. In 1986 he joined Telenor and is presently a chief engineer on fibreoptic cables.

FIGURES

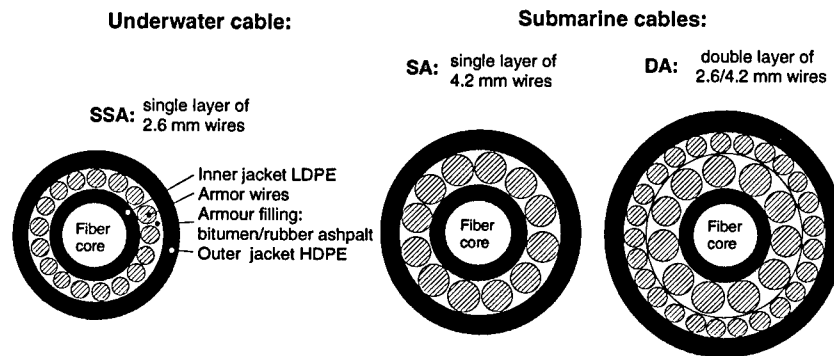


Figure 1: Underwater and submarine cable constructions.

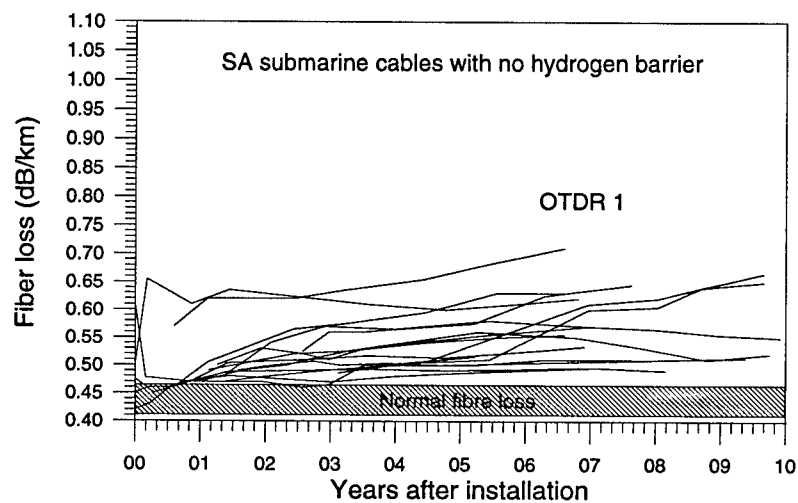


Figure 2: Long term fibre losses in single armoured (SA) submarine cables measured with hydrogen sensitive OTDR 1.

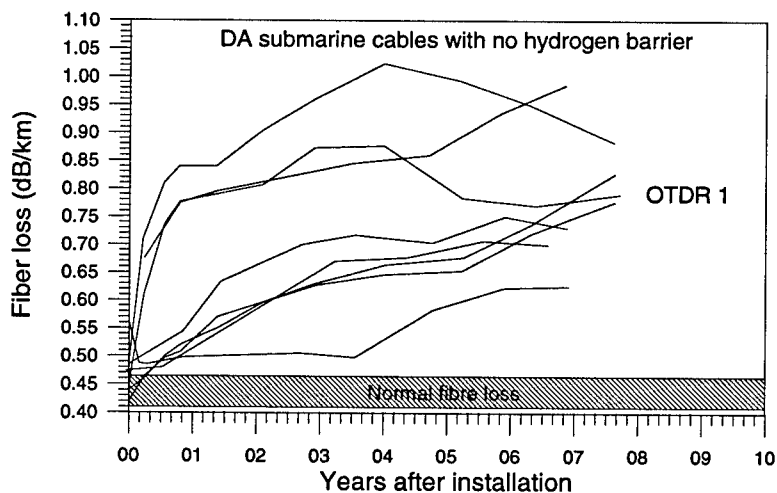


Figure 3: Long term fibre losses in double armoured (DA) submarine cables measured with hydrogen sensitive OTDR 1.

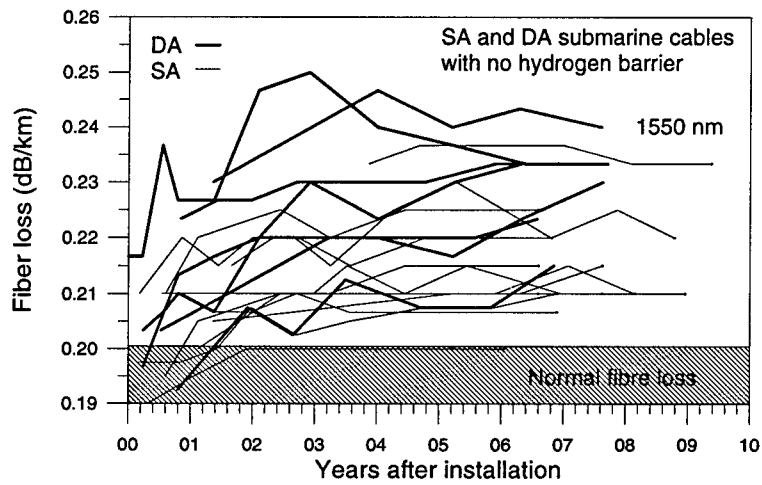


Figure 4: Long term fibre losses in SA and DA submarine cables at 1550nm.

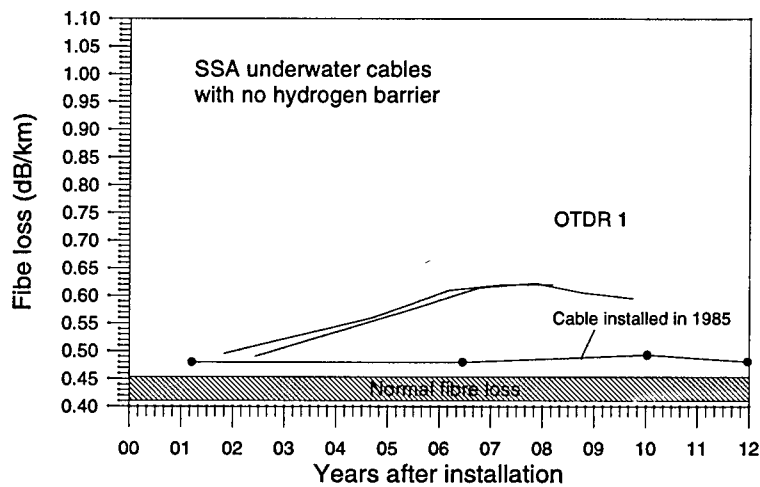


Figure 5: Long term fibre losses in underwater cables (SSA) measured with hydrogen sensitive OTDR 1.

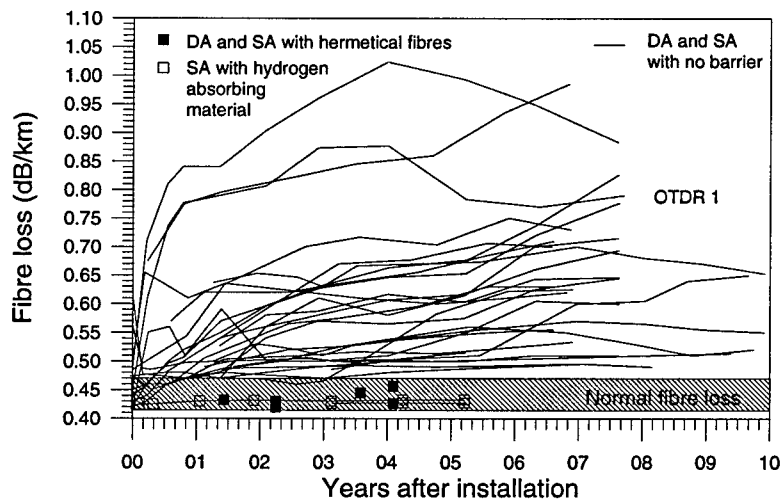


Figure 6: Long term losses in submarine cables measured with hydrogen sensitive OTDR 1.

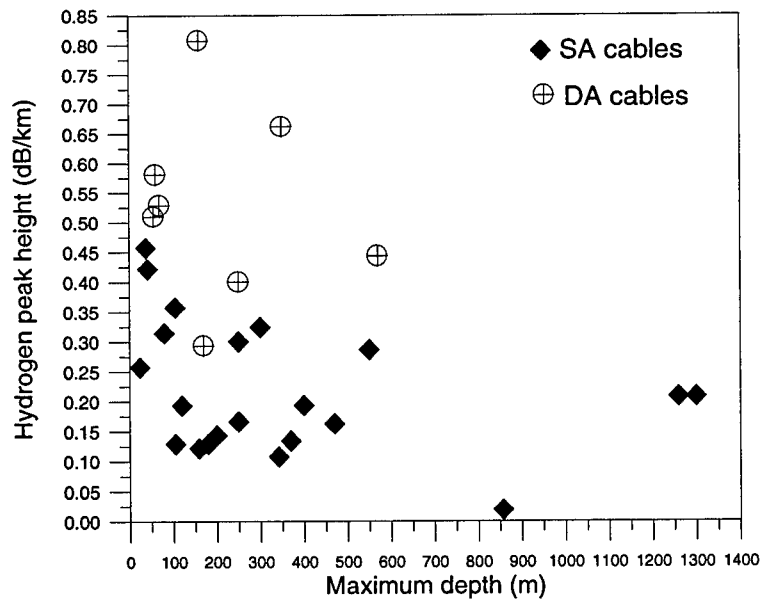


Figure 7: Hydrogen induced losses at 1244 nm in SA and DA submarine cables versus maximum route depth.

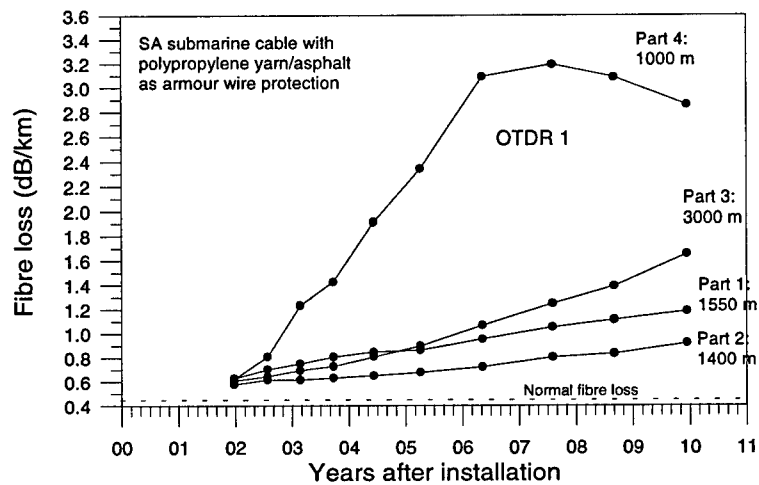


Figure 8: Long term fiber loss in SA submarine cable with polypropylene yarn/asphalt as armour wire protection, measured with OTDR 1.

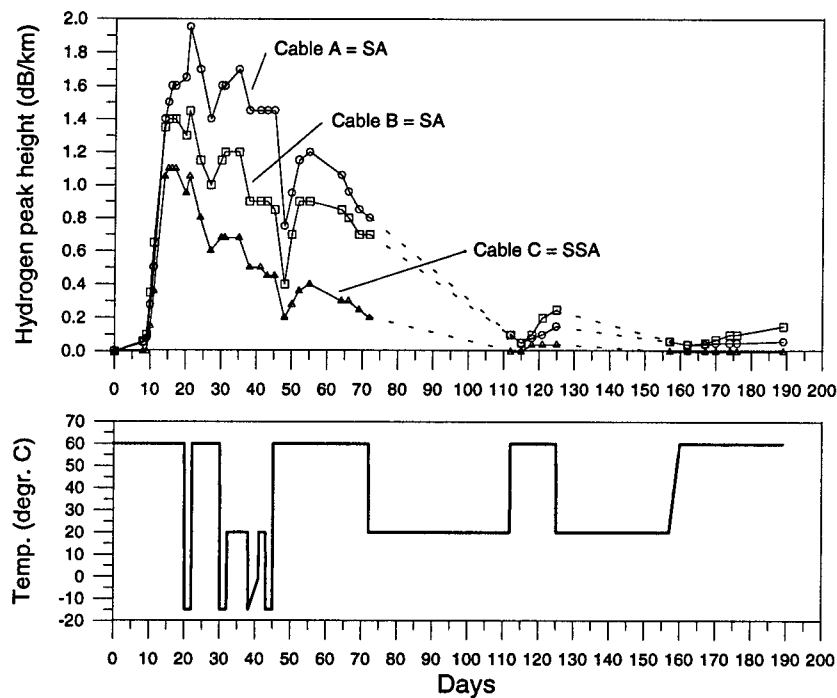


Figure 9: Hydrogen induced losses and temperature versus time in SA and SSA cables heated in dry air.

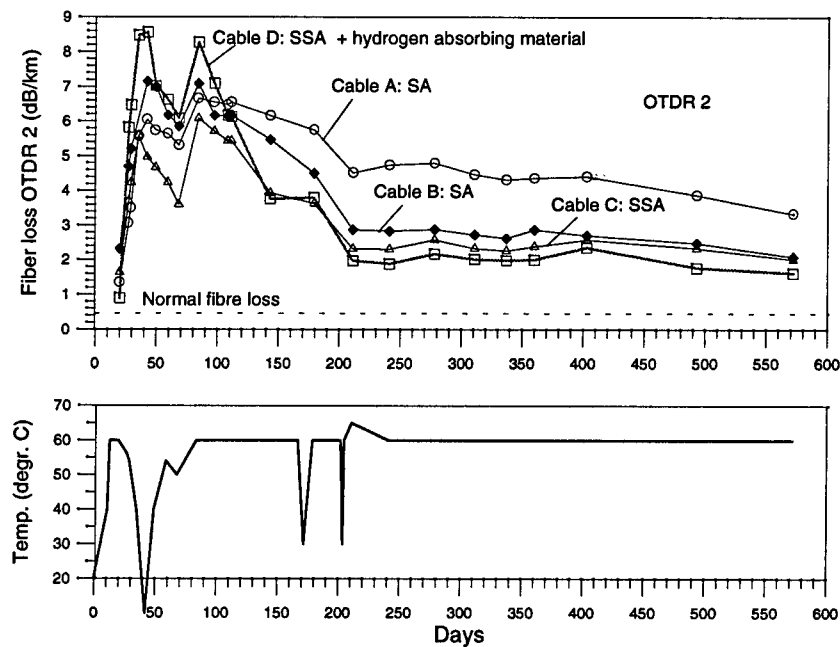


Figure 10: Fibre losses and temperature versus time in SA and SSA cables heated in sea water, measured with with hydrogen sensitive OTDR 2.

ASSESSMENT OF HYDROGEN INGRESS IN SUBMARINE CABLES AT JOINTS AND TERMINATIONS

Jean-François LIBERT - Franck RUELLE - Peter WORTHINGTON

**ALCATEL SUBMARINE NETWORKS
536 Quai de la Loire - BP 849 - 62225 CALAIS CEDEX - FRANCE -**

ABSTRACT

Stability of optical attenuation of submarine systems is a key issue for system designers because of the spectacular increase of their performances.

Submarine cable manufacturers have developed cable designs that avoid any additional losses due to hydrogen ingress. One remaining issue is the discontinuities made by jointing boxes where metallic components may generate hydrogen because of corrosion.

Choice of material is a key stage in development. Some simple rules are explained to allow preliminary selection of materials and an experimental technique is described to validate selection.

Different joint designs including different materials have been tested using these technique and designs, selection of materials and their protection have been validated.

1. INTRODUCTION

Requirements for reliability of optical submarine systems are becoming more and more stringent : increase of point to point lengths (10 000 km is a common figure) and spectacular increase of bit rates thanks to Wavelength Division Multiplexing could lead to dramatic economical consequences in case of system failure. That is why customers ask system designers to pay more and more attention to the reliability of current and future systems keeping in mind that the design target is to ensure a lifetime of 25 years.

For optical submarine cable manufacturers, that means that new product developments must include a detailed study of the design, a careful choice of materials and finally a full qualification test range : this generally loads a development program for several years.

One of the main risks to assess is the increase of the fibre attenuation caused by external factors that could be either mechanical stress or chemical effect. A lot of studies are made by cable manufacturers in order to evaluate the possible change of optical loss in cable versus time. Ageing margins are then calculated in order, for example, to define system performances.

One of the possible phenomenon that leads to the increase of optical loss in cable is the poisoning of the fibres themselves by hydrogen. The effect of hydrogen on the attenuation of optical fibres is now well known and well understood.

Possible sources of hydrogen are polymer degradation, metallic outgassing as well as corrosion. In this last case, hydrogen can be generated by self corrosion of the metallic components in contact with sea water, for example the outer armour wires.

That is why, in order to minimise the risk, Alcatel Submarine Networks has developed a full cable range that exhibits high resistance to radial ingress of hydrogen [1] : the cable structure is based on a steel tube in which fibres are embedded in a thixotropic jelly. More over, in depth studies have been made in order to ensure that the chosen raw materials are those which generate the minimum amount of hydrogen during ageing.

The steel wire strength member around the steel tube is enclosed in a continuous welded hermetic copper tube. The copper and steel tubes provide a very effective double barrier to radial penetration.

However, all under sea fibre optic networks include all or some of jointing boxes, repeaters or branching units. Hydrogen may enter through these joints and then longitudinally ingress along the cable. Risk is especially acute at these points because they are generally made of metallic components in contact with sea water : corrosion of these components can generate a significant amount of hydrogen. Again, a careful choice of design and materials must be made in order to minimise the hydrogen risk.

This paper describes the work that has been done to understand the corrosion phenomena that leads to hydrogen formation and explains trials that have been performed in order to validate the choice of design and materials for submarine jointing boxes.

2. CORROSION AS HYDROGEN SOURCE

Corrosion can generally be defined as in the degradation of metallic materials under the action of the environment because of a chemical reaction.

Two main corrosion mechanisms can be identified :

- Electrochemical corrosion.
- Corrosion due to bacterial action.

In this paper, we will only consider the first mechanism, the second one too mainly depends on the natural environment. Moreover, we will only focus on the way hydrogen is generated during corrosion which is not a current approach! Indeed, most of the corrosion specialists first take into consideration the mechanical effect of corrosion, but our experience shows that, in our particular case, the effect of hydrogen on fibres is the first consequence that can be observed on optical submarine cables, long before potential mechanical problems.

2.1 - Electrochemical corrosion mechanisms

2.1.1 - General

Because components under study are working in a submarine environment, we will only consider aqueous corrosion mechanisms and more precisely we will try to assess the influence of the marine environment which is probably the most aggressive common environment in which metals are expected to operate.

In most case, the corrosion of metals is due to an irreversible oxidation/reduction reaction between a metal and an oxidising agent. Oxidation of the metal leads to the reduction of the oxidising agent following the above reaction :

metal + oxidising agent \rightarrow oxidised metal + reductioning agent

- For example, corrosion of iron in hydrochloric acid is due to the reaction :



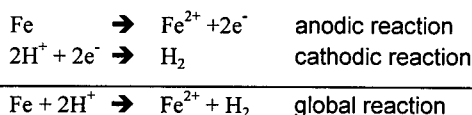
- In an aqueous environment, hydrochloric acid and chloride of iron are under their ionic form. The above reaction can also be written the following way :



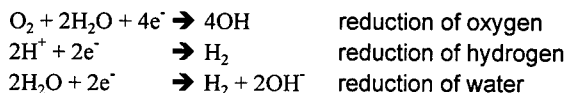
- And because chloride ions do not directly participate in the global reaction, this one can be simplified :



But, every oxidation/reduction reaction can be split into two partial reactions which are named anodic and cathodic partial reactions :



In sea water, main cathodic reactions are the reduction of dissolved oxygen, the reduction of hydrogen ions and the reduction of water :



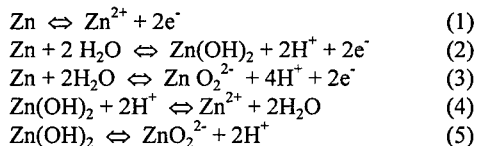
The reaction occurring depends on a lot of parameters such as pH, aeration or composition of the solution. These reactions demonstrate that oxygen is not necessarily involved in corrosion reaction to evolve hydrogen.

Finally, if two dissimilar metals are in electrical contact in an electrolyte, then galvanic effects can drastically increase the corrosion speed of the less noble metal.

2.1.2 - Pourbaix diagrams

The study of the Pourbaix diagrams can give a good idea of how a metal will behave in a solution and more precisely can give some reliable information on the possible formation of hydrogen because of corrosion.

These diagrams are designed to illustrate how the stability of different species are affected by potential and pH. The result is a graph which shows the conditions under which a metal will be corroding, immune or passivated. Let us take the example of zinc corroding in pure water. Up to four species can be present over the complete range of potential and pH : Zn , Zn^{2+} , $\text{Zn}(\text{OH})_2$ and ZnO_2^{2-} . Therefore five reactions must be written to describe the interconversion of each species.



Those reactions which involve the generation of electrons (1, 2, 3) must be influenced by variations of electrode potential, whereas those in which hydrogen ions are formed (2, 3, 4, 5) will be controlled by pH. Reactions 2 and 3 are controlled by both potential and pH.

All reactions define domains separated by lines of which equation is given by the Nernst relationship :

$$E = E^0 - RT/nF \ln ([\text{products}]/[\text{reactants}])$$

where E^0 is the standard potential, n the number of electrons exchanged during reaction, F the Faraday constant and $[\text{species}]$ the activity of the involved species that can be here considered as the concentration of the species. The lines can be plotted on a graph like on **graph 1** showing the Pourbaix diagram of the zinc in pure water.

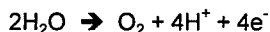
Each domain indicates a region in which one species is the most thermodynamically stable. If the metal is the most stable species then it is considered immune to corrosion, but if a soluble ion is most stable then the metal should corrode.

Additional information of real interest in our application is given by the dashed lines in **graph 1**. They represent two other reactions which are possible in aqueous solutions :

- Line 1 defines the limit of the reduction of hydrogen ions to liberate hydrogen gas.



- Line 2 defines the limit of the oxidation of water to liberate oxygen gas.



That means that below line 1, hydrogen gas is the most stable species, while above it the hydrogen ion is stable. Hydrogen gas is always liberated at a cathode and this will occur when the cathode is in the domain of potential and pH below line 1.

If we take the example of the zinc corroding in pure water (**see graph 1**), that means that there is a lot of chance that hydrogen will be generated when zinc is in water whatever the pH of the solution.

This is a thermodynamic approach which does not give an estimate of the kinetics. Experiments are necessary to determine the rate of reaction in a particular case.

3 - SUBMARINE CABLE JOINTS FOR LONG-HAUL REPEATERED SYSTEMS

3.1 - General

The main function of a submarine cable joint is to ensure the full continuity between two lengths of cable : the joint has to maintain the mechanical, electrical and optical integrity of the cable.

In the case of long haul repeatered cable-high dielectric insulation is given by the polyethylene insulant, surrounding the composite conductor made of wire steel strand and copper tube (**See Figure 1**).

The joint is generally made of a metallic « box » ensuring mechanical and electrical continuity in which an excess of fibre is placed and spliced together in order to reinstall the optical path. The whole is then overmoulded with a polyethylene sheath in order to insulate the joint from the sea water.

This is the basic structure of the lightweight (LW) joint which is used to joint LW cable in depth of typically 2000 to 8000 m.

In some design of LW joint there is also an outer metallic sea case used to protect the joint from damage during deployment.

In the case of armoured cables using galvanised steel armour wires, the same basic LW design is used to joint the central cable. An outer sea case is used to protect the joint and to reinstall the mechanical strength of the outer armouring.

This outer sea case is generally made of metallic components that are then in contact with sea water: the self corrosion or the galvanic corrosion of the chosen materials may induce hydrogen formation that can then enter the joint and then ingress in the cable each side.

Some experiments have then to be made in order to validate the joint design.

3.2 - Tested cable joints

Two configurations designated A and B are tested. General drawings of the different joints are given in appendix.

Figure 2 shows the Lightweight cable joint A and **Figure 3** shows Lightweight cable joint B. From a corrosion point of view, the main difference between the two joints is that joint B is surrounded by a metallic sea case : this component is made of zinc coated steel and is in contact with sea water. On the contrary, the Lightweight cable joint type A has no metallic part in contact with sea water.

Figure 4 shows the armoured cable joint A and **Figure 5** shows the armoured cable joint B. These types of joints are used in shallow water down to 2000 m. The main differences between these two joints are; the use of different materials for the outer protection, the way armouring wires are anchored and the electrical continuity of the cable armouring layer through the joint.

In armoured cable joint A, the outer sea case is made of nickel plated cast iron. Armoured joint B uses a zinc coated steel outer sea case. The used nickel plating is a Ni-P alloy obtained using the reduction of a nickel salt by sodium hypophosphate in aqueous solution. Thickness of coating is around 75 μm . This method of coating nickel gives a better corrosion protection than the electrolytical method.

In armoured cable joint A, armouring wires are anchored by ferrules and embedded in epoxy resin. In the armoured joint type B, the armour wires are gripped by conical steel wedges which are then secured to the outer sea case. This method of anchorage gives an electrical connection between the armouring and the sea case.

4 - TESTS

4.1 - Hydrogen generation of raw materials

An experiment was designed to quantify the hydrogen generation on the two different sea cases (zinc coated steel and nickel plated cast iron). **Figure 6** shows the apparatus whereby a sea case is placed under a glass funnel in a container of artificial sea water. At the start of the experiment, the funnel was completely filled with water by applying suction via the tap at the top. Gas evolved during the experiment would rise to the top of the funnel and displace the water, enabling the volume of the gas to be measured.

When nickel-plated, other hand, cast iron was placed in such equipment, no gas evolution was noticed at all.

On the other hand, the zinc-coated steel sea case exhibited significant hydrogen outgassing as shown

in **graph 2**. For the first eighty days, the test was carried out at an ambient temperature of about 15°C, after which it was moved to an environment where the average temperature was near to 22°C. By day eighty one, the evolution of hydrogen had settled to a rate of about 1.7 cc/day. However, this must be taken as a minimum estimate as there would have been an unknown amount of hydrogen dissolved in the water which may explain the apparent low rate up to day thirty. Since the sea case is in a funnel containing about 6 litres of sea water, then, assuming a solubility in water of 0.018 cc/cc, there would be a total of 108 cc of dissolved hydrogen. Hence, the upper estimate for the evolution rate, averaged over the first 81 days of the test is 2.6 cc/day.

Thanks to this test, we are already able to predict the corrosion behaviour of the two materials.

The study of the Pourbaix diagrams can explain the differences between the behaviour of the two materials. As said previously, the Pourbaix diagram of the zinc shows that there is a lot of chance for hydrogen to be generated when zinc corrodes in water. On the contrary, the Pourbaix diagram of nickel (**see graph 3**) shows that above pH = 6 (which is generally the case for the marine environment), there is little chance that hydrogen will be generated by nickel corrosion.

Experiment and Pourbaix diagrams are in agreement but, like always when corrosion mechanisms are studied, these results have to be cautiously taken into account : lab conditions are often far from actual conditions ! For example, if we take the case of the nickel-plating, we have to remember that nickel is sensitive to pitting corrosion because of the action of chlorides : galvanic corrosion between the nickel layer and cast iron could occur at localised corroded points.

That is why it is absolutely necessary to perform tests on the finished product.

4.2 - Joints tests

4.2.1- Principle

Sample joints were made up to test for corrosion and hydrogen generation in sea water.

A 4 km fibre bobbin was inserted in the tested joint and spliced to the line fibre. There were 5 metres of cable each side of the joint allowing the connection of the fibre for optical measurement purposes. The fibre bobbin was used as an hydrogen sensor.

Figure 6 gives a general view of a sample.

The whole sample was then immersed in an aerated flow tank in the following conditions :

- Electrolyte : water containing 3.5% NaCl
- Ph of electrolyte : 6.9 to 7.5
- Temperature : $40^{\circ}\text{C} \pm 2^{\circ}\text{C}$
- Flow speed : 0.1 m/s along the samples

An increase of temperature accelerates the corrosion phenomena and leads to results in a shorter time. In these tests, an increase of 10°C in temperature approximately doubled the rate of the chemical reaction.

Because molecular state hydrogen produces a strong and narrow absorption peak at 1240 nm, the change of loss by hydrogen is monitored using a 1240 nm OTDR.

This gives a very sensitive detection of increase of hydrogen pressure inside the joint.

4.2.2 - Measurements

4.2.2.a - Calibration of the fibre bobbin

A calibration of the fibre bobbin was conducted to measure the increase in attenuation due to hydrogen using the 1240 nm OTDR. A fibre bobbin identical to the ones used in the joint experiments was wound with 4 km NDS fibre. The fibre was sealed in a dessicator with a fibre end glanded off to facilitate optical measurement. The dessicator was then purged with a hydrogen/nitrogen mixture, at atmospheric pressure by venting the purged gas through an air lock. The attenuation increase was monitored regularly over a period of three weeks to ensure that a hydrogen equilibrium had been reached. The dessicator was regularly purged with a fresh gas mixture during this time. The dessicator and gas bottle was maintained at a constant temperature of 20°C . After equilibrium had been attained, the dessicator was purged with a higher concentration of hydrogen and the three weeks procedure repeated. Hydrogen concentrations in the range 10 to 80% were used. The increase in loss for each concentration is shown in **graph 4**. The slope of the graph equates to a loss increase for the tested fibre of 9.8 dB/km/atm. This value will be used for all future calculations of the hydrogen concentration within tested joints.

4.2.2.b - Results

Lightweight joint type A and B, and armoured joint type A and B were tested following the conditions described above.

Results are summarised in the **graph 5**.

The difference in performance between the two designs can easily be seen on the graph. Solutions B show significantly higher hydrogen generation than solutions A.

Within six days from the start of the test, all joints type B showed an increase in attenuation at 1240 nm. This showed that the hydrogen could readily diffuse into the joint cavity. The initial rate of loss for the armoured joint B was equivalent to 0.11 dB/km/day, with the lightweight joint B showing a lower rate of 0.018 dB/km. Over the test period, the armoured joint B reached a mean equilibrium value of around 4.0 dB/km, equivalent to a hydrogen pressure of around 0.36 atm. The lightweight joint B reached a lower equilibrium pressure of around 0.14 atm of hydrogen.

The difference in the results from the different samples can be also explained by the difference in the amount of metallic components surrounding the joint. For example in armoured joint type B, galvanised steel wires anchored close to the moulded box are in contact with sea water, they are not in the armoured joint type A.

Results of joints A showed no significant loss increase within the accuracy of the measurements.

The differences in the results from joints A and B are in agreement with test results described in section 4.1.

4.2.2.c - Additional tests

In order to confirm that zinc-coated components are the major cause of hydrogen problem, the following tests were performed.

Test 1

A Lightweight joint type A was tested following the test method described above but after 180 days ageing, a sea case of the kind used on Lightweight joint type B was placed around it.

As shown in **graph 6**, loss increased in a similar manner to the previous tests. The zinc-coated sea case caused hydrogen evolution when placed around a Lightweight joint type A.

Test 2

It was thought that the main source of hydrogen diffusing into the joints was generated on the inside of the zinc-coated sea case. This test was designed to eliminate this generating surface by filling the gap between the moulded joint and sea case with a silicone rubber compound.

The modified joint type B was then tested following the same procedure and results are given in **graph 7**.

The merits of filling the joint with silicone is clearly shown by comparing the result with that of a standard joint.

5. - CONCLUSION

This paper described a simple method of assessing hydrogen risk in submarine cable joints

We showed that a preliminary selection can be made thanks to a simple theoretical study of the behaviour of materials.

An experimental technique has been developed to validate the choice of metallic components of joints in contact with sea water.

Material type must be carefully selected and the amount of metallic components must be as small as possible.

When used for long-haul repeatered systems :

- For Lightweight joints, it is preferable not to use any metallic component in contact with sea water, because of the high hydrogen pressure build up that can be seen due to high depth.
- For armoured cable joints where there are metallic components in contact with sea water, it is preferable to select materials which do not produce hydrogen by corrosion (for example, stainless steel or nickel-plated iron as used in the type A joints described in the paper).
- For designs using galvanised parts, improvements in performance can be made by resin injection to reduce corrosion at the inner surface of the sea case.

Bibliography :

- [1] : «New submarine cable design for long haul, high bit rate systems», JF Libert, Y. Charles, IWCS proceedings 1996 pages 8-12
- [2] : «Corrosion et chime de surfaces des métaux», Dieter Landolt
- [3] : «Corrosion for science and engineering , KR Trethewey and J Chamberlain
- [4] : «Corrosion en milieux aqueux des métaux et alliages», JM Defranoux, Techniques de l'ingénieur Vol. M111
- [5] : «Corrosion engineering», Mars G. Fontana
- [6] : «Corrosion marine», R Collee

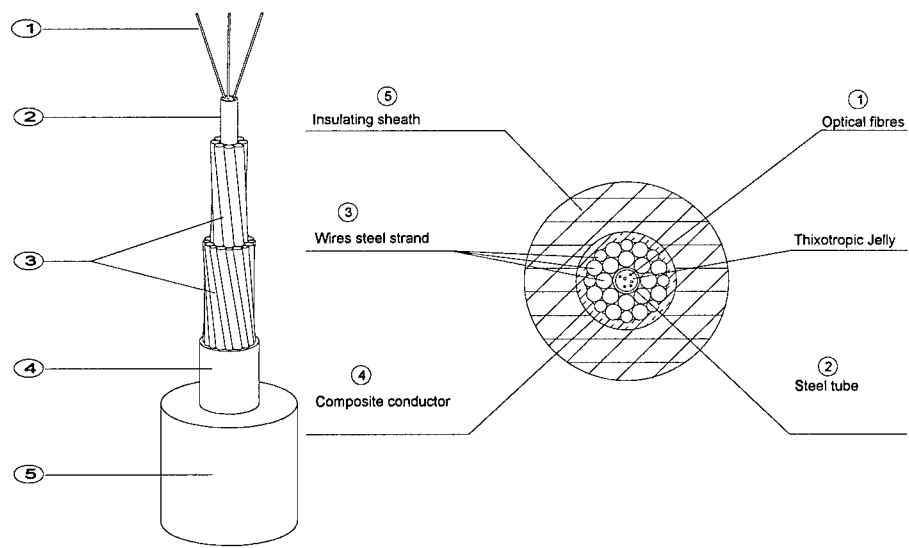


Figure 1
Example of lightweight cable
used in long-haul repeatered systems
The insulated sheath 5 is surrounding the
composite conductor 4, made of wire steel
strand 3 and copper

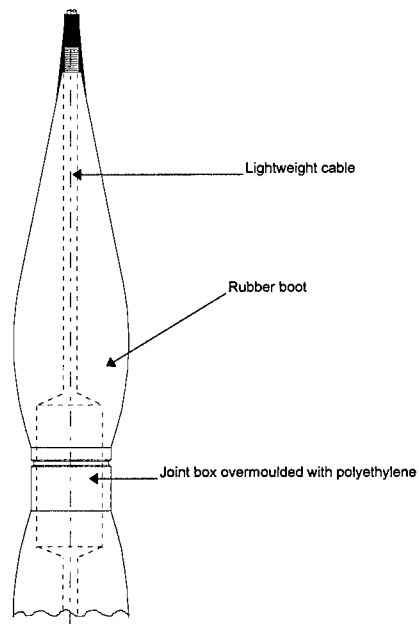


Figure 2
Lightweight joint type A. No metallic components
in contact with sea water

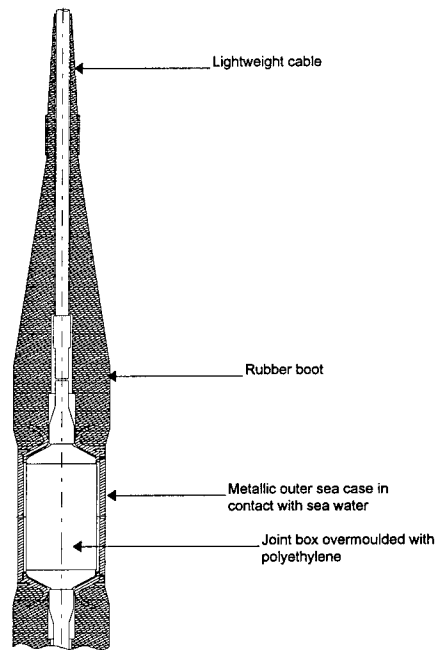


Figure 3
Lightweight cable joint type B

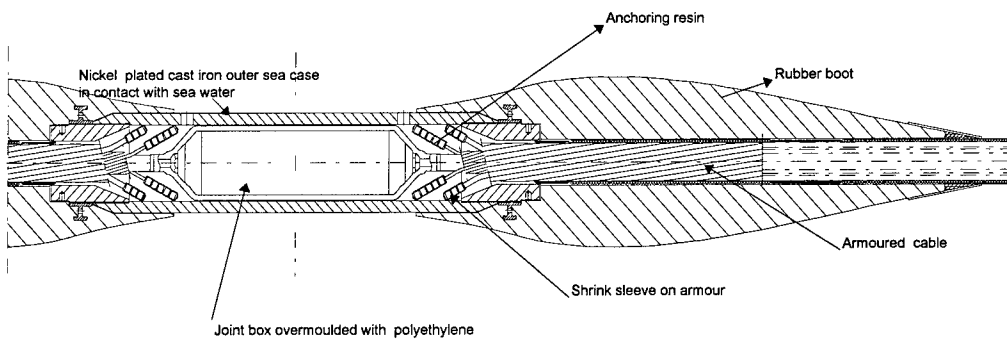


Figure 4
Armoured cable joint type A

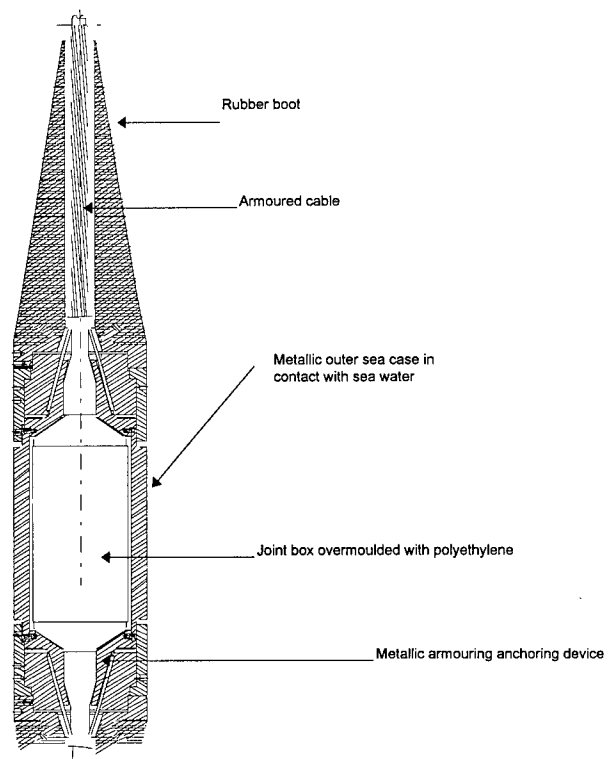


Figure 5
Armoured cable joint type B

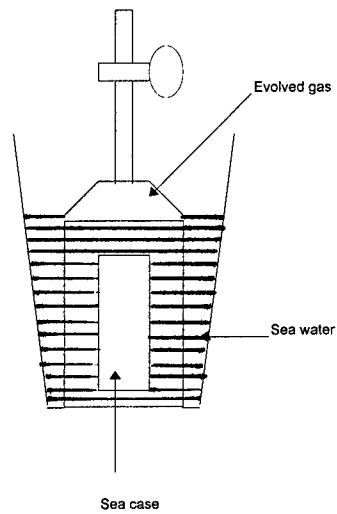


Figure 6
Test arrangement to measure hydrogen generation during corrosion of sea cases

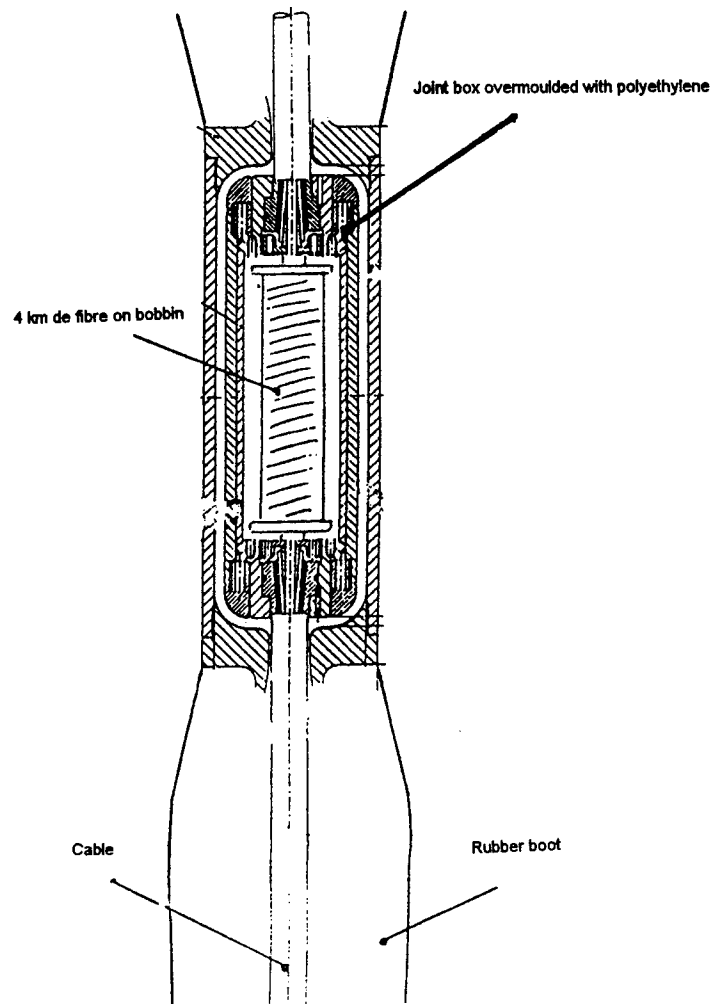
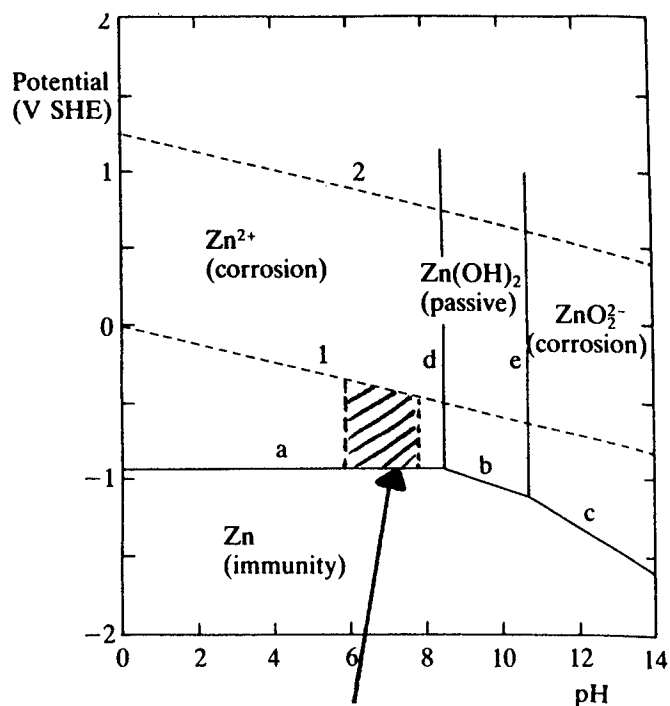
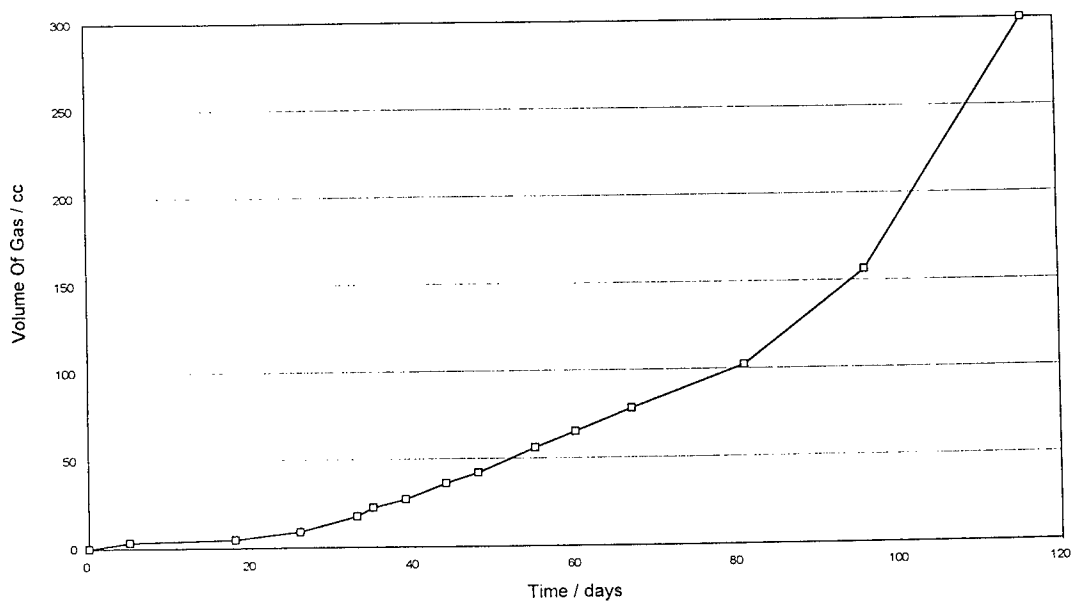


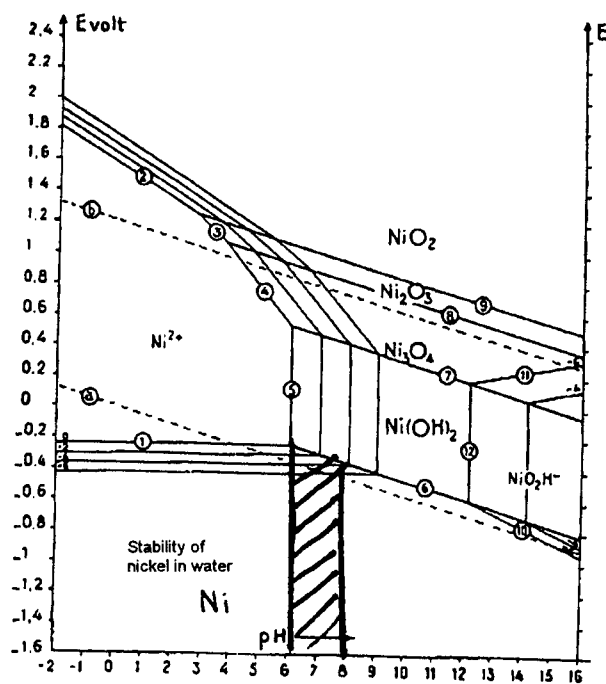
Figure 7
Diagram showing arrangement
of fibre bobbin in joint



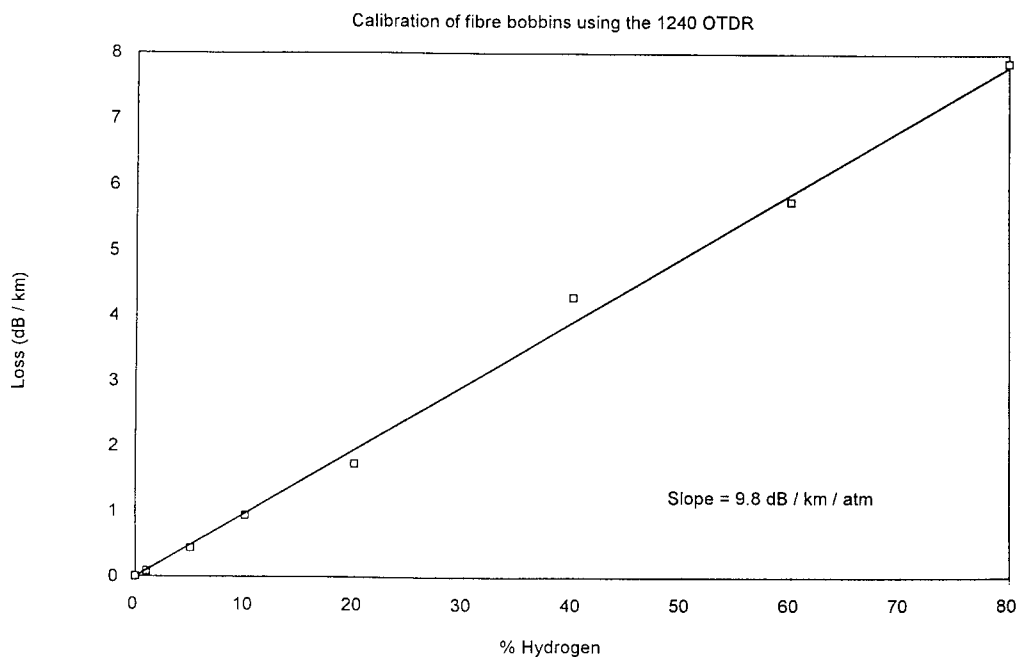
Graph 1
POURBAIX Diagram of zinc in water



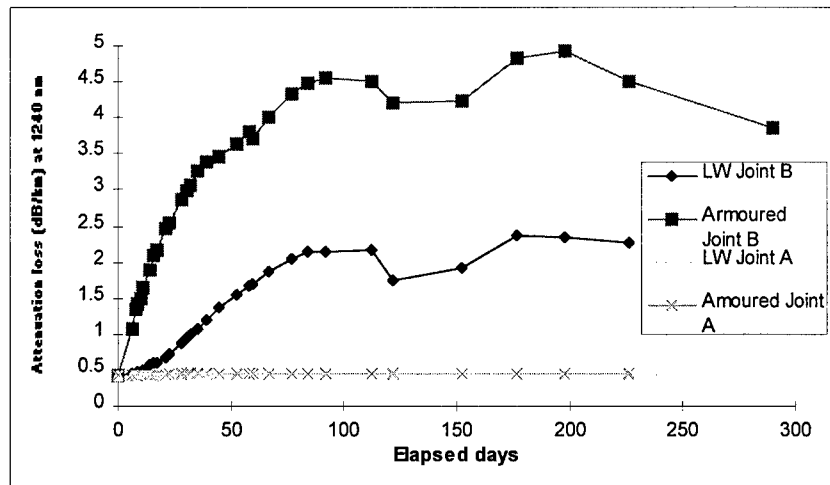
Graph 2
Hydrogen evolution from zinc coated sea case
in sea water.
Slow rate at beginning of test is due to solubility
of hydrogen in water



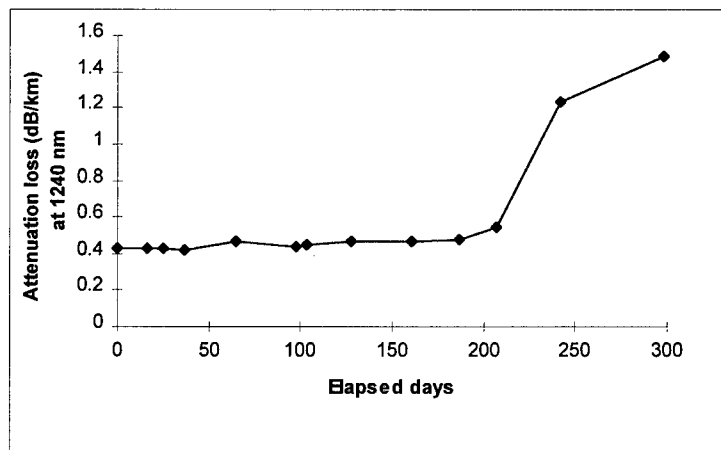
Graph 3
POURBAIX Diagram of nickel in water



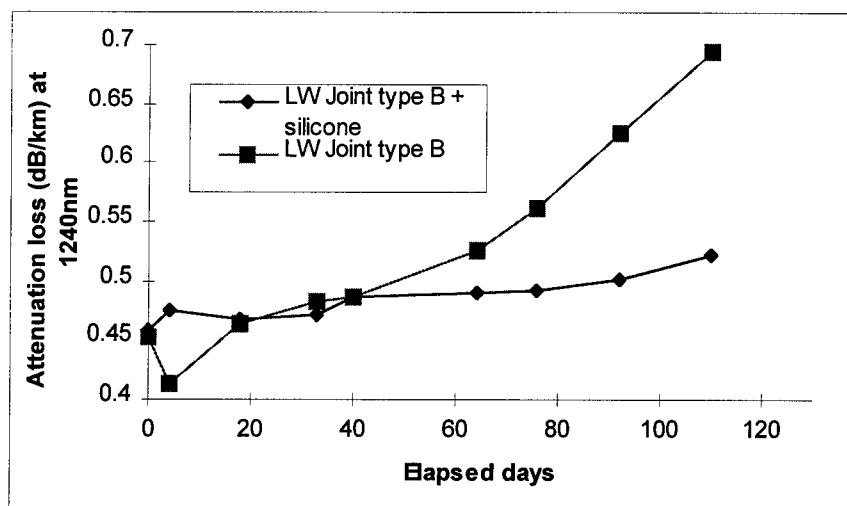
Graph 4
Calibration plot of 1240 nm OTDR
the fibre exhibits attenuation loss linearly
depending on the hydrogen pressure



Graph 5
1 240 nm attenuation evolution.
Joints B which have the more important
amount of metallic components in contact
with sea water exhibit the highest hydrogen generation



Graph 6
1 240 nm attenuation evolution
of lightweight joint type A when surrounded,
after 180 days, by sea case of joint type B



Graph 7
Protection of metallic surfaces
may increase their corrosion resistance

Authors

J.F LIBERT
Alcatel Submarine Networks
536 Quai de la Loire
62225 Calais Cedex

Jean-François LIBERT received his engineering degree from «Hautes Etudes Industrielles» of Lille (FRANCE). He joined Alcatel in 1984. He is now Technical Manager for Optical Submarine Cable in Calais.

F. RUELE
Alcatel Submarine Networks
536 Quai de la Loire
62225 Calais Cedex

Franck RUELE was born in 1965. He is graduated in chemistry from the «Ecole Nationale Supérieure de Chimie de Clermont-Ferrand». He joined Alcatel in 1991 where he is in charge of cable materials development.

P. WORTHINGTON
Alcatel Submarine Networks
536 Quai de la Loire
62225 Calais Cedex

Peter WORTHINGTON is a development engineer in Alcatel Submarine Networks. He received a BSc in Electronics and Electrical Engineering from the University of Birmingham in 1971. Since 1977 he has been involved in the development of optical cables for submarine systems.

A study of Air Blown Fiber for a Long Distance Tube

Itaru Sakabe, Wataru Katsurashima, Hiroaki Sano and Shigeru Tanaka

Yokohama Research Laboratories, Sumitomo Electric Industries, Ltd.

1, Taya-cho, Sakae-ku, Yokohama, 244 Japan

Phone: +81-45-853-7164 / Fax: +81-45-851-1557 / E-mail: sakabe@yklab.sei.co.jp

Abstract

To extend the installation length of optical fiber unit for ABF system [1], we have studied the blowing performance and found out that the blowing velocity of optical fiber unit is explained by the calculated viscous blowing force at the inlet of tube caused by compressed air. Using this relation, we can estimate the blowing velocity provided that the tube length and the inner diameter of tube are decided. And in our experiment, we optimized the outer diameter of 6-fiber unit and succeeded to blow it into the 3000m tube within 2 hours at the pressure of 10kg/cm².

gy to data transmission and subscriber networks is well under way. It is difficult to predict the future increase in information traffic or the expected scale of the optical fiber system required. Optical fiber lines that are not initially needed are often installed to avoid future replacement or expansion of existing optical fiber paths, which is not economical in terms of cost and conduit space.

The air blown fiber (ABF) system is a unique optical fiber cable installation technique which blows a fiber unit into a previously installed tube by utilizing the viscous drag of compressible air. Fig.1 depicts the concept of the ABF system.

1. Introduction

The application of optical fiber technolo-

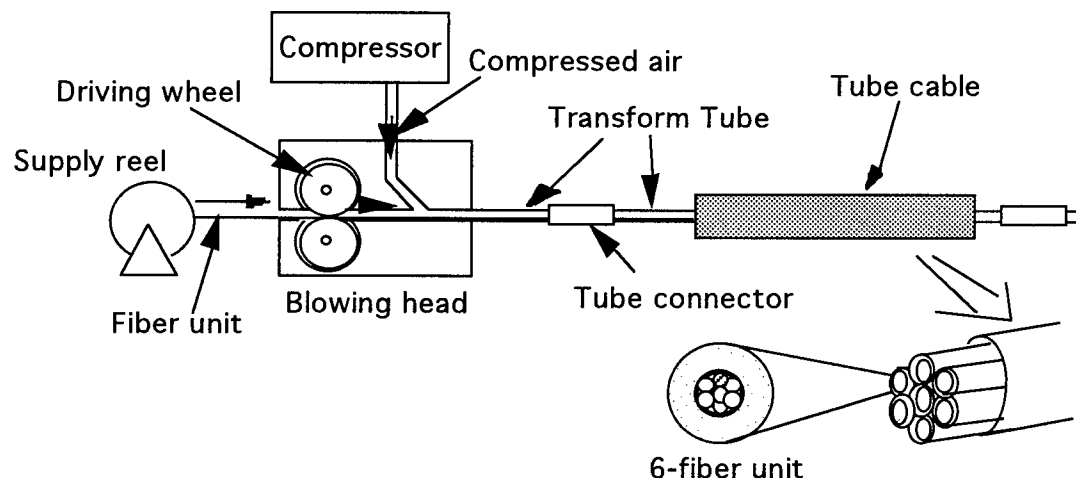


Fig.1 Construction of Air Blown Fiber system

The optical fiber unit is blown into the tube by the blowing head, together with compressed air fed from the compressor, and is drawn through the tube by the viscous drag of the air. The ABF system has the following characteristics:

(1) An optical fiber unit can be blown into an existing tube when need arises, provided that the tube (pipe cable) has been installed in the section where the need for an optical fiber line is expected. This allows the user to avoid over-installation of optical fibers and reduces the initial cost.

(2) The blowing pressure distributing over the entire length of the unit is causing almost little tensile stress to the optical fibers during and after installation since the optical fiber unit is transferred by compressed air whose blowing force per unit length is small.

(3) A continuous splice-free optical fiber unit can be installed provided that the tubes are jointed at the necessary lengths in advance. This dramatically reduces the number of optical fiber splices.

For the third characteristics, the long distance blowing has been studied further to reduce the number of optical fiber splices and to improve the efficiency of blowing operation. As a long distance blowing installation method, tandem operation using plural blowing heads was proposed and reported that 13600m length optical fiber unit was blown through the whole length tube [2]. On the other hand as a conventional blowing installation method using only one blowing head, the long distance blowing characteristics of at most 2000m length tube have been reported [3]. In this paper we describes the blowing performance of optical fiber unit into the long distance tube using only

one blowing head.

2. Pressure Gradient and Blowing Force

The blowing force per unit length f is given by Eq.1 [1].

$$f = \frac{\pi d_1 d_2}{4} \frac{dP}{dl} \quad \text{Eq.1}$$

where d_1 and d_2 in Eq.1 indicate the inner diameter of tube and the outer diameter of optical fiber unit respectively as shown in Fig.2; dP/dl indicates the pressure gradient in the tube.

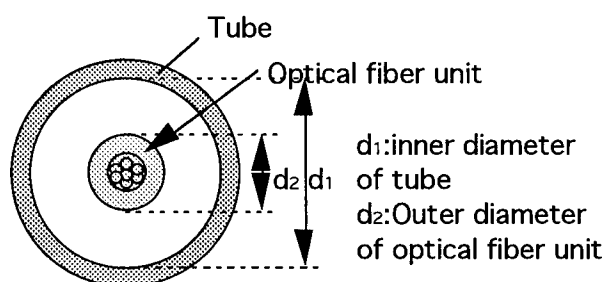


Fig.2 Cross section of tube and optical fiber unit

All terms except dP/dl in Eq.1 are constant, and the pressure gradient dP/dl is not uniform over the entire length of the tube because air is compressed fluid. The blowing force varies in relation to the insertion length of the unit since the effective space clearance of the tube changes as the insertion length of the optical fiber unit is gradually increasing.

After the unit is inserted into a tube by the length of l , the pressure at the position u from the inlet of the tube is given as Eq.2 and Eq.3

$$P(u) = \sqrt{P_{in}^2 - \frac{u}{l}(P_{in}^2 - P_1^2)} \quad \text{Eq.2}$$

$$P_1 = \sqrt{\frac{d_1^{19/4} l P_{out}^2 + d_2^{19/4} (L-l) P_{in}^2}{d_1^{19/4} + d_2^{19/4} (L-l)}} \quad \text{Eq.3}$$

where P_{in} is the absolute pressure at the tube inlet, P_{out} is one at the tube outlet equal to atmospheric pressure. Symbols are shown in Fig.3.

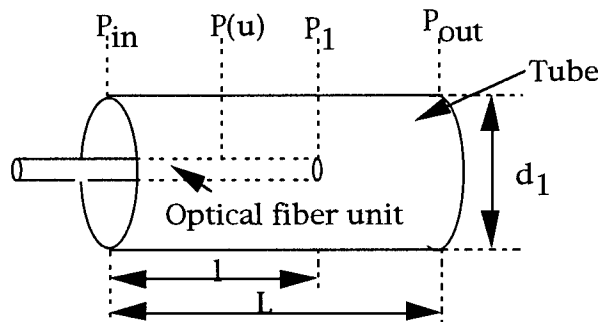


Fig.3 Parameters of blowing force

From Eq.1 and Eq.2, the blowing force per unit length at the position u , $f(u)$, is expressed as Eq.4.

$$f(u) = \frac{\pi d_1 d_2}{8} \frac{P_{in}^2 - P_1^2}{l^{1/2} \{l P_{in}^2 - u(P_{in}^2 - P_1^2)\}^{1/2}} \quad \text{Eq.4}$$

Fig.4 shows the calculated blowing force distribution and the three lines (A,B,C) indicates the condition that the insertion length of the unit is 1000, 2000 and 3000m. The pressure at the inlet is 10 kg/cm². The viscous drag force is the smallest at the inlet of tube and becomes smaller as the insertion length of the optical fiber unit is increased.

This viscous drag force at the inlet, $f(0)$, is derived by substituting $l=0$ in Eq.4 and is described as Eq.5

$$f(0) = \frac{\pi d_1 d_2}{8} \frac{P_{in}^2 - P_1^2}{l P_{in}} \quad \text{Eq.5}$$

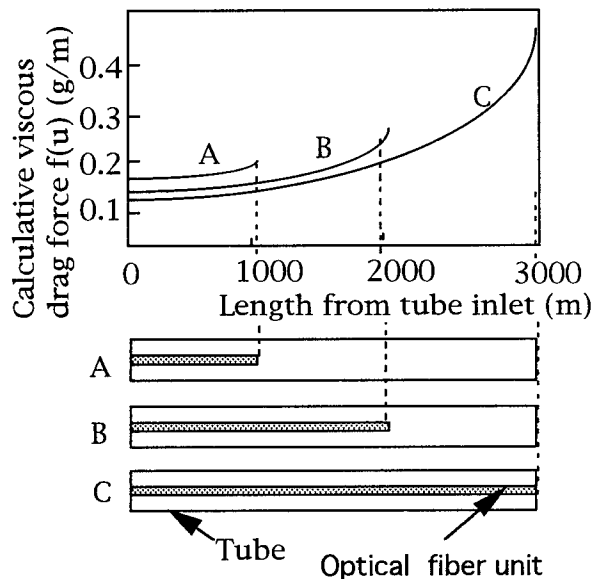


Fig.4 Calculative viscous drag Force

3. Tube configuration

The maximum blowing installation of 2000m at one shot is already reported [3]. To expand the installation length, it is inevitable to hold the viscous drag force on the unit under the regulated air pressure, and raising up the inner diameter of the tube is effective for it. We set the target of 3000m-installation, which coincides with the distance between neighboring railway stations in urban area. And for a blowing experiment, we prepare the tubes whose inner diameter are 6mm and 8mm; former is 8mm O.D./6mm I.D. tube widely adopted for blowing fiber system and the latter is

10mm O.D./8mm I.D. tube which has larger inner diameter than the conventional usual one.

4. Optical fiber unit design

Our test unit is depicted in Fig.5. Six fibers are stranded around central member and coated by UV curable resin to the diameter of 0.8mm. Foamed polyethylene is sheathed around it.

The viscous drag force on a unit is the smallest at the inlet of the tube, and it is important to know this minimum force for deciding whether the unit can be installed through a tube or not.

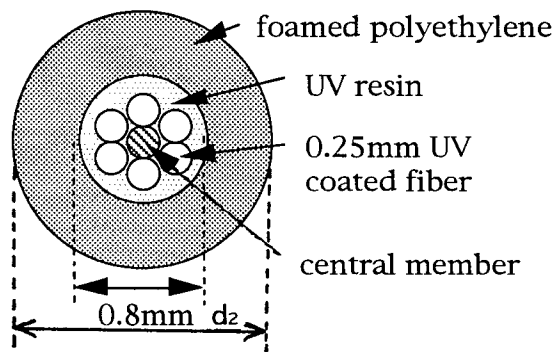


Fig.5 Cross section of optical fiber unit

We determined the outer diameter of optical fiber unit so that the effective viscous drag force f_{eff} as denoted as Eq.6, is the largest as possible.

$$f_{\text{eff}} = f(0)_{l=L} - \mu mg \quad \text{Eq.6}$$

where $f(0)_{l=L}$ and μmg are the inlet blowing force and the friction resistance between the tube and the optical fiber unit respectively. μ is the friction factor. m is the mass of the optical fiber unit per unit length and g is the acceleration of gravity. The suffix $l=L$ indicates that the optical fiber unit reaches the end of the

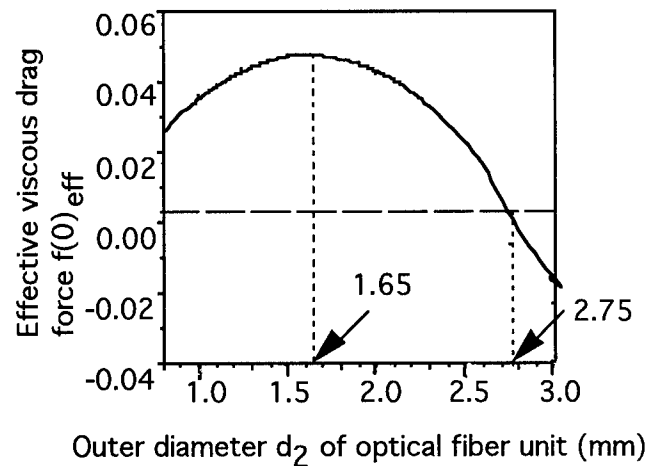


Fig.6 Optimization of optical fiber unit outer diameter

tube.

The relation between the effective drag force and the outer diameter of the optical fiber unit is calculated and described in Fig.6. The calculative condition is that the tube length L is 3000m, the tube inner diameter is 8mm, the inlet pressure of compressed air is 10kg/cm^2 and the friction factor μ is 0.1. The mass of optical fiber, m , is calculated in Eq.7 as a function of the unit diameter d_2 .

$$m = 0.360 \cdot d_2^2 + 0.423 \quad \text{Eq.7}$$

If the unit diameter is smaller than 2.75mm, f_{eff} is larger than zero and the unit is expected to blow the whole length.

The best diameter of optical fiber unit which has the largest effective viscous drag force is 1.65mm. The effective drag force f_{eff} has the peak when the outer diameter is 1.65mm, so we manufactured a test unit whose outer diameter was from 1.6mm to 1.7mm.

5. Performance of horizontal long distance blowing

We examined the performance of horizontal long distance blowing using the unit whose diameter was 1.65mm. The experimental set-up is shown in Fig.7.

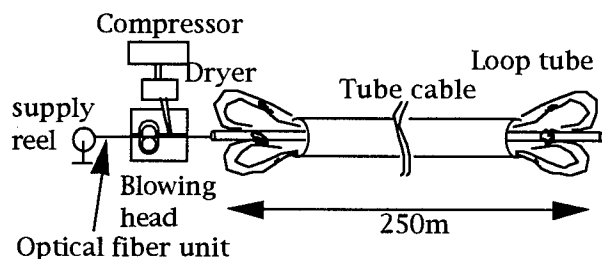


Fig.7 Experimental set-up

We assume that the effective drag force dominates the blowing performance, that is to say, the blowing velocity. 2000m-long distance blowing was reported[2]. In order to make the effective drag force with 3000m length tube equivalent to one with 2000m, which is the maximum length reported blowing unit reaches in a shot so far, we have to raise the inner diameter of the tube to 8mm. Then we manufactured two size of tube cables. These cables whose inner diameters are 8mm and 6mm respectively are laid straightly and

Table 1 Experimental conditions of horizontal long distance blowing

Tube inner diameter	Tube length	Pressure at the inlet of tube
8mm	3000m	from 7 to 12kg/cm ²
	2000m	from 4 to 8kg/cm ²
	1000m	from 2 to 4kg/cm ²
6mm	2000m	from 5.5 to 7kg/cm ²
	1000m	from 2 to 4kg/cm ²

horizontally on the ground. The lengths of tube cables are both 250m. We made the 1000m, 2000m and 3000m length tube route by connecting the tubes at both ends of the cable. The maximum blowing velocity is limited to 30m/min. The experimental conditions are listed on Table 1.

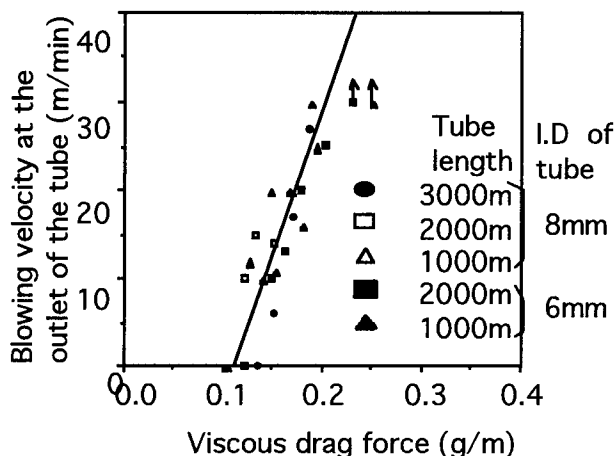


Fig.8 Experimental blowing performance of horizontal long distance blowing

The experimental results of horizontal long distance blowing is shown in Fig.8.

The x-axis in Fig.8 shows the calculated viscous drag force caused by compressed air and the y-axis shows the experimental blowing velocity of optical fiber unit under the condition that the unit reaches the end of the tube. The x-intercept is interpreted as the friction resistance between the tube and the optical fiber unit. The experimental blowing velocity of optical fiber unit has a linear relationship to the calculated viscous blowing force. The deviation of viscous blowing force is about 0.05g/m at the same blowing velocity regardless of the inner diameter and the length of the tube.

From the experiment, the effective blowing force of 0.2g/m is required for

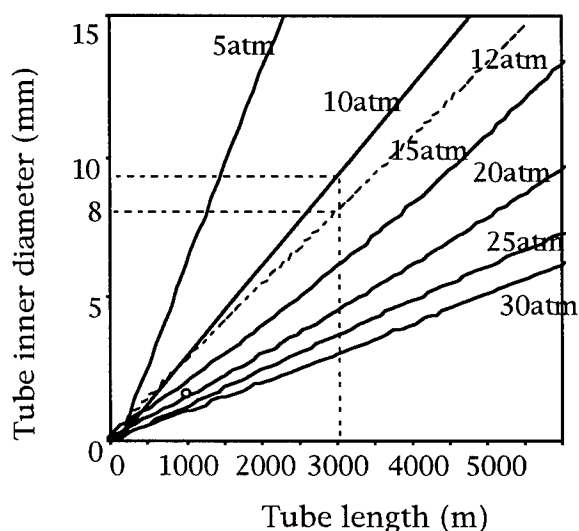


Fig.9 Desired pressure to blow the whole distant of tube

30m/min installation.

Fig.9 indicates the necessary pressure to blow the optical fiber unit at the blowing velocity of 30m/min.

To blow an optical fiber unit into 3000m length tube with the blowing velocity of 30m/min at the pressure of 10kg/cm², tube inner diameter should be more than 9mm. In our experiment using 8mm inner diameter tube, the unit had been progressing at 30m/min until 2500m installation, however, decreased its velocity to 27m/min at the termination of 3000m tube. The total blowing time took one hour and fifty minutes which is sufficiently tolerable for blowing operation.

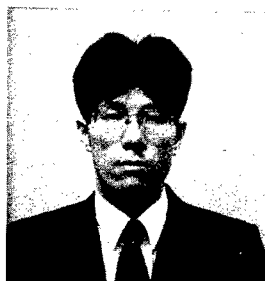
6. Conclusion

We found out that the blowing velocity of the unit is proportional to the effective viscous drag force defined as the difference between the calculative drag force and the friction residence created during the blowing installation. And in our experiment, we succeeded to blow a 6-fiber

unit through 3000m tube in one shot within 2 hours at the pressure of 10kg/cm² by optimizing the outer diameter of the unit and tube. Longer possible blowing length will extend the flexibility of blowing installation technique.

Reference

- [1]S.A.Cassidy and M.H.Reev, "A radically new approach to the installation of optical fibre using the viscous flow of air ",proceedings of IWCS 1983, pp250-254
- [2]Nicholas J.Medlen, "Blown fiber field trial "Lightwave May 1992, p23,30
- [3]S. Takaoka et.al., "Investigation of Long Length Installation to Air Blown Fiber Unit "proceedings of the 1993 spring IEICE general conference B-878



Itaru Sakabe

Sumitomo Electric
Industries, Ltd.
1, Taya-cho, Sakae-ku,
Yokohama, Japan

Itaru Sakabe received the M.E. degree in electronics and communication engineering from Electro Communication University in 1993. He joined Sumitomo Electric Industries, Ltd. and then has been engaged in the development and design of communication cables. Mr. Sakabe is an engineer of Communication R&D Department in Yokohama Research Laboratories.



Hiroaki Sano

Sumitomo Electric
Industries, Ltd.
1, Taya-cho, Sakae-ku,
Yokohama, Japan

Hiroaki Sano was born in 1960, and received his M.E. degree in Polymer Science from Kyoto University in 1984. He joined Sumitomo Electric Ind., Ltd. and has engaged in development of optical fiber manufacturing process and fiber-optic cable design. He received JSPMI (Japan Society for the Promotion of Machine Industry) Prize for "Commercial Application of Air Blown Fiber System" in 1994. He is a senior engineer of Intellectual Property Department and a member of the Institute of Electronics, Information and Communication Engineers of Japan.



Wataru Katsurashima

Sumitomo Electric
Industries, Ltd.
1, Taya-cho, Sakae-ku,
Yokohama, Japan

Wataru Katsurashima was graduated from Tokyo University in 1987. He joined Sumitomo Electric Industries, Ltd. in 1987 and has been engaged in optical fiber and cables. He is an engineer of Communication R&D Department in Yokohama Research Laboratories. Mr. Katsurashima is a member of Institute of Electronics, Information and Communication Engineers of Japan.

Shigeru Tanaka

Sumitomo Electric
Industries, Ltd.
1, Taya-cho, Sakae-ku,
Yokohama, Japan

Shigeru Tanaka received the B.S. and M.E. degree from Tokyo University in 1974 and 1976. He received Ph.D degree in 1989. He joined Sumitomo Electric Industries Ltd. in 1976 and has been engaged in the design and characterization of optical fibers and cables. He is a manager of Communication Department in Yokohama Research Laboratories. Dr. Tanaka is a member of Institute of Electronics, Information and Communication Engineers of Japan.

BLOWN FIBRE – A REFERENCE TEST BLOWING ROUTE

Keith Cockrill, Jon Nixey, Ray Studd, BT Laboratories, UK
Martin Davies, Ralph Sutehall, Pirelli Cables, UK

ABSTRACT

Blown Fibre (BF) systems have grown rapidly during the last six years. The manufacture of enhanced performance fibre unit (EPFU) and BF tube assemblies has moved from the laboratory to volume production. Previous performance tests simulated a real access network but did not allow investigation of climatic performance. A Reference Test Method (RTM) was needed to enable the preparation of purchase specifications, and to provide quality assurance measures after manufacture. A RTM has been developed to assess the climatic installation window of Blown Fibre systems. The new test is compact, uses non-specialised equipment, and provides a cost-effective and detailed means for assessing the properties of EPFU, BF tube assemblies and/or the blowing equipment itself.

GENERAL PRINCIPLES OF BLOWN FIBRE

The BF installation technique provides point-to-point fibre communication links. The technique is based on a network of pre-installed tubes (in customer buildings and/or the access network) into which an EPFU can be installed on a 'Just-In-Time' basis. EPFU is fed into the tube using a pair of motorised pinch wheels. Compressed air fed into the tube propels the EPFU via viscous drag along the tube length imparting minimal strain to the fibre (see figure 1).

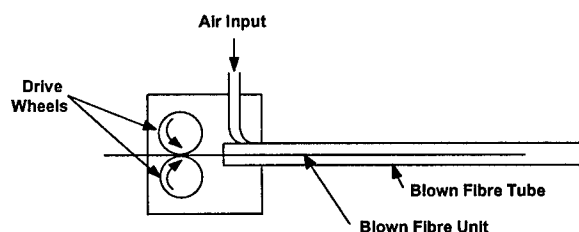


Figure 1: blowing schematic

BACKGROUND

Climatic window

Air, typically at 10 bar pressure and flowing at 80 Litres/min, is used to propel fibre into tubes of 3.5 and 6.0 mm bore at installation rates of 25 m/min. The temperature and moisture content (dewpoint) of the compressed air has been found to have an important effect on blowing performance and figure 2 shows the moisture content possible in the two tube sizes⁽¹⁾ used in the BT access network.

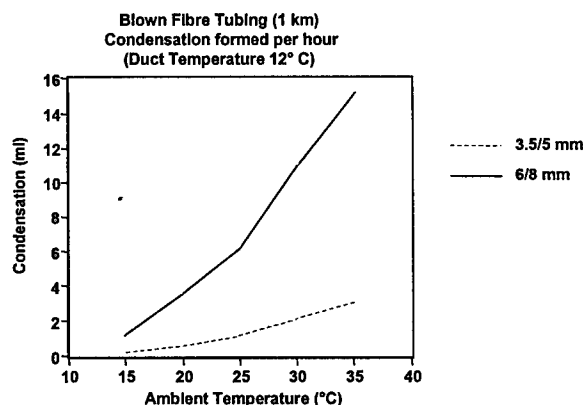


Figure 2: condensation in blown tube

In particular, the affect of the temperature differential between the blowing system and duct needs to be understood and controlled for repeatable and reliable installation performance.

The UK climate can show warm, humid conditions above ground and cold, dry conditions below ground. During extreme conditions variable installation performance was noted. Prior to the RTM these conditions were simulated by making use of an 'ocean simulator' – a 450 m long twin pipe temperature controlled vessel. BF tubing was installed in the vessel and maintained at a constant temperature of

12° C (the UK duct mean), whilst the blown air ambient temperature was varied between 5° C and 30° C to create a good representation of the UK diurnal range. These initial tests provided a benchmark for a range of BF tube and EPFU as a forerunner to the development of a Reference Test Method.

Preliminary test routes

Product qualification tests required an installation of over 700 m (3.5/5 mm) and 1200 m (6/8 mm) of BF tube with a prescribed number and diameter of bends. These test routes were based on typical duct layouts within the BT access network. Such a 'typical route' (figure 3. for example) was neither practical for factory quality assurance testing of BF tube or EPFU nor useful for comparison purposes because of local climatic variations at the test sites. Very often the routes were miniaturised on the assumption that straight routes could be simulated by large radius bends. None of these 'compact' routes were truly identical which further made comparison difficult. The original tests were destructive of cable product and therefore could not be used economically as a quality assurance batch test. In addition, the methodology did not aid the preparation of performance specifications. The inconsistencies indicated the need for development of a reliable Reference Test Method.

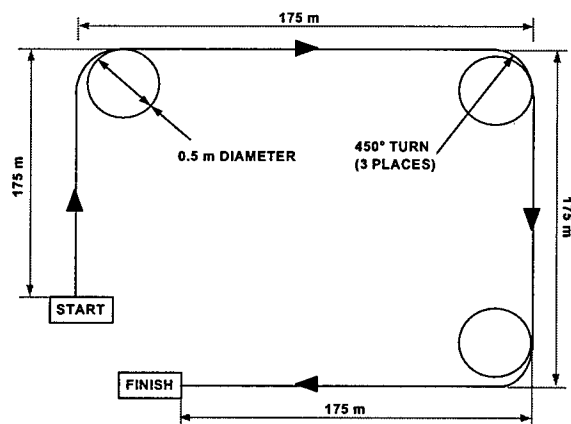


Figure 3. Initial Test Route for 3.5ID/5 mm OD BF Tube

Reference Test Method Requirements

Over recent years manufacturers and users of BF systems have developed the requirements for a performance Reference Test Method. The fundamental demands are:

- A compact test route suitable for use indoors independent of external climatic conditions or geographical location.
- A test route able to replicate or exceed the full range of environmental conditions of the blowing air temperature, dewpoint and tube temperatures experienced at installation sites – the 'climatic window'.
- The number of bends used in a test route shall exceed those found in customer buildings or the access network.
- A test route able to evaluate the blowing performance of existing and new BF tube linings and EPFU materials including physical parameters of surface finish and electrostatic characteristics.
- A test route using 'standard' equipment such as delivery drums, BF tubes and connectors, blowing compressors and equipment.
- No requirement for large environmental chambers working at extreme temperatures or humidity.

TEST PROGRAMMES

Ocean simulator

Many tests were conducted on the BT ocean simulator in order to evaluate the characteristics of blowing performance with respect to environmental conditions. The results of this work are summarised in the graphs below. All graphs plot maximum blowable distance versus temperature difference between blowing air and duct (ΔT).

In figures 4 and 5, plot 1 shows the limited performance window offered by early EPFU and both diameters of BF tube. Plots 2, 3 in the figures show the performance window for current EPFU and BF tube. Plot 4 shows the improved performance of the current products when the blowing equipment is equipped with a membrane dryer to dehumidify the air. The dryer has been adopted as a modification for all field installations.

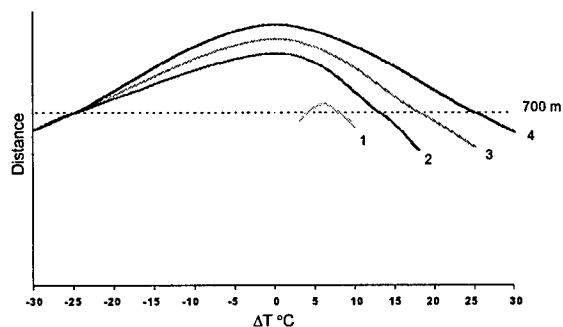


Figure 4: 700 m of 3.5 mm ID/5 mm OD tube

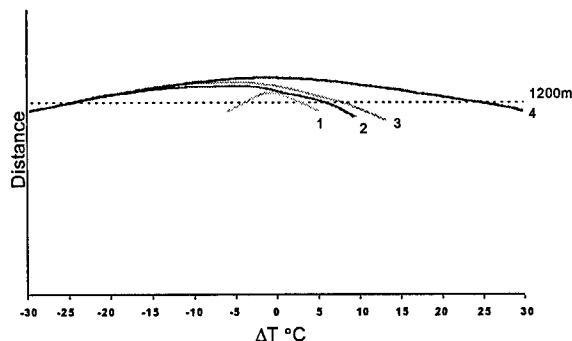


Figure 5: 1200 m of 6 mm ID/8 mm OD tube

Drum based test

The ocean simulator test is representative of climatic conditions, but not the convoluted routes found in the network. Much of this testing was repeated using a drum based test for each BF tube diameter and figures 6 and 7 show how the operating window is reduced. This is due to the number of coils.

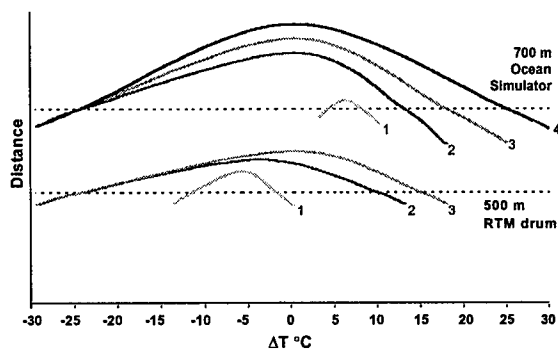


Figure 6: 3.5 mm ID/5 mm OD tube in ocean simulator and drum tests

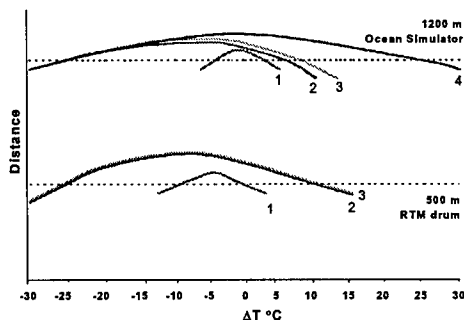


Figure 7: 6 mm ID/8 mm OD tube in ocean simulator and drum tests

REFERENCE TEST METHOD DEVELOPMENT

Various options existed for the RTM and these are discussed below.

Drum with axis horizontal

Early attempts to blow EPFU into tubes on standard drums with their axis horizontal had met with only limited success. The number of coils was believed to be excessive, particularly with the need for the EPFU to travel vertically up and down each coil. The small radius of the coils was also thought to be a factor. A large belly drum was used to try and improve blowing distances up to 500 m (i.e. a full drum length). However, non-standard drums would not be of particular benefit to quality assurance activities and this route was not considered further.

Drum with axis vertical

The horizontal axis trials were repeated with the drum axis placed vertically. These trials showed that a 500 m installation could be achieved but only with the blow carried out in a particular direction.

Verification

The work showed that the drum tests would form a good basis for product qualification, routine quality assurance and for assessment of modified blowing equipment. Tests using a standard drum with axis vertical were pursued to verify the methodology.

A tube and EPFU combination that had been known to perform well in the ocean simulator was re-tested according to the regime described above. Using the same blowing conditions the

performance window narrowed due to the number of coils on the drum. Adjustment of the temperature differential (ΔT = blowing air temperature - duct temperature) was then made in order to produce a set of limiting conditions similar to those achieved in the ocean simulator. The dewpoint of the blowing air at the tube entry was also controlled in order to avoid local variables giving optimistic results.

BF TUBE AND EPFU COMBINATIONS

An early version of EPFU which was known to be a poor performer in the ocean simulator and not acceptable in the field was tested using the drum test. The results showed a curtailed performance window indicating that the test was indeed discriminating.

A range of products which were acceptable in the field were tested in the drum test and appropriate acceptance limits were chosen. These chosen limits are now the product acceptance benchmark.

EPFU variability

Certain pre-production 'varieties' of EPFU are known to be more flexible and prone to buckle in tortuous network routes. Tests conducted in the ocean simulator were acceptable, but re-testing on the drum produced failures. Similar failures occurred during trial network installations.

This evidence shows the ability of the drum test to segregate marginal product. Straight test routes such as the ocean simulator, whilst satisfactory for assessing temperature differentials, are not the complete answer for demonstrating real network performance.

Climatic window and equipment variables

Results over a wide range of dewpoints, blowing air and tube temperatures have demonstrated that the drum test is able to produce a repeatable climatic window of performance limits. In effect, ΔT and the dewpoint affect the level of the moisture likely to be found in the tube, providing neither the blowing air or tube temperature is below 0°C . The range of test conditions is sufficiently large to make the drum test independent of geographical location whilst providing the required assurance of 'blowability'.

RTM DESCRIPTION

The rigorous evaluation described, allowed an easily applied Reference Test Method (figure. 8) that makes use of industry standard equipment to be defined. Standard wooden cable delivery drums, environmental chambers used for cable testing and BF installation equipment are used to provide a realistic test regime. The RTM may be used for product qualification, quality assurance, product and installation equipment development.

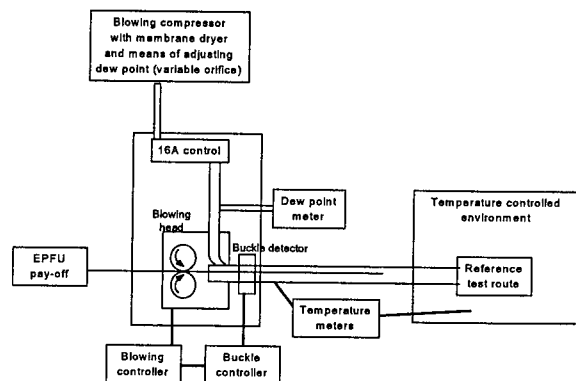


Figure 8: Schematic of typical test arrangement

The BF tube to be tested is placed with drum axis vertical in an environmental chamber. A range of blowing air dewpoints and temperature differentials is used to assess blowing speed and distance. The method requires control and/or knowledge of the climatic simulation parameters;

- the dewpoint of the compressed air used for blowing, and
- the temperature difference between the compressed blowing air, and the duct into which the BF Tube is installed.

If ΔT is positive, condensation in the BF Tubes may occur. If the dewpoint is low and ΔT is negative, static attraction between the BF Tube wall and the EPFU may occur. These two conditions influence blowing speed and blowable distance. By varying ΔT and the dewpoint temperature, the blowing conditions may be simulated and minimum performance levels assessed for world-wide deployment of blown fibre systems.

The number of bends in the BF tube wound on the drum in the RTM exceeds those of a test route and the linear ocean simulator. They can

therefore be used to predict the minimum performance of the BF tube and EPFU.

The EPFU installation rate is controlled with an upper and lower bound. The maximum speed is restricted to ensure that the EPFU does not buckle within the blowing head. A buckle detector is used to stall the equipment if this does occur, and may be reset to continue blowing. The minimum speed reflects the lowest acceptable field installation rate.

SUMMARY

The Reference Test Method is quick and easy to use, compact, using standard environmental test chambers and independent of test location and environmental conditions.

The product is unaffected by the non-destructive test, making it suitable for product qualification and quality assurance.

It is representative of the most convoluted installation, gives indication of access network performance and allows correlation of blowing performance and materials' limiting conditions with field experience.

In particular, the method gives the ability to demonstrate the suitability of blown fibre installation in world-wide markets by using appropriate blowing conditions.

ACKNOWLEDGEMENTS

The authors recognise the valuable contributions of colleagues within both BT and Pirelli. Special thanks are due to Rebekah Davey and Peter Hale for compiling and editing the paper.

REFERENCES

1. P A Barker & R Lowe. Blown Fibre - Second Generation Development. Plastics in Telecommunications, September 1995.

AUTHORS



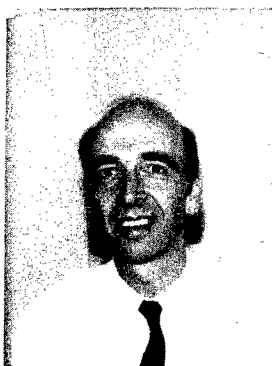
Martin Davies
Pirelli Communication
Cables Limited
Wednesbury Street
Newport, S. Wales
UK. NP9 0WS

Martin Davies is Chief Engineer with the Communications Cables Division of Pirelli Cables UK, where he is responsible for product design and development. He has been an active member of a number of standardisation bodies, including BSI, ETSI and IEC. Currently, he is a member of the CENELEC joint working group, developing standards for optical cables to be used along electrical power lines.



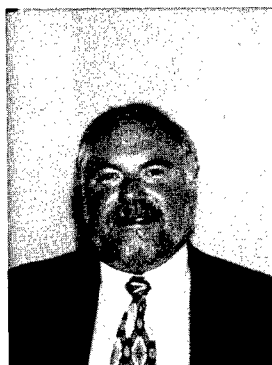
Ralph Sutehall
Pirelli Communication
Cables Limited
Wednesbury Street
Newport, S. Wales
UK. NP9 0WS

Ralph Sutehall is a Senior Engineer with the Communications Division of Pirelli Cables in the UK, where he is responsible for installation development. He has been working with optical fibre cables for 24 years and is an active member of the CIGRE working group on fibre optics.



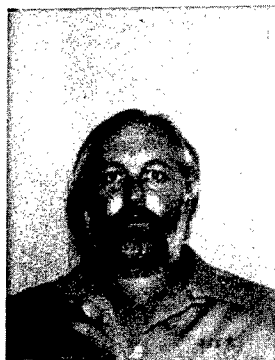
Jon Nixey
BT Network &
Systems
BT Laboratories
Martlesham Heath
IPSWICH, UK
IP5 7RE

Jon Nixey joined BT (then the GPO) in 1967 to work on development models of future electronic telephone exchanges. In 1977 he transferred to work on the quality and reliability of electronic components, particularly their assembly quality during manufacture. As a committee member, much of his work has been transferred to International standards such as IEC, BSI and CECC. In 1994 he transferred to the Optical Fibre and Cable unit to support standardisation work on cables and recently Blown Fibre installation solutions.



Keith Cockrill
BT Network &
Systems
BT Laboratories
Martlesham Heath
IPSWICH, UK
IP5 7RE

Keith Cockrill joined BT (then the GPO) in 1967, working on vendor quality of submarine and land cables and later on the maintenance of complex test equipment. In 1975 he transferred to BT Laboratories to work on submarine system projects. His 27 years of work in the submarine area has given him an international reputation for universal solutions of moulding problems. In 1994 he transferred to lead the Optical Fibre and Cable unit to use his expertise in novel solutions to reliability aspects of cable and Blown Fibre.



Ray Studd
BT Network &
Systems
BT Laboratories
Martlesham Heath
IPSWICH, UK
IP5 7RE

Ray Studd joined BT (then Post Office Telecommunications) in 1971, to work at the Post Office Research Department on high reliability transistors for submarine repeaters. He transferred to BT Laboratories to work on reliability projects for integrated circuits and other novel opto-electronic semiconductor devices. In 1994 he transferred to the Optical Fibre and Cable unit to work on reliability aspects of fibre and cable. In particular, he has carried out assessment of Blown Fibre for installation in the public access network.

Study on Additional Fiber Blowing Technique

Wataru Katsurashima, Hiroki Ishikawa, Hiroaki Sano, Shigeru Tanaka

Sumitomo Electric Industries, Ltd.

1, Taya-cho, Sakae-ku, Yokohama, 244 Japan

ABSTRACT

A new blown fiber technology of the additional blowing technique was studied with theoretical and experimental investigation. Preliminary experiment suggests that four Ny coated fibers can be installed through a 150 m length 4.5 mm inner diameter tube via additional 40 m drop tube, which enables us to establish the practical aerial fiber distribution network to subscribers.

1. Introduction

The Air Blown Fiber (ABF) system has become used in many applications for special advantages caused by its unique fiber installation method. Blowing technique has advantages such as,

- (1) few access points and fiber splices at jointing points
- (2) few tensile stresses on fiber bundles thanks to very small blowing force over the entire length
- (3) enables system engineer to avoid over-installation of fibers and to reduce initial cost.

To extend its abilities of network flexibility and to increase the fiber density of ABF system, a technology of "additional fiber blowing technique," in which an additional fiber bundle is blown into a tube where one or more fiber bundles are pre-installed have been studied[1][2]. A smaller

cable including less numbers of tubes supports network flexibility as conventional ABF system, which leads to the cable cost reduction and saving of cable installation space.

We have studied this additional fiber blowing technique in use for aerial subscriber distribution network, whose lines are constructed by relatively short length of 100-150 m distribution line and at most 40 m leading pass for drop to the subscriber. And test results shows the configuration of 2.5 mm inner diameter (I.D.) drop tube and 4.5 mm I.D. distribution tube enables us to install four fiber bundles in a tube.

2. Aerial subscriber distribution configuration

In the experiment, we assumed the aerial subscriber distribution configuration as shown in Fig. 1. Feeder cable (ribbon-fiber cable accommodating up to 100 or 200 fibers) and distribution tube cable is connected at the access points on a telephone pole, and drop tube cable is connected at the drop point near the residence. In the drop point, star-figured tube module^[3] connects tubes of drop and distribution tube cable and the fiber bundles are propelled into tubes from the residence to access point through the tube module.

Widely prevailed 0.9 mm ϕ outer diameter Ny coated fiber is selected as fiber bundle for a additional fiber blowing experiment, in terms of easy connection and

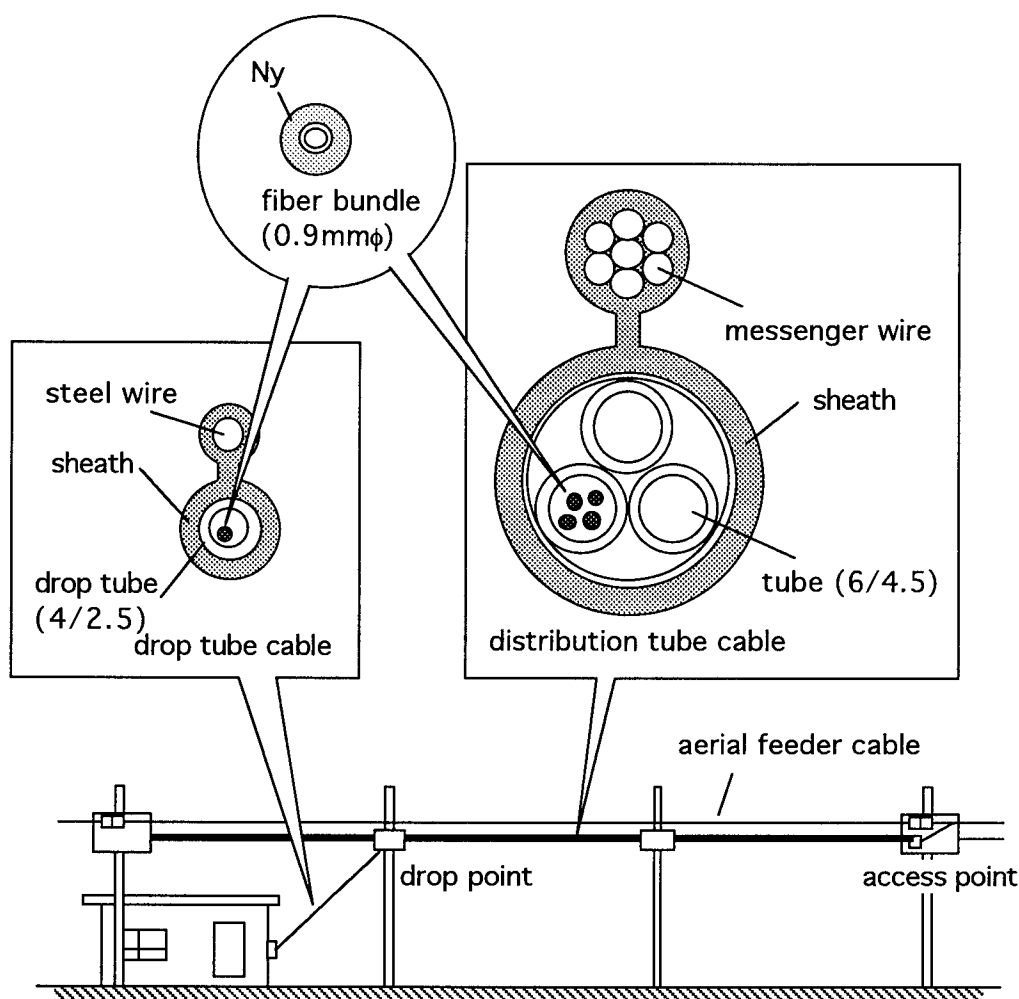


Fig. 1 aerial subscriber distribution configuration by blowing fiber technique

cheaper cost. Ny coated fibers are thinly coated with lubricative powder to lessen the friction loss between each fiber and the tube.

3. Theory and preliminary experiments

3-1 effective inner diameter

After the fiber bundle is inserted in a tube, effective space for air flow decreases. Equivalent tube inner diameter after bundle insertion (d_e) is easily calculated using following equation,

$$d_e = \left[\frac{0.3164L}{g(P_n^2 - P_{out}^2)} \left(\frac{\pi}{4} \right)^{7/4} P_{out} \rho_0 v_0^{1/4} Q^{7/4} \right]^{4/19} \quad \dots (1)$$

where, P_n and P_{out} are the air pressure at the inlet and outlet of the tube, Q is the air mass flow, L is the length of the tube, ρ_0 and v_0 are the mean density of air and the kinematic viscosity of air.

Fig. 2 indicates the relationship between d_e and the bundle-count (n). Effective inner diameter d_e is estimated with eq. (2) by the tube diameter d_t by fitting the measured data.

$$d_e = d_t \exp \left[-1.22 \exp(-0.68 d_t) n \right] \quad \dots (2)$$

3-2 driving force on a fiber bundle

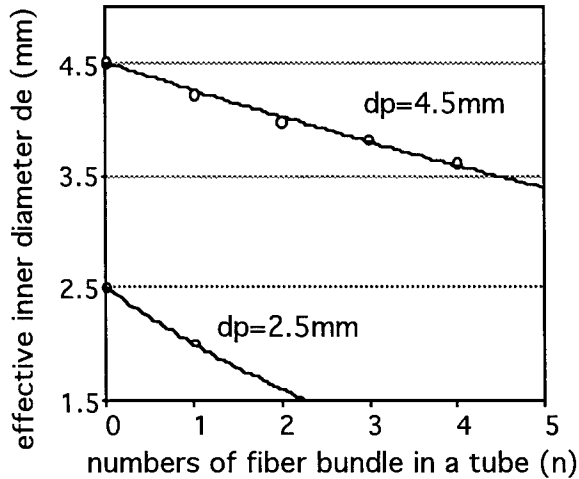


Fig. 2 effective inner diameter after insertion of bundles

When a bundle propels through tubes with different inner diameters, we can calculate the air pressure distribution by substituting them with cascaded three tubes with different inner diameters (fig. 3).

Air pressure distribution is acquired under the condition that air mass flow is consistent throughout the whole length of connected tubes. The pressure at the intermediate points are expressed as follows,

$$P_1^2 = \frac{L_1 P_{out}^2 + (m_1 L_2 + m_2 L_3) P_n^2}{L_1 - m_1 L_2 - m_2 L_3} \quad \dots (3)$$

$$P_2^2 = \frac{m_2 L_3 P_n^2 + (L_1 - m_1 L_2) P_{out}^2}{L_1 - m_1 L_2 - m_2 L_3} \quad \dots (4)$$

where $m_1 = (d_1/d_2)^{19/4}$, $m_2 = (d_1/d_3)^{19/4}$.

The viscous force on a fiber bundle is relatively small in a larger I.D. tube rather than in smaller I.D. tube, because the pressure gradient tends to concentrate in narrower tube. Fig.4 indicates the example of calculative driving force on a fiber bundle under the condition of $P_n=7.5 \text{ kgf/mm}^2$, $d_{drop}=2.5 \text{ mm}$ ($L_{drop}=40 \text{ m}$), $d_{dist} = 4.5 \text{ mm}$ ($L_{dist}=100\text{m}$). Where the suffix 'drop' is related to drop tube, and 'dist' to distribution tube. The plain line is the case that the fiber bundle is inserted from the drop (narrower) tube to the distribution (wider) tube and the viscous driving force on the bundle decreases rapidly at the junction point to the degree of 0.25 gf/m , small but enough driving force to propel a bundle. The bold line indicates the opposite case and the minimum driving force at the junction falls to 0.07 gf/m , too small for the bundle to move along the path. The fiber bundle is preferably inserted from the drop (narrower) tube to the distribution tube for the longer installation.

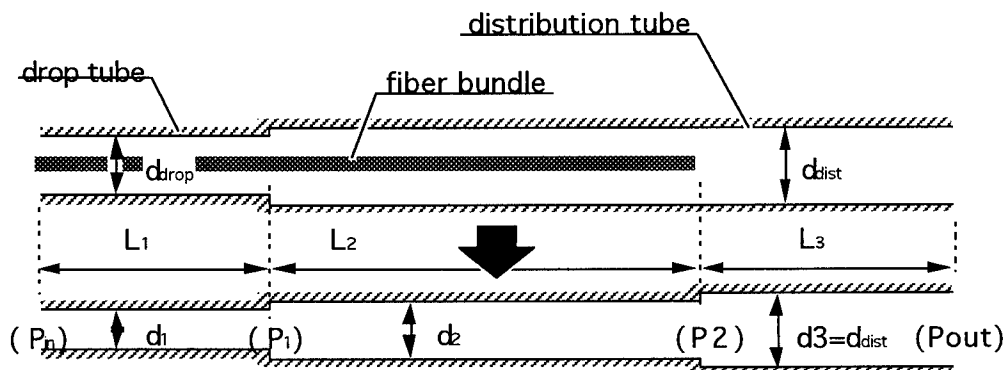


Fig. 3 equivalent connection of tubes

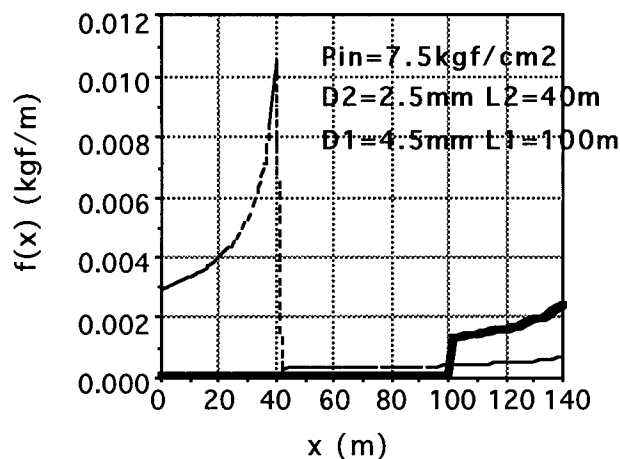


Fig. 4 viscous force on fiber bundle

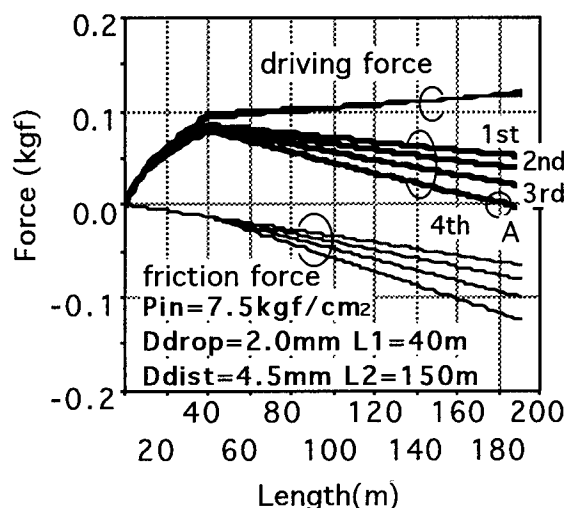


Fig. 5 calculative driving force and friction force

3-3 friction force

Fiber bundle ceases propelling when the friction loss exceeds the viscous driving force. We introduce friction force per unit length m [gf/m] and assume the equilibrium condition between friction and driving force as follows,

$$\int_0^{L_s} f[x] dx = m_{\text{drop}} L_{\text{drop}} + m_{\text{dist}} (L_b - L_{\text{drop}}) \quad \dots (5)$$

where $f[x]$ is the calculative driving force and m_{drop} and m_{dist} is the friction force in drop and distribution tube respectively. L_{drop} indicates the drop tube length and L_b the length of the bundle going into tube.

Friction force for the fiber bundle to move along the tube or the tube with the bundles already installed is obtained by experiment. Inner diameter 2.5 mm of drop tube and the length of 40 m were fixed during the friction force measurement, and the friction force is fitted regressively by the numbers of the bundles (n) and inner diameter of the distribution tube (d_{dist}). The result is as follows,

$$m = (5. - 1.8 d_{\text{dist}} + 0.29 d_{\text{dist}}^2) \exp [0.2 n] \quad \dots (6)$$

3-4 estimation of the possible installation length

Fig. 5 indicates calculative result of the driving force, friction force and the remainder of these. Each branch is for 1st, 2nd, 3rd and 4th bundle installed in turn to a tube. Calculative condition is described in the figure. The graph shows that the 4th bundle cannot reach the terminal under a written condition, because the friction force exceeds driving force at the point A in the fig. 5. In this case the length of distribution tube is rather longer for the 4th bundle to be accomplished the installation and we must estimate the tube length shorter.

Using above techniques further discussed, we calculated the possible installation length using additional fiber blowing technique. Bundle diameter of 0.9 mm, drop tube length of 40 m and the compressed air pressure of 7.5 kgf/cm² are consistent in calculation and we estimated the possible installation length of 4th bundle

in a tube. Fig. 6 indicates the result. Provided D_{drop} to be 2.5 mm and D_{dist} to be 4.5 mm, we can expect 200m length installation of four fiber bundles in a tube. And $D_{\text{drop}}=3.0\text{mm}$ and $D_{\text{dist}}=5.0\text{mm}$ is the best combination that suggests 300m length installation.

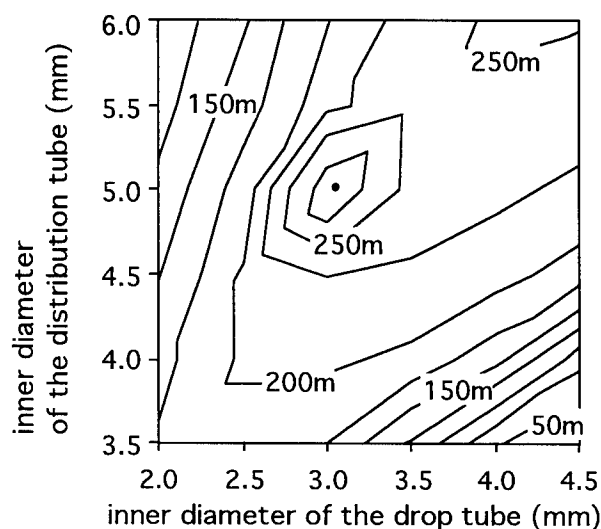


Fig. 6 possible installation length

4. Experiment

4-1 Long haul additional blowing experiment

To confirm the installation length estimation, we sent bundles one by one into a 190 m tube; 40 m of it is for drop part and 150 m is for distribution part. I.D. of distribution tube is 4.5 mm, and we installed fiber bundles through drop tubes with three different inner diameter; 2.0 mm, 3.5 mm and 4.5 mm. Installation tests were conducted twice in the same condition. Fig. 7 to 9 indicate the results. Four fiber bundles were successfully blown into the tube in the experiment and some 5th and 6th bundles completed installation. Fig. 6 suggests that four fiber bundles are expected to be blown 200 to 225 m length through a 4.5 mm distribution tube via drop tube, whose inner diameter is within 2.0 to 4.5 mm. Our experimental results are in good agreement

with the expectation.

4-2 Transmission properties during installation

Pre-installed fiber bundle ought not to be disturbed during additional blowing and the transmission quality should be guaranteed under any conditions. Optical loss fluctuation of pre-installed fiber bundle was observed during the additional bundle installation. Measurement configuration is illustrated in fig. 10. The drop tube has 40 m length and 2.5 mm inner diameter and distribution tube cable has 150 m length and I.D. of 4.5 mm. Light emitted from 1.55 μm LD is launched into a pre-installed fiber bundle that returns back at the far end of the cable and leads to the optical detector through a empty tube. Optical power was monitored through a high speed detector and recorded on a paper chart and a digital oscilloscope whose sampling time is 25ns (40MHz). Even a sudden, sharp loss change more than 0.1 dB could be detected if there were a disturbance on existing lines. During the measurement, no sudden loss change more than 0.1 dB was observed and the optical loss deviation from the initial power was within 0.03 dB that is as much as the emitting power fluctuation without any disturbance but ambient temperature change. The actual transmission line has some toughness to the loss change, and the sudden loss change within 1 dB or gradual larger loss change is considered safe.

And additional transmission experiment was conducted in analogue and digital lines. Experimental configuration is depicted in fig. 11. Analogue signal (1.55 μm) and digital signal (1.3 μm , 622Mb/s) are mixed through optical coupler and pass through a common fiber bundle. Modulation rate is 4%/ch and the number of channels is 60ch in analogue transmission and we measured CNR, CSO, CTB, and XM before and during the additional

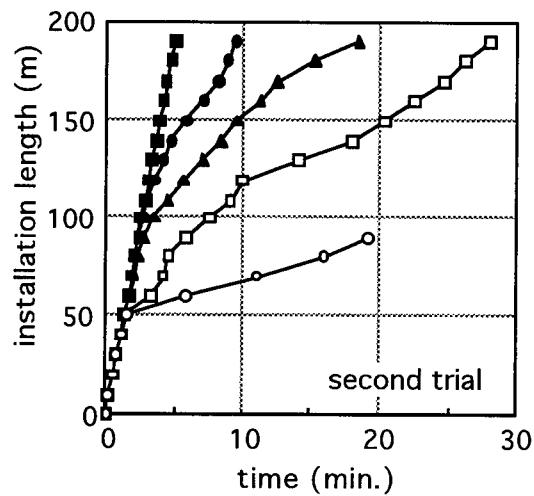
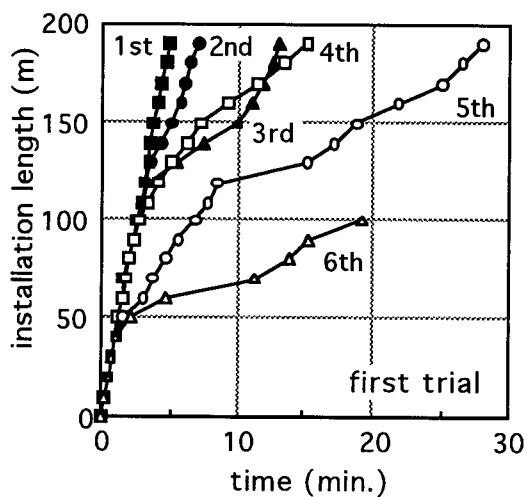


Fig. 7 result of additionalblowing of the bundles via 2.0 mm inner diameter drop tube

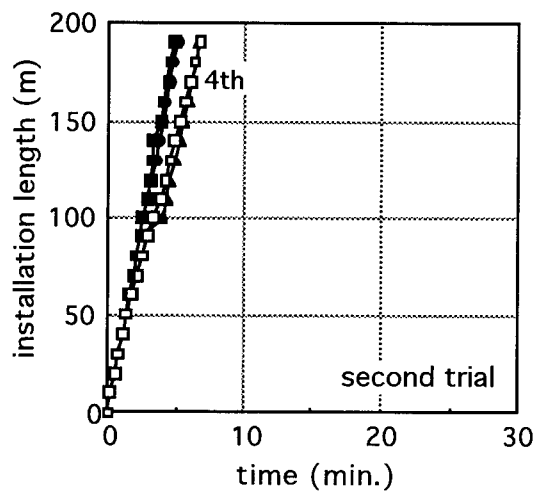
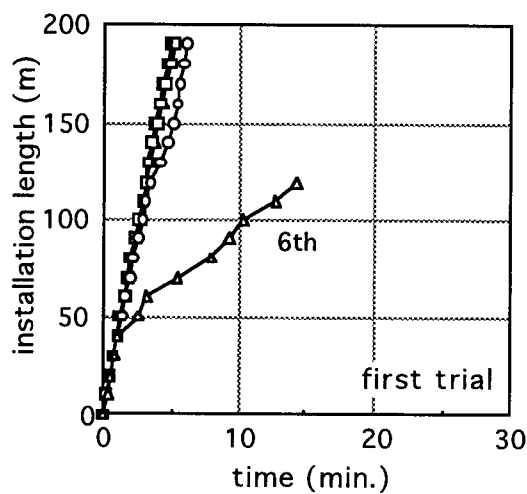


Fig. 8 result of additionalblowing of the bundles via 3.5 mm inner diameter drop tube

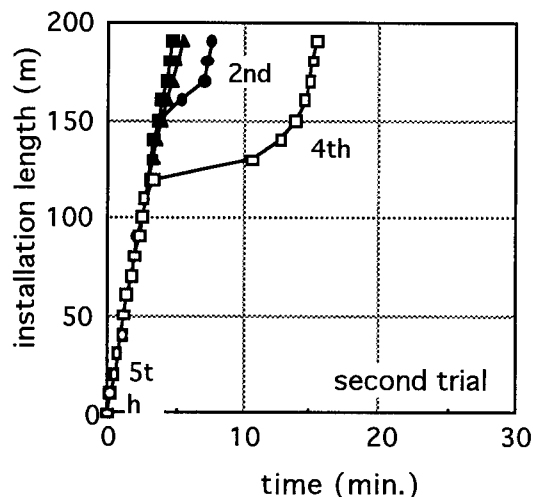
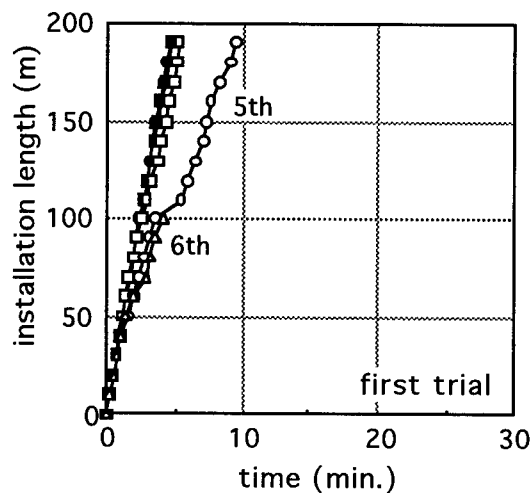


Fig. 9 result of additionalblowing of the bundles via 4.5 mm inner diameter drop tube

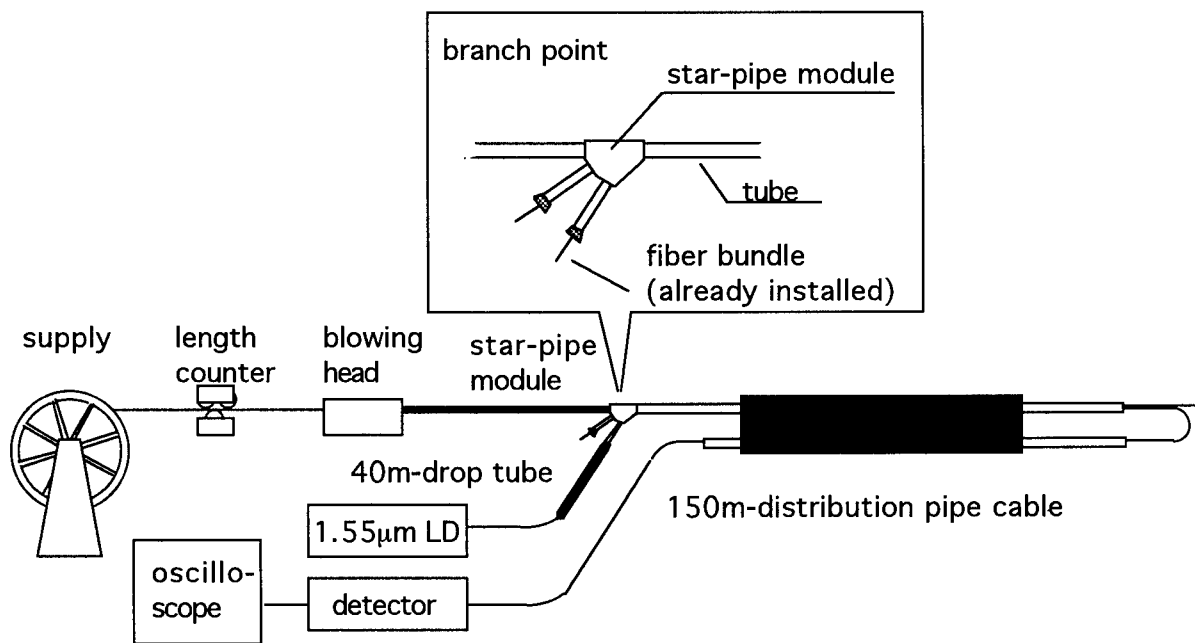


Fig.10 optical power measurement during additional installation

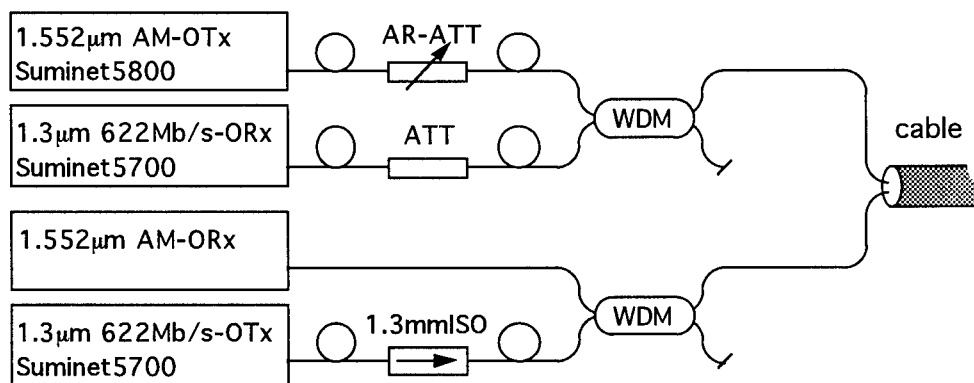


Fig. 11 transmission experiment configuration

installation. BER was measured on digital transmission and initial optical power is lowered to -31.52 dBm to generate some bit errors intentionally. The analogue signal distortion properties are indicated in fig. 12. Measurement accuracy expected on CNR and other parameters are 0.5 dBs and the measured fluctuations are within 0.5-1.0 dBs, which make no detectable problems on transmission quality. In the digital signal, we can see some BER change during our

experiment in fig. 13. That is translated as at most 0.5 dB optical power fluctuation in our equipments, that is as much as the optical power fluctuation detected in previous experiment, and it suggests that we can expect high transmission quality during the additional installation by setting initial transmission powers as regular condition.

5. Conclusion

We have investigated the additional fiber blowing technique for subscriber distribution lines. Four fibers were successfully blown one by one into 150 m distribution tube, and few BER and loss change were observed during additional fiber blowing process.

This technique enables us to use the installed facilities effectively and saves

installation times and money. It can be one of the promising candidates for the distribution configuration.

6. References

- [1] K. Hogari et al, communication society technical reports, OCS96-3, pp.15-21
- [2] H. Sano et al, conference proceeding of 6th International Workshop on Optical Access Networks, Oct '94, S3.8
- [3] H. Ishikawa et al, Proceeding of the 1996 communications society conference of IEICE B-961 (in Japanese)

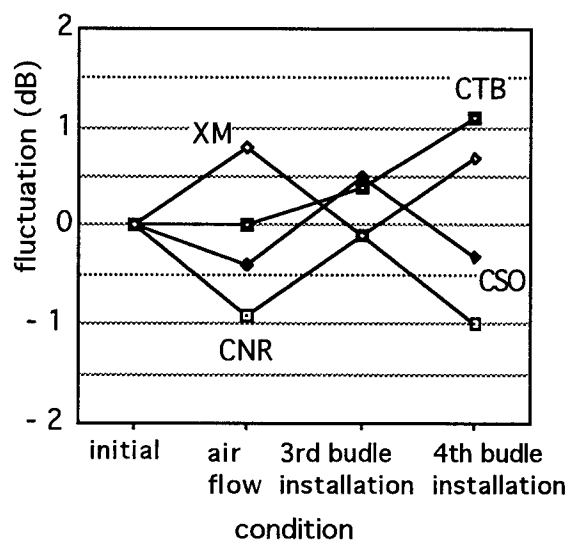


Fig. 12 analogue signal distortion during installation

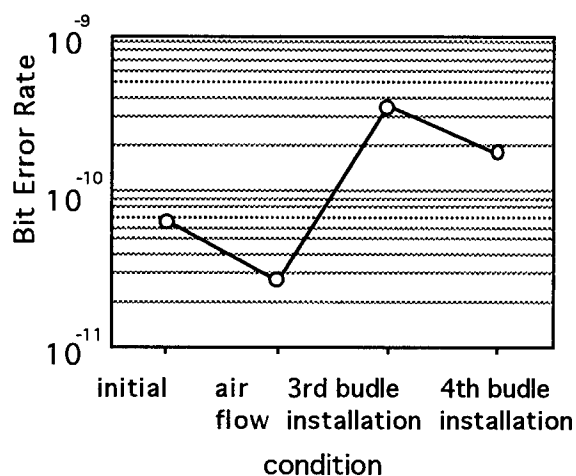


Fig. 13 BER on digital signal during installation



Wataru Katsurashima

Sumitomo Electric
Industries, Ltd.

1, Taya-cho, Sakae-ku
Yokohama, Japan

Wataru Katsurashima graduated from Tokyo University in 1987. He joined Sumitomo Electric Industries, Ltd. in 1987 and has been engaged in developing optical fiber and cables. Mr. Katsurashima is a member of Institute of Electronics, Information and Communication Engineers of Japan.



Hiroki Ishikawa

Sumitomo Electric
Industries, Ltd.

1, Taya-cho, Sakae-ku
Yokohama, Japan

Hiroki Ishikawa was born in 1965 and received his M.E. degree in applied physics from Tohoku University in 1990. He joined Sumitomo Electric Industries, Ltd. in 1990 and he has been engaged in the research and development of fiber-optic cables. Mr. Ishikawa is a member of Communication R&D dept. in Yokohama Research Labs.



Hiroaki Sano

Sumitomo Electric
Industries, Ltd.

1, Taya-cho, Sakae-ku
Yokohama, Japan

Hiroaki Sano was born in 1960, and received his M.E degree in Polymer Science from Kyoto University in 1984. He joined Sumitomo Electric Industries Ltd. and has engaged in development of optical fiber manufacturing process and fiber-optic cable design. He received JSPMI (Japan Society for the Promotion of Machine Industry) Prize for "Commercial Application of Air Blown Fiber System" in 1994. He is a senior engineer of Intellectual Property Department and a member of the Institute of Electronics, Information and Communication Engineers of Japan.

Shigeru Tanaka

Sumitomo Electric Industries, Ltd.

1, Taya-cho, Sakae-ku, Yokohama, Japan

Shigeru Tanaka received the B.S. and M.S. degree from Tokyo University in 1974 and 1976. He received Ph.D degree in 1989. He joined Sumitomo Electric Industries, Ltd. in 1976 and has been engaged in the design and characterization of optical fibers and cables. He is a manager of Communication R&D department. Dr Tanaka is a member of Institute of Electronics, Information and Communication Engineers of Japan.

CURRENT DEVELOPMENTS IN CABLE-IN-DUCT BLOWING TECHNIQUES

W. Griffioenⁱ, G. Plumettazⁱⁱ

ⁱKPN Research, Leidschendam, The Netherlands, ⁱⁱPlumettaz SA, Bex, Switzerland

ABSTRACT

Installing optical cables in ducts by synergetic pushing and blowing is becoming the standard technique now in most countries. A review is given of this technique and its appliances and a comparison is made with traditional techniques. Some current developments are addressed: remote installation units powered by the airflow through the duct, blowing in of (multi) tubes and the use of water instead of air. Remarkably it is the copper telecommunications access network, where both small and very large cables are used, demanding new breakthroughs today.

INTRODUCTION

Traditionally cables were installed in ducts by pulling. The lengths per pull were limited because of the "exponential effect": the friction between cable and duct in bends and undulations of the trajectory is proportional to the built-up tension in the cable, causing an exponential build-up of the pulling force.^{1,2} The introduction of optical fibers in telecommunications stimulated the development of new installation techniques. The low attenuation of these fibers makes the splices the dominant loss contributors, causing a demand for long spliceless cable lengths. Fortunately, the small size and low weight of optical fibers allow longer cable lengths. But, the "exponential effect" becomes more serious when lengths become longer and more bends have to be passed.

In 1983 British Telecom developed a technique to install lightweight and flexible fiber members into small bores by means of the viscous drag of air, the blown-fiber technique.³ When injecting air into the bore, and not using a shuttle at the end of the fiber member, a high-speed airflow is obtained. This airflow exerts a distributed drag-force on the fiber member. A length of the bore can be chosen such that the drag-force is larger than the friction between fiber member and bore-wall at every lo-

cation, and no tension is built-up. Hence, the "exponential effect" is eliminated. Therefore this technique, where forces exerted on the fiber member are an order less than for pulling, allows long continuous lengths to be installed.

In 1988 KPN Research developed the technique of synergetic pushing and blowing larger optical cables into ducts.^{4,5} It was recognized that the pressure drop along a duct is not linear: in the first part the pressure gradient is much smaller than at the end, and the same is true for the drag-force. Therefore additional pushing of the cable improves the blowing performance considerably. For pushing to be effective, the cable must possess enough stiffness to avoid blocking due to buckling. Theoretical analysis, confirmed by practical experience, learned that stiff cables can be blown into ducts with unexpected ease.⁵

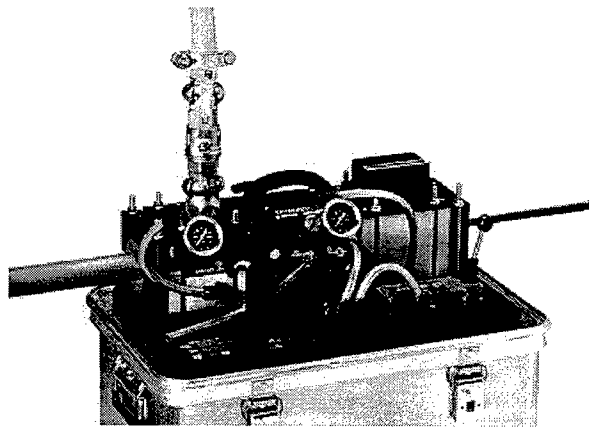


Figure 1 *Example of an installation unit for blowing cables into ducts.*

The technique of synergetic blowing and pushing cables into ducts was a big success. After the first test the prototype never returned from the field and the technique immediately became the

standard for PTT Telecom (The Netherlands). Now the technique is used more and more all over the world. Not only optical cables are installed with this technique, also copper cables, e.g. coaxial or twisted-pair cables. Even blowing of cables into ducts already occupied with another cable is possible, using a special Y-connector.⁷ The technique improved since it first showed up. Some impressive records have been obtained: 3.5 km with one installation unit, 8 km or 12 km (buffered) with cascaded units, 15 km in one day, 34 mm cable-diameter, 12 N/m cable-weight and 1.4 tons of cable with one unit in "one blow". The improvements made over the last few years were attributed to developments of lubricants and new machinery. Another improvement was the "sonic-head", a semi-open shuttle at the end of the cable. The latter uses a small amount of the airflow (which remains mainly intact) to exert a small force at the cable end.⁵ It helps to pass the "critical point", at about two third of the trajectory, and is also useful when the cable is not stiff enough.

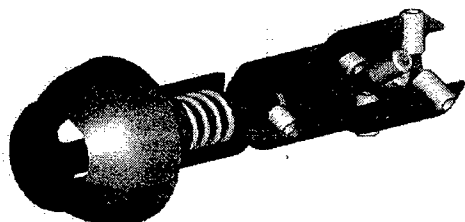


Figure 2 Example of a "sonic-head", to be used with the blowing technique.

In this paper an overview is given of past and current developments of the blowing (+ pushing) technique (patents granted/pending). Possibilities and limitations of the technique will be summarized and compared to other techniques. Some examples of current developments will be treated, such as an intermediate installation unit that does not need to be powered by a local compressor but which uses a remote compressor. The "blowing technique" with water instead of air will also be addressed. The cable will partially float, but also many other effects occur. Advantages and disadvantages will be listed. Not only cables, also tubes can be blown into ducts, surprisingly easy and without the need to open the far end of the duct. Finally the blowing technique marches up towards copper cables in access networks, where cables from small (like in ⁶) to extremely large, e.g. 900-pairs, are used. Boundaries of what we think is "blowable" will be passed.

COMPARISON CURRENT TECHNIQUES

A lot of practical experience with various kinds of cables and ducts has been obtained with the blowing technique. In this paper a comparison is made with other techniques for an average reference cable in average duct trajectories, tortuous and a less tortuous, using a computer program. This program is based on the theory of ⁵ and has been proven by experimental practice.

The reference cable has a weight of 1 N/m, a diameter of 12 mm, a stiffness of 2 Nm² and a friction coefficient with the duct wall of 0.15. The duct of the tortuous trajectory has outer/inner diameter 32/26 mm, undulations with an amplitude of 5 cm (free space in trench) and a period of 5 m, and a bend with bend-radius of 1 m occurs every 200 m. The duct of the less-tortuous trajectory has outer/inner diameter 40/32 mm and undulations with a period of 8 m. A compressor with a pressure of 9 bar and a capacity of 180 l/s is used. The installation unit for blowing pushes with 400 N. The winch pulls with a force equal to the maximum pulling force of the cable, 2000 N. The intermediate capstans, which grip on the cable jacket, push/pull with a lower force of 500 N.

Table 1 Lengths per pull for tortuous trajectory.

Technique	Cascading	Length (m)
Pushing	no	350
Winch pulling	no	800
"Figure-8" capstan	yes	500
Caterpillar capstan	yes	600
Air-powered shuttle	no	200
Same with pushing	no	800
Blowing with pushing	yes	1150
Same with "sonic head"	yes	1250

Table 2 Lengths per pull for less-tortuous trajectory.

Technique	Cascading	Length (m)
Pushing	no	350
Winch pulling	no	1200
"Figure-8" capstan	yes	700
Caterpillar capstan	yes	800
Air-powered shuttle	no	500
Same with pushing	no	1200
Blowing with pushing	yes	1400
Same with "sonic head"	yes	1600

In Tables 1 and 2 the results are given for the tortuous and less-tortuous trajectories, respectively. Also cascading possibilities are given. The winch can only pull at the cable head, the capstans also halfway. The caterpillar capstan reaches more than the "figure-8" capstan because it can push as well as pull. For acceptable

results the air-powered shuttle needs mechanical feeding. If not, the entrance of the cable into the pressurized space causes a considerable stress in the cable from the beginning, growing soon by the "exponential effect". The tables show that blowing is favorable (moreover, no extra step to install a rope is needed), as expected especially in the tortuous trajectory. Here suppression of the "exponential effect" pays off most. Blowing the cables with use of a "sonic head" clearly gives the best results. It is very difficult to find a cable/trajectory where this is not true! Note that cascading is effectively possible when using a "sonic head": once the cable has been installed in a first section the "sonic head" is not needed anymore in that section because the "critical point" has been passed already.⁵

BUFFERING TECHNIQUES

Longer cable lengths can be installed by, instead of cascading installation units, by buffering lengths of cable. Most techniques, like laying the cables in "figure-8"s, are simple but require a lot of handling. The hand-operated "Van de Akker" reel can be used for clean processing of the cable.^{4,5} Recently mechanically driven buffer systems have been developed, a passive coiling buffer (driven by a blowing unit), see Figure 3, and a true "Figure-8" machine.⁷

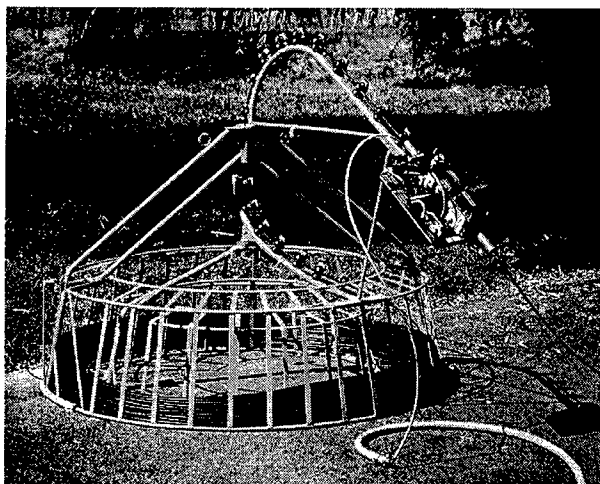


Figure 3 *Passive coiling buffer (blowing unit driven).*

REMOTE-POWERED INSTALLATION UNIT

It is possible to power a pneumatically-driven blowing-unit, positioned along the trajectory, by means of a remote compressor which feeds through the duct in which the cable is installed (or through a separate pipe). A certain pressure needs to be maintained for the blowing unit to be

driven. This means that less pressure difference is available along the cable, hence, less drag-force and less installation length for a section. But, the net result is usually positive because of the extra push/pull point. Several remote-powered units can be positioned in cascade when the airflow is bypassed, see Figure 4. The powering airflow can also move against the cable insertion direction. The method can be used without or with a shuttle at the cable head. In the latter case many cascaded units can be powered, as long as the airflow can be transported through the duct, filled with cable. Many kilometers can be installed using one single compressor powering many blowing units along the trajectory. In this way the large capacity of the compressor is used far more effectively than with traditional blowing.

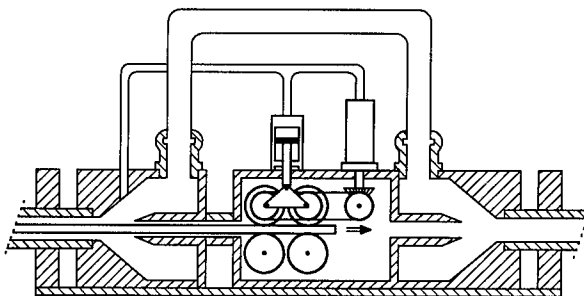


Figure 4 *Schematic view remote-powered blowing unit.*

The remote-powered blowing units can be used together with "ordinary" blowing units and are extremely useful when the planned distances with "normal" blowing cannot be overcome in practical situations. At the location where the cable gets stuck, or at another suitable location where the cable has already passed, the duct is opened and a remote-powered unit is placed (no shuttle needed). Installation becomes possible then without moving all kinds of heavy equipment (compressors), which was always a worry in urban environments.

Also positioning several cascaded remote-powered units along the trajectory, combined with a shuttle at the end of the cable, has typical advantages: when long lengths of a cable route cannot be accessed by trucks with their compressors, when no other power source is available along the route, or when duct diameters are such large that traditional compressors cannot maintain enough pressure difference.

In a first (short) experiment a cable with diameter of 13 mm was installed in a 1 km long, tortuously

laid, 32/27 mm tube. This is not an ideal combination for remote-powered blowing units because the duct filled with cable has a high flow resistance. Also the location of the remote blowing unit was too far ahead, 650 m. This is what happened. Installation with a single blowing unit went too quickly. With the cable already at 650 m the pressure had to be reduced down to 4.5 bar to stop the cable and to reach a "non-blowable" condition. Then a remote unit was placed at 650 m (the first prototype was not splittable) and the installation was completed with the same pressure at the beginning of the duct. The pressure for the remote unit of 1,4 bar (1,8 bar when the cable reached the end) was higher than calculated, but, rather low for powering a pneumatic motor. With longer tubes ("non-blowable" condition at higher pressure), larger tube diameters (less flow resistance) and the remote unit placed more close to the beginning much better results are expected.

INSTALLATION WITH WATER

Instead of an airflow also a flow of liquid, e.g. water (only water considered in this paper), can be used to propel the cable.^{5,8} Advantages compared to blowing can be recognized:

- The cable will (partially) float, diminishing the friction. Longer lengths can be "flown".
- The pressure drop along the duct becomes linear. This leads to longer installation lengths in very tortuous trajectories.
- Less pump capacity is needed. Water has a much higher viscosity than air resulting in much lower flow velocities.

Also disadvantages compared to blowing exist:

- Installation time is longer because of lower flow velocities. This is especially a problem for ducts with small diameters.
- Because of the linear pressure drop the synergetic effect of pushing and blowing disappears, resulting in shorter installation lengths for less tortuous trajectories.
- Supply and exhaust of water can be a problem. For small ducts tanks can be used. Recycling, e.g. using a fire hose, is another solution. Sometimes nearby canals can be used.
- Every 10 m elevation must be balanced by 1 bar. When recycled in a closed system, the return flow can compensate this pressure. But care shall be taken that ducts and equipment can withstand the excess pressures.
- Air gaps can occur, especially at up/down routes, worsening the "flowing" performance.

- Water cannot always be removed in a simple way. This might cause problems when cables cannot withstand prolonged exposure to water. Also freezing can cause problems.

In situations where "flowing" with water is possible theory predicts tremendous installation lengths, e.g. 6500 m in one "flow" as follows with the computer program for the previously mentioned example with tortuous trajectory. This length can even increase for less stiff cables (the effect of stiffness in bends, especially at the cable head, becomes more dominant for "flowing") or when using a "sonic head". No such results have been reported until now, although experiments on shorter lengths have confirmed the theoretical predictions.⁸

BLOWING TUBES INTO TUBES

Not only cables, also tubes (empty or not), or bundles of them, can be blown into larger tubes. An experiment has been performed with a bundle of 7 loose 8/6 mm tubes, blown into a 750 m long 32/27 mm HDPE tube with not a straight part in it. The bundle of tubes, being 380 m long, could be easily installed with use of about ½ l of silicon-based lubricant. The tubes did not cross, but formed a helix with a period of about 10 m.

It is not necessary to close the end of the tube which is installed. In fact, the backflow through the tube can be used advantageously. Even blowing a tube into a tube with closed end becomes possible then. This is proven in the following experiment.^a A 5/3.5 mm tube was inserted in a 8/6 mm tube with closed end, wound on a reel with diameter of 1 m (first 5 m straight). Only 20 m could be inserted when the backflow through the inserted tube was blocked (at the end, still on the reel). Removing this block resulted in 70 m insertion length.

COPPER ACCESS NETWORK

Developments of installation techniques for optical cables now also stimulates new ways to install copper cables, e.g. for telecommunications access networks. Unarmored cables can be installed in direct-buried "fit-to-protect" tubes, with diameters only a little larger than those of the cables. This concept is studied now for PTT Telecom (The Netherlands). For future migration to optical fiber the copper cables must be replaced by fiber-containing cables in the part of the net-

^a this also proves the effect of the hydrostatic part of the pressure gradient on advancing the cable.^{3,5}

work close to the homes, where bundles of guide-tubes run through larger protective tubes.⁶ In the primary part of the network enough space is left for additional optical cables, but techniques to install them have to be studied. A variety of installation techniques is needed in such access networks.

Especially the high-count cables demand new installation techniques. To install e.g. a 300-pair cable into a 75/61 mm duct by blowing (pulling lengths are too short) requires too much compressor capacity. The solution is found by using remote-powered units positioned along the trajectory combined with a shuttle at the cable-head, or by using water instead of air. Experiments with these cables are in preparation.

CONCLUSIONS

A comparison of installation techniques learns that the technique of synergetic blowing and pushing gives the longest lengths in most situations, especially in combination with a "sonic head". Cascaded use and buffering is simple so that longer cable lengths can easily be installed. For unplanned stagnation of the cable, or when the route is difficult to access, a remote powered unit is a nice accessory. Its functioning has been demonstrated in a simple test. Also blowing (multi)tubes into larger tubes has been proven experimentally. Using water instead of air has the potential of reaching dramatic lengths, but some limitations are recognized. Currently tests are planned to install large copper cables into ducts.

ACKNOWLEDGEMENTS

The authors wish to acknowledge A.B. Wacinski and H.G. Nobach for their valuable contributions to developing the blowing techniques and writing the software program, respectively.

REFERENCES

1. F.H. Buller, "Pulling tension during cable installation in ducts or pipes", *General Electric Review*, August 1949, pp. 21-23.
2. R.C. Rifenburg, "Pipe-line design for pipe-type feeders", *Trans. AIEE Power Apparatus and Systems*, vol.72, part III (1953) 1275-1284.
3. M.H. Reeve, S.A. Cassidy, "Installation of optical fibre units using viscous drag of air", *Proc. ECOC* (1983) 239-242.
4. W. Griffioen, "A new installation method for conventional fibre optic cables in conduits", *Proc. 37th IWCS* (1988) 172-178.

5. W. Griffioen, "Installation of optical cables in ducts", Plumettaz, Bex (CH) 1993.
6. W. Griffioen, H. Nijstad, A.T.M. Grooten, A. van Wingerden, G. Brown, D.F. Hawkins, G. Plumettaz, "A new, extremely versatile, access network cabling concept for migration to optical fiber", *Proc. 45th IWCS* (1996) 485-489.
7. Product documentation of Plumettaz SA (CH-1880 Bex, Switzerland) and Sherman & Reilly, Inc. (400 West 33rd St., Chattanooga, TN 37401-1267 USA).
8. D.L. Walters, M.J. Parry, C.J.W. Thomson, D.F. Harrison, "Cable installation by hydrodynamic drag: theory and practice", *Proc. 42th IWCS* (1993) 202-210.

BIOGRAPHIES



Willem Griffioen received a MS degree in Physics and Mathematics from Leiden University (Netherlands) in 1980. Worked there until 1984. Joined KPN Research, St. Paulusstraat 4, 2264 XZ Leidschendam, The Netherlands. Responsibilities R&D of Outside-Plant and Installation Techniques. Worked at Ericsson Cables, Hudiksvall (Sweden) and at Telia Research, Haninge (Sweden) in the scope of exchange/joint projects with KPN Research. Received Ph.D. (Reliability of Optical Fibers) in 1995 from the Technical University of Eindhoven (Netherlands).



Gerard Plumettaz received a MS degree in mechanical engineering at the Swiss Federal Institute of Technology, Zürich, in 1970 with an emphasis on machine tool techniques. Joined his family business, Plumettaz SA, CH-1880 Bex, Switzerland, in 1971 and became instrumental in product design, development and marketing.

Initial task was to design and develop winching concepts for military tank retrieval. Here specialized winching techniques led to the design of underground placement methods. Today, president and chief operating officer of Plumettaz SA continuing to be active in the pursuit of advanced methods in underground placement/technology.

CHARACTERISTICS OF A RIBBON TYPE 16-FIBER PASS UNIT

K. Ishida, K. Kobayashi, A. Mogi, K. Oohashi, and M. Miyamoto

Fujikura Ltd.

1440 Mutsuzaki, Sakura, Chiba 285, Japan

Tel: +81-43-484-3946 Fax: +81-43-484-3988

ABSTRACT

As part of our development of ribbon type units for PASS cables, we conducted a free coil test on experimental ribbon type 16-fiber PASS units. The results showed that the units that have no ribbon twisting are less likely to show deformation. Accordingly, we produced several types of ribbon-type 16-fiber PASS units with no ribbon twisting and examined the characteristics of the units. The result is that optimizing the material for the unit's buffer layer and its outer diameter enables the design of units with a excellent peeling property and a low-temperature loss characteristic. We further conducted the pressure feed test of these experimental units and verified that 1-km units can be successfully pressure-fed into a pipe wound on a drum.

INTRODUCTION

As more optical fiber networks are constructed, the demand for an optical fiber wiring system that is adaptable to different demands and can be easily installed is increasing. One expected means to achieve easy wiring to feed optical fiber units into pipe cables by using compressed air. This is known as a pressurized air carrying fiber system (PASS). This system can be easily installed, and the number of cable fibers is easily increased as needed, provided that pipe cables are laid, which is an economical feature of the system. This system is particularly suitable for the lines of networks that will be extended in the future or for wiring that will be changed. We believe that the demand for PASS cables will increase in the future as optical fibers come into increasing use.

Therefore, we are examining multi-fiber units for the purpose of increasing cable density. We experimentally produced 16-fiber PASS units using four normal 4-fiber ribbons, taking into account the easy handling of units and connectivity with existing ribbon cables. This article describes the results of our examination of the characteristics of these units.

EXPERIMENT

STRUCTURE OF EXPERIMENTAL UNIT

We prepared ribbon-type 16-fiber PASS units, as shown in Figure 1. The unit consists of four four-fiber ribbons, a buffer layer made of UV resin, and an outside layer made of polyethylene foam (PEF).

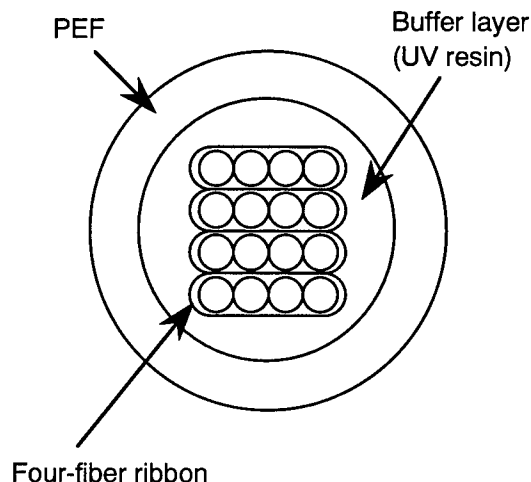


Fig. 1 Structure of an Experimental Unit

FREE COIL TEST

First, we experimentally produced units coated only with buffer layers that have twists on the ribbons at three different twist intervals: 100 mm, 200 mm, and 300 mm. We made free coils of units at a diameter: 100 mm, 200 mm, and 300 mm and conducted a test to observe the deformation of the free coils. Table 1 shows the extent of holding these shapes. The units with no twisting on the ribbons of 100 mm dia. showed no changes in state, while units with twisting on the ribbons deformed. This may be caused by longitudinal changes in the bending rigidity of units with twists on the ribbons. When such units are made into a free coil, an uneven twisting force is exerted, thus deforming the unit. For units without twists on the ribbons, the bending rigidity of the unit is evenly distributed in the longitudinal direction. Therefore, no twisting force is exerted on the unit, and deformation is prevented. From these test results, we experimentally produced units that have no twisting on ribbons to investigate its characteristics.

Table 1 Extent of holding the free coil's shape

Diameters of free coils (mm) Twist intervals(mm)	100	200	300
100	Bad	Poor	Good
200	Bad	Poor	Good
300	Poor	Poor	Good
No twist	Excellent	Excellent	Excellent

COATING STRUCTURE OF EXPERIMENTAL UNITS

We prepared six types of units (A,B,C,D,E,F). The coating structures of these experimental PASS units are shown in Table 2. All of the units had the same 1.3-SM optical fiber ribbons. The fibers had similar parameters, but the buffer layers of units A, B, C, and D were made of UV-curable resins with different Young's moduli and elongation. The buffer layers of units B, E, and F were made of the same UV resin, but their outer diameters were different.

Table 2 Coating structure of the units

Units	Fiber	Young's modulus of the buffer layer (Relative value)	Outer diameter (mm)
A	1.3-SM (MFD= 9.1~9.5 μ m)	1	2.5
B		5	
C		10	
D		20	
E		5	2.3
F		5	2.8

CHARACTERISTICS OF EXPERIMENTAL UNITS

Peeling property

We designed a unit with a buffer layer that can easily be peeled off without the use of any tools. Among these experimental units, the buffer layer of unit A was most easily peeled off for removal of the ribbons. In the case of unit D, an extended period was required to peel off the buffer layer. The peeling property between the units was based on the differences in the Young's modulus and elongation of the buffer layer. The buffer layer of unit D has the highest Young's modulus and the lowest elongation. When a resin with a high Young's modulus is used for the buffer layer, buffer braking becomes difficult, and when resin with a low elongation is used, peeling becomes difficult as it breaks down into small pieces.

Bending property

We wound each unit onto mandrels of various diameters (30~60 mm) for 10 turns and measured the transmission loss at $\lambda = 1.55 \mu\text{m}$. The results are shown in Figure 2. At a bending diameter of 30 mm, loss increases were less than 0.05 dB in all the units.

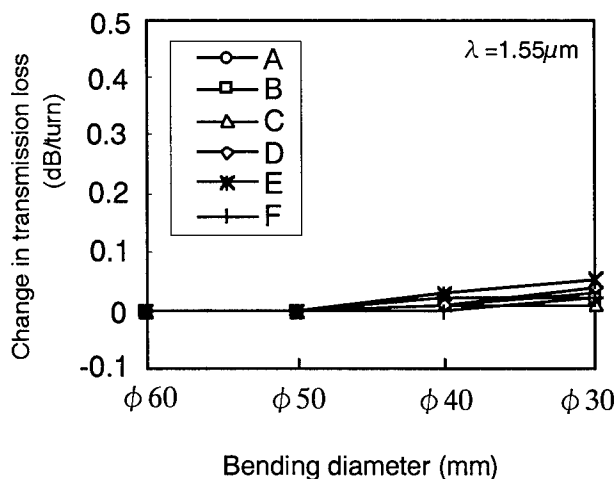


Fig.2 Results of a bending test

Effects of the process and temperature on transmission Loss

The changes in transmission loss following the processing, cooling, and heating of the experimental units are given in Figure 3. Small loss increases were observed following the PEF coating process. The units also showed slight loss increases at low temperatures. The corner fibers tend to show poorer transmission characteristics than the others. In particularly unit A and E, which have a lower Young's modulus and a thinner buffer layer, respectively, showed greater loss increases than the others. The loss increase apparently depends on the Young's modulus and the thickness of the buffer layer. Therefore, we believe that the stress caused by the PEF shrinking can lead to the loss increase of the units.

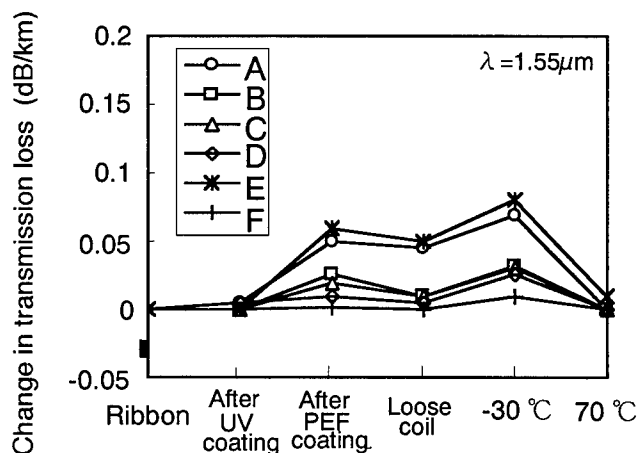


Fig. 3 Change in Transmission Loss after Processing, Cooling, and Heating

Effect of lateral pressure

We used two polished steel plates to apply lateral pressure to the experimental units and measured transmission loss. Figure 4 shows the results for pressures up to 500 N/100 mm. No unit showed any significant losses.

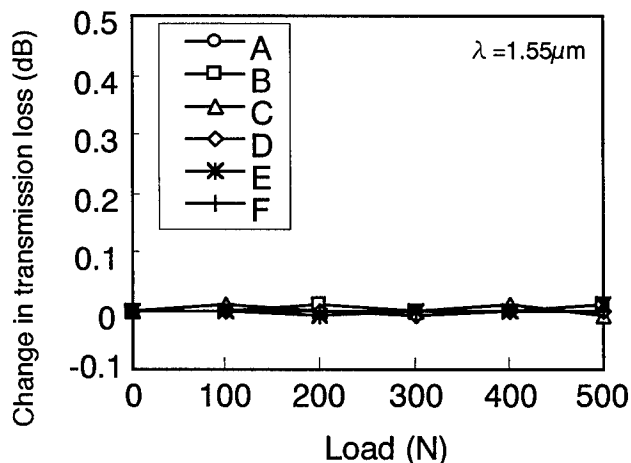


Fig.4 Results of a Lateral Pressure Test

Feeding apparatus

The present feeding test measured the feeding length and the feeding time when experimental units were fed into a pipe 1,000 m in length, 6 mm in inner diameter, and 8 mm in outer diameter that was in turn wound onto a drum 1,000 mm in diameter by using air compressed by a compressor and the feeding apparatus.

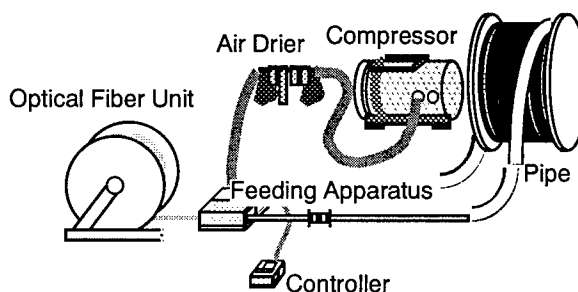


Fig. 5 Test Method of Pressure Feed Performance

Pressure feed performance

It is known that the surface state of the unit has a strong influence on the pressure feed performance. We employed PEF with optimized foaming and surface properties for all the prototype units made for the present test. The test results on the pressure feed performance of these units indicate that, as shown for an initial rate of 20 m/min in Figure 6, there was no significant reduction in rate for any unit. All of the units were carried within one hour per km. No transmission loss increase through the fibers observed after the test.

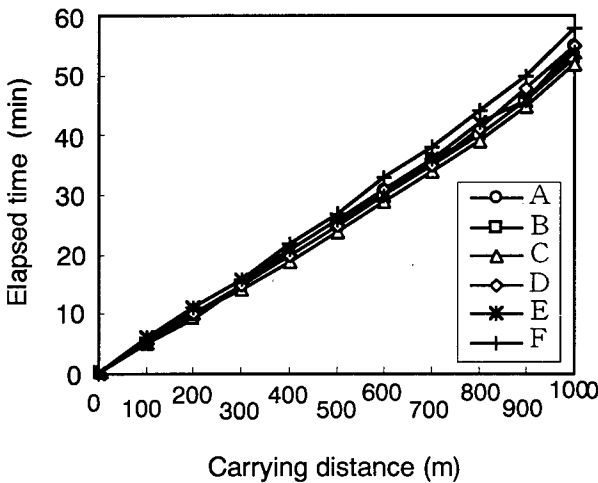


Fig.6 Results of a Pressurized Air Carrying Test

Long-term reliability

We investigated the long-term reliability of these units at +70 °C , +60 °C with a relative humidity of 95 %, and -30 °C severally. The results are shown in Figure 7. Under these conditions, no changes were observed for any units after one month. We also examined the feed performance of the units following the aging, and no significant changes were found.

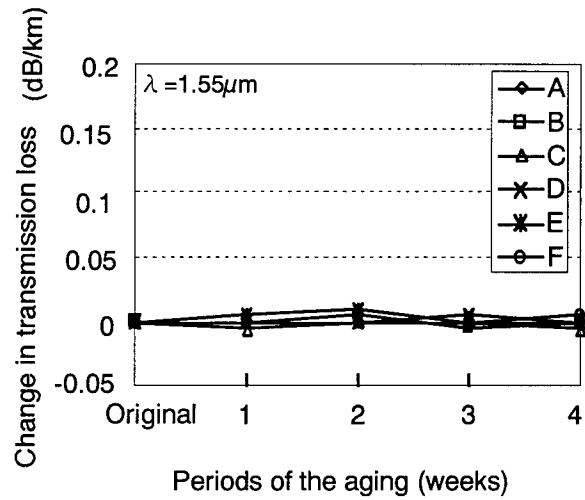


Fig. 7-1 Result of long-term reliability at +70 °C

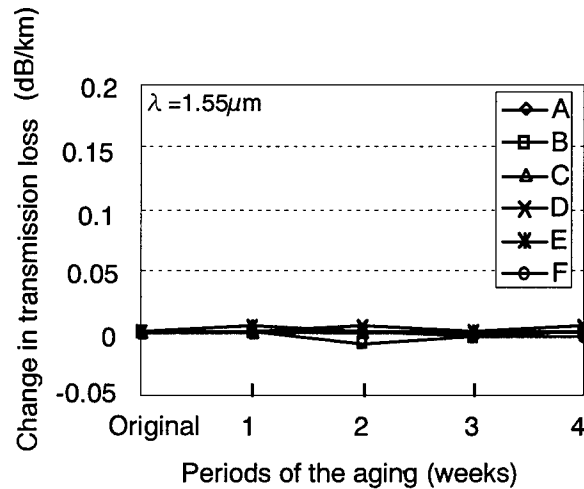


Fig. 7-2 Result of long-term reliability at +60 °C, 95%RH

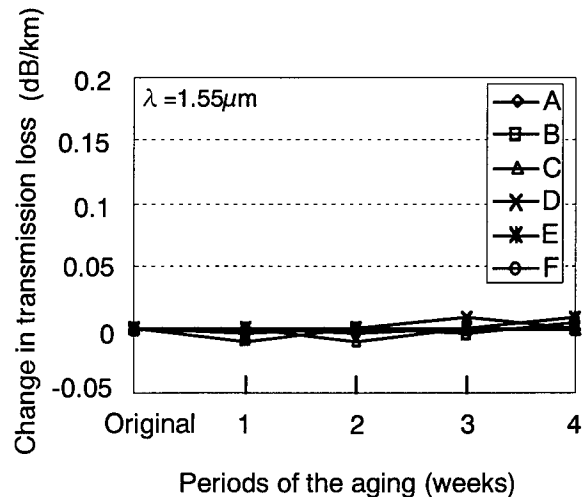


Fig. 7-3 Result of long-term reliability at -30 °C

CONCLUSIONS

We experimentally produced and examined various types of 16-fiber PASS units using four four-fiber ribbons. As a result, we were able to develop units featuring both good transmission characteristics and peel performance to optimize the structure of the ribbon twisting and the coating structure of its buffer layer. We intend to continue to study on the ribbon-type 16-fiber PASS unit, including its long-term reliability, and to conduct field experiments.

REFERENCES

- 1) S.A. Cassidy and M.H. Reeve
"A RADICALLY NEW APPROACH TO
THE INSTALLATION OF OPTICAL FIBER
USING THE VISCOUS FLOW OF AIR"
IWCS Proceedings, 1983, pp. 250-254
- 2) A. Sano, A. Mogi, and M. Miyamoto
"LONG LENGTH,HIGH SPEED AIR
FEEDING OF OPTICAL UNITS BY
PRESSURIZED AIR"
IWCS Proceedings, 1991, pp. 457~462
- 3) K. Horii, Y. Tomita, T. Hamade, Y. Shimo
and Y. Matsumae
"NOVEL SPIRAL-AIR SYSTEM FOR
OPTICAL FIBER AND CABLE INSTALL-
ATION"
IWCS Proceedings, 1992, pp. 481~485

AUTHORS

Katsuyoshi Ishida



Opto-electronics
Laboratory
Fujikura Ltd.

1440 Mutsuzaki
Sakura-shi
Chiba-ken
285 Japan

Katsuyoshi Ishida was born in 1967. He joined Fujikura Ltd. after his graduation from Gunma University with a B.E. degree in 1991 and has been engaged in research and development of optical fibers. He is now an engineer in the Telecommunication Cable Material Section and a member of the IEICE of Japan.

Kazunaga Kobayashi



Opto-electronics
Laboratory
Fujikura Ltd.

1440 Mutsuzaki
Sakura-shi
Chiba-ken
285 Japan

Kazunaga Kobayashi was born in 1961. He joined Fujikura Ltd. after his graduation from Gunma University with a M.E. degree in 1985 and has been engaged in research and development of optical fibers. He is now the assistant-chief in the Telecommunication Cable Material Section and a member of the IEICE of Japan.



Akio Mogi

Opto-electronics
Laboratory
Fujikura Ltd.

1440 Mutsuzaki
Sakura-shi
Chiba-ken
285 Japan

Mr. Mogi was born in 1946. He joined Fujikura Ltd. After graduation from Haneda Institute High school in 1967 and has been engaged in research and development of the metallic cables and optical cables. He is now the chief of a Telecommunication Cable section and a member of IEICE of Japan.



Matsuhiro Miyamoto

Opto-electronics
Laboratory
Fujikura Ltd.

1440 Mutsuzaki
Sakura-shi
Chiba-ken
285 Japan

Matsuhiro Miyamoto was born in 1953. He graduated from Nagoya Institute of Technology with a B.E. degree of electrical engineering. He joined Fujikura Ltd. after his graduation from Tokyo Institute of Technology with a M.S. degree in 1978 and has been engaged in research and development of optical fiber cables. He is now the chief of a Telecommunication Cable department and a member of IEICE of Japan.



Keiji Oohashi

Opto-electronics
Laboratory
Fujikura Ltd.

1440 Mutsuzaki
Sakura-shi
Chiba-ken
285 Japan

Keiji Oohashi was born in 1956. He graduated from the Tokyo Institute of Technology in 1980 with a B.E. degree in chemistry. After eight years of work as an engineer in the field of materials for motor vehicles, he joined Fujikura Ltd. in 1988. He has been engaged in research and development for optical fibers and optical fiber coatings. He is now chief of the Telecommunication Cable Material section and member of the IEICE of Japan.

“ NEW COPPER CABLING SYSTEMS FOR RESIDENTIAL HOME NETWORK ”

Authors: M. Lissillour - O. Bouffant - H. Le Cozic - P. Guillas

France Telecom - BD/CNET/DTD - Lannion, FRANCE

ABSTRACT

This paper describes the new copper home wiring retained by the National Research Center (C.N.E.T.) of France Telecom for TAMARIS [1] trials for the introduction of new broadband services in the residential home networks, and the Full Services Access Networks (FSAN) works in the Network Termination - Home Network Working Group.

After the introduction of new broadband services like video and multimedia applications, and the presentation of the working groups taken as reference in standardization, the first part of the document focusses on general conditions defined for ADSL, VDSL, FTTB/FTTC or FTTH access networks. These conditions involve the nature of the network termination (NT), the separation of narrowband and broadband services (and networks) and the different interfaces. The second part examines the residential home network for each configuration in terms of applications, interfaces and bit rates, new cabling system alternatives or potential re-use of the existing home network, etc. and tests conducted in order to determine the copper network for the field trials in France.

INTRODUCTION : NEW SERVICES FOR THE RESIDENTIAL HOME NETWORK

The convergence of audiovisual, computing, and telecommunications techniques results in important mutations in the way we communicate at the office and at home.

These mutations concern voice, data, text, images, and video, and imply an increase toward higher bit rates.

Each customer can use a wide range of services, from the analog telephone (POTS) to digital television or digital services like ISDN and

multimedia with Internet, video services like Video On Demand (VOD), games, etc. Others services can be used such as group communications, remote working or distance teaching.

Services such as digital TV or VOD can be accessed on TV via a Set Top Box (STB) while multimedia services are on a PC.

For telecommunications services, the terminal depends on the proposed service (POTS, ISDN, Fax, etc.).

Different access technology can be deployed to connect customer to the access node :

- ADSL or xDSL networks using the existing copper network,
- FTTB/FTTC or VDSL networks using both optical fibers and copper pairs,
- FTTH network using optical fibers from end to end.

At the time being, for the broadband services delivery, the Home Wiring (HW) inside the customer premises is made up of copper pairs or coaxial cable. Two options could be used : either installing a new cabling system or re-using the existing one with or without modifications. This paper defines the engineering rules for the experimental installation of cabling systems in trials.

REFERENCE STANDARD DOCUMENTS

The documents taken as reference are the following ISO/IEC and CENELEC standards :

- ISO/IEC IS 11801 “ Information technology - generic cabling for customer premises ”,
- CENELEC EN 50173 “ Information technology - generic cabling systems ”

as well as the working document edited by the Full Services Access Networks Working Group :

- FSAN - GX, Network Termination - Home Network, Functional requirements [2],
- and the France Telecom specifications concerning cables, connecting hardware, and patch cords.

FSAN HOME ARCHITECTURE AND ACCESS NETWORK

FSAN general conditions (ADSL, VDSL, FTTH)

For the three access networks, the general conditions defined by the FSAN Working Group are described on table 1.

Access network type	ADSL	VDSL	FTTH
Terminal	2 BroadBand terminals : 1 PC and 1 STB		
Topology	Star : point-to-point interface		
Reach	> 50 meters		
Cable type	FTP-5 or UTP-5 or STP-5		
Down-stream bit rate	2 - 8 Mbit/s	13 - 26 Mbit/s	5 - 155 Mbit/s
Up-stream bit rate	up to 800 kbit/s	2 Mbit/s	0.5 - 25 Mbit/s

Table 1 : FSAN WG general conditions

Home wiring models

Two general architecture models are defined by the FSAN WG, firstly for the ADSL and VDSL access networks, described in figure 1, and secondly for the FTTH network (figure 2).

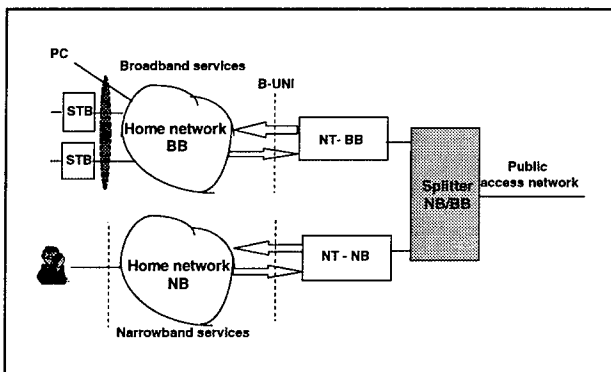


Figure 1 : general architecture for ADSL and VDSL access networks

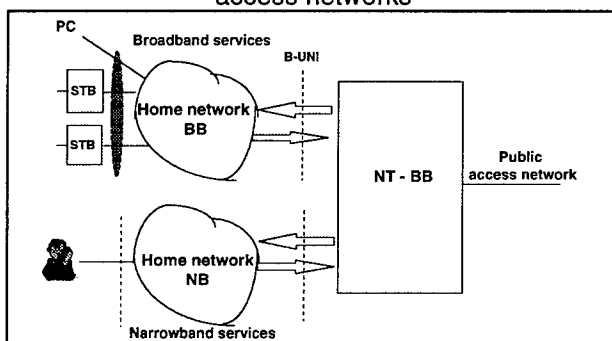


Figure 2 : general architecture for FTTH access network

For the ADSL and VDSL architectures, the first device is the POTS Splitter which makes the separation between the two cabling systems, one for the narrowband (NB) services and the other for the broadband (BB) services. Each cabling system is connected to its network termination (NT).

For the FTTH architecture, the two networks (NB and BB) have the same active NT with two separate cabling systems.

Home topology and interfaces.

Concerning home wiring for broadband services, the chosen topology, regardless of the number of connectors, is the star topology, with a point-to-point configuration for the interfaces. This topology is shown in figure 3.

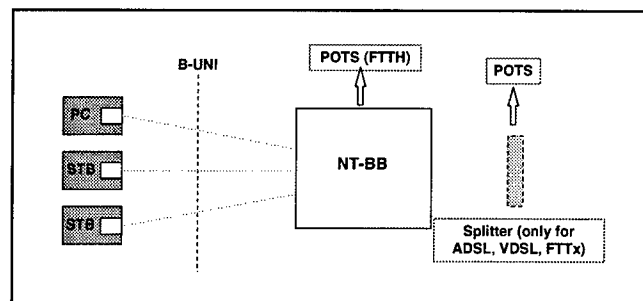


Figure 3 : Star topology for home wiring

The POTS Splitter is located before the NT in ADSL / VDSL configuration. The separation of narrowband and broadband signals is inside the NT in the FTTH configuration. From this active NT, each terminal is reached by a point-to-point link from an NT interface up to the same interface on the terminal, for both TV (with Set Top Box) and PC. At this point, the interface is called B-UNI for Broadband User-to-Network Interface.

The interfaces used in these two configurations, as described in figures 4A and 4B, are 10BaseT or 25.6 Mbit/s interfaces.

With the 10BaseT interface, an ATMF 25.6 Mbit/s interface can be used in the NT with an 10BaseT adaptor near the terminal.

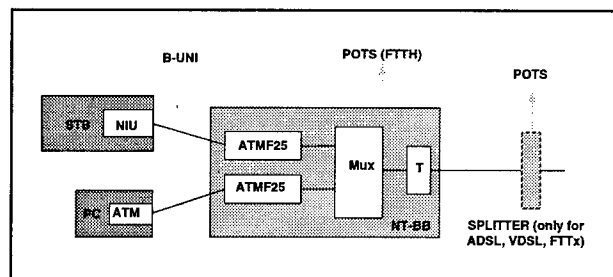


Figure 4A : ATMF interfaces

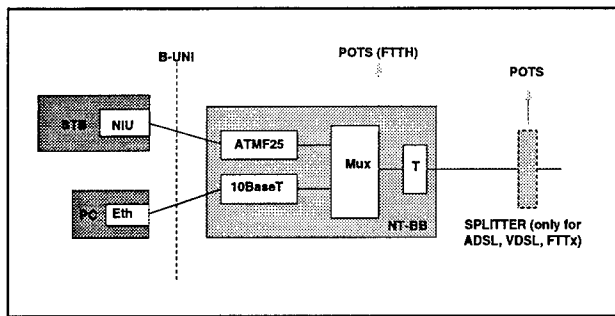


Figure 4B : ATMF and 10BaseT interfaces

Each type of architecture for the ADSL, FTTB/FTTC, and FTTH access networks, is described in the next paragraph in terms of :

- NT,
- interfaces,
- re-use of the cabling system,
- type of existing or new cables,
- length,
- measurements over different configurations.

HOME WIRING FOR TAMARIS FIELD TRIALS

FTTB/FTTC Architecture

The architecture [3] between the Optical Network Unit (ONU) and the terminal plug is a point-to-point configuration with a passive NT. The transmission system uses the ATM 25.6 Mbit/s interface to carry the broadband services over two pairs.

These services are video services on STB (digital TV, Video On Demand, Near VOD, etc.) and multimedia on PC (Internet access, local services including movie trailers, news, etc.). In figure 5, Foiled Twisted Pairs cables (FTP) are used from the ONU to the terminal plug.

The drop is a FTP multipair cable called "88/98" (France Telecom specification) which has a category 4 cable performance in ACR, NEXT, etc. It has a 4-pair capacity (2 pairs for ATM interface and one pair for POTS). The passive NT is a wall-mounted box located at the entrance of the house. The home network includes a 4-pair FTP category 4 cable, called "L122" (France Telecom specification) for broadband services. The existing wiring is used for the POTS. Due to the chosen system (ATM forum 25.6 Mbit/s) and electromagnetic compatibility requirements, the configuration retained for the FTTB/FTTC Field Trial called "Multimedia sur Armor" is a maximum copper cable length of 250 meters. So, the copper network is constituted with the following maximum lengths : 200 meters for the "88/98" drop cable and 50 meters for the "L122" home wiring.

The differences between this configuration and the FSAN requirements are the passive NT and the category 4 cables. Today, France Telecom is specifying new cables called "Lita" for the new multimedia home network, which are category 5 screened cables (FTP-5) with 2, 4 or 8-pair capacities under the same Zero Halogen sheath.

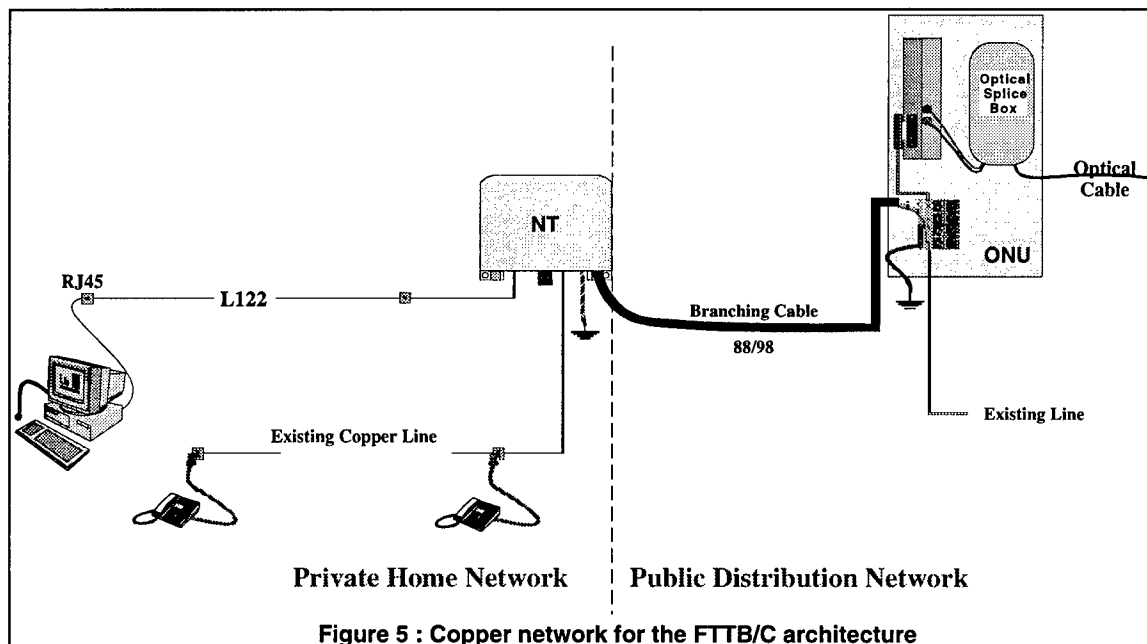


Figure 5 : Copper network for the FTTB/C architecture

ADSL architecture

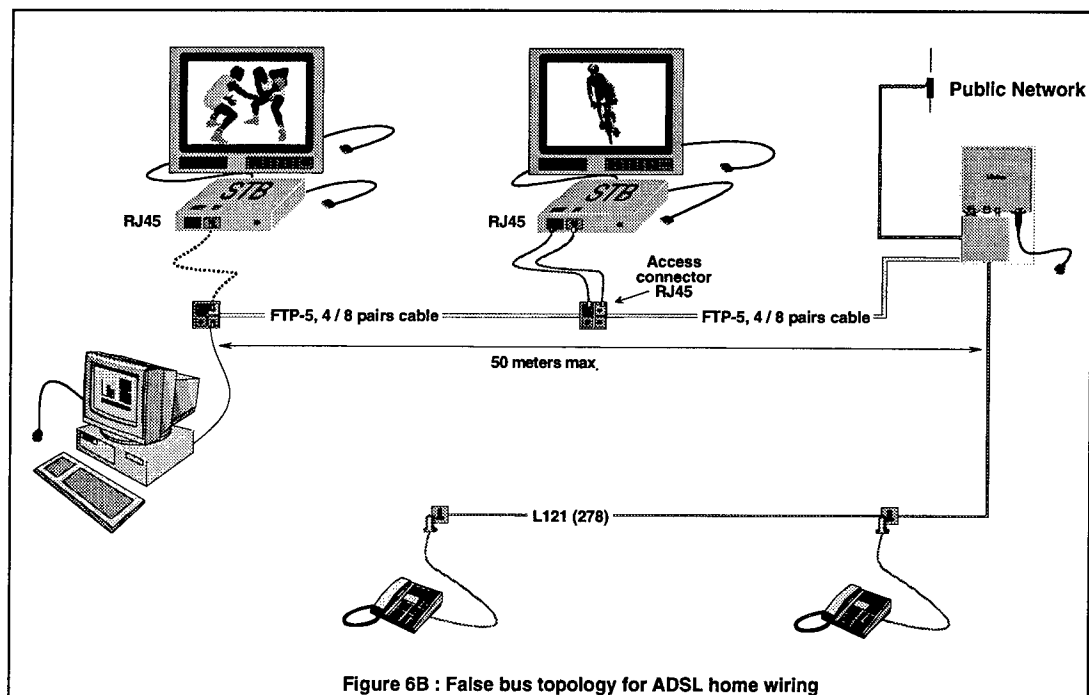
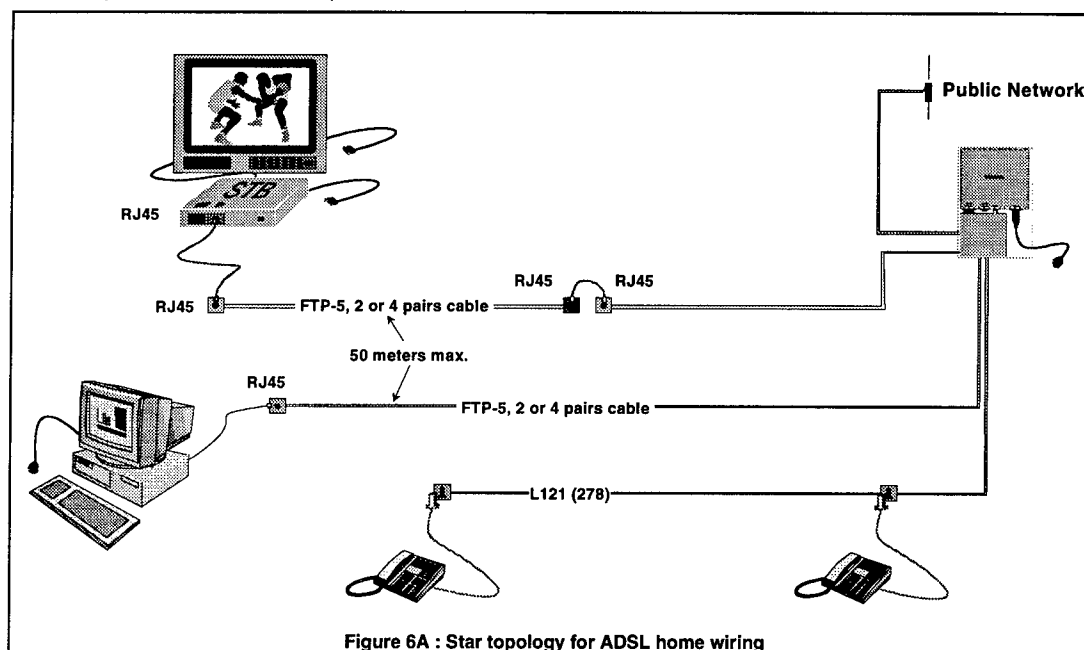
Studies are devoted to three types of home wiring for ADSL :

- New cabling systems,
- Re-use of existing cabling with modification,
- Re-use of existing cabling without modification.

New cabling. This cabling is in accordance with the FSAN requirements, with an active NT and the use of a new category 5 cabling for the broadband network. As mentioned before, the cabling system carrying the broadband signals and the cabling system carrying the narrowband signals are separated after the splitter, so the re-

use of existing home wiring for narrowband services is possible. This new cabling offers two possibilities described in figures 6A and 6B ; the use of one branch, so one cable per service (PC or TV) is possible, or the integration of the two services over the same cable (false bus notion). This is possible due to the high performances of FTP-5 cable, notably with respect to electromagnetic requirements.

In the two configurations, the in-house cable is a FTP-5 cable called "Lita" (France Telecom specification) with 2, 4 or 8-pair capacity and a maximum length of 50 meters for each branch. The physical accesses are, for the star topology,



one for PC and two for TV services (no simultaneous) and for the false bus topology, two (no simultaneous) for both services.

These are the two first configurations retained for the "CAMILLE" field trial conducted in Lannion, with 8 Mbit/s downstream bit rate and around 600 kbit/s upstream bit rate. One hundred customers are now using the video on STB and multimedia on PC services.

Re-use of existing cabling with modification. The FSAN WG did not study the re-use of the existing copper cabling system for the broadband services but it seems very interesting from an economic point of view, for the telecommunications operator and mainly for the customer (who does not always appreciate new cabling in his house).

For the narrowband (POTS) services, France Telecom has deployed, since the 70's, a 4-pair capacity cable. But, if some pairs are free, this home network has poor quality with "T" connectors and UTP-3 cable.

So, adaptation is needed.

The first solution for the re-use of existing cabling requires modification of the wiring. This solution, shown in figure 7, is for mono-terminal applications.

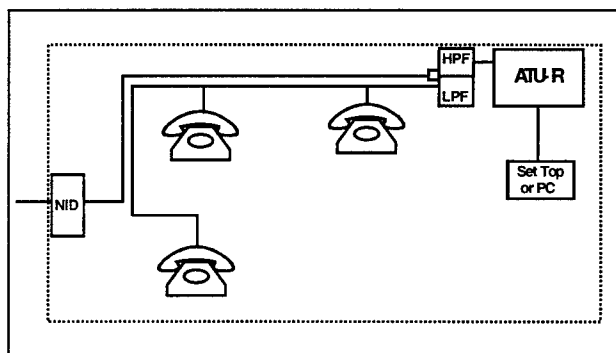


Figure 7 : modification of the existing home wiring for ADSL

It consists of using an extra pair in the cable to connect the customer ADSL modem to the Network Interface Device (NID) on the existing connector where the terminal and its connection system (RJ31X connector + ATU-R + STB or PC) will be installed. So, after this point, the existing cabling is re-used for narrowband services. For measurements in this configuration, different lengths of network and in-home cable have been tested. Bit rates between the two ADSL modems are set to 4 Mbit/s. Table 2 shows the line attenuation and the maximum up and downstream bit rates reached by modems under test.

6/10 cable L1 (m)	4/10 cable L2 (m)	6/10 Home wiring cable (m)	Up-stream bit rate (Mbit/s)	Down-stream bit rate (Mbit/s)	Total att.(dB) at 150kHz
2064	535	30	0.816	6.648	23.29
1010	1140	"	0.820	7.292	23.38
1010	1210	"	0.832	7.240	24.20
2150	605	"	0.816	6.200	24.70
3290		"	0.784	4.888	25.20
3744		"	0.692	3.500	28.28

Table 2 : bit rates and attenuation

For the use of ADSL modems at a 4 Mbit/s bit rate, the maximum attenuation is 26 dB at a frequency of 150 kHz.

This third configuration has been also retained for the "CAMILLE" field trial conducted in Lannion, with 2 Mbit/s downstream bit rate and around ten kbit/s upstream bit rate. Some customers are now using multimedia on PC services.

Re-use of existing cabling without modification. A second solution can be realised without modification of the existing cabling (figure 8). Some devices have to be added : low-pass filter on connectors for POTS and the high-pass filter of the ADSL modem on the broadband services multimedia-dedicated connector.

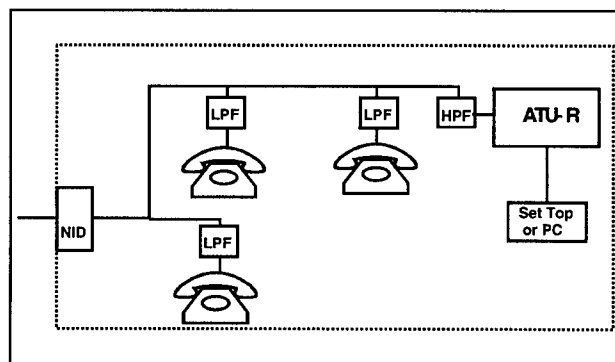


Figure 8 : adaptation of the existing home wiring for ADSL

For both solution, using UTP cable, it would be important to make a particular attention to the electromagnetic perturbations. The use of FTP cable in noisy environment is preferable.

FTTH architecture

Architecture and system. For the FTTH access network, the general architecture is described in figure 2 with an active NT. The optical access network is deployed up to the customer household with the ONU at the entrance of the home.

A POTS interface is used for the narrowband services and an ATMF 25.6 Mbit/s interface for the broadband services on PC.

A third interface is used for the broadband video services (same as others trials over the existing CATV services) ; this interface is connected to the existing customer coaxial network.

Cabling system. The two types of existing home cabling systems are :

- copper cabling for POTS,
- coaxial cabling for CATV services.

In the new cabling shown in figure 9, the ONU is located at the entrance of the home. The existing POTS cabling is not modified. The FTTH ONU brings three services: a new POTS line, multimedia on PC and video on STB services.

POTS services use a new UTP-3, 2-pair capacity cable from the POTS interface on the ONU ("Z") to its "T" connector, or a branch of the existing

cabling is re-used.

For multimedia on PC services, a “L122” or category 5 “Lita” is installed between the ATMF interface and a RJ45 connector.

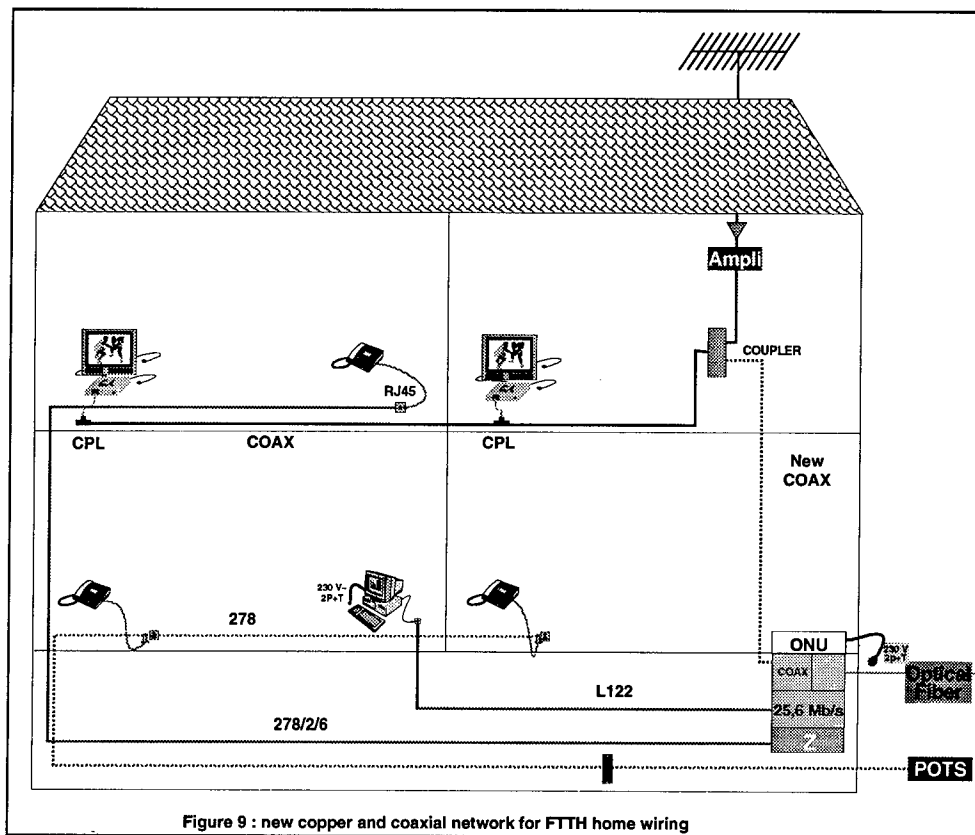
For video on STB services (digital TV, VOD, NVD, etc.), the coaxial customer network is re-used, being connected to the ONU by a coupler, which permits access to the new services and existing CATV services at the same time.

This is the solution retained for « ODET » field trial conducted in Lannion. Forty customers are identified and about ten are connected yet to the services.

CONCLUSION

All these works are conducted in field trials in Lannion with TAMARIS (CAMILLE, MULTIMEDIA sur ARMOR, ODET) and in other places (Rennes, Paris, etc.) concerning ADSL, FTTB/FTTC and FTTH access networks. For TAMARIS in Lannion, about 250 customers will be connected in september 97, using video on STB and multimedia on PC services on their new home network.

The main point of our works is now concentrating in ADSL deployment, re-using existing public copper network. For home wiring, there are interesting solutions for the re-use of existing



home network in France. The knowledge of the existing topology and cabling is very important. How to know it, how to re-use it? Another important point is to make attention to electromagnetic perturbations with UTP existing cables. The use of FTP cables is better in noisy environment, etc.

All these studies are geared toward defining a universal cabling system for home wiring in the next century.

REFERENCES

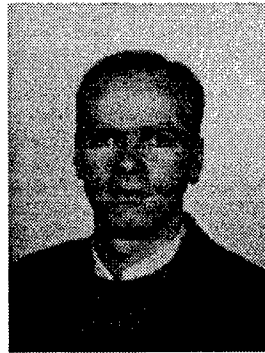
- [1] TAMARIS field trials - 8th International Workshop of Optical Hybrid Access Networks - Atlanta, March 97,
- [2] Full Services Access Networks - GX, Network Termination - Home Network, Functional requirements - 8th International Workshop of Optical Hybrid Access Networks - Atlanta, March 97,
- [3] Optical fiber and copper cables and passive components for FTTB/FTTC network - E.Cressan, O.Bouffant, G.Le Traon, O.Daguillon, R.Petit, J. Moalic, France Telecom / BD / CNET - 45th IWCS 1996

AUTHORS



Michel LISSILLOUR began his career with the National Research Center (C.N.E.T.) of France Telecom in 1967. He worked in the Test Laboratory for Computers from 1967 to 1989. After four years managing the LAN (Physical Layer) group, he joined the

Telecom Cables and Connection Equipment Department. He became the manager of the Optical and Copper Cables group working on specifications, performing tests and implementation of cables and cabling in Field Trials. He is also working on the new high bit rate applications on Customer Premises Cabling Systems



Olivier BOUFFANT was graduated from the University of Toulon in Electronics in 1992. He joined the National Research Center (C.N.E.T.) of France Telecom in 1994. Working in the Telecom Cables and Connection

Equipment Department, he is in charge of the new high bit rate applications on the Customers Premises Cabling Systems.



Herve LE COZIC began his career in the National Research Center (C.N.E.T.) of France Telecom in 1981. After six years in Physical-Chemical Laboratory, he joined the Telecom Cables and Connection Equipment Department in 1987. Working on standardization for data

cables, he is in charge of the telecom cables, connectics and home wiring tests.

Pierrick GUILLAS began his career with the National Research Center (C.N.E.T.) of France Telecom in 1976. After six years in Research and Development at the Computer Center in Paris, he joined the Telecom

Cables and Connection Equipment Department in 1982. Working on standardization for data cables, he is an expert on copper cables, for outside and inside plans, establishing specifications, and test methods.

FIELD TEST OF TELEPHONY SERVICE BY UTILIZING A CABLE TELEVISION NETWORK

Yukihiko Sato(*1), Shinji Zenimura(*2), Keiji Yoshikawa(*2),
Terutaka Anada(*3), Shingo Masumitsu(*3), Hiroyuki Ishida(*1), Mitsunori Kato(*1)

(*1) The Furukawa Electric Co., Ltd. Hiratsuka, Japan

(*2) Tokyo Electric Power Co., Inc. Tokyo, Japan

(*3) Tokyo Telecommunication Network Co., Inc. Tokyo, Japan

ABSTRACT

The cable television system has been used as a multi-channel video signal distribution system.

But now, in Japan, its cable network is attracted as a transmission network for other new services, on account of its wide-band and 2-way(Forward/ Reverse) transmission; and the telephony service has begun to be studied as one of the possibilities.

We have carried out a field test using an existing cable television network for 1994 and 1995. The field test was conducted using two optical links of the network and about 50 subscribers in total participated in the test as monitor, who actually used the telephony service for six months. During this period, system transmission performances were measured and the monitor's usage of the telephony system was systematically surveyed.

And we got a result, that the telephony service using an existing cable television network is entirely feasible without any influence onto the video transmission signals.

INTRODUCTION

In the course of fusion of communication and broadcasting in recent years, there is a growing demand for a new cable television system which readily realises such communication services as telephone, facsimile, and electronic mail in addition to conventional broadcasting services viz. video-signal distribution. With a view to implement and promote such a new system, the New-Generation Network Study Group(we are the members of the group) has commissioned us to do a verification study on technological as well as operational aspects of telephony service utilizing a cable television network; and we carried out a field test

of telephony service which utilizes the cable television network of Nihon Network Service Co., Ltd. (NNS) in Kofu city, Yamanashi prefecture for 1994 and 1995.

The field test was conducted using two optical links of the network and about 50 subscribers in total participated in the test as monitor,

Six other cable television operators were running similar field tests at their own network at the same time, so that every system could communicate each other through a public telephony network of TTNNet. And TTNNet's network is connected with NTT's public network, so the monitors could also talk with TTNNet subscribers and NTT subscribers.

SYSTEM CONFIGURATION

Figure 1 shows the system configuration of the field test. As shown, a TIU (Trunk Interface Unit) and a PBX for cable telephony system are included in the center facility, and a VIU (Voice Interface Unit) for cable television terminal and a commercially available analog telephone set in the subscribers' premises.

The terminal is connected via cable television transmission line to the PBX, so that one can talk with other subscribers within the same cable television network. And the PBX is connected with the TTNNet public network, so one can also talk with TTNNet subscribers, monitors within the six cable television networks under experiment, and NTT subscribers as well.

In the field test, about 50 cable television subscribers kindly took part in the test as monitor; they were from the Kobuchizawa route in Kobuchizawa-cho, Yamanashi prefecture, and from the Kofu Shiobe route in Kofu city, Yamanashi

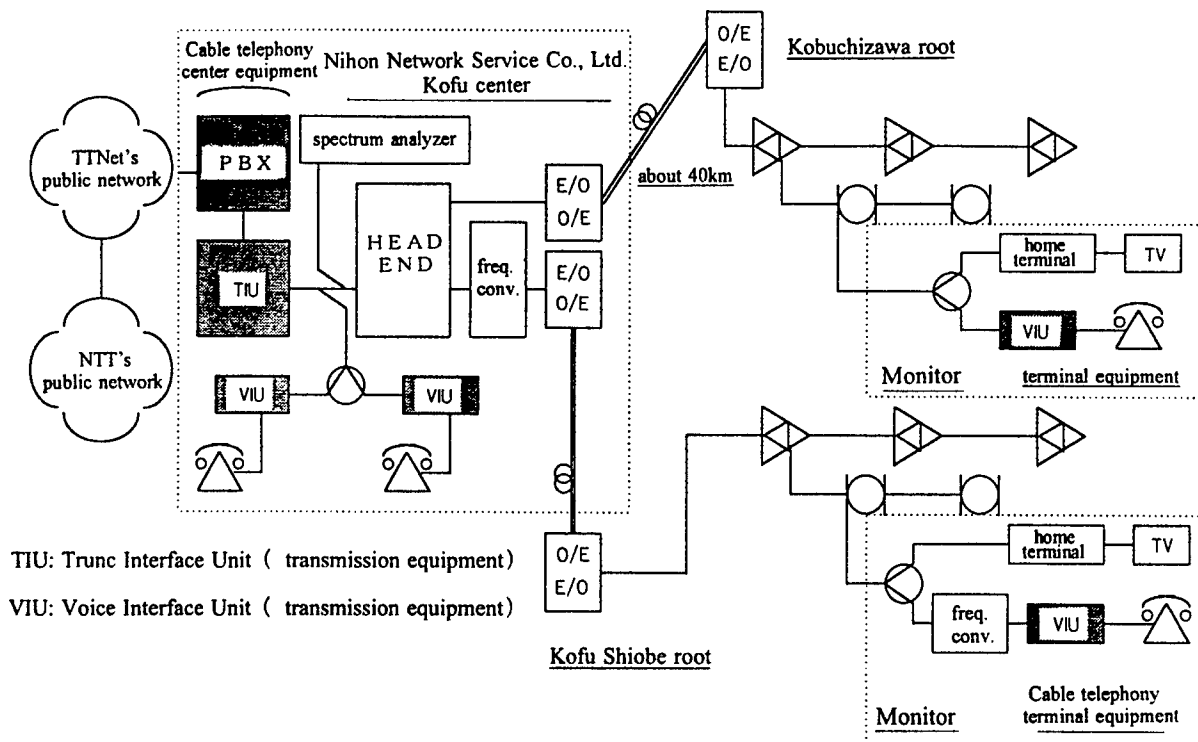


Figure 1 Field test system configuration

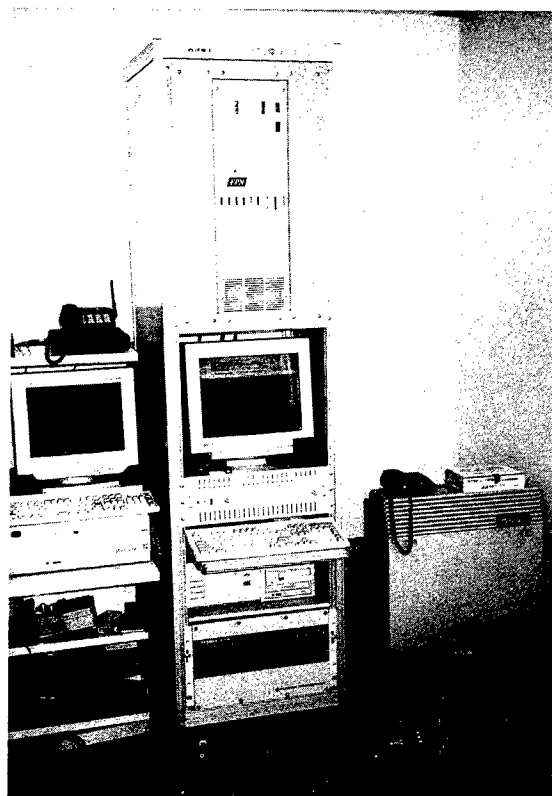


Photo 1 Cable telephony center equipment



Photo 2 Cable telephony terminal equipment

prefecture.

A transmission band of 330–336 MHz was used for the downstream channel. As for the upstream channel, the actual transmission line situation that was measured beforehand was taken into consideration; and it was decided to use a band of 18–24MHz for the Kobuchizawa route, and by introducing a frequency converter, a band of 30–36 MHz was used for the cable television transmission line of the Kofu Shiobe route.

Photo 1 shows the cable telephony system equipment at the center facility; the PBX is seen on the right, and the cable telephony center transmission equipment is housed in the rack at the center. Photo 2 shows the cable telephony terminal equipment seen under the telephone set.

ADVANCED MEASUREMENTS

Results of System Characteristics Confirmation before Shipping for Field Test

System Specifications. Table 1 gives the outline of system specifications. The system adopts the TDMA (Time Division Multiple Access) scheme for the upstream signal and the TDM (Time Division Multiplex) scheme for the downstream signal, so that subscribers can make an efficient use of the system. The digitized signals are transmitted with a bandwidth of 6MHz per one carrier, by using SQPSK (Staggered Quadrature Phase Shift Keying) modulation method for the upstream signal, and AMPSK (Amplitude Phase Shift Keying) modulation method for the downstream signal.

Influence on Video Signal. A confirmation test of the influence of telephone signal working on the video signal was carried out. Figure 2 shows the result. In the test, the downstream video signal level was fixed (60dBuV at the input of home terminal), and the influence on the video signals of above-adjacent and below-adjacent channels were investigated by varying the telephone signal level on the downstream channel.

As a result, it has been confirmed that the telephone signal does not exert any adverse effect on the downstream video signal (that is, image and sound quality) when the DU ratio of video signal (video signal to telephone signal) is better than –5dB and –12dB, in the cases of below-adjacent and above-adjacent, respectively.

Table 1 System specification

	Terminal Equipment	Center Equipment
Manufacturer (Model NO)	First Pacific Networks, Inc. (FPN1000)	
Multiplexing scheme	Time Division Multiple Access	Time Division Multiplex
Transmission frequency	12~30 MHz	294~342 MHz
RF input level	50~70 dBuV	58~78 dBuV
RF output level	109~115 dBuV	109~115 dBuV
CN ratio	30 dBuV or better	30 dBuV or better
Number of carriers per 6MHz	1 wave(s)	1 wave(s)
Modulation scheme	Staggered Quadrature Phase Shift Keying	Amplitude Phase Shift Keying
Transmission speed per carrier	5.018 MHz	5.018 MHz
Telephone channel per carrier (Telephone channel per trunc line)	56 (112)	56 (112)
Channel assignment scheme	Demand assign	
Number of terminals per trunc line	1,360 at call traffic: 0.07erl, degree of traffic loss: 1%	
Transmission distance	80 km maximum at one-way	

Downstream transmission frequency: 333MHz
 Upstream transmission frequency: 21MHz
 Downstream video signal input level: 60dBuV
 Upstream telephone signal input level: 68dBuV

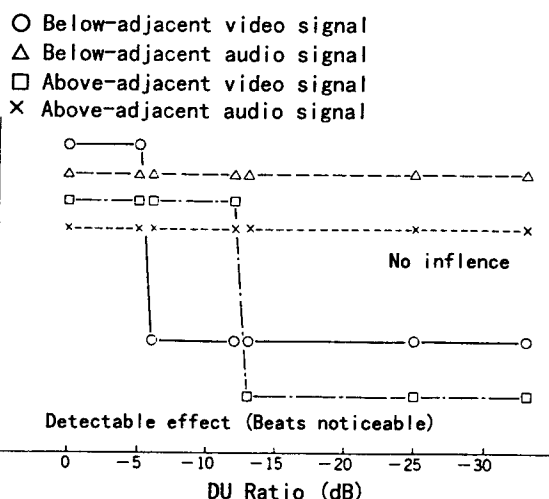


Figure 2 Influence of telephone signal on video signal

Influence of Video Signal on Telephony Signal.

A confirmation test of the influence of telephone signal working on the telephone signal was measured. Figure 3 shows the result. In the measurement, the telephone signal level was fixed (60dBuV at the VIU input of downstream channel, and 68dBuV at the TIU input of upstream channel, and the influence on the telephone signal was evaluated by measuring the BER, while varying the video signal level of adjacent (above and below) channels on the downstream channel.

As a result, it has been confirmed, as indicated by no occurrence of bit errors, that the video signal does not exert any adverse effect when the DU ratio of telephone signal (telephone signal to video signal) is better than -20dB and -16dB, in the cases of above-adjacent video transmission and below-adjacent, respectively. Thus, it is concluded that a telephone signal level of -10dB with respect to the video signal is sufficiently safe to operate the telephony system.

Input Power vs. BER Characteristics.

Figure 4 shows the relationship between telephony quality (bit error rate) and input power level of the telephone signal. The relationship was measured with input levels fixed: the downstream signal level at VIU was set to 60dBuV for the measurement of upstream signal, and the upstream signal level at TIU to 68dBuV for the measurement of downstream signal. The remarks in the figure, "available" and "not available", mean respectively that the cable telephony terminal become ready for use or not, via. initialization, when the power supply is turned on.

It is seen from the figure that, on the upstream channel, bit errors do not occur when the TIU input level is 55dBuV or higher; and the terminal is available for use when the level is 54dBuV or higher. On the downstream channel, in contrast with this, bit errors do not occur when the VIU input level is 45dBuV or higher; and the terminal is available for use when the level is 40dBuV or higher.

CN Ratio vs. BER Characteristics. The CN ratio vs. BER characteristics of telephone signal was measured and is shown in Figure 5. The measurement was done with a noise bandwidth of 4.2MHz so as to ease comparison with the video signal; and the telephone signal level was set fixed (60dBuV at the input of VIU, and 68dBuV at the

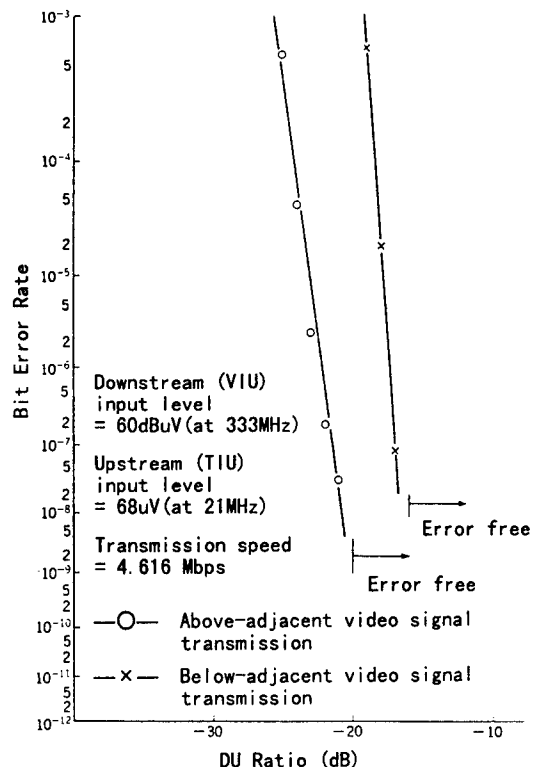


Figure 3 Influence of video signal on telephone signal

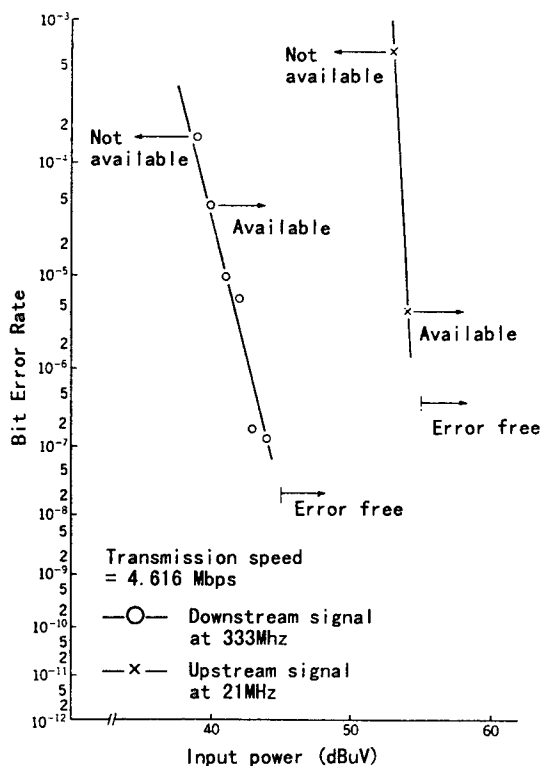


Figure 4 Characteristics of input power vs. BER

input of TIU), and the influence on the telephone signal was evaluated by measuring the BER, while varying the noise level.

As a result, it has been found that the audible noise does not exist when the CN ratio is better than 21dB (corresponding to a BER of 6.6×10^{-6}) for the downstream signal, and 26dB (corresponding to a BER of 6.8×10^{-6}) for the upstream signal.

Interference DU Ratio vs. Telephony Quality.

Figure 6 shows the frequency characteristics of telephony quality when a single frequency interference near the telephone carrier frequency was introduced into the cable television transmission line in order to simulate the ingress noise on the upstream channel. The figure also shows two limiting DU ratios for the frequency band of 18-24 MHz that is occupied by the upstream telephone signal carrier, a DU ratio which allows a critical availability of telephone, and the one which allows an audible-noise-free availability.

The critical DU ratio corresponds to a situation where telephone calling is approaching interruption due to a single frequency interference. Figure 6 indicates that telephone calling is ensured as long as the interference DU is higher than 17dB in the frequency band in use. Whereas, the noise-free DU ratio corresponds to a situation where the audible noise starts to be present in telephone calls due to a single frequency interference. It is seen that the audible noise is absent in telephone calls when a DU ratio higher than 24 dB is secured in the frequency band in use.

Results of Advance Measurement of Transmission Line

The ingress noise on the upstream channel is one of the dominant system parameters in the telephony service utilizing a cable television network. Figures 7 and 8 show the results of ingress noise measurements for the Kobuchizawa route and the Kofu Shiobe route, respectively.

These figures show the variation of the maximum ingress noise in the frequency band in use measured by a spectrum analyzer in the maximum-hold mode.

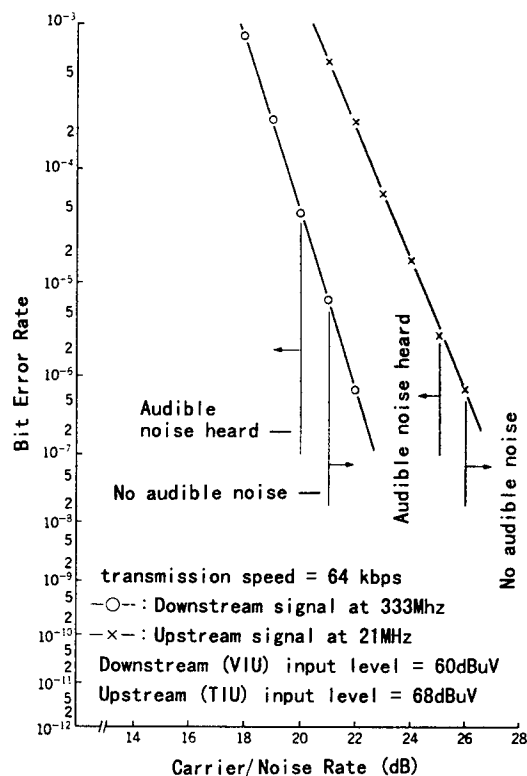


Figure 5 Characteristics of CNR vs. BER

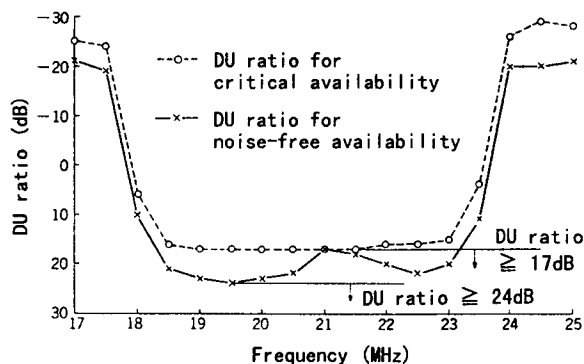


Figure 6 characteristics of Single tone interference vs. telephone quality

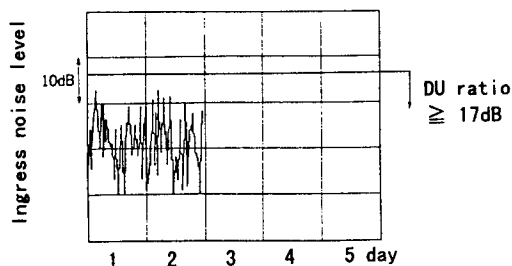


Figure 7 Maximum ingress noise in the transmission band width of 18-24 MHz at Kobuchizawa route

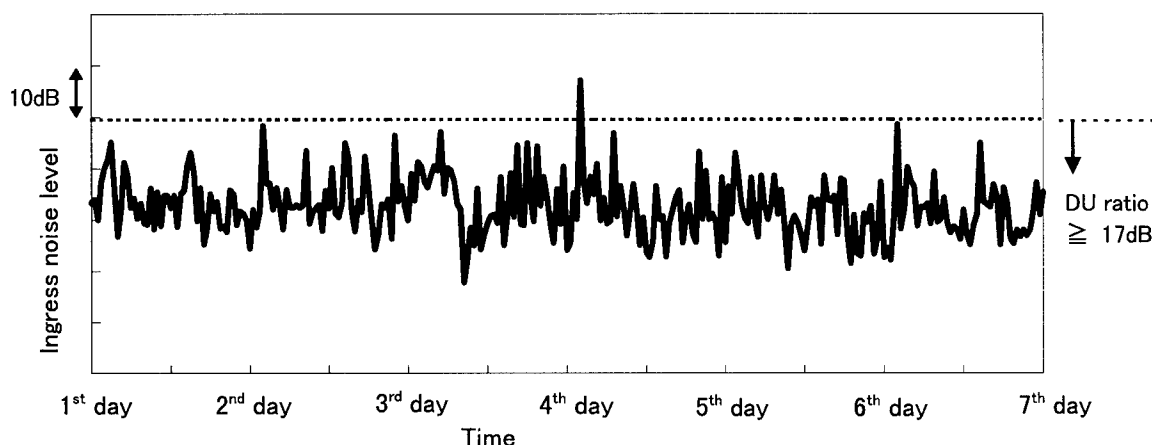


Figure 8 Maximum ingress noise in the transmission band(30-36MHz) at Kofu Shiobe route

lead to a possible interruption of telephone calling so far as the noise level is concerned. While in the Kofu Shiobe route, an ingress noise leading to a possible interruption occurs just once in the measurement of 6 days so far as the noise level is concerned.

It was concluded that the result above mentioned —there is a possibility of telephone calling interruption once in 6 days so far as the noise level is concerned— was not very crucial from the standpoint of practical service; and we decided to carry out the field test utilizing these

two transmission lines.

MEASUREMENT RESULTS OF TRANSMISSION QUALITY AT FIELD

Simultaneous Measurement of Ingress Noise and BER on Co-axial Transmission Line

Before installing a monitoring terminal, the relationship between ingress noise and BER was measured by a VIU at the center facility, with a loopback BER test measuring. The results are shown in Figure 9.

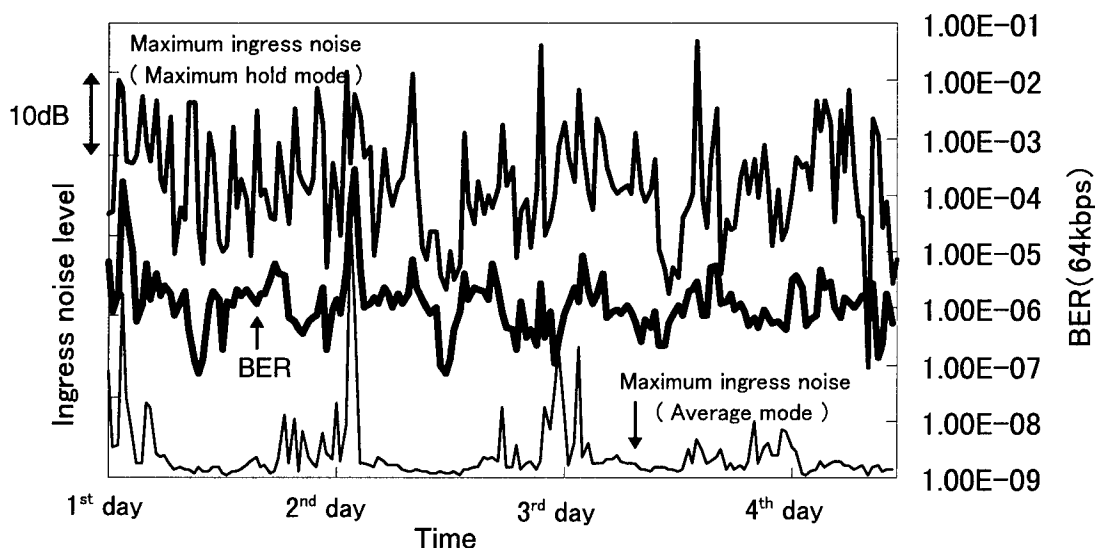


Figure 9 Relationship between ingress noise level and BER

The ingress noise was measured by repeating measurement in the maximum-hold mode for 27 min followed by a measurement in the averaging mode for 3 min; and the variation of maximum values of the maximum-hold mode and the averaging mode in the frequency band in use are shown in the figure. The bit-error rate was measured every 30 min at a transmission rate of 64 kbps. Figure 9 shows a tendency in which the ingress noise increases as the BER increases, thus suggesting the bit error is caused by the ingress noise.

Bit error measurements were also done during the monitoring period for 9 days (211h 30 min) and Table 2 summarizes the results in terms of total BER and error performance. As is seen, the total BER is three times the target value, and the error performance is inferior to the ITU-T recommendations.¹⁾ It is necessary to reduce the ingress noise to satisfy the target values, because, as shown in Figure 9, the bit error is clearly caused by the ingress noise. The target values will probably be achieved, while using the current cable telephony equipments, by such means as providing independent transmission equipment for each transmission line so that the ingress noise is reduced. However, referring to a conclusion reached by the questionnaire to be mentioned hereafter that the telephone calling quality is not problematic, we consider these target values are not necessarily essential prerequisites.

Measurement of

Telephone Transmission Path Quality

In this field test, telephone calling is possible not only with other cable telephony subscribers within the same network, but also with TTNNet subscribers and with NTT subscribers in addition to the cable telephony subscribers in the six other cable television networks under experiment. Various analog transmission qualities among these subscriber terminals were measured. Figure 10 shows an example of the relationship between modem connection speed and analog transmission quality. In the measurement, the connection speed of audio modem was to be set automatically, so that the connection speed is adjusted to lower speeds autonomously when a connection fails at the maximum speed of 28.8 kbps.

Both total distortion and talker echo affect the modem connection speed as shown in Figure 10, but they remained the same when measured with

Table 2 Results of total bit error measurement

Evaluation scale	Result	Recommendation
B E R	1.56×10^{-6}	4.5×10^{-6} (*1)
% E S	11.6 %	less than 1.2 % (*2)
% D M	39.2 %	less than 1.5 % (*2)
% S E S	0.10 %	less than 0.015 % (*2)

(*1) Recommendation of BER is derived by assigning 15 % of the value of 3×10^{-5} which is the general requirement for bit error rate for audio service, to the subscribers' one-way portion.

(*2) ITU-T G.821 recommendation

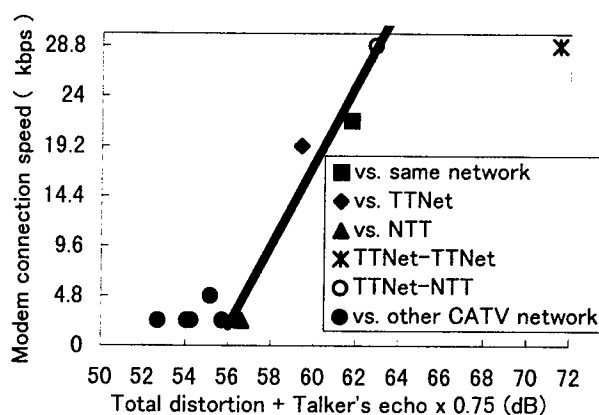


Figure 10 Relationship between analog transmission quality and modem connection speed

the cable television transmission line disconnected. From this fact, it may be concluded that the modem connection speed doesn't depend upon the ingress noise, but depends upon the system configuration, in particular, on A/D conversion of the telephone path.

SURVEY OF MONITORS FOR USAGE OF THE SYSTEM

Result of Traffic Survey

In this field test, about 50 monitors took part in the test and actually made use of telephone service about half a year. Telephone calls within the network were toll-free, but those to TTNNet subscriber and NTT subscribers were tolled and the monitors paid the tolls respectively.

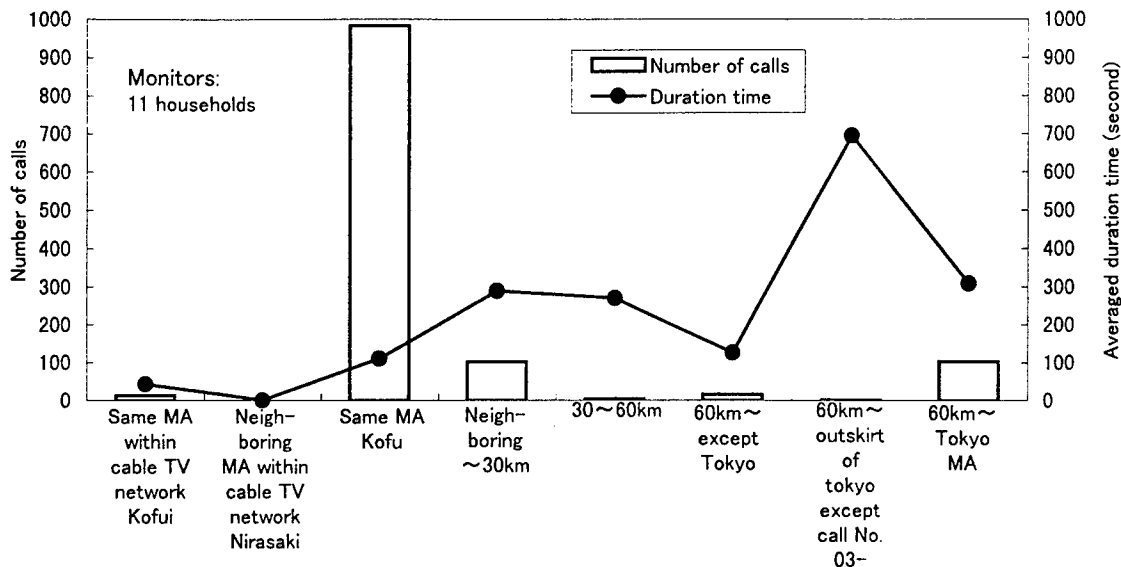


Figure 11 Traffic volume according to call destinations (Kofu Shiobe route)

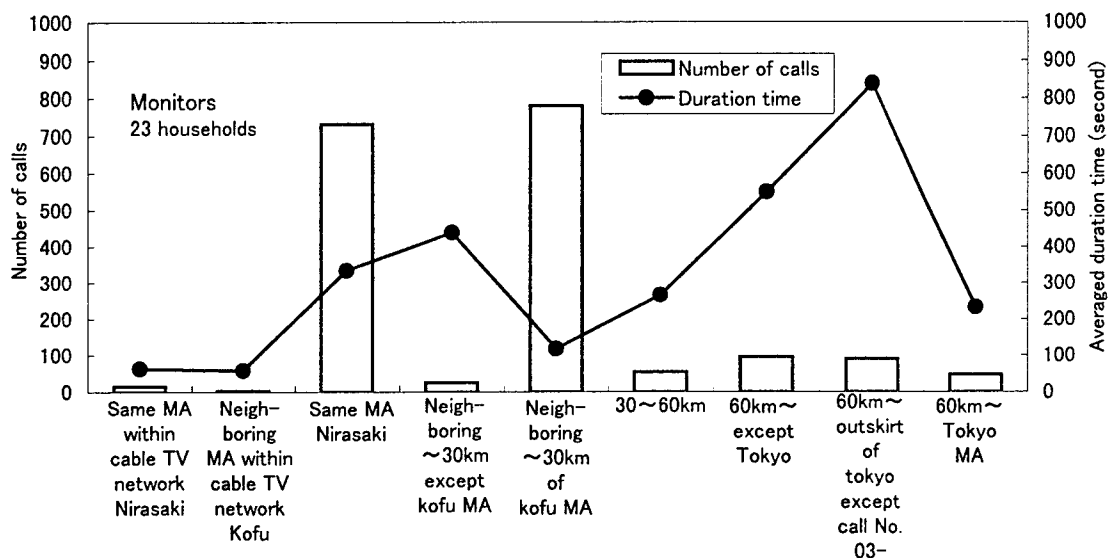


Figure 12 Traffic volume according to call destinations (Kobuchizawa route)

Calls from monitors may be grouped into those from businesses and those from common households according to their behaviors, but most of them were to NTT subscribers. Calls from businesses concentrate on the business hours of 9-17 o'clock in terms of number of calls and duration of calls. While, calls from common households increase in number in the morning (9-10 o'clock) and in the evening (18-19 and 20-21 o'clock), and their durations tend to increase toward midnight (22-23 o'clock). These tendencies

are common with NTT subscribers calls.

Figures 11 and 12 show traffic volumes of common households of Kofu Shiobe route and Kobuchizawa route, respectively, classified according to the call destinations. It is seen that the average duration of calls increases with the call distance; and the majority of calls in the Kofu Shiobe route (Figure 11) is addressed to within the same MA (message area) in terms of the number of calls, whereas many monitors in the Kobuchizawa route make a call to the neighboring

Kofu MA rather than to the same MA.

Results of Questionnaire

A questionnaire was issued to all monitors in order to survey and evaluate their usage of cable telephony.

Although some monitors answered that the noise was heard, there was no complaints about the interruption of telephone calling, so that it might be concluded that the telephone quality was appropriate. About 40 % of monitors answered that the cable telephony terminal equipment is oversized or they preferred the equipment should be placed outdoors; however, 60 % of monitors answered they don't care about the size of equipment. Furthermore, many monitors responded that they wished to enjoy comparable services as for NTT such as outgoing and incoming calls across the country and the availability of emergency calls. As to the telephone toll, many monitors answered they wished a toll level 30 % lower than that of NTT.

In summary, the monitors think that the telephone quality is acceptable as it is now, that the service content should be comparable with NTT, and that the toll should be cheaper than NTT.

CONCLUSIONS

A field test of telephony service utilizing a cable television network was conducted and the following results were obtained:

- (1) It is technologically possible to run a telephony service utilizing the existing cable television facilities.
- (2) A telephone signal, the same level as of the video signal, does not have an adverse influence on the system operation.
- (3) The occurrence of bit error is always accompanied by an increase of upward(reverse way) ingress noise. That is, the ingress noise is a dominant factor controlling the occurrence of bit error.
- (4) A bit error rate of 1.56×10^{-5} was obtained as a result of measurement for a week. However, it is confirmed that this level of bit error rate is not influential in telephone calls, because the monitor concluded that the telephone quality was good.
- (5) The traffic survey indicated that the diurnal pattern of calls was similar to that of NTT subscribers. In terms of destination, the greater part of calls in the Kofu Shiobe route were

directed to the same MA, whereas in the Kobuchizawa route they were to the neighboring Kofu MA.

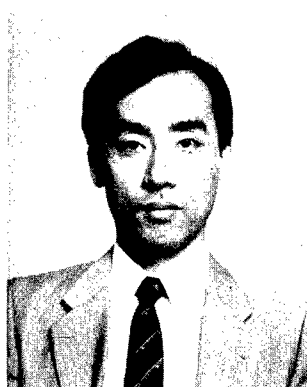
- (6) The result of questionnaire indicated that the monitors were desirous to have a telephony service whose service contents are the same as of NTT and whose tolls are cheaper than NTT.

To conclude this report, we would like to thank deeply those gentlemen concerned of the New-Generation Network Study Group and Nihon Network Service Co., Ltd. for their help and guidance in conducting this field test.

REFERENCE(S)

- 1) NTT R & D Division (eds.):
"Notes for a better understanding of NTT networks" (Revised), (1994), 302. (in Japanese).

AUTHORS

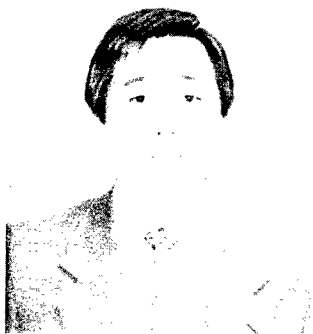


Yukihiro Sato

Furukawa Electric
Co., Ltd.

5-1-9, Higashiyawata,
Hiratsuka, Kanagawa,
254 JAPAN

Yukihiro Sato received the B.E. degree in electronics and communication engineering from Waseda University, Tokyo, Japan in 1983. Since 1983, He has been with Furukawa Electric Co., Ltd. where he has been engaged in the development and maintenance of the Factory Automation system. At present he is working in Communication Service research section of Information & Electronics Laboratory.



Shinji Zenimura

Tokyo Electric Power
Co., Inc.

1-1-3, Uchisaiwai-chou,
Chiyoda-ku, Tokyo,
100 JAPAN

Shinji Zenimura received B.E. and M.E. degrees in electronics and communication engineering from Waseda University, Tokyo, Japan in 1977 and 1979. He has been with Tokyo Electric Power Co., Inc. and he has been engaged in facilities planning, construction and maintenance management. Since 1997, he has been working in Telecommunication Research Division.



Shingo Masumitsu

Tokyo
Telecommunication
Network Co., Inc.

Shibauya Square Bldg.
4-9-25, Shibaura,
Minato-ku, Tokyo,
108 JAPAN

Shingo Masumitsu received the B.S. degree in telecommunication engineering from University of Electro-Communications, Tokyo, Japan in 1991. Since 1991, He has been with Tokyo Telecommunication Network Co., Inc., where he has been engaged in the development of telecommunication systems.

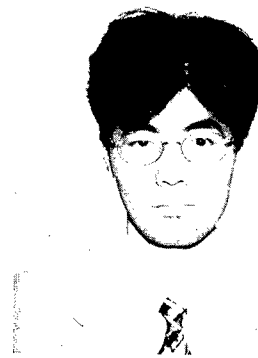


Keiji Yoshikawa

Tokyo Electric Power
Co., Inc.

1-1-3, Uchisaiwai-chou,
Chiyoda-ku, Tokyo,
100 JAPAN

Keiji Yoshikawa received the B.E. degree in electrical engineering from Meiji University, Tokyo, Japan in 1980. He joined Tokyo Electric Power Co., Inc. and he has been engaged in facilities planning and maintenance management. Since 1996, he has been working in Telecommunication Engineering Division.



Hiroyuki Ishida

Furukawa Electric
Co., Ltd.

5-1-9, Higashiyawata,
Hiratsuka, Kanagawa,
254 JAPAN

Hiroyuki Ishida received the M.E. degree in electronic engineering from University of Electro-Communications Tokyo, Japan in 1994. Since 1994, he has been with Furukawa Electric Co., Ltd. where he has been engaged in the research and development of cable telephony system.

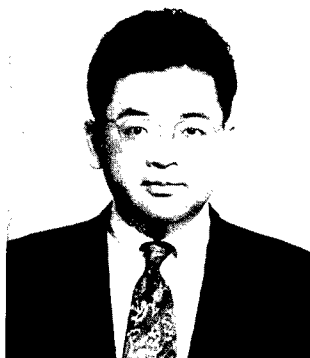


Terutaka Anada

Tokyo
Telecommunication
Network Co., Inc.

Shibauya Square Bldg.
4-9-25, Shibaura,
Minato-ku, Tokyo,
108 JAPAN

Terutaka Anada has been with Tokyo Electric Power Co., Inc. since 1965. In 1970, he received the B.E. degree in electrical engineering from Nihon University, Tokyo, Japan. He has been on loan to Tokyo Telecommunication Network Co., Inc., where he is currently a Manager of Cable Television Group in Multimedia Business Division.



Mitsunori Kato

Furukawa Electric
Co., Ltd.

5-1-9, Higashiyawata,
Hiratsuka, Kanagawa,
254 JAPAN

Mitsunori Kato received the B.E. degree in instrumentation engineering from Keio University Kanagawa, Japan in 1981. Since 1991, he has been with Furukawa Electric Co., Ltd. where he has been engaged in the research and development of automotive electronics system and in the research and development of multimedia communication system.

BUILDING ITALIAN HFC BROADBAND DISTRIBUTION NETWORK: FIELD EXPERIENCES AND SPECIAL INSTALLATION SOLUTIONS

Mauro Bottanelli, Edoardo Cottino

SIRTI S.p.A.
Cassina de' Pecchi (MI) - ITALY

ABSTRACT

In 1995, Telecom Italia chose an Hybrid Fiber Coax (HFC) architecture for the distribution of broadband and multimedia services in the Italian access network according to a Sub-Carrier Multiplexing (SCM) Passband transmission technique.

Two years later, the so called "SOCRATE project" (consisting of about 5.5 million passed homes) is having a strong impact in terms of infrastructure installation in the field.

HFC network design and construction are particularly complex in Italy, due to the Telecom Italia high quality level requirements and to the variety of urban and administrative situations.

This paper summarizes the last two years field experiences and the most important particular solutions developed by SIRTI for the HFC SOCRATE project, from the designer and the installer point of view.

THE SOCRATE PROJECT

Recently, growing availability of broadband services, higher quality requirements for traditional services and the liberalization of the European telecommunication market, have forced operators towards new access network technologies.

In the case of Telecom Italia, the "SOCRATE" (Sviluppo Ottico Coassiale della Rete di Accesso Telecom, that is: Optical-Coaxial development of the Telecom access network) project has the target to gradually develop a broadband network platform according to the following three phases:

- Phase 1: analog video services distribution

and preparation for digital video transmission;

- Phase 2: video distribution and multimedia interactive on-line services;
- Phase 3: video distribution and multimedia interactive services with integration of traditional narrow band services.

In the technical solution for the SOCRATE project phase 1 (Sub-Carrier Multiplexing Passband transmission) analog and digital signals are multiplexed by means of suitably spaced radiofrequency (RF) sub-carriers [1]: the resulting signal modules an optical carrier which is transmitted to the network peripheral nodes.

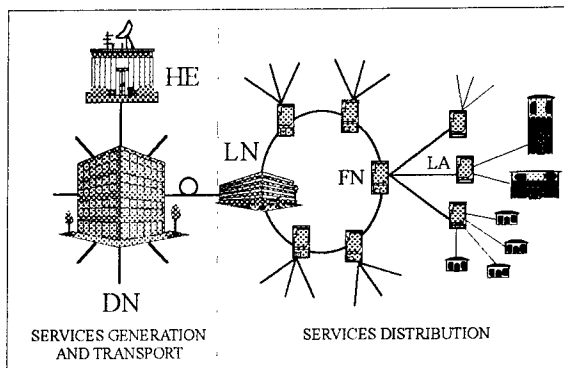


Fig. 1 - HFC architecture for the SOCRATE project phase 1

The reference architecture for the SOCRATE project phase 1 is sketched in figure 1, according to the following node classification:

- Head End (HE): the center where different video signal sources are processed and organized to become available on the network;
- Distribution Node (DN): the network entry point for channels coming from different

HEs. In the DN, video signals are put on the available transmission band by means of frequency multiplexing. A DN typically serves a metropolitan area and its suburbs;

- **Local Node (LN):** this network node receives signals from the DN and parts them on the urban distribution area FNs;
- **Fiber Node (FN):** this network node converts the optical signal into an electric one and distributes it by means of a tree like coaxial network. A FN typically serves a 400 homes maximum distribution area;
- **Last Amplifier (LA):** the last amplification point before the distribution to the customers. In the case of low signal levels (very broadened customer area) it is often necessary to add a further amplification point on the trunk network between FN and LA ("Line Amplifier").

From HE to DN channels are transported by means of SDH 34 Mbit/sec links; from DN to LN analog transmission is carried out by means of optical regional network; from LN to FN optical fibers of the primary distribution network are used; finally, from FN to LA and up to the customer NT ("Network Termination") transmission is carried out by means of a tree like amplified coaxial network for 500 meters typical maximum link lengths.

The coaxial part of the network limits the available bandwidth to 1 GHz according to the following targets:

- from 5 up to 30 MHz for network control signaling and interactive services upstream transmission;
- from 54 up to 470 MHz for analog video distribution;
- from 470 up to 862 MHz for digital video distribution, telephony and data transmission;
- from 862 up to 1000 MHz, the band is available for future applications.

NETWORK INFRASTRUCTURE FOR THE ITALIAN COUNTRY

Different problems had to be solved in order to implement the above described HFC architecture in the field, because of both Telecom Italia requirements and the different urban and administrative situations of the Italian country. Table 1 summarizes in very general terms the three basic cable installation techniques for the access network according to

their cost, reliability and flexibility characteristics.

Table 1 - Cable installation techniques

	COST	RELIABILITY	FLEXIBILITY
AERIAL	Low	Low	Medium
BURIED	Medium	Medium	Low
DUCT	High	High	High

As in the past, Telecom Italia chose cable in duct installation with operation, connection, and distribution manholes. This is the most expensive solution but the most reliable and flexible too, considering the Italian country needs and network future evolution. Less expensive HFC architectures can be design for simplified contexts by means of the following solutions (see table 2):

Table 2 - Solutions for less expensive HFC networks

• Frequent wall and pole installation
• Low depth cable duct installation (30 cm)
• More than a cable in the same duct
• Limited cabinets number and typology
• Different services (HFC+FTTC) in the same cabinet
• Twin cables (coax and t.p.) for customer connection

In every case, an HFC architecture automatically implies the presence of active elements in the field. Figure 2 summarizes coaxial components according to their cabinet or their housing in the network.

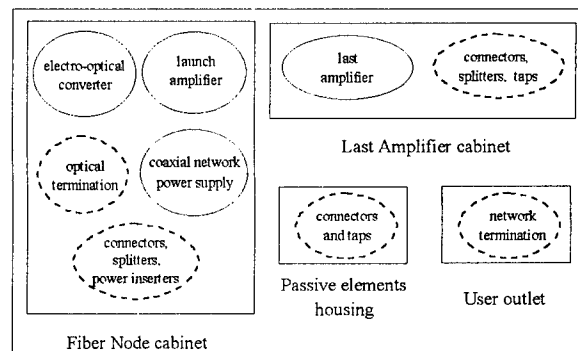


Fig. 2 - Coaxial network elements and cabinets

Among them, the continuous line circled ones are active, and may dissipate from 15-35 watts

(RF amplifiers) up to 100-150 watts (FN coaxial network power supply).

FN and LA cabinets are commonly installed on curbs, while passive component housings can be installed both on curbs and into customer buildings. The following simple estimate can give an idea of the HFC network environmental impact: in the circular area around a FN, there are typically 6 LA cabinets and about 20 passive component housings.

For these reasons, the physical construction of such a network has to face a lot of limitations, according to the ground morphology, the customers distribution, the administration requirements, the presence of historical monuments and so on.

Limitations and requirements may change according to different cities in a very dramatic way, so that what is requested in some areas is strictly forbidden in some others. Table 3 summarizes some of the typical HFC network different installation requirements or situations for the Italian country.

Table 3 - HFC network different installation requirements

• Underground LA installation only
• Forbidden underground LA installation
• Built in wall LA cabinets
• On curb excavations only
• On grade excavations only
• Forbidden parallel excavations
• Crossing excavations near cross-roads only
• Use of no-dig techniques when possible
• Air installation highly recommended (Venice)
• Frequent use of line amplifier

In order to meet so different requirements, SIRTl developed and experimented different solutions concerning installation techniques and cabinet types and locations. Examples of these solutions are listed in the following points:

- Directional drilling (fig. 3), air, pole, and wall installation techniques has been adopted to limit HFC network environmental impact;
- On curb FN and LA cabinets have been derived from traditional twisted pairs distribution cabinets by means of careful calculation and proper design of heat dissipation (more than 300 watt) louvers for natural convection;
- 300 twisted pairs Telecom Italia old cabinet modules have been adapted for building installation of a LA and two taps;
- Underground waterproof sheet molding

compound LA cabinet (fig. 4) has been developed for installation into manholes;

- Finally, a whole FN underground cabinet has been recently developed and first prototypal installations are now under test.

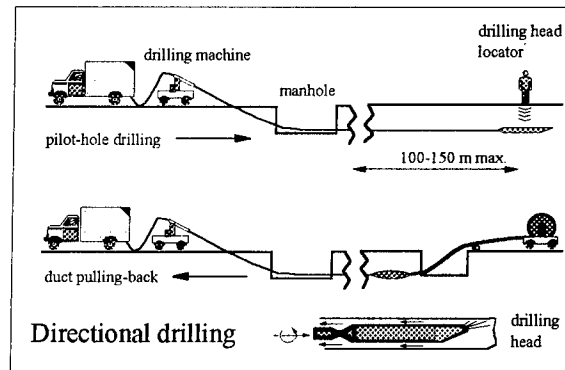


Fig. 3 - Scheme of the directional drilling technique

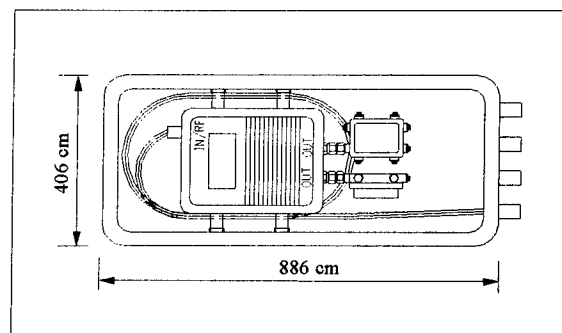


Fig. 4 - Underground LA cabinet sketch

COAXIAL NETWORK DESIGN

The optimization of the HFC network infrastructure with reference to field requirements is one of the basic coaxial network design target. This activity proceeds according to the following different steps:

- Broadband connections definition;
- Walk-in;
- Walk-out;
- Catchment areas definition;
- RF design;
- Civil design;
- Bill of materials;
- Drawing.

In the Telecom Italia HFC network design

reference guide, customer premises are classified according to broadband connection requirements as summarized in table 4.

Table 4 - Customer premises classification

TYPE	DESCRIPTION	Nr. of BB LINES
A	apartments, offices, shops	1
B	commercial centers, schools, < 20 rooms hotels/residences	4
C1	20-80 rooms hotels/residences	40 (1 LA)
C2	81-150 rooms hotels/residences	80 (2 LA)
D1	>400 circuits business customers	1 FN
D2	101-400 circuits business customers	1 FN
D3	51-100 circuits business customers	as B or C
D4	> 150 rooms hotels/residences	1 FN

This first classification is followed by a detailed analysis of the horizontal and vertical premises layout ("walk-in maps") in the considered area. Moreover, by means of the so called "walk-out maps", the network designer is informed of buildings entrances, suitable places for cables and cabinets installation, and of already existing infrastructures.

The RF coaxial network design is then obtained by means of an automatic CAD system (developed by SIRT I LTD for UK CATV installations and adapted by SIRT I S.p.A. to the Italian situation) according to a typical bottom-up approach, proceeding from LA areas definition ("Catchment areas definition") up to FN. On the basis of a highly detailed RF components database, the designer can easily dimension all parts of the coaxial network in order to ensure at least 12 dBmV electrical signal level at the customer network termination.

15.8 mm (.625 in.) and 19.1 mm (.750 in.) aluminum based trunk cables are used to connect FN to LAs and LAs to taps, while type 6 and type 11 drop cables are used for customer premises cabling. The availability of different cable types and attenuations allows to minimize the number of RF line amplifiers in the network. The civil design immediately follows the RF one: the CAD operator has to chose cabinets, manholes, and ducts typology and locations, exploiting already existing infrastructures as much as possible.

Finally, the CAD system can automatically extract from the network design the bill of materials and draw the requested documentation (coaxial and civil planimetries).

EVOLUTION TOWARDS ALL OPTICAL NETWORKS

With reference to future developments, it is worth considering the following consequences of the SOCRATE project:

- Introduction of broadband services transmission technologies in the Italian access network;
- Arrangement of infrastructures for a possible future network expansion towards new architecture types.

While the first well known aspect is directly related to the SOCRATE project mission, the second one often risks to be underestimated. However, it is even obvious that the SOCRATE project main features (about 5.5 million passed homes from 1996 to 1999; new broadband services supplying; hybrid fiber-coax network) constitute a first step towards a fast technological evolution of the Italian distribution network, especially considering the present dynamic situation of the European telecommunication market.

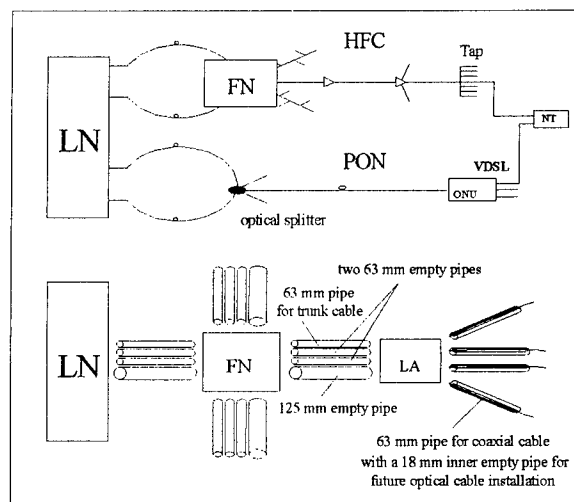


Fig. 5 - Evolution towards all optical networks: HFTTB

Figure 5 illustrates an example of the SOCRATE project evolution potentiality (Hybrid Fiber To The Building architecture). Here the present HFC infrastructure is compared to a possible future passive optical network (PON) experimentation, as a first step towards all services integration. HFC infrastructure is in fact already arranged to support a passive optical network, with optical splitters located near FN

cabinets. From FN to LA cabinets and for every HFC network directrix, two 63 mm and one 125 mm empty pipes have been already prepared for future applications. Moreover, from LA to customer premises, every 63 mm pipe for coaxial cable has been equipped with an inner 18 mm empty pipe for future optical cable installation.

From LN to FN, HFC network and PON share the same optical cable ring on different fibers; from FN to customer premises they lean on the same infrastructure; finally the two networks match at the user outlet. Broadband distribution services are transmitted on the HFC network; traditional and broadband interactive services are integrated and transmitted on the PON. The final goal of such an experimentation might be the future integration of all the services on the same optical network.

CONCLUSION

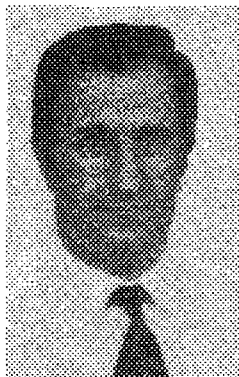
Last two years field experiences and the most important particular solutions developed by SIRT I for the HFC Telecom Italia SOCRATE project have been described from the designer and the installer point of view. New services availability, technological solutions and European market situation move towards future all optical networks.

REFERENCES

- [1] G. Aureli, V. C. Di Biase: "Un'architettura di rete in fibra ottica e coassiale per il trasporto di segnali video con tecnica SCM (Sub-Carrier Multiplexing)", Proceedings of Fotonica '95, pp. 69-80, Sorrento, Italy -1995.

ACKNOWLEDGMENTS

Authors would like to thank A. Marcone, G. Proietti Silvestri and HFC Design Center operators for their invaluable remarks and suggestions.



Edoardo Cottino

Cables and Optical
Technologies - R&D Dep.
SIRT I S.p.A.
Via E. Fermi, 2 - 20060
Cassina de' Pecchi (MI)
ITALY

Edoardo Cottino was born in Turin, Italy, in 1957. He received his degree of electronic engineering from the Polytechnic of Turin in 1982. He joined AET Telecomunicazioni in 1983 in the fiber optic laboratories, and moved to SIRT I in 1995, where he currently holds the position of manager of the Cables and Optical Technologies R&D Division. Dr. Cottino is a member of SPIE and his present responsibilities include ITU-T activities.



Mauro Bottanelli

Cables and Optical
Technologies - R&D Dep.
SIRT I S.p.A.
Via E. Fermi, 2 - 20060
Cassina de' Pecchi (MI)
ITALY

Mauro Bottanelli was born in 1963. He received the Dr. Ing. degree in Nuclear Engineering from the Polytechnic of Milan. After a two years activity in the field of industrial automation, he joined SIRT I in 1990 as research engineer in the field of optical fiber and optical component characterization, and of broadband access network design. He is a member of the ITU-T SG 6 National Working Group.

NEW CATV-COAXIAL CABLES AND COMPONENTS FOR HYBRID FIBER/COAX (HFC) NETWORKS WITH HIGH-SPEED DATA TRANSMISSION

**Peter E. Zamzow
Alcatel Kabel
Mönchengladbach, Germany**

**Heinrich Schürmann
Alcatel Cable Benelux
Seneffe, Belgium**

**Anton Ludl
Consultant to Alcatel
Mönchengladbach, Germany**

ABSTRACT

The emerging market for interactive media services requires new network solutions with high quality CATV components. Return data streams from the subscriber site complete the existing pure distribution network into a universal bi-directional communication network. Existing CATV networks for unidirectional transmission contain components that are useful for return path applications, such as conventional coax amplifiers, passive outdoor and indoor distribution devices and outlets to the subscriber. Coaxial cables for T & D applications with welded or extruded outer conductors are capable for return path. For drop cables with an outer conductor of foil and braid this is not assured. State-of-the-art CATV distribution systems are normally designed for 85 dB screening efficiency but only in the frequency range above 30 MHz. Through the additional use of upstream services the frequency range is expanded down to 5 MHz where the screening efficiency of coaxial cables decreases. Only a few cable constructions fulfill the 85 dB screening efficiency in this case. In the 5 to 50 MHz frequency range optimized constructions of the outer conductor are necessary to meet this value. Especially selected combinations of materials lead to technical and commercial solutions. Thorough examinations in testing confirm that the selection of coaxial cables has a strong influence on the electrical transmission parameters. We will demonstrate which parameters are

important for the dimensional design of HFC networks. Test results will be introduced. Requirements placed on coaxial cables and components with their technical solutions will be compared. As a result we conclude that a screening efficiency of 85 dB is required for drop cables in the access area.

INTRODUCTION

Return path for multimedia applications.

New telecommunication services are offered under the "multimedia" label¹. The acceptance of these new services, in addition to their contents, is driven by cost and degree of user-friendliness. The combination of audio, video-graphics and text satisfies most customer requirements (Fig. 1). The reception of only partial information from TV does not satisfy many subscribers. Once they have acquired their own experience from their video recorders subscribers are eager to have a hand in the creation of their own programs as well as a dialogue with the offering service. This falls under the concept of interactivity. The technical solution for interactive programming is offered by the introduction of the return path in the TV distribution network. Combined with the appropriate system technology the return path offers the following multimedia services²:

Type of service	Bit rate (upstream) kbit/s	Bit rate (downstream) kbit/s
Cable telephone	64	64
Video-on-demand	1.2	4,000
Internet	64	15,000
LAN/WAN	10,000	10,000
Telemetry	19.2	19.2

Table 1. Bit rates per subscriber for various services.

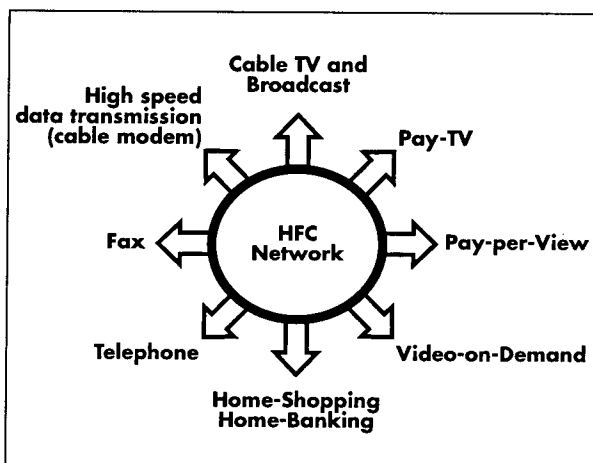


Fig. 1. HFC Network services

- Analog and digital TV and audio
 - Pay-per-channel
 - Pay-per-view
 - Audio on demand
 - Video on demand
 - Near-video on demand
- Telecommunication services
 - Telephone
 - Fax
 - Telemetry (network monitoring, remote control)
 - Data transmission
- Multimedia services
 - Banking, learning, shopping, teaching, office at home
 - On-line services
 - Gateway to the Internet
 - Games
- Local services
 - Information channels
 - Local TV services
 - Social and security services

In order to permit the exchange of operating data and information between the programming service (Server) and the subscriber, a return path to the server is required. In turn, a control channel from the server to the subscriber becomes necessary. The return path can be installed over the CATV net or through a telephone, radio or satellite broadcasting network. This paper, however, will deal only with return paths in coaxial CATV networks which, by their nature, lend themselves to the implementation of wide bandwidth and high immunity to interference. This is particularly the case when the subscriber's system renders possible a qualitative improvement through the use of cables and components with high shield attenuation and low transfer impedance. For the control channel it has the following functions:

- Customer identification for billing purposes
- Monitoring of connections (system additions, removals)
- Interaction with the server during use for menu selection or control of the "virtual" video recorder.

An important characteristic of the return path is the bit rate available to the customer. Table 1 lists the bit rates available to a subscriber for various services.

The implementation of the return path in present tree-structured coaxial networks for Service on Demand (SoD) requires access technology in the design of the return path to reflect customer wishes.

Based on currently available systems technology it is useful to assign a frequency range between 5 and 50 MHz for the return path operation in coaxial distribution networks. Hereby it is important that the signals distributed between the main entry point in the house and the antenna receptacles and TV set be compatible for use with the return path. In addition to transmissions from short wave

broadcasts and CB transmitters, interference may be generated into the return path by radio telephones and electrical home appliances. For the implementation of coaxial cables it is therefore proposed to specify their radiation resistance in the 5 to 50 MHz range to 114 dB (μV) or a transfer impedance of $< 1 \text{ m}\Omega/\text{m}$. The corresponding nominal values are derived in this paper and they are confirmed experimentally through measurements of the transfer impedance in the return path range.

TECHNICAL REQUIREMENTS FOR THE COAXIAL CABLE INSTALLATION FOR BI-DIRECTIONAL TRANSMISSION IN AN HFC NET

The hybrid fiber/coax network architecture is usually implemented as a ring-star or as an active or passive double-star. This means that the transport net requires a minimum radius in excess of 25 km. It is connected to the main transmitter by single-mode fibers at the 1310 or 1550 nm wavelength between individual nodes (Fig. 2). The nodes maintain the connecting net with a surface radius of $>10 \text{ km}$. The individual nodes are connected to the Broadband Optical Network Termination (BONT) through optical splitters.

The cable design for the optical transmission uses mostly single-mode fibers in loose-tube construction. The standard SM-type 9/125 μm fibers are rated for 0.3 dB/km attenuation at the 1310 nm wavelength and 0.2 dB/km at 1550 nm. The required number of fibers is given by the net topology. Each BONT connects, in general, between 250 and 500 subscribers through the coaxial cable network.

The transmission characteristics of hybrid fiber/coaxial networks are determined by the noise level at the receiver. The minimum level at the connector should be 60 dB (μV) and the maximum 78 dB (μV). This ratio must not be allowed to be deteriorated by the coaxial cables or passive components used. A distinction must be made between coaxial cables for external and internal use. External cables which connect the last amplifier to the transition point in the house have an aluminum or copper outer conductor with cellular polyethylene or bamboo-type (PE-air dielectric) insulation. The required transmission characteristics such as conductor attenuation, return path or shield attenuation can be determined through suitable design. The coaxial cables used as feeder cables in

HFC networks with a length of several 100 m exhibit the following attenuation at 450 MHz:

- Line attenuation: 8 to 12 dB/100 m
- Return loss: $>20 \text{ dB}$
- Shield attenuation: $>120 \text{ dB}$

On account of the required bending characteristics flexible coaxial cables are selected for internal use. To achieve the required flexibility the outer conductor of these cables consists of one or more braids; these, in turn, are combined with metal or plastic foils for the improvement of the shield density. Depending on the size of the building the cable length between the entry point and the subscriber's receptacle is between 50 and 100 m. Cables with different dimensions and/or attenuation characteristics are used to achieve the required operating load level.

Line attenuation (α) at 450 MHz:

- Single-family dwelling: 14 dB/100 m
- Tall buildings: 9 dB/100 m

Adequate shielding precautions must be taken to suppress external interference sources in order to ensure good in-house transmission. This applies to the cables as well as to associated components such as connecting hardware, etc.

A measure of the quality of the shielding is the screen dimension or the shield attenuation. The magnitude of the shield attenuation can be determined through extensive calculations. However, it must still be confirmed through measurements. The effect of bends, in particular, on the attenuation must be determined, as it may take on different values depending on the design of the outer conductor¹⁰.

In the transmission range between 5 and 50 MHz of the return path it is not possible to measure the shielding factors with sufficient accuracy. An alternate solution consists in measuring the transfer impedance^{3,4}.

The relationship between the shielding factor and the transfer impedance will be described later on. However, one must consider that an interference-free media application must not lie below 85 dB within the transmission range of the return path.

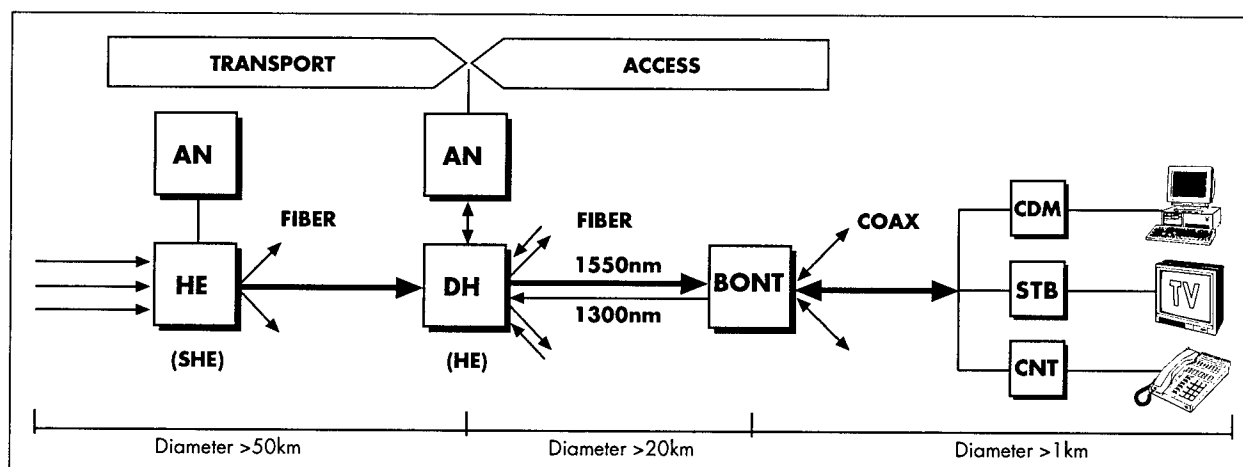


Fig. 2. HFC network topology with Alcatel 1570 BB

Frequency Range:	Interference source (with example):	Transmitted power:
0.0157 MHz to 0.143 MHz (0.0775 MHz)	Extra long-wave band • Newscast	50 kW
0.148 MHz to 0.5 MHz (0.148 to 0.255 MHz)	Long wave band • LW Broadcast stations	2,000 kW
0.525 MHz to 3.4 MHz (0.526 MHz to 1.6 MHz)	Broadcast band • Broadcast stations	1,200 kW
3.4 MHz to 47 MHz (3.4 MHz to 26 MHz) (26.965 MHz to 27.275 MHz) (27.12 MHz to 40.68 MHz) (3.5 MHz to 29.7 MHz) (36.64 MHz to 37.98 MHz)	Short wave band • Short wave broadcast • Walkie-talkies, CB radio • Industrial, Scientific & Medical Equipment • Amateur radio (80, 40, 30, 20, 17, 15, 12, 10 m bands) • Wireless public address systems	500 kW 0.5 W no defined range 750 W 0.1 W
20 – 30 MHz	• Radio telephones (analog)	0.1 W

Table 2. The effects of interference on coaxial in-house cables in return path applications.

THE EFFECTS OF INTERFERENCE ON IN-HOUSE COAX CABLES IN THE RETURN PATH

Table 2 illustrates how electromagnetic fields affect all coaxial systems. This means that currents are induced into the outer conductor or shield. These currents can raise the interference level to the operating load level^{6,7,8}. At lower frequencies between 25 and 400 Hz the interference level is caused by industrial machinery (Table 3). At audio levels between 100 Hz and 3.4 kHz and up to radio frequencies in the GHz range interference is generated mostly by rf transmitters. The radiation of various interferences into the coaxial net renders the inner conductor of a coaxial pair into a receiving antenna. Fig. 3 shows how the physical relationship between interference and the cable net should be visualized. Proper consideration has been given to the fact that all buildings or buried cables contribute considerably to a reduction of the attenuation of the

interfering signal. This means that the field strength inside a building varies in dependence of the frequency between 15 and 25 dB with respect to the following rf interference sources:

- Radio transmitters (broadcast and short wave, other transmitters, CB and radio telephones)
- Electric railroads (switches, shorts to ground, control pulses, rectifiers)
- Trucks (switching operations, spark plugs)
- Generating stations (shorts to ground, switching operations, electrical discharges, coronas)
- Household appliances(fluorescent lamps, vacuums, washing machines, drills)
- Various other industrial, scientific and medical apparatus

Protective measurement procedure applicable to: ⇒	Reduction factor		Transfer impedance		Shield attenuation	
Frequency range ↓	Cable	Receptacles Connectors Branch-offs	Cable	Accessories	Cable	Accessories
0 to 3.4 kHz	X	-	-	-	-	-
3.4 kHz to 50 MHz	-	-	X	X	-	-
50 MHz to 3 GHz	-	-	-	-	X	X

Table 3. Measurement criteria for determining the screening efficiency of coaxial components

A particularly susceptible range is the result of short wave transmission between 5 and 15 MHz. CB and other similar radio telephone transmissions are the source of interference between 20 and 30 MHz. So as to ensure that the cable networks fulfill the nominal requirements, Table 4 was created. This Table serves to define the freedom from interference as a function of transfer impedance within the frequency range of 5 to 50 MHz

PROTECTIVE MEASURES AGAINST RF-INTERFERENCE

A HFC network comprises the distribution net (fiber optic cables) and the access net. The access net consists of coaxial cables⁹. Customarily coaxial trunk and distribution cables are used for the last half-mile before the building's entry point. In modern networks these cables include a welded outer

conductor⁶. This design with the aluminum outer conductor has become accepted during the past 5 – 8 years. The shield attenuation for this cable type with welded outer conductor is in excess of 120 dB and therefore a secure protection from external interference.

On the other hand, for internal use and within the feeder range the design consists mainly of braids or, in more sophisticated installations, of a mixture of foil and braid (Fig. 4). It is important that these cable types, unlike the buried welded tubes, be fully flexible and capable of installation with small bending radii.

There exist a multitude of cable designs for conventional TV distribution. These exhibit a shield attenuation between 40 and 80 dB. If the return path - which lies within the 5 – 50 MHz frequency range - is to be used, a shield attenuation of at least 85 dB is required for multimedia transmission. If these conditions are not met, the network may be affected and the quality of the return path will not meet international specifications.

Frequency MHz	Immunity to radiated interference dB(μ V/m)	Building Attenuation dB	S/N ratio dB	Signal dB(μ V)	Transfer impedance mohm/m
1	114	25	60	70	5.0
5	114	25	60	70	2.0
10	114	20	60	70	1.0
20	114	20	60	70	0.4
30*	114	15	60	70	0.5
50*	114	15	60	70	0.8

* above 30 MHz the shield attenuation is >85 dB

Table 4. Transfer impedance in a coaxial TV distribution network with return path.

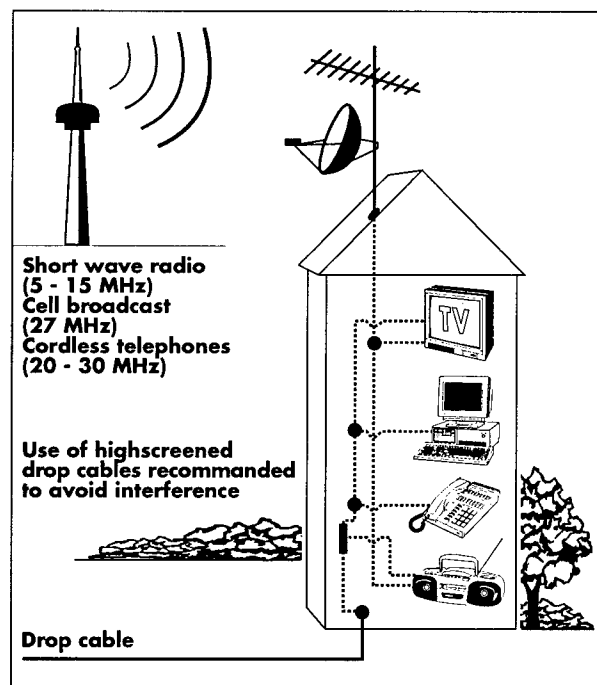


Fig. 3. Sources of interference in CATV in-house cabling.

The protective measures required for interference protection are classified as a function of the transmitted frequencies, as follows:

- Reduction factor
- Transfer impedance
- Shield attenuation

Table 3 illustrates the effect of frequency on HFC cable system components.

In the application of preventive measures to ensure adequate RF shielding it is important to include the building attenuation. This means that the building attenuation improves the immunity to radiated interference in accordance with Table 4. The relationship between transfer impedance (R_k) and shield attenuation (a_s) is represented by the equations in the following chapter.

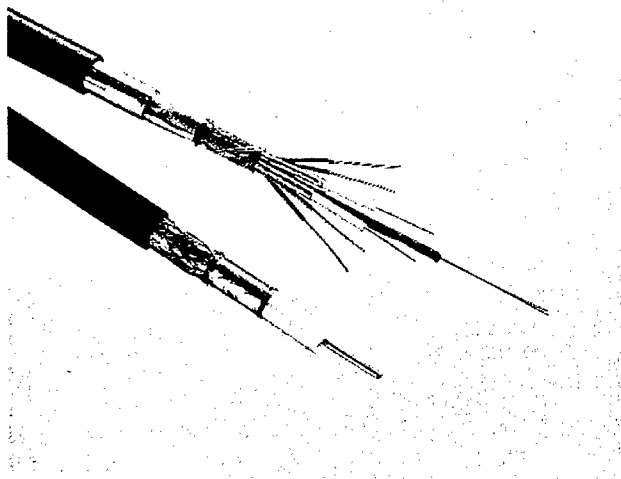


Fig. 4. Construction of flexible in-house cables.

RELATIONSHIP BETWEEN IMMUNITY TO RADIATED INTERFERENCE AND SHIELDING OF THE COAXIAL OUTER CONDUCTORS

The immunity to radiated interference can be calculated from the radiation density of the half-wave dipole (max. gain = 1.64).

Radiation density:

$$S = \frac{1.64 \cdot P}{4\pi d^2} \quad (1a)$$

Relationship between radiation density in free space and electrical field strength E:

$$S = \frac{E^2}{120\pi} \quad (1b)$$

Immunity to radiated interference:

$$E = \frac{7.01 \cdot \sqrt{P}}{d} \quad (2)$$

where:

P = delivered power

d = distance (m)

E = electrical field strength in V/m or
20 log in dB μ V/m

S = radiation density in W/m^2

Table 4 reflects the calculated values for the immunity to radiated interference as a function of frequency. The transfer impedance results from the immunity to radiated interference factor in dB(μ V/m), the frequency-dependent housing attenuation in dB and an assumed 60 dB S/N ratio and average 70 dB load level at the connector to the TV set.

Transfer impedance:

$$R_K = \frac{U_{St}}{I_{St}} \cdot \frac{1}{l} = R_{KR} + j\omega L_i \quad (m\Omega / m) \quad (3)$$

wherein

U_{St} = interference voltage induced into the inner conductor

I_{St} = interference current induced into the outer conductor by external fields

R_{Kr} = transfer impedance of a coaxial cable with tubular outer conductor in mohm/m

$$R_{Kr} = R_0 \cdot \frac{jkd}{\sinh(jkd)} \quad (4)$$

where

$$k = \sqrt{j\omega\mu_0\mu_r\chi}$$

d = wall thickness of the tube

L_i = longitudinal inductance (depending on the construction and the nature of the material of the outer shield)

Shield attenuation

$$a_s = 20 \cdot \log \frac{\sqrt{Z_1 \cdot Z_2 \cdot 2 \cdot \pi \cdot f \cdot (\sqrt{\epsilon_{r1}} - \sqrt{\epsilon_{r2}})}}{c_0 \cdot R_K} = 20 \cdot \log \left(181 \cdot \frac{f}{R_K} \right) \quad \text{in dB} \quad (5)$$

wherein:

a_s = shield attenuation in dB

Z_1 = Cable impedance (primary circuit, 50 ohms)

Z_2 = Cable impedance (secondary circuit, 150 ohms)

$\omega = 2 \pi f$ (angular frequency)

ϵ_{r1} = dielectric constant in primary circuit (1.21)

ϵ_{r2} = dielectric constant in secondary circuit (1)

c_0 = speed of light

f = frequency (MHz)

R_K = transfer impedance in mohm/m

At the 30 MHz frequency a 0.3 mohm/m transfer impedance results in a shield attenuation of >85 dB.. Any further frequency increase results in a constant 85 dB shield attenuation in the cable.

MEASUREMENT TECHNIQUES TO DETERMINE THE SHIELDING DENSITY OF COAXIAL CABLES AND COMPONENTS

The measurement techniques for determining the shielding density of coaxial cables and components are divided into three frequency ranges^{11,12}.

- Low range: 0 to 1 MHz
- Middle range: 1 to 50 MHz
- Upper range: 50 MHz to 3 GHz

The interference sources in the lower frequency range are primarily generated by power plants, electric railroads and lightning. It is possible to diminish their effects through electro-magnetic shielding to the point that dangerous voltages or currents are prevented from perturbing the telecommunication system. Interference currents are also avoided in the audio frequency range. The measure for defining the shielding effect of the jacket is the reduction factor.

The central frequency range, which includes the return path, is affected mainly by broadcast transmitters, including radio telephones. The shielding effect of the cables and components described here is characterized by the surface transfer impedance (Fig. 5).

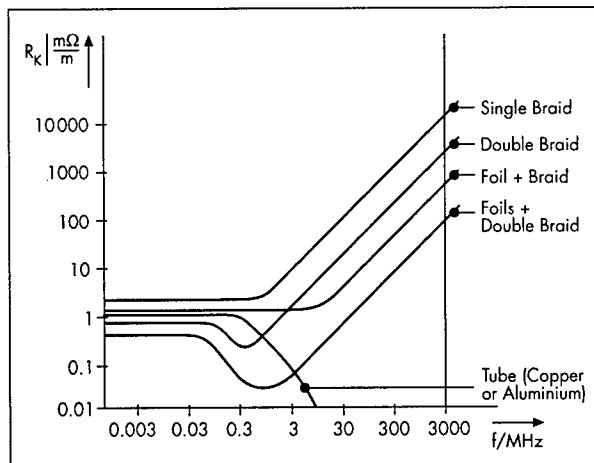


Fig. 5. Transfer impedance for different cable construction types

The upper frequency range falls within the transmission channels of TV systems. CATV channels are situated in the range of 450 to 862 MHz and intermediate frequency channels for satellite systems at 3 GHz. The prevailing interference here is caused primarily by radio transmitters, such as "ERMES" (European Radio Message System), for example⁸. As a measure for evaluating the shielding effectiveness of the cable jacket against rf electrical fields the shield attenuation was introduced.

All three of the above terms define the effectiveness of the cable shield. They can be confirmed through measurements. The measurement procedures are laid out in Standards such as, for example, DIN VDE 0472 and DIN IEC 61196-1^{10,11}. The measuring set-up is illustrated in Fig. 7. A brief description of the test procedures explains the differences.

N°	Properties	Measurement Methods	Frequency Range
A	Shielding Factor $r_k = \frac{U_a}{U_M}$		0 - 3.4 kHz
B	Transfer Impedance $R_K = \frac{U}{I_{ST} \cdot l}$		3.4 kHz - 50 MHz
C	Screening Attenuation $\alpha_s = 20 \log \frac{I_w}{I_i}$		50 MHz - 3000 MHz

Fig. 6 Measurement procedures
a) determining the shielding factor
b) determining transfer impedance
b) determining shield attenuation

Reduction factor

The reduction factor is important for the evaluation of interference caused by electrical railroads, high power transmission lines and lightning. The reduction factor is determined in accordance with DIN VDE 0472 (Fig. 6a).

Transfer impedance

The transfer impedance serves to determine the shielding of a cable exposed to electrical fields. In the case of closed, homogeneous outer conductors the transfer impedance can be gathered from the dimensions and the material properties. On the other hand, a precise determination cannot be made for shields consisting of single braids or braids in combination with foil. Instead, measurements must be conducted as illustrated in Fig. 6b. A detailed description is furnished in DIN IEC 611 96-1.

Shield attenuation

The determination of the screening efficiency of coaxial cables in the upper frequency range is conducted through measurements shown in Fig. 6c. For the coaxial cable together with the applicable connecting components (plugs, receptacles, couplings) this measurement method can be used universally. It is imperative, however, that a perfectly electrically impervious coaxial cable (tube cable) be used for this test.

The description and measurement procedure is in accordance with DIN IEC 611 96-1. It is important to note that there exist three distinct measurement methods:

- Tri-axial method up to 500 MHz
- Absorbing clamp method up to 1 GHz
- Line injection procedure up to 3 GHz

Item	Transfer impedance					Shield attenuation dB
	mΩ/m					
Cable construction	DC	5 MHz	10 MHz	30 MHz	50 MHz	5-50 MHz
Single braid	20	17	33	100	170	35
Double braid	10	1	2	6	10	60
Foil + braid	15	0.5	1	3	5	65
Foils + double braid	5...8	0.017	0.033	0.1	0.17	95
0.25 mm copper tube	1...3	0.16	< 0.01	< 0.01	< 0.01	> 120
Aluminum tube	0.4..1.5	0.18	< 0.01	< 0.01	< 0.01	> 120

Table 5. Transfer impedance and shield attenuation of CATV drop cables

MESUREMENT RESULTS

To determine the suitability of the return path of coaxial cables and components we are limiting ourselves here to the 5 – 50 MHz frequency range. The open literature lists the reduction factors and shield attenuations that can be expected for various cable designs in the lower and upper frequency ranges. Our examinations of cables and components covered the following subjects:

- Single braid
- Double braid
- Foil with braid
- Foils with double braid
- Copper tube
- Aluminum tube

Table 5 summarizes the results for the 5 – 50 MHz frequency range, including the DC components.

As expected tube cables are resistant to interference. They confirm the lowest values of transfer impedance and the highest shield attenuation (Fig. 7). Major differences in the quality of indoor or feeder cables have been found as a result of cables that do not meet Standards or cables with inadequate shielding characteristics.

The required shield attenuation at 50 MHz and the transfer impedance of <0.1 mohm/m can be achieved through proper optimized design with special foils and braiding (Fig. 8).

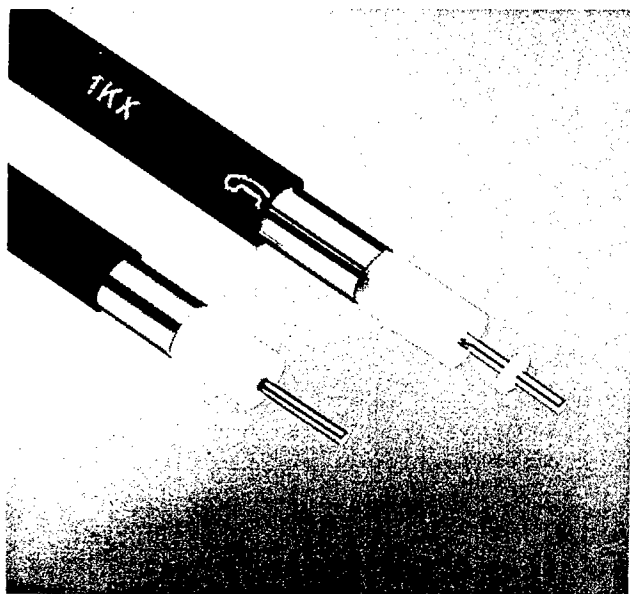


Fig. 7. Trunk and distribution cables in trunk construction (aluminum or copper)

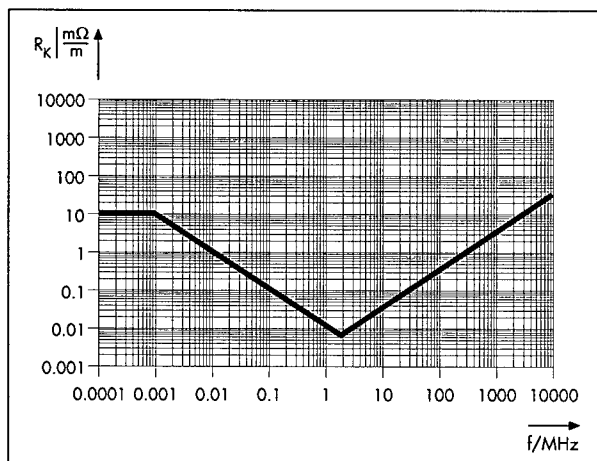


Fig. 8. Test results of transfer impedance on shielded in-house cables.

SUMMARY

Our examinations demonstrate that induced radiation into indoor cabling can lead to considerable interference with TV transmission and into the return path (5 to 50 MHz). These interferences are caused by broadcast transmitters, radio telephones, and household appliances. They are the result of:

1. Poor quality of the cables and components
2. Improper installation

In many cases the indoor cabling was often conducted under the responsibility of the landlords or building proprietors and no upgrade to the latest state-of-the-art, such as EN 50 117, was carried out. One can therefore conclude that many indoor cable installations are not suited for the transmission of multimedia. This includes not only the cables from the interconnection point to the receptacle in the house but also the flexible connecting cables to the TV set or to the set-top box. The implementation of symmetrical telephone cables using, for example, Digital Subscriber Loop (DSL) Technology (e.g. Asymmetric DSL, Very High DSL) as proposed by Deutsche Telekom may solve the problem of rf interference while, on the other hand, considerably reducing the bandwidth capability offered by coaxial cables. Examinations of our cables demonstrate the benefits of proper shielding of coaxial indoor cables. Adequate transfer impedance values and proper screen attenuation in the TV distribution network and satellite intermediate frequency range can be achieved.

The resulting transfer impedance values of <1 mohm/m and shield attenuation of 114 dB (μ V) for immunity to radiated interference are considered adequate. Upon first investigations following the introduction of ERMES additional results for the improvement of screening efficiency and bending requirements for TV transmission were presented at the European Cable Conference in Antwerp in June 1997. In this paper we have presented the most recent results of our investigations and proposals for further improvement of indoor CATV cable wiring for multimedia applications using the return path.

The results demonstrate that the use of high-quality shielded coaxial cables with 85 dB shield attenuation in indoor cabling renders possible interference-free multimedia application through the use of the return path in the 5 – 50 MHz range.

A recommendation is therefore made to consider the 85 dB attenuation figure as minimal value for cable standards.

ACKNOWLEDGMENTS

The authors wish to acknowledge the valuable assistance received from Mr. Henry Hofheimer of Cable Consultants Corporation Larchmont NY in translating and editing this paper.

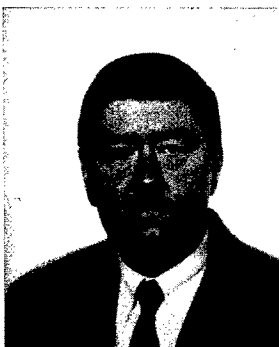
REFERENCES

- [1] BMPT: Technische Perspektiven für die Multimedia-Zukunft in Deutschland, 1996
- [2] ANGA-ZVEI: TV-Kabelnetze; Zukunftssicherheit durch Ausbau zu interaktiven Breitbandnetzen, 1996
- [3] Ochem, H.: Der Kopplungswiderstand koaxialer Leitungen, Hochfrequenz- und Elektroakustik 48/1935 H.6
- [4] Kaden, H.: Wirbelströme und Schirmung in der Nachrichtentechnik, Springer-Verlag 1959
- [5] Halme, L. et Szentkuti Bb.: the background of electromagnetic screening measurements of cylindric screens, Techn. Mitt. PTT, 1988
- [6] Belich, U. u. Schüler, H.: Schirmungskonzept des Liniennetzes, taschenbuch der fernmeldepraxis 1989
- [7] Morgenstern, J.: Electromagnetische Verträglichkeiten (EMV) von TK-Einrichtungen, ntz 46/1993 H.12
- [8] Ludl, A.: Kein Problem mit "ERMES" bei Verwendung normgerechter HF-Empfangskabel ntz 48/1995 H.12
- [9] Ludl, A.; Vellinga, J.; Zamzow, P.: Low cost solution for introduction of optical fibres in existing coaxial CATV networks, Montreux International Symposium 1997
- [10] Guery, D.; Ludl, A.; Schürmann, H.; Zamzow, P.: High Screened CATV Drop Cables For Future Broadband Transmission, Proc. ECC Antwerpen, 1997
- [11] DIN VDE 0472 Prüfungen an Kabeln und isolierten Leitungen
- [12] DIN IEC 61196-1 (Entwurf 1997): Hochfrequenzkabel
Teil 1: Fachgrundspezifikationen-
Allgemeines, Definitionen, Anforderungen und Prüfverfahren



Peter E. Zamzow
Alcatel Kabel
Mönchengladbach,
Germany

Peter E. Zamzow (57) is director of the Telecommunication Division. He completed his post-graduate studies in telecommunications in Munich and Graz as Dipl.-Ing. He joined AEG KABEL in 1970. He has been engaged in development and production of telecommunication cables. In 1980 he became head of the fiber optic division at AEG KABEL and in 1982 he was nominated as a senior engineer. From 1992 on he was plant manager of the new Optical Fiber Cable Plant Rheydt. Since July 1994 he is director, manager of the product group CATV, Telecommunication product line for Germany..



Heinrich Schürmann
Alcatel Cable Benelux
Seneffe, Belgium

Heinrich Schürmann (53) is responsible for engineering of CATV cables and components. He obtained his Dipl.-Ing. degree from the RWTH Aachen, Technical University of Aachen/Germany. In 1971 he joined KABEL RHEYDT where he was being engaged in the development of symmetrical and coaxial cables. In 1980 he transferred to the optical fiber department where he was responsible for data processing. In early 1996 he again joined the CATV product group. Since May 1997 he is engaged in engineering and technical support for the CATV production at Alcatel Cable Benelux in Seneffe/Belgium.



Anton A. Ludl
Consultant
Alcatel Kabel
Mönchengladbach
Germany

Anton A. Ludl received his Dipl.-Ing. degree in 1964 from the Technical University of Aachen. He joined Alcatel SEL, Stuttgart in the same year. In 1970 he became head of the development of telecommunication cables. From 1974 to 1983 he was the head of the quality department for the production plants in Stuttgart and Berlin. In 1983 he became responsible for cable installation projects in different countries outside Germany. He joined AEG KABEL, now Alcatel Kabel, in 1991, where he became the head of the construction department for symmetrical CATV and optical cables. Later on he became responsible for the product management of communication cables. Since 1982 he is a member in different standardization bodies, e.g. ITU, IEC, CENELEC and VDE. Since early 1996 he is a communications cable consultant to Alcatel Cable for outside plant projects.

NEW COATINGS DEVELOPMENTS AND CHARACTERIZATIONS AND MULTI-USES CABLES MATERIALS FOR FTTH

A. Morgand, D. Boscher, B. Cadier, A.C. Reau, Y. Ruello

CNET Laboratory, France Telecom, Lannion, France

ABSTRACT

This paper reports on works accomplished to develop new approaches on optical fibers and cables, in preparation of the access network deployment.

Most fibers available on the market are not adapted to the distribution fiber which must have a greater fatigue resistance (improved corrosion parameter) to support important curvature and harsh environment (humidity...).

A part of the works has consisted of developing new coating types permitting to improve the corrosion parameter and to maintain its value after aging.

The distribution fiber will be introduced in small drop cables. Like the current cables are too big and heavy, a new multi-uses microcable structure has been developed : diameter around 1 mm, light (2g/m), easy and fast to install, excellent global behavior.

The principal characteristics of the new fibers and microcable, some fields trials in indoor and outside configurations are presented. A new DMA measurement method developed to optimize the coatings and their compatibility with the microcables is also described.

INTRODUCTION

For long-haul applications, optical fiber has demonstrated during the last ten years great qualities for transmission : capacity to transmit very high bit rates, insensitivity to electromagnetic perturbations, very good bit error

performances, reliability better than coaxial links. For the access network, the fiber will present another advantage which is a greater cabling facility due to lower cables diameter and weight. These characteristics will permit to install very small cables in aerial with low tensions, almost invisible cables on a facade or in an apartment, under carpet...

The cables, in this network terminal section, are more submitted to the environment (humidity...) and to mechanical (important curvature...) and thermal stresses. According to the life time prediction model, the distribution fiber must have an improved fatigue resistance.

Some studies already exists on technologies which seem to improve the fibers resistance [1,2,3,4].

As the consequences are very important for the future infrastructure definition, France Telecom started investigations on these fibers and internal studies on two complementary ways.

These two ways are briefly described in this paper. Their common aim is to obtain low cost resistant fibers, fulfilling the following specification :

- curvature radius : 10 mm (fiber diameter between 180 and 250 μ m)
- permanent elongation : 0.6 % or more
- very good coatings intrinsic resistance
- good adhesion and strippability

All these characteristics have to be maintained after aging and during all the cable life.

Two resistant fiber types with improved corrosion parameters have been obtained. These fibers can be introduced in very small drop cables.

Like the current cables are too big and heavy to be used as drop cables, a new low cost multi-uses microcable designed to support important curvature and harsh environment has been also

developed [5] : diameter and weight around 1 mm and 2g/m, easy and fast to install, with excellent thermal, mechanical and aging behaviors.

To compare different fibers behavior, classic and improved fibers have been introduced in these microcables and some field trials in aerial and building configurations have been performed.

The paper presents the principal characteristics of the microcable and the aging behavior of the fibers before and after cabling ; a new very sensitive method developed to optimize the new coatings and permitting optical fiber in-situ characterizations is described.

RESISTANT OPTICAL FIBERS FOR DROP CABLES

The fibers for the access network must have an improved corrosion resistance. A first approach shows that it is easy and cheap to increase the bending and microbending fiber resistance, but the most effective technologies (like carbon coatings) seem generally too costly for distribution applications. So, new ways have been studied and have provided first promising results.

One of them is based on thin hydrophobic polymers, the other is based on a new ultra-thin hermetic coating technology. They permit to improve the corrosion parameter, without degradation after aging and without decreasing the initial fiber breaking strength.

Thin Hydrophobic Polymer (fiber F1)

This new type of resin is deposited as an inner layer. A new adhesion promoter is introduced in its structure in order to block the fragile sites present on the silica surface. The adhesion promoter permits to improve the coating adhesion to the silica, which avoids water penetration during aging.

The deposited layer has a thickness around 1 μm (observed by Atomic Force Microscopy) and is protected with one layer of a classic coating (thickness between 30 and 45 μm). The global coating cost of this new fiber is equivalent to a classic fiber.

The corrosion parameter « n » and the breaking strength of this fiber have been measured ; the

results, compared to classic or quasi-classic fibers (F3,F4,F5,F6) are reported in the table 1.

Ultra-thin Hermetic Coating (fiber F2)

A new type of hermetic « metalloid molecules » which permits to improve the optical fiber corrosion parameter without decreasing its breaking strength has been developed.

With the associated technology (medium pressure deposition system which allows non-limited drawn lengths), it will be possible to manufacture low cost resistant fibers compared, for example, to the carbon technology.

The thickness of the deposited layer is around 30 nm (observed by High Resolution Electron Beam Microscopy).

The corrosion parameter and the breaking strength obtained are presented in the table 1. An example of a Weibull and a static « n » curve is shown on the fig. 1 and 2.

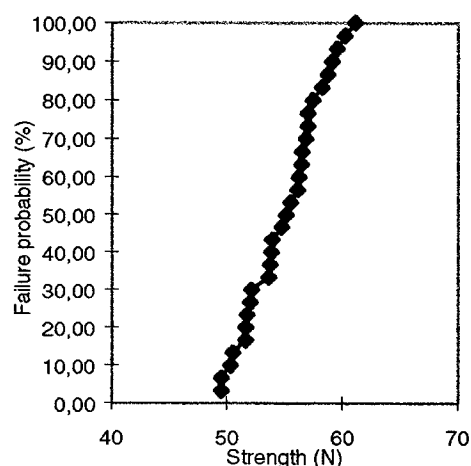


Fig.1 : Weibull obtained with fiber F2

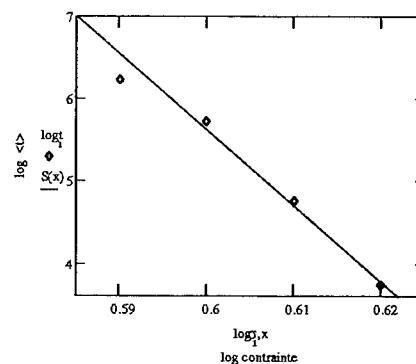


Fig.2 : F2 static « n » curve

The breaking times corresponding to the static n curve are :

mandrels diameter	time to failure
2.4 mm	1h30
2.45 mm	15 h
2.5 mm	6 Days
2.55 mm	20 Days

	n ref.	n after 30d at 85°C/85%RH	F _{63%} (N)
F3*	23	21	~ 55
F4*	> 40	20	~ 55
F5	> 100	40	~ 40
F6	> 100	> 100	~ 40
F1*	30	28	~ 55
F2	~ 100	in progress	~ 55

* static corrosion parameter

Table 1 : principal characteristics of new resistant fibers (F1 and F2)

Comments

Table 1 shows that, in opposition to F3, F4 and F5, the thin hydrophobic polymer permits to preserve the corrosion parameter after aging. The hermetic coating allows to achieve very long failure times (several months on 2.6 mm diameter mandrels) and a « n » > 100, without decreasing the breaking strength.

We have also verified that these 2 fibers are easy to splice and connect, with losses lower than 0.1 dB.

Two types of low cost resistant optical fibers for the access network have been developed and introduced in a new microcable structure (described below) to compare their behavior with classic fiber's one.

MULTI-USES MICROCABLE FOR THE ACCESS NETWORK [5]

Description

The new distribution fibers seem to be promising elements which make possible the fabrication of new microcables designed to support important curvature and harsh environments, to be small and light, to simplify connection and installation and to reduce the global cost of the link.

The distribution fiber is introduced in a structure which does not stress it : the fiber is tight in an external hard composite and "decoupled" of this structure with a "decoupling agent" (fig. 3). This agent damps down the mechanical and thermal stresses and facilitates the fiber extraction out of the cable.

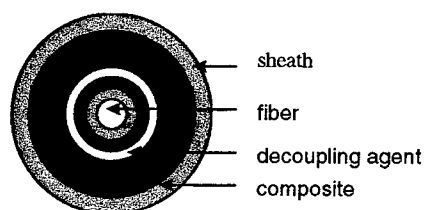


Fig 3 : microcable structure

Characteristics

The main parameters which can be specified are :

- cable diameter : 1.2 mm
- fiber diameter : between 180 and 250 µm.
- cable weight : 2 g/m
- minimum bending radius : 10 mm
- ES = 2000-4000 daN,

Curvature Resistance. Several curvatures of 10 mm radius are applied on the cables according to the fig.4. This system allows also curvature fatigue evaluations.

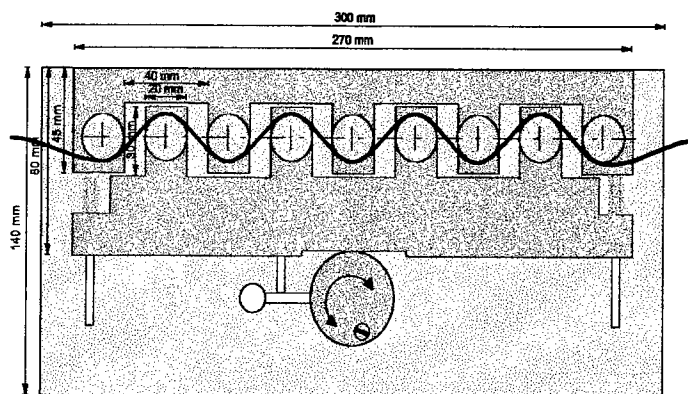


Fig.4 : curvature resistance measurement system

All the tests performed provided attenuation increases lower than 0.03 dB. After the tests, the coatings are analyzed.

Crushing Resistance. This test has shown that the microcables do not attenuate up to 25 daN/cm applied during 15 minutes.

Temperature Behavior. The microcables were subjected to a thermal cycle, between -30°C and +70°C : the attenuation variation was lower than 0.05 dB/km, like shows the fig.5 :

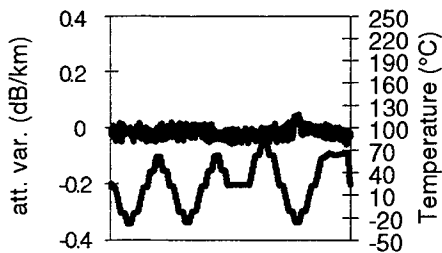


Fig. 5 : attenuation variation during thermal cycling

FIELD TRIALS CONDUCTED, INCLUDING OUTSIDE AND INDOOR INSTALLATIONS [5]

Several installations in real conditions of a terminal line and indoor cabling have been realized. The characteristics of the microcables allow fast (around 1 hour to install 200 m in aerial/building), easy and low cost installation methods for duct, building and aerial configurations (easy blowing, pushing..., low cost and miniaturized connectors, crimping clamps...)

Blowing-Pushing Field Trials

Several trials which demonstrated that only a few minutes are sufficient to blow / push 200 m of the microcable in a microduct of 6 mm internal diameter with 20 bends of 30 mm bending radius, without added loss after blowing, have been carried out.

Aerial and building installations

These fields trials show the multi-uses application of the cables and the excellent behavior of the fiber after several months on the field.

The fig. 6 schematizes the installation on our experimental site : around 250 m of different microcables are installed in outside and indoor

configurations including several crimping systems, connectors and door wedges.

On the outside circuit, 2 microcables (bimodule) are associated according to the fig.7 ; the sheath can be easily torn to separate the microcables for a mono-fiber indoor installation.

If a greater tensile strength is necessary, one or two microcables can be associated with one strength member ; a structure example is shown on the fig. 8.

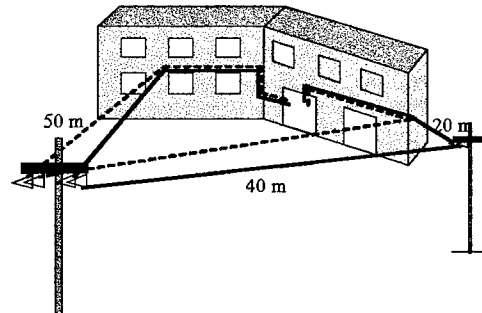


Fig.6 : test line in real conditions

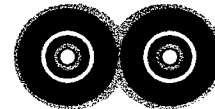


Fig. 7 : two microcables association

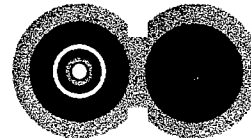


Fig. 8 : microcable and strength member association

The fig. 9, 10 and 11 represent some photos of the installations.

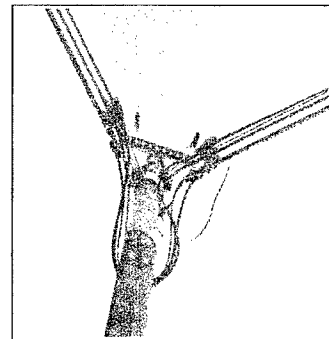


Fig. 9 : bimodule size compared to classic cables

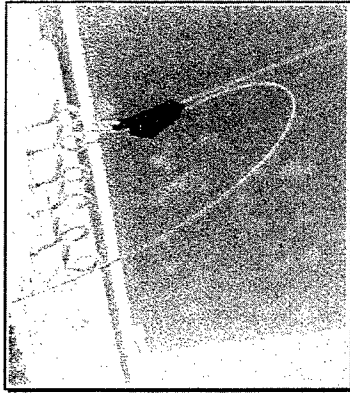


Fig. 10 : low cost and simplified crimping clamp

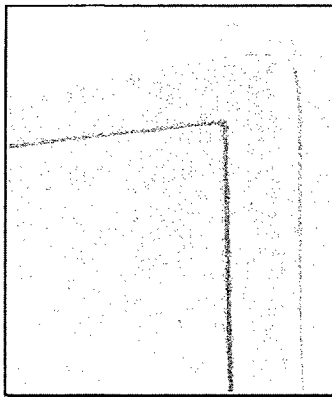


Fig. 11 : sticking or fastening of almost invisible cable in an apartment

The fig. 12 represents the OTDR graph of one line comprising 5 connectors, 4 crimping clamps and 5 door wedges : after one year installation, the global loss has not changed and is lower than 1 dB at 1.55 μm .

Some values of the added loss in harsh conditions (wind, snow...) are reported in the table 2 and show the excellent behavior of the microcables.

	wind 95km/h	T°= - 5°C	T°= +30°C	snow
$\Delta\alpha$ (dB)	0.005	-0.03	-0.02	0.02

Table 2 : added loss, in harsh conditions, of the microcables installed since one year

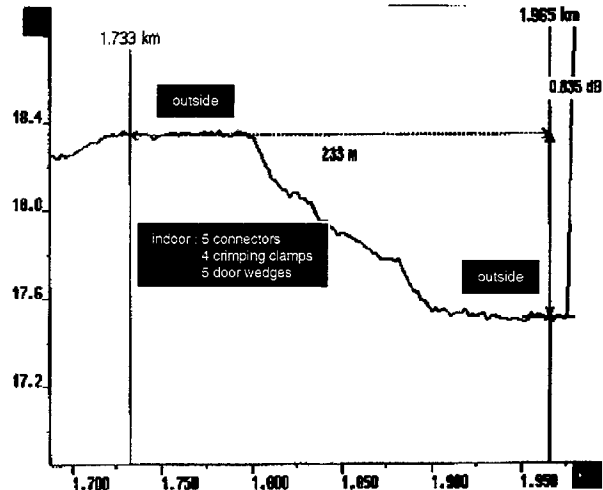


Fig. 12 : OTDR graph at 1.55 μm of one global line after 1 year installation

The evolution of the fibers characteristics (corrosion parameter, coatings behavior and adhesion to the silica...) after several months installation will be also analyzed.

In view of this excellent global behavior, a pre-industrialization of the microcables and their accessories is in progress to realize more important field trials during the next months.

A NEW VERY SENSITIVE METHOD FOR IN-SITU OPTICAL FIBER CHARACTERISATION

Different populations of fibers have been tested in microcables :

- industrial fibers : F3, F7
- studying fibers : F1, F2, F4

Their coatings have been observed and their adhesion to the silica after microcabling has been analyzed.

The following table 3 summarizes the results obtained :

	coatings in classic cables	observation * in micro- cables	adhesion after micro- cabling **
F7	good	good	good
F3	limit	damaged	bad
F4	/	damaged	bad
F1	/	good	good
F2	/	good	/

* microscopy observation

** DMA measurement

Table 3 : fibers behavior after cabling

These observations show that some fibers are not usable in the microcables whereas they are used without problems in classic cables. The microcables, having a tight structure and undergoing important bending radius, stress the fibers more than a loose structure. To support this environment, the fibers must have coatings more adherent to the silica.

Coatings Degradation

After F3 and F4 extraction out of the microcables, an important coatings degradation has been observed (fig. 13 and 14).

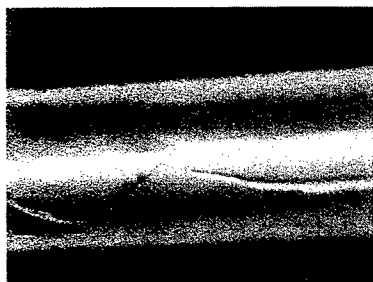


Fig. 13 : coating crack

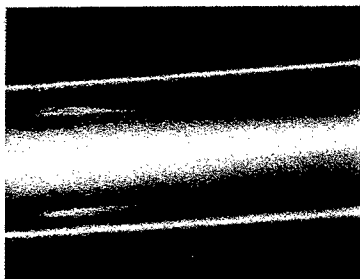


Fig 14 : primary coating detachment

These phenomena are generally observed after maintaining a 10 mm radius curvature during a few days but can also occur without stresses. They are due to a low initial coating adhesion on the silica.

So, to maintain the fiber resistance during all its cable life and in order to elaborate new specifications for distribution fibers and cables, it is necessary to understand the different behaviors observed. For that, it is essential to analyze the coatings characteristics before and after aging and cabling.

The most important characteristic is the adhesion on the silica and its evolution after aging or cabling.

In this chapter, a DMA (Dynamic Mechanical Analyzer) method developed for in-situ analysis on fibers is described.

A New DMA Measurement Method for optical fibers in-situ analysis [5]

DMA Principle. DMA permits to measure the modulus, glass transition temperature, $\tan\delta$, stress damping, flowing or relaxation characteristics,... by applying to a sample a sinusoidal stress and measuring the resultant deformation. The sample response can be studied according to temperature, time, frequency and amplitude of the stress.

The DMA is schematized on the fig. 15.

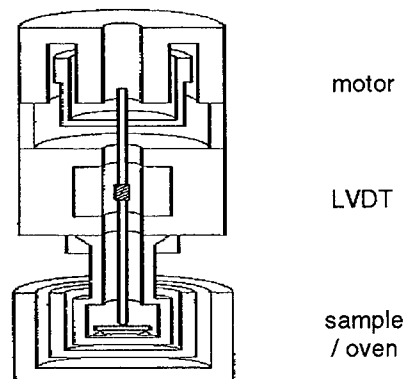


Fig. 15 : DMA schema

DMA specifications :

- Force : 1 to 2500 mN \pm 1 mN
- Temperature : -170 to 500 °C \pm 2°C
- Amplitude : 1 to 650 μ m \pm 0.01 μ m
- Frequency : 0.01 to 51 Hz
- Modulus range : 10^4 to 10^{12} Pa \pm 10 Pa

DMA is used to evaluate the adhesion of the inner coating directly on the fiber. This type of measurement permits to follow the adhesion evolutions after aging or cabling in real conditions.

The sample type used for analysis, the corresponding measurement procedure, the evolutions observed after fibers aging, microcabling and microcables aging are presented.

Sample Definition. The following sample allows to measure the primary coating adhesion characteristics (fig. 16).

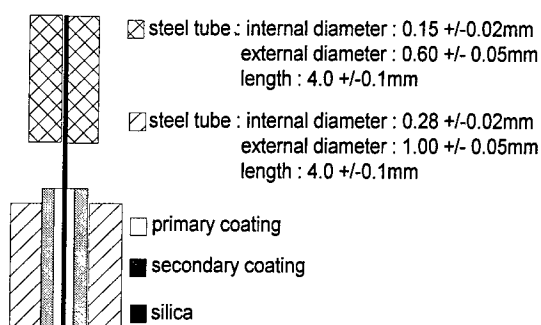


Fig. 16 : sample used for the adhesion characterization on optical fibers

Measurement procedure. The procedure gave below permits to obtain the coating strip temperature on typical curves like the one shown on the fig. 17 ; a sample before and after stripping is represented on the photo of the fig.18.

Procedure :

mode : temperature scanning
temperature range : from -25°C to 140°C
speed : 5°C/min
dynamic force applied : 490 mN
static force : 540 mN
frequency = 1Hz

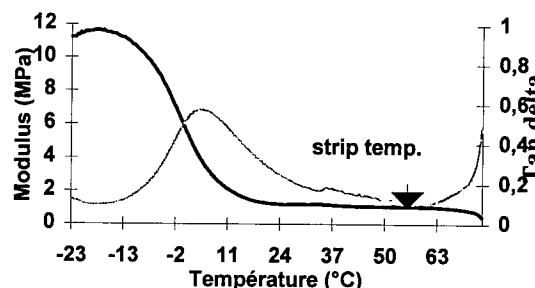


Fig. 17 : curve type obtained with the adhesion measurement method

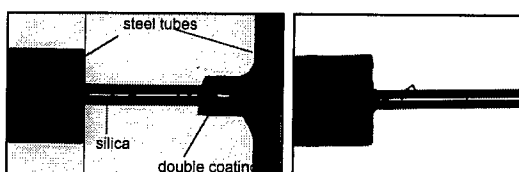


Fig. 18 : a sample before and after stripping

The comparison of different optical fibers strip temperatures gives a very good idea about the relative adhesions and their evolutions according to the studied coating type.

Results. A fiber will have a good fatigue resistance and a good behavior in cable if its initial coating adhesion on the silica is good (corresponding to a high strip temperature) and if it does not vary after aging and cabling. So, the strip temperature (T_s) for different fibers after fiber aging, cabling and cable (without sheath) aging has been measured.

The table 4 gives our principal results obtained on fibers with polymeric coatings ; T_s evolutions for fibers with hermetic coatings are under investigation.

The results show that :

- F1 has the higher initial adhesion
- after cabling, T_s increases for fibers F3 and F4 ; in fact, the fibers receive a supplementary UV dose during the cabling. So, we measured the polymerization degrees (by IRTF) for all the fibers and found that F3 and F4 had a lower initial polymerization degree which increased after cabling, explaining the T_s increases.

- F1 is the only fiber for which Ts does not vary after aging and cabling.
This conclusion is well correlated with the corrosion parameters previously measured.

	F3	F7	F4	F1
initial Ts	60°C	100°C	50°C	135°C
ΔTs after 2d. in 60°C water	-55°C	-65°C	-25°C	< ±5°C
ΔTs after cabling	+40°C	-5°C	+20°C	< ±5°C
ΔTs after 2d. in 60°C water (in cable)	+10°C	-20°C	+10°C	< ±5°C

Table 4 : strip temperature evolutions
for different fibers after aging

CONCLUSION

In preparation of the access network, two new types of low cost coatings have been developed. They permit to obtain distribution fibers with an improved fatigue resistance, maintained after aging and without initial breaking strength decrease.

These resistant fibers have been introduced in a new low cost multi-uses microcable structure designed to support important curvature ($r_c = 10$ mm) and harsh environments ; the microcables are easy and fast to install (small diameter and weight), allow the use of fast, easy and low cost installation and connection methods for duct, aerial and building configurations.

The DMA method used to evaluate the coating adhesion to the silica has permitted to see that, to be used in small and tight cables, the distribution fibers must have coatings presenting a better initial adhesion than the classic fibers. This adhesion has to be maintained after aging and cabling. The DMA is an apparatus very useful to define the future access network fiber and cable specifications.

The works performed have permitted to obtain two distribution fiber types and a drop microcable presenting an excellent global behavior.

ACKNOWLEDGMENT

The authors want to express their thanks to Mr. ERIKSON from « Fibres et Techniques » for his collaboration in the microcables development.

REFERENCES

- [1] « Recent trends in and new applications for carbon-coated optical fibers »
NTT - IWCS 95
- [2] « Hermetic and polymeric coatings for military and commercial applications »
ALCATEL - IWCS 95
- [3] « Manufacturing and characterization of colored, fatigue resistant optical fiber »
ALCATEL - IWCS 96
- [4] « A new multi-purpose coating for optical fibers with excellent aging behavior »
Plasma Optical Fiber - EFOC&N' 94
- [5] « Influence de l'environnement immédiat de la fibre optique sur son comportement en câble »
Anne -Cécile REAU thesis - 26/11/96

BIOGRAPHY



Annie MORGAND, born in 1968, received her diploma of Engineer in Sciences of Materials in 1991. She joined CNET to study optical fibers and cables materials. Since 1994, she works on resistant fibers and drop cables for the access network.

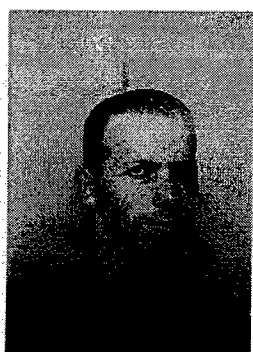


Yves RUELLO received his engineering degree from Ecole d'Application des Hauts Polymères of Strasbourg in 1981 and joined CNET in 1983. He is in charge of the « Resistant optical fiber and drop cable for the access network » group.



Daniel BOSCHER, born in 1951, received his engineering degree from the Ecole Nationale Supérieure des Arts et Métiers and joined CNET in 1973. Working on circular waveguide until 1979, he then joined the optical fibers and cables department.

Since 1993, he is manager of the « Fibers, Cables and Measurement » Department.



Benoît CADIER, born in France in 1972, received in 1995 his engineering degree in Physics and Chemistry of Materials (Magistère Matériaux) and his DEA (Diplôme d'Etudes Approfondies) in Solid Chemistry from the University of Rennes, Fr.

In 1995, he joined the CNET to prepare his Ph. D. degree.



Anne Cécile REAU, born in Bordeaux (FRANCE) in 1969 received her engineering degree in ceramics in 1993. She joined C.N.E.T. in 1993 and obtained her Doctorate degree in science of materials in 1996.

APPLICABILITY OF UV CURABLE URETHANE ACRYLATE COATING AT HIGH DRAWING SPEED

Masanobu Sugimoto, Yuji Naito, Hirofumi Uchida, Zen Komiya, Takashi Ukachi

Tsukuba Research Laboratory, Japan Synthetic Rubber Co. Ltd., Tsukuba Japan

ABSTRACT

As an increase of the drawing speed of optical fiber, applicability of UV curable coatings to the drawn glass or to the primary coating is becoming important characteristics for the coatings. At high share rate, the UV curable coatings are expected to behave as non-Newtonian fluid, which means the viscosity would change non-linearly at high share rate. Flow behaviors of some representative coatings were measured by using a slit-die rheometer (SDR), and the structure-property relationship was investigated. The coatings were applied to a metallic wire running up to 1800 m/min using a drawing tower for optical fiber to evaluate their practical applicability. The drawing experiments revealed that the absolute viscosity is one of the most important factors which controls the applicability at high drawing speed.

INTRODUCTION

Recent strong demand for optical fiber cable is resulting in shortage of optical fibers. It is necessary not only to construct new drawing towers but to increase the drawing speed for high productivity. There are several subjects to be solved to achieve high speed drawing. For example, effective cooling methods for the drawn glass fiber would be necessary. Consistency of the fiber configuration from the beginning of the production to the end would be another subject to be maintained. Regarding UV curable urethane coatings for the optical fibers, fast cure speed and stable application at high drawing speed would be the most important characteristics.

UV curable urethane coatings are the most widely used material for the protection of the optical glass fiber. Usually the coatings consist of polymeric urethane acrylate (oligomer), acrylate monomers, and photo initiator. Since the urethane acrylate coatings are polymeric material, the viscosity would change non-linearly at high share rate, which is called non-Newtonian flow. Non-Newtonian flow has been studied and well-established for conventional polymers.¹ Especially in the wire and cable industry, flow behavior of polyethylene has been studied very well.² In contrast to polyethylene, studies on the UV curable urethane acrylate coatings are rare. The most significant difference of the UV curable coatings from polyethylene is that they are essentially a mixture of low molecular weight acrylate monomers and urethane acrylate oligomer of which molecular weight is relatively low compared with that of polyethylene. In this paper, we report the evaluation of the flow behavior of the UV curable urethane acrylate coatings for fiber optics and relation to the applicability at high drawing speed.

EXPERIMENTS

Materials

Urethane acrylate based secondary coatings with oligomers with various molecular weights were prepared (Table 1). The content of oligomer for each coating was kept constant. A secondary coating S-3 has an oligomer with twice of molecular weight as the one in S-1. Tensile properties of the cured film of these coatings are included in Table 1.

Table 1. Formulation and Physical Properties of Coatings.

Formulation	S-1	S-2	S-3
Oligomer A(Mn=1466) ¹⁾	50.2		
Oligomer B(Mn=1816) ¹⁾		50.2	
Oligomer C(Mn=2816) ¹⁾			50.2
(Oligomer content)	(50.2)	(50.2)	(50.2)
Monomer A	19.7	19.7	19.7
Monomer B	9.9	9.9	9.9
Monomer C	20.2	20.2	20.2
Tensile properties of cured film ²⁾			
Young's modulus (MPa)	1450	745	441
Tensile strength (MPa)	56	42	63
Tensile elongation (%)	57	63	94

1) Number molecular weight calculated from the stoichiometry of the raw materials for the oligomer preparation.

2) Cured at 1 J/cm² under air. Film thickness is 200 μ m.

Viscosity measurements

For low share viscosity, type B rotating viscometer was used. We defined that the data obtained by the type B viscometer as zero-share viscosity. For high share viscosity, a Slit-Die Rheometer (SDR) was used. Structure of the SDR is depicted in Figure 1.

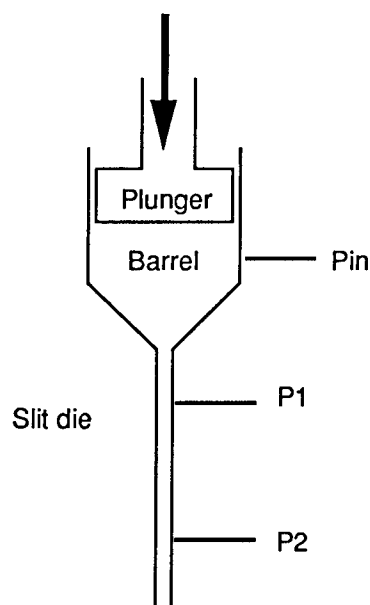


Figure 1. Structure of the Slit-Die Rheometer (SDR).

The slit-die has square cross section so that pressure sensors can be placed on the flat surface. This is the most remarkable difference from a capillary rheometer which has cylindrical

surface to which a pressure sensor is difficult to attach (see Figure 2).

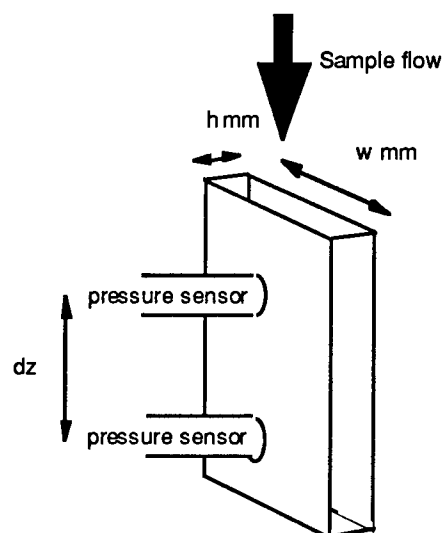


Figure 2. Structure of the slit die.

The instrument was made by Japan Synthetic Rubber Co. Ltd., called JSR-SDR. The share rate can be controlled in the range of $10^0 \sim 10^6$ sec⁻¹ by varying size of the slit and the speed of the plunger. The temperature is controlled from 27 °C to 60 °C. A measurement at given temperature and four different share rates takes about 10 ~ 15 minutes. The details of the

measurements are discussed in the following section.

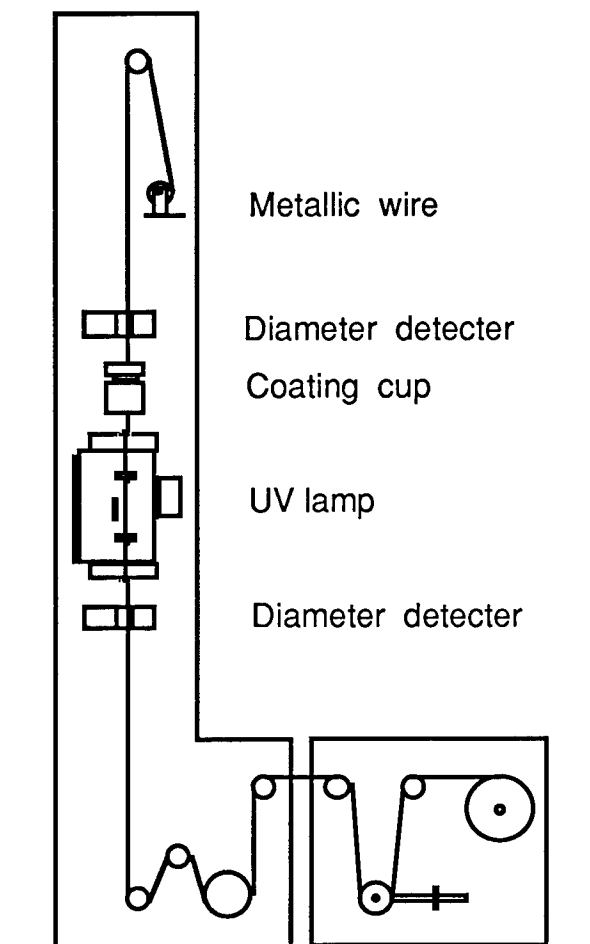


Figure 3. Schematic diagram of drawing experiment.

Drawing experiments

Drawing experiments were carried out using metallic wire of 125 μm in diameter instead of optical fiber glass because one does not need to worry about the cooling of the drawn fiber. By using a metallic wire, one can eliminate the effect of the temperature of the substrate to which the coatings are applied. Configuration of the drawing experiments is depicted in Figure 3. The urethane acrylate coating was applied on the wire with a thickness of 40 μm . The temperature of the coatings was controlled at the reservoir. The coating was lead to the coating cup through an insulated nylon pipe. The draw speed was increased from 200 to 1800 m/min. The diameters of the wire and the coated wire were monitored by laser detector. The coating was

cured by using QRU-2373-C UV lamp with 7 kW input power made by ORC manufacturing Co., Ltd.

RESULTS AND DISCUSSION

Non-Newtonian behavior of the coatings

The share rate applied to the liquid coating on the optical glass fiber can be calculated assuming linear flow rate distribution in the coating cup. When the fiber glass runs at 600 m/min and the coating is applied to 30 μm thickness, the share rate is $3.3 \times 10^5 \text{ sec}^{-1}$. At 2000 m/min of draw speed, it reaches more than $1 \times 10^6 \text{ sec}^{-1}$. There are several methods to measure viscosity at high share rate. The most popular method would be a capillary rheometer. This method uses the pressure difference between inlet and outlet of the capillary for calculation of viscosity. Usually the outlet pressure is atmospheric one and the inlet pressure is the one applied to the sample. Since the capillary is very thin, the pressure loss at the inlet of the capillary is unavoidable. For accurate measurements, it is necessary to use several types of capillary with different length to cancel the pressure loss. In contrast to the capillary rheometer, the SDR does not need to consider pressure loss at the approach into the slit-die.³ As shown in Figure 2, the SDR has flat face in the slit-die, two pressure sensors can be put *inside* of the slit. These pressure sensors enable us to measure the pressure difference directly and in a real-time way. By using pressure values of two sensors, the share stress (τ) is calculated using equation (1) shown below, where h is the thickness of the slit and dp/dz indicates pressure gradient between two pressure sensor.

$$\tau = \frac{h}{2} \times \frac{dp}{dz} \quad (1)$$

The apparent share rate ($\dot{\gamma}_a$) is calculated by the amount of flow (Q) and the shape of the slit (w and h) as follows.

$$\dot{\gamma}_a = \frac{6Q}{wh^2} \quad (2)$$

Figure 4 shows viscosity - share rate plot at three different temperatures for the coating S-2. The

share rate was varied in the range of $10^3 \sim 10^6$ sec^{-1} .

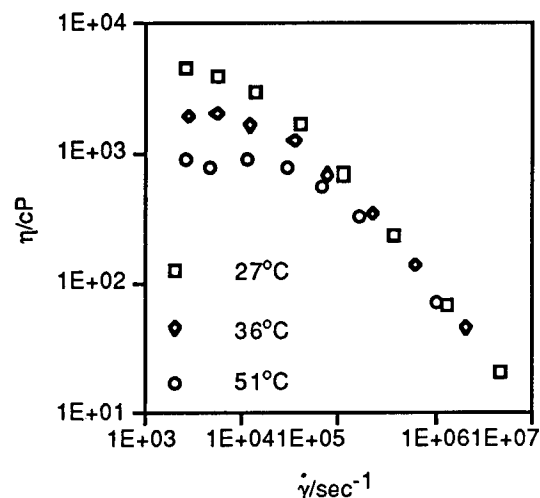


Figure 4. Viscosity-share rate plot of S-2 obtained by SDR measurements.

The viscosity of the coating decreased non-linearly as the increase of the share rate exhibiting clear non-Newtonian flow. Comparing to conventional polyethylene, decrease in viscosity starts relatively high share rate region because of lower average molecular weight of the oligomer in the coating, S-2. For example at 57 °C, when the share rate exceeds 10^4 sec^{-1} , the viscosity of S-2 starts to decrease. The share rate of 10^4 sec^{-1} corresponds to the draw speed of 60 m/min. This suggests that the coating always behaves as a non-Newtonian fluid when it is applied to the optical fiber. By using a time-temperature superposition method, a master-flow-curve for coating S-2 was made. The calculated shift factor (ΔT) plot is shown in Figure 5 and the master-flow-curve for S-2 at 27 °C is depicted in Figure 6.

All these results are completely the same as what is observed for high molecular weight polymers. Namely, non-Newtonian behavior and master-flow curve complying with time-temperature superposition are commonly observed. If the coatings behave similarly as high molecular weight polymer, the molecular weight of the oligomer in the coatings would have a large effect on the flow behavior.

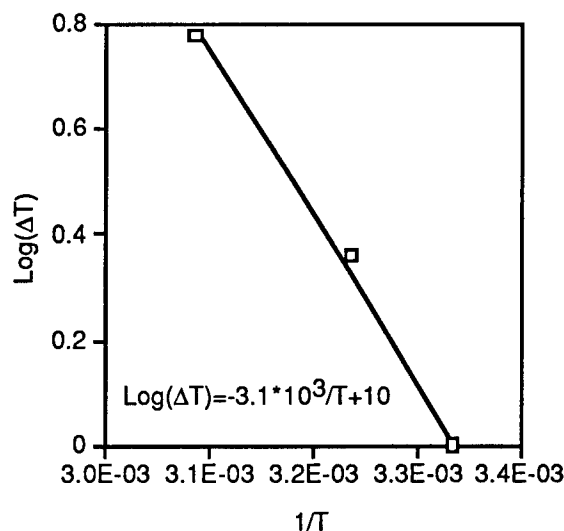


Figure 5. Shift factor plot for S-2.

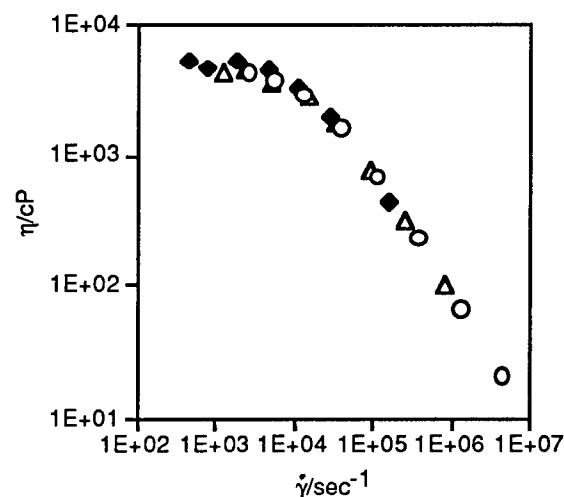


Figure 6. Master-flow curve for S-2 at 27 °C; ○ : derived from the data at 27 °C, Δ : derived from the data at 36 °C, and ♦ : derived from the data at 51 °C.

The other two coatings were evaluated by the SDR and their master-flow-curves were plotted in Figure 7. The master-flow-curves were plotted at the temperatures that all coatings have the same zero-shear viscosity for the sake of comparison of their non-Newtonian behavior. As

shown by the magnified plot inserted in Figure 7, the difference among the coatings is very small.

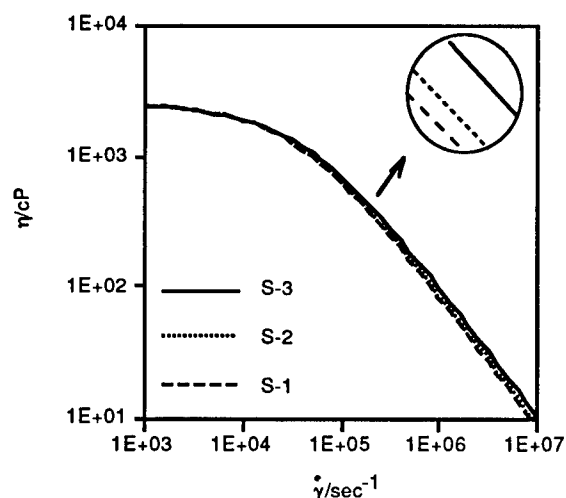


Figure 7. Master-flow-curves of S-1, S-2, and S-3. Flow-curves are plotted at temperatures at which all the coatings have the same zero-share viscosity.

It is regarded that the non-Newtonian flow of polymer is originated from the entanglement of long polymer chain and the interaction between each chemical component. Although the UV curable coatings contain polymeric component, the molecular weight was too small to see the effect of the entanglement by changing molecular weight from 1500 to 2800. This result suggests that the main factor which controls the flow behavior of the UV curable coating is the interaction between each chemical component. It is known that the most strong interaction between chemical components is dipole-dipole interaction. Especially in the case of the UV curable urethane acrylate, strong hydrogen bonding between urethane group constitutes one of the strongest dipole-dipole interaction. Since such interaction can easily lost at high temperature, it is expected that the viscosity is greatly affected by temperature. Figure 8 shows the temperature dependence of the zero-share viscosity of the three coatings. Table 2 lists the viscosity data, molecular weight of the oligomer, and urethane group concentration of each coating.

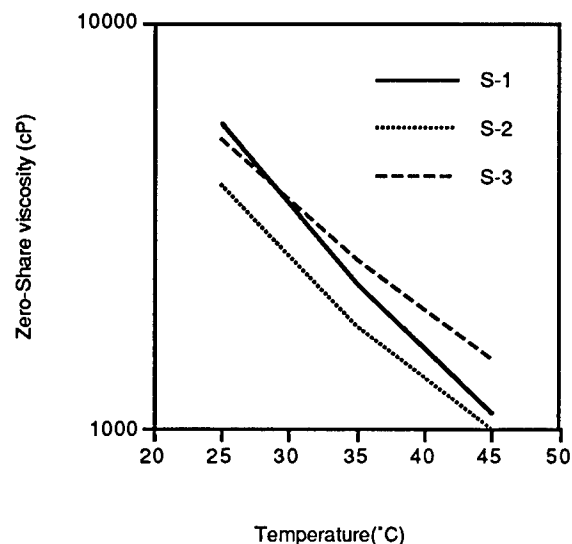


Figure 8. Temperature dependence of zero-share viscosity of the coatings.

It is clear that the temperature dependence is not directly related to the molecular weight of the oligomer but to the urethane group concentration which engages in strong hydrogen bonding. It should be noted that, the absolute viscosity can be affected not only by urethane group concentration but also by molecular weight of the oligomer. However, it is true that the higher the urethane group concentration becomes, the greater the viscosity changes by temperature change.

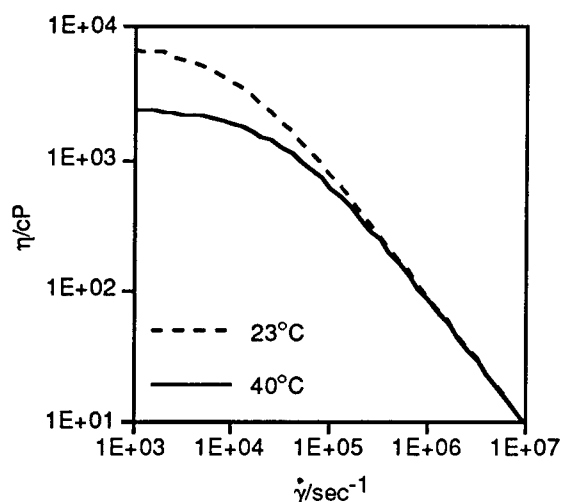
Figure 9 shows viscosity-share rate curves of S-2 at 23 °C and 40 °C. Nevertheless the changes in the curve by the molecular weight of the oligomer were small, the plot is affected dramatically by changing the temperature. The viscosity of the coating becomes less sensitive to the share rate at high temperature. It seems that the best way to make the viscosity change as small as possible at high share rate would be to increase the temperature of the coating.

Table 2. Zero-share viscosity and urethane group concentration of the coatings.

	S-1	S-2	S-3
Viscosity (cP)			
@ 25 °C	5600	4000	5200
@ 35 °C	2300	1800	2600
@ 45 °C	1100	1000	1500
Urethane concentration (mmol/g)	2.0	1.6	1.1
MW of oligomer	1466	1816	2816

Table 3. Maximum drawing speed of S-1, S-2, and S-3 on metallic wire.

Coating	Temperature (°C)	Zero-share viscosity (cP)	Max. drawing speed (m/min)
S-1	40	1600	1500
S-2	37	1600	1500
S-2	23	5000	1250
S-3	43	1600	1500

**Figure 9. Viscosity-charge rate relationship of S-2 at different temperature.**

Drawing experiments

The viscosity data at high temperature suggest that the changes in the molecular weight of the oligomer have little effect on the applicability of the coating at high draw speed. To confirm this speculation, coatings S-1, S-2, and S-3 were applied to a metallic wire using a coating cup for optical fiber coating. The temperature of each coating was controlled to the one at which each coating showed the same zero-share viscosity. The drawing experiments were started at slow drawing speed monitoring the diameters before and after coating. The drawing speed was gradually increased by adjusting the pressure

applied to the coating to keep the coating thickness constant. Usually, as the increase of the drawing speed, a sudden fluctuation of the coating thickness started and the average coated layer became thinner. We defined that the draw speed where the fluctuation started as maximum drawing speed. The maximum drawing speed for the coatings are listed in Table 3 including the experiments done by changing the temperature of the coating S-2. As expected from the SDR measurements and other results mentioned above, three coatings which behave similarly at high share rate gave the same maximum drawing speed. In contrast, S-2 at low temperature showed poor applicability. At a glance it seems that this result is also in good accordance with the viscosity-flow curves obtained by the SDR measurements. However, the fact that S-2 at 23 °C reached 1250 m/min of draw speed indicates the share rate must be more than 10^5 sec^{-1} . Figure 9 indicates negligible difference in viscosity between curves at 23 °C and 40 °C more than 10^5 sec^{-1} of share rates. In this case, the flow-curve did not represent the results of the drawing experiments. This implies that there must be other factors which contribute to the applicability of the coating at high drawing speed.

CONCLUSION

It was demonstrated that the UV curable urethane acrylate coatings behaved as non-Newtonian fluid at high share rate. The

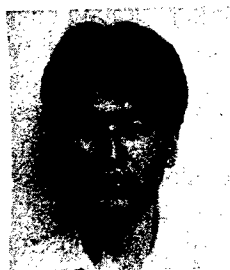
sensitivity of the viscosity to the share rate was mainly controlled by changing the temperature not by the molecular weight of the oligomer different from conventional high molecular weight polymers such as polyethylene. The drawing experiments showed good agreement with the results obtained from the SDR measurements as far as the molecular weight of the oligomer concerned.

It was shown that stable applicability at high drawing speed could be realized by keeping the coating temperature high. It seemed that the high temperature had made the coating less sensitive to the changes in the share rate. However, the viscosity-share rate data did not indicate the difference in the applicability. It is

necessary to consider other factors such as affinity with the substrate and the coating.

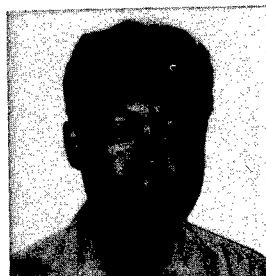
REFERENCES

- ¹ C. D. Han, *Rheology in Polymer Processing*, Academic Press, New York, 1976. D. Romanini, *Polym.-Plast. Technol. Eng.*, **19**, 201 (1982).
- ² For example, S. T. E. Aldhouse, D. McMahon, J. E. Robinson, *Plastics in telecommunication IV*, **32**, 1, (1987).
- ³ C. D. Han, T. C. Yu, *Poly. Eng. Sci.*, **12**, 81 (1972). C. D. Han, K. U. Kim, *Trans. Soc. Rheo.*, **17** : 1, 151 (1973). C. D. Han, *Trans. Soc. Rheo.*, **18** : 1, 1633(1974).



Masanobu Sugimoto
Tsukuba Research
Laboratory,
Japan Synthetic Rubber
Co., Ltd.
25 Miyukigaoka,
Tsukuba, 305 Japan

Masanobu Sugimoto received his M. E. degree in Material Science from Nagoya Institute of Technology and joined Japan Synthetic Rubber Co., Ltd. in 1991. He has been engaged in research and development of radiation curable materials for optical fiber coatings.



Zen Komiya
Tsukuba Research
Laboratory,
Japan Synthetic Rubber
Co., Ltd.
25 Miyukigaoka,
Tsukuba, 305 Japan

Zen Komiya received his Ph. D. in Organic Chemistry Hokkaido University in 1984 and joined Japan Synthetic Rubber Co., Ltd. He was engaged in research and development of new transparent plastics and currently has been engaging research and development on radiation curable materials.



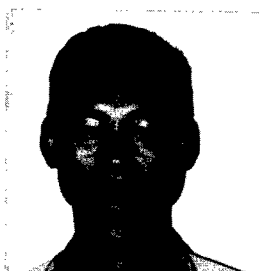
Yuji Naito
Tsukuba Research
Laboratory,
Japan Synthetic Rubber
Co., Ltd.
25 Miyukigaoka,
Tsukuba, 305 Japan

Yuji Naito graduated in Chemical Engineering Course of Sagamidai Technical High School in 1971 and joined Japan Synthetic Rubber Co., Ltd. He has been engaged in research and development on plastics and rubber. He is now a chief engineer of radiation curable materials group.



Takashi Ukachi
Tsukuba Research
Laboratory,
Japan Synthetic Rubber
Co., Ltd.
25 Miyukigaoka,
Tsukuba, 305 Japan

Takashi Ukachi received his B. E. degree in Biophysics and Bioengineering from Osaka University and Ph. D. in Material Science from Kyushu University. He started his professional carrier at Japan Synthetic Rubber Co., Ltd. in 1976 and has been engaged in research and development of radiation curable materials.



Hirofumi Uchida
Tsukuba Research
Laboratory,
Japan Synthetic Rubber
Co., Ltd.
25 Miyukigaoka,
Tsukuba, 305 Japan

Hirofumi Uchida received his B. E. degree in Material Science from Hokkaido University and joined Japan Synthetic Rubber Co., Ltd. in 1990. He was involved in thermo plastics processing and has been engaged in the research and development of radiation curable materials.

ENVIRONMENTALLY FRIENDLY STRATEGIES FOR TELECOMMUNICATIONS PROVIDERS

Trevor N. Bowmer

**Bellcore - Network Integrity Solutions
445 South Street, Morristown NJ 07960**

ABSTRACT

The management of environmental risks is becoming increasingly costly and complex. In this paper, we review the business drivers raising these environmental issues and their possible solutions from the standpoint of telecommunications companies. Various case studies of wire and cable products are used to illustrate rationales for environmental strategies as well as to examine the positive and negative collateral effects of "green" material choices.

INTRODUCTION

The management of environmental risks is becoming increasingly costly and complex for telecommunications companies¹⁻³. Disposal of products requires knowledge of their chemical composition and the multitude of associated laws and regulations. Local, state, federal and international laws/regulations are impacting not only the disposition and disposal of many telecommunications products, but also adding to the initial purchase price.

Recent trends have developed around "Industrial Ecology" concepts using cost/benefit analysis tools¹⁻⁴ to identify, trace, track and quantify dollar and environmental costs for individual products and materials from a total life-cycle assessment (LCA)^{2,3,5}. As these costs are incorporated into the manufacturer's design and processing decisions, environmental costs will become a more visible component in the purchase price of equipment. The best environmental solutions are designed to be

- (a) proactive, not simply reactive to laws
- (b) incorporated early in product idea/design
- (c) open and flexible to new opportunities/data
- (d) broadly based rather than local

From the perspective of a telecommunications provider (TP), there are numerous business drivers that insert environmental factors into their long term business plans including -

- (a) Regulatory and Legal Compliance
- (b) Reduced Disposal Costs
- (c) Reduced Liability
- (d) Competitive Advantage of a "Green" Image
- (e) Increased Operating Efficiencies
- (f) Reductions in Product Total Life-Cycle Cost

The consequences of environmental regulations and standards will be most sharply felt by TPs in the range of available products and in the disposal options for plant at the end of its useful life. The economic choice between disposal in a landfill, reuse as very low value products or use as fuel (i.e., incineration) is time dependent in that today's answer may change as regulations and disposal costs change^{6,7}.

As older plant and equipment is retired or replaced by fiber optic, hybrid-fiber-coaxial (HFC), or wireless architectures; the disposal of old central office switch equipment, cables and plant hardware components and other material assets will become significant in terms of asset value, recycling and reuse potential, and landfill/disposal costs. Partnerships with equipment suppliers or recycling companies can help minimize disposal costs². Partnerships with resellers/recyclers of equipment can enhance the dollar value of out-dated equipment as well as reducing the overall disposal costs and any future liability.

The introduction of any new product or material can result in unforeseen consequences and costs associated with new capital equipment, different installation practices/procedures, disposal of replaced equipment, and accommodation to changes in product performance or characteristics. Purely reactive strategies towards compliance and regulations

are typically more expensive and less effective from a pollution control aspect compared to the more cost-effective approach of proactive planning and partnerships with regulators and manufacturers^{1,3}.

MATERIALS PERSPECTIVE

The variety and amount of materials used in telecommunications networks are large. Over \$16 Billion dollars are spent each year to maintain, upgrade and expand the \$200 Billion dollar telecommunications network within the USA with an estimated \$2+ Billion dollars of apparatus and materials being purchased each year⁸.

Metals Pure metals are easily recycled since they can be melted and reformed, which avoids the high costs of mining/refining of metals from ores. Lead from batteries, steel from automobile bodies and aluminum from beverage cans are all excellent illustrations of good economics and environmentally-sound recycling. The prime problem in telecommunications equipment is one of separation of metals from plastic and ceramic components as well as separating the individual metallic elements from one another. The cost of disassembly to the individual element stage can not compete with the low cost of current feedstocks. The most effective remedy is to design products for disassembly so that the product or individual components are easy to reuse or replace.

Plastics Plastics are ubiquitous throughout the network not only in telecommunications cables but also found in structural supports, protective insulations, environmental seals, dielectric isolators, anti-corrosion coatings, encapsulants, water-resistant filling compounds and gels, battery cases, epoxy-based circuit boards, acrylic adhesives, and so forth. Thermoplastic resins can be mixed with each other along with a myriad of additives such as lubricants, fire retardants, impact modifiers, fillers, colorants, and pigments to customize materials for specific applications in the telecommunications plant.

Thermoplastic resins can be re-formed by heating to a high temperature (typically 150→300°C) and shaping the plastic by molding and extrusion processes. Thermoplastic polymers are more recyclable than thermoset plastics. Thermosets are crosslinked plastics

that are cured during processing with heat, Ultraviolet (UV) light or ionizing radiation (e.g., electron beam). Thermoset plastics cannot be easily melted and reformed since they typically degrade at high temperatures (>300°C) rather than melt and flow.

Although some polymers can be used as pure polymers with only a few percent of stabilizers and colorants, most plastics are a combination of polymer resins with an array of additives and property modifiers to customize the material properties. This ability to modify a polymer's properties provides the material scientist and design engineer with versatility in selection of the optimum material for specific products or applications. With the complex mixture that is a modern plastic material, care is required to ensure a uniform product with the desired properties is made from batch to batch over many millions of kilograms of production. The additives and modifiers include

- Plasticizers
- Hydrolysis Inhibitors
- Inorganic Fillers
- Colorants
- Impact Modifiers
- Lubricants
- Mold Release Agents
- Thermal Stabilizers
- Flame Retardants
- Ultraviolet Stabilizers
- Pigments
- Flow Modifiers
- Antistatic Agents

The "art" of mixing these components into a plastic resin that will process quickly and correctly with minimal degradation during manufacture, a long reliable life, at the lowest possible cost and fastest production speeds is not simple. The interactions between components can be complex and apparently minor changes in formulation have led to disastrous field failures⁹.

The plastics used in telecommunications applications have typically been high-end, high-value products carefully designed for long life (30+ years) with excellent dielectric and mechanical properties. Traditionally, a high premium has been placed on the quality and reliability of the materials used in these telecommunications products.

CABLE AND WIRE EQUIPMENT

There are over three million kilometers of buried cable containing 400 million wire pairs installed across the USA, which is evolving into an optical

Table 1. Materials Lists for Telecommunications Cables(*)

Component	Copper	Coaxial	Fiber	Power
Ducts/Outer Cover	PE or PVC	PE or PVC	PE or PVC	FR Cotton Braids
Jacket/Sheath	Lead PE or PVC Fluoropolymers	PE PVC	PE or PVC Fluoropolymers	CSPEs, Rubbers, CPEs, Polyolefins, Thermosets
Adhesive/Flooding Compounds	Acrylic Adhesives Hydrocarbon Gels	Hydrocarbon Gels	Hydrocarbon or Silica Gels	N/A
Shielding (Electrical)	Terneplate (tin- lead coated steel)	Aluminum Mesh or Foils	N/A	N/A
Outer Conductor	N/A	Aluminum	N/A	N/A
Inner Wraps Shielding	Polyester Wraps	Acrylic Adhesives	Polyester Wraps	Polyester Wraps
Plastic Core Components	Polyester Wraps Polyester Tapes	Acrylic Adhesives	PBT Buffer Tubes Polyester Rip Cords	N/A
Conductor/Fiber Insulations	Colored/Pigmented PE and/or PVC	Foamed PE Solid PE	Colored/Pigmented Urethane-Acrylates	N/A
Pigments and Colorants	Inorganic/Organic Dyes and Paints	N/A	Inorganic / Organic Dyes and Paints	Paints
Transmission Medium	Copper & Tin-Coated Copper	Copper-Clad Aluminum	Glass Fiber (Si,Ge,O)	Copper & Tin/Lead Coated Copper

(*) PE = Polyethylene,

PVC = Poly(Vinyl Chloride),

PBT = Poly(Butylene Terephthalate)

(*) FR = Fire Retardant,

CPEs = Chloro-PolyEthylenes,

CSPEs = ChloroSulfonated-PolyEthylenes

fiber (FTTC/FTTH) and hybrid-fiber-coaxial (HFC) networks. Although predictions of the copper cable plant being totally replaced before the turn of the century were made in the 1980s, transmission strategies and protocols extended the lifetime and capabilities of the copper network so that these cables will be around well into the next century. Large amounts of coaxial cables and intrabuilding copper cables are being placed to accommodate the broadband service and data demands from customers¹⁰. As the older vintage copper and coaxial cables are replaced, environmental issues will arise during the disposal and recovery of copper and aluminum material.

All copper and coaxial and fiber optic cables use similar plastic jackets, insulations, filling compounds and other protective materials. The same environmental issues about lead stabilizers and pigments that contain heavy metals need to be resolved for these new fiber-coaxial transmission technologies.

The oldest cables are sheathed with lead (Pb). Studies^{11,12} showed that lead compounds on cable sheaths are non-soluble or very sparingly soluble, and lead release into the environment from such lead cables is limited with 98% of the

released lead being retained within 50 mm of the cable surface. Therefore leaving superseded lead cables in place is a viable option or they can be mined/recycled for their copper and lead metals. Removal of lead sheath cable requires care to minimize dispersal of lead and lead compounds caused by abrasion of the sheath¹³.

Economics of Recycling

The components within telecommunications cables include a wide variety of materials as summarized in Table 1 above. Plastics and metals used in cables have been recycled (or at least recovered) in the manufacturing plant for many years. Scrap produced at the processing line can often be recycled or reused in the manufacturing plant since the separation and collection is straightforward and efficient. The composition of this scrap is accurately known and therefore easily handled, reformulated with additional stabilizers and reused.

Once combined into cables with filling compounds, bonded sheaths and other composite materials; the separation and collection issues make recycling and reuse much more difficult. The recycling of cable and wire products after many years of useful service has been actively pursued to reclaim the

valuable copper resource in the conductors. Such intermingled plastic components can only be recycled into low value products (plastic cones, mats, park seats, etc.). Currently the economic driving forces for recycling are the price of copper (~\$2.20/Kg) and the disposal costs of up to a maximum of \$300-400/tonne for PVC wastes contaminated with lead.

Table 2. Economics of Cable Recycling¹⁴

Cable Type	Material Value of Scrap Cable (\$/meter)	
	Copper	"Fluff" landfill cost
Indoor Switchboard	\$0.52	- \$0.06
Outdoor Aircore Duct PIC Cable	\$14	- \$0.015

The "fluff" in Table 2 is non-toxic fibrous waste consisting of paper, cotton, shredded plastic with trace metal contamination. For a single TP, the cost of landfilling this fluff could be approximately \$250,000 to \$300,000 per year. The cost for landfilling is prorated by the hazard classification of the "fluff" as defined by TCLP test results. The TCLP test¹⁵ for "leachable" lead (Pb) contamination in waste simulates a worst case leaching situation where highly acidic seepage is envisioned percolating through a landfill.

Across the USA, about 180 million Kilograms (Kg) of cable are scrapped annually. A major fraction (40%) of this weight comes from lead sheath cable that is being replaced with newer technology. Approximately, 16-18 million Kg of plasticized PVC and polyethylene recovered from these operations is landfilled. The opportunities for telecommunications companies in this recycling/scrap business include (1) selling plastic byproducts from scrap cable, and (2) purchasing cables with recycled plastics.

The 16 million Kg of recovered plastic could be worth as much as \$3 million if the contamination and quality issues that surround the recovered plastics could be solved. Currently, companies pay to landfill this plastic byproduct and these costs could be as high as \$300-400/tonne if this waste is designated hazardous waste owing to the presence of lead. The lead comes from lead-based stabilizers in the insulations and tin-lead coatings on Terneplate shielding and the copper conductors. The ability of recyclers to deal with these materials and re-use these

plastics economically is limited by this lead and the complicated mixture of plastics that typically comes off a cable chopping line. Such a polymer mixture will not melt and flow uniformly and therefore can not be extruded or molded consistently.

The cost of recycling even a well defined plastic product streams is considerable - e.g. PET soda bottles costs \$185/tonne and PE costs \$190/tonne not including collection. The gathering, transport and separation steps required to transform cable scrap materials into useful commodities will only add to these costs. The recovery process delivers a product of inconsistent quality that passes through too many players including telecommunications companies, disposal companies, cable miners, materials recyclers, materials formulators and product manufacturers to make the plastics recycling process economically attractive at present. If landfill costs did rise dramatically, then incorporation of this plastic scrap into "low-value products" such as road cones, park seats, plastic/concrete composites for piers and other low-end products may become more attractive from a disposal cost and a total lifetime cost view. The ultimate low value product is to use the recovered plastics as fuel for burning to retrieve the heat of formation. Although technically this could still be called recycling, it would only be "green" in the very broadest sense of the word.

Optical fiber cables contain SiO₂ glass fibers doped with germanium (Ge) and phosphorous (P) and protected by crosslinked urethane/epoxy coatings. These coated fibers are placed inside plastic (PET) buffer tubes filled with water resistant gels of fumed silica suspensions in low molecular weight hydrocarbon oils. An ensemble of various buffer tubes or ribbon arrays containing multiple fibers are gathered together and further protected with filling/flooding compounds and sheathed in a polyethylene (HDPE) or poly(vinyl chloride) jacket. Recycling of materials in a fiber cable is difficult and not economically attractive. The costs associated with separation and purification of the glass and plastic components in a fiber cable far exceeds the manufacturing/processing costs of the virgin materials. Unlike copper cables, where the price of the copper helps drive the recycling business, there is no high-value material easily reclaimed from the fiber cable.

Perhaps as specific fiber cables become obsolete or unable to accommodate the new broadband demands, the cable may be reused for services requiring less stringent bit error rates or data speeds. That is, the traffic from copper cables and coaxial cables will migrate to older fiber cables as those fiber cables are replaced/superseded with new fiber cable systems. This traffic switch is an example of "software" recycling as opposed to the hardware recycling that reclaims materials and fabricates a new product.

Below we shall examine three case studies that illustrate the major issues surrounding the introduction of "green" material solutions into telecommunications wire and cable products.

CASE STUDY #1 - Power Cable Insulation

Conventional central office power and battery cables consist of tin/lead coated copper conductors insulated by crosslinked chlorinated rubbers and an outer cotton/rayon braid. Outer cotton braids and sleeveings are used to enhance the mechanical toughness of the softer rubbers and these braids are coated in fire-retardant coatings and paints. Various polyester wraps are used to protect the copper wires in the cable core from water and chemical attack (e.g., from sulfur in the insulation that can corrode unprotected copper). Environmental concerns with power cables arise from three materials -

- Tin-lead coatings on conductors
- Lead-based stabilizers in insulations
- Ozone-depleting chemicals in manufacture

Therefore these cables raise both a disposal issue and a "green" opportunity if a substitute insulation material can be found or developed.

Before candidate materials can be considered to replace traditional power cable insulations, the critical performance requirements need to be established or be re-assessed¹⁶. Purchasing requirements for mature products such as power cable typically contain implicit requirements that need to be made explicit when a new material is introduced. For example, if cables without braids are permitted then abrasion, cut-through and compression resistance all become

important and necessary additions to product testing.

With the braid in place, a certain level of mechanical robustness and toughness is assumed. After the new product is purchased and deployed, field questions and complaints will be generated simply from the new appearance and different physical texture of the cable. Retraining or education of craftpeople is often necessary to get the most reliable performance out of any new cable design.

The electrical power requirements (voltage/ampere capacity) primarily determine the gauge and number of copper conductors needed. The insulation's purpose is to protect and isolate these conductors. Damaged jackets and insulations have contributed to expensive electrical shorts and fires. Mechanical damage during installation or cable mining operations are well known. These field failures, technology advances and environmental concerns require that any new insulation or cable design should

- (a) be mechanically tough and robust
- (b) have high cut-through, compression and creep resistance
- (c) have excellent fire resistance
- (d) eliminate need for braid coverings
- (e) not use lead-based wire coatings

Let us consider the consequences of a change from a braided power cable with chlorosulfonated polyethylene (CSPE) insulation to a non-braided cable design using non-halogen polyolefin (e.g., crosslinked polyethylene filled with 50-60% aluminum trihydrate) insulations.

These "green" non-halogen materials are designed around the removal of the halogen compounds while maintaining fire resistance. As the temperature increases, the aluminum trihydrate filler breaks down producing water vapor which quenches the fire. With the reduced use of lead stabilizers and no sulfur in the insulations, tin-lead coatings on the copper wires will no longer be needed. However, the first generation of non-halogen polyolefin materials were not robust, being susceptible to abrasive wear, point penetration and compressive stresses. If the braids are eliminated, then the mechanical robustness and toughness of this new "green" material will become a major concern.

Table 3. Cut-Through Resistance for Power Cable Insulations
— V-Blade Penetration Test Method —

Cable Insulation (All insulations were 2.8 mm thick)	Cut-Through Resistance (kg)	
	No Braid	With Braid
CSPE Insulation	20.5±1.5	22.5±2
Composite CSPE/EPR Insulation	16.0±1.5	---
Non-Halogenated Thermoplastic (Crosslinked Ethylene Copolymer filled with Aluminum Trihydrate)	13.5±1.5	18.0±2
Composite - Neoprene/EPR Insulation	11.5±1.5	----

Past field experience with hydrocarbon rubbers, chlorinated rubbers and other insulation materials for power cables implied that braids were necessary for abrasion resistance, toughness and color coding. New insulation materials and designs may have sufficient toughness without the braid, but mechanical tests will be needed in functional performance document used for product procurement. These test would include -

- an abrasion test
- cut-through and/or penetration tests
- durability tests for cable markings

Power cables in central offices are placed along cable trays, down cable falls and around/through equipment. Field failures of these cables have been found (i) when cable was mined and pointed instruments were used to pry apart individual cables, and (ii) where unbraided cables were laced to superstructure. Some insulations are quite soft and will need the added protection of "Fiber Sheathing" where vertical drops in cable runs are laced with twine. "Fiber-Sheathing" consists of wrapping the power cable with protective fiberglass or plastic cloth before the cable is laced to the cable tray rack with twine.

Penetration/cut-through resistance for the power cable insulations can be tested using a V-blade penetration test where a V-shaped blade is pushed into the power cable insulation until the blade tip contacts the copper conductors in the cable core. Table 3 lists the results of such V-blade tests for a selection of power cables insulations. These results show that neoprene/EPR rubber insulations are less tough than non-halogenated polyolefins which were less tough than CSPE-type insulations. Woven braids added 10-30% to the cut-through resistance.

Distinguishing between the different rubbers and insulations may not be possible without a laboratory analysis. With no well defined cut-through/penetration criteria, standard installation and maintenance procedures must include "fiber sheathing" to protect any unbraided cable unless the cable insulation can be clearly shown to be a material with high penetration/cut-through resistance. Therefore, elimination of braids from power cable may require

- a) Improved test requirements ("cut-through")
- b) Revised cable placement procedures
- c) Long term reliability testing.

to help ensure the power cable will meet functional performance needs.

In conclusion, this power cable example showed that drop-in "green" materials are not readily available to replace traditionally used materials in telecommunications products. In selection of "green" material replacements for products, thorough technical review is needed to

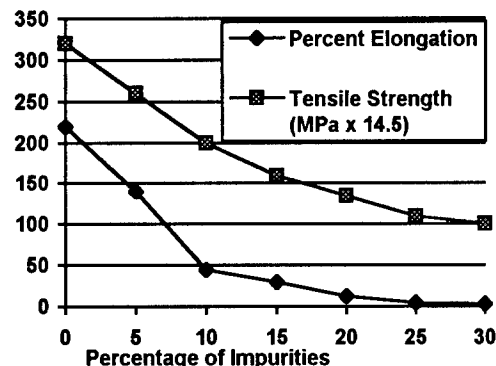
- maintain product reliability/ performance,
- revise criteria for product requirements,
- identify major environmental impacts/costs,
- evaluate collateral benefits or costs to associated products (e.g., cable connectors).

Any new material ("green" or not) has to compete with the long field history of a mature product like CSPE insulations which includes not only knowledge of CSPE's limitations and problems, but also the well known and tested solutions to these problems.

CASE STUDY #2 - Recycled Cable Jackets

In this case study, we will analyze the technical issues associated with the use of recycled plastic scrap from cable mining operations in the manufacture of new telecommunications cables.

Figure 1 Effect of Impurity Levels on PVC Mechanical Properties¹⁷



If the impurity levels in the vinyl plastic exceed five-to-ten percent, then the mechanical properties deteriorate (Figure 1). The dielectric requirements on materials used for telecommunications cables are stringent to reduce electrical noise, avoid crosstalk and minimize bit error rates. These requirements will become even more critical at the higher data rates and video transmission criteria needed for the new broadband services.

The recycling of PVC scrap into durable goods can be accomplished if the material stream is sufficiently cleaned up and reformulated. Some of the potential products that can be formulated using the recycled plastics from wire and cable include truck mud flaps, floor mats, garden hose, shoe soles, floor tiles, steel coil separators, fillers, bumper guards, sound dampening and vibration dampening materials. Most of these applications are low-end, low-value products where appearance is not critical.

It is possible to use recycled PVC materials at levels of 20-30% for higher value products like telecommunications cable jackets with certain provisos. Additional stabilizers are needed to process a reasonable cable jacket. Table 4 compares the properties of cable jackets formulated from mixtures of recycled and virgin PVC materials.

The results in Table 4 highlight some of the generic problems with using recycled materials for high performance products such as telecommunications wire and cable.

- Maximum Recycle Content = 20-30%
- Color Limitations
- Physical Texture Degrades

- Mechanical Toughness Degrades
- Processing Stability Decreases

The level of impurities present in recycled PVC plastics limits the recycle percentage to 20-30% that can be safely incorporated into new products. At these levels, care is needed to reformulate with additional processing stabilizers and thermal stabilizers to compensate for the impurities and reduced thermal stability. These recycled materials have already been through one manufacturing process along with any environmental degradation during use. Further mechanical and thermal stresses occur in the recycling operation (e.g., chopping and separation). All these processes degrade the polymer and make it more susceptible to further degradation. The difficulties in mixing and extruding the recycled materials is evident from the reduced processing (Brabender) stability and the diminution in mechanical toughness and abrasion requirements. Since processing stability is reduced, the materials can not be as well mixed under high shear stresses and high temperature for sufficiently long time to obtain the well mixed plastic that produces a smooth jacket with high mechanical toughness.

Color changes are indicative of dehydrochlorination of the PVC molecules and account for the fact that recycled products have a pinkish/brownish tint and some problems may arise in effective color coding of jackets and insulations. Fortunately, jacket materials have a wider color tolerances than individual wire insulations which need to be clearly distinguishable in poor light found in wiring closets and manholes.

This diminution of performance does not mean that recycled materials cannot be used for telecommunications product. Realistic levels of performance need to be incorporated into specifications and requirements documents. Recycled cable jackets materials can perform adequately in low stress applications where installation stresses are low and maintenance/repair activity after placement is minimal. Furthermore, plasticizers, stabilizers and processing aids can be added to overcome these stability problems to a certain degree as shown by the relatively good tensile strength and ultimate elongation values found for the recycled jacket materials. Ironically, the most effective stabilizers

Table 4 Jacket Properties of General Purpose 6-Pair Cables Made With Recycled PVC Materials

Cable Jacket Properties	Manufacturer #1			Manufacturer #2	
	Virgin	20% Recycle	30% Recycle	Virgin	25% Recycle
Appearance	Smooth	Pimply	Pimply	Smooth	Few Pimples
Color	Olive Gray	Pinkish Gray	Mauve	Gray	Pinkish Gray
Thickness	0.61 mm	0.41 mm	0.43 mm	0.89 mm	0.81 mm
Cut-Through Strength	1.8 kg	1.6 kg	1.5 kg	4.6 kg	3.5 kg
Brabender Stability	>60 min	44 min	41 min	>60 min	>60 min
Tensile Strength (MPa)					
Initial -----	18.1	20.2	18.9	19.4	16.4
After 7 days @ 100°C--	18.8	21.7	19.9	19.7	16.5
Ultimate Elongation					
Initial ---	330 %	300 %	300 %	350 %	340 %
After 7 days @ 100°C	320 %	290 %	260 %	370 %	350 %
Oxygen Index	31.5	31.0	30.5	29.0	27.5
Scrape Abrasion Test (# Cycles to Failure)	850-900	200-250	200-250	650-700	350-400
Cold Impact Test at					
-10 deg C	passed	failed	failed	passed	passed
-20 deg C	passed	failed	failed	failed	failed
-30 deg C	failed	failed	failed	failed	failed
Cold Bend Test at					
-10 deg C	passed	passed	passed	passed	passed
-20 deg C	passed	passed	passed	passed	passed
-30 deg C	passed	failed	failed	failed	failed

(*) Brabender Stability measures stability under shear stress which simulates processing conditions with longer times being preferred. Oxygen Index measures fire resistance.

to add are the very lead-based stabilizers which contribute to the disposal problem in the first place. The next case study reviews some of the non-lead based stabilizers for these materials.

CASE STUDY #3 - Green Stabilizers for PVC

Stabilizers based on barium-zinc and calcium-zinc chemistry can be used, but they are usually not as effective as the lead-based compounds. Publicity like that received for lead stabilizers in miniblinds¹⁸ may cause increased regulations and restrictions on lead-based stabilizers.

The alternative stabilizers that have been developed to replace lead-based and cadmium-based compounds¹⁹⁻²¹ can reduce the environmental impact of plastics and enhance their recycle potential. Table 5 shows the Brabender stability times for a selection of the commercial PVC formulations designed to meet the dielectric requirements of cable jacket and

wire insulations. In general, the lead-based thermal stabilizers out-perform their "green" replacements. Increasing the Ca/Zn or Ba/Zn stabilizer concentrations to improve the Brabender stability times would lower the volume resistivity values to unacceptable values and reduce the transmission performance of the cable product.

However, these results show that "green" stabilizers can perform adequately. In general, the processing window is smaller for these "green" alternatives and manufacturers will need good process control to help ensure jackets and insulations are not damaged during the high temperature mixing and extrusion steps. Following product requirements such as tensile strength, elongation-at-break, volume resistivity (dry and wet) and color retention after aging should help provide the quality control to detect and eliminate any inadequate insulation and jacket products.

Table 5. PVC Material Properties using "Green" Stabilizers

Cable Jackets & Wire Insulations Materials	Stabilizer Type	Brabender Stability in minutes	Volume Resistivity in ohms	Tensile Strength in MPa	Percent Elongation
Jackets					
A	Lead	46	2×10^{14}	20.0	290 %
B	Barium-Zinc	42	2×10^{13}	18.2	275 %
C	Barium-Zinc	34	5×10^{12}	18.7	295 %
D	Barium-Zinc	27	9×10^{11}	18.6	315 %
E	Calcium-Zinc + Magnesium-Zinc	30	6×10^{12}	18.3	300 %
GR-492 Requirement	----	> 30	$> 5 \times 10^{12}$	> 17.2	> 200%
Insulations					
A	Lead	45	2×10^{15}	22.8	295 %
B	Barium-Zinc	25	3×10^{15}	23.1	320 %
C	Barium-Zinc	33	3×10^{15}	23.4	320 %
D	Barium-Zinc	51	3×10^{15}	22.6	325 %
GR-492 Requirement	----	> 16	$> 5 \times 10^{13}$	> 20.7	> 200%

"GREEN" STRATEGIES FOR PURCHASING

There are a variety of effective strategies that can enhance a company's "green" reputation while simultaneously reducing their day-to-day operating costs, decreasing current and future disposal costs and minimizing their liability towards future environmental problems that may develop. Promising strategies include (1) partnerships with scrap/disposal companies or equipment suppliers to reduce waste volume and cost, (2) specific "green" material choices and/or environmental criteria in product requirement documents, and (3) improved operational practices to reduce energy needs and consumption.

Purchasing requirement strategies can provide a powerful vehicle to suggest, encourage or mandate the use of environmentally friendly products in telecommunications products. Bellcore's GR documents or a company's RFP (Request-For-Proposal) requests are two such means that can implement these "green" strategies. For example, incorporation of -

- ◆ Optional Life-Cycle-Assessments
- ◆ "Green" Certification/Label Uses
- ◆ Product "Take-Back" Policies or Contracts
- ◆ ISO-14000 Certification Requirements

within the product requirements and contract documents can prove very useful in advancing a company's environmental goals.

Which strategy is to be preferred are determined by business factors of implementation time and economic payback. For example, Table 6 lists the status and estimated payback for some of the problems and solutions discussed in this paper.

CONCLUSIONS

In this paper, we have reviewed environmental issues and their possible solutions from the standpoint of telecommunications companies. We used various case studies of wire and cable products to illustrate rationales for environmental strategies as well as to examine the possible positive and negative collateral effects of "green" material choices for network products

ACKNOWLEDGMENTS

Joe D'Amico and John Shelburne III are thanked for supplying data for this paper.

REFERENCES

1. Proceedings of USTA (United States Telephone Association) Environmental Subcommittee Conference - "Environmental Management in the Telephone Industry" April 1995, San Diego, CA.
2. Proceedings of IEEE (Institute of Electrical and Electronics Engineers) on "Electronics and the Environment" conference (Dallas, TX) May 1996
3. T.E. Graedel and B.R. Allenby, "Industrial Ecology" - Prentice Hill (1995)

4. J. Bjorkman, B. Heyman and H. Serrander, "Green Perspective on Telecommunications", *TELE*, February 1993.
5. R.A. Frosch, "The Industrial Ecology of the 21st Century", *Scientific American*, September 1995.
6. "Concerns Broaden over Chlorine and Chlorinated Hydrocarbons", (B. Hileman), *C&EN News*, p11, April 19th Issue, 1993.
7. A. Davey, "Mandatory Re-Use Quotas for Plastics", *Plastics and rubber weekly*, No.1487, p6, May 1993
8. "Telephone Company Statistical Data" - Reports to FCC (Federal Communications Commission) and SEC (Security Exchange Commission).
9. P.C. Warren, "Plastics Failures in Loop Applications", *Proceedings of International Conference on Plastics in Telecommunications (PIT VI - London, UK)*, p29/1, 1992.
10. C.A. Glew, "Evolution of Materials for Communications Wiring", *Wire Technology International*, p30, September 1995.
11. G. Schick, "Lead Sheathed Cable Corrosion and Its Effect on the Environment", *Bellcore proprietary report*
12. S. Forsberg and J. Bjorkman, "Release of Lead from Lead-Sheathed Telecom Cables in Soil", *Proceedings of 1994 International Wire and Cable Symposium*, p478 1994.
13. Bellcore Practice BR-877-112-001, "Removal of Lead Sheath Cable from Outside Plant - Aerial, Underground and Buried" Issue 1 August 1996
14. P.C. Warren, private communications.
15. T.M. McKee and D.L. Syhre, "TCLP : A Flawed Method", *Environmental Lab.*, Feb./Mar., 1991.
16. Bellcore's GR-347 "Generic Requirements for Central Office Power Cable", (1996).
17. W. Alan Sell and H-Khim Boo, "Recycling Vinyl Wire and Cable - A New Approach", *Wire Technology International*, p44, January 1994
18. Lead Danger Prompts Vinyl Miniblind Alert", (J.S. Cohen), *USA Today* July 1996.

19. E. Tucza and F. Cortolano, "Reformulating PVC to Eliminate Heavy Metals and Protect Performance", *Modern Plastics*, October 1992.
20. "Heat Stabilizers : Lead-Free Systems for Wire and Cable Arrive", *Modern Plastics*, Sept. 1994.
21. "New Products Improve Productivity and Performance", (D. Smock), *Plastics World*, p33, March Issue 1996.



Trevor Bowmer is a member of Network Integrity Solutions Group in Bellcore's Professional Services organization. After receiving his Ph.D. in Chemistry from the University of Queensland (Australia), he joined Bell Labs in 1980 and investigated radiation-cured systems and lithographic materials. Since 1984, his research at Bellcore has focused on materials-related reliability problems in the telecommunications industry. Current interests include assessing the impact of current and future material technologies and developing appropriate product requirements, as well as installation practice & procedures.

Table 6. Status and Payback Expectations for Environmental Strategies

Strategy	Implementation	Payback/Savings(*)
<u>Material Management of</u> Old/Scrapped CO Equipment	Legally Required Now	Immediate Savings (\$)
<u>Hazard Reduction</u> Help Generate Market for Recycled Products	Possible Now - review needed for product performance requirements	Long Term (\$)
<u>Operational/Software Solutions</u> Use Old Copper Plant for Broadband	Possible and Happening Now	Near Term Savings (\$\$)
<u>Material Replacements/Substitutions</u> Mandate Recycled Content in Products Replace Lead-Based Stabilizers	Possible Now - review needed for product performance requirements	Long Term (\$)
<u>Technology Paradigm Shifts</u> Copper --to--Coaxial/Fiber--to--Fiber	Is Happening Now	Long Term (\$\$\$)

(*) \$\$\$ = large or rapid return to operating costs \$\$ = medium savings or savings over long term
 \$ = small savings per unit (may accumulate to significant savings over entire plant)

LIFE-CYCLE ASSESSMENT OF CABLES

Roger Färlin, Karin Nygård-Skalman

Ericsson Cables AB, Hudiksvall, Sweden

ABSTRACT

The aim of this investigation is to carry out, as completely as possible, a life-cycle analysis of three different cables. The analysis is to follow the product from the cradle to the grave and, with the help of the Environmental Priority Strategies in Product Design (EPS) system, establish where in the life-cycle the greatest loading occurs.

The result shows that the co-axial cable gives the greatest loading if the effect in service is neglected. The assumption that the energy consumption per cable and subscriber is much lower for optical cable implies that it is the most environment friendly.

It can be concluded that negative environmental effects can be reduced if cables are designed to be recovered. This can imply that copper wires are produced without tinning and that polymers from the same group are used.

Transport should be with environmentally acceptable electricity. Energy consumption, for production and when in service, needs to be minimised.

INTRODUCTION

A long term aim of environmental protection is to ensure a good environment in the future. Natural resources are not to be used at future generations expense. This view has commonly been called sustainable development. An important starting point to achieve this aim is environmentally adapted product development.

Many of today's environmental problems stem indirectly from the way products are manufactured and used. The environment, as a competitive argument, is an ever increasing factor in showing a company's readiness to design and manufacture environmentally acceptable products

Consequently a need has arisen for an environmental system to assess the relative environmental effect during the whole of a

products lifetime, so as to be able to choose rational and correct priorities during product development. It can be said that there has arisen a new parameter, environmental adaptation, to add to the existing; *function, achievement, cost, reliability and ease of servicing.*

This work aims at deciding, as far as is possible, the environmental effects that the three different telecom cables have by making a life-cycle analysis primarily of manufacturing but also the effects in service.

LIFE-CYCLE ASSESSMENT, LCA

LCA aims at checking the product inventory from the cradle to the grave. Ideally the assessment should begin with the procurement of the raw materials, through manufacturing and use and end with the handling of the residual materials. The inventory, if complete, should include the consumption of raw material, energy, additives and their production. Moreover the analysis should include, transport and by-products including those released into the atmosphere, ground and water. LCA is a study of the whole life-cycle but it is not necessarily a study in depth. The amount of detail can vary greatly and the life-cycle analysis can be both qualitative and quantitative.

The use of a life-cycle analysis

The most important application is the identification of where in the life-cycle or from which product the greatest negative environmental effects are generated. Cost effective measures can then be taken to reduce or eliminate this effect.

Comparison of different design solutions and manufacturing alternatives with respect to environmental loading become possible. This can be included at the product development stage to ensure that new products cause the least possible loading of the environment.

Increased environment protection demands by the public, community, customers and industry has to be satisfied. Comparing life-cycle

analyses is a good way to ensure that these demands are met and is a good starting point for continued environmental involvement.

Life-cycle analysis can also be used as an argument in marketing especially if it can be shown that environmental improvement was accomplished.

Further uses can be in selecting waste disposal strategies, providing a basis for environmental marking criteria and for contributing information and as a source for education.

Procedure

Primarily through the efforts of the Society of Environmental Toxicology and Chemistry (SETAC), the LCA method has received a generally accepted structure and terminology. This structure defines LCA in 4 categories:

- 1 Definition of aims and scope
- 2 Inventory Analysis
- 3 Impact Assessment
- 4 Improvement Assessment

Definition of aims and scope is the first step and denotes the extent and limits of the analysis. The aim is to express unequivocally what the results can be used for by indicating what restrictions have been applied.

Inventory Analysis is the next step and it is objective and factual. It quantifies energy use, material flows, waste disposal etc. A flow scheme is made and data collected. Every conceivable environmental effect which is connected with the product under scrutiny is considered.

Impact Assessment is the third step and implies all data collected during the inventory is weighted according to an environmental index system where different environmental effects are differently weighted.

Improvement Assessment is the final step and systematically evaluates the results, often yielding guide lines for the future. This emphasises that a LCA is to produce a basis for future environmental improvement measures.

Evaluating

The evaluation stage, which is included in environmental effect determination, is the most controversial part of a life-cycle analysis and consequently the least acceptable. The aim is to sum up all the inventory data to ascertain the overall environmental effect.

There is a number of different ways of evaluating environmental effects:

The EPS-system is based on how resource consumption and contaminated waste influence five categories. The evaluation leads to a simple environmental index which is a weighted assessment of the influence on the categories, where even economic factors are included in the assessment.

The Tellus Institute's model relies on the documented "willingness to pay" by the community to avoid other emissions. *The principals of ecological scarcity* expresses the relationship between the present total environmental load and the maximum acceptable load.

The effect classification method re-assesses subsidies for different environmental effects (effect categories). These are then weighted against each other considering different assessment aspects i.e. political or economic decisions.

EPS-system

The acquired experience coupled with the easy to use results has led to the EPS-system being chosen for future investigations.

The evaluation system aims at determining and assessing different types of environmental effects that products have. This effect is categorised on an environmental index expressed in ELU (Environmental load unit). An ELU represents the amount society is willing to contribute to hinder or reverse negative environmental effects. An ELU is equivalent to an ECU in the OECD countries.

The evaluation is based on five categories:

- health
- biological multiplicity
- biological production
- natural resources
- aesthetic values

The different effects these categories have are defined by basic assessments. The system relies on the evaluation of a primary environmental index for emissions and consumption of natural resources from which a secondary environmental index is established for transport, energy consumption, design material and one off processes.

Finally, an environmental loading figure is deduced for the product which yields a quantitative value for the total environmental effect during the entire life-cycle.

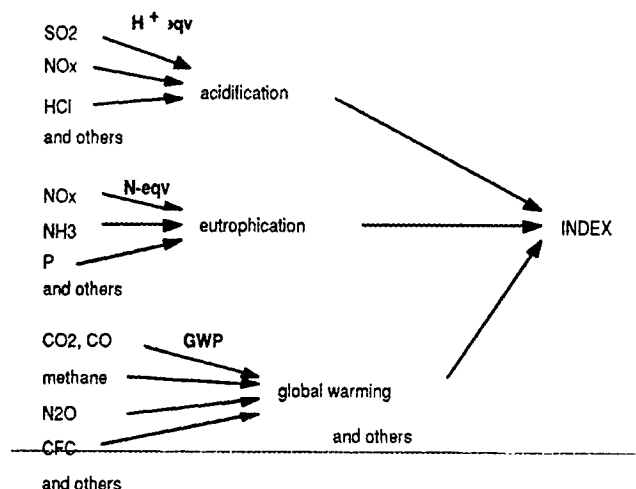


Fig.1. The environmental index

The environmental index is often the main part of an environmental evaluation system including the EPS-system. By using the environmental index a versatile, easy to use evaluating system is produced. The EPS-evaluations relate to the primary environmental index for the use of natural resources and emissions. The construction of an environmental index is somewhat complicated incorporating a range of assessments and evaluations, see Fig.1. The primary environmental index is evaluated with reference to the material's effect and concentration. An environmental index for design material, such as steel, can be extracted from these primary environmental indices. This is done by analysing the processes that are necessary for production, material and energy consumption, and waste that the process causes multiplied by the relative environmental index. In this way the secondary index is produced which in turn leads to higher EPS-ratings, i.e. for a cable.

CABLE CATEGORIES

The following were examined. A screened cable with 10 conductor pairs, a coaxial cable with flame retardant sheathing and an optical cable with 24 loose tubes.

The limitations within the analysis include the absence of the emissions that come from material that is not thought to be an environmental load due to the limited mass in the cable or because the supplier will not divulge this information.

Indicator colouring, swelling agents and pigments fit this category.

The cable is designed for a 40 year lifetime.

10-pair cable

This is a local cable for permanent outdoor use where moisture is present. The conductors have a diameter of 0.5 mm insulated with expanded PE. The cable is compound filled, and wrapped with woven fibre and screened with aluminium foil. The sheath is LLDPE.

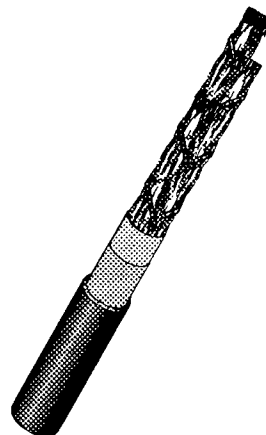


Fig.2. 10 pair cable

Material	w%	Production
8 mm Copper	28.87	Drawing
Tin	0.033	Tinning
Marking wire	0.022	Wrapping
PET-yarn	0.451	Wrapping
Marking tape	0.128	Wrapping
Woven fibre	0.872	Wrapping
Swellable woven fibre	2.812	Wrapping
Screening foil	13.20	Wrapping
Colour	0.068	Colouring of insulation
Ink	0.004	Labelling of sheath
LLDPE	27.97	Sheathing
Cellular PE	6.96	Insulation
Filling compound	17.66	Filling
Hot melt	0.940	Wrapping
Drum	2.2 (p)	

Table 1. Material and mass % for 10 pair cable.

Coaxial cable

A copper cable for indoor use primarily telephone exchanges. The conductors are 0.5 mm tinned copper wire insulated with LDPE. The screen comprises two cross woven tinned copper layers. The sheath is a flame retardant halogen free polymer.

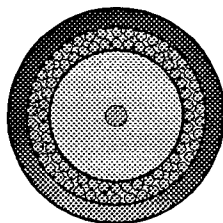


Fig.3. Coaxial cable

Material	w%	Production
8 mm Copper	2.67	Drawing
Tinned wire	62.00	Braiding
Tin	0.035	Tinning
Colour	0.243	Colouring of sheath
Ink	0.010	Labelling of sheath
LLDPE	10.91	Insulation
HFLSFR-plastic	24.13	Sheathing
Drum	2.2 (p)	

Table 2. Material and mass % for coaxial cable.

Optical cable

A dielectric cable designed for duct use. The slotted core is MDPE with a strength member of glass reinforced plastic. The loose tubes are of PA and they are filled with cable filling compound. There are four fibres to a tube. The sheathing is LLDPE and the cable is water proofed longitudinally by filling with cable compound.

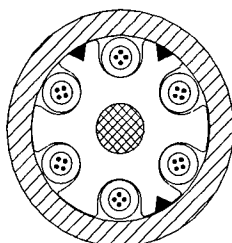


Fig.4. Optical cable

Material	w%	Production
Preform	0.4	Fibredrawing
Acrylate	0.5	Coating
PA	5.0	Loose tube
FRP	8.8	S-Z sheathing
Filling compound	20.2	S-Z sheathing
MDPE	30.4	S-Z sheathing
Marking tape	0.01	S-Z cabling
LLDPE	34.0	Sheathing
Drum	0.25 (st)	

Table 3 Material and mass % for optical cable.

Raw material production

The copper used consists of about 70 % from Swedish ore and 30 % from reclaimed material. The ore passes through several processing stages, i.e. dressing, converting and electrolysing before it is incorporated into the copper from which conductors are drawn. Polymers are manufactured in Europe.

The oil used for manufacturing PE comes from the North Sea and is refined and cracked in Sweden. The raw material is then sent for polymerising and subsequently additives, needed for a complete product, are incorporated.

Other materials, i.e. PET, PA, tin and aluminium are analysed in the same way as copper and PE.

Transport

All materials have to be moved from place to place before they reach their final form and destination. This transportation imposes an environmental load i.e. diesel consumption and exhausts and nuclear power. For the three cables analysed, boat, lorry and rail form the mode of transport. The total environmental load is dependant on whether the goods come from Japan by boat or from another part of Sweden by lorry.

Energy consumption

Energy consumption comprises primarily the energy used to accomplish the various process stages but includes the functional units proportional part of illumination and heating of the manufacturing plant.

Heating comes mainly from a central incinerating station fuelled by home produced peat, pine oil and sump gas. The remaining heating comes from a heat pump.

The electrical consumption is derived from an average value for Sweden where hydroelectric generation and nuclear power dominate.

Handling and waste management

An analysis has shown that practically no material permeates into the ground surrounding the cable rather the environmental loading of the cable in service comes from the plant and the use of the cable. A calculation or estimate of the energy consumption in service has proved to be very difficult due to the different uses, systems and ancillary equipment. It can be fairly safely stated that the optical fibre cable requires less energy for transmission per conversation than the two copper cables.

The waste handling existing today concentrates mainly on the metals in the cables i.e. copper, aluminium and tin. A great deal of research is being carried out in the

hope of considerably increasing the amount of polymer re-cycling compared with today. Whilst re-cycling is the best solution incineration is also an acceptable alternative for utilising the energy capacity of the polymer provided the temperature can be held high enough to prevent the emission of toxic material.

In general, the emissions, energy and material needs for all processes and transport stages are presented in tabular form for all materials. These data are normalised against the functional unit and summarised for each cable type.

RESULTS

The functional unit was chosen as kg cable to eliminate the influence of heavy material such as metals. If the functional unit is chosen as 1 km cable, the environmental effect of cable with a low mass % of metal will diminish. The power need with continuous service during the 40 year cable lifetime is unknown but the tabulated results show the magnitude of the power level which gives a significant addition to the total environmental load.

10 pair cable

For the 10 pair cable the greatest environmental loading occurred with the acquisition of the raw materials. If the material categories are broken down it can be seen that the copper definitely gives the greatest addition. It is today feasible to recycle cables due to their high copper content. Energy consumption in service can also be a relatively large addition that is to be minimised.

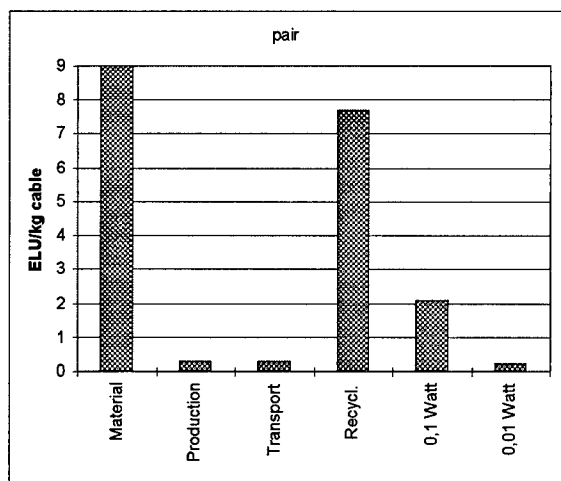


Fig.5. 10 pair cable

Coaxial cable

Coaxial cable presents a substantial environmental load both for the material and

the manufacturing. The screen in the form of the two woven layers is the culprit. The tinning of every strand of the weave is energy demanding and processing is relatively slow. Moreover the production of tin places quite a load on the environment

The re-cycling process does not allow separation of the tin from the copper which leads to a lower recovery value compared with 10 pair cable. The material cannot be recycled for use in cable production.

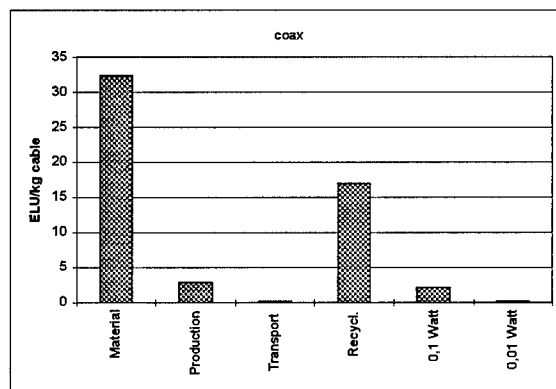


Fig.6. Coaxial cable

Optical cable

The result for the dielectric optical cable shows a distinctly lower level of environmental loading. The absence of metals lies behind these results. The values for transport gave a somewhat higher figure than for the two others due to the longer transport distances involved. Note there was no re-cycling.

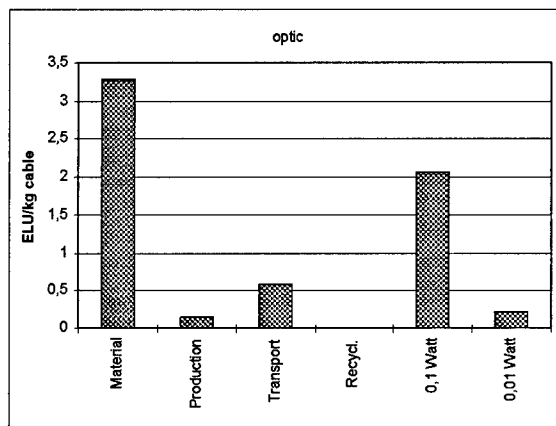


Fig.7. Optical cable

Comparisons

A comparison of the three cables shows that the coaxial cable loaded the environment the most and the 10-pair cable the least.

It should be noted that consumption in service is not included as explained previously. It can be suspected that a great deal of the copper cable environmental effects occur in service and that should benefit the optical cable if the

loading is divided by the number of subscribers.

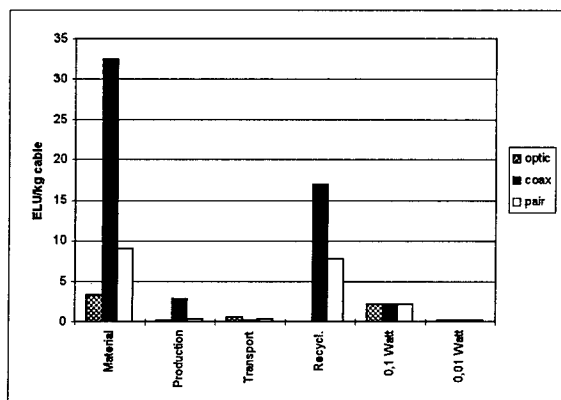


Fig.8. Comparison.

If the re-cycling is subtracted from the total loading, excluding service loading, the following results:

10 pair cable	1.8 ELU/kg
Optical cable	4.0 ELU/kg
Coaxial cable	18.4 ELU/kg

With the functional units changed to 1 km cable:

10 pair cable	236.8 ELU/km
Optical cable	582.6 ELU/km
Coaxial cable	1067.8 ELU/km

The coaxial cable has a high tin content per strand, which complicates recovery. Eliminating the tin in the design would effect an improvement by facilitating recovery thus raising the amount of re-cycling and reducing the loading of the material value.

Increasing the re-cycling amount also has an effect on the environmental loading.

Transportation, i.e. by using electric trains instead of aircraft should be considered. also the use of cleaner fuels and more efficient engines that already exist ought to be implemented.

The energy requirement for all electronic and mechanical products needs to be minimised so as to use the existing energy resources in the best way for sustainable development.

CONCLUSION

Of the cables analysed the coaxial cable proved to yield the greatest environmental loading. However the cables are not directly comparable and the true service consumption has not been included allowing some distortion of the result presented. Dividing the environmental loading by the number of

estimated subscribers shows the optical cable as the best of the alternatives.

Future analyses should examine a number of different production and installation methods. The environmental load produced by different methods of communication may also be of interest.

ACKNOWLEDGEMENTS

The author wishes to thank Peter Fickling for help with translation, Jens Malmödin for discussions concerning LCA and to all the suppliers who contributed material data.

REFERENCES

Bengt Steen "EPS-Default Valuation of Environmental Impacts from Emission and Use of Resources" Version 1996, Report 111, Swedish Environmental Research Institute, IVL, Gothenburg

Göran Finnveden "Valuation Methods within the Framework of Life Cycle Assessment", Report B1231, Swedish Environmental Research Institute, IVL, Stockholm

J.Malmödin "LCA on a microchip", Ericsson Radio System AB, Kista

J.Malmödin "LCA on RBS 882/RBS 884", M.Sc. thesis work 1995, Ericsson Radio Systems AB, Kista.

L-G Lindfors et al "Nordic guidelines on Life Cycle Assessment", Nordiska ministerrådet, Nord 1995:20, Århus, 1995

M.Sune'r "Life Cycle assessment of Aluminium, Copper and Steel", Technical environmental planning, Chalmers Tekniska Högskola 1996.

AUTHORS



Mr Roger Färlin received his M.Sc. in Mechanical Engineering and Material Science from the University of Luleå in 1994 and joined Ericsson Cables AB, Hudiksvall Sweden, in 1995. Since joining Ericsson Cables he has been working in the Material Technology Department, mainly with polymers and LCA.



Mrs Karin Nygård-Skalman received her M.Sc. in Chemical Engineering at the Royal Institute of Technology, Stockholm 1982. She has been working at Ericsson Cables Telecom Cables Division since 1984. At present she is responsible for the Material Technology Department.

RECYCLING OF PLASTIC SCRAP FROM OUTSIDE PLANT IN NTT

Tsuneo Konaka, Shinjiro Murai and Shiro Nishi

Nippon Telegraph and Telephone Corporation, Tsukuba Ibaraki, Japan

ABSTRACT

In 1995, we adopted a recycling system in which the plastic scrap from stray guards and access terminal boxes are recycled. The stray guard scrap is recycled as the inner layer of a stray guard and the access terminal box cover scrap is recycled as the bottom sheet of the box. In each case, more than 100 tons was recycled in 1996.

We have also examined the possibility of recycling two types of cable sheath material, polyethylene type and nonhalogenated flame retardant type. The properties of the recycled sheath material were almost same as those of virgin material. The performance of optical cable with a sheath made of recycled material satisfied requirements.

INTRODUCTION

Recycling can reduce the environmental pollution caused by the disposal of waste and allow us to use natural resources effectively. This makes recycling an important subject in relation to sustainable development. NTT's telecommunication installation work generates about 200,000 tons of scrap per year. Most of the metal scrap is recycled. However, plastic scrap is rarely recycled because of cost and is mainly disposed of as landfill or burning. This is because it is very difficult to separate different plastics from equipment economically. Therefore, we began by recycling stray guard scrap (polyethylene PE) and access terminal box cover scrap (polypropylene PP) which can be easily separated and collected.

The rapid proliferation of optical cables will lead to a large increase in cable scrap. Currently, optical cable waste amounts to about 500 tons and it is estimated that this will grow to more than 10,000 tons in the next twenty years. It is difficult to dismantle optical

cable because it has a complex structure consisting of a bundle of tens to thousands of optical fibers together with other materials. We have examined the possibility of recycling the sheath, because it can be easily separated from the cable and is composed of a single material.

STRAY GUARD AND ACCESS TERMINAL BOX COVER RECYCLING

Outline of Recycling

The scrap from stray guards and access terminal box covers is recycled as the inner layers of stray guards and the bottom sheets of boxes, respectively. Since 1995 NTT has been using a 20%-recycled stray guard and a terminal box with a 50%-recycled bottom sheet (100%-recycled since 1996). Recycled stray guard and access terminal box cover scrap amounted to about 190 and 122 tons, respectively, in 1996 as shown in Table 1.

Table 1 Stray guard and access terminal box cover recycling

Scrap	Recycled amount (ton)		Use of recycled material
	1995	1996	
Stray guard	66	190	Inner layer of stray guard
Access terminal box cover	39	122	Bottom sheet of box

Recycling System

Figure 1 shows a flow chart of the recycling process from scrap to finished products. At a construction site or office, the stray guard scrap and terminal box covers are collected into bundles. The collected

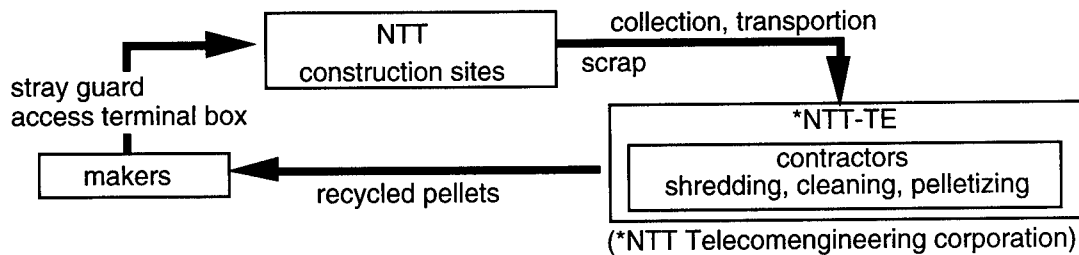


Figure 1 Stray guard and access terminal box cover recycling system

stray guard and cover scrap are shown in Figs. 2 and 3, respectively. NTT Telecomengineering (NTT-TE) which is a subsidiary of NTT, buys this scrap from NTT very inexpensively and directs the recycling processes. The scrap is transported to a contractor where it is chopped, cleaned and pelletized. NTT-TE pays the contractor and then sells the recycled materials in pellet form to the stray guard and access terminal box makers. The price of the recycled pellets is equal to or lower than that of new pellets. The makers manufacture the stray guards or access terminal boxes using these recycled pellets. Finally, NTT buys the recycled stray guards and access terminal boxes. This recycling system help to use natural resources effectively and to reduce the need for waste disposal. The costs of waste disposal and this recycling system paid by NTT are compared in Fig. 4. The above system eliminates the cost of the waste disposal process. This system also benefits NTT-TE because the cost of the recycling process is less than the price they charge for the pellets. Recycled stray guards and access terminal boxes are the same cost as those manufactured using new pellets and there are no disadvantages to the manufacturer.

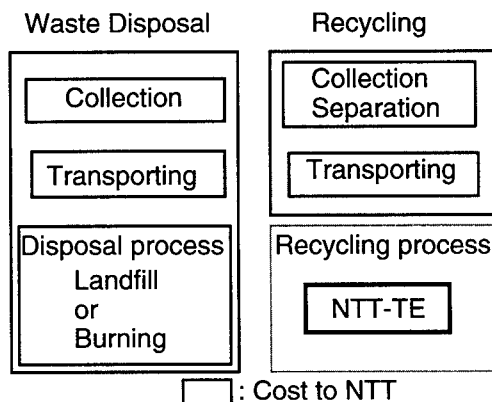


Figure 4 Comparison of waste disposal cost and recycling costs for NTT

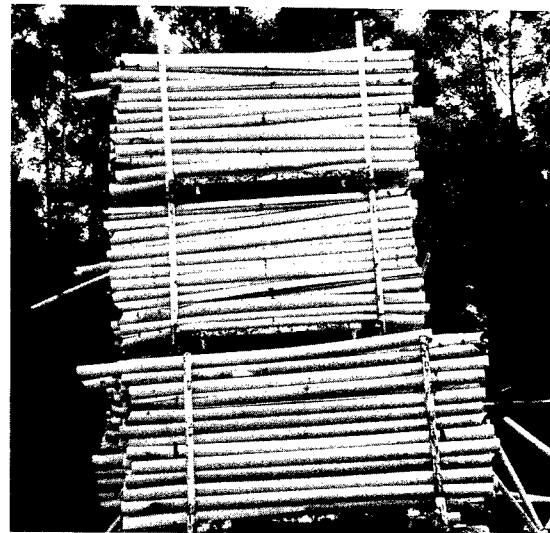


Figure 2 Stray guard scrap

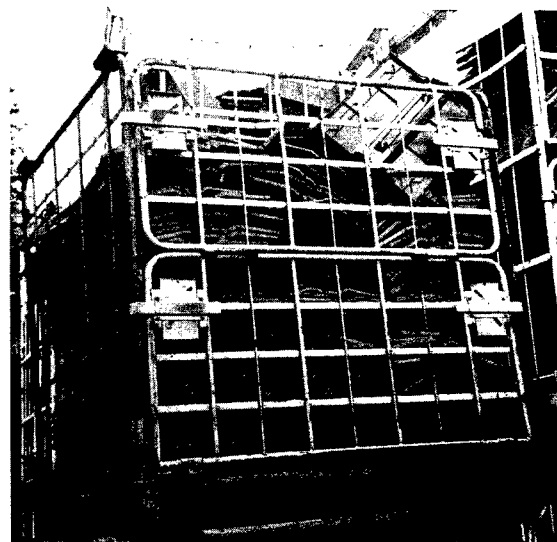


Figure 3 Access terminal box cover scrap

Properties of Recycled Materials

The mechanical properties of recycled and virgin material are shown in Table 2. The tensile strength, elongation at break and brittleness temperature of the recycled material are almost the same as those of virgin material. The use of recycled rather than virgin material has posed no problems to date.

Table 2 Mechanical properties of recycled and virgin material

Property	Recycled material	Virgin material
<u>Stray guard</u>		
Tensile strength (MPa)	18.4	17.6
Elongation at break (%)	622	590
Brittleness temperature F ₅₀ (°C)	< -60	< -60
<u>Bottom sheet of Access terminal box cover</u>		
Tensile strength (MPa)	21.3	20.8
Elongation at break (%)	610	522
Brittleness temperature F ₅₀ (°C)	- 44	- 41

OPTICAL CABLE RECYCLING

As the first step towards optical cable recycling we have tried to recycle the sheath materials from cable scrap as sheath materials for new cable because the sheath accounts for about 30% of an optical cable and is easily removed from it.

Cable Disassembly

In general, an optical cable is composed of many components such as a sheath, wrapping tape, optical fiber, fiber coating, a slotted rod and a strength member. At first NTT used optical cable with a stranded unit structure but today slotted rod cable is mainly. We evaluated the ease with which three types of optical cable can be disassembled. They were the stranded unit type, the single slotted rod type and the multi-slotted rod type. Optical cables about 1 m long were disassembled by three people using a slotting machine. Figure 5 shows the result of this experiment. The sheath could be removed in a short time in each case. However, a long time was required to disassemble the cable

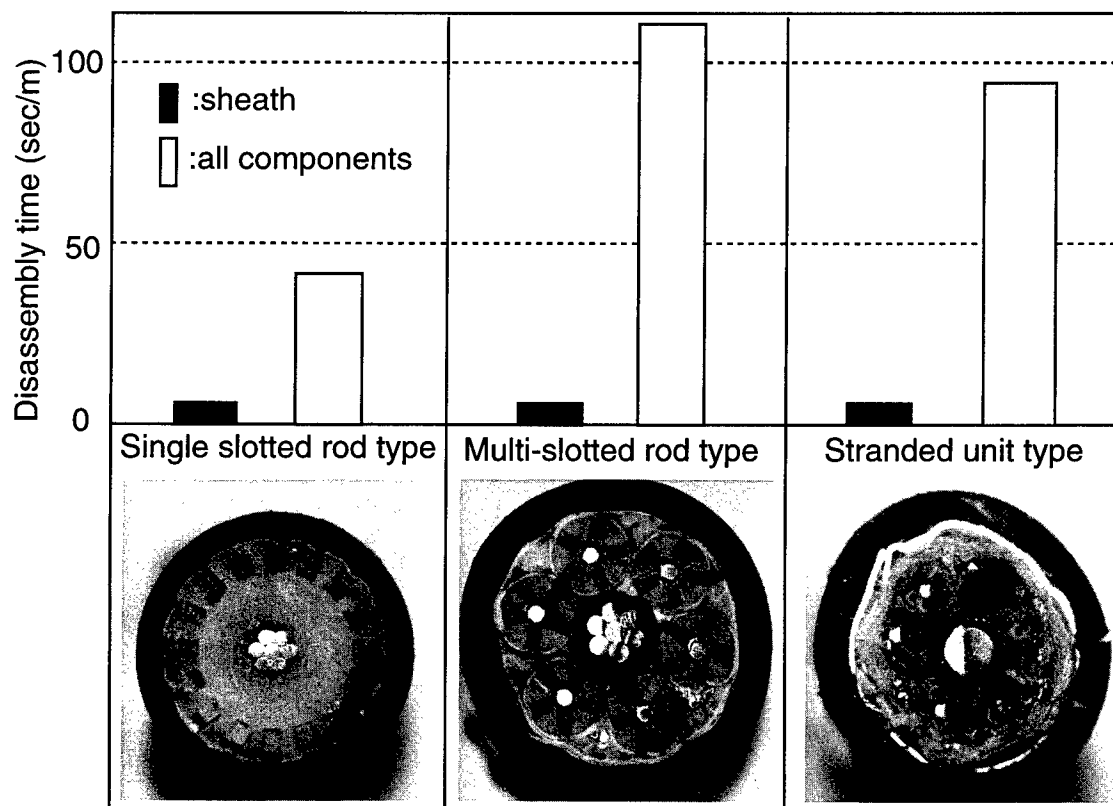


Figure 5 Result of disassemble experiment of optical cables

components and this time increased in relation to the complexity of structure. It is therefore clear that, in practical terms, only the sheath can be recycled.

Sheath Material

NTT has used the same three types of sheath material for metal cable and optical cable for many years. They are low density polyethylene type (PE), nonhologenated flame retardant compound type (FR) and polyvinylchloride (PVC). We have studied the recycling of PE and FR sheaths which are mainly used for optical cables.

Sheath Recycling Process

The sheath scrap was collected from metal and optical cable scrap. The recycling process is shown in Fig. 6. The sheaths were removed from the cables using a slotting machine and attached wrapping tapes were also removed. Then the sheaths were chopped into pieces of about 10 mm which were cleaned using water and dried. They were molded into rods of about 3 mm in diameter by using an extruder and the rod was cut into 3 mm pellets. The pellets were dried to remove absorbed water and then packaged. Figure 7 shows pellets made of recycled sheath material.

Properties of Recycled Sheath Material

We examined the melt index (MI), density, tensile strength, elongation at break, thermal aging after 48 hrs at 100°C, brittleness, environmental stress crack resistance (ESR) after 500 hrs, oxygen index (OI), smoke density and acid gas generation of a mixture of recycled and virgin material. Figures 8, 9 and 10 show the results. The MI of recycled materials is higher than that of virgin materials. The mechanical characteristics, thermal stability and ESR of the recycled materials were almost the same as those of virgin materials. The brittleness temperature for zero failure (F_0) of the recycled PE and FR sheath materials was below -60°C and -35°C, respectively. These brittleness temperatures are sufficiently below the NTT required values. The density and oxygen index of the recycled FR sheath material were slightly lower than those of virgin material. There are two FR compounds grade, normal and high. The high grade type contains more flame retardant agent than the normal type. We compared the recycled material with a high grade type. The recycled material was a mixture of normal and high grade types. Consequently, we observed a

decrease in the density and oxygen index. The smoke density and acid gas generation were almost the same.

Molecular weight distribution curves of virgin and recycled PE materials are shown in Fig. 11. The curve of the recycled material shows a decrease at high molecular weight indicating slight decomposition. This decomposition caused the increase in the MI of the recycled material shown in Fig. 8. But, it is apparent that this decomposition does not influence its use as sheath material because there is no serious lowering of other properties as shown in Figs. 8, 9 and 10.

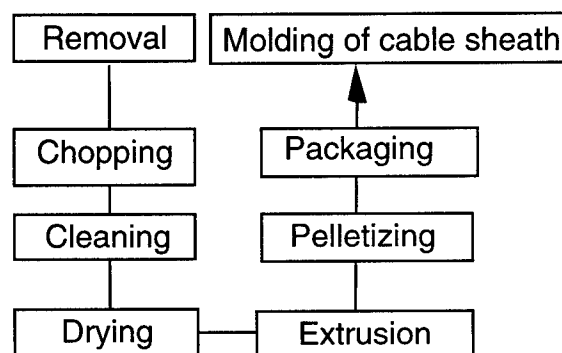


Figure 6 Cable sheath scrap recycling process

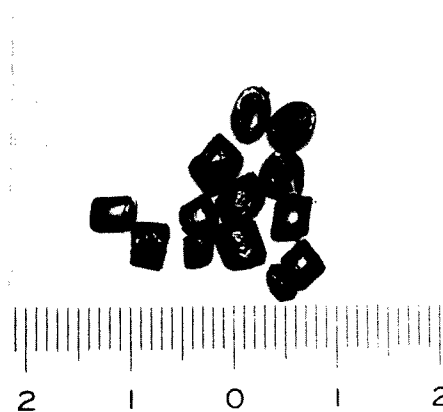


Figure 7 Pellets of recycled sheath material

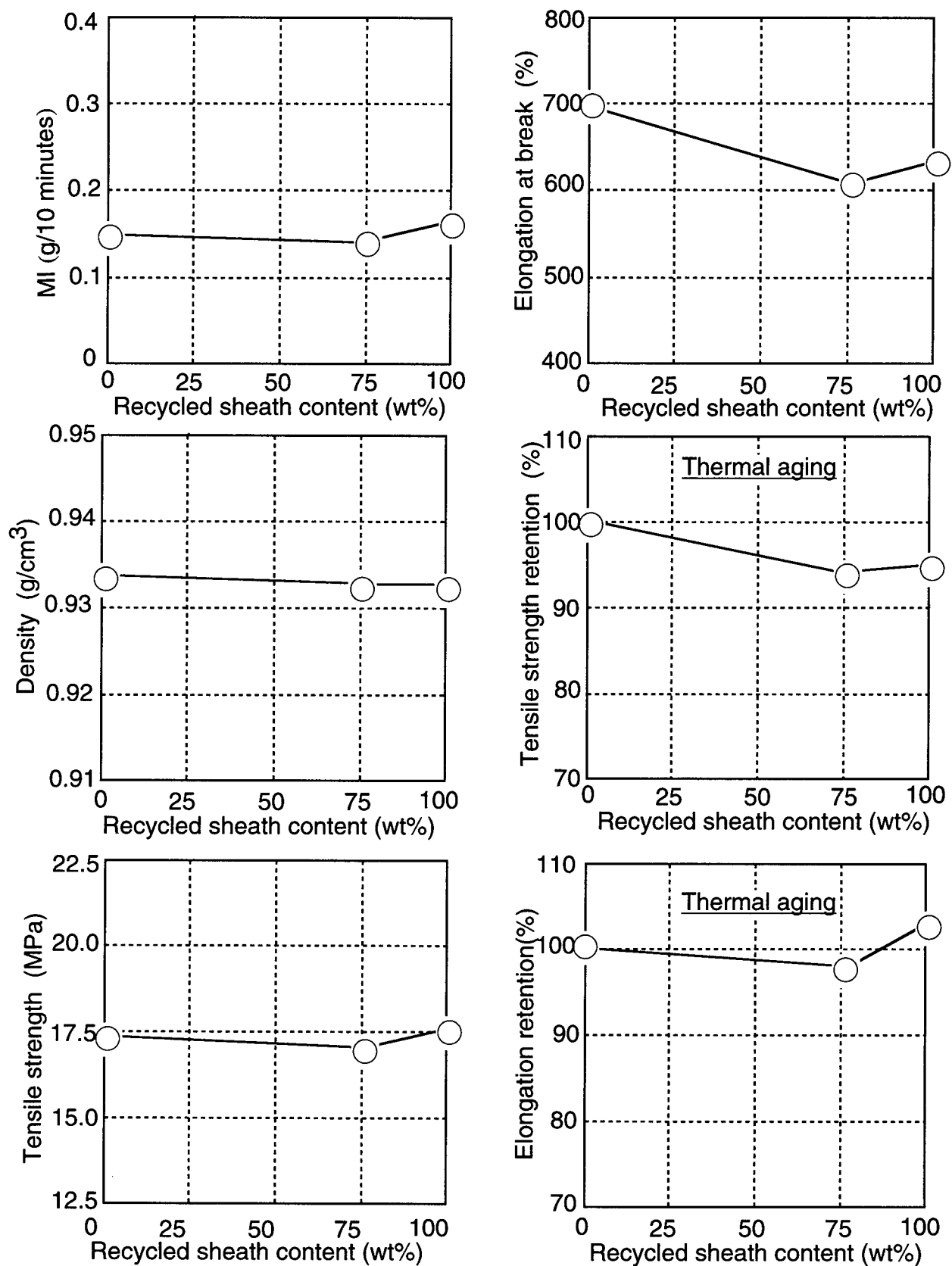


Figure 8 Properties of recycled PE sheath materials

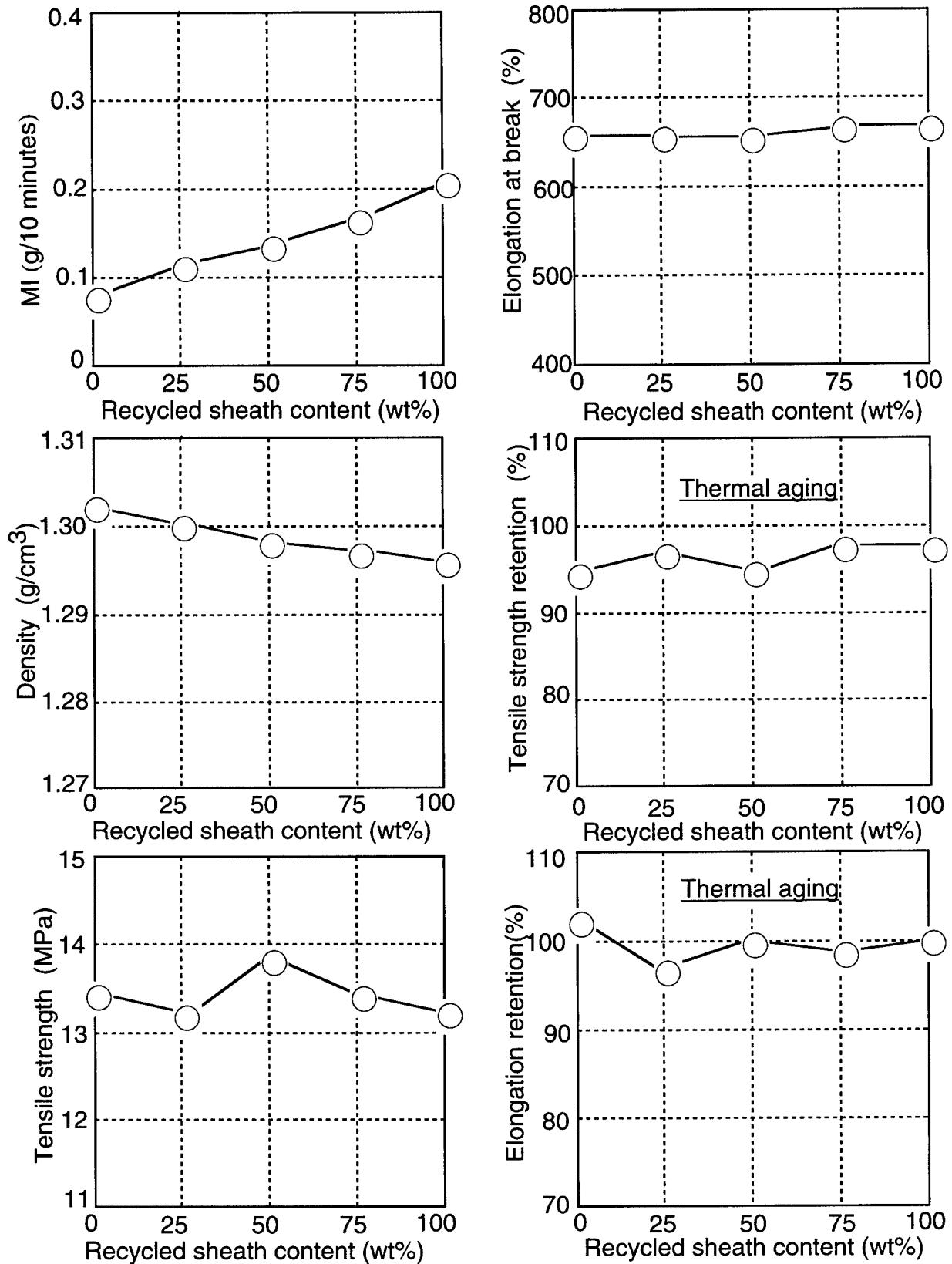


Figure 9 Properties of recycled FR sheath materials

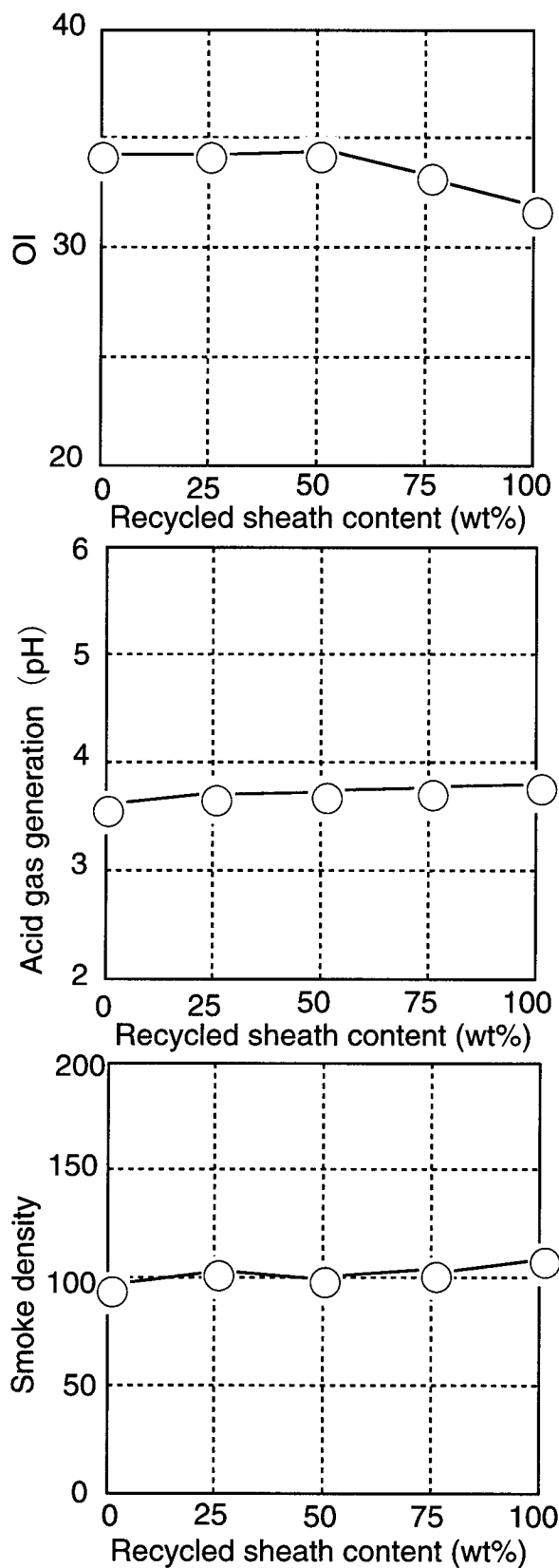


Figure 10 Flame retardant properties of recycled FR sheath material

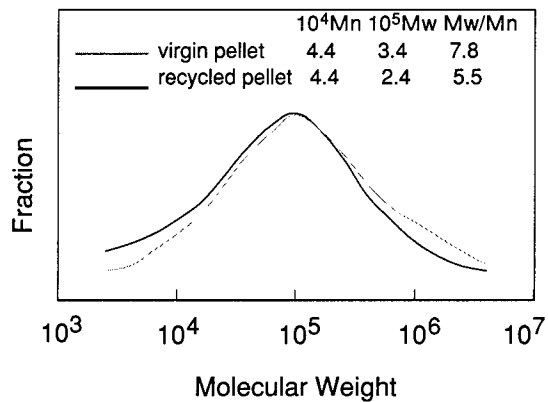


Figure 11 Molecular weight distribution curves of virgin and recycled PE materials

Performance of Optical Cable with Recycled Sheath

We produced 300-fiber SM optical cables with PE and FR sheaths containing 50 % and 100 % recycled sheath material. The properties of optical cables with 50%-recycled sheaths and the properties of the sheaths, themselves, which are similar to those of new sheaths, are shown in Table 3. The performance of recycled optical cables in, crush, squeezing, torsion, impact, repeated bending and flame retardant tests is similar to that of current cable. The performance also was same with 100%-recycled sheath. These results show that recycled sheath material is sufficient for use with optical cable. It was necessary to reduce adequately the amount of water and dust in the recycled materials by controlling the cleaning and drying processes because the water and dust had such detrimental effects on the molding of the cable sheath as causing an increase in surface roughness and the generation of voids in the sheath.

CONCLUSION

We have introduced recycling systems for stray guards and access terminal box covers. Their scrap is recycled as inner layers of stray guards and bottom sheets of access terminal boxes, respectively. These systems operate economically . We showed that the recycled sheath material has similar properties to virgin material and the performance of recycled sheath optical cable is similar to that of current cable. We will try to construct an economical system for sheath recycling and study methods for recycling other core parts.

ACKNOWLEDGMENTS

The authors are grateful to N.Murata, H.Haraguchi, M.Takeshima, K.Shyoji, and H.Yonezawa for helpful suggestions and comments.

Table 3 Properties of optical cables with 50%-recycled sheaths

Properties	PE sheath	FR sheath
<u>Sheath</u>		
Tensile strength (MPa)	16.3	13.0
Elongation at break (%)	608	624
Thermal aging		
Tensile strength retention (%)	99	99
Elongation retention (%)	98	97
Brittleness temperature F_0 (°C)	< - 60°C	< - 15°C
<u>Cable</u>		
Crush (dB)*	< 0.1	< 0.1
Squeezing (dB)*	< 0.1	< 0.1
Torsion (dB)*	< 0.1	< 0.1
Impact (dB)*	< 0.1	< 0.1
Repeated bending (dB)*	< 0.1	< 0.1
	(no damage)	
Combustion length (cm)	-	85

*Optical loss increment



Tsuneo Konaka

NTT Access Network Systems Laboratories
1-7-1 Hanabatake, Tsukuba-shi, Ibaraki, 305 Japan

Tsuneo Konaka is a senior research engineer. He was born in 1949 and received B.S. and M.S. degrees in nuclear engineering from Hokkaido University in 1972 and 1974.

He joined NTT in 1974. Since 1994 he has engaged in research on recycling and environmental matters related to outside plant.



Shiro Nishi

NTT Science and Core Technology Laboratory
Group
Musashino-shi, Tokyo, 180 Japan

Shiro Nishi is a senior research engineer. He was born in 1957 and received B.S. and M.S. degrees in macromolecular science from Osaka University in 1980 and 1982.

He joined NTT in 1985. Since 1996 he has engaged in research on the recycling of plastics.



Shinjiro Murai

NTT Procurement & Supply Department
Tokyo Opera City, 26th Floor
20-2 Nishishinjuku 3-Chome, Shinjuku-ku, Tokyo,
163-14 Japan

Shinjiro Murai was born in 1950. He joined NTT in 1972. Since 1988 he has developed scrap recycling systems.

$$\tau = \eta \frac{\partial v}{\partial r} \quad \eta = \text{viscosity} \quad (2)$$

Deviating (2) to ∂r and introduced in (1) we get the differential equation:

$$\frac{\partial p}{\partial z} = \eta \left(\frac{1}{r} \frac{\partial v}{\partial r} + \frac{\partial^2 v}{\partial r^2} \right) \quad (3)$$

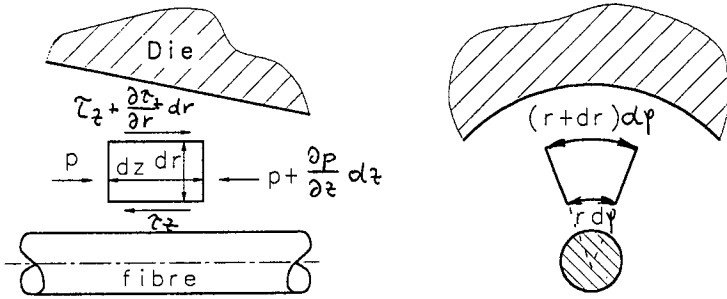


Fig. 2: Equilibrium on a volume element

which can be found also in literature. The simplifications made (flow in z-direction only, constant temperature of the fluid, ideal newtonian fluid) will not seriously influence the results to be obtained. As in fibre colouring the colour layer is very small (4 μm) compared to the fibre radius (125 μm) we neglect the term $\frac{1}{r}$ in

(3) and get the following equation

$$\frac{\partial p}{\partial z} = \eta \frac{\partial^2 v}{\partial r^2} \quad (4)$$

which can be integrated in general way (no numerical methods needed). Together with the boundary conditions of the speed and the pressure an expression for the pressure and velocity distribution is obtained.

With $h = H - \frac{H-h_s}{t_0}z$, $z \in [0, t_0]$ we get for the taper part

$$v(r) = \frac{2\eta v_f}{\left(\frac{H-h_s}{t_0}\right)} \left(\frac{3}{h-f} - \frac{1}{2f} \ln \frac{h+f}{h-f} \right) + \frac{3\eta A}{\pi r^2 \left(\frac{H-h_s}{t_0}\right)} \left(\frac{2f-h}{(h-f)^2} + \frac{1}{2f} \ln \frac{h+f}{h-f} \right) - \frac{12\eta B}{\pi} \quad (5)$$

$$v(r) = \frac{2v_f(h+2f)(r^2 - r(f+h) + fh)}{(h-f)^2(h+f)} - \frac{6\eta v_f}{\pi(h-f)(h+f)} + v_f \frac{h-r}{h-f} \quad (6)$$

$$A = \frac{\frac{\pi v_f}{6} \frac{H-h_s}{t_0} \left(\frac{3(H-h_s)}{(H-f)(h-f)} - \frac{1}{2f} \ln \frac{(h+f)(H-f)}{(h-f)(H+f)} \right) - \frac{\pi}{12\eta} \delta p_0}{\frac{1}{4f^2} \frac{H-h_s}{t_0} \left(\frac{(2f-h)(H-f)^2 - (2f-H)(h-f)^2}{(h-f)^2(H-f)^2} + \frac{1}{2f} \ln \frac{(h+f)(H-f)}{(h-f)(H+f)} \right)} = q[t_0]$$

$$B = \frac{\pi \left(\frac{2f-H}{(H-f)^2} + \frac{1}{2f} \ln \frac{H+f}{H-f} \right) \delta p_0}{12\eta \left(\frac{(2f-h)(H-f)^2 - (2f-H)(h-f)^2}{(h-f)^2(H-f)^2} + \frac{1}{2f} \ln \frac{(h+f)(H-f)}{(h-f)(H+f)} \right)} - \frac{\pi(\Delta p + p_s)}{12\eta}$$

$$\delta p_0 = \frac{\pi \left(\frac{\Delta p(h-f)^2(h+f)}{4\eta(t-t_0)} + v_f(h+2f) \right) (h-f)}{\left[\frac{4f^2}{12\eta} \frac{H-h_s}{t_0} \left(\frac{(2f-h)(H-f)^2 - (2f-H)(h-f)^2}{(h-f)^2(H-f)^2} + \frac{1}{2f} \ln \frac{(h+f)(H-f)}{(h-f)(H+f)} \right) + \frac{(h-f)^2(h+f)}{(t-t_0)} \right] + \frac{4\eta^2 v_f}{\pi} \left(\frac{3(H-h_s)}{(h-f)(H-f)} - \frac{1}{2f} \ln \frac{(h+f)(H-f)}{(h-f)(H+f)} \right) + \frac{(2f-h)(H-f)^2 - (2f-H)(h-f)^2}{(h-f)^2(H-f)^2} + \frac{1}{2f} \ln \frac{(h+f)(H-f)}{(h-f)(H+f)} \right] + \frac{\pi}{12\eta} \left[\frac{4f^2}{12\eta} \frac{H-h_s}{t_0} \left(\frac{(2f-h)(H-f)^2 - (2f-H)(h-f)^2}{(h-f)^2(H-f)^2} + \frac{1}{2f} \ln \frac{(h+f)(H-f)}{(h-f)(H+f)} \right) + \frac{(h-f)^2(h+f)}{(t-t_0)} \right]}$$

For the cylindrical part the equations are (with $h = H = h_s$, $z \in [t_0, t]$):

$$p(z) = p_a + \frac{t-z}{t-t_0} \delta p_1 \quad (10)$$

$$q[t_0, t] = \frac{\pi v_f(h-f)(h+2f)}{3} + \frac{\pi(h-f)^2(h+f)}{12\eta(t-t_0)} \delta p_1 \quad (11)$$

$$v(r) = (h_s - r) \left(\frac{v_f}{h_s - f} + \frac{r-f}{t-t_0} \frac{\delta p_1}{2\eta} \right) \quad (12)$$

$$\delta p_1 = \Delta p + \delta p_0 \quad (13)$$

The tension force F_R on the fibre is

$$F_R = \pi f(h-f) \delta p_1 - 2\pi \eta v_f \frac{t-t_0}{h_s-f} + \frac{6A\eta t_0}{(h_s-f)(H-f)} + \frac{3A\eta v_f}{f} \frac{H-h}{H-h} \ln \frac{(h-f)(H+f)}{(h+f)(H-f)} + \frac{2\pi \eta v_f}{H-h_s} \left(4 \ln \frac{h_s-f}{H-f} - \ln \frac{h_s+f}{H+f} \right) \quad (14)$$

And finally the coating thickness on the fibre can be computed with

$$s = \sqrt{\frac{q_{[0,t_0]}}{\pi v_f}} + f^2 - f. \quad (15)$$

2.2 Optimization of die dimensions

Using the dimensionless characteristic values

$$\bar{H} = \frac{H}{h_s} \quad \text{and} \quad \bar{t} = \frac{t_0}{t}$$

been done, allowing to optimise the die dimensions according to the chosen optimisation criteria. Very often in technical applications the best form is the one giving the smallest hydraulic friction of the fibre in the die (note that the die form **and** the feed pressure act on the friction created in the die). We optimized the die form for highest pressure generation in the die. The highest pressure gives the highest spring - and attenuation constants characterising the self centering behavior (an only small eccentricity of the fibre in the die creates the highest possible pressure unbalance pressing the fibre back to its centered position). Optimized pressure generation is obtained for

$$2 \leq \bar{H} \leq 2.4$$

$$\text{and } \bar{t} = 0.9.$$

Both optima are relatively flat (not very pronounced). For manufacturing reasons $\bar{t} = 0.7$ had been chosen. The difference to the optimum value of $\bar{t} = 0.9$ is negligible.

3 CASE STUDY

For conditions typical in the fibre colouring application, the pressure distribution in the die has been calculated with these values $2f = 250\mu\text{m}$, $h_s = 7.5\mu\text{m}$, $\bar{H} = 2.2$, $\bar{t} = 0.7$, $\eta = 1 \text{ Pas}$. Fig. 3 shows pressure distributions at different colouring speeds calculated for a negligible supply pressure. The high absolute peak pressure may be surprising; they are due to high viscosity of the ink, the high line speed and the pressure optimized die design. Fig. 4 shows generated pressures in the die as a function of the supply pressure. As long as the supply pressure is small ($0 \leq \Delta p \leq 5 \text{ bar}$) there is no significant influence on pressure generation. On 4 selected locations in the die, the velocity profile of the ink has been calculated (Fig.5). Again the small variations of the supply pressure do not alter the velocity profile significantly. Necessarily the thickness at the colour layer cannot vary either (Fig. 3-5 for $\eta = 1 \text{ Pas}$).

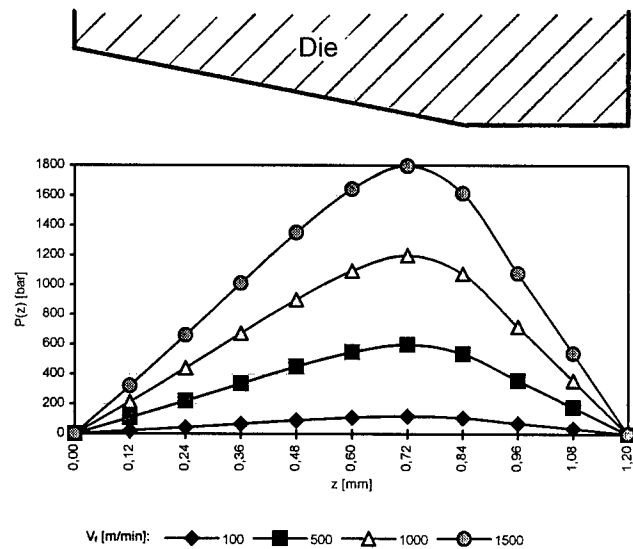


Fig. 3: Pressure distribution in the die at different fiber velocities [m/min]

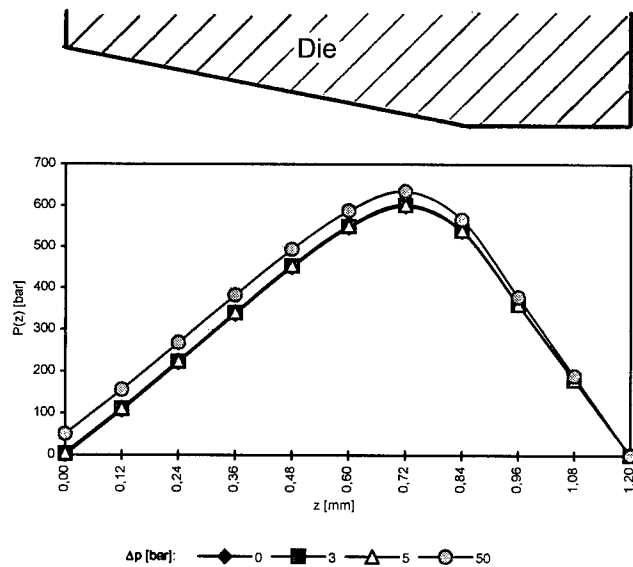


Fig. 4: Pressure distribution in the die with different supply pressures [bar] at 500 m/min

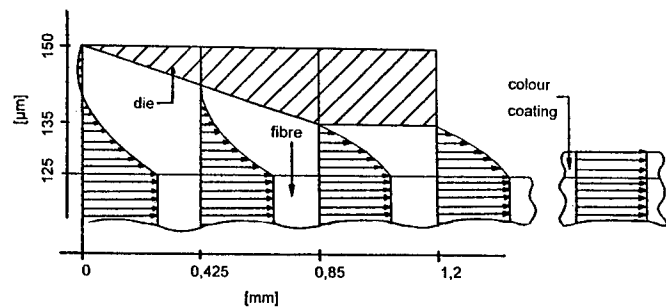


Fig. 5: Calculated velocity profiles at 500 m/min

A convenient way to verify whether all calculated values coincide to reality is to compare at least one calculated parameter to the same one measured. Our fibre optic colouring line is equipped with a pressureless colour feeding system and a load cell for the continuous display of the fibre tension force. (the purpose of this load cell in a production line is to function, via chosen thresholds, as an early warning system to, e.g. a dirt accumulation in the colouring die, lack of ink, etc.).

Fig. 6 shows calculated and measured friction forces of the fibre in the die. The right interpretation needs a few precisions. The viscosity of colour "D" at 20, 40 and 50°C is 14, 1.5, 0.8 Pas. This colour has additionally a thixotropic behavior (=shear thinning). The viscosity of colour "H" at 20, 40 and 50°C is 2.6, 1.3, 1.0 Pas. This colour is a newtonian fluid (no shear thinning). Measurements have been made at a controlled temperature of 40°C, nevertheless the colour temperature in the die is higher: with increasing speed the friction power ($F_R \cdot v_f$ [Nm/s]) increases and heats up the colour.

Velocity dependent friction forces have been calculated for $\eta = 2.8$ and $\eta = 1.0$. The higher viscosity ($\eta = 2.8$) represents the viscosity at low speed, the low viscosity ($\eta = 1.0$) anticipates the fact, that viscosity drops with increasing temperature created by friction. All measured values lie between these limits, the points calculated for low viscosity fitting well the measured values for high speeds and vice versa. For the needs of this study the calculation of colour temperature increase with increasing speed (via an energy balance) was not necessary.

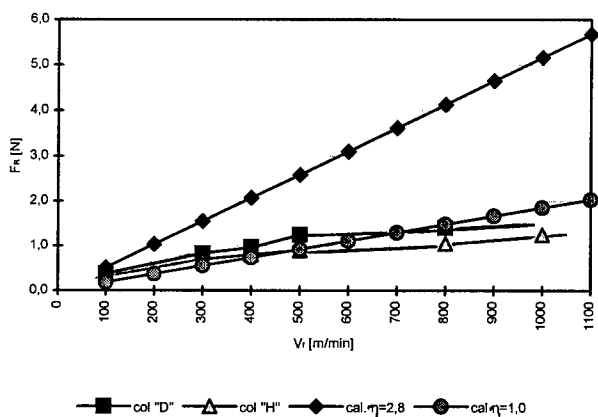


Fig. 6: Measured and calculated friction forces in the die on the fibre during colouring

4 COMPARISON

The examples presented allow for at least a qualitative comparison of a pressureless and pressurized colouring system.

4.1 Layer thickness

Using a pressureless colouring system, the colour layer thickness depends on the dimensions of the fibre and the die only. The layer thickness does not depend on the viscosity (temperature), line speed and naturally not on ink pressure.

On pressurized systems the same is true as long as the feed in pressure is small ($0 \leq \Delta p \leq 5$).

High feed pressures would naturally increase the layer thickness. For a constant thickness the feed pressure has to be adapted to the line speed and to the viscosity of the ink.

4.2 Layer thickness variation

Colouring optical fibres has the additional effect that existing diameter variations of the fibre normally are reduced to half of this variation. This is a very welcome effect when manufacturing optical fibres ribbons. Let us assume that a given fibre has a diameter variation of 10 µm between the thinnest part of 245 µm and the thickest part of 255 µm. After colouration through a 265 µm die, the outer diameter will become 253 µm for the 245 µm part and 258 µm for the 255 µm part. The original variation of 10 µm has been reduced to the half of 5 µm after colouring. This is true for a pressureless colouring system and for low supply pressures. This equalizing effect decreases with increasing feed pressure.

4.3 Self centering

The highest centering pressure at a given eccentricity is obtained with no or only small feed pressures. When interpreting Fig. 4, one has to keep in mind that this comparison has to be made for a given layer thickness, not for a given die dimension. Samples produced on an intentionally badly aligned die (angle of about 5° between center line of die and fibre) and on a pressureless feed system showed layer thickness variations (eccentricity) smaller than what could be measured from a photograph taken with a scanning electron microscope. It is true that surface tension effects might also contribute to maintain concentricity.

4.4 Practical considerations

4.4.1 Die size

No or only small supply pressures allow the use of the biggest possible die. As the gap between the fibre and the die is a few microns only this effect brings on appreciated contamination tolerance to the inking process.

4.4.2 Replenish

A pressureless open ink container may be refilled anytime during colouring without influencing the process in any way.

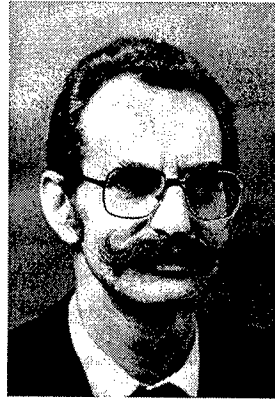
4.4.3 Simplicity

The simplicity of a pressureless colouring system cannot be beaten.

5 CONCLUSION

The investigations made have shown that the influence of feed pressure to the colouring process have been overestimated. For small feed pressures (<5 bar) there is no significant difference between a pressurized and pressureless system. High feed pressures would influence the process negatively. For practical reasons a pressureless colouring system is preferable, mainly due to its simplicity.

An optimized design of the die is most important. A die form optimized for maximum selfcentering has been calculated. All results and conclusion made here apply for thin layers only; conditions become rapidly very different as soon as the layer thickness becomes more important.



Bruno E. Bulushek graduated in mechanical engineering at the Technische Hochschule, Munich. In 1968, he started as a research engineer at the Federal Institute of Technology in Zürich, Switzerland, and received his PhD in 1979. He joined Maillefer SA where he was in charge of the R&D Department and of the Extrusion Department. In 1988 he started his own engineers office and is now technical manager at SWISSCAB Switzerland.

Dr.-Ing. Bruno E. Bulushek
SWISSCAB E.Kertscher S.A.
CH - 1462 Yvonand
Switzerland
Tel.: +41-24-4300-160
Fax: +41-24-4300-124



Miroslav Blánarik was born 1974 in Slovakia. Since 1990 he lives in Austria (Bruck an der Mur), where he finished the school. Since 1993 he is a student at Technische Universität Graz, Austria, where he studies technical mathematics, branch computer science. He is currently working as a summer intern for SWISSCAB.

Study of the relationship between optical fiber strength after splicing and the method of optical fiber cleaning prior to splicing

J. Suzuki S. Yaguchi M. Yoshinuma

Fujikura Ltd. Sakura-shi, Chiba-ken, JAPAN

ABSTRACT

The strength of optical fiber is generally 4.8GPa, but if optical fibers are spliced by arc fusion splicing, the strength of the splice drops dramatically. The spliced fiber strength averages about 0.64GPa when typical fusion splicing methods are used. This strength is easily varied by the detail of the method of splicing. The fiber cleaning process prior to splicing especially affects the fiber strength. There are various methods of fiber surface cleaning and various types of wipes that can be used. We studied the relationship between spliced fiber strength and the method of fiber surface cleaning. The results are as shown below:

<u>Cleaning Method</u>	<u>Average Strength</u> (GPa)
Acid cleaning	2.01
Cotton wipe	0.67
Gauze wipe	0.67
Paper wipe	0.59
Arc cleaning	0.52

1. INTRODUCTION

Arc fusion splicing is the most common splicing method when a good splice loss is required, and stable, long splice life is needed. The following are the common splicing processes:

1. Stripping the coating
2. Cleaning the fiber surface
3. Cleaving

4. Arc fusion splice
5. Proof test
6. Reinforcing the spliced fiber

A "proof test" is done in order to guarantee the life of the spliced fiber, and weak fibers are eliminated in this process. The strength of optical fiber is generally 4.8GPa, but the strength decreases when fibers are spliced. The lower strength occurs due to stress concentration at microscopic cracks on the optical fiber surface. The microscopic cracks arise from various causes.

The strength of spliced optical fiber is 0.64GPa when arc fusion splicing is employed. This numerical value may change according to the methods of fiber preparation used. We particularly stress the relationship between optical fiber strength after splicing and the method of cleaning the fiber before splicing. The most commonly used fiber cleaning processes are:

- Cleaning with cotton, paper or gauze wipes
- Cleaning with chemicals (acids, organic solvent, or organic solvent + ultrasonic waves)
- Cleaning by burning (electric arc discharge)

There are other methods for cleaning optical fiber, such as $H_2 - O_2$ torch or ozone cleaning, but these are not common. The most useful cleaning method is by use of an alcohol soaked wipe.

There are various types of wipes. We studied the spliced fiber strength when we cleaned the fiber with

different wipes, and we studied the relationship between spliced fiber strength and methods of arc cleaning and acid cleaning.

2. METHOD OF ARC FUSION SPLICING

2.1 Splicing processes other than cleaning

These processes were standardized in order to clarify the effect of cleaning upon spliced fiber strength.

Stripping the fiber coating

The fiber coat stripping was done by a mechanical stripper. The hole diameter in the stripper blade is large enough so that the fiber surface does not touch the edge. (Fig. 1)

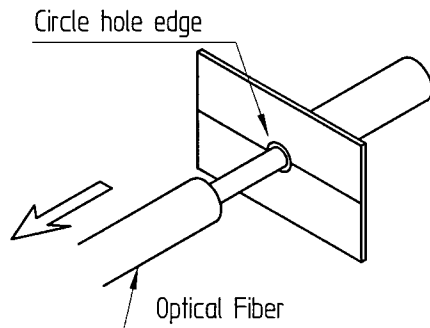


Fig.1 Stripping the fiber coating

Cleaving

A general (industry standard) cleaving tool was used to cleave the fiber (Fig. 2).

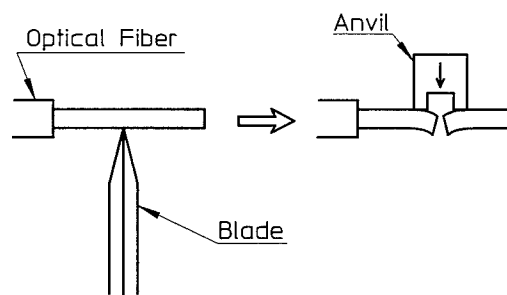


Fig2. Cleaving

Arc fusion splice

A high strength splicer was used for the splicing process. The fiber surface did not directly touch the splicer, because the coated part of the fiber was inserted into the splicer V-groove. (Fig. 3)

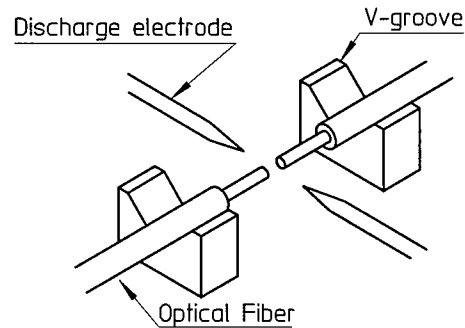


Fig3. Fiber position in V-groove

2.2 The cleaning process

Acid cleaning

We soaked the glass surface of the optical fiber in acid to clean thoroughly, then soaked it in volatilization chemicals to remove the acid.

Wipe cleaning

We wiped the glass surface of the optical fiber four or five times with an alcohol-dampened wipe. Three types of wipes were used:

- Cotton
- Gauze
- Paper (lint-free tissue)

Arc cleaning

As shown in Fig. 4, we cleaned the dust from the optical fiber by using an electrical arc. The arc power and the distance between arc and fiber were adjusted so that the fiber did not melt.

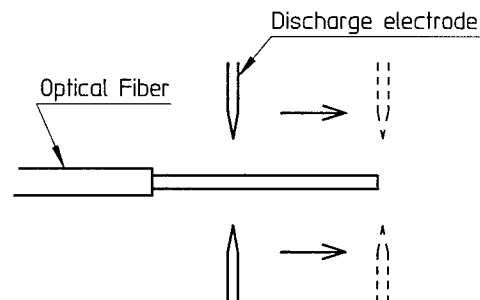


Fig4. Arc cleaning

3. RELATIONSHIP BETWEEN SPliced FIBER STRENGTH AND EACH CLEANING PROCESS

The relationship between fiber and cleaning method and fiber strength is as follows:

Cleaning Method	Strength (F=50%)
Acid cleaning	2.01GPa
Cleaning with cotton wipe	0.67GPa
Cleaning with gauze wipe	0.67GPa
Cleaning with paper wipe	0.59GPa
Arc cleaning	0.52GPa

Test parameters were:

Number of splices	200 (wipe cleaning) 20 (acid and arc cleaning)
Gage length	0.1 m
Strain rate	20% /min.
Test environment	23° C 45%RH

Weibull plots of the strength values are shown in Fig. 5-1 through Fig. 5-5

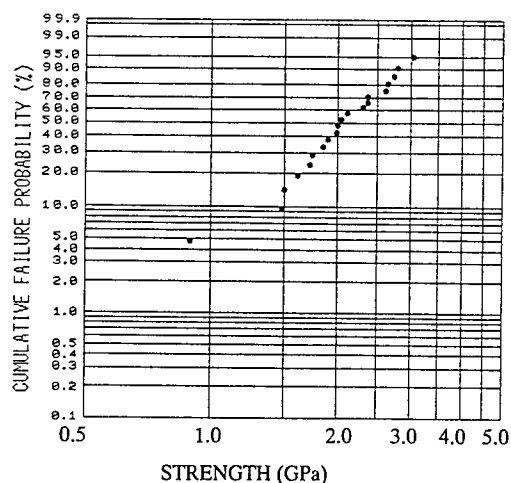


Fig. 5-1 Optical fiber strength after aplicing (Acid cleaning)

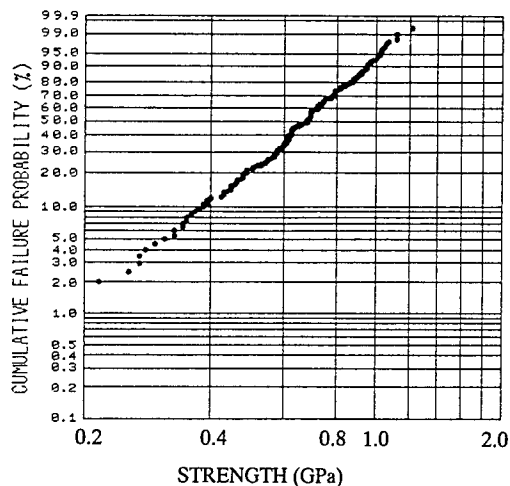


Fig. 5-2 Optical fiber strength after aplicing (cleaning with cotton wipe)

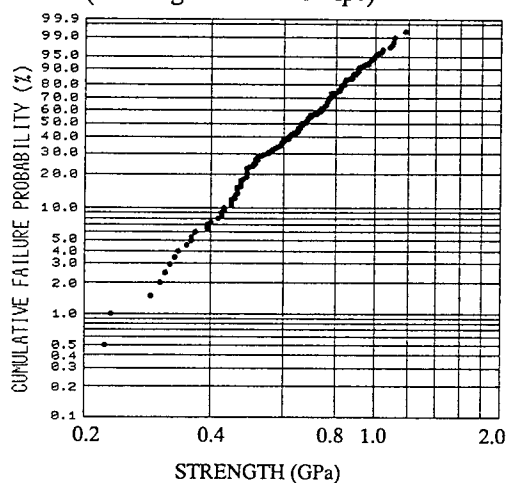


Fig. 5-3 Optical fiber strength after aplicing (cleaning with gauze wipe)

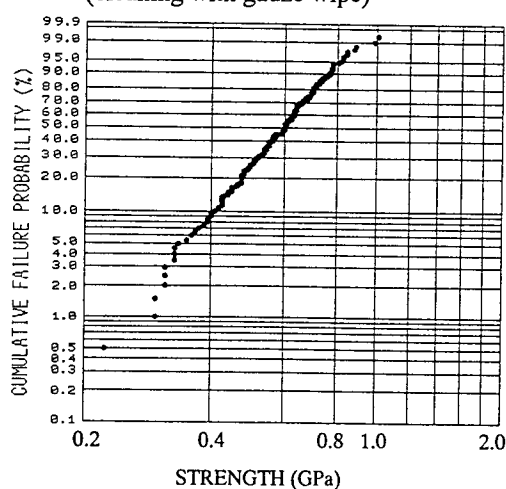


Fig. 5-4 Optical fiber strength after aplicing (cleaning with paper wipe)

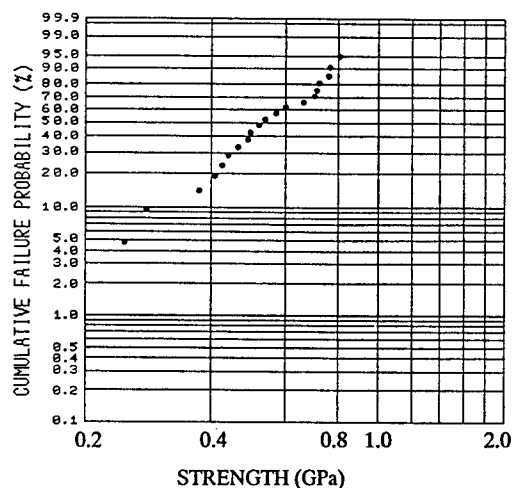


Fig. 5-5 Optical fiber strength after applying (Arc cleaning)

4. RELATIONSHIP BETWEEN THE DYNAMIC FATIGUE OF SPLICED FIBER AND EACH CLEANING PROCESS

We investigated the dynamic fatigue of spliced fiber. There were no differences in dynamic fatigue among the cleaning processes tested.

Cleaning Method	n
Acid cleaning	18
Cleaning with cotton wipe	17
Cleaning with gauze wipe	19
Cleaning with paper wipe	18
Arc cleaning	18

The dynamic fatigue test results are shown in Fig. 6.

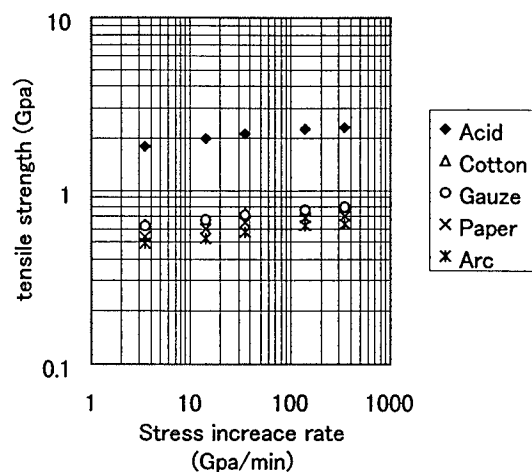


Fig.6 Dynamic fatigue test results

5. CONCLUSION

As stated above, we investigated the strength of spliced optical fiber which was cleaned using various methods prior to splicing. We investigated the dynamic fatigue and showed that there are no differences in dynamic fatigue among the cleaning processes tested.

REFERENCE

T. Wei, C.H. Hasz and P.L. Key
 "DEGREDDATION OF FIBER STRENGTH DURING COATING STRIPPING"
 International Wire & Cable Symposium
 Proceedings, p.199-204, 1989



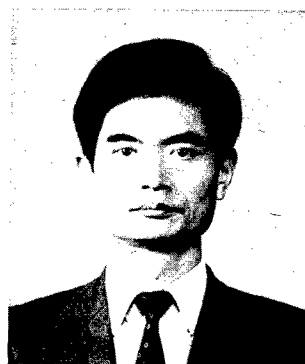
Junichi Suzuki

Precision Instruments
R&D Dept.
Fujikura Ltd

1440,Mutsuzaki,
Sakura-shi,
Chiba-ken, 285,
JAPAN

Junichi Suzuki was born in 1963. He graduated in precision mechanical engineering from Shizuoka University in 1986.

He joined Fujikura Ltd. In 1986 and had been optical fiber production engineering section for 7 years and has been engaged in the research and development of an optical fiber splicers and related products.



Mikio Yoshinuma

Precision Instruments
R&D Dept.
Fujikura Ltd

1440,Mutsuzaki,
Sakura-shi,
Chiba-ken, 285,
JAPAN

Mikio Yoshinuma was born in 1947. He graduated in mechanical engineering from Chiba University in 1971.

After graduation, he joined Fujikura Ltd. And has been engaged in research and development on mechanical equipment and tools for communication wires, cables, and parts. He is now a general manager of the Precision Instrument R&D Department, including responsibility for fusion splicer R&D.



Shonosuke Yaguchi

Precision Instruments
R&D Dept.
Fujikura Ltd

1440,Mutsuzaki,
Sakura-shi,
Chiba-ken, 285,
JAPAN

Shonosuke Yaguchi was born in 1955. He graduated in mechanical engineering from Keio University in 1979.

He joined Fujikura Ltd. In 1979 and had been engaged in the Plant Engineering Section for 12 years and currently is a manager of the Precision instruments R&D department.

Evaluation of Color Stability of Optical Fiber Coatings

S.-H. Chou, J.-C. Lin, C.-M. Hsiao, H.-F. Lin, H.-P. Hsu, Y.-c. Lin, Y.-K. Tu

OSP, Telecommunication Laboratories, Chunghwa Telecom, Taiwan, R.O.C.

ABSTRACT

The factors to influence the color stability of optical fiber coatings have been evaluated in this study. The colored fibers were aged at 100°C in the oven for a period of one year. The data shows a clear feature that the fibers colored with different curing processes result in different discoloration mechanisms. The fibers colored with thermally-cured inks have the greater part of color changes during the first three months to one year and then the color changes approach to equilibrium. On the other hand, for the fiber colored with UV-cured inks, the colors remain almost unchanged for the first one month, and then changed in demonstrating a monotonous increase over the aging time. Furthermore, regardless of the curing processes made, its own essence of the color is another important discoloration factor. The effects of the essential properties of color — lightness (value), hue and chroma — on the color stability of optical fiber coatings are also discussed in this paper.

INTRODUCTION

The optical fiber utilized in telecommunication and data transmission is usually coated with polymeric materials. In order to identify polymer-coated optical fibers, visually distinct inks are applied to the fiber surface.⁽¹⁻⁴⁾ The color stability of colored fiber is adversely influenced by aging and is related to the characteristics of the inks, the characteristics of the secondary coating, and the interactions with the environment to which the fiber is exposed.

The inks may be solvent-based and thermally cured, or cured by exposure to UV light.⁽⁴⁻⁵⁾ The specific characteristics of the inks in the colored fiber are normally affected by the manufacturing processes. Generally, the coloring layer obtained by UV-cured method provides a more transparent, thinner and more uniform surface. Exposed to the service environments with time, coating materials have been observed to exhibit color changes. Thermal oxidative process may cause the secondary coating to yellow.⁽¹⁾ If the coloring layer is not thick or opaque enough to mask this yellowing, the fiber coating can contribute to the color changes during aging. However, aging process also may produce the coloring layer to discoloration; the color change of optical fiber

therefore is a complicated problem due to the contribution from both secondary coating and coloring layer.

Color has three essential properties, lightness (V, value), hue (H), and chroma (C). Munsell symbol (H V/C) and (L*, a*, b*) color notation are used to describe the color in this paper.^(1,3,4,6) Munsell symbol (H V/C) can provide a very clear color sense; the main disadvantage however is the calculation problem and color difference description. Based upon the CIE system (Commission Internationale de l'Eclairage), the L*a*b* space uses an xyz coordinate system to describe a color, including the lightness coordinate L*, the red-green coordinate a*, and the yellow-blue coordinate b*. Compared with Munsell notation, the main advantage of the L*a*b* notation is the simplicity of the calculations; however, hue and chroma senses are not clear enough.

Furthermore, color difference, ΔE^*_{ab} , is used to describe the distinction between color₁ (L*₁, a*₁, b*₁) and color₂ (L*₂, a*₂, b*₂), which is expressed as the linear distance between these two points. On the other hand, it also can be introduced to represent the deviation from the unaged sample.

$$\Delta E^*_{ab} = ((\Delta L^*)^2 + (\Delta a^*)^2 + (\Delta b^*)^2)^{1/2} \quad (1)$$

The color identification of fibers is adversely influenced by aging. The curing process is an important factor to affect the discoloration mechanisms. The nature of the color, including its lightness, hue and chroma stabilities, is another factor. The objectives of this work are to study the effect of aging on colored fibers and evaluate the factors to influence the color stability of optical fiber coating.

EXPERIMENTAL

The samples were supplied from five suppliers, identified as fibers A, B, C, E and F. Twelve differently colored fibers (blue, yellow, green, red, violet, white, brown, black, aqua, orange, rose and slate) were provided from each supplier. Fibers from A were colored with thermally-cured inks, whereas the others were with UV-cured inks.

The fiber samples were enclosed in a buffer tube and already submerged in filling compounds supplied from their original suppliers. Colored fibers were aged at 100°C in the oven, and then removed from the aging environment after one month, three months, six months

and one year for examining.

The main problem to measure the color of the optical fiber is attributed to the small size of the fiber, 250 μm in diameter, which is inherent to the optical fiber. For providing a large viewing area, the fibers have to be laid parallel and touching in a holder which is a square hollow with 20 mm in each side and about 0.5 mm in depth and is made of Teflon plate. Furthermore, the fiber sample containing two layers of fibers orthogonal to each other avoiding background effect is necessary. Due to the pseudo-plane including several curved surfaces, different orientations between illumination/receiving and fiber direction may result in different color data. Macro-P method, which has been introduced previously, was used to measure the colors of all samples.⁽⁶⁾

The colorimeter includes an Otsuka MCPD-1000 Spectro Multi Channel Photo Detector using an accessory, MC-955, for a large-area sample and an available software for color measurement. The D_{65} standard source was used as the light source. The instrument equipped with a Y-shaped optical fiber to connect the light source and the photo detector. The Y-shaped optical fiber directed the light at a 0° angle to the fiber surface and guided it at 45° back to the photo detector which monitored the reflected light by a photodiode array. The $0^\circ/45^\circ$ illumination and receiving geometry was used. The measurement area was 5 mm in diameter and the sampling time was 2.4 sec. Color data were calculated via the colorimeter software using a data processing unit. Each data point was the average of three individual measurements.

RESULTS AND DISCUSSION

Due to a large number of fiber samples, the data obtained in this study were numerous. However, the color data obtained from the samples using UV-cured processes show similar patterns of color changes; only the data of fibers obtained from suppliers A, B and C therefore are shown to be discussed in this paper.

Furthermore, it should be noted that the color data of fibers obtained by macro-P method are given by the $L^*a^*b^*$ notation. To discuss the color data, transformation of the data into Munsell symbol (H V/C) is necessary. JIS color chips were measured by the colorimeter to provide (L^* , a^* , b^*) data corresponding to original (H V/C) symbols as calibration references. The relationships between them have been introduced in previous paper,⁽⁶⁾ it therefore should not be noted here again.

The initial color data of fibers from these three suppliers measured by the colorimeter are summarized in Table 1. The data are presented by Munsell symbols which provide a very clear color sense: There are some features in this Table. First of all, it clearly shows that the colors provided

from different suppliers can be quite different color data, including different hue, different lightness, different chroma, and/or even all. Secondly, the achromatic samples (white, black and slate) have somewhat chroma values. Moreover, they own the hue ranges around Y (yellow) and YR (yellow-red) except the slate samples from A. Finally, the white and yellow fiber samples from these suppliers display the highest lightness values comparing with the other colors. On the other hand, the yellow, red and orange samples have much higher chroma values.

It is well-known that the colors are perceived as darker and duller after aging. By calculations, the color changes of fiber samples provided from A, B and C under aging environments are presented in Figures 1, 2 and 3, respectively. The fiber samples were removed from aging after one month, three months, six months and one year. Each Figure includes the color difference, ΔE^*_{ab} , values of 12 colors for four aging periods. The ΔE^*_{ab} value below 5 is assumed within experimental error. Higher ΔE^*_{ab} values indicate larger deviations from the original color. These Figures display several general features.

Black fibers, having the ΔE^*_{ab} value below 2.5 even aging for one year, seem inert to the aging environment no matter what the supplier is. Regardless of the aging periods, except black, the brown and slate samples also display good color stability comparing with the other colors. On the other hand, the blue and yellow samples exhibit the worst color stability. In addition, the fiber samples from C possess much better color stability comparing with those from the other two suppliers.

Another important feature in these Figures is the rate of color change of fiber samples during one year aging. The data shown in Figures clearly exhibit two quite different discoloration mechanisms. The samples from A, which were colored with thermally-cured inks, experienced most of their color changes during the first three months, and then the equilibrium amount of color change for each color was generally reached. On the other hand, the colors of the samples from the other suppliers, which were with UV-cured inks, remained almost unchanged for the first one month, and then changed in demonstrating a monotonous increase over time. The data conclude that the curing process is an important factor to influence the discoloration mechanisms.

The comparison of the ΔE^*_{ab} data obtained from the fibers colored with thermally-cured and UV-cured inks showed that thermally-cured colored fibers supplied from A had obviously color changes at the beginning, especially for the yellow sample having the ΔE^*_{ab} value up to 41.5 during the first one month. In contrast, the yellow samples colored with UV-cured inks from B and C had the color

differences only 7.4 and 2.5, respectively. However, after aging for one year, the ΔE^*_{ab} values of the yellow samples from A, B, and C were 45.6, 52.3 and 32.0, respectively. It implies that although different discoloration mechanisms are provided by the fiber samples colored with different curing processes, the data show that the color changes have similar magnitudes after aging for one year.

However, for understanding the discoloration factors, the ΔE^*_{ab} values cannot clearly depict the direction of color change. L^* diagram and a^*-b^* diagram can be used to present more detailed description about this problem.

Figures 4, 5 and 6 show the L^* data for 12 colors graphically through L^* diagrams corresponding to suppliers A, B and C, respectively. The points marked the same symbol display that they are experienced for the same aging period. As shown in Table 1, the white and yellow fibers possess highest lightness values. The data shown in these Figures indicate that the lightness stabilities of these two colors are the worst.

Considering the rate of lightness change, the samples from A experienced most of their lightness decreases during the first one month, whereas those from B did most of their lightness changes occurred from sixth month to one year. However, during aging for one year, among the fiber samples from these suppliers, ones from B exhibit the worst lightness stability, whereas ones from C have the best lightness stability. Therefore, the curing process is not a unique factor for the color change. Although the fiber samples are colored with the same process, thermal stability may be different due to the other factors, such as raw materials of the coloring layer and the manufacturing processes.

Figures 7, 8 and 9 show all (a^* , b^*) data for chromatic colors graphically through the a^*-b^* diagrams that correspond to suppliers A, B and C, respectively. The (a^* , b^*) data are used to depict hue and chroma. Chroma (C^*) and hue angle (h) can be calculated by equations (2) and (3), respectively.

$$C^* = ((a^*)^2 + (b^*)^2)^{1/2} \quad (2)$$

$$h = \tan^{-1} (b^*/a^*) \quad (3)$$

In these Figures, the points marked the same symbol exhibit that they are experienced for the same aging period. The points from the same colored samples are drawn with a line. The distance between the data point and the zero point expresses the chroma value of this point. The longer the distance, the higher the chroma. The hue change is considered to be the angle change between two points moved around the zero point.

Among the (a^* , b^*) data, no matter what the supplier is,

ones aged for a longer period are much near to the zero point having lower chroma. Besides, the length of the line shown in the Figures can be used to explain how the color stability is. It has to be noted that the shorter the length, the better the stability of hue and chroma properties.

The data show clearly that the rates of color changes based upon the (a^* , b^*) data behave in similar trends to those based upon the ΔE^*_{ab} data presented in Figures 1, 2 and 3. Furthermore, after aging one year, all brown samples and the red samples from A and C have much more stable hue and chroma properties. On the contrary, all blue, yellow and aqua samples exhibit very bad stability. Therefore, it ensures that different colors behave various degrees of color stability. In addition, some colors are remarkably sensitive to the aging process, such as blue, yellow and aqua. The results suggest that its own essence of the color is another important discoloration factor regardless of the curing process used.

Blue, yellow and aqua have the worst color stability whatever the supplier is. More interesting problem is what the major contribution to their discoloration behavior is, lightness, hue or chroma contribution. Their color data from these three suppliers experienced for several aging periods are presented in Table 2. These data are offered by Munsell notations which can provide more detailed information. Generally, for the blue samples, the major contribution to the color change is from hue and chroma. Whereas, for the yellow ones, the color change is attributed to the bad stability of lightness and chroma, possibly due to the high lightness and chroma values of the unaged fibers. On the other hand, the most important discoloration factor of the aqua samples can be attributed to the hue changes.

Considering the thermal stability of chroma, if the chroma value of the color is higher, then the thermal stability of the color is generally worse. The chroma data show that yellow and blue samples have the worst chroma stability. As shown in Table 1, the yellow, red and orange samples have much higher chroma values. It therefore is reasonable that the chroma values of the yellow ones drop fast. However, the red samples having high chroma values display quite stable results comparing with yellow and orange samples. On the other hand, before aging, the chroma values of blue samples only are about half of those of yellow ones. After aging for one year, the chroma changes of both samples are similar. This suggests that the chroma stability of blue colors exhibit remarkably sensitive to the aging environment. Furthermore, the result can conclude again that its own essence of the color is an prominent discoloration factor.

By comparison, the hue changes move in the direction in a curve, changing the hue from PB, B, BG, G, GY, Y, and

then to YR. However, also considering the a^*-b^* diagrams, no matter what the hue is before aging, the hues of all colors move toward YR range, clockwise (including blue, aqua, yellow) or anti-clockwise (such as violet and red), after aging. The farther the distance from YR area, the less stable the hue. It means that after aging all colored samples turned brown color. Therefore, the blue and aqua samples having the worst hue stability can be attributed to the original hues having the farthest distance from YR.

SUMMARY

For evaluating the factors to affect the color stability of optical fiber coatings, the colored fibers were aged at 100°C in the oven for a period of one year. This study concludes that the curing process used and its essential properties of the color are two important discoloration factors. The rate of color change can be dominated by the inking technology used. Optical fiber coatings colored with thermally-cured inks experienced the majority of their color changes during the first three months to one year, whereas those with UV-cured inks remained almost unchanged for the first one month. The effects of the essential properties of color present different features. First of all, the higher the lightness value (yellow and white), the worse the lightness stability. Secondly, the chroma stability is affected by both its value and its own essence of the color. The yellow samples have the bad chroma stability due to the high chroma value. However, the bad chroma stability of blue ones can be attributed to its own unstable inner nature. Finally, after thermal aging all colored samples turn brown color. The farther the distance from YR area (blue and aqua), the less stable the hue.

REFERENCES

1. R. A. Frantz and I. M. Plitz, *Proc. 42nd IWCS*, 850, 1993.
2. J. R. Petisce, M. D. Kinard, S. Siddiqui and C. Taylor, *Proc. 42nd IWCS*, 552, 1993.
3. J.-C. Lin, S.-H. Chou, C.-M. Hsiao, H.-P. Hsu, Y.-c. Lin and K.-Y. Chen, *Proc. 44th IWCS*, 502, 1995.
4. B. J. Keon and R. A. Frantz, *Proc. 43rd IWCS*, 522, 1994.
5. R. A. Frantz, E. M. Vogel and B. J. Keon, *Proc. 44th IWCS*, 146, 1995.
6. S.-H. Chou, J.-C. Lin, C.-M. Hsiao, H.-P. Hsu, Y.-c. Lin and K.-Y. Chen, *Proc. 45th IWCS*, 561, 1996.

Table 1. Initial color data (H V/C) of colored fibers from three suppliers

Color	supplier A	supplier B	supplier C
Blue	3.0PB 3.0/10.7	10.0B 3.0/8.5	5.5B 3.9/9.0
Yellow	2.5Y 7.8/13.0	6.5Y 8.0/10.0	2.5Y 7.8/12.0
Green	2.5G 4.4/8.5	10.0G 3.4/8.0	1.8G 5.0/9.8
Red	2.0R 3.4/12.0	2.0R 4.1/13.0	3.5R 3.8/12.5
Violet	2.5P 4.2/9.5	4.0P 4.3/8.0	8.0P 3.4/7.0
White	5.0Y 8.7/0.3	4.0Y 8.6/1.1	10.0YR 8.4/0.7
Brown	6.5YR 4.1/3.5	4.5YR 4.4/5.2	4.0YR 4.4/5.5
Black	6.0Y 1.1/0.5	10.0YR 0.8/0.2	1.0Y 0.6/0.1
Slate	10.0G 4.6/0.8	5.0Y 4.2/0.3	5.0Y 4.1/0.1
Aqua	8.5B 6.3/7.5	4.5B 6.4/5.0	7.5B 6.2/6.5
Orange	0.5YR 5.8/12.5	2.5YR 5.7/12.5	6.0YR 6.7/10.5
Rose	1.5R 6.3/7.5	7.5R 6.9/7.0	8.5R 6.6/8.0

Table 2. Color data of blue, yellow and aqua from three suppliers for aging several periods

color	aged time	supplier A	supplier B	supplier C
BL	Initial	3.0PB 3.0/10.7	10.0B 3.0/8.5	5.5B 3.9/9.0
	aged 1 M	1.5PB 2.9/7.6	6.6B 3.1/ 7.6	5.0B 3.9/8.8
	aged 3 Ms	9.1B 2.6/4.8	4.5B 2.7/6.4	1.7B 3.8/8.0
	aged 6 Ms	7.0B 2.7/ 4.6	8.6BG 2.7/5.3	7.5BG 3.5/6.4
	aged 12 Ms	5.9B 2.5/ 4.4	5.0BG 1.9/2.9	5.0BG 2.9/4.6
YL	initial	2.5Y 7.8/13.0	6.5Y 8.0/10.0	2.5Y 7.8/12.0
	aged 1 M	2.1Y 5.6/ 7.7	5.0Y 7.8/9.0	2.5Y 7.9/11.7
	aged 3 Ms	8.9YR 4.7/ 6.7	3.9Y 7.3/8.6	2.0Y 7.5/11.3
	aged 6 Ms	8.0YR 5.0/ 7.6	0.8Y 6.5/8.1	0.9Y 6.9/10.3
	aged 12 Ms	8.3YR 5.3/8.0	6.2YR 4.8/6.1	10.0YR 6.1/8.7
AQ	initial	8.5B 6.3/7.5	4.5B 6.4/5.0	7.5B 6.2/6.5
	aged 1 M	1.4B 5.7/2.1	9.8BG 6.6/4.5	4.1B 6.4/5.6
	aged 3 Ms	5.8Y 4.8/0.8	0.6BG 6.3/3.4	9.5BG 6.2/4.4
	aged 6 Ms	6.1Y 4.9/1.8	5.9GY 5.8/2.5	5.0BG 5.9/3.0
	aged 12 Ms	8.7Y 4.9/2.0	5.5YR 4.3/1.5	5.5BG 5.5/2.0

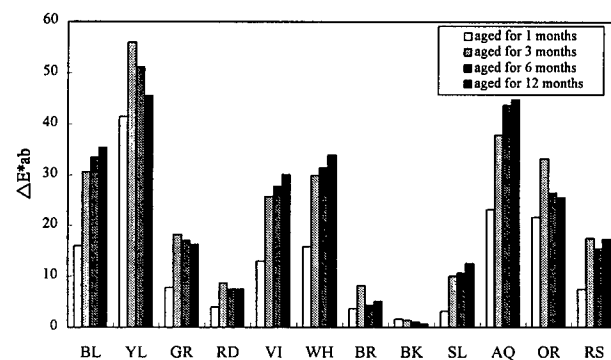


Figure 1. Color changes ΔE^*_{ab} for colored fibers from A.

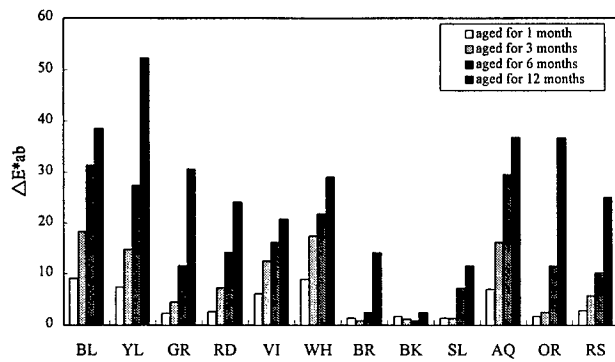


Figure 2. Color changes ΔE^*_{ab} for colored fibers from B.

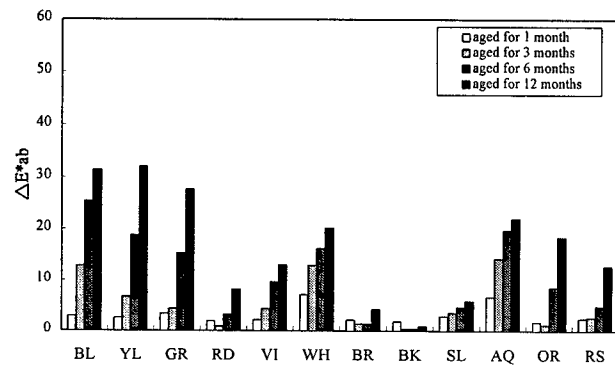


Figure 3. Color changes ΔE^*_{ab} for colored fibers from C.

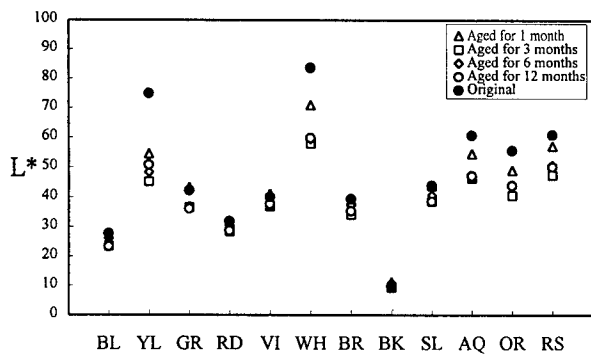


Figure 4. L^* diagram for colored fibers from A, the points marked the same symbol experienced the same aging period.

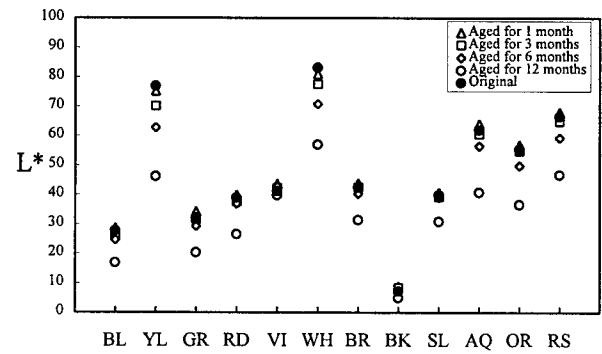


Figure 5. L^* diagram for colored fibers from B.

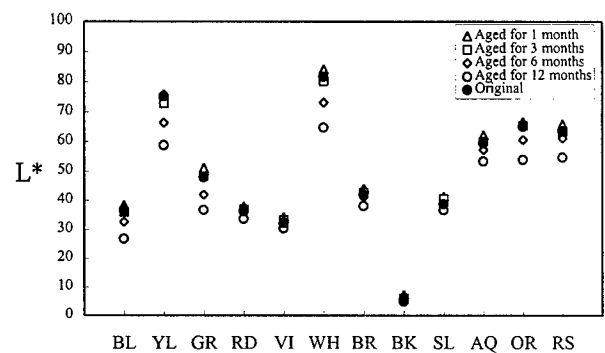


Figure 6. L^* diagram for colored fibers from C.

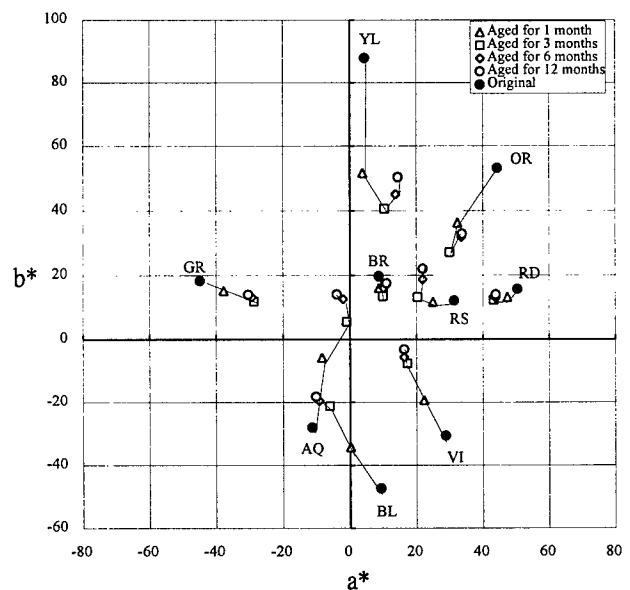


Figure 7. Color data of nine colors (without achromatic colors) from A graphically through a^* - b^* diagram, the points marked the same symbol experienced the same aging period.

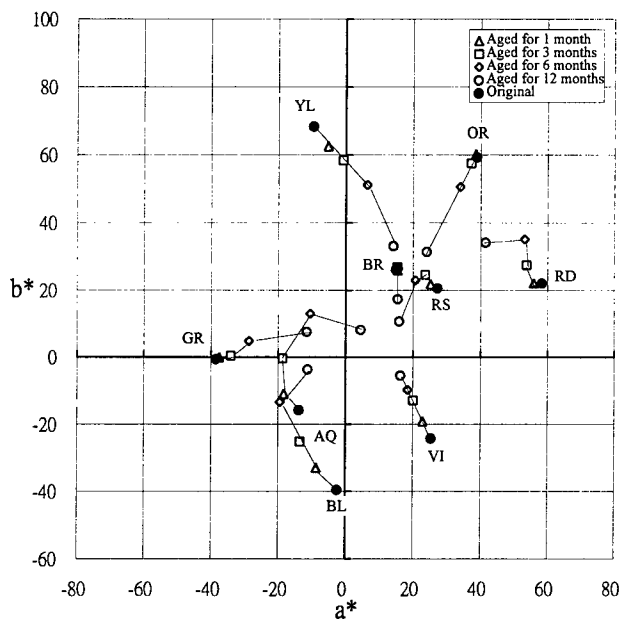


Figure 8. Color data of nine colors (without achromatic colors) from B graphically through a^* - b^* diagram.

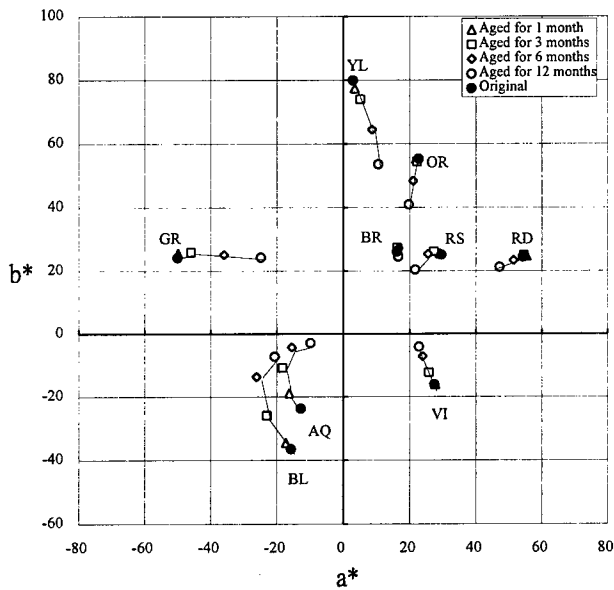


Figure 9. Color data of nine colors (without achromatic colors) from C graphically through a^* - b^* diagram.

NUMERICAL SIMULATION OF OPTICAL FIBER COATING PROCESS

Katja J. Lyytikäinen

Nokia-Maillefer, Vantaa, Finland

ABSTRACT

One of the main difficulties in achieving high drawing speeds relates to the primary coating of the fiber. Good quality of the coating must be maintained also at high speeds. To meet the prerequisites for high speed drawing of optical fiber, detailed knowledge of the coating process is essential. Major advances in computer technology and computational mechanics attract the use of numerical modeling. In this work a fluid dynamics analysis package using the finite element method is used to model the optical fiber coating process. The main object of the work is to gain better knowledge of the physical phenomena in the coating die and to determine the relationship between coating parameters such as pressure, temperature, geometry of the die, etc., and the internal centering forces in the die. This paper describes the results of the simulations covering pressure, temperature and flow profiles with different taper angles of the die.

INTRODUCTION

For years, optical fiber has been the main information transmission medium. In pace with technological development there is a growing need to transfer larger and larger volumes of information. Today the production of optical fiber is around 30 million kilometers per year, which is less than the demand. In consequence the demand for higher production capacity generates the need for increased research and development work in the field of optical fiber and cable manufacture.

The most important part in the manufacturing process of optical fiber is the fiber drawing process. In order to draw high quality fiber a

successful coating process is of utmost importance. Thus it is vital to understand the physical phenomena inside the coater during processing. In order to optimize the process the relationship between major process parameters and the product quality must be known. Increasing the knowledge of the coating process enables more reliable design criterion resulting in improved coating construction.

In past years effort has been made to construct analytical models that describe the coating process. The relation between coating thickness and process parameters such as drawing speed, die geometry and surface tension effects have been studied by Dunn¹, Paek and Schroeder^{2,3}, Chida et al.⁴, Mitsoulis⁵ and Panoliaskos et al.⁶. The theories were mainly constructed in 1980's for low drawing speeds. To enable an analytical approach assumptions such as constant properties for coating material are usually made and viscous heating is neglected. However, for high speed drawing such assumptions are not necessarily valid^{5,6}.

COATING PROCESS

The fundamental process of the manufacture of optical fiber is the fiber drawing process. A quartz-based optical preform is drawn out into fiber in a drawing tower. The preform is fed into a furnace which is heated to 2200°C. At the same time the fiber is drawn down and out of the furnace. After cooling down the bare fiber is coated with two layers of UV-curable acrylate. High quality coating with good concentricity and accurate dimensions is essential for a successful optical fiber drawing process.

The purpose of the coating on the optical fiber is to protect the fiber from contact and foreign

particles as these significantly reduce the strength of the fiber. Besides strength preservation, the coating must protect from microbending by being concentric and bubblefree around the fiber and by having a stable performance in different environments. Usually the fiber is coated with two layers of UV-curable acrylate; a soft inner layer protects the fiber and a hard outer layer ensures good mechanical properties. The layers can be applied simultaneously by one applicator (wet-on-wet method) or separately by two different applicators (wet-on-dry method). Irrespective of the application method the quality of the primary coating is mainly characterized by the concentricity and diameter variation of the coating. Figure 1 shows a schematic diagram of coating and Figure 2 the usual dimensions of a coated optical fiber.

The coater die has the property of producing concentric coating due to centering forces in the coater die. In respect of controlling the concentricity of the coating, the main task is to understand the relationship between the centering forces in the die and the geometry of the die.

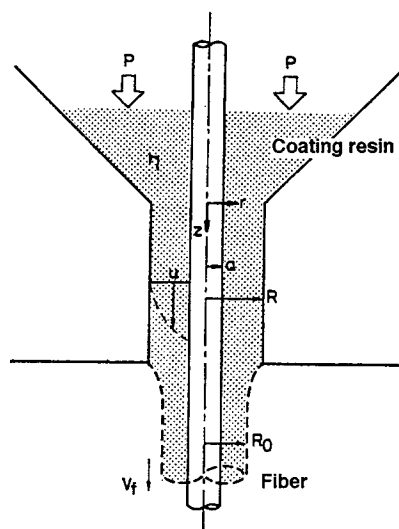


Figure 1. Schematic diagram of coating

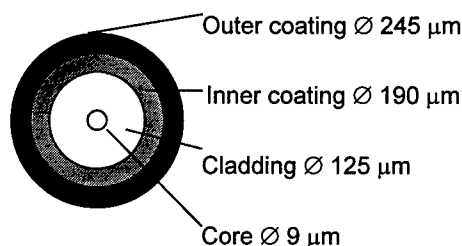


Figure 2. Cross-section of optical fiber with two layers of coating

NUMERICAL ANALYSIS

In this work the optical fiber coating process is approached from the computational fluid dynamics (CFD) point of view. The computational approach allows investigating of different model configurations under different physical conditions in a relatively short time and reducing the number of expensive and time consuming tests. Successful utilization of CFD on similar applications as optical fiber coating has been reported in literature⁷.

Fluid dynamics analysis package FIDAP is used to study the fluid flow inside the coating applicator. This general purpose CFD software package is based on the Finite Element Method and is extensively used for applications in the field of material processing.

The following steps describe the process of numerical modeling.

1. The creation of a model which describes the acrylate flow in the primary coating process of optical fiber.
2. The verification of the model through appropriate tests.
3. The use of numerical simulation to determine the optimal process parameters.

In the simulation typical input parameters are die geometry, die wall temperature, drawing speed, fiber temperature and the physical properties of the coating material. The simulation produces e.g. pressure, temperature, velocity and material property fields of the acrylate in the die.

MODEL

The geometry of the coater is simplified to be axisymmetric. The free surface at the outlet of the die is fixed. The acrylate flow is described by Navier-Stokes equations for incompressible fluid. Navier-Stokes equations are connected to heat equation via the temperature dependency of the viscosity of the fluid. It is reasonable to assume that the flow is laminar and independent of time. Heat transfer consists of heat conduction in the acrylate and in the fiber as well as of forced convection in the acrylate and advection in the fiber. Also the production of heat due to viscose dissipation is included in the heat equation.

The following assumptions are made in the model:

1. Acrylate flow is laminar and incompressible
2. The flow and temperature fields are fully developed at the outlet of the die
3. Axisymmetric constant feed of the acrylate
4. The "free" surface is fixed at the outlet of the die
5. No-slip condition is valid on the coater walls
6. The temperature of the coater wall is constant
7. The temperature of the acrylate feed and inlet fiber temperature are constant.

For these assumptions to be valid the coating process must be stable and the coater geometry modified such that the third assumption of constant, axisymmetric acrylate feed is reasonable.

Typical input parameters for the simulations were:

- fiber diameter = 125 μm
- acrylate viscosity, see Figure 3
- temperature of acrylate feed = 30°C
- drawing speed = 13 - 17 m/s
- temperature of the fiber at the inlet = 60°C
- applicator wall temperature = 40°C

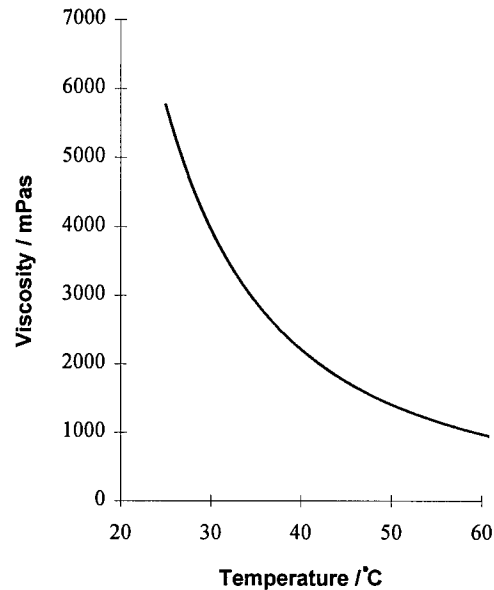


Figure 3. Viscosity of the coating material

The geometry of the model is shown in Figure 4. For the simulations the geometry remained unchanged except for the lower part of the die where the taper angle was changed. The die has a short cylindrical part at the outlet.

SIMULATION RESULTS

From Figure 4 can be seen that the flow field is smooth and that the speed of the fluid slows down from the fiber speed (13 m/s) to zero on the applicator wall being 0.7 m/s halfway the tank radius. The 'cold' acrylate (30°C) warms up at a relatively short range as it flows slowly towards the fiber. The temperature stabilizes to that of the applicator wall (40°C) at the upper part of the coater. The fiber entering at 60°C temperature cools down quickly and does not heat the surrounding material. However, as is seen in Figure 5 the effect of viscous heating is considerable at the lower part of the die. The temperature is at its maximum at the cylindrical part of the die. For this particular geometry the temperature rise at the cylindrical part is approximately 3°C. Depending on the temperature this accounts to hundreds of mPas drop of viscosity for this particular coating material, see Figure 6. The pressure in the

applicator is quite even except for a peak at the upper corner of the die. This probably indicates the advantage of using a smooth die without sharp corners to avoid any source of instabilities in the flow.

A simulation with increased drawing speed was also conducted. The fiber speed was increased from 13 m/s to 17 m/s, other parameters left unchanged. The shapes of the velocity and pressure profiles are the same in both cases. However, as was expected, the pressure level was higher for the higher drawing speed. The temperature profile was also the same but the temperature rise due to viscous heating was more severe for the higher drawing speed. The maximum temperature was at the cylindrical part of the die being 3°C higher for the 17 m/s drawing speed. The temperature increase in the lower part of the die was 9°C for the lower drawing speed and 11°C for the higher speed. The effect on the values of viscosity are not however that drastic as at higher temperatures the decrease of viscosity is smaller for temperature rise of same magnitude.

Simulations with altering taper angles of the lower part of the die were conducted to clarify the function of the die geometry. The temperature, velocity and pressure fields did not show any major differences. The temperature rise due to viscous heating increased as the taper angle was decreased. As the model was axisymmetric, no real centering forces could be directly derived. However, the trends were estimated using two models, the other having a tighter geometry simulating the situation of horizontally dislocated fiber. The results showed an increasing centering effect of the die as the taper angle was increased to a certain level. The cylindrical part appeared not to have any centering effects as was the case with the upper part of the applicator.

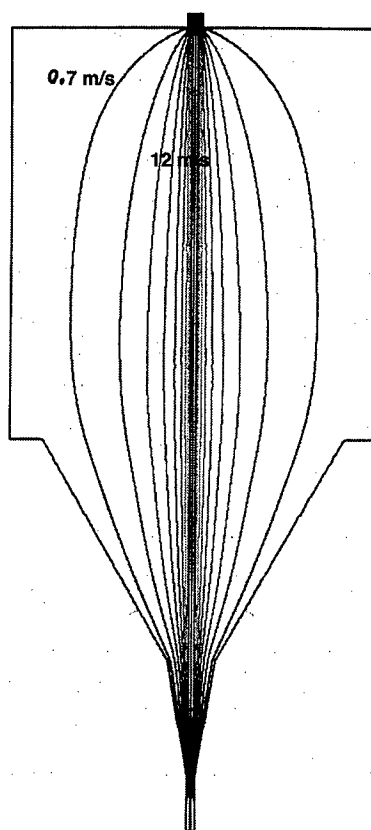


Figure 4. Speed contour plot of the acrylate in the applicator.

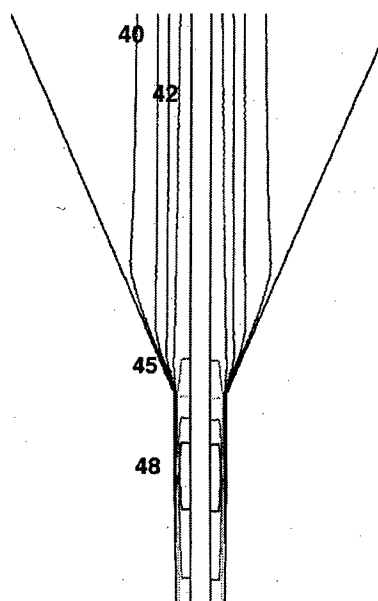


Figure 5. The temperature of the acrylate in the coater die.

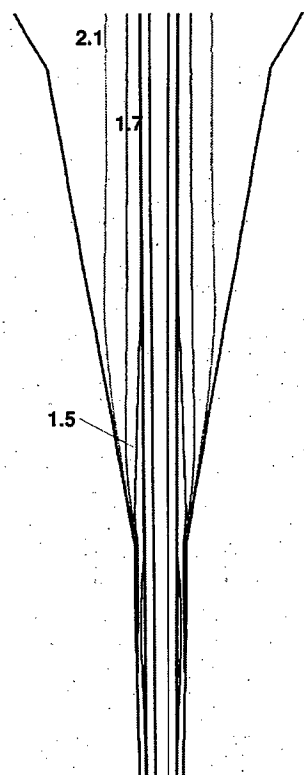


Figure 6. The viscosity of the acrylate in the coater die.

CONCLUSIONS

In this work computational fluid dynamics was used to simulate the fluid flows in the optical fiber coating applicator. The results show the potential of using a numerical approach to the problem of studying flow behavior of a fluid in micro dimensions. The function of the lower die was studied thus excluding the effect of the guiding die at the entrance of the incoming fiber.

AUTHOR



Katja Lyytikäinen
Nokia-Maillefer Oy
P.O.Box 44
FIN- 01511 Vantaa
Finland

Katja Lyytikäinen is currently studying at the Helsinki University of Technology, Finland. This work is part of her Master of Science Theses for Chemical Engineering Department. She joined Nokia-Maillefer in 1997 and is presently engaged in high-speed coating techniques for optical fibers.

The preliminary test results showed a promising support for the simulations, however, indicating the complexity of the coating process showing the importance of proper material feed and the guiding die as emphasized also in literature⁸.

In order to gain additional knowledge of the process and to accommodate the nonidealities, the model will be further modified. For example a 3D-model will be constructed and free surfaces studied at the outlet of the die.

REFERENCES

1. France and P.L. Dunn, "Optical Fiber Protection by Solution Plastic Coating", *Proceedings, Second European Conference on Optical Fiber Communication*, 1976, p.177.
2. U.C. Paek and C.M. Schroeder, "High Speed Coating of Optical Fibers with UV Curable Materials at a Rate of Greater Than 5 m/sec", *Applied Optics* **20** (23), 4028-4033.
3. U.C. Paek and C.M. Schroeder, "Coating of Optical Fibers with a Conical Shape Applicator", *Fiber and Integrated Optics* **2** (1979), 287.
4. K. Chida et al., "High-Speed Coating of Optical Fibers with Thermally Curable Silicone Resin Using a Pressurized Die", *Electronics Letters* **18** (1982), 713.
5. E. Mitsoulis, "Finite Element Analysis of Wire Coating", *Polymer Engineering and Science* **26** (2), 171-183.
6. A. Panoliaskos et al., "Prediction of Optical Fiber Coating Thickness", *Applied Optics* **24** (15), 2309-2312.
7. P. Ehrhard and W. Kaumanns, "FEM-Simulations of the Free-Interface Flow in a Gap", *Computational Fluid Dynamics '96*, 797-801.
8. E. Seppäläinen, "Increasing the Drawing Speed of Optical Fiber", *MSc Theses, Nokia Cables*, 1996.

INSTALLATION ADVANTAGES WITH RIBBON TECHNOLOGY

Hans Serrander, Hans Olofsson

Ericsson Business Networks AB, Sundbyberg, Sweden

ABSTRACT

This paper deals with the physical aspects of installing optical fibre cables in the access network duct system. The development of products and methods means that considerable benefits, including cost savings are achieved by using the methods described below together with products containing the right properties.

A slim, light, flexible and crush-resistant cable, such as slotted-core, optical fibre ribbon cable, is ideal to use where long installation lengths are required. This type of cable allows access to individual fibres by using the midspan splicing technique. Midspan splicing makes it possible to install the distribution cable first and then to connect Optical Network Units at virtually any point along the cable.

One advantage is that when the distribution cable is installed in a ring configuration, a choice is made at each splice whether to keep the ring intact to maintain fibre diversity, or whether to allow access from both ends for maximum fibre use. The concept is applicable for both ring and full star topologies. There is less need for detailed network planning. Install the main cable and make branch splices wherever and whenever needed.

It is also very important to choose the right dimensions for the duct system for optimum cable installation performance.

Measurements are reduced to a minimum as ribbons rather than individual fibers are handled at installation time. Using ribbon components reduces errors to a minimum and installing with either floating or blowing techniques minimises fibre stress and thus the risk for fibre breaks.

NETWORK TOPOLOGY

Fibre diversity and redundancy is inherent in the ring structure, where direct fibre and SDH transmission

are supported. Both full star and PON topology are equally suitable for the fibre ring which, when installed efficiently, is the first choice for an access network where different solutions coexist in the same cable.

Modern access solutions are normally only upgraded at the head end and at the customer premises to either change or add services. Service re-routing and switching is managed by the OA&M system for SDH and ATM networks, thus allowing the physical optical access network to be constructed and left.

It is recommended that all ribbon splicing is done using simple joint-sealing techniques rather than handling individual fibers on organisers which are placed in expensive, special joint closures.

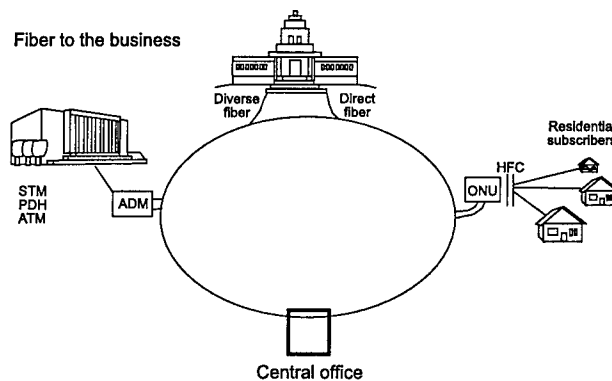


Fig.1 Fibre ring

CABLE INSTALLATION

By using blowing or floating techniques, and in some cases special cable coiling equipment, very long lengths of light, flexible optical cables can be installed (see figures 2 and 3).

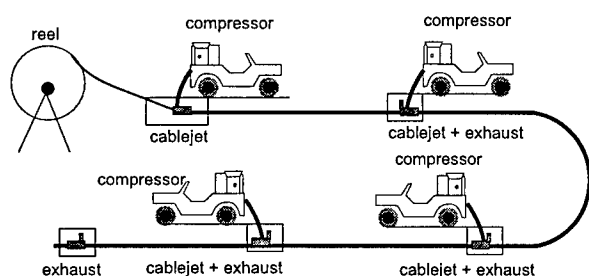


Fig.2 Blowing optical cable

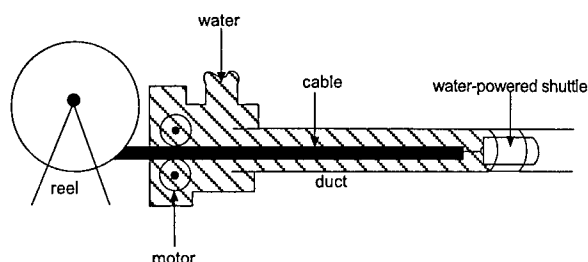


Fig. 3 Floating optical cable

The floating technique allows installation of long cable lengths, even in ducts with many bends. However, cable and duct design must be balanced correctly, in which case more than 7 km of cable can be inserted into a duct during one operation.

The ratios between the cable and duct diameter and the cable weight and flexibility must be selected carefully to ensure a successful installation.

The maximum length of a cable that is installed without any splices can be doubled if rewinding equipment is used. However, this is only possible if the cable design allows for a temporary twist when it is re-wound onto a special drum. After installation the cable returns to its normal, relaxed state. Ribbon cables with slotted-core and single sheaths have proven ideal for this purpose. (See figure 4)

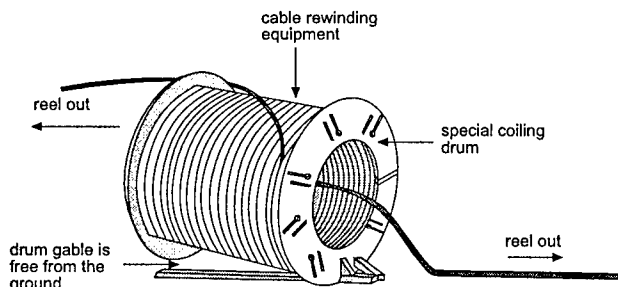


Fig.4 Rewinding equipment

Other important factors affecting installation costs are; the choice of duct (i.e. type, dimensions, material) and duct splicing method.

CABLES

Slotted-core ribbon cable designs have high fibre-density, allow easy splicing, fast repair and easy midspan access. A non-metallic cable with an FRP element for its strength member has all the properties necessary for installation by blowing and floating techniques. This type of cable is also ideal when using the midspan coiling technique.

DUCTS

The dimensions, inner surface, material and mechanical strength are important duct parameters. Installation and splicing of the duct must also be adapted for using blowing or floating techniques. Lay the duct as straight as possible to obtain the maximum performance. The inner diameter of the duct should be at least twice the cable diameter.

ACCESSORIES

Flexible wrap-around ducts can be fitted to provide extra mechanical protection if the cable is removed from the main duct. Handholes which are used for splicing and for storing cable slack must be designed for optical cables. Do not use handholes for copper cables, although if this is the only alternative verify that optical cables can be installed.

In new installations, handholes used for splicing and for containing cable slack should be specially designed for optical cables - not for copper-type cables

SPLICING COMPONENTS

Splicing optical ribbon cables is generally fast and safe. Fibres are spliced keeping the ribbon intact. Special ribbon components (see figs. 5 and 6) are used for re-routing and cross connection of either individual fibres or between ribbons.

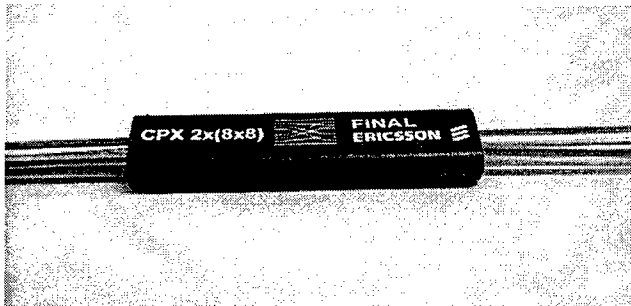


Fig.5 Cross connect component

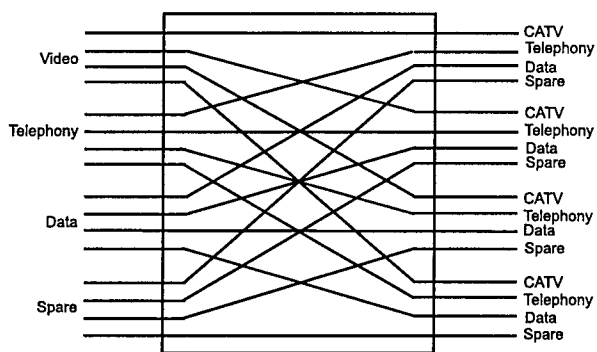


Fig.6 Cross-connection of fibre ribbons carrying different traffic flows

SPLICING CLOSURES

Splice protection and closures must be both low-cost and allow a fast installation in the access network. A method of gaining midspan access is described below: (See fig. 7)

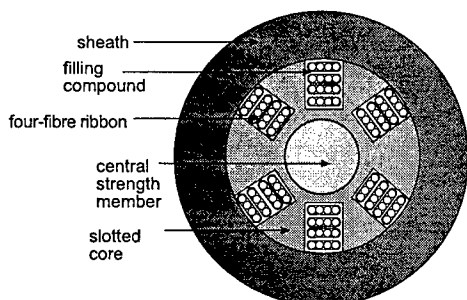


Fig.7 Cable profile

1. Remove 5 cm of the sheath to gain access to the ribbon for mid-span connection. This is the top ribbon in the slot. The desired ribbon can now be cut without cutting the central strength member.
2. The ribbon is drawn out from the cable via the nearby opening in the sheath to a maximum length of 2 m. (fig. 8) The minimum length needed for fusion splicing is 30 cm and even less for the mechanical splice technique.
3. The opening where the ribbon has been cut is repaired neatly and efficiently either by a special taping technique or is included inside the splice. No other fibres are affected by the operation. (Fig.8)

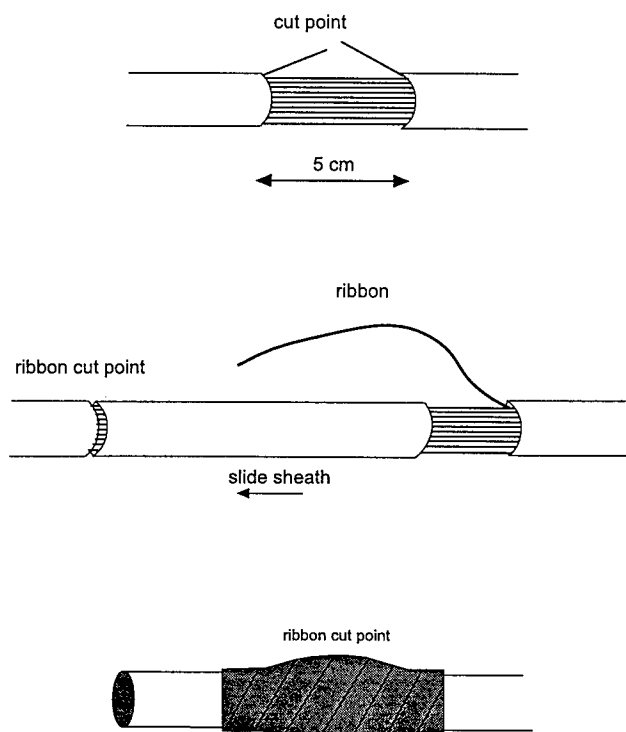


Fig. 8

4. The cut fibre ribbon (4F) is connected to a 4F-ribbon cable and protected by a simple tape or gel closure. No box or organiser is needed and the branch-off ribbon is separated from the other fibres. (Fig. 9)
5. If the 4F-ribbon cable is connected to a fibre ring where redundancy is required, then connections can be made from both sides by making two slim splices (fig. 9).
6. Normally slack is provided at midspan connection points but in some cases it could be necessary to work on a straight cable (fig 9)

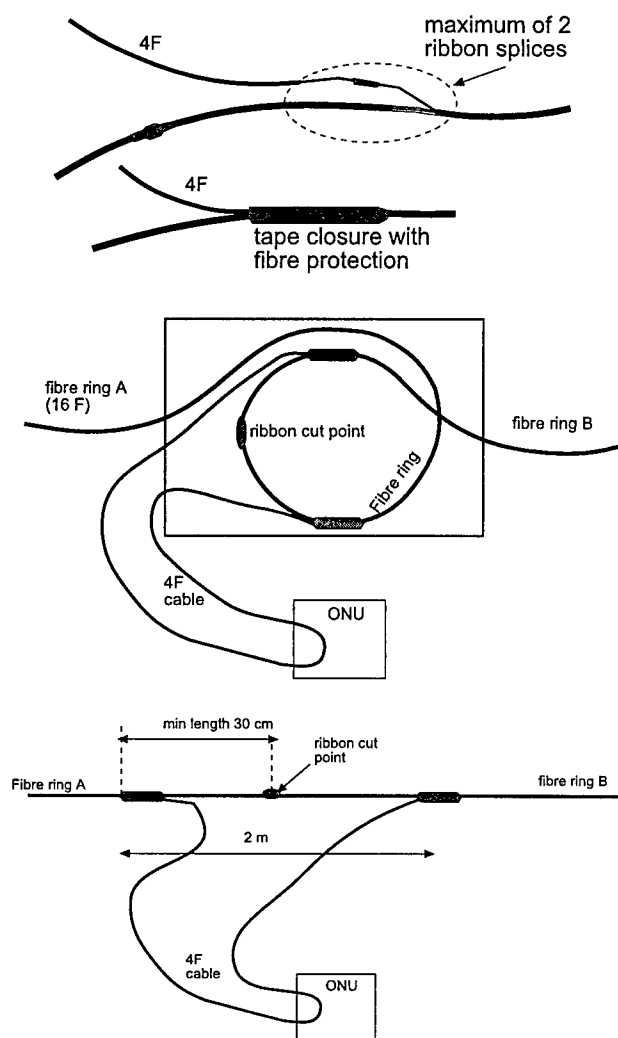


Fig.9 Fibre cable arrangements

7. All 8 fibres (double stub 4F) can be connectorised if necessary. For example, if they are needed for certain cross-connect purposes i.e. as reserves, or if looped to another ONU. This unit can be prefabricated, for example, an Optical Distribution Frame (ODF) is manufactured with connectors and stub cables of a certain length. (Fig. 10)

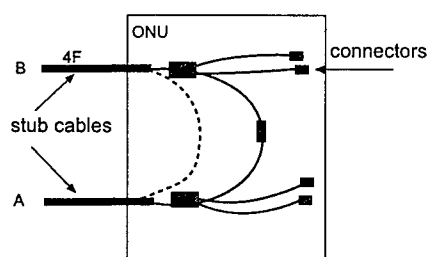


Fig 10 The ONU is connected with two fibres coming from each direction in a ring topology

TERMINATION

Pre-terminated, connectorised cables with either single-fibre or MT-connectors for an individual ribbon, can be used. These cables, including racks and/or boxes for ODF arrangements ensure an easier and faster installation and guarantee the best connector quality. Cables can be manufactured in lengths up to 300 m. Ribbon connectors can reduce the amount of tangled patch cords and ensure a more compact termination.

MEASUREMENT

Measurement time is drastically reduced with ribbon accessories such as fan-out connectors with mechanical ribbon splices. Also, it has been shown that OTDR measurements are only needed when the loss values of a fibre loop significantly exceed the typical loss values, and for maintenance and fault location.

MAINTENANCE

If fibre cables are damaged due to excavation activities, then ribbon cables are very fast and easy to repair either with fusion splicing or mechanical ribbon splices.

ADVANTAGES

The advantages of the described concept are:

- ◆ easy to install in duct systems, by blowing or floating technique.
- ◆ no splice box or cassettes necessary for midspan - lower material cost.
- ◆ only the actual ribbon is handled when midspan splicing - not the other fibres.
- ◆ midspan splice possible on straight cables. the central strength member is uncut.
- ◆ generally, fewer splices necessary due to long cable lengths.
- ◆ midspan access is faster to install compared to the conventional box methods.
- ◆ prefabricated ODF with stub cables (good quality)
- ◆ environmentally well designed installation.

AUTHORS

Hans Serrander is a Senior Outside Plant Engineer BSC Telecom Engineering, SSTA Stockholm, Sweden. Hans has been employed by both Ericsson and Telia (Swedish Telecom) for many years. He has professionally worked abroad for Ericsson and Swedtel in Mexico, Egypt and Brasil in different telecom projects. Currently he is working within Ericsson Transport & Cable Networks, and the group Network Technologies with a focus on HFC-networks.



Hans Olofsson received his M.S. degree in electronics engineering from Chalmers University of Technology, Gothenburg, Sweden in 1983. He joined Ericsson Cables in 1984 working in the transmission laboratory until 1991 when he was engaged in Ericsson's applied research. Since 1995 he has been working for Ericsson Business Networks and is currently responsible for the Network Technologies department within Business Line Cable Networks, Sundbyberg, Sweden.



NEW CLOSURE SYSTEM WITH SINGLE FIBER ACCESS FOR CONTINUOUS NETWORK OPERATION

Werner Stieb, Franz Grajewski

ALCATEL KABEL; Telecom Components Product Line, Germany

ABSTRACT

ALCATEL has an entirely new closure system to report which consists of a combination of a conventional underground branch-off closure equipped with standard splice cassettes for the main cable and a fully premounted dome-type closure with a stub cable, which can be equipped with up to 48 single subscriber cassettes. The premounted dome-type closure is installed in a small, robust and easily accessible composite housing. The premounted and cascable single subscriber cassette modules allow the access to the pre-installed fibers for the connecting of new subscribers without interrupting the operation of already active fibers. Additional advantages of the new closure system are the systematic and uniform marking of the fibers in the cassettes as well as the high economic efficiency and safety due to the storage of the uncut fibers of the main cable in a underground standard closure, which is designed to employ mass splicing technique.

INTRODUCTION

New telecommunication system operators generally design optical networks for local loop applications as ring structures for redundancy.

The connection of new subscribers in these networks is made gradually. That means that during the first installation of the network the time and place for the connection of a new subscriber is not predictable. Therefore, one requires access points in the network which allow an easy and quick connection of a new subscriber. This connection must not interrupt the operation of already active fibers. These factors identify the need for closure systems, which make a trouble-free single fiber access possible.

CONCEPT OF THE CLOSURE SYSTEM

The intended purpose of the closure system is to provide several access points to the fibers along an optical cable line. In order to avoid the expensive and time-consuming splicing of all fibers at each access point along a cable run only those fibers of the main cable for a potential

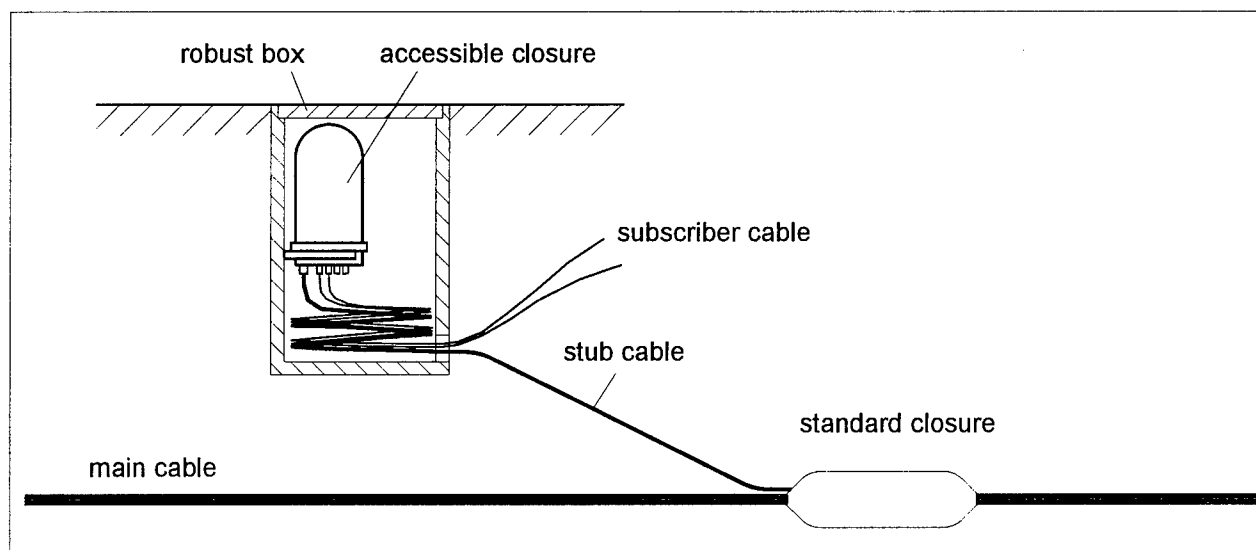


Fig. 1. Closure concept

subscriber are spliced and looped to the access point. The experience of such network installations, e.g. the TKN 2000 project in Germany, have proven that usually 15% to 30% of the main cable fibers provided for access at one point are sufficient.

In Fig. 1 the basic elements of the concept are shown.

Out of the main cable, e.g. 144 fibers loose tube construction in 12 tubes, the fibers of 4 tubes are cut and spliced to the stub cable serving the pre-mounted dome-type closure of the access point. The splices are stored in standard cassettes using time and cost-saving standard splicing methods. There is no general limitation for the fiber count of the main cable, because the choice of the buried closure is unrestricted.

The remaining tubes are looped in the standard closure without cutting.

The accessible dome-type closure is completely pre-mounted with a splice organizer for single subscriber access and is equipped with a stub cable and additional ports for the subscriber cables. The closure is stored in a small robust composite box with a spare coil of the stub cable of about 2 m length which allows removal of the closure from the composite box for connecting a new subscriber cable to the line.

Today's market offers some different closure systems with organizers for single subscriber access.

Common to most of these solutions is a relatively complicated procedure for the first installation of the closure.

For protection against damage the fibers from each tube of the main cable are fed through individual tubes to the different subscriber cassettes of the organizer. This is a very time-consuming process. Evaluations of the quoted TKN 2000 project report 30% to 50% extra time compared to a standard closure using standard splice technique. Furthermore, the feeding of fiber through tubes can cause breakage of a fiber which requires a complete new installation of the closure.

All these disadvantages and risks are avoided using ALCATEL's new pre-mounted closure system because the installation work on site is reduced to standard splicing technique.

SINGLE SUBSCRIBER ACCESS SPLICE ORGANIZER

Subscriber splice cassette

Fig. 2 shows schematically the design of the pre-mounted single subscriber cassettes. Each

cassette contains the two fibers which are generally determined for one subscriber. Before a subscriber is connected the two fibers are uncut. The fibers are bridged through some successive series of closures in the line and they are available for the connection of a new subscriber.

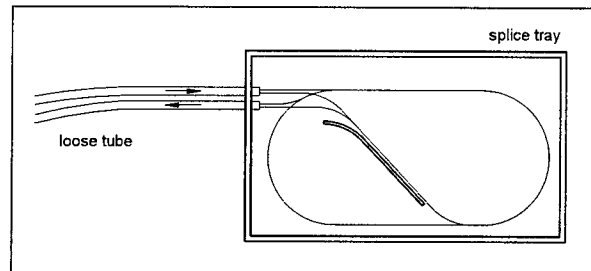


Fig. 2. Pre-mounted Single Subscriber Cassette

Fig. 3 illustrates the situation after a subscriber is connected. The two fibers were cut and spliced to two fibers of a subscriber cable which should ideally use a 2-fibers per tube design or the network should be built as a ring structure using fibers connected through at a subscriber, a 4-fibers per tube design. In the last-mentioned case the returning fibers from the subscriber are spliced to the remaining fiber ends in the same cassette as shown in Fig. 3.

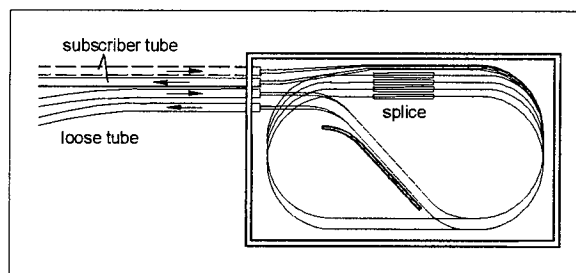


Fig. 3. Single Subscriber Cassette with connected subscriber

Organizer

Fig. 4 shows the organizer as part of the open dome-type closure. The modules for the subscriber splice cassettes are mounted on a base which forms an integrated whole with the closure's base. The maximum capacity of the closure is designed for 4 modules with 12 subscriber splice cassettes each. This enables the connection of up to 48 subscribers per access point. Each module is designed such that the splice cassettes can be handled like drawers. The tubes of the stub cable and of the subscriber cables are guided through a cable rack with outlets for the tubes at each splice cassette. This

guarantees that moving a cassette, e.g. for connecting a new subscriber, the tubes of all other cassettes are not moved and a disturbance of active fibers is prevented.

In addition, the organizer's design prevents installers and splicers from exceeding the minimum bend radius of the fiber.

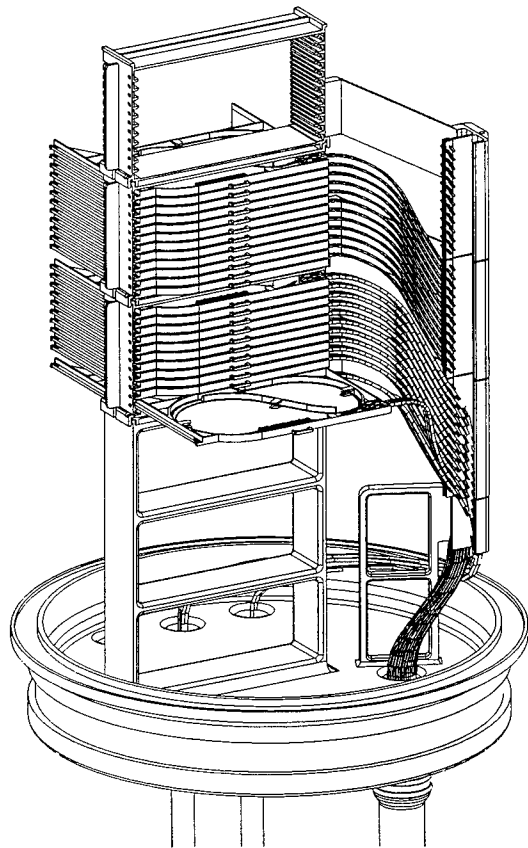


Fig. 4. Organizer

PRE-FABRICATED STUB CABLE

The dome-type closure is delivered with a pre-mounted stub cable of approximately 8 m length. The stub cable contains the tubes with two fibers each. The fibers are already looped (without a splice) in the subscriber cassettes, prepared for the connection of a new subscriber. 2 m of the stub cable are stored as a spare coil in the concrete box. Therefore, 8 m of the stub cable are available for the connection to the buried standard closure. The stub cable is designed without a central strength member which is normally used in fiber cables. This is permissible due to the short length of the stub cable. The advantage out of this is that the bending radius of the stub cable is only limited by the minimum

bending radius of the fiber tubes. The spare coil in the concrete box does not require a larger volume of the box than the dome-type closure needs for easy handling.

The stub cable shows a circular shape and the closure does not require an oval port (as conventional closure concepts require if the main cable is spliced in the dome-type closure). The sealing of the stub cable at the closure's base can be done very economically and reliably by using e.g. a heat-shrinkable tube.

For sealing the stub cable against propagating water - in case of damage to the cable's outer sheath - the cable can be delivered with a water-swelling material or a water block inserted at the entrance of the buried standard closure.

SUBSURFACE HOUSING CONCEPT

Normally for the installation of telecommunications equipment polymeric cabinets are used. While traveling through the country one can easily notice the increasing number of gray boxes of various sizes located at many corners.

Three years ago we introduced to Deutsche Telekom an underground system, which was especially designed for a new transmission concept. It consists of a two-shell housing whose outer shell is made from concrete as protection against mechanical forces. The inner part is a polymeric box which covers the electronic components and seals them hermetically against dust and moisture.

This system has confirmed the advantages of underground technology over the last three years:

- no defacing the landscape, especially in old towns;
- no exposure of the equipment to traffic accidents and vandalism;
- optimal thermal conditions for all components.

Fig. 5 illustrates the subsurface housing concept using a similar design as described before. The dome-type closure is mounted in a small 450 x 450 x 900 mm concrete box which is segmented into three pieces, in order to limit the weight of each piece for easy installation of the box. The box is closed with a cast iron cover.

The dome-type closure is fixed at its base on a adapter using a metallic rod with a thread which allows to remove the closure out of the housing comfortably from the pavement.

Under the closure there is sufficient space for approximately 2 m loop of the stub cable.

For splice works the fixing rod has to be unscrewed. Then the rod is again fixed at the second adapter. The position of this adapter is exactly on the opposite side of the box. Fig. 6 shows the position of the closure ready for splice works. Here the fixing rod acts as a mounting

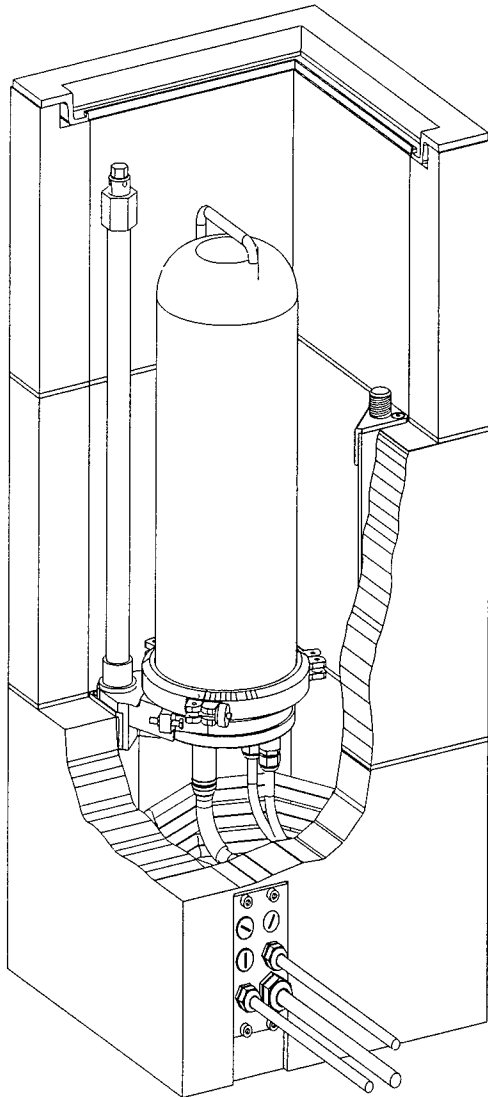


Fig. 5. Housing Concept

support for the closure.

While lifting the closure from the fixed position to the position for splice works the closure must be turned by 180°. This turn opens the loop of the stub cable and allows a complete control of the stub cable and the subscriber cables when the closure is put in the fixed position again. So it is guaranteed that the bending radius allowed for

the fibers will never be undercut during the splice works and active fibers will not be disturbed.

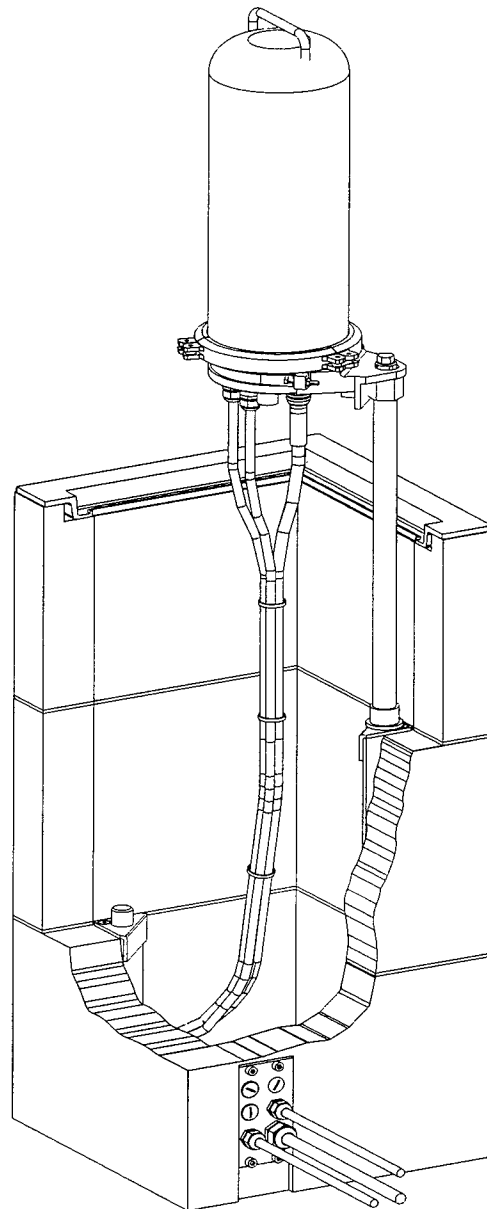


Fig. 6. Housing Concept – Position for splice works

SUMMARY

The described design of a new closure system offers the following features for operators and installers:

- Only fibers for potential future access are cut

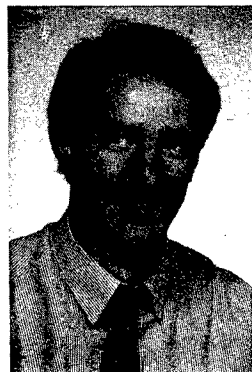
and spliced using economical standard splice and closure technique.

- High safety due to the fact that most of the fibers are stored in the buried standard closure.
- Optimum access to each single fiber without disturbing active fibers with the new organizer concept.
- The flexible stub cable allows small bending radii and, therefore, a small outer box and easy and controlled handling of the closure.
- The pre-mounted closure concept reduces installation costs, creates reliability and allows tailor-made solutions.



Franz Grajewski
ALCATEL KABEL
31655 Stadthagen
Germany

Dr.-Ing Franz Grajewski (41) studied mechanical engineering at Aachen's Technical University. From 1984 to 1988 he assumed a scientific fellowship at the University's Institute of Polymer Processing. After graduation he joined ALCATEL KABEL as manager R&D/Heat-Shrink Technology. Since 1991 he is General Manager of the product group Accessories and Heat-Shrink Technology.



Werner Stieb
ALCATEL KABEL
31655 Stadthagen
Germany

Dipl. Ing. Werner Stieb (39), after receiving his electrical engineering degree from the University of Kaiserslautern in 1986, he joined ALCATEL KABEL as a development engineer in the field of telecommunication cables and fiber optic components. Today he is Sales Manager of the product group Accessories and Heat-Shrink Technology.

DEVELOPMENT OF COMPACT FUSION SPLICER FOR AERIAL OPTICAL FIBER CABLE

Hidetoshi Hongu, Tomomi Sano, Yoshifumi Hishikawa,
Hiroshi Takayanagi, Keiji Osaka

Sumitomo Electric Industries, Ltd.
1, Taya-cho, Sakae-ku, Yokohama city, 244, Japan

ABSTRACT

A compact fusion splicer is developed which is able to splice 1-4 optical fibers of SM/MM in the manholes under the street or for aerial use, conveniently. Including a battery unit, the weight of this splicer is less than 3.0(kg). The splicer is able to perform more than 30 splices and reinforces per one battery charge and the splice sequence is automatic from setting, butt-joint, fusion and inspection.

The splicer is lightweight, small-sized and has lower power-consumption by introducing the techniques of "power management" and "2-way optical system".

1. INTRODUCTION

Recently optical fiber cables have been extending to subscriber network. It is an important technique to joint an optical fiber in order to establish such network. Among various jointing techniques, fusion splicing technique has higher reliability and produces lower loss, lower reflection than other jointing techniques. However it was very difficult to splice aerial optical fiber cable as shown in Figure 1 because conventional fusion splicers were big and heavy.

2. SPECIFICATIONS

For an aerial use, a compact fusion splicer was developed considering specific function necessary for aerial situation such as:

1) easy carrying:

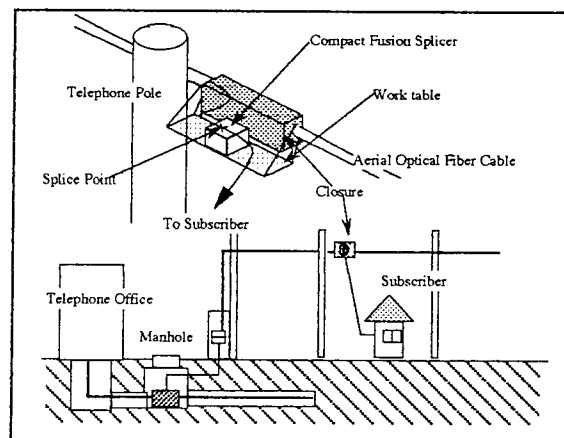


Figure 1 Schematic view of aerial splice

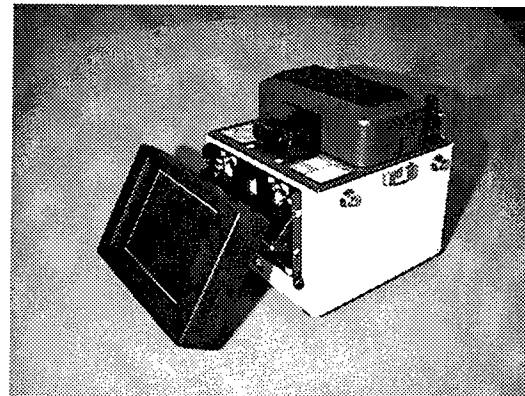


Figure 2 Appearance of the newly developed splicer

Table.1 Specifications of the newly developed fusion splicer

Items	Specifications
Applicable fiber	Number of Fibers: 1,2,4
	Fiber Type: SM,MM
Dimensions	155(W)×145(D)×135(H)(mm) including a battery unit
Weight	less than 3.0(kg) including a battery unit
Splice sequence	Automatic splice sequence
Loss Estimation	±0.1dB
Average splice loss	0.05dB (SM)
Tact time	35 sec (typ.)
Wind-shield	against 10m/s
Battery	30 splices and reinforcements at room temperature
Monitor	4 inch-TFT-LCD

lightweight and compact so as to carry up to high place using ladder or lift

2) easy operation:

built-in automatic splice function, easy splice point observation and low power consumption with attached battery unit

3) full automatic:

splice loss estimation, cleave quality measurements and axis-offset measurements

An appearance is shown in Figure 2. Specifications of the fusion splicer are shown in Table 1.

The maximum number of applicable fiber is 4-fiber ribbon of SM or MM, because 4-fiber ribbon is the highest fiber number for aerial cable in Japan. For easy operation at the aerial place, automatic function was built-in enabling easy observation of fibers or messages, with 4-inch TFT LCD monitor.

3. POWER MANAGEMENT TECHNIQUE

In order to use splicers in a construction field, how many splice is possible per battery charge is important. However, to make the splicer and the battery smaller and lighter, power consumption performance is also important.

The actual splice sequence is shown in Figure 3. When turning on, conventional splicer is always at active status and is with ready to splice. By carefully examining the power consumption along the splice sequence, we found it more effective to save power during when the splicer is waiting (idling) rather than to save power during fusing or heating. The hatched area in Figure 3 is the saved power by our power management system. Supposing one splice cycle is 5 minutes,

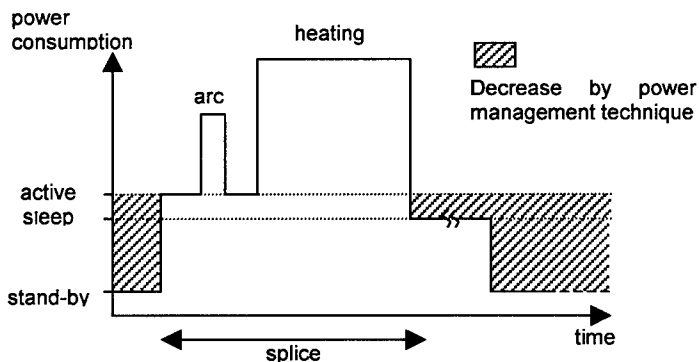


Figure 3 Profile of power consumption

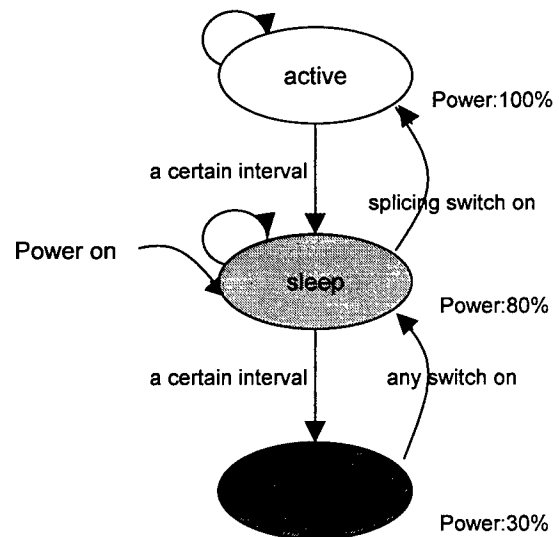


Figure 4 Diagram of power management

Table 2 Power management mode

Mode	Status	Notes
Active	All devices are power-on	Splicer is active (spliceable)
Sleep	Microscope power-off Image processing circuit power-off	Can display messages on the LCD monitor Wake-up by pushing any console switch
Stand-by	Superimpose circuit power-off LCD monitor power-off CPU's clock stops	Display function is also powered-off Wake-up by pushing any console switch

90% of the period is 'idling'.

Other than turning off the splicer so often, we developed self-power saving function. The electric power of the splicer is CPU-controlled for adequate power management of each device and CPU itself through changing 3 modes: "active mode", "sleep mode" and "stand-by mode", as shown in Figure 4 or Table 2.

active mode

In this mode, all devices are powered and the fiber is to be spliced. If the splicer don't receive an input from an operator for a certain interval (programmable), it shifts to "sleep mode" after warns the operator by buzzer and displays a warning message.

sleep mode

By turning on the power switch, the splicer enters this splice mode. In this mode, the LCD monitor is powered-off but is powered again only when the fiber image is necessary to the operator. Thus, the power consumption is reduced to 80% (typical) than that of "active mode".

When any console switch is pushed, the splicer returns to "active mode". But if the splicer is not used for a certain interval, it beeps and warns the operator and shifts to "stand-by mode".

stand-by mode

During the "sleep mode", if the splicer is not awoken still more(programmable), it beeps again and shifts to "stand-by mode". This mode does not supply power to LCD monitor and stops CPU's clock. In this mode, the power consumption is reduced to 30% (typical) than that of "active

mode".

Total consumption through the splice is kept very low by controlling three power modes. Therefore, this splicer was realized to perform more than 30 splices and reinforcements per one charge at normal condition.

4. 2-WAY OPTICAL SYSTEM

For the ease of splice work under unstable conditions, reliable and repeatable performance of the splicer is the key technology. For that purpose, full automatic splice sequence including our high-precision loss estimation is realized. The axis offset of the mating fibers are measured precisely by viewing from 2 directions alternatively. Optical resolution as low as 0.2 μ m is necessary to assure low-loss(less than 0.1dB) and high loss-estimation accuracy(within 0.1dB). In the conventional Sumitomo splicer, a mirror and a camera is used, both were motor-driven to have 2-direction image of the fibers(Figure 5(A)). However, it is effective to fix a pair of an LED illumination and a lens onto a

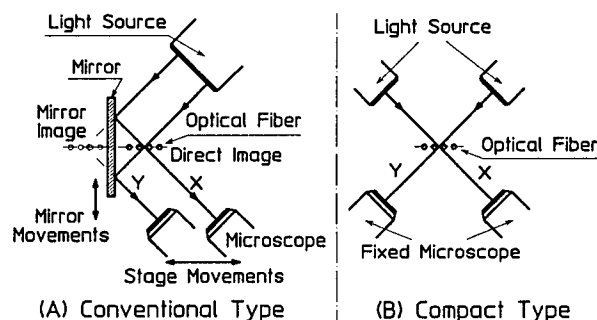


Figure 5 Comparison of 2-way optical system

base plate for stable observation(Figure5(B)). It is also useful

---to reduce the splice time by eliminating the focussing process

---to reduce power consumption by eliminating motors

---to minimize the size of the mechanism by omitting the driving system of mirror and microscope

Thus splice time of this splicer is reduced to less than 35 seconds(typical) when splicing 4-fiber ribbons against that of conventional splicer:45 seconds. No driving system for focusing contributed the improvement of splice time.

In the 2-way optical system, LEDs and microscope are not always powered. By electronically switching from one side to the other, necessary power of the optical system is at the same level as the conventional viewing system.

5. TOTAL PERFORMANCE

The reliability test conditions are shown in Figure 3. Under this conditions or after this conditions, an average splice loss of 0.05(dB) was obtained for SM1,4-fiber ribbons, respectively, as shown in Table 4 as well as loss estimation accuracy of 0.1(dB). The loss value and the estimation is same as those of the conventional splicer. The splice time was 35 seconds (typical) by automatic sequence.

6. CONCLUSION

The compact fusion splicer adopting power management technique and 2-way optical system was developed. The splicer realized more than 30 splices and reinforcements per one charge.

Thus our new splicer has high performance and is suitable for field use from installation to maintenance of optical cable. We hope the machine play an important role in realizing FTTH networks throughout the world.

Table 3 Splice Characteristics

Fiber	SM1f	SM4f
Splice Loss	0.05 dB typ.	0.05 dB typ.
Loss estimation	$<\pm 0.1$ dB	$<\pm 0.1$ dB

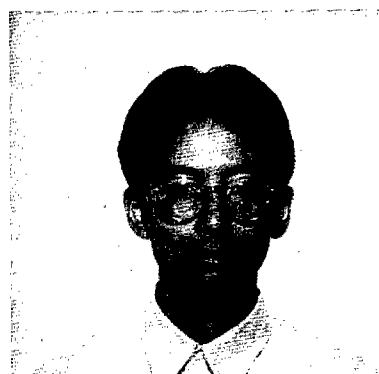
Table 4 Reliability test

High temperature	50°C
Low temperature	-10°C
High humidity	90%RH at room temperature
Vibration	± 5 mm,2hr x,y,x-direction respectively
shock	30G

REFERENCES

- 1) NTT REVIEW Vol.6 No.4 July 1994
- 2) Ziff-Davis Publishing Company "BatteryMark" 1996.

AUTHORS



Hidetoshi Hongu

E-mail:hongu@yklab.sei.co.jp.

Sumitomo Electric Industries, LTD.

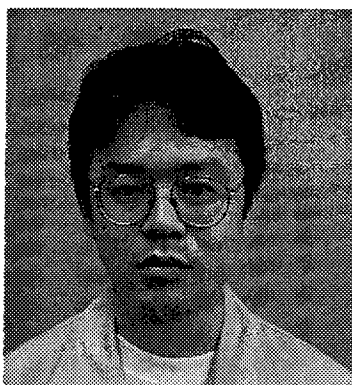
1,Taya-cho, Sakae-ku, Yokohama, Japan

Hidetoshi Hongu was born in 1967 and received his M.S. degree in electric engineering from Tokyo University of Agriculture and technology in 1992. He joined Sumitomo Electric Industries the same years and has been engaged in research and development of fusion splicing technologies for optical fibers.



Tomomi Sano
E-mail: tomo@yklab.sei.co.jp.
Sumitomo Electric Industries, LTD.
1, Taya-cho, Sakae-ku Yokohama, Japan

Tomomi Sano was born in 1965 and received his M.S. degree in electric engineering from Tokai University in 1990. He joined Sumitomo Electric Industries the same year and has been engaged in research and development of fusion splicing technologies for optical fiber. He is a member of Japan Applied Physics.



Hiroshi Takayanagi
E-mail: hiroshi@yklab.sei.co.jp.
Sumitomo Electric Industries, LTD.
1, Taya-cho, Sakae-ku Yokohama, Japan

Hiroshi Takayanagi was born in 1970 and he joined Sumitomo Electric Industries in 1996 and has been engaged in research and development of fusion splicing technologies for optical fibers.



Yoshifumi Hishikawa
E-mail: hishi@yklab.sei.co.jp.
Sumitomo Electric Industries, LTD.
1, Taya-cho, Sakae-ku Yokohama, Japan

Yoshifumi Hishikawa was born in 1965 and received his M.S. degree in information engineering from Hokkaido University in 1991. He joined Sumitomo Electric Industries the same years and has been engaged in research and development of data communication system and fusion splicing technologies for optical fibers.



Keiji Osaka
E-mail: osaka@yklab.sei.co.jp.
Sumitomo Electric Industries, LTD.
1, Taya-cho, Sakae-ku Yokohama, Japan

Keiji Osaka joined Sumitomo Electric Industries in 1981 and has been engaged in research and development of fusion splicing technologies for optical fibers and optical switch technologies. He is now a chief research associate of Optomechatoronics System R&D Dept. Yokohama Research Laboratories and a member of Electronics, Information and Communication Engineering of Japan.

Development of Small Size and High Performance Flat Intra-Office Optical Fiber Cable using Fiber Cord and Fiber Ribbon Cord

Yoichi Nagase, Hajime Tamura, and Masaaki Yoshida

TOYOKUNI ELECTRIC CABLE CO., LTD.

4125, Sakitama, Gyouda-City, Saitama, 361 Japan

Abstract

A compact fiber-optic cable is effective for low cost and easy handling. Intra-office optical fiber cable has also been studied as a suitable structure for telephone offices with terminals. In this paper, we will introduce the newly designed Flat Intra-Office Optical Fiber Cable, and its high and stable optical performances.

1. Introduction

Recently, smaller cross section and easily ripping the cable sheath during installation has been required for intra-office optical fiber cable using fiber cords and fiber ribbon cords.

Conventional intra-office cables with circular structure which are stranded fiber cords and fiber ribbon cords during the central tension member has the great potential to realize stable optical performances.

Instead, We have adopted the flat intra-office optical fiber cable which is arranged a fiber cord, a fiber ribbon cord and a tension member on a single plane sheath. A torn slot is formed on the flat sheath in order that it is easy to take out optical fiber cords and fiber ribbon cords during installation. Therefore, even though a sheath is not cut off by a cutter knife as before, it can be cut off by pulling a torn slot to both directions. For the Intra-Office Optical Fiber Cable design, the following three matters have been carefully considered:

- (1) Decrease of interaction between fiber cords and a plane sheath

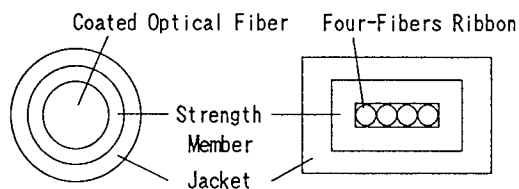
- (2) Design of flat cable to improve the characteristics of lateral force of the cable since the cable is subjected to external force during production and installation.
- (3) Easily ripping the cable sheath for taking out optical fiber cords.

2. Cable design

2.1. Single Fiber Cord and Four-Fibers Ribbon Cord

The single fiber cord with PVC resin and polyaramido yarn is adopted a diameter of 1.7mm, that is smaller than conventional standard. Single-mode fibers, Graded-index fibers of 0.9mm coating diameter which is coated by using silicone resin and polyamido resin are used.

The four-fibers ribbon cord with PVC resin and polyaramido yarn has dimensions to be 1.5×2.5mm. The four-fibers ribbon which are used Single-mode fibers of 0.25 mm coating diameter has the dimensions of of the common cating to be 0.30×1.1mm. Figure 1 shows the design of Single Fiber Cord and Four-Fibers Ribbon Cord.



Single Fiber Cord Four-Fibers Ribbon
Cord

Figure 1, The design of Single Fiber Cord and Four-Fibers Ribbon Cord

2.2. The Flat Intra-Office Optical Fiber Cable

We have adopted the Flat Intra-Office Optical Fiber Cable which is arranged a fiber cord, a fiber ribbon cord and a tension member on a single plane sheath. Figure 2 and Figure 3 shows the design of the Flat Intra-Office Optical Fiber Cable using single fiber cord with Optical Fiber Cord Number. The cable containing two fiber cords and a tension member has the dimensions of the common sheath to be $3.6 \times 6.6\text{mm}$. The cable sheath which is formed the torn slots on the flat sheath is adopted the flame retardant polyethylene resin. The cable containing four fiber cords and a tension member has the dimensions of the common sheath to be $5.2 \times 10.8\text{mm}$. This cable is also formed the torn slots on the flat flame retardant polyethylene sheath.

Figure 4 and Figure 5 shows the design of the High-density Intra-Office Optical Fiber Cable using four-fibers ribbon cords with Ribbon Cord Number. The Cable containing a four-fiber ribbon cord and two tension members has dimensions of the common sheath to be $5.0 \times 7.9\text{mm}$. The Cable containing two fiber ribbon cords and two tension members has the dimension of the common sheath to be $5.0 \times 10.4\text{mm}$. These cable is also formed the torn slots on the flat flame retardant polyethylene sheath. In order to decrease of interaction between fiber cords and a plane sheath, the suitable manufacturing conditions are chosen.

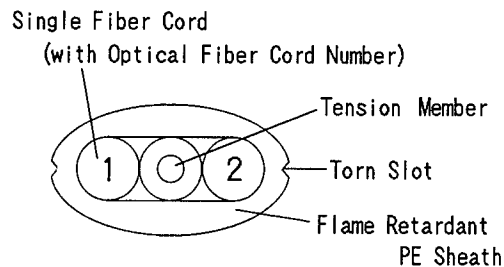


Figure 2 : Design of Two-Fibers Intra-office Cable

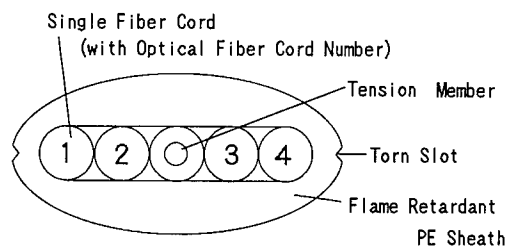


Figure 3 : Design of Four-Fibers Intra-office Cable

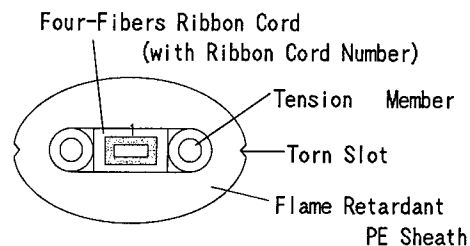


Figure 4 : Design of Four-Fibers High-density Intra-office Cable

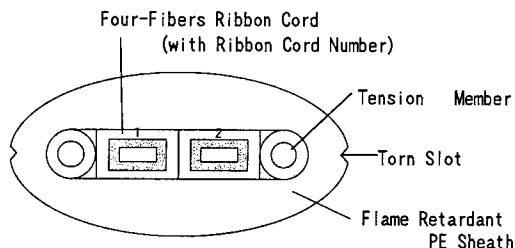


Figure 5 : Design of Eight-Fibers High-density Intra-office Cable

3. Ripping Process

Easily ripping the cable sheath for taking out optical fiber cords has been carefully considered. The newly designed Flat Intra-Office Optical Fiber Cable has the torn slots on the flat sheath which is formed in sheathing process. In ripping process as shown in Figure 6 and Figure 7, each of fiber cord is easily take out from the cable sheath during installation. Therefore, even though a sheath is not cut off by a cutter knife as before, it can be cut off by pulling a torn slot to both directions.

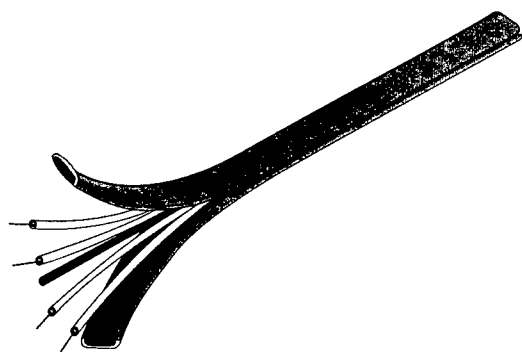


Figure 6 : Four-Fibers
Intra-office Cable
(Ripping the Sheath)



Figure 7 : Eight-Fibers
High-density
Intra-office Cable
(Ripping the Sheath)

4. Optical Performance

4.1. Crush Resistance

Design of flat cable to improve the characteristics of lateral force of the cable since the cable is subjected to external force during production and installation has been carefully considered. The crush resistance is one of the important parameter for the Flat Intra-Office Cable. To measure the crush resistance, the Flat Intra-Office Cable was placed between two aluminum plates, and the required pressure of 9.8N/mm ($100\text{Kg}/100\text{mm}$) was applied. As shown in Figure 8, the Flat Cable was bended $6D$ (cable diameter $\times 6$) and the weight was applied to direction of long length sheath. Loss increase caused by the required pressure was measured at $1.55\mu\text{m}$.

Relationship between loss increase and average thickness of sheath in the case of the Four-Fibers Intra-Office Cable is shown in Figure 9. Loss increase should be reduced less than 0.10dB at $1.55\mu\text{m}$ for Intra-Office Cable. We have determined that average sheath thickness of 1.4mm give best results for the Four-Fibers Intra-Office Cable. Average sheath thickness of the Flat Intra-Office Cable shown in Figure 2 ~ Figure 5 was determined using the same method.

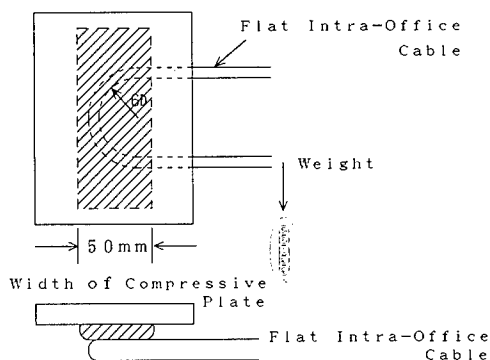


Figure 8 : Crush Resistance
Test Method

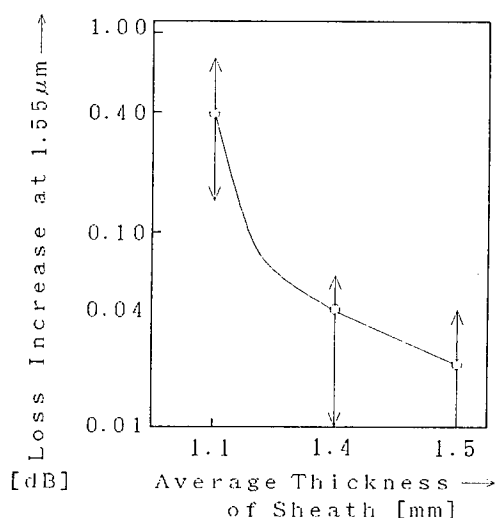


Figure-9 Compressive Strength of Four-Fibers Intra-Office Cable.

4.2. Temperature Cycling

The characteristics of temperature cycling has important design considerations. As shown in Figure 10, the Four-Fiber Intra-Office Cable was evaluated transmission property within operation temperature from -10°C to $+40^{\circ}\text{C}$ (6hr/a temperature step). The newly designed the Flat Cable was recognized to have the stable and excellent characteristics with no loss increase which was continuously monitored at $1.55\mu\text{m}$.

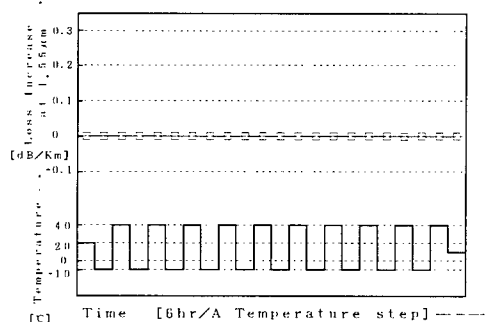


Figure 10 : Temperature Cycling of Four-Fibers Intra-office Cable

4.3. Summary of Tests and Results

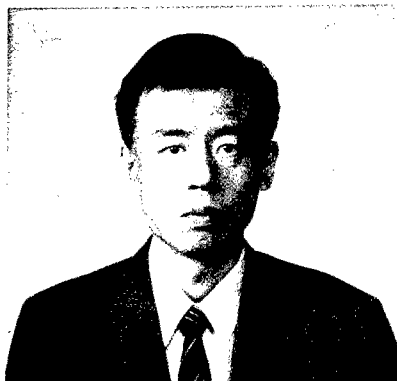
As summarized in Table 1, various kinds of mechanical tests and temperature cycling test were conducted on the manufactured Flat Intra-Office Optical Fiber Cable of the proposed design with fiber cords and fiber ribbon cords. Optical loss was continuously monitored at 1550nm during those tests. The newly designed Flat Cable have the stable and excellent results with no loss increase.

Table 1 : Summary of Tests and Results

Test Item	Conditions	Results
Temperature Cycling	$-10\sim 40^{\circ}\text{C}$ 10Cycles 6hours duration at each temperature	$\Delta\alpha\leq 0.1\text{dB}$ at 1550m
Crush Resistance	9.8N/mm 1 minute duration	$\Delta\alpha\leq 0.1\text{dB}$ at 1550m
Cable Bend	1 Wrap on Mandrel Dia. = 60mm	$\Delta\alpha\leq 0.1\text{dB}$ at 1550m

5. Conclusion

The newly designed Flat Intra-Office Optical Fiber Cable using fiber cord and fiber ribbon cord was realized by the proper design. The stable and excellent results with no attenuation increase has given the prospect of the Intra-Office Optical Fiber Cable for the use in optical cable transmission systems linking telephone offices.



Yoichi Nagase is a Member of Technical Staff in the Network & Fiber Optics Engineering Department at Toyokuni Electric Cable Co., Ltd in Gyouda-City, Saitama. He is responsible for design and development of Optical Fiber Cable products.

Mr. Nagase joined Toyokuni Electric Cable Co., Ltd. in 1975. He has a B.S. degree in Industrial Chemistry from Meiji University. He is a member of the Institute of Electronics, Information and Communication Engineers of Japan.



Masaaki Yoshida is a Director & Executive Manager of Research and Development Department at Toyokuni Electric Cable Co., Ltd. in Gyouda City, Saitama.

Mr. M. Yoshida joined Sumitomo Electric Industries, Ltd. in 1966, and transfer to Toyokuni Electric Cable Co., Ltd. in 1995.

He has a B.S. degree in chemical Engineering from Kyushu University. He is a member of the Institute of Electronics, Information and Communication Engineers of Japan.



Hajime Tamura is a Manager in the Network & Fiber Optics Engineering Department at Toyokuni Electric Cable Co., Ltd. in Gyouda-City, Saitama. His group's responsibilities include design, development and process engineering for Optical Fiber Cable and Connector products.

Mr. Tamura joined Toyokuni Electric Cable Co., Ltd. in 1969. He has a B.S. degree in Chemical Engineering from Chuo University. He is a member of the Institute of Electronics, Information and Communication Engineers of Japan.

Design of compact optical fiber identification (ID) tester and talk set for optical subscriber loops.

Yoshitaka ENOMOTO, Nobuo TOMITA, Hiroshi TERUI, Yasufumi YAMADA,
and Naoto UCHIDA.

NTT Access Network Systems Laboratories, and NTT Opto-electronics Laboratories.
Tokai-mura, Naka-gun, Ibaraki, JAPAN

ABSTRACT

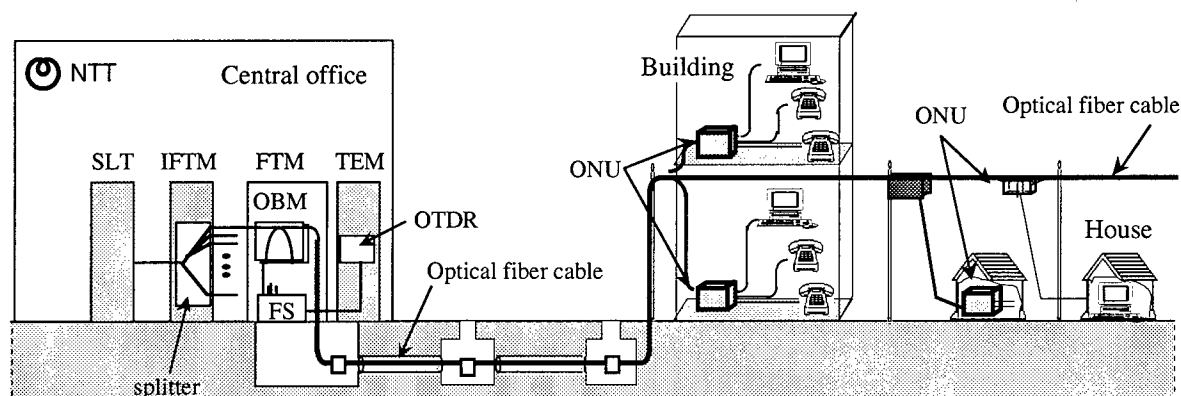
Compact and low-cost optical measurement equipment is essential for reducing construction and maintenance costs for optical subscriber loops. We have designed a compact and lightweight optical fiber ID tester and talk set with the hybrid optical module technology used for optical subscriber transmission systems. The hybrid optical module we developed consists of an LD, an LED and a PD installed with or on a planar lightwave circuit (PLC) platform. The prototype optical fiber ID tester is 140 x 90 x 30 mm and weighs 0.6 kg. This size and weight are, respectively, one fourth and one third those of a conventional ID tester. The prototype optical talk set is 130 x 80 x 25 mm and weighs 300 g. It is very compact and light and has a dynamic range of more than 20 dB for communication between two locations.

1. Introduction

Single-mode optical fiber cables have been introduced in local subscriber areas in order to

provide a high speed and broadband communication service [1]. Figure 1 shows the outline of an optical access network system [2]. When we construct and maintain an access network system, it is necessary to measure and evaluate fiber characteristics, fiber loss, connection loss, return loss, and to identify fibers, and fault locations as shown in Table 1. Optical loss comprises fiber section, connector, and fusion splice loss. The test equipment is a light source (LS), an optical power meter (OPM), and an optical time domain reflectometer (OTDR). For return losses, connectors are tested with an OTDR. In addition, fiber identification is necessary when checking the object fiber during cable removal and rejoining work. The test equipment consists of an LS and an OPM with a special local detector which can detect the radiated light from a fiber bend. Faults can be located with an OTDR.

Compact and low-cost optical measurement equipment is essential for reducing the construction and maintenance costs of optical subscriber loops. A test equipment module (TEM) with an OTDR is installed in a central office [3]. And we can measure



SLT: Subscriber line terminal.
IFTM: Intermediate fiber termination module.
FTM: Fiber termination module.
OBM: Optical branch module.

OTDR: Optical time domain reflectometer.
FS: Fiber selector.
TEM: Test equipment module.
ONU: Optical network unit.

Figure 1. Outline of optical access network system.

Table 1. The test items when measuring and evaluating fiber characteristics

Items	Components	Equipment	Measurement factors
1 Optical loss	Fiber (Point to point)	LS and OPM	Insertion loss
	Connector and splice	OTDR	Relative change in backscattering
2 Return loss	Connector	OTDR	Difference between backscattering and Fresnel reflection levels
3 Fiber identification	Fiber	LS and OPM	Direct incidence and local detection of test light
4 Fault location	Fiber	OTDR	Relative change in backscattering

the optical fiber characteristics with the OTDR in the field. Moreover, we have already developed a portable testing device with LSs and OPMs which is called an optical fiber identification (ID) tester [4][5]. It consists of a 1.31 μm LED and a 1.55 μm laser diode (LD) which operate as light sources, an optical power meter, a fiber identifier with a bending unit and a detector, and an optical talk set. The functions it provides include the measurement of optical fiber loss, fiber identification, and spoken communication between two locations for construction and maintenance work.

This optical fiber ID tester must be made more compact and lighter in weight because of its use in such confined spaces as on a pole and in a manhole. Moreover, as high density optical fiber cable has no metal wires, we have to communicate with other locations using a dark fiber. This paper describes the design of the compact optical fiber ID tester and talk set.

2. Compact optical fiber ID tester and talk set

2.1 Design of optical fiber ID tester and talk set

Our design target for the optical fiber ID tester and the talk set was that they should be small enough to be hand held without there being any detrimental effect on their characteristics and functions. Table 2 shows the characteristics of an optical fiber ID tester and a talk set. The currently used devices consist of optical components including fiber couplers, filters, LD, LED, and photo diode (PD) modules and each part is connected using fibers which makes it impossible to achieve compactness. We therefore employed the hybrid optical module technology

Table 2. Characteristics of an optical fiber ID tester and talk set

Units	Functions	Values
Light source	Loss test	Wavelength
		Output power
		Stability (10 - 40 °C)
	Identify	Wavelength
Receiver and sensor	Power meter (1.31 μm)	Output power
		Minimum power
	Identify (1.55 μm)	Accuracy
		Insertion loss
		Minimum power
Talk set	Dynamic range	Coupling efficiency

* For trunk line

used for optical subscriber transmission systems [6][7][8]. Moreover, the optical fiber ID tester uses a dry battery and one PD is shared between the optical power meter and the detector of the identifier. A conventional optical talk set requires a value of over 35 dB for trunk line construction and maintenance work. Our target for the dynamic range is over 20 dB because it will be used for subscriber line construction and maintenance work. Table 3 shows the characteristics of conventional and proposed optical talk sets.

Table 3. Characteristics of conventional and proposed optical talk sets

Functions	Conventional	Proposed
Wavelength	1.31 / 1.55 μm (WDM)	1.31 μm
Modulation / demodulation	FM	PAM
Dynamic range	≥ 35 dB	≥ 20 dB

2.2 Structure of optical fiber ID tester and talk set

(1) Optical fiber ID tester

Figure 2 shows the structure of an optical fiber ID tester. It consists of a light source unit, a receiver unit and a sensor unit. The light source unit has a 1.31 μm light source for optical loss tests and a 1.55 μm light source for fiber identification. The 1.31 μm light source consists of a 1.31 μm LED, a band pass filter (BP filter), a coupler, a PD, and an LED driver circuit. The 1.31 μm light source is stabilized by the forward feedback (FFB) method to provide a very stable measurement [9]. The 1.55 μm light source consists of a 1.55 μm LD, a monitor PD (M-PD), and an LD driver circuit. The 1.55 μm light source is modulated by 270 Hz to distinguish it from the communication light.

The receiver and sensor units consist of a PD to receive a test light, a power meter circuit, a CPU, and an LCD. The received power is displayed on the LCD in dBm. The sensor unit requires an attachment of which there are three types. One is an SC type attachment for an SC connector. Another is an MT type attachment for 4MT and 8MT connectors. These attachments are used for the optical loss test. The third is a bending attachment for fiber identification. The sensor unit uses one PD which is shared between the optical power meter and the detector of the identifier.

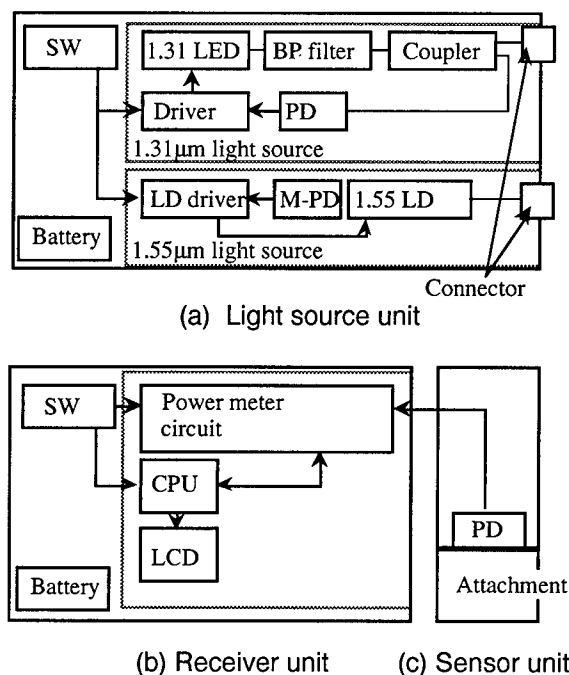


Fig. 2. Structure of optical fiber ID tester

the pulse amplitude modulation (PAM) method [10]. The LD sends the modulated signal light to a second optical talk set. Moreover, the PD receives a signal light from this optical talk set. The received signal is demodulated and sent to the earphone of the headset.

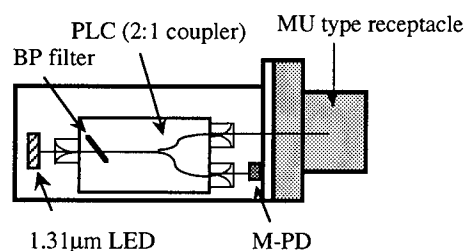
2.3 Hybrid optical module

(1) Light source module

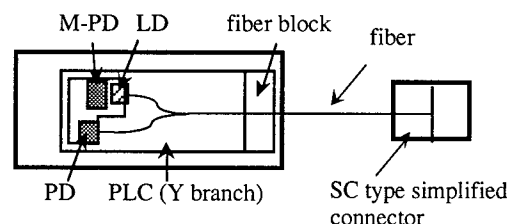
Figure 4(a) shows the light source module for the optical fiber ID tester. The hybrid optical module consists of a 1.31 μm LED and a PD installed with a planar light wave circuit (PLC). The PLC is composed of a BP filter and a 2:1 optical coupler circuit. The PLC connects an output fiber, and the fiber pigtails of an LED module and a PD module using fiber guide holes. The PLC, and the LED and PD modules were assembled in a Au-plated KOVAR package with an MU type receptacle and then sealed by seam welding. The size, including an MU type receptacle, is 60 x 15 x 8.5 mm.

(2) Optical talk module

Figure 4(b) shows an optical talk module. The hybrid optical module consists of a 1.31 μm LD and two PDs all mounted on a PLC platform. The PLC is composed of a Y branch coupler circuit. The PLC connects an input/output fiber with an SC type simplified connector using a fiber block part. Table 4 shows the performance of the optical talk module which is 35 x 15 x 5.5 mm in size.



(a) Light source module



(b) Optical talk module

Fig. 4. Hybrid optical module

(2) Optical talk set

Figure 3 shows the structure of an optical talk set. It consists of a 1.31 μm LD light source, an M-PD, a PD, a coupler, an LD driver circuit, and a modulation/demodulation circuit. This talk set uses a headset with an earphone and a microphone. The voice signal from the microphone is modulated with

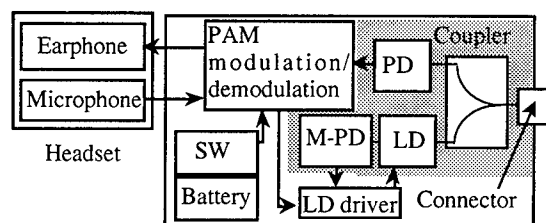


Fig. 3. Structure of optical talk set

Table 4. Performance of the module

Performance (25°C)	Item
Output power	- 5 dBm (14 mA)
Center wavelength	1.30 μ m
Responsivity	0.32 A/W
Dark current	< 1 nA
Crosstalk	- 27 dB

2.4 Characteristics of prototype optical fiber ID tester and talk set

(1) Optical fiber ID tester

Figure 5 shows our prototype optical fiber ID tester which is 140 x 90 x 30 mm in size and weighs 0.6 kg. This size and weight are, respectively, one fourth and one third those of a conventional ID tester with no deterioration in the optical characteristics.

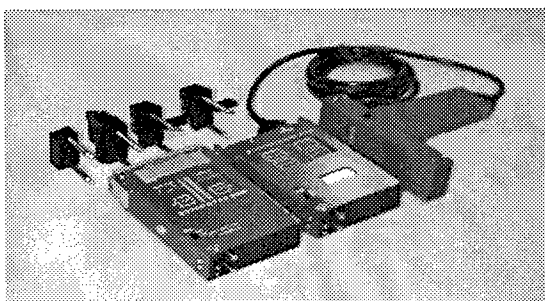


Fig. 5. Prototype optical fiber ID tester

(2) Optical talk set

Figure 6 shows our prototype optical talk set which is 130 x 80 x 25 mm and weighs 300 g. This makes it very compact and light. Figure 7 shows the experimental setup for measuring the dynamic range which is more than 20 dB for communication between two locations.

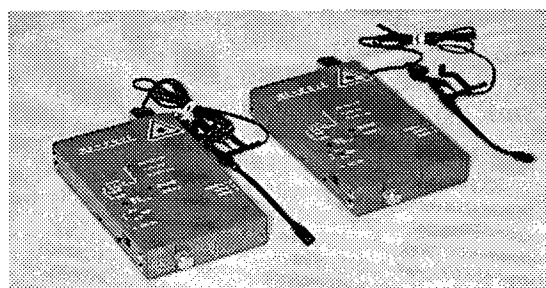


Fig. 6. Prototype optical talk set

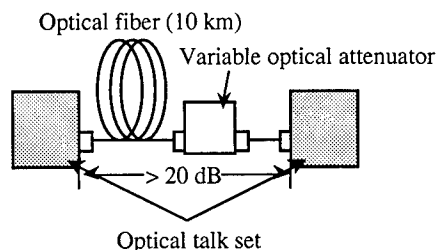


Fig. 7. Experimental setup for measuring dynamic range

3. Application of the optical talk set

When in the field, we need to access the telephone network to speak to the telephone office about construction and maintenance work. We confirmed that it was possible to access the telephone network with our optical talk set by using a dial and equipment installed in a central office. Figure 8 shows this telephone network access equipment and an optical talk set with a dial. The equipment consists of a 1.55 μ m LD light source, PDs, a 1.31/1.55 μ m WDM coupler, a PD level monitor circuit, a switch controller circuit, switches, and a PAM modulation/demodulation circuit. The optical talk set has a dial for selecting telephone numbers. The equipment is connected to the optical talk set

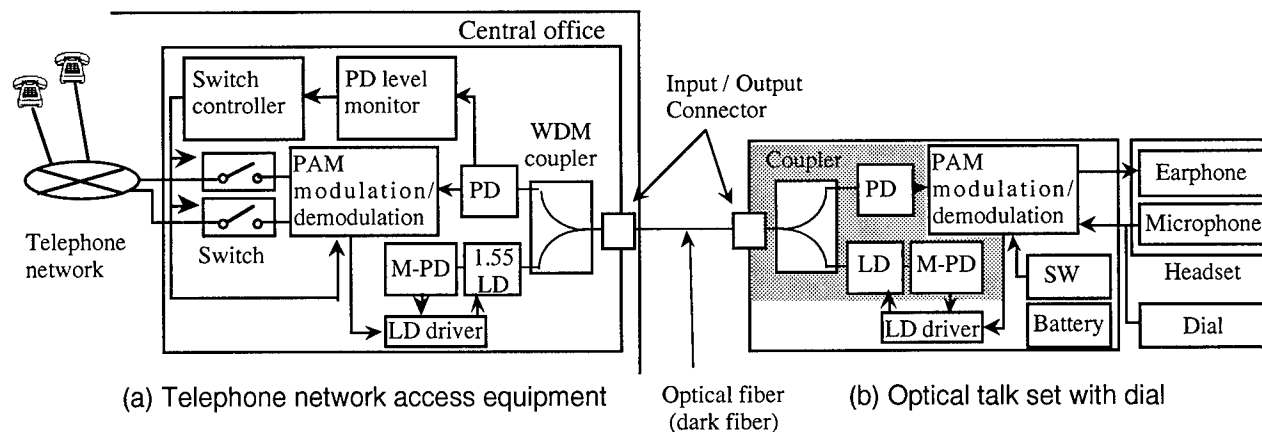


Fig. 8. Structure of telephone network access equipment and optical talk set with dial

through a dark fiber.

The access method is as follows; (1) A worker connects an optical talk set with a dial to a dark fiber which is already connected to the equipment in the central office. (2) He turns on the optical talk set, which then transmits a signal light to the equipment. (3) The PD of the equipment receives the signal light, then a switch control circuit closes switches to provide connection with the telephone network. (4) After closing these switches, it is possible to transmit tone or voice signals through the fiber from an exchange or a headset.

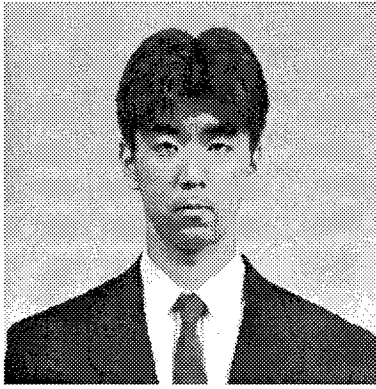
When the worker has completed his communication, he turns off the optical talk set to stop the signal light. The switch controller circuit of the equipment then opens the switches to disconnect the telephone line.

4. Conclusions

We have described a compact and lightweight optical fiber ID tester and talk set which uses hybrid optical module technology. The hybrid optical module we developed consists of an LD, an LED and a PD installed with or on a PLC platform. The prototype optical fiber ID tester is 140 x 90 x 30 mm and weighs 0.6 kg. This size and weight are, respectively, one fourth and one third those of a conventional ID tester. The prototype optical talk set is 130 x 80 x 25 mm, and weighs 300 g. It is very compact and light and has a dynamic range of more than 20 dB for communication between two locations. Furthermore, we confirmed that it was possible to access the telephone network with our optical talk set by using a dial and equipment installed in a central office.

References

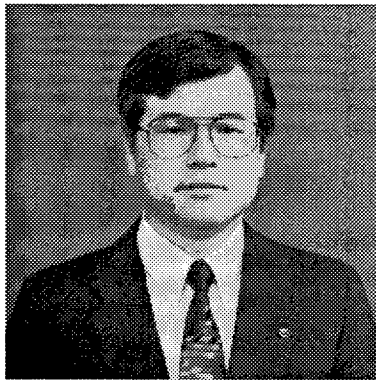
- [1] M. Kawase, T. Fuchigami, T. Haibara, S. Nagasawa, S. Takashima, "Loop-network configuration for subscriber loops and single-mode optical fiber ribbon cable technologies suitable for mid-span access", Proc. 37th IWCS, pp. 141-149, 1988.
- [2] "New optical access system -accelerating the opticalization of access network-", NTT Review, pp. 10-11, 1997.
- [3] N. Tomita, H. Takasugi, N. Atobe, I. Nakamura, F. Takaesu, and S. Takashima, "Design and performance of a novel automatic fiber line testing system with OTDR for optical subscriber loops", IEEE J. Lightwave Technol., Vol. 12, No. 5, pp. 717-726, 1994.
- [4] E. Maekawa, K. Yamashita, and Y. Koyamada, "Measurement equipment for subscriber optical lines", Review of the Electrical Communication Laboratories (NTT), Vol. 34, No. 6, pp. 669-675, 1986.
- [5] K. Arakawa, K. Yoshida, H. Ikeya, "A method for identifying single-mode fibers in an operating fiber cable system", Proc. 38th IWCS, pp. 88-93, 1989.
- [6] H. Terui, T. Kominato, K. Yoshino, S. Hata, S. Sekine, M. Kobayashi, J. Yoshida, K. Okada, "Optical module with a silica-based planar lightwave circuit for fiber-optic subscriber systems", IEEE Photon. Technol., vol.4, no. 6, pp. 660-662, 1992.
- [7] Y. Yamada, S. Suzuki, K. Moriwaki, Y. Hibino, Y. Tohmori, Y. Akatsu, Y. Nakasuga, T. Hashimoto, H. Terui, M. Yanagisawa, Y. Inoue, Y. Akahori and R. Nagase, "A hybrid integrated optical WDM transmitter/receiver module for optical subscriber systems utilizing a planar lightwave circuit platform", Proc. OFC '95, PD12, 1995.
- [8] N. Uchida, Y. Yamada, Y. Hibino, S. Suzuki, and I. Ishihara, "Low-cost WDM module consisting of a spot-size converter integrated laser diode and waveguide photodiode on a PLC platform for access network systems", IEICE Trans. Elec. vol. E80-C, pp. 88-97, 1997.
- [9] Y. Unami, M. Tanaka, and T. Yamada, "Optical power measuring system for fiber ribbon", Proc. 39th IWCS, pp. 435-439, 1990.
- [10] Y. Unami, K. Sakurai, T. Yamada, N. Kuwaki, M. Yomoto, "Wide dynamic range optical talk system using external loss modulation", Proc. 41th IWCS, pp. 88-96, 1992.



Yoshitaka Enomoto

NTT Access Network Systems Laboratories
162 Shirakata-shirane, Tokai-mura, Naka-gun,
Ibaraki, 319-11 JAPAN

Yoshitaka Enomoto joined NTT Telecommunication Field Systems R & D Center Ibaraki, Japan in 1992, and is engaged in the research and development of an optical fiber line testing system, and optical components for the central offices of access network systems.

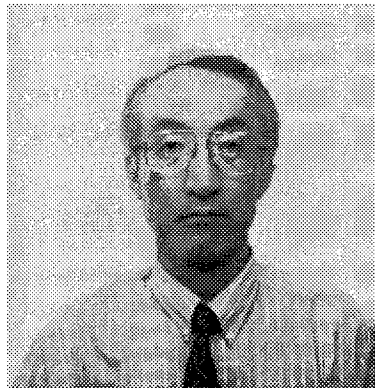


Nobuo Tomita

NTT Access Network Systems Laboratories
162 Shirakata-shirane, Tokai-mura, Naka-gun,
Ibaraki, 319-11 JAPAN

Nobuo Tomita is an executive research engineer at NTT Access Network Systems Laboratories. In 1974, he joined NTT Ibaraki Electrical Communication Laboratory, Ibaraki, Japan, where he engaged in research on broadband and digital subscriber loops and the development of optical fiber cable components. Since 1987, he has been engaged in the research and development of operation and

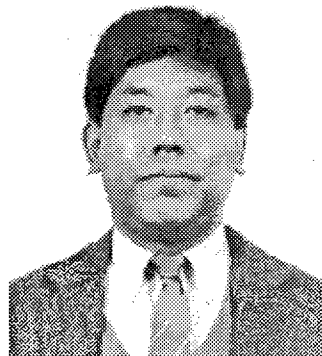
maintenance systems for optical trunk and subscriber lines.



Hiroshi Terui

NTT Opto-electronics Laboratories.
162 Shirakata-shirane, Tokai-mura, Naka-gun,
Ibaraki, 319-11 JAPAN

Hiroshi Terui is an executive research engineer at NTT Opto-electronics Laboratories. In 1974, he joined NTT Ibaraki Electrical Communication Laboratory, Ibaraki, Japan, where he engaged in research on materials for magnetooptic recording. Since 1976, he has been engaged in research on guided-wave optical devices.

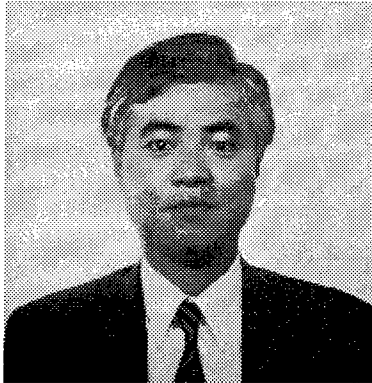


Yashufumi Yamada

NTT Opto-electronics Laboratories.
162 Shirakata-shirane, Tokai-mura, Naka-gun,
Ibaraki, 319-11 JAPAN

Yashufumi Yamada is an executive research engineer at NTT Opto-electronics Laboratories. He joined NTT Ibaraki Electrical Communication

laboratory, Ibaraki, Japan in 1982, where he engaged in the research and development of silica-based waveguides for planar lightwave circuits. His current interest is in the hybrid integration of optical devices on planar lightwave circuits.



Naoto Uchida

NTT Opto-electronics Laboratories.
3-1, Wakamiya, Morinosato, Atugi-shi,
Kanagawa, 243-01 JAPAN

Naoto Uchida is an executive research engineer at NTT Opto-electronics Laboratories. In 1985, He joined the Electrical Telecommunication Laboratories, NTT, where he engaged in research on the hetero-epitaxial growth of III-V materials such as InP on Si, GaAs on Si for opto-electronic integrated circuits (OEIC) and solar cells. He also engaged in research on OEICs of receivers. He is currently engaged in the development of integrated optical modules for access networks.

Design and Development of Optical Fiber Jointing Techniques for Efficient Construction of Aerial Distribution Cable Systems

Masaaki Takaya, Toshiaki Katagiri, Shinji Nagasawa, and Norio Kashima

NTT Access Network Systems Laboratories
Tokai, Naka, Ibaraki, 319-11 JAPAN

Abstract

In this paper, we describe the design and performance of newly developed optical fiber jointing techniques for aerial distribution cables. One employs a compact mass-fusion splicer and the other involves a small mechanical splice. These techniques exhibit excellent performance for use in aerial sites and enable aerial distribution cable systems to be constructed efficiently.

They will be useful for the economical construction of optical access networks for fiber-to-the-home.

1. Introduction

To provide customers over a wide area with broadband services, it is essential to enhance optical-fiber access networks. To achieve this, economical aerial distribution cables and jointing techniques must be developed. Various jointing techniques have already been developed including fusion splicing, mechanical splicing, and connecting [1][2][3][4][5]. However, these techniques were designed mainly for use in underground sites, and some aspects must be improved in order to use them for aerial distribution cables.

In this paper we propose three novel and simple jointing techniques for aerial use.

2. Compact mass-fusion splicer

Various fusion splice machines have already been developed for use in realizing optical subscriber systems. However, there are some problems as regards their weight and compactness when they are used for aerial distribution cables.

We developed a compact mass-fusion

splicer for joining 4-fiber ribbons. Figure 1

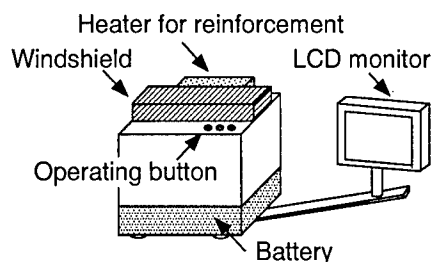


Fig. 1 Structure of a compact mass-fusion splicer.

shows the structure of this machine. The machine consists of a main body and a liquid crystal device (LCD) monitor. The main body includes fusion splicing mechanisms, the battery needed to supply electric power, a windshield at the glow-discharge region, and a heater for reinforcement. The number of mechanical and electrical parts in the splicer is reduced by simplifying both the fusion mechanisms and the image processor. In this way, we succeeded in reducing the size of the equipment to $150 \times 150 \times 150 \text{ mm}^3$, and its weight is less than 3 kg. We can complete more than 30 fiber joints with a fully-charged battery, and the windshield makes it possible to operate the machine in wind speed of up to 10 m/s. These characteristics are summarized in Table 1.

Table 1 Characteristics of the compact fusion splicer

Applicable fibers	SM	1,2,4-fibers
	GI	1,2,4-fibers
Dimensions	Width	< 150 mm
	Depth	< 150 mm
	Height	< 150 mm
Weight	3 kg	
Battery capability	30 times	
Condition	Wind velocity of less than 10 m	

2. Small mechanical splice

We also developed a small mechanical splice for joining single fibers. Figure 2 (a) shows the structure of the device. The splice

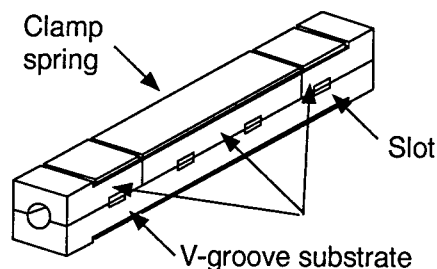


Fig. 2 Structure of the small mechanical splice.

is a pre-assembled structure consisting of a V-groove substrate, three coupling plates, and a clamp spring. It is only $4 \times 4 \times 40 \text{ mm}^3$ in size and less than 2 g in weight. Figure 3 shows an exploded view of the device.

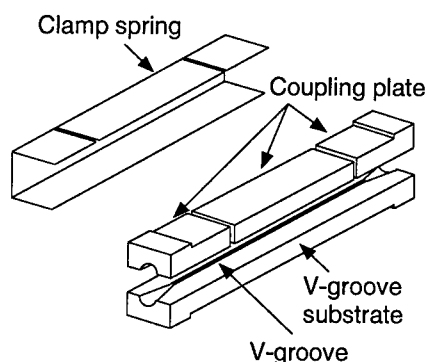


Fig. 3 Exploded view of the mechanical splice.

Optical fibers are placed in the V-groove on the substrate, and covered with the coupling plates. They are then clamped in position by the clamp spring. A jointing tool is used during the splicing. Figure 4 shows the

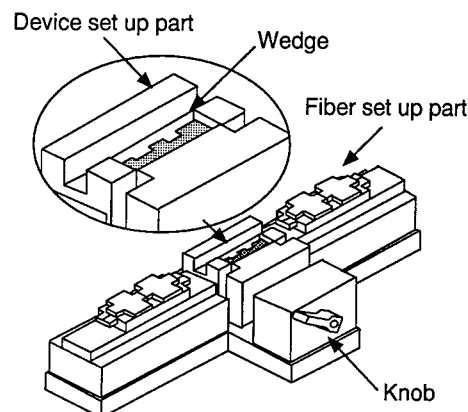


Fig. 4 Structure of the jointing tool.

structure of the tool. It consists of three parts, a device set up part, fiber set up parts, and a wedge. We can easily move the wedge by turning a knob. The tool is less than 1 kg in weight, and is suitable for use with aerial distribution cables. The jointing procedure is simple as described below. First we make a gap between the substrate and the coupling plate by inserting the wedge into slots formed in the side of the device (see Fig. 5).

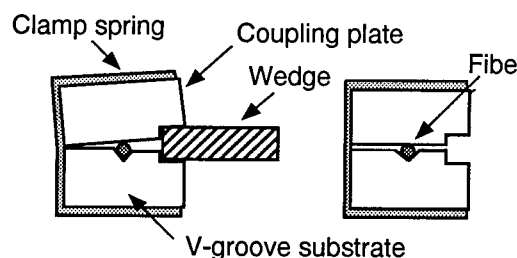


Fig.5 The jointing process.

Next we insert fibers into each end of the device. Then we remove the wedge after confirming that the fiber endfaces are touching, and the joint is completed. The jointing time is only 3 minutes.

A modified version of this splice has been designed which has the same size but which can join four fibers.

We performed optical, mechanical and environmental tests on the mechanical splice for single fibers. The results are summarized in Table 2.

Table 2 Results of optical, mechanical and environmental tests on small mechanical splices.

Tests	Conditions	Results
Insertion loss	Wavelength 1.31 μm	0.09 dB
Return loss	Wavelength 1.31 μm	> 40 dB
Vibration	10~50 Hz, amplitude 1.5 mm, 2 hours, 3 directions	$\Delta\text{Li} < 0.1 \text{ dB}$
Straight pulling	3.0 N	$\Delta\text{Li} < 0.2 \text{ dB}$
Temperature change	-40~70 $^{\circ}\text{C}$, 4 hours/cycle, 10 cycles	$\Delta\text{Li} < 0.2 \text{ dB}$
Temperature & humidity cycling	-10~65 $^{\circ}\text{C}$, 93 % (at 65 $^{\circ}\text{C}$) , 1 day/cycle, 10 days	$\Delta\text{Li} < 0.2 \text{ dB}$
High temperature endurance	70 $^{\circ}\text{C}$, 240 hours	$\Delta\text{Li} < 0.2 \text{ dB}$
Low temperature endurance	-40 $^{\circ}\text{C}$, 240 hours	$\Delta\text{Li} < 0.2 \text{ dB}$

We then performed environmental tests according to the Bellcore Standard to confirm splice reliability over long periods. The tests consisted of high temperature endurance (85 $^{\circ}\text{C}$), high humidity endurance (60 $^{\circ}\text{C}$, 95%RH) and temperature cycling (-40 - 75 $^{\circ}\text{C}$). The insertion loss change was less than 0.2 dB during these tests for eight samples.

3. Field trial results

We carried out a field trial. Figure 6 shows the trial circuit configuration. We used a 200-

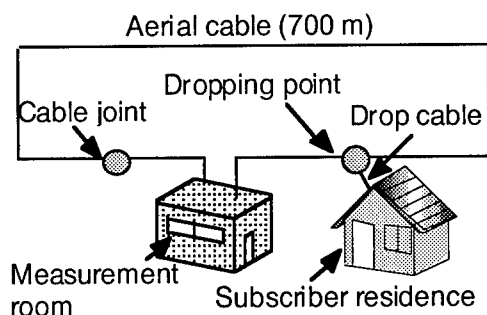


Fig. 6 Trial circuit

fiber self-supporting (SS) cable about 700 m

in length. We formed two aerial joints. One was in the SS cable, and the other was between the SS cable and the drop cable.

Figure 7 shows the working environment.

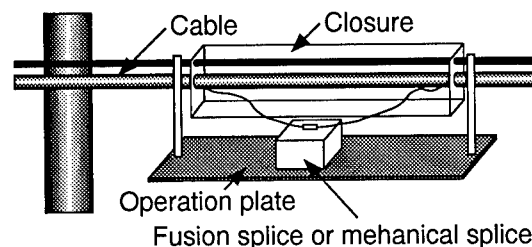


Fig. 7 Operation environment

We joined fibers on an operation plate, which was suspended beneath the cable.

3.1 Jointing time results

We measured the time needed to form joints. Figure 8 shows the times required when using mechanical and fusion splices.

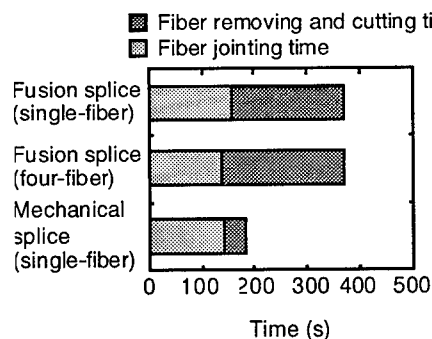


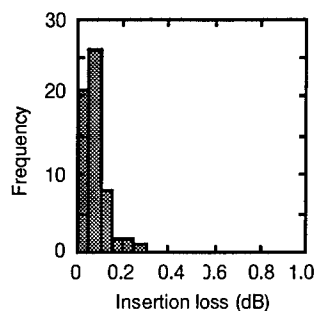
Fig. 8 Jointing times using fusion and mechanical splices.

As shown in this figure, the total jointing time using the mechanical splice is about 3 minutes. This is about half the time needed for a fusion splice.

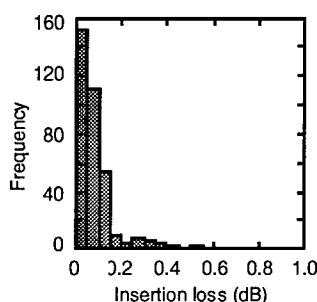
3.2 Jointing loss results

We measured the jointing losses of the fusion and mechanical splices using an optical time domain reflectometer (OTDR).

Histograms of the single- and four-fiber fusion splice losses obtained in our field trial are shown in Fig. 9 (a) and (b), respectively.



(a)



(b)

Fig. 9 Insertion loss histograms for fusion splices (a) single-fiber (b) four-fiber.

We obtained a low average insertion loss of 0.07 dB for single-fiber and 0.09 dB for four-fiber fusion splices, respectively.

A histogram of single-fiber mechanical splice losses obtained in the field trial are shown in Fig. 10.

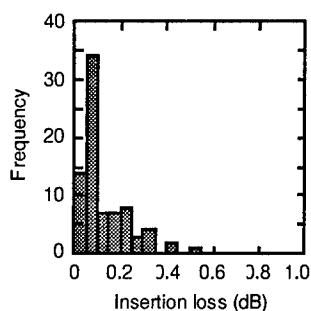


Fig. 10 Insertion loss histogram for mechanical splice.

We obtained a low average insertion loss of 0.13 dB for single-fiber. The return losses were more than 40 dB.

4. Quickly assembled multifiber connector

In addition to the completed work described above, we are currently developing a quickly assembled multifiber connector for future applications. The connector ferrule has a structure compatible with the 4-fiber mechanically transferable (MT) connector ferrule.

A feature of the connector is that the assembly process is very easy. This process is shown in Fig. 11. First fibers with cleaved

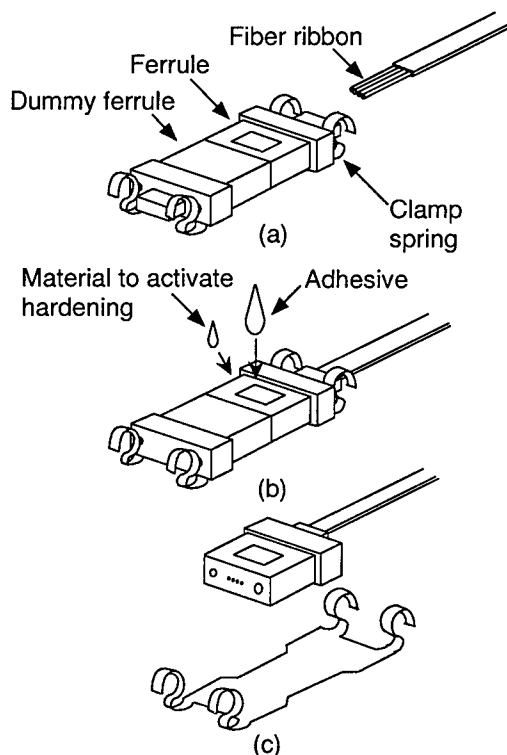


Fig. 11 Assembly process of the quickly assembled multifiber connector

endfaces are inserted into fiber-holes in the ferrule. The actual ferrule and a dummy ferrule are held by the clamp spring, and the fiber endfaces make contact with the dummy ferrule's endface. They are then fixed in place with an adhesive. The adhesive is hardened instantaneously using a solidifying medium. Next we remove the clamp spring, and detach the dummy connector. This process eliminates the need for endface

polishing. The ferrule assembly time is 3 minutes, which is about one-fifth that with the conventional field assembly method.

The insertion losses were measured using an LED operating at 1.3 μm . Histograms of the insertion losses for connectors with 4-fiber ribbons are shown in Fig. 12.

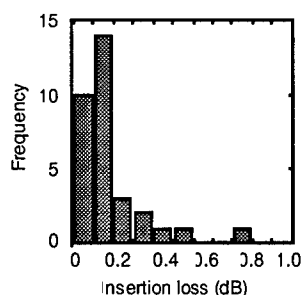


Fig. 12 Insertion loss histogram for the quickly assembled multifiber connector

We obtained an average insertion loss of 0.18 dB and a return loss of more than 40 dB for 4-fiber joints.

5. Conclusion

We have developed two new optical fiber jointing techniques for aerial distribution cables. One employs a compact mass-fusion splicer and the other involves a small mechanical splice. We measured the jointing losses of fusion and mechanical splices in a field trial. We obtained a low average insertion loss of 0.07 dB for single-fiber fusion splices and 0.09 dB for four-fiber fusion splices. We also obtained a low average insertion loss of 0.15 dB for single-fiber mechanical splices.

We have proposed a quickly assembled multifiber connector for future applications. This makes it possible to achieve high productivity, and also contributes to cost effectiveness. The ferrule assembly time is 3 minutes, which is about one-fifth that with the conventional field assembly method. We obtained an average insertion loss of 0.18 dB.

Our new jointing techniques exhibit good

levels of performance and are promising with regard to upgrading the access networks for fiber-to-the-home.

References

- [1] C.M. Miller, S.C. Metter, and I.A. White, "Optical Fiber Splices and Connectors," Marcel Dekker, Inc., 1986
- [2] N. Kashima, "Passive Optical Components for Optical Fiber Transmission," Artech House, Inc., 1995
- [3] M. Tachikura and N. Kashima, "Fusion Mass-splices for Optical Fibers Using High-Frequency Discharge," *Journal of Lightwave Technology*, Vol. LT-2, No.1, pp. 25-31, 1984
- [4] S. Nagasawa and I. Sankawa, "Reliability of V-groove Optical Fiber Mass Splice," *IEIE of Japan*, J-67-B, 4, pp. 369-376, 1984
- [5] F. Ashiya, T. Satake, and S. Nagasawa, "Development of Multifiber Connectors and their Application," *E-FOC '87*, pp. 304-308



Masaaki Takaya

NTT
Access Network
Systems
Laboratories
Tokai, Ibaraki,
319-11, JAPAN

Masaaki Takaya is a research engineer at NTT Access Network Systems Laboratories.

He joined NTT in 1992. Since 1993 he has been engaged in research on optical connector.

Mr. Takaya is a member of IEICE of Japan.



Toshiaki KATAGIRI

NTT
Access Network
Systems
Laboratories
Tokai, Ibaraki,
319-11, JAPAN

Toshiaki Katagiri is a senior research engineer at NTT Access Network Systems. He joined NTT Electrical Communications Labs., Ibaraki, Japan, in 1974. From 1974 to 1981, he was engaged in developmental research on construction machinery. Since 1982, he has been engaged in developmental research on optical fiber joint and switching technology.



Shinji NAGASAWA

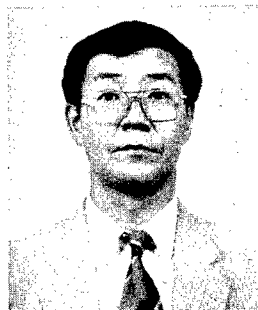
NTT
Access Network
Systems
Laboratories
Tokai, Ibaraki,
319-11, JAPAN

Shinji Nagasawa is an executive research engineer at NTT Access Network Systems

Laboratories.

He joined NTT in 1976. He has been engaged in research and development on multifiber connectors.

Mr. Nagasawa is a member of IEEE.



Norio KASHIMA

NTT
Access Network
Systems
Laboratories
Tokai, Ibaraki,
319-11, JAPAN

Norio Kashima is an executive research engineer at NTT Access Network Systems Laboratories.

He joined NTT in 1975. He has been engaged in research and development of fiber design, fusion splicing, optical connectors, transmission systems, and access network operation systems, and optical cables.

Dr. Kashima is a senior member of IEEE.

NEW CONNECTOR BLOCK MECHANISM APPLIED TO CABLE CONNECTION

Sok-ho Kim, Keun-ha Chin, Seong-kyu Kang, Chang-ha Kim
Korea Telecom, Outside Plant Technology Research Laboratory
62-1, Whaam-dong, Yusong-gu, Teajon, Korea
e-mail: obird@rcunix.kotel.co.kr

ABSTRACT

For copper cable connection, cam type connector block offering connection forces above 50 Kgf for 1 pair of outdoor wires (conductor diameter 1.0mm, insulation diameter 3.0mm) is designed and fabricated. By changing curvatures of the outer several faces of cam fixture, effective dispersion (15 ~20 kgf) of connection force can be obtained and performances of test-product is confirmed.

INTRODUCTION

Among various electrical connection techniques applied to copper cable, IDC(Insulation Displacement Connection) is the technique inserting wire into slotted pin without stripping. At insertion of 1 pair of 1.0mm diameter outdoor wire, big forces above 50 Kgf would be needed because wire travels straightly in a definite distance to be inserted into slot of the pin. Therefore insertion & disconnection tools or screw-nut type mechanical blocks are designed for ID connection using in outdoor terminal box.

But in this study new connector mechanism is developed to use fingers to complete connection readily and easily on the pole. And this is for the connection needed big forces to insert wires in the range of 0.4mm conductor to 1.0mm (maximum insulation : 5.0mm).

IDC MECHANISM

The process of ID (Insulation

Displacement) connection is shown in Figure 1. Wire is arrayed on IDC pin and moves into slot of the pin. Insulation of the wire is teared and conductor is deformed. In this process insertion forces is changed with the changes of displacement point as the curve of Figure.2. The connection forces of a IDC type connector are determined by design and material of IDC pin, conductor , insulation diameter and materials of the cable. The size of the connection force according to insertion position is not uniform because of mixed structure (insulation and conductor) in wire and increase of contact area between wire and IDC pin.

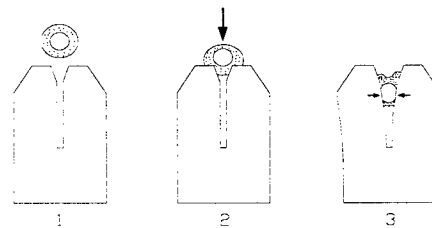


Figure1. Connection process of typical ID connection

For the connection of 1 pairs of 1.0mm outdoor wire, big connection force above 50kgf are needed and can not be applied by hand and even on the pole. Moreover repulsive force, the same size of insertion force, are applied to opposite direction and so continuous force downward have to be applied from the block. This is the reason why outdoor IDC connector block is hard to design using insertion tools and screw type block. Besides this kind of connector block need tools, long connection time and dependence on worker's expertness. The major point of

this mechanism is small connection force by hand, no tools and independence on worker's expertness.

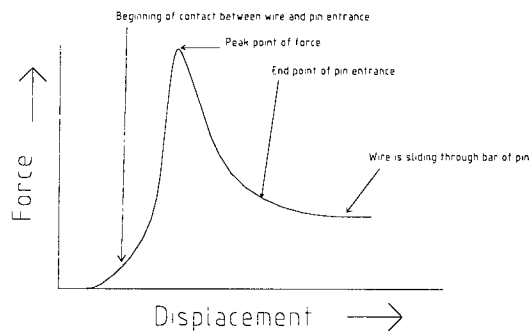


Figure 2. The changes of insertion forces by displacement of cable

BLOCK DESIGN

The major object of block design is the effective dispersion of the big connection forces by transforming rotation to straight movement. In considering connection position and applied force for that, block is designed to disperse insertion forces unevenly according to various position. By changing curves of the cam the applied force at a certain point can be adjusted under minimum level. The mechanism is applied from movement principles of the cam and the lever, and we proposed design techniques usable in ID Connection. The Figure 3 shows connection mechanism of designed block and dispersion of insertion forces by changing curvatures of the several outer faces of cam fixtures.

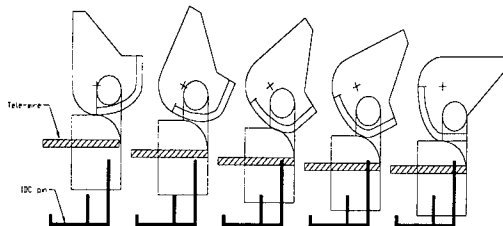


Figure 3. The connection mechanism of design block

To transform the rotation movement of cam to vertical movement of cables,

1-pair holder holding cables in it's holes is hanged on cam. One side of cam has the shape of lever to apply rotation force. The flat face of cam makes connection complete because upward repulsive force blocks backward-rotation of the cam. The correlation of insertion forces according to 1.0mm wire displacement is shown in Figure 4.

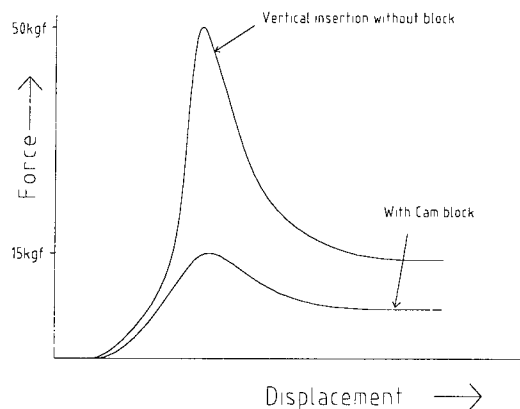


Figure 4. Insertion forces VS displacement of 1 pair 1.0mm wire between direct insertion and with cam block

The curve down in the Figure 4 shows broadening peaks meaning that big insertion force(upper curve) required of insulation of wire to be cut by the developed universal pin is dispersed by cam mechanism. The designed block is shown in Figure 5 and wire displacement according to rotation angle of cam and accordingly the changes of insertion force is shown in Figure 6.

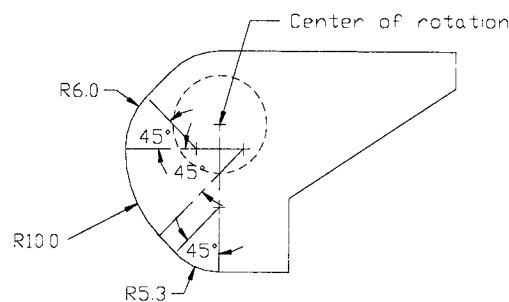


Figure 5. Drawing of designed Cam

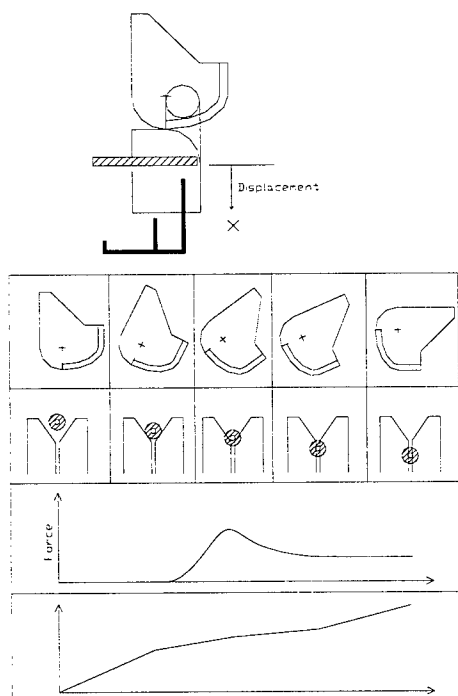


Figure 6. The changes of insertion forces of designed block according to increase of rotation angle of cam

FABRICATION OF CAM-TYPE CONNECTOR BLOCK

The cam type terminal block devised is shown as follows in Figure 7.

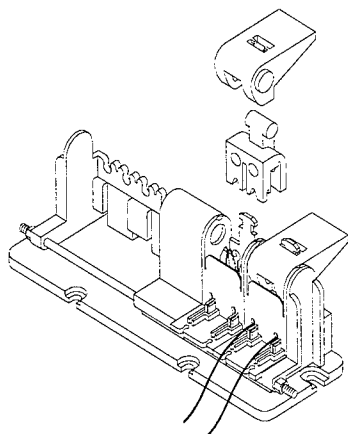


Figure 7. Fabricated Cam-type Terminal Block

The housing materials is PC and pin

material is phosphate bronze. Fabricated block afford to connection of cable ranged from 0.4mm to 1.0mm conductor diameter in one hole. 1-Pair modular connector can be assembled to various terminal blocks.

The increase of connection resistance under various environment (temperature cycling, humid, stress relaxation, 100 times repeated insertion, etc) are measured and appeared the values within $2m\Omega$ after test. The tested insertion forces are measured values between 15 ~ 20kgf which is one third values of direct insertion force (50kgf).

CONCLUSION

By changing curvatures of the outer several faces of cam fixture, effective dispersion (15 ~ 20 kgf) of connection force can be obtained and good performances of test-product is confirmed. Therefore this block design can be applied to connector block for various cable connection, cutting tool and other big vertical force needed tools.

REFERENCES

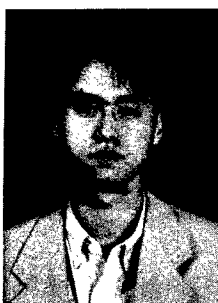
1. Outside Plant Lab Yearly Report, "The Development of Fiber Optic products", 1992 ~ 95, Korea Telecom
2. Connectors and Interconnection Handbook, vol. I ~ V, IICIT Inc., 1990
3. W.E. Pugh, "An Evaluation of the Insulation displacement Electrical Contact", IICIT symp., Holm conference, 1979
4. Horn Heneth W, et.al., "Understanding Stress Relaxation in Copper Alloys", Fifth Annual Proceeding of IICIT, 1982.
5. N.K. Mitra, "An Evaluation of the Insulation Displacement Electrical Contact", In Holm Conf. Proc., 1979, p99 ~ 108.

AUTHORS



Sok-ho Kim
Korea Telecom
Outside Plant Technology Research
Laboratory
62-1,Whaam-dong,
Yusong-gu,Teajon,
Korea
305-348

Sok-ho Kim graduate from Hanyang University in 1988 with a M.S. Degree on Material Engineering. After 3 yrs developing electronic materials in Korea Advanced Institute of Science and Technology, he joined in Korea Telecom and is engaged in outside plant products, fiber optic products..



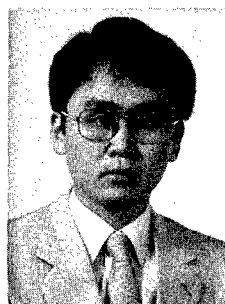
Keun-ha Chin
Korea Telecom
Outside Plant Technology Research
Laboratory
62-1,Whaam-dong,
Yusong-gu,Teajon,
Korea
305-348

Keun-ha Chin graduate from Seoul National University in 1993 with a M.S. Degree on Mechanical Engineering. He then joined Korea Telecom and is engaged in development of terminal box.



Seong-Kyu Kang
Korea Telecom
Outside Plant Technology Research
Laboratory
62-1,Whaam-dong,
Yusong-gu,Teajon,
Korea
305-348

Seong-kyu Kang graduate from Kunkuk University in 1982 with a B.S. Degree on Electronic Engineering. He is engaged in development of terminal box.



Chang-ha Kim
Korea Telecom
Outside Plant Technology Research
Laboratory
62-1,Whaam-dong,
Yusong-gu,Teajon,
Korea
305-348

Chang-ha Kim graduate from Korea University in 1986 with a B.S. Degree and KAIST with a M.S. and Ph.D on Material Scienc Engineering. He is engaged in development of outside plant products.

MINI-MPO CONNECTOR

Naoko SHIMOJI Jun YAMAKAWA

THE FURUKAWA ELECTRIC CO., LTD.
6, Yawata-Kaigandori, Ichihara, Chiba 290 JAPAN

ABSTRACT

We have recently developed mini-MPO connector, which is based on existing MPO (Multi-fiber Push-On) connector and is a more compact and simpler structure than MPO. Mini-MPO connector is capable of connecting a 2- or 4-fiber ribbon. This connector is sized to a cross section of $7 \times 10 \text{ mm}^2$, which is approximately half the size of a conventional MPO. The 2-fiber single-mode mini-MPO connector shows optical characteristics of less than 0.2 dB in insertion loss and of more than 50 dB in reflectance. In a connection-disconnection test, the connector was found to be stable enough to show an insertion loss of less than 0.2 dB. In a 9.8 N side pull test, it showed an increase in insertion loss by less than 0.2 dB. Mini-MPO connector could achieve equivalent performance to conventional MPO.

1. INTRODUCTION

Because optical fiber connectors equipped on the panel of equipment subject to cycle

connection and disconnection, they are required to be better connectability. Consequently, it is preferable that connection and disconnection can perform in an action such as push-on / pull-off basis and appropriate optical performances can be got without index matching material. Moreover, optical connectors are strongly required to be compact and keep high density, to meet needs in recent years for high count and high density optical fiber cables^[1]. MPO (Multi-fiber Push-On) connector using a multi-fiber MT (Mechanically Transferable) ferrule has been already put into practical use^[2]. It is an optical connector capable of connecting a 12-fiber cable at the maximum. And the 12-fiber MPO connector is capable of meeting the above-mentioned requirements sufficiently.

It could not be said, however, that MPO connector has achieved a satisfactory level of high density in a 2-fiber or a 4-fiber connection. The proposed mini-MPO connector is focused on an applicable to a maximum of 4-fiber ribbon, thereby achieving a sufficiently compact low-cost structure in comparison with a conventional MPO connector.

2. DESIGN CONCEPT

2.1 Fundamental Structure

Fig. 1 is a schematic of mini-MPO connector.

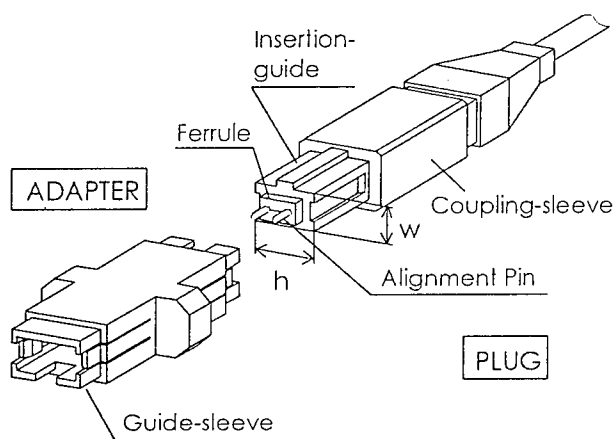


Fig. 1 The structure of mini-MPO connector

Mini-MPO connector is designed to be fundamentally analogous to an existing MPO connector. Similarly to MPO connector, mini-MPO connector consists of two plugs and one adapter. The connector aligns itself by two alignment pins. The ferrule end of the connector is polished obliquely and the optical fibers protrude from ferrule surface slightly. This permits fiber to connect mutually even. In addition, it reduces Fresnel reflection without index matching material. Consequently, a stable optical characteristic is available with mini-MPO connector.

Mini-MPO connector has a ferrule size of 2.6 mm in alignment pin pitch as compared with 4.6 millimeters of the conventional MPO connector. Between alignment pins, the four fibers are aligned at a pitch of 250 μ m at the maximum. The smaller alignment hole pitch allows the ferrule to have smaller dimensions in height.

2.2 Tilt and Bending by Side-Pull Force

Mini-MPO connector adapter does not have the shell which a conventional MPO adapter has, shown in Fig. 2. As a result, mini-MPO adapter is of simple structure, having smaller dimensions not only in height but also in width. A conventional MPO adapter has a size of 15 x 10 mm² while mini-MPO adapter has 10 x 7 mm². In terms of cross section, mini-MPO connector is approximately half conventional MPO.

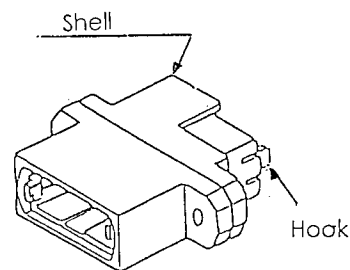


Fig. 2 Conventional MPO adapter

A conventional MPO connector has the shell perform a role of protecting the plug for a possible tilt by a side-pull force applied on the plug coupling-sleeve. An tilt of the plug would induce a bend of the optical axis at the ferrule splice, resulting in a deterioration of optical characteristics. Mini-MPO connector which does not have the shell has this tilt controlled by the adapter guide-sleeve. This tilt angle θ is dependent upon a connected length of the adapter guide-sleeve and of the plug housing insertion guide and upon a clearance between adapter and insertion guide.

$$\theta = \arctan [(clearance) / (connected length)].$$
Detail dimensions of the guide-sleeve, therefore, are important to control an tilt of the plug. Once the side-pull force has become very large, not only the tilt due to a clearance between adapter and plug but also a plug-

bending deformation will take place. Mini-MPO connector has a smaller plug cross section than the conventional MPO connector. The bending deformation due to a side pull force, however, tends to be larger according as the cross section becomes smaller. A relation with the bending due to a bending force is proportional to:

$$(\text{side-pull force}) / (h \times w^3)$$

where, h and w, respectively, are the high and wide dimensions of the plug housing. A usual MPO adapter does not have a guide-sleeve and has a sufficient clearance between the plug housing insertion guide and the coupling sleeve. In addition, the insertion-guide engages with the adapter to a very small extent. Then, the insertion guide is liable to bend-deform independently. The insertion guide of MPO connector plug has cross-sectional dimensions of 7.2 mm high and 4 mm wide. Mini-MPO connector, however, has the adapter guide-sleeve come in close contact with the plug housing. As a result, the plug has a bending deformation controlled by the cross-sectional dimensions of the adapter guide-sleeve. Therefore, the bending of the plug engaging the adapter results in a sufficiently small deformation as compared with that of a separated plug.

2.3 Alignment Mechanism

Both conventional MPO and mini-MPO connector plugs align themselves using two alignment pins per connector assembly. The alignment pin of one plug is allowed to have a misalignment smaller than the alignment hole diameter just before inserting the alignment hole of the ferrule of the other connector. The main causes of this offset are a misalignment of

the plug due to a clearance between adapter and plug, and a misalignment of an alignment pin at the tip due to a tilt of the plug. To reduce the tilt-induced misalignment, it is necessary to increase the connected length between adapter and plug.

Mini-MPO has a larger length connected with the plug housing due to the adapter guide-sleeve than that of the conventional MPO connector. As a result, the plug is less tilt against the adapter so that the alignment pin can be aligned more accurately just before connecting the plugs.

In mini-MPO connector referred to above, a dimensional shape of the adapter guide-sleeve is an important factor, which is influential over not only side-pull characteristic but also alignment accuracy.

3. CHARACTERISTICS

3.1 Optical Characteristic

Based on the design concept already referred to, we have trial-manufactured single-mode 2-fiber mini-MPO connector and have studied its optical characteristic. The ferrule was polished by 8 degrees obliquely at the endface. In all measurements, no index-matching material was applied to a splice of connectors.

Fig. 3 shows an insertion loss characteristic at measuring wave-lengths of 1,310 nm and 1,550 nm. A mean insertion loss is 0.19 dB. Next Fig. 4 shows a reflectance characteristic at 1.310 nm and 1,550 nm wavelengths. A mean reflectance is 60 dB and a minimum is 53 dB.

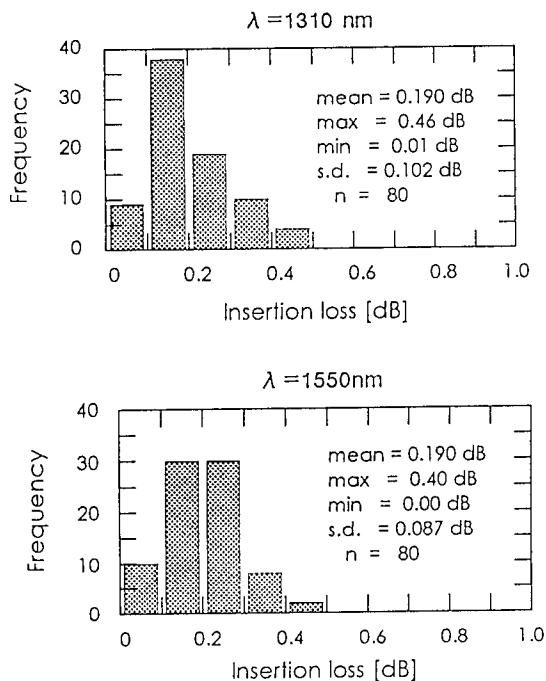


Fig. 3 The characteristic of the insertion loss

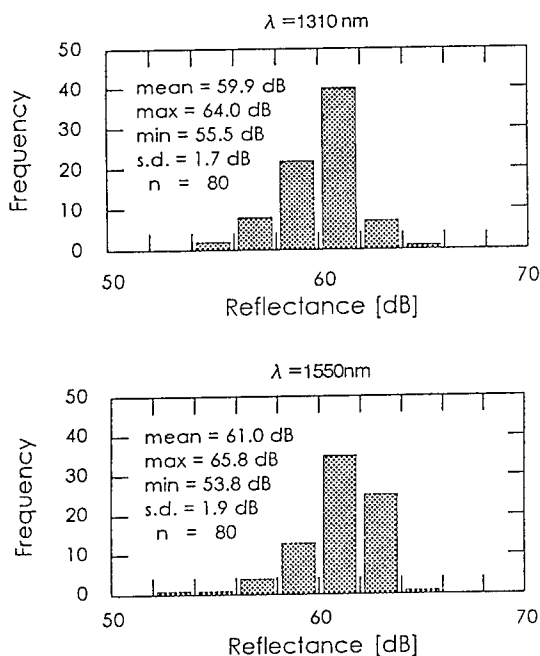


Fig. 4 The characteristic of reflectance

3.2 Connection-Disconnection Test

To look into the alignment accuracy and durability of mini-MPO connector, a

connection-disconnection test was performed. Fig. 5 shows the insertion changes loss when connecting and disconnecting 2-fiber mini-MPO connector in 500 cycles without index-matching material. The insertion loss changes are less than 0.2 dB. This slight insertion loss fluctuation is assumed to be attributable to a change of splice offset due to connections and disconnections. Nevertheless, the connector showed a very stable optical characteristic for a repetition of connections and disconnections. From this, it is considered that mini-MPO connector has alignment accuracy stabilized irrespective of the number of connection-disconnection cycles.

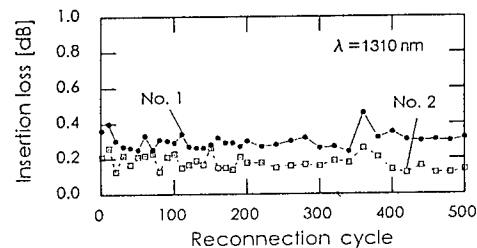


Fig. 5 The results of the connection-disconnection test for 500 cycles

3.3 Temperature Cycling Test

Mini-MPO connector may be really used in a pyrogenic or cryogenic atmosphere. Fig. 6(a) and Fig. 6(b), respectively, show the insertion loss changes and the reflectance of 2-fiber mini-MPO connector in a temperature cycle of -25 through +70 °C without index-matching material. The maximum insertion loss change is less than 0.2 dB. The reflectance is more than 50 dB over the entire range of temperatures. From these findings, it is considered that mini-MPO connector ensures a

high reflectance and a stable insertion loss characteristic within that temperature range.

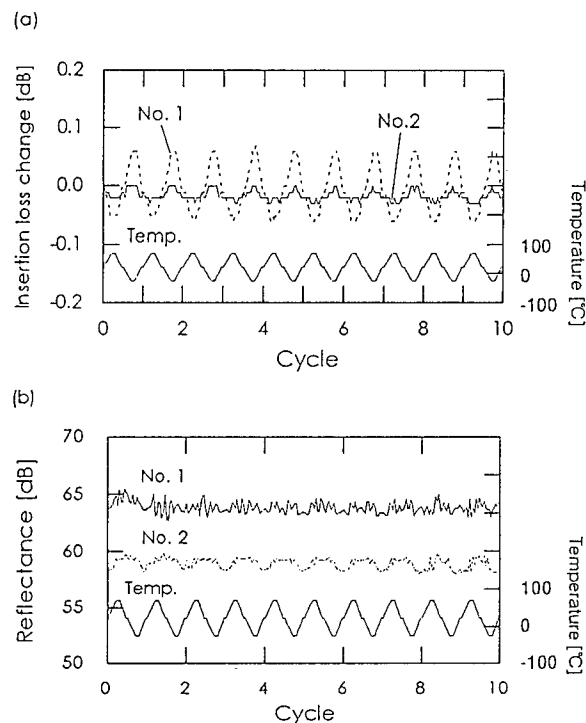


Fig. 6 The insertion loss change and the reflectance in $-25^{\circ}\text{C}/70^{\circ}\text{C}$ temperature cycling test ($\lambda=1310\text{ nm}$)

3.4 Side-Pull Test

To verify the design of the adapter guide-sleeve in mini-MPO connector, furthermore, a side-pull test was performed. For testing, the connector was secured at 90 degrees, to which a load of 9.8 N was applied. And the insertion loss was measured in 10 or more seconds after applied a load. The results are shown in Table 1. All of the results show that the insertion loss tends to increase by less than 0.2 dB. For this test, we designed an adapter-plug clearance of approximately 0.7 degrees in tilt of the plug to the adapter. When single-mode fiber has an optical axis bent to 0.7 degrees at a splice, the insertion loss will theoretically increase by about 0.25 dB. This nearly coincides with the

test results. From these findings, it is gathered that the plug will have a tilt equivalent to the adapter-plug clearance, with a side load of 9.8N applied. Besides, there are possibilities that no bending deformation may have taken place with this load. Thus, it is concluded that the clearance design is appropriate.

Side-pull force[N]	9.8
The maximum of the insertion loss change [dB]	< 0.2
n	6

Table 1 Side-pull test

4. CONCLUSION

We have developed mini-MPO connector of smaller and simpler structure than that of an existing MPO connector. And this mini-MPO connector is applicable to 2- and 4-fiber optical ribbons. It has a connector size of $10 \times 7\text{ mm}^2$ in cross section of the adapter, which is approximately half that of a conventional MPO connector. For adapter structure, mini-MPO connector does not have a shell unlike the conventional MPO connector but has a guide-sleeve instead.

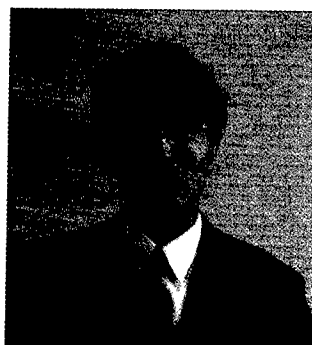
For optical characteristics, mini-MPO connector is favorable in terms of both insertion loss and reflectance. A connection-disconnection test and a $-25^{\circ}\text{C} / +75^{\circ}\text{C}$ temperature cycling test have offered that mini-MPO connector has an insertion loss characteristics stabilized. In addition, a high reflectance was available over that temperature range. From the side-pull

characteristic, moreover, the adapter-plug clearance is confirmed designed appropriately.

REFERENCES

[1] S. Nagasawa, T. Tanifuji, M. Matsumoto, and M. Kawase, "Single-Mode Multifiber Connectors for Future Large Scale Subscriber Networks", ECOC'93, pp. 29-32, 1993.

[2] S. Nagasawa, Y. Yokoyama, F. Ashiya, and T. Satake, "A High-Performance Single-Mode Multifiber Connector Using Oblique and Direct Endface Contact between Multiple Fibers Arranged in a Plastic Ferrule", *IEEE Photon. Technol. Lett.* vol. 3, NO. 10, pp. 937-939, 1991.



Jun YAMAKAWA

The Furukawa
Electric Co., Ltd.

6, Yawata-kaigandori,
Ichihara, Chiba 290
JAPAN

He was born in Hokkaido, Japan, in 1965. He received the B.E. degree in applied electronic engineering from University of Electro Communications, Tokyo, Japan, in 1989.

He was joined The Furukawa Electric Company, in 1989. Since then he has been engaged in the research and development on optical component.



Naoko SHIMOJI

The Furukawa
Electric Co., Ltd.

6, Yawata-kaigandori,
Ichihara, Chiba 290
JAPAN

She was born in Tokyo, Japan, in 1968. She received the B.S. and M.S. degrees in Physics from Chuo University, Tokyo, Japan, in 1991 and 1993, respectively. She joined The Furukawa Electric Company, in 1993. Since then she has been engaged in the research and development on optical component.

Development of 72-channel optical fiber connector

Ken Kanai*

Osamu Suzuki**, Takayuki Watanabe**, Seiji Toda**

*THE FURUKAWA ELECTRIC CO., LTD.

6, Yawata-kaigandori, Ichihara, Chiba 290 Japan

**FUJITSU LIMITED

4-1-1, Kamikodanaka, Nakahara-ku, Kawasaki, Kanagawa 211 Japan

Abstract

72-channel Multi-pass Push-on connector (72MPO connector) has been developed. This type of connector consists of one adaptor and two plugs, and the plug consists of 6 pieces of 12MT ferrule within one plug housing, so it can connect 72 fibers in one action.

Dimension of 72MPO connector is almost the same as half of the one which 6 pieces of conventional 12MPO connector are stacked.

Insertion loss of 72MPO is 0.378dB in average and this value is almost the same as of 12MT ferrule measured before assembling them into the plug housing.

1. Introduction

MPO connector^[1] has been developed and used in the place where connections are repeated many times, for example, at the terminals of equipment. This type of connector consists of a conventional MT ferrule^[2] and a few housing parts, and has push-on pull-off coupling mechanism, so it can be connected in one action.

In the meantime, to get higher throughput of computer system, more and more number of CPU must be connected in a computer system. That means CPU networking size becomes bigger and bigger. Consequently, the connection number of the fiber cable is increasing. In this situation, to get higher reliability of the optical connector coupling and easy network construction, multi connector coupling system is required in these computer system.

On this point of view, we developed 72MPO connector which contains 6 pieces of 12MT ferrule in the plug housing and can connect 72 fibers in one action.

2. Structure of 72MPO connector

Fig.1 shows the structure of 72MPO connector. This type of connector consists of one adaptor and two connector plugs, and the connector plug has 6 pieces of conventional 12MT ferrules within its housing. The type of fibers assembled into the ferrule was multi-mode 12-fiber ribbons, and core diameter was $62.5 \mu\text{m}$.

Fig. 2 shows the mating face of 72MPO connector plug. The dimension is 33mm in height and 16mm in width. This is as same as half of one which 6 pieces of conventional 12MPO connector are stacked.

The adaptor consists of two parts and one metallic plate shown in Fig. 3. The two pieces of adaptor parts are assembled back to back each other, and the metallic plate is inserted between them. This metallic plate prevents electromagnetic wave leaking from the cabinet.

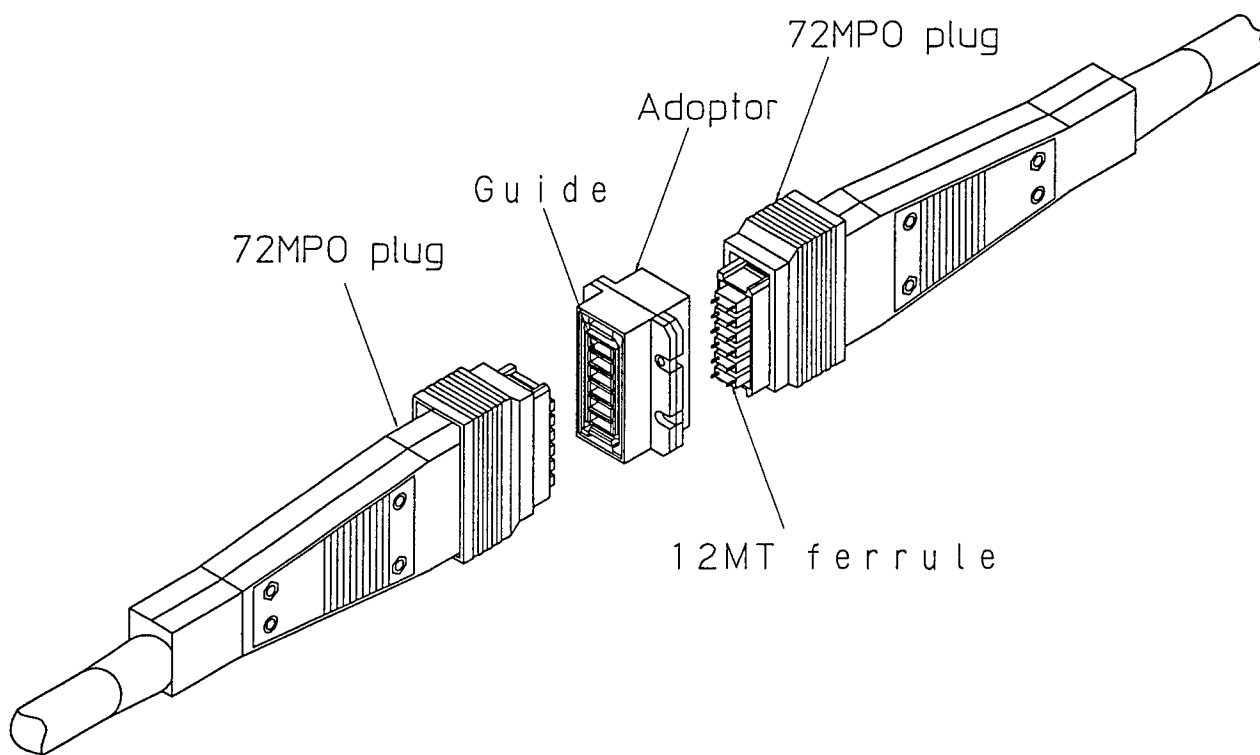


Fig. 1 Structure of 72 MPO connector

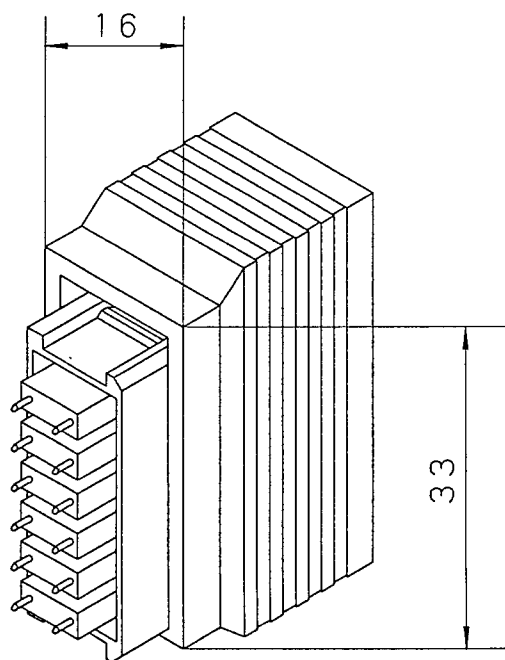


Fig. 2 Mating face of 72 MPO connector plug

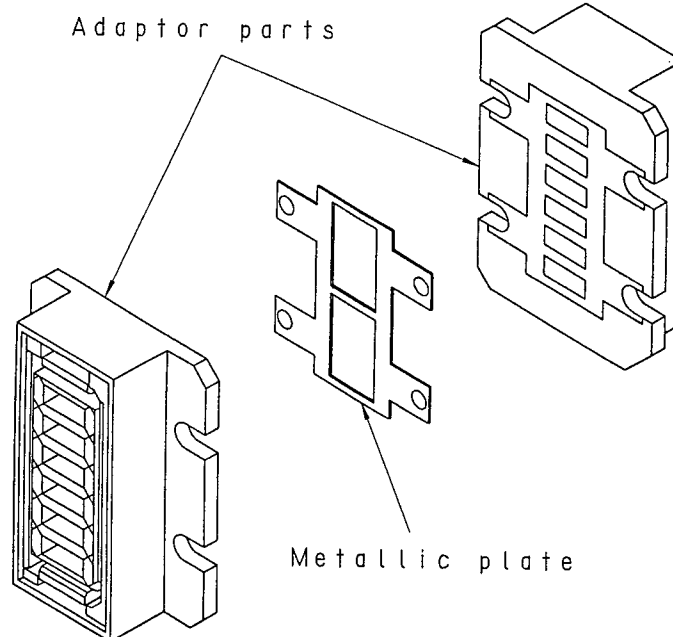


Fig. 3 Adaptor parts and metallic plate

3. Coupling sequence of 72MPO connector

Fig. 4 shows coupling sequence of 72MPO connector.

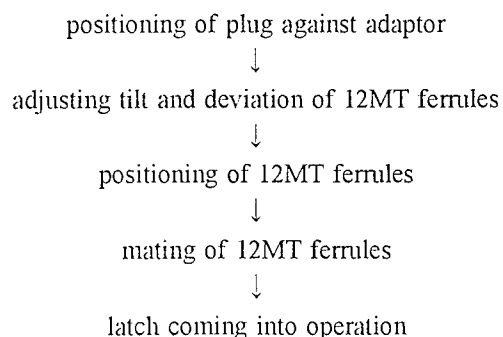


Fig. 4 Coupling sequence

As the connector plug is inserted into the adaptor, firstly, tilt and deviation of the plug against the adaptor is adjusted by the shape of both the plug and the adaptor. As the plug is inserted into the adaptor furthermore, tilt and deviation of 6 pieces of 12MT ferrule are aligned by the guides in the adaptor shown in Fig. 5 and 6. Then, each 12MT ferrule are positioned by the alignment pins which are previously inserted into the alignment pin holes of 12MT ferrules shown in Fig. 7 and they are mated shown in Fig. 8. At this point optical connections of each 12MT ferrule are completed, and as the plug is inserted into the adaptor furthermore, latch function comes into operation and this latch keeps the connections of 6 pairs of 12MT ferrule.

This coupling mechanism was designed based on almost the same concept of MPO connector. Different point from conventional MPO connector is that 72MPO connector has 6 pieces of 12MT ferrule in the plug housing and should connect 12MT ferrules at one time. To connect each 12MT ferrule with certainty, the plug housing was designed each 12MT ferrule to be able to move individually in the plug housing, we call this as independent floating mechanism, and the adaptor has the guides, and the tip of the guide is rounded to absorb tilt and deviation of 6 pieces of 12MT ferrule. We decided dimensions and tolerance of ferrule, housing and adaptor to operate the mechanism described above.

After each 12MT ferrule are mated, 72MPO connector should keep the connections of MT12 ferrules. Each connection causes repulsive force of 9.8N, so 72MPO should absorb repulsive force of 58.8N, which is six times higher than conventional MPO connector. From the result of examination of the dimension of the latch, 72MPO connector achieved to decrease its size keeping the coupling force of over 60N.

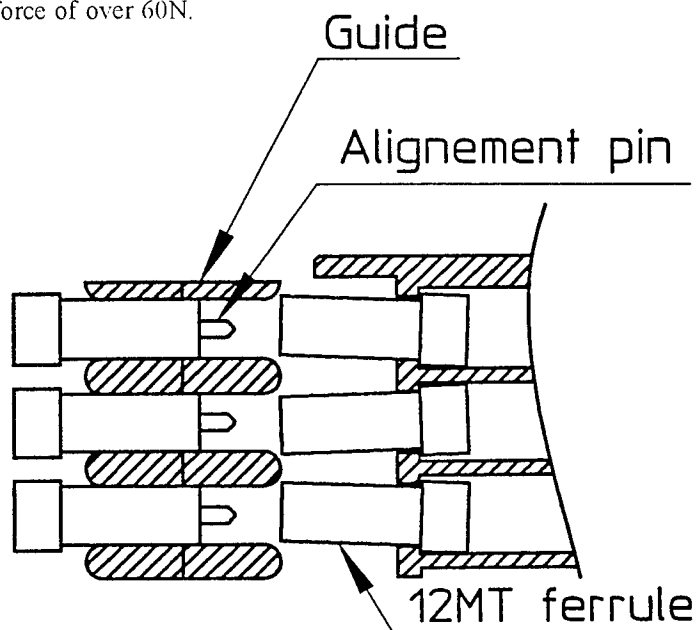


Fig.5 Tilt and deviation of 12MT ferrules

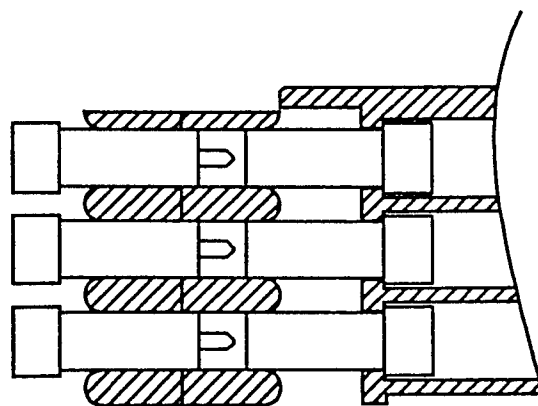


Fig.6 Adjusting tilt and deviation of 12MT ferrules

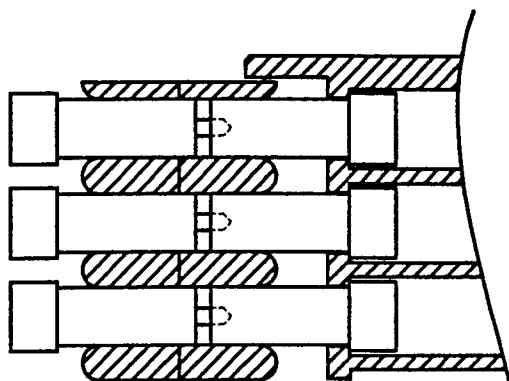


Fig.7 Positioning of 12MT ferrules

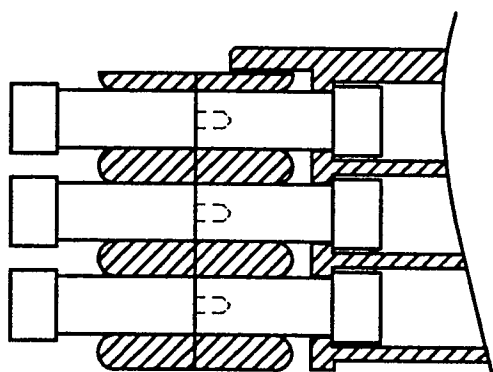


Fig.8 Mating of 12MT ferrules

4. Optical property

Insertion loss of 72 MPO connectors was measured with multi-mode (62.5/125) 12-fiber ribbons.

Fig. 9 and 10 show the insertion loss measured as 12MT connectors and as 72MPO connectors, respectively. From the comparison of these two figures, it is said that the optical property of 12MT connectors were kept after those connectors were assembled into the plug housing. No optical performance degradation caused by housing design has not been observed.

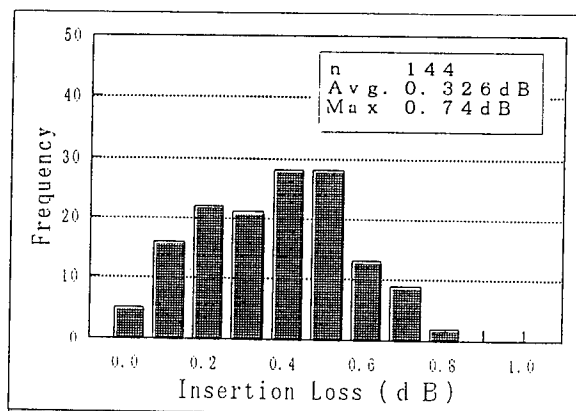


Fig. 9 Insertion loss measured as 12MT connector

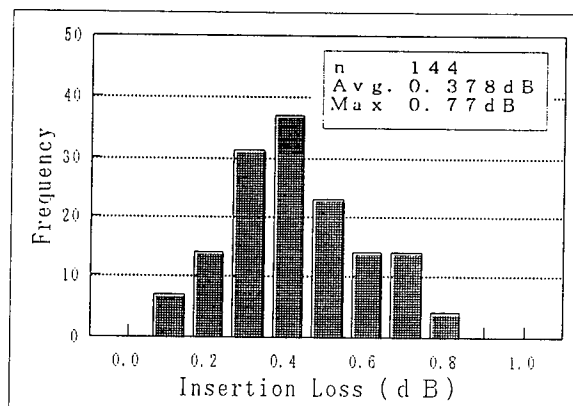


Fig. 10 Insertion loss measured as 72MPO connector

5. Conclusion

This time we have developed 72MPO connector by stacking 6 pieces of conventional 12MT ferrule in one housing. The structure and optical property are as follows.

72MPO connector consists of one adaptor and two plugs. The plug contains 6 pieces of conventional 12MT ferrule which are stacked in plug housing. It achieved to reduce the mating face of the plug by half compared to the one where 6 pieces of conventional MPO plug were stacked.

Plug and housing were designed to keep the coupling force of 6 pieces of 12MT ferrule, and to connect each 12MT ferrule in one action.

Insertion loss of 72MPO connectors was measured with multi-mode (62.5/125) 12-fiber ribbons. The results are as follows.

Ave.: 0.378dB Max.: 0.77dB

Insertion loss of the 12MT connectors, which were the same ones stacked in the plug housing, measured before assembly was 0.33dB in average. No optical performance degradation caused by housing design has not been observed.

References

[1] S. Nagasawa, Y. Yokoyama, F. Ashiya and T. Satake, "A High-Performance Single-Mode Multifiber Connector Using Oblique and Direct Endface Contact Between Multiple Fibers Arranged in a Plastic Ferrule", IEEE PHOTONICS TECHNOLOGY LETTERS, VOL3, NO.10 October, 1991, pp937-939

[2] T. Satake, S. Nagasawa and R. Arioka, "A New Type of Demountable Plastic-molded Single-mode Multifiber Connector", J. of Lightwave Technology, Vol.L4, No.8, August, 1986, pp1232-1236

Osamu Suzuki

FUJITSU LIMITED

4-1-1, Kamikodanaka,
Nakahara-ku, Kawasaki,
Kanagawa 211 Japan

Takayuki Watanabe

FUJITSU LIMITED

4-1-1, Kamikodanaka,
Nakahara-ku, Kawasaki,
Kanagawa 211 Japan



Ken Kanai

The Furukawa Electric
Co., Ltd.

6, Yawata-kaigandori,
Ichihara, Chiba 290
Japan

Ken Kanai was born in Niigata, Japan, in 1967. He received the B.E. and M.E. degree in materials science engineering from Keio University, Kanagawa, Japan, in 1990 and 1992, respectively.

He joined The Furukawa Electric Co., Ltd., in 1992. Since then, he has been engaged in development of optical fiber connectors.

Seiji Toda

FUJITSU LIMITED

4-1-1, Kamikodanaka,
Nakahara-ku, Kawasaki,
Kanagawa 211 Japan

RADIATION AGING AND DEGRADATION MECHANISM OF POLYMER INSULATION FOR ELECTRIC CABLES

Masahiko Sugiyama, Makoto Nitta, Tsuneo tani
Yazaki Electric Wire Co.,Ltd.
Numazu, Shizuoka, Japan

Tadao Seguchi, Toshiaki Yagi
Japan Atomic Energy Research Institute
Takasaki, Gunma, Japan

ABSTRACT

The degradation mechanism of insulation materials for electric cables was studied on the point of the relation of radiation-induced oxidation to gel fraction and tensile properties. Flame retardant crosslinked polyethylene (FR-XLPE) and special heat resistant polyvinyl chloride (SH-PVC) were investigated by volume resistivity, gel fraction, and tensile property. Furthermore, the oxidation profile by Electron Probe Microanalysis (EPMA), Ultra Micro Hardness Measurement and Scanning Acoustic Microscopy (SAM) after ^{60}Co gamma-ray irradiation in various oxidative conditions were investigated.

As a result of the experiments, it was confirmed that the electric property is changed by radiation oxidation, gel fraction corresponds well to the proportion of oxidation layer, and a surface oxidation layer induces the fracture of specimens during the tensile test, as a notch effect.

INTRODUCTION

A large number of electric cables have been used in nuclear facilities, where the cables are subjected to radiation, and degrade gradually with time in electric properties and also mechanical properties. The cables must be highly reliable in such circumstances to remain safe under operation. The polymers used as cable insulation should degrade through chemical reactions such as molecular chain scission and / or crosslinking by radiation and thermal aging, and properties such as electric resistance and mechanical strength change with the degradation.

In this report, the relation of radiation oxidation to volume resistivity, as well as to gel fraction,

tensile property and oxidation profile in polymer insulation used for electric cables in nuclear facilities was minutely investigated.

EXPERIMENTAL METHOD

Samples

Two types of insulation materials were prepared. FR-XLPE was formulated by chemical crosslinking using Dicumyl peroxide after mixing some flame-retardant agents and some stabilizers. SH-PVC contains plasticizer which has high heat resistance, and some stabilizers.

Irradiation

Samples were irradiated by ^{60}Co gamma-rays at room temperature under three different conditions. (1) High dose rate irradiation in air (8kGy/h), (2) Low dose rate irradiation which induced oxidation throughout the cross-section of sheet samples (5kGy/h under 0.6MPa oxygen pressure), and (3) Irradiation without oxidation (6kGy/h in a vacuum).

Volume Resistivity (VR) Measurement

Volume resistivity measurement was carried out, using a high resistance meter at room temperature.

Gel Fraction (GF) Measurement

Gel fraction was measured by solvent extraction. For FR-XLPE, Xylene was used as the solvent, and stored for 24h at 138 °C ; for SH-PVC, Tetrahydrofuran was used and stored for 5h at 65 °C .

Tensile Test

Tensile test of dumbbell shape specimens was carried out, with the speed of the jug separation at 200mm/min at room temperature. The residual elongation and tensile strength were determined.

Electron Probe Microanalysis (EPMA)

The sliced specimens from the sheet samples were immersed in Potassium hydroxide isopropanolic solution, to stain the carboxylic acid sites in the sample with K atoms. The K atoms trapped at the carboxylic acid sites were counted by EPMA with the accelerated voltage of 25kV and current of 2.0×10^{-8} A.

Micro Hardness Measurement

Sample sheets were cut into slices for the measurement of the micro hardness in a cross-section to observe the hardness profile. The hardness was measured by a Ultra Micro Hardness Tester at room temperature.

Scanning Acoustic Microscopy (SAM)

Sample sheets were cut into slices for the observation of the radiation oxidation layer in the cross-section by a Scanning Acoustic Microscope. The frequency of acoustic lens was 200MHz.

RESULTS AND DISCUSSION

Volume Resistivity

Fig. 1 shows the relation between dose and volume resistivity of FR-XLPE. The values for irradiation in air decrease by two orders at 2MGy, and under pressurized oxygen decrease by three orders at 2MGy. For irradiation in a vacuum, the values decrease by one order after a brief increase with the dose from 0 to 0.6MGy.

Fig. 2 shows the relation between dose and volume resistivity of SH-PVC. The values for irradiation in air decrease sharply with the dose from 0 to 0.5MGy, and gradually to 2MGy. For irradiation under pressurized oxygen, the values decrease by three orders at 2MGy, and in a vacuum decrease about one order at 2MGy. What is evident on comparing the irradiation conditions such as in the presence of oxygen with the irradiation without oxygen, is the difference of the degree of decrease in the volume resistivity. It is considered that the decrease of the volume resistivity is accelerated by the oxidation.

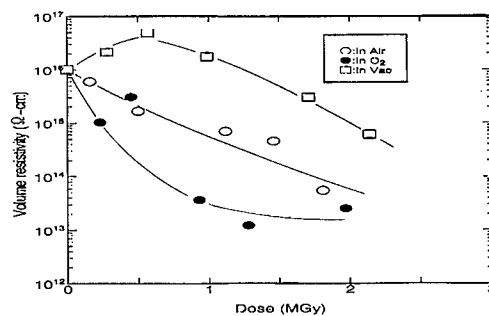


Fig. 1. Relation between dose and VR of FR-XLPE.

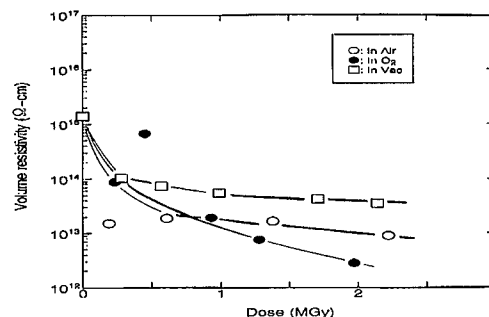


Fig. 2. Relation between dose and VR of SH-PVC.

EPMA Profiles

Fig. 3 shows the oxidation profiles analyzed by EPMA for FR-XLPE irradiated in air and under pressurized oxygen. For the sample irradiated in air, the K intensity shows the two peaks in the cross-section, which means the oxidation takes place only at the surface layer (70μm) of FR-XLPE sheet. The concentration of the oxidation products at the surface layer increases in proportion to the irradiation dose. The K intensity is very low between two layers, which indicates the oxidation at the inside area is scarce even when irradiated at higher doses. The thickness of the sheet is 935μm, and the oxidation layer is 70μm in Fig. 3(a). Therefore, the oxidation layer and the non-oxidation layer are calculated 15% and 85% of the total thickness, respectively.

In the case of irradiation under pressurized oxygen, the profile is almost uniform throughout the sheet, which means the oxidation proceeds homogeneously in the sheet. When the sample was irradiated in a vacuum, the K intensity was very low throughout the sheet, the same as the non-oxidation layer in the inside of the sheet in air.

The oxidation profiles of SH-PVC irradiated in air and in pressurized oxygen are shown in Fig.4.

The profiles of SH-PVC irradiated in air and under pressurized oxygen indicate similar results to FR-XLPE, respectively. The oxidation layer and the non-oxidation layer are 24% and 76% of the total thickness, respectively.

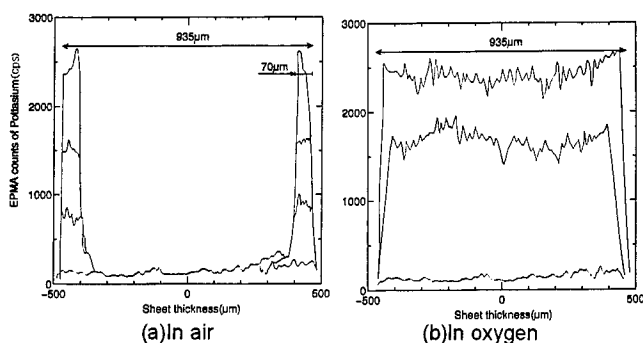


Fig. 3. Oxidation profiles of FR-XLPE.

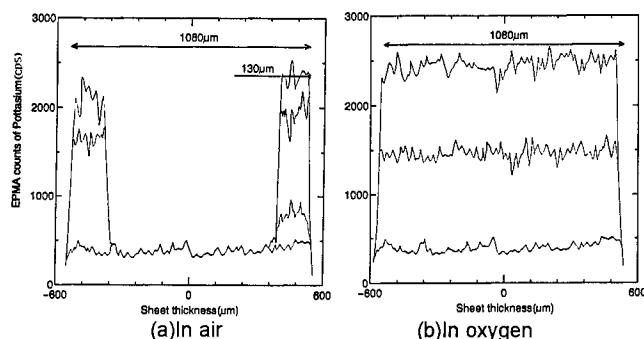


Fig. 4. Oxidation profiles of SH-PVC.

Gel Fraction

Fig. 5 shows the relation between dose and gel fraction of FR-XLPE. The values for irradiation in air decrease about 10% at a dose of 2MGy, and under pressurized oxygen reaches nearly 0 at a dose of 1MGy. However, the values for irradiation in a vacuum increase with a dose. These results indicate that the chain scission occurs in the oxidation layer, and the crosslinking proceeds in the non-oxidation layer.

In accordance with the results in the EPMA analysis already given, two oxidation layers in the cross-section are formed for irradiation in air. The estimated values in gel fraction for irradiation in air, as shown in Fig.5, is calculated by a supposition which means the gel fraction in the oxidation layer has the same dependency on a dose as that of the sample under pressurized oxygen. And also, that the gel fraction in the non-oxidation layer has the same dependency on a dose as that of the sample in a vacuum. The estimated values which were calculated by the superposition of the values in a vacuum and under pressurized oxygen are similar to the

measured values for irradiation in air.

Fig. 6 shows the relation between dose and gel fraction of SH-PVC. The gel fraction increases up to 75% in air and up to 85% in a vacuum, and does not increase at all under pressurized oxygen, which means that the radiation-induced crosslinking does not occur in the oxidation layer. The estimated values, which were calculated using the same method of FR-XLPE, are still more similar to the measured values of SH-PVC than the estimated values in FR-XLPE.

In the results of the comparison of the measured values for irradiation in air with estimated values, it is found that the change of gel-fraction corresponds well to the proportion in both an oxidation layer and crosslinked layer.

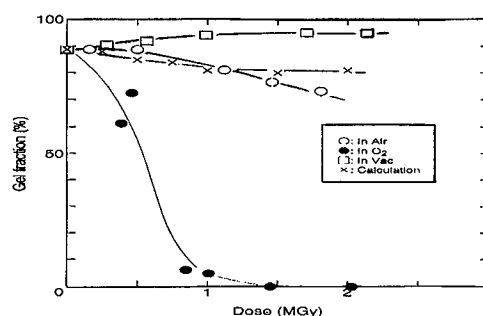


Fig. 5. Relation between dose and GF of FR-XLPE.

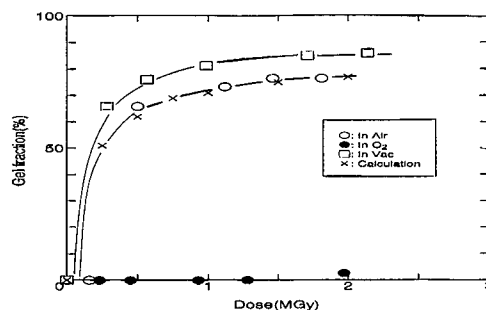


Fig.6. Relation between dose and GF of SH-PVC.

Tensile Property

Fig. 7 shows the dose versus residual elongation and tensile strength of FR-XLPE. The decrease of the residual elongation is small in a vacuum, and large under pressurized oxygen. The values for irradiation in air rather show a nearer match of the values for irradiation under pressurized oxygen than irradiation in a vacuum.

The tensile strength for irradiation in air rather show a nearer match of the values for irradiation under pressurized oxygen than irradiation in a vacuum, as the same as the residual elongation.

Fig. 8 shows the dose versus residual elongation and tensile strength of SH-PVC. The values for irradiation in air rather show a

nearer match of the values for irradiation in a vacuum than irradiation under pressurized oxygen. This tendency also can be seen the tensile strength.

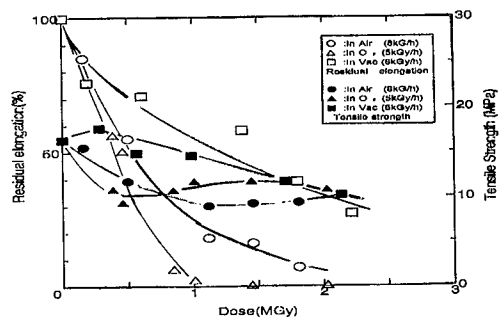


Fig. 7. Relation dose versus residual elongation and tensile strength of FR-XLPE.

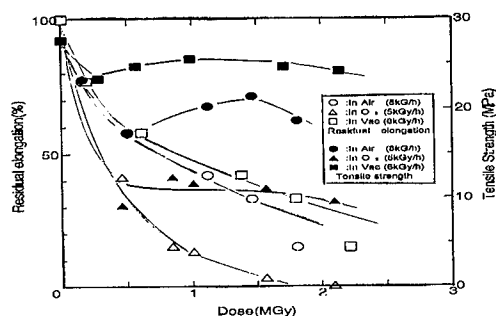


Fig. 8. Relation dose versus residual elongation and tensile strength of SH-PVC.

Micro Hardness Profiles

Fig. 9 shows the micro hardness profiles in the cross-section of FR-XLPE and SH-PVC irradiated in various doses in air. The values of both samples increase with the dose, especially on the surface area. However, the edge of SH-PVC decreases a little with an increasing dose.

Fig. 10 shows the crack development by tensile test for both specimens after irradiation in air. In FR-XLPE, the specimen is broken with a clear crack development throughout the sheet. However, in SH-PVC, many small cracks develop, but the cracks do not extend to the inside area.

The micro crack developed in the surface layer of FR-XLPE specimen grows progressively into the non-oxidation layer, due to the hardening of the surface layer caused by radiation oxidation. This behavior is called "notch-effect". However, such propagation of the cracks were not observed in SH-PVC, due to the softening of the surface layer caused by radiation oxidation.

This means the notch effect in the tensile test occurs in FR-XLPE, but does not occur in SH-PVC by radiation oxidation.

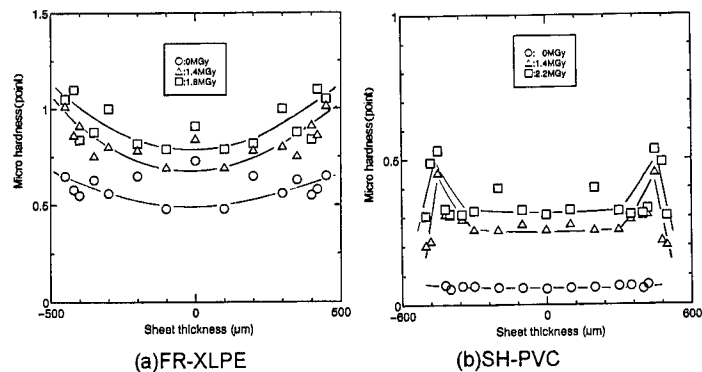


Fig. 9. Micro hardness in the cross-section after irradiation in air.

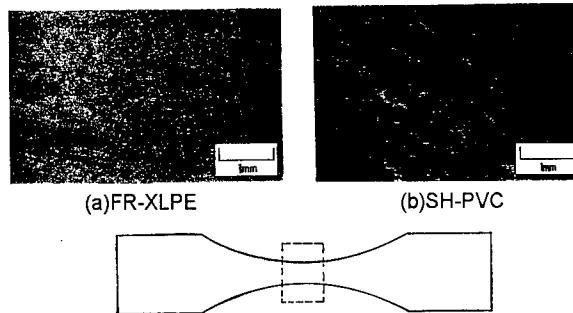


Fig. 10. Crack development on the surface by tensile test after irradiation in air.

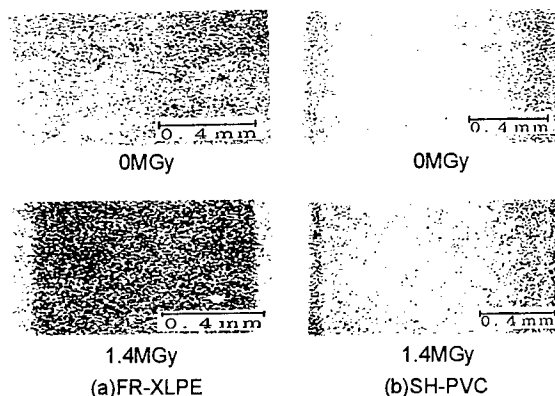


Fig. 11. Observation of the cross-section after irradiation in air by SAM.

SAM Image

Fig. 11 shows the SAM image of the cross-section of FR-XLPE and SH-PVC before and after irradiation in air. The contrast of the image is different between the surface and the inside areas of both specimens. The SAM indicates the difference of the hardness as a result of the contrast. In these image, the dark area indicates soft matter, and the light area indicates hard matter.

The SAM corresponds well to the results of the micro-hardness.

CONCLUSIONS

We conclude from the experiments as follows:

- (1) Volume resistivity was influenced significantly in the presence of oxygen, which is caused by radiation oxidation;
- (2) Gel fraction corresponds well to the proportion of the oxidation layer and the crosslinked layer;
- (3) The notch effect which induces the fracture of specimens during the tensile test was confirmed in FR-XLPE, but it was not observed in SH-PVC. It is considered that the radiation oxidation layer becomes hard in FR-XLPE, and soft in SH-PVC.

REFERENCES

- (1) M.Sugiyama, et al. : Radiation Degradation Mechanism of Polymer Materials, DEI-94-88 of I.E.E. Japan.
- (2) M.Sugiyama, et al. : Observation of Oxidation Layer in Polymer Materials for Electric Cables using Scanning Acoustic Microscope, 1996 National Convention of I.E.E. Japan.

AUTHORS



Masahiko Sugiyama
Yazaki Electric Wire
Co., Ltd.
2771, Ohoka, Numazu,
Shizuoka, JAPAN.

M.Sugiyama received his BE degree from Tokai University in 1991, and joined Yazaki Electric Wire Co., Ltd. He has been engaged in R&D of insulation materials for electric cables.



Makoto Nitta
Yazaki Electric Wire
Co., Ltd.
2771, Ohoka, Numazu,
Shizuoka, JAPAN.

M.Nitta received his BE degree from Waseda University in 1977, and joined Yazaki Electric Wire Co., Ltd. He has been engaged in R&D of insulation materials for electric cables.



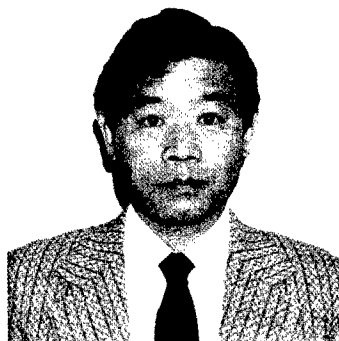
Tsuneo Tani
Yazaki Electric Wire
Co., Ltd.
2771, Ohoka, Numazu,
Shizuoka, JAPAN.

T.Tani received his BE degree from Tohoku University in 1963, and joined Yazaki Electric Wire Co., Ltd. He has been engaged in R&D of insulation materials for electric cables.



Tadao Seguchi
Japan Atomic Energy
Research Institute.
(JAERI)
1233, Watanukimachi,
Takasaki, Gunma,
JAPAN.

T.Seguchi received his MS degree in 1966 and Dr. of technology degree in 1977 from Hokkaido University, and joined JAERI Takasaki in 1966. He has been engaged in R&D of polymer materials by radiation application such as radiation resistance, synthesis of advanced materials.



Toshiaki Yagi
Japan Atomic Energy
Research Institute.
(JAERI)
1233, Watanukimachi,
Takasaki, Gunma,
JAPAN.

T.Yagi received his BS degree from Gunma University in 1973, and joined JAERI Takasaki. He has been engaged in R&D of polymer synthesis and degradation by radiation.

NOVEL CONDUIT INSPECTING SYSTEM

**R.-S. Kuo, Wen-Long Lin, Min-Sung Lu, Chang-Ho Chen, Lian-Jehn Huang,
Shih-Teng Chang, Shih-Wei Lai, Hsi-Pai Hsu, Y.-C. Lin, Yuan-Kuang Tu**

OSP, Telecommunication Labs, Chunghwa Telecom Co. Ltd., Taiwan, ROC

ABSTRACT

The major reason that causes the underground conduits deformed and broken and results in difficulty in cable lay-out is largely due to the traffic loading and the nearby construction activity. To reveal the conduit condition such as deformed locations, breakage...etc., an efficient system for conduit inspection is developed. An useful information to determine the status of the conduit is the radius variation of the conduit. The new conduit radius measurement system consists of four major elements. From core to peripheral, there are: conduit caliber probe, power winch assembly, data processing unit and pulley reaction frame.

Conduit caliber probe measures the conduit radius by six ribs outstretching from the body shank. The power winch assembly pulls the probe forward and offers the location reading. Data processing unit receives the data transmitted from both the probe and the winch and gives the effective cross section radius data of the conduit. The pulley reaction frame is used to transfer the power from the hydraulic power winch to the probe. With the novel system, the inspection of the conduit condition can be made very easily.

INTRODUCTION

Telecom conduit plant, usually routed along roads, is surrounded by many other utility delivery systems. Therefore, the underground conduits are vulnerable to the traffic loading and the nearby

construction activity which are the major reasons that cause conduits deformed and broken. Those damaged conduits, sometimes with ingress of soil and water, pose difficulties in cable lay-out.

For cable installation, the conduit is first cleaned by high pressure waterjet and iron brush. Then, a flexible plunger rod or a section of cable is pulled through to inspect the conduit. The purpose of such inspection is to determine whether there is enough space for new cable^{1,2}. However, this simple inspection procedure can only determine whether the conduit is intact or not. For an old and aged conduit, whether occupied by cable or not, the conduit is occasionally either deformed or broken due to accumulated stress and ingress sediment.

A deformed conduit may be useful if damaged location can be detected and parts of the deformed conduit can be repaired. Therefore, inner space inspection of deformed conduit becomes important. In order to examine the conduit space and detect the damaged location, a novel conduit inspecting system has been developed by TL OSP Lab.

CONVENTIONAL METHOD REVIEW

Besides plunger rod, several other inspection techniques have been proposed. With mini-camera sent into the conduit the inner condition can be examined by visual image. Infrared devices can indicate the radius change by comparing the transmitted and reflected signals³. The electro-

magnetic induction sensor can detect the intensity change of the magnetic field when approaching obstacle. A major problem with the above systems is that all these devices are very delicate and fragile and is not robust enough for practical field use.

An ideal system for conduit inspection should provide more detail about the status of conduit than the plunger rod method and should be small and robust for easy use in the conduit. The new equipment should also be easy to operate and maintain and can tolerate outside plant toughness. Therefore, mechanical equipment is chosen as our solution for radius measurement.

DESIGN CRITERIA

Design criteria are set-up in the early stage of development, there are:

1. Application domain: Within 3" and 4" PVC conduit
2. Effective measurement length: 250 m or more
3. Device features: Waterproof and mudproof
4. Driving speed: about 10 m/min.

CONFIGURATION OF THE CONDUIT INSPECTING SYSTEM

This newly developed inspection system included four basic elements as shown in Fig.1. Functions of each part will be described in details.

Conduit Caliber Probe

The probe is the key module of the system which detects the desired conduit condition. In order to operate inside the conduit, compact design of the probe is one of the major concerns in design.

Conduit caliber probe measures the conduit radius by six ribs outstretching from the body shank⁴ as shown in Fig.2. The probe has rollers that move along the inner wall of the conduit. The movable

arm attached to the rollers can move the movable sleeve and in turn push a LVDT(Linear Variable Differential Transformer). With the roller movement, the radius variation can be measured as the displacement of the LVDT tip.

A guiding line in front of the probe drives the probe moving forward and a transmission line behind the probe transmits the signal to the processing unit.

Signal Processing Unit

The LVDT send out an analog voltage signal. The amplitude is in proportional to the tip displacement of the LVDT. The unit processes the data and provides a constant visual display of the radius variation in real time. A chart recorder is used to provide a permanent record of each meter of the conduit. The record is extremely useful for documenting repair data and cost estimation job. The processed output also facilitate the control of power winch. If the radius reading has abrupt change, the unit alerts the event by red lamps as well as a sounding buzzer to stop the power winch operation.

Power Winch Assembly

The system has two winches located in the target and starting manhole respectively. Electrical power winches provide the pulling force for the probe. Pulling lines drawn from the winch are connected to the ends of the probe as shown in Fig. 1. The front pulling line is the guiding line that drives the probe moving forward. The one behind is the idle line pulled by the probe. The counter attached to the winch take the reading of the guiding line length wound on to the shaft. The winch may provide the location mileage of the probe by converting the length readout. The winch can be operated manually or by automatic control. Both pulling force and speed are easily adjustable by assigning power output and rotation speed of the winch. The winch can also be programmed with a load limit. If the loading output exceed the programmed limit,

the puller automatically ceased the operation, thereby eliminating the possibilities of damaging the pulling line and the probe.

Pulley Reaction Frame

The reaction frame is made of aluminum alloy or stainless steel. The purpose of the frame is to transfer the pulling force from the vertical direction above the ground to the horizontal direction inside the manhole. Pulley set functioning as guiding rail, reduces the friction force between the pulling line and the manhole surface.

CONCLUSION

A novel conduit inspecting system is developed to inspect the conduit radius variation. The result can be recorded and visually displayed. This inspection is important for cable lay-out task. The major elements of the system include Conduit Caliber Probe, Signal Processing Unit, Power Winch Assembly and Pulley Reaction Frame. Field trials have indicated that the system functions well and the task of the cable installation in the conduit plant can be made easier and more precise.

REFERENCES

- 1."Construction Specification of Underground Cable in Local Outside Plant," CLC-CL1001-1, Spec. of Chung-Hwa Telecom Co., 1983 (in Chinese).
- 2."Acceptance Test Specification of Telecom OSP Construction," CLA-AL0003-2, Spec. of Chung-Hwa Telecom Co., 1992 (in Chinese).
- 3."Instrumentation," No.6, Bi-Monthly, Precision Ltd. Co., Jan. 1992 (in Chinese).
- 4.Chang, C.-F. : "Handy Manual of Standard Mechanical Design Table," Tai-Long Book Co., Inc., Taipei, 1980 (in Chinese).

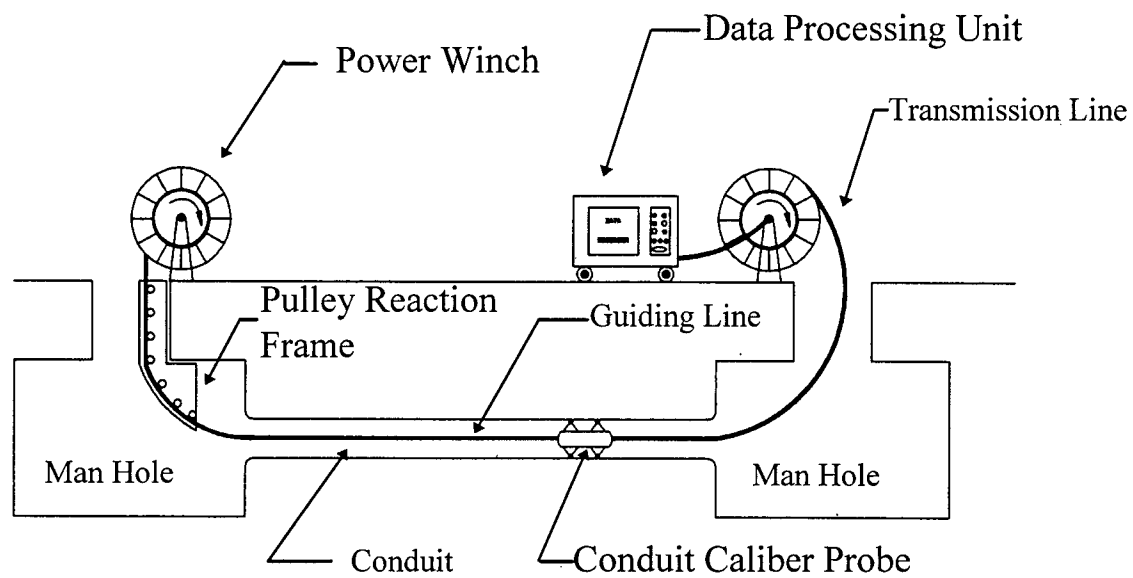


Fig. 1 Schematic Diagram of Conduit Inspection System

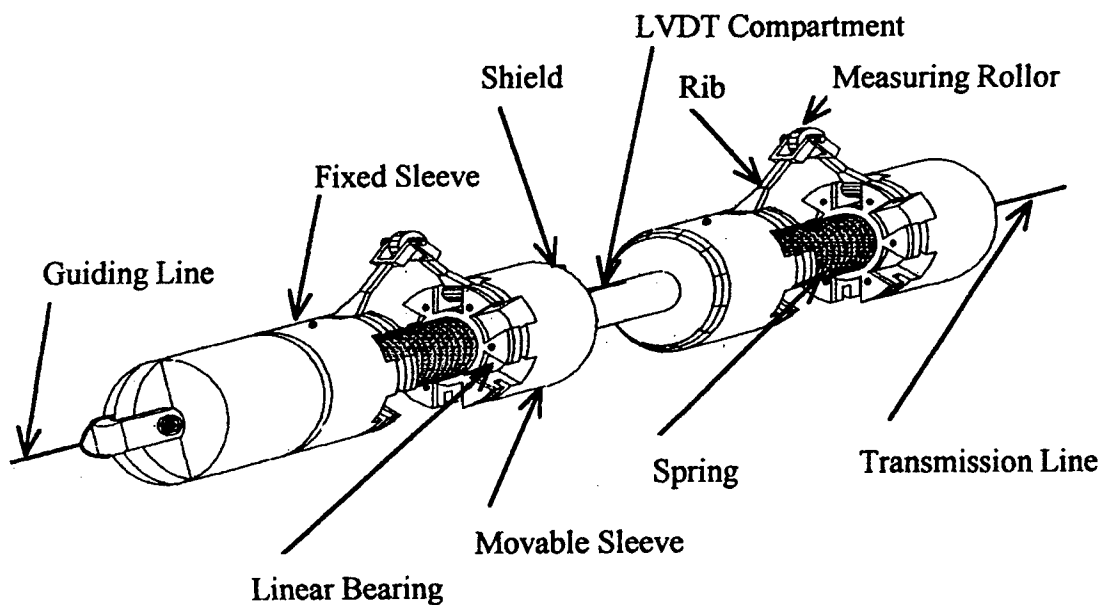


Fig. 2 Configuration of Conduit Caliber Probe

A NEW APPROACH ON OPTICAL FIBER CABLE NETWORK SUPERVISION SYSTEM

Hélio Silvino de Almeida Prata

Telebrás, Campinas, São Paulo, Brasil

ABSTRACT

The propose of the work is to show how the Optical Supervision System can became also an Administration System of the local and trunk optical network. It can be done by transforming each landmark belongs to the optical route on an Network Element to be monitored. In that way will be possible, for instance, evaluated the reliability of a WDM - Wavelength Division Multiplexed - used to introduce the supervision signal onto active fiber.

Another example is, when any kind of trouble occur on the fiber or in the cable , the systems try to find where its happened based on the information that the user introduced on the Landmarks. The right place showed by the system depend of the actual geographic Landmark position, the quality of the fiber signature, the nature of the fiber degradation and mainly the ability of the user to identify the cause of the problem.

INTRODUCTION

Most of the Brazilian telecommunications companies are already using and others are installing the Optical Supervision System developed by the Telebras R&D Center.

The System is very simple to operate and one of its great advantage is that the companies can buy the cheapest Optical Time Domain Reflectometer (OTDR) and Optical Selectors on the market that we implement the drivers to control the equipments.

Another important fact, that became our system a success in Brazil, is the two curses that are give to the companies. One of them is to teach how to plan and design an Optical

Supervision System, the other one is how to install and operate the system.

As the companies are using the system we have note that some improvements must be include in the system, otherwise, the user will need to understand very well how to interpret a fiber signature. The problem is that the operators are not specialists in OTDR, so the interpretation of the fiber signature representing an attenuation increases, because of a bending on the cable, can be misunderstood with an water sensor actuated.

PLANNING AND DESIGNING THE SYSTEM

After the company makes the plan and design of the System using the knowledge got on the course, we make a revision on the project to see if it is possible to became it cheaper and better.

With the final project on the hand, the company team go to the field to check if all the fibers used on the project really exist and more important than that where are them on the switches and where are the paths of the routes. It is probably the most important part to assure that the system will work properly.

At this time the system begins to bring the first collateral advantage to the companies, because to install all the components to form a route that will be monitored is necessary to have a very good agreement between Transmission and OutSide Plant areas. On the end of the installation, at least an up date file with the information about the fibers terminators and transmission equipments is ready to be used also for others companies's areas, like an OutSide Plant Administration . Many times we have found informations about terminator fiber inconsistent with the actual position of the fiber on the transmission equipments.

ARCHITECTURE OF THE SOFTWARES

The system is made up Remote Supervision Points (RSP) connected to a Centralized Supervision Point (CSP) by any kind of network TCP/IP supported.

On the Remote Supervision Point has a Hardware Server that makes all different types of OTDR talk by the same manner with the Client User, represented by the Graphic User Interface. This technology make possible have different OTDR models running under the same CSP. The Hardware Server is also responsible to control the local Optical Selector via General Purpose Interface Bus (GPIB) and the Remote Optical Selectors via RS232 Interface.

The Data Base of each RSP has a replica of the main information on the CSP, so from the CSP is possible to operate any RSP that makes part of the system.

OPERATING THE REMOTE SUPERVISION POINT

To illustrate the main features of the system that run on the RSP, let's use the fig. 1 that shows a single system configuration to surveillance one trunk optical outside route, composite by 2 optical cables interconnecting 2 optical transmission systems, with by-pass on station B, and an water sensor installed between Stations A and B.

The first action of the operator is manipulate carefully the controls of the OTDR to obtain a fiber signature that shows as many events as possible, example:

- WDM location,
- Water Sensor Location,
- Splices Location,
- others.

If it is impossible to see all the events in one signature, you must divide the signature in pieces that make possible show the more important events of the route. This first signature, called Reference Curve, is the base of the system, so it must be done by a person that know how to work with OTDR, otherwise many problems can occur on the route and the system will not detect. The up

date measurements on this route will be always compared, point by point, with the Reference Curve considering the safety threshold. If the up date measurement overtake the threshold, the system will calculate where it occur, based on the Landmark, and what is the probably cause of the problem. The alarms issued by the system can assume the following status:

1. Rupture Alarm

This is an urgent alarm. The system look for a abrupt drop of the signal until the noise level.

2. Open connection

This is an urgent alarm. The system look for an abrupt raise and drop of the signal until the noise level.

3. Bad optical coupler near OTDR

This is a not urgent alarm. The system take care with the off-set optical power on the begin of the signature.

4. Water Sensor.

This is a not urgent alarm, but if it happen often it became a urgent alarm. To assure that the alarm is because of water penetration, the Landmark that represent the optical closure splice was introduced on the system as a Network Element that can be managed.

5. WDM alarm

This is a not urgent alarm, but if it happen often it became a urgent alarm. This kind of alarm occur because the housing that the WDM is installed need an adaptation, and if it is not make with the appropriated device, the WDM can follow down increasing the attenuation on this point.

6. General Alarms

This kind of alarm can happen because of a bending on the cable, that increase smoothly the attenuation in many points

of the signature not associated with an specific landmark .

The system also manage the quality of the splices checking periodically the variation of their attenuation, and the quality of any connection make by connector by measuring the return loss of that components.

OPERATING THE CENTRALIZED SUPERVISION POINT

The system running on the CSP gives to its user practically the same environment that the RSP user has. The most important feature of the CSP is its open interface to communicate with Transmission Equipment Supervision Systems (TESS). As we have many different TESS already installed and many others been installed, it will be very difficult to keep the same data base between all this systems to try to have at first time an Integrated Management Network and later on an indeed Telecommunication Management Network. To minimize the problem, our system has a very simple protocol that is responsible for the change of information between the TESS and CSP. By this protocol when the TESS have an alarm that can be because of fiber fault, it give to the CSP the address of the equipment with alarm. The

CSP consult its data base and if that equipment has fiber under surveillance, the system make the measurement and return the result to the TESS with 100% of assurance that the problem is or not because of fiber. If that specific equipment has no fiber on the data base of the CSP, but the fiber just beside has been under surveillance, the CSP return to TESS that the problem is quit sure because of fiber, if after make a measurement found a break.

CONCLUSION

As we don't sell equipment, our system try to use as less OTDR as possible to surveillance the optical outside plant. To give an idea the capital of Sao Paulo state that has hundreds of kilometer of optical cable is installing just 5 Remote Supervision Point and one Centralized Supervision Point to surveillance at least one fiber of each single mode cable. The system is already installed in 10 telecommunication companies and until the end of this year more 10 companies intend to install.

The key of our success is to be in constant contact with the final user of the system - the operators. They are the people which really give to us all informations we need to make our system better day by day.

References:

1. Telebras - Magazine 95/05
2. ITU-T COM 6-R 6-E

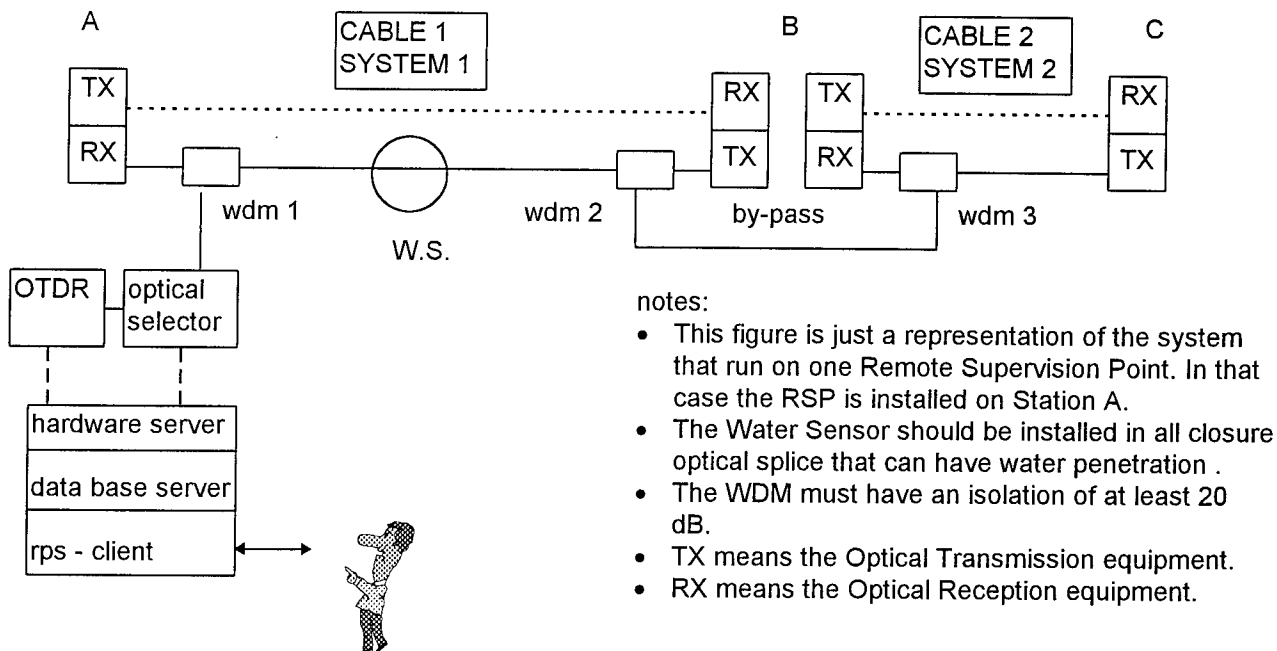


fig. 1 - A single Remote Supervision Point

Contact : Eng. Silvino
 Address : Rod. Campinas / Mogi-Mirim Km 118
 Campinas SP. Brazil - CEP 13088-061
 Phone : (55) 019 - 239-6459
 Fax : (55) 019 - 239-6558
 Email : silvino@cpqd.br

I am an electronic engineer working on Telebras R&D Center since 1986. Nowadays I am responsible for the development of the optical supervision system. I am involved also on the measurements necessary to qualify wide band network using Hybrid Fiber Coaxial Topology.

MEASUREMENT OF COUPLED NOISE ATTENUATION

Dirk Wilhelm

GHMT, Bexbach/Saar, Germany

ABSTRACT

After the initial problems affecting the transmission of data services at bit rates of 100+ Mbit/sec along twisted-pair (TP) cables had fully been solved through the introduction of state-of-the-art technologies for the production of cables, it became quite clear that – besides the parameters specific to the transmission technology – still other parameters had to be taken into account in order to be able to proceed from lab-type units to proven systems which are suitable for everyday operation by end users.

In this connection, the so-called electromagnetic compatibility (EMC) is of crucial importance for these systems. EMC means, on the one hand, that running systems do not disturb the function and/or operation of other devices and systems, and, on the other hand, that such systems are not disturbed either by the operation of different devices and systems.

The present article reviews how cable manufacturers, designers and end-users can exactly test the influence of cable technologies on the EMC characteristics of systems without, however, having to use a large number of measuring devices.

INTRODUCTION

Within the European Union, the electromagnetic compatibility of devices is regulated by the EMC directive which was passed into law in Germany on 1st January 1996. All devices which comply with this act are allowed to bear the so-called CE symbol (conformité européenne). In other countries, the compliance with the EMC regulations is examined similarly by other measures, e.g. by tests in accordance with FCC standards and application of FCC notes.

Initially, not much attention was given to the problem that these standards almost exclusively apply to devices and only insufficiently deal with the issue of connecting such devices to form an entire system.

The electromagnetic compatibility of systems, however, also comprises other parameters than simply the EMC of devices. By locating a large number of defects in systems which had been

disturbed by electromagnetic interference, it was possible to gather critical information which has been grouped in the following 5-pillar model.

The EMC behaviour of a system consists of the following individual influences:

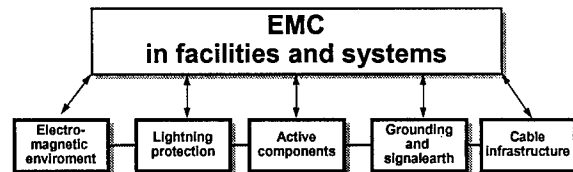


Figure 1: EMC of the overall system

As can be seen from the above diagram, the EMC of devices which is regulated by the relevant EMC standards is only part of the overall system.

For this reason, a lot of efforts have been made to examine such systems with respect to their interference immunity and behaviour (i.e. if they themselves cause interference), for example in shielded absorber chambers.

In addition to the obvious benefits, these tests, however, also had disadvantages, in particular for manufacturers of passive components such as cables, patch panels, or mains sockets.

1. Since large systems required a lot of space, only minimum configurations could be tested.
2. Regarding data services with different transmission rates and key frequencies, the measured values also differed, and it was not possible to ascertain whether these differences were caused by the active or the passive components.
3. The test results were heavily influenced by the specific model and hence by the manufacturer of the active components.
4. Although the measurements were not very conclusive for manufacturers of cables and components, their execution required a large number of devices and a lot of time.

Thus such measurements were comparatively expensive.

To date, only inaccurate auxiliary parameters, which are e.g. originally used in the coaxial or telephone cable technologies, have been applied. These parameters include the transfer impedance, the screening attenuation as well as the unbalance attenuation.

A decisive disadvantage of procedures allowing to determine EMC-relevant parameters is, however, that – in the case of the shielded data cables – balanced and coaxial cables must be pre-cut. Another disadvantage is that procedures with and without the use of shields can only be compared by using different methods of measurement. Thus the IEC 96-1 method is used to determine the transfer impedance of shielded TP cables while ITU 0.121 is applied in order to determine the unbalance attenuation of unshielded TP cables.

Result: when dealing with less informed end users, there are some difficulties in explaining why unshielded TP cables also may have good EMC characteristics – in spite of a screening attenuation of 0 dB.

For these reasons, there are currently several approaches in Europe to introduce a parameter which would allow to close these gaps. The following sections present the measurement procedure developed by GHMT mbH in order to determine the suppression of interference power and compare this procedure with other possible procedures which are discussed at the moment.

COUPLED NOISE ATTENUATION

Basics

First of all some basic terms will be explained to clarify the principle of measurement.

Primary System. The term “primary system” was first used for coaxial lines where it consists of the inner conductor and the outer conductor or shield serving as return wire. The data transfer shall be effected along the primary system, and the impedance of this primary system should be equal to that of the connected devices.

In case of TP cables, this primary system consists of the electrical and mechanical characteristics of the corresponding (if possible, balanced) wire pair. The shield, if existing, only has a protective function and is not included in the description of the primary system. Anything related to objects outside of this primary system (which is closed under ideal conditions) is considered to be no part of the primary system.

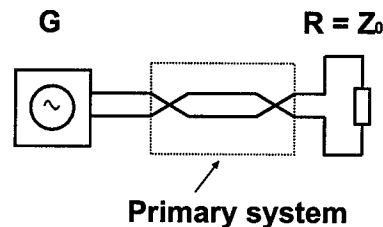


Figure 2: Primary system of unshielded or shielded TP-cables

Hence the primary system has been defined in such a way that it does not distinguish between shielded and unshielded cables.

Typical parameters of the primary system are, e.g. the impedance with 100, 120 or 150 Ω , or the image attenuation.

Secondary System. The secondary system describes the behaviour of the cable within its electromagnetic environment. In case of coaxial cable, it mainly consists of the characteristics of the shield, i.e. how well the shield insulates the primary system from the environment.

However, TP cables may be available both as unshielded and shielded types.

Nevertheless even unshielded cables have a secondary system because unshielded TP cables, too, only have a finite symmetry just as shields only have a limited effect. Therefore there will be – inevitably – a certain grounding. In case of unshielded TP cables, this characteristic is described by the secondary system.

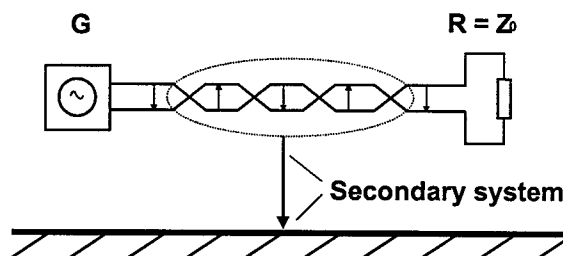


Figure 3: Model of secondary system (e.g. unshielded cables)

In case of shielded TP cables, there will be, in addition to the existing wire pair (which is more or less balanced), one or several shields to separate the primary system from its environment. The term “in addition” should be regarded as a qualifier because the symmetry of a wire pair can be deteriorated through the use of a shield.

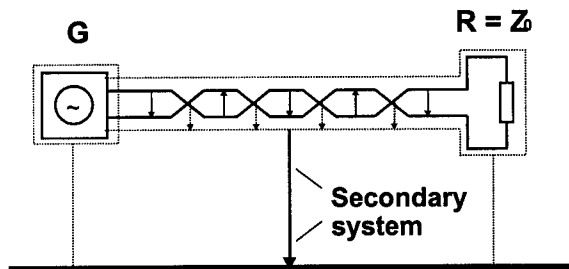


Figure 4: Model of secondary system (e.g. shielded cables)

Typical parameters which can be used to describe the secondary system are the transfer impedance, the screening attenuation, and the unbalance attenuation.

Traditional Procedures

Determination

of Shielding Parameters.

Example: measurement of the shielding factor a_{SCREEN} according to the absorber clamp method (IEC 96-1).

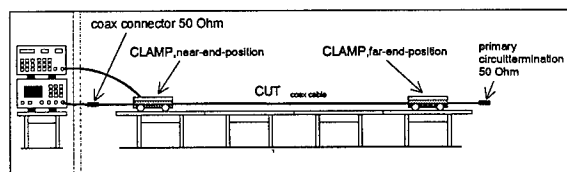


Figure 5: Test setup for the measurement of a_{SCREEN}

You can see that, when this procedure is applied, shielded TP cables must be converted to coaxial cables. One or several inner conductors are connected to a common potential while the shield serves as return wire. When examining the now existing secondary system, one decisive quantity, however, is not taken into account, i.e. the symmetry of the twisted pair.

Determination of the Symmetry of Twisted-Pair Cables.

Example: determination of unbalance attenuation to ITU 0.121.

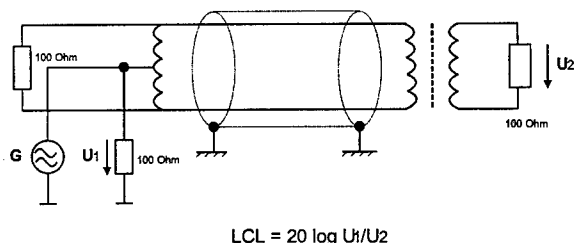


Figure 6: Test setup for the measurement of the unbalanced attenuation

The problem of this procedure consists in the fact that it was originally developed for telecommunication lines with a small bandwidth. In case of the bandwidths of 600+ MHz which are today aimed at for data transfers, there are heavy dependencies on the measuring environment because of earth-coupling effects.

Definition of a

Universal Descriptive Parameter

It is obvious that the EMC response of unshielded or shielded TP cables cannot be described by traditional parameters alone. However, the above explanations show that the new parameter to be introduced can be computed from the traditional parameters provided that the used measuring procedures are comparable.

From this follows:

$$a_{\text{CNA}} = \text{LCL} + a_{\text{SCREEN}} \quad (1)$$

You can recognize that the coupled-noise attenuation (a_{CNA}) is an attenuation, i.e. an insertion attenuation between the primary system (signal path) and the secondary system (electromagnetic environment) which is as large as possible.

The above equation applies both to unshielded and shielded TP cables.

Example: In case of unshielded cables, the screening attenuation (a_{SCREEN}) is zero while there is still a separating effect between the signal path and the environment because of the large longitudinal conversion loss (LCL).

Measurement of Coupled-Noise Attenuation

The new procedure must take into account both the symmetry of a cable and, if existing, the screening quality. Hence the specimen must be connected during the measurement in such a way that is equal to its operation in a real-world environment. Therefore the specimen will not be connected coaxially, as in the procedures used so far, but balanced (e.g.: twinax connections).

The coupling should be effected unbalanced just as under practical conditions. Most environment-induced interference signals cause an interference with the common mode (directed to earth).

Not only the balanced connected primary system but also the secondary system into which earth-related interference signals are to be coupled should be connected with the right impedance.

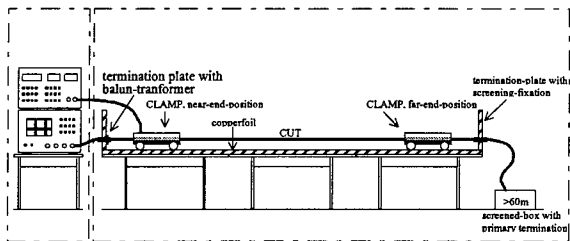


Figure 7: Test setup for the measurement of coupled noise attenuation

The specimen will be mounted at a certain height above the test bench (length: approx. 6 m). A conductive reference plate is fastened on the bench in the longitudinal direction of the specimen. The distance from the reference plate to the specimen as well as the outer diameter of the possibly existing shield determine the characteristic impedance of the secondary system (target to be aimed at: approx. 150 Ω). Both ends of the bench are equipped with terminating resistors suitable for high frequencies which allow to terminate the secondary system with the correct impedance.

Using a so-called EM coupling link (known from the EMC standard IEC 1000-4-6), a certain HF power P_2 is supplied to the secondary system.

The decoupling of the power P_2 reduced by the coupled-noise attenuation shall be carried out from the primary system which is balanced connected via a balun.

By means of scalar or vector network analyzer, the indicated attenuation is as follows:

$$a_{CNA} = 10 \log \frac{P_2}{P_{1bal}} \quad (2)$$

The power can also be coupled into the primary system if it is decoupled from the secondary system via the clamp (reciprocity theorem).

The reading of the attenuation must be corrected by the attenuation of the balun, of the connecting cable and by the insertion attenuation of the coupling clamp.

Measured Values

The attenuation values which were determined amounted to 120 dB for heavily screened cables and were high, as was expected, because they were partly caused by the addition of screening attenuation and LCL. However, it was possible to prove that insufficiently shielded cables have a lower a_{CNA} than highly balanced, unshielded TP cables.

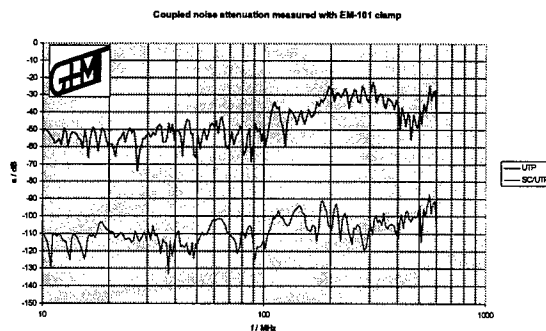


Figure 8: Coupled noise attenuation measured with EM-101 clamp

Moreover the influence of single-pair screens (S/STP) on the symmetry of wire pairs showed by the fact that an S/UTP cable with a comparable screening effect has an improved coupled-noise attenuation (better by several dB).

CONCLUSION

The EM coupling clamp of the type Lüthi EM 101 which was used for the GHMT procedures considerably differs from the MDS 21 clamp which is used for other procedures that are currently also examined. MDS 21 is a current-transformer clamp equipped with ferrit rings and is used for the measurement of screen currents along coaxial cables.

Because of the rudimentary propagation medium existing for longitudinal waves, the wave propagation in case of unshielded TP cables differs from that of shielded specimens. Since this would exclude a comparability of UTP and STP cables, the electromagnetic coupling link is used which, additionally, has a lower insertion attenuation and thus does not restrict the system's dynamics as much as the MDS 21 clamp.

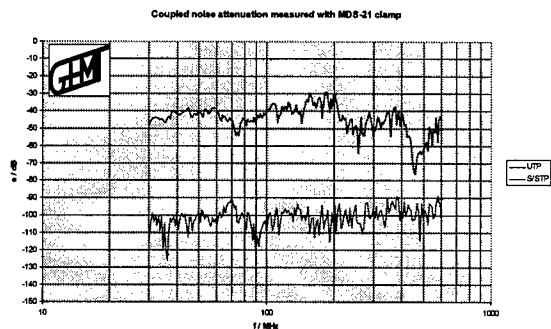


Figure 9: Coupled noise attenuation measured with MDS-21 clamp

The above diagrams show that UTP cables would be evaluated incorrectly when using current-transformer clamps because the wave propagation within the secondary system of a UTP cable is mainly effected through a TEM wave.

OUTLOOK

The measurements of the coupled-noise attenuation which have been carried out so far were well received by the various European committees because the results appear to be suitable in order to provide a considerable support to manufacturers and designers of cabling systems and also to manufacturers of active units when specifying their requirements regarding the cabling system.

For this reason, we are currently working on the further development of the procedure to include test of entire links.

It is also possible to adapt the system to larger bandwidths and attenuations.



Dirk WILHELM is a graduate engineer (Dipl.-Ingenieur), 30 years old, and studied information and communication technology at the University of Kaiserslautern, Germany.

In the course of his diploma thesis carried out at GHMT in 1993, he developed a measuring procedure for the analysis of EMC characteristics of balanced data cables.

This measuring procedure has been adopted as the German proposal for a European standard covering this problem.

Currently Mr. Wilhelm is responsible for the technical area related to electromagnetic compatibility, particularly within distributed systems.

Mr. Wilhelm is a general manager of GHMT mbH, an independent test lab for the worldwide certification of cables, components, and active devices of LAN/WAN technologies.

Mailing address

GHMT
Gesellschaft für Hochfrequenz-Meßtechnik mbH
In der Kolling 13

D 66450 Bexbach/Saar
Germany

Phone: ++49 / (0) 68 26 / 92 28 - 0
Fax: ++49 / (0) 68 26 / 92 28 - 99
e-mail: WILHELM@GHMT.COM

Review On The Correlation Between Residual Strain Of Fibers In Ribbon And Ribbon Property

G. W. Seo, Y. H. Jeon, S. H. Kim

Daewoo Telecom Ltd.
531-1, Kajwa-dong, Seo-gu, Incheon, Korea

ABSTRACT

In general, the residual strain of fibers in ribbon has an important effect upon the geometry and the attenuation property of ribbon. Thus, it is a necessary to make the fiber obtain minimum residual strain after ribbon process so that we may make the best ribbon fiber. Because the residual strain like this also affects the life span of optical cable and long distance installation, we have studied the above phenomena that may originate during ribbon process theoretically and experimentally. Our paper shows that there is close correlation between ribbon property and the residual strain of fibers in ribbon and proposes the theoretical method to lower the residual strain.

1. Introduction

The fibers being inserted into the ribbon die are easily subject to the lateral pressure caused by fiber pay-off tension & incidence angle into the die, vibration by static electricity among fibers and friction by velocity difference among fibers in ribbon die. These cause serious fiber strain in ribbon process and its quantity depends on fiber position. In other words, the inner fibers are subject to electro-static force and frictional force one another, the outer fibers (two fibers on both sides) have severe lateral force because the width of guide roller before ribbon coating die is generally larger than that of the die. After all, these strain can affect the geometry of the ribbon and attenuation, we should release this fiber strain in respect to long term reliability after installation of optical cable. So, in this paper, we have carried out several experiments as BOTDA (Brillouin Optical Time Domain Analysis), optical attenuation and ribbon geometry to confirm residual strain distribution of fibers in ribbon. And, for the theoretical approach, we compared the theoretical equation on the lateral force effect for each pay-off condition of fibers with the experimental results. From the comparison, we can get the correlation factor. The factor approaches to the value 1 with going from center to outer fiber in ribbon. This means that the inner fibers are affected by vibration and friction force among fibers

as well as the lateral force. From these consideration, we presented the method to reduce the residual strain of fibers in ribbon and went through procedures as follows for completing our paper. Firstly, we used 6 resins for our work and selected the best resin and the condition of UV lamp. Secondly, fiber pay-off conditions and incidence angles of fibers into ribbon coating die were selected and theoretical calculation of the lateral pressure ratio for each was done. BOTDA measurement theory to obtain proper data on strain distribution of fibers in ribbon was handled, also. Thirdly, we made ribbon fibers according to the pay-off conditions and measured optical attenuation, strain, geometry and degree of curing on them. Finally, we analyzed and summarized these results in detail. In conclusion, we could show the method to make ribbon fiber to ensure the long term reliability of the fiber by presenting the theoretical equation which can minimize residual strain of fibers in ribbon.

2. Theoretical Background

2.1 Theoretical Formula For Pre-estimate Of Strain Due To Lateral Force [In Ribbon Process]

In ribbon process, the fibers inserted into the ribbon coating die basically have a constant incidence angle. Therefore, two fibers on each edge among 8 fibers in a ribbon to be touched on both sides of ribbon die suffer serious strain by lateral force and the others on inner side undergo serious vibration by static electricity and friction one another. Of course, the vibration has close correlation with ribbon property such as optical attenuation and ribbon geometry. Thus, it is difficult to solve all of the phenomena only with lateral force effect but we could induce proper formula at second hand by means of comparing theoretical result with experimental data. The derivation procedure is as follows.

As appeared in Fig.1, incidence angle of each fiber is simply calculated by Eq.(1) in order.

$$\theta = \tan^{-1} \frac{\left[\frac{(W_g - W_c)}{2} + \nu R_f - \nu \left(\frac{1}{2} \times \frac{W_g}{8} \right) \right]}{L_o} \quad (1)$$

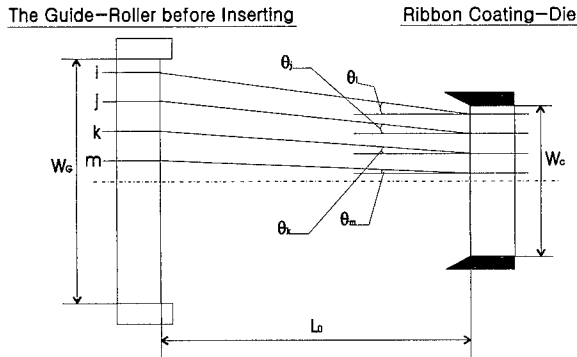


Fig.1 Schematic Diagram of Guide-Roller & Die

i, j, k, m : Fiber Identification
 W_c : Width of Ribbon Coating Die
 W_g : Width of The Last Guide Roller
 L_0 : Distance Between Coating Die and The Last Guide Roller
 θ_{i-m} : Incidence Angle
 R_f : Radius of Colored Fiber

Above Eq.(1), the value of ν has 1,3,5 and 7 in turns from the i^{th} to m^{th} fiber. So, the lateral force in ribbon process, F_l is expressed as Eq.(2)

$$F_l = \sum_i F = \sum_i T_f \sin \theta \quad (2)$$

F_l : Lateral Force
 T_f : Back Tension Loaded To Fiber By Pay-Off

The fibers in ribbon are easy to get residual strain due to pay-off tension of optical fibers, friction force by ribbon die & fibers and interaction one another and vibration by electrostatic force among fibers. In the long run, this strain causes the increase of fiber attenuation. The residual strain of fibers in ribbon, ϵ is calculated as follows.

$$\epsilon_i(\%) = K \cdot \left[\frac{T_f + \mu_{f-s} \sum_i F - \mu_{f-f} \sum_i F}{A_f E_f} \times 100 \right] \quad (3)$$

ϵ_i : Strain of i^{th} fiber
 A_f : Cross Section of Colored Fiber
 E_f : Young's Modulus of Colored Fiber
 K : Correlation Factor For Correction Of Distributed Strain
 μ_{f-s} : Coefficient of Friction, Film to Steel
 μ_{f-f} : Coefficient of Friction, Film to Film

By the way, we must take to heart that there are two more factors to be considered for getting more confidential data. One is the vibration of fibers by electrostatic force among

fibers and the other is fiber hunting by minute vibration of equipment itself when pay-off tension is loaded. In this paper, instead of inducing an adequate formula directly to take a consideration of above two factors, they were expressed as K factor to correct the difference between experimental and theoretical data. That is, because it is difficult to quantify and measure the vibration effect of fibers, we cannot help estimating its effect by analyzing experimental & theoretical data only. However, K factor to be induced like this has important effect on analyzing residual strain distribution of fibers in ribbon.

$$K = f(F_{\text{Electrostatic}}, F_v) \quad (4)$$

K : Correlation Factor For Correction Of Distributed Strain

$F_{\text{Electrostatic}}$: Electrostatic Force Among Fibers

F_v : Force From Fibers Vibration Caused By Pay-Off

2.2 Distributed Strain Measurement Theory By BOTDA System

In the area of no light absorption, the molecules on the path of light play a role to radiate or scatter light through the transition of electron density. At this time, the energy interchange called "Inelastic Phenomenon including Brillouin Scattering" is done. This shows how to obtain induced amplifying CW(Continuous Wave) light frequency out of pulse light frequency of fiber's origin Brillouin wavelength. In other words incident light interacts with a sound wave to be happened in material and its original frequency is scattered into different one, thus we call the frequency difference 'Brillouin frequency shift' depending on material, given strain and outer temperature. As for the intensity and the location of strain distribution in fiber, we put to use Brillouin spectroscopy and time domain measurement technique to analyze nonlinear interaction between sound wave and light wave frequency-shifted. The experimental configuration of distributed strain measurement system is as following Fig. 2.

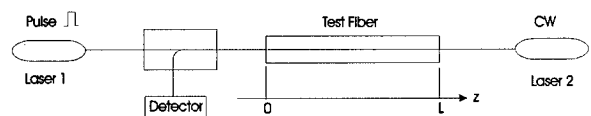


Fig. 2 Experimental Configuration of BOTDA(Brillouin Optical Time Domain Analysis)

BOTDA system has a pulse light source and a CW light source at both ends of the test fiber as Fig. 2. If the frequency of pulse light is ν_p and one of CW light is ν_{cw} , the difference of frequencies of both light sources is $\Delta\nu$, $\Delta\nu = \nu_p - \nu_{cw}$. If the difference of frequencies of both light sources, $\Delta\nu$ is controlled to be the same as Brillouin

frequency shift of the test fiber, ν_b , pulse light is optically modulated into CW light by the induced Brillouin scattering. That is, the CW light make Brillouin amplification in test fiber. Consequently this phenomenon makes signal analysis possible. The amplified CW light signal is modulated to electric one by detector and its signal wave to time domain is as Fig. 3.

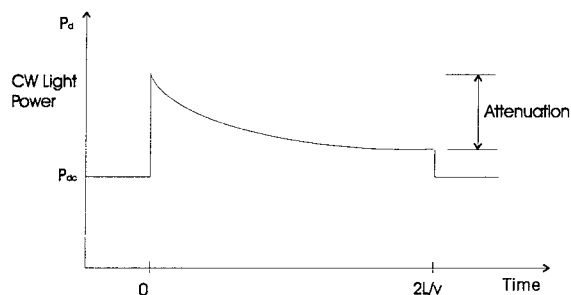


Fig. 3 Signal Wave Profile of BOTDA

If the Brillouin frequency shift, ν_b , is constant in all points of test fiber, the decrease of Power(P_b) at the location(z) will accord with the coefficient of fiber attenuation. Also the Brillouin frequency shift, ν_b , largely rely upon the residual strain in test fiber, ϵ , which is as follows.

$$\nu_b(\epsilon) = \nu_b(0) (1 + C \times \epsilon) \quad (5)$$

$\nu_b(0)$: The Brillouin Frequency Shift In Case Of No Strain
C : The Coefficient Of Strain Of The Brillouin Frequency Shift

Lastly, we can measure the strain of fiber by making use of the signal wave shape in Fig. 3 and the equation (5).

3. Experimental Method

In this paper, we will show for fibers to have different residual strains in accordance with the location of fibers in ribbon after ribbon making process and proved that they are closely related with pay-off tension. Also the method to make strain-free ribbon was suggested. For these results we carried out the experiment as follows.

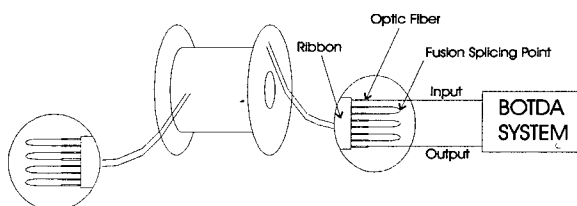
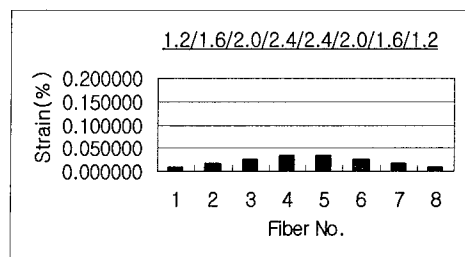


Fig. 4 Schematic Diagram of Strain Measurement By BOTDA

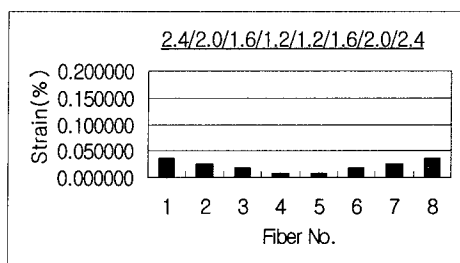
At first, we selected five proper experimental conditions to compare residual strain in ribbon among all the conditions allowed by our ribbon making equipment. After making ribbons under above conditions, we measured geometry of ribbon and attenuation. The curing degree of each ribbon was almost same and more than 96%. The geometry and attenuation have some relation with the residual strain in ribbon. Thus, in order to get reliable data the strain distribution in fiber was measured by BOTDA. The test was carried out as Fig. 4. Moreover to obtain accurate data we measured the basic frequency of a reference fiber before ribbon process, which is 11.940 GHz. The result showed that the reference fiber has uniform residual strain of 0.01% that is supposedly caused by Spool Take-Up tension. In using the basic Brillouin frequency we measured the residual strains of ribbons with BOTDA and found out that there were some differences among them. For getting the adequate formula to make strain-free ribbon, we related the theoretical formula to the experimental results.

4. Theoretical and Experimental Results & Analyses

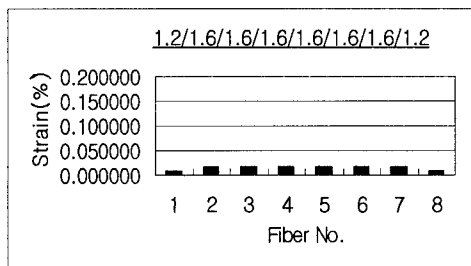
The theoretical strain by lateral pressure is calculated and its result is as Fig. 5. Here, the Fig. 5 shows the result that the effect of Take-Up tension (about -0.01~ -0.02%) was considered. Of course, there is still some differences between theoretical and experimental result.



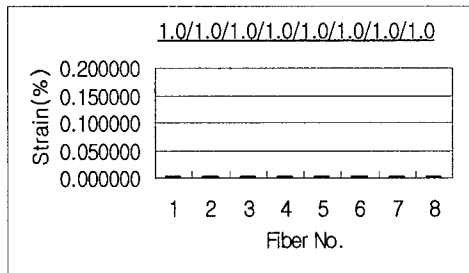
(a)



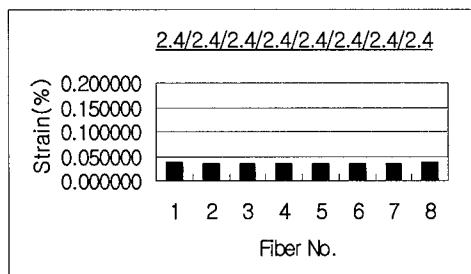
(b)



(c)



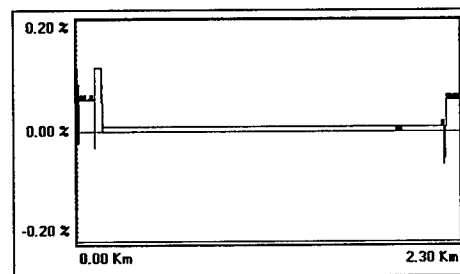
(d)



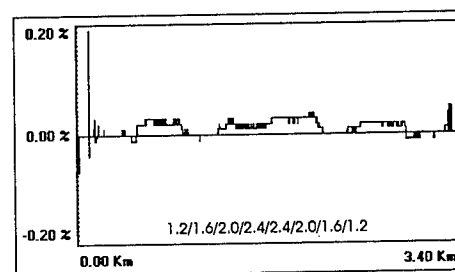
(e)

Fig. 5 Theoretical Result(I) of Strain Distribution of Ribbon

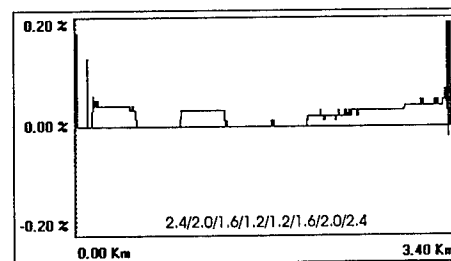
In Fig. 5, each graph shows the thoretical strain distribution of fibers in ribbon manufactured under the pay-off conditions such as Table.1. Each pay-off tension was expressed as a relative proportion on a basis of the minimum pay-off tension (the relative value = 1). Also, the test results with BOTDA is as Fig. 6.



(Reference)



(a)

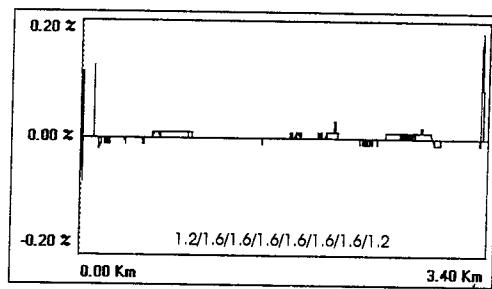


(b)

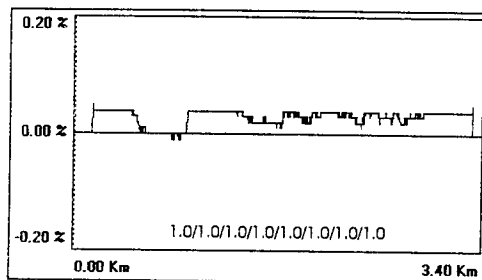
Fig. 6 Strain Distribution of Ribbon by BOTDA

Experiment Condition	Pay-off Tension Ratio	Remark
a	1.2 / 1.6 / 2.0 / 2.4 / 2.4 / 2.0 / 1.6 / 1.2	* Each optical fiber pay-off tension ratio correspond to the 1 st , 2 nd , 3 rd , 4 th , 5 th , 6 th , 7 th and 8 th fibers in ribbon from left to right.
b	2.4 / 2.0 / 1.6 / 1.2 / 1.2 / 1.6 / 2.0 / 2.4	
c	1.2 / 1.6 / 1.6 / 1.6 / 1.6 / 1.6 / 1.6 / 1.2	
d	1.0 / 1.0 / 1.0 / 1.0 / 1.0 / 1.0 / 1.0 / 1.0	
e	2.4 / 2.4 / 2.4 / 2.4 / 2.4 / 2.4 / 2.4 / 2.4	

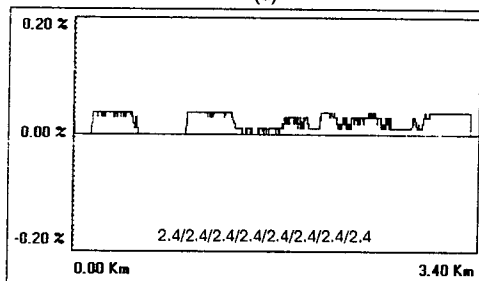
Table. 1 Pay-off Tension Ratio At Each Experimental Condition



(c)



(d)



(e)

Fig. 6 Strain Distribution of Ribbon by BOTDA

In Fig. 6, x-axis of each diagram expresses the total length of test fiber, 3.2km [(8fibers/ribbon)x(400m/fiber)]. Fiber No. in a ribbon increases from left to right. If we observe the results minutely, we can know that edge fibers, which are the 1st, 2nd, 7th and 8th fibers, show the tendency similar to theoretical result but inner fibers, which are 3rd, 4th, 5th and 6th fibers, give little differences with being compared with theoretical one. In other words, taking a consideration of real ribbon making process, the nearer the fibers are located toward center of ribbon, the more the result of BOTDA disagrees with theoretical one. It means that the inner fibers in a ribbon are affected by some factors besides the lateral force. As mentioned in the introduction, the vibration, caused by the electrostatic force among fibers and minute hunting of pay-off part, makes the experimental result deviate from theoretical one. Thus we introduced a correlation factor K to compensate for the deviation. Here, we define that K factor is just 1 when theoretical result is the same with the experimental one. Then, our test results

show that K factor depends on a position of the fiber and approaches to 1 as the fiber moves from center to edge in a ribbon. Especially, under the condition of very low pay-off tension, the variation of K factor is larger than ones of others. The theoretical result corrected by K factor is given as following Fig. 7 and Fig. 8.

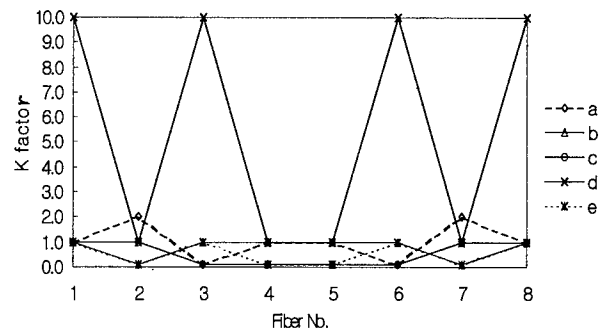
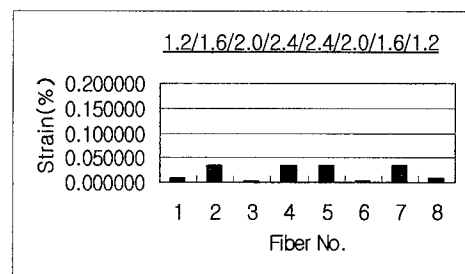
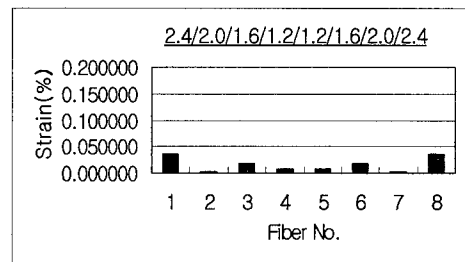


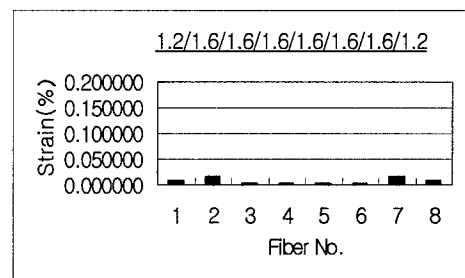
Fig.7 The Variation of K factor as for each fiber at respective test conditions.



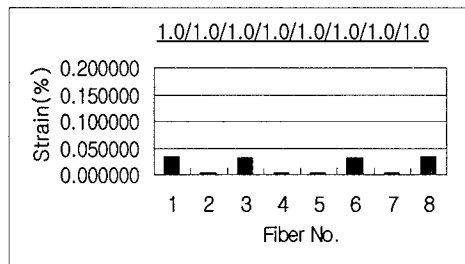
(a)



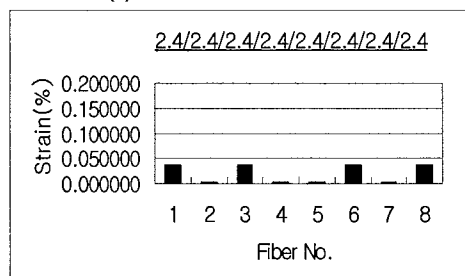
(b)



(c)

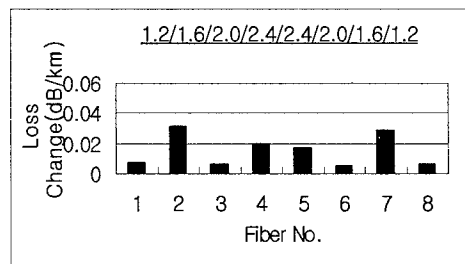


(d)

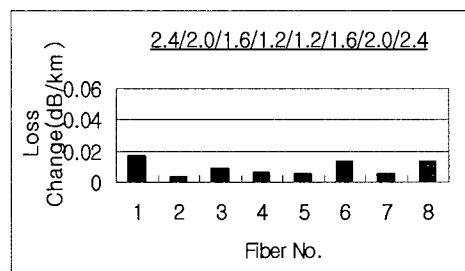


(e)

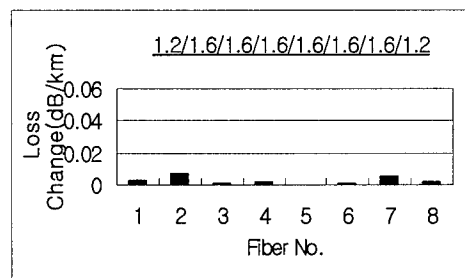
Fig. 8 Theoretical Result(II) Corrected by K factor



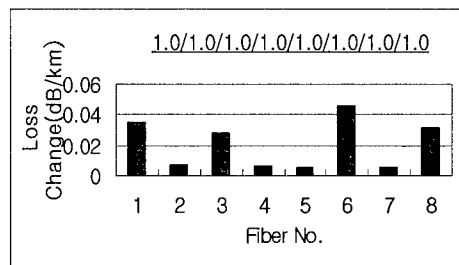
(a)



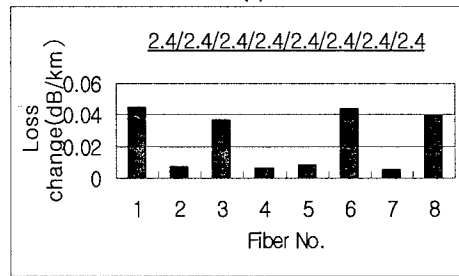
(b)



(c)



(d)



(e)

Fig. 9 Loss change of each fiber at respective test conditions

When this corrected Fig. 8 is compared with Fig. 6 obtained by BOTDA and Fig. 9 by fiber loss measurement, they have a lot of similarity one another. Therefore, we can know that the residual strain of fiber in ribbon has a close relation with the loss of fiber and it is very important to decrease the residual strain in fiber for the best ribbon. That is, so as to improve the optical property of ribbon the residual strain has to be minimized. From the above result we can predict that the vibration caused by interaction or electrostatic force among optic fibers is increased with the increase of pay-off tension. The higher pay-off tension causes a great deal of tensile strain in ribbon and relatively, the lower tension increases the vibration of optical fibers when inserted into ribbon coating die. These physical phenomena result in irregular geometric structure of ribbon or distribution make the ribbon property bad. The results are shown in Fig. 10. This figure gives the fact that from the optimum pay-off tension, which is similar to the experimental condition (c), we can get the ribbon with the better characteristics such as optic attenuation, residual strain, geometrical structure and so on. Finally we can control the property of residual strain and optic loss in ribbon making process if we make use of our theoretical formula.

Next, we measured the polished section of ribbon to check the geometrical structure of ribbon for each pay-off tension with the geometry measuring equipment and the results are appeared as Fig. 11. In this figure, irregular profile of ribbon is derived from partly irregular polishing or breakage and does not means real thickness, outline and shape. But there is no problem for discerning the planarity property of ribbon.

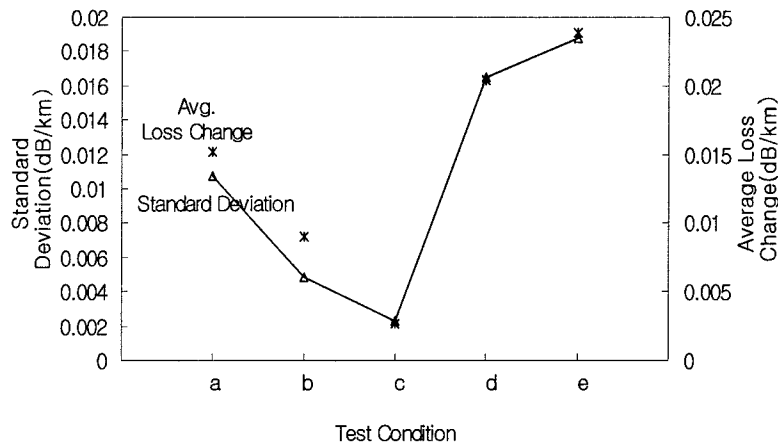
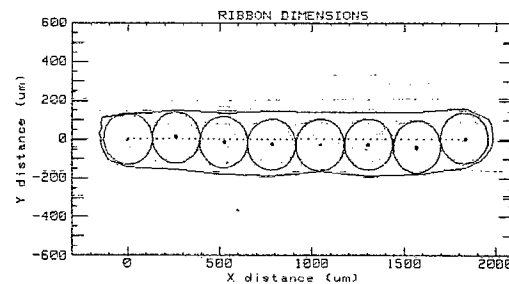


Fig. 10 Both Average and Standard Deviation of Loss Change at Each Test Condition

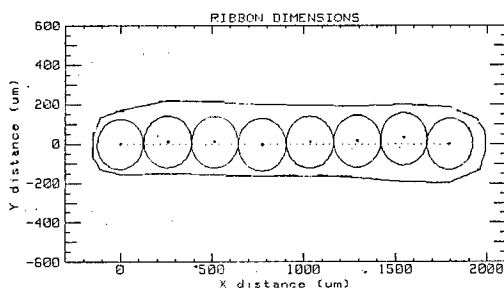
Experiment Condition	Planarity(μm)								Standard Deviation	Average
	1	2	3	4	5	6	7	8		
a	0.0	10.1	11.0	-3.3	10.1	17.1	33.0	0.0	11.7	9.8
b	0.0	12.9	-16.4	-25.4	-28.6	-29.4	-43.2	0.0	18.9	-16.3
c	0.0	1.7	10.7	14.5	24.1	5.9	-9.2	0.0	10.3	6.0
d	0.0	-30.2	-60.0	-35.2	5.3	-2.4	-10.1	0.0	23.0	-16.6
e	0.0	9.3	-4.6	30.5	-6.9	-55.2	-10.2	0.0	24.1	-4.6

Table. 2 The Variation of Planarity of Ribbon

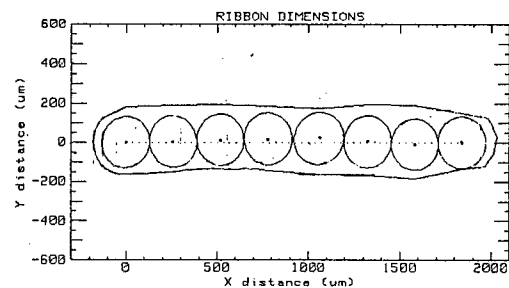
Substantially it is supposed that the geometry of ribbon should not entirely affect on the characteristics of optical fiber ribbon but has close relation with residual strain. So we found out the trend at Table. 2 and Fig. 11. Also if we consider the planarity of ribbon, which is related with the splicing and connecting property of fibers in ribbon, the ribbon of the best state can be produced at the experimental condition (c) and these data correspond with all the data above-mentioned.



(b)

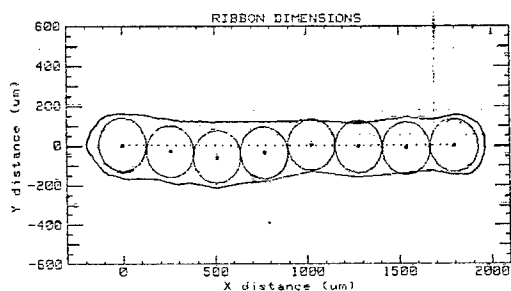


(a)

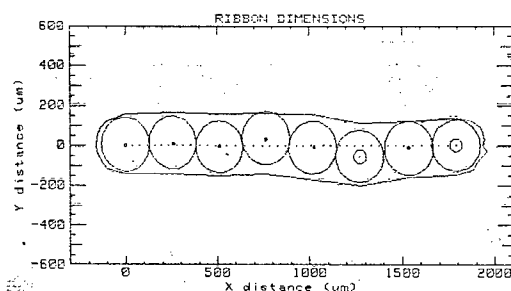


(c)

Fig. 11 The Geometry of Ribbon at Each test condition



(d)



(e)

Fig. 11 The Geometry of Ribbon at Each test condition

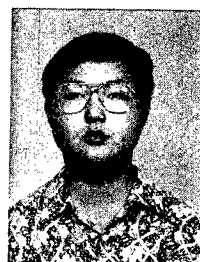
5. Conclusion

Up to now, we studied the correlation between residual strain of fibers in ribbon and ribbon property through the theoretical and the experimental approach method. It was established that the fiber strain did harm to the ribbon property in our research. Thus, we could know that it is essential to make ribbon without any residual strain in fibers for the best one. Of course, it is a common-sense fact that the fiber strain affects ribbon property but there was neither trial to quantify it nor to suggest the theoretical method to remove it until now.

In conclusion, we could show the method to make ribbon fiber to ensure the long term reliability of the fiber with the theoretical equation which can minimize residual strain of fibers in ribbon.

6. References

- [1] T. Horiguchi, M. Tateda, "Optical fiber attenuation investigation using stimulated brillouin scattering between a pulse and a continuous waves", Opt. lett., vol. 14, no. 8, pp. 408-410, 1989
- [2] K. Shimizu, T. Horiguchi, Y. Koyamada, T. Kurashima, "Brillouin OTDR employing self-heterodyne detection and its application to fiber distributed strain and temperature measurement", IEICE Technical report OCS93-2, pp. 9-16, 1993
- [3] T. Kurashima, T. Horiguchi, M. Tateda, Y. Koyamada, "distributed strain measurement equipment for silica optical single mode fibers", NTT field systems research and development center Technical report, 1992
- [4] T. Horiguchi and M. tateda, "BOTDA - Nondestructive measurement of single mode optical fiber attenuation characteristics using brillouin interaction : Theory", Journal of lightwave tech., vol. 7, no. 8, pp.1170-1176, 1989



G.W.Seo
DAEWOO TELECOM Ltd.
531-1,Gajwa-Dong,Seo-Gu,
Inchon-City,Korea

He joined Daewoo Telecom.LTD. after graduating from Pusan University with M.S. degree in the inorganic material engineering in 1993 and, since then, has been engaged in Fiber Optic R&D Center. He is now senior engineer and is working as the cable designer.



Y.H.Jeon
DAEWOO TELECOM Ltd.
531-1,Gajwa-Dong,Seo-Gu,
Inchon-City,Korea

He is a researcher of Fiber Optic R&D Center. He graduated from KAIST with bachelor's degree in the electrical material engineering in 1991 and joined it after military service in 1996. He is working as the cable designer in the optical cable part.



S.H.Kim
DAEWOO TELECOM Ltd.
531-1,Gajwa-Dong,Seo-Gu,
Inchon-City,Korea

He is a member of CCITT(Study group 6) and in charge of development of multi-fiber cable. He obtained bachelor's degree in the precision mechanical engineering from Hanyang University and joined DAEWOO TELECOM. LTD.in 1982. Since then, he has been engaged in Fiber Optic R&D Center. He is now chief engineer of the optical cable part.

DEVELOPMENT OF NEW MECHANICAL SPLICE

Toshiyuki Tanaka, Yasuaki Fujiwara, Yasuhiro Tamaki and Hiroshi Yokosuka

Fujikura Ltd., Opto-Electronics Lab., Sakura, Chiba, Japan

ABSTRACT

We have developed a low cost mechanical splice for use in single fiber splicing. It is simple to use and it requires no specific training, and its optical performance is the same as fusion splices and connectors.

The optical characteristics of the mechanical splice which we have measured are as follows: the mean splice loss is 0.04 dB (same single-mode fiber, $\lambda = 1.31 \mu\text{m}$), the mean splicing time is less than 3 minutes (from fiber preparation to splicing) and it is reliable for practical use.

1. INTRODUCTION

In order to realize FTTH; Fiber To The Home, economically, it is necessary to construct optical access networks with the same cost compatible to that of metallic cable networks. This easy and low cost technologies for splicing optical fibers in place of using normal fusion splices and connectors [1], [2], have to be developed.

We have developed the new mechanical

splice as the splicing technology corresponds to these requirements. Fig. 1 shows its external view.

2. DESIGN AND STRUCTURE

2.1. CONCEPT OF DESIGN

The features required when we developed this mechanical splice are as follows:

- Low loss
- Low cost
- Easy operation
- Small size and light weight
- No power supply needed
- to be able to re-join fibers

Our concept of the design is shown in Fig. 2.

First of all, we compare the method of alignment of bare fibers with that of prepared fiber ends. The result is shown in Table 1. We decided to use V-groove alignment with flat cover plate; type B structure in Table 1 for the structure of mechanical splice [3].

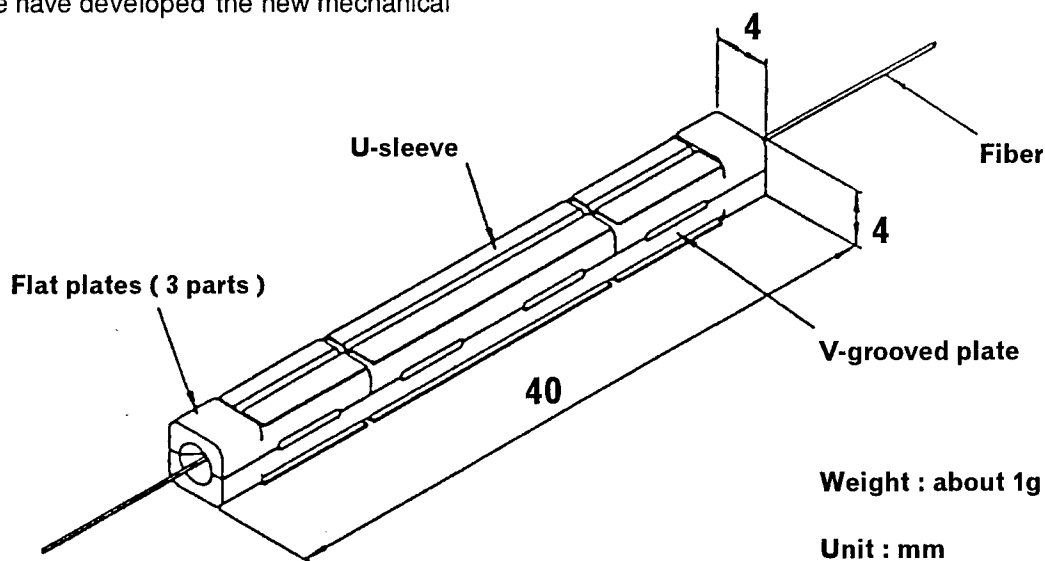


Fig.1 External view of mechanical splice

2.2 STRUCTURE

The mechanical splice that we have developed is designed to obtain the required characteristics and functions with consists of as few parts as possible. It consists of U-sleeve; a leaf spring with an alloy of copper, a V-grooved plate and flat cover plates: which are precision molded plastic. Optical fibers are aligned between the V-grooved plate and the flat cover

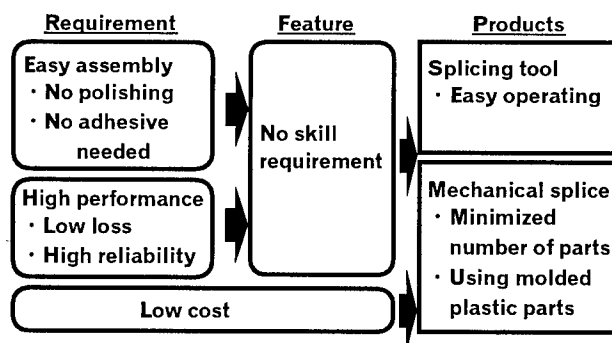


Fig. 2 Concept of design

plates, and fixed by the spring force of U-sleeve.

It consists of only 5 parts. As shown in Fig. 3, flat plates consists of 3 parts, which are used to fix the contact point at bare fiber's ends and their coatings separately. Before shipment, these parts have been assembled as mechanical splice in factory and index matching gel has been filled inside.

The principle and process of splicing fibers are shown in Fig. 4. Before splicing fibers, the gap between the V-grooved plate and the flat cover plates is slightly opened by inserting a wedge into the grooves at the side. The bare fibers with prepared ends; stripped, cleaned and cleaved by the same method as fusion splice, are inserted into the each port of mechanical splice, and end surfaces are aligned. After removing the wedge, splicing is done. There is a gap between V-grooved plate and flat plates to keep spring force against the damage of V-groove. A

Table 1 Methods to alignment bare fibers

Type	A	B	C	D
Alignment				
Example	Micro capillary	V-groove + Flat plate	Slitted micro capillary + Elastic plate	Metal element
Accuracy of alignment	△	○	○	○
Simplicity of fiber setting	△	○	△	○
Simplicity of structure	○	○	○	△
Simplicity of manufacturing	○	○	△	△
Total	○	○	○	△

In alignment, bare fibers are fixed by 3 points; a,b,c.

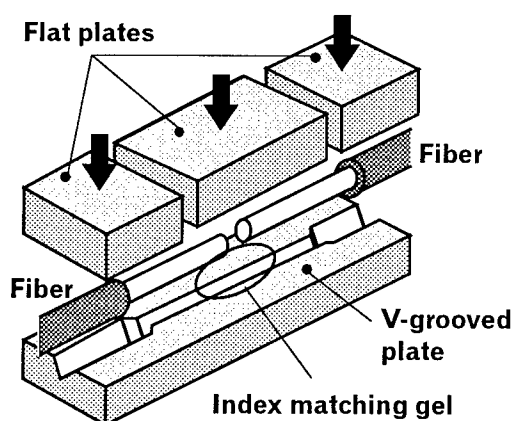


Fig. 3 Structure of mechanical splice

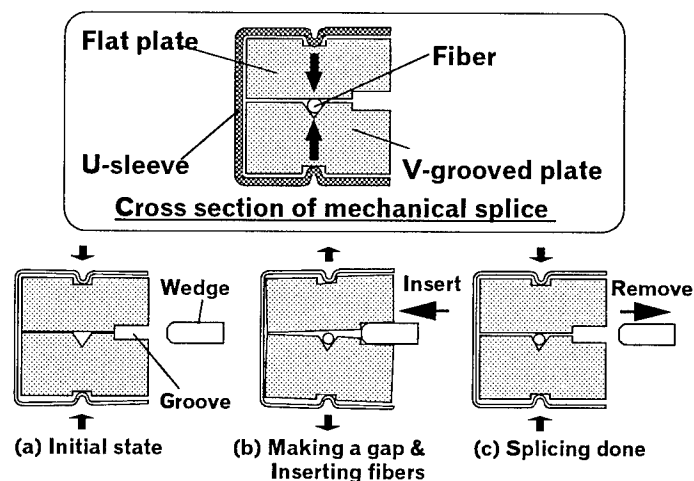


Fig. 4 Principle of splicing fibers

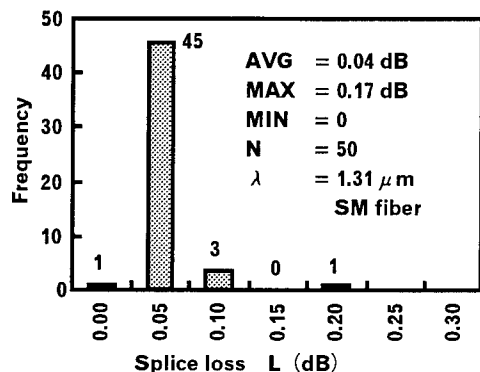


Fig.5 Splice loss of mechanical splice

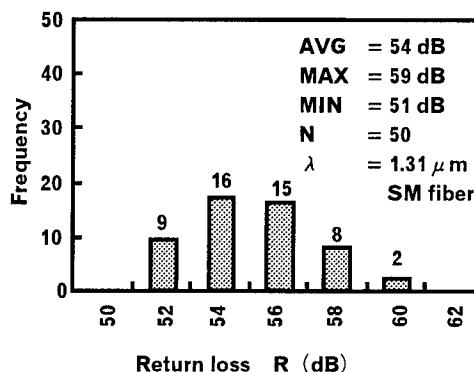


Fig.6 Return loss of mechanical splice

Table 2 Reliability performance

• Fiber : 10/125 (SM)
• Wavelength : 1.31 μ m

Test Item	Duration	Test Parameters	Loss fluctuation during test (dB)		Loss increase after test (dB)	
			Average	Maximum	Average	Maximum
Temperature cycling	10 cycles	-40°C to +70°C	0.05dB	0.07dB	0.01dB	0.03dB
Temperature & humidity cycling	10 cycles	-10°C to +65°C 93%RH at +65°C	0.05dB	0.09dB	0.01dB	0.02dB
High temperature	240 hours	+70°C	0.04dB	0.08dB	0.01dB	0.02dB
Low temperature	240 hours	-40°C	0.04dB	0.07dB	0.01dB	0.02dB
Straight pull	—	4.4N 60 sec	—	—	< 0.01dB	0.01dB
Impact	3 times / axis for 3 axis	980mm/sec 2 6msec	—	—	< 0.01dB	0.01dB
Vibration	2 hours / axis for 3 axis	Freq : 10 to 55Hz Amp : 1.5mm	—	—	< 0.01dB	0.01dB
Neutral salt spray	24 hours	Dens : 5 wt% (35°C) Press : 1 kgf/cm ²	—	—	0	0

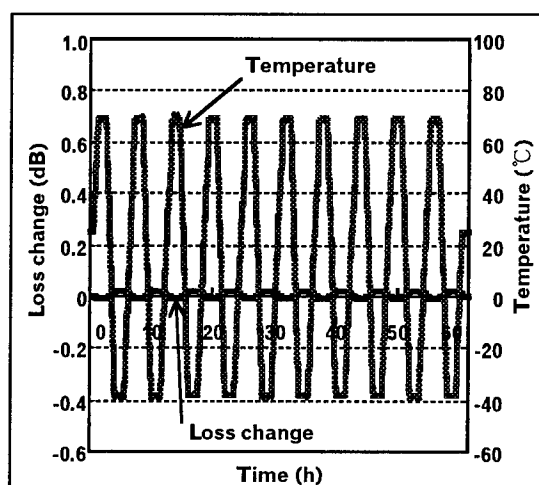


Fig.7 Temperature cycling test

fibers is the most useful feature of the mechanical splice.

3. PERFORMANCE

3.1. OPTICAL PERFORMANCE

We have evaluated the optical characteristics of mechanical splice with single-mode fibers at a wavelength of 1.31 μ m under laboratory conditions.

With same single-mode fibers, the mean splice loss is 0.04 dB. Fig.5 shows the histogram.

The return loss is more than 50 dB with same single-mode fibers at room temperature (Fig. 6), and it is more than 35 dB at -40°C~+70°C range. The characteristic of the return loss depends on the characteristic of index matching gel inside the mechanical splice.

splicing tool is used to insert and remove the wedge.

In this structure, it is possible to remove spliced fibers and insert new fibers after splicing is done, by inserting the wedge into the mechanical splice again. This function to re-join

3.2. RELIABILITY

We have evaluated the reliability of mechanical splice, it was shown that the mechanical splice was reliable for practical use. The results are shown in Table 2, and Fig. 7 shows a typical loss fluctuation during the temperature cycling.

In addition to these tests, we tested long temperature cycling of -40°C to $+70^{\circ}\text{C}$ during 3 month. About 20 samples in series, the total loss fluctuation during test is 0.40 dB and the total loss increase after test is 0.08 dB.

4. OPERATION

Tools that are needed to splice fibers with this mechanical splice are as follows:

- (a) Fiber holders (Fig. 8)
- (b) Mechanical stripping tool
- (c) Wiping paper and alcohol
- (d) Fiber cleaver with spacer for mechanical splice
- (e) Splicing tool for mechanical splice (Fig. 8)

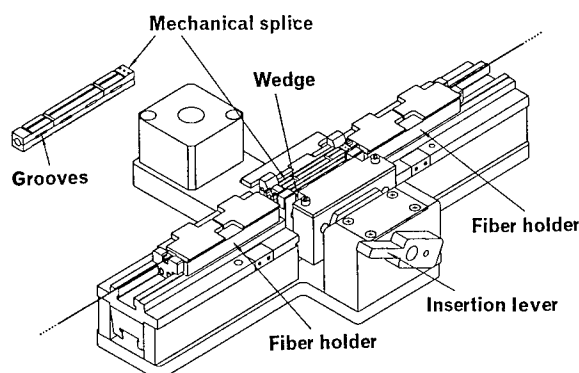


Fig. 8 Splicing tool and fiber holders

To prepare fibers before inserting them into mechanical splice, we use tools from (a) to (d) which is almost the same as the tools used for fusion splice.

It is simple to perform fiber splicing with the mechanical splice. The procedure is as follows:

- (1) Place a mechanical splice into holding cradle in the splicing tool.
- (2) Insert a wedge into the grooves at the side of mechanical splice with the splicing tool.
- (3) Clamp a first fiber in a fiber holder.
- (4) Strip the coating of first fiber with a mechanical stripping tool.

- (5) Clean the stripped fiber with alcohol and a wiping paper.
- (6) If a spacer is not installed, install it in the slot of cleaver for fusion splice. The spacer acts as a gauge in order to set cutting length.
- (7) Cleave the first fiber with the cleaver.
- (8) Insert the first fiber into the end port of mechanical splice.
- (9) Repeat the stripping, cleaning and cleaving for the second fiber.
- (10) Insert the second fiber into the other end port of the mechanical splice.
- (11) Push the fiber holder slightly to ensure the ends of fibers are in contact. If the other fiber holder is moved accordingly, the fibers' contact is confirmed.
- (12) Remove the wedge from the grooves at the side of the mechanical splice.
- (13) Pick up the mechanical splice from splicing tool.

Preparation of fibers takes up most of the operation time; i.e. stripping, cleaning and cleaving before inserting them into mechanical splice. The mean splicing time is less than 3 minutes, from step (1) to (13). If operator has the experience of fusion splice, he will be able to splice fibers at less than about 2 minutes 30 seconds with this mechanical splice.

5. CONCLUSION

We have developed the new mechanical splice for single fiber splicing. It is a simple and low cost technology for splicing optical fibers, and its optical characteristics are the same as fusion splices and connectors.

The features are as follows: The mean splice loss is 0.04 dB (same single-mode fibers, $\lambda = 1.31 \mu\text{m}$). The mean splicing time is less than 3 minutes (from fiber preparation to splicing). The size is 4 mm \times 4 mm \times 40 mm (almost the same size as the protect sleeve for fusion splice). The weight is about 1 g.

With all its advantages, this mechanical splice will be useful in the construction of optical access networks with cost compatible to that of metallic cable networks, in order to realizing FTTH economically.

6. REFERENCE

- [1] M.Nozawa et al. : "Field test results of areal cable jointing techniques for access network", Proceedings of the 1997 IEICE general conference, B-10-49.
- [2] M.Takaya et al. : "Design and Development of Mechanical Splice for Areal Distribution Cables", Proceedings of the 1997 IEICE general conference, B-10-50.
- [3] T.Tanaka et al. : "Development of New Mechanical Splice", Proceedings of the 1996 IEICE general conference, B-1084.

AUTHORS



Toshiyuki Tanaka

Fujikura Ltd.

1440 Mutsuzaki
Sakura, Chiba,
285, Japan

Toshiyuki Tanaka was born in 1961. He received his B.E. degree in electrical & electronics engineering from Sophia University in 1984. He joined Fujikura Ltd. after his graduation, and has been engaged in research and development of optical fibers and accessories. He is now an assistant manager of Fiber & Cable Accessory Department within Opto-Electronics Laboratory.



Yasuaki Fujiwara

Fujikura Ltd.

1440 Mutsuzaki
Sakura, Chiba,
285, Japan

Yasuaki Fujiwara was born in 1967. He

received his B.E. and M.E. degrees in Mechanical engineering from Nagaoka University of Technology in 1992. He joined Fujikura Ltd. after his graduation, and has been engaged in research and development of optical fiber manufacturing and accessories. He is now an engineer of Fiber & Cable Accessory Department within Opto-Electronics Laboratory and a member of IEICE of Japan.



Yasuhiro Tamaki
Fujikura Ltd.

1440 Mutsuzaki
Sakura, Chiba,
285, Japan

Yasuhiro Tamaki was born in 1955. He received his B.E. degrees in mechanical engineering from Saitama University in 1977. He joined Fujikura Ltd. in 1982, and has been engaged in research and development of telecommunication cables and accessories. He is now a manager of Fiber & Cable Accessory Department within Opto-Electronics Laboratory and a member of the IEICE of Japan.



Hiroshi Yokosuka

Fujikura Ltd.

1440 Mutsuzaki
Sakura, Chiba,
285, Japan

Hiroshi Yokosuka graduated in mechanical engineering from Tokyo Metropolitan Technical Junior College in 1967. He has been engaged in development of telecommunication cables and accessories. He is now a general manager of Fiber & Cable Accessory Department within Opto-Electronics Laboratory and a member of the IEICE of Japan.

CABLE REFERENCE MEASURING CLAMP KRMZ 1200

Frank Streibert

GHMT, Bexbach/Saar, Germany

ABSTRACT

At the begin of the 90's, the cabling structure of building facilities experienced a surprising renaissance, although quite a few experts thought that glass fiber cables would be introduced as transmission medium up to the desktop. By further developing copper-based cables for applications focusing on frequencies of up to 100 MHz, a more economical and easier to install alternative vis-à-vis glass fibers became available.

In order to enable this rapid of development, it was a matter of course that measuring techniques required for quality assurance purposes had to be developed at the same pace.

OVERVIEW

The automatic cable measuring systems which up to that time had been available at the cable manufacturers' only allowed (within the course of an automated measuring process) to determine the high-frequency transmission parameters up to a maximum frequency of 25 MHz. At that time, measurements up to 100 MHz were mostly carried out by means of separate baluns which had to have excellent transmission characteristics to carry out reproducible measurements.

The diagram below shows the typical measuring setup for determining the transmission characteristics of data cables up to 100 MHz.

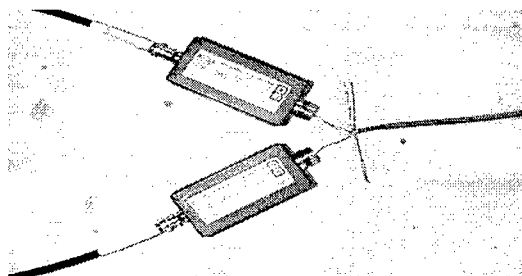


Figure 1: Traditional measuring technique for determining the transmission characteristics of data cables

This type of measurements requires measuring engineers to answer the following questions:

- How large is the maximum admissible stripping length of the individual wire pairs?
- How should the transformers be positioned?
- How should the cable shield be fastened (if existing)?
- etc.

Unless these open questions had been clearly answered, it would have been difficult to carry out reproducible measurements.

To answer the above questions, first of all the following requirements were defined:

- It must be possible to determine the high-frequency transmission parameters of a data cable in a reproducible way, i.e. independently of any location or person.
- An exact stripping length of the individual wire pairs must be specified.
- The arrangement of the baluns must be realized unambiguously.

The first cable reference measuring clamp having a transmission bandwidth from 25 kHz to 100 MHz was developed in 1992 / 1993 and is shown in figure 2 below.

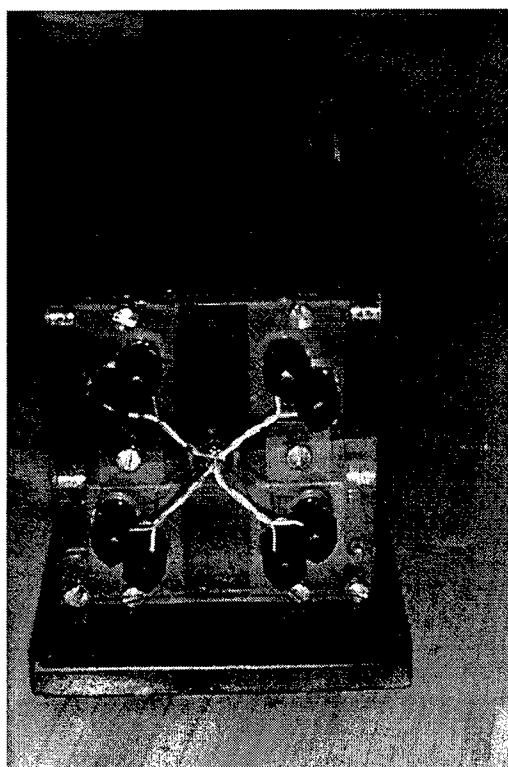


Figure 2: Representation of the first cable reference measuring clamp, KRMZ 100, which allowed the simultaneous connection of up to 4 wire pairs (the measuring head of KRMZ 100 included 4 equivalent baluns)

Technical data of KRMZ 100

1. Frequency range: 25 kHz – 100 MHz
2. Impedance at balanced gate: 105 Ω
Impedance at unbalanced gate: 75 Ω
3. Active return loss at 75 Ω
at F = 10 MHz: ≥ 40 dB
in the frequency range
5 ... 100 MHz: as a rule, 30 dB
4. Effective attenuation constant
at F = 5 MHz: ≤ 0.5 dB
5. Effective unbalance attenuation
to CCITT 0.9
up to F = 10 MHz: ≥ 60 dB
up to F = 100 MHz: ≥ 20 dB
6. Connections:
balanced gate: snap-on connectors
unbalanced gate: 75 Ω – BNC

Figure 2 shows that the requirements applying to the mechanical components could be covered satisfactorily.

Using the cable reference measuring clamp KRMZ 100, parameters such as attenuation, near-end crosstalk (NEXT) attenuation, return loss coefficient and input impedance (in combination with an upstream reflection coefficient measuring bridge) could be measured in a reproducible way, i.e. independently of specific persons.

By arranging the baluns on a plexiglass plate at distances of approx. 5 cm, no mutual interference was expected within a frequency range of up to 100 MHz.

On account of the introduction of paired shielded data cables in the mid of the 90's for applications with key frequencies of up to 300 MHz or – in individual cases – up to 600 MHz, the original model of the cable reference measuring clamp KRMZ 100 could no longer be used because of coupling effects occurring between the individual measuring gates. That is why an optional facility allowing to decouple the individual measuring gates had to be implemented into the cable reference measuring clamp.

The new generation of cable reference measuring clamps was milled from a piece of solid brass and completed with a matching cover (also made of solid brass). The cover included altogether 4 chambers which are arranged exactly above the individual measuring gates. Thus it is possible to determine the excellent NEXT attenuation values of the new generation of cables across the entire frequency range and at a very high dynamic range of measurement of more than 100 dB.

At the end of the 90's, cable manufactures are increasingly requested to develop balanced data cables which allow to operate applications with frequencies of close to 1 GHz.

In order to accompany these ongoing development activities by corresponding measuring techniques, GHMT developed the cable reference measuring clamp KRMZ 1200 which allows to determine the attenuation as well as the NEXT attenuation within the frequency range of 100 kHz – 1.2 GHz.

By connecting a reflection coefficient measuring bridge in series to KRMZ 1200, it is possible to measure the impedance and the return loss coefficient at frequencies of up to 600 MHz.

The figure below shows the KRMZ 1200 during the measurement of a paired shielded data cable.

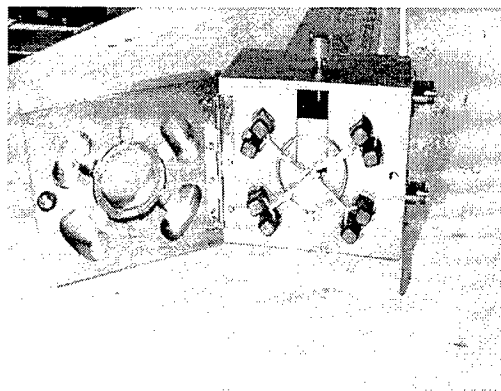


Figure 3: Representation of the reference measuring clamp KRMZ 1200 with lockable cover in order to decouple the individual balanced measuring gates

Technical data of KRMZ 1200

1. Frequency range: 100 kHz – 1.2 GHz
2. Terminal impedance
at the balanced gate: 100 Ω
Impedance at unbalanced gate: 50 Ω
3. Active return loss
at the balanced gate:
at F = 100 kHz ... 100 MHz: ≥ 20 dB
4. Power attenuation
 $a = 10 \times \log(P_{in}/P_{out})$
at F = 10 MHz: 3 ± 0.3 dB
5. Unbalance attenuation
LCL at F = 100 MHz: ≥ 30 dB
6. Side-to-side crosstalk attenuation
within the measuring head
at F = 100 kHz ... 1.2 GHz ≥ 100 dB

The following measuring diagram shows the intrinsic attenuation of two baluns which have been connected in series.

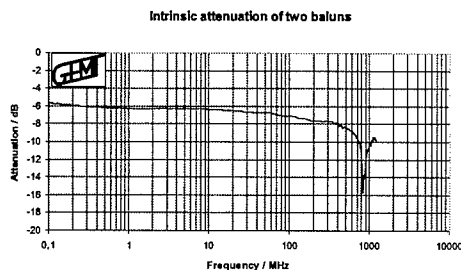


Figure 4: Intrinsic attenuation of two baluns

The following measuring diagram shows the crosstalk attenuation of two adjacent baluns with the cover closed.

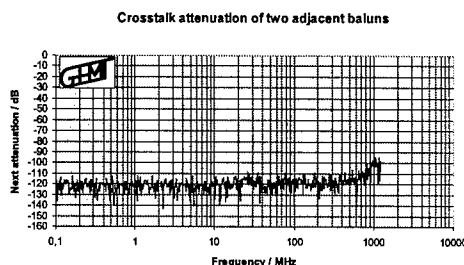


Figure 5: Crosstalk attenuation of two adjacent baluns

OUTLOOK

On account of the high reproducibility of the measured values and the very high dynamic range of measurement across the entire frequency range, a number of cable manufacturers have already included the cable reference measuring clamp KRMZ 1200 in their lab equipment. To integrate this high quality of measuring results into the cable production processes, it is planned to automate the operation of KRMZ 1200 in the near future. Then it would be possible to carry out continuous quality assurance tests of large cable volumes within the cable manufacturing halls.



Frank STREIBERT is a graduate engineer (Dipl.-Ingenieur), 32 years old, married, and father of 2 children.

He studied information and communication technology at the University of Kaiserslautern, Germany. In the course of his diploma thesis carried out a GHMT in 1992, he examined the application of traditional HF measuring techniques to the increased requirements of category 5 cables and components.

Currently he is responsible for link performance and cable measurements to EN 50173 and E DIN 44312-5.

Mr. Streibert is a general manager of GHMT mbH, an independent test lab for the worldwide certification of cables, components, and active devices of LAN/WAN technologies.

Mailing address

GHMT
Gesellschaft für Hochfrequenz-Meßtechnik
mbH
In der Kolling 13

D 66450 Bexbach/Saar
Germany

Phone: ++49 / (0) 68 26 / 92 28 - 0
Fax: ++49 / (0) 68 26 / 92 28 - 99
e-mail: STREIBERT@GHMT.COM

INVESTIGATION OF A DUAL PURPOSE CABLE COMPONENT: A WATER-BLOCKING TENSILE GLASS FIBER STRAND

Thomas P. Hager

Owens Corning, Granville, OH

Anne G. Bringuier

Siecor Corporation, Hickory, NC

ABSTRACT

Since the introduction of dry water swellable technology to replace flooding compounds, a natural evolution has occurred where traditional cable components are modified to perform waterblocking duties as well as their original role. This paper investigates the engineering of an impregnated glass fiber tensile yarn to be used as a water-blocking medium meeting tensile strength and processing requirements. Its use in a single tube, riser-rated cable reduces terminations and their associated costs.

INTRODUCTION

Initially, optical fiber cables were used as the trunk or backbone of a telecommunication system. Installation of the cable was simple, only requiring the end of the cable to be spliced to a dispatch panel where twisted pairs or coaxial cable would then transport the signal. The introduction of broadband services employing optical fiber cables has made splicing more frequent and termination environments more diverse in terms of hardware, locations and procedures. Cable constructions utilizing greaseless water-swallowable materials started to be designed^{1,2,3,4} to provide field personnel with craft friendly and cost effective methods of accessing the cable core for re-entries and mid-span access.

In these dry core designs, waterblocking is usually ensured with the use of water swellable tapes and yarns. This paper

introduces a dual-purpose cable component, an impregnated glass fiber tensile yarn called AquaBlok™ reinforcement and made with proprietary water-swallowable technology. In a single tube design, the path available for the water to travel is limited to the space between the buffer tube and the jacket. The water passage areas are small and easily blocked with swellable tensile yarns. These swellable yarns provide for a compact cable design with fewer elements to contend with during field installation and repair.

The dual-purpose tensile yarn fulfills the roles of both tensile strength provider and waterblocking medium. The installer needs to only install the cable without the clean-up and flammability concerns associated with greasy water-resistant compounds. If a cut in the cable jacket allows moisture to enter the cable, the yarn swells and plugs the cut, thus blocking further fluid from entering.

CABLE DESIGN

Multiple building networks, such as campuses, are starting to use indoor/outdoor cables that need to meet UL flammability requirements as well as outdoor requirements. Because flooding compounds are flammable, alternate means of waterblocking are necessary. In the two indoor/outdoor cables described here, the waterblocking feature is transparent to the craftsman. A water-swallowable tensile yarn enables field

personnel to rapidly perform cable termination and mid-span access.

The cable consists of: a buffer tube, two layers of the water-swellaable yarns helically stranded, and the jacket material. The cable can accommodate 1 to 12 fibers. Figure 1 shows the cross section of this 12f indoor/outdoor drop cable. Figure 2 shows an isometric view of it.

Buffer Tube

The cable utilizes a polyolefin tube chosen for its superior hydrolytic stability in hot humid environments and improved flexibility in limited space applications. The tube is filled with a compatible thixotropic compound. The 3.0 mm diameter of the tube allows compatibility with standard stranded loose tube fan-out kits for rapid, simple termination.

Jacket Material

Two materials may be used for this indoor/outdoor cable: a PVC cable (called FREEDM™/LST) or a low smoke zero halogen flame retardant polyolefin (cable called LSZH™/LST). The PVC cable construction provides good flame resistance and meets UL-1666 riser requirements. The low smoke polyolefin meets the international flame standard IEC 332-3, "Tests on Electrical Cables under Fire Conditions."

CABLE PERFORMANCE

Cables were produced with fiber counts ranging from 2 to 12. The cables were tested to different optical, mechanical and environmental industry requirements. Both PVC and low smoke polyolefin cables contained dispersion-unshifted single mode fibers and multimode 62.5/125 µm core fibers.

Environmental

Environmental tests are shown in Table 1. Attenuation results include a 0.05 dB/km allowance for measurement repeatability. Both the PVC and low smoke polyolefin cables met major industry performance requirements including ICEA S-83-596.

Mechanical

Both the PVC and low smoke polyolefin cables were subjected to various

mechanical requirements. The results shown in Table 2 indicate all major performance levels were met.

Water Penetration

Water penetration was tested in accordance with EIA/TIA-455-82A (FOTP-82). This procedure consists of exposing the cross section of a one meter section of cable to a one meter head of tap water for 24 hours. After aging in an oven for 1 and 3 weeks at 85°C, cables were tested, then dissected to obtain the water ingress measurements. In Table 3, results were normalized against the water ingress in the unaged cable. The standard deviation for these comparative results is 0.2. Each value represents the average of four measurements. All cables subjected to the different conditions in Table 3 passed the one meter industry requirement.

TENSILE YARN PERFORMANCE

The glass fiber tensile yarn provides the tensile strength for the fiber optic cable during installation. Tests were conducted to examine any potential effects the waterblocking coating may have on the ability of the yarn to perform its initial protective purpose.

Tensile Properties

Three different strand properties associated with tensile stresses were evaluated: 1) tensile strength, 2) modulus of elasticity and 3) force at specified elongation (FASE).

For each tensile property, two series of tests were conducted: 1) performance of the yarn as-received, and 2) performance of the yarn after heat aging for 4 weeks at 85°C. Each test series measured the specific property of the yarn in three different conditions: 1) the original yarn without the waterblock coating, 2) the yarn with the waterblock technology in a dry state, and 3) the yarn with the waterblock technology in a wet state.

According to the test data, yarn with the waterblock coating in a dry state experienced a moderate drop in tensile strength at break between as received and aged glass fiber reinforcement (Table 4). However, there is no significant

differences between as received and aged for the two critical properties of modulus of elasticity (Table 5) and FASE (Figure 3). Furthermore, for aged material in the dry state, percentage changes from the original impregnated fiber were: +12% for as received and +2% for aged for tensile; -2% for as received and +0.5% for aged material for modulus of elasticity; and no changes for FASE over the range of 0.1 to 2.50% strain. Properties remained within the ranges required to effectively protect against tensile stresses.

Yarn with the waterblock coating in a wet state experienced additional declines in all three properties (Table 4 and 5, Figure 4) but are still within required performance parameters. Furthermore, the need for tensile stress protection significantly diminished after cable installation, when moisture attack most likely occurs.

Water Absorption Properties

The effectiveness of the water swellable coating was tested by measuring the effect of water on the individual yarn. Two different physical properties were measured when the coated yarn was exposed to water: 1) the percent swell (Table 6) measured by the increase in cross sectional area, and 2) the percent weight increase (Table 6).

For each physical swell property, two series of tests were conducted: 1) performance of the yarn as-received, and 2) performance of the yarn after heat aging for 4 weeks at 85°C. Each test series measured the specific property of the yarn under two different conditions: 1) the coated yarn exposed to deionized water and 2) the coated yarn exposed to 1% saline solution. As the results in Table 6 and 7 show, the increases in swelling and weight were higher in the deionized water. Percent changes for aging from the as received material were: 1) -1.5% in deionized water and -48% in 1% saline solution for swelling; and 2) -25% in deionized water and -10% in 1% saline solution for weight gain.

Coating Consistency

Loss on ignition tests were conducted to measure the variability in the application of

the waterblocking powder. Loss of ignition is commonly used in the glass fiber reinforcement industry. The test measures the weight of a given length of yarn before and after it is exposed to flame. The difference indicates the amount of organic materials on the inorganic fiber.

Measuring the loss on ignition for over 7 separate production runs yields a standard deviation of 2.20% with an average loss on ignition of 13.39%. The testing population was 27 individual packages. The confidence interval at 95% confidence limit, using Student's t distribution:

$$\text{Confidence Interval} = \text{average} \pm (t)(\text{std. dev.})/(N)$$

where N is the number of tests, and t is from the t table.

$$\text{C.I.} = 13.39 \pm (1.706)(2.20)/(27) = 13.39\% \pm 0.72\%$$

Thus at 95% confidence, of the measured losses on ignition are expected to fall within 0.75% of the above stated average⁵.

CONCLUSIONS

In summary, an impregnated glass fiber strand traditionally used in cables for tensile strength inherently performs an auxiliary role of waterblocking when the strand is treated with a coating. The reliability of the swellable material and strand was investigated in terms of aging, tensile properties, swellability and cable processing. The dual-purpose material in cable form met all relevant industry requirements for outdoor use.

REFERENCES

1. A. Bringuier and C. Clyburn III: "Development of a Loose Tube Cable With Non-Flooded Core For Outdoor Plant Environment," Proceedings of the Eleventh Annual National Fiber Optic Engineers Conference, pp. 376-386, June 1995.
2. R. Gravely III and S. Stokes: "An Improved Loose Tube Cable With Dry Water Blocking Elements,"

Proceedings of the Eleventh Annual National Fiber Optic Engineers Conference, pp. 367-375, June 1995.

3. C. Clyburn III and A. Bringuier, "A Dry Core Loose Tube Cable for Outside Environments," Proceedings of the 44th International Wire and Cable Symposium, pp. 29-36, 1995.
4. P. Gaillard, C. McNutt, J. Holder, A. Bouvard and O. Tatat, "Significant Improvement of Loose Tube Cable Spliceability Based on New Cable Dry Design," Proceedings of the 45th International Wire and Cable Symposium, pp. 353-358, 1996.
5. CRC Standard Mathematical Tables, 17th Edition, 1969.

BIOGRAPHIES

Anne G. Bringuier
Siecor Corporation
PO Box 489
Hickory, NC 28603, USA

Anne Bringuier received an engineering degree in Materials Science and Engineering from the Institut National des Sciences Appliquées (INSA) in Lyon, France, an Advanced Studies Diploma (DEA) in Macromolecular Science from the University of Lyon in 1985, and a M.S. in Polymer Science and Engineering from

Pennsylvania State University in 1987. From 1987 to 1993, she worked at Raychem Corporation in the area of telecommunications closures. In 1993 she joined Siecor where she has been involved with materials selection and design of optical fiber cables. Anne is currently a Senior Product Development Engineer.

Thomas P. Hager
Owens Corning
Science & Technology Center
2790 Columbus Rd., Route 16
Granville, OH 43023-1200, USA

Thomas P. Hager is a Senior Scientist with Owens Corning at their Science and Technology Center, Granville, Ohio. He has been with Owens Corning since 1978. He is currently in the Composites Group involved with product and applications development for telecommunication cable reinforcements. Hager has also developed coatings for glass fiber materials for braided skis, filtration products, electrical laminates and carpet backings. He received an M.S. degree in Polymer Science from the Institute of Polymer Science, the University of Akron, Ohio, and a B.S. degree in Chemistry, also from the University of Akron.

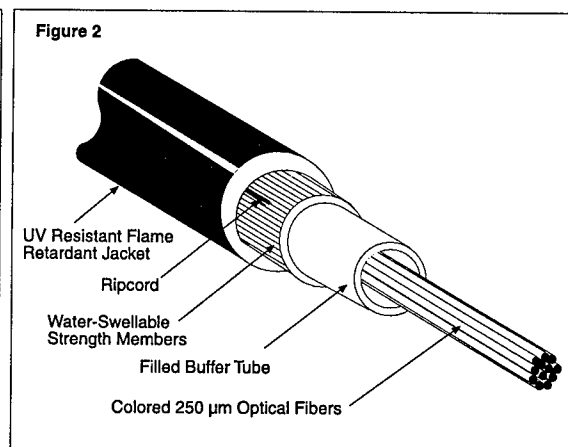
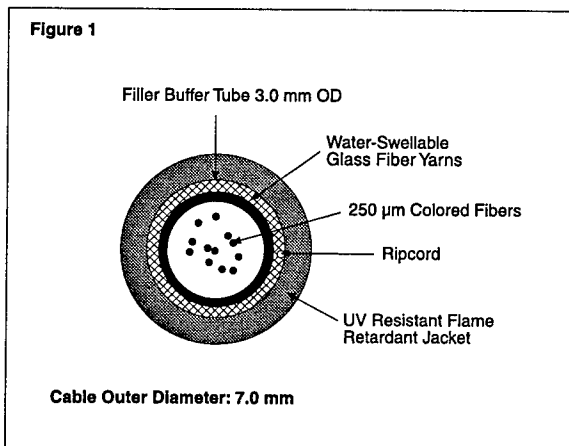


**Figure 3. Force at Specified Elongation
Glass Fiber Dry State -- Unaged**

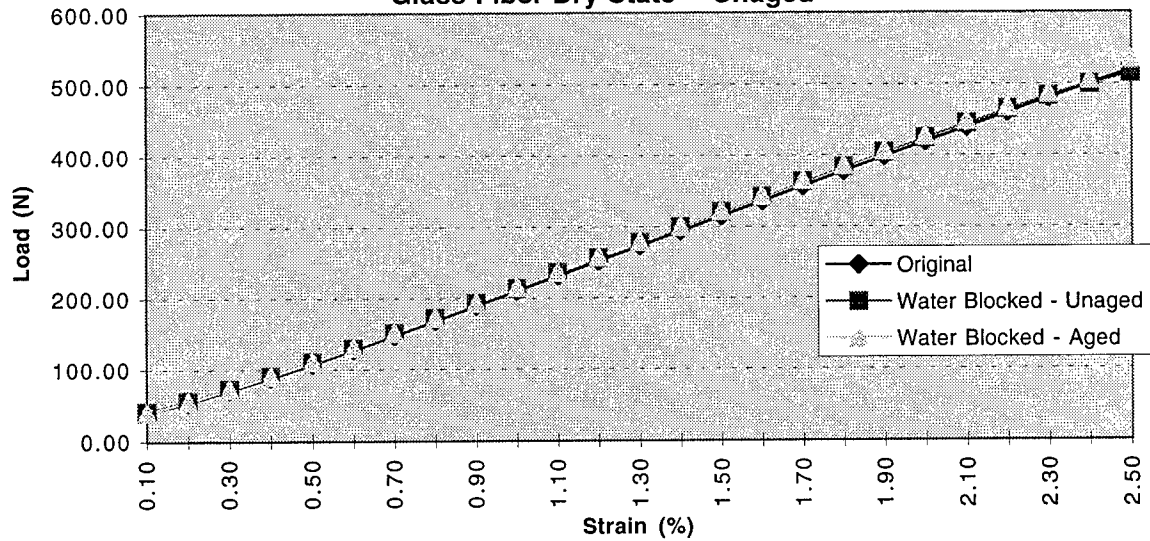


**Figure 4. Force at Specified Elongation
Glass Fiber Wet State -- Unaged**

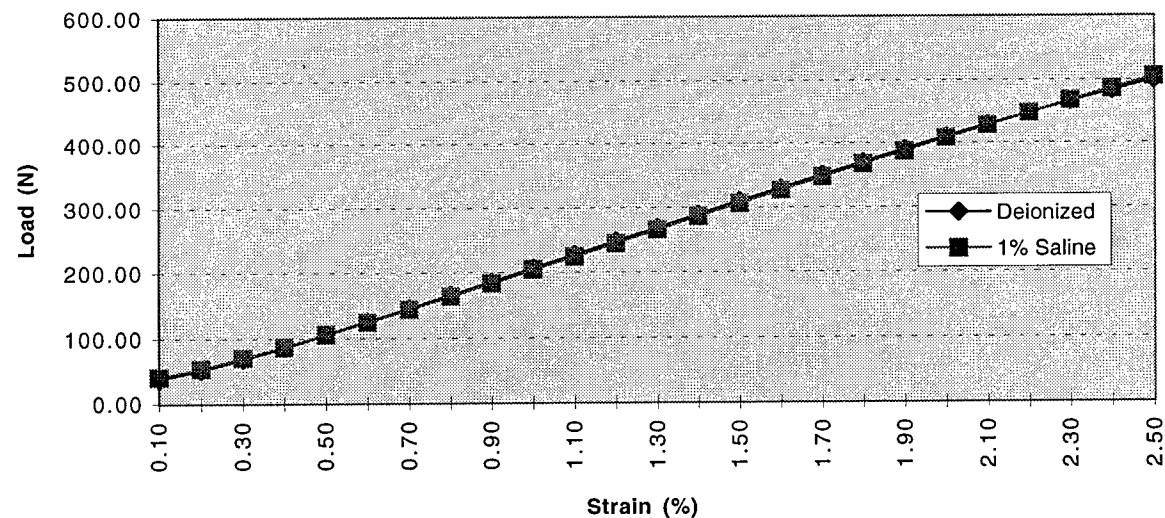


Table 1: Environmental Tests on Cable

Test	Results	Method
Temperature cycling* -40° to +70°C	Maximum change (SM/MM in dB/km) <0.3/0.6	FOTP-3
Cable Aging* 85°C 168 hrs	Maximum change (SM/MM in dB/km) <0.6/01.2	FOTP-3
Water penetration	No water leakage 24 hrs unaged, 1 hr aged 168 hrs @ 85°C	FOTP-82
Jacket shrinkage 110°C, 2 hrs	<5%	FOTP-86
Filling compound flow 80°C	No compound flow	FOTP-81
Resistance to fungus growth	Grade 0 - 0% growth	ASTM G-21
Material compatibility	Buffer tube elongation >10% 45 days in 85°C water	ASTM D2105
Corrosivity of gases from combustion**	Passed pH and conductivity requirements	IEC 754-2

*Note: Attenuation measurements @ 1550 nm

**For LSZH/LST cable

Table 2: Mechanical Tests on Cable

Test	Results	Method
High/low temperature bend 50°C, 0°C, 4 turns	Maximum change (SM/MM in dB/km) <0.2/0.5	FOTP-37
Impact 20 cycles	Maximum change (SM/MM in dB/km) <0.2/0.4	FOTP-25
Compression 8.9 N/mm	Maximum change (SM/MM in dB/km) <0.2/0.4	FOTP-41
Tensile strength 1320 N	Maximum change (SM/MM in dB/km) <0.2/0.5	FOTP-33
Cable Twist/Bend	Maximum change (SM/MM in dB/km) <0.2/0.4	FOTP-91
Cyclic Flex 25 cycles, 20X cable OD	Maximum change (SM/MM in dB/km) <0.2/0.4	FOTP-104

Table 3: Water Penetration Tests on Cable

Conditions	Time	Normalized Water Ingress*
Aged @ 85°C	0 days	1.0
Aged @ 85°C	7 days	1.1
Aged @ 85°C	21 days	1.2
Aged @ 85°C, 95% RH	21 days	1.3
-40°C/+70°C cycles	21 days	1.9
1% salt solution	21 days	2.0

*Normalized against water ingress in unaged cable.

Table 4. Tensile (N) Measurements of Original and Water Blocked Glass Fiber Reinforcement

		As Received		Aged	
		Dry	Wet	Dry	Wet
			Dionized 1% Saline		Dionized 1% Saline
Original	549				
Water Blocked	617		589 596	557	528 535

Table 5. Modulus of Elasticity (GPa) of Original and Water Blocked Glass Fiber Reinforcement

	Dry		Wet			
	As Received	Aged	DI Water		1% Saline	
			As Received	Aged	As Received	Aged
Original	74.2					
Water Blocked	72.9	74.5	71.8	72.7	71.7	81.0

**Table 6. % Swell of as Received and Aged Water Blocked Glass Fiber Strand
(Cross Sectional Area Increase)**

	As Received	Aged
Deionized Water	570%	561%
1% Saline Solution	354%	183%

Table 7. Percent Weight Gain of as Received and Aged Water Blocked Glass Fiber Strand

	As Received		Aged	
	Deionized	1% Saline	Deionized	1% Saline
1 min	327%	109%	258%	95%
10 min	655%	180%	502%	158%
20 min	800%	185%	601%	167%

FIBER GRATING BASED CHROMATIC DISPERSION COMPENSATORS: PACKAGING AND SYSTEM PERFORMANCES

Piergiuseppe Peretta, Francesco Pozzi, Marco Signorelli

SIRTI S.p.A. Cables and Optical Technologies
Cassina de Pecchi (Milano), Italy

ABSTRACT

In this paper a description of the packaging of chromatic dispersion compensators based on fiber gratings is reported. These devices are well known to be very sensitive to thermal fluctuations therefore they generally require a careful stabilization of their working wavelength. In the following, the design of the package based on Peltier cells for temperature control is described along with the experimental tests for system performance evaluation on the packaged device in critical environmental conditions (i.e. $+10^{\circ}\text{C}$ - $+40^{\circ}\text{C}$).

INTRODUCTION

The continuously growing demand of broadband services is expected to require an impressive increase of the channel capacity in the next future in particular in repeaterless transmission links.

In case of G.652 fiber, it is well known that system performances can be dramatically affected the chromatic dispersion (about 17 ps/nm*km); therefore dispersion compensators appear to be very promising devices for exploiting already installed cables at higher bit rates (10 Gbit/s or more) either in single or in multi-channel systems in a cost effective way.

Several kind of dispersion compensating techniques have been experimented so far (e.g. soliton transmission, midway spectral inversion, dispersion compensating fibers) [1]. However these solutions may be not completely satisfactory due to the high cost

and complexity or to excessive insertion loss. Nowadays, there is a considerable interest in fiber gratings directly written on optical fibers using UV light (at about 290nm) [2, 3].

In particular, chirped fiber gratings have been demonstrated to be very efficient chromatic dispersion compensators (CDC) [4, 5, 6] when used in combination with optical circulators. These components appear to be very attractive for their potential compactness, low insertion loss and low cost.

However they are intrinsically fragile, sensitive to temperature as well as to axial stress [7]. Therefore packaging appears to be a key factor for this kind of components as it should be able to overcome any device sensitivity as well as to give protection from any external stress.

In this paper, after a short theoretical analysis of the phenomenon of chromatic dispersion compensation and a brief description of fiber grating based CDCs, the design of the package by means of Peltier cells is reported. Moreover the system measurements in case of environmental temperature changes are shown in order to demonstrate the effectiveness of the stabilization technique.

THEORETICAL ASPECTS

The degradation of the BER in case of chromatic dispersion is well known to be caused by the spreading of the pulse due to the different propagation speed of frequency components of the optical pulse. The effect is a reduction of the peak power as well as an increase of the intersymbolic interference from adjacent bits. Both effects are well known to cause a degradation of the eye

diagram which results in an increase of error probability.

Many theoretical analysis have been carried out in order to model this effect and the predictions are greatly affected by the assumptions made on the transmitter and receiver actually used. A rule of thumb relationship of the dispersion limit for an ideal transform limited NRZ signal is given by the well known formula [8]:

$$B^2DL=10^5$$

where B, D and L represent the bit-rate, the fiber chromatic dispersion coefficient and the maximum link length respectively.

However depending on the amount of transmitter chirp (typical of directly modulated lasers), the dispersion limit can be much more severe, reducing the available transmission distance below 100 km even at 2.5 Gbit/s.

In case of linearly chirped fiber Bragg gratings, the dispersion compensation mechanism is obtained by the reflection of the different frequency components of the optical pulse at different sites in the grating (in particular the longer wavelengths are reflected before and the shorter ones afterwards).

This behaviour, in combination with the use of an optical circulator, make it possible to introduce a different delay to the various spectrum components and therefore enables a proper compensation of the dispersion due to G.652 optical fibers.

The delay introduced by the grating depends on many physical parameters and in particular on grating length, peak reflectivity and bandwidth. They depend on the actual realization technique adopted by the manufacturer and are related as follows [3]:

$$\Delta\tau = 2 \frac{L}{v_g}$$

$$\Delta\lambda = \frac{\Delta\tau}{D}$$

where $\Delta\tau$ represents the total delay of the grating, $\Delta\lambda$ its bandwidth, v_g the group velocity and D the slope of the grating delay curve (dispersion parameter).

PACKAGE DESIGN

The design of the package has the aim of reducing as much as possible the thermal excursion of the chromatic dispersion compensator in the range 10°C-40°C (usual temperature interval assumed for a central office environment) while keeping packaging cost and electrical power consumption as low as possible.

In figure 1, a scheme of the chromatic dispersion compensator is shown. Since the grating behaves as an optical reflector, it is placed at the common arm of an optical circulator. The other end of the grating is immersed in index-matched gel in order to prevent any backreflection effect or could possibly be used for monitoring purposes.

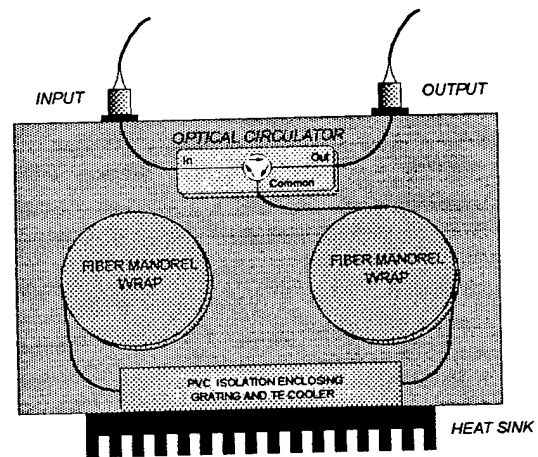


Fig 1. Scheme of the CDC package layout

The core of the package is reported in figure 2.

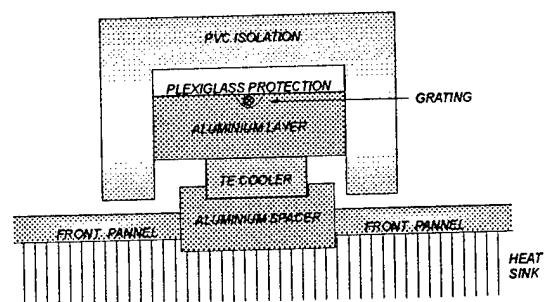


Fig 2. Transversal section view of the housing for CDC

It consists of a suitably designed housing with a submillimetric groove used to host the unpretentioned grating in straight line position. As the grating length for 0.5 nm bandwidth and 1700 ps/nm dispersion compensation is about 10cm-13cm, a 14 cm long housing has been realized.

The aluminium holder is placed in full contact with the Peltier cells on one side and is thermally insulated on the other by a cover of suitable material.

At the hot side of the Peltier cell a heat sink has been placed dissipating the power necessary for grating temperature stabilization.

Both the holder dimensions and the the cover have been designed in order to reduce the thermal conductivity of the package with the outside environment as well as with the aim of minimizing the heat capacity of the system.

The thermal design of the package takes into account either thermal conduction between the holder and the insulating cover or the thermal convection between the last one and the external environment which has been supposed to be in non turbulent state.

According to the electric equivalent model of the heat transfer theory, the two contributions mentioned before can be modeled using resistors (R_{cond} and R_{conv}) which represent the ratio between the heat flow between two given surfaces and the corresponding temperature difference. The conduction and the convection contributions can be taken into account with the following terms:

$$R_{cond} = \frac{s}{k * A} \quad R_{conv} = \frac{1}{h * A}$$

where s is the thickness and A is cross sectional area of the material while k and h are the thermal conductivity of the material and heat transfer coefficient respectively.

After having minimized the holder size, the cover dimensions have been determined in order to reduce thermal flow while maintaining a reasonable size for the packaged device. Finally a suitable low thermal resistance heat sink have been used.

In the device reported in this paper, the main geometrical limit is represented by the quite large size of the commercially available Peltier cells. Further reduction of this dimension could result in an improvement of package performances.

Concerning the electronic control scheme, a thermistor enables to monitor the actual temperature of the package and therefore of the grating. An electronic circuit designed for this application exploits the error signal of the thermistor on a Wheatston bridge to drive the Peltier cells with a suitable feedback current in order to keep a predefined temperature for the device.

The temperature is controlled within 2-3 °C peak-to-peak for an external temperature from 5°C to 45°C.

Moreover through the variation of the value of a resistor at the input bridge, a precise tuning of the grating on the transmitter wavelength is made possible.

Such feature appears to be very useful for this kind of component with very low bandwidth and is not made available by any kind of passive packaging.

EXPERIMENTAL RESULTS

The performance of the packaged grating has been tested in CSELT by performing a spectral characterization of the device and by inserting it in a transmission experiment. The chirped grating was provided by a partner of PHOTOS project (BT labs).

In particular in figure 2 the transmission spectrum of the CDC for different environmental temperatures along with the laser transmission spectrum are reported. The useful bandwidth has been measured to be about 0.15 nm and is determined both by the reflectivity profile and by the region of linearity of the delay curve.

As shown in figure 2, a change in the environmental temperature results in a translation of the center wavelength with a rate of 0.0081 nm/°C.

In the case under consideration, the transmitter is tuned on the grating at room temperature (25°C) and its bandwidth is quite large (about 0.2 nm@-20 dB) so any detuning is expected to results in high penalty at the receiver. This is the reason why tight temperature control of the grating is strictly needed for this kind of application.

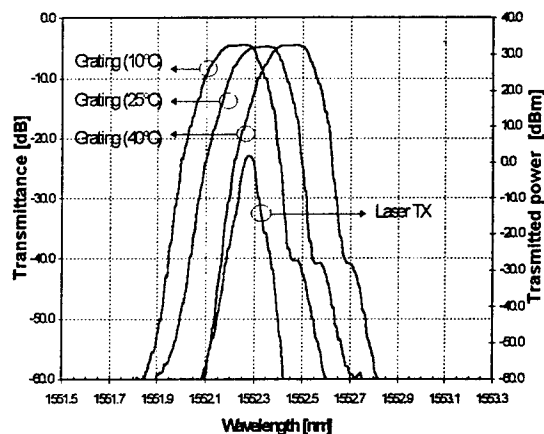


Fig 2. Reflection spectrum of the CDC at different temperatures as well as laser transmission spectrum

The measurement set-up for system performance evaluation consists in a

transmitter and a receiver with a pseudorandom pattern generator. A booster amplifier allows output powers as high as +16.5 dBm and the dispersion compensator is placed just in front of the receiver (post-compensation).

In figure 3 the Bit Error Rate (BER) curves in the back-to-back configuration and with 150 km of G.652 fiber are shown. Moreover the performances in case of use of thermally stabilized CDC for different environmental temperatures are reported. The CDC causes a slight power penalty with respect to the back-to-back case but allows penalty reduction with respect to the uncompensated condition and in any case prevents the system from floors due to excessive chromatic dispersion.

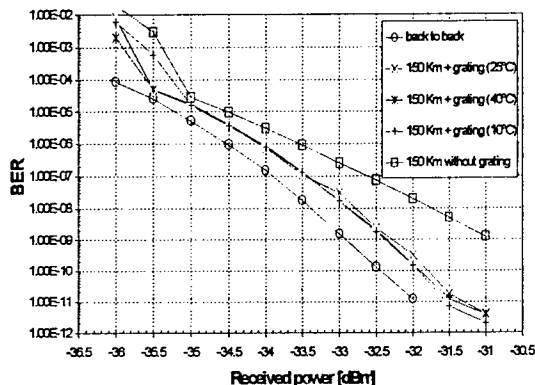


Fig 3. BER performance with stabilized grating.

The curves for temperatures from 10°C to 40°C, show a good degree of overlap which confirms the optimum thermal stabilization provided by the package.

For the same values of environmental temperatures used for the BER measurements, the electrical power consumption of the packaged device has been measured and reported in figure 4. As the electronic circuitry has been designed for room temperature operation, the electrical power consumption is negligible at 25 °C and increases either at 10°C and at 40°C.

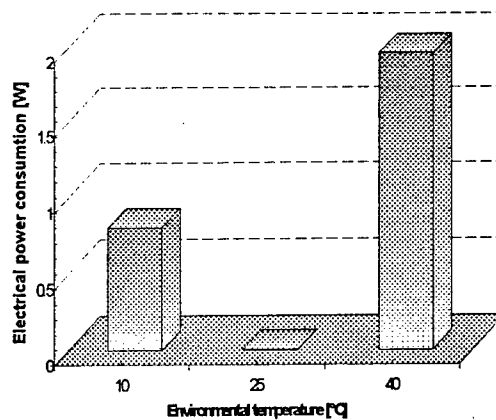


Fig 4. Electrical power consumption against environmental temperature

In figure 5 the effect of grating temperature variation on the BER in case of non stabilized CDC are shown for a received power of -32.5 dBm. As expected, the optimum behaviour has been found at 25°C while the performances are completely degraded at 40°C. The diagram is asymmetric in temperature due to the fact that at 25°C the central wavelength of the transmitter is placed slightly at the left side of the CDC spectrum (see fig. 2). Therefore a downward shift of the CDC spectrum is less critical than a corresponding upward variation.

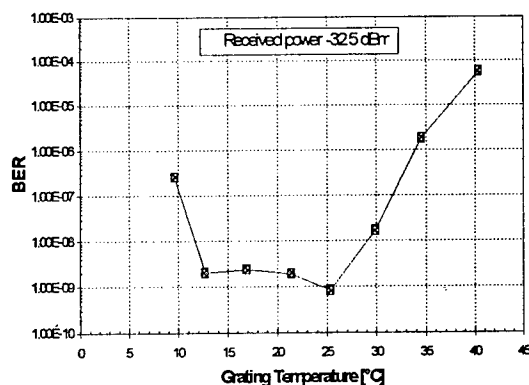


Fig 5. BER degradation due to grating temperature variation.

CONCLUSIONS

In this paper packaging problems related to fiber grating based CDCs are described and the sensitivity to environmental parameters, in particular to temperature, have been reported. Moreover the design of the package used to overcome this problem has been described either from both the optical and the electronic point of view. The design is based

on the use of Peltier cells and a suitable electronic circuitry in order to keep a desired temperature on the grating. The electronics enables a fine tuning of the CDC on the transmitter wavelength, feature believed to be very important in case of high density WDM systems. Moreover a suitable external housing can protect the fiber from unwanted mechanical stresses and shocks.

BER measurements showing the correct operation of the CDC in the range between 10°C and 40°C have been reported.

Moreover sensitivity to detuning has been demonstrated, confirming the necessity of a tuning option for CDCs having such a reduced bandwidth. This aspect obliges the adoption of an active packaging approach as any passive packaging technique could make this option available.

ACKNOWLEDGMENTS

The authors desire to thank Dr. Emilio Riccardi (CSELT-TO/IA) for the fruitful discussions and his valuable help in the system measurements as well as CSELT laboratories for providing the BER experimental test-set.

This study has been partially supported by the EEC, ACTS Project A046 PHOTOS.

REFERENCES

- [1] M. Artiglia: "Upgrading the capacity of installed systems to multigigabit bit-rates by means of dispersion compensation", *MoB.4.1, Optical Fiber Technology* 1, pp.17-34, 1994.
- [2] R.Kashyap: "Photosensitive optical fibers: devices and applications", *Optical Fiber Technology* 1, pp.17-34, 1994.
- [3] R.Kashyap et al.: "Novel method of producing all fiber photoinduced chirped gratings", *Electronic Letters* Vol. 30, N. 12, pp. 996-997, 1994.
- [4] K.O.Hill et al.: "Aperiodic in-fiber Bragg gratings for optical fiber dispersion compensation", *Proceedings of Optical Fiber Conference 1994*, PD2.
- [5] R.I. Laming et al., "Fiber gratings for dispersion compensation", *Proceedings of Optical Fiber Conference 1997*, ThA3.
- [6] R. Kashyap, "Eight wavelength x 10Gbit/s simultaneous dispersion compensation over 100 km single-mode fiber using a single 10 nanometer bandwidth, 1.3meter long, super-step-chirped fiber Bragg grating with a continuous delay of 13.5 nanoseconds"

Proceedings of European Conference on Optical Communications 1996, ThB.3.2.

[7] S.Pitassi et al. "Fiber gratings: temperature and mechanical sensitivity of narrow band transmission filters using different packaging solutions", *Proceedings of International Wire and Cables Symposium Conference, 1996*.

[8] G. P. Agrawal *Fiber optic communication systems*, John Wiley & Sons, 1992.

Authors

Piegiuseppe Peretta was born in Turin, Italy, in 1965. He received the doctor degree in Electronic Engineering from "Politecnico di Torino" in 1990. After a brief period of work in CSELT, he joined AET where he dealt with optical monitoring systems. In 1995 he joined R&D Dept. of SIRT I where he is currently engaged in passive optical components as a Senior Engineer. He is involved in national and international standard committees and had some papers published in national and international conferences.

Francesco Pozzi was born in Gallarate, Italy, in 1968. He received the doctor degree in Electronics Engineering from "Politecnico di Milano" in 1993. He joined the R&D Dept. of SIRT I in 1995 where he is currently engaged in optical components as well as in testing of equipment based on WDM-SDH-ATM technology and networking as a Senior Engineer. In particular he has been working on optical amplifiers, fiber grating based components as well as high capacity communication systems. He is involved ACTS PHOTOS and PROMETEO project with Telecom Italia and had some papers published in national and international conferences.

Marco Signorelli was born in Milano, Italy, in 1972. He is studying Electronic Engineering at the "Politecnico di Milano" with specialization in Optoelectronics.

Mailing address: SIRT I S.p.A.

via E.Fermi 2,
20060 Cassina de Pecchi
Milano, Italy

E-mail: f.pozzi@sirti.it

Tel. +39.2.6677.5154

fax +39.2.6677.5199

TYPHOON TOUGHENED ADSS CABLES

Scott G. Kipp, Anthony Peng & Kaofeng Tsai

Baycom Opto-Electronics Technology Co. Ltd.,
Hsinchu Science Based Industrial Park, Taiwan, ROC

ABSTRACT

Taiwan is annually battered by typhoons that destroy aerial cables with wind speeds of up to 160 mph (266 kph). These strong winds fatigue the cables and cause micro-cracks in the fibers that increase attenuation. A new All Dielectric Self Supporting, ADSS, cable was designed to withstand these forces and extend the life of the cable. Novel installation techniques were employed to alleviate acute strain points. The combination of the new cable design and typhoon proof installation techniques extends the life of the cables.

Typhoons place extreme strain on optical fiber cables. During extreme strain, the cable is stretched beyond the strain window and stress is placed on the optical fiber. Under extreme strain, the signal attenuation did not increase significantly until the fibers broke. Strains of over 2% did not increase the attenuation or have long term effects on the cable's performance.

STORM DAMAGE

Background

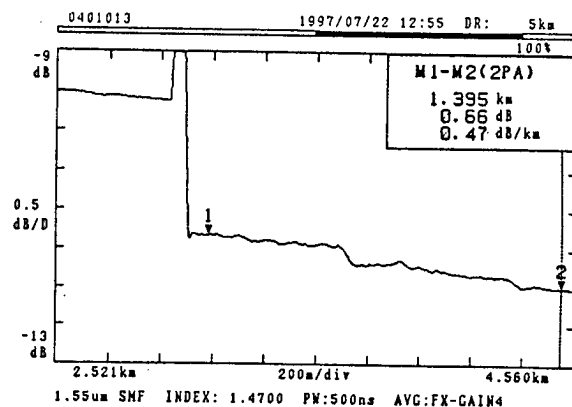
Typhoons are tropical cyclones that torment Taiwan and the North Pacific basin an average of 25 times a year.¹ Similar tropical disturbances are experienced in six other global regions including the Atlantic Basin where they are called hurricanes. These storms wreak havoc across the land and have sustained surface wind speeds of at least 71 mph (118 kph), typical speeds of 120 mph (200kph) and maximum recorded wind speeds of 183mph (306 kph).

Aerial CATV cables are replaced approximately every five years on the north-east coast of Taiwan due to damage caused by the severe wind conditions there. When regular service checks note unacceptable attenuation in the

cables, they are replaced so that high quality service is maintained.

Damage Analysis

An Optical Time Domain Reflectometer, OTDR, measurement in Graph 1 shows how the beaten cable's reflections fluctuate much more than the bare spooled fiber at the left of the splice. The weather beaten cables had much higher attenuations of up to 0.8 dB/km at 1310 nm and 0.47 dB/km at 1550 nm. Attenuation in the cable was more than double the original value of 0.367 dB/km and 0.21 dB/km measured when the cable was manufactured in 1993. Permanent deformations in the cable developed near the deadend locations as shown in Photo 1. Micro-cracks in the fiber were observed near the fastening locations. The distortions in the cable and the microcracks are the result of many years of abuse experienced during typhoons.



Graph 1: Weather Beaten Cable Attenuation

Other common experiences during typhoons are felled utility poles. One recent incident was during the worst typhoon to strike Taiwan in 30 years. In one location, two adjacent poles fell down under the conditions shown in Figure 1. The messengered cable was strong and flexible enough to support the two downed poles and

service was uninterrupted under these extreme conditions.

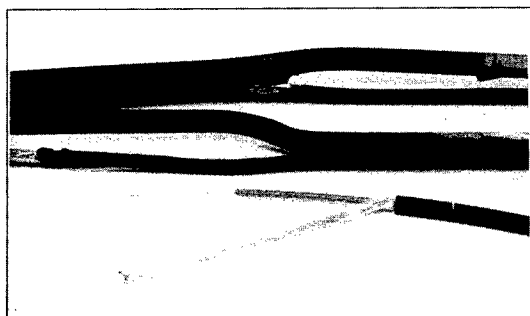


Photo 1: Weather Beaten Cable and New Cable

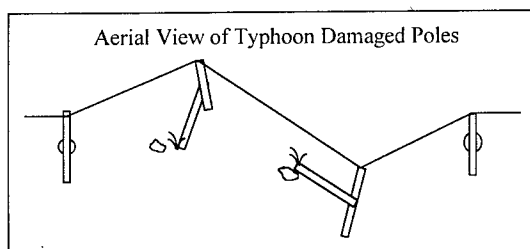


Figure 1. Damage From Typhoon

Field Analysis

In aerial plants, the ADSS cable is usually supported with deadends that restrict the cable movement in both directions. Under gusty winds, varying lateral forces whip the cables into a gallop around these constrained points. Examination of the weather worn cables showed that microcracks in the fiber and sharp bends in the cable were primarily near the deadends. Thus, the majority of the destruction of the cable was due to the localised strain at the deadends. To alleviate the acute strain placed on the cables, either the force applied to the cable can be reduced or the force can be dispersed over a longer length of cable. The force on the cable is decreased by reducing the wind load and the force is dispersed with novel installation techniques.

The wind load or force on the cables is directly proportional to the cable's outer diameter and the square of the wind velocity. The weather worn cables that were replaced had considerably larger outer dimensions than the new design. With a messenger wire, the old cable had an outer diameter of 0.87" (22 mm) and a width of 0.55" (14 mm) as shown in Figure 2. During typhoon force winds, the cable was seen to twist

around the messenger wire to show a smaller cross section to the wind. This twisting motion placed additional torsional forces on the cable.

The new cable's outer diameter was reduced to only 0.30" (7.6 mm) and is symmetrical. The smaller diameter cable decreases the wind load of the cable by at least 66%. The symmetry of the cable avoids additional torsional loads that were placed on the previous asymmetric design. The new cable cuts through the wind with a smaller outer diameter and still contains twice as many optical fibers as the replaced cable.

New Design

Figure 2 contrasts the new cable design with the old design. More elegant and flexible than the old design, the ADSS cable is without a central strength member or messenger wire. Lightweight and flexible, the cable is easily installed and spliced with a minimum of handling.

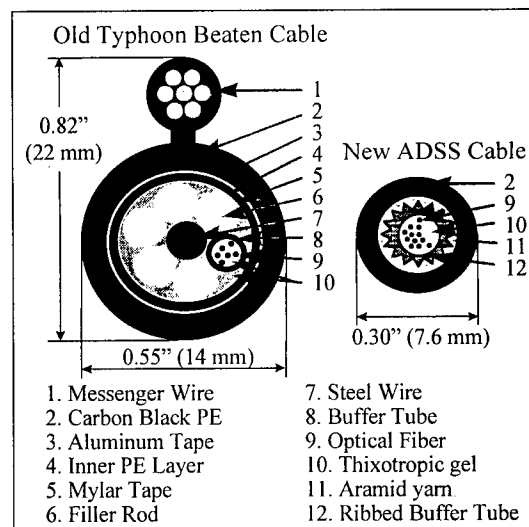


Figure 2: Old and New Cable Designs

Using a patent pended design, the buffer tube holds the fibers loosely in a thixotropic gel. The buffer tube is designed with grooves that increase the lateral strength of the cable without increasing the weight of the cable. The buffer tube grooves also grip the aramid yarn and keep the tube from slipping in the cable. Abundant aramid yarn is employed for its outstanding tensile strength and high packing density. The outer polyethylene sheath encases the yarn and resists abrasions. The outer cable diameter was kept below 0.32" (8 mm) to reduce wind load.

The cable can support up to 12 fibers and is ideal for CATV applications and moderate data rate transmission systems. The compact design and dense packing make the cable resistant to external forces.

Experiments

The new cable design was tested per FOTP 33 to measure attenuation increases due to stress placed on the fiber. The cable was stressed until failure to see how the fiber and cable responded under extreme strain. The calculated breaking force of the cable was 853 lbf (388 kg). No significant attenuation change was measured after a force of 905 lbf (411 kg) broke some of the aramid yarns and the cable slipped. The cable strain at this time was only 1.65%. The aramid yarn was supposed to support a strain of 2.4%. So while the strength of the cable exceeded expectations, the elongation of the cable was less than expected. No attenuation change was noted until the cable was strained to 2.65% and the fiber broke. During testing, the attenuation usually did not increase at all and it never increased more than 0.08 dB/km until the fibers broke.

If the density of the fiber remains the same as the fiber is stretched, the strain on the fiber will alter the shape of the fiber according to Figure 3. D1 and D2 are the core diameters and L1 and L2 are the fiber lengths. A strain of 2.65% would alter the physical dimensions of the fiber to those shown in Table 1. The small decrease of about 110 nm in the core diameter did not change the attenuation of the fiber significantly. Figure 4 shows how a considerable portion of the HE₁₁ wave already propagates through the cladding. Strain on the fiber does not affect the transmission of the signal to a considerable degree.

The performance of the cable under extreme strain was studied to see if strain increased transmission losses. Basically, there was no increased attenuation until catastrophic failure. Most studies on stressed fiber measure attenuation increases due to microbending and macrobending.² Macrobending and microbending losses occur because the fiber is distorted laterally and stable modes couple to lossy modes. Cables are designed to avoid these bending losses and even under typhoon conditions, the bending losses are minimal. The problems created by typhoons are not due to

temporary losses in the cable but due to fatigue over the life of the cable.

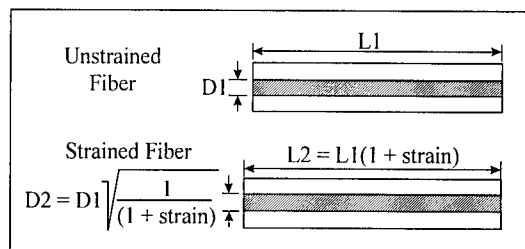


Figure 3: Strained Dimensions

Table 1: Fiber Strain and Mode Field Diameter

Fiber	Unstrained	2.65% Strain
Fiber diameter	125 μm	123.4 μm
Core diameter	8.3 μm	8.19 μm
Mode Field Diameter (μm)	9.3 +/- 0.50 10.5 +/- 1.00	@1300 nm @1550 nm

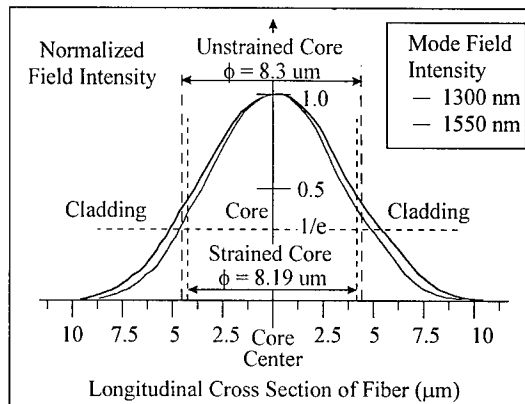


Figure 4: Fiber Distortions and Mode Fields

Novel Installation Techniques

The smaller cable diameter reduces the force on the cable but there is still a concentration of force at the deadends. Since the wires of the standard deadend terminate at the same point, pressure builds up at these points and can cut or weaken the cable. To decrease the acute pressure at the deadends, a tapered deadend was created by cutting some of the wires as shown in Photo 2. The modified deadend still grips the cable well and is much more flexible at the point of termination. The result of this simple modification is that the cable receives less acute strain at the deadends.

Another common problem associated with high winds are due to the cables being abraded on nearby objects such as advertising billboards or

streetlights. The most common nearby objects are other utility poles or guy wires that run parallel paths along roadways. To alleviate the abrasive forces on the cables when they are whipped into these obstructions, a thin Poly Vinyl Chloride, PVC, pipe or spiral wrapping band is placed over the area of the cable near the obstruction. This has proven to be another simple and effective way to protect the cable from damage and stress.

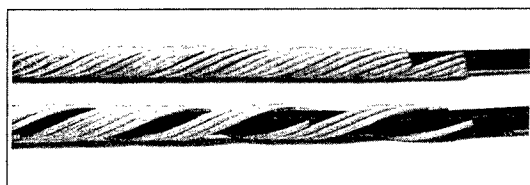


Photo 2: Standard and Modified Deadend

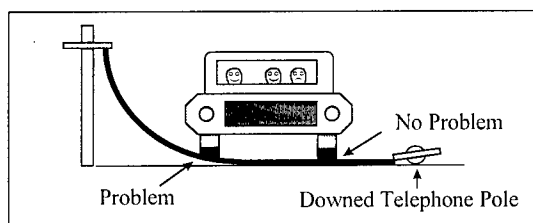


Figure 6: Traffic Problems

The last problem cables routinely face is the downing of utility poles. The majority of poles in Taiwan are concrete and thus very heavy. When these 30' (9m) poles are blown over or washed loose in heavy rains, cables are usually pulled to the ground. This usually does not harm the cable because there is sufficient slack cable that can be pulled to the ground. The weight of the pole is often supported by many other wires as well.

A problem that has been experienced is when the cable falls across the road. The crushing force of a car or truck is usually not a problem unless the scene is as shown in Figure 6. If the cable is raised from the ground as on the left of the diagram, then the cable will be ripped to the ground by the passing cars. The weight of the car cannot be supported in this situation. Breakaway deadends are one solution to this problem, but it was not deemed cost effective to implement. Since this situation is extremely rare, the most plausible solution is to repair the

downed pole as soon as possible before this unfortunate situation materialises.

CONCLUSION

Several adaptations of the cable design and the installation have been implemented in Taiwanese and Indonesian cable plants to reduce detrimental effects of typhoons. A new simple ADSS cable design reduces wind load by almost 70% and is more flexible than previous messengered designs. Protective measures to reduce typhoon abuse include modifying deadends, encasing the cable in a PVC pipe and using spiral wrapping bands to alleviate acute strain points.

Strain on the cable causes long term degradation on the transmission properties of the cable instead of short term increases in attenuation. The wear and tear on the cable after many years of typhoons causes microcracks in the fiber and sharp bends in the cable that increase attenuation. A thinner more flexible cable that uses proactive installation techniques will avoid and deter cable damage. These new steps towards longer cable life help Taiwan's cables weather the storm.

ACKNOWLEDGEMENTS

The authors would like to acknowledge the help that the Quality Control department has given for this paper. Their thorough testing and inspection offered insight into the old cable's problems. Manufacturing has also played an important role in building high quality new cables.

REFERENCES

1. http://www.yahoo.com/Earth_Sciences/Meteorology/Weather_Phenomena/Typhoons
2. Gardener, W. B., Bell Systems Tech. J. 54, 457 (1975)
3. Fiber Optic Cables, Gunther Mahkle and Peter Gossing, John Wiley & Sons, 1987
4. 144 Fiber All Dielectric Aerial Cable For Railway Applications, Ralph Bohme, p. 500, IWCS, 1996

Authors

Scott G. Kipp
Baycom
Opto-Electronics
Technology
Company, Inc.
23 R & D Rd. 2
Science Based
Industrial Park,
Hsinchu City,
Taiwan, ROC



Scott G. Kipp was born in Kansas City, Kansas in 1966. He has studied at Kansas State University, Kingston University in Kingston-upon-Thames, England and received a BS and MS Degree in Electrical Engineering from California Polytechnic State University in SLO, CA. Scott's concentration has been in photonics and travel. He completed Santa Barbara Research Center's Engineering Rotator's Program in 1995. Scott has a keen interest in digital video and lives in Taiwan to see what the East is all about.

Kaofeng Tsai
Baycom
Opto-Electronics
Technology
Company, Inc.
23 R & D Rd. 2
Science Based
Industrial Park,
Hsinchu City,
Taiwan, ROC



Kaofeng Tsai was born in Taiwan in 1955. He received a BS in Nuclear Engineering from National Tsing-Hua University in 1979 and an MS in Electrical Engineering from the University of California in Santa Barbara. Since 1986, Mr. Tsai has been involved in a variety of optical fiber projects including communications system design, CATV networks, cable design, outside plant engineering and systems integration. He has also designed and worked with many opto-electronic devices and components. Mr. Tsai is the president of Baycom.

Anthony Peng
Baycom
Opto-Electronics
Technology
Company, Inc.
23 R & D Rd. 2
Science Based
Industrial Park,
Hsinchu City,
Taiwan, ROC



Anthony Peng was born in Hsinchu, Taiwan in 1959. He graduated from the Mechanical Department of Ta-Hua Polytechnic Institute in 1980. Mr. Peng joined Baycom in 1991 and has been in charge of optical cable design and tooling since. He is the chief supervisor of Baycom's Technical Division. Anthony is responsible for research and development in cable design and production process improvement.

A MECHANICAL MODEL FOR STUDYING STRESS AND STRAIN CAUSED BY TEMPERATURE VARIATIONS IN FIBRE OPTIC CABLES

José Luis Rodríguez
Victoria Latorre
Valentín Abadía

BICC Cables de Comunicaciones, S.A
P.O. Box 581, 50080 Zaragoza, Spain

ABSTRACT.

Temperature changes undergone by fibre optic cables lead to variations in size of their elements. These variations and related stresses may cause an increase in attenuation, due to the curvatures created by the difference of the length of the fibre and the secondary protection. The method used to predict this effect is based upon the balance of strengths between the different elements making up the cable, hence it is necessary to determine all the forces involved in this balance (expansion, contraction and friction). Young's modulus and the coefficient of thermal expansion, both depending on the temperature, are the material parameters used to calculate the expansion and contraction stresses in fibre optic cables. A more exact method may be obtained by measuring these stresses directly in an experimental way. This paper shows the results of the above mentioned methods to determine the mechanical stresses linked to temperature changes and a model to study the thermomechanical behaviour of fibre optic cables.

1.- INTRODUCTION.

Thermal changes undergone by fibre optic cables during their working life lead to length variations and induced stresses in their components. This fact may lead to attenuation increases caused by the curvatures which take place when there is a variation in the length between the fibre and the secondary protection due to the different coefficient of thermal expansion of both materials. Should the cable expand and the secondary protection length be too great for the fibre, the latter may undergo oversteering, which also leads to attenuation increases, albeit to a lesser degree, and a premature mechanical ageing of the fibre.

Optic fibre cable designs try to minimize these effects. For example in loose protection cables the fibre is longer than the PBT tubes in an attempt to prevent stresses which would result from the expansion of the cable. Moreover, when the cable contracts the fibre readjusts with a certain degree of ease in the tixotropic compound filling the tube, which partly reduces the risk of curvature formation. Therefore to be able to optimize the design of the cable it is essential to predict as accurately as possible the length variations caused by thermal

changes and above all the length differences which may occur between the fibre and the secondary protection.

The calculation of dimensional variations due to temperature changes is based upon dynamic balance of the different components making up the cable. This balance is determined by the stresses resulting from expansion/contraction and by the forces of friction:

- The stress related to the phenomena of expansion and contraction can be calculated in two ways: Based on determining the coefficient of thermal expansion, α , and Young's modulus, E ; or by direct experimental measurements.
- Friction is caused by the interaction of different layers of the cable made out of different materials.

A physical model for the study of the mechanical behaviour of fibre optic cables which have undergone different thermal changes is presented in this paper. For the development of this model it is necessary to first include an experimental part to determine all the parameters involved: the coefficient of thermal expansion, $\alpha(T)$, Young's modulus, $E(T)$, the contraction stress, $\sigma(T)$ and the friction forces between the different layers making up the cable, F_{ij} .

2.- THERMAL EXPANSION COEFFICIENT.

The coefficient of linear expansion, α , has been determined by measuring the variation in thickness at different temperatures, $L(T)$, in samples of each of the materials making up the cable. The measurement was carried out in a DMA-7 Perkin-Elmer dynamic mechanical analyser. Each of the trials was performed in a static mode (TMA), at a scan rate of 1 °C/minute. A quartz kit measuring system was used on account of its low LTEC and a gas purge of He (40 cc/minute) used as an inert cooling system due to its low heat capacity. Hence, the variation of the coefficient of linear expansion at different temperatures is obtained directly from the derivative of this function, $L(T)$:

$$\alpha(T) = \frac{1}{L_0} \cdot \frac{dL(T)}{dT} \quad [1]$$

where L_0 represents the initial thickness of each of the samples at the initial temperature of each scan.

Test samples of 3 mm thick parallelepipeds cut from molded slabs (M) and extruded material (E) have been used. Each of the samples tested has been marked with the direction in which each of the trials has been carried out:

- Longitudinal (L): In a parallel direction to extrusion or parallel to the direction of the milling of the slabs.
- Transversal (T): In a perpendicular direction to the one previously described.

Furthermore, each of the test samples has been previously heated a number of times in order to remove any possible stress present in the material.

The curve-fit of the experimental results obtained following the third and latter heatings gives rise to the following equations:

$$\alpha_{\text{Aramide}}(T) = -10^{-7} \text{ }^{\circ}\text{C}^{-1}$$

$$\alpha_{\text{FRP}}(T) = 5.9 \cdot 10^{-6} \text{ }^{\circ}\text{C}^{-1}$$

$$\alpha_{\text{LDPE,M,T}}(T) = 10^{-7} \cdot \exp(7.6222 + 0.0112T) \text{ }^{\circ}\text{C}^{-1}$$

$$\alpha_{\text{LDPE,M,L}}(T) = 10^{-7} \cdot \exp(7.7864 + 0.0119T) \text{ }^{\circ}\text{C}^{-1}$$

$$\alpha_{\text{LDPE,E,L}}(T) = 10^{-7} \cdot \exp(7.7011 + 0.0098T) \text{ }^{\circ}\text{C}^{-1}$$

$$\alpha_{\text{MDPE,M,T}}(T) = 10^{-7} \cdot \exp(7.3584 + 0.0078T) \text{ }^{\circ}\text{C}^{-1}$$

$$\alpha_{\text{MDPE,M,L}}(T) = 10^{-7} \cdot \exp(7.4540 + 0.0077T) \text{ }^{\circ}\text{C}^{-1}$$

$$\alpha_{\text{MDPE,E,L}}(T) = 10^{-7} \cdot \exp(7.3807 + 0.0069T) \text{ }^{\circ}\text{C}^{-1}$$

$$\alpha_{\text{PBT,M,L}}(T) = \begin{cases} (795.46 + 3.4265T) \cdot 10^{-7} & T \leq 30^{\circ}\text{C} \\ [-1664.2 + 766.41 \cdot \ln(T)] \cdot 10^{-7} & T \geq 30^{\circ}\text{C} \end{cases}$$

The following effects can be noted:

- The existence of *anisotropism* seen in PE is shown with a higher value than the origin ordinate in the longitudinal direction and a slight change of curvature.
- The coefficient of thermal expansion of PBT is affected by the *glass transition* which this material undergoes at about 30 °C (Fig. 1). This transition gives rise to a change in the way the expansion coefficient depends on the temperature, which implies the need to use an expression of $\alpha(T)$ for temperatures lower than T_g and another for higher temperatures (1) (2).
- β relaxation in PE was observed but the low energy involved in this kind of transition makes detection difficult using this experimental method and has no significant influence on the dependence between α and the temperature (3).

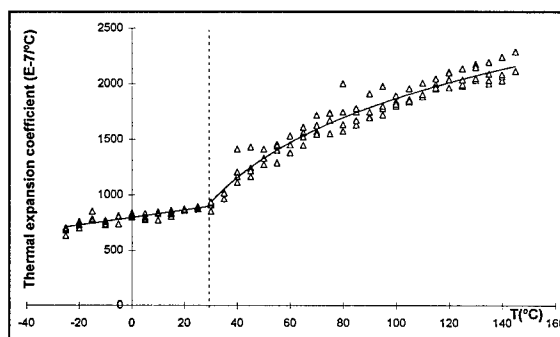


Figure 1.- Temperature dependence of the coefficient of thermal expansion ($10^{-7} \cdot ^{\circ}\text{C}^{-1}$), PBT.

- The coefficient of thermal expansion of PE both for LDPE and MDPE can be fairly accurately expressed by the following exponential law:

$$\alpha(T) = 10^{-7} \cdot \exp(a + bT)$$

where a and b are two characteristic parameters of the PE type, the values of which increase with density.

- The coefficient of thermal expansion tends to have the same value both for LDPE and MDPE at very low temperatures, therefore this value may represent a typical characteristic of the inherent nature of the material.

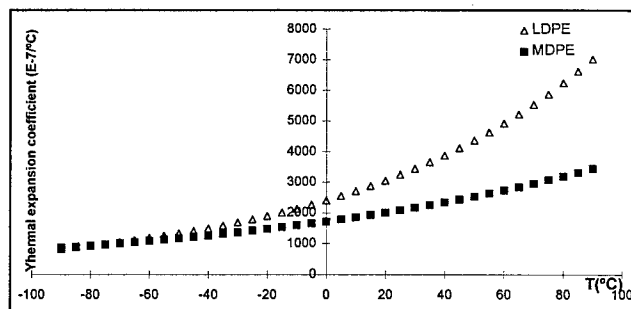


Figure 2.- Temperature dependence of the coefficient of thermal expansion ($10^{-7} \cdot ^{\circ}\text{C}^{-1}$), PE.

- The coefficient of thermal expansion both of Aramide and FRP were considered as constant at different temperatures. These values correspond to those given in the manufacturers' specifications.

3.- YOUNG'S MODULUS.

Within the limits of the validity of Hooke's Law the normal stress, σ , and the relative strain $\varepsilon = \frac{\Delta L}{L_0}$ are proportional:

$$\sigma = E \cdot \varepsilon \quad [2]$$

where the proportionality constant E is referred to as Young's Modulus (4). Out of these limits, for greater strains, the relationship between σ and ε is no longer

linear. Two clearly defined regions may be seen in a σ vs ϵ plot:

- Elastic region: Where Hooke's Law is followed.
- Plastic region: The material can no longer completely recuperate its former state.

For most polymeric materials the first part of the σ - ϵ curve is not linear and therefore Young's Modulus can no longer be defined as the slope of this curve, and other quantities such as the tangent modulus, the origin tangent modulus or the secant modulus need to be defined (5).

In this paper, the secant modulus has been determined between 0.025 and 0.5 % elongation as a function of temperature, $E(T)$, for different materials used in fibre optic cables. These measurements were performed on a ZWICK/Materialprüfung 1445 equipment which is made up of a dynamometer and a temperature programmable camera.

The values thus obtained depend largely on the chosen experimental conditions. This fact makes the way of obtaining the modulus by this experimental technique uncertain due to the selection of the parameters used. A previous study of all the parameters involved was carried out in order to obtain the most suitable experimental conditions:

- *Secant Modulus*: Secant Modulus is defined as the slope of a line joining the origin and a selected point on the σ - ϵ curve. Due to the initial shape of the curve initial point considered is not the origin but a 0.025 % elongation ($\epsilon=2.5 \cdot 10^{-4}$). On the other hand, it is necessary to choose a suitable point of the curve, near the origin, so as not to go beyond the elastic limit but far enough so that the equipment may have enough data and calculations to be accurate. The point which leads to the lowest dispersion in the results is a 0.5 % elongation.

	0.1 %	0.5 %
Test sample 1	358.6	504.7
Test sample 2	386.3	480.2
Test sample 3	594.8	487.7
Test sample 4	601.7	493.9
Test sample 5	689.3	484.2
Test sample 6	543.8	461.7
Test sample 7	360.9	504.4
Test sample 8	705.5	493.5
Test sample 9	150.8	442.7

Table 1.- MDPE Secant Modulus (Mpa) between 0.025 % and 0.1-0.5 %.

- *Preload (F_p)*: As the test samples are not tense enough in the dynamometer a preload strength needs to be applied to avoid this problem. The ideal preload should be as little as possible, enough to tense the test sample but without surpassing the yield point of the material. It seemed convenient to use a preload of 0.5 N at 70 °C and lower values for

lower temperatures, reaching a zero value at temperatures below 40 °C.

- *Preload velocity (v_p)*: It was considered that preload velocity must be the lowest one possible. 0.1 mm/minute seemed most suitable.

- *Clamp separation velocity (v)*: The experimental parameter which shows the most important influence on the modulus value is the clamp separation velocity. It was seen that the secant modulus corresponding to $v=200$ mm/minute is double the one corresponding to a velocity of 1.5 mm/minute. Hence, a velocity of 1.5 mm/minute was considered suitable as it is a slow velocity and is widely used by other authors.

Therefore, all the experiments were carried out with a precharge velocity of 0.1 mm/minute, a preload of 0-0.5 N and a clamp separation velocity of 1.5 mm/minute. The curve-fit of the experimental values leads to the following equations:

$$E_{\text{Aramide}}(T) = 100 \text{ GPa}$$

$$E_{\text{FRP}}(T) = 52 \text{ GPa}$$

$$E_{\text{LDPE}}(T) = \exp(6.1105 - 0.0291 \cdot T) \text{ MPa}$$

$$E_{\text{MDPE}}(T) = \exp(6.7900 - 0.0245 \cdot T) \text{ MPa}$$

$$E_{\text{PBT}}(T) = \begin{cases} 2217.5851 - 3.6007 \cdot T & T \leq 30^\circ \text{C} \\ \exp(8.4368 - 0.0292 \cdot T) & T \geq 30^\circ \text{C} \end{cases}$$

The following points should be highlighted:

- The glass transition experimented by the PBT at about 30 °C has an enormous effect on the modulus behaviour at different temperatures.

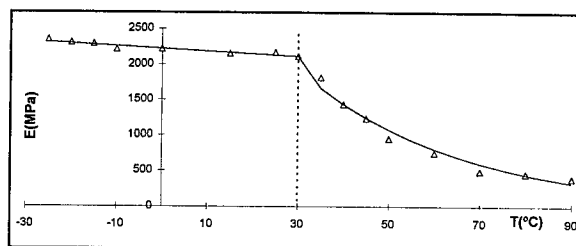


Figure 3.- Young's Modulus as a function of temperature for PBT.

- The analysis of the experimental values for PE leads to a dependence curve of the secant modulus at different temperatures of the following kind:

$$E(T) = \exp(a - b \cdot T)$$

where a and b are two parameters dependant on the experimental conditions and the type of polyethylene tested. It may be seen that b is approximately equal in both types of polyethylene (low and medium density) and seems to be less influenced by the experimental conditions. However, a increases

according to the density of the type of polyethylene tested.

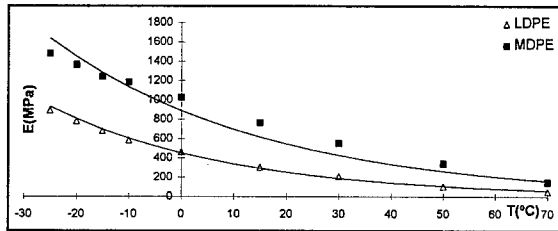


Figure 4.- Young's Modulus as a function of temperature for PE.

- The modulus of Aramide and FRP was considered constant with temperature. These values correspond to those given in the manufacturers' specifications, contrasted with the average results obtained internally on receipt of the materials.

We have already highlighted the enormous influence of the experimental parameters on the value we obtain for Young's modulus in this kind of trial. For this reason, an experimental method to determine the stress suffered by the material on expansion was developed. This method enables the modulus value to be determined with a lesser degree of uncertainty with regard to possible varying factors in the trial. This new method and the results thus obtained are presented in the following point.

4.- STRESS ASSOCIATED TO THERMAL CHANGES:

The necessary stress to prevent size changes, ΔL , of any material when it is subjected to thermal change, ΔT , is expressed in the following integral:

$$\sigma(T) = \int_T^{T+\Delta T} \alpha(T) \cdot E(T) \cdot dT \quad [3]$$

from T to T+ ΔT .

4.1.- Numerical method: Once the temperature dependence of α and E is known (as shown above), the stress may be calculated by equation [3]. The calculation of these integrals for the materials tested is expressed in the following formulas for the stress (MPa):

$$\sigma_{\text{Aramid}}(T) = -0.01 \cdot \Delta T$$

$$\sigma_{\text{FRP}}(T) = 0.31 \cdot \Delta T$$

$$\sigma_{\text{LDPE}}(T) = -1.62 + 5.18 \cdot 10^{-6} \cdot \exp(13.812 - 0.019T)$$

$$\sigma_{\text{MDPE}}(T) = -2.39 + 5.96 \cdot 10^{-6} \cdot \exp(13.244 - 0.017T)$$

$$\sigma_{\text{PBT}}^*(T) = \begin{cases} 12.35 - 0.18T & T \leq 30^\circ \text{C} \\ 14.02 - 0.28T + 0.0014T^2 & T \geq 30^\circ \text{C} \end{cases}$$

(*) NOTE: Due to the complexity of the equation obtained for PBT the formula calculated by integration was adjusted to the equation given above.

The formulas for the stress obtained by direct calculation are somewhat inaccurate as a result of the experimental uncertainty in obtaining the modulus because of trial condition, as was discussed in the preceding section. For this reason, an experimental method to measure the stress in a direct way was developed which will enable the Young's modulus of each material to be determined.

4.2.-Experimental method: The stress measurement was carried out on a ZWICK/Materialprüfung 1445. The trials were performed in a static mode without any movement between the clamps. Samples of different materials cut from a PKP cable with a length of approximately 42 cm to minimize the effect of the expansion or contraction of the clamps and metallic arms were used.

The sensitivity of the experimental equipment and the thermoplasticity of the materials studied only allow the stress associated to their contraction to be determined. For this reason the cycles begin above room temperature and at suitable temperature for each material. The experimental method used for the measuring of $\sigma(T)$ is described below:

- Each of the test samples is placed in the dynamometer attached to the upper clamp and heated at a temperature of 10 or 15°C above the initial temperature of the trial.
- The test sample is kept in this way as long as is needed to avoid the subsequent bending between the clamps caused by the thermoplasticity of the material.
- Once the test sample is free from stress, it is attached to the lower clamp and is cooled until it reaches the initial temperature for the experiment, so that the test sample is properly tensed between the clamps.
- When the equipment is stabilized it is reset and the test sample is submitted to a series of thermal cycles in which the strength made by each test sample and its corresponding temperature are periodically recorded.

This method tries to describe as faithfully as possible the real conditions endured by a fibre optic cable, and to show the stress changes in an environment in which there are gradual temperature changes.

The analysis of the experimental results offers the following equations for the stress (MPa):

$$\sigma_{\text{Aramid}}(T) = -0.011 \cdot \Delta T$$

$$\sigma_{\text{FRP}}(T) = 0.413 \cdot \Delta T$$

$$\sigma_{\text{LDPE,E}}(T) = 10.981 - 2.587 \cdot \ln(T + 33)$$

$$\sigma_{\text{MDPE,E}}(T) = \exp(13.16 - 0.036T)$$

$$\sigma_{\text{PBT}}(T) = \begin{cases} 23.615 - 0.444T & T \leq 30^\circ \text{C} \\ 20.278 - 0.387T + 0.002T^2 & T \geq 30^\circ \text{C} \end{cases}$$

By comparing the formulas given by both methods, the following differences may be noted:

- FRP: Both methods lead to a linear dependence of stress with temperature. However, the experimental result is greater than the one obtained by integration.
- LDPE: The experimental stress value is lower than the one obtained by direct calculation.
- MDPE: In this case, the experimental stress is greater than the one obtained by direct calculation, above all at low temperatures.

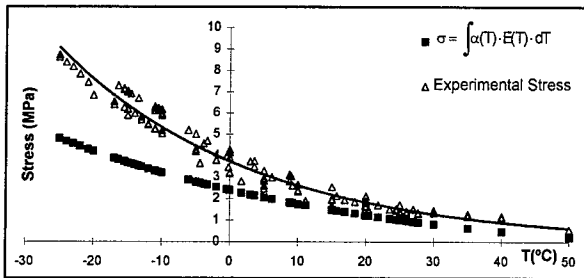


Figure 5.- Stress (Mpa) as a function of temperature for MDPE.

- PBT: An analogous dependence was seen in both methods although the greater stress value is given by the experimental method.

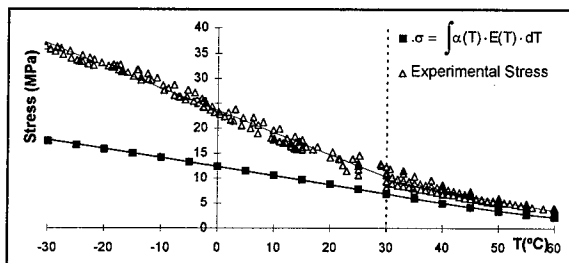


Figure 6.- Stress (Mpa) as a function of temperature for PBT.

- Aramide: Experimental difficulties did not allow the stress to be determined accurately by this method. However, a linear dependence with temperature can be deduced, and a greater value than the one obtained by integration estimated.

4.3.- Young's Modulus Correction: Taking into account the negligible uncertainty of the thermal expansion coefficients, the difference between the stress value given by both the experimental and numerical methods enables the modulus to be determined from the experimental stress and coefficient of thermal expansion. Young's Modulus is expressed by:

$$E(T) = -\frac{1}{\alpha(T)} \cdot \frac{d\sigma(T)}{dT} \quad [4]$$

The formulas for the modulus as a function of temperature obtained from the stress equations given in section 4.2 are the following:

$$E_{\text{Aramide}}(T) = 110 \text{ GPa}$$

$$E_{\text{FRP}}(T) = 70 \text{ GPa}$$

$$E_{\text{LDPE}}(T) = \frac{2.5867 \cdot 10^7}{T + 33} \cdot \exp(-7.7011 - 0.0098T) \text{ MPa}$$

$$E_{\text{MDPE}}(T) = 0.0358 \cdot \exp(-6.065 - 0.0427T) \text{ MPa}$$

$$E_{\text{PBT}}(T) = \begin{cases} \frac{0.444 \cdot 10^7}{795.46 + 3.4265T} & T \leq 30^\circ \text{C} \\ \frac{(0.387 - 0.0036T) \cdot 10^7}{-1664.2 + 766.4 \cdot \ln(T)} & T \geq 30^\circ \text{C} \end{cases} \text{ MPa}$$

These results show that the modulus calculated from the stress is greater than the one measured in traction trials. The biggest differences appear in the more rigid materials (Aramide, FRP and PBT) whereas for PE, they concord more although they begin to differ at temperatures lower than 0 °C.

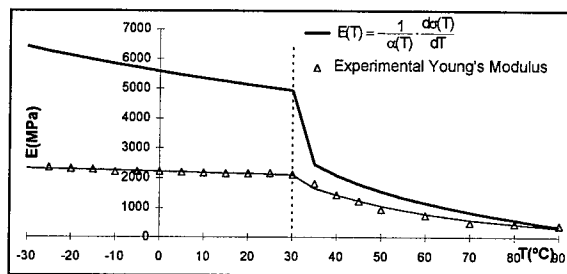


Figure 7.- Young's Modulus (MPa) as a function of temperature for PBT.

The following points should be highlighted:

- Should the clamp separation velocity (1.5 mm/minute) be modified, both methods would give the same modulus values. The velocity of the trial must be suitable for both the material as well as the thermal range in which the modulus is determined. For example, for MDPE a velocity of 1.5 mm/minute could be used for temperatures above 10 °C, whereas the velocity should be increased for lower temperatures.
- A reason for the different values of both methods is due to the use of direct measuring in section 4 whereas in section 3 the secant modulus between 0.025 and 0.5 % elongation was determined.
- On the other hand, even though this method reduces the number of experimental parameters for the trial, it may also offer some uncertainty due to the expansion/contraction of the measuring equipment. For this reason, experimental conditions must be carefully controlled. For example, the temperature of the arms holding the clamps must be constant, ensure that the length of these arms in the chamber be as short as possible, etc.

5.- FRICTION.

Maximum friction is understood as the strength which has to be applied to one layer of the cable to make it slide on another. Friction between cable components is approximately proportional to their distance from the end of the cable when the axial strength is considered an additive quantity:

$$F_{R,ij} = CF_{ij} \cdot L \quad [5]$$

where CF_{ij} is the friction coefficient between i and $i-1$ layers, given in N / m.

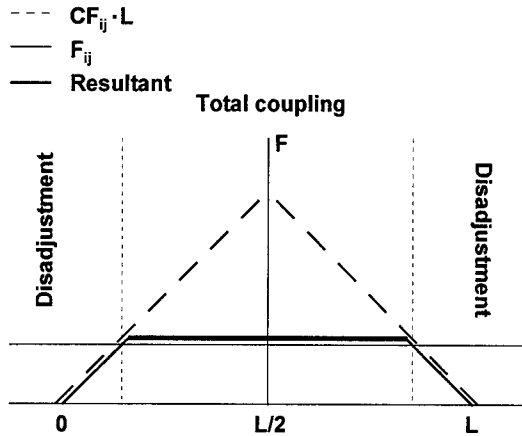


Figure 8.- Strength's diagram on the boundary layers as a function of the distance from the end of the cable.

It can be seen that when the distance to the ends of the cable is enough, friction does not allow the different elements to slide freely and at these distances the cable behaves as a whole in which length changes due to expansion or contraction are equal for all elements. For points nearest the end, expansion or contraction strengths are greater than the corresponding friction and movements between different layers are produced.

The coefficient of friction CF_{ij} was determined for a PKPR 24FO cable, designed and manufactured during 1993 and 1994. An INSTRON 1075 traction device was used.

The results show a dispersion between different samples, as seen in table 2 below. In this table and future reference the following ij notation is used:

- 1: FRP dielectric strength member
- 2: PBT loose protection tubes
- 3: LDPE inner jacket
- 4: Aramide yarn layer
- 5: MDPE outer jacket

	Range (N / m)	Taken value (N / m)
$CF_{1,2}$	75 - 110	82
$CF_{2,3}$	250 - 450	300
$CF_{3,4}$	400 - 475	375
$CF_{4,5}$	225 - 550	375

Table 2.- Friction coefficients between PKPR24FO cable layers.

6.- CALCULATION MODEL.

In order to develop a physical model to study fibre optic cables behaviour when they are subjected to temperature changes, we first need to consider the effects of stress on the cable elements and the strains they produce.

6.1.- Theoretical aspects. Should a rigid element of L_o length be considered:

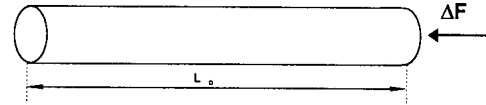


Figure 9.- Isolated tube of L_o length.

subjected to a temperature change from T to $T+\Delta T$ experiments a unit length variation:

$$\frac{\Delta L_{dil}}{L_o} = \alpha(T) \cdot \Delta T \quad [6]$$

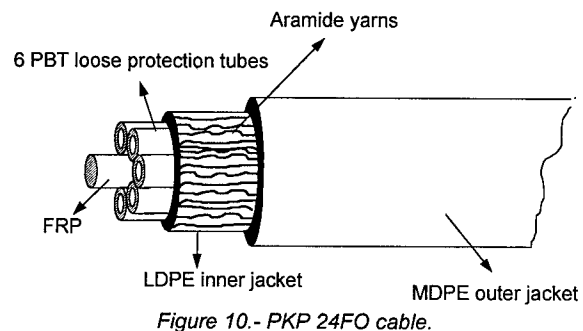
where $\alpha(T)$ is the thermal expansion coefficient of the material making up the element.

If a restoring force ΔF is applied simultaneously, the unit length variation will now be:

$$\frac{\Delta L_{Efec}}{L_o} = \alpha(T) \cdot \Delta T - \frac{\Delta F}{A \cdot E(T)} \quad [7]$$

in which A is the element cross section area (assuming A is constant with temperature), and $E(T)$ is the Young's modulus. For $\frac{\Delta L_{Efec}}{L_o}$ to be zero; that is, to prevent the material from expanding or contracting (depending on the ΔT sign), the strength ΔF must equal the mechanical stress $\sigma(T)_{T+\Delta T}$ determined in the experiments to measure the expansion and contraction without any size alteration as described in section 4 (equation [3], $A=1$).

If a fibre optic cable, as shown in the figure below is now considered:

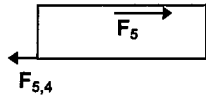


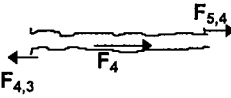
and all components are assumed parallel, according to equation [7] for each component:

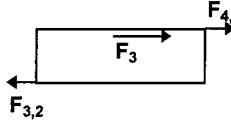
$$\frac{\Delta L_{Efec,i}}{L_o} = \alpha_i(T) \cdot \Delta T - \frac{\Delta F_i}{A_i \cdot E_i(T)} \quad [8]$$

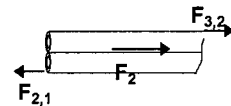
when the temperature changes from T to $T+\Delta T$.

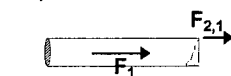
Friction between the layers is the only strength which prevents free expansion or contraction. Therefore, dynamical equilibrium for the whole cable and for its different layers can be expressed as:

MDPE  $F_5 - F_{5,4} = 0$ [9]

Aramide  $F_4 + F_{5,4} - F_{4,3} = 0$ [10]

LDPE  $F_3 + F_{4,3} - F_{3,2} = 0$ [11]

PBT  $F_2 + F_{3,2} - F_{2,1} = 0$ [12]

FRP  $F_1 + F_{2,1} = 0$ [13]

Cable $F_1 + F_2 + F_3 + F_4 + F_5 = 0$ [14]

Figure 11.- Strengths acting on the different cable components.

which fulfil the condition $\Sigma F=0$ in each component and in the cable as a whole.

The sign criterion derives from equation [8] when the temperature increases after heating. That is, F_i are positive when they are opposed to expansion (or favour contraction), and negative otherwise. For friction stress, F_{ij} , the sign corresponding to the lower layer is taken, i.e., the sign corresponding to $i-1$ layer is taken by $F_{i,i-1}$.

Two different cases appear in the study of length variations of cable elements when it undergoes a temperature change:

a) *Total coupling*: When a longitudinal element is far enough from the cable end so that there is an equilibrium of friction strength between the different layers, all the cable components will expand or contract as a whole and

the unitary length variation $\frac{\Delta L_{Efec,i}}{L_{o,i}}$ will be the same for all of them:

$$\varepsilon = \frac{\Delta L_{Efec,1}}{L_o} = \frac{\Delta L_{Efec,2}}{L_o} = \dots = \frac{\Delta L_{Efec,5}}{L_o} \quad [15]$$

where $\frac{\Delta L_{Efec,i}}{L_{o,i}}$ corresponds now to the effective unitary cable expansion between T and $T+\Delta T$, referred to as ε .

Taking into account equations [8] and [14], ε may be computed by substituting F in an element by the addition of the other strengths F_i . For example, consider component 1:

$$\varepsilon = \frac{\Delta L_{Efec,1}}{L_o} = \alpha_1(T) \cdot \Delta T + \frac{\sum_{i=2}^5 \Delta F_i}{A_1 \cdot E_1(T)}$$

and

$$\Delta F_i = A_i \cdot E_i(T) \cdot \alpha_i(T) \cdot \Delta T - A_i \cdot E_i(T) \cdot \varepsilon$$

we have:

$$\varepsilon = \frac{\sum_{i=1}^5 A_i \cdot E_i(T) \cdot \alpha_i(T)}{\sum_{i=1}^5 A_i \cdot E_i(T)} \cdot \Delta T$$

and therefore:

$$\varepsilon \Big|_{T_1}^{T_2} = \int_{T_1}^{T_2} \frac{\sum_{i=1}^5 A_i \cdot E_i(T) \cdot \alpha_i(T)}{\sum_{i=1}^5 A_i \cdot E_i(T)} \cdot dT \quad [16.a]$$

or:

$$\varepsilon \Big|_{T_1}^{T_2} = \int_{T_1}^{T_2} \frac{\sum_{i=1}^5 A_i \cdot \sigma_i(T)}{\sum_{i=1}^5 A_i \cdot E_i(T)} \cdot dT \quad [16.b]$$

The derivative of equation [16.a] gives the effective coefficient of thermal expansion considering the cable as a whole:

$$\alpha_{Efec}(T) = \frac{\sum_{i=1}^5 A_i \cdot E_i(T) \cdot \alpha_i(T)}{\sum_{i=1}^5 A_i \cdot E_i(T)} \quad [17]$$

(Rule of mixtures, (5) (6)).

Both equations [16] and [17] would be exact if the Poisson coefficient were identical for all cable materials. However, if the section changes of different components as functions of temperature are considered as negligible compared to variations of E and α , these equations can be taken as good approximations.

b) *Disadjustment*: If a point near the end is considered, friction can no longer balance strengths from other sources and, according to equations [9] to [13], a relative displacement between elements will be produced.

If, for example, $F_{3,2}$ is less than $CF_{3,2} \cdot L$ (equation [5]), L being the distance from the considered point to the nearest end, the dynamical equilibrium given by equations [9] to [13], will now be expressed:

$$\begin{aligned} F_5 - F_{5,4} &= 0 \\ F_4 + F_{5,4} - F_{4,3} &= 0 \\ F_3 + F_{4,3} - CF_{3,2} \cdot L &= 0 \\ F_2 + CF_{3,2} \cdot L - F_{2,1} &= 0 \\ F_1 + F_{2,1} &= 0 \end{aligned}$$

with $F_1 + F_2 + F_3 + F_4 + F_5 = 0$.

Physically, this means that elements 3, 4 and 5 present a unitary length variation ε_{345} and elements 1 and 2 a different one ε_{12} . Hence the preceding equations may be solved by ε_{345} and ε_{12} :

$$F_3 + F_4 + F_5 = CF_{3,2} \cdot L$$

$$F_1 + F_2 = -CF_{3,2} \cdot L$$

and we obtain:

$$\varepsilon_{345}(T, L) = \frac{-L \cdot CF_{3,2} + \sum_{i=3}^5 A_i \cdot \int_T^{T+\Delta T} E_i(T) \cdot \alpha_i(T) \cdot dT}{\sum_{i=3}^5 A_i \cdot \bar{E}_i}$$

$$\varepsilon_{12}(T, L) = \frac{L \cdot CF_{3,2} + \sum_{i=1}^2 A_i \cdot \int_T^{T+\Delta T} E_i(T) \cdot \alpha_i(T) \cdot dT}{\sum_{i=1}^2 A_i \cdot \bar{E}_i}$$

where \bar{E}_i is the average modulus of all materials in the interval from T to $T+\Delta T$.

If disadjustment between more layers takes place, the calculations of different ε may be carried out in a similar way. It can be seen that the ε are functions of the distance to the cable end due to the appearance of L in the preceding equations.

6.2.- Calculation programme. A calculation model based on the equations given in section 6.1 above was developed. This model is valid for the study of the mechanical behaviour and the dimensional variations of a fibre optic cable as shown in figure 10. The programme based on this calculation model is also valid for the study of other designs or other types of cable if the corresponding formulas are used.

The programme shown in figure 12 works in the following way:

- i) *Data for the programme:* As initial data the cross section measurements of the different components making up the cable, A_i , the formulas of $\alpha_i(T)$, $E_i(T)$ and $\sigma_i(T)$ of the materials and the temperatures ($T_1=T$ and $T_2=T+\Delta T$) at which the cable is going to be simulated must be given.
- ii) *T loop for total coupling:* In the case of total coupling, the programme carries out the numerical integration of equation [16]. This integration with equation [8] gives:
 - $\varepsilon(T)$ and $F_i(T)$ for each step of the integration,
 - ε and each F_i for the total integration interval (from T_1 to T_2),
 - From equations [9] - [13] the effective strength between different layers, F_{ij} , are determined.
- iii) The F_{ij} interfaces strengths, calculated for total coupling in the previous loop, are compared with the

maximum friction strengths according to the length, $CF_{ij} \cdot L$. When $CF_{ij} \cdot L < F_{ij}$ the programme goes on to the loop for disadjustment and indicates the layers between which there is sliding.

iv) *L loop for disadjustment:* In this loop each ε_i and each F_i as functions of L is calculated. In each of these steps the programme checks again if some new layer becomes uncoupled. Should this be so, the calculation is carried out taking into consideration all the layers which slide.

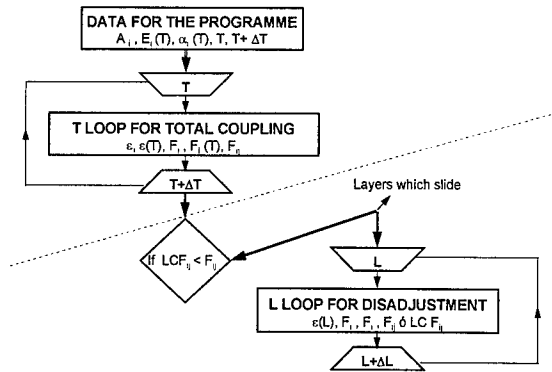


Figure 12.- Programme algorithm.

6.3.- Simulation results: A PKP cable as shown in figure 10 was used applying the equations developed in the calculation model as described in point 6.1. For the curve fit, the equations of points 2, 3, 4 and 5 were used. A series of simulation tests were carried out with this particular equations. Here are some of the most representative examples.

Example 1: In the case where the cable acts as a whole, the expansion behaviour has been simulated from 20°C to 50°C using the data corresponding to the ones deduced from a direct measurement of the contraction strengths (point 4). In this test the following cases have been assumed depending on the resistance of the aramide yarns to expansion.

- k=0: the aramide yarn layer does not affect the expansion,
- k=0.2: It intervenes proportionately until there is an elongation of 0.2% after which it stands up to the expansion totally,
- k=0.1: It intervenes proportionately until there is an elongation of 0.1% after which it stands up to the expansion totally, and
- k=1: The aramide resists totally from the beginning

In figure 13 $\varepsilon(T)$ is represented in the four cases under consideration. It can be observed that $\varepsilon(T)$ is much less when the aramide yarns resist the expansion of the other components. The change of the slope at about 30°C, the cause of which is the PBT glass transition, can also be seen.

In figure 14 the strengths which resist (or favour) the expansion of each of the elements are represented, taking into account that the layer of aramide yarns does not intervene mechanically (k=0). In this case it can be noted that the element which bears the strains to

counteract the expansion of the others is the FRP reinforcing element. Figure 15 corresponds to the same kind of representation assuming that the aramide layer totally stands up to the expansion of the other elements ($k=1$). It can be seen that in this last case the aramide yarns bear the brunt of the expansion of the other elements.

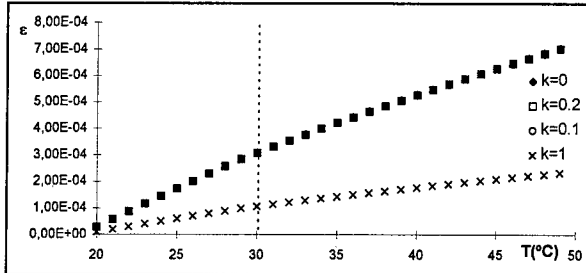


Figure 13.- Length increase according to the temperature and influence of the aramide yarns.

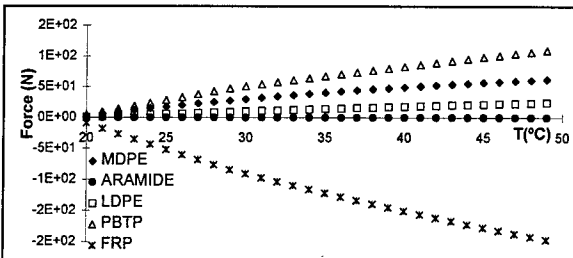


Figure 14.- Variation of F_i as a function of temperature (with an assumed lack of effect of the aramide layer).

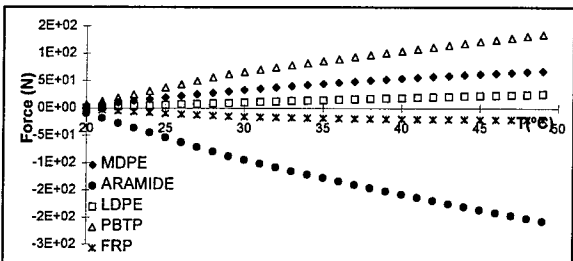


Figure 15.- Variation of F_i according to the temperature (with an assumed total effect of the aramide layer).

Example 2: In this example the contraction of the cable from 28 to -20°C is simulated assuming that the layer of aramide yarns does not stand up to the contraction of the other component ($k=0$) as is really the case. In figure 16 $\epsilon(T)$ is shown, a unitary contraction of the cable as a whole for lengths in which total coupling can be considered, calculated using the experimental traction data (point 3) and trials to establish the contraction strengths directly (point 4). It can be seen that this contraction is slightly less when it is calculated using the direct experimental data due to the higher value of the modulus obtained from materials with a lower α . On the other hand, the strengths which should stand up to the contraction of the components are slightly higher (figure 17 for FRP).

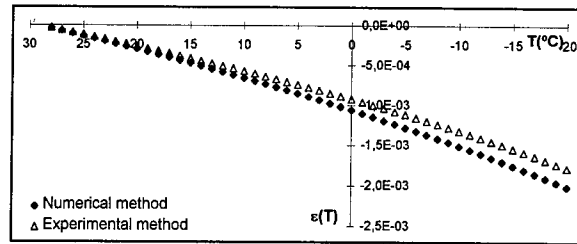


Figure 16.- Unitary contraction as a function of temperature, $\epsilon(T)$.

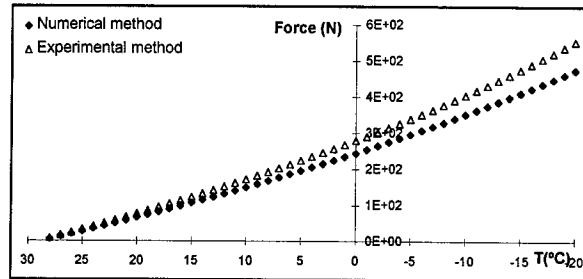


Figure 17.- Contraction strength applied to the FRP strength member.

Finally, the possible dimensional disadjustment of the components is studied. The results are shown in the following figures, in which the distance to the end of the cable is now shown in abscissae, $L(\text{cm})$.

Figure 18 shows the unitary elongation values of the different components of the cable in relation to the distance from the end. The decrement of the length of the PBT tubes increases with their proximity to the end of the cable. This fact is due to the tubes sliding on the FRP dielectric strength member and they have to withstand the contraction of the sheath. It can also be seen that the bulk jackets and the aramide layer slide 50 cm from the end of the cable. Hence, even though there maybe a certain rearrangement of the fibre along the secondary protection tubes, the highest attenuation increase values will be procured at the points nearest the end of the cable as a result of cooling the cable at low temperatures.

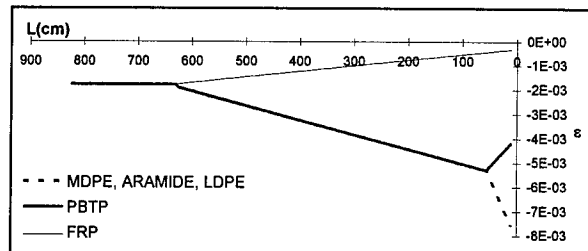


Figure 18.- Unitary length decrement of the different components in relation to the distance from the end of the cable (cooling).

Figures 19 and 20 show the F_i strengths which stand up to (< 0) or favour (> 0) the contraction of the different components and effective friction strengths on the end layers, F_{ij} , depending on the distance from the end of the cable.

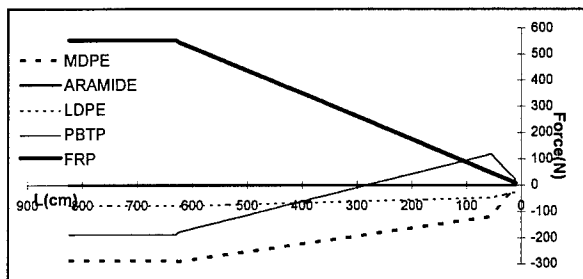


Figure 19.- Contraction strength applied to the different components as a function of the distance to the end of the cable (cooling).

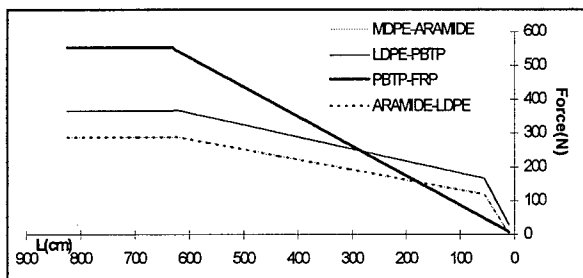


Figure 20.- Friction strength between layers in relation to the distance from the end of the cable (cooling).

7.- CONCLUSIONS.

The calculation programmes based on a physical model as presented in this paper allows the simulation of real conditions and experimentation, in an comfortable, economic way, on different possible designs and materials in order to optimize the design of cables. These programmes require reliable data of the physical properties of materials and cable. This data has to be determined previously in trials.

In this paper the experimental results are shown to determine the coefficient of linear expansion and Young's modulus (traction) of materials used in the manufacturing of a PKP fibre optic cable. The Young's modulus measurement offers a certain degree of experimental uncertainty stemming basically from the velocity of separation of the clamps used in traction trials, above all with polymeric materials. It is, therefore, difficult to determine accurately the modulus value which results from slow processes like the dimensional change caused by temperature change around the cable.

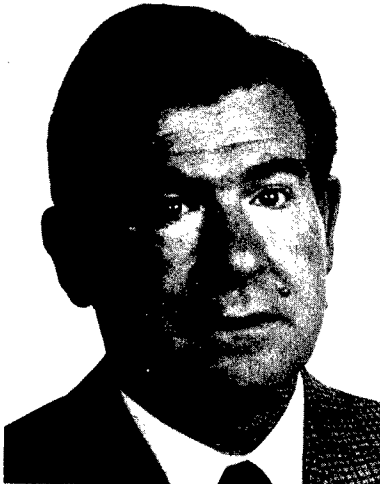
As a result of this uncertainty a trial method has been developed for the direct measurement of the stress associated with slow expansion and contraction processes. The results tend to show that the modulus value in slow processes is slightly higher than expected, after it had been determined in traction trials at slow velocities. This leads to an increase in the σ - ϵ slope. A similar increase can also be seen when the traction trials are carried out at different velocities (7).

It has also been pointed out that the way in which this method was carried out offers a certain degree of inaccuracy. However, once it has been perfected it may offer reliable results to determine the thermomechanical behaviour of fibre optic cables. It should also be noted that the trials carried out using this method are easier and require less time than it takes to determine the modulus in relation to temperature in traction trials.

8.- BIBLIOGRAPHY AND REFERENCES.

- 1.- Nielsen, L.E. **Mechanical Properties of Polymers**. Van Nostrand Reinhold, New York 1962. Chapter 2: *Transitions in High Polymers*.
- 2.- González de Posada, F. **Fundamentos de la Termodinámica Clásica**. Departamento de Publicaciones de la Universidad Politécnica de Madrid, 1992. Chapter 10: *Cambios de fase*, p. 91.
- 3.- Perry, B.C. *Relaxation Behavior of the β Phase of Poly(butylene terephthalate)*, *Macromolecules*, Vol 20, No.2 (1987), pp 422-427.
- 4.- Marin, J. *Mechanical Relationships in Testing for Mechanical Properties of Polymers*, Chapter 3, in Vol 1 of **Testing of Polymers**, Schmitz, J. V. (ed.), John Wiley and Sons, New York, 1965.
- 5.- Cooper, S.M.; Coupe, K.L.; Zimmermann, B. D. *The effect of Temperature dependent Materials Properties on Fiber Optic Cable Design*. 35th I.W.C.S. Proceedings (1986), pp 148-158.
- 6.- Lenahan, T.A. *Thermal Buckling of Dual-Coated Fiber*. AT&T Technical Journal, Vol 4, No. 7 (September 1985), pp. 1565-1584.
- 7.- Ref. 1, pp 111-113.

Acknowledgements: The authors wish to thank Mr. Ignacio Rodríguez and Mr. Mark Chapelle for their invaluable help in translating this paper.



José Luis Rodríguez, came to BICC Cables de Comunicaciones S.A. in 1973 after working for 3 years as an assistant teacher for the Chemistry Department at the University of Zaragoza. Since then, until 1989, he was responsible for the selection and development of dielectric cable materials. In 1985/89 he was incharge of the selection of the materials for optical cables. In 1993/97 he was responsible for the Instrumental Analysis Laboratory. Currently, he heads the Environment Departament. Dr. José Luis Rodríguez is qualified in Chemical Sciences by the University of Zaragoza (1969) and Ph. D. in Sciences (1987) from the same University.

Victoria Latorre began her professional career in June 1995 as a work experience student in the Instrumental Analysis Laboratory, BICC Cables de Comunicaciones. Her first tasks were dedicated to the study of thermal properties of polymeric materials. In July 1996 she was employed to carry out the measurement of properties shown in this paper amongst other studies. Since April 1997 she has formed part of the Environmental Departament. Miss Latorre is qualified in Physical Sciences, University of Zaragoza, specializing in Materials.



Valentín Abadía began working for BICC Cables de Comunicaciones as an engineer in R&D Departament responsible for the Electrical Laboratory. In 1977 he was incharge of the Cables Engineering Department. After holding other positions related to the design of communication networks he was named Quality and Technology Director in 1996. Presently, he is Plant Director. Mr. Valentín Abadía is a Telecommunications Engineer, University of Madrid (1974) and qualified by the University of Zaragoza in Business Administration (1983).

MANUFACTURING AND CHARACTERIZATION OF MULTICORE FIBERS

J.-F. Bourhis, R. Meilleur, P. Nouchi, A. Tardy and G. Orcel

Alcatel, Conflans-Sainte-Honorine, France

Abstract

We are proposing a new process for manufacturing single-mode multicore fibers (MCF) with a low number of operations. The process has been fully developed for 4 core fibers. The performances of the obtained fiber comply with the needs of FTTH networks at a much lower cost compared to standard singlemode fibers. The crosstalk is below -50dB. The mechanical strength is 70 N. A seven-core fiber is briefly presented to demonstrate the ability to manufacture fibers with a higher number of cores. The cleaving and splicing performances of the MCF are also investigated.

Introduction

The deployment of fibers closer to the subscriber in FTTH networks is impeded by the high cost of installation of the actual optical fiber cables. A real breakthrough is needed to lower cost and increase density for drastic reduction of installation and civil engineering costs. This can be achieved by new concepts¹ as the singlemode multicore fiber (MCF). The MCF we propose includes 4 single mode guides for the same size (245 μm coated fiber OD) as a classical single mode fiber. It offers higher waveguide density than any existing product.

As early as in the late 70s, multimode multicore fibers² were proposed to increase the core density in optical fiber cables. To our knowledge, this concept did not lead to a commercial product used in the field.

The aim of this paper is to demonstrate that singlemode multicore fibers match the requirements of FTTH network and that they can be manufactured without the need for complex procedures or tools. In the following sections, the MCF structure design is briefly described. The optical crosstalk and geometry accuracy, which are probably the most challenging parameters, are presented in details. The mechanical strength is also discussed in details because of its importance for the cabling process and installation.

Finally, the cleaving and splicing performances of the MCF are presented.

Design of the multiguide structure

In order to correctly design the MCF for subscriber network, one has first to define the specific requirements of the FTTH systems.

FTTH System key requirements

The FTTH system requires fibers to operate in the 1.3 and 1.55 μm windows. The fiber lengths involved in these networks are short and 10 km was set as the maximum span. Therefore the constraints on the wavelength of minimum dispersion and attenuation are relatively low. The crosstalk is of prime concern and should not be higher than -35 dB. The performance of the final cabled and jointed link requires first, a high degree of control of the geometry leading to accurate core pattern, and second, fan out devices at both ends which provide individual access to the optical guides. Another critical point is cable repair. It requires the corresponding cores to be aligned for splicing. Therefore, each core must be easily identifiable. Finally, the mechanical strength of the MCF should be of the same level as for standard singlemode fibers, such as to withstand the stresses associated with cabling and installation processes.

Fiber geometry

The geometry of the core array is characterized by a rotational axis, which is the fiber axis, and by the distribution of core axes at the vertices of regular polygons (see figure 1).

This study focuses on 4-core fibers. One core has a distinct profile for identification purpose. It shows a ring index profile while the other cores exhibit a step index structure. The core spacing is chosen large enough to reduce crosstalk and to ease access to the individual guide in fan-outs. The distance between 2 cores of 51.78 μm allows to use fan-out devices with 125 μm ferrules.

Design of the single mode waveguide

The fiber has both loss and crosstalk minimized at the two operating windows. Increasing the core refractive index difference, Δn , gives a more strongly confined guided mode and results in lower crosstalk and microbending losses. The refractive index difference of the core, the spacing of the cores, the core refractive index difference and the ratio of the operating wavelength to λ_c are computed according to the mode coupled theory³ to minimize the level of crosstalk. The following simplified rules can be used as guides : each Δn increase of 1×10^{-3} improves the crosstalk by 10dB and each core spacing increase of $1 \mu\text{m}$ improves the crosstalk by 5 dB. These rules of thumb are valid close to the nominal values given below.

The core index difference for the step index profile is of $\Delta n = 6.2 \times 10^{-3}$. The spacing between 2 adjacent cores is set to $51.78 \mu\text{m}$. The ring profile is designed to give a power confinement similar to other guides which requires a peak Δn of 10×10^{-3} . The cut-off wavelength is set below $1.3 \mu\text{m}$ to allow single mode operation at both windows.

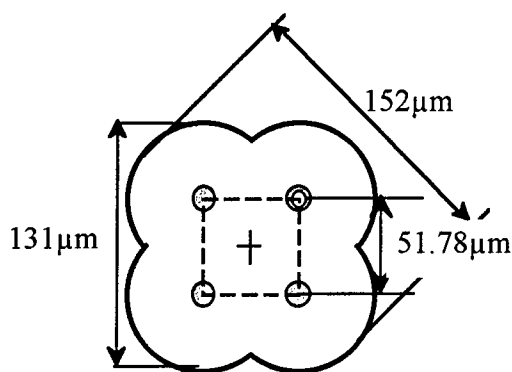


figure1. Schematic cross section of 4-core fiber with chosen dimensions and geometry.

Manufacturing process of the MCF

Primary preform

The first step consists in producing primary single core preforms by the MCVD process. Standard deposition procedures are used. However, particular care must be taken during the collapse procedure to insure that the geometrical characteristics of the preforms remain within the set limits.

Assembly of primary preforms

Four primary preforms and a silica rod are closely packed together by means of a V-groove. The silica rod has a diameter of about 40 % of the primary preform diameter and is set in the middle of the 4 preforms to minimize the air gap. The array is secured and introduced inside a sleeving tube as can be seen in figure 2. The quality of the glass used for the rod and sleeving tube is chosen such as to minimize the residual stresses in the multicore fiber.

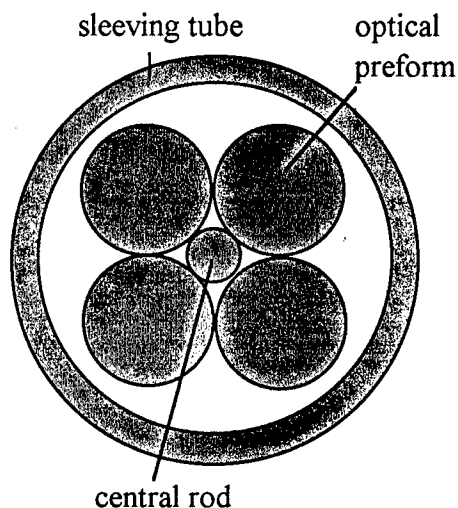


figure 2 structural components of multicore preform

The assembly is then collapsed under vacuum so that the preforms join together and all gaps are filled with silica glass. It is a very critical step as the final quality of the MCF depends upon its good control both in terms of geometry and mechanical strength.

Both off-line sleeving and rod-in-tube drawing techniques have been used successfully. Off-line sleeving was achieved on a sleeving lathe. A slight vacuum is applied so that the inner part of the tube is in depression. This technique allows a good control of the overall geometry of the sleeved preform. The absence of bubbles at the numerous interfaces between the different elements of the assembly can be easily checked. It was demonstrated that bubbles can be fully eliminated if the sleeving tube is well cleaned by thermal polishing. Attention has also been paid on the cleanliness of the primary preforms and the rod prior to assembly. The process was optimized to reduce contamination and flaws.

In the rod-in-tube technique, the multicore preform assembly is set in the drawing oven. The sleeving tube is kept under depression by a vacuum pump. Sleeving occurs in the hot zone of the furnace during draw. This approach reduces the number of processing steps and associated preparation.

As both techniques are equally successful, the rod-in-tube technique is preferred because of the lower number of processing steps involved.

MCF Drawing

The MCF drawing process differs from the one used for singlecore fiber in two ways. First, the geometry of the fiber can be modified by changing the drawing tension and speed and second there is no single diameter to rely on for dimension control. Furthermore, for the rod-in-tube technique, the draw speed and tension must be set so that the elements of the assembly join well and no air gap is left.

MCF drawing speed and tension The shape of the MCF results of the flowing of the preform components in the draw furnace. Therefore it depends on the neckdown region which is determined by the draw tension and speed. This is a major difference between multicore and single core fibers. An almost round shape can be obtained for very low tension (below 40 g). If tension is set at higher than 80 g, the shape is more similar to a clover leaf. A square-like shape is obtained at intermediate draw tensions (40 g to 80 g). Silica glass fills the gaps between the lobes. Speed is found to have a lower impact on the shape than tension.

A deformation factor was defined as the ratio between the minimum and maximum dimensions. It is equal to 0.86 +/- 0.01 for a 4-core fiber. In the present process, this is obtained by keeping the draw tension at 95 g +/- 10 g. The large range of allowable tensions means that this parameter can be used to control the shape of the MCF.

The draw speed has also an impact on the mechanical strength of the fiber. For a given draw tension, the mechanical strength increases with the draw speed and reaches a plateau around 300 m/min. The longer preform neck and the higher temperature are probably responsible for this behavior.

MCF dimension control The MCF is not cylindrical and thus it cannot be characterized by one single diameter value. It is impossible to know from variations of the signal from one single diameter gauge if the fiber size is changing or if the fiber is

simply rotating. As can be easily seen on figure 1, the measurement of a MCF of perfect size varies between 131 and 152 μm depending upon the angular position of the sensor. Two diameter gauges are set at an angle of 45°. From those 2 measurements one computes the largest dimension ϕ_{max} by using equation 1:

$$\phi_{\text{max}} = A \frac{\phi_1 + \phi_2}{2} + B * (\phi_1 - \phi_2)^2 \quad (1)$$

where ϕ_1 and ϕ_2 are the measurements from the 2 gauges. A and B are shape factors. They depend on the number of cores and on the chosen ratio between the largest and smallest dimension ϕ_{max} and ϕ_{min} . For a 4-core fiber and a ratio of 0.86, A equals 1.05 and B equals 0.021.

Once ϕ_{max} is known it can be used in the dimension control loop. The proportional gain and integration time are very similar to the ones used for singlecore fiber drawing.

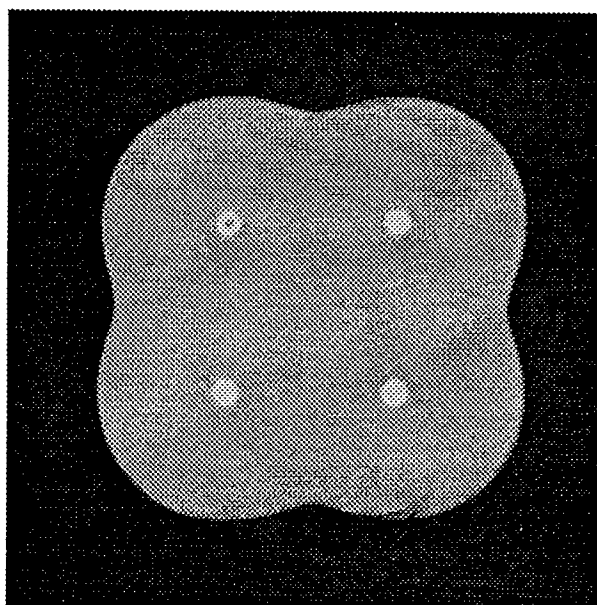


figure 3 end view of a 4-core fiber

Feasibility of MCF with a larger number of cores

One of the asset of the proposed manufacturing process is the easy adaptation to higher number of cores. In order to illustrate this point, a 7 core MCF was realized by sleeving 6 primary preforms around a 7th one.

The angle between the 2 diameter gauges was modified to account for the different shape of the 7-core fiber. It was set at an angle of 60°. Furthermore, B equals to 0.01 in equation 1.

The 7 core MCF has a geometry as precise as the 4 core MCF (see MCF characteristics section below).

MCF characteristics

Optical performances

Attenuation results are reported in table 1. The attenuation values are reproducible within 0.01 dB/km. The guide with a ring index profile systematically shows higher losses due to the higher germanium content necessary to get a 10×10^{-3} index difference. Single core fibers with the same ring profile exhibit similar optical losses.

Table 1 : Attenuation of multicore fibers

Measurement wavelength	core with a step index profile	core with a ring index profile
1310 nm	0.37 dB/km	0.45 dB/km
1550 nm	0.23 dB/km	0.28 dB/km

The bending and microbending tests have shown negligible incremental loss at longer wavelengths. They are obviously favored by the relatively small mode diameter : $8.4 \pm 0.2 \mu\text{m}$ at 1310nm and $9.75 \pm 0.25 \mu\text{m}$ at 1550nm.

The crosstalk is measured on a 10 km long fiber, wound onto a 15cm-diameter drum with 30g tension. The measured values are less than -50dB at 1550nm and less than -70dB at 1310nm (see table 2). The crosstalk is much lower than the required - 35 dB level which is necessary for digital systems. It actually is adequate for Amplitude Modulated analog systems.

Table 2 : typical crosstalk of a 10 km long MCF

type and position of the cores	crosstalk 1310nm	crosstalk 1550nm
adjacent cores (one is ring index profile)	< - 70 dB	- 57 dB
adjacent cores (step index profiles)	< - 70 dB	- 58 dB
opposite cores (step index profiles)	< - 70 dB	< - 70 dB
opposite cores (one is ring index profile)	< - 70 dB	< - 70 dB

Mechanical strength

The MCF mechanical strength was evaluated by performing 10m-gauge length tensile tests. Figure 4 shows a typical Weibull probability plot. The mean strength is close to 70N while a $125\mu\text{m}$ single core conventional fiber typically breaks around 60 N. The 25% larger section area of the MCF results in a 16 % gain in mechanical strength.

In terms of stress a MCF breaks at a level of 4.6 GPa which is 94 % of the stress level of a $125\mu\text{m}$ single core fiber .

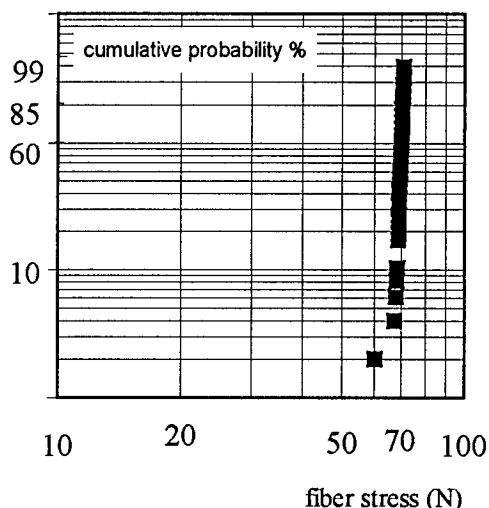


figure 4 Weibull probability plot of 4-core fiber. The test was realized on 10 m long samples at a speed of 500 mm/mn.

Geometry of the MCF

The standard deviation on the outer diameter achieved during a specific draw is $0.2 \mu\text{m}$. The standard deviation on the outer diameter achieved for multiple draws is within $\pm 2 \mu\text{m}$ and the standard deviation on the distance between adjacent cores is within $\pm 1 \mu\text{m}$. The splicing performance of MCF which is described below, illustrates that the accuracy which has been achieved is adequate.

MCF splicing

Joining single core singlemode fibers is not a simple task, so connecting multicore fibers could appear a risky venture. Looking more closely at the specific features , one can note :

- the single core is replaced by a core array with rotational symmetry and to achieve proper alignment the jointing process needs the rotation of at least one fiber,

- for link restoration purposes, the cores must be identified and connected to each other. The multicore fiber jointing process requires a core identification operation and means to localize the singular core,

- besides these constraints, and because 4 optical paths are spliced at one time, this new fiber shows the advantages of mass-spliceability.

Core identification

Core identification is an operation specific to multicore fiber. Two techniques were evaluated to detect the singular core. The first one uses a local injection device to launch 'white light' inside the refractive index structure; the second one uses diffusion to launch 'white light' into the cladding so the inner structures appear dark. Viewing instrument can be a microscope linked to CCD camera. The ring shaped core can be also detected using an inspection microscope for field applications with a 400 X magnification.

Fusion splicing

Tests were made using commercially available cleaving tool and automatic fusion splicing machine.

The breaking tension on the cleaving tool can be adjusted resulting in mirror-like endfaces with a mean angle of about 1°. There is some evidence that the stress distribution due to the multiguide structure could introduce slightly more end-face angle than in the case of single core fiber. This characteristic could impair fusion splice performances since it is well known that perpendicular endfaces are required for avoiding core deformation. However, the angles obtained after cleaving are well within the recommended values, and high quality splices were obtained, as shown below.

The fusion splicing machine was developed for polarization maintaining fibers and it has rotary alignment capability. When the 4-core fiber is illuminated from one side, the circular-shaped corners act as lenses and the relative light intensity is a function of the rotational position of the fiber. By calculating the correlation between two profiles, the system properly aligns the fibers before fusion.

A first experiment was carried out by cutting a fiber and splicing the 2 well matched endfaces. The splicing process parameters were tuned to minimize surface tension effects and fiber roundness. The most suitable fusion current and time were defined. The average 0.2dB and standard deviation 0.12dB of losses (4x19 splices) are directly related to the multicore geometry quality and instrument splicing ability. It also shows that the quality of cleaved endfaces is satisfactory.

In a second experiment, two fibers from different preforms were spliced together. The dispersion about the core spacings is estimated to be around $\pm 0.5\mu\text{m}$. The distribution of splice losses is shown in figure 5. The mean loss is 0.27dB and the standard deviation is 0.2dB.

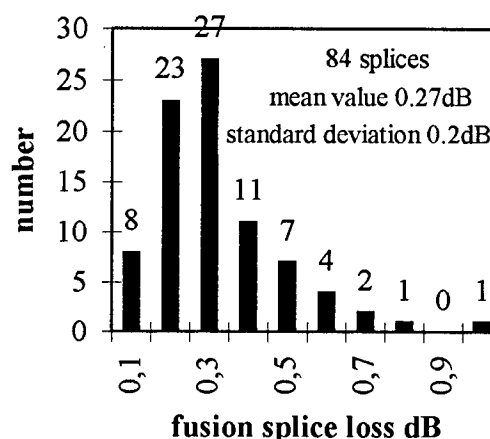


figure 5 distribution of splice losses achieved with an automatic fusion splicing machine

Mechanical splicing

For local networks, the mechanical splice is of great interest, at least for quick repairs. It was desirable to investigate this technique by using commercially available mechanical splices. The Placoptic system from A.T.I. was chosen because it can readily be used despite the specific geometry of the MCF. Each endface was oriented prior to insertion in the mechanical splice. On 10 splices (i.e. 40 core joints), the mean insertion loss is 0.2 dB with a standard deviation of 0.2 dB.

System and commercial aspects

In order to deploy the multicore fiber in the field, some dedicated devices like fan-outs are required. They connect each of the cores of the MCF to the

single core of a 125 μm fiber and thus to the other parts of the network. A major difficulty associated with multicore fiber is how to excite and detect the signals in each core because of their relatively close proximity. A proposed solution³ is being engineered by RADIALL. Single-mode conventional fibers are chemically etched to exhibit diameter reduction corresponding to core spacing of MCF. The diameter is nominally 51.78 μm since compact assembly of four elements can be inserted into the 125 μm diameter bore of ceramic ferrule.

Due to the very high core density compared to other fibers, cables and ribbons, the MCF concept is very attractive in terms of cost. The process described in this paper has a capacity of 100 km of 4 core fibre per meter of preform. The cost per core of MCF is already competitive compared to standard single mode fibres. Further cost reductions are anticipated by increasing preform size and draw speed.

Conclusion

The attenuation, crosstalk and mechanical strength of the MCF which have been presented in this paper, meet the requirements of the FTTH networks. The low crosstalk is a major achievement as it was a strong concern in the MCF concept. The high mechanical strength of the fiber demonstrates that there are no flaws at the primary preforms and tube interfaces. The good geometry, which is maintained throughout all the processing steps, allows to obtain good splicing performances.

The multicore fiber described in this work can be manufactured by using simple, traditional processing techniques, similar to those used for standard singlecore fibers. Due to higher core density, the installed 4-core fiber is expected to be less expensive than two conventional fibers.

In addition, it must be noted that many existing tools and apparatus developed for traditional fibers can be used for multicore fibers with minor adaptations. For example: breaking tension for cutting tools or arc-fusion conditions for fusion splicing machine. This makes the MCF easy to deploy in the field.

Acknowledgments

The authors are very grateful to Max Matau and Pascal Mazabraud for their strong involvement in

developing the MCF manufacturing process. Gérard Le Ber took a large part in the MCF splicing program. The authors wish to thank France Telecom which sponsored this work under the « Subscriber Fiber » project 95 6M 821.

References

- (1) G. Le Noane and al. « Ultra high density cables using a new concept of bunched multicore monomode fibers: a key for the future FTTH networks » IWCS'94 Proceedings pp 203-209
- (2) S. Inao and al. « High density multicore-fiber cable » IWCS'79 Proceedings pp 370-384
- (3) A.W.Snyder and J.D.Love « Optical Waveguide Theory » Chapman and Hall Ed. (London, 1984)
- (4) R. Le Marer, G.Perrin « composant d'éclatement pour fibres multicoeurs monomodes. L'éclateur : un composant clé » Opto n°81 (Mars-Avril 1995)

Biographies

Jean-François Bourhis joined Alcatel in 1990 and received his Ph. D. in Optoelectronics in 1992 while working on passive Integrated Optics waveguides and associated pigtailling techniques. His current interest is in Optical Fiber Drawing Technologies.

Rosine Meilleur graduated from the Ecole Nationale Supérieure de Sciences Appliquées et de Technologies in 1990. She joined Alcatel in 1990 to work on optoelectronics module. Her current interest is in Optical Fiber Drawing Technologies.

Pascale Nouchi received her Ph.D. degree in Optical Sciences from the University of Southern California in Los Angeles in 1992. She then joined Alcatel. Her current interest is in Guided Optics.

A Tardy received his engineering degree in 1966 from the Institut National des Sciences Appliquées. He joined CGE which later became Alcatel working on optical fiber connection and testing systems. His current interests are distribution fiber and components

Gérard Orcel received his Ph.D. degree from the University of Florida in 1987. He held positions at GelTech and Spectran before joining Alcatel in 1992. Since then, he has been involved in preform design, CVD and draw technology and coating development.

DESIGN STRATEGIES FOR HIGH FIBER COUNT PLENUM CABLES

J. T. Chapin, M. F. Marx, Parry A. Moss,
Wayne M. Newton, Montri Viriyayuthakorn, and Carla G. Wilson,

Lucent Technologies, Bell Laboratories, Norcross GA.

ABSTRACT

Premises optical fiber communications cables are designed in various fiber counts. As the customer needs for capacity and data-rate service has increased so has the need for higher fiber count cables. Therefore, high fiber count cables have been recently developed, 18 through 72 fibers. Cables are designed to meet the mechanical, optical and fire safety requirements for many applications using various materials, process conditions and constructions. Optimizing plenum cables to meet all of these performance requirements is difficult. The challenge is to design flexible high fiber count plenum cables using inherently rigid flame retardant materials. The purpose of this paper is to present the strategies used in overcoming the many obstacles to design high fiber count plenum cables.

INTRODUCTION

The typical medium used to transmit information in the telecommunications industry is cable. Plenum cables, though difficult to design, offer the most economical solution to installed cable cost. Cables are classified as plenum cables by meeting the requirements of the most stringent fire test in industry.

We chose a building block approach in this development. The strategy was to identify suitable cable materials, develop a robust buffered fiber, develop a robust multiple fiber sub-unit and combine the sub-units into a high fiber count cable meeting all the required objectives. Using Design of Experiment (DOE)

techniques we were able to optimize the mechanical, optical, and fire safety (UL-910) performance of the cable. Several variables, input and response, were investigated to select an optimum window of performance. Some of the variables and responses used in the DOE included: buffered fiber micro-bend sensitivity, buffer processing, buffer strippability, sub-unit construction, jacket thickness, cabling lay, and diameters. In addition, simplicity, manufacturing flexibility, minimizing components, maximizing yields, minimizing manufacturing cost, ease of entry, and connectorization were considered throughout each phase of the development and incorporated in the final design. Each sub-unit is fully qualified for mechanical, optical and fire safety specifications and can be used as a stand alone cable. This design also eliminates installer safety concerns with exposed glass rods.

The result is a family of cables that meet the most stringent fire safety requirements, and is flexible, easy to handle, craft friendly and has excellent mechanical and optical performance.

CONCEPT OF BUILDING WIRING

Optical Fiber Premises cables are divided into three basic categories:

1. Interconnect
2. Distribution
3. Backbone or Riser

Interconnect cables are primarily used as patch cords in main frames. Distribution cables are those that are used in the horizontal distribution

of cables within a floor. Backbone or riser cables are used to connect floor-to-floor in a building. Figure 1 indicates schematically the typical use of fiber optic premises cables.

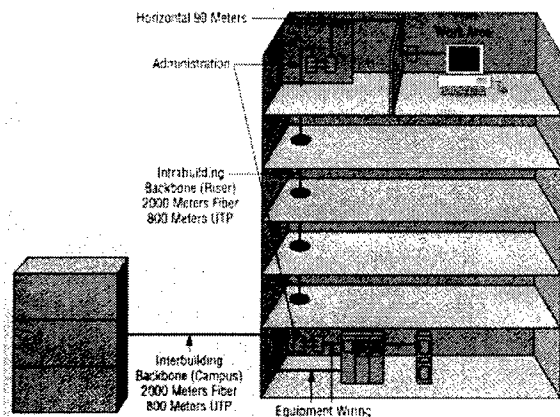


Figure 1: Building Cable Layout

PLENUM CABLE DEFINED

Optical fiber and copper communications cables are often installed in buildings employing structured wiring systems. That is, all of the components of a telecommunications network (transmission and cross connect equipment, etc.) are divided into structured, horizontal and vertical spaces within a building as shown in Figure 1. In the US, most commercial buildings incorporate drop ceilings. These ceilings support things such as light fixtures, air vents, and sprinkler system heads. Often the space between the drop ceiling and the building structure becomes a return-air conduit for heating and air conditioning systems. When this space is used for the air-return of the buildings environmental air it is called a *plenum*. Plenum spaces are often continuous throughout the width and length of each floor of the building. These spaces are also avenues for flame spread and smoke evolution due to the combustion of materials present within those spaces. As a result, it is important to ensure that cables placed in plenum spaces have adequate protection or fire resistance to minimize the propagation of a fire. Cables installed in plenum spaces are required to be placed within metal conduit or meet stringent fire specifications. The US National Electrical Code

(NEC) has established installation and fire performance requirements for optical fiber cable in Article 770 "Optical Fiber Cable and Raceways." The hierarchy of NEC fire tests is found in Table 1.

Table 1. US National Electrical Code Fire Test Hierarchy for Fiber Optic Cables

Large Scale Fire Test	Metallic Cable	Non-Metallic Cable
UL 910 Plenum	OFCP	OFNP
UL 1666 Riser	OFRC	OFNR
UL 1581 Vertical Tray	OFC	OFN

The NEC defines *plenum* as a compartment or chamber to which one or more air ducts are connected and that forms part of the air distribution system. The plenum concept in buildings has become popular over the past 20 years in the US and more recently overseas due to the advantages of reduced construction costs and energy efficiency. These spaces often have high airflow due to the movement of environmental air (heating or air conditioning) and is considered the most hazardous from a fire hazard standpoint. The UL 910 test (also known as NFPA 262-1994, "ANSI Standard Method of Test for Fire and Smoke Characteristics of Wire and Cables",) was developed to assess the flame spread and smoke performance of cables installed in plenum spaces. A diagram of the test is found in Figure 2. The test involve placing a single layer of cable on a 11.25 inch ladder in a horizontal orientation. The cable is exposed to a 270,000 BTU burner for 20 minutes with an airflow of 245 ft³/minute. To pass the test the cable must have a maximum peak optical density of 0.5, a maximum average optical density of 0.15, and a maximum allowable flame distance of 5 ft (1.52 m).

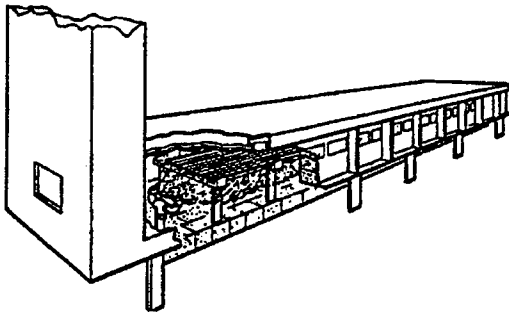


Figure 2. UL 910 Test Diagram

This test has the most stringent combined flame and smoke requirements for a large scale fire test in the cable industry. In addition, the cables are not exempt from meeting the mechanical toughness, optical transmission performance, and handling specifications and requirements of the customer.

The key to the design success of plenum cable is the design configuration and material selections.

Optical Fiber Cable Requirements

The primary function of an optical fiber cable is to provide: fiber protection, stability of the fiber transmission characteristics, strength and identification of fibers within the cable. Cables are tested to determine their optical, mechanical, physical and fire resistance characteristics. The test methods and procedures are established by the EIA Committee. Typical premise cable requirements and specifications are found in Appendix I.

Many of these test are a measure of the stress and strain transferred to the fiber when subjected to certain conditions and are reflected in the fiber's attenuation response. Others are a measure of the physical performance and ease of the cable installation process. Materials and cable design configuration play a major role in the cable's mechanical, optical, physical, and flame retardant properties. The building block strategy provides the opportunity for a cable to be optimized for each performance characteristic.

BUILDING BLOCK THEORY

The intent was to optimize the overall cable performance by developing and optimizing the building blocks that make up the cable, i. e.,

buffered fibers, and sub-units.. A buffered fiber that was made with materials and processes to provide the optimum results with reference to Bellcore mechanical tests should perform optimally through out the cable design, whether tested in Buffer, Sub-Unit, or Cable form. Similarly, a sub-unit that was made with materials and processes to provide the optimum results in sub-unit form should perform optimally in the cable design. The design decision matrix also included less defined criteria such as flexibility, ease of entry, safety, customer satisfaction, and ease of manufacture. Several combinations of processes and materials were found that would meet all the UL and Bellcore tests, but different design decisions could be made that would make the cable more flexible, easier to manufacture, install, enter, and connect.

The sub-unit design objective was to make individual sub-units capable of being used as a stand alone cable meeting the requirements of Appendix 1 before they could be considered as a building block for a high fiber count cable. This allows the network designer to have the cable installed to a central location, remove the jacket, and distribute the sub-units to different parts of the building.

Component Optimization using DOE

Design of Experiments were used to determine the window of manufacturing conditions that produced cable components that met the Bellcore mechanical requirements. The best set of operating conditions could then be identified. The initial examination of the process identified twelve variables as possibly important in controlling the process. In the buffer process, the controlling variables identified were: buffer modulus, melt temperature, line speed, preheat temperature, preheat distance from extruder, cooling gap, cooling temperature, buffer diameter. In the sub-unit cabling process, the controlling variables identified were: jacket material modulus, jacket ID, jacket thickness, and fiber lay length. Due to the large number of control variables identified, the buffering process and the cabling process were studied separately. The steps used in the DOE were the same.

In developing a robust design and a robust production process for buffers or sub-units, we must find values of the control variables which cause the cable to constantly perform well

according to a set of responses. This involves several important steps:

1. The range of the control variable setting must be found through screening trials.
2. The key responses must be identified through collecting and studying cable data.
3. The effect of unavoidable variation in response measurements must be reduced through study of variance of the replicate trials and variance of cable measurements.

In this study, an initial screening trial was carried out to identify key design variables for the cabling process. The responses include loss measurements during several Bellcore mechanical and environmental tests. After the data were collected, the DOE analysis fits a polynomial equation to these data, and standard quadratic response surface designs were created. The equation is a multidimensional curve that is useful in displaying a picture of the relationship between the response and design variables.

Finding the optimum point on a multidimensional response surface is not always easy. However, with the key control variables identified, we simultaneously minimized the losses for each of the key responses, resulting in a window of robust operation.

Cable Construction

Cables which contain 18, 24, 30, and 36 fibers are made of sub-units containing 6 color coded buffered fibers as shown in Figure 3. Cables which contain 48, 60 and 72 fibers are made of sub-units containing 12 color coded buffered fibers as shown in Figure 4. The 6 or 12 buffered fibers are formed into sub-units by a reverse oscillated lay process around aramid yarn central strength members. The fibers are then covered with helically served aramid yarn and jacketed with a plenum rated jacket.

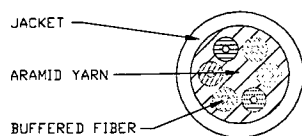


Figure 3: 6 Fiber Subunit

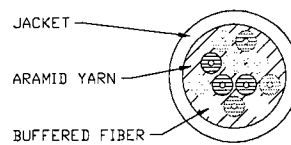


Figure 4: 12 Fiber Subunit

To obtain the desired number of fibers in the final cable, the appropriate number of these color coded jacketed sub-units are cabled by a second reverse oscillated lay process around a central organizer and jacketed. Spacers, which are hollow tubes may also be included for some fiber count sizes in order to maintain the structural geometry of the cable. Examples of the resulting cable structures are shown in Figure 5 and 6. Note that this construction does not contain core binders which have to be removed when opening the cable, rip cords which can damage the sub-units when removing the jacket or exposed glass rods which can be a safety concern to the installer. The jacket can be easily removed by ring cutting with a simple hand tool and sliding the jacket off the cable. Sub-unit jackets can be similarly removed providing quick and easy access to the fibers.

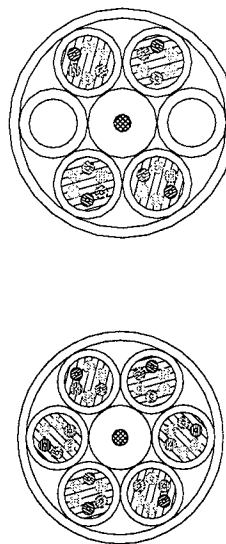


Figure 5: 24 and 36 Fiber Cables

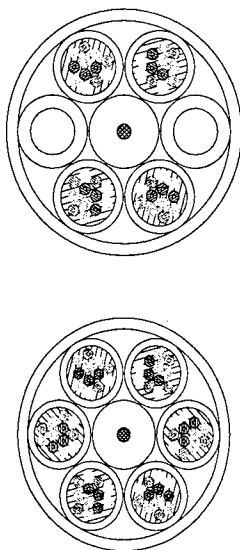


Figure 6: 48, and 72 Fiber Cables

MATERIALS

In order to design the family of high fiber count plenum cable that also meets a wide array of customer transmission, installation and reliability requirements, a range of materials and formulations were evaluated. The predominant materials used in copper and fiber optic plenum cables are highly flame retarded and smoke suppressed. Examples of these materials would be fluoropolymers, copolymers with fluorine and chlorine and low smoke PVC compounds.

Mechanical Properties

The mechanical properties of jacket and buffer materials can significantly affect a wide variety of performance characteristics of fiber optic cable, such as: cable stiffness and bending, impact behavior, transmission performance, surface friction and/or abrasion resistance. We have characterized the modulus behavior of various plenum materials as a function of temperature by mechanical spectroscopy. A plot of two representative plenum materials is found in Figure 7.

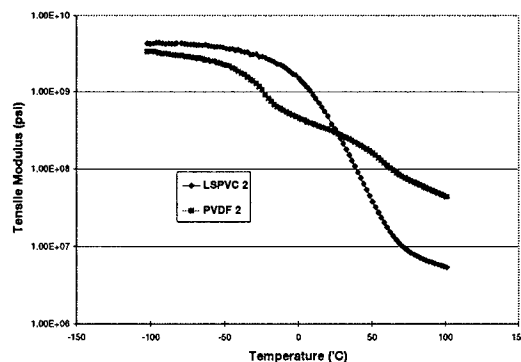


Figure 7. Modulus Behavior of Various Plenum Materials

Note that the LSPVC material has a broad transition from the glassy modulus plateau (below -10°C to the rubbery region approaching 100°C . In contrast the PVDF shows a reasonably linear change in modulus with temperature. By using this information, we can select materials for buffer and jacket applications that best suit the requirements for storage, installation and operating temperatures.

Processability of Low Smoke Flame Retarded PVC (LS FR PVC)

PVC wire compounds are inherently flame retardant, however in areas where they are used for plenum applications, additional ingredients are added to further reduce flammability and to suppress smoke. These additives increase melt viscosity, reduce processing thermal stability and increase gravity. To offset viscosity and stability changes, a compounder can modify a formulation by reducing resin molecular weight, using processing aids, choosing a new plasticizer system, adjusting lubricants, and/or adding additional stabilizer along with using other state of the art additive technology. Therefore, LS FR PVC compounds have become complex formulations, requiring process as well as fire performance evaluations.

Static Thermal Stability, Metrastat Automatic Oven Test

The Metrastat automatic oven parallels earlier oven stability testing where hanging samples are removed periodically from a high temperature

oven with controlled air circulation and affixed to a time chart.

In the automatic oven test, compound pellets are placed in a 1 inch wide sample tray lined with aluminum foil. The 12 inch long tray retracts into the oven, preheats the sample and is ejected at a preset rate. Usually several, up to 5 samples are run side by side for comparison. Conditions used for LS FR PVC were 200°C and 2 hours travel. Color development signifying stages of degradation is continuous compared to manual oven testsamples.

Test results in the static mode were not conclusive. Difference in color development was not significant enough to choose between samples. More significant results came from dynamic thermal stability tests.

Dynamic Thermal Stability, Torque Rheometer and Capillary Rheometer

To evaluate processing, melt viscosity and thermal stability, laboratory tests were run to confirm extrusion degradation observations that were found during lab extrusion trials. Dynamic torque rheometer testing of LS FR PVC was performed using conditions similar to those used for testing other vinyl wire and cable compounds. The conditions were:

205 °C
100 RPM
#5 electrically heated roller head
60 cc sample charge

The severe test conditions produced stability curves shown in Figure 8. Although curves A and B had reasonable stability times (>40 minutes) taken from the distance between 30° tangent slopes, curve B produced a more defined, ever increasing melt viscosity, with no clear end point.

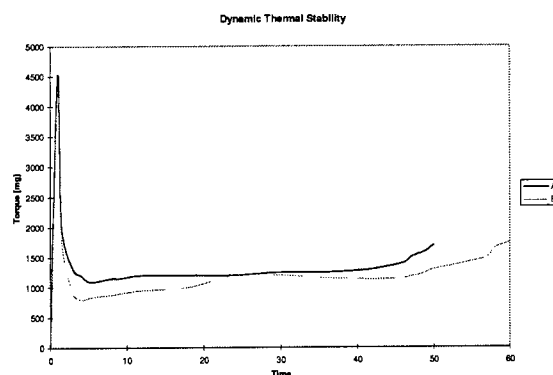


Figure 8. Dynamic Thermal Stability, Torque Rheometer

This steady crosslinking effect was also seen in a capillary rheometer. Using a Kayeness Galaxy V Rheometer, the shear rate was held constant and apparent viscosity was plotted with a delay of 6 minutes between runs held to 200°C. Figure 9 shows the constant viscosity increase with time (curve B) which relates to less desirable processing stability and more compound degradation, particularly in the restrictive flow passages of extruder tools. In further processing development, material B was found to offer acceptable processing at optical fiber processing line speeds.

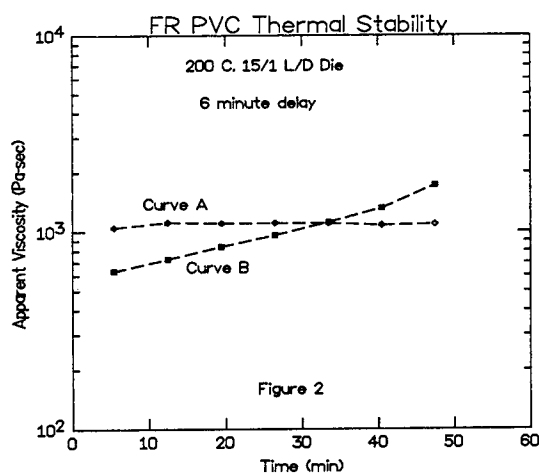


Figure 9. Dynamic Thermal Stability, Capillary Rheometer

Processing Melt Viscosity

To verify melt processing, new compounds can be readily compared to known processable formulations that have been used or are being used today. Poly vinyl-chloride compounds are typically tested at 175°C. Using a Kayeness Galaxy V Rheometer, viscosity vs. shear rate curves were run on a new LS PVC formulation and on a proven processable buffer compound. The lower melt viscosity curve of the two plotted in Figure 10 indicates that the new LS FR PVC compound would run at similar extrusion conditions, i.e. not generating an increased melt temperature or a higher head pressure. Buffer conditions during manufacture support these findings.

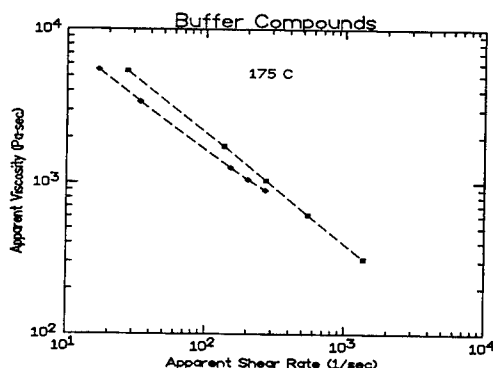


Figure 10. Process Melt Viscosity Comparing New Material to Old Material

Combustion Properties

The flame spread and smoke requirements for UL 910 require a comprehensive understanding of the combustion properties of plenum cable materials. Several methods can be utilized, including Cone Calorimetry per ASTM E1354, heat of combustion (H_c), per ASTM 2015 and limiting oxygen index (LOI), per ASTM 2863. For most polymeric materials H_c varies from a low value of 2,000 BTU/lb., for perfluoropolymers to 20,000 BTU/lb., for polyethylene. Likewise, LOI varies typically from 18% for polyethylene to >95% for fluoropolymers. Typical H_c and LOI values for various materials used in this investigation are found in Table 2.

Table 2. Typical H_c and LOI Values for Plenum Materials

<u>Material</u>	<u>H_c</u>	<u>LOI</u>
PVDF1	6399	45
PVDF2	5982	65
PVDF3	5044	99
LSPVC1	5809	49
LSPVC2	5230	48

Although LOI is not a predictor of fire performance, it is a parameter along with others that offers guidance into choosing preferred compounds. From LOI tests, subtle observations can be made. The nature of smoke and char should be noted. Did the sample burn vigorously or did it glow. As long as the sample glows, we consider burning to be taking place even though this is not the ASTM description of "candle like burning".

As more ingredients are added to formulations for better flame retardance and increased LOI, the final end point of a LOI test becomes more obscure. Samples will burn, fold, break off, drip, smoke, glow, and sputter. No doubt, early oxygen index testing was more simple when fewer additives were used to suppress burning and smoke evolution.

Another more sophisticated method is to test materials using a Cone Calorimeter. This method yields a range of information about materials during the process of combustion, such as: gravimetric analysis, heat release rate (HRR), smoke release rate (SRR) and CO/CO₂ evolution. Of these properties, HRR and SRR can be used to estimate the behavior of materials in the UL 910 test (flame spread and smoke evolution.) The data for total SRR and HRR for various plenum materials tested at 75 kW/m² is found in Figures 11 and 12. The data indicates that by selective modifications to the material, one can have substantial variations in flame spread and smoke performance. This can then be used in the design and development of optimized plenum cable constructions.

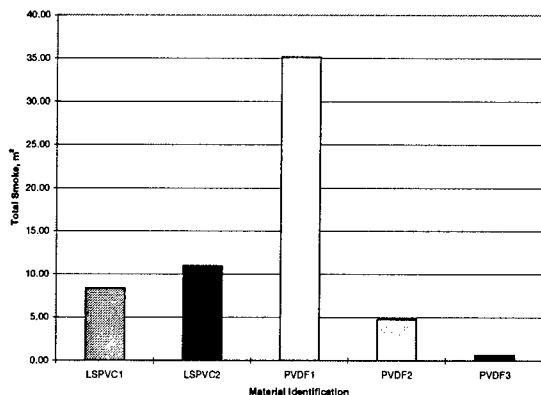


Figure 11. Total Smoke for Various Plenum Materials

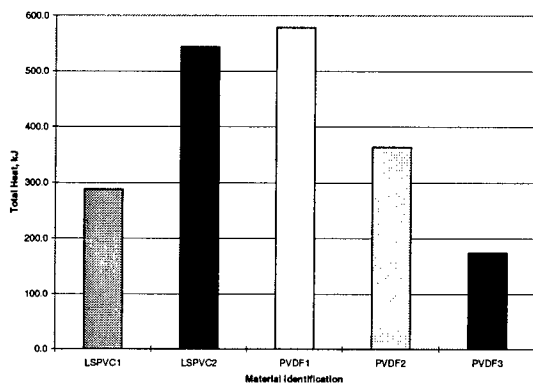


Figure 12. Total Heat Released for Various Plenum Materials

Completed cable constructions and components can be burned to help rank configuration changes. Thin samples will have a lower LOI than a standard 3 mm (.118 inch) thick X 25 mm (0.256 inch) wide ASTM D 2863 Type A sample. A Type B sample is allowed which is 2 mm (0.78 inch) thick and is convenient when other physical tests are made using what is commonly referred to as 75 mil test sheets. Cable jackets when tested in a tubular configuration, will generally have a lower LOI than an ASTM samples made of that material.

UL 910 Fire Test Results

A typical smoke trace for plenum cable is shown in Figure 13. This trace provides insight into the behavior of the smoke characteristics of the cable. As indicated the peak smoke (0.38) occurs at 18 minutes into the test. The average smoke value is determined by the area under the curve.

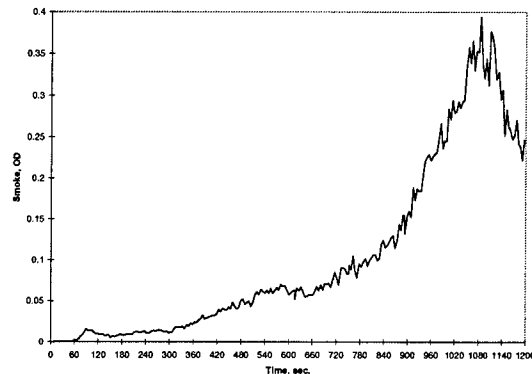


Figure 13. Typical Smoke Trace for a Plenum Cable

In addition, typical flame spread and peak smoke results are shown in Figures 14 and 15. These curves indicate the variation in the performance of different fiber counts and design configurations. They also validate the building block approach by allowing the designer to choose the best fire performer that should be used for the next stage. For example, the cable identified as 12-Fiber A is a better performer than 12-fiber B with regards to peak smoke but cable B has better flame spread characteristics than cable A. Having this type of information allows the engineer to minimize the guess work and select sub-units that will provide a high fiber count cable that will meet the UL-910 test requirements with predictable margins, thus, saving development time and the cost associated with the development and testing of plenum cables.

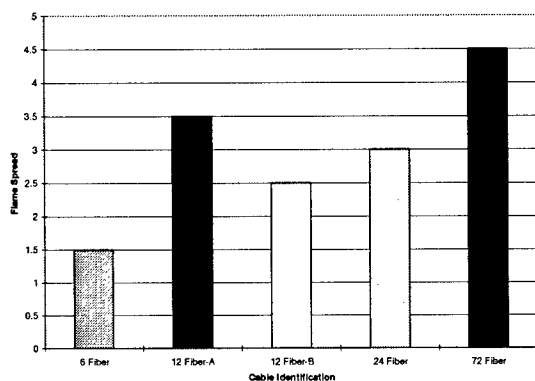


Figure 14. Flame Spread for Plenum Cables

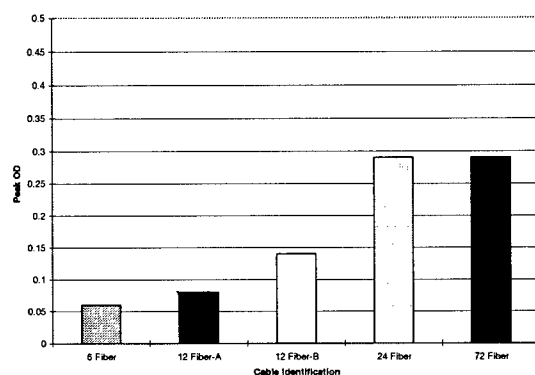


Figure 15. Peak Optical Density for Plenum Cables

CONCLUSIONS

A family of High Fiber Count plenum rated cables, from 18 through 72 fiber count, have been developed using the building block approach that meet all the Bellcore mechanical and optical requirements. In addition, the cables are flexible, easy to install, and easy for the installer to enter. The total cable structure and the individual sub-units meet the most stringent fire requirements in the cable industry.

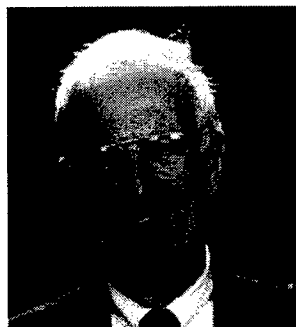
As indicated in this text, there is much to be considered in the development of plenum cables. As a result, the "building block" approach proved essential to the success of developing products that are desirable and customer friendly.

APPENDIX I
GENERIC REQUIREMENTS FOR PREMISES CABLES

NO.	TEST DESCRIPTION	INTERCONNECT CABLE	DISTRIBUTION CABLE
1	TEMPERATURE CYCLING	EIA-455-3A 0°C to 50°C	EIA-455-3A 0°C to 50°C
2	AGING	EIA-455-3A Continuation of Temp. cycling 85°C, 336 hours	EIA-455-3A Continuation of Temp. cycling 85°C, 336 hours
3	FIRE RESISTANCE	VW1, UL-1666, UL-910	VW1, UL-1666, UL-910
4	STRIPPABILITY	EIA-455-178 15mm (0.6 in) ≤ 13.4N (3lbf)	EIA-455-178 15mm (0.6 in) ≤ 13.4N (3lbf)
5	CYCLIC FLEXING	EIA-455-104 Mandrel Dia. = 20X Dia. 300 cycles	EIA-455-104 Mandrel Dia. = 20X Dia. 100 cycles
6	IMPACT	EIA-455-25 0.74 N-M (0.54 ft-lb), 20 cycles 150mm (5.9 in)	EIA-455-25 0.74 N-M (0.54 ft-lb), 20 cycles 150mm (5.9 in)
7	TWIST	EIA-455-85 Length = 0.3 meter (11.8 in)	EIA-455-85 Length = 1 meter (3.3 ft)
8	LOW & HIGH TEMPERATURE BEND	EIA-455-37 Mandrel Dia.=20X Dia./ 50mm (2.0 in) X kg, 10 Turns 0°C & 50°C	EIA-455-37 Mandrel Dia.= Dia./ 15.2cm (6.0 in) X kg, 10 Turns 0°C & 50°C
9	COMPRESSION	EIA-455-41 10.16cm (4 in) Dia, 3.5N/mm (20 lbf/in)	EIA-455-41 10.16cm (4 in) Dia, 10 N/mm (57 lbf/in)
10	TENSILE STRENGTH	EIA-455-33 220N (50 lbf)	EIA-455-33 ≤12f 444N (100 lbf), >12f 665N (150 lbf)
11	CABLE JACKET SHRINKAGE	EIA-455-86 15cm(6in) long, 0.6cm(0.24 in) wide 121°C, 2 Hrs, Shrinkback ≤ 5%	EIA-455-86 15cm(6in) long, 0.6cm(0.24 in) wide 121°C, 2 Hrs, Shrinkback ≤ 5%



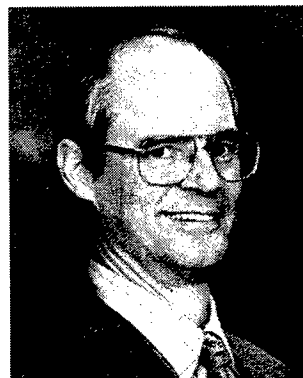
J. Thomas Chapin is a Member of Technical Staff in the Chemistry, Environment and Safety Group at Lucent Technologies, Bell Laboratories in Norcross, Georgia. He is responsible for fire technology research and materials development for copper and fiber optic cables. He joined AT&T Bell Laboratories in 1980 after working at the Upjohn Company for three years. He received his B.S. in Chemistry and Ph.D. in Polymer Science from the Institute of Materials Science at the University of Connecticut. Since 1980 he worked in the areas of outside plant materials failure phenomena, optical fiber coating development and fiber optic cable development. He has been awarded 11 patents and has 15 publications.



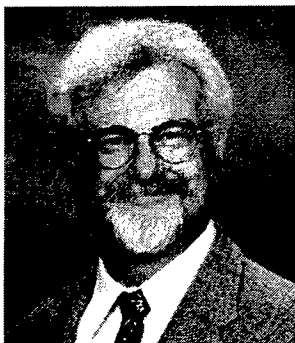
M. F. Marx is a Member of Technical Staff with Lucent Technologies, Chemistry Group, formerly AT&T Bell Laboratories, Norcross Georgia. He is responsible for plastic materials used in the manufacture of optical fiber cable, and copper wire and cable for Network Cable Systems

He is past President of SPE Southern Section, and has been active in all capacities including

numerous RETECs. He is also a past Chairman of the Vinyl Division and a current member of the Vinyl Division Technical Program Committee. Fred graduated from the University of Maryland with a BS in Engineering and is a Registered Professional Engineer. He has presented several technical papers, has two patents, and is an author in Ed Wickson's "Handbook Of PVC Formulating".



Parry A. Moss is a Member of Technical Staff in the Fiber Optic Premises Cable Group at Lucent Technologies Inc., Norcross, GA. After he obtained his BSME from the University of Nebraska in 1975, he worked for General Electric as a Field Engineer installing and starting Large Steam Turbines. He joined Western Electric in 1980, and worked in the Ribboning and Fiber Color Code areas for 5 years. He then started working in the Premises Area, and has had responsibilities in Buffer, Interconnect, and Cable, manufacturing and design. He attended Clarkson University and received a Masters of Science in Engineering and Manufacturing Management. His current responsibility is the manufacture of premises distribution cables. He has been awarded four patents in the cable design and processing areas, and is a Registered Professional Engineer



Wayne M. Newton is a Distinguished Member of Technical Staff in the Fiber Optic Premises Cable Development Group at Lucent Technologies Inc., Norcross, GA. After obtaining a BSEE from Clemson University in 1965, he began his Western Electric-AT&T-Lucent career in 1966 in Switching Systems Engineering. In 1970, he joined the Atlanta Works working in Copper Cable Development Engineering assigned to new product and process development. In 1979, he was assigned to the Copper Cable Product Engineering Group where he continued to work in product and process development in addition to his product engineering responsibilities and received a MSIE from Texas Tech University in 1985. In 1990 he was assigned additional responsibilities of technical support for international joint venture initiatives. Since 1993 he has been responsible for process development for new fiber optic premises cable designs and has been awarded 3 U.S. patents in the cable design and processing areas.



Carla G. Wilson is a Member of Technical Staff in the Fiber Optic Cable & Materials Development & Engineering Department at Bell Laboratories of Lucent Technologies in Norcross, Georgia. She is responsible for the

design and development of optical fiber premises distribution and interconnect cables. Her current assignment emphasis is on plenum cable applications.

Ms. Wilson joined Bell Laboratories in 1975. She received her B.S. degree in Electrical Engineering Technology from Southern Polytechnic State University, and a M.S. degree in Manufacturing Engineering from Brigham Young University.

She has been granted four patents on cable design with one more pending.



Montri Viriyayuthakorn is a Member of Technical Staff in the Fiber Optic Cable and Materials Development and Engineering Department, at Lucent Technologies, Inc., in Norcross, Georgia. He is responsible for product design and manufacturing process development for Fiber Optic Building and Specialty Cables.

Dr. Viriyayuthakorn joined AT&T Bell Laboratories in 1979. He has a B. S. degree in Civil Engineering and an M. S. degree in Mechanical Engineering from Worcester Polytechnic Institute, and a Ph. D. degree in Chemical Engineering from Brown University.

He has been granted 11 patents.

Development and actual environment testing of optical fiber cables with small diameter stainless pipe

Yasushi Sudo, Takuya Ohsako, Kazumasa Nemoto, Hiroshi Ishizaki

Ocean Cable Co., Ltd.
Kita-Kyushu, Japan

ABSTRACT

The trend in recent telecommunication network is to introduce optical fiber cables into trunk line systems in order to make the best use of their advantages, which include reduction of transmission loss, improvement in frequency characteristics and decrease of number of repeaters. Moreover, optical fiber cables are being developed for the subscriber lines.

We developed optical fiber cables with the unit structure of stainless steel pipe covering optical fibers. This cable structure has excellent characteristics such as mechanical performances, corrosion resistance and small diameter. The cable will be suitable for subscriber network. Then we evaluated optical loss and distortion characteristics of the cable in field installation conditions. Consequently we have had excellent test results that the cable is available for subscriber network.

The cables developed are superior in thermal expansion coefficient, yield strength and moisture-resistance as against loose tube structure cables, and also are superior in weight and outer diameter as compared with slotted structure cables.

1. INTRODUCTION

Optical fiber cable have been recently used

under various environments such as aerial, underground and submarine in order to take advantage of their transmission capacity and small space requirement. The cable developed can be used under all of the above environments. The cable are superior in thermal expansion coefficient, yield strength and moisture-resistance as against loose tube structure cables which used PBT(polybutylene terephthalate), and also showed light-weight and smaller diameter as compared with slotted structure cables. The basic structure of the cable is similar to that of loose tube cable and maximum 12 coloring fibers can be inserted in the pipe per unit.

One of the requirement of aerial cable is to maintain their initial performances for a long time under actual environment. Evaluation tests in factory of such as tensile and temperature characteristics, and other acceleration deterioration tests, are conducted by individual tests based on assumed effects. It goes without saying that such tests are significant because evaluation data shows individual cable characteristics. However, it is necessary to distinguish such data from actual environment data, upon which heavy weather, humidity and sunshine irradiation have complicated effects. Taking this into consideration, we installed the self-supported optical fiber cables to the outdoor with stainless steel pipe to evaluate their characteristics and reliability. We examined aging characteristics of the optical loss after

3.5 years, and the optical fiber distortion characteristics in summer and winter.

We used a high-stable laser and an optical power meter for measurement of optical attenuation loss change, and made two kinds of measurements for optical fiber distortion: BOTDA (Brillouin optical time domain analysis) and a phase method, in order to evaluate local distortion of the fiber in the longitudinal direction and mean distortion. As the result of this evaluation test, we successfully verified that the optical attenuation loss change was within 0.02dB/km even after 3.5 years of its installation, that local distortion was within 0.1% and that it was mostly uniform. In this paper, we show the cable structure, the characteristics, the evaluation test results of the developed cable and the results after installation.

2. CABLE STRUCTURE

The structure and parameter of developed cable are respectively shown in Figure 1 and Table 1. The cable are available with two types of stainless steel pipe :one with 12 single-mode fibers and an outer diameter is 0.25mm, and the other with 4 fibers ribbon. The former type is described in this paper. The fiber and jelly are introduced into tube stainless steel pipe with 0.15mm thickness during tube forming, and then the formed pipe by with outer diameter 2.3mm is welded by a CO2 laser. This pipe covered by PE(Polyethylene) with 0.15mm thickness as a unit of cable provides full yield strength as a unit, thus allowing for simple unit structure.

Considering external force effects during field installation, we adopted the structure of prestranded cable. As an example, Table 2 gives a comparison between a stainless unit and a loose tube unit. In this samples used for comparison, the stainless steel unit has the structure mentioned herein and the loose tube unit has the structure of 3mm outer diameter and 0.5mm thickness using PBT material. In the test result of the compression characteristic in the above-mentioned

structure, stainless is about 3 times as strong as PBT. In the case of the same compression strength with PBT, the stainless steel pipe can make its thickness more thinner by down to 0.1mm.

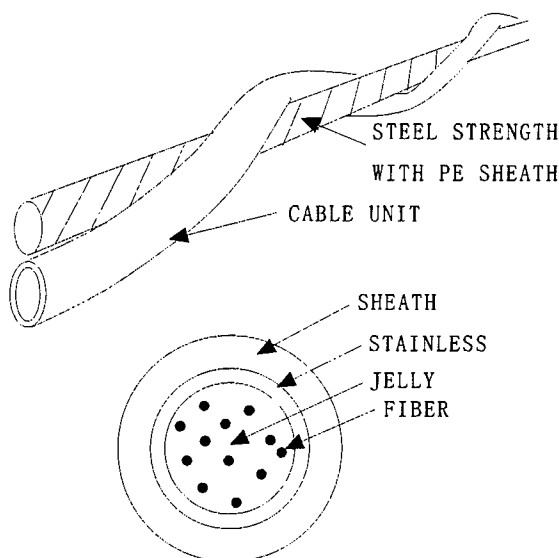


Figure 1 Cable Construction

Cable parameter	Specification
Stainless steel pipe outer diameter	Max: ϕ 2.3mm Min: ϕ 1.8mm
Stainless steel thickness	0.15mm
Cable diameter	Max: ϕ 5.3mm Min: ϕ 4.8mm
The maximum number of fiber	12 fibers
Cable weight	Max: 0.78N/m
Outer diameter of steel strength with PE sheath	ϕ 4.6mm

Table 1 Cable Parameter

	Stainless tube	Loose tube
Unit diameter	ϕ 2.3mm	ϕ 3.0mm
Unit weight	0.088N/m	0.098N/m
Young modules	137KMPa	2.35KMPa
Thermal expansion coefficient	1.6×10^{-5} (cm/cm/°C)	8×10^{-5} (cm/cm/°C)
Compression	3.5~4 (KN/100mm)	1~1.5 (KN/100mm)

Table 2 Comparison between loose tube unit and stainless steel tube unit

3. CABLE ADVANTAGES

In addition to high corrosion resistance, this cable has the following two merits. The first merit is a small diameter. This is useful for installation and carrying when developing for subscribers. For example, the cable unit which is described in this paper has an outer diameter of 5.3mm and the steel strength with PE sheath has an outer diameter of 4.6mm. The gross cable weight is about 0.78N/m.

The second one is the stainless steel pipe unit that is resistant to external force. That is, the cable can be applied for various environment. The unit has excellent performance such as a tensile strength with 10 times or more as high as plastic cable unit, no moisture penetration and thermal expansion coefficient close to fiber.

Another advantage of the cable is the prestranded structure that allows for easy separation between the messenger wire and the cable unit. After separation, the stainless steel pipe ensures enough strength, and is excellent in low thermal expansion and formability as against plastic loose tubes.

4. OPTICAL PERFORMANCES

4.1 OPTICAL ATTENUATION LOSS CHANGE DURING MANUFACTURING PROCESS AND INSTALLATION

Figure 2 shows the optical attenuation loss change during manufacturing process and after installation. In general, it is known that the fiber inside a cable unit is slackened as though a helical trail were being drawn. It is therefore thought that the fiber is loose. As shown in figure 2, there is no prominent increase in optical attenuation loss between processes, and the optical attenuation loss level after installation remains unchanged and is stable.

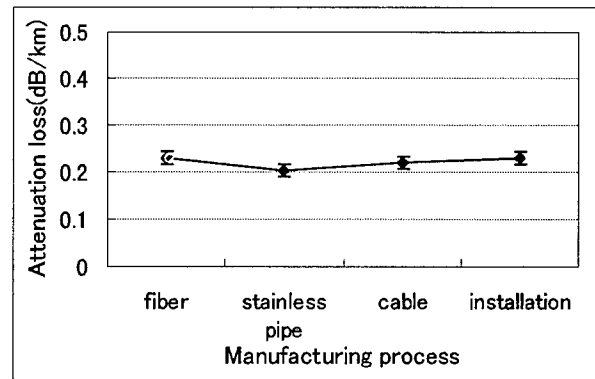


Figure 2 Attenuation change during manufacturing process

4.2 CABLE CHARACTERISTICS AFTER MANUFACTURING

Table 3 shows the results of the evaluation test. Aerial cables are required to withstand various loads applied during installation and service periods, and have to maintain their transmission characteristics. Then we have conducted various tests such as impact, compression, tensile strength, cable bending, temperature cycling, water penetration and so on. The tensile strength characteristic is considered to be important in terms of reliability because it is related directly to the fiber elongation characteristic on a transmission line. With this evaluation, a tensile test was conducted to clarify the relation of elongation between the cable and fiber when the cable are stretched. Figure 3 shows the evaluation results of the tensile test. As seen from the figure, the optical fiber has an elongation of 0.01% or less, when applying a tensile that causes a cable elongation of 0.2%. It is therefore recognized that little load is applied to the optical fiber structurally. The compression characteristic shows the maximum advantage of stainless steel pipe. There is no increase in optical loss even if 15kN/100mm is applied. It is clear that the stainless steel pipe shows a very good characteristics. Figure 4 shows the results of the compression characteristic evaluation test.

Figure 5 shows the results of the evaluation of the attenuation optical loss vs temperature

characteristic. Because the optical loss change was 0.02dB/km within a cycle temperature range from -40℃ to 70℃, the characteristic was seen as good.

Test	Result
Impact	9.8N×1m <0.01dB
Compression	2000N/100mm <0.01dB
Tensile strength	2500N <0.01dB
Cable bending	r=100mm 180° <0.01dB
Temperature cycling	-30~70℃ <0.02dB/km
Water penetration	1m 24hours No water leakage

Table 3 Test result

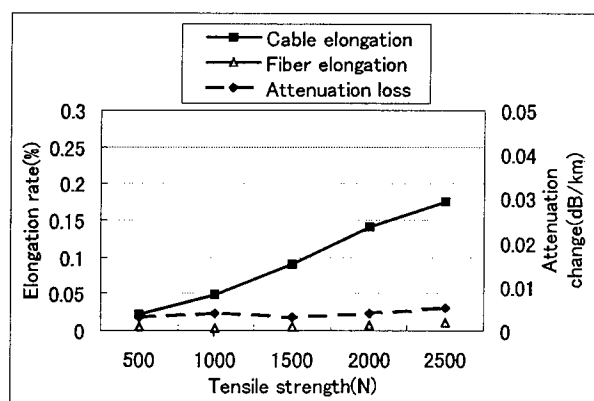


Figure 3 Tensile - strength testing

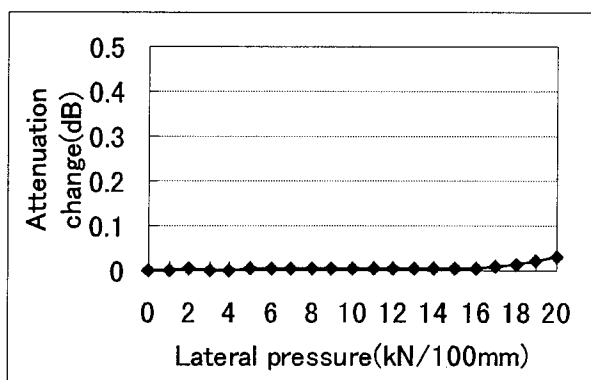


Figure 4 Compression testing

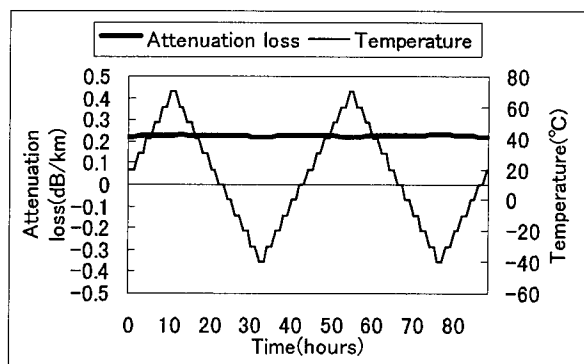
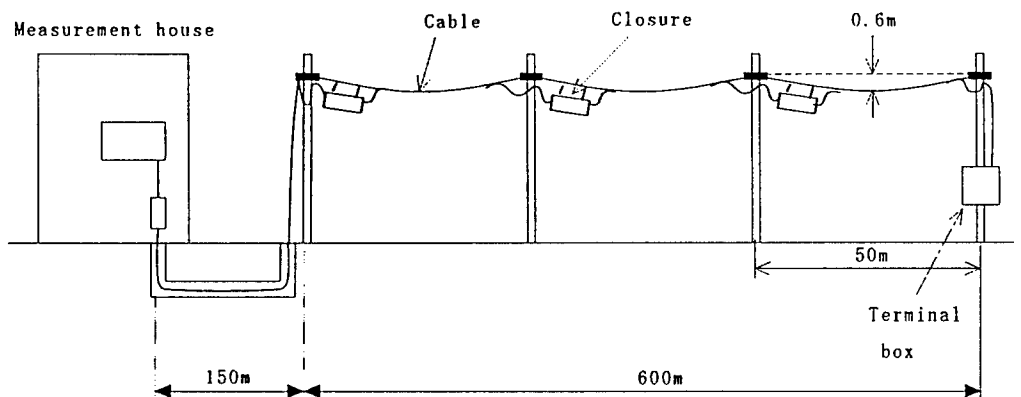


Figure 5 Attenuation vs temperature characteristics

4.3 CABLE CHARACTERISTICS IN FIELD TESTING

We installed the stainless steel tube covered optical fiber cable in outdoors and evaluated their characteristics under field condition to verify reliability further. We assume that in the worst conditions they would undergo a wind pressure of 110kg/mm² at a distance of 50m between supporting points. Figure 6 shows the route diagram. The cable was looped at seven points on the optical fiber, 3.2km in overall length and fusion spliced at 17 points. The newly developed closure was used for all the connections. 3.5 years have passed since the cable was installed. We measured the optical attenuation loss during this period. Figure 7 shows the results of the attenuation loss characteristic. Based upon the evaluation, the cable was proven to have good, stable characteristics because no particular increase in optical attenuation loss was found within the period of 3.5 years after installation.

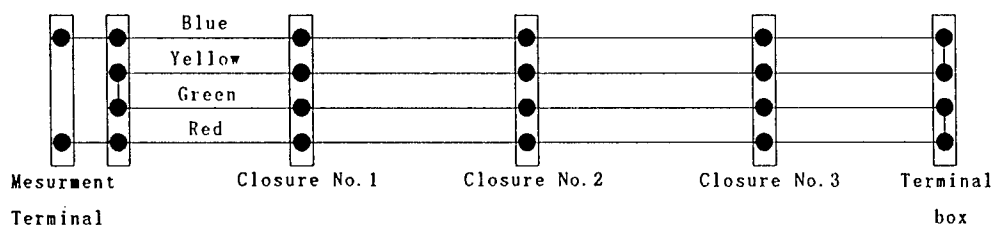
Then, we made measurements of the distortion in the longitudinal direction using BOTDA, in order to investigate local distortion of the optical fiber of the installed cable. It is thought that local concentration of the distortion with optical fiber should be verified because such as dancing or galloping occurs in actual environments due to various causes, including wind pressure. As a result of the evaluation, we verified that local fiber distortion was 0.1% at maximum and was



Installation environment

Temperature $-8 \sim +38^{\circ}\text{C}$ (Ave. 18°C)

Wind $0 \sim 28\text{m/s}$ (Ave. 22m/s)



Total length : about 3,000 m

Figure 6 Field testing route diagram

mostly uniform in the longitudinal direction. Figure 8 shows the result of BOTDA measurement.

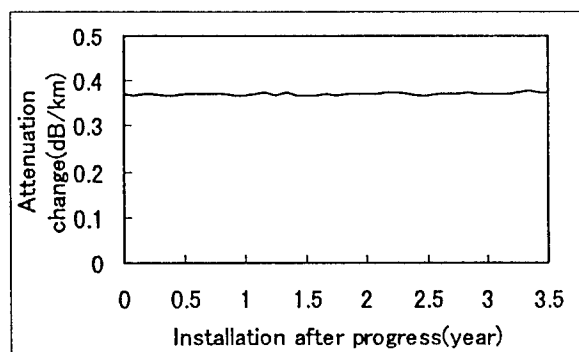


Figure 7 Attenuation change after installation

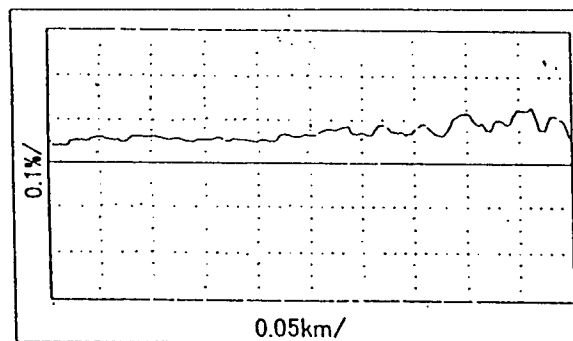


Figure 8 BOTDA testing

Along with this evaluation test, we measured optical fiber distortion during summer and winter seasons that were different in environment temperature, in order to investigate the change of optical fiber inside the stainless pipe due to the temperature changing. Figure 9 and 10 show the test results of the evaluation of optical fiber distortion. It can be seen that optical

fiber distortion follows temperature changes in the summer and winter season. In the summer season, the optical fiber distortion for a temperature change of 15°C was about 0.01%; in the winter season, that for a temperature change of about 20°C was about 0.02%. The maximum optical fiber distortion was about 0.02% in the direction of elongation at a temperature of about 36°C , and the minimum was about 0.01% in the direction of shrinkage at a temperature of about 0°C . From the above results, the total optical fiber distortion was assumed to be about 0.03% throughout the year, and very little change due to temperature was verified.

Incidentally, we can see the part which has a big distortion change in figure 10. This is the important data when typhoon was passing through. The velocity of maximum wind in this case was 23.2m/s.

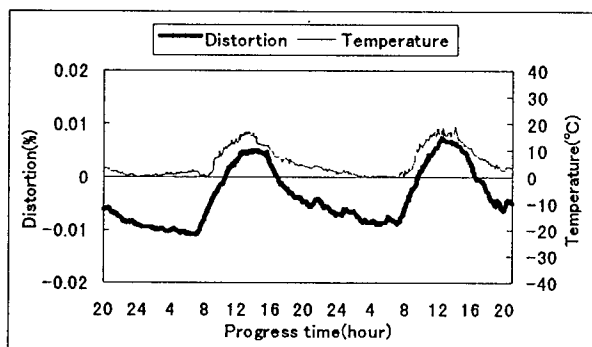


Figure 9 Distortion during day in winter

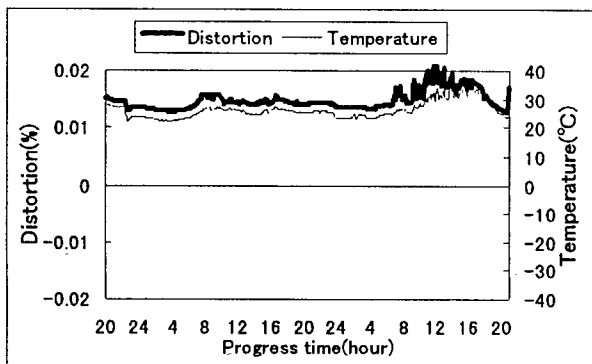


Figure 10 Distortion during day in summer

5. CONCLUSION

We have developed optical fiber cables which have their optical fiber inserted into stainless steel pipe. These cables have excellent characteristics in external environments. We evaluated them using which include outdoor installation testing. At the test result of the evaluation, we verified that the optical attenuation loss change and the local distortion were small respectively and the distortion was mostly uniform. The cable structure has a features of small diameter and very strong. The cables will perform fully in a year-round heavy-weather area or heavy-snow area.

Also, the cables will be able to be applied for indoor uses, such as under-carpet cables, by making the most of the above features.

REFERENCE

- 1.H.Ishizaki, S.Imamura, H.Momma, "Development of Electro-fiber optic cable containing metal tube armored fiber for deep sea tow", 45th IWCS,1996
- 2.T.Ohsako, Y.Sudo, K.Nemoto, "The changing characteristic of M-PAC after installation (2)", Record of Annual Meeting of IECE Japan, 1997, March
- 3.Andrew S.Dodd, Harvey R.McDowell III, Richard S.wagman, "Design and test considerations for fiber optic aerial cables ", 39th IWCS,1990



YASUSHI SUDO

Submarine System Div, Ocean Cable Co., Ltd.
1-105-2 Hibikimachi Wakamatsuku, Kitakyushu 808
Japan

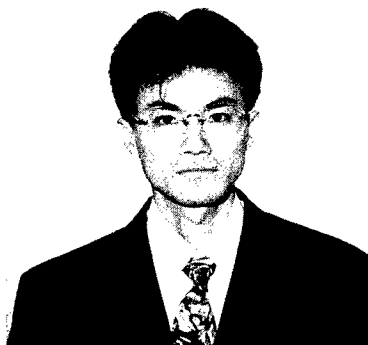
YASUSHI SUDO was born in 1969. He joined Ocean Cable Co., Ltd. after his graduation from Chiba University with a B.E in 1994, and has been engaged in research and development department of wire and cable. He is an engineer of the Submarine System Division.



KAZUMASA NEMOTO

Submarine System Div, Ocean Cable Co., Ltd.
1-105-2 Hibikimachi Wakamatsuku, Kitakyushu 808
Japan

KAZUMASA NEMOTO was born in 1953. He received the B.E. degree in electrical communication engineering and the M.E. degree in electronic engineering from Tokyo Denki University in 1976 and 1979, respectively. He joined Ocean Cable Co., Ltd. in 1979 and engaged in the development of submarine optical fiber cable. He is a member of the Institute of Electronics, Information and Communication Engineering (IECE) of Japan.



TAKUYA OHSAKO

Submarine System Div, Ocean Cable Co., Ltd.
1-105-2 Hibikimachi Wakamatsuku, Kitakyushu 808
Japan

TAKUYA OHSAKO was born in 1967. He joined Ocean Cable Co., Ltd. after his graduation from Tokyo Denki University with a B.E in 1990, and has been engaged in engineering department cable and wire division. He is an engineer of the Submarine System Division.



HIROSHI ISHIZAKI

Submarine System DIV Ocean Cable Co., Ltd.
1-105-2 Hibikimachi Wakamatsuku, Kitakyushu 808
Japan

HIROSHI ISHIZAKI was born in 1952. He joined Ocean Cable Co., Ltd. after his graduation from Sophia University with a B.E in 1976, and has been engaged in research and development of fiber, oceanographic cable. He is an engineer of the Submarine System Division, member of the IEICE of JAPAN Society of Applied Physics.

DEVELOPMENT AND DESIGN FOR OPTIMIZING HIGH-COUNT OPGW

C.H JUNG, S.C PARK, Y.I LEE, H.J KANG

**TAIHAN ELECTRIC WIRE CO., LTD.
785, KWANYANG-DONG, ANYANG-CITY, KYUNGKI-DO, KOREA**

ABSTRACT

In order to establish the current tendency for longer distance and larger capacity communication, it is essential for developing the high count optical cable. Besides, in case of OPGW, the superior optical characteristics against heat resistant and macrobending loss is required to be used for severe environment condition. So, it is necessary to develop the OPGW which has a high count fibers with low transmission loss, easy splicing and high reliability. In order to achieve above recent demand, we manufactured rectangular unit using of three stacked edge-bonded 8-fiber ribbon which was coated by UV-acrylate resin, and this unit are inserted into AL spacer with three grooves for a 72-core OPGW. This paper describes the characteristics of 72-core OPGW such as heat resistant properties and ribbonized structure to give an optimized residual strain in cable.

1. INTRODUCTION

The general need for compact high fiber

count cable design is leading to a widespread interest in OPGW. Recent trends in OPGW design include the production of cables which are small size, high count fiber and low manufacturing costs. Therefore, We considered a comprehensive design and development which has resulted in the creation of a family of new OPGW design. In order to make a high count OPGW, we design the ribbonized OPGW cable by using the rectangular unit and analyzed the cable properties such as heat resistance, tensile strength and attenuation. Thus, the ribbonized rectangular type unit for successful optical performance and high count fiber was attempted to design a new kinds of OPGW. The optical units with 72-core fibers were placed in a AL spacer of three grooves. Based on the analysis of optical characteristics, we made trial cables and carried out the various test. The ribbonized OPGW is required to endure 200 °C aging for heat shock and 120°C aging for long term heat test under high voltage power cable. In addition, it is very important to evaluate the residual strain of fiber in the AL spacer for optimized cable design as well as mechanical

characteristics. We will discuss the concepts of OPGW design, the theoretical strain analysis, the MAC properties according to the macrobending loss of ribbon, heat shock test, long term heat test and mechanical test for new ribbonized OPGW.

2. OPGW DESIGN

2.1 Structural Design of Optical Unit

To design the allowable strain and easy manufacturing conditions, the dimension of rectangular unit can be represented by equation (1) and (2) respectively.

$$H = 2(U_t + C + S_R \cdot R_t) + S_R \cdot F_D \quad (1)$$

$$W = 2(U_t + C + R_{et}) + F_N \cdot F_D \quad (2)$$

Table.1 illustrates various parameters of unit by using above equations. Therefore, we calculated the manufacturing conditions required to make a cable with an efficient

ITEM	DESCRIPTION	VOLUME
U_t	Unit thickness	0.2mm
S_R	Number of stacked ribbon in a unit	3
R_t	Ribbon coating thickness	0.025mm
R_{et}	Ribbon coating thickness of edge-section	0.05mm
F_D	Coated fiber diameter	0.250mm
F_N	Fiber count in a ribbon	8
C	Clearance	C_h 0.6mm
		C_w 0.4mm
H	Unit height	2.5mm
W	Unit width	3.3mm

(Table.1) Explanation of design item

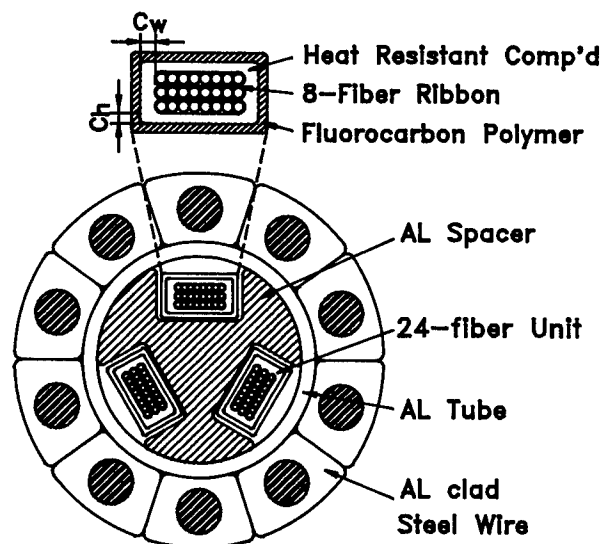


[Fig. 1] Cross section of 72-core OPGW with ribbon unit of rectangular type

clearance value ($C_h=0.6\text{mm}$ and $C_w=0.4\text{mm}$) to optimize the residual strain in cabling process.

2.2 Design of Rectangular Type Unit

As the OPGW is affected by the stress during manufacturing process and installation, we developed the edge bonded 8-fiber ribbon coated by UV acrylate resin which is the most widely used in the world, and then this unit was coated by fluorocarbon polymer for rectangular type and injected by heat resistant filling compound as shown in Fig. 1. Mainly, the heat resistance properties depend on the materials which make up optical sub-unit in OPGW. The heat resistant filling compound is used for improving the heat resistance and preventing each ribbon from adhesion. Also, the rectangular unit coated

by fluorocarbon polymer offers the buffering layer against stress during manufacturing process. To evaluate design of the optimized OPGW unit and the characteristics of performance, the 72-core OPGW which is composed of three layers of 8-fiber ribbons for each groove is developed. Especially, for giving an optimized residual strain and decreasing the attenuation of edge part in ribbon during manufacturing process, the ribbon is positioned into the rectangular unit that has a sufficient excess length and heat resistance.

2.3. Theory of Residual Strain

To design the optimized OPGW structure, we investigated the ribbon strain of a newly developing ribbonized OPGW. Basically, the strain in cabling process, shown in Fig. 2, is composed of fiber elongation, bending and twist.

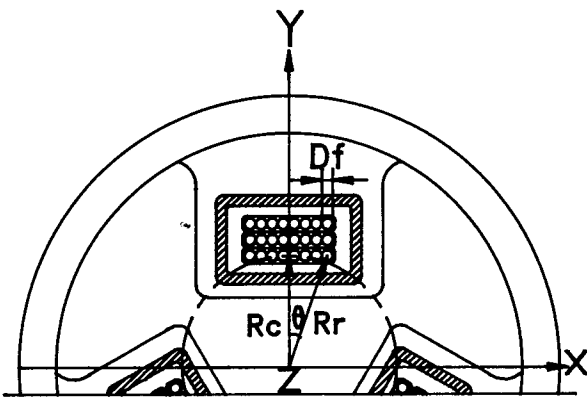


[Fig. 2] Analysis of strain

① Fiber elongation strain

Fiber elongation strain(ϵ_e) is the strain

produced by back tension on the ribbon and came from the additional fiber path length with accommodation into the AL spacer. This is expressed as eq. (3).

$$\epsilon_e = \frac{\sqrt{(2\pi R_r)^2 + P^2}}{L_f} - 1 \quad (3)$$

where, R_r : bending circle radius for each fiber

P : AL spacer pitch

L_f : the each fiber path length into the AL spacer

② Fiber bending strain

The fiber curvature and the fiber strain are dependant on cable bending radius. The strain of the fibers along the cable is caused by the length difference of fibers when the cable is straight and bent in AL spacer groove. The effective bending radius of each ribbon(R_b) is expressed as eq. (4).

$$R_b = \frac{D_r}{2} + \frac{P^2}{2\pi^2 D_r} \quad (4)$$

where, D_r is pitch circle diameter for each fiber. Fiber bending strain (ϵ_b) is calculated as

$$\epsilon_b = \frac{D_f}{2R_b} = \frac{\pi^2 D_f \cdot D_r}{\pi^2 D_r^2 + P^2} \quad (5)$$

where, D_f is the fiber diameter

③ Fiber twist strain

The fiber length difference in a ribbon is a function of twist. As the ribbon is

twisted, the fibers in the center of the ribbon are compressed while those on the outside are in tension. The fiber twist strain can be represented by eq. (6)

$$D_t = \frac{P}{2\pi} + \frac{2\pi R_r^2}{P}$$

$$\varepsilon_t = \frac{D_f}{2R_t} = \frac{P/2\pi}{R_r^2 + (P/2\pi)^2} \times \frac{D_f}{2} \quad (6)$$

The total fiber strain (ε_{total}) during the cabling process is given by synthesizing the three kinds of strain as eq. (7)

$$\varepsilon_{total} = \frac{1}{2} \left[\varepsilon_e + \varepsilon_b + \sqrt{(\varepsilon_e + \varepsilon_b)^2 + (2G_f \varepsilon_t / E_t)^2} \right] \quad (7)$$

where, G_f : the modulus of elasticity

E_t : the Young's modulus of a ribbon and fluorocarbon polymer

Fig. 3 shows the characteristics of strain value of 8-fiber ribbon that has a rectangular type coated by fluorocarbon polymer and compared to the strain of ribbon unit without rectangular type during manufacturing process. As a result, Occurring the strain from tensile strength during installation and thermal expansion, the allowable strain value was less than 0.02% in rectangular type ribbon. On the other hand, the strain of stacked ribbon unit without rectangular type was more than 0.04%. In addition, we consider MAC value of optical fiber to improve the macrobending loss characteristics. Especially, since the edge part of ribbon is affected by stress during manufacturing process, it has a possibility of increasing

the attenuation. So, we investigated the relation between the attenuation and MAC properties.

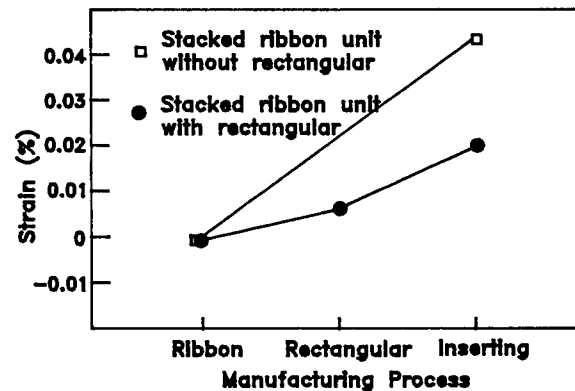


[Fig. 3] Strain analysis during manufacturing process

3. TEST RESULT

3-1 Heat Shock Test

This is an important test item to investigate the practicability of OPGW because it is occasionally affected by accidental fault from adjacent power cable and flash light resulting from lighting on the cable. The transmission loss in wide range temperature was experimentally investigated and continuously monitored at wavelength of $1.55\mu\text{m}$ for rectangular ribbon unit with and without heat resistant filling compound. The specimens, ribbon unit with length 500m was looped at both ends, exposed to heat hysteresis in chamber under bundled condition (Peak temperature were 100, 120, 150, 170 and 200°C). Fig. 4 shows the variation of transmission loss in

accordance with peak temperatures for 8-cycle. The change of transmission loss in ribbon unit with heat resistant filling compound was less than 0.05dB/km. But, in case of ribbon unit without heat resistant filling compound, the variation of transmission loss was more than 0.1dB/km and the deterioration of coating material was severe.

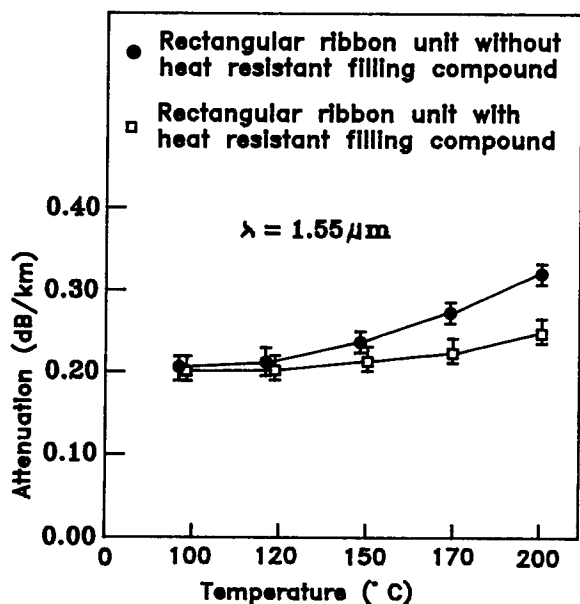


[Fig. 4] Attenuation versus heat shock

3-2 Long Term Heat Test

The purpose of this test is to determine the time to failure at a elevated temperature and to guarantee long compatibility. The exposure of optical fiber to high temperature characteristics can affect not only the mechanical and optical properties but also their aging behavior in the long term. Two types of rectangular ribbon unit in a bundle condition were

placed in an oven. The change of transmission loss of the rectangular ribbon unit under long term temperature condition is measured at 1.55 μ m as shown in Fig. 5. Consequently, the variation of transmission loss of rectangular ribbon unit with heat resistant filling compound is less than 0.05dB/Km, and this optical rectangular unit shows a good performance in long term heat test. From these investigations, we can prove that the rectangular ribbon unit has a stable characteristics under range of temperature from 80°C to 120°C for 400 hours.

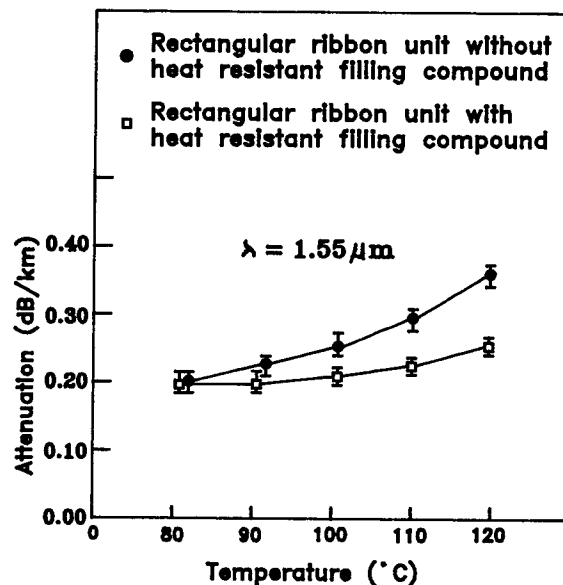


[Fig. 5] Attenuation versus long term heat resistance

3-3. Mechanical Test

The changes in transmission loss and fiber strain that caused by application of tensile force were measured. As a tensile load of 50kN, the fiber strain reached 0.15% and the optical attenuation was no change shown in Fig. 6. After removing

the loading from the cable, a remaining fiber strain of 0.02% was observed.

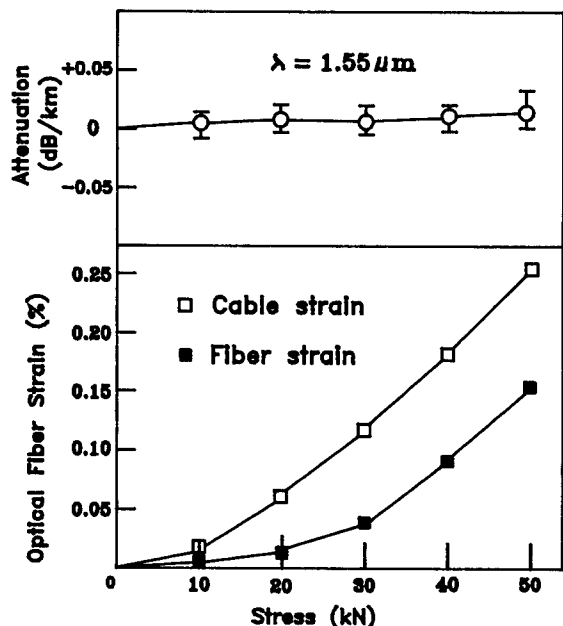


[Fig. 6] Attenuation and fiber strain versus tensile strength

3-4. MAC Value

The sensitivity of optical fibers to macrobending at $1.55\mu\text{m}$ wavelength is critical to their performance in cables. In order to ensure the optical loss below 0.25dB/Km at $1.55\mu\text{m}$ wavelength, it is indispensable to recognize the possibility of attenuation increase by macrobending in the ribbonized OPGW cable. The definition of MAC value is the ratio of the measured fiber mode field to the measured fiber cutoff. During cable manufacturing process, ribbon is apt to get damaged by stress and friction, and the attenuation of optical fiber can be increased at that time. We manufactured 8-fiber ribbon which is used the strong fiber at edge part of ribbon, namely good MAC properties, against stress. We theoretically analysed attenuation increase according to MAC

value, and the prediction derived from theory was consisted with experiment. Fig.7 shows the relation with MAC value versus attenuation obtained when AL spacer is wound in bobbin with \varnothing 800mm barrel diameter in order to compare the characteristics of rectangular type ribbon with and without heat resistant filling compound at edge fiber of 8-fiber ribbon.

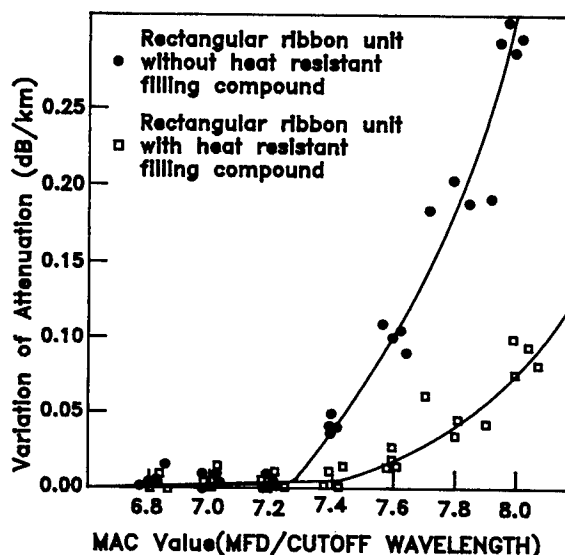


[Fig. 7] Attenuation increase and MAC value at edge fiber of 8-fiber ribbon

4. CONCLUSION

A newly developed OPGW cable has been designed, manufactured, and tested. Also, the theoretical and experimental analysis was performed with respect to fiber strain. Accordingly, we found that the proposed ribbon OPGW cable shows excellent optical and mechanical properties less than 0.05dB/km and fiber strain is less than 0.15% in 50kN tensile strength, and a remaining fiber strain of 0.02% was

observed after removing the loading from the trial cable. Through the testing of rectangular ribbon unit with heat resistant filling compound and consideration of MAC value, especially for both edge fibers of ribbon, it is verified that the ribbonized OPGW has a excellent characteristics enough to ensure heat shock test and long term heat test and has a satisfactory performance for practical use. The construction of the rectangular ribbon unit with heat resistant filling compound offers many advantageous features of new OPGW such as excellent heat resistance, easy splicing of the fibers and increase of the optical fibers number. The new ribbonized cable can be expected to contribute to the further expansion for application of OPGW.

5. REFERENCE

- (1) I. Matsubara, Y. Kitayama, S. Nishiyama, T.Kikuta. "Development of large-capacity composite fiber optic ground wire" , confarence of the Institute of Electric Engineers of Japan, 1065, 1986.
- (2) IEEE std. 1138-1994 "IEEE standard Construction of composite Fiber Optic Ground Wire(OPGW) for use on Electric Power Utility Lines"
- (3) H. Kawahira, T. Ishibashi "Development of a Composite of Fiber-optic Ground Wire" Sumitomo Technical Review. No. 23. 1984
- (4) T. Horiguchi et al., "Brillouin Characterization of Fiber Strain in bent slot type Optical Fiber Cable" Journal of lightwave technology, vol. 10, No. 9, September 1992.
- (5) Sadao Mori, Takeshi Ishibashi, Susumu, Ihara, Kouichi Kurebayashi, Yuji Kimura. "Development of a Fault-locating System using OPGW". Sumitomo Electric Technical Review. No.25, January 1986.

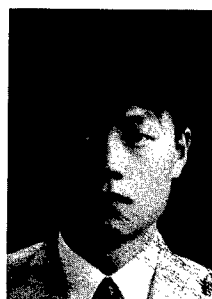
BIOGRAPHIES



Chang-hyun, JUNG

Taihan Electric Wire Co., Ltd. Korea

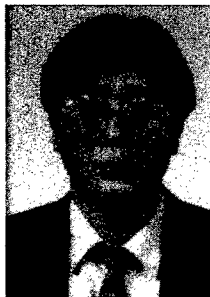
C.H. JUNG received his B.A. degree from Hanyang University in 1994. He joined Taihan Electric Wire Co., Ltd. and has been engaged in engineering department of optical fiber. Now he is a engineer of Fiber Optics Engineering Department.



Sang-cheol, PARK

Taihan Electric Wire Co., Ltd. Korea

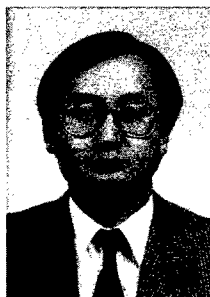
S.C. PARK received his B.A. degree from A-juo University in 1994. He joined Taihan Electric Wire Co., Ltd. and has been engaged in engineering department of optical fiber. Now he is a engineer of Fiber Optics Engineering Department.



Young-ik, LEE

**Taihan Electric Wire
Co., Ltd. Korea**

Y.I. LEE received his M.S. degree from Yonsei University in 1981. He joined Taihan Electric Wire Co., Ltd. and has been engaged in engineering department of optical fiber. Now he is a section manager of Fiber Optics Engineering Department.



Hee-jeon, KANG

**Taihan Electric Wire
Co., Ltd. Korea**

H.J. KANG received his B.A. degree from Hanyang University in 1979. He joined Taihan Electric Wire Co., Ltd. and has been engaged in engineering department of optical fiber. Now he is a general manager of Fiber Optics Engineering Department.

LOW PMD FIBERS BY AN ON-LINE SPINNING APPARATUS

M.Caiata, F.Cocchini, A.Mazzotti, A.Monetti, and A.Schiaffo

FOS Fibre Ottiche Sud, Battipaglia, Italy

ABSTRACT

A novel method has been experimented to apply a variable spinning to the fiber during the drawing process. The apparatus is able to torque the fiber through a rotating die while the protective primary coating is applied. This is effective in reducing the Polarization Mode Dispersion (PMD) of the fiber.

INTRODUCTION

Polarization Mode Dispersion (PMD) has become an issue in high bit rate telecommunication systems, especially when Optical Amplifier are used on long distances. Not negligible PMD values, larger than $0.15 \text{ ps/km}^{1/2}$, can be observed in optical fibers, especially in as highly doped fibers as Dispersion Shifted (DS) ones.

PMD is due to birefringence, i.e. the relative propagation delay between the two polarization states of the fundamental mode. On turns, the fiber birefringence is induced by the superposition of core ellipticity, asymmetric lateral stresses and twisting. Usually, all these events vary randomly along the fiber, thus producing mode coupling, i.e. the exchange of optical energy between modes.

Mode coupling and birefringence have opposite effects on PMD, since increasing mode coupling reduces PMD, while increasing birefringence increases PMD.

The application of a frozen-in twist in the fiber (spinning) at 2-10 turns/m is known to substantially reduce PMD [1], via mode coupling. The method is known to be more effective with an alternate rotation [2].

Up to now the spinning of the fiber has been obtained either by rotating the preform in the drawing furnace or by manipulating the coated fiber, close to the capstan. Both the methods have their shortcomings: the former needs to rotate an heavy, large and usually not well equilibrated preform in the furnace at high speed; the latter needs complex rotating machinery and usually adds an elastic twisting on the wound fiber.

In this paper we present a novel apparatus which is able to spin the fiber while drawing, through the rotation of the coating applicator.

THEORY

The novel apparatus is based on a rotatable die for the coating application. The flow in the rotating die is able to turn the naked fiber and to transfer the twisting to the neckdown region, to be frozen-in (see fig.1a-b, where for the sake of simplicity only one coating applicator has been considered).

The flow region in the die in standard application has been often described as an annulus with a fully developed flow [3]. Following that approximation, a rotatable die can be modeled through a Couette flow between two cylinders, of radii R_0 and R_1 , and height h (fig.2a-b).

The torque exerted on the fiber (i.e. the internal cylinder) by the rotating die (i.e. the external cylinder) is

$$(1) \quad M_1 = 4\pi\mu h \frac{R_0^2}{1 - \left(\frac{R_0}{R_1}\right)^2} (\Omega - \dot{\theta}_1) \equiv \\ \equiv K_1 (\Omega - \dot{\theta}_1)$$

where μ is the coating viscosity, Ω is the die angular speed, and $\dot{\theta}_1 = \frac{\partial \theta_1}{\partial t}$ is the fiber angular speed in the die (fig.1b).

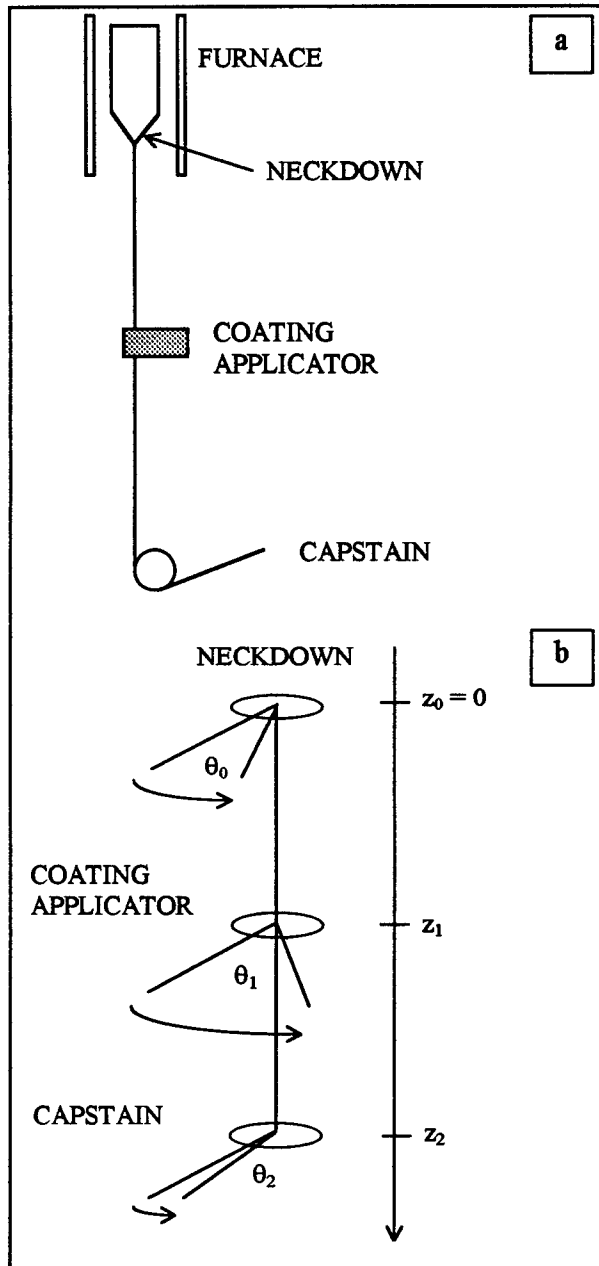


Figure 1 - Draw tower plan and torsion coordinates.

To achieve detectable results it should be $\Omega \gg \dot{\theta}_1$. Therefore eqn.(1) simplifies to

$$(2) \quad M_1 \approx K_1 \Omega$$

This torque is transferred through the solid elastic fiber up to the neckdown region and down to the capstan.

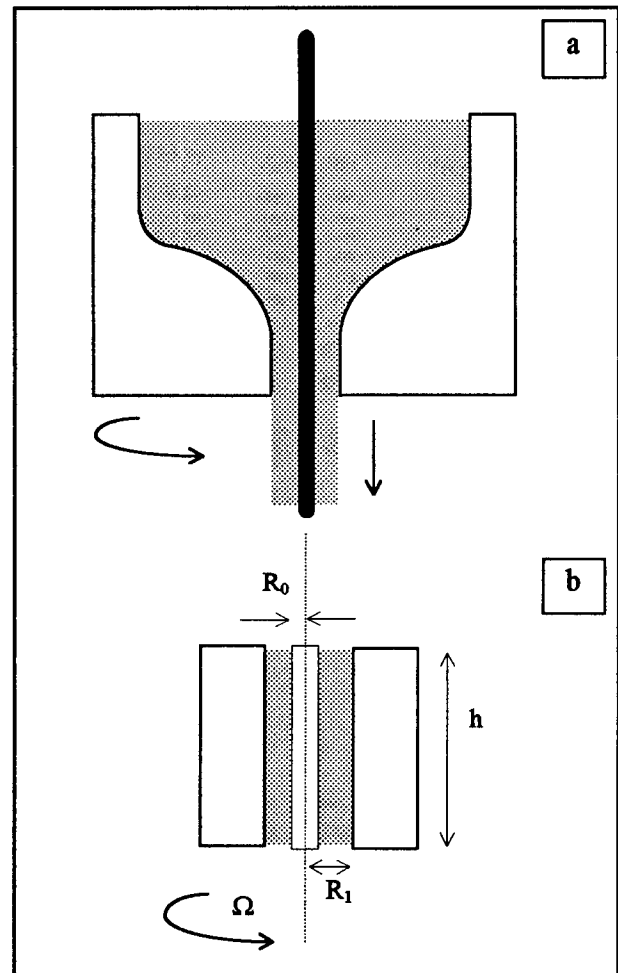


Figure 2 - Coating applicator and equivalent Couette flow.

The neckdown region in the furnace gives a torque associated to the viscous shearing. A uniform angular speed is assumed for simplicity on each section, i.e. $v_\theta = \omega(z) r$; therefore, the shearing stress is

$$(3) \quad \tau_{z\theta} = -\mu_{\text{glass}}(z) \frac{\partial v_{\theta}}{\partial z}$$

where $\mu_{\text{glass}}(z)$ is the glass viscosity depending on the local temperature. The torque in each neckdown section of radius $R(z)$ is

$$(4) \quad M_0 = 2\pi \int_0^{R(z)} \tau_{z\theta} r^2 dr = \frac{\pi}{2} R^4(z) \mu(z) \frac{d\omega}{dz}$$

Integrating in the neckdown region with the boundary conditions

$\omega(z < \text{neckdown}) = 0$ (i.e. the preform does not rotate in the furnace)

$\omega(z > \text{neckdown}) = \dot{\theta}_0 = \frac{\partial \theta_0}{\partial t}$ (angular speed of the fiber just below the neckdown)

the torque can be written as

$$(5) \quad M_0 = \frac{\pi}{2} \frac{1}{\int_{\text{neckdown}} \frac{dz}{R^4(z) \mu(z)}} \dot{\theta}_0 \equiv K_0 \dot{\theta}_0$$

The capstan will assure a torque M_2 which is dependent on how and if the fiber rotates in it. If the rotation of the die is alternated at a sufficiently high rate with respect to the time in which the fiber travels from the die to the capstan, a negligible rotation is observed at the capstan, thus avoiding at all residual elastic twisting on the wound fiber. Therefore it is assumed $\theta_2 = \text{constant} = 0$, which is, furthermore, the worst case for the die to be able to apply a torque to the fiber. The elastic torsion of the fiber depends on the torsion rate $d\theta/dz$. The torque associated is

$$(6) \quad m(z) = \frac{\pi}{4} \frac{E}{1+\nu} R_0^4 \frac{d\theta}{dz} \equiv H \frac{d\theta}{dz}$$

where E is the Young modulus of glass (72 Gpa) and ν the Poisson ratio (0.4).

For a standard fiber radius, 62.5 μm , the constant H turns out to be about $6.16 \cdot 10^{-7} \text{ N m/(rad/m)}$.

Neglecting inertia of the fiber the torques should be equilibrated along the z coordinates. Therefore between the neckdown region and the rotating die it results

$$(7a) \quad K_0 \dot{\theta}_0 = H \frac{\theta_0 - \theta_1}{z_1}$$

while between the die and the capstan it results

$$(7b) \quad K_1 \Omega = H \frac{\theta_1}{z_2 - z_1}$$

Since K_0 is usually small the above equations can be reduced to

$$(8) \quad \Omega = \frac{H}{K_1} \frac{\theta_0}{(z_2 - z_1)}$$

which relates the die angular speed Ω to the frozen-in rotation of the fiber θ_0 .

As an example let us consider a sinusoidal variation of the die speed

$$(9) \quad \Omega(t) = \Omega_0 \sin(2\pi\Gamma t)$$

where Γ is the inversion frequency.

From eqn.(8) it turns out that the frozen-in torsion of the fiber is

$$(10) \quad \frac{d\theta_0}{dz} = \frac{\dot{\theta}_0}{v_{\text{draw}}} = \frac{2\pi\Gamma K_1 \Omega_0}{H v_{\text{draw}}} (z_2 - z_1) \sin(2\pi\Gamma t)$$

where v_{draw} is the drawing speed. Let us consider a numerical example:

$$v_{\text{draw}} = 10 \text{ m/s}$$

$$\Gamma = 4 \text{ hz}$$

$$\Omega_0 = 10000 \text{ rpm} \approx 1000 \text{ rad/s}$$

$$z_2 - z_1 = 5 \text{ m}$$

$$\begin{aligned}
 h &= 4 \text{ mm} \\
 R_1 &= 120 \text{ } \mu\text{m} \\
 \mu &= 5 \text{ Pa s} \\
 K_1 &= 1.35 \cdot 10^{-9} \text{ N m/(rad/s)}
 \end{aligned}$$

From eqn.10, the maximum fiber torsion turns out to be about 4.4 turns/m. Therefore, this simplified analysis shows how it is possible to achieve fiber torsions of practical interest.

The analysis of eqn.10 suggests, furthermore, which are the key parameters to achieve the requested fiber torsion (at least 2-10 turns/m). In increasing order of practical feasibility or manufacture efficiency, it is possible:

- i) to reduce H , by reducing the glass fiber diameter (which will become not standard),
- ii) to increase the distance between the rotating coating applicator and the capstan,
- iii) to reduce the drawing speed,
- iv) to increase the K_1 constant, through a specific die design or by increasing the coating viscosity (see eqn.1),
- v) to increase the maximum angular speed Ω_0 and/or the inversion rate Γ of the rotating die.

Experimental results

An apparatus has been built according to the theory mentioned above [4]. The high angular speed of the die has been assured by mounting the die itself on ball bearings, supplied by an electric motor.

The motor has been driven by an electronic device which allow to vary the electric tension with time.

The actual frozen-in twist has not been monitored directly, but through PMD measurements, which is actually the quantity of interest, carried out by the Fixed Analyzer method on 1 km long samples.

In agreement with the theory (eqn.10 and following discussion), the effect of changing the maximum angular speed Ω_0 and/or the inversion rate Γ of the rotating die (during the drawing of the same preform) are quite

evident on the PMD values. In particular the PMD dependence on the die rotational speed has been reported in fig.3 and that on the inversion rate in fig.4. A substantial reduction of the PMD can be obtained by a suitable choice of the process parameter, e.g. $\Omega_0 = 10000 \text{ rpm}$ and $\Gamma = 4 \text{ hz}$.

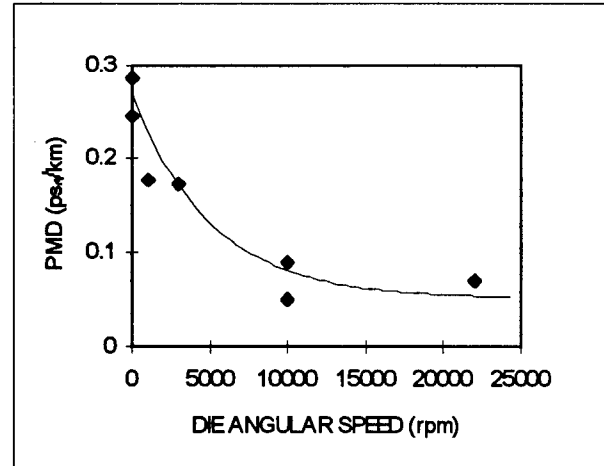


Figure 3 - PMD vs Die angular speed Ω_0 at an inversion rate $\Gamma = 4 \text{ hz}$.

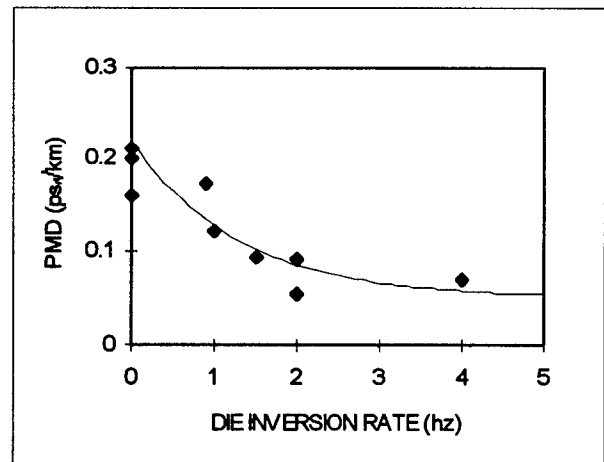


Figure 4 - PMD vs inversion rate Γ at a die angular speed $\Omega_0 = 22000 \text{ rpm}$.

The residual elastic torsion on the wound fiber has been verified to be negligible ($< 1 \text{ turn/m}$) by the visual observation of the recovery.

The high rate of the die rotation does not affect the coating application. On the contrary a slight increase of the coating concentricity has been observed since the rotation increases the axial symmetry of the application.

Conclusions

A substantial reduction of the PMD has been obtained by spinning fibers while drawing by a rotating coating applicator. Stable values below $0.1 \text{ ps/km}^{1/2}$ have been obtained by a suitable choice of the process parameters. The interplay of various parameters have been discussed theoretically and experimentally proven.

Acknowledgments

The assistance of G. Malafronte is acknowledged for the design of the apparatus.

References

- [1] A.J.Barlow, J.J.Ramsgov-Hansen, and D.N.Payne, *Applied Optics* 20 (1981) 2962.
- [2] A.F.Judy *IWCS 1994 Proc.* (1994) 658.
- [3] K.Chida, S.Sakaguchi, M.Wagatsuma and T.Kimura *Electron. Lett.* 18 (1982) 713.
- [4] F.Cocchini and A.Schiaffo, European Patent n. 96203170.4

Marco Antonio Caiata (first from the left) was born in 1966 in Basel (CH). After graduating from the Technical School of Chemistry "A. Avogadro" in Salerno in 1986 he joined FOS, where he is currently involved in drawing technological development.

Franco Cocchini (second from the left), after graduating in Physics from the University of Pisa in 1983, received a PhD in Solid State Physics from the Scuola Normale Superiore of Pisa. He has worked with EniChem R&D on the rheological and mechanical properties of polymeric materials. He joined FOS in 1990 where he dealt with the development of coating materials for optical fibers. He is now currently involved in modeling the process for fiber manufacturing and the fiber performances.

Andrea Mazzotti (first from the right) after graduating in Mechanical Engineering from UNICAL in 1992, joined FOS in 1994, where he dealt with mechanical reliability of optical fibers and coating properties. He is an active member of COST 246. He is currently involved in technological development of the manufacturing process.

Antonio Monetti (second from the right) was born in 1965 in Battipaglia (Italy). He graduated from the Technical School of Chemistry "A. Avogadro" in Salerno in 1985. He has been responsible of the Chemical Laboratory of MERAL (Metal Treatment). In 1991 he joined FOS, where he is currently involved in technological development of the drawing process.

Antonio Schiaffo (in the middle), after graduating in Mechanical Engineering from the University of Salerno in 1991, has been involved in Factory Automation in Comau/Fiat. After one year, he joined FOS where he is responsible for the technological development of the optical fiber manufacturing.



APPLICABILITY OF ALL-DIELECTRIC SELF SUPPORTING CABLE SYSTEMS TO VERY HIGH VOLTAGE OVERHEAD POWER LINES

Chris N. Carter, Jimmy Deas, Neil R. Haigh*, Simon M. Rowland*

The National Grid Company plc, Leatherhead, UK.

*BICC Cables Ltd, Helsby, UK.

ABSTRACT

It is well known that dry-band arcing provides a significant obstruction to the installation of All-Dielectric Self-Supporting (ADSS) cables in high voltage overhead power line environments. This paper reviews the aspects of high voltage overhead power line installations which need to be borne in mind when consideration is given to the deployment of ADSS cables. Progress is reported upon an ongoing (15 month long) field trial to investigate the phenomenon of dry-band arcing within HV ADSS installations, and in particular, the extent to which catastrophic failure of the ADSS cable can be prevented by utilising a length of semiconductive rod, installed alongside the ADSS cable span, as an arc control mechanism. In addition to presenting the results from the trial, which has included extensive environmental data monitoring, an example is shown of catastrophic dry-band arcing damage which has occurred to an installed ADSS cable on the trial site.

INTRODUCTION

Optical Cables for Overhead Lines

The de-regulation of the telecommunications and electricity distribution industries now taking place world-wide, has led to a dramatic increase in the demand for optical cable systems which can be installed on high voltage power networks. The competition and increased commercial pressures within these industries, has resulted in a number of means by which the optical cable may be deployed, depending upon various issues such as bandwidth, number of discrete fibres, cost, speed of installation and long term

system reliability. Currently, there are three dominant types of optical cable which are deployed¹: the optical ground wire (OPGW), the spiral wrap cable and the all-dielectric self supporting optical cable (ADSS). The OPGW cable is a popular choice if the overhead line system requires a new earthwire for refurbishment purposes or if a new overhead line circuit is being built. The spiral wrap cable which can be wrapped around an existing earthwire is attractive for transmission lines with existing earthwires which have a significant remaining lifetime, or if low installation costs and rapid deployment are important. The ADSS cable offers particular advantages in that it can be installed without the need to de-energise the power circuits, and, being separate from the power system, it offers unique benefits in terms of system maintenance and asset management in general. It is also of use as a short term repair cable where there is an urgent need to maintain an optical communications link, whilst repairs or refurbishments are made to the overhead power line carrying the existing communications channel. In such an instance, an interruption of several weeks (or possibly only a few days) to the communications link whilst the circuitry is repaired, might be completely unacceptable to the telecommunications service provider. In the UK, Energis, the telecoms carrier owned by the National Grid Company, use ADSS product for such rapid repairs.

The main drawback with ADSS cable, is that under certain circumstances, it can be catastrophically damaged by a phenomenon known as dry-band arcing². In the UK for example, concern with regard to dry band arcing damage has resulted in a situation where ADSS

cable will not be deployed on overhead lines at 275 kV and 400 kV unless as a short term repair section, whereas, it has been installed and performed reliably on 132 kV lines for around a decade.

Dry-Band Arcing

On a typical UK lattice tower, the ADSS cables are usually suspended at the level of the bottom or middle cross arm on a tower (Figure 1) and for a standard twin circuit tower, this will usually be at a point midway between the bottom four conductors. As a consequence, the ADSS cable, which will be at, or close to, ground potential where it is attached to the tower, is situated in an electromagnetic field which can give rise to a significant voltage gradient occurring along the length of the cable. Whilst the cable remains dry, this voltage gradient, which can be of the order of tens of kilovolts dropped over several metres, will not in itself present a problem. However, if the surface of the cable becomes conductive, due to the presence of moisture and/or pollution, the gradient can induce milliamp sized currents along the cable. By the nature of the system this current will be greatest at the point where the cable is joined to the tower, and, for reasons of symmetry, zero at the midspan position³. Figure 2 schematically shows the voltage gradient and associated leakage current for a typical ADSS cable, from which it can be noted that the majority of electrical activity is confined to a region of the span referred to as the 'active length.' Dry-band arcing takes place as the cable surface dries out, either naturally, or as a result of electrical Joule heating. The occurrence of such a dry band around the cable will lead to a break in the previously continuously conductive cable surface, and thereby, a large voltage may be dropped across the short section of cable which constitutes the dry-band gap. If electrical breakdown occurs across the gap, then the corresponding arcing activity can lead to erosion of the cable surface, and ultimately, a deep furrow being cut into the cable sheath. In extreme cases, the strength member within the cable may become exposed and weakened, leading to catastrophic failure of the cable altogether. However, for commercial reasons, such failures have not been widely reported or discussed in the literature. Therefore, in the following section, we describe those parameters

which we believe to be critical for the safe deployment of ADSS cables in high voltage environments. We also report on the progress to date on the development of a device which will prevent dry-band arcs in situations where they would otherwise have occurred.

DEPLOYMENT OF ADSS CABLE

System Voltage and Space Potential Contours

As described above, the threat of dry-band arcing has resulted in the situation where, in general, ADSS cables have been used routinely on overhead line systems at 150 kV or below, but not for example at, 220, 275 and 400 kV. This is a consequence, not only of the reliable performance to date of such cables in the field in 132 and 150 kV installations, but as a result of assessments made upon the magnitude of the space potential within which the ADSS cable is to be strung. Such an assessment is useful because it can be used to estimate the likelihood of the occurrence of dry-band arcing, and in this regard, formulae⁴ and indeed, commercial software now exists, which can use the configuration and geometry of the phase conductors to estimate the space potential around the ADSS cable when strung in the overhead line system. The output of the software is usually displayed in the form of a plot of the electrical space potential contours³ in planes perpendicular to the cable span, although it is capable of much more. The desired outcome of such a calculation is the identification of regions of low, preferably zero, space potential, within which the ADSS cable may be strung. Experience in the field to date has led to a general heuristic which associates a 'safe' ADSS installation location as lying within space potential contours of 12 kV or less, and potentially hazardous locations as being above this threshold value. Because the construction, geometry, and location of the overhead line towers is likely to vary considerably along the overhead line route, the above field calculations may not necessarily be undertaken in simplistic terms for the route in its entirety, and accordingly there may be a need to take into account the specific tower geometries. More importantly, but less obviously, the effect of a line outage of one of the circuits if it is a twin circuit system, and the impact of extreme environmental conditions such

as wind induced 'blow out', need to be considered. Even in conditions where the cable is typically in a low space potential, such changes in conditions can increase this to a level where the threat is high. It must not be forgotten that the ageing mechanism is not a gradual one but occurs suddenly and quickly depending upon the environmental conditions⁷.

Leakage Currents and Arc Properties

A further refinement of the assessment of the in-service environment around an ADSS cable is the evaluation of the magnitude of the leakage currents which may be drawn along the cable by the capacitively coupled voltage gradient. In particular, considerable effort has been made to investigate how the nature of the damage occasioned to the cable sheath is related to the magnitude of such currents and the properties of their associated electric arcs^{3,6,7}. It has been established that the greatest damage to the cable occurs when the earth leakage currents are in the range of 1-5 milliamps⁶, and accordingly, a nominal threshold of 1 mA can be chosen below which arcing activity is considered to be acceptable, and highly unlikely to lead to damage to the cable sheath. Support for such a threshold level can be drawn from the observations of laboratory tests utilising high voltage, low current arcs on wetted cables^{3,6}, as well as from field experience on the performance of ADSS in 400 kV installations, such as the recent UK field trial at Hunterston⁵.

Geographical and Environmental Considerations

It is clear from the above analysis that the combination of the overhead line space potential and resulting current induced on the ADSS cable are of primary importance in assessing the potential for dry-band arcing damage to occur. The situation is however further complicated by the difficulty in predicting (and indeed verifying) the electrical resistance of the ADSS cables when in service, as this directly affects the magnitude of the leakage currents which may be driven by the induced space potential. For example, when dry, the resistance of the cable is estimated to be in the region of 10's of Megohms per metre, such that when in a 400 kV overhead line installation and a corresponding worst case space potential position of 35 kV, the available

current on the cable will be much less than 0.5 mA and, consequently, damaging arcing is unlikely to take place.

However, the presence and combination of rain, dew, salt-spray and pollution upon the cable can alter the situation, such that the leakage currents are high enough that damaging arcing is initiated. The resistance per unit length of any real cable will vary, from very high when dry, down to a variable lower limit, determined by the prevailing conditions, when polluted and wet. Humid, marine locations will often result in values of the order of 10^5 ohms/m, whereas inland rural areas well away from industry may rarely see less than 10^7 ohms/m. However, although these more conducting conditions may be rare they can be damaging. Even in the cleanest areas it would be prudent to assume that 10^6 ohms/m will be attained infrequently. Thus it is not simple to use the geographical location of the route (e.g. coastal/inland/rural/industrial) as a guide to the suitability of ADSS cable to an application. In marginal cases there may be a need for the severity of pollution that may be precipitated onto the cable to be assessed, in order that the worst case electrical resistance of the cable can be estimated and the magnitude of the earth leakage current derived. An indication of such an estimation technique is illustrated in Table 1, which shows how the space potential threshold level at which damaging arcing may occur varies with the resistance per unit length of the cable. Furthermore, the table also shows how the resistance per unit length may vary with the level of pollution (classified arbitrarily as light, medium and heavy). Further work is required in order for meaningful pollution levels to be associated with specific geographic locations. For example, marine pollution, which can be classified in this case as heavy, may be fairly frequent close to the sea, but cannot always be ruled out 50 km or more from the coast; rural areas which might be thought of as pollution free (i.e. light) may on occasion, have agricultural pesticides and fertilisers, applied in aerosol form from the air, which may become deposited as pollution upon the cable. Industrial pollution itself is emitted from a large number of sources, is often poorly documented, and can be redistributed almost anywhere by the prevailing meteorological conditions.

HIGH VOLTAGE ADSS SYSTEMS

A number of solutions have been proposed to enable ADSS cables to be installed in very high voltage overhead line systems, and these can be broadly divided into two areas:

- i Use of arc resistant (Anti-Tracking) sheaths;
- ii Development of arc control methods.

Arc Resistant Cable Sheaths

With the advent of ADSS cable failures in the field, it was generally recognised that polyethylene (PE) cable sheaths were unlikely to provide reliable, long term protection against arcing damage, even within 132 kV installations. Consequently, attention has been focused within the last 5 years or so, upon the development of sheath materials that offer resistance to arcing and the growth of arc tracks or erosion⁴. Certainly, ADSS cables with such arc resistant sheaths have led to an improvement in the performance of the cables. However, such resistance will not always protect the cable over its required service lifetime. Such protection has certainly not been proven, and it is difficult to see how this could be achieved until many more years of experience have passed. The evidence of laboratory testing is not strong since this has been with unrepresentative high current tests which are less onerous than low current service conditions⁷.

Arc Control Mechanisms

Several means have been described in the literature^{8,9} by which electrical activity within the vicinity of the ADSS cable may be modified or controlled to the extent that damaging arcing does not take place. For example, the cable sheath itself can be made to be semiconductive. However this has drawbacks, not only in terms of cable processing, but in finding the balance in cable conductivity per unit length such that dry band arcing is prevented, whilst electrical Joule over-heating does not, in itself lead to failure of the cable. In this paper we report upon the progress made to date for an arc-control system which comprises of a semiconductive rod which is attached to the ADSS cable, and pushed out from the tower over the first 50 metres of the

span. Details of this technique were first described at IWCS '95⁹, and at IWCS '96 last year¹⁰. Briefly, the retrofit rod system comprises of a rod with a resistance per unit length in the range 300 to 1300 kilohms per metre, attached to the ADSS cable by a series of semiconductive clips spaced typically at around 30 cm apart. The rods are pushed out by hand from the tower to a distance of 50 metres, covering the so called 'active length' of the ADSS cable, where the leakage currents might exceed the damaging arcing threshold. Details of the field trial used to assess the performance of the retrofit rod system are described below.

An issue associated, but different from the threat of dry-band arcing, is corona discharge. This can occur at the ends of the metallic clamps, which act as stress raisers, and can lead to slow, gradual, erosion. This is different from the type of dry-band arcing described here, which can be an all-or-nothing event, with damage occurring over a very short space of time, possibly days. It is our experience that in some locations, dry-band arcing is very rare, but when and where it does occur, maybe after many arcing-free years, damage can be very rapid indeed.

FIELD TRIAL OF RETROFIT ROD ARC CONTROL SYSTEM

Trial Configuration

As first reported at IWCS '96 last year¹⁰, a field trial of now 15 months duration, is underway, to evaluate the performance of the retrofit rod system in a very high voltage 400 kV installation. The overhead line system is located in a coastal region of Southern England, in conditions which are particularly aggressive because of the local environment. Furthermore, prior to the installation, the ADSS cable sheath was 'pre-aged' by hand, using a mild abrasive process, estimated to provide a preliminary weathering of the cable sheath surface equivalent to around 2-3 years of exposure in the field. This was necessary, as the strongly hydrophobic nature of standard cable sheaths can be quite efficient in preventing dry banding (and hence arcing) from taking place during the first few years following installation of a cable. To further provide acceleration of the conditions liable to promote dry band arcing, the ADSS cable was not strung in the optimum space potential location on the

tower, but was instead, offset by around 1 metre from the tower centre axis, such that the space potential at the cable midspan was of the order of 20 kV during the continuous in-service condition of the cable. In addition, it was also estimated that for such an offset position, an outage of one of the transmission circuits would, in the worst case, raise the space potential to around 35 kV, thereby representing an extremely aggressive environment for the cable.

The trial configuration comprises two ADSS cable spans as illustrated schematically in figure 3, one of the spans (section A to B) has been used as an experimental control, and it therefore was not fitted with the retrofit rod device. The other span (section C to D) has been used to evaluate a range of retrofit rods, and associated component hardware, such that the optimum rod system could be identified, for use in the most aggressive of environments. An intelligent, solar powered data logging workstation was installed upon the central tower on the span, to provide continuous data for a range of environmental and electrical parameters, deemed to be of interest to the analysis (see below). The installation has been visited every few months, at which time the cable spans are lowered, and the cable sheaths inspected for damage. Figure 4 shows the cable line engineer at work, installing the retrofit rod system live-line on the 400 kV installation.

Parameters Analysis

The following performance parameters have been explored to date during the trial:

Rod System Hardware. Critical to the optimisation of the retrofit rod system has been the assessment of the performance of a range of rods of differing resistivities per unit length, and a variety of components for terminating the rod at both its tower and span ends.

Installation. The rod system is designed to be installed without switching circuits out, and as a consequence resolution of health and safety critical factors such as the techniques for earthing the rod system before, during, and after installation of the rod has been paramount.

Leakage Current Monitoring. At the central tower position, the earth leakage current has

been measured from both the control span and the span fitted with the retrofit rod system. The mean, minimum and maximum currents are measured every 10 seconds for an interval of 10 minutes and automatically recorded. In addition, a 50 Hz notch filter has been used to allow high frequency currents associated with electrical arcing activity to be resolved separately from the continuous earth leakage current.

Environment. Air temperature, relative humidity, the amount of rainfall, the wind speed and wind direction have all been monitored continuously during the trial.

Pollution precipitation. To measure how the precipitation of pollution could affect the surface resistance of an ADSS cable, two orthogonal 30 cm length glass rods were installed on the tower and their end-to-end resistances measured continuously.

Field Trial Result Analysis

The primary outcome of the year long trial to date has been the confirmation of the highly aggressive nature of the field trial site and installation, which has resulted in the occurrence of electrical damaging activity as described below. The leakage current monitoring system was also found to be successful in recording the electrical activity upon the cables, where it should also be noted that the measured currents, of the order of a few milli-amps, agreed well and were typical of those expected within such a very high voltage environment. For example, figure 5 shows the changing leakage currents detected during outages of the overhead line system. Similarly, it was also found that the leakage current from the semiconductive rod system correlated as expected when rods of differing resistance per unit length were installed onto the span. All the measurements have verified the two software packages used to model the rod and cables' performance.

ADSS Control Span

For the ADSS control span (sections A to B in figure 3), severe tracking damage due to dry band arcing was found to occur within 6 months at span location B, and 9 months at span location A, after which time, due to the severity

of the damage, it was decided to remove the cable from the trial. Figure 6 shows the severity of the damage which occurred at span location A, wherein it can be seen that a severe furrow was cut into the cable sheath for a distance of around 20 cm from the cable suspension armour rods. Damage of a similar nature was noted upon the monitored end of the ADSS cable (Span section B) after only 6 months, and, in this case, the associated electrical activity upon the cable was detected by the leakage current monitoring system for several weeks prior to the site inspection (see figure 5). The physical nature of this damage was consistent with dry-band arc compression, rather than the gradual damage associated with continuous arcing⁷.

ADSS Cable Fitted with Retrofit Rod system

For the cable span fitted with the retrofit rod component hardware, a range of performance data has been obtained allowing the system to be optimised. Retrofit rods which had a resistance per unit length of the order of a few hundred kilohms per metre were found to be too conductive, giving rise to a very low level of damage at the end of the rod on the span. The physical nature of this damage being that associated with continuous arcing damage rather than that of arc compression. No damage was observed under the retrofit rod itself. The upper limit of the rod resistance is currently being probed using rods of resistances of the order of 1-10 Megohm per metre, for which no damage has been observed to date. The aggressive environment of the location has also served to focus attention upon the mechanical and environmental performance of the rod attachment hardware; this has been modified and developed accordingly, to ensure its long term performance.

Environmental Data

With regard to the environmental data monitoring, there has been only limited success in reliably correlating any single environmental factor with the occurrence of electrical activity upon the cables. For example, figure 8 shows the filtered leakage current on the ADSS control cable simultaneously with a measured rainfall event, suggesting perhaps that the rainfall served to initiate the arcing activity. However, such conclusions cannot always be drawn from

the data. For example, it is the case that for highly polluted cables, heavy rainfall is beneficial in terms of washing the pollution based contaminants off the cable surface, light rainfall is detrimental if the moisture serves only to convert the pollutants into an active electrolyte. Figure 9 also shows electrical activity upon the control cable, correlated in this case with the measured relative humidity over the period. Incidentally, for the period of time shown in this figure, the control cable was fitted with a device, attached to the cable suspension armour rod which was designed to reduce and control corona activity. The electrical activity data shown in the figure suggests that elimination or reduction of corona is not in itself sufficient to prevent electrical activity from occurring upon the cable, and in this case dry-band arcing can still be seen to occur.

CONCLUSIONS

The design parameters of high voltage ADSS cable installations have been reviewed in relation to the likelihood of occurrence of dry-band arcing activity and related damage to ADSS cables. It is proposed that ADSS cables only be strung in locations on the tower where the midspan space potential is at or below a nominal threshold level of 12 kV. However, this threshold level may vary for particular ADSS installations, depending upon how environmental conditions, such as the deposition of pollution upon the cable, can alter the cable resistance per unit length.

The progress of a field trial to investigate dry-band arcing upon an ADSS cable in a 400 kV high voltage overhead line system has been described. In particular, an arc control method has been developed in the form of a retrofittable rod, which can be installed alongside the ADSS cable to reduce arcing activity to an acceptable level. In addition the trials have led to a better understanding of the ageing of traditional ADSS cables with so called dry-band arc resistant sheaths, both with and without corona protection. This has reinforced the belief that these have a very limited application on high-voltage power lines above 150 kV.

ACKNOWLEDGEMENTS

The authors would like to acknowledge the support of their colleagues in carrying out this work. In particular, Andy Platt, Ian Nicholls, Malcolm Shaw, Andy McDowell and Mark Latham at BICC Cables, and Simon Neve at Balfour Kilpatrick.

The authors are grateful to BICC and The National Grid Company for permission to publish this work.

REFERENCES

- 1/ S C Sharma, 'Solution for fibre optic cables installed on overhead power transmission lines. A review'. IETE Technical Review 11 p. 215-222, 1994.
- 2/ C N Carter 'Dry Band Electrical Activity on Optical Cables Strung on Overhead Power Lines.' Proc. 37th International Wire and Cable Symposium, p. 117-121, 1988.
- 3/ C N Carter and M A Waldron 'Mathematical Model of dry band arcing on self-supporting, all dielectric optical cables strung on overhead power lines' IEE Proc. C, 139, p. 185-196, 1992.
- 4/ A J Peacock and J C Wheeler 'The development of Aerial Fibre Optic Cables for Operation on 400 kV Power Lines' IEE Proc. A 139, p. 304-313, 1993.
- 5/ G Carlton, C N Carter, A J peacock and R Sutehall, 'Monitoring Trials on All-Dielectric Self Supporting Optical Cable for Power Line Use,' 41st Proc. International Wire and Cable Symposium, p. 59 - 63, 1992.
- 6/ S M Rowland and I V Nichols 'The effects of dry-band arc current on ageing of self-supporting dielectric cables in high fields' IEE Proc.- Sci. Meas. Technol. 143 , p. 10-14, 1996.
- 7/ S M Rowland and F Easthope 'Electrical Ageing and Testing of Dielectric Self-Supporting Cables for Overhead Power Lines,' IEE Proc. A 140, p. 351-356, 1993.
- 8/ C N Carter, 'Arc Controlling Devices for use on Self-supporting Optical Cables,' IEE Proc. A 140, p. 357-361, 1993.
- 9/ A J Taha, I V Nichols, C A Platt, S M Rowland, 'A novel system for the installation of all-dielectric self supporting optical cables on high voltage overhead power lines' 44th Proc. International Wire and Cable Symposium, p. 171 - 177, 1995.
- 10/ N R Haigh, S M Rowland, A J Taha, C N Carter, 'A Fully Instrumented Installation and Trial of a Novel All-dielectric Self-supporting Cable System for Very High Voltage Overhead Power Lines,' 45th Proc. International Wire and Cable Symposium, p. 60 - 67, 1996.

Table 1: Relationship Between 'Safe' Space Potential Threshold Level and Cable Resistance per Unit Length

Space Potential Threshold Level (kV)	Cable Resistance per Unit Length (Ω)	Associated Pollution Level (Arbitrary)
10	10^5	Heavy
18	10^6	Medium
30	10^7	Light

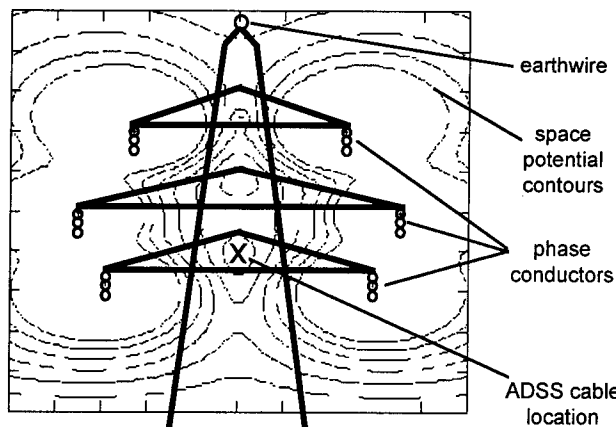


Figure 1: Schematic of a Typical Twin Circuit Tower (UK) & associated Space potential contours

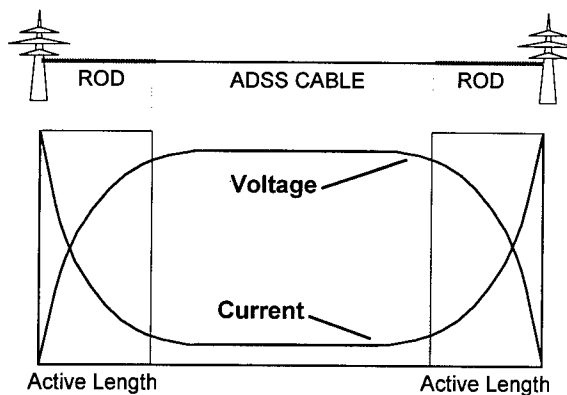


Figure 2: Schematic showing the relationship between the Induced Voltage and Current on an ADSS Cable strung in an overhead power line.

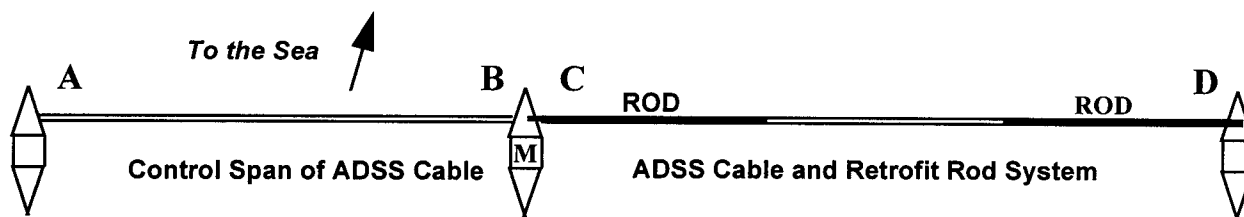


Figure 3: Schematic of Configuration of HV ADSS Field Trial

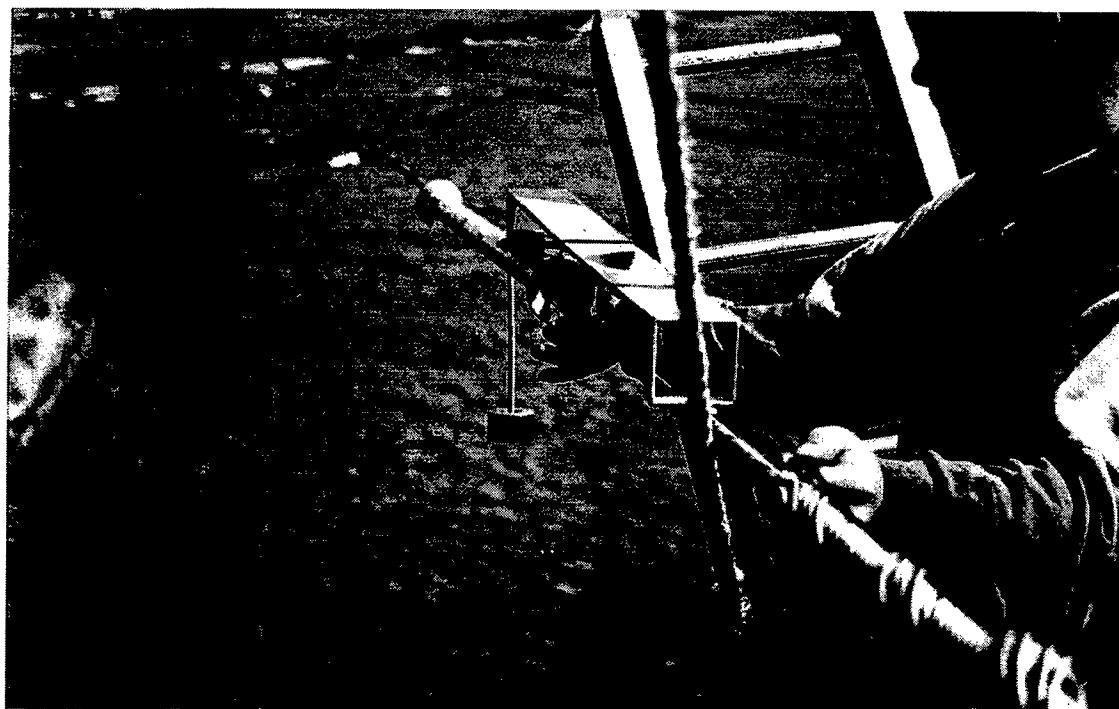


Figure 4: Live-Line Installation of Semiconductive Retrofit Rod System

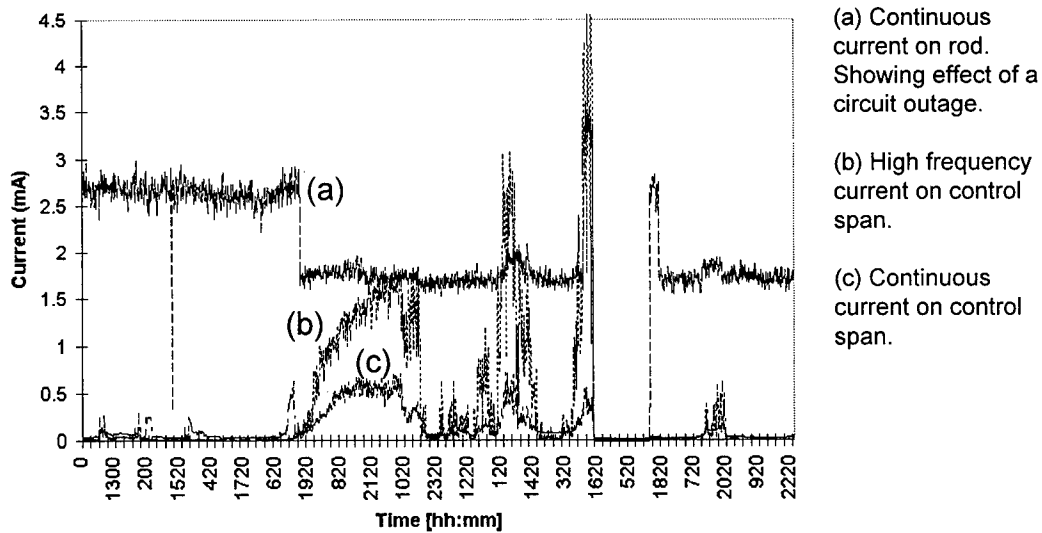


Figure 5: Detection of Dry-Band Arcing Activity on ADSS Cable during Field Trial

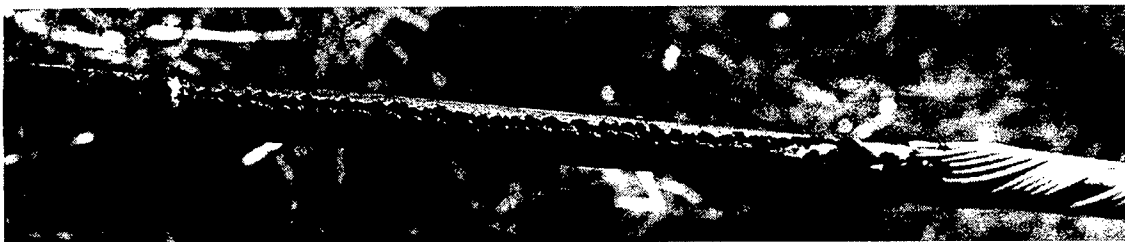


Figure 6: Damage to ADSS Cable due to Dry-Band Arcing

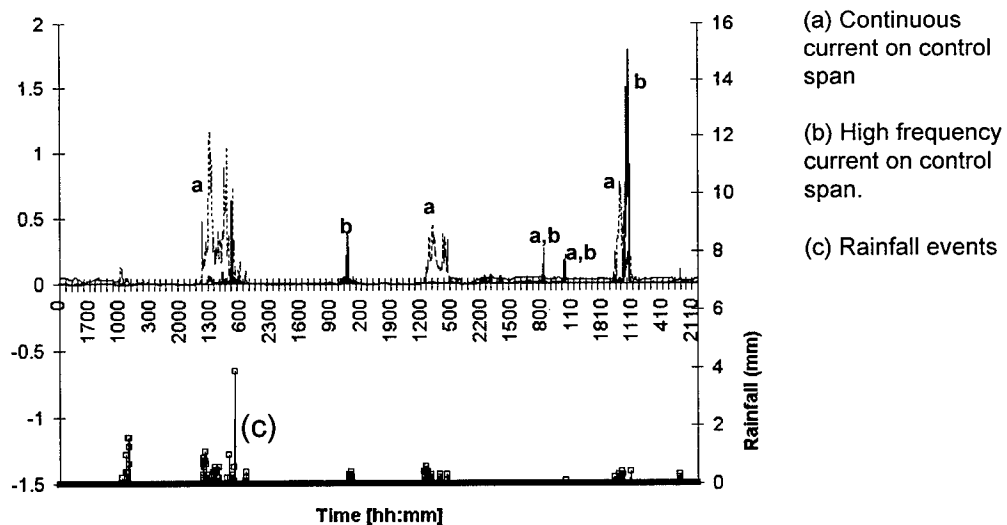


Figure 8: Dry-Band Arcing Activity Correlated against Rainfall

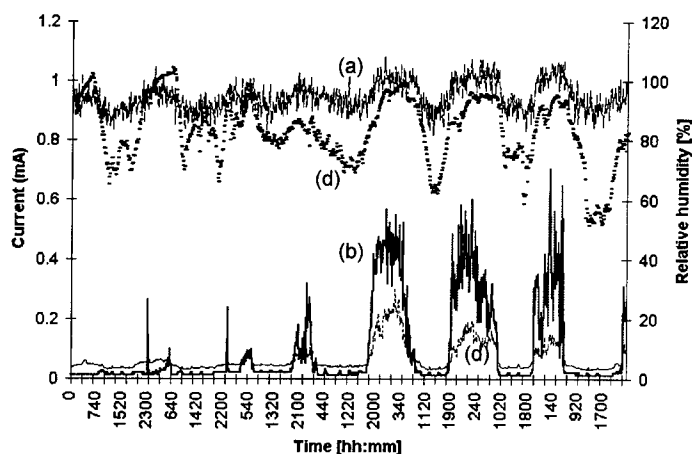


Figure 8: Dry-Band Arcing Activity Correlated against Relative Humidity

- (a) Continuous current on rod span
- (b) High frequency current on control span.
- (c) Continuous current on control span
- (d) Relative Humidity



Chris Carter

National Grid Co. plc
Kelvin Avenue
Leatherhead
Surrey KT22 7ST
United Kingdom

Chris Carter graduated in 1963 from the University of London. He has since worked on magnetohydrodynamic power generation, superconducting magnet design, AC loss measurements in superconductors, failure mechanisms in the joints of power cables and since 1979, the development of optical communications on power lines.



Jimmy Deas

National Grid Co. plc
Kelvin Avenue
Leatherhead
Surrey KT22 7ST
United Kingdom

Jimmy Deas was born in Walton-on-Thames, Surrey, England. He has an HNC in Electronic Engineering and an HND in Software engineering, and has worked at the National Grid Company on a number of overhead lines projects since 1989. He has been responsible for establishing the field based data monitoring system for the HV ADSS project.



Simon Rowland

BICC Cables Ltd
Helsby Tech. Centre
Helsby
Cheshire WA6 0DJ
United Kingdom

Simon Rowland was born in London, England. He obtained a BSc from the University of East Anglia and a PhD from the University of London. He joined BICC Cables from STC Technology Ltd in 1989 where he worked on power cable insulation materials. He is Programme Manager for Telecoms Research and Development at the Helsby Technology Centre.



Neil Haigh

BICC Cables Ltd
Helsby Tech. Centre
Helsby
Cheshire WA6 0DJ
United Kingdom

Neil Haigh was born in Cheshire, England. He graduated with a BSc and PhD from the University of London, specialising in the field of Applied Optics. He joined BICC in 1988 and is actively involved in the area of optical fibre measurements. He is a Principal Research Engineer at the Helsby Technology Centre, and Project Manager for the HV ADSS development.

AN APPROACH TO INCREASING MULTIPLEXED OPTICAL SIGNALS ON THE OPTICAL MULTI-COUPLER SYSTEM

Hideyuki Nasu, Hideyuki Omura, Yukihiisa Shinoda*, Yusuke Kuze*
The Furukawa Electric Co., Ltd., Hiratsuka, Kanagawa, Japan
*Tokyo Electric Power Company, Chiyoda, Tokyo, Japan

ABSTRACT

We propose to use external modulators in the transmitter for the optical multi-coupler systems. Since the external modulator does not cause frequency chirping, the wavelength spacing between channels can be narrowed and the number of channels can be increased. We estimate the required channel spacing for FM video and 1.5 Mb/s QPSK data transmission by investigating the transmission characteristics. For the case of FM video, the required channel spacing is a half of that of direct modulation. This approach is useful especially for the systems with optical amplifiers where the wavelength region with flat gain is limited.

INTRODUCTION:

We have demonstrated the configuration, advantages and applications of the optical multi-coupler systems [1]-[4]. Schematic configuration of the system is shown in Fig.1. The systems are now widely used as supervisory systems employing FM-SCM video transmission to monitor electric power transmission, road and railroad construction, and accidents and security services. In such applications, terminals equipped with optical transmitters are located at all of the monitoring points. Therefore, number of multiplexed signals increases according to the increase in the monitoring points. On upward link in the system, the multiplexed optical signals are detected by a single photo-diode. Therefore, the beat interference between the signals [5]-[7] can deteriorate the transmission quality. To achieve the required CNR (Carrier to Noise Ratio) for FM video transmission, wavelength spacing between the signals should be larger than 0.2 nm when directly modulated DFB lasers are used in the transmitters. The number of signals is limited by the required wavelength spacing and the available optical

bandwidth. In this paper, we propose an approach to increase the number of optical signals by using light sources with narrow chirping width to reduce the required wavelength spacing. Since the intensity modulation with LiNbO_3 external modulators provides non-chirping, FM components of the beat spectrum can be eliminated. AM components generated on the beat are, however, remained. We investigate the interference characteristics of AM components upon the subcarrier signal allocated at the same frequency. Furthermore, we estimate the wavelength spacing between the signals to achieve the required quality of FM video and 1.5Mb/s QPSK data transmission.

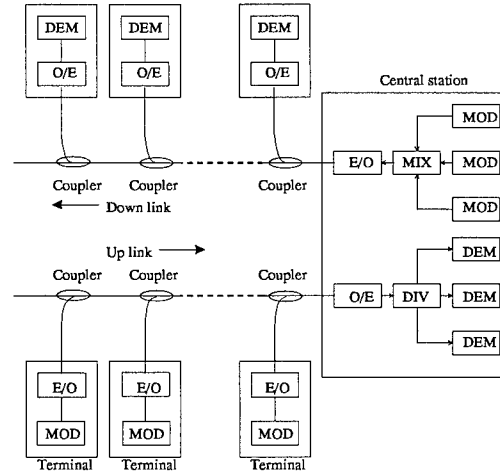


Fig.1 Schematic configuration of the optical multi-coupler system.

EFFECT OF MODULATION METHOD VARIATIONS UPON THE OPTICAL BEAT SPECTRA:

The optical beat spectra depends on modulation methods. To confirm the effect upon the spectra, an

experiment was implemented. Experimental setup is illustrated in Fig.2. In Fig.2(a), a DFB laser at 1.55 μ m wavelength range was directly modulated with sine-wave. On the other hand, in Fig.2(b), a DFB laser was externally modulated with a LiNbO₃ intensity-modulator. The external modulator consist of two cascaded modulators for distortion compensation to be used in analog transmission, such as optical CATV systems. OMI(Optical modulation index) of each experiment was adjusted to 90%. Spectral linewidth of both lasers are 20MHz. Each modulated lightwave was coupled with local lightwave launched from a DFB laser using a 1 \times 1 optical coupler. Polarization states of the signal and the local lightwave were adjusted so that the beat level can be maximum.

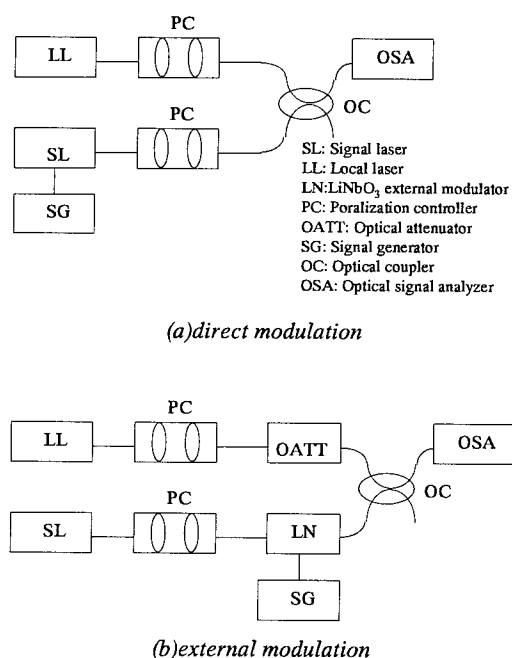
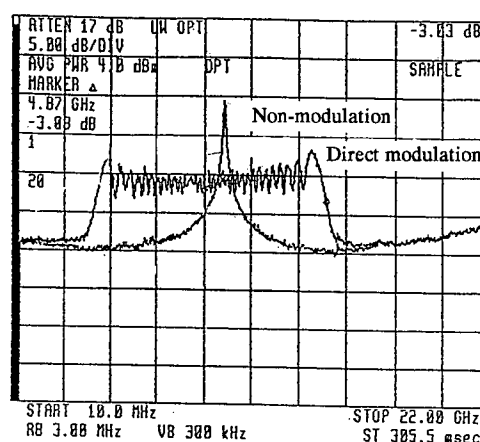


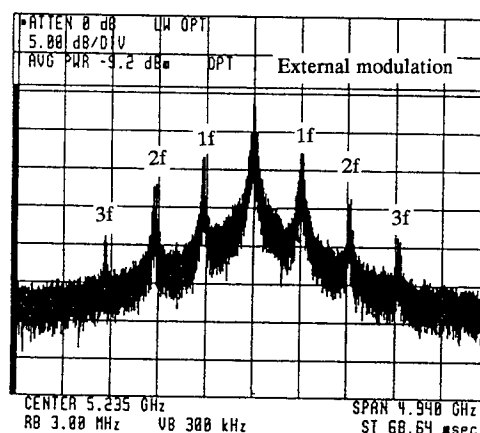
Fig.2 Schematic illustrations for experimental setup.

Fig.3 shows the spectra obtained in the experiment. Two spectra are shown in Fig.3(a). A curve with the Lorentzian shape is the spectrum without modulation. A curve widely expanded toward lower and higher frequencies is the spectrum with direct modulation. This frequency distribution is due to chirping phenomena which is caused by the refractive index change of the semiconductor laser with modulated injection current. When subcarrier

signals are allocated in the bandwidth of generated optical beat, transmission quality of subcarrier signal will be deteriorated. A spectrum shown in Fig.3(b) is the spectrum with external modulation, where FM components are eliminated because of non-chirping. However, AM components are symmetrically generated on Lorentzian distribution. The highest peak corresponds to the center frequency of the optical beat. Frequencies of AM components are uniformly spaced from the center of optical beat. The frequency difference between AM components is equal to modulation frequency. For distinction of AM components, those are named 1f, 2f and 3f as shown in Fig.3(b). Up to OMI of 90%, higher AM components than 3f were not detected.



(a) non-modulation and direct modulation



(b) external modulation

Fig.3 The optical beat spectra. (a) shows a spectrum of non-modulation and a spectrum of direct modulation. (b) shows a spectrum of external modulation with a LiNbO₃ intensity modulator.

REQUIRED RIN_{beat} FOR FM VIDEO AND 1.5 Mb/s QPSK DATA TRANSMISSION:

As described in [1]-[4], interference resulted from the optical beat can be expressed with RIN_{beat} . RIN_{beat} is defined as RIN(Relative intensity noise) caused by the beat between optical signals. In this section, required RIN_{beat} is investigated theoretically for FM video transmission utilized in supervisory systems and 1.5 Mb/s QPSK data transmission utilized in circuits exchange of N-ISDN and so on. The required RIN can be derived from the required CNR and the number of channels. For FM video transmission, we specify the required CNR to be 14 dB by evaluating the quality of transmitted picture. On the other hand, the CNR for 1.5 Mb/s QPSK required to achieve the BER(bit error rate) of 10^{-8} is 20 dB. The number of signal channels is assumed to be 100. The total RIN for the two channel transmission $RIN_{total(2w)}$ is given by;

$$RIN_{total(2w)} = \frac{RIN_{laser(1)} P_{r(1)}^2 + RIN_{laser(2)} P_{r(2)}^2}{(P_{r(1)} + P_{r(2)})^2} + RIN_{beat(1,2)} \quad (1)$$

$RIN_{laser(1)}$ and $RIN_{laser(2)}$ are RIN for laser1 and laser2, respectively. $P_{r(1)}$ and $P_{r(2)}$ are received optical power for each channel. The total RIN for the simultaneous transmission of n optical signals $RIN_{total(nw)}$ is expressed as the following equation;

$$RIN_{total(nw)} = \frac{\sum_{i=1}^n (RIN_{laser(i)} P_{r(i)}^2)}{\left(\sum_{i=1}^n P_{r(i)}\right)^2} + \sum_{i=1}^{n-1} RIN_{beat(i,i+1)} \quad (2)$$

Where $RIN_{laser(i)}$ is RIN for each laser. $P_{r(i)}$ is received optical power for each channel. In practice, RIN_{beat} is much larger than RIN_{laser} . Therefore, following relationship is obtained from equation (1).

$$RIN_{total(2w)} \approx RIN_{beat(1,2)} \quad (3)$$

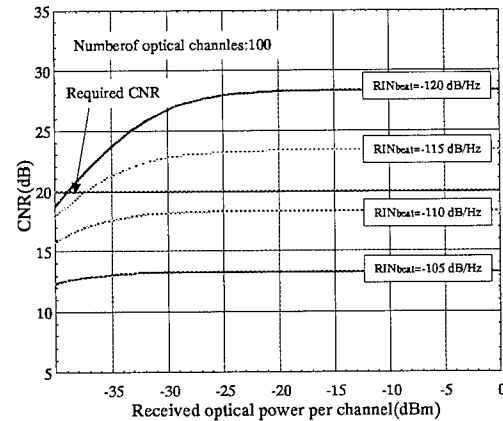
When the RIN_{beat} for each nearest channels $RIN_{beat(i,i+1)}$ is the same for all combinations by adjusting wavelength spacing,

$$RIN_{beat} = RIN_{beat(1,2)} = RIN_{beat(i,i+1)} \quad (4)$$

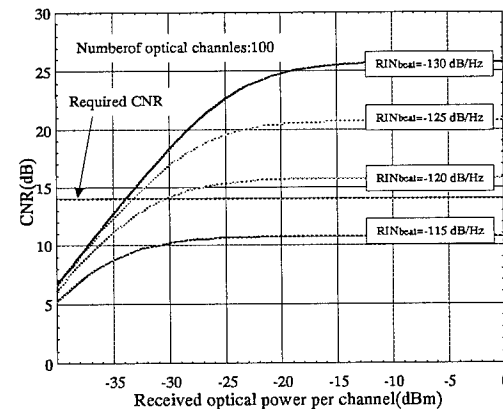
When received power for each channel is the same, equation (2) can be replaced as the following equations;

$$RIN_{total(nw)} = \frac{\sum_{i=1}^n (RIN_{laser(i)} P_{r(i)}^2) + \sum_{i=1}^{n-1} rin_{beat} (P_{r(i)} P_{r(i+1)})}{\left(\sum_{i=1}^n P_{r(i)}\right)^2} \quad (5)$$

$$rin_{beat} = 4RIN_{beat} \quad (6)$$



(a) 1.5 Mb/s QPSK



(b) FM video

Fig.4 Calculated CNR as a function of received optical power per channel(P_r). (a): 1.5 Mb/s QPSK (b): FM video. Number of optical channels is assumed as 100.

As shown in equation (5), $RIN_{total(nw)}$ is expressed with $RIN_{laser(i)}$, $P_{r(i)}$, and a proportional constant rin_{beat} which is expressed as equation (6). CNR is given using $RIN_{total(nw)}$ as the following equation;

$$CNR_{(i)} = \frac{\frac{1}{2} (m_{(i)} MSP_{r(i)})}{\left[2e \left\{ I_{da} + M^{2 \cdot x} \left(I_{da} + \sum_i SP_{r(i)} \right) \right\} + I_t^2 + \left(\sum_i MSP_{r(i)} \right)^2 RIN_{total(nw)} \right] B} \quad (7)$$

where $m_{(i)}$ is optical modulation index for each channel, M is the optimized multiplication factor of APD, S is the sensitivity of APD at low bias voltage, X is the excess noise index of APD, I_{do} is the dark current of APD, I_m is the multiplication current of APD, I_t is thermal noise current of amplifier and B is band width of modulation. Under the condition that $P_{r(i)}$ and $m_{(i)}$ is the same for each channel and RIN_{beat} is constant, calculation of CNR was implemented. Fig.4 shows characteristics between CNR and received optical power per channel under the condition of 100 channels simultaneous transmission. Fig.4(a) is for 1.5 Mb/s QPSK data transmission, where the bandwidth B is 910 kHz and Fig.4(b) is for FM video transmission, where the bandwidth is 27.0 MHz. Assuming that minimum received optical power per channel is -30 dBm, we specify the required RIN_{beat} for the 1.5 Mb/s QPSK data and FM video transmission to be -120 dB/Hz and -130 dB/Hz, respectively.

MEASUREMENT OF RIN_{beat} :

RIN_{beat} with external modulation was measured using experimental setup illustrated in Fig.2(b).

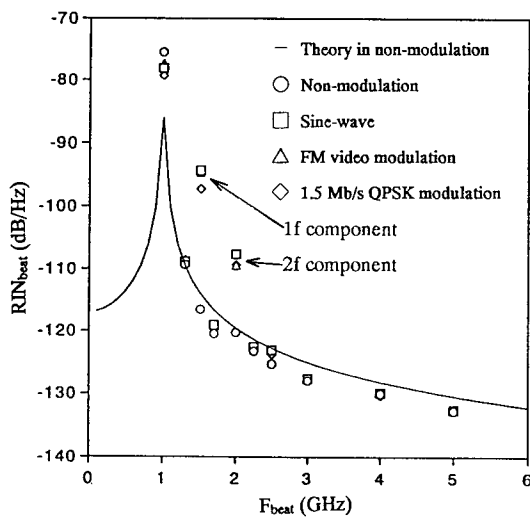


Fig.5 RIN_{beat} as a function of center frequency of generated optical beat. The solid line denotes theoretical curve without modulation. The circles denote the experimental result without modulation. The squares, triangles, and lozenges denote the experimental results with sine-wave, 1.5 Mb/s QPSK, and FM modulation, respectively.

For every modulation method, modulation frequency was fixed at 515 MHz and OMI was 50%. Center frequency of generated optical beat (F_{beat}) was varied by adjusting the wavelength of local laser. The subcarrier frequency allocation of the conventional video monitoring system using multi-coupler system employing FM-SCM method is the same as the allocation used in satellite broadcasting in Japan, where subcarriers are allocated around 1.0 GHz. Therefore, RIN_{beat} is measured at 1.0 GHz. Fig.5 shows RIN_{beat} as a function of center frequency of the generated optical beat. The solid line is theoretical RIN_{beat} in the case of non-modulation. The circles shows the measured RIN_{beat} in the case of non-modulation. The circles have good agreement with theory. The squares, triangles and lozenges are the measured RIN_{beat} with sine-wave, FM video and 1.5 Mb/s QPSK, respectively. The experimental results with modulation agree with the theory without modulation except at the frequency of AM components. The level of RIN_{beat} at AM components are approximately the same regardless of the modulation signals.

INTERFERENCE CAUSED BY AM COMPONENTS GENERATED ON THE OPTICAL BEAT:

In our previous work [1] on the systems using directly modulated DFB lasers, the interference caused by the optical beat is regarded as random noise which can be represented with RIN .

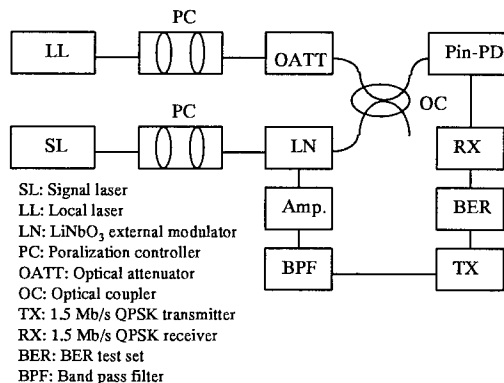
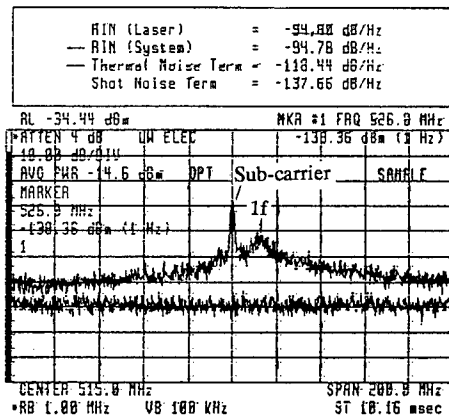
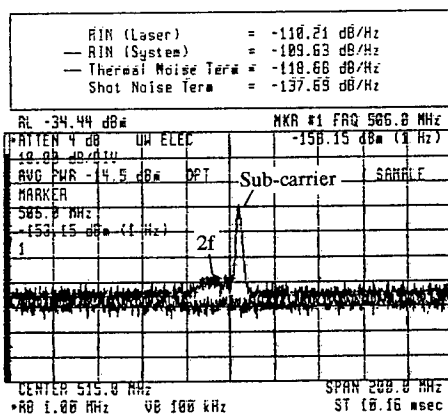


Fig.6 Illustration of experimental setup for BER measurement.

In order to investigate whether the interference can be regarded as random noise in the system using external modulation, the relationship between CNR and BER was measured for the 1.5 Mb/s QPSK data transmission. The experimental setup is illustrated in Fig.6. Received optical power of the optical signal is adjusted to be -17.8 dBm, which is equal to that of local laser.



(a) around 1f component



(b) around 2f component

Fig.7 Beat spectra around subcarrier frequency of 515 MHz. 1f and 2f components generated at subcarrier frequency are shown in (a) and (b) respectively. Measured RIN at each component is shown above each spectrum.

Fig.7 shows the beat spectra around subcarrier frequency of 515 MHz and measured RIN at the

peak of AM components, where Fig.7(a) and Fig.7(b) corresponds to 1f and 2f component, respectively. The measured RIN_{beat} are -94.8 dB/Hz and -110.21 dB/Hz for 1f and 2f, respectively.

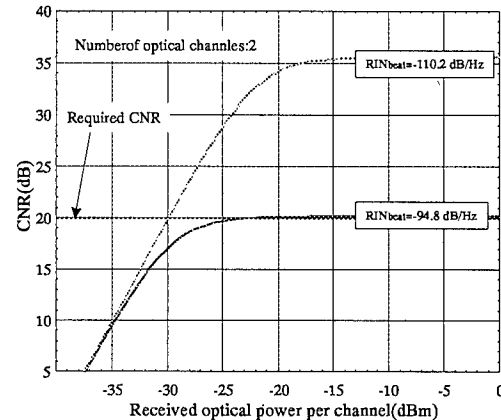


Fig.8 Calculated CNR characteristics as a function of received optical power per channel (P_r), where number of channels is 2. At P_r of -17.8 dBm, CNR for each RIN_{beat} are estimated as 20 dB and 35 dB for 1f and 2f, respectively.

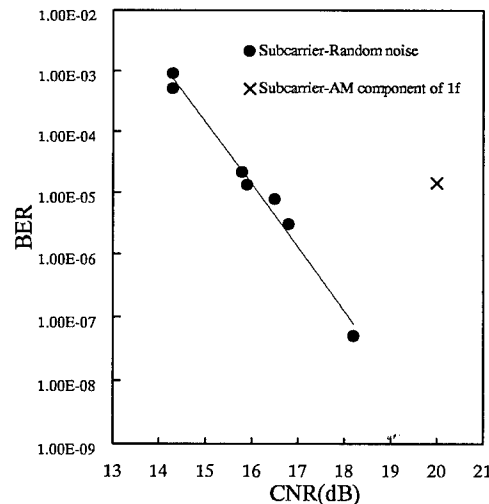


Fig.9 Relationship between CNR and BER for case (i) and case (ii). BER for 2f in case (i) is out of range.

Fig.8 shows the calculated CNR as a function of received optical power. From this graph, CNR are estimated to be 20 dB at 1f and 35 dB at 2f. BER was measured for the following two cases where:

- (i) Subcarrier frequency is exactly at 1f and 2f components,

(ii) Subcarrier frequency is on the noise floor of the beat spectrum.

For the case (i), the measured BER was 1.4×10^{-5} at 1f and $<10^{-8}$ at 2f. In Fig.9, BER is plotted as a function of CNR for case (i) and case (ii). BER for 1f in case (i) remarkably differs from case (ii). Therefore, we conclude that the interference due to AM components cannot be regarded as random noise. Since the AM components have narrow bandwidth, the interference caused by the AM components can have the nature similar to that of single-tone interference. In order to confirm this, BER was measured with the experimental setup shown in Fig.10.

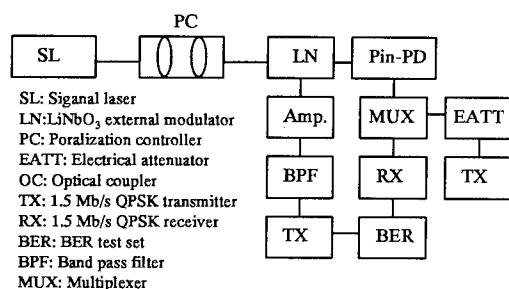


Fig.10 Illustration for experimental setup for the single-tone interference.

In the experiment, single-tone interference generated by a 1.5 Mb/s QPSK signal was coupled with transmitted signal before the receiver. In Fig.11, BER is plotted as a function of D/U (Desired/Undesired) ratio, which is defined as the ratio of signal carrier level to the single-tone interference level. If we regard the 1f and 2f components as single-tone interference, D/U ratio are 11.8 dB and 26.0 dB, respectively. BER for 1f plotted in Fig.11 have good agreement with the BER with single-tone interference. From Fig.9 and Fig.11, we conclude that interference caused by AM components can be regarded as a single-tone interference, not as random noise. Table.1 shows D/U ratio for 3f component in the case of OMI of 90% per channel. The measured D/U ratios are approximately the same regardless of subcarrier frequency.

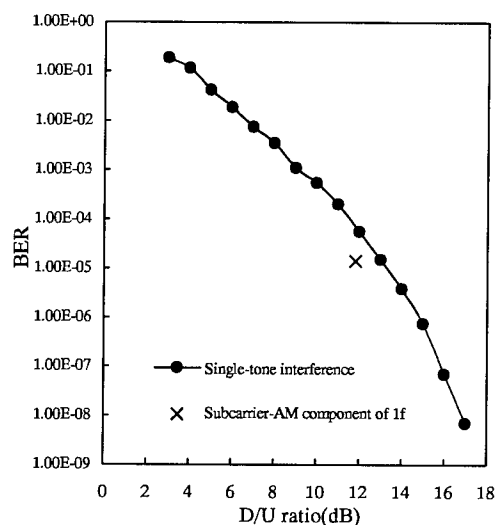


Fig.11 Relationship between D/U ratio and BER for case(i) and the single tone interference. BER for 2f in case(i) is out of range.

Table 1 Measured D/U ratios at 3 f components for different subcarrier frequencies, where a DFB laser is modulated externally.

Frequency(MHz)	D/U ratio(dB)
515	30.7
625	31.2
930	29.2

The D/U ratio was also measured for the case where two DFB lasers were externally modulated as shown in Fig.12.

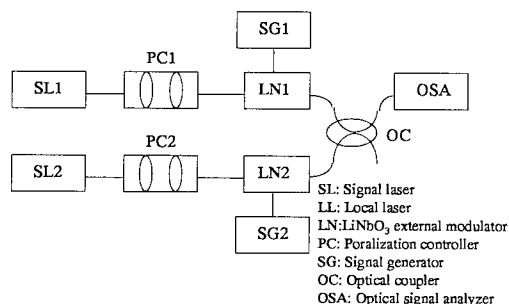


Fig.12 Illustration for experimental setup to measure D/U ratio of AM components on the beat, where both signals are externally modulated with different frequencies.

In this case, inter-modulation components IM2 and IM3 are detected. D/U ratio for detected components are summarized in Table.2. Frequency difference between the 3f component and the center of beat is larger than the difference between other AM components and the center of beat.

Table 2 Measured D/U ratio for each AM component on the beat, where two DFB lasers are modulated externally.

AM components	D/U ratio(dB)
1f	10.5
2f	20.8
3f	30.0
IM2	17.8
IM3	27.5

INVESTIGATION OF REQUIRED WAVELENGTH SPACING FOR NEAREST CHANNELS:

In this section, we investigate the required wavelength spacing for 100 channel multi-coupler system with externally modulated lasers as transmitters. The required RIN_{beat} and D/U ratio are summarized in Table 3 for 1.5Mb/s QPSK data and FM video transmission. The required D/U ratio for 1.5 Mb/s QPSK is estimated as 17 dB when BER is $<10^{-8}$ according to relationship between BER and D/U ratio shown in Fig.11. On the other hand, the required D/U ratio is estimated as 31 dB from evaluating transmitted picture.

Table 3 Required RIN_{beat} and D/U ratio for 1.5 Mb/s QPSK data and FM video transmission.

Modulation method	$RIN(dB/Hz)$	D/U ratio(dB)
1.5 Mb/s QPSK	-120	17
FM video	-130	31

(i) 1.5Mb/s QPSK data transmission:

From Fig.5 and the required RIN_{beat} of -120dB/Hz, F_{beat} should be separated by 1 GHz the maximum subcarrier frequency(f_{max})

$$F_{beat} \geq 1GHz + f_{max} \quad (7)$$

On the other hand, since the required D/U ratio is

17dB, 1f is the only AM component which deteriorates the transmission quality when a subcarrier frequency is exactly at the component (see Table 2). In order to avoid the deterioration, the maximum subcarrier frequency f_{max} should be lower than the frequency of 1f component $F_{beat}-f_{max}$. Therefore,

$$F_{beat} > 2f_{max} \quad (8)$$

From (7) and (8), we derive the following design criteria;

- If f_{max} is lower than 1GHz, required frequency spacing is $1GHz+f_{max}$.
- If f_{max} is higher than 1GHz, required frequency spacing is $2f_{max}$.

This result is summarized in Table 4.

Table 4 Required wavelength spacing of optical signals for 1.5 Mb/s QPSK modulation.

F_{max}	F_{beat}	Wavelength spacing
$< 1.0 \text{ GHz}$	$1GHz+f_{max}$	$F_{beat} \lambda^2/c$
$\geq 1.0 \text{ GHz}$	$>2 f_{max}$	

(ii)FM video transmission:

From Fig. 5 and the required RIN_{beat} of -130dB/Hz, F_{beat} should be separated by 4 GHz from f_{max} .

$$F_{beat} \geq 4GHz + f_{max} \quad (9)$$

In this case, since the required D/U ratio is 31dB, all AM components in Table 2 deteriorate the transmission quality. In order to avoid the deterioration, the maximum subcarrier frequency f_{max} should be lower than the frequency of 3f component $F_{beat}-3f_{max}$. Therefore,

$$F_{beat} > 4f_{max} \quad (10)$$

The design criteria are summarized in Table 5.

Table 5 Required wavelength spacing of optical signals for FM video modulation

f_{max}	F_{beat}	Wavelength spacing
$< 1.33 \text{ GHz}$	$4 \text{ GHz}+f_{max}$	$F_{beat} \lambda^2/c$
$\geq 1.33 \text{ GHz}$	$>4 f_{max}$	

COMPARISON OF WAVELENGTH SPACING WITH THE SYSTEM UTILIZING DIRECT MODULATION:

To compare the specified wavelength spacing between direct modulation and external modulation, minimum wavelength spacing as a function of maximum subcarrier frequency is plotted in Fig.13, where the wavelength region is assumed to be $1.55 \mu\text{m}$. The solid lines and dotted lines shows minimum wavelength spacing for FM video modulation and 1.5 Mb/s QPSK, respectively. The required transmission quality is satisfied when wavelength spacing is larger than the minimum wavelength spacing. And the quality is satisfied when the wavelength spacing is on the lines, except 0 to 1.0 GHz and 0 to 1.33 GHz regions in external modulation. The minimum wavelength spacing on external modulation method is remarkably narrower than that of direct modulation method for both FM video and 1.5 Mb/s QPSK.

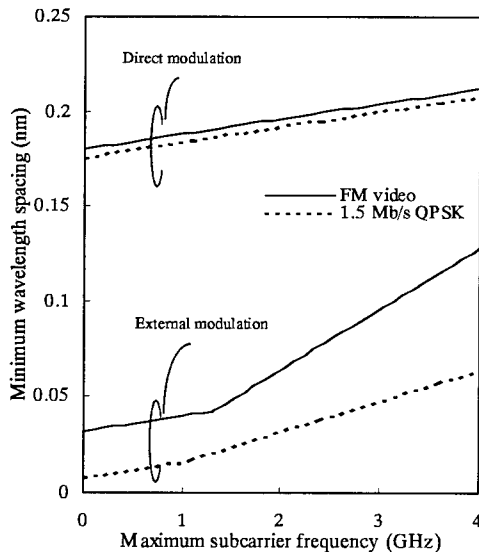


Fig.13 Relationship between the minimum wavelength spacing and maximum subcarrier frequency. The difference between direct modulation and external modulation is shown. The solid lines shows the characteristics for FM video transmission and the dotted lines shows the characteristics for 1.5 Mb/s QPSK data transmission.

Table.6 shows the required wavelength spacing for conventional system using directly modulated lasers

and proposed system using externally modulated lasers. The FM video transmission with the highest subcarrier frequency of 2.5GHz is assumed. The frequency is equal to the maximum subcarrier frequency of 50 channels FM-SCM transmission system which we have engineered. The required wavelength spacing for the proposed system is a half of that of conventional system and therefore the number of signal channels can be doubled.

Table 6 Comparison with the conventional system ($f_{\text{max}}=2.5 \text{ GHz}$).

System type	Wavelength spacing
Conventional	0.2 nm
Reported in this paper	0.1 nm

CONCLUSIONS:

We described an approach to increasing multiplexed signals by utilizing light sources with narrow chirping width. As a method of non-chirping, we have investigated the transmission characteristics with external modulators. The interference caused by AM components on the beat can be regarded as the single tone interference. We described the method to determine the wavelength spacing needed to meet the required transmission quality. Compared with the conventional system, the wavelength spacing can be narrowed. Consequently, the maximum number of multiplexed signals can be increased.

ACKNOWLEDGMENTS

The authors would like to thank N. Kagi for helpful discussions, and N. Matsuo, K. Omac and H. Hondo for their encouragement.

REFERENCES

- [1]N. Matsuo et. al: 'The experimental study of the influence of optical beat interference on FM-video transmission system employing 30ch multiple optical carriers', ECOC'94, We.P.21,

1994

- [2]H. Omura et. al: 'Development of multi-coupler bi-directional optical communication system employing FM-SCM video transmission', 44th IWCS, pp380-386, 1995
- [3]H. Omura et. al: 'Development of the portable terminals for the Information Free Access System employing FM-SCM transmission method', 45th IWCS, pp618-622, 1996
- [4]H. Nasu et. al: 'Design of the novel supervising network using the Information Free Access System', 45th IWCS, pp669-678, 1996
- [5]C. Desem; 'Optical interference in lightwave subcarrier multiplexing systems employing multiple optical carriers', Electronics Letters, vol.24, pp.50-52, 1988
- [6]C. Desem; 'Measurement of optical interference due to multiple optical carriers in subcarrier multiplexing', IEEE, Photonics Technology Letters, vol.3, pp387-389, 1991
- [7]T. H. Wood et. al; 'Operation of passive optical network with sub-carrier multiplexing in the presence of optical beat interference', IEEE Journal of Lightwave Technology, vol.LT-11, pp.1632-1640, 1993



Hideyuki Nasu
Furukawa Electric Co., Ltd.
5-1-9, Higashiyawata,
Hiratsuka, Kanagawa, 254,
JAPAN

Hideyuki Nasu received the B.E. and M.E. degrees in electrical engineering from college of science and technology, Nihon University, Tokyo, Japan in 1993 and 1995, respectively. He joined Furukawa Electric Co., Ltd. in 1995 and he has been engaged in the development of optical devices and optical communication systems. He is working in the video transmission system and equipment research section of Information and Electronics Laboratories. He is a member of the Institute of Electrical and Electronics Engineers and the Institute of Electronics, Information and Communication Engineers of Japan.



Hideyuki Omura
Furukawa Electric Co., Ltd.
5-1-9, Higashiyawata,
Hiratsuka, Kanagawa, 254,
JAPAN

Hideyuki Omura received the B.E and M.E. degrees in electrical engineering from Tokai University, Kanagawa, Japan in 1985 and 1987, respectively. He joined Furukawa Electric Co., Ltd. in 1987. Since he has been engaged in the development of bi-directional CATV system. At present, he is working in the video transmission system and equipment research section of Information and Electronics Laboratories. He is a member of the Institute of Electrical Engineers of Japan.



Yukihiisa Shinoda
Tokyo Electric Power
Company
1-1-11, Babadori,
Utsunomiya, Tochigi, 320,
JAPAN

Yukihiisa Shinoda received the B.E and M.E degrees in electrical engineering from Chiba University, Chiba, Japan in 1985 and 1987, respectively. He joined Tokyo Electric Power Company(TEPCO) in 1987. He pursued the development of optical transmission system until 1996. At present, he is working in the electronic telecommunication section of branch office of TEPCO in Tochigi, Japan. He is a member of the Institute of Electronics, Information and Communication Engineers of Japan.



Yusuke Kuze

Tokyo Electric Power
Company

4-1, Egasaki-cho, Turumi-
ku, Yokohama, 230,
JAPAN

Yusuke Kuze received the B.E and M.E degrees in electrical engineering from Tokyo Institute of Technology , Japan in 1985 and 1987, respectively. He joined Tokyo Electric Power Company(TEPCO) in 1987. He has engaged in developmental research on optical transmission systems. At present, he is working in Computer & Communications Center.

TESTING OF EXPENDABLE OPTICAL FIBERS FOR UNMANNED GROUND VEHICLES APPLICATIONS

D. Keith Anderson

**U.S. Army Aviation and Missile Command, UGV/S Joint Project Office
Redstone Arsenal, Alabama**

Sherrie J. Burgett

**U.S. Army Aviation and Missile Command, Missile Guidance Directorate
Redstone Arsenal, Alabama**

Thomas B. McAlpin

**U.S. Army Aviation and Missile Command, System Engineering and Production
Directorate, Redstone Arsenal, Alabama**

James R. McMinn

Morgan Research Corporation, Huntsville, Alabama

ABSTRACT

The Unmanned Ground Vehicles/Systems Joint Project Office (UGV/S JPO) is developing a Tactical Unmanned Vehicle (TUV) for the U.S. Army and Marine Corps. The TUV is a teleoperated vehicle capable of conducting forward reconnaissance and surveillance missions. In a series of engineering tests, both military specialty and commercial telecommunications fiber optic cable were successfully payed out in unmanned ground vehicle scenarios. The system design and testing are unique in that commercial off-the-shelf (COTS) optical fiber and data transceivers were utilized in a battlefield scenario to teleoperate an unmanned ground vehicle in over-the-hill, non-line-of-sight missions. Multiple crossings of the fiber with military vehicles, all-terrain vehicles, and human pedestrians failed to terminate the link in off-road environments. This testing provides further substantiation that optical fiber is a viable datalink alternative for teleoperated, unmanned ground vehicles; providing true non-line-of-sight, covert

communications capabilities, under less than ideal conditions, with enormous bandwidth capabilities. These efforts are also significant in that they mark the first-known successful precision winding of standard telecommunications fiber optic cable.

INTRODUCTION TO UNMANNED GROUND VEHICLES

The UGV/S JPO was established in 1990 at Redstone Arsenal, Alabama, to act as the focal point for ground robotics in the U.S. Military. The goal of the UGV/S JPO is to field the first generation UGV for tactical applications. This program is referred to as the Tactical Unmanned Vehicle (TUV). The TUV mission is to conduct forward reconnaissance and surveillance missions that are currently conducted by manned scouts.

The TUV system consists of two major components: the Remote Controlled Multi-Mission

Platform (RCMMP) and the Operator Control Unit (OCU). The RCMMP is the vehicle that is teleoperated forward, conducting the reconnaissance and surveillance mission with a variety of sensors. The OCU provides the man-machine interface required to teleoperate the RCMMP. It has the capabilities to control the RCMMP during driving and reconnaissance operations. It also provides visual data from the RCMMP to the operator, allowing him/her to maneuver the RCMMP, search for and identify targets, and disseminate this information throughout the battlefield.

The OCU and RCMMP are connected via a datalink. This datalink will be either a physical link, such as fiber optics, or a non-physical link, i.e. radio frequency (RF). The preferred datalink is RF because it offers more flexibility in movement and positioning of the TUV components. The drawbacks of an RF datalink are that it has limited bandwidth, is effected heavily by terrain features, and is susceptible to detection and jamming systems.

A fiber optic datalink offers a solution to the above mentioned drawbacks. It has essentially unlimited data bandwidth, is not effected by terrain features, and is very covert. The only drawbacks are that it is a physical tether and is susceptible to breakage.

Fiber optic datalinks are not new to UGV applications. Several demonstration vehicles employed fiber optic datalinks. All of these datalinks used jacketed, reinforced, single mode, fiber optic cable. These cables were, as now, spooled off with the forward motion of the vehicle, and without mechanical intervention. After the cable had been payed out, it was retrieved and rewound for another mission.

It has become more evident, after extensive RF testing, that fiber optics could provide a way for successfully conducting non-line-of-sight missions. Previous fiber optic payout systems were expensive, heavy, cumbersome, and logistics intensive. A 5 km spool of jacketed fiber optic cable weighs approximately 100 lbs. (45 kg), and costs more than \$1.00 per meter. A spool, of this weight, requires at least two soldiers to remove and replace the payout spool. For fiber optics to become viable as a datalink for UGVs, the size, weight, supportability, and costs had to be reduced.

ENGINEERING TESTING OF A TUV FIBER OPTIC PAYOUT SYSTEM

Rapidly developing optical fiber technologies have allowed fiber vendors to achieve impressive improvements in manufacturing and quality control, while also lowering costs. Such revolutions led the UGV/S JPO, along with the U.S. Army Aviation and Missile Command (AMSAM), Research, Development and Engineering Center (RDEC) to investigate the use of expendable, thin-buffered optical fiber for remote operation of TUVs. A complete non-line-of-sight optical fiber payout system was designed, leveraging from the Man-portable Non-Line-of-Sight (MANLOS) missile and Fiber Optic Guided Missile (FOG-M) programs. This payout system was adapted to ground vehicles and a series of payout tests were conducted to prove the viability of fiber optics for TUVs.

The main objective of the payout tests was to determine if a small, buffered-only fiber optic cable and expendable payout system are applicable to unmanned ground vehicle operation. Criteria for this determination included whether or not the unjacketed fiber could withstand being run over by vehicles in certain types of terrain and if the fiber optic dispenser could withstand the vibrations experienced during ground payout. These tests also served as a testbed for identifying design changes and improvements required to make the MANLOS and/or a modified FOG-M dispenser a fieldable addition to the TUV program.

Prototype TUV Fiber Optic System

Fiber optic bobbins from the MANLOS program were considered for the TUV application. The small MANLOS bobbin, that is approximately the size of a cola can, was particularly appealing due to its small size, however, it was also limited in range. The 14ounce (397 g) bobbin will hold up to 2.5 km of fiber.

The fiber optic cable that was initially tested was Corning's "Dev Coating" optical fiber, the precursory name for TA-20® fiber. The TA-20® fiber is a military specialty fiber designed for low bending loss and increased tensile strength. It is a single mode, 1550/1310 nanometer wavelength fiber, and is the payout standard for all of the Army's fiber-guided missile programs. It costs approximately \$0.50 per meter and is often

difficult to obtain. However, being the payout standard, it was the most logical choice for the expendable fiber investigations.

(Note: TA-20 is a registered trademark of Corning Glassworks, Inc.)

Prototype Fiber Optic Dispenser Mount

The first step in the development of a TUV fiber optic system was to design a vehicle mount assembly (VMA) for the fiber optic dispenser. The original mount was designed around the MANLOS dispenser, and was developed as a working prototype. Several design lessons were learned during this initial design phase and later incorporated into the final design. It was determined that the height of the bobbin above ground level and the payout angle with respect to horizontal needed to be variable. The VMA was designed to allow for bobbin centerline height adjustment from 19 to 22 inches (48 to 56 cm) above ground level and payout angle adjustment from +45 to -45 degrees with respect to the horizontal.

A fiber guide was also designed to allow the fiber to pay out easily around turns and during vehicle backup. This guide consists of an adjustable bracket mounted on the side of the dispenser mount, an adjustable rod, and a Teflon eyelet. The eyelet guides the fiber off the dispenser as the host vehicle performs maneuvers.

A brushguard was also incorporated into the VMA to keep grass and limbs from coming in direct contact with the dispenser during payout tests. The brushguard hung down beneath the dispenser approximately 8 inches and pushed the grass and limbs away from the dispenser during forward motion of the vehicle.

Field Testing of the Prototype Fiber Optic Datalink

A payout test course was defined at the UGV/S JPO Practice Facility at Redstone Arsenal, Alabama. Each payout test consisted of a variety of maneuvers -- including high and low speed bumps, straight-aways, high and low grass maneuvers, and criss-cross/back-across maneuvers. The ultimate goals of the testing were to verify that this type of fiber optic payout mechanism is suitable for TUV operations and that the lightweight optical fiber is capable of performing TUV missions.

A payout system based upon the MANLOS dispenser was mounted and tested on two platforms: a Highly Mobile Multi-Wheeled Vehicle (HMMWV) and an All-Terrain Vehicle (ATV). Initial testing monitored the mechanical functionality, testing signal transmission passively only (i.e. vehicle operation was not dependent upon the data link). A series of maneuvers was performed by the vehicle while under manual operation. Test data was recorded manually and via cameras -- one mounted to observe the payout dynamics and one mounted to view the forward terrain and provide visual data similar to that used for remote operation. This test setup is shown in Figure 1.

A total of ten dispensers were wound for this initial testing. All ten were wound with Corning "Dev Coating" fiber on bobbins made from the MANLOS design drawings. The first payout test was designed to optimize the payout height and angle of the dispenser, familiarize test participants with the payout mechanism, and to identify any modifications that would be required prior to conducting further testing.

A problem unique to ground vehicles applications was identified while paying out around turns. It was noted that when turns were made at angles more acute than approximately 120 degrees, the payout angle became such that the fiber was pulled taught against the surface of the dispenser and could not payout. The increase in tension caused the already-deployed fiber to drag across the ground, and if left to proceed, would have broken the fiber. The solution to this problem was to design the fiber eyelet guide discussed earlier. The guide was designed and built for incorporation into subsequent runs. The guide forces the fiber to be pulled away from the bobbin before traversing any maneuver angle, and thus eliminates the problem.

Nine of the ten dispensers were tested in eleven test runs. Dispenser #10 was kept for demonstration purposes. Six runs were conducted from a HMMWV platform and five from an ATV. Two runs were conducted completely non-line-of-sight through heavily wooded terrain, where RF was known to fail. All tests were successful. The fiber exceeded all expectations of robustness, and even withstood considerable cross-traffic in grassy terrain.

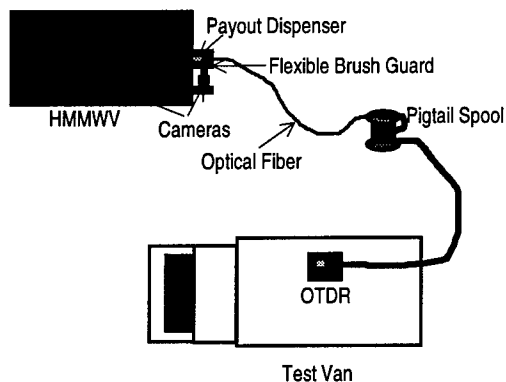


Figure 1: Initial Test Setup

TELECOMMUNICATIONS FIBER INVESTIGATIONS

Based upon the extreme success of the initial tests, the increasing unavailability of military payout fiber, and the cost associated with the specialty fiber, the decision was made to pursue testing of a commercial off-the-shelf (COTS) telecommunications optical cable (TELCO). The issues of greatest concern for implementation of a TELCO fiber were: 1) the 'windability' of the telecommunications fiber, 2) the tensile strength of the fiber, and 3) the bend-loss sensitivity of the fiber.

After investigating specifications for various TELCO fibers -- the most important being diameter variation tolerance and tensile strength -- it was found that the Corning Titan[®] fiber was closely related to the TA-20[®] fiber, readily available, and 1/5th the cost of the specialty version. Samples of this fiber, as well as Corning's SMF-28[®] TELCO fiber were obtained for preliminary testing.

(Note: Titan and SMF-28 are registered trademarks of Corning Glassworks, Inc.)

TELCO Fiber Tensile Testing

The rated tensile strength of the Corning Titan[®] fiber is 100 kilopounds per square inch (kpsi). The method Corning uses to evaluate whether or not the fiber meets the minimum strength rating is to stress it at the 100 kpsi level. If the fiber does not break, it meets the minimum requirements. It was suspected that this type of proof testing might, in some way, degrade the strength of the fiber. In order to determine if the suspicion was true, an additional series of proof

tests were conducted. A total of 100 samples of the Titan[®] fiber were tested individually, with each sample measuring 5 meters in length. Each sample was tested to failure, and the maximum sustained force was measured prior to fracture. The results of the tests were surprisingly high. Over 90 percent of the samples measured endured forces of over 600 kpsi. There were, however, samples that fractured near the 100 kpsi rating. Therefore, the conclusion drawn from the tests is that, for the most part, this TELCO fiber is highly underrated in tensile strength, but it cannot be expected to withstand greater forces 100 percent of the time.

TELCO Fiber Bend Loss Testing

A series of tests were conducted to investigate the effects of bending the fiber around different radii. The motivation for doing the tests was to compare the losses of TELCO fiber with the losses of payout fiber given the same stress levels. Two different samples of Titan[®] fiber were tested along with a sample of SMF-28[®] fiber. The results were then compared to an existing database for TA-20[®] payout fiber. The SMF-28[®] TELCO fiber is generally the same as the Titan[®] fiber except that the titania doped buffer, which makes the Titan[®] fiber more fatigue resistant.

A test matrix was set up to include three different stress angles: 0°, 90°, and 170°. A sample of fiber was placed in the test fixture, positioned around a small diameter rod, and the weight of a small brass chuck was used to provide the stress at the desired angle. Two rod diameters were used, one 0.032 inches and one 0.063 inches. The wavelength of the light source used for the tests was 1300 nm. Figure 2 shows a plot of the test results for the 90 degree bend on the smaller diameter rod. There are several observances of particular mention for the collected data. First, it was discovered that there was no prior database for payout fibers at the 170 degree pull angle, and very little data at the 90 degree angle; thus no real basis for comparison with the payout standard was achieved. Second, although the SMF-28[®] achieved better loss performance on average, there is no ready technical reason for why it should be any different than the Titan[®] fiber. Likewise, there is no explanation for the superior performance of Titan[®] sample #1 over Titan[®] sample #2. The only useful conclusion obtained

from this testing was that the bending loss levels, although much greater than those of TA-20® fiber, remained reasonably low. Given the slow speeds of ground vehicles, as compared to missiles, the maximum bending stresses will not, theoretically, reach the levels to which this testing was conducted.

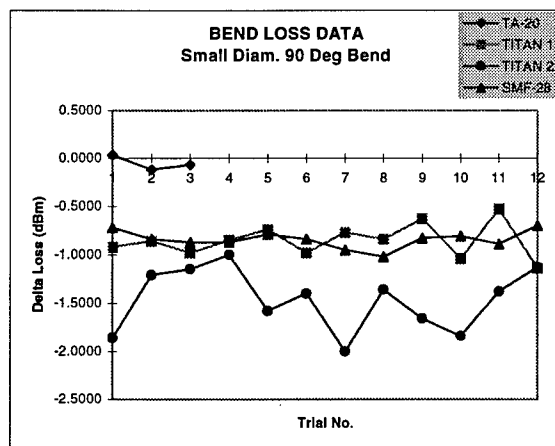


Figure 2: TELCO Fiber Bend Loss Data

Winding the TELCO Fiber

One of the biggest concerns regarding the TELCO fiber was the ability of the manufacturer to maintain a tight tolerance on the diameter of the fiber. Since the fiber is wound in a precise manner, and a precision-wind requires an almost constant diameter fiber, it was necessary to conduct an optical inspection of the fiber. After continuous inspection of 21 km of the TELCO fiber, the diameter remained very consistent throughout the entire spool.

The only unresolved issue was the windability. Once again, the MANLOS bobbin design was used for testing. There were no abnormal winding problems associated with winding the TELCO fiber. A total of four 2.5 km dispensers were wound on the MANLOS bobbin design with the Titan® fiber in this initial COTS fiber testing.

Field Testing of the TELCO Fiber Dispenser

Three of the four TELCO dispensers were payed out in the field. Testing was conducted in environments and under conditions as nearly identical to the previous testing as possible. ST® type connectors were chosen to match up with existing instrumentation, and were installed on the dispensers to allow for connection of a video transceiver. Consequently, video images were

broadcast back to the OCU via the fiber optic datalink. Again, all tests were successful. The video clarity was exceptional, both visually and when observed using a videoscope.

These tests mark two extremely significant events in fiber-guided weapons research: 1) the first successful precision winds of telecommunications fiber, and 2) the first successful payouts of telecommunications fiber in a battlefield scenario.

(Note: ST is a registered trademark of AT&T, Inc.)

TESTING OF A MODIFIED FOG-M DISPENSER

To increase the length of fiber optic cable, and therefore the system range, from a maximum of 2.5 kilometers to 10 kilometers, a new bobbin was designed based upon the Army's Fiber Optic Guided Missile (FOG-M). This was done in order to meet the non-line-of-sight requirements specified in the Joint Operational Requirements Document (JORD).

The axial dimension of the FOG-M bobbin was shortened by 42%, but the 2-degree taper angle was maintained. This taper angle has a well-documented history in the high-speed payout arena, therefore conforming to this parameter was considered to be the least-risk design. The modified FOG-M bobbin somewhat increased the size and weight of the dispenser, making it about the size of a coffee can and weighing about 5 lbs. (2268 g).

With this new bobbin design, came a new, more sophisticated mount design, as well as, a shroud to replace the brushguard and experimental eyelet designs. (See Figure 3.)

Four modified FOG-M dispensers were wound and tested in this new series of tests. All four were wound with 5 kilometers of the Corning Titan® fiber and were deployed from a HMMWV platform. All four of these tests used a fully operational, two-way data link to remotely control the Technical Test Bed HMMWV. These four dispensers were payed out on the same test course used previously. Each payout test consisted of a variety of maneuvers including high and low speed bumps, straight-aways, high and low grass maneuvers, and criss-cross/back across maneuvers. The fiber again exceeded all

expectations. Multiple crossings of the fiber failed to break the link. Video transmission through the fiber link was excellent. All tests were highly successful.

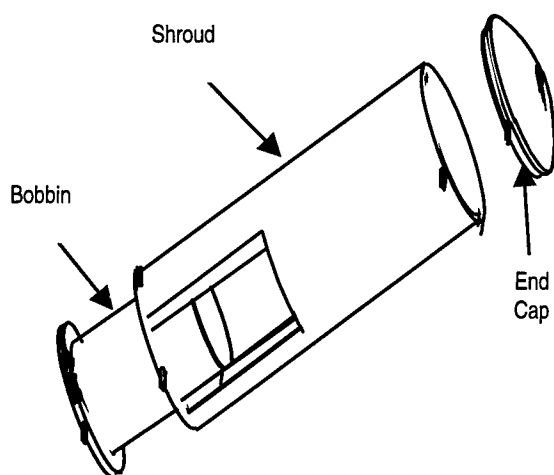


Figure 3: Shroud Assembly Design

IMPLEMENTATION OF THE FIBER OPTIC DATALINK

The prototype modified FOG-M payout system has been partially integrated on a Surveillance and Reconnaissance Ground Equipment (SARGE) vehicle, and tested. Two 5 km dispensers wound with the Titan® fiber have been successfully payed out while teleoperating a SARGE vehicle, integrated with the fiber optic datalink system. (See Figure 4.)

A 'mini-production' run of optical fiber dispenser assemblies has begun. In this effort, thirty-four 5 km dispenser/shroud packages will be fabricated and utilized in SARGE missions. This premanufacturer stage is providing valuable insight into the producibility of the dispenser design. Several sideline research topics are being further explored: such as the issues of optical winding tension for longterm pack stability and manufacturing quality control.

All total, eighteen (18) fiber optic dispensers were payed out in these series of engineering tests. Nine were wound with TA-20® fiber and nine with a COTS fiber. Tests were conducted from three different vehicle platforms, in temperatures varying from 45° F to 95° F (7° C to 35° C), over terrain varying from gravel roadway to open field to heavy woods. Speeds

of 30 MPH (48 KPH) were reached. Two sizes of bobbins were tested, and two different types of optical transceivers were utilized. Every test was deemed successful. This very successful series of testing is considered a milestone accomplishment for tethered military vehicles.

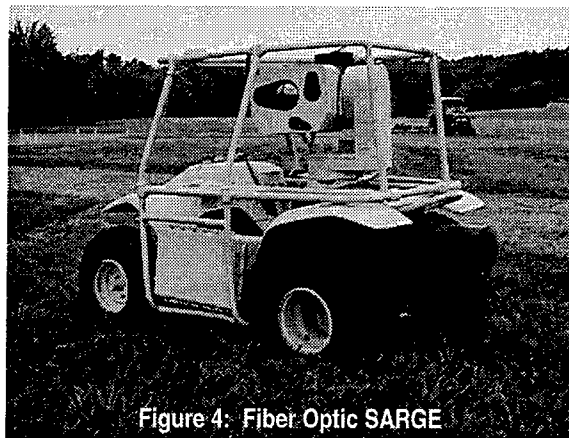


Figure 4: Fiber Optic SARGE

CONCLUSIONS AND RECOMMENDATIONS

The test results clearly indicate that both military payout optical fiber and telecommunication fiber are viable means of communication for the UGV program. Testing conducted under this project demonstrates that optical fiber can be used effectively as a data link between the RCMMP and the OCU under certain scenarios.

A fiber optic data link offers advantages over current RF technology for certain applications. Several advantages are listed below:

- Fiber allows the vehicle to operate in a non line of sight application
- A Fiber optic link provides advantages over RF where countermeasures are a concern
- Fiber has much greater bandwidth than RF technology
- Use of Fiber optic data links can offer reduced set up and configuration time as compared to RF systems

It is recommended that a fiber optic data link be considered in conjunction with the RF data link to broaden the range of UGV applications and missions. To support future use of fiber optics on the UGV program, more testing and development is recommended. Specifically the following recommendations are made:

- The feasibility of using commercial grade telecommunications optical fiber on UGV has been proven to be of significant value, but other telecommunication fibers should also be investigated to prevent limiting the availability to one source. Use of commercially available fiber would significantly reduce the cost of the fiber and fiber optic transmit/receive hardware on future production programs.
- Investigate the use of composite materials to replace the aluminum used in these prototypes in order to reduce the overall weight of the shroud assembly.
- Also, a new bobbin size should be designed for the UGV program. Efforts should focus on design and testing of fiber bobbins that minimize the number of layers of fiber for the given range requirements.

Based on preliminary test results and past performance of fiber optic systems on unmanned vehicles, fiber optics have a very bright future for specific applications on Tactical Unmanned Vehicles for the U.S. Army and Marine Corps. Future testing will be conducted to familiarize soldiers and marines with fiber optics, and to verify that fiber optics has a place on the unmanned battlefield of the future.

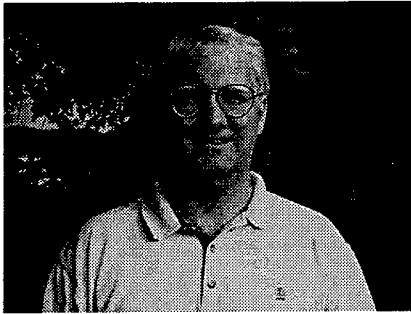
It is envisioned that fiber optic hardware, such as developed under this effort, will become an integral part of the electronics on the TUV system. It will be software configurable and selectable. The fiber optic dispensers will be packaged such that they are very user friendly and easily installed and replaced. Fiber optic technology developed for the Non-Line-of-Sight Missile System will be utilized to the maximum extent. Several million dollars have been spent in the research and development of bobbins, winding mechanisms, computer models, adhesives, and other related technologies. Every effort will be made to draw upon that database for the UGV programs.

FUTURE OF FIBER OPTICS ON UNMANNED GROUND VEHICLES

The future of fiber optics for unmanned vehicle applications is bright. It offers an uninterrupted, covert datalink capable of very high data rate, wide bandwidth data transmission. It also helps eliminate the ElectroMagnetic Interference (EMI) and Radio Frequency Interference (RFI) problems. Frequency allocation is not an issue with fiber optics. Whether fiber optics becomes the primary datalink is still a question. While it does have the above mentioned advantages it also has disadvantages. These include being tethered to a fixed point, not allowing the operator to move the OCU while operating the RCMMP. The fiber is also vulnerable to breakage due to vehicle crossover. Fiber optic cable is still expensive, on the order of \$0.50 per meter for military fiber and \$0.10 per meter for TELCO fiber, at present; although, the cost per meter would be reduced when procuring production quantities.

It is anticipated that both fiber optics and RF will be integrated into one datalink. The RF could be used in line-of-sight, short range missions and the fiber optics could be used in the non-line-of-sight, longer range missions. When the soldier needs to get the unmanned vehicle to a non-line-of-sight reconnaissance point quickly, fiber optics may be the way to go. When he needs to perform a short range, line-of-sight mission such as route clearing, RF may be the datalink of choice.

ABOUT THE AUTHORS



D. KEITH ANDERSON

AMSAM-DSA-UG-E, BLDG. 3221
REDSTONE ARSENAL, ALABAMA 35898
anderson-dk@fhssmtp.redstone.army.mil

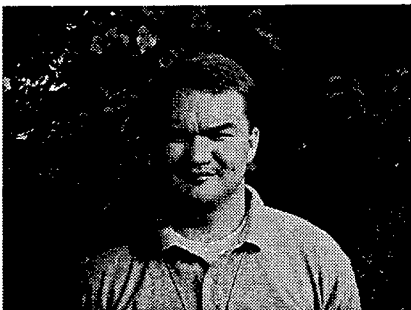
Dennis K. Anderson graduated from the University of South Alabama in 1987 with a BSEE degree, and is currently pursuing a Masters Degree in Engineering Management at the University of Alabama in Huntsville. Since graduation, he has been employed by the U.S. Army Aviation and Missile Command as an Electrical Engineer. He is currently assigned to the Unmanned Ground Vehicles/Systems Joint Project Office as the lead engineer on Unmanned Ground Vehicle datalinks.



SHERRIE J. BURGETT

AMSAM-RD-MG-NC, BLDG. 5400
REDSTONE ARSENAL, ALABAMA 35898-5254
sburgett@redstone.army.mil

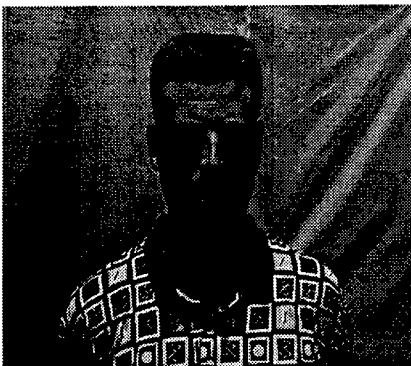
Ms. Burgett obtained a B.S. degree in Electronic and Computer Engineering from the University of Alabama in Huntsville. She has over ten years of experience in research and development of optical fiber winding and payout technologies at AMCOM. She is well published in several areas relating to optical fiber technologies, pioneering several applications of both optical fiber payout and optical fiber sensors as related to Fiber Optic Guided Vehicle missions.



THOMAS B. MCALPIN

AMSAM-RD-SE-PT, BLDG. 4762
REDSTONE ARSENAL, ALABAMA 35898
MCALPIN-RD-SE-PT@redstone.army.mil

Mr. McAlpin graduated in 1991 from Auburn University with his B.S. degree in Electrical Engineering. He has worked since 1992 for the US Army Missile Command (now the Aviation and Missile Command (AMCOM)) in Huntsville, Alabama, as an Electronics Engineer. His major duties include electrical and mechanical design of prototype modifications to the various weapon systems managed at the AMCOM.



JAMES R. MCMINN

MORGAN RESEARCH CORPORATION
2707 ARTIE STREET, SUITE 17
HUNTSVILLE, ALABAMA 35805-4769
jmcminn@morganres.com

Mr. McMinn is a Research Engineer for Morgan Research Corporation (MRC). At MRC, Mr. McMinn manages the production of fiber optic dispensers for Unmanned Ground Vehicle applications. He is currently the Field Support Engineer for the Tactical Unmanned Vehicle Surveillance and Reconnaissance Ground Equipment program. Mr. McMinn is also developing fiber optic data link technologies as applied to other types of teleoperated systems. He has been employed at MRC for the past seven years. Education: BSEE, Magna Cum Laude, University of Alabama in Huntsville.

AN OPTICAL-CABLE IDENTIFICATION SYSTEM USING OPTICAL INTERFERENCE BETWEEN TWO OPTICAL FIBERS

Yuji Azuma*, Koichi Matsuno, Koji Arakawa, and Koji Yoshida

* NTT Maintenance and Service Operations Department

NTT Technical Assistance and Support Center

Tokyo, Japan

ABSTRACT

The proposed optical-cable identification system makes it possible to identify a specific optical cable from among many cables installed side by side. This system uses the changes in output intensity caused by optical interference between the optical paths of different fibers in the specified cable. It will be very useful for identifying optical cables in future multimedia networks.

1. INTRODUCTION

NTT is continuing to install optical-fiber cable for new multimedia services. We are also expanding the capacity of our trunk and subscriber optical fiber networks.^[1] The result is that many optical cables now run parallel through conduits and along utility poles. An example of the crowded conditions in our underground route is shown in Fig. 1. It is sometimes necessary to identify a particular optical cable from among these many similar optical cables very quickly.

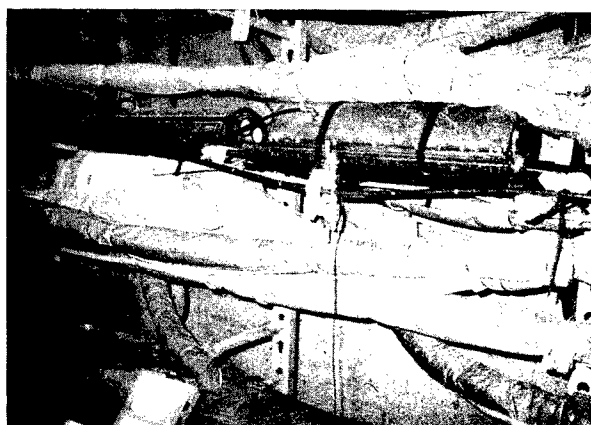


Fig. 1 Crowded condition of optical cables
in an underground route.

The conventional identification method is the "push-pull method", in which a cable is identified at a second location by pushing and pulling it from a location where it has already been identified. However, when an optical cable is pushed and pulled, the transmitted signals are sometimes broken due to optical loss caused by the pushing and pulling. Moreover, for a long cable span, it is impossible to identify a particular optical cable by using this method. Identification can also be done using electromagnetic induction, in which the cable is identified by transmitting and detecting an induced signal along its metallic components. However, this method works only for short cable spans. Moreover, it cannot be used for a non-

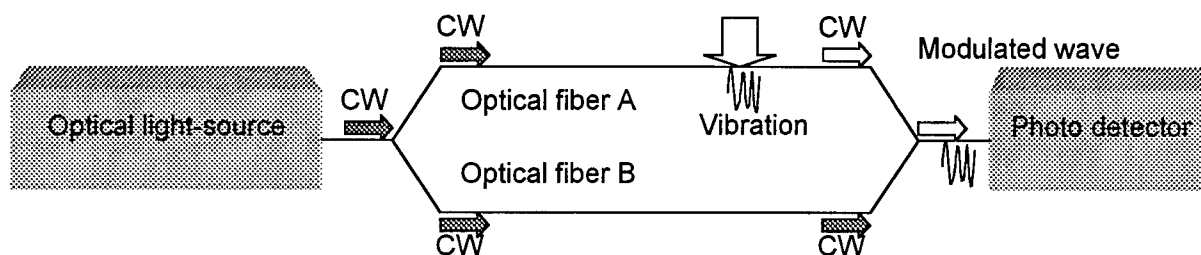


Fig. 2 Principle of cable identification using optical interference.

metallic optical cable. On the other hand, there is optical-polarizing-rotation method^[2] by using an optical fiber. However, the exact detection of polarizing angle is difficult and expensive. Cables that have been tagged with a specific code name or bar code can be easily identified, but these codes must be attached when the cable is manufactured.

We have developed an optical-cable identification system that uses the optical interference between two optical fibers in the cable. This system can quickly identify a particular optical cable, even one over 40 km long, without having to slice it open.

2. SYSTEM DESCRIPTION

2-1 Identification using optical interference

As shown in Fig. 2, our proposed optical-cable identification system uses two optical fibers. These two fibers are constructed in the same optical cable, because each fibers must have the same length roughly. A continuous lightwave from an optical light-source is divided between the two fibers, transmitted over each, mixed at the fiber end, and detected at a photo detector. The lightwave transmitted along one

fiber, fiber A in Fig. 2, is vibrated with a specified signal for identification. The strain caused by the vibration changes the optical length and polarizing angle of the lightwave. The optical intensity of the lightwave mixed at the fiber end changes to the same vibration frequency because the lightwave results from the interference between the two lightwaves. By detecting the specified vibration frequency at the photo detector, we can identify a specific optical cable with certainty.

Because the vibration originates from outside the optical cable, it cannot be isolated onto only one fiber in the optical cable. Although it is transmitted onto both of the fibers we use, the strains caused on each fiber differ due to the differences in their positions and initial strains.

The optical intensity of the interference $\zeta(t)$ is given by

$$\zeta(t) = \zeta_0(1 - \cos \theta(t) \cos \phi(t))/2,$$

where $\theta(t)$ and $\phi(t)$ are the differences in the phases and polarizing angles, respectively. Clearly, the optical intensity is sensitive to changes in both the phase and polarizing angle.

2-2 Generation of vibration

As shown in Fig. 3, the vibration is induced by a piezo-electric actuator set on the optical cable. The vibration signal is supplied by a signal generator through a switching device, the frequency of the signal is from 0.1 to 30 kHz. The switching device controls the supply of the signal frequency to the actuator. The maximum offset of the actuator is approximately $2\text{ }\mu\text{m}$ from a position without an input voltage. The vibration is transmitted into the optical cable, placing a strain on all the fibers.

We used one actuator in our study, but for a thick optical cable, several actuators around the cable could be used.

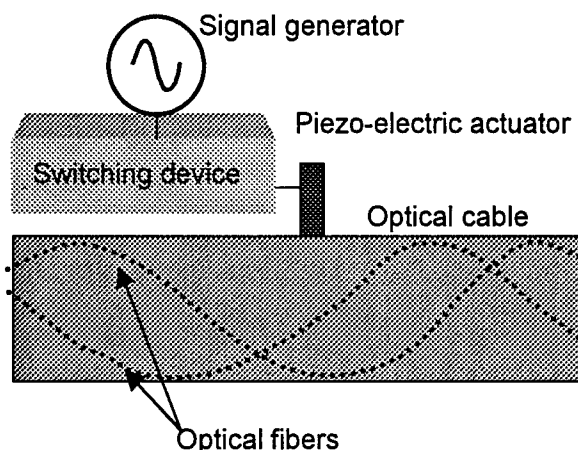


Fig. 3 Location of cable actuator.

3. EXPERIMENTAL RESULTS

3-1 Measurement Methods

The experimental setup we used to measure the signal-to-noise ratio (SNR) is shown in Fig. 4, the specifics of the optical

fiber and cable we used are in Table 1. The lightsource was a DFB laser diode with a $1.55\text{-}\mu\text{m}$ wavelength, and the output light was a continuous wave divided by a 2x2 single-mode optical-fiber coupler. The two lightwaves were then mixed by another 2x2 optical-fiber coupler after being transmitted through the two fibers. The mixed lightwave was detected by a photo detector. A piezo-electric actuator was set on the optical cable. Using the signal provided by a signal generator through a switching device, it

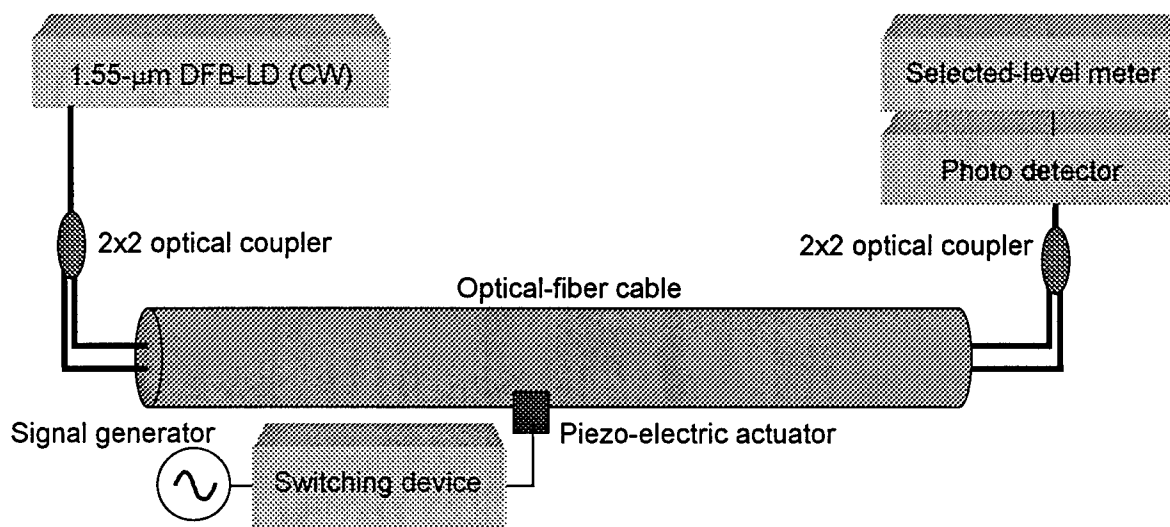


Fig. 4 Experimental setup.

Table 1 Specifics of optical fiber and cable.

Cable: 40-fiber slotted rod
Slotted-rod twist pitch of 500 mm
Diameter of 15 mm
Fiber: Single-mode for 1.3- μ m-wavelength
4-fiber ribbon

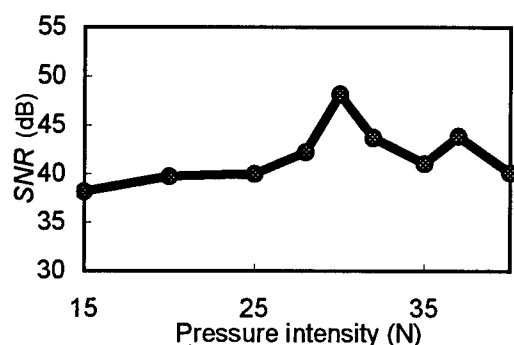


Fig. 5 Dependence of SNR on pressure intensity.

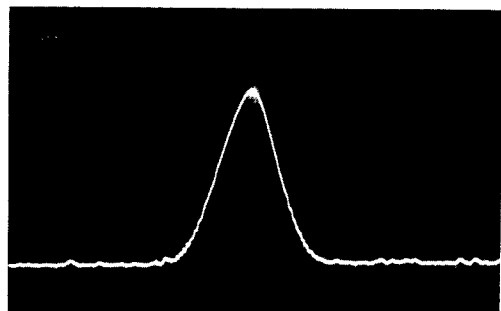


Fig. 6 Spectrum of detected signal.

vibrated the optical cable at an amplitude of about 0.1 mm. The switching device frequently passed the signal from the generator. The frequency of the generated signal was f . The vibration caused a strain on the optical cable. Normally, the piezo-actuator would be set at a location where

cables are identified, such as at an access hole. In our experiment, we set it at the center position, between the two ends of the cable. The two fibers were affected differently by the strain. The lightwaves on the two fibers is differently changed each optical path length. The detected-signal frequency was measured by a selective-level meter. The SNR at frequency f was calculated as

$$SNR_f = P_f / P_{f0},$$

where P_f was the detected power when signal frequency f was transmitted by the switching device, and P_{f0} was the detected power when signal frequency f was not transmitted by the switching device. We calculated the SNR of the object cable. Moreover, we must evaluate also the SNR of the adjacent cable. Because the other cable is identified mistakenly if the frequency is detected at the adjacent cable.

3-2 Pressure intensity

Because the piezo-electric actuator vibrates the optical cable directly, the pressure intensity between the actuator and the cable affects the SNR characteristics. As shown in Fig. 5, when the pressure intensity was 30 N, the SNR reached a peak between 15 and 40 N. For our next experiment, we used a pressure intensity of 30 N.

3-3 Frequency characteristics

The spectrum of the interference signal detected by the photo detector, when the frequency modulated by the signal generator was 5 kHz, is shown in Fig. 6. The SNR

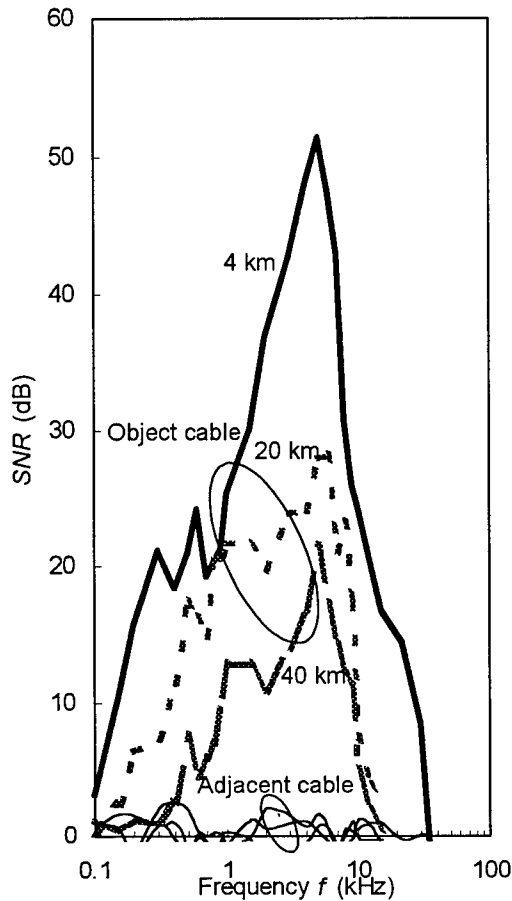


Fig. 7 Frequency characteristics of SNR.

frequency characteristics are shown in Fig. 7. The pressure intensity between the actuator and the cable was 30 N. Cable lengths of 4, 20, and 40 km were used. The upper and lower set of lines show the SNR of the object cable and of the adjacent cable, respectively. The highest SNR was at around 5 kHz for all these cable lengths. The adjacent cable, which was 10 cm from the object cable at the vibration location, had an SNR of around 0. Therefore, the cable vibration has little effect on the other cables.

3-4 Fiber-length characteristics

The measured and approximated relationships between the SNR and cable

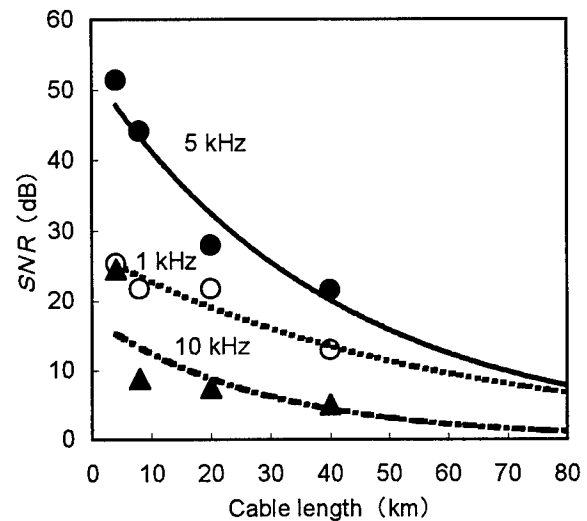


Fig. 8 Dependence of SNR on cable length.

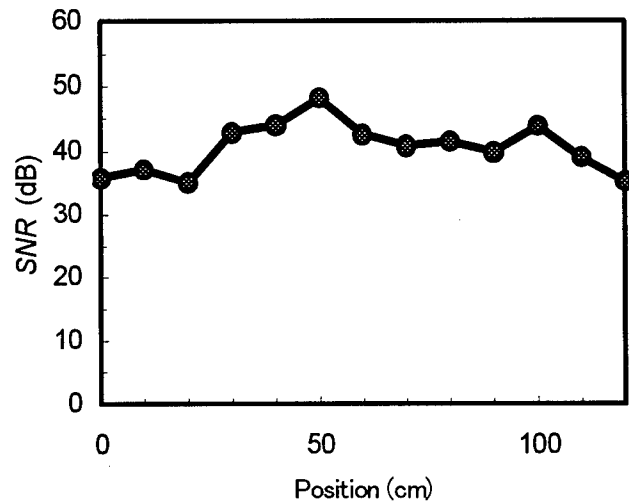


Fig. 9 Dependence of SNR on vibration position along cable.

length at 1, 5, and 10 kHz are shown in Fig. 8.

As the cable length increases the SNR decreases. When the frequency is 5 kHz, the SNR is more than 20 dB at 40 km and about 10 dB at 80 km. These SNR levels are sufficiently high to enable signal f to be detected, and thus a cable to be identified.

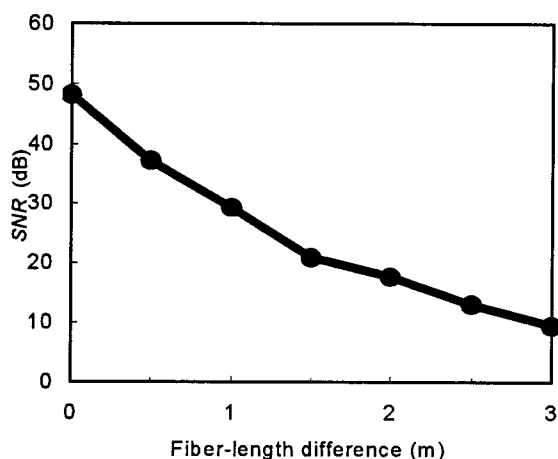


Fig. 10 Dependence of SNR on length difference.

3-5 Effect of cable-slot pitch

The dependence of the SNR on the vibration position along the cable is shown in Fig. 9. When the vibration position is changed, the cable must not be twisted. The measured SNR characteristics follow an approximate sine waveform. The span of the peak-to-peak is about 500 mm. The interval span is identical to the slotted-rod twist pitch of the cable. It is clearly to cause the difference of the distance between the actuator and each optical fiber.

3-6 Dependence on fiber-length difference

Because our proposed identification system uses optical interference, the SNR is affected by length differences between the two optical fibers. As shown in Fig. 10, as the length difference increases, the SNR decreases. For instance, when the difference is 1 m, the SNR decreases by approximately 10 dB. Therefore the two optical fibers used between two optical couplers have to be same length as strict as possible. However it is almost satisfied with this condition to use two optical fibers in the same cable.

4. FIELD APPLICATION

An example application of our optical-cable identification system is illustrated in Fig. 11. The cable to be identified runs between network centers A and B. The lightsource and a 2x2 optical-fiber coupler are in network center A, and another coupler and a photo-detector are in network center B. A field worker at the access hole sets the piezo-electric actuator on one of the optical cables. A worker at network center B then advises the field workers if a vibration frequency is detected. If not, the field worker

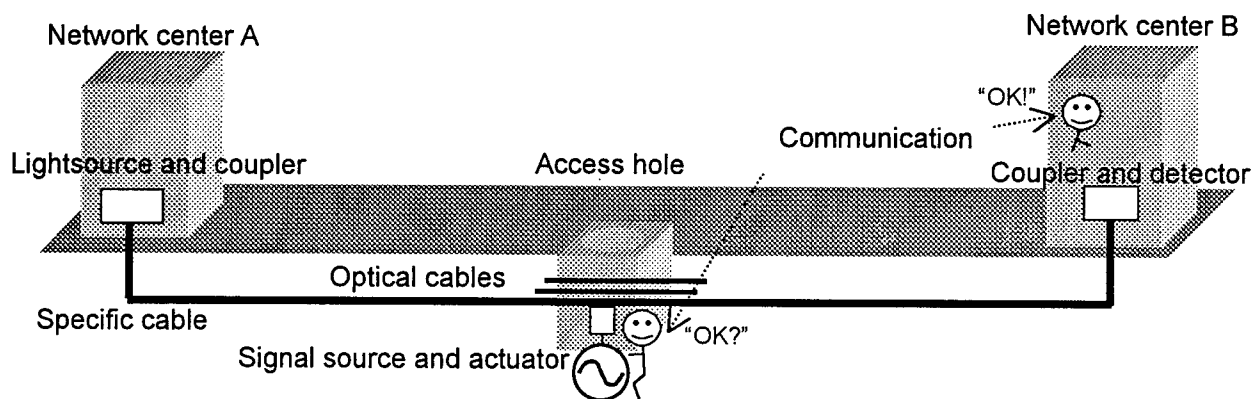


Fig. 11 Field application example.

sets the actuator on a different cable. This process continues until the specific cable is identified.

5. CONCLUSION

Our proposed an optical-cable identification system can be used at any point along on optical-fiber cable without having to slice open the cable. It was demonstrated to work for cables over 40 km long. This system is a suitable tool for optical-fiber cable maintenance for future multimedia networks.

ACKNOWLEDGMENTS

We are grateful to Dr. Masaaki Kawase, Mr. Yasuyuki Imori, and Mr. Nobuyuki Ikawa for their helpful suggestions and encouragement, and to Mr. Masaru Kobayashi for his insightful discussion.

REFERENCES

- [1] T. Miki, "Fiber-optic access networks and services", NTT Review, Vol. 6, No. 3, pp.17-25, 1994.
- [2] A. Fujisaki, H. Ogoshi, S. Sentsui, M. Kurokawa, M. Mizutani, and M. Miyazaki, "Optical talk set and optical identifier using polarised-wave-external-modulation method", 39th IWCS, pp.418-423, 1990.



Yuji Azuma

NTT Maintenance and Service Operations Department

Nishi-Shinjuku, Shinjuku-ku, Tokyo 163-19, Japan

Yuji Azuma is an Associate Manager in the NTT Maintenance and Service Operations Department. After receiving his B.E. degree in electrical engineering from Doshisha University, Kyoto, Japan, in 1984, he joined NTT Laboratories. He has researched the characteristics of high-density optical-fiber cables, evaluated the reliability of optical devices, and developed optical-fiber maintenance equipment. Mr. Azuma is a member of the Institute of Electronics, Information and Communication Engineers of Japan.



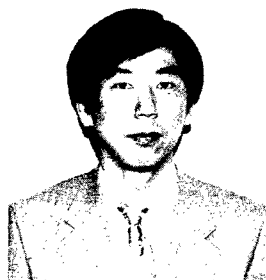
Koichi Matsuno

NTT Technical Assistance and Support Center

Midori-cho, Musashino-shi, Tokyo 180, Japan

Koichi Matsuno has worked as an Engineer in the Technical Assistance and Support Center, NTT Maintenance Service and Operations Department. He joined NTT in 1981. He has designed optical-fiber-cable identification systems and has developed of optical-fiber

maintenance equipment. Mr. Matsuno is a member of the Institute of Electronics, Information and Communication Engineers of Japan.

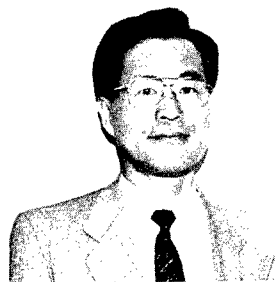


Koji Arakawa

NTT Technical Assistance and Support Center

Midori-cho, Musashino-shi, Tokyo 180, Japan

Koji Arakawa is an Executive Engineer in the Technical Assistance and Support Center, NTT Maintenance Service and Operations Department. After receiving his B.E. degree in electrical engineering from Osaka Prefecture University in 1978, joined NTT. He has researched optical-fiber-cable reliability and developed optical-fiber maintenance equipment. Mr. Arakawa is a member of the Institute of Electronics, Information and Communication Engineers of Japan.



Koji Yoshida

NTT Technical Assistance and Support Center

Midori-cho, Musashino-shi, Tokyo, 180 Japan

Koji Yoshida is an Executive Engineer in the Technical Assistance and Support Center, NTT Maintenance Service and Operations Department. After receiving his B.E. degree in communications engineering from Osaka University in 1973, joined NTT. He has developed optical-testing instruments and researched on optical-fiber-cable reliability. Mr. Yoshida is a member of the Institute of Electronics, Information and Communication Engineers of Japan.

A Novel Surveillance System for Installed Fiber Optics Cables using Stimulated Brillouin Interaction

M. Niklès, L. Thévenaz, A. Fellay, M. Facchini, P. A. Robert

Swiss Federal Institute of Technology of Lausanne, Metrology Laboratory, Switzerland

P. Salina,

Swiss Telecom PTT, Bern, Switzerland

Abstract: A novel surveillance system for installed fiber optic cables is presented. It is based on the analysis of the local stimulated Brillouin scattering interaction. The configuration of the instrument rely on the use of a single laser source and the required light signals are all generated using an electro-optic modulator, resulting in a high stability and an excellent reliability of the setup. Some results of the first field measurements are discussed. They have provided important information on the strain distribution actually experienced by the fibers, fiber uniformity, local birefringence, temperature variations. The system can operate over 100 km and the spatial resolution, which remains sub-metric over the first 10 km, is below 10 m over the full range.

1. Introduction

During the last two decades fiber optics telecommunications have experienced a spectacular progress. Thousands of kilometers of cables are being installed every year to complete an ever growing network. Besides high-speed transmission systems have become

more and more sophisticated to achieve higher bit rates for long-haul fiber optic links. At highest bit rates the performances of these systems rely on the quality of the propagation medium. Silica rapidly became the preferred transmission medium because of its low-loss characteristics and the design of single-mode fibers has given to the transmission link a extremely large available bandwidth. However it is known that cable installation procedure and fiber ageing can affect these performances and therefore can impose severe limitations to the whole communication system. Up to date the tests of a fiber link only rely on the traditional OTDR which is suitable for the detection of excess loss and the localization of breaks. It turns out that there is an urgent need for a surveillance equipment for installed fiber optic cables that could diagnose fiber and cable degradation and provide important information such as strain distribution and local birefringence. The instrument should also grant a long-term preventive maintenance and allow to remotely localize possible problems.

The present paper describes the operation and the performances of a new instrument that has

been designed for optical fibers surveillance. It is based on the local analysis of stimulated Brillouin inter-action along optical fibers. Brillouin gain spectrum (BGS) measurement has been pointed out several times in the past for its potentiality for strain monitoring in installed telecommunication cables^[1]. The purpose of this paper is twofold: to show on one hand that this potentiality has been made effective, since field measurements of installed fiber optics cables *currently in operation* are demonstrated, and on the other hand that the application of BGS analysis is not limited to strain measurements.

2. Theory of operation and instrument configuration

Stimulated Brillouin Scattering (SBS) shows the lowest threshold among all non-linear processes observed in optical fibers. It is also strongly dependent on local physical parameters of the fiber, since the scattered light experiences a frequency downshift ν_B with respect to the incident light proportional to the acoustic velocity within the fiber, this latter being function of temperature and strain. SBS is therefore naturally used to achieve distributed

sensors measuring these quantities, and numerous contributions in this field have been presented in the past few years^[1, 2, 3, 4].

The basic configuration of a distributed Brillouin sensor is simple: a strong light pulse, hereafter called pump, is launched into the fiber. It crosses a weak CW lightwave, called signal or probe wave, that propagates in the backward direction. SBS occurs when pump and probe overlap, resulting in an amplification of the probe wave provided that the difference between the two frequencies lies within the BGS of the fiber. This BGS shows a Lorentzian distribution centered on the Brillouin shift ν_B that is the quantity to determine. To obtain the BGS and thus determine ν_B , one simply measures the amplification of the Stokes wave while making a frequency scan. The spatial resolution for distributed measurements is directly related to the pulse length. For a given pump power the ultimate spatial resolution is determined by the narrowest pump pulse that leaves a sufficient gain for a BGS measurement to be performed with minimum contrast. Instead of using the now traditional configuration using two laser sources^[1, 2, 3], a

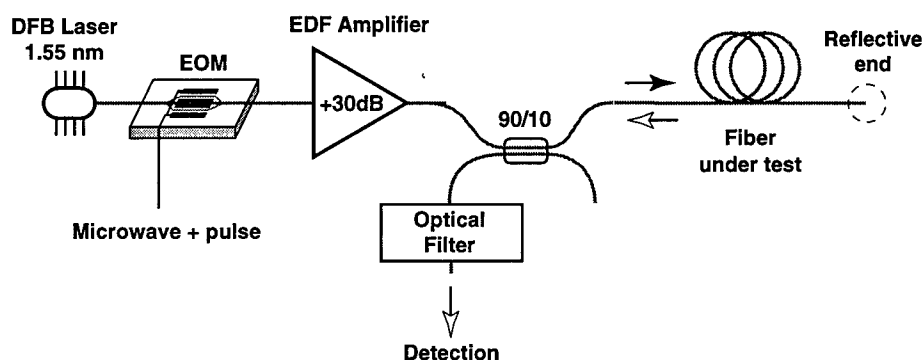


Fig. 1: Experimental configuration of the Brillouin scattering based system.

novel experimental setup has been developed in our laboratory ^[5]. Its main original feature is the presence of a single laser source that is modulated through an Mach-Zehnder electro-optic modulator (EOM) to generate both pump and probe lightwaves. This gives to the system an inherent stability, as far as frequency drifts of the laser are concerned. In addition, access to a single fiber end is required to perform the measurements, what is an obvious advantage in the field. On-site measurements have been so far performed using a 150 mW Nd:YAG laser at 1319 nm, leading to a 3 m best resolution ^[6]. To improve this figure, it was necessary to boost the intensity of the pump wave, what can be ideally performed using an optical amplifier at 1550nm. The experimental setup is schematically shown in Fig. 1. In proper working conditions of the EDFA peak pump powers in the Watt range can thus be obtained and sub-meter spatial resolution can

be reached. Minimal absorption loss is a further advantage of the 1550 nm transmission window, making a 100 km sensing range possible.

3. Applications

The first field measurements using the local analysis of stimulated Brillouin interaction (LASBI) have provided essential information on: fiber identification, local strain, fiber uniformity, fiber local birefringence, temperature distribution.

3.1 Fiber identification (manufacturing process, profile)

The LASBI investigation gives access to the value of the local Brillouin frequency shift, which depends on fiber parameters such as dopant concentration and refractive index profile. The Brillouin frequency shift can in fact

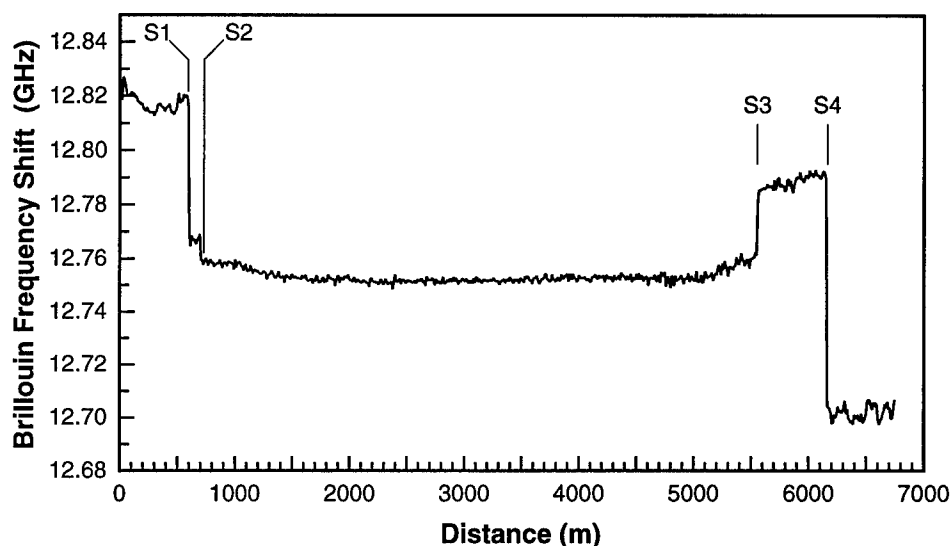


Fig. 2: Identification of different sections of a fiber optic cable installed under the lake of Geneva. The five segments of fiber are identified by their different Brillouin frequency shift. The splices are indicated S1 to S4 on the graphic.

be considered as a sort of fingerprint of a specific fiber, and can be used to identify different fibers. Fig. 2 presents the result of a measurement carried out on a 6.8 km-fiber optic cable of the Swiss Telecom PTT network. The Brillouin shift profile shows that this link has been made of 5 fiber segments coming from different preforms spliced together (the splices are indicated S1 through S4). The third segment (from S2 to S3) corresponds to an underwater section of the link. The Brillouin shift of the last segment, by far under the value of standard telecom fibers, indicates that the geometry of the refractive index profile is different for that fiber.

3.2 Local strain detection;

Localization of excessive strain was the first foreseen application of LASBI systems [1]. The strain dependence of the Brillouin frequency shift is approximately 60 MHz/ $\mu\epsilon$ (50 MHz/ $\mu\epsilon$) for standard fibers at 1.3 μm (at 1.55 μm) [7, 8]. The spatial resolution achieved by our instrument actually reaches the physical limits. A 80 cm fiber segment experiencing a 1.5 %

elongation can be clearly identified, as shown in Fig. 3. A fiber optic link can thus be checked for the absence of strain, which is the key information for a long-term reliability.

3.3 Fiber uniformity evaluation;

The dependence of the Brillouin frequency shift on the dopant concentration can be used to check the fiber uniformity, which is an important condition for a constant cut-off wavelength all along an optical fiber. An ideal fiber placed with no strain in a temperature controlled environment should show a constant value of Brillouin frequency shift throughout the length. Any deviation from this value can be attributed to non-uniformity in the fiber constitutive parameters. In practice another fiber can be used to monitor the environmental conditions, as can be seen in Fig. 4.

3.4 Determination of local birefringence;

It has been demonstrated over the past few years that polarization mode dispersion (PMD) may limit the ultimate data rate through an optical fiber. The basic reason for PMD is the

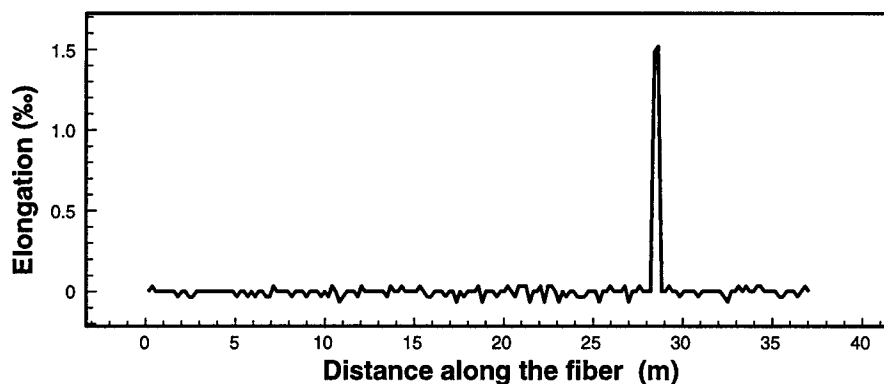


Fig. 3: Detection and localization of the presence of local strain. Here a 80cm fiber segment stretched by a 155g weight is clearly identified, resulting in a 1.52% elongation.

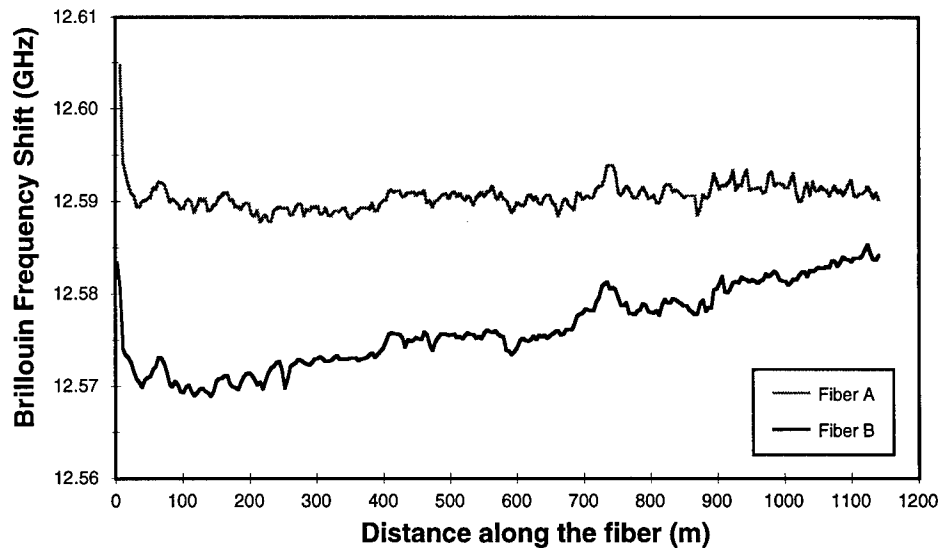


Fig.4: Two different fibers out of the same tube in the same cable present different Brillouin characteristics. They both experience the same temperature fluctuations but Fiber B presents a non-homogenous dopant concentration, resulting in a variation of the Brillouin frequency shift, corresponding to a 1.3 % wt. mol. decrease of the GeO_2 concentration over 1 km.

presence of intrinsic or induced birefringence within the fiber. Measuring the local birefringence would thus provide key information to localize the fiber segments mainly contributing to PMD, so that an efficient action could be undertaken for cable upgrade. The amplification rate at any location depends on local features of the fiber, such as temperature and strain, but also on the relative polarizations of the waves crossing at this point. The time recording of the intensity of the reflected light gives the spatial distribution of the Brillouin gain along the fiber, that is directly related to the polarization variations experienced by light during its propagation. The local gain is actually polarization-dependent, being maximal for aligned fields and zero for crossed fields. The gain varies along the fiber as the relative polarizations of

pump and probe are changed by birefringence, as shown in the measured gain profile in Fig. 5. The information about the birefringence beat length can be extracted from such a gain profile, provided that the beat length is larger than the spatial resolution of the system. The distance between a maximum and the next minimum of the gain corresponds to a quarter of the local beat length. Fig. 5 shows the local beat length obtained from a typical gain profile, as well as the gain profile itself.

3.5 Other applications

Distributed Brillouin scattering based systems have been first proposed to analyze the attenuation characteristics of optical fibers [9]. The use of Brillouin scattering instead of Rayleigh scattering brings a 10 dB improvement in the dynamic range, but

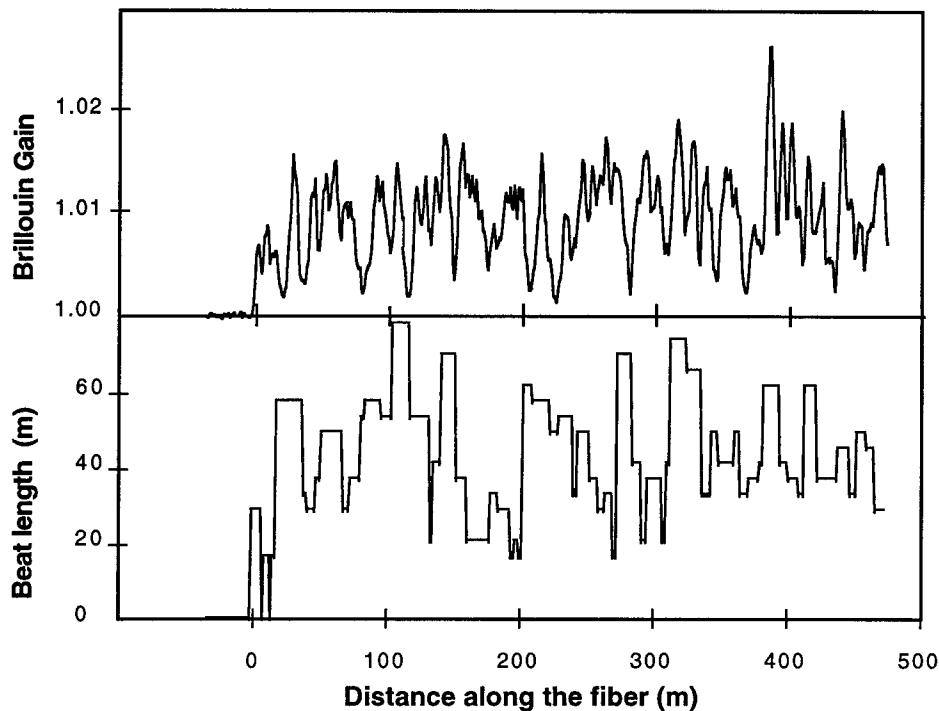


Fig. 5: Brillouin gain distribution along a segment of fiber (top) and calculated corresponding local beat length (bottom).

require some complicated processing to get rid of fluctuations due to polarization variations (see Fig. 5).

The temperature dependence of the Brillouin frequency shift (approximately 1.3 MHz/°C at 1.3 μm for standard fibers) can be used to perform distributed temperature measurements [2, 3, 4]. Again the temperature and strain cross-sensitivity of the Brillouin frequency shift must be taken into account. However it can be compensated by calibration measurements in temperature controlled environment.

4. Conclusions

A novel surveillance system for fiber optic cable has been developed. The high stability and

reliability of the experimental configuration of the instrument is very promising for the further development of an industrial prototype. The system specifications are illustrated by the figure of merit shown in Fig. 6. The most remarkable feature shown on this graph is the maintained resolution over a long distance: it remains below 3 meters over 50 km, as a consequence of the low loss at 1550 nm. On the other hand, the optimal resolution for very short fibers is slightly less than 1 m. This kind of sensors is thus definitely dedicated for long range measurements with meter resolution and is not suitable for a centimeter resolution.

Local analysis of stimulated Brillouin interaction measurements have been carried out on different installations of the Swiss Telecom PTT

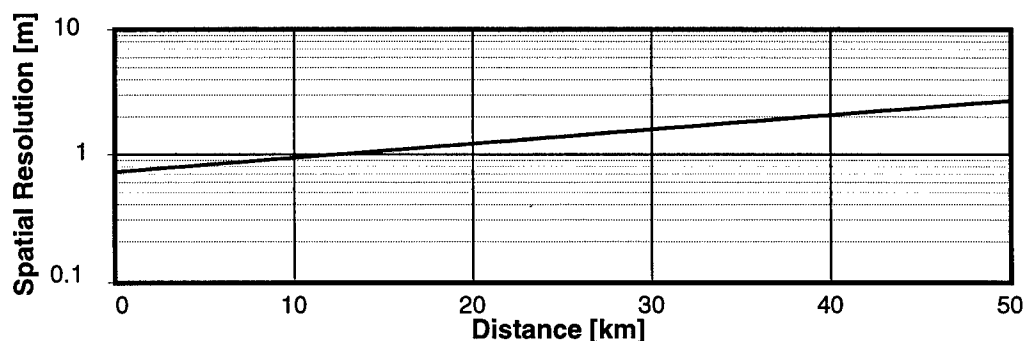


Fig. 6 Spatial resolution as a function of the distance along the fiber at a wave length of $1.55 \mu\text{m}$.

currently in operation. Important information was collected for the first time on the actual strain experienced by the fiber, fiber non-uniformity, local fiber birefringence, leaving demonstrative charts. Measurements have been repeated over a one year period to check the long term stability of the fiber links in different seasonal conditions.

In spite of the metric limitation of the spatial resolution, the applications of Brillouin sensing technique remain numerous: the figure of merit shown in Fig. 6 indicates in particular that the LASBI instrument is very competitive when a resolution in the meter range is needed over a considerable distance. Some typical applications are the detection of defects in telecom fibers, the monitoring of deformations in large-sized concrete structures like tunnels or dams, and the centralized temperature survey of building at a city scale.

References

- [1] T. Horigushi, T. Kurashima, M. Tateda, "A technique to measure distributed strain in optical fibers", IEEE Photonics Technol. Lett., Vol. 2, p. 352, 1990.
- [2] X. Bao, J. Dhliwayo, N. Heron, D.J. Webb, D.A. Jackson, "Experimental and theoretical studies on a distributed temperature sensor bases on Brillouin scattering", IEEE J. Lightwave Technol., Vol. 13, p. 1340, 1995.
- [3] T. Kurashima, T. Horigushi, M. Tateda, "Distributed-temperature sensing using stimulated Brillouin scattering in optical fibers", Optics Lett., Vol. 15, p. 1038, 1990.
- [4] M. Niklès, L. Thévenaz, Ph. Robert, "Simple Distributed Temperature Sensor based on Brillouin Gain Spectrum Analysis", Proceedings of the 10th. Optical fiber sensors conference (OFS'94), Glasgow, Scotland, 11-13 oct 1994, pp. 138-141, 1994.
- [5] M. Niklès, L. Thévenaz, Ph. Robert, "Simple Distributed Fiber Sensor based on Brillouin Gain Spectrum Analysis", Optics Lett., vol. 21, no 10, pp. 758-760, 1996.
- [6] M. Niklès, L. Thévenaz, P. Salina, Ph. A. Robert, "Local Analysis of Stimulated Brillouin Interaction in Installed Fiber Optics Cables", Technical Digest of the Symposium on Optical Fiber Measurements, Boulder Colorado, October 1-3, 1996, NIST Special Publication 905, pp. 111-114, 1996.
- [7] M. Niklès, Ch. Gabioud, L. Thévenaz, Ph. Robert, "Highly Accurate Measurement of Temperature and Strain-dependence of Brillouin Gain in Single-mode Fibres", 3rd Optical Fiber Measurement Conference (OFMC '95), Liège, Belgique, 25-26 septembre 1995, paper VII.2, 1995.
- [8] M. Niklès, L. Thévenaz, Ph. A. Robert, "Brillouin Gain Spectrum Characterization in Single-Mode Optical Fibers", to be published in IEEE J. of Lightwave Technol., Vol. 15, N° 10., 1997.
- [9] T. Horigushi and M. Tateda, "Optical-fiber-attenuation investigation using stimulated Brillouin scattering between a pulse and a continuous wave", Optics Lett., Vol. 14, p. 408, 1989.

Biography of the authors

Marc Niklès

EPFL, Metrology Laboratory,
CH-1015 Lausanne, Switzerland

Marc Niklès received the Dipl.-Ing. degree in Microtechnology from the Swiss Federal Institute of Technology of Lausanne (EPFL) in 1989. He received the Ph.D. degree from the Electrical Engineering Department of the Swiss Federal Institute of Technology of Lausanne in 1997. In 1990 he joined the Metrology Laboratory of the Swiss Federal Institute of Technology of Lausanne, Switzerland, where he developed metrological facilities for characterizing integrated optical devices and applications using optical signal processing. For his doctoral research he investigated stimulated Brillouin scattering in optical fibers and developed a new fiber optic distributed temperature sensor.

Luc Thévenaz

EPFL, Metrology Laboratory,
CH-1015 Lausanne, Switzerland

Luc Thévenaz received the B. Sc. degree in astrophysics from Observatory of Geneva, Switzerland, in 1982, and the Ph.D. degree in physics from the University of Geneva in 1988. In 1988, he joined the Laboratory of Metrology of the Swiss Federal Institute of Technology in Lausanne, where he presently occupies a research manager position. His research interests include Brillouin scattering in fibers, optical fiber sensors and laser spectroscopy. In 1991, he visited the University of Rio de Janeiro and Stanford University.

Alexandre Fellay

EPFL, Metrology Laboratory,
CH-1015 Lausanne, Switzerland

Alexandre Fellay earned the Ing. Dipl degree in Physics from the Swiss Federal Institute of Technology of Lausanne (EPFL) in 1996. Since 1996 he has worked for the Metrology Laboratory of the same Institute in the domain of fiber optics, focusing more specifically on Brillouin scattering and distributed sensors.

Massimo Facchini

EPFL, Metrology Laboratory,
CH-1015 Lausanne, Switzerland

Massimo Facchini earned his degree in Electronical Engineering from the Politecnico of Milan, Italy, in 1996. In 1997 he joined the Metrology Laboratory of the Swiss Federal Institute of Technology (EPFL), Switzerland, where he actually works in the domain of distributed fiber optic sensors.

Pascal Salina

Swiss Telecom PTT, Ostermundigenstr. 93,
CH-3029 Bern, Switzerland

Pascal Salina received the Dipl. Ing. degree in Material Sciences from the Swiss Federal Institute of Technology of Lausanne (EPFL) in 1987. In 1988 he joined Swiss Telecom PTT where he worked in the group for Cable Technique which he has headed since 1995, dealing with both copper and optical fibre cable characterisation as well as material analysis, mainly in the field of polymers. He is also involved in COST 246 "material science and reliability of optical passive components" where he acts as vice-chairman and in different standardisation bodies such as CENELEC/CECC SC 86 "optical fibre cables" and UIT-SG 6 "outside plant".

Philippe Alain Robert

EPFL, Metrology Laboratory,
CH-1015 Lausanne, Switzerland

Philippe Alain Robert received his diploma in physics engineering in 1961 and his Ph.D. in 1968 from the Swiss Federal Institute of Technology of Lausanne (EPFL). From 1968 to 1974 he was with Les Câbleries et Tréfileries de Cossonay where his research interests lay in new products and new manufacturing processes, including optical fibers. From 1974 to 1979 he has been engaged in the development and installation of the first optical cables made in Switzerland. Since 1979 he is a professor at the EPFL and head of the Laboratory of Metrology. His current research activities concern guided optics: optical fibers and integrated optics with applications in optical signal processing, sensors and telecommunications.

REFLECTIVE INFLUENCE CONSIDERATION FOR SUB-CARRIER MULTIPLEXING SYSTEM

Tomoyuki KATO, Hideyuki OMURA, Shin-ichi TAKASHIMA

THE FURUKAWA ELECTRIC CO.,LTD. Hiratsuka, Kanagawa, JAPAN

ABSTRACT

We investigate, both theoretically and experimentally, the transmission characteristics of a SCM system under the influence of optical reflection. In order to satisfy the specifications for AM-VSB and FM transmission, the reflected signal into LD should be suppressed below -40dB and into PD should be suppressed below -50dB. The use of optical isolators is effective to suppress the reflection into the LD. The influence of reflection into the PD can be suppressed by the use of LDs with shorter coherent length than the distance between connectors.

1. INTRODUCTION

Sub-carrier multiplexing (SCM) is an important technique for high speed optical transmission systems, such as optical CATV systems. The influence of optical reflection is one of the important factors we have to consider in designing SCM systems. There are two types of reflection in optical transmission paths. One is the optical feedback into a laser diode (LD) caused by the reflection from optical connectors and Rayleigh backscattering in optical fibers. The other is the reflection into a photo-diode (PD) caused by multiple Rayleigh backscattering and multiple reflection between connectors. These reflection could deteriorate the transmission characteristics of SCM systems, such as RIN (Relative Intensity Noise), CSO (Composite Second Order), CTB (Composite Triple Beat) and XM (Cross Modulation). Therefore systems with few optical connectors would be desirable because of the reduced optical reflection. However, for system maintenance such as inspection and route switching, it would be convenient to have some optical connectors in the system. Thus for optimum system design it is necessary to investigate the quantitative relationships

between transmission characteristics mentioned above and the reflected signal intensity induced in optical transmission paths.

In this paper we investigate, both theoretically and experimentally, the transmission characteristics of a SCM system under the influence of optical reflection. The methods to suppress the influence of reflections are also discussed.

2. SPECIFICATIONS FOR SCM SYSTEMS

Specifications for analog video transmission systems with SCM are shown in Table 1. Fig.1 shows the carrier-noise ratio (CNR) as a function of received optical power. CNR was calculated by the following formula; ⁽¹⁾

$$CNR = 10 \log \frac{(1/2)(mMSP_r)^2}{\left[2q(I_{do} + M^{2+x}(I_{dm} + SP_r) + I_t^2 + (MSP_r)^2 RIN) \right] B} \quad (1)$$

where m is the optical modulation index for each channel, M is the optimized multiplication factor of APD (Avalanche Photo Diode), x is the excess noise index of APD, S is the sensitivity of APD, q is the electronic charge, I_{do} is the dark current of APD, I_{dm} is the multiplication current of APD, I_t is the thermal noise current amplifier, P_r is the average received power, and B is the bandwidth of the signal.

As shown in Fig.1, when an optical modulation index for each channel is 5%/ch, in order to satisfy the CNR specifications shown in Table 1, RIN has to be less than -140dB/Hz for AM transmission and less than -120dB/Hz for FM transmission.

Table 1 Specifications for analog video transmission systems with SCM

	AM-VSB ($B=4.2\text{MHz}$)	FM ($B=27\text{MHz}$)
CNR	42dB	14dB
CSO	55dB	42dB
CTB	55dB	42dB
XM	55dB	—

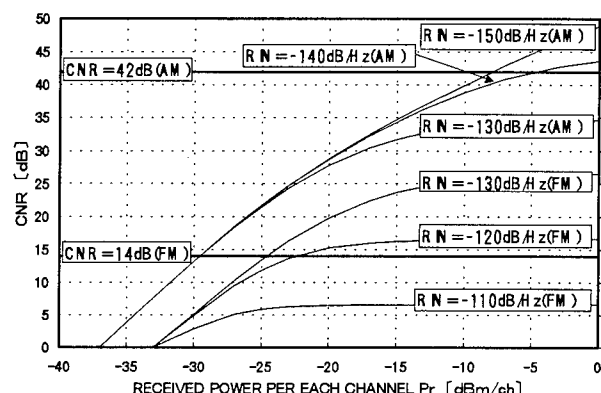


Fig.1 Relationship between CNR and received power per channel, calculated for each RIN value ($m=5\%/ch$).

3. INFLUENCE OF REFLECTION INTO LASER-DIODE

3-1. EXPERIMENTS

3-1-1. METHOD FOR EXPERIMENT

In optical transmission systems in service, a part of the optical signal is reflected back to the light source (LD) from connection points as shown in Fig.2.

We have investigated the effects of the reflected signal on transmission characteristics. Fig.3 shows the experimental setup to measure the noise and distortion characteristics under the influence of direct reflection. A light source was modulated with 40 channel sine waves in measuring distortions, and was CW in measuring RIN. The optical signal was launched into a 3-dB optical coupler. A part of the signal was reflected back to the light source from port 4 with a reflection terminal. The intensity of the reflected signal was controlled with a variable optical attenuator and was measured with a power meter at port 2. Polarization of the reflected optical signal was controlled with a polarization controller.

Two types of LDs were used as the light source. One is with an optical isolator and the other is without isolator.

The measured items in this experiment are shown in Table 2.

The characteristics of LDs are shown in Table 3.

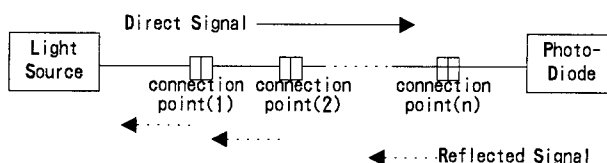


Fig.2 Direct reflection model

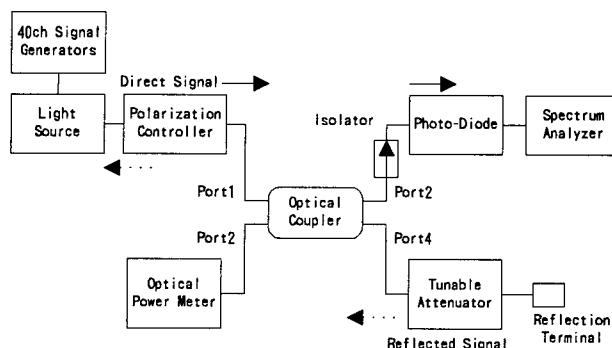


Fig.3 Experimental setup to evaluate the influence of direct optical reflection

Table 2 Measured items

items	measuring contents
RIN	measuring relative intensity noise at Photo-Diode in non-modulation (100MHz and 400MHz)
CSO	measuring composite second order distortion at Photo-Diode in 40ch-modulation (91.25MHz and 331.25MHz)
CTB	measuring composite triple beat distortion at Photo-Diode in 40ch-modulation (91.25MHz and 331.25MHz)
XM	measuring cross modulation distortion at Photo-Diode in 40ch-modulation (91.25MHz and 331.25MHz)

Table 3 Characteristics of LD used in experiment

LD type (A,B)	DFB-LD A : without isolator B : with isolator(35dB)
output power	A : +4.0dBm B : +5.5dBm
wavelength	A,B : 1.31 μ m
RIN	A,B : -160 d B/Hz
modulated index	A,B : 7%/ch
number of channels	A,B : 40ch(AM-VSB)

3-1-2. RESULTS

Fig.4, 5, 6 and 7 show RIN and distortion characteristics versus reflection power ratio under the worst polarization conditions. The reflection power ratio is defined as the ratio between the output power of the light source and the measured optical power at port 2.

RIN :

In the case without isolator, RIN deteriorates with increasing reflection power. The amount of deterioration depends on the polarization state of the reflected signal. RIN becomes -130dB/Hz at the reflection power ratio of -20dB at the *worst* polarization state. In the case with an isolator, RIN deterioration is small. Intensity noise spectra with and without isolator are shown in Fig.8 and 9, respectively. Both spectra were measured at the *worst* polarization state. As in these figures, the periodic noise peaks are induced by the reflection. The height of the peaks are suppressed in the case with an isolator.

DISTORTION :

In the case of without isolator, CSO, CTB and XM deteriorate with increasing reflection power. The amount of the deterioration is 10 dB at maximum. In the case of with isolator, the deterioration is small.

These results shows that the reflection power ratio should be kept below -40 dB in order to satisfy the specifications of system shown in Table 1 using a LD without isolator.

The isolator used in the experiment has the isolation of 35dB, which is almost enough to suppress the reflection power to the level where the influence of reflection is negligible.

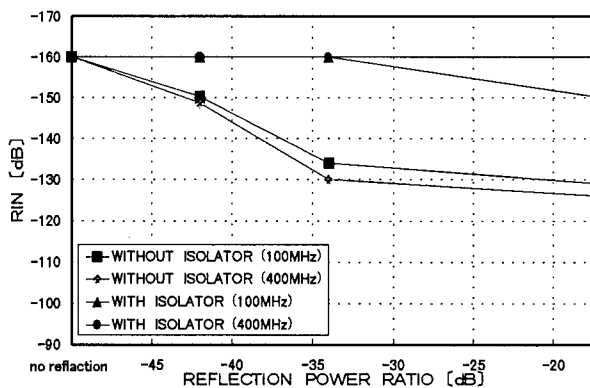


Fig.4 RIN versus the reflection power ratio under the worst polarization condition

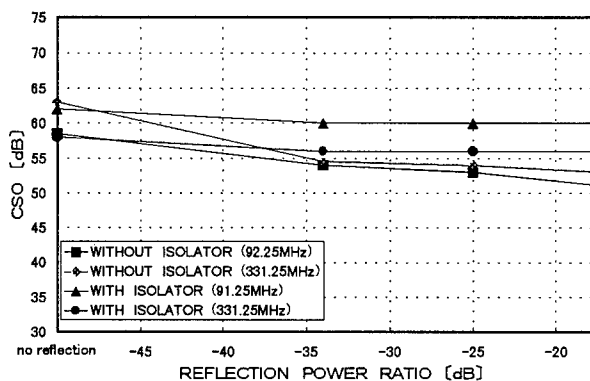


Fig.5 CSO versus the reflection power ratio under the worst polarization condition

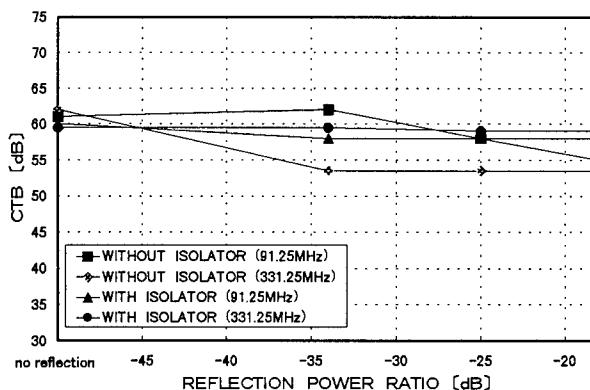


Fig.6 CTB versus the reflection power ratio under the worst polarization condition

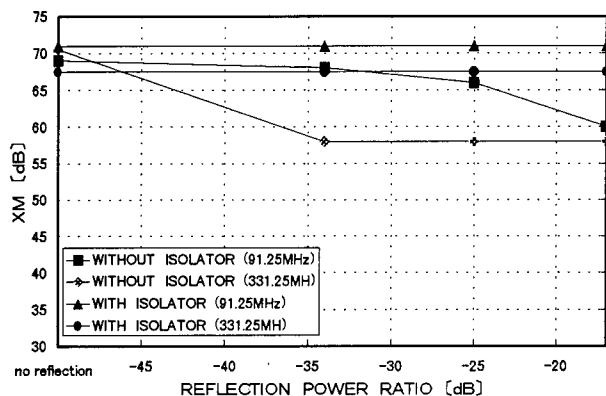


Fig.7 XM versus the reflection power ratio under the worst polarization condition

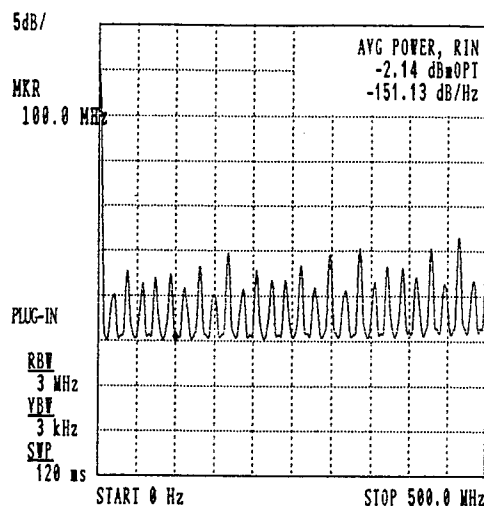


Fig.8 Intensity noise spectrum without isolator at reflection power ratio of -30dB under the polarization condition where the periodic noise peaks are the highest.

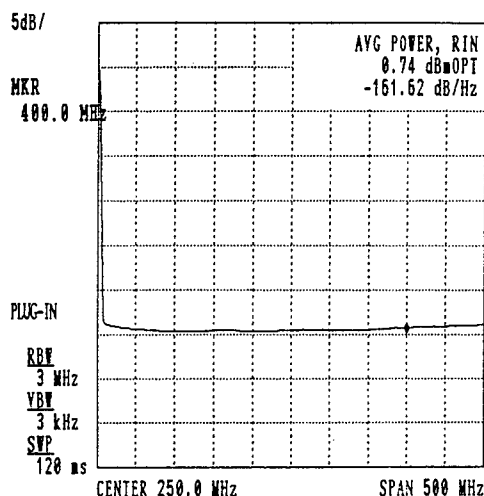


Fig.9 Intensity noise spectrum with isolator at reflection power ratio of -30dB.
(The periodic noise peaks are little induced.)

3-2. DISCUSSION

3-2-1. THEORETICAL ANALYSIS

It has been reported that laser diode noise significantly increases when there are reflected optical signals from optical transmission paths. This phenomenon is explained based on mode competition theory as follows.

The reflection-induced noise of LD is mainly due to the reflection from the laser-fiber coupling and optical components (in particular, optical connectors) in optical paths. Reflected optical waves build up a standing wave between LD and reflection point and form a new cavity mode. This new mode is called an external cavity mode. Even if an oscillation continues on laser mode, the noise increases by competition with the external cavity mode. The excess noise immediately comes up from the level of quantum noise when effective feedback ratio reaches Γ_c .^[2]

$$\Gamma_c = 22R_2 \left[\frac{n_{eq}l}{L(1-R_2)} \right]^2 \quad (2)$$

where R_2 is the reflectance of the laser faces, n_{eq} is the refractive index of on the lasing mode, l is the length of the laser cavity, L is the length between the laser and the reflection point.

Considering typical LD, it is estimated that $R_2 = 10\%$, $n_{eq} = 3.5$ and $l = 300 \mu m$. In the experiment, $L = 4m$. Therefore, Γ_c is estimated as 1.9×10^{-6} ($\approx -67dB$). In the experiment, direct signal power to minimum reflected power ratio was -42dB, RIN can be sufficiently increased due to reflected signal.

When a part of the laser output is reflected back into the laser from the reflection point of distance L , the intensity of the laser output fluctuates. The spectrum of the fluctuation has periodic peaks with the fundamental frequency component f_p , which is nearly equal to the reciprocal of the round-trip time of the fiber, as is given by;^{[3], [4]}

$$f_c = \frac{c}{2nL} \quad (3)$$

where c is the velocity of light, n is refractive index of the optical fiber.

In the experiments L is a few meters. Therefore, as in Fig.8 f_p in the experiments almost agree with the calculated result by eqn.(3).

The influence of reflection on the distortions has little

been reported, further theoretical study is necessary based on the experimental results.

3-2-2. METHODS TO SUPPRESS THE INFLUENCE OF REFLECTION IN SCM SYSTEM

The frequency peaks and the noise spectrum depend on the condition of reflected signals. In order to suppress the reflection from laser-fiber coupling, anti-reflection coating at the facets of optical components and spherical or angled polishing of the optical connector facets are useful. For suppressing the reflection from connection points in paths, in addition to the techniques mentioned above, inserting an optical isolator is effective.

As in the experimental results, in order to satisfy the specifications of system shown in Table 1 using a LD without isolators, the reflection power ratio has to be suppressed below -40 dB. Therefore when we employ SCM systems, it is necessary to keep the reflection power ratio below -40 dB, or to install an isolator to decrease the influence of reflection.

4. INFLUENCE OF REFLECTION INTO PHOTO-DIODE

4-1. EXPERIMENTS

4-1-1. METHOD FOR EXPERIMENT

In optical transmission systems in service, a part of the optical signal is reflected into the photo-diode (PD) by multiple reflections from connection points as shown in Fig.10.

We have investigated the effects of the reflected signal on transmission characteristics. Fig.11 shows the experimental setup to measure the noise and distortion characteristics under the influence of multiple reflections. The LD with isolator shown in Table 4 was used as a light source. The LD was modulated with 40 channel sine waves in measuring distortions, and was CW in measuring RIN. The optical signal was divided by an optical coupler. Two divided optical signals were combined after transmitted through a direct path and a delay path. In the delay path the optical signal power and polarization state were controlled with a variable optical attenuator and a polarization controller, respectively.

The measured items in this experiment are shown in Table 2. In this experiment the noise and distortions

were measured for two delay length. One is nearly equal to 0 meter which is shorter the coherent length of the LD. The other is about 1000 meters which is much longer than the coherent length.

The coherent length ($2 \Delta l$) is given by

$$2\Delta l = \frac{c}{n\Delta\nu} \quad (4)$$

where $\Delta\nu$ is the linewidth of LD. The LD used in the experiment has the coherent length of about 20 meters.

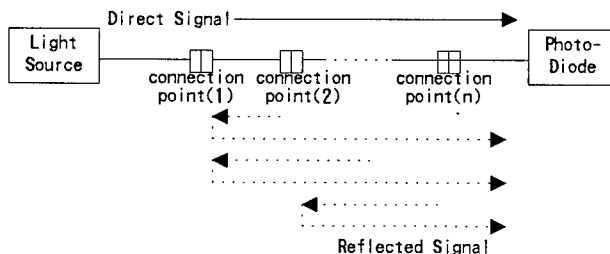


Fig.10 Multiple reflection model

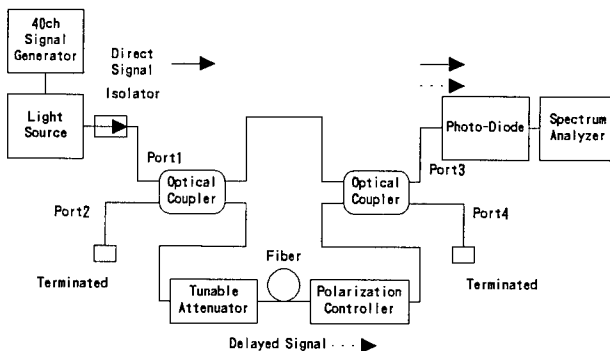


Fig.11 Experimental setup to evaluate the influence of multiple optical reflections

4-1-2. RESULTS

Fig.12, 13, 14 and 15 show RIN and distortion characteristics versus reflection power ratio under the worst polarization conditions. The reflection power ratio is defined as the ratio between the optical powers in the direct path and in the delay path.

RIN :

RIN depends on the polarization state of the reflected signal. There is little difference between the worst RIN for the delay length of 0m and that for the delay length

of 1000m. However, the best RIN for delay $\approx 1000\text{m}$ is smaller (better) than that for delay $\approx 0\text{m}$. Intensity noise spectrum for the two delay lengths are shown in Fig.16 and 17.

RIN at low frequency is larger than RIN at high frequency. This is because the direct signal and the reflected signal are received by the photo-diode at the same time and induce beat noise near DC.

DISTORTION :

CSO, CTB and XM also depend on the polarization state of the reflection signal. Distortion for delay $\approx 0\text{m}$ is worse than that for delay $\approx 1000\text{m}$. For delay $\approx 0\text{m}$, the amounts of deterioration are 25dB for CSO, 25dB for CTB, and 33dB for XM at the reflection power ratio of -20dB. For delay $\approx 1000\text{m}$, the amounts of deterioration are little for CSO and CTB and 25dB for XM.

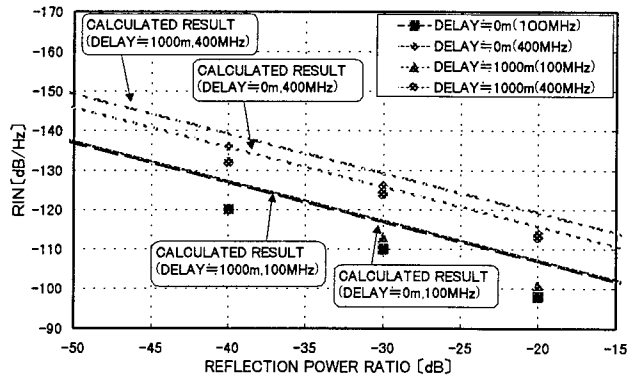


Fig.12 RIN versus the reflection power ratio under the worst polarization condition

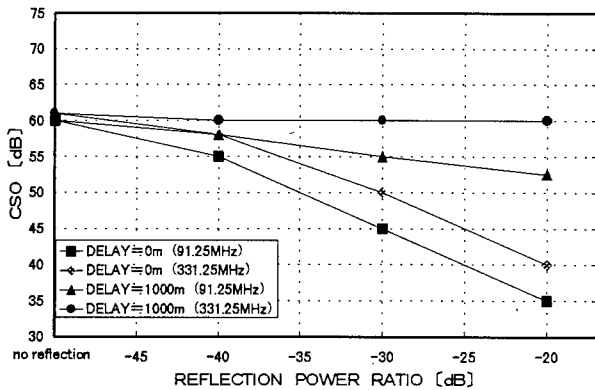


Fig.13 CSO versus the reflection power ratio under the worst polarization condition

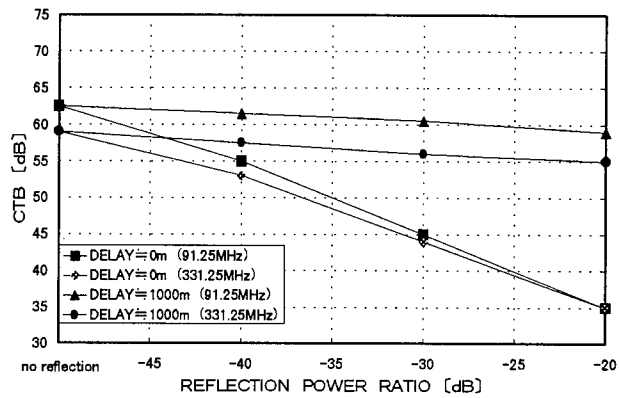


Fig.14 CTB versus the reflection power ratio under the worst polarization condition

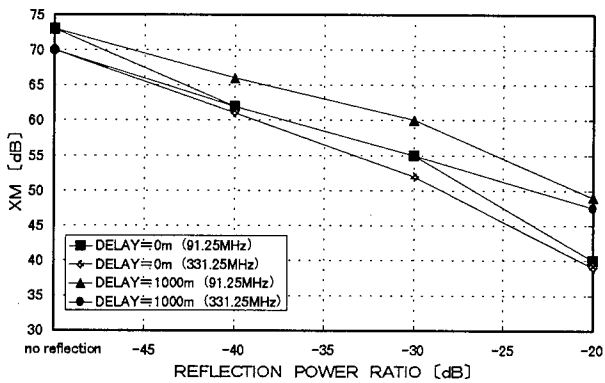


Fig.15 XM versus the reflection power ratio under the worst polarization condition

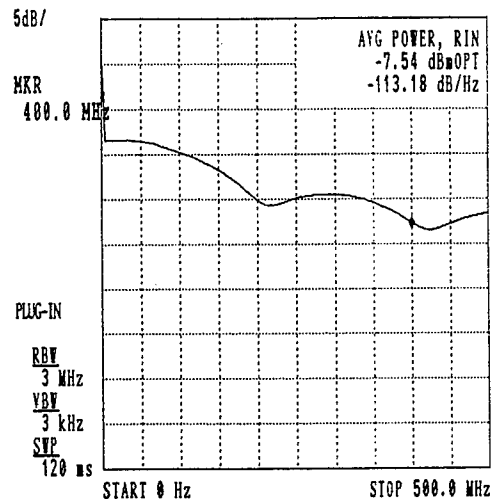


Fig.16 Intensity noise spectrum at the reflection power ratio of -20dB (delay $\approx 0\text{m}$)

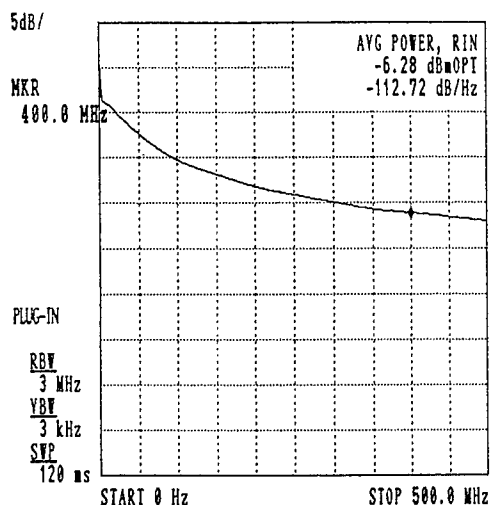


Fig.17 Intensity noise spectrum at the reflection power ratio of -20dB (delay \approx 1000m)

4-2. DISCUSSION

4-2-1. THEORETICAL ANALYSIS

RIN :

In optical transmission systems with multiple connection points, phase noise of a laser is converted into intensity noise by the optical interference between the direct optical signal and the reflected signals with delays. When there are two connection points with the reflectance of R_1 and R_2 , the resultant RIN can be expressed by; ^[5]

$$RIN(f) = p \frac{4}{\pi} \left[\frac{\Delta\nu}{f^2 + (\Delta\nu)^2} \right] \eta_{12} R_1 R_2 \cdot \left\{ 1 + \sin^2(\omega_0 \tau) \left\{ e^{-4\pi\Delta\nu\tau} - 2e^{-2\pi\Delta\nu\tau} \cos(2\pi f\tau) \right\} \right. \\ \left. \cdot \cos^2(\omega_0 \tau) \left\{ e^{-4\pi\Delta\nu\tau} + 2e^{-2\pi\Delta\nu\tau} \cdot (\Delta\nu / f) \sin(2\pi f\tau) \right\} \right\} \quad (5)$$

where η_{12} is the optical transmittance between the two connection points, f is the noise frequency, ω_0 is the angle optical frequency of the laser, p is the coupling coefficient between a polarization component of the direct signal and that of the reflected signal, and τ is the delay time between the reflected signal and the direct one.

We calculated RIN with experimental parameters using eqn. (5). The calculation results are shown in Fig.12 by solid lines with measured data.

As one can see from Fig.12, experimental results almost agree with the calculated ones.

If there are multiple connection points, the resultant RIN can be estimated by summing the RINs calculated by eqn.(5) for all possible combinations of two connection points.

In practical system RIN is varied by the following two factors;

- (1) Loss: In the experiment with delay \approx 1000m there are no optical connections in the 1000m fiber span. In the practical systems the intensity of the reflected signal is lower since the reflected signal is transmitted through multiple connection points with optical loss.
- (2) Polarization: In the experiment polarization states were adjusted so that the worst RIN could be obtained, corresponding to $p=1$ in eqn.(5). However, in the practical systems, p is smaller than 1 because the reflected signals have various polarization states.

DISTORTION :

In optical transmission systems with multiple connection points, distortions are induced by the optical interference between the direct optical signal and the reflected signals with delays. The amount of the distortion is large particularly when the delay length is shorter than coherent length of LD.

The following formulae have been reported for calculating CIR (Carrier-to-Interference Ratio) which comprises of CSO and CTB. ^{[6], [7]}

$$CIR = \frac{16R_1 R_2}{m^2} \cdot J(N, z) \cdot C(\Delta\nu, \tau) \quad (6)$$

where

$$J(N, z) = N_2 \left[J_2(z) J_1(z) J_0(z)^{N-2} \right]^2 \\ + N_3 \left[J_1(z)^3 J_0(z)^{N-3} \right]^2 \quad (7)$$

$$C(\Delta\nu, \tau) = \exp(-2\pi\Delta\nu\tau) \quad (8)$$

$$z = 2m_f \cdot \sin\left(\frac{\omega_i \tau}{2}\right) \quad (9)$$

In these expressions, N is the number of channels, $J_i(z)$ is i th order Bessel function, $J(N, z)$ is the spectrum related to distortion, $C(\Delta\nu, \tau)$ is a function of

representing correlation between the direct signal and the reflection one, N_2 and N_3 are the numbers of two-tone and three-tone intermodulation distortions respectively which are generated in the bandwidth of the signal, ω_i is the angle frequency of i th channel, and m_f is the FM-modulation index.

As in formulae (6) and (8), when the delay time τ is much longer than the reciprocal of the linewidth, $C(\Delta\nu, \tau)$ approaches 0 and CIR deterioration is little. When the delay time is short, CIR (CSO and CTB) deteriorates depending on the reflection intensity, frequency, FM-modulation index, and linewidth of LD. The experimental results, where the CIR for delay ≈ 0 m is worse than that for delay ≈ 1000 m, agree with above consideration.

The theoretical analysis on XM has little been reported. In our experiments, the amounts of deterioration for XM are large for delay ≈ 0 m and are small for delay ≈ 1000 m. This behavior is similar to that of CIR. Further theoretical study is necessary.

Multiple Rayleigh backscattering and the combination of Rayleigh backscattering and the reflection from the connection points could also affect the transmission characteristics. The effect of Rayleigh backscattering becomes important when long optical fibers with small reflection from connection points are used. However in most cases the reflection from the connection points are dominant. For example, it is reported that the main cause of RIN deterioration is the reflection from connectors in a 7 km long transmission system with 10 connection points where the reflection power ratio is -35dB/connector.

4-2-2. METHODS TO SUPPRESS THE INFLUENCE OF REFLECTION IN SCM SYSTEM

In most systems in service, the distance between the connection points range from few tens of meters to several hundreds of meters, which are longer than the coherent length of LD. From the experimental results for delay ≈ 1000 m, we conclude that reflection power ratio has to be suppressed below -50dB in order to satisfy the specifications shown in Table 1, particularly because of deterioration of RIN and XM.

However, although the use of isolators is effective to suppress the reflections into the LD, it is not effective to suppress the multiple reflections into the PD since the reflected signals propagate in the same direction as

the direct signal. For this reason it is necessary to decrease the reflection at the connection points in the optical transmission paths by using connectors with low reflection.

Even if we use superior connectors such as SPC (Super-PC) type connectors with a typical reflection of -40dB, the reflection power ratio could be as high as -25dB, which is a typical value for PC type connectors, when the connector facets are stained or the connections are loose. Therefore, care should be taken in using optical connectors. If we use APC (Angled-PC) type connectors with care, we can suppress the reflections even more.

5. CONCLUSION

We have investigated, both theoretically and experimentally, the transmission characteristics of a SCM system under the influence of optical reflection. The relationships between transmission characteristics and the amount of reflections are measured. In order to satisfy the specifications for AM-VSB and FM transmission, the reflected signal into LD should be suppressed below -40dB, and into PD should be suppressed below -50dB. The use of optical isolators is effective to suppress the reflection into the LD. The influence of reflection into the PD can be suppressed by the use of LDs with shorter coherent length than the distance between connectors.

6. REFERENCES

- [1] H.Nasu and H.Nakayama and H.Omura, "Design of the Novel Supervising Network using the Information Free Access System," 45th IWCS, PP669-678 (1996)
- [2] M.Yamada and M.SUHARA, "Analysis of Excess Noise Induced by Optical Feedback in Semiconductor lasers Based on Mode Competition Theory," Trans., IEICE, vol.E73, No.1, pp77-82 (1990)
- [3] K.Sato, "Intensity Noise of Semiconductor Laser Diodes in Fiber Optic Analog Video Transmission," IEEE, J.Quantum Electron., QE-19, 9, pp1380-1391 (1983)
- [4] I.Ikushima and M.Maeda, "Self-Coupled Phenomena of Semiconductor Lasers Caused by an Optical Fiber," IEEE, J.Quantum Electron.,

QE-14, 5, pp331-332 (1978)

- [5] J.L.Gimlett and N.K.Cheung, "Effects of Phase-to-Intensity Noise Conversion by Multiple Reflection on Gigabit-per-Second DFB-Laser Transmission Systems," J.Lightwave Technol., Vol.7, 6, pp888-895 (1989)
- [6] J.H.Angenent, "Distortion of Multicarrier Signal due to Optical Reflection," Proc. ECOC'91, WeC8-4 (1991)
- [7] W.Domon and M.Shibutani and K.Emura, "Reflection Induced Degradations in Optical Fiber Feeder for Microcellular Mobile Radio Systems," Trans., IEICE, vol.E76-C, 2, pp287-292 (1993)



Hideyuki Omura

Furukawa Electric Co.Ltd
5-1-9, Higashiyawata
Hiratsuka, Kanagawa, 254
JAPAN

Hideyuki Omura received the M.E. degrees in electronical engineering from Tokai University, Kanagawa, JAPAN, in 1987. He joined Furukawa Electric Co.Ltd in 1987 and he has been involved in the development of bi-directional CATV for 4 years. At present he is working in Video Transmission System and Equipment research section of Information & Electronics Laboratory.

Mr. Omura is a member of the Institute of Electrical Engineers of Japan.

AUTHORS

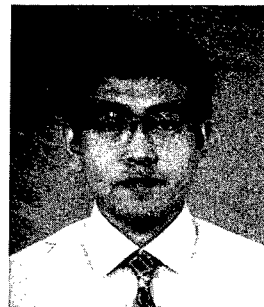


Tomoyuki Kato

Furukawa Electric Co.Ltd
5-1-9, Higashiyawata
Hiratsuka, Kanagawa, 254
JAPAN

Tomoyuki Kato received the B.E. degrees in electronical engineering from Nihon University, Tokyo, JAPAN, in 1993. He joined Furukawa Electric Co.Ltd in 1993. At present he is working in Video Transmission System and Equipment research section of Information & Electronics Laboratory.

Mr. Kato is a member of the Institute of Electronics, and Communication Engineers of Japan.



Shin-ichi Takashima

Furukawa Electric Co.Ltd
5-1-9, Higashiyawata
Hiratsuka, Kanagawa, 254
JAPAN

Shin-ichi Takashima received the M.E. degrees in crystalline materials from Nagoya University, Nagoya, JAPAN, in 1994.

He joined Furukawa Electric Co.Ltd in 1994. At present he is working in Optical CATV System and Access Network Designing section of Fitel System Division.

Mr. Takashima is a member of the Institute of Electronics, and Communication Engineers of Japan.

AUTOMATIC OPTICAL CABLES SHEATH MONITORING SYSTEM

Edoardo Cottino, Andrea Damiano, Igor Piffari

SIRTI S.p.A.
Cassina de' Pecchi (MI) - Italy

Andrzej Regini

RADIODETECTION LTD
Bristol - UK

ABSTRACT

This paper describes a new automatic Sheath Monitoring System (SMS) for the supervision of underground optical cables. The system can remotely and automatically provide an up to date report about the cables condition. The system consists of a Central Monitoring Station linked to some Base Stations through the telephone network; every Base Station can monitor up to 15 cable sheaths, each of them having a maximum length of 100 km. Each cable section is monitored by an element, the Outpost, (up to 50 Outposts per cable) placed near the splice enclosure, sending all the data to the own Base Station.

INTRODUCTION

This paper describes a new remote Sheath Monitoring System (SMS) which automatically supervises the condition of underground optical cables. The main problem the system has to face is the penetration of humidity inside the fiber cable, which is undesirable as it can lead to internal degradation and consequent loss of service.

At present, the control of cable insulation consists of making manual measurements of the cable-sheath resistance to ground. Such operation requires the intervention of a technician to verify the various sections of the cable-sheath along the whole installation path.

A manual measurement of dielectric insulation is required within every section but it gives imprecise results which cannot be recorded systematically. It is therefore impossible to survey the behavior of the measured resistance, except by empirical comparison between the former and the latter measures.

Because of the complexity of the procedure, such a method results in high costs in terms of time, human resources and equipments.

The automated control performed by the SMS offers many benefits with respect to traditional methods:

- * all the benefits deriving from the most recent and advanced techniques concerning cable fault location and identification;
- * a single Central Monitoring Station, connected by the telephone network to the theoretically unlimited number of Base Stations;
- * up to fifteen 100-km-length underground cables can be monitored by each Base Station for a total of 1500 km;
- * the time-consuming task of routinely visiting cable sections points is avoided;
- * early warning is provided: the system can be configured to generate an alert if the cable-sheath resistance to ground falls below a user-configured value;
- * network reliability improves. Damages to a cable outer insulation can be quickly identified and repaired before internal degradation and loss of service occurs;
- * both local and remote monitoring are possible. Base Stations can be controlled and monitored locally or by the Central Monitoring Station;
- * frequent monitoring is allowed. The cable-sheath resistance to ground can be tested once a day to give early warning in case of problems;
- * human errors are avoided (i.e. when measuring and recording the cable resistance at every point);
- * unusual trends in spatial and temporal behavior can be easily noticed. From the ancient data bases of each Base Station the Central Monitoring Station is able to show any variation in the cable-sheath resistance to ground;
- * all monitoring operations are performed by means of the metallic sheath: it supplies power to Outposts and allows data transmission and reception, while ground is used as the return path for DC power and signals.

DESCRIPTION OF THE SYSTEM

The SMS controls automatically the underground cable conditions through the measure of the metallic cable-sheath resistance to ground. It can be generally employed for all the cable types having a metallic sheath and an outer insulator.

The system requires: the *Central Monitoring Station*, the *Base Stations*, the *Outposts*, and the *Surge Arresters*. A diagram of the whole system is reported in figure 1.

The main functions the SMS can accomplish are three:

- * **sheath monitoring:** this function measures the cable-sheath resistance to ground, the humidity and the temperature inside the splice enclosures along the cable route, and generates alert signals in case the user-configured threshold values are exceeded;
- * **cable location:** this function determines the position of an underground cable up to several tens of kilometers away from the Central Office;
- * **fault location:** this function finds out the position of cable low insulation points within a section.

In the case of optical telecommunication networks, the typical configuration under test is a cable span between two Central Stations along a backbone line: it is divided in sections correspondent to the splice enclosures locations, that is a typical length of 2/3 kilometers per section. Branch joints are also present on the backbone line and branch sections can measure from some tens of meters up to a few kilometers.

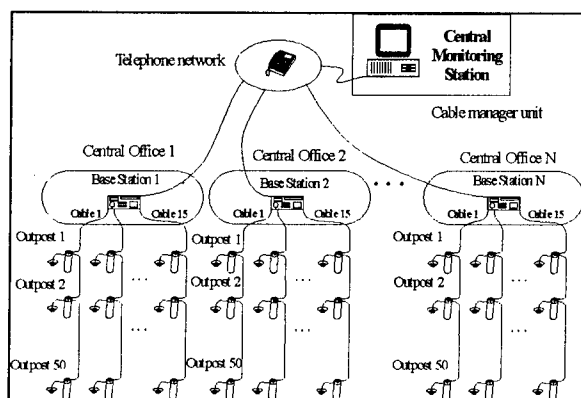


Figure 1 - Sheath Monitoring System

BASE STATION

The cables under test are terminated at the Base Station, which is programmed by the Central

Station through the telephone network. Every Base Station can monitor up to 15 cables, by means of 3 switching modules supporting 5 cables each. For every cable under test, the Base Station "sees" the Outposts and can dispose the measurements in the different sections of the cable. A maximum of 50 *Outposts* can be installed along a 100-km-long cable (sheath resistance p.u.l. = 30 Ω /km, capacity to ground p.u.l. = 1 μ F/km). The Outposts send the measurement results back to the Base Station which stores data for any future Central Monitoring Station elaborations the user may require.

The Base Station electrically supplies Outposts through the cable-sheath, which is also used by the Outposts to transmit to the Base Station the measures carried out on every cable section.

As far as cable-sheath monitoring is concerned the frequency at which the measures are performed is decided by the Central Monitoring Station by properly configuring the Base Station.

The Base Stations can perform the measurements even when the Central Monitoring Station is off.

The Base Station generates alert signals and files if the values of the measured parameters exceed the user-configured threshold values.

As far as the functions cable location and fault location are concerned, the Base Station contains a unit that enables advanced techniques for cable location and identification. For instance, even at tens of kilometers away from the Central Office, a field operator can ask the Base Station to send a signal on the line in order to locate the exact position of an underground cable or a fault.

The man-machine interface is really user friendly thanks to the vocal messages the Base Station can produce in answer to the operator's requests through a telephone/order wire telemetry interface.

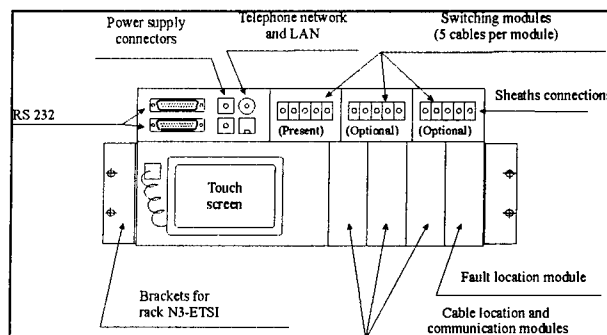


Figure 2 - Base Station

The Base Station structure is given in figure 2: the Central Monitoring Station can execute *sheath monitoring*, *cable* and *fault location* using a modem and the *Switching modules* which are

connected to the *Cable Manager Unit* (3 switching modules in case 15 cables are connected to the Base Station).

The Base Station consists of a module of compact dimensions, for installation in a N3-ETSI rack.

OUTPOSTS

The Outposts are small units to be installed at splice enclosures. The housing case is provided with three connections, one taken to the cable-sheath and the other two to ground (Signal and Power), as illustrated in figure 3.

The presence of two ground links allows self-testing and better accuracy in the measures of the cable-sheath resistance to ground. The power ground must be realized with a proper ground rod, while the Signal ground can be obtained by a simple connection to the metallic frame of the manhole lid.

Within the cable connecting the Outpost to the Splice enclosure, there are wire links to the cable-sheaths as well as to the sensors of humidity, temperature and presence of water inside the enclosure itself.

Every Outpost carries out the insulation measurements on the respective downstream cable section and sends them back to the Base Station via the upstream one. The cable section monitored by the Outpost can be either backbone or branch: every Outpost supplies up to 5 links to correspondent metallic sheaths, making it possible to monitor a maximum of four sections per enclosure (the backbone section downstream and up to three branch sections) as shown in figure 4.

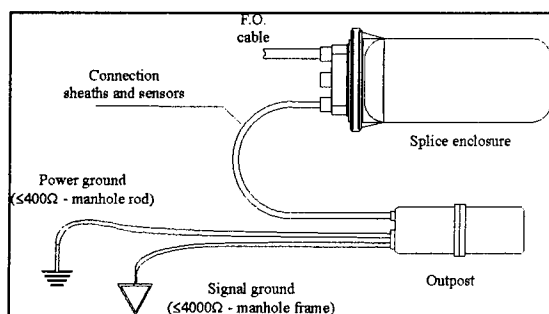


Figure 3 - Outpost connections

The total Outpost capacity in terms of cable length to be monitored relies on three factors: the electrical capacity to ground, the electrical sheath resistance, the network topology. As a reference a 100-km-long cable, having specific sheath resistance of $30\Omega/\text{km}$ and electrical capacity to ground of $1\mu\text{F}/\text{km}$, allows the installation of

maximum fifty Outposts, each with a connection to ground having a resistance inferior to 400Ω . Whenever the parameters above are increased all the others should be decreased.

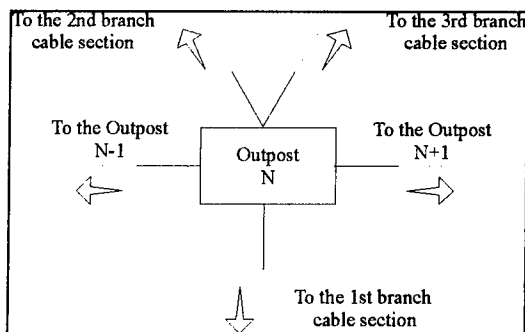


Figure 4 - Outpost links

The presence of a Signal ground connection enables the Outpost self-test, as prescribed by ISO 9000 quality standard, and assurance of upstream measurements in case of Power ground failure, which is therefore seen by the referring Base Station. The maintenance intervention can be limited to the mere substitution of the damaged Outpost, as identification and new settings are performed automatically by the Base Station in occasion of the successive measurement.

The Outpost electronics housing has two partitions: the left side contains a unique cable-sheath termination port, which allows the partition of the cable sections without opening the splice enclosure, while the measure and control electronics are placed in the right side. Two versions are available: one with three cable-sheath connections (able to monitor a downstream backbone section and a branch one), the other with five cable-sheath connections (able to monitor a downstream backbone section and three branch ones).

SURGE ARRESTERS

Surge arresters are placed at the end of each branch cable section with two main purposes:

- ensure cable-sheath to ground insulation to prevent the upstream Outpost from seeing an artificially build up ground connection at the end of the section;
- protect the conductive sheath, performing lightning arrest.

They are compact in size, they can easily be installed in the fiber termination rack of the central station.

CENTRAL MONITORING STATION

The Central Monitoring Station collects data and eventual warnings coming from the monitored cables. It is also called Remote Station, due to its position with respect to the points of measure. It is linked to the Base Stations through the telephone network and via the Base Stations monitors all the Outposts installed along the cable route.

It is possible to visualize the data relative to every monitored section concerning sheath insulation, humidity, temperature and presence of water inside the splice enclosure.

From the Central Station the user can configure cable number, Outposts number per cable, measurements frequency and alarm thresholds of each Base Station independently.

SMS USAGE IN FIELD

SMS usage is simple and easy for any of the three functions for which it is designed (sheath monitoring, cable location, fault location).

Sheath monitoring is performed by the software of the Central Monitoring Station, on the contrary cable and fault location are performed *in field* through the Base Station telephone/order wire telemetry interface.

Independently from the Central Monitoring Station, a field operator can easily find out the position of an underground cable coming from a station where a Base Station is installed.

Several services are supplied to the user by making a phone call to the Base Station and tapping on the telephone dial the proper codes which will be converted to the so-called DTMF tones.

The management software is able to generate vocal answers to the operator who asked for the service. In that way, by means of a portable instrument and even if there is nobody in the Central monitoring station, the operator is able to get a test signal from the Base Station to locate the cable in the range of several tens of kilometers away from the Central Monitoring Station.

SMS supplies a guided procedure for exact fault location: referring to figure 5, the steps are as follows:

- 1) automated location of the low insulation section, detected by the upstream Outpost (Outpost in G_n).
- 2) make sure that the low insulation point is not near the splice enclosures at the section ends (G_n and G_{n+3}). This test is performed by ground telemetry at splices. A ground value measurement at G_n and G_{n+3} can reveal if the low insulation is emphasized by a manhole

water flood. One can estimate that in 30% of the cases the fault location is at splices.

- 3) instrumentation usage for fault location near the intermediate splices enclosures (G_{n+1} and G_{n+2}). An operator can reach these splices and ask the Base Station, through a cellular phone (DMTF tones), the transmission of a signal for fault location. Using a portable instrument the operator can find the fault within a range of some tens of meters away from the enclosure.
- 4) if the 3rd step fails, the fault is situated along the run between the two enclosures. Linking two portable instruments to the Outposts placed at G_n and G_{n+3} (by means of two cellular phones), a joint measure of cable-sheath to ground insulation lets the operator know the fault distances from the two end Outposts. Cable-sheath partition operations in G_{n+1} and G_{n+2} are therefore avoided.

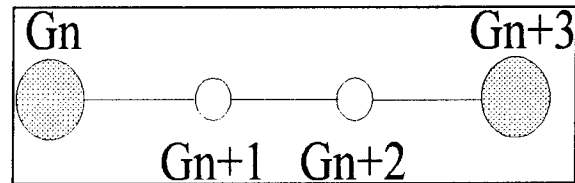


Figure 5

The activation of test signals to cable and fault location can also be done from the Central monitoring Station through a touch screen display.

MEASUREMENT RESULTS

Field trials on a test SMS installation over a 30km fiber link have been carried out in the Telecom Italia regional network from August 1996 to June 1997. A single Base Station and 13 Outposts were installed to perform the sheath monitoring. Measures of cable-sheath to ground resistivity and of temperature at splice enclosures were taken daily during the whole period. Figures 6 and 7 show the measurement results elaborated by the Central Monitoring Station.

Cable-sheath to ground resistivity

The user-configured threshold resistivity of 1000 $k\Omega.km$ is clearly visible in figure 6: below this value the Base Station sends an alert signal to the Central Monitoring Station.

Each trace refers to a single cable section of about 3km-length. Nine sections out of thirteen showed good insulation (constant overlapped traces), two sections experienced temporary

failures until a ready intervention restored good cable-sheath insulation (round markers), one section showed a ground fault due to both temporary enclosure flood and mechanical damage (square marker) and one section showed poor near-to-threshold performance (trace entirely below alert threshold).

CONCLUSIONS

We designed a new automatic Sheath Monitoring System (SMS) for underground optical cables supervision. Three main functions are provided: sheath monitoring, cable and fault location. Within sheath monitoring the user can get some information about humidity, temperature and water presence at splice enclosures as well as an efficient elaboration capability on the measured data. SMS is a user friendly system and its installation procedure is quite simple as well as the intervention in case of fault location.

Temperature at splices

Temperature trends (see figure 7) follows the general weather conditions with a fall of about 6/8°C in all splice enclosures, except for the two placed at the Central Office. These measures are taken at Outposts beside splice enclosures.

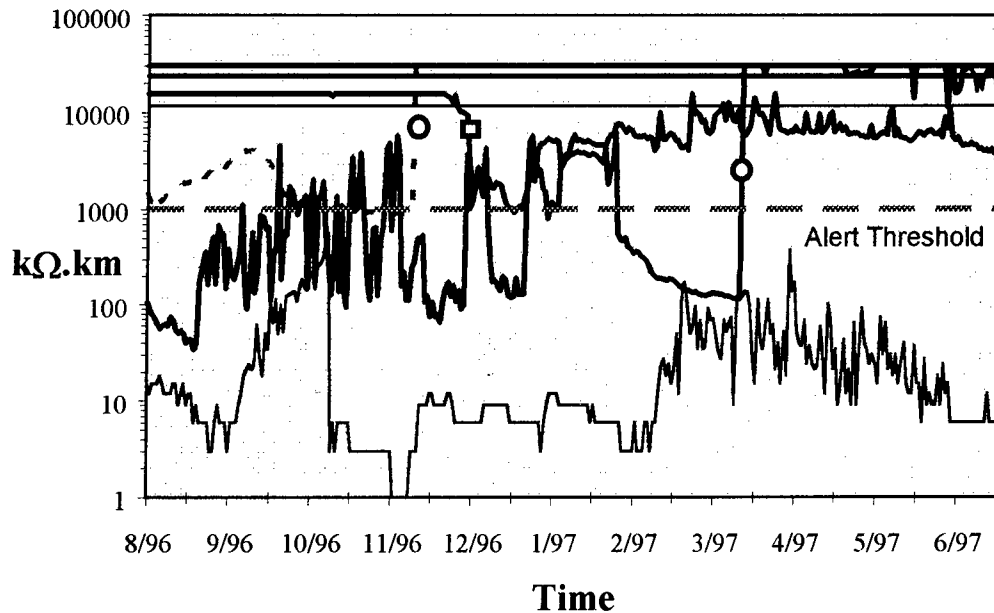


Figure 6 - Cable-sheath to ground resistivity

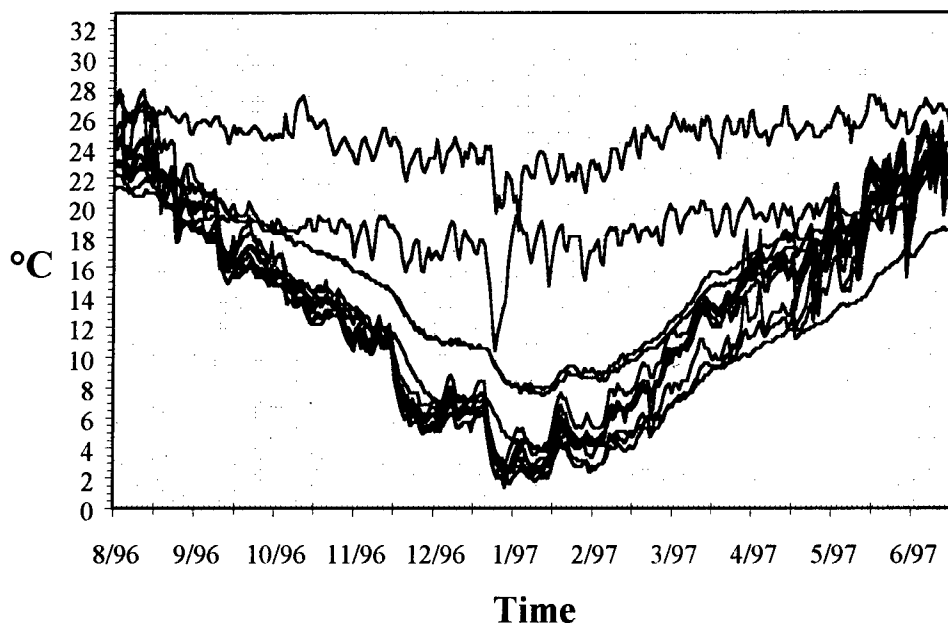
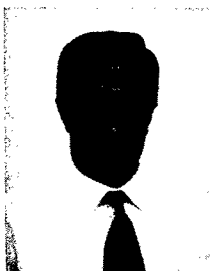


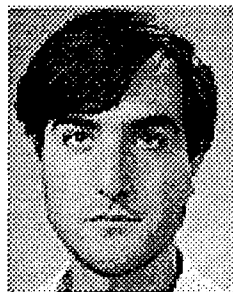
Figure 7 - Temperature at splice enclosures



Edoardo Cottino

Cables and Optical
Technologies - R&D
Dep. SIRT I S.p.A.
Via E. Fermi, 2 - 20060
Cassina de' Pecchi (MI)
ITALY

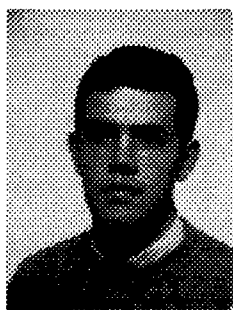
Edoardo Cottino was born in Turin, Italy, in 1957. He received his degree in electronic engineering from the Polytechnic of Turin in 1982. He joined AET Telecomunicazioni in 1983 in the fiber optic laboratories, and moved to SIRT I in 1995, where he currently holds the position of manager of the Cables and Optical Technologies R&D Division. Dr. Cottino is a member of SPIE and his present responsibilities include ITU-T activities.



Andrea Damiano

Cables and Optical
Technologies - R&D
Dep. SIRT I S.p.A.
Via E. Fermi, 2 - 20060
Cassina de' Pecchi (MI)
ITALY

Andrea Damiano was born in 1963. He started working as an R&D Engineer at Sirti since 1980. His main areas of interest are fiber optics, monitoring systems design and field installation problem solving.



Igor Piffari

Cables and Optical
Technologies - R&D
Dep. SIRT I S.p.A.
Via E. Fermi, 2 - 20060
Cassina de' Pecchi (MI)
ITALY

Igor Piffari was born in Bergamo, Italy, in 1969. He received his doctor degree in Opto and Micro Electronics Engineering from Polytechnic of Milan (1994), where he studied Kerr lens mode locking from Ti:sapphire lasers. He joined R&D Dept. of SIRT I in 1996 where he has been engaged in optical cables and fibers monitoring systems design.



Andrzej Regini

RADIODETECTION Ltd.
Bristol
BS14OAZ
Western drive
UK

Andrzej Regini was born in 1960 in Bristol, England. Studying Electrical and Electronic Engineering at Plymouth Polytechnic, he graduated in 1984 with a Higher National Diploma. Since that time, he has been with Radiodetection Ltd., the recognised world leaders in pipe and cable location technology. Based in the UK office, he has progressed through the engineering division, and is at present a Senior Design Engineer involved with all aspects of research, design and development. During his period with the company, he has played a central role in the development of cable location equipment and been responsible for some of the most significant inventions and advances in the field. These include patents on cable fault finding methods, rotating magnetic fields, metal detection and remote detection of corrosion faults on pipes. But undoubtedly the most important of these has been CD (current direction), a revolutionary method by which previously un-identifiable cables can be uniquely traced from the surface. Although based in the UK, he has gained significant experience abroad investigating the problems of cable location and fault detection on long line fibre networks. This has culminated in the recent design and development of the system for the automatic and remote monitoring of fibre sheath integrity.

Assessment of the Uniformity of Twists.

J.- H. Walling*, J.- F. Richard* and V. LeNir**

*NORDX/CDT, Montreal, Canada

** V.P.S. Enterprises, Montreal Canada

Abstract

We measure the overall diameter of twisted pairs in order to obtain indicators describing their geometric balance and configuration.

We use a laser scanning diameter gauge, a Holix 5007 from Target Systems, with a measurement rate of 1833 measurements per second.

Our results are preliminary and indicate that it is advantageous to use an instrument with a narrower window in the direction of the twisted pair to be measured, in order to gain more resolution in the area of the diameter minimum.

The method we use here requires substantial refinement, in order to allow the definition of a descriptive numerical expression for the degree of geometric balance of a twisted pair.

Our results highlight at the moment an immediate need for more precise scanning instruments.

Background

The performance requirements for data grade wires and cables are subject to a steady increase. This renders the quality assessment of these wires during the manufacturing process increasingly important. It is with this in mind, that Nordx/CDT tries to evaluate

the quality of twisted pairs. Towards this goal we try to use the geometric configuration and uniformity of the pairs as prime quality assessment tools. The uniformity of twisted pairs alone can be understood as being strictly a time series. This implies that the speeds as well as the cumulative tension in the twistings are well defined and controlled.

Time series are easy to deal with using Fourier transforms and yield basically information about the twist frequency distribution. Thus a Fourier transform yields information regarding the uniformity of twists.

Our aim here is more ambitious and covers basically the question if it is possible to assess the geometric balance of twisted pairs with respect to uniform tension while at the same time checking the diameter of the wires.

Towards this purpose we use conventional measuring equipment and evaluate it for its suitability. One of our objectives in this regard is to verify if there is a need to develop more accurate measuring instruments.

It is well known that the twist lays of modern data grade wires are short, in order to meet the stringent performance requirements with respect to crosstalk isolation.

Additionally, the electrical balance requirements become more stringent. The electrical balance is tightly correlated to the geometric balance of the pairs.

Here we understand under geometric balanced pairs those pairs which are produced using insulated conductors of perfectly equal individual diameter, and which have a straight center line.

In the past twisted pairs are considered using a model assuming a shape of the wires which is essentially helical. In this model, the two-dimensional projection of the pair yields a sinusoidal shape both of the center line as well as of the outer contour.

However, for short twist lays these assumptions are too simplifying and no more correct.

In the following we assume that the cross sections of the conductors during the twisting operation remain circular and perpendicular to the wire axis. This assumption is, from a metal deformation point of view justified, provided the bending radii are sufficiently larger than the radii of the conductors.

This is normally the case for data grade wires. For smaller bending to conductor radii ratios, the cross section of the wire deforms somewhat elliptical, which is, from a transmission point of view desirable, as it decreases the copper loss. However, metal deformation instabilities render such the twisting operation uncontrollable. Furthermore, the insulation is to all likelihood more deformed than the copper.

The bending deformation instabilities are accentuated and amplified by eccentric conductors inside the insulation.

In our model only the center line of each conductor of a pair follows a helix, whereas in the projection the outline of the twisted pair is formed by the envelope of circles moving along a sinusoidal axis. We call this a "sliding pearl on a helix" model.

Introduction

Diameter measuring equipment for the wire and cable industry is readily available. However, most gauges use rather large measuring windows in the direction of the wire axis. Hence, they are not suitable for our purpose. We strive for a scanner with a window comparable to a knives' edge, i.e. a window in form of a very sharp line perpendicular to the axis of the twisted pair. The width of the beam we aim for should be approximately 0.0001 to 0.00005 inch. We use for our initial trials a commercially available laser scanner from Target Systems, the Holix 5007 which has a window width of approximately 0.0015".

Methodology and Calculations

Our objective is to gather information about the profile of the twisted pair, to get an insight in the geometric balance of the pair. This allows to derive data about the twist lay, its longitudinal distribution, as well as the diameter of each conductor forming the pair.

Our ultimate goal is a better manufacturing process control. In this

sense, our initiative represents a challenge to all those companies building instrumentation for the wire and cable industry. Our expectation is that they come up with suitable equipment meeting these needs, accompanied by the corresponding algorithms for the treatment of the collected data.

We consider first an ideal twisted pair. We calculate the geometric shape of twisted pairs using the equations given in the appendix. As the system of equations yielding the precise projection of the twisted pair is very difficult to solve, we use a simplified approach.

We calculate, using the "sliding pearl on a helix model" the coordinates of the normal to the helix and the circle. We obtain thus for each center point of the circle two coordinate pairs for the envelope. That means: the x coordinate for the center point of the circle and the intersections of the normal with the circle are not the same. We use a 10th order Fourier rational, yielding the best approximation, for the curvefitting and the interpolation of the coordinates of the contour for a given x coordinate of the center of the circle on the sinusoid.

We note that a Fourier rational of 10th order limits of course to some extent the usefulness of the computed results if they are used to obtain a Fourier transform.

We calculate the coordinate values for a twisted pair which is perfectly balanced with respect to its geometry, and compare these to the profiles for pairs having conductors with different diameters. We assume, furthermore, that a tension deviation between both conductors forming a twisted pair, yields

a defined geometric unbalance. However, it has to be noted that we are not able to assign to these geometric unbalances of our model any tension differences, acting on the conductors as occurring in real twisting operations.

We calculate the results of our modeling in a spread sheet. Our model yields data which do not cover the same range with respect to the number of twists as the measurement data described in the following. Nor do we have any model to correlate numerically "geometric unbalance" to tension unbalance during the twisting operation.

We then use some twisted pairs with:

- same diameter of both wires.
- increased diameters of one wire.
- perfect tension control on each wire.
- intended tension differences in both wires to create a geometric unbalance.
- with both varying tensions and diameters.

The production of these pairs has been done under meticulous supervision, and this with respect to the manufacture of the singles as well as the pairs.

The pairs are then measured running through the scanner at a constant speed of 7.12 m/min. We use a precision capstan, to be able to check the uniformity of our twist lays. We record in each case the data over a defined time period. The same data were recorded for check of consistency five times in a row for each pair type.

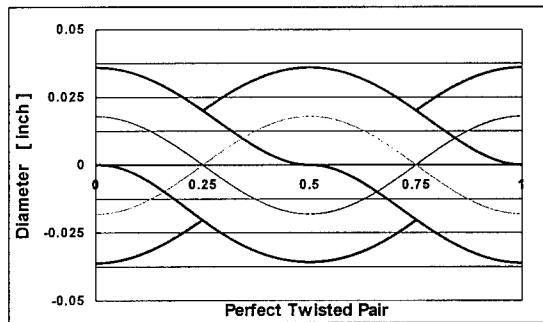


Fig. 1: Perfect twist of two wires with 0.038 inch diameter.

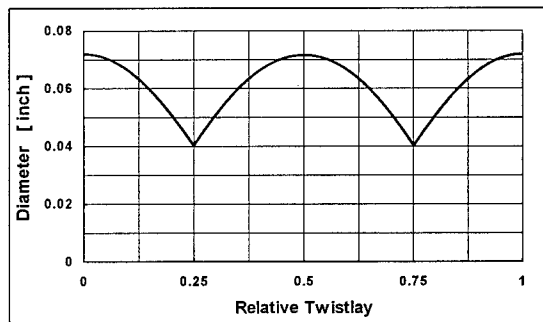


Fig. 2: Diameter as measured on a pair depicted in Fig. 1.

Results

We show some of the computed results, using our model. The Fig. 1 gives the profile of a perfectly twisted pair with a twist lay of 0.55 inch. The twist lay depicted here is normalized. This pair fulfills the two geometric conditions for a balanced pair, i.e. a straight center line resulting out of equal tension on both wires. Additional conditions are of course centered conductors within the insulation and equal bending and/or deformation properties.

In Fig. 2 the diameter of this pair is shown, as it appears when measured.

We see that the minimum is substantially higher than half the maximum, which is equivalent to the sum of both wire diameters. Though in the figures the twist lay is normalized, it

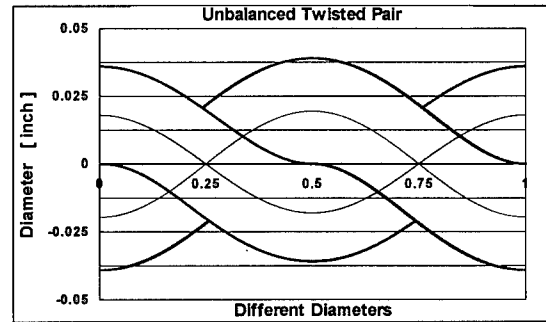


Fig. 3: Twisted pair with balanced tension and different wire diameters.

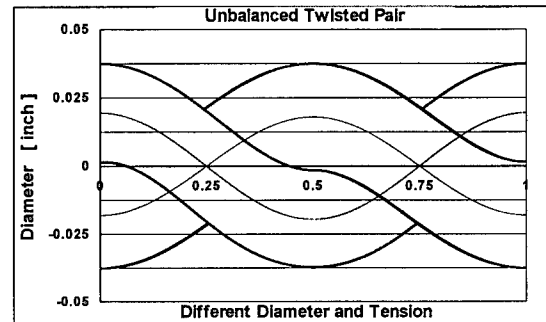


Fig. 4: Same as in Fig. 3, but more tension on the larger wire.

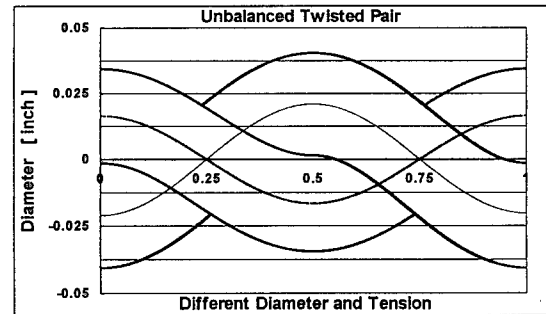


Fig. 5: Same as in Fig. 3, but more tension on the smaller wire.

has to be remembered, that the shape of the measured curve as well as the level of the minima changes with the absolute twist lay.

In the next three figures we have the shape of twisted pairs with different conductor diameters. Fig. 3 shows a perfectly balanced pair. Here we assume that the tension is equal on both wires and yields a straight center line.

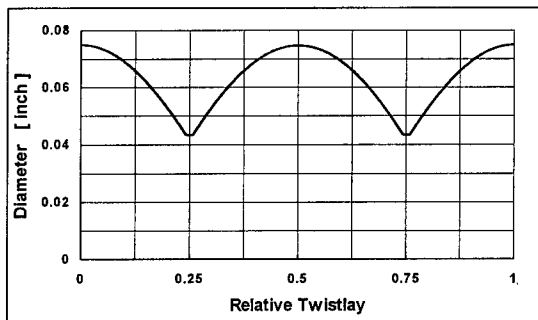


Fig. 6: Diameter of the pair in Fig. 3.

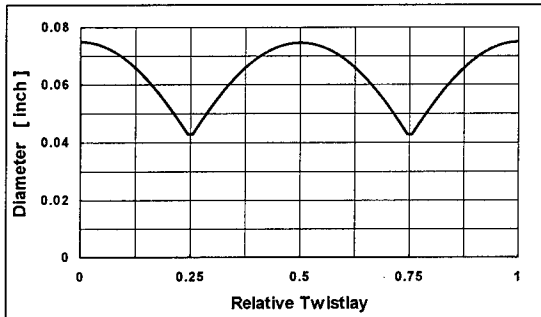


Fig. 7: Diameter of the pair in Fig. 4

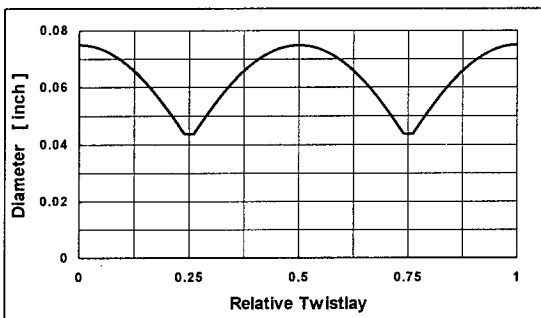


Fig. 8: Diameter of the pair in Fig. 5

In Fig. 4 and Fig. 5 we use the same wire in our model as depicted in Fig. 3, but apply different "tensions" to the wires. In fact, as already mentioned, we can assume here only a discrete displacement of the center line of the twisted pair, depending upon on which wire a higher tension is applied.

The following three pictures show the diameter as it appears to a suitable measuring instrument. To be noted here is the fact that diameter differences yield a plateau in the measured diameter.

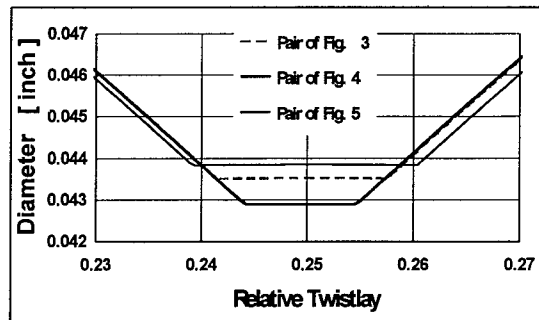


Fig. 9: Diameter of the pairs of Fig. 3 to Fig. 5 at their the minima.

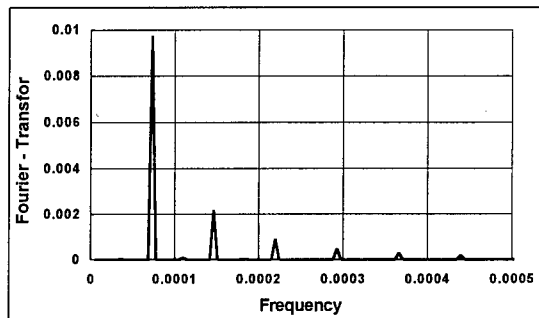


Fig. 10: Fourier transform of the computed data as depicted in Fig. 6.

This is more evidenced in the Fig. 9. Here the different curves indicate:

- a relatively large plateau, approximating 3.5 to 4% of the twist lay length for a wire with different diameters.
- the height of this plateau is increasing if the smaller wire is subjected to more tension, i.e. approaches a more straight line.
- The level of the plateau decreases if the larger wire is subject to higher tensions.

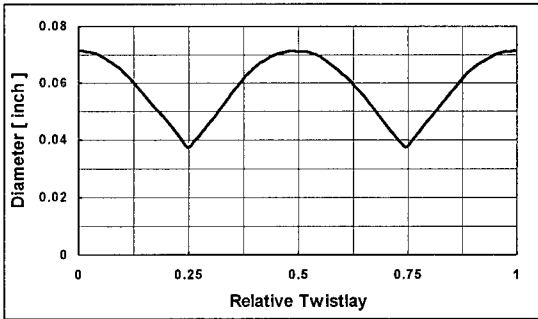


Fig. 11: Diameter of an ideal pair with same diameters and equal tension on each wire during twisting.

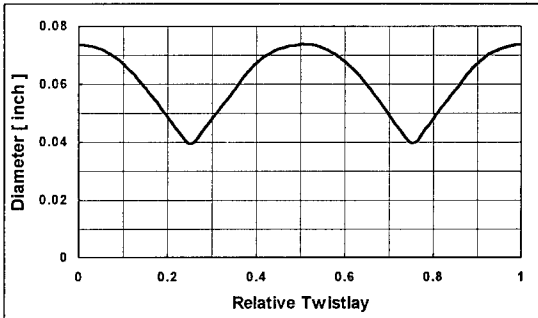


Fig. 12: Diameter of a pair with different diameters and different tensions on each wire.

Fig. 10 indicates a Fourier transform of the data according to Fig. 6. Interesting here is the fact that at the beginning some very small peaks in between the others are visible, indicating the effect of the different symmetries of the sin- and cos-function, which highlights the already mentioned fact that a Fourier rational is not the best curvefit function, if a Fourier analysis is aimed for.

In the following pictures, i.e. Fig. 11 and Fig. 12 are shown real measurements.

The Fig. 11 shows an ideal pair with equal conductor diameters, twisted with the same tensions. Fig 12 shows a pair with different conductor diameters. We apply a higher tension to the larger of both conductors during the twisting operation.

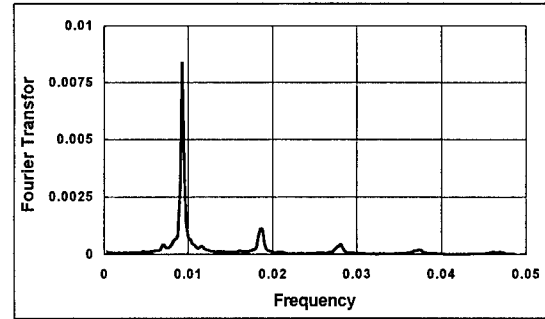


Fig. 13: Fourier transform of an ideal pair as depicted in Fig. 11.

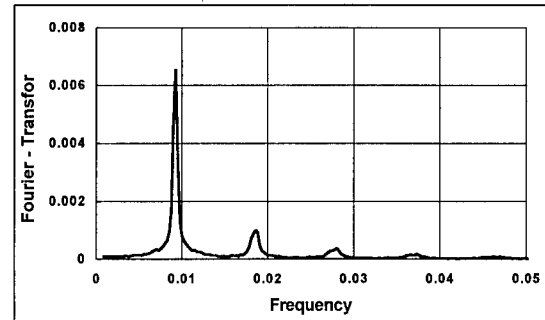


Fig. 14: Fourier transform of a pair having conductors with different diameters, where a higher tension is applied to the larger conductor.

In the Fig. 13 we have the Fourier transforms for an ideal pair with uniform conductor diameters. Here we use different frequency scaling than in our model.

In Fig. 14 the larger wire is subject to a higher tensions during twisting.

Discussion of Results and Solutions pursued

Continuous measurements of the diameters of twisted pairs can yield information about the degree of uniformity of the pairs. However, as most of the indications are concentrated in a range not exceeding approximately 2 to 4% of the length of the twist lay, continuous and highly precise measurements are mandatory.

However, the resolution of the data obtained with the used gauge are not yet of the desired precision, mainly with respect to the sharpness of the edges between the flanks and the plateaus. This can be seen from both the Fig. 2 and Fig. 11 and Fig. 6 and Fig. 12, respectively. This lack of resolution has of course an influence upon the shape of the peaks representing the harmonics in a Fourier transform.

The ratio of maximum diameter to the minimum diameter of a twisted pair, though decreasing with decreasing lay length, is also an indication about the balance of a twisted pair.

We find that the flanks of the measured humps of the twisted pairs are different. This is difficult to show graphically, as these differences are small. Though the differences are subjectively clearly perceptible, they are difficult to substantiate numerically.

A Fourier analysis of the measurement data yields indications on uniform twist lay of the wires as well as uniform capstan speed, as can be seen from the Fig. 13 and Fig. 14. The Fourier transform yields also the linear offset of the time series ("DC-offset"), and we can use this value in conjunction with the minima and maxima of the diameters of the pairs measured. This gives us some indication about the shape of the flanks.

In a Fourier transform we lose the time information to get a precise frequency response. Time and frequency are interchangeable with twist length and twist frequency. Therefore, we are losing all local information in the time

or twist length domain. Hence we are losing all information concerning the shape of the humps as well the length of the plateaus in relation to the humps.

We give some data in Table I and Table II, which refer to the calculated and measured data, respectively.

Concerning the interpretation of these data it has to be kept in mind that a direct correlation between calculated data and measured data is not possible, as we do not have any information about the degree of a geometric distortion induced by different tensions on each conductor.

Generally we find that the minimum diameter of the twisted pairs of our model yield slightly higher values than we are able to find in reality. This has to do with a certain crush of the insulating material during the twist formation. We find this also confirmed in the "DC - offset" of the twisted pair. The values for the real twisted pairs are also lower than those calculated from our model. The magnitude of this difference is approximately one half of the previously mentioned difference, confirming thus a crush of the insulation in the forming process of the twist. It has to be noted, that this crush is not occurring along the centerline between both conductors. The magnitude of this crush may surprise, but it has to be remembered that the minimum and the maximum diameter here refers to the absolute extremes of approximately 165,000 measurements. In so far this value represents only a "minimum spot crush". A certain unroundness or "crush" of the wires has been verified consecutively before and after twisting.

Sample	1. Wire Diameter inch	2. Wire Diameter inch	Tension on Small-Large Conductor	Diameter		DC-Offset inch
				Min. Dia. inch	Max. Dia inch	
1	0.03600	0.03600	Equal	0.04044	0.07200	0.06091
2	0.03600	0.03600	Low - High	0.03999	0.07200	0.06086
3	0.03600	0.03700	Equal	0.04130	0.07300	0.06171
4	0.03600	0.03700	Low - High	0.04108	0.07300	0.06171
5	0.03600	0.03700	High - Low	0.04141	0.07300	0.06166
6	0.03600	0.03800	Equal	0.04241	0.07400	0.06252
7	0.03600	0.03800	Low - High	0.04199	0.07400	0.06251
8	0.03600	0.03800	High - Low	0.04263	0.07400	0.06244
9	0.03600	0.03900	Equal	0.04352	0.07500	0.06334
10	0.03600	0.03900	Low - High	0.04290	0.07500	0.06332
11	0.03600	0.03900	High - Low	0.04384	0.07500	0.06325
Sample	1. Wire Diameter inch	2. Wire Diameter inch	Tension on Small-Large Conductor	Ratio		
				Max./Min inch	Max./DC inch	Min./DC inch
1	0.03600	0.03600	Equal	1.78037	1.18216	0.66399
2	0.03600	0.03600	Low - High	1.80026	1.18300	0.65713
3	0.03600	0.03700	Equal	1.76759	1.18302	0.66929
4	0.03600	0.03700	Low - High	1.77682	1.18304	0.66582
5	0.03600	0.03700	High - Low	1.76295	1.18385	0.67152
6	0.03600	0.03800	Equal	1.74481	1.18369	0.67841
7	0.03600	0.03800	Low - High	1.76239	1.18382	0.67171
8	0.03600	0.03800	High - Low	1.73604	1.18506	0.68262
9	0.03600	0.03900	Equal	1.72326	1.18416	0.68716
10	0.03600	0.03900	Low - High	1.74845	1.18451	0.67747
11	0.03600	0.03900	High - Low	1.71086	1.18579	0.69310

Table I : Minimum and maximum diameters for the different twisted pairs modeled. Also given are the different ratios and the "DC"-offset of the Fourier transform.

Summary and Conclusion

We try to characterize the uniformity of twisted pairs with respect to their geometric balance. Unfortunately we are not yet able to give a numeric indicator for the geometric balance of a twisted pair itself.

We used readily available equipment to measure the diameter of twisted pairs in

an equidistant manner at relatively high scanning rates. However, we find that the resolution of the gauge we use is not high enough, to resolve the required details close to the minima of the diameter of twisted pairs. An alternative are high speed and high resolution line-scan cameras. However these are to date relatively very expensive.

Sample	1. Wire Diameter inch	2. Wire Diameter inch	Tension on Small-Large Conductor	Diameter		DC-Offset inch
				Min. Dia. Inch	Max. Dia inch	
1	0.03590	0.03590	Equal	0.03680	0.07229	0.05888
2	0.03590	0.03590	Low - High	0.03678	0.07170	0.05884
3	0.03590	0.03690	Equal	0.03745	0.07301	0.05964
4	0.03590	0.03690	Low - High	0.03741	0.07271	0.05949
5	0.03590	0.03690	High - Low	0.03742	0.07306	0.05953
6	0.03590	0.03738	Equal	0.03811	0.07427	0.06055
7	0.03590	0.03738	Low - High	0.03819	0.07429	0.06041
8	0.03590	0.03738	High - Low	0.03829	0.07395	0.06043
9	0.03590	0.00385	Equal	0.03887	0.07608	0.06112
10	0.03590	0.00385	Low - High	0.03921	0.07438	0.06100
11	0.03590	0.00385	High - Low	0.03936	0.07451	0.06100
Sample	1. Wire Diameter inch	2. Wire Diameter inch	Tension on Small-Large Conductor	Ratio		
				Max./Min Inch	Max./DC inch	Min./DC inch
1	0.03590	0.03590	Equal	1.96443	1.22788	0.62506
2	0.03590	0.03590	Low - High	1.94941	1.21870	0.62516
3	0.03590	0.03690	Equal	1.94989	1.22423	0.62785
4	0.03590	0.03690	Low - High	1.94353	1.22218	0.62884
5	0.03590	0.03690	High - Low	1.95249	1.22715	0.62851
6	0.03590	0.03738	Equal	1.94904	1.22666	0.62937
7	0.03590	0.03738	Low - High	1.94510	1.22989	0.63230
8	0.03590	0.03738	High - Low	1.93140	1.22376	0.63362
9	0.03590	0.00385	Equal	1.95706	1.24480	0.63605
10	0.03590	0.00385	Low - High	1.89699	1.21938	0.64280
11	0.03590	0.00385	High - Low	1.89280	1.22140	0.64529

Table II : Minimum and maximum diameters for the different twisted pairs measured. Also given are the different ratios and the "DC"-offset of the Fourier transform.

We note that for a suitable assessment of the twists we need absolutely a correlation between model and reality as far as it concerns the tensions on each wire and the thereout resulting geometric off-set of the center line. This is a subject which will have to be addressed in more detail. The geometric offset of the center line and

its impact on electrical unbalances can be evaluated and this for resistance as well as for capacitive unbalances.

We mentioned already that the Fourier transform yields for a time function only the frequency components, while loosing any time or local information. However, in our case this information is vital.

We pursue, therefore, the utilization of wavelet transforms or pseudo spectral methods. We are confident that this will yield more detailed information about the shape distortions of the diameter profile of twisted pairs, and this not only with respect to the plateaus, but also with respect to the differently shaped flanks.

An additional interesting observation is the numerical confirmation of a crush of the insulation material but not along the center line of both conductors.

Acknowledgment

The authors like to express their gratitude to Mr. Alexandre Rousseau from the Ecole Polytechnique in Montreal for his support in carrying out the measurements.

Authors



Jörg-Hein (Jo) Walling received his diploma in Mechanical Engineering in 1966 at the Technical University of Berlin. In 1974 he obtained a Doctor's degree (Dr.-Ing.) at the same University. In 1974 he joined Northern Electric in the Research and Development Department. Since 1976 he is senior engineer at the Northern Telecom, now Nordx/CDT Lachine Cable Plant, responsible for the design of Outside Plant and Data Grade Wires and Cables.



Jean-François Richard received his bachelor's degree in electrical engineering from the Ecole Polytechnique in Montreal in 1991.

From 1991 to 1995 he worked both at the "Ecole Technologique Supérieure" and at the Ecole Polytechnique as a research and teaching assistant. In 1995 he joined Nordx/CDT in the Engineering Department, and works since on a continuous quality improvement program.



Victor LeNir received a B.Sc in Physics from Manchester University, England in 1960 and a M.Sc. in Computer Science from London University in 1968. He was employed at the Northern Telecom Cable Division in Lachine, Quebec in the Research & Development Group from 1963 to 1991. Since then he is with V.P.S. Enterprises working on the development of specialized, dedicated software packages, especially with regard to data grade wires and cables.

APPENDIX

For the centerline of the twisted pair we have:

$$y_o = a \cdot \cos(b \cdot x_o)$$

and:

$$b = \frac{2 \cdot \pi}{T}$$

Here is:

- a - the amplitude of the centerline of the twist
- b - the pitch of the twist
- T - the twist lay length

If our conductor diameter is r , then we have for the circles on the sinusoid:

$$F(X, Y, x_o) = r^2 - (X - x_o)^2 - (Y - a \cdot \cos(b \cdot x_o))^2 = 0$$

In order to obtain the envelope of the circles, we have to get the partial derivation of above equation with respect to x_o , i.e. :

$$\frac{\partial F}{\partial x_o} = 0 = -(X - x_o) + a \cdot b \cdot \sin(b \cdot x_o) \cdot (Y - a \cdot \cos(b \cdot x_o))$$

To solve the system of the last two equations, we have to eliminate x_o from both equations, in order to get a function between X and Y . That route to a solution is very awkward, and we do not pursue it here further.

Here we calculate only from the first equation the coordinates X and Y still with x_o as an implicit parameter and determine

the intersections with the normal to the sinusoid. These values are points of the envelope.

We get for the coordinates of the intersection of the normal to the sinusoid and the circle X and Y , respectively:

$$X = x_o \pm \frac{r \cdot a \cdot b \cdot \sin(b \cdot x_o)}{\sqrt{a^2 \cdot b^2 \cdot \sin^2(b \cdot x_o) + 1}}$$

$$Y = y_o \pm \frac{r}{\sqrt{a^2 \cdot b^2 \cdot \sin^2(b \cdot x_o) + 1}}$$

We then use a curve fit for the coordinates X and Y , and calculate therefrom the coordinates y_{upper} and y_{lower} of the upper and lower envelope respectively. To do this we use a Fourier rational of 10th order, i.e.:

$$F_{rational} = \frac{\left(a_o + \sum_{n=1}^{n=5} (a_n \cdot \cos(x_o) + b_n \cdot \sin(x_o)) \right)}{\left(1 + \sum_{m=1}^{m=5} (a_m \cdot \cos(x_o) + b_m \cdot \sin(x_o)) \right)}$$

We get then respectively:

$$y_{upper} = F_{rational}(x_o)$$

$$y_{lower} = F_{rational}(x_o)$$

Overlaying of such envelopes yields, if the phase shift is 180 degrees, the projection of a twisted pair. The difference of the absolute maxima and minima yields the diameter of the twisted pair.

TERMINATION OF A SCREEN IN PRACTISE: EARTHING VERSUS GROUNDING.

M. Pelt, P. De Win

Alcatel Cabling Systems Competence Center
Brussels, Belgium

ABSTRACT

Termination of a screen influences its performance. The choice depends on multiple parameters like the type of screen, the frequency range of interest and the environment in which the cable is installed. In this paper we will focus on the termination of an overall screen inside a building. This will be done on what is published in text books and illustrated with some simple qualitative experiments. Misconceptions inside cabling standards will be pointed out.

INTRODUCTION

An earthing network inside a building is used for many purposes like diverting fault currents, diverting lightning currents, providing a reference voltage to apparatus, increasing the EMC performance, etc.. The multiple inherent phenomena give arise to seemingly conflicting requirements. Moreover since the sixties the data transfer speeds has increased drastically. As a consequence the optimum screening requires different connection regimes today. This creates a large amount of misconceptions about termination of screens.

When all possible safety rules are respected the screen can be terminated at both extremities resulting in the optimal EMC performance. Nevertheless this situation is not always favourable. As manufacturer of generic cabling systems it is not admitted to rely on other building utilities to assure the performance of its product. Independent of the quality of the earthing structure, the low voltage power supply, the presence of lightning protection, etc. the optimal performance must be pursued. This requires a great amount of knowledge and understanding which can not be expected from a cabling installer. Hence the concept behind a screened cabling system must take into

account all possible circumstances in which the cabling is installed.

In the following the parameters which have an impact on the termination of an overall screen are analysed. The discussion is focused on screened category 5 cabling as specified in the cabling standards¹⁻³. This means that a link consists of maximum 90 meters of cable, the interfaces of the active equipment are screened or unscreened RJ45 connectors, the overall screen is not used for the signal transfer, the frequencies of interest go up to 100 MHz, etc.

REVIEW ON CATEGORY 5 DATA TRANSFER

By analysing the current loops the consequences of terminating the screen can be predicted. Data signals are transferred in the differential mode loop formed by the twisted conductors of a cable. Hence electromagnetic fields which interact with this loop - directly or through the transfer impedance and the balance - interfere with the data transfer causing bit-error-rates.

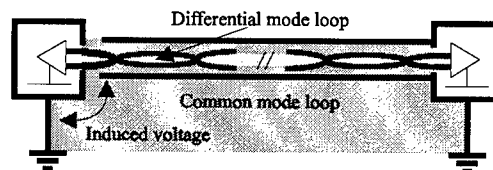


Figure 1: Current loops in case of single sided termination

The common mode loop is dependent on how the screen is terminated. If the screen is terminated at a single side, the common mode loop is formed by the signal carrying conductors and the earthing network. In this case the surface of the loop can become very large. As a consequence magnetic fields can induce voltage peaks at points where the loop is left open. This

may lead to damage of the equipment's electronic circuitry in the long term.

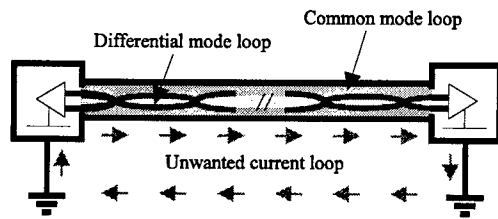


Figure 2: Current loops in case of double sided termination

In the case that the screen is terminated at both ends the common mode loop is formed by the signal carrying conductors and the screen. Hence the loop surface is nearly reduced to zero.

The magnitude of the currents along the screen also depend on the termination. When the screen is terminated at a single side the currents are small. However when terminating the screen at both ends an alternative path is created for low frequency currents on the protective earth. This applies when the screen is connected to safety class I¹² equipment which implies that the metallic housing of the equipment is earthed. Under extreme conditions these currents can have large magnitudes which can damage the screen. In this case the low frequency currents should be blocked using a capacitor^{4, 10} in the screen such that high frequency surges can go through. Doing so makes the termination of the screen independent of the presence of high power currents on the earthing network.

REVIEW ON IMPEDANCE OF A WIRE

It is well known that the impedance of an electrical wire is characterised by its resistance and its inductance⁴⁻⁸. For low frequencies, such as 50 Hz mains supplies, inductance is usually negligible and only resistance needs to be considered. As a consequence the cross-sectional area of the conductor determines the current path. For high frequencies, such as those related to data transfer over a link, inductance dominates. As a consequence the impedance increases linearly with frequency and is proportional to the length of the conductor.

This has numerous consequences on the screen termination. At first a protective earth is made up of a network of wires with sufficient cross-section to carry away high power low frequency currents. Due to the

rise of impedance with frequency high frequency currents are unable to propagate along the protective earth. Hence a protective earth can only divert low frequency currents from the screen. Secondly by earthing the screen at both ends an unwanted current loop can be created. However an overall screen of a cable can be considered as a single hollow conductor which blocks high frequency currents. Hence only low frequency currents are able to propagate inside an earth loop.

Finally it also determines how a screen should be terminated. When using a wire (pigtail) it will only divert low frequency currents. Hence a low inductive connection must be realised when terminating the screen.

REVIEW ON EMC PERFORMANCE

In most text books the issue about terminating a screen has been dealt with extensively⁴⁻⁸. A screen earthed only at one end provides good screening from electric fields but none for magnetic fields. In contrary a screen earthed at both ends provides good screening from both electric and magnetic fields above the cut-off frequency. A screen should be earthed at least every tenth of the wavelength in order to be effective. However this electric and magnetic coupling applies only to the near field. It will not affect the category 5 data transfer as will be illustrated experimentally further in this paper.

About the far field most text books address the issue of screening effectiveness in general⁴⁻⁸. They deal with the skin-effect which forces currents to remain on the surface of the conductor. Hence current propagation along the screen is not a problem due to the separation between the inner and outer currents. However only very few text books mention what the impact is of terminating the screen under these circumstances⁷⁻⁸.

Once the cable length approaches a quarter wavelength the screen currents create a standing wave pattern whether or not there is an external connection. Resonances occur for each frequency when the length of the cable corresponds to a quarter of a wavelength. The height of the resonances depend on the load at each end of the transmission line formed by the cable and the screen. Thus single or multiple earthing is not an issue at these frequencies. The induced currents on the screen generate noise on the signal

carrying conductors due to the non-zero transfer impedance of the screen. There are two ways to minimise the effect of these resonances: either by reducing the transfer impedance at high frequencies or eliminate the reflections on the screen conductors by matching them in their characteristic impedance.

In case of category 5 cabling the frequencies of interest are between 1 MHz and 100 MHz. Hence the performance do not rely on earthing the screen but on the effect of separation of the inner and outer currents on the screen. Earthing the screen is not an issue for the EMC performance but making an external connection with the terminal equipment. However in practice the screen load is unknown. In the worst case the terminal equipment has an unscreened RJ45 jack generating large reflections whereas in the best conditions the terminal equipment has a screened RJ45 jack minimising the reflections. This is also demonstrated in the experimental part of the paper.

IMPACT OF BUILDING UTILITIES

When terminating the screen at one side no currents can propagate along the screen. Hence screen's performance is not affected by the building utilities but a safety problem may occur. When terminating the screen at both ends an earth loop is created in which currents may propagate. These currents do not affect the data transfer due to their low frequency. However due to their magnitude they may damage a screen which is not designed to carry them.

These issues are covered within multiple standards which deal directly or indirectly with the topic of termination of screens. There are cabling design standards¹⁻³, safety standards¹¹⁻¹⁴, and soon installation standards⁹⁻¹⁰. The variety of standards makes it unclear for a reader. Moreover some basic misconceptions exist in these documents.

Impact of earthing network

A single protective earth should be present inside each building to interconnect all metallic parts which may assume a hazardous voltages. This should be accomplished by a network of conductors with sufficient cross-sections in order to divert the low frequency currents¹³.

In each building conductive parts like pipes supplying services (gas, water) or structural metallic parts shall be connected

to the protective earth¹³. In reality the screens of a category 5 cabling systems are interconnected to each other at the floor distributor or at the campus distributor. As consequence the screens themselves create a conductive network which may transfer hazardous voltages or currents like the gas or water pipes. For this reason we believe that a screen of a cable should be earthed.

In the case of generic cabling¹⁻³ the safety class¹² of the equipment attached to the cabling can not be foreseen. If only safety class I¹² equipment is attached to the link an earth loop is created. In contrary if only safety class II¹² equipment is attached to the cabling the screen is left unearthed. For this reason the screen must be earthed through the connecting hardware - like the outlet or the patch panel - independent of the peripheral equipment.

As long as the cabling extends over a single protective earth the point where the cabling is earthed has no importance. Mostly this is the case inside a building but certainly not when the cabling interconnects an entire campus. When the screen is terminated at a single side the potential difference that exists between the earthing networks will be found back at the not terminated side. This is an intolerable safety hazard which must be avoided by making equipotential connections¹⁴ between the earthing networks or choosing for optical fibres.

Up to now no regulations exist which define earthing requirements for the overall screen of a cable. It is considered that the voltages during data transfer so low that they will never cause any safety hazards. The only possible danger comes from the active equipment attached to the cabling which must fulfil safety regulations¹². However if a cabling is generic its safety performance may certainly not rely on other building utilities to our opinion.

According to the cabling standards¹⁻² it is not possible to use screened cabling when the potential difference exceeds 1 V r.m.s.. This is an old requirement for low frequency data transfer using coaxial cables that does not apply for category 5 cables. At first the frequencies during data transfer lie much higher than the power frequencies. Hence the interference will be negligible. Moreover as the dc-resistance of the screen is about 30 mΩ/m depending on the type of screen the magnitude of the currents will remain low. Inside an equipotential zone there may not be any

hazardous voltage difference which create large currents inside the earthing network. Introducing a capacitor in the screen will block these currents if the quality of the earthing network is poor.

Impact of grounding network

The purpose of a grounding network is not to carry away fault currents but to create an equipotential surface. Grounding is unlike earthing something for higher frequencies. As currents with higher frequencies do not propagate along wires a network of conductor must be created. Inside a building the grounding network is created by interconnecting all metallic parts of the building in a high frequency way⁹⁻¹⁰. The impact on the performance of an overall screen depends on the quality of the connection between the screen and the grounding network. In practice when cabling is installed inside an office building this can only be accomplished by a wire which affects the lower frequencies. It is impossible to bring the grounding network to each outlet of the cabling to make a low inductive connection. Nevertheless the grounding network will have its impact as it diverts these currents from the screen like a parallel earth conductor⁹⁻¹⁰.

Impact of the low voltage power supply

Inside a building with a PEN conductor the function of the protective earth is combined with that of the neutral. Multiple safety standards¹¹ point out the risk for neutral current that would pass along the screen creating EMC problems. For this reason the earth loop should only be terminated at a single end. This applies certainly when the screen is used for low frequency data transfer. However in the case of category 5 cabling the data signals will not be disturbed by the power frequencies. Moreover the magnitude of the current in the screen is very limited due to the low voltage drop between the ends of the cable. So under normal working conditions no interruption of the screen is required. However in case of a fault the magnitude of the current may become very large when the TN-C system is not designed correctly.

Impact of lightning

In case of lightning a strong magnetic field will couple with the common mode loop. In case of double side termination the common mode loop is small and as a consequence no large voltage is induced.

Introducing a capacitor in the screen will not block the lightning induced voltages or transients.

EXPERIMENTS

During our tests a "line injection" method is used to evaluate the overall EMC performance on an electrically long sample. Hereto an unscreened and a screened cable are bundled together over their entire length. The bundle is rolled out isolated from the earth and ground. By injecting a signal into the unscreened cable currents are induced on the outside of the screen. Depending on the transfer impedance of the screen noise is generated on the signal pairs. This coupling is measured using a network analyser together with an linear wideband amplifier to increase the dynamic range. The network analyser scans the frequency from 1 MHz up to 100 MHz in steps of 0.123 MHz. As a balun is used to inject and retrieve the signals the overall EMC performance is evaluated. The far end of the cable is terminated with its nominal characteristic impedance.

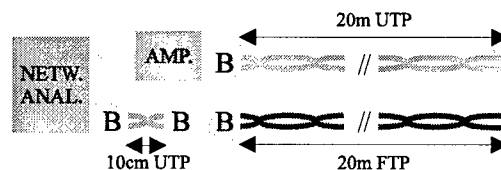


Figure 3: Set-up of "Line injection" method

As can be seen in figure 3 the set-up is totally isolated from any earthing or grounding networks. As the signal is injected through a balun on an UTP cable no physical connection exists with the earth or ground of the amplifier. Likewise at the retrieving side two supplementary baluns are used interconnected with a piece of UTP wire in order to avoid any physical connection.

Doing so a current is induced on the outside of the screen. This generates a resonance each time the cable length equals a quarter of the wavelength. This can be seen on the graph below where a peak can be observed on regular distances on a linear horizontal scale. This indicates the presence of a standing wave patterns.

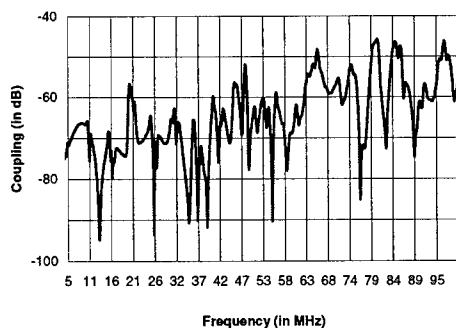


Figure 4: A resonance peak can be found on each vertical line of the grid (separated 5,26 MHz from each other)

During the following tests nothing is changed except for the way the screen is terminated. This means that the induced current on the outside of the screen remains the same but the standing wave pattern changes.

When terminating the screen at both ends optimal results are observed. This is done by connecting the screen to the metallic housing of the baluns. In this way both the differential mode and the common mode impedance are nearly matched. As a consequence the resonances nearly disappear as the transmission line - formed between the signal conductors and the screen - is matched at both ends. Terminated versus not terminated screens gives rise to peaks of about 10dB - 20dB as can be observed in the graph below:

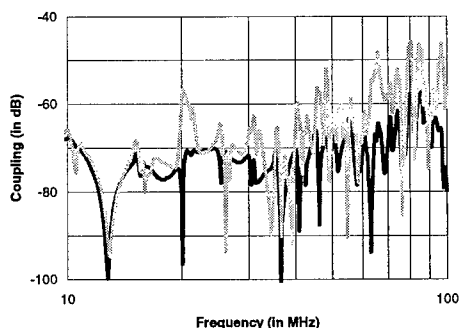


Figure 5: Screen terminated at both ends (dark trace) or not terminated at both ends (light trace).

In the following graph it can be observed that the termination at the far end seem to have little impact on the standing wave pattern. This can be explained due to the increase of impedance with frequency which makes that currents will find it difficult to propagate along the screen.

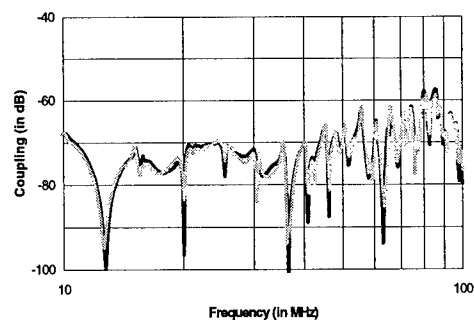


Figure 6: Screen terminated at near end. At the far end screen terminated (dark trace) or not terminated (light trace)

In practise the load of the screen can not be controlled but will be determined by the housing of the terminal equipment. This was simulated using a metallic box to terminate the screen. This gave results which are better than when leaving the screen not terminated.

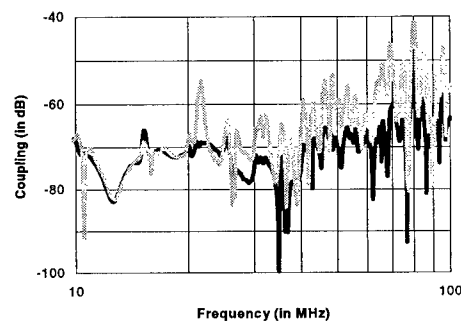


Figure 7: At near screen terminated to a metallic box (dark trace) or not terminated (light trace). Screen not terminated at far end.

By leaving the screen not terminated the worst case performance of a screened cable is obtained. Nevertheless this provides more EMI protection than when using no screen. This is proven when repeating the test with two unscreened cables as illustrated in the graph below.

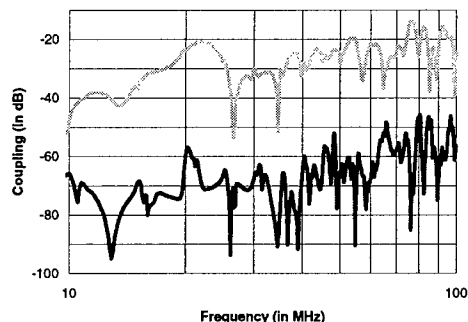


Figure 8: Not terminated screen at both ends (dark trace) and unscreened instead of screened cable (light trace).

The above experiment illustrates clearly that from 1 MHz - which is the frequency range of interest in case of category 5 cabling - the EMC performance of the screen is not influenced by an earthing network.

CONCLUSION

In this paper we have illustrated both theoretically and experimentally that the earthing network inside a building has no impact on the data transfer of category 5 cables. For the frequencies of interest terminating the screen at one or both extremities influences only the standing wave pattern that arises on the screen surface. By connecting the screen to the active equipment the resonances are reduced and as a consequence less noise is coupled into the differential mode loop. When connecting the screen at a single side the common mode loop is formed by the signal conductors and the earthing network. By connecting the screen at both ends the common mode loop is practically reduced to zero and as a consequence the immunity against transients like lightning is increased. Doing so creates an earth loop in which high power currents can propagate in case of fault conditions. In this case it may be favourable to block the low frequency currents without degenerating the screening integrity by introducing a capacitor into the screen. This solution is independent of the building utilities and their quality.

REFERENCES

- [1] EN 50173, 1995.
- [2] ISO / IEC 11801, 1995.
- [3] TIA/EIA-568-A, 1995.

- [4] Clayton R. Paul, *"Introduction to Electromagnetic Compatibility"*, New York: John Wiley & Sons, 1992.
- [5] Henry W. Ott, *"Noise reduction techniques in electronic systems"*, New York: John Wiley & Sons, 2nd ed., 1992.
- [6] John D. Kraus, *"Electromagnetics"*, McGraw-Hill, 4th ed., 1991.
- [7] Tim Williams, *"EMC for product designers"*, Butterworth - Heinemann, 1992.
- [8] Anatoly Tsaliovich, *"Cable shielding for electromagnetic compatibility"*, New York: Chapman & Hall, 1995.
- [9] prEN 50174-2, 1997.
- [10] ISO / IEC 1000-5, 1997.
- [11] ISO / IEC 364-5-548, 1996.
- [12] ISO / IEC 950, 1991.
- [13] ISO / IEC 364-4-41, 1992.
- [14] ISO / IEC 364-5-54, 1980.

AUTHOR



Michiel Pelt
Alcatel Cabling Systems
Bd. Paepsemalaan 16
B-1070 Brussels
Belgium

Received the degree in Engineering (Applied physics) from the Free University of Brussels in 1992. Currently responsible for the EMC research on generic cabling systems within Alcatel Cabling Systems. Active member of various standardisation committees within CENELEC like TC 215 / WG 2 and TC 46 X / WG 3 (Secretary).

Performance Assessment of Baluns

J.- H. Walling, M. Belanger* and J. Scharf**

* NORDX/CDT, Montreal, Canada

**Analog-Elektronik, Metzingen, Germany

Abstract

We measure several types of baluns, using commercially available standards. We build also some special standards and adapting hardware to verify the performance of these baluns.

The characterization of the baluns is done primarily with respect to the CMR and the LCL. The reason for this is the need for a verification of performance of the baluns with respect to balance, before setting standards on the balance of cables, links or channels.

We come to the conclusion that minimum CMR levels of 45 to 50 dB at 100 MHz and 50 dB for the LCL are required to measure reliably LCL levels of up to approximately 35 dB at 100 MHz. Exceeding this LCL measurement range requires more work with respect to the attainable accuracy and in comparison to the balun intrinsic LCL.

Background

In two previous papers we describe the impact of the baluns on measurements on cables and connecting hardware [1];[2]. In these articles it has been concluded that the difference of the obtained results is due to the difference of the baluns, especially with respect to their balance and impedance performance.

In the last couple of years the performances of data grade cables and related connecting hardware improved substantially. It becomes increasingly important to describe the performances of the baluns used for testing these better, to obtain consistent results.

The present article targets specifically wideband baluns and tries to establish criteria to comprehensively describe their behavior with respect to single port balance measurements. Our objective is to assess the performances of the baluns, to obtain information regarding their suitability for measuring the balance of cables and corresponding connecting hardware.

Though it is well understood, that balance is an important factor to be dealt with upon striving for higher link or channel performance, work on the standards level started only recently. All the previous work on balance measurements relates to frequencies, as prevailing in telephone systems [3];[4];[5].

Thus the ITU Recommendation 0.9 and the IEEE Standard 455-1985 indicate both different test circuits to measure LCL in a very low frequency range. Only few more recent public papers deal with higher frequency ranges of up to 100 MHz [6];[7];[8];[9].

The performances of baluns have to be well understood when using them. For this reason we shortly describe their performance behavior with respect to certain characteristics.

For the definitions of single and two-port network balance measurements and the corresponding parameters, we refer to the ITU - Recommendation G.117 [5].

We then characterize some of the commercially available baluns with respect to their performance and compare them using measurements on identical standards.

Introduction to the Characterization of Baluns

We understand a balun as a wideband signal transformer which converts balanced to unbalanced signals and vice versa, while at the same time matching the corresponding impedance at input and output ports to the best possible degree to those of the connected circuitry. Baluns, suitable as measurement signal transformers have to be characterized, and the corresponding results normally have to accompany any balun.

This, though not yielding any traceability to a national or international standard, allows a certain traceability to a reference balun kept by the manufacturer for calibration purposes.

The data to be indicated are listed consecutively with an explanation of their effect:

- Transformer impedance ratio (i.e. 50/100, 50/150 Ohm etc.)

- Insertion loss at a specific reference frequency. This value should be as low as possible. However, to obtain a larger frequency response it is possible to obtain a pre-defined insertion loss by compensating with an attenuator. It should be noted that this requires generally slightly higher power levels at the input.

- Frequency response of the insertion loss. The limits of the useable frequency range of a balun should be kept to a range, in which the insertion loss does not vary more than 1.5 dB.

The total insertion loss, for two port measurements, shall not exceed the 3 dB level. This can be easily measured by connecting both baluns in series with leads as short as possible. The attenuation of the baluns can be measured and taken into account.

The winding ratio of the balun yields also a difference between the balanced and unbalanced side of the balun. Generally a 3 dB difference is cited, independent of frequency. However, this value is difficult to verify by the user so that there remains an error source. We compensate in the following for the winding ratio with the values indicated by the manufacturers.

- Return loss. The return loss is the magnitude of the reflection coefficient. As such it indicates the impedance transformation range within the balun. At low frequencies, the return loss is predominantly influenced by the main inductance of the balun. At higher frequencies, however, the transforming characteristic of the balun, and hence also the return loss, is increasingly affected by several parameters.

These parameters are normally referred to as parasitics. To enumerate only some, we mention the degree of coupling of the balun, the frequency performance due to the complex permeability of the ferrites used, and the internal stray capacitances. In the latter case we have the circuit to circuit capacitance and the capacitance to ground as well as their respective capacitance unbalances.

A value of 20 dB is for frequencies exceeding 100 MHz quite acceptable, provided that the cabling and the instrument have also an acceptable and adequate return loss performance. A too low return loss of the balun yields easily multiple reflections, if the balun is used to measure cables or short links.

The return loss at the differential port is always referred to as a return loss with a nominal termination of 50 Ohm at the coaxial side of the balun. The return loss at the common mode port is then measured with a nominal impedance termination at the differential port of the balun.

If both ports are fully characterized, then the balun can be used bi-directionally. This bi-directionality is in most cases a design objective. However, it is not required for the measurement of the attenuation (insertion loss). To obtain a higher frequency range the bi-directionality is, therefore, often sacrificed. It has to be mentioned that the reflected wave is absorbed at the unbalanced port of the balun in the network analyzer. On the differential side of the balun a relative high return loss is generally specified.

However, it is stated clearly here that the use of such baluns entails a higher degree of variability of the results especially if cable impedance is measured.

- Common mode impedance (CMI). This value is so far only specified for very few baluns, though it is important to also absorb common mode signals as occurring due to conversion losses with a suitable impedance termination on the common mode port.

Note: It is our recommendation to develop a test method for the common mode impedance measurement. However, elaborating upon this subject exceeds the objective of our present work.

The magnitude of the common mode signal depends upon the overall symmetry of the entire circuit. Therefore, the CMI value of the balun has to be tailored to the common mode impedance of the entire circuit or cable. Aimed for is a general standard of a CMI level of 50 Ohm.

The observation of this objective will help to avoid "spikes" and resonance while measuring NEXT and FEXT.

- Common mode rejection. The common mode rejection of the balun can be assessed using a short or a highly balanced resistance pair (resistor with center tap) across the differential input port. The unbalanced input is then connected to the center tap of the short or the resistance pair. As the differential signal is not measured, we have to take into account the internal attenuation of the balun if we want to determine the CMR value. Towards this purpose the

attenuation of two baluns is measured, and then one balun is replaced by the center tapped resistance or by the short. As attenuation of the baluns the average of both S_{21} and S_{12} is taken, and half the value attributed to each balun.

A high value of CMR yields a high noise immunity. Thus a high CMR value is an indicator for both the EMI and crosstalk performance.

Too low CMR values of the balun yield substantial errors when measuring NEXT, FEXT, and also attenuation.

- Input Signal level. Indications concerning the signal level refer always to the unbalance port of the balun. The maximum allowable signal level depends upon the lowest measuring frequency and the ferrite core of the transformer itself. The maximum signal level, which can be connected to the unbalanced port, without damaging the balun, has to be clearly indicated.

Methodology

We characterize in the following different balun types, and show their performance in measurements of LCL and crosstalk.

For these measurements we build some adapters which we tried to balance very well. This is verified by poling. Additionally we use for the LCL measurements a commercially available standard with 100 Ohm impedance and an infinite longitudinal conversion loss. We use also a resistive 100 Ohm load. With both these standards we measure the LCL on the baluns by poling the loads and using the average of the measurements. We note that the

differences of poling the loads are negligible.

We then measure the CMR on the same baluns. For these measurements we use balanced input adapters for the 100 Ohm port, which are essentially short circuiting the 100 Ohm port. We make also measurements, using a very well balanced 100 Ohm common mode test head, which is also commercially available.

We then carry out some measurements with the baluns (at least with those which have 100 Ohm impedance on the differential side). We measure the LCL of a 20 dB standard, and additionally the LCL of two other standards. These standards we build specially for this purpose. They yield, to all practical purposes an identical LCL, sloping down over frequency with approximately 30 dB/decade.

We then measure the LCL of two pairs of a so called short link, in order to see if we have some evidence of the so called resonance effect. The short link has been build out as a "standard" and yields very repetitive results. In fact this standard is connectorized with Twinax connectors and is frozen in position to get long term repeatability.

Finally we take the previously mentioned standards and the short link to verify the crosstalk performance in comparison.

Results

We note that all the measurements are carried out in the laboratories of Nordx/CDT to avoid any potential bias.

We investigate the behavior of 8 balun types. Here we cannot report all results in detail, but have to quote often simply based upon the accumulated data.

Fig. 1 to 3 show the LCL measurements obtained on three different balun types. It has to be noted that the balun winding error has been compensated for. Two different loads were used.

The Fig. 4 shows the CMR for some baluns without a common mode port. What has to be noted here is that the 100 Ohm balun, which is widely used has only a CMR of approximately 15 dB at 100 MHz. Crosstalk measurements with these baluns may yield easy error prone results.

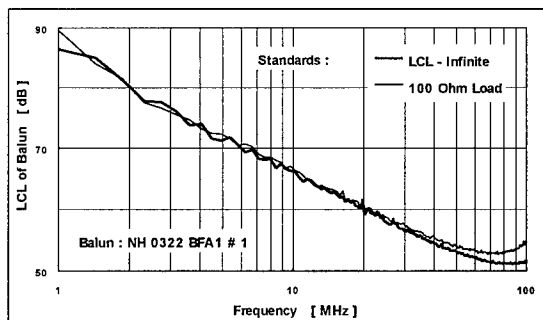


Fig. 1: LCL of North Hills 0322BFA1 balun

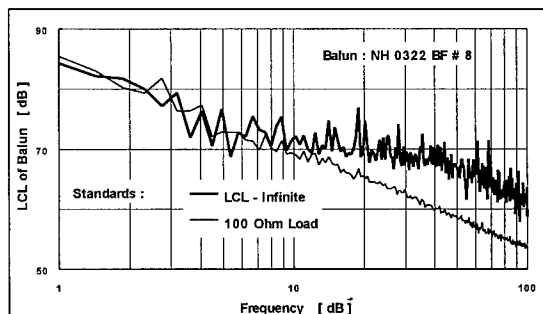


Fig. 2: LCL of North Hills 0322BF balun

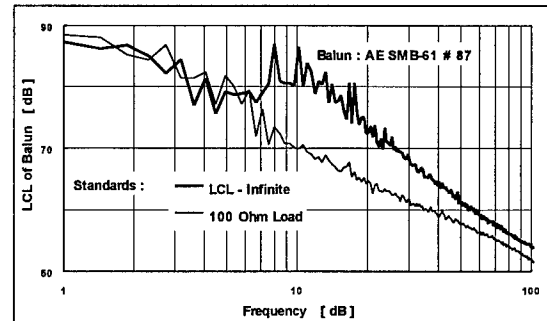


Fig. 3: LCL of Analog Elektronik SMB-61 balun

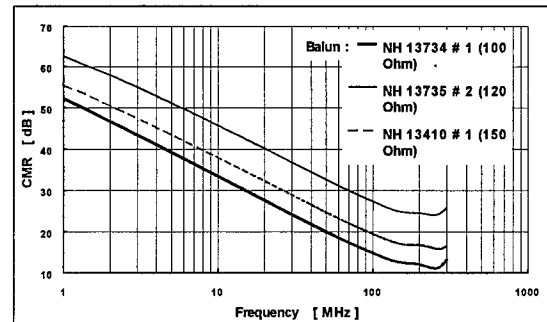


Fig. 4: CMR of some baluns without common mode port

In the Fig. 8 to Fig. 10 we have each three LCL measurements on a 20 dB standard and two on our specially build standard.

Fig. 5 to Fig. 7 show CMR measurements on three different balun types using as an input head either a short or a resistor network across the 100 Ohm port.

In Fig. 11 to Fig. 13 we have the LCL measurements for each of the balun types on two pairs of the short link.

Finally in the Fig. 14 to 16 we have crosstalk measurements for some baluns for comparison purposes. These measurements were taken on both pairs of the previously mentioned standard, and on the short link.

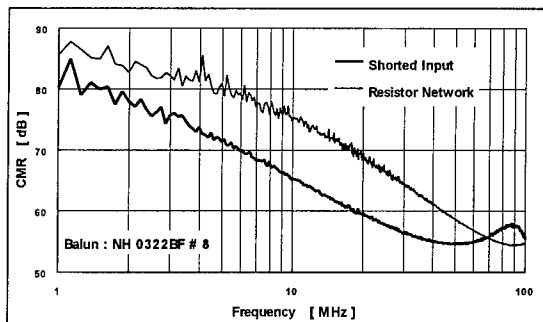


Fig. 5 : CMR of Balun with common mode port, measured with short and with a center tapped resistor network across the differential mode port.

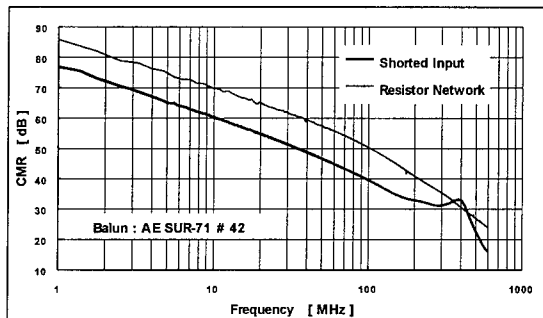


Fig. 6 : CMR of Balun without common mode port, measured with short and with a center tapped resistor network across the differential mode port.

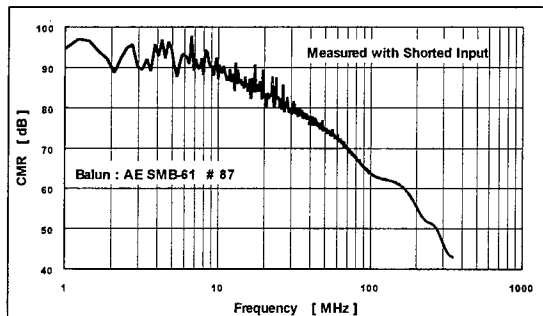


Fig. 7 : CMR of balun with common mode port, measured short across the differential mode port.

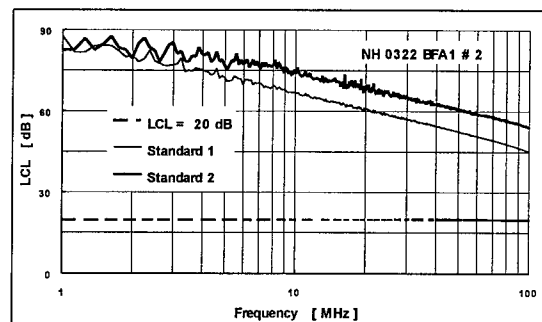


Fig. 8 : LCL measurements with balun on different standards.

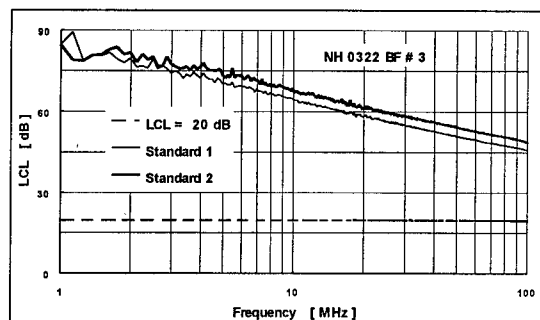


Fig. 9 : LCL measurements with balun on different standards.

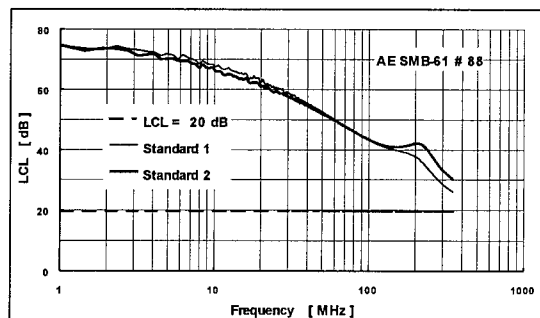


Fig. 10 : LCL measurements with balun on different standards.

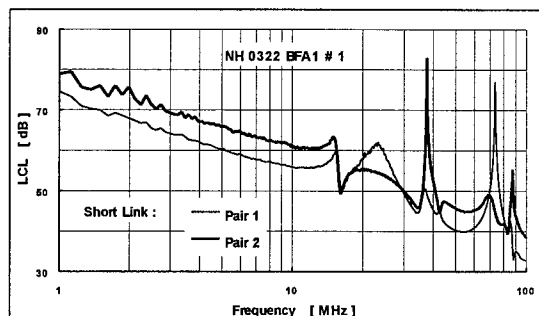


Fig. 11 : LCL measurements with balun on short links.

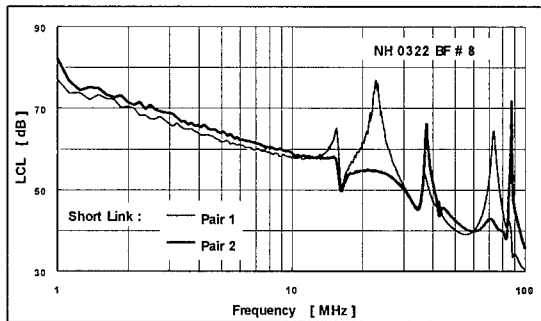


Fig. 12 : LCL measurements with balun on short links.

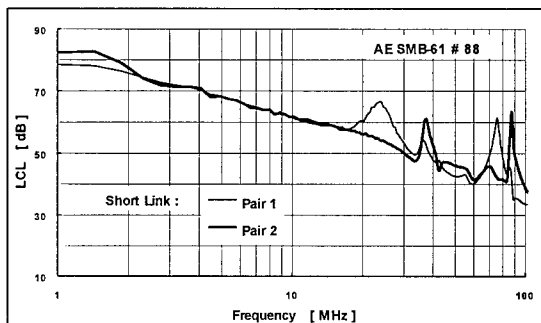


Fig. 13 : LCL measurements with balun on short links.

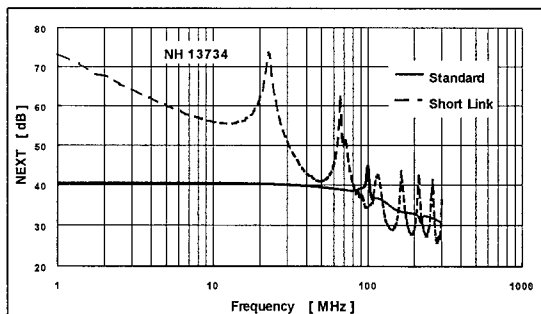


Fig. 14 : NEXT measurements with balun on a short link and a standard.

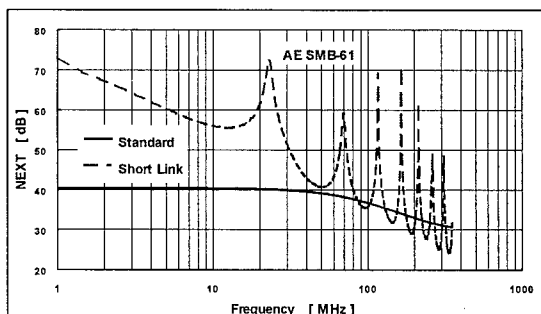


Fig. 15 : NEXT measurements with balun on a short link and a standard.

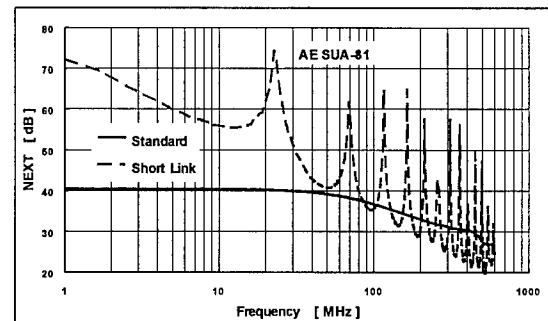


Fig. 14 : NEXT measurements with balun on a short link and a standard.

Discussion of Results

We limit the discussion of our results to a frequency range of up to 100 MHz. We note that the LCL of the baluns is generally better than 50 dB at 100 MHz for the baluns measured. We note slight differences in the LCL using either an impedance of 100 Ohm with infinite LCL or a 100 Ohm resistive load on the differential port as can be seen in Fig. 1 to Fig. 3.

The Fig. 4, indicates the CMR of three balun types without common mode port. The CMR slopes down over frequency with approximately 20 dB/decade, leveling out at higher frequencies to a more constant value.

Fig. 5 and Fig. 6 show the CMR for two balun types with common mode port, both measured with a short and a center tapped resistor at the differential output port. The results indicate a difference of approximately 10 dB in the measured CMR values. We carried out some more measurements with different types of resistor networks across the differential output port, and come to the conclusion, that for the characterization of the baluns themselves, it is best not to use center tapped resistors, but to

stay with a shorted output at the differential port.

The Fig. 7 shows such a measurement up to 350 MHz for one of the balun types. It is noteworthy that the CMR in this case is approximately 45 dB at 350 MHz.

The Fig. 8 to Fig. 10 represent the data obtained measuring our standards with different balun types. It is clearly visible that the standard, having a LCL of 20 dB is perfectly captured in its behavior by all the balun types.

However for the standard, which we build, the picture is slightly different. This standard has a LCL which slopes down with frequency, thus that we are reaching at low frequencies with all the balun types into the noise floor. The first two baluns show marked differences in the results. Thus the measurements in case of the regular North Hills 0322 BF balun are more comparable. In fact they show only a difference of approximately 4 dB, whereas the North Hills 0322 BFA1 indicates a difference of approximately 10 dB. This confirms also the results reported by Lucent Technologies [10], and presented to TIA TR 41.8.1 in 1997, indicating that the 0322 BFA1 balun may be slightly inferior to the regular 0322 BF balun.

The Analog Elektronik balun SMB-61 shows nearly identical values of approximately 44 dB at 100 MHz.

It has to be noted that these LCL values are very high and the respective balun measurement accuracy may have to be verified in more detail. The main reason for this is that the balun intrinsic LCL

becomes predominant. In this context we refer to a paper about LCL accuracy [9].

In the Fig. 11 to Fig. 13 we have LCL measurements on two pairs of a short link. We see again a difference in the measurements with the North Hills 0322 BFA1 vs the 0322 BF balun. Here the differences are markedly smaller, as the entire LCL level is substantially lower (approx. 15 dB) than previously.

Additionally, the results with both baluns indicate a tendency to resonance effects.

The same measurements with the Analog Elektronik SMB-61 in Fig. 13 balun show no resonance at lower frequencies. In the higher frequency range, the results are very much comparable.

Our crosstalk results are nearly identical for all balun types, see Fig. 14 to Fig. 16. An exception are the results obtained for the North Hills balun 13734, which show resonance at 100 MHz and approximately 220 MHz. This may have to do with the fact that the CMR for this balun is very low, and that the impedance is not matched to the 100 Ohm standard.

Generally the crosstalk levels of our standards are lower as compared to the levels of their individual LCL on the pairs. This may be an explanation for our near perfect match of all crosstalk measurement data for nearly all baluns.

Though the CMR values for the baluns with common mode port are comparable, the results show some differences in balance measurements, especially in the higher LCL range.

Here we can only suspect, that this may have to do with the common mode impedance. However, the North Hills balun 0322 BFA1 is reported to have a common mode impedance in the range of 50 Ohm for the considered frequencies [11]. Else we do not have any explanation which we can support with our results.

Summary and Conclusion

Our results indicate that for adequate balance measurements we need CMR levels of the baluns in the range of minimum 45 to 50 dB at a 100 MHz. The intrinsic LCL of the baluns themselves should exceed at the same frequencies the 50 dB mark.

In all cases, the common mode impedance should be in the vicinity of 50 Ohm.

However, even under these conditions the measurement of LCL levels exceeding approximately 35 dB will have to be studied in more detail, mainly with respect to the attainable accuracy and without measuring an increasing proportion of the balun intrinsic LCL.

Preliminary and basic work in this direction has already been started [9]. As to verification of the attainable accuracy levels, it would be helpful, to have 100 Ohm impedance reference standards with different LCL levels, covering the range from approximately 10 dB to approximately 45 dB. This will allow a direct measurement comparison.

References

- [1] B. Lord et al.: Balance Measurements of UTP Connecting Hardware.
45th IWCS, 1996, p. 287-294
- [2] J.-H. Walling et al.: Crosstalk Measurements as a Means to Characterize the Balance of Data Grade Wires.
45th IWCS, 1996, p. 751-761
- [3] NN: Transmission Aspects of Unbalance about Earth
ITU-T Recommendation G.117 (2/96)
- [4] NN: Unbalance about Earth of Telecommunication Installations
ITU-T Recommendation K.10 (3,93)
- [5] NN: Measuring Arrangements to Assess the degree of Unbalance about Earth
CCITT Recommendation 0.9 (Geneva 1972, amended at Malaga-Torremolinos, 1984 and at Melbourne, 1988)(Revision 1996 : see [3])
- [6] NN: Verification Test Procedure for Measuring Balun Output Signal Balance and Common Mode Rejection.
A contribution of Microtest Eng. to TIA TSB 67, August 1995.
- [7] L. Staschover: Measurements Unbalance to Ground of Balance Systems.
North Hills Electronics
Contribution to JTC1/SC25/WG3 in Munich (Green Paper 25)
45th IWCS, 1996, p. 751-761
- [8] L. Staschover: Wideband Signal Transformers.
North Hills Electronics. Application Note # WB-1 (3,1994)

- [9] H. Koeman and A. Bennet : LCL Measurements Accuracy Test Procedure.
Results for North Hills 0322 BF Baluns.
Submitted by the Fluke-Corporation to TIA TR41.8.1-97-08-45
- [10] NN: Comparative results on North Hills baluns 0322 BF and 0322 BFA1. Presented to TIA TR41.8.1 in 1997
- [11] P. Chandra, North Hills Signal Processing.
Personal communication.

Authors



Jörg-Hein (Jo) Walling received his diploma in Mechanical Engineering in 1966 at the Technical University of Berlin. In 1974 he obtained a Doctor's degree (Dr.-Ing.) at the same University. In 1974 he joined Northern Telecom in the Research and Development department. Since 1976 he has been a senior engineer at the Nortel, now Nordx/CDT, Lachine Cable Plant, responsible for the design of Outside Plant and Data Grade Wires and Cables.



Martin Bélanger received his B.E. in Electrical Engineering from University of Sherbrooke. He joined the Technology Cable Group of Northern Telecom Canada Limited, now Nordx/CDT, in 1992.

He was initially responsible for cable design and electrical test methods. He is at present responsible for the manufacturing aspects of data grade cables, for quality assurance and for the development of new manufacturing test facilities.



Joachim Scharf, born in 1945, was for more than 20 years a research and development engineer in the research facilities of Wandel & Goltermann in Germany. He has specialized in the design and evaluation of narrow band crystal filters.

Since 1993 he is heading an engineering office for high frequency measurements (Analog-Elektronik, D-72555 Metzingen, Beim Häusle 12, Tel. 01149-7123-14001). His main task is the design and development of balanced measurement accessories.

About the Influence of Residual Elongation and Thermal Expansion on the Sagging Performance of Glass Fiber Reinforced Aerial Service Wires.

J.- H. Walling

NORDX/CDT, Montreal, Canada

Abstract

Two standards deal with glass fiber reinforced aerial service wires. Both indicate maximum elongation and residual elongation of the wire under specified loads. The present paper verifies the validity of these elongation requirements, and demonstrates that the values will have to be modified. This is based upon sag calculations, derived from the load elongation values directly. We demonstrate that the sags based upon the standardized values are excessive and must be reduced. The proposed values are 0.75 to 0.8 % and 0.2 % for the elongation and residual elongation, respectively.

Another objective of this paper is the investigation of thermally induced sag increase. We show ways to reduce it by modifying the linear expansion coefficient of the strength member of these wires.

Finally we present a new and patented design of an aerial service wire with superior sag characteristics. This wire has virtually zero residual elongation, resulting in low sag variations.

Background

Up to the early eighties a self supporting type of aerial service wire, which used copper clad steel conductors, has been

widely used in North America. The copper clad steel conductors give the wire sufficient strength to support reasonable span length. The design of these wires has been initially based upon a common insulating layer, which is covered by a textile braid and an outer jacket to provide for the long term protection of these wires. Over time the jacket, textile braid and insulation have been combined to a multipurpose single layered insulation/jacket.

Since their introduction glass fiber reinforced aerial service wires have been increasingly deployed. However, very little is known about the mechanical performances of these wires, and their long term behavior. In the relevant standards mechanical performance requirements of the traditional copper clad steel reinforced self supporting aerial service wires have been directly transposed to the glass fiber reinforced aerial service wires. The increasing deployment forced a fast action on the elaboration of relevant standards, though very little in depth knowledge about these wires has been acquired by then. One of the few adjustments concerns the load for the static load test. The only new requirement introduced into these standards is the residual elongation. Historically Phillips Cable (BICC) introduced first limiting values for

the residual elongation of such aerial service wires. Since 1988 Northern Telecom, now Norcom, a Division of Nordx/CDT is studying the electrical and mechanical performances of such wires, in order to be able to improve the design and to lay the basis for a more comprehensive description of basic performance requirements. In this context we focus in a paper [1] on the impact of the clamps on the sagging performance. We come to the conclusion that an improvement of the clamp design is desirable. Alternately the wire has to be designed such as to fill the clamp at the outset in its width as much as possible. We show [1] that wires with reduced thermal expansion are definitely an asset.

The breaking strength of the copper clad steel self supporting aerial service wire is such that the wire has to fail absolutely before the wedge clamp failure. This is mandatory due to the high strength of the copper clad steel conductors which are terminated to the binding posts inside the terminal. Otherwise the terminal is exposed to breakage, if the clamp fails during a mechanical overload.

Glass fiber reinforced aerial service wires have 22 AWG soft copper conductors, which will not damage the binding posts, even if the clamp fails. The glass fiber reinforced aerial service wires have substantially high tensile strength, which exceeds by far the maximum load the clamps can sustain. However, this higher tensile strength yields also a high elastic elongation, and, due to design specific aspects also a residual elongation component, which cannot be neglected.

A better understanding of the mechanical performances of the glass fiber reinforced aerial service wires is useful to allow adjustments in their design and to reflect more realistic requirements in the relevant standards on these wires to avoid service problems by avoiding life line service interruptions following an extreme ice-storm or another mechanical overload.

Introduction

Glass fiber reinforced aerial service wires are according to their design subject to a residual elongation, i.e. they show a permanent elongation after being subjected to a high load for a short duration. Such load cycles are experienced during a hurricane or a sleet storm and induce a certain permanent or residual elongation in the wire. This residual elongation has a significant impact upon the sag.

In a previous reporting [1] we referred to the general load-elongation curve of aerial service wires. In this article, we introduce both, the original and the hysteresis modulus of service wires [2].

The exclusive use of the hysteresis modulus implies that the span considered is re-tensioned after application of a high load for a certain time. However, in reality this is not done, as it is unlikely that the linesmen will re-tension the spans after a sleet storm. Therefore both moduli have to be considered.

Towards this purpose it is important to know the impact of this residual elongation upon the sag of the spans. We investigate here the sag increase,

remaining after a sleet storm if the ice load is taken off, either by shedding or melting, i.e. the residual sag increase.

We assess the impact upon the sag performance of aerial service wires for which the relevant standards, are indicating standard values of elongation and residual elongation under the specified loads.

Hence, the objective of our study is the verification of the validity of the standardized values for elongation and residual elongation [3];[4] and to check if a revision of these values is warranted.

The impact of the linear thermal expansion of aerial service wires on the sag is well known. Though the relevant standards do not reflect any requirements of thermal expansion in the standards.

However, it is possible to compensate for the linear thermal expansion by combining fibers with positive and negative expansion coefficients. Glass fibers have a positive, and polyaramid fibers have a negative linear thermal expansion coefficients. Thus, by combining both fiber types in proper proportions, we can design a wire with virtually zero thermal expansion, or at least with substantially reduced linear thermal expansion. Such a wire is only subject to sag variations under different load conditions.

We show that a design of glass fiber reinforced aerial service wires is feasible having virtually no residual elongation. We present such a patented wire design. This design optimizes the

sag with respect to the thermal expansion and negligible clamp induced sag increases.

Rationale

In the present paper we use the same basic formulæ for the sag of wires after a length increase which are reported in an earlier paper [1]. The length increase is calculated from the residual elongation caused by exposure to heavy ice or storm loading. The tension in the wire resulting from these loads is computed and used to determine the residual elongation. For these calculations we use the length specific load increase on the span based upon the standard values for such calculations (0.5 inch conformal ice load and a wind load of 8 lbs/sqft, which add up vectorially. The relative density of the ice is assumed to be 0.9). We calculate the sag due to residual elongation, if the entire span would have been stretched by an average force, i.e. the average of the force at the suspension point and the horizontal force in the wire.

It is obvious that the real result lies between these two values, thus that the average of both length increases is sufficient to describe the sag performance of the span after being stretched with a residual elongation remaining.

This paper does not include the detailed derivation of the rigorous formulæ, describing precisely the sag with residual elongation. This derivation has been made, and has been used for comparison purposes [5]. However, we find the use of the previously described method of the average of the maximum

and minimum residual elongation to calculate the sag performance of aerial service wires to be sufficiently precise, and easy to use.

We assess the sag performance of aerial service wires under the assumption that the reinforcement is based upon a glass-polyaramid fiber mix, using different proportions of both fiber types. The general formulæ for the sagging performance are given in the Appendix, though limited only to straight elastic wires.

We show, that the linear thermal expansion coefficient is zero for a specific proportion of the glass and polyaramid fibers. However, due to tex count availability of each fiber type, this 'ideal' fiber mix is in most cases not feasible. Data on a two pair aerial service wires with different proportions of glass and polyaramid fibers are presented.

Data of a regular six pair aerial service wire (Figure-H design), which is subject to residual elongation and thermal expansion are compared to a new design concept, which

- reduces the impact of the clamps to a minimum
- has a substantially reduced thermal expansion, and
- is characterized by having no residual elongation.

This new design is exposed to the same elastic elongation. This has to be taken into account in the installation practice of these wires, i.e. the installation practice has to have provisions for free

longitudinal movement of the copper conductors within the core.

Methodology and Calculations

We describe the behavior of glass fiber reinforced drop wires with a residual elongation by an original and a hysteresis modulus. These moduli refer to the slope of the load elongation curve, i.e. the entire cross section of the wire is considered, without trying to calculate a so called composite elastic modulus. We have (see Fig. 1):

$$E_o = \frac{F}{\varepsilon} \dots\dots\dots(1)$$

$$E = \frac{F}{\varepsilon - \varepsilon_R}$$

Hence we get:

$$\varepsilon_R = F \cdot \frac{E - E_o}{E \cdot E_o} \dots\dots\dots(2)$$

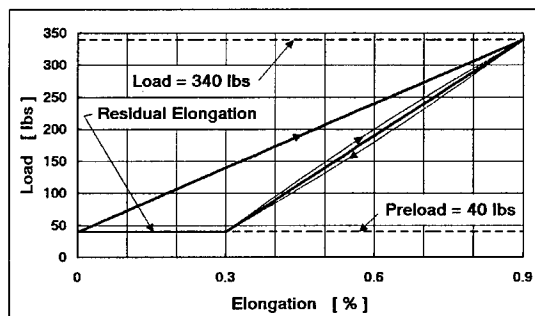


Fig.1 : Load elongation curve of a two pair glass fiber reinforced aerial service wire, based upon the standardized values. Schematically shown is also the hysteresis for cyclic loading.

Using equations (1) and (2) we can calculate the cable moduli from the values given in [3] in ICEA S-89-648-1993, Section 8.1.7 for 2 and 6 pair

glass fiber reinforced aerial service wires. Using the indicated loads and under consideration of the preloads we can calculate the corresponding wire moduli. We obtain then respectively:

$$E_o = 33,335 \text{ [lbs]}$$

$$E = 50,002 \text{ [lbs]}$$

$$E_o = 43,123 \text{ [lbs]}$$

$$E = 64,684 \text{ [lbs]}$$

These are the values which we verify for their practical applicability. Towards this purpose we calculate the sag which is obtained on some spans of different length with an original string-up tension close to the preload level indicated in [3]. We then expose these spans to the loads under combined standard ice and wind loads [5]. From there we calculate the sag upon unloading to the string-up tension level using the resultant residual elongation.

Results

In the following we neglect the impact of the clamps upon the sag. We assume a linear thermal expansion coefficient of $+7.2 \cdot 10^{-6} \text{ [ft/ft } ^\circ\text{C]}$ for the glass fibers and, as they are predominant for the mechanical performance of the wire, we use the same figure also for the entire wire. We assume as well a length specific weight of the wire of typically 0.046 lbs/ft and 0.084 lbs/ft for two and six pair aerial service wires, respectively. These weights represent typical average values of the products actually on the market.

Fig. 2 and Fig. 3 show the sag of a two pair wire according to the standards for spans of 50 and 100 feet, respectively. Additionally there is indicated the sag for

reduced residual elongation allowances, that is for 0.1 and 0.2 % residual elongation.

In Fig. 4 and Fig. 5 we show the sag for a two pair wire for two different string-up tensions as a function of the span length again with the residual elongation as a parameter.

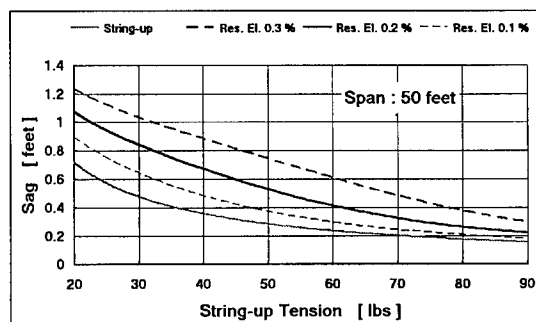


Fig. 2 : Sag as a function of the string-up tension for a span of 50 feet with the residual elongation as a parameter. (Two pair wire)

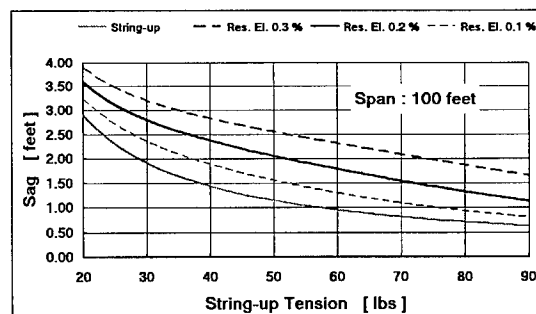


Fig. 3 : Sag as a function of the string-up tension for a span of 100 feet with the residual elongation as a parameter. (Two pair wire)

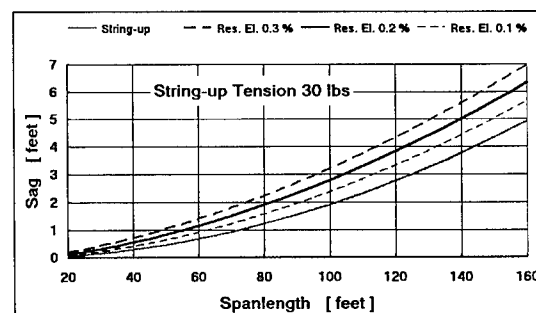


Fig. 4 : Sag as a function of the span length for a string-up tension of 30 lbs with the residual elongation as a parameter. (Two pair wire)

In the Fig. 6 and Fig. 7 the behavior of a six pair fiber reinforced aerial service wire is shown for two span length.

In Fig. 8 and Fig. 9 show the sag of a six pair wire for two different string-up tensions depending upon the span length, with the residual elongation as a

parameter. Six pair wires, due to their higher length specific weight need higher string-up tensions.

For the differential temperature range, i.e. the temperature range between actual and string-up temperature, this yields an operating window for the

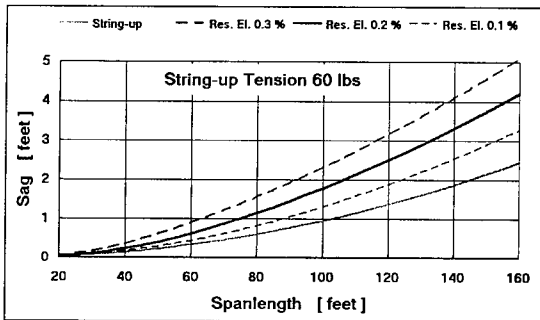


Fig. 5 : Sag as a function of the span length for a string-up tension of 60 lbs with the residual elongation as a parameter. (Two pair wire)

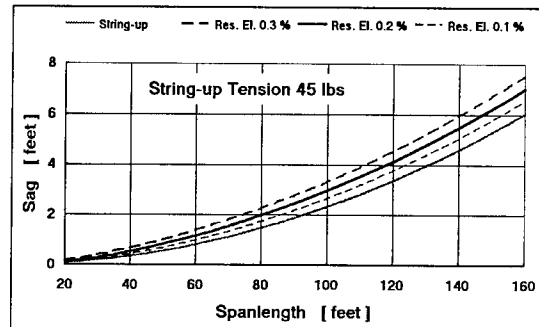


Fig. 8 : Sag as a function of the span length for a string-up tension of 45 lbs with the residual elongation as a parameter. (Six pair wire)

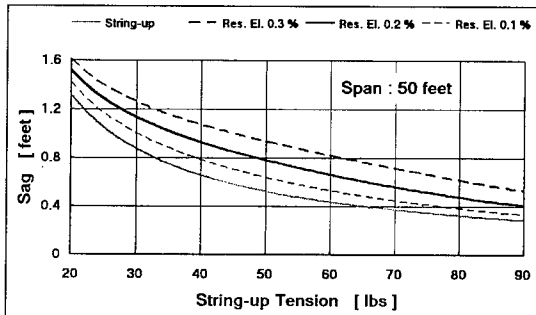


Fig. 6 : Sag as a function of the string-up tension for a span of 50 feet with the residual elongation as a parameter. (Six pair wire)

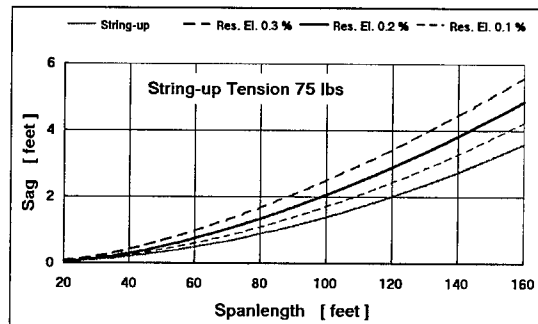


Fig. 9 : Sag as a function of the span length for a string-up tension of 75 lbs with the residual elongation as a parameter. (Six pair wire)

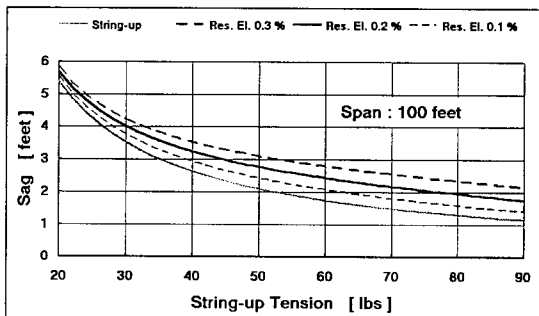


Fig. 7 : Sag as a function of the string-up tension for a span of 100 feet with the residual elongation as a parameter. (Six pair wire)

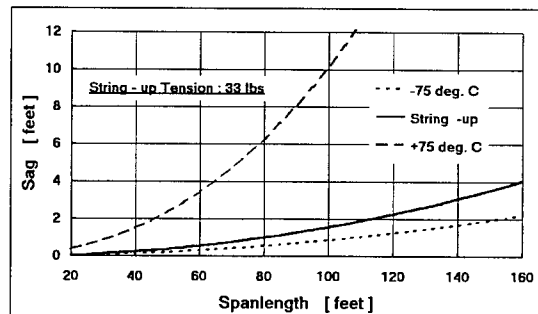


Fig. 10 : Sag as a function of the span length for a two pair service wire for different temperature differentials relative to the string-up time.

wire from -40 °C to +60 °C if we assume we use the range from -75 °C to +75 °C an acceptable installation temperature range for the installers from -15 °C to +35 °C.

Fig. 10 shows the sag performance of a 2 pair aerial service wire under the extreme temperature conditions, defined above. In this case the cable elasticity has been calculated from the standardized elongation allowance of 0.9%. The string-up tension in this case is 33 lbs (This value has been selected, as the algorithm for long span length and at the high temperatures selected becomes unstable). Due to the thermal expansion coefficient of the glass fibers, we obtain a relatively wide range of sag variation with temperature. Here the sag for the full differential temperature range, that is the temperature range between actual and string-up temperature is shown.

Discussion of Results and Solutions Pursued

We show first for each wire type the sag for two span length. The sag is indicated as a function of the string-up tension. It has to be mentioned that at least the two pair wires are hand strung, which generally limits the string-up tension to approximately 60 lbs. For higher string-up tensions as often required for the six pair wires, a "come-along" has to be used.

Fig. 2 to Fig. 5 and Fig. 6 to Fig. 9 indicate for the two pair and six pair aerial service wires, respectively, the sag, which is to be expected at string-up time. Additionally shown is the sag which results due to the residual elongation, if the span is exposed to a

high load condition, which then ceases due to shedding of the ice. It has to be noted, that this sag increase is only due to the residual elongation after a high load condition. The sag under high load condition is not shown here.

The sag is more than doubling at average string-up tensions even for span length of only 50 feet, if we allow a residual elongation of 0.3 %. This effect is even more dramatic for longer span length, if the string-up tension is kept to acceptable levels. On the other hand, it can be seen clearly that for lower residual elongation allowances the sag increase due to this residual elongation is markedly smaller, and is already for a residual elongation allowance of 0.2% very acceptable. A differential temperature raise shows this effect even more dramatically.

Thus an excessive sag is depicted in Fig. 10 which is due to:

- a relatively high linear thermal expansion coefficient
- due to the relatively low cable elasticity.

In fact, this sag can be substantially improved by:

- lowering the values for the elongation allowance to 0.75 or 0.8 % , thus increasing the cable elasticity.
- reducing the linear thermal expansion coefficient of the wire.

We see, that especially for longer span length and under high temperatures, as

are occurring under direct sunlight exposure, the sag performance is relatively poor, using the string-up tensions indicated. The high sag can be partially compensated for by higher string-up tensions. However, there is a limit to the higher string-up tensions when the wire is exposed to high temperatures. This limitation is the result of the relatively high plasticizer content of the jacketing materials required for low temperature exposure. Under the conditions mentioned above an adhesion failure results easily between the coated fibers and the jacket. This failure happens inside the clamps, and yields a span breakdown.

Fig. 11 shows the sag performance of a comparable 2 pair aerial service wire as depicted in Fig. 10, but with different proportions of polyaramid and glass fiber as reinforcement. We see that the thermal expansion is substantially reduced, even with the addition of only small amounts of polyaramid fiber.

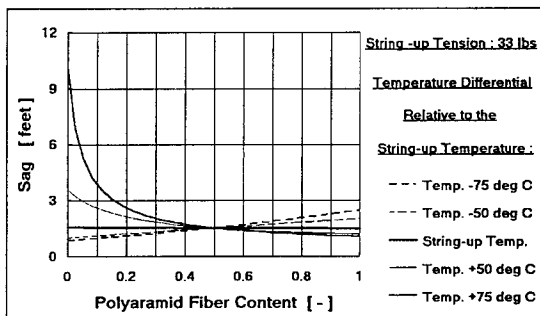


Fig. 11: Sag as a function of polyaramid content with the temperature differential as a parameter.

We pursue this concept of adjusting the thermal expansion coefficient by mixing different fiber, i.e. polyaramid and glass fiber, both having different signs in their respective linear thermal expansion coefficients (polyaramid fibers have a linear thermal expansion coefficient of

-3.6×10^{-6} to -4.0×10^{-6} [ft/ft °C]). The Appendix gives formulæ for the sag of service wires with different fiber content.

Presentation of an Highly Improved Aerial Service Wire

It is obvious from Fig. 11 that a full compensation of the linear expansion coefficient is not required. In fact, it is sufficient to add a relatively small amount of polyaramid fiber, to substantially reduce temperature induced sag variations.

In Fig. 12 we present a new design concept of Norcom, Division of Nordx/CDT for a multiple pair aerial service wire. This design offers virtually zero residual elongation.

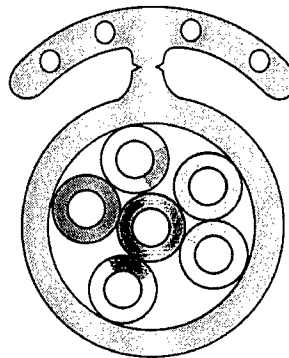


Fig. 12: Cross section of Norcom's new multiple pair aerial service wire.

This is a result of the total separation of the strength member and the core. Only the strength member is clamped in the wedge clamp. Thus the core may move free axially inside a core wrap, which in turn is bonded to the surrounding jacket.

The strength member is designed in a shape to follow the contour of the core of the wire itself. This is to reduce aeolian vibrations and to minimize sleet

or ice build-up. The strength member is attached to the core by a web with a separation groove. For installation the core and strength member are separated, such that only the strength member is introduced into the wedge clamps.

The wedge clamps are the same as for the two pair aerial service wire, to avoid the carrying of two types of clamps. Furthermore, the design of the strength member is such as to fill the width of the wedge clamp entirely so that the clamp setting is reduced to a minimum. This contributes to a substantial reduction in sag.

In order to avoid the stretching of the copper conductors under heavy loading, they will have to be given some slack at the suspension points, in order to be able to move free longitudinally. This is shown schematically in Fig. 13 for a pole in midspan position.

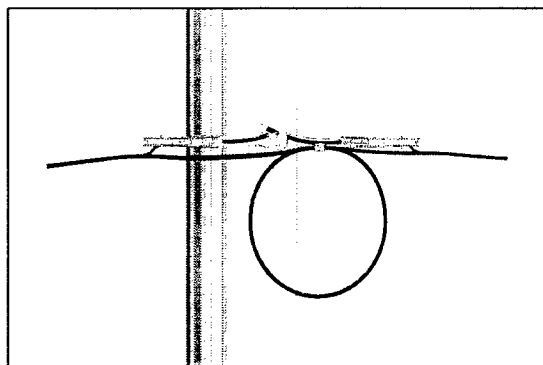


Fig. 13 : Installation of the new multiple pair aerial service wire on a midspan pole, leaving slack for the core in an expansion loop.

This wire design yields the highest performance of fiber reinforced aerial service wires which is economically achievable. However, our wire may be further improved by using glass polyaramid fiber mixtures as reinforcing strength members.

Summary and Conclusion

We show that the actually allowed values for the residual elongation are too lenient, and will have to be tightened in the interest of line service reliability. In this context, a reduction of the elongation allowance has to be considered, in order to increase the elasticity of the service wires. We propose towards this purpose to reduce the residual elongation to 0.2% and the elongation allowance to 0.75 or 0.8% under the same load conditions.

As already mentioned in the introduction, the test methods for these service wires will have to be tailored to the specific characteristics of these wires. We find in this context a strong correlation between long-term static load test results and residual elongation. Thus we find generally for a higher residual elongation frequent failures in the static load testing even after several days. We strongly emphasize this point, as the actual standardization of the static load test, i.e. a 24 hour testing is definitely insufficient to guarantee proper life expectancy.

We present furthermore a new type of wire with specific patented design features which allows us to:

- optimize the sag performance of aerial service wires by avoiding virtually any residual elongation.
- reduce next to nil the clamp induced sag increase.
- improve thermally induced sag increases to very acceptable levels, and this also under extreme climatic conditions.

References

- [1] J.- H. Walling et al : The sag behavior of aerial service wires using different wedge clamps. 44 IWCS, 1995 p. 702-712
- [2] E.R. Kaswell: Wellington Sears Handbook of Industrial Textiles Wellington Sears Co., Inc. 1963, p. 214
- [3] NN: ICEA S-89-648-1993 : ICEA Standard for Aerial Service Wire. Insulated Cable Engineers Association, Inc.
- [4] NN: Bellcore Technical Reference TR-NWT-001069, Issue 1, June 1992: Generic Requirements for Non-Metallic Reinforced Aerial Service Wire.
- [5] J.- H. Walling: The sagging of service wires. Monography, Northern Telecom Canada, Ltd., Montreal (Restricted)

Author

Jörg-Hein (Jo) Walling received his diploma in Mechanical Engineering in 1966 at the Technical University of Berlin. In 1974 he obtained a Doctor's degree (Dr.-Ing.) at the same University.



In 1974 he joined Northern Electric in the Research and Development Department. Since 1976 he is senior engineer at the Northern Telecom, now Nordx/CDT Lachine Cable Plant, responsible for the design of Outside Plant and Data Grade Wires and Cables.

APPENDIX

Sag Calculation for Wires with Fibers of Different Linear Thermal Expansion Coefficients

We use the following abbreviations:

- a,b,c - Abbreviations
- E - Wire elasticity modulus
- f - Sag
- F - Force on the wire
- g - Gravitational acceleration
- i - Tex count of polyaramid
- j - Tex count of the glass
- l - Span length
- L - Length of wire on the span
- n - Constant
- p - Slope of sag curve under ice load
- T - Temperature, Total tex count
- α - Linear thermal expansion

- Δ - coefficient Differential between string-up and actual state
- ϵ - Elongation
- μ - Length specific weight of wire
- \mathcal{E} - Tex specific elasticity

Indices :

- 0 - Indicating the minimum of parameters or the original unstressed state
- 1 - Indicating the maximum of parameters or polyaramid fibers
- 2 - Indicating glass fibers
- C - Indicating combined characteristics

We assume that only the reinforcing fibers are contributing to the strength of the wire. That is we consider only the problem where two

different fiber types are used. We introduce two parameters i and j , describing the proportioning of the two different fibers according to their respective tex count. The cross sectional area of the fibers is proportional to their tex count and respective density.

The Poisson ratio of both fiber types is different but the impact of the Poisson ratio upon the cross-sectional changes in the elongation ranges considered here ($> 2\%$) can be neglected. We consider the elasticity which is characteristic to each fiber and which refers to their respective tex count. We use gothic letters to describe the tex count specific elasticities. Only as a reminder : In the previous derivations [1];[5] we consider an integral elasticity of the wire, but not the elasticity of its components. However, here our intent is to obtain a general description of the wire elasticity, if two different types of reinforcing fibers are used simultaneously, and we calculate therefrom an integral value for the entire cable.

The tex count specific elasticity is the hypothetical force required to stretch the fibre by one hundred percent. This tex specific elasticity relates to the cross section represented by one tex of a fiber. Fig. 1 shows schematically the force required per tex for both fibre types as a function of the elongation. For a given temperature mechanical and thermal elongation are additive. This is shown in Fig. 2.

For a composite we have to take the corresponding tex count of each fibre type into account as well. This is shown in Fig 3. The schematics refers only to one tex of each fiber type, respectively. Let j be the tex count of the glass fibre rowing used in a specific wire design, and i the corresponding tex count of the polyaramid fiber. We then get for the force in each fiber type, under consideration of the thermal expansion :

$$\begin{aligned} F_1 &= i \cdot \mathcal{E}_1 \cdot (\varepsilon - \alpha_1 \cdot \Delta T) \\ F_2 &= j \cdot \mathcal{E}_2 \cdot (\varepsilon - \alpha_2 \cdot \Delta T) \end{aligned} \quad \dots\dots\dots(1)$$

For the entire force we have then:

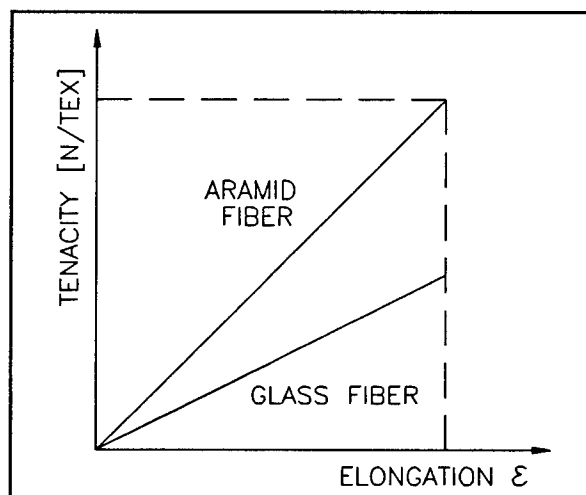


Fig. 1 : Indication of the tex count specific elasticity for glass and polyaramid fibers

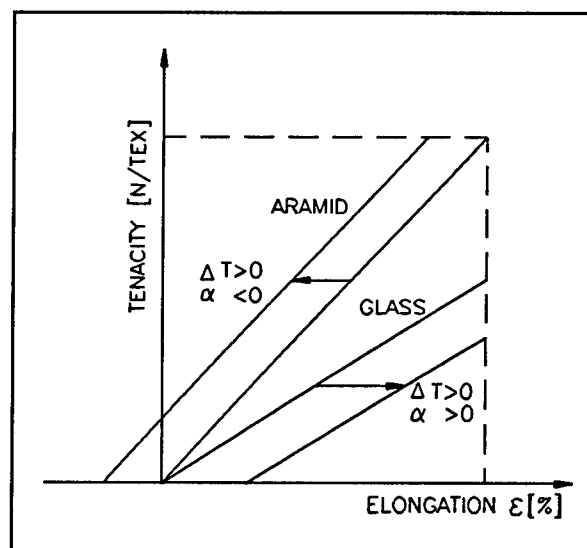


Fig. 2 : Changes of tex specific force elongation curve due to linear thermal expansion

$$\begin{aligned} F &= (i \cdot \mathcal{E}_1 + j \cdot \mathcal{E}_2) \cdot \varepsilon \\ &\quad - (i \cdot \alpha_1 \cdot \mathcal{E}_1 + j \cdot \alpha_2 \cdot \mathcal{E}_2) \cdot \Delta T \quad \dots\dots\dots(2) \end{aligned}$$

We establish at a fix temperature (reference temperature) the glass-polyaramid content such as to always obtain the same force for the same elongation. We then get:

$$i = \frac{F}{\varepsilon \cdot \mathcal{E}_1} - \frac{\mathcal{E}_2}{\mathcal{E}_1} \cdot j \quad \dots\dots\dots(3)$$

At the reference temperature we have $\Delta T = 0$, hence we obtain:

$$i \cdot \mathcal{E}_1 \cdot \alpha_1 = -j \cdot \mathcal{E}_2 \cdot \alpha_2 \quad \dots\dots\dots(4)$$

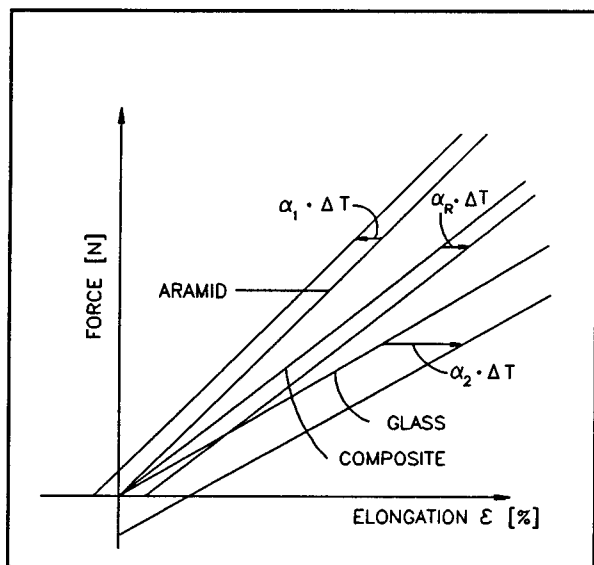


Fig. 3 : Indication of the tex count specific elasticity for a glass - polyaramid fiber mix with nearly zero thermal elongation.

The last two equations represent a linear system for the two unknown values of i and j for zero thermal expansion.

For the combined expansion coefficient, i.e. for all combinations from i and j we obtain then:

$$\alpha_c = \frac{i \cdot \mathcal{E}_1 \cdot \alpha_1 + j \cdot \mathcal{E}_2 \cdot \alpha_2}{i \cdot \mathcal{E}_1 + j \cdot \mathcal{E}_2} \quad \dots\dots\dots(5)$$

For the combined elasticity of the wire we have then:

$$E_c = i \cdot \mathcal{E}_1 + j \cdot \mathcal{E}_2 \quad \dots\dots\dots(6)$$

We can rewrite equation (2) under consideration of equation (5) and (6) and obtain then:

$$\begin{aligned} F &= (i \cdot \mathcal{E}_1 + j \cdot \mathcal{E}_2) \cdot (\varepsilon - \alpha_c \cdot \Delta T) \\ &= E_c \cdot (\varepsilon - \alpha_c \cdot \Delta T) \end{aligned} \quad \dots\dots\dots(7)$$

For the total tex count we have:

$$\begin{aligned} T &= i + j \\ &= \frac{F}{\varepsilon \cdot \mathcal{E}_1} - \frac{\mathcal{E}_2 - \mathcal{E}_1}{\mathcal{E}_1} \cdot j \end{aligned} \quad \dots\dots\dots(8)$$

For the sag we get then according to [1]:

$$\begin{aligned} f &= \frac{F_0}{\mu_0 \cdot g} \cdot \left[\frac{F_0}{2 \cdot E_c} \cdot p_1^2 \right. \\ &\quad \left. + (1 + \alpha_c \cdot \Delta T) \cdot \left(\sqrt{1 + p_1^2} - 1 \right) \right] \end{aligned} \quad \dots\dots\dots(9)$$

and:

$$\begin{aligned} \frac{l \cdot \mu_0 \cdot g}{2 \cdot F_0} &= \frac{F_0}{E_c} \cdot p_1 \\ &+ (1 + \alpha_c \cdot \Delta T) \cdot \operatorname{arcsinh} p \end{aligned} \quad \dots\dots\dots(10)$$

We can now proceed to solve (10) numerically by iteration as indicated in [1], using the following abbreviations:

$$a = \frac{l \cdot \mu_0 \cdot g}{2 \cdot (i \cdot \mathcal{E}_1 + j \cdot \mathcal{E}_2)} \quad \dots\dots\dots(11)$$

$$= \varepsilon_{\max} - \frac{i \cdot \mathcal{E}_1 \cdot \alpha_1 + j \cdot \mathcal{E}_2 \cdot \alpha_2}{i \cdot \mathcal{E}_1 + j \cdot \mathcal{E}_2} \cdot \Delta \quad \dots\dots\dots(12)$$

$$c = \varepsilon_{\max} - b + 1 \quad \dots\dots\dots(13)$$

If the length specific weight of the wire has to be taken into account, then the varying tex count has to be introduced into the length specific weight of the entire wire. In case of a load change following string up, the corresponding equations are as follows:

$$\begin{aligned} f &= \frac{L_o}{2} \cdot \left[\frac{\mu \cdot g \cdot L_o}{4 \cdot E_c} \right. \\ &\quad \left. + (1 + \alpha_c \Delta T) \cdot \frac{\left(\sqrt{1 + p_1^2} - 1 \right)}{p_1} \right] \end{aligned} \quad \dots\dots\dots(14)$$

$$\begin{aligned} \frac{l}{L_o} \cdot p_1 &= \frac{\mu \cdot g \cdot L_o}{2 \cdot E_c} \\ &+ (1 + \alpha_c \cdot \Delta T) \cdot \operatorname{arcsinh} p \end{aligned} \quad \dots\dots\dots(15)$$

The numerical treatment follows exactly as outlined in [1].

DEVELOPMENT OF CROSS-INDUCTIVE CABLE FOR TRAIN LOCATION DETECTION IN THE SUPERCONDUCTING MAGLEV TRAIN CONTROL SYSTEM

Motoharu Ono*1 Yoshifumi Sakai*2 Mitunori Ohta *3 Osamu Koyasu*4 Kohei Tazumi*5 Kyouji Mita *6

*1 Central Japan Railway Co. Tokyo Japan *2 Railway Technical Research Institute Tokyo Japan

*3 Japan Railway Construction Public Corporation Tokyo Japan *4 Fujikura Ltd. Chiba Japan

*5 Hitachi Cable Ltd. Tokyo Japan *6 Sumitomo Electric Industries Ltd. Osaka Japan

Abstract

We have developed a cross-inductive cable which serves to detect precisely the current location of a train on the superconducting Maglev railway. In the cross-inductive cable, six paired wires each composed of a twisted and a parallel portions repeated at fixed intervals are arranged so as to be able to detect the train location by calculating the voltages induced to the parallel portions from the signals transmitted from the on-board antennas of the train.

The train is levitated and driven forward by the repulsive and attractive forces of the propulsion and levitation coils in the track called "guideway" and the superconducting magnets installed to the train. Train control is effected by the frequency and phase of the electric current applied to the coils, so it is necessary to detect the train location with high accuracy. As the cross-inductive cable is laid with high tension to prevent its expansion and contraction by the wind pressure from the train traveling at high speed as well as by temperature changes, mechanical strength and length accuracy under high tension become also important. The cross-inductive cable that meets these specifications was laid on the Yamanashi Maglev Test Line, and various running tests have been conducted with good results.

1. Introduction

In November 1990, construction of a new test line was started by Central Japan Railway Co., Railway Technical Research Institute and Japan Railway Construction Public Corporation.

The superconducting maglev train system is expected to be a new generation ultra-rapid transit system succeeding Japan's existing rapid transit system "Shinkansen." At present, this system is being tested in the first-phase section about 18 km long between two cities, Ohtsuki and Tsuru, in Yamanashi Prefecture. In this system, a train equipped with superconducting magnets travels in the levitated state at high speed on the track (guideway) equipped with propulsion and levitation coils, by the repulsive and attractive forces of these magnets. Train operation is performed by detecting the train location precisely and controlling the frequency and phase of the current applied to the propulsion coils at the train location. Therefore, it is important to detect the current train location with high accuracy.

Location detection errors should be very small, on the order of several centimeters or less. To meet this requirement, it is necessary to make the cross-inductive cable high in length accuracy as well. Taking these into account, the cross-inductive cable is required to possess mechanical properties such as tensile properties, bending performance, vibration performance under high tension, and length accuracy of about 0.04%, and electrical properties such as characteristic impedance, attenuation, protection against crosstalk, insulation, and coupling performance with the on-board antennas of the train. The cross-inductive cable should satisfy high requirements for these properties.

2. Brief Description of Maglev Train

In the superconducting Maglev system, the train travels on the guideway shown in Fig. 1. Levitation and propulsion coils are attached to the sidewalls of the guideway. When the traveling speed exceeds 100 km/h, the levitation coils work as electromagnets by the action of the superconducting magnets installed to the train, and the train is levitated about 10 cm by the repulsive force as shown in Fig. 2. For propulsion, the propulsion coils are varied in polarity by controlling the frequency of the current applied to them, and the train is driven forward by the repulsive and attractive forces produced between the coils and the superconducting magnets of the train as shown in Fig. 3. For frequency and phase control of current, it is necessary to detect precisely at which coils the train is currently located. This location detection is made by the cross-inductive cable laid on the bottom of the guideway.

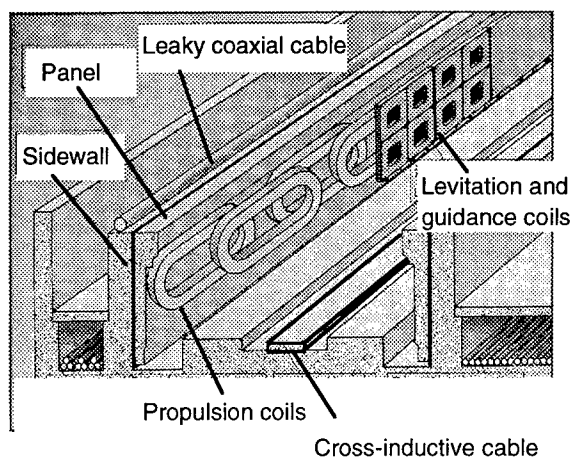


Fig. 1 Guideway

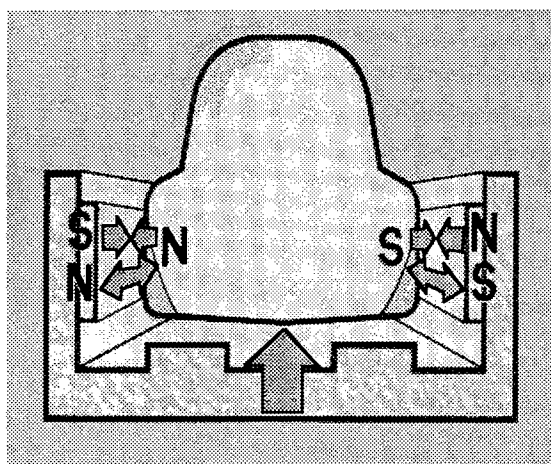


Fig. 2 Principle of Levitation

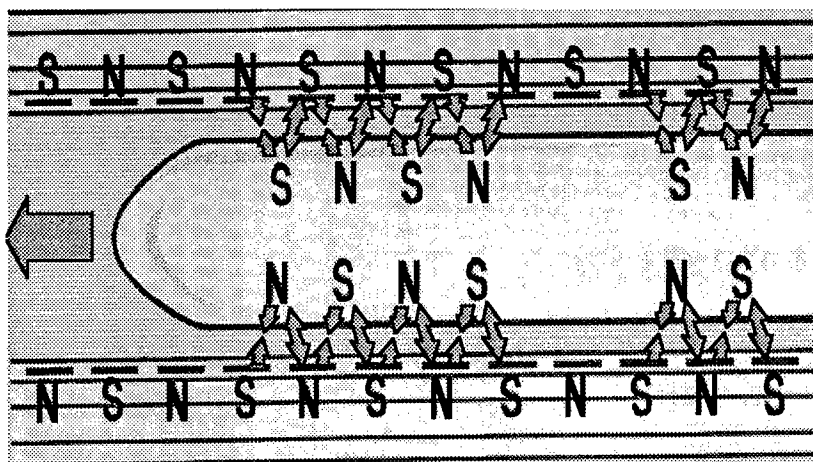


Fig. 3 Principle of Propulsion

3. Structure of Cross-inductive Cable

Fig. 4 shows the cross section of a cross-inductive cable, and Fig. 5 shows the arrangement of inductive core wires. In the cross-inductive cable, six location detection pairs each composed of a portion twisted at fixed pitches and a parallel-opened portion, which are repeated at fixed intervals, and two information pairs each having a crossing at fixed intervals are arranged on a base plate, and these are wrapped with a fastening tape and are coated together with polyethylene so that one each messenger wire is positioned on both sides of the base plate. The major specifications are given in Table 1.

Table 1 Structure of Cross-inductive Cable

Item	Description
Basic structure	Number of pairs housed: 6 location detection pairs 2 information pairs Maximum width: 170 mm Maximum thickness: 25 mm
Core	Conductor: Annealed copper wire, tinned Core identification: blue, yellow, green, red, violet, black, white, brown, and gray
Cable length	151.2 m
Messenger wire	2.9 mm galvanized steel wire x 7 pcs.

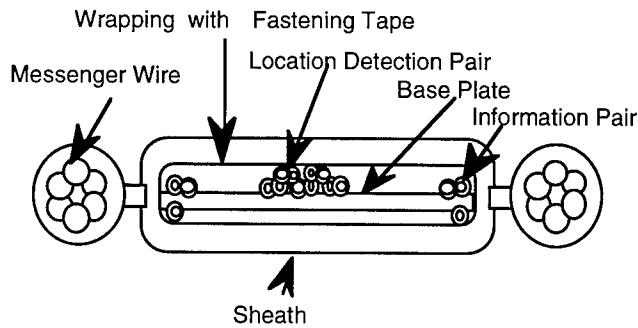


Fig. 4 Cross Section of Cross-inductive Cable

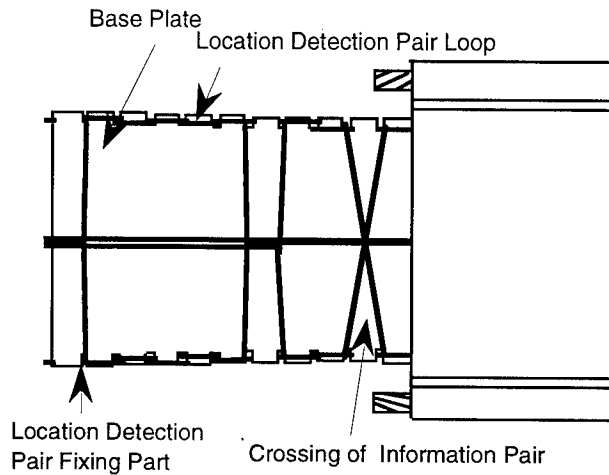


Fig. 5 Structure of Cross-inductive Cable

In the cross-inductive cable, two each location detection pairs shifted by half a pitch are grouped into one set, and waveforms of three phases are obtained by combining the voltages induced from the on-board antennas as shown in Fig. 6. By processing these waveforms arithmetically and determining from one cycle of the obtained waveform and the location detection pair interval of 2.7 m the phase of the combined waveform, it becomes possible to calculate the location.

4. Design of Cross-inductive Cable

After laying cross-inductive cable, it is necessary to make the installation pitch of propulsion coils in the guideway correspond to the cable laying pitch and to minimize length changes by effects of wind pressure and temperature change. For this reason, the length of the cross-inductive cable has to be made smaller than that of one control section of the coils. The tension necessary to make the length of the cross-inductive cable agree with that of the coil section can be determined by formula (1) as shown in Fig. 7:

$$T = E \times D \times (L_s - L_c) / L_c \quad (1)$$

where T = tension

E = longitudinal elastic modulus of cross-inductive cable

D = cross sectional area of cross-inductive cable

L_c = length of cross-inductive cable

L_s = section length

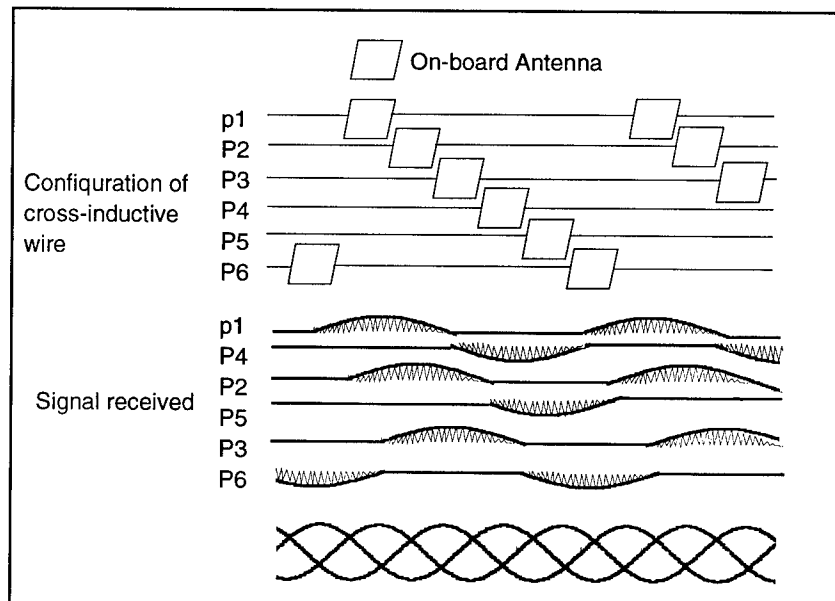


Fig. 6 Location Detection theory

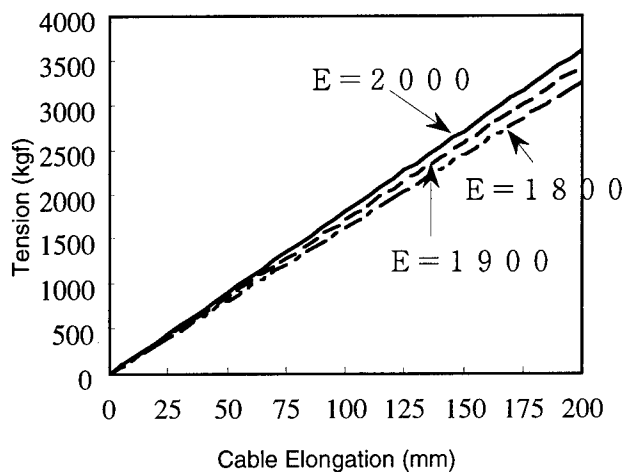


Fig. 7 Elongation and Tension of Cross-inductive Cable

Length changes of the cross-inductive cable include expansion and contraction by temperature. The temperature range is from -20 to +60°C. The length change of the cable in this range can be determined by formula (2):

$$\Delta L = L_c \times \alpha \times \Delta t \quad (2)$$

where ΔL = amount of change in cable length

α = linear expansion coefficient

Δt = amount of temperature change

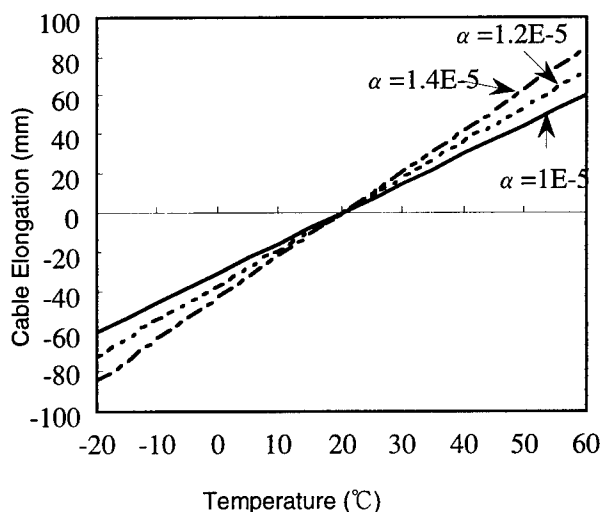


Fig. 8 Temperature Vs. Elongation of Cross-inductive Cable

From these results, it has been decided to use a messenger wire composed of seven 2.9 mm galvanized steel wires and an FRP plate as the base plate. In this case, the tension for laying is about 1,000 kgf, and the tension change by temperature is 900-3,000 kgf, i.e., less than 1/3 the breaking strength of the messenger wire, so there is no problem with safety.

5. Mechanical Properties

5-1 Tensile performance

The cross-inductive cable was laid in the actual guideway and measured for changes with time of elongation and tension. The results are given in Figs. 9 and 10. Measurements were made in the tunnel section. The air temperature was about 10°C with virtually no change, the length of the cross-inductive cable was not more than 151.2 m \pm 3 cm, and the laying tension was as good as 915 kgf. Changes during a period of about 10 days were small as well.

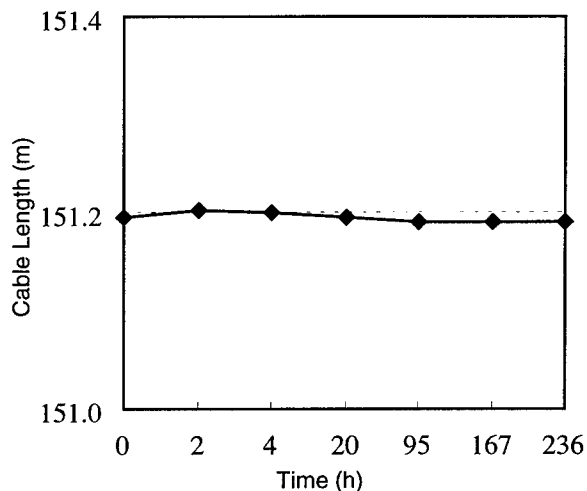


Fig. 9 Length Change with Time

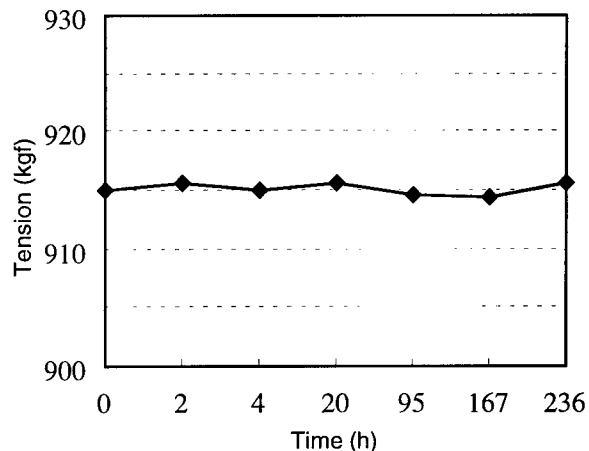


Fig. 10 Tension Change with Time

The cross-inductive cable laid was divided into sections about 20 m long, and the length of each section was measured. The results are given in Fig. 11, from which it can be seen that the cable was elongated uniformly on the entire length.

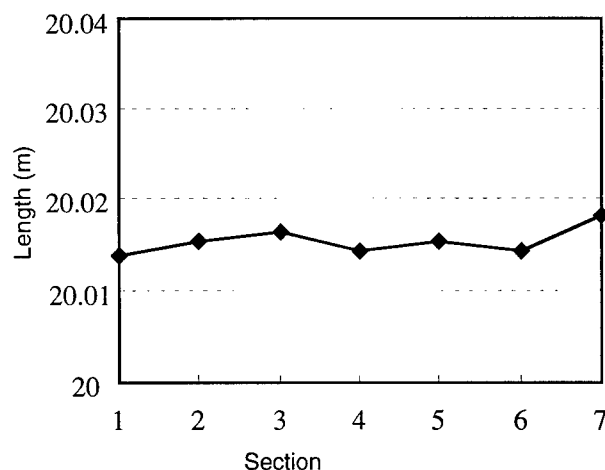


Fig. 11 Elongation of Each Section

5-2 Vibration performance

It was confirmed that there was no abnormality on the external appearance and inductive core wires even when the cable was made to vibrate 260,000 times with an amplitude of 28 mm at a frequency of 13Hz, with the left and right supports spaced 900 mm from the vibrating center and with a 1000kgf tension applied to one messenger wire.

5-3 Bending performance

When the cross-inductive cable was bent 180° back and forth twice around a 600 mm dia. mandrel, there was no damage on the external appearance and inner cores.

6. Electrical Properties

6-1 Characteristic impedance

Fig. 12 shows the frequency characteristic of the location detection pair. The characteristic impedance at a working frequency of 180kHz was about 170 Ω for the location detection pair and 370 Ω for the information pair.

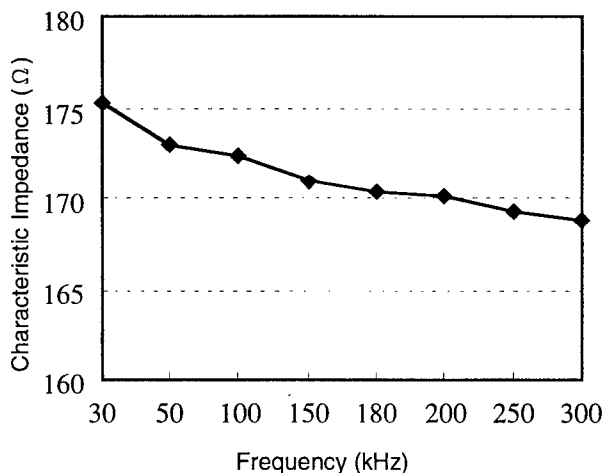


Fig. 12 Frequency Characteristic of Characteristic Impedance

6-2 Attenuation

Fig. 13 shows the frequency characteristic of the attenuation of the location detection pair. The attenuation at 180kHz was about 2.3 dB/km for the location detection pair and 1.6 dB/km for the information pair.

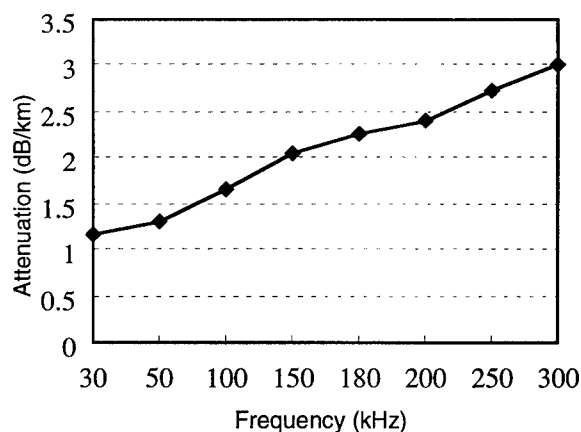


Fig. 13 Frequency Characteristic of Attenuation

6-3 Other electrical properties

Other electrical properties at 180kHz are given in Table 2.

Table 2 Electrical Properties of Cross-inductive Cable

Item	Maximum	Minimum
Crosstalk at far end	71dB	35dB
Conductor resistance	24.4 Ω /km	22 Ω /km
Insulation resistance	72 M Ω /km	32 M Ω /km
Dielectric strength	No abnormality at 4,000V for one minute	

6-4 Coupling performance

To measure induced voltages, the antennas 350 mm high by 500 mm wide were moved parallel at right angles to the cross-inductive cable, with a horizontal clearance of 250 mm and a vertical clearance of 530 mm, and the voltages induced at the end of each pair with a transmission output of -2.6 dBm at a frequency of 180kHz were measured. The induced voltages at each pair are shown in Fig. 14. The differences in voltage between each pair were small, and a sufficient SN ratio of about 30 dB was obtained. Fig. 15 shows the waveform obtained by combining these signals and its phase. Fig. 16 shows the location detection errors determined from the phase of the combined waveform. A good result of less than ± 3 cm was obtained.

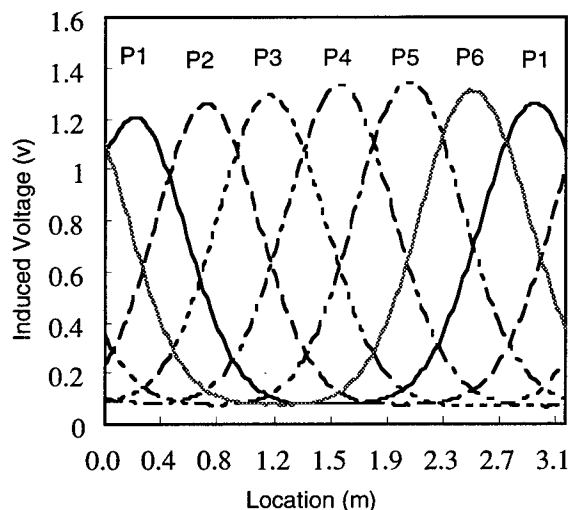


Fig. 14 Induced Voltage at Each Pair

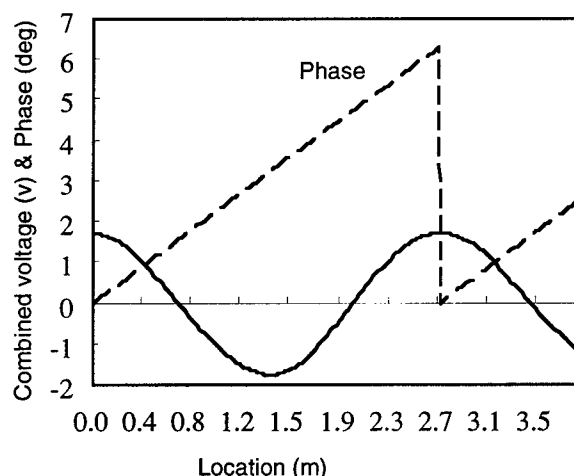


Fig. 15 Combined Waveform

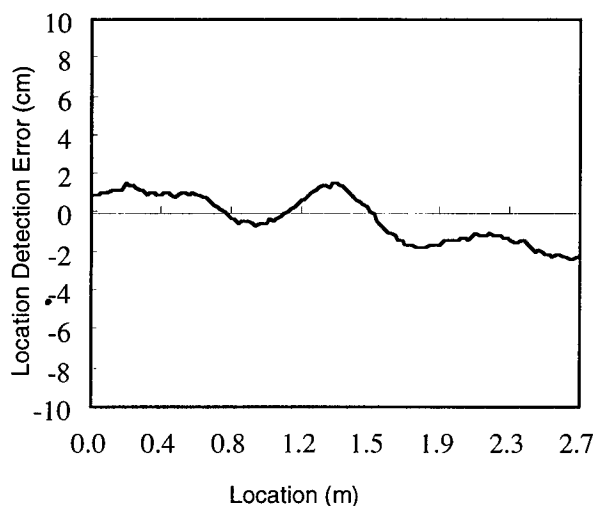


Fig. 16 Location Detection Error

7. Conclusion

We developed a cross-inductive cable capable of detecting the location of a Maglev train with high accuracy. It was confirmed that the cable when laid with high tension exhibits good performance in terms of mechanical properties such as vibration, expansion and contraction, length accuracy, etc., electrical properties, and location detection. The cross-inductive cable began to be laid in the first-stage section of about 18 km in the Yamanashi Maglev Test Line in March 1997. Its electrical properties and coupling performance have been measured with good result.

At present, various running tests are being carried on with the aim of achieving the world's highest speed. We believe this cross-inductive cable can contribute to attaining this project.

Acknowledgement

The authors wish to acknowledge the help of all the persons involved in the design, fabrication, testing, and installation of the cross-inductive cable. We want to thank in particular member of linear project, from Railway Technology Research Institute, who have been of great help in research and development of cross-inductive cable. Also Japanese government subsidy is covered this project.

Reference

- (1) Fundamental Features of Systems for Continuous Detection of Vehicle Position by Inductive Lines
E. Itakura, T. Sasaki IEE 50-C4 (1975)
- (2) A Construction of Inductive Lines for Continuous Detection of Linear Motor Vehicle Position and Detecting Accuracy
T. Sasaki IEE 55-C29 (1980)

Authors

Motoharu Ono



Yamanasi Control
Center
Central Japan Railway
Co.

271-2 Ogatayama, Turu-
shi, Yamanasi, 402,
Japan

M. Ono was born in 1947. He joined Central Japan Railway Co. after graduated from Niihama Technical College in 1968 and has been engaged in research and development of safety devices of signal and a member of the IEE of Japan.

Yoshifumi Sakai

Electric Dept.
Railway Technical
Research Institute

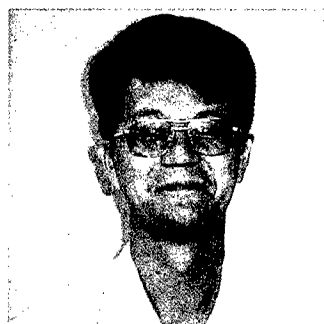
1-6-6 Yaesu,
Chuuou-ku Tokyo
103 Japan

Mitunori Ota
Kantou Branch
Japan Railway
Construction Public
Corporation



1-10-14, Kitaueno,
Taitou-ku, Tokyo
110 Japan

M. Ota was born in 1948. He joined Japan Railway Construction Public Corporation after graduated from Taira Technical Highschool in 1968.



Osamu Koyasu
Opto-Electronics
Laboratory
Fujikura Ltd.

1440, Mutuzaki,
Sakura-shi, Chiba,
285 Japan

O. Koyasu was born in 1953. He joined Fujikura Ltd. from Kisarazu Technical College in 1973 and has been engaged in research and development of cable. He is now engineer in the Telecommunication Cable Section and a member of the IEICE of Japan.

Kohei Tazumi
Engineering Dept.
Telecommunication Div.
Hitachi Cable Ltd.



2-1-2 Marunouchi,
Chiyoda-ku, Tokyo
100 Japan

K. Tazumi was born in 1941. He joined Hitachi Cable Ltd. after graduated from Osaka University in 1964 and has been engaged in design, inspection and construction of telecommunication cable.



Kyouji Mita
Radio Wave System
Dept.
First Engineering
Sect.
Sumitomo Electric
Industries Ltd.

1-1-3 Shimaya,
Konohana-ku,
Osaka, 554, Japan

K. Mita was born in 1952. He joined Sumitomo Electric Industries Ltd. after graduated from Maizuru Technical College in 1973 and has been engaged in engineering of new traffic system, cellular phone and detection system of car location.

TRENDS AND DEVELOPMENTS IN FLAME RETARDANTS FOR CABLES

Stephen C. Brown

Alcan Chemicals Limited
Banbury
England

ABSTRACT

This paper discusses flame retardant and smoke suppressant additives for cables. It begins with a general discussion of the inorganic flame retardants known to the author which find significant application in cables. Some organic flame retardants including organo-bromine and organo-phosphorus compounds are also mentioned. The first part of the paper considers flexible PVC formulations of the type which can be used for plenum cables. The second part considers flame retarded polyethylene copolymers and polyethylene most notably EVA and metallocene polyethylenes.

INTRODUCTION

It is obvious, at least with the benefit of hindsight, that a fire involving a product of great length can potentially present a greater hazard in spreading fire than a discreet smaller item. Cables, pipes and conveyor belts are examples. Other items such as flooring, wall cladding, ceiling and roofing materials can present the same problem (particularly in public buildings which may contain long corridors). The design of installations can mitigate the threat eg incorporation of barriers or other protection at regular intervals. In addition to the threat of flame spread there is the ever present hazard of generating and spreading smoke and toxic gases.

The cable industry, legislative bodies and specifiers that work with the cable industry have been, and continue to be, at the forefront of confronting and minimising these threats. In the USA the UL910 test for plenum cables is a good example of a

requirement for a high level of both resistance to flame propagation and smoke generation. In Europe the EU is conscious of the need to derive tough new standards and specifications which will be implemented across the continent. Cables and flooring are both noted as being particularly important categories requiring ongoing progress. Tests already widely used in Europe include the IEC 332/3, which does not have a smoke requirement. The IEC 1034 (three metre cube test) is often used for smoke assessment.

Cable jacket isolates the internal construction of the cable from the outside world. The outer layer of a wire or cable does not have to be polymeric - lead, steel and aluminium outer jackets are obvious examples, but the various benefits of a more or less flexible polymeric outer jacket have led to their dominance. Perhaps the first example of such a jacket was in 1847 when Werner Siemens supplied 3,000 miles of gutta percha insulated telegraph wire to the Prussian Post Office. Over the years a variety of other polymers have been used with natural rubber being the most significant¹. Also, in recent decades polymers with a degree of inherent flame retardancy have been much used. These include PVC, polychloroprene, CSM, silicone rubbers and FEP. Of these, PVC has dominated many wire and cable applications. Whilst PVC is inherently resistant to ignition it needs to be made more flexible by the addition of plasticisers and because many plasticisers are flammable it is usually necessary to add flame retardants. Among the flame retardants used in PVC wire and cable are antimony trioxide, Sb_2O_3 , aluminium trihydroxide (ATH), $Al(OH)_3$, zinc borates of

which there are various, a commonly used form is $4\text{ZnO} \cdot 6\text{B}_2\text{O}_3 \cdot 7\text{H}_2\text{O}$, ammonium octamolybdate, $(\text{NH}_4)_4 \text{Mo}_8 \text{O}_{26}$, zinc stannate, ZnSnO_3 , zinc hydroxy stannate $\text{ZnSn}(\text{OH})_6$, magnesium hydroxide, $\text{Mg}(\text{OH})_2$, magnesium carbonates including Huntite, $\text{Mg}_3\text{Ca}(\text{CO}_3)_4$, and hydromagnesite, $\text{Mg}_4(\text{CO}_3)_3 (\text{OH})_2 \cdot 3\text{H}_2\text{O}$. Additionally, flame retardant plasticisers and co-plasticisers can be used with PVC and these include phosphates, chlorinated paraffins and brominated plasticisers. Some of the issues of PVC flame retardancy are discussed in more detail below.

A further development in recent years has been the gradual adoption for various high risk or sensitive environments of jacketing with reduced corrosive gas emission in the event of a fire. Such environments include some ships, particularly warships and submarines, computer installations, telephone exchanges, mass transit systems, power stations etc. In practice these requirements have often been met by use of a polyethylene or polyethylene copolymer with an ATH flame retardant filler. Polyethylene vinyl acetates (EVA) have been the main polymers of choice for these ATH based systems in recent years. The reasons are presumably due to the cost / performance ratio of these systems. Developments in polyethylenes and polypropylenes particularly metallocene catalysed grades look likely to have an increasing impact on these types of jacketing in the near future. Other flame retardant fillers that are also used in these low corrosivity jacketings include magnesium hydroxide, zinc stannate, zinc hydroxy stannate and magnesium carbonates. Aspects of low corrosivity flame retarded jackets are discussed further below.

PVC Plenum Formulations

The UL 910, 'Test for Flame-Propagation and Smoke Density Values for Electrical and Optical Fiber Cables Used in Spaces Transporting Environmental Air', is one of the most demanding fire and smoke test for cables in the world today. For many years the polymer combination of choice for this

market has been an FEP (Fluoro-Ethylene Polymer) jacket with either an FEP or PE insulation polymer. FEP has a very high degree of inherent flame retardancy. However, in recent years there has been a growth in the use of PVC as the jacketing material. Usually the insulation polymer used in conjunction with a PVC jacket has been FEP but some developments have managed to meet the test requirements with one or more of the (usually four) conductor pairs being PE insulated. PVC has scope for good flame retardancy due to its high chlorine content but is not noted for good smoke performance. Consequently the challenge for formulators has been to improve smoke outputs whilst maintaining good flame retardancy^{2,3,4}. This has been achieved in a variety of ways including the addition of other flame retarding polymers including CPE and CPVC, flame retardant plasticisers and co-plasticisers, flame retardant and smoke suppressant additives. Generally speaking no single additive achieves the required performance and in practice it seems that a combination of additives based on various of the following elements are used - Al, B, Br, Cl, Mg, Mo, P, Sb, Sn, Zn. It is thus the case that the formulator is usually trying to achieve a synergistic interaction of the various flame retardants and smoke suppressants. A variety of studies have been published on combinations of flame retardants and smoke suppressants for flexible PVC and each sheds light on aspects of what is clearly a complex set of interactions eg for B/Mo/Zn/Sn⁵, Sb/Zn/Sn/Mo⁶, Mo/Sn/Zn⁷. In addition to these mixed systems, which are usually effective at relatively low loadings it is not uncommon to add a fire retardant/smoke suppressant filler which is present in larger amounts. ATH is the most commonly used, but also magnesium hydroxide and the magnesium carbonates described above can have merit.

Wire and cable developments are commercially sensitive. It is thus difficult to generate any 'typical' plenum formulations. However a reading of the patent literature and information published by suppliers keen to promote their own products for use in these markets can give some useful insight.

The data below shows how four formulations perform by cone calorimetry. Formulation A was judged to be adequate by UL910 flame spread criteria but of inadequate smoke performance. The formulation B is believed to have merit as a PVC jacket over an FEP insulation. The cone data for this second formulation was validated to a very limited extent by larger scale testing (Steiner Tunnel)⁶. Formulations C, D and E show much improved performance and would be

of interest to compounders wishing to develop formulations which will allow some replacement of FEP insulation with PE. It must be stressed that the intention here is give examples of flame retardant formulations that are illustrative. The author would not suggest commercial adoption of these formulations without further testing and a review of the patent literature.

Table 1. - Formulation Details (by weight)

	A	B	C	D	E
PVC DS7060	100	100	100	100	100
Elvaloy HP441	-	-	15	15	15
Santisizer 148	30	30	10	10	10
DP45	20	20	25	25	25
ATH	30	30	40	40	40
* H / H	-	-	10	10	10
Irgastab EZ-712	7	7	4	7	7
TBLS	-	-	3	-	-
Antimony Trioxide	-	3.3	3	3	3
** AOM	-	3.3	25	-	10
Zinc Stannate	-	3.3	-	25	15

* H / H = Hydromagnesite / Huntite

** AOM = Ammonium Octamolybdate

Table 2. - Ingredients Functionality and source

PVC DS7060	PVC Resin	Hydro Polymers
Elvaloy HP441	Plasticiser	Dupont
Santisizer 148	Phosphate Plasticiser	Monsanto
DP45	Brominated Plasticiser	Great Lakes
ATH	Flame Retardant/Smoke Suppressant	Alcan Chemicals
H / H	Flame Retardant	Microfine Minerals
Irgastab EZ-712	Stabiliser	Ciba
TBLS	Stabiliser	Cookson
Antimony Trioxide	Flame Retardant	Cookson
AOM	Smoke Suppressant/Flame Retardant	Climax
Zinc Stannate	Flame Retardant/Smoke Suppressant	Alcan Chemicals

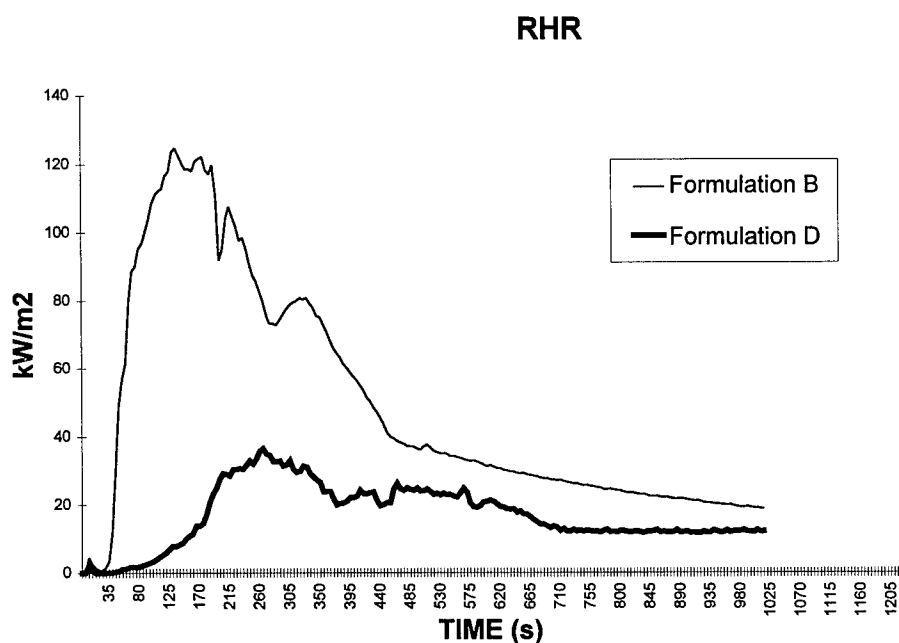
Table 3. - Cone Calorimetry Data (Irradiance = 40 kW/m²).

	A	B	C	D	E
Time to Ignition (s)	48	49	897	705	Did not
* Peak RHR (kW/m ²)	131	128	35	35	-
** Av SEA m ² /kg	777	385	433	342	-

*RHR = Rate of Heat Released.

** Av SEA = Average Specific Extinction Area (a measure of smoke production).

Figure 1. Rate of Heat Release For Formulations B and D.



This data shows the tremendous differences in fire, and particularly smoke, performance that can be achieved in flexible PVC. A comparison of the formulations shows the benefits of trying to maximise synergy between the flame retardant and smoke suppressant ingredients (whilst at the same time minimising the various antagonisms). Relatively high loadings (25 phr) of the key ingredients - AOM or zinc stannate - can give greatly increased resistance to ignition and lowered heat release as is shown in table 3 and in Figure 1.

Interestingly these increased loadings (Formulations CDE) do not dramatically

improve average smoke performance versus the earlier optimized lower loading formulation (B). Formulation E is a material that has sufficient flame retardancy that, at 40 kW/m² irradiance, it does not ignite at all (as defined in the test standard although there is occasional short lived flaming). We can say that 40 kW/m² irradiance is around or below the critical radiation flux for this material. We are now conducting future work at higher irradiance (70 kW/m²). Of course the actual UL910 test utilises a heat flux gradient across the sample in a Steiner Tunnel. So it is not clear that any particular flux is best suited for indicative tests by cone calorimetry. Based on our own work, which

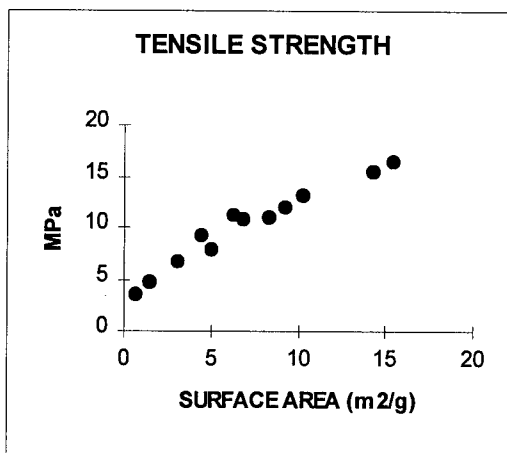
now comprises evaluations of over five hundred test formulations - zinc stannate, ATH, zinc borate, AOM and hydromagnesite / huntite are the additives most notably tolerant of the presence of other FR/SS ingredients. Put another way, they seem usually to give synergistic or additive effects with each other and with other flame retardants such as antimony trioxide.

POLYETHYLENE AND POLYETHYLENE CO-POLYMER FORMULATIONS

There has been considerable commercial growth in recent years of cables jacketed and / or insulated with polyethylene and polyethylene copolymers rendered flame retardant and giving low smoke emission by the addition of flame retardant fillers. The main such filler has been ATH and, to a lesser extent magnesium hydroxides and carbonates. Many commercial cable formulations are a blend of polymers though usually with one type predominating. In practice for many years the major polymer of has been EVA (Polyethylene vinyl acetate) either for 'elastomeric' products with a relatively high vinyl acetate (VA) content (40-50%) or for 'thermoplastic' material containing lower VA (18-24%). PE itself along with EPR, EPDM, EAA and Vamac® also find application in these products. For higher temperature application, such as underbonnet wiring, PP would have merit.

Figure 2 below illustrates the first criterion that is usually addressed when choosing an appropriate flame retardant grade. The formulation for this graph, and indeed the succeeding graphs is a basic formulation and does not contain the various additional and confidential ingredients which compounders and cable companies use to boost the tensile strength further. However it is the case that the same trends are observed in sophisticated commercial formulations. Tensile strength is seen to be a nearly linear function of surface area (all other things being equal).

Figure 2. Tensile strength of ATH in EVA (40% VA)* at 150 phr addition



* Levapren 400

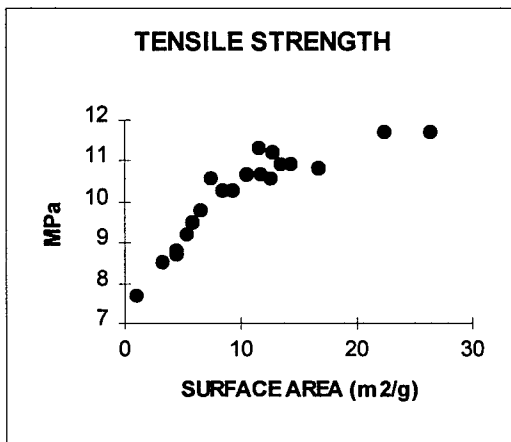
For precipitated ATH, surface area is a function of the reciprocal of median particle size. Therefore the graph above could have been plotted as tensile strength versus particle size to yield a plot in which tensile strength increases as particle size decreases. For commercially available magnesium hydroxides the relationship between surface area and particle size is less clear because of the presence of micro crystallites that can lead to a high surface area at a relatively high particle size. We can simplify this by saying that such grades have a high surface roughness or rugosity. For performance in a cable jacket high surface roughness is usually undesirable, so that choice of an appropriate magnesium hydroxide grade is less simple and generally requires an engineered grade which minimises rugosity. The matter is more simple for magnesium carbonate products since these seem to be derived from a small number of mined deposits and have a basic crystal size of about one micron.

The reasons why tensile strength is an important factor when choosing the flame retardant are twofold. Firstly from a historical perspective these systems have often been used to displace PVC. Jacketing made of PVC had a high tensile strength (above 20 MPa). The new PE based products initially had a much lower tensile strength (below 10 MPa) and so compounders and cable

companies were very keen to find ways and means to narrow this differential. They have succeeded well in this regard in recent years. Secondly, tensile strength is one property where choice of flame retardant grade can have a major impact on performance. Other properties such as elongation, water swell, tear strength and indeed the fire and smoke performance itself are of course affected by FR grade but often in interrelated, rather complex and formulation specific ways. Some of the published literature on these effects is included in the reference section below^{1,8,9,10}.

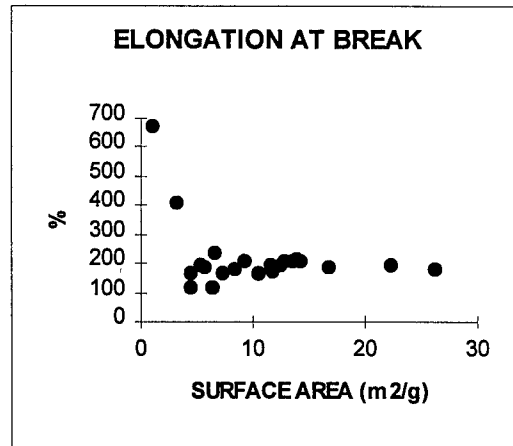
A compounder can blend fillers to fine tune a formulation for various properties. Almost inevitably this involves a set of compromises. The graphs below illustrate the case for blends of ATH products at 150 phr loading in Escorene Ultra 00119 EVA.

Figure 3. Tensile strength of ATH in EVA (19% VA) at 150 phr addition.



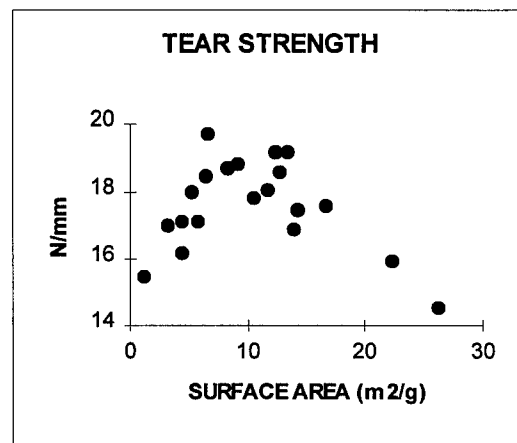
We again see a trend with surface area but no longer the near linearity we saw with a single (monomodal) additive.

Figure 4. Elongation at break.



Elongation seems insensitive to change in surface area except at low surface area i.e. where the particles are mostly relatively large (2-5 microns). Elongation can be dramatically increased by other means including various surface modifications of the filler.

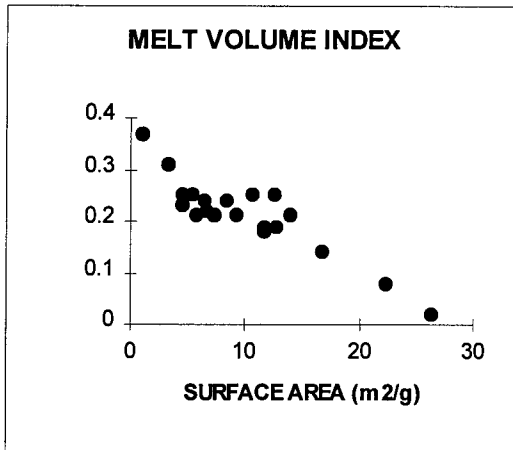
Figure 5. Tear Strength.



Interestingly, we see clear evidence of an optimum surface area of around 9 m²/g in this system at this loading. The possible connection between this curve for a 'thermoplastic' EVA formulation and the very similar curve that can be obtained for impact strength in polypropylene with the same loading of various ATH grades in polypropylene is intriguing¹¹.

Our final figure in this set graph shows us the well known effect of finer fillers giving higher viscosity (decreased MVI).

Figure 6. Melt Volume Index.



It can be seen that despite the scatter there is good scope for selecting a particular set of properties by simple admixture of fillers.

METALLOCENE POLYETHYLENES

Another way the compounder can alter properties is by use of polymer blends. In this regard the relatively recent development of metallocene polyethylenes (mPE) have added useful new options to the cable industry. The suppliers of mPE products suggest that certain grades be blended for different applications. The graphs below show the properties for blends of Dow Engage 8003 with Engage 8411 containing a loading of 180 phr ATH (1 micron - Alcan Superfine 7E).

Figure 7. Tensile Strength with mPE blends containing 180 phr of ATH.

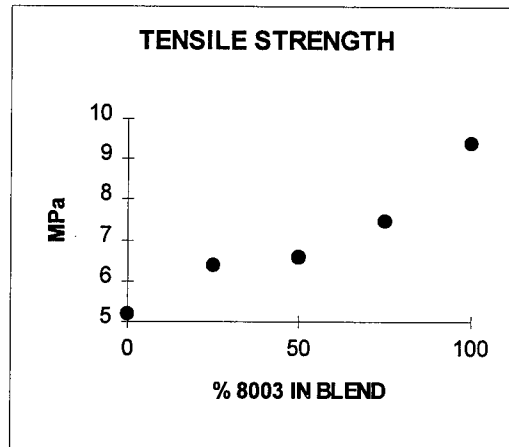
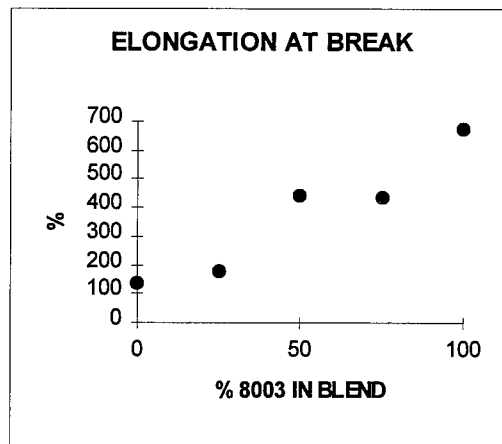
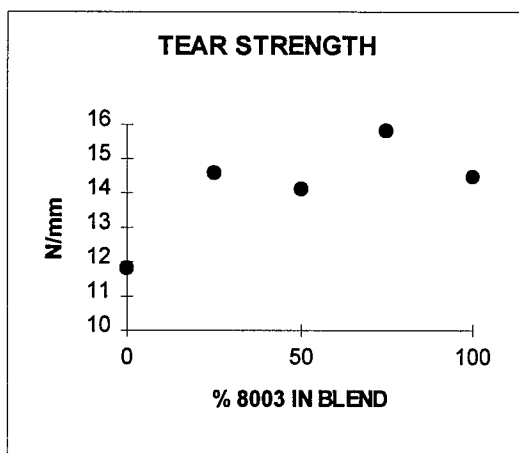


Figure 8. Elongation with mPE blends containing 180 phr of ATH.



In figures 7 and 8 we see elongation trending in the same direction as tensile strength. A useful and fairly unusual finding. Traditionally the trends go in opposite directions as for example in Figures 2 and 3 above. That is, if you modify a formulation to improve tensile strength you make usually elongation worse and vice versa.

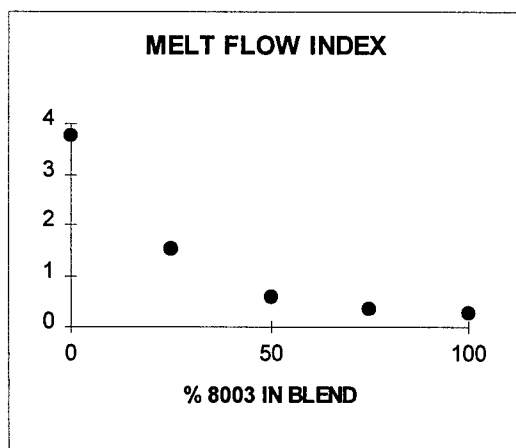
Figure 9. Tear Strength with mPE Blends.



Tear strength seems to show a less clear trend, apparently increasing with % Engage 8003 in the blend, but further work would be needed for greater confidence since unlike the other graphs in this set, tear strength data seems to have significant scatter.

The final figure shows, unsurprisingly, that there is a smooth curve for viscosity of the blends. NB here we use MFI rather than MVI as the viscosity parameter. It has been our experience that the compounding industry are interested in these types of measure but some prefer MFI while others prefer MVI.

Figure 10. MFI with mPE Blends.



When we consider the wide range of options in polymer blends, filler blends and additive

types it is not surprising there are such a wide range of compounds for the cable manufacturer to consider.

From a European perspective it would probably be fair to say that these types of polyethylene co-polymer formulations containing flame retardant / smoke suppressant fillers are now well established in their particular market areas. The initial large differences in technical performance by comparison with previous polymers, notably PVC, have been narrowed in many respects. Significant further commercial expansion, is likely to be due to cost reductions - both materials costs and processing / production costs. To this end the suppliers of flame retardants have to both address the costs of their products and look for ways of helping the compounder and / or cable company to process more cost effectively. This entails improvements in powder characteristics to improve handling and improvements in compound rheology to enable increased production rates.

REFERENCES

1. M.J.Herbert. Fire Retardant Polyolefines in Wire and Cable - Overcoming the Barriers to Better Processing. Conference: COMPOUNDING 92, Sheraton Hotel, Brussels 19-20/2/92.
2. W.Coaker. European Patent 0364717, 1989, assigned to B F Goodrich.
3. H.Naseem. US Patent 4892683, 1990, assigned to Gary Corp.
4. P.Kroushl. US Patent 5227417, 1992, assigned to Cooper.
5. D.J.Ferm , K.K.Shen. The Effect of Zinc Borate in Combination With Ammonium Octamolybdate or Zinc Stannate on Smoke Suppression in Flexible PVC. Journal of Vinyl & Additive Technology, March 1997, Vol 3, No. 1.
6. M.J.Herbert. PVC Cable Sheathing With Improved Smoke Characteristics. Conference: FR96. Queen Elizabeth

Conference Centre, London, 17-18 Jan 96, pub by Interscience, pp 157-172, ISBN 0 9516320 8 6.

7. P.M.Cook, L.L.Musselman. New Test Results on Mechanism and Performance of Molybdenum, Tin and Zinc Based Flame and Smoke Suppressants for Halogenated Polymers. BCC Flame Retardancy Conference - June 2-4, 1997, Stamford, CT.

8. M.J.Herbert. Cone Calorimetric Evaluations of ATH filled EVA. Conference: Flame Retardants 94, Queen Elizabeth Conference Centre, London, 26-7 Jan 94, pub by Interscience , pp 59-71, ISBN 0 9516320 5 1.

9. M.J.Herbert. Optimization of ATH Filler Properties in EVA Copolymers for Flame Retardant Cable Applications. Conference (supp): CABLES AND FIRE PROTECTION, Heathrow Penta, 16/1/92.

10. S.C.Brown, M.J.Herbert. New Developments in ATH Technology and Applications. Conference: FR 92, Queen Elizabeth Conference Centre, London 22-23/1/92 ISBN 1-85166-758-X pp 100-119 PUBLISHER:Elsevier.

11. S. C. Brown unpublished data. Available on request.

BIOGRAPHY

Steve Brown is Manager for flame retardant developments at Alcan Chemicals research headquarters in Banbury, Oxfordshire, England. He has worked on flame retardants for twenty years and holds several patents in the field. He has a B.A. in mathematics and computer science. His business address is:- Alcan Chemicals Ltd, Southam Road, Banbury, Oxon, Great Britain.



THE LONG TERM BEHAVIOUR OF HALOGEN FREE, FLAME RETARDANT MATERIAL UNDER DIVERSE CONDITIONS

Marie Nilsson, Karin Nygård-Skalman, Marie-Cristin Ljung
Ericsson Cables AB, Hudiksvall, Sweden

ABSTRACT

The ageing properties of four flame retardant halogen free (FRHF) jacketing materials have been studied and evaluated. The material was subjected to accelerated ageing in two ways. Firstly, by varying the temperature whilst holding the ambient conditions constant; i.e. the material was surrounded by air, water or cable filling compound for 10700 h. Secondly by applying Weather-O-Meter ageing; an artificial ageing test to simulate outdoor conditions, i.e. sunlight, humidity and temperature in varying combinations and intensities.

The material degradation has been followed by observing the change of the mechanical properties and oxygen induction time.

On the basis of the accelerated test results a life time prediction has been made.

INTRODUCTION

During the last few years the cable industry has experienced an increased demand for halogen free, flame retardant materials. As a part of this development, the requirements for the use of these materials has broadened.

The halogen free flame retardant material is relatively new to the market whereas material like polyethylene (PE) and polyvinyl chloride (PVC) have been used for decades.

Although these materials have been studied^{1,2} intensively during the last ten years, predictions about life time have still to be based on simulation by short term accelerated ageing tests.

The drawback to accelerated ageing is partly that the raised temperature can initiate chemical breakdown that would not have occurred at room temperature and partly that account is not taken of the energy interaction that may occur. Weather-O-Meter ageing, which is carried out in an artificial climate, can be used to study the interaction of humidity, heat and UV radiation.

The readily available FRHF material is often a thermoplastic polyolefin, based on co-

polymers of PE and/or ethylene vinyl acetate (EVA). To make the material flame retardant, aluminium oxide trihydrate ($2[Al_2O_3(H_2O)_3]$) or magnesium hydroxide ($MgO(2H_2O)$) is usually added.

Materials with high filler concentration like FRHF material can be sensitive to external influence from, for example, water or chemicals. The study of this influence is important to ensure the right environment for the material.

This study aims at understanding the changes over time which may influence the efficacy of the flame retardant halogen free material in use and determine the lifetime when exposed to different environments.

FLAME RETARDANTS

Polymers containing halogens, i.e. PVC, have been used by the cable industry for many years. The advantages of the PVC type of material are low cost, easy production processes and the accumulation of knowledge after many years of use. The disadvantage is that toxic and corrosive gases evolved during thermal breakdown are harmful to people and equipment. PVC also may create enough smoke to hamper the normal fire fighting procedures. Moreover, a burning PVC cable may spread the fire zone.

It is probably these factors which have led to the interest in flame retardant halogen free polymers.

There is today a number of flame retardant polymers. The commonest flame retarder for polyolefines has been aluminium oxide trihydrate but the use of magnesium hydroxide is increasingly being used.

The flame retardant process³ occurs in three stages. The total reaction for the previously mentioned material is shown in Figure 1.

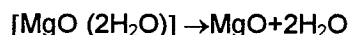
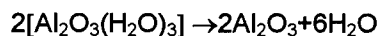


Figure 1. The flame retarding reaction during a fire.

Stage one is the endothermal dehydration process which cools the breakdown products. Then, water produced by the flame retardant material thins the evolved volatile products. Finally, aluminium oxide (Al_2O_3) or magnesium oxide (MgO) ash deposits on the surface protecting the underlying polymer.

MATERIAL

The materials which have been evaluated are thermoplastic compounds based on PE and EVA. The amount of EVA differs as does the choice of flame retarder. The material data is shown in Table 1.

Material	A	B	C	D
Polymer Base	EVA	PE/EVA	PE/EVA	PE/EVA
Flame Retardant Agent	Mg(OH)	Al(OH)	Al(OH)	Mg(OH)
LOI, %O ₂	45	35	42	39
Specific gravity, g/cm ³	1.46	1.58	1.58	1.50

Table 1. Material data.

PROCESSING

The test pieces were prepared by extruding a ribbon in a laboratory extruder, see Table 2. A single flight screw, 20D/30 mm, compression ratio 2.5:1 and a ribbon die with an orifice of 29.4 x 1.1 mm were used during extrusion. No strainer was used. The draw down is the ratio between the die orifice and the ribbon cross sectional area (Table 2).

Material	Draw down ratio	Screw speed (rpm)	Temperature set (°C)
A	1.3:1	40	150-160-170-180-190
B	1.4:1	40	130-140-150-160-165
C	1.2:1	40	130-140-150-160-165
D	1.6:1	40	150-180-190-200-210

Table 2. Processing data.

It is preferable to use a low compression screw with the extrusion of material B and C. The reason is that these materials, which are filled with inorganic flame retarder, have a tendency to generate heat through friction and excess pressure in the extruder.

This does not apply to material A or D even though these too are filled but with magnesiumhydroxide rather than aluminium oxide trihydrate.

A screw with higher compression ratio may be used with materials rich in magnesium hydroxide as they can stand a higher extruding temperature than aluminium oxide trihydrate rich materials.

METHODS

The study aimed at simulating the varying environments a material might experience. Four different surroundings were chosen:

- 1: Dry air
- 2: Tap water
- 3: Cable filling compound
- 4: Weather-O-Meter (UV-exposure)

Item 1: simulates indoor conditions, 2 : underground outdoor conditions, 3: application for cables filled with cable filling compound and 4 :simulates outdoor UV-radiation. A complete test schedule is shown in Table 3.

Environments	Time (h)	Temperature (°C)
Air	1350, 2400, 5400, 10700	80, 90, 100
Water	1350, 2400, 5400, 10700	60, 70, 80
Cable filling compound	1350, 2400, 5400, 10700	70, 80, 90

Table 3. Ageing test schedule

The Weather-O-Meter method is an artificial outdoor simulator where humidity, heat and UV-radiation are periodically applied to the material. An Atlas Weather-O-Meter Ci65 is used. The tests for materials B and D were carried out in accordance with DIN 53387.

The categorising of polymer material lifetime⁴ is usually made in accordance with IEC 216 which estimates the material life time at different temperatures. From these data the life time is extrapolated using the actual service temperature. This extrapolation assumes that material breakdown follows the Arrhenius relationship.

Breakdown is measured, utilising the tensile strength, the elongation at break⁵ and the oxygen induction time⁶ (OIT).

The material life time was considered to have been determined when the tensile strength and the elongation had fallen to 50 % of the initial value.

RESULTS

Ageing in air

Ageing in air is normally carried out in an oven to test the stability against oxidation of that material. No mechanical or OIT breakdown was detected for material B, C or D at any measured temperature.

Figure 2 shows that the tensile strength for B, C and D is unchanged for ageing at 90°C. Material A shows a rapid decrease in tensile strength subsequently levelling out to a constant value. The difference of breakdown is more pronounced for the elongation at break (see Figure 3) where elongation for material A reduces substantially whilst the other materials are hardly changed in value. Material A consists mostly of EVA which is thermally unstable over 100°C. For the same reason it was not possible practically, to measure the mechanical properties at 100°C because the test pieces hanging in the oven fell.

Oxidation is the commonest breakdown mechanism⁷ during the ageing of polymers in dry air. During the initial stage of the reaction there is normally no visible evidence that any change in the material has occurred. Subsequently the rate of oxidation increases rapidly due to self catalysing. This oxidation often leads to a change in colour and a reduction of the molecular mass (chain scission). It is also possible for cross linking to occur thus increasing the ultimate tensile strength of the material. By adding antioxidants and stabilisers the onset of oxidation can be delayed. The process can be followed by OIT or by FTIR (Fourier Transform InfraRed spectroscopy).

FTIR observations⁸ could not reveal any sign of breakdown products. The materials B, C and D showed a significant colour change after 10700 h compared with 5400 h indicating that an oxidation reaction had begun. Since there was no change in the molecular structure of the material the reaction is, in all probability, a chain scission process. Common breakdown products⁹, especially from polyethylene, are hydroperoxides, which display a characteristic absorption peak at 3550 nm. However, it is difficult to be sure whether such a peak was generated after ageing in air as the stabiliser system peaks occur in the same area.

The Arrhenius relationship could not be utilised with the ageing in air for materials B, C and D because, at the test temperatures used, no breakdown occurred. To determine the lifetime, the Montsinger rule was used instead.

This rule assumes that the breakdown rate doubles for every 10°C rise in temperature. Using this rule and with a minimum of 5400 h at 80°C the predicted lifetime is 40 years at 20°C. A life time prediction for material A was not possible to accomplish because of too rapid degradation of the material in the tested temperatures. Since the material is thermally unstable in high temperatures a new test with lower temperature would be more suitable.

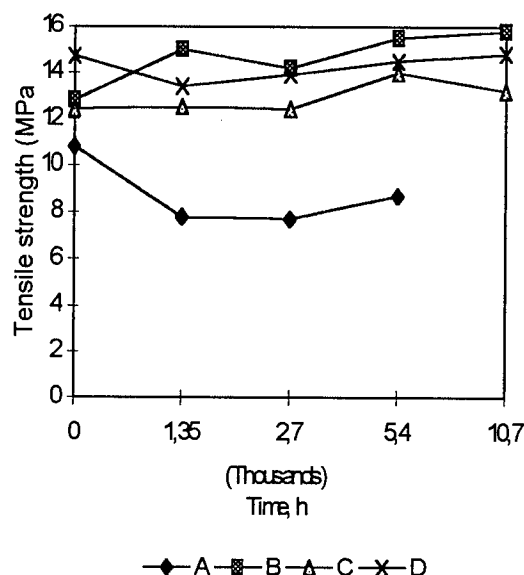


Figure 2. Tensile strength after ageing in dry air at 90 °C.

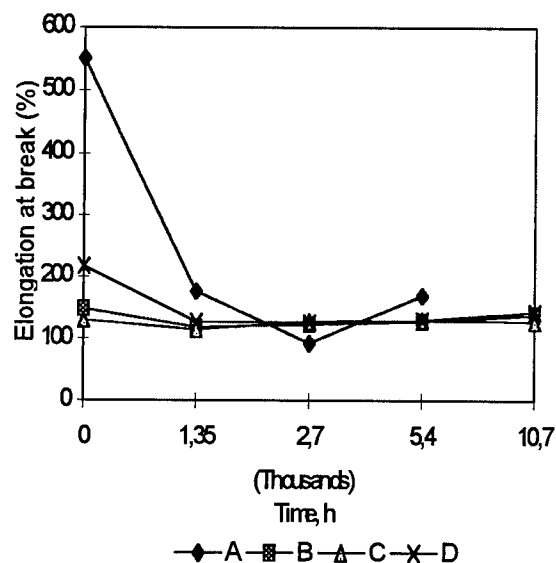


Figure 3. Elongation at break after ageing in dry air at 90 °C.

Ageing in water

Ageing in water showed a great diversity in mechanical properties between materials. The test results (Table 4) shows that material A and C breaks down rapidly between 70° and 80° C. It can be noted from Figures 5 and 6 that the reduction in the ultimate tensile strength and the ultimate elongation occurs during the first 1350 hours subsequently levelling out to a constant value.

A visual inspection of test pieces for A and C shows blistering of the material. This indicates that water has probably diffused in between the flame retarder and the polymer chain. Along this water barrier the interfacial strength is lower thereby reducing the mechanical properties.

For material B a reduction in the mechanical properties can clearly be seen at 80° C which probably is a critical migration temperature.

This can be confirmed by a visual inspection of the test pieces which shows much more blistering at 80° C than at 70° C. The rate with which the diffusion process progresses may dominate at elevated temperatures whilst being much slower during normal conditions.

Material D shows the lowest breakdown in the water ageing mechanical properties which occurred after 4700 h at 80° C (Figure 4).

This predicts a life expectancy of 34 years at 20° C.

It was not possible to determine the lifetime for other materials because the breakdown progressed too quickly.

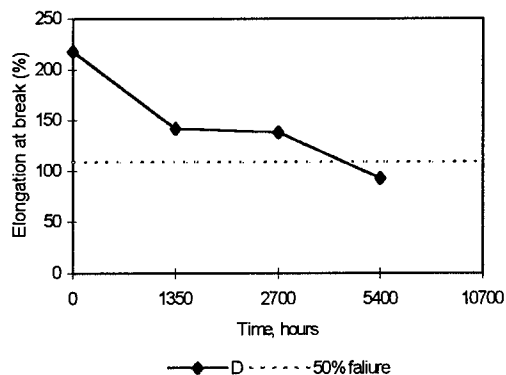


Figure 4. Elongation at break for material D after ageing in water at 80 °C.

Colour change in the material is a typical indication of thermal breakdown. For materials A and D this colour change is clear. This can be confirmed using an FTIR which shows a reduction of the stabilisers over time.

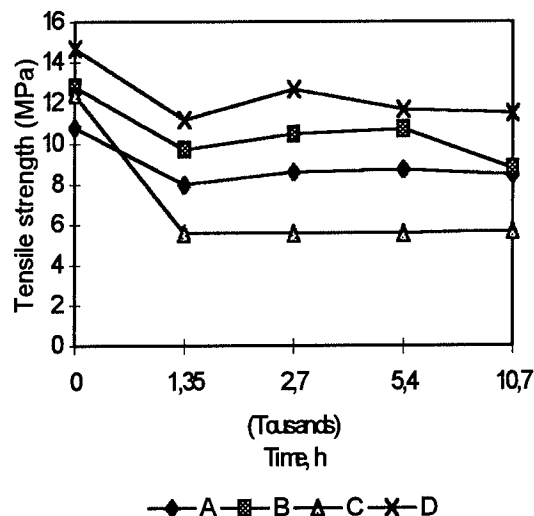


Figure 5. Tensile strength after ageing in water at 70 °C.

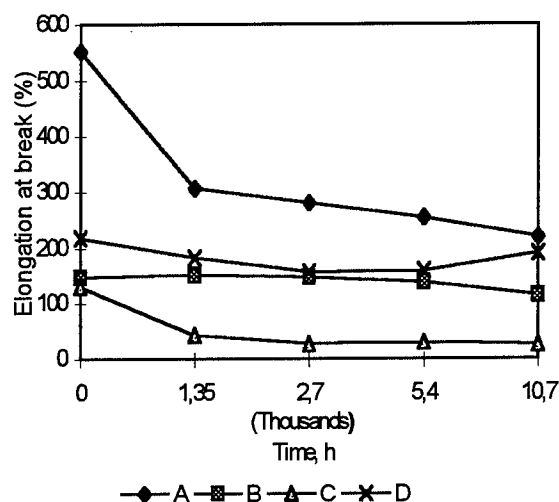


Figure 6. Elongation at break after ageing in water 70 °C.

Time (h)	Temp (C)	A		B		C		D	
		Tensile Strength (MPa)	Elongation (%)	Tensile Strength (MPa)	Elongation (%)	Tensile Strength (MPa)	Elongation (%)	Tensile Strength (MPa)	Elongation (%)
Prior ageing		10.8	552	12.8	148	12.4	130	14.7	218
1350	60	8	333	10.5	160	9.4	125	11.6	214
	70	8	306	9.7	151	5.6	43	11.2	183
	80	8.1	174	6.7	32	5.1	35	10.7	142
2700	60	8.3	237	10.8	169	9.2	120	13.1	172
	70	8.6	281	10.5	148	5.6	28	12.7	157
	80	8.9	147	6.4	20	5	27	11.3	138
5400	60	8.7	370	10.9	168	9.6	123	12.8	173
	70	8.7	254	10.7	138	5.6	30	11.7	159
	80	7.9	100	6.8	29	5.3	30	9	93
10700	60	8.8	226	11.2	165	8.4	95	12.1	213
	70	8.4	219	8.8	115	5.7	26	11.5	190
	80								

Table 4. Mechanical properties after ageing in water.

Ageing in cable filling compound

The compound used for the tests is a thixotropic compound consisting of polyalphaolefins. Material breakdown in the compound has proved to be highly temperature dependant. This can be observed in Table 7 where it can be seen that ageing at 70° C alone produced approved values. (Figures 7 and 8)

With ageing at 80° and 90° C the mechanical properties deteriorated rapidly and a significant mass increase could be observed (Table 6).

OIT measurements show that materials B and C were subject to less breakdown whilst A and D have a lower OIT-value by 1350 hours at 70° C. (see Table 5). The test pieces for material A were in such bad condition that they disintegrated when lifted from the filling compound after 2700 h. Material B has a critical temperature at 80° C as it had for water. After 5400 h at 80° C and 90° C the samples B, C and D had broken down to the extent that they disintegrated when lifted from the filling compound.

Ageing/Material	B (min)	C	D
1350 h, 80 °C	27	>60	10
2700 h, 80 °C	26	>60	2
5400 h, 80 °C	10.5	>60	---

Table 5. OIT after ageing in cable filling compound.

An FTIR examination of the aged polymers shows an increase in the peaks characteristic for cable filling compound. This result, together with the increase in mass after ageing, indicates absorption of the compound by the material.

These ageing test signify that non of the tested flame retardant material should be subjected to cable filling compound.

Time (h)	Temp (C)	A (%)	B (%)	C (%)	D (%)
1350	70	11.3	8.1	7.6	10.0
	80		19.4	13.2	12.9
	90		13.3	23.4	17.1
2700	70	7.4	5.4	5.7	7.7
	80		14.7	13.0	11.8
	90		8.4	16.5	13.5
5400	70	7.7	5.3	7.5	7.4
	80		11.9	11.7	9.3
	90		9.5	17.5	11.2
10700	70	11.1	9.7	8.7	8.4
	80		14.5	11.9	8.8
	90				15.5

Table 6. Percentage mass increase after ageing in cable filling compound. The shaded areas represent totally broken down test samples.

Time (h)	Temp (°C)	A		B		C		D	
		Tensile Strength (MPa)	Elongation (%)	Tensile Strength (MPa)	Elongation (%)	Tensile Strength (MPa)	Elongation (%)	Tensile Strength (MPa)	Elongation (%)
Before ageing		10.8	552	12.8	148	12.4	130	14.7	218
1350	70	7.2	609	8	151	7.5	140	8.8	159
	80			3.1	151	5.1	149	6.5	146
	90			2	92			5.1	142
2700	70	7.7	632	9.2	149	8.6	133	8.9	146
	80			2.6	113	4.9	147	6.9	137
	90			2.3	79	2.2	61	4.9	110
5400	70	7.4	588	8.8	153	8.5	136	9.2	142
	80								
	90								
10700	70	7.2	634	8.6	174	7.8	151	9.4	166
	80								
	90								

Table 7. Mechanical properties after ageing in cable filling compound.

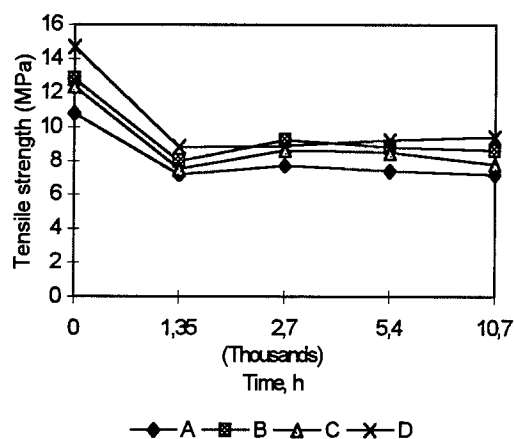


Figure 7. Tensile strength after ageing in cable filling compound at 70 °C.

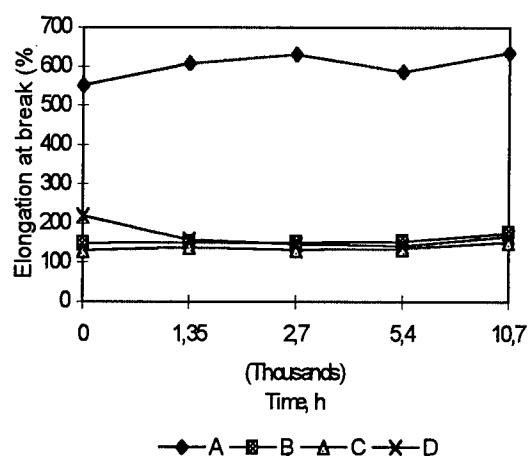


Figure 8. Elongation at break after ageing in cable filling compound at 70 °C.

Ageing in Weather-O-Meter (W-O-M)

An Atlas Weather-O-Meter Ci65, using a Xenon-Arc lamp, was used for UV-radiation ageing at 340 nm. The ambient temperature in the test area was 25° C, the relative humidity 65 % and the black panel temperature 45° C. The test cycle comprised 18 minuets water spraying, 120 minuets irradiation (simulated sun light) and 18 minuets drying.

Only materials B and D had acceptable values when aged in water and were, therefore, suitable for use in this test.

It can be observed from Figures 9 and 10 that the breakdown of material B is rapid. Conversely material D exhibits good mechanical properties. The explanation is that D is UV-stabilised and B is not.

An FTIR spectrum was acquired for material D after ageing for 8000 h. The material was broken down totally in respect of mechanical properties. Despite this the FTIR spectrum did not reveal any changes in the molecular structure of the material. This implies that the breakdown mechanism is a chain scission process.

To determine the lifetime, the rule that 1000 h is equivalent to 1 year outside implies that material D is good for 7 years.

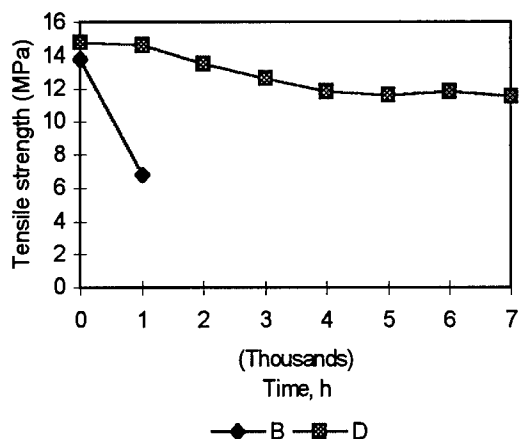


Figure 9. Tensile strength after ageing in Weather-O-Meter.

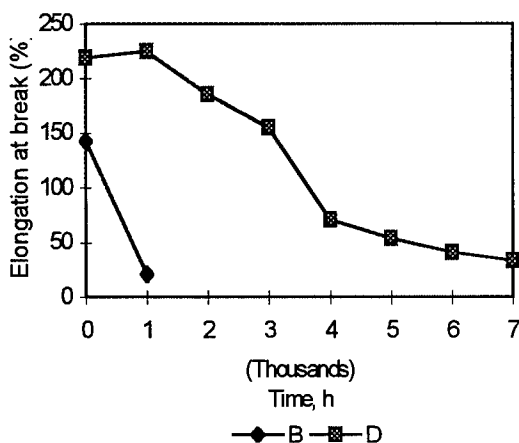


Figure 10. Elongation at break after ageing in Weather-O-Meter.

CONCLUSIONS

The flame retardant halogen free materials which have been tested exhibit substantially different susceptibilities to differing environments.

The Montsinger, rule, that breakdown doubles for every 10° C rise in temperature, has been used in determining the lifetimes of the materials. In some cases breakdown was so rapid that it was not possible to distinguish the

time in relation to the temperature. In other cases it was so slow that, at best, only one breakdown value could be registered. These two factors precluded the use of the Arrhenius relationship in determining the material lifetime.

Determination of material lifetime in dry air proved difficult due to the material stability under those conditions. Using Montsingers rule, for materials B, C and D, it was possible to determine a service lifetime of over 40 years at a service temperature of 20° C. A life time prediction for material A was not possible because of too rapid degradation.

Determination of material lifetime in water yielded a greater variation between materials than in air. Material D has a slow degradation process in water giving it an expected lifetime of 34 years at 20° C. It was not possible to determine the lifetime for other materials because the breakdown progressed too quickly.

Ageing in cable filling compound shows that the tested FRHF materials should not come into contact with this compound.

Weather-O-Meter ageing showed that material D possessed relatively good outdoor properties.

As already mention, the four materials tested incorporated differing amounts of EVA. Material A had most EVA followed by C, B and D. The low melting temperature of EVA accounts for the thermal instability of A at raised temperatures.

Ageing in water confirmed that the greater the amount of EVA in a material the poorer were the mechanical properties.

In conclusion, to be able to choose a flame retardent material for telecommunication cables the environmental conditions has to be clearly defined.

To establish these condition the material requires continuous testing.

REFERENCES

1. Grüner-Nielsen L., Hasløv P. and Skovgaard N. H.; "Short and Long Term Behaviour of Halogen Free Fire Retardant Cable Materials in Different Environments". Proceedings of the 41th IWCS, pp 321-331. 1992.
2. Artingstall S., Taylor J. and Pyle A.J.; "Recent Advances in Thermoplastic, Zero Halogen, Low Smoke, Fire Retardant Cable Compound Technology". Proceedings of the 36th IWCS, pp 254-264. 1987.
3. Troitzsch J.; "International Plastics Flammability Handbook". 1990
4. IEC 216 part 1 to 5, "Guide for determination of thermal endurance properties of electrical insulating materials". 1990.
5. IEC 811-1-1-9, "Common test methods for insulating and sheathing materials of electric cables-Test for determining the mechanical properties". 1985
6. ASTM 4565, "Physical and Environmental Performance Properties of Insulation and Jackets for Telecommunication Wire and Cable". 1990
7. Kelen T.; "Polymer Degradation". Van Nostrand Reinhold Company Inc..1983
8. Grassie N. and Scott G.; "Polymer Degradation and Stabilisation". Cambridge University Press. 1985.
9. Silverstein R.M., Bassler G.C. and Morrill T.C.; "Spectrometric Identification of Organic Compounds". John Wiley & Sons Inc. 1991.

AUTHORS



Mrs. Marie Nilsson received her M.Sc. at the University of Gothenburg in Chemistry 1994. She has been working at Ericsson Cables Telecom Cables Division since 1996. At present she is working as group manager of polymer materials at the Material Technology Department.



Mrs. Karin Nygård-Skalman received her M.Sc. in Chemical Engineering at the Royal Institute of Technology, Stockholm in 1982. She has been working at Ericsson Cables Telecom Cables Division since 1984. At present she is responsible for the Material Technology Department.



Mrs. Marie-Cristin Ljung received her M.Sc. in Chemical Engineering at the Royal Institute of Technology, Stockholm in 1990. She has been working at Ericsson Cables Telecom Cables Division since 1992. At present she is working as a production leader.

HIGHLY STABILIZED FLAME RETARDED POLYOLEFIN INSULATION COMPOUNDS

L. Y. Lee

Millennium Petrochemicals Inc., Cincinnati, Ohio

ABSTRACT

Polyolefin compounds used in many residential and industrial wire insulations are often required to have a balance of properties in electrical, physical, processability, and flame retardancy to meet material specifications. In applications which demand high service temperatures and thermal stability, these compounds are further crosslinked either chemically or with irradiation, and stabilized with high levels of antioxidants.

Strategies to design flame retarded (FR) insulation materials with a specific target for a 150° C rated appliance wire insulation is the subject of this paper. Approaches to use different technologies in FR, antioxidants (AO), and crosslinking to achieve a balance of properties are discussed as well as the effects of base resin, halogenated vs. non-halogenated FR additives, and copper catalyzed thermal degradation. Experimental design was used to optimize the compound's performance in oven aging and cure efficiency.

INTRODUCTION

Polyolefinic materials used to make cable insulation in low voltage (less than 1kv) applications such as power cables, control cables, and appliance wire are required to have a multitude of properties compliant with the UL 44 standard and the various application-specific styles. Often times, end users demand even higher performance levels than those specified in the standards. Hence this class of compounds represents significant technical and development challenge to the material suppliers. A broad knowledge of flame retardant, antioxidant, base resin, filler, and processing to achieve a balance of properties is critical in designing these compounds.

Recent advances in areas of flame retardant, antioxidant, and related technologies¹⁻⁴ signal there are opportunities to improve product performance and cost effectiveness. The current specifications for the 150° C rated appliance wire insulation require heat aging at 158°C for 150 days and VW-1 flame resistance.

The intrinsic difficulty in achieving long term heat stability is the need to have a high level of antioxidant which causes problems in compatibility (blooming), chemical interference leading to poor cure and high cost. Another issue in thermal stability is the detrimental copper effect as a result of the insulation having direct contact with the conductor. Conventional metal deactivating antioxidants are effective only in lower temperature ranges and are limited to thermoplastic applications.

The need for high levels of antioxidants creates a difficulty in crosslinking. Hindered phenolics which are effective long term thermal stabilizers invariably interfere with peroxide crosslinking, and to a lesser extent, with irradiation crosslinking.⁵ Simple addition of more AO or peroxide does not necessarily improve their performance, but rather may diminish their effectiveness.

It is the intent of this paper to describe work to design crosslinkable FR insulation compounds with high thermal stability. Experimental results in studying the effects of base resin, FR additives, and copper-catalyzed degradation in oven aging are presented. These results were used in the design of a 150° C compound. Experimental design was employed in the study to optimize heat aging and cure and its performance was compared to a commercial product.

EXPERIMENTAL

Sample Preparation

Heat age samples were made by blending the components in a 240 cc Brabender for 8 min. at a melt temperature applicable to the base resin. All additives were commercial grade and used without further purification. The resulting mixture was prepared according to ASTM D638 method for tensile and elongation testing. The samples were compression-cured for 20 min at 375° F. The specimens were aged in a convection oven at the preset temperature. The test for brittleness was determined by bending and pulling the specimen several times. The specimen fails if any crack appears. Three replicates were used for each sample.

Wire Coating

Wire samples were made on a 3.5 " dia. extruder with a 20/1 L/D. The temperature profile was set at 220-235° F on the various zones. The wire construction consisted of #18 16/30 tin coated copper conductor with 30 mil wall thickness.

Experimental Design Program

Experimental design, model fitting and analyses were done with JMP version 3.1 from SAS Institute Inc. on an IBM PS/2E computer. The Box-Behnken table was generated from the response surface design selection. Model fitting was done in the response surface/effects screening mode. The resulting parameters were analyzed. Higher order terms (other than the liner coefficients) that contained probability t values greater than 0.01 were deleted and the fitting step was repeated. This iteration process continued until the remaining terms had t values < 0.001.

RESULTS AND DISCUSSION

Screening of AO Systems and Copper Effects in Accelerated Heat Aging

Long term thermal stability of polyolefin compounds is inherently difficult to assess due to the length of testing period. The accepted requirement for the 150° C rated appliance wire is >50% retention of elongation after 150 days at

158° C. To reduce the test duration an accelerated test at 180° C for 21 days was chosen to evaluate several primary AO systems. There are concerns in the validity of accelerated testing, however. It is recognized that there are controversies in applying the Arrhenius law in heat aging.⁶ Physical processes such as deformation, molecular diffusion, and annealing all contribute to the overall temperature dependence in addition to chemical degradation. These factors, however, are less significant in crosslinked filled polymers where chain mobility is severely limited.

After screening nearly thirty different AO formulations covering the general classes of stabilizers used in polyolefins, three systems were selected for further study. They were AO1, a package currently used in a commercial XL polyethylene compound which consists of a hindered phenol and a thioester; AO2, a system consisting of a hindered phenol and a sulfur-containing additive and AO3, a proprietary system developed internally which contains no phenolics. The AO's were tested at normal levels and high levels in two types of ethylene-copolymers which were selected for filler/additive compatibility. The copolymers chosen were ethylene-n-butyl acrylate (EnBA) and ethylene-vinyl acetate (EVA) at comparable monomer content (18% w/w). Copper powder was added at 100 ppm for evaluating copper-catalyzed degradation. Plaque samples containing 1.3% Vulcup[®] were cured and heat aged at 180° C until cracking or brittleness was observed. The results are given in Table 1.

TABLE 1 SCREENING OF AO SYSTEMS
(Days to brittleness)

AO SYSTEMS	XL-EVA	XL-EVA	XL-EnBA	XL-EnBA
	No Cu	100 ppm Cu	No Cu	100 ppm Cu
A01 (NORMAL LEVEL)	10	7	11	6
A02 (NORMAL LEVEL)	9	7	13	10
A02 (HIGH LEVEL)	15	11	14	10
A03 (NORMAL LEVEL)	11	8	12	9
A03 (HIGH LEVEL)	21	11	17	10

As seen, both commercial AO systems failed to reach 21 days even in the absence of copper. The new AO package at high level reached 21 days without copper but fell to 11 days with copper. The copper effect is significant as polymer integrity was decreased 20-50%.

The mechanism of copper catalyzed autooxidation of polymers is well-documented.⁷ It is believed that copper ions (I and II) accelerate the decomposition of polymer hydroperoxides to chain degrading radical species. Utilization of chelate chemistry to immobilize copper ions has been used to develop deactivators. The copper deactivator currently used in telecommunication insulation, Irganox[®] 1024 is very effective because of its hydrazine functional group in addition to the hindered phenolic groups. However, its commercial success is largely limited to thermoplastics where aging temperatures seldom go above 120° C. To determine whether Irganox 1024 is useful at higher temperatures, it was added to AO1 in EVA and aged at 165 and 180° C. In this experiment, passing was >50% elongation retention. The results are given in Table 2.

TABLE 2 EFFECTS OF Cu DEACTIVATOR

SAMPLE	AO1Level	Irganox 1024 (%)	Cu (ppm)	165 C	180 C
1	NORMAL	NONE	200	FAIL	FAIL
2	NORMAL	0.1	200	PASS	FAIL
3	HIGH	0.1	200	PASS	FAIL
4	NORMAL	0.1	NONE	PASS	FAIL
5	HIGH	0.1	NONE	PASS	PASS

Samples 1-3 are controls to show that 200 ppm Cu was sufficient to cause AO1 to fail at the normal level (Sample 1). In the absence of Cu, adding 0.1 % Irganox 1024 to AO1 at the normal level enabled the resin to pass at 165° C (but not at 180° C) and passed both temperatures at the higher AO1 level. Samples 4 & 5 show that the metal deactivator is ineffective at 180° C.

FR and Base Resin Effects in Accelerated Heat Aging

The knowledge of how FR additives influence resin thermal stability (not combustion property) is largely empirically based. In theory, additives that produce reactive species that catalyze polymer degradation are detrimental to heat aging. Conversely, additives that scavenge harmful species help stabilize resins. Bromine FR additives are not known to have harmful effects in polyethylenes although corrosive bromine species may be produced at higher temperatures. Hydrated fillers such as aluminum trihydrate and magnesium hydroxide which have basic surfaces can neutralize acidic species. There are very few published studies⁸ on these effects, thus it was

instructive to compare several FR packages their impact on heat aging. Four bromine-antimony oxide systems (11% total) and one non-halogenated additive (30%) were tested with AO3 and the results are given in Table 3.

TABLE 3 EFFECTS OF FR IN HEAT AGING

FR SYSTEM S	DAYS TO BRITTLINESS	Br TYPE
NONE	10	-----
BR-FR 1	19	AROMATIC Br, WITHO, N
BR-FR 2	17	AROMATIC Br ONLY
BR-FR 3	15	AROMATIC Br, WITHO
BR-FR 4	12	ALIPHATIC Br, WITHO
NON-HAL	15	-----

There is no systematic similarity in the bromine additives except that they are all commercially available. BR-1 contains aromatic Br, O, and N; BR-2 contains aromatic Br only; BR-3 contains aromatic Br and O; and BR-4 contains aliphatic Br and O. Oven aging at 180° C indicated that the FR additives improved stability substantially in the presence of copper. With BR-1 the extension of stability to 19 days was particularly encouraging.

The mechanism of the observed enhancement due to Br additive and whether this synergy exists in other AO systems remains unknown. The fact that BR-1 contains both O and N and also gave the best improvement suggests that the additive itself or its impurities may have some copper complexation properties thereby counteracting some of the copper effects. Although not addressed in the current study, this apparent synergy would be an interesting area to investigate with more refined analytical techniques such as TGA. An understanding of the mechanism could lead to developing a more robust metal-deactivator that is useful in high temperature applications.

Copolymers such as ethylene-vinyl acetate and ethylene-ethyl acrylic acid are generally used to make highly filled compounds because of their good flexibility and additive compatibility. The disadvantages, however, are their lower thermal stability and electrical insulation due to the presence of large number of polar side chain. In this study we have investigated three resins for heat aging. They were EVA, EnBA, and EMA. AO3 and BR-1 were added to each

and aged at 180° C until brittleness. As seen in Table 4, EnBA yielded the best results while EMA gave the poorest.

TABLE 4 EFFECTS OF BASE RESIN IN HEAT AGING

RESIN	HEAT AGE (DAYS)
EVA	16
EnBA 1	17
EnBA 2	16
EMA	13

Several factors have to be considered in speculating the heat aging performance of the resins. First, copolymer stability is largely determined by the ease of breaking the side chain from the polymer backbone. Since EVA contains C-O bonds (60-65 kcal/mole) which are weaker than C-C bonds (70-75 kcal/mole) in EnBA and EMA, one would expect EVA to be the least stable. Another factor is diffusion of decomposed species within the polymer matrix to catalyze degradation, especially if they are acidic. It is speculated that EnBA would decompose to give n-butyric acid or butanol which diffuses slower than acetic acid or methanol as in EVA or EMA. Finally, crosslinking via ester groups in these polymers leading to loss of elongation (brittleness) could be significant, especially with EMA. It is very difficult to establish which of these factors is the main reason for EnBA's superior heat stability.

Flame Retardance and Physical Properties of Insulation Compounds

The UL 44 standard specifies a VW-1 FR rating for most of the low voltage appliance wires. To achieve this level of fire resistance requires substantial amount of flame retardants. Invariably the electrical insulative and physical properties of the resin suffer. Non-halogenated FR additives such as ATH and magnesium hydroxide have advanced in recent years mainly in coating technologies to improve polymer compatibility. This allows a larger processing window and restores some elongation. Yet the hydrated fillers remain unsuitable for insulation particularly in applications such as XHHW, RHH, SIS, and USE where wet dielectrics and insulation resistance are critical. Hence halogenated additives are still preferred in these applications.

However, there remain some formulation drawbacks in using halogen additives. The levels of halogen/antimony oxide to provide good flame retardance are in the 20-30% range. This implies that the polymer content is about 60% when all other minor components are included (peroxide, AO's, processing aids, pigments, etc.). Because PE is such a good fuel source (H/C greater than 2), compounds containing more than 50% PE are difficult to pass vertical burn tests. Test failure usually occurs when flaming particles drip and cause the cotton to ignite below. To overcome this deficiency 20-30% of inert fillers such as talc or calcium carbonate are required. The filler improves FR by acting as both a resin diluent and reinforcing agent to reduce dripping. Consequently some processability and physical properties are compromised. Optimization of this type of compounds is, therefore, always a balance of FR, processing and physical properties.

Formulations containing AO3, BR-1, and an inert filler were optimized to achieve UL94 V-0 and acceptable tensile/elongation properties. The samples also contained 100 ppm Cu and aged at 180° C to insure there is no detrimental effects to the AO system. The results are given in Table 5. Two BR-1 levels were used. The incentive to try a lower level (less than 10%) was for economic reason since the FR package usually is the highest cost component in the formulation. As the result indicates, it is

TABLE 5 FR OPTIMIZATION

SAMPLE	RESIN	BR-1 LEVEL	FILLER	UL94	T/E	HEAT AGE
1	36.7	NORMAL	35	V-0	2400/440	20
2	41.7	NORMAL	30	V-0	2400/530	20
3	46.7	NORMAL	25	V-1	2390/640	19
4	41.9	LOW	35	V-1	2420/500	18
5	46.9	LOW	30	F	2330/560	18
6	51.9	LOW	25	F	2330/710	16

essential to have FR levels greater than 10% to achieve a V-0 rating although at higher filler level (35%) a V-1 rating was obtained with the lower FR level. It is also encouraging that heat aging performance remained suggesting the new AO system was not detrimentally affected by the filler.

The optimization of BR-1 and AO3 in EnBA formed the basis of an experimental 150° C compound. The critical properties in long term heat aging are outlined in Table 6 in addition to the FR and cure requirements for this application.

TABLE 6 150° C RATED COMPOUND PROPERTIES

CURED PLAQUE		TARGETED WIRE PROPERTIES
1830 psi	UNAGED TENSILE	>1800 psi
302%	UNAGED ELONG.	>250%
92%	AGED ELONG.	
	7 DAYS @180 C	>85% RETENTION
	@158 C	
	90 DAYS	>70% RETENTION
	120 DAYS	>85% RETENTION FROM 90 DAYS
	150 DAYS	>85% RETENTION FROM 120 DAYS
	MANDREL	PASS 150 DAYS
UL94 V-0	FLAME TEST	VW-1
0%	HEAT DEF.	<15%

The material properties of the experimental compound are also included for comparison. However, It is important to recognize that finished wire properties are often different from cured plaque due to the impact of processing. Both line speed and temperature profile can cause substantially different cure characteristics. Incorrect temperature profile can result in loss of stabilizers and polymer degradation which will diminish heat aging performance.

Wire Properties of 150° C Rated Compound

A test run of the experimental 150° C compound was carried out on a commercial-scale wire line using typical process parameters for this product. A #18 AWG tin coated copper wire was insulated with 30 mils wall at 400, 500, 600 ft/min line speeds. The compound extruded well with a glossy surface with no detectable difference at different line speed. The head pressure also was normal (<3000 psi) indicating proper filler loading and dispersion. No premature crosslinking (scorching) was observed. Overall, the processability was deemed excellent.

Stripped insulation samples were aged at 158° C for 150 days. Concomitantly wire samples were coiled around a small metallic cylinder and tested for cracks under the same condition (mandrel test). A commercial 150° C rated wire was also prepared and tested simultaneously. Additionally, wire

samples were tested for VW-1, gel content, and heat deformation. The results are given in Table 7.

TABLE 7 150° C RATED WIRE PROPERTIES

UNAGED TENSILE STRENGTH		1400 psi
UNAGED ELONGATION (break)		320%
TENSILE/ELONGATION @158 C		
30 DAYS		1960 psi/200%
90 DAYS		1900 psi/170%
120 DAYS		1560 psi/140%
MANDREL TEST		PASSED 120 DAYS
		FAILED 150 DAYS
COMPETITIVE 150 C WIRE		FAILED 90 DAYS
FLAME TEST		PASSED VW-1
LINE SPEED	GEL CONTENT	HEAT DEFORMATION
400 ft/M IN	43%	69.4%
500 ft/M IN	37%	72.9%
600 ft/M IN	22%	96.5%

It is important to note that both our experimental compound and commercial wire failed the long term heat aging test. The experimental compound performed better (failed at 120 days) compared to the commercial sample (90 days). It is also evident that our wire was undercured based on the gel and heat deformation data.

The deficiencies in our experimental compound are attributable to insufficient stabilization and peroxide loss during processing. Theoretically, heat stability can be improved by higher AO levels. However, it is not recommended in crosslinkable compounds due to the detrimental interaction with peroxide. Most antioxidants function by deactivating free radicals which is in direct conflict with peroxide action to generate free radicals. Mere addition of more AO's would only result in poorer cure with little or no improvement in heat aging.

Optimization of Heat Stabilization and Cure

The AO-peroxide antagonism required a change in design strategy to improve both cure and heat stabilization. The antioxidant system which is multi-component was examined further to identify the free radical scavenging component. This component is denoted A and the other components are denoted B. The chemical curing system was also modified to improve cure. A cure coagent (C) was used to

increase crosslinking rate without causing extensive AO interference.

The components A and B from AO3, and C were optimized for 180°C oven aging (day) and Monsanto oscillating disk rheometer (ODR) measurement based on a 3-factor, 3-level Box-Behnken design. Experimental design can be used in formulation and development programs not only to derive optimized formulations but also to detect and measure interaction between components.⁹ The Box-Behnken design is particularly useful to generate response surfaces such as heat aging and ODR for a set of continuous factors such as A, B, and C. These response surfaces when projected onto the component planes, define the ranges of components for optimization. The levels are designated L (low), M (medium), and H (high) for the AO's and 0 (none), L, and H for the coagent. The design pattern and the data obtained are given in Table 8.

TABLE 8 3-FACTOR 3-LEVEL BOX-BEHNKEN DESIGN

RUN #	PATTERN	A	B	C	ODR	HEAT AGE
1	--0	M	L	0	21	33
2	-+0	M	L	H	64	28
3	+ -0	M	H	0	32	41
4	++0	M	H	H	67	39
5	0--	L	M	0	53	35
6	0-+	H	M	0	17	36
7	0+-	L	M	H	85	32
8	0++	H	M	H	54	37
9	-0-	L	L	L	75	25
10	+ -0	L	H	L	80	38
11	-0+	H	L	L	46	35
12	+0+	H	H	L	45	41
13	000	M	M	L	54	37
* 14	000	M	M	L	57	37
* 15	000	M	M	L	58	35
* 16	++0	M	H	H	64	40
* 17	0-+	H	M	0	17	39
* 18	-0-	L	L	L	77	26

* REPLICATES

The response surfaces derived from these data are graphed as a function of two factors giving rise to three surfaces for ODR and heat age. They are shown respectively, in Figure 1 and 2.

FIGURE 1 ODR RESPONSE SURFACES

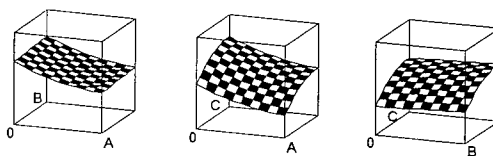
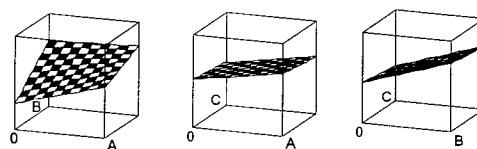


FIGURE 2 HEAT AGE RESPONSE SURFACES



A prediction profile and coefficients for the components are also derived for each property (Figure 3 and 4).

FIGURE 3 ODR PREDICTION PROFILE

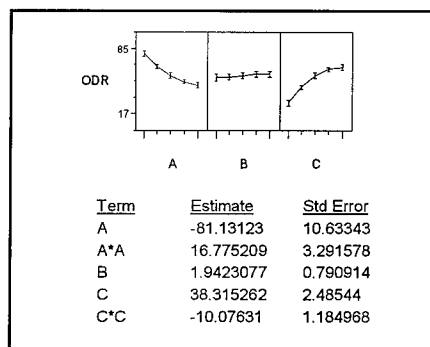
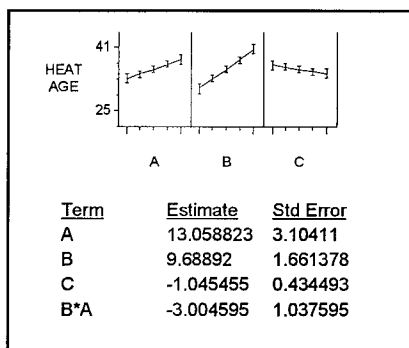


FIGURE 4 HEAT AGE PREDICTION PROFILE

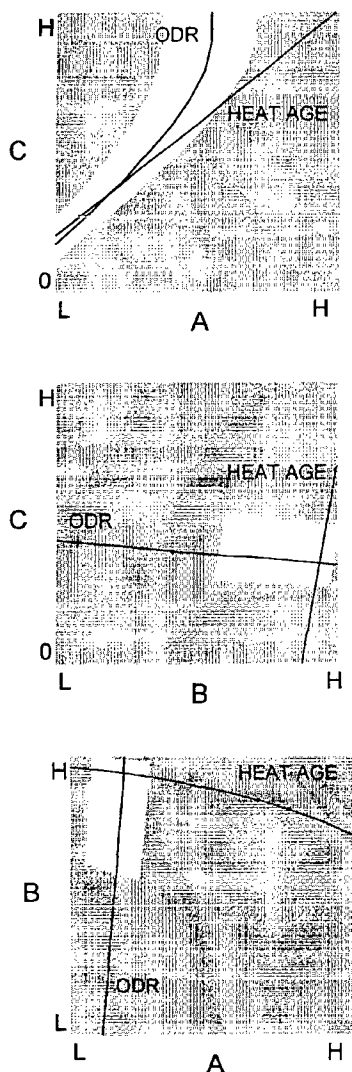


As expected, heat age is positively dependent on the AO system (A&B) while the cure coagent has a slight negative impact. For ODR, it is clear that C is the main contributor to cure. But more interestingly, negative response for A and the relatively weak or lack

of dependence on B verifies the hypothesis that component A is the cause of free radical consumption.

Conceptually, optimization of the components points to a formulation that maximizes B for heat age and balances between A and C to obtain reasonable cure. Targets of 60-70 ODR and 35-40 days heat age were used for optimization. The basis for the ODR value is from independent gel and heat deformation experiments that cure was shown to be sufficient. The length of heat age is estimated from a 50% improvement on the previous material which had a 21 day accelerated heat age that corresponded to 120 days long term. These targets define regions in the component planes (AB, AC, BC) shown as white areas in Figure 5.

FIGURE 5 OPTIMIZED ODR & HEAT AGE



Projection of the ODR and heat age surfaces onto these regions determines the component levels to achieve these values. The intersection of the projected curves for each component plane defines the levels for the two components. The three intersected points in Figure 5 corresponds to a unique set of A, B, and C. The predicted ODR and heat age for this set are 64 and 39 days, respectively.

The improved formulation based on the experimental design was compared to the previous material in ODR and 180° C heat aging. The result is shown in Table 9. It is clear that both cure and thermal stability were improved in the new formulation. Currently, the 158° C/150 day oven aging is being tested.

TABLE 9 IMPROVED ODR AND HEAT AGING

150 C	ODR	ACC. HEAT AGE
OLD	30-35	21DAYS
NEW	60-65	30-35 DAYS

SUMMARY

A peroxide crosslinkable compound suitable for the 150° C rated appliance insulation was developed. The design combined screening of AO, FR, and base resin to derive the formulation. Laboratory studies showed that the presence of copper metal degraded thermal stability 20-50% in accelerated oven aging. Commonly used metal deactivator such as Irganox 1024 is effective at lower temperatures but not useful in higher temperatures up to 180° C. Certain brominated FR additives enhance the compound's thermal stability most likely due to some oxygen and nitrogen containing impurities that could act as copper chelating agents. A proprietary non-phenolic AO system was developed to provide the long term thermal stability. Its components and a cure coagent were optimized through a Box-Behnken experiment design for cure and heat aging. Wire samples exhibit good processability and superior long term heat aging performance when comparing to a commercial product.

REFERENCES

1. U.S. Patent No. 4,797,323
2. U.S. Patent No. 5,139,875
3. U.S. Patent No. 5,216,059
4. U.S. Patent No. 5,358,991
5. S.K. Dutta, et al., Polym. Deg. & Stab., **50**, 75-82 (1995).
6. W.O. Drake, et al., HAS as HATS, 14th Annual Conference, Advances in Stab. and Deg. of Polym. (1992).
7. Z. Osawa, Polym. Deg. & Stab., **20**, 203-236 (1988).
8. M.T. Bryk, Degradation of Filled Polymers, Ellis Horwood Limited (1991).
9. G.E.P. Box and N.R. Draper, Empirical Model-Building and Response Surfaces, John Wiley & Sons (1987).

BIOGRAPHY

Lester Lee is a Senior Research Specialist of the Wire and Cable Group at Millennium Petrochemicals Inc. . He holds a B.S. degree in chemistry from University of Washington and a Ph.D. degree in physical chemistry from Oregon Graduate Institute of Science & Technology. Since joining Millennium in 1988, he has worked in developing polyethylene products in flame retardant and other specialty applications.



TESTING OF CABLES DESIGNED FOR FIRE RESISTANCE A COMPARISON OF U.S. AND EUROPEAN STANDARDS

Siegfried Richter; Rüdiger Schmidt*

Consulting Engineer, Eckental, Germany

*Martinswerk GmbH, Bergheim, Germany

ABSTRACT

Fire is a global issue. It therefore follows that the use of cables with special fire-retardant characteristics should be subjected to similar regulations all over the world. At present, the existence of numerous different test specifications suggests that they reflect the actual practice. This is a fatal error. To understand the behavior of cables under fire conditions and their relevant test methods it is necessary to know how fire affects the cables. These effects and the principal US and European flame test methods on cables are described. A proposal regarding worldwide harmonization of flame test methods on cables is given. To avoid misunderstandings, in addition to the test methods and test requirements relevant terms and definitions should also be globally harmonized. This will increase the safety of cable installations and remove trade barriers.

INTRODUCTION

Cables designed, manufactured, installed and operated in accordance with public standards are safe. They do not cause fire. However, it is possible that cables are effected by fire from other sources and these may enhance the magnitude and propagation of the fire.

For better interpretation of the variety of test methods it is first necessary to understand how fire affects the behavior of cables.

CABLE INSTALLATIONS IN BUILDINGS

Many different systems are used to install electrical cables in buildings. These depend, among other factors, on the intended use of the building, the cable types, the cable environment and, last but not least, on the legal requirements of the governing authorities.

Cables are installed:

- inside or outside of walls, ceilings and floors. Some or all of these may be thermally insulated,
- under, in or over the sheet rock or wooden panels,
- in voids of the masonry, in the plenum, in tunnels or in shafts which may be ventilated,
- directly or in conduits, trunks, pipes, ducts, trays, on brackets or ladders,
- with or without fastening devices.

Cables are laid:

- as individual single cables,
- in bundles, in loose or compact arrangements, together with cables of the same type and dimension or in a mix with other cable types and dimensions,
- horizontally or vertically.

The American practice to install cables in air conditioning ducts or to use the plenum for air conditioning purposes is not allowed in Europe. In case of fire the cables would be supplied with additional oxygen, thus supporting fire propagation as well as smoke distribution.

In Europe, to the contrary, the building code requires that areas in excess of 400 m² (4,300 sq.ft.) be divided up into fire zones. In the event that cables pass from one zone to the other, the walls between zones must be provided with fire resistant bushings.

Cables have different fuel loads and they show different behavior under fire conditions. They are either flammable, flame-retardant, flame-resistant or fire-resistant. When exposed to fire, cables may emit flammable gases (flash over), smoke, corrosive gases or toxic gases.

Every cable installation is different and so is every fire scenario.

BEHAVIOR OF CABLES UNDER FIRE CONDITIONS

Thermoplastic insulations and jackets soften when exposed to the heat of the fire before the flames reach the cable. Insulations and jackets may be deformed and they may drip while burning. If the cables are pressurized, short circuits may occur between adjacent conductors and/or the grounded surroundings. Crosslinked materials are heat-resistant and will not be deformed by the heat of the fire.

If the flames reach the cable, the insulating and jacketing compounds are decomposed and may start burning by themselves. The burning of the cable and the propagation of the fire depend on:

- cable design,
- cable position,
- cable installation,
- type of compound,
- number of cables,
- cable environment.

The nature and the quantity of compounds determine the energy level of the cable. The fuel load of power cables is significantly higher than the fuel load of communication cables. Large air-filled interstices in communication cables, promote the fire through the supply of air. Flame barriers like mica coated glass-woven tapes protect the insulation from direct flames. This permits emergency operation for a certain period of time.

Insulation and jacketing compounds may be classified from easily flammable to severely flammable and from flame propagating to self-extinguishing.

An indicator for the flammability is the Limiting Oxygen Index (LOI). Self-extinguishing materials are materials which may burn while exposed to supporting ignition; they will extinguish themselves once the ignition source disappears.

Provided there is no air stream, such as in an air-conditioning duct, cables in horizontal position propagate fire slowly or not at all. Cables in vertical position may propagate fire quickly. The „chimney“ effect is supported by rising of hot fire gases.

Single cables and bunched cables, even cables of the same type under the identical conditions, may exhibit completely different behavior in

case of fire. Besides the number of cables, the arrangement of cables has an important influence on the fire behavior. Fire propagation is most significant if the distance between adjacent cables is approximately equal to the diameter of the cables. Close packed bundles have less tendency to propagate the fire. The dimensions of the installation shaft in relation to the dimension of the cable bundle also is important.

FIRE GENERATED GASES

Every fire generates gases. These are distinguished as smoke, flammable gases, corrosive gases and toxic gases.

Smoke hinders the vision of people trying to escape from the fire area as well as for the fire fighters.

Flammable gases may support the fire propagation of the cables itself and their surroundings and they may contribute to an early „flash over“.

Corrosive gases, when mixed with water, may form aggressive acids, which may attack metal objects in the surroundings of the fire. Many cases are known where the corrosive secondary damages were more severe than the direct damage caused by the fire. Corrosive gases can also hinder sight and breathing.

Toxic gases do not have any influence on the fire itself, but they are dangerous to the people trapped in the fire zone and to the fire fighters.

PROPERTIES OF CABLES UNDER FIRE CONDITIONS

The properties of cables under fire conditions are classified as follows:

- low fuel load,
- flammable,
- flame-retardant,
- flame-resistant,
- fire-resistant,
- low smoke,
- fire gases halogen-free,
- fire gases non-corrosive,
- fire gases with low toxicity.

No conclusion can be drawn from the given definition of one individual property to any other. The properties can be combined at the risk of increased cost.

„Fuel load“ is the amount of energy which can be released from burning materials. The fuel load of a cable is calculated from the calorific value and the compound quantity used in the cable. It is expressed in kWh/m and should be kept as small as possible, to minimize its contribution in the case of fire.

„Flammable“ means, that cables may readily be set aflame an ignition source and that they will continue to burn, after the ignition source is removed. Flammable cables will not self-extinguish; they propagate fire with ease.

„Flame retardant“ cables may start burning when ignited. However, they extinguish themselves as soon as the ignition source is removed. Flame retardant cables do not propagate fire when tested as individual cables but they may fail the test when bunched together with other cables.

„Flame resistant“ cables are flame retardant. They extinguish themselves if the ignition source is removed. They do not propagate the fire, neither in a single cable nor in a cable bundle test.

„Fire resistant“ cables are suited for emergency operation over a limited period of time, although the cable insulation and/or jacket may have burnt down completely. This property may be negatively influenced by water or other quenching media and/or mechanical attacks. Mineral insulated cables are a special kind of fire resistant cables. They do not burn at all, withstand very high temperatures over several hours, do not emit fire gases and they resist water and chemical quenching agents.

„Low smoke“ cables develop little smoke in a fire and the smoke should be bright and transparent to light.

„Corrosive fire gases“, generated in particular from halogen-bearing materials, may develop corrosive acids from contact with the humidity of the environment or with the quenching water. To avoid this possibility „halogen-free“ cables are implemented. They shall not contain any chlorine, bromine, fluorine or iodine components. Halogen-bearing materials are not the only ones to develop such corrosive acids.

N → → → HNO₃
 S → → → H₂SO₃, H₂SO₄, H₂S
 P → → → H₂PO₃, H₃PO₄
 C → → → H₂CO₃, organic acids

„Toxic gases“ are generated in every fire. Carbon monoxide, in particular, is extremely dangerous because it is not visible and has no smell. Most of the other gases may be detected by their strong smell. Every fire extracts oxygen from the surrounding air. People trapped in a fire area therefore are threatened by death from suffocation. Experts find that more than 80 % of the people killed in a fire die by suffocation but they are not burned. Dioxins and furanes, created from chlorine or bromine sources, can not absolutely be avoided. But dioxins and furanes are developed only at lower fire temperatures due to carbonization and they decompose at higher temperatures of 800 °C and above.

MATERIALS FOR CABLES UNDER FIRE CONDITIONS

The cable design often has to combine different polymers for insulation and jacketing compounds. Typical polymers which are often chosen are:

- polyolefins (PE, PP), homopolymers and copolymers, without or with flame retardants,
- hydrocarbon elastomerics (EPDM) without or with flame retardants,
- plasticized PVC without or with flame retardants,
- fluoropolymers.

Polyolefinic or elastomeric insulations and jackets based on hydrocarbons do easily burn if they are used without any additive flame retardants. The main difference between thermoplastic and elastomeric materials is that thermoplastics may melt at the high temperatures of the fire and may drip down burning or non-burning, but crosslinked polymers do not. Therefore, if used for jacket compounds, such thermoplastic polymers have to be highly filled with inert minerals like chalk to reduce fuel load and ignitability. Much more effective in achieving flame retardancy are fillers which are not only inert, but which really act as flame retardants. Aluminium hydroxide (ATH) or magnesium hydroxide (MDH) are such flame retardants that function via endothermic decomposition and the release of water. Other available options include halogenated flame retardants or those based on phosphorous components

If using PVC or chlorinated elastomers, the ignitability of the polymer itself is lower compared to hydrocarbons. Unfortunately, usual

plasticizers like phthalates are used to optimize the flexibility of the polymer compound which leads to drastically reduced flame retardancy. This effect has to be overcome by adding some flame retardants like ATH or magnesium hydroxide (MDH). In addition to the cooling reaction as described for ATH, MDH works as smoke suppressant in such applications. Antimony trioxide is very effective regarding the reduction of ignitability, but due to the fact that it supports smoldering conditions it leads to increased amounts of smoke and carbon monoxide during any fire.

The third alternative are fluoropolymers showing a much higher thermal stability compared to other polymers mentioned. Nevertheless, still being organic materials, fluoropolymers will also decompose if the temperature of the fire is high enough. In cases of such high temperatures, it is under discussion that extremely toxic gases, „supertoxins“, may be created by fluoropolymers during a fire.

Cable designs should take all these arguments into account to create a cable being „fit for use“ regarding the intended individual application.

TEST METHODS FOR CABLES UNDER FIRE CONDITIONS

In general, the test methods given in standards are not intended and not suitable to prove that the cables really are reliable in use. Only the combination of specified cable design, specified materials, specified test procedures and the use in accordance with the specified „guide to use“ guarantees that the cables are reliable in the intended use. This is not only valid for the general properties, but in particular for any tests under fire conditions. In practice, there is neither a standard installation nor a standard fire. Each real fire and each real installation are different and not predictable. All test methods given in the standards allow only a comparison of the behavior of different cables under the same specified conditions.

Furthermore, it is important to realize, that all test methods use an ignition flame to initiate the burning of the cables. There is no test procedure in the standards taking into account, that the cable itself starts burning. This indicates that cables are safe and they are not the cause of any fire if they are manufactured, tested, installed and used in accordance with the standards.

The following comparison includes the European CENELEC standards for fire tests and the similar US-standards. The CENELEC standards are very close to IEC. National standards of individual European countries are not taken into account, due to the CENELEC rules these standards are already withdrawn or will be withdrawn in the near future.

In the following comparison the test procedures are grouped as follows:

- fire propagation,
- fire gases,
- fire resistance,
- integrity of service.

FIRE PROPAGATION

In most cases, fire propagation of cables is tested using the more severe vertical position. The test procedures distinguish between tests for single and for bunched cables.

The test procedures for single cables in vertical position (IEC 332-1, EN 50265-2, UL 1851-1060, 1061, 1080) follow the same principle.

The cable is vertically mounted in a metal enclosure and an ignition flame is positioned on the cable. More or less different are the dimensions of the metal enclosure of the test equipment, the length of the sample, the kind of burner, the used gas and the time of ignition. On the other hand the required test results are nearly the same, with one exception: only the UL-specifications require that the burning cable shall not ignite materials in its vicinity (cotton on the bottom of the test equipment; indicator flag on the upper end of the tested cable). This requirement is reasonable and should be integrated also in the IEC- and European standards.

The European test standards for bunched, vertically installed cables follow very close the IEC-standard 332-3, while the American standards are totally different, although the IEC 332-3 traces back to the American standard IEEE 383, intended for cables in nuclear power stations.

For the IEC 332-3 test a certain number of cables is mounted on a ladder, 3,6 m high. The ladder is installed in a thermal insulated steel chamber (4 x 1 x 2 m) and a gas ribbon burner ignites the cables for 20 min. (small cables) or 40 min. (big cables). After the flames ceased,

the length of the charring is measured. The damages shall not reach the upper end of the tested cables.

The revised IEC 332-3 (at present under consideration), will be adopted as European Norm EN 60332-3. This revised standard includes a better differentiation between the requirements for smaller and bigger cables. Big energy cables shall be mounted in the front and in the rear of the ladder and for small cables a new „category D“ with a combustible volume up to 0,5 l/m will be introduced. For very small cables, e.g. optical fibers, it is proposed to strand several of the test cables before mounting them on the ladder.

For the test according to UL 1666 a concrete test cabinet is used, with two test chambers in two floors, connected by a slot. The total height is 5.7 m and the inner space is 2.44 x 1.22 m. The test cables are mounted on a metal frame, running through the two floors. The cables are not ignited by a gas ribbon burner positioned to the cables as in the IEC test, but by a burner diffusion plate on the floor, with a vertical flame, in front of the test cables and in parallel to them. The ignition time is 30 min. The flame height shall not exceed 3.6 m and the max. temperature measured in the upper test chamber shall not exceed 850 °C.

Besides this test of vertical installed cables in a shaft the UL-specification 1581 contains further tests for cables vertically installed in trays. The European standards do not cover equivalent test procedures. According to UL 1581-1160, the cables are mounted in a single layer in a steel ladder tray in a vertical position. No further enclosure is required and the same gas ribbon burner is used as required for the IEC- and European tests of vertical installed bunched cables, but the burner is positioned behind the tray. After 20 min. the burner has to be removed and the time the cables continue to flame has to be reported and the length of charring on the cables is to be measured.

UL 1581-1164, which is equal to CSA FT4 - vertical tray test, also describes the behavior of cables in vertical trays. For this test an enclosure is required to eliminate external influences. The same tray type and the same gas ribbon burner is used as in the test mentioned before. The burner is positioned in front of the open vertical tray with the installed test cables inside. The ignition time is 20 min. After the burner has been removed, the length of char on

the surface of the test cables has to be determined.

There is only one test for a single cable in a horizontal position (UL 1581 - 1100). For this test the same metal enclosure and the same ignition flame are used as for the UL-tests on single cables vertically installed. The blue inner cone of the test flame of a tirril burner shall be applied to the cable for 30 s. After the test flame is removed, the length of char has to be measured.

According UL 910 horizontally installed bunched cables are tested in a preheated tunnel, more than 70 m in length, in which 7.3 m long test samples are installed on a horizontal ladder. The cables are ignited for 20 min. by a gas burner and the tunnel is flowed through by an air stream. At the end of the tunnel the smoke density is measured. During the test the velocity of the flame spread and the optical density have to be reported. After the test the cables have to be removed for examination regarding flame propagation (> 1.37 m).

The European standards do not cover similar tests for horizontally installed cables, neither as single cables nor as bunched cables in tunnels.

ISO 5660, the „cone calorimeter test“, originally developed by NBS, also is used in the laboratories of European cable manufacturers. In this test, the samples are exposed to a constant heat flow combined with a calorimeter. By means of the oxygen consumption, the heat released during the combustion and the effective heat of combustion is determined. The heat release rate may be plotted against the time taking into account the radiant heat flux. In this way, for the investigated sample, the phases in the course of a fire become detectable.

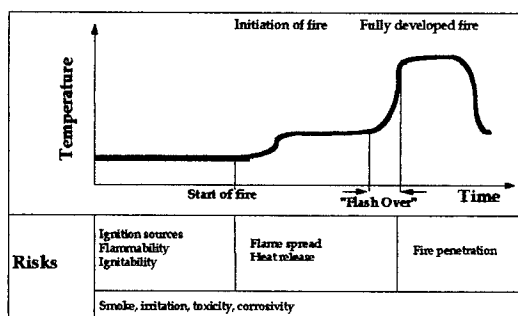


Fig.: 1 Phases in the course of a fire

Furthermore, the „time to ignition“ , the „mass loss rate“ and additionally the „smoke density“ may be measured. Originally, this test procedure was intended to investigate the behavior of materials only, but many tests have been done on completed cables. It seems that the test results received from the cone calorimeter tests are comparable with the results from other fire propagation tests. More investigations are necessary to prove whether it is possible to replace the present fire propagation tests for small and medium sized cables by the cone calorimeter test. In any case, this test delivers very valuable and comprehensive knowledge about the behavior of insulation and jacket materials as well as completed cables under fire conditions.

FIRE RESISTANCE

According to the present IEC 331 a single cable, 1.2 m long, is horizontally fixed 75 mm above a tube type gas burner, 0.61 m in length. The test flame, with a temperature of 750 °C is applied for 180 min. During the test a continuous current shall pass through the conductors of the cable provided by a voltage source with the rated voltage of the cable and of at least 3 A capacity, connected to the cable through fuses. The current is achieved by connecting a suitable load, e.g. a lamp, between the conductors at the other end of the cable. During the test no fuse shall fail, no lamp shall extinguish, no conductors shall be interrupted and the voltage shall maintain during the whole test procedure.

Some European countries adopted IEC 331 as national standards and some of them furthermore require to expose the cables to mechanical shocks during the test. IEC 331 is not yet harmonized in Europe, but an European standard is under preparation.

A new European standard EN 50200 - „Method of test for resistance to fire of unprotected small cables for use in emergency circuits“ - is under consideration. It is proposed to mount the test cables on a defined heat resisting, non-combustible board by means of steel supports. The dimensions of the board are in the range of 900 x 300 mm. The cables are mounted like an „U“. The used burner is a gas ribbon burner similar to the burner described in IEC 332-3 for the tests of vertical bunched cables, but 500 mm wide instead of 257 mm. It is proposed that the board is exposed to defined mechanical shocks at the upper edge of the board. The

required test results for energy and control cables are the same as in the present test. For communication cables the requirements are similar and for optical fiber cables the increase of the attenuation shall be reported.

FIRE GASES

For the determination of the smoke density and corrosivity, again different test methods are used in the US and Europe. The test according ASTM E 662 is carried out in a test chamber, well known as „NBS-chamber“, of the inner dimensions 914 x 610 x 914 mm. A sample of the material or a test cable is mounted in the chamber. For the nonflaming test, the sample is heated by a radiant-energy source. Using the flaming mode, the sample is in addition ignited by a multiple flamelet gas burner. A photometric system with a vertical light path measures the transparency of the smoke and the optical smoke density is calculated.

The test procedure used in Europe traces back to a test developed by London Underground. The test chamber is a cube 3 x 3 x 3 m. The test may be used for samples of materials or for completed cables. It is possible to test one or more cables. The samples are positioned in the test chamber and ignited by 1 litre of alcohol. In the big chamber the uniform distribution of the smoke is achieved by a vent. The optical density is determined by a photometric system measuring a horizontal light path through the test chamber.

The present European standard HD 602, adopted from IEC 754, will be extended and issued as EN 50257. This standard describes the test on gases evolved during combustion of cables. The test material is stored in a combustion boat, inserted in a tube furnace.

There are 3 test procedures:

Following the first procedure, the sample is heated up to 800 °C for 20 minutes in a stream of dry air. Combustion gases are absorbed by sodium hydroxide solution in wash bottles. The amount of halogen is determined by analytical methods. This procedure is not suitable for materials containing hydrofluoric acid, for materials creating less than 5 mg/g halogen acid or to define materials to be „halogen-free“.

Following the second procedure, the samples are heated up to 935 °C for 30 minutes. In the wash bottles, containing distilled water, the di-

electric permittivity ($\epsilon > 4.3$) and the conductivity ($\kappa < 100 \mu\text{S/cm}$) are measured. The intention for this procedure is to test materials creating less than 5 mg/g halogen acid and so to distinguish between „halogen- containing“ and „halogen-free“ materials.

Following the third procedure, three specimens of each non-metallic material of a cable are tested according to the second procedure. From the results, mean value, standard deviation and coefficient of variation are calculated. From these values, the weighted average mean values of pH and conductivity of the constituent materials related to the unit length of the cable are determined.

It was tried to find other possibilities to judge the corrosivity of fire gases. The French telecom uses a test procedure where the fire gases condense on printed copper circuits. After the test the corrosion on the surface of the circuit is visually judged. In the USA, a similar procedure is under consideration, but for this procedure it is proposed to measure the leak currents between the printed circuits. European experts are of the opinion that both methods are up to now not ripe to adopt one of them as European standard. The results of these tests depend not only on the nature of the fire gases. They depend also on the material of the printed circuits, the influence of the temperature of the fire gases attacking these materials and the influence of soot and other conductive particles on the leakage current.

It is rather difficult to find out the toxicity of fire gases. Therefore, up to now no international test standard is available.

With the so-called „Pittsburgh-test“ it was tried to determine the toxicity by means of the lethal dose of the fire gases created by different cable materials, expressed as LC_{50} values (LC = lethal concentration). This is the amount of gases which killed 50 % of mice exposed to the fire gases.

The effect on humans survivability is unknown and tests with animals will not be accepted in Europe for humanitarian reasons.

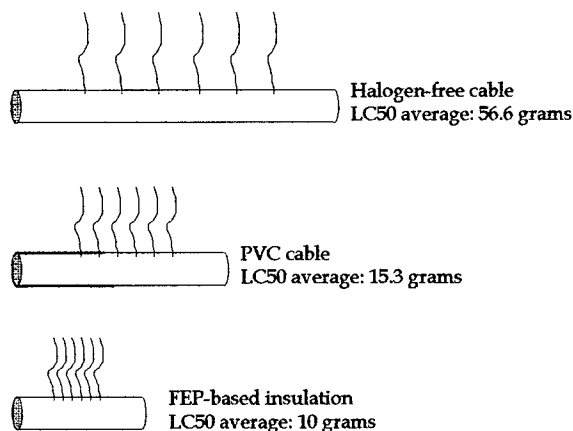


Fig.:2 LC 50 values for compounds used in cables

(Source: Data Communications, July 1996, page 63)

Instead of such biological tests, in Europe the insulation and jacket compounds are burned or decomposed and the different chemical agents of the fire gases are evaluated. The added evaluation values give the „toxicity-factor“ of the investigated compound. In the past mainly two test procedures have been used. In the test developed from the British Marine (NES 713) a sample of the material is burned in an open flame in a small test chamber. The fire gases are analyzed by indicator tubes. Using this procedure, more carbon dioxide is formed and the test results are not as accurate as in the test developed by the French railways (NFC 20454). In this French test the sample of the material is in a combustion boat which is inserted in a tube furnace and the fire gases are properly analyzed. The French specification does not evaluate nitrogen. But it is now proposed to introduce the French test including nitrogen in the European standards for railway cables. It is to be expected that this test will then also be applied for all the other cables covered by European standards.

INTEGRITY OF SERVICE UNDER FIRE CONDITIONS

In Europe and in particular in Germany, the integrity of service under fire conditions becomes more and more important in the discussions about the safety of cables under fire conditions. „Integrity of service“ means that cable systems continue their service for a certain, agreed time, e.g. 30 min. or 3 h, even if the insulation and/or the jacket burnt down to ash. This integrity of service can be achieved e.g. by woven glass tapes coated with mica, applied on

the conductor and/or the insulation and/or underneath the jacket. The integrity of service is tested in accordance with the German standard DIN 4201 part 12 in a test chamber with inner dimensions of approx. 3 x 3 x 3 m.

The cables are installed in the same way as in the intended actual installation, using the same cables, the same trays or racks, the same clamps and all the other installation elements, in the same configuration as later on intended in the actual installation. The test chamber is heated by oil-burners on the side of the chamber. The temperature follows the ISO-temperature curve and heats the chamber over 3 hours up to 1200 °C. As in the fire resistance test a continuous current shall pass through the conductors of the cable provided by an energy source with the rated voltage of the cable and of at least 3 A capacity, connected to the cable through fuses. The current is achieved by connecting a suitable load, e.g. a lamp, between the conductors at the other end of the cable. During the test no fuse shall fail, no lamp shall extinguish, no conductors shall be interrupted and the voltage shall maintain during the whole test procedure.

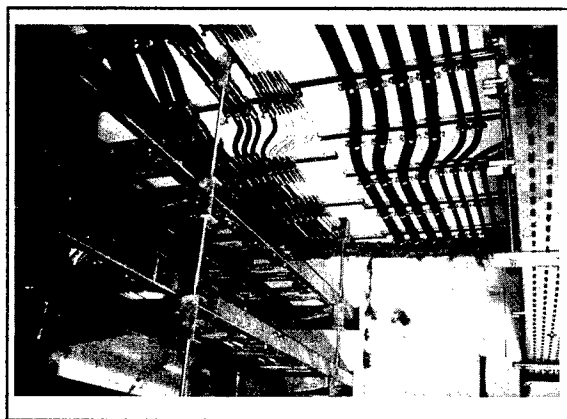


Fig.: 3 Installation for test of integrity of service according DIN 4201
(by courtesy of Kabelwerke Ehlers, Hamburg)

The approval gained by this test is valid only for cable systems using cables, installation equipments and installation arrangements as used in the test and some similar elements extraordinarily mentioned in the approval.

Although this is a test for a complete installation system and not only for cables, there is a discussion in Europe, whether such test should

be introduced in the European cable standards or not.

EUROPEAN STANDARDS AND THE LAW

Over a long period of time the use of standards was voluntary. But there is now a significant change in Europe which creates an important difference in the use of standards in Europe and the USA. The treatment of Rome requires to delete trade barriers between the European countries. It was said explicitly that different technical standards are one such trade barrier which has to be removed. For that reason, the National Standard Bodies in Europe are forced by the rules of the European standard organization CENELEC to withdraw their national standards which are equal, comparable or in competition with European Harmonization Documents (HD) or European Norms (EN). Harmonization Documents have to be implemented in the national standards. Due to the different structure of the standards in the different countries a comparison of the standards is difficult and an exchange of goods within the European Union is prevented. Therefore the Harmonization Documents will be replaced by European Norms which are absolutely equal, word by word and page by page in all CENELEC-countries.

Furthermore the European Commission issues more and more European Directives which become part of the national legislation. For cables, the most important European Directives are

- Low Voltage Directive
for all electrical equipment in the range of 60 V AC to 1000 V AC.
- Constructive Products Directive
for all materials and elements used and fixed in or on constructions.
- Magnetic Directive
for the interference of electrical and electronic systems, in particular in the field of telecommunication.

The European Directives are amended by lists of the standards, which are applicable for the relevant European Directive and in this way they become compulsory for manufacturers and users in the European Union.

CONCLUSION

The diversity of different tests, which is in particular true for the test of fire propagation, may confuse the architects, installers and users. They may have the impression that these different tests mirror the practice. But this is a fatal error. The present manifold of tests feign an accuracy which is not existing. All these tests only compare the behavior of different cables under defined testing conditions. On the other hand, most of the tests do already follow the same principle with more or less important deviations in details. Therefore it should be possible to harmonize the conditions of these tests worldwide. A good base for such harmonization are the IEC standards which have been agreed already from many countries, including USA and the European countries. All European standards fulfill already the existing IEC standards. Missing test procedures should be agreed on and the present standards if necessary should be amended and improved. To avoid misunderstandings, other standards which are not in agreement with the global harmonization should be withdrawn. In parallel, the terms of properties of cables under fire conditions should be defined and should also be globally harmonized. This offers not only more transparency for the users of such standards, it also increases the overall safety of cable installations and removes trade barriers between different parts of the world.



Siegfried Richter was born in 1929. He studied Electrical Engineering. From 1952 to 1994 he was engaged in the cable industry, responsible for cables design and in his last position for the development of special cables. After his retirement he worked as consultant. In the field of power and data cables he was a member of several national, European and international standard organizations, like VDE, CENELEC and IEC for more than 30 years, up to the end of last year.

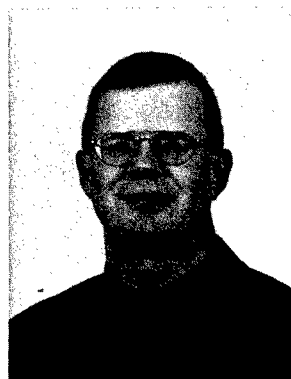
The following simple scheme is proposed to achieve a worldwide harmonization of standards for the testing of cables under fire conditions:

Property of cable	Test Standard
low fuel load	still missing
flame retardant	IEC 332-1
flame resistant	IEC 332-3
fire resistant	IEC 331
heat release/course of fire	ISO 5660
low smoke fire gases	IEC 1034
halogen-free fire gases	IEC 754 *)
non-corrosive fire gases	IEC 754 *)
low toxic fire gases	ENxxx (under consideration)
integrity of service	DIN 4102 part 12

*) amended by EN 50257

Fig.:4 Proposed harmonized test scheme

Martinswerk GmbH
Koelner Strasse 110
D - 50127 Bergheim
Tel.: +49 2271 902 -371



Dr. Rüdiger Schmidt was born in 1958. He studied Chemistry at the university of Hannover. From 1988 to 1996 he was engaged in the rubber industry. His main focus was on the development of flame retardant building products based on elastomerics. In 1996, he joined Martinswerk where he is responsible for market development of high purity mineral flame retardants like ATH and magnesium hydroxide, mainly for the cable industry.

NANOCOMPOSITES:
RADIATIVE GASIFICATION AND VINYL POLYMER FLAMMABILITY

Jeffrey W. Gilman*, Takashi Kashiwagi, Sergei Lomakin†
National Institute of Standards and Technology, Gaithersburg, MD

Joseph D. Lichtenhan, Paul Jones
Phillips Laboratory, Edwards Air Force Base, CA

Emmanuel P. Giannelis, Evangelos Manias
Cornell University, Ithaca, NY

ABSTRACT

In the pursuit of improved approaches to flame retarding polymers a wide variety of concerns must be addressed. The low cost of commodity polymers requires that the fire retardant (FR) approach be of low cost. This limits the solutions to the problem primarily to additive type approaches. These additives must be easily processed with the polymer, must not excessively degrade the other performance properties, and must not create environmental problems in terms of recycling or disposal. Currently, some of the commonly used flame retardant approaches for polymers can reduce the thermal and mechanical properties of the polymer.^{1, 2, 3}

Polymer-clay nanocomposites are hybrid organic polymer inorganic layered materials with unique properties when compared to conventional filled polymers. The mechanical properties for nylon-6 clay nanocomposite, with clay mass fraction of 5 %, show excellent improvement over those for the pure nylon-6. The nanocomposite exhibits a 40 % higher tensile strength, 68 % greater tensile modulus, 60 % higher flexural strength, 126 % increased flexural modulus, and comparable impact strengths. The heat distortion temperature (HDT) is increased from 65 °C to 152 °C.⁴ Previously, we reported on the flammability properties of nylon-6 clay nanocomposites.⁵ Here, we will briefly review these results, present the results of radiative gasification experiments and report on our initial studies of the flammability of *intercalated* polymer-clay nanocomposites prepared from polystyrene, PS, and polypropylene-graft-maleic anhydride, PP-g-MA.

EXPERIMENTAL

Cone Calorimeter

Evaluations of flammability were done using the Cone Calorimeter.⁶ The tests were done at an incident heat flux of 35 kW/m² and 50 kW/m², using a cone shaped heater. A heat flux of 35 kW/m² represents a typical small-fire scenario.⁷ Peak heat release rate, mass loss rate and specific extinction area data, measured at 35 kW/m², are reproducible to within ± 15 %. The carbon monoxide and heat of combustion data are reproducible to within ± 10 %. The uncertainties for the Cone calorimeter are based on the uncertainties observed while evaluating the thousands of samples combusted to date. Typically two samples were combusted in each case in the Cone, and the results averaged. Cone samples were prepared by compression molding the samples (20g to 50g) into rectangular or round plaques, 4mm to 15 mm thick, with a typical area of ~ 0.004 m², using a press with a heated mold.

Radiative Gasification

Figure 6 shows a gasification apparatus which is similar to the Cone calorimeter. The gasification apparatus allows pyrolysis, in a nitrogen atmosphere, of samples identical to those used in the Cone calorimeter, at heat fluxes like those experienced in a fire (30 kW/m² to 100 kW/m²). It allows study of the condensed phase decomposition processes decoupled from the gas phase combustion and resulting heat feedback from the flame. In a typical experiment thermocouples are imbedded in the sample to monitor the temperature at which the pyrolysis and decomposition processes occur. A load cell gives mass loss rate data which can be compared to mass loss rate data from the Cone calorimeter experiments. A video camera records the pyrolysis and charring phenomena.

Nylon-6 clay nanocomposites

Nylon-6 clay nanocomposites (clay mass fraction of 2 % and 5 %) and nylon-6 were obtained from UBE industries and used as received.⁸ The above nanocomposites will be referred to as; nylon-6 clay nanocomposite (2%) and nylon-6 clay nanocomposite (5%), respectively.

PS-clay-nanocomposite

Preparation of PS-clay-nanocomposite (clay mass fraction of 3 %) by melt blending PS with bis(dimethyl)bis(octadecyl)ammonium-exchanged montmorillonite, yields a nanocomposite with the *intercalated* structure (see Scheme 1). The intergallery spacing, by X-ray diffraction, XRD, is 3.1 nm ($2\theta = 2.7^\circ$). In the *intercalated* form and at this low clay concentration this nanocomposite is essentially a blend, with *intercalated*-PS-clay domains dispersed in pure PS. The *immiscible* PS-clay mix, where the clay is only mixed in at the primary-particle size scale ($\sim 5 \mu\text{m}$), is prepared under the same melt blending conditions except the alkylammonium used to compatibilize the montmorillonite has only one octadecyl R group instead of two. This renders the ion exchanged montmorillonite slightly less organophilic and intercalation does not occur. The PS used was Styron 6127 from Dow Chemical Co.

PP-g-MA-clay-nanocomposite

Preparation of PP-g-MA-clay-nanocomposite (clay mass fraction of 5 %) by melt blending was accomplished by pressing the PP-g-MA mixed with the bis(dimethyl)bis(tallow)ammonium-exchanged montmorillonite, Closite 15A, at 160 °C for 30 minutes using a Carver press, followed by heating in a vacuum oven for several hours at 160 °C. This yields a nanocomposite with the *intercalated* structure (see scheme 1). The intergallery spacing, by XRD analysis, is 3.6 nm. PP-g-MA (m.p. 152°C) was purchased from Aldrich and contains a mass fraction of 0.6 % maleic anhydride. It has a melt index of 115 g/600 s and a Mw of $\sim 10\text{K}$, Mn $\sim 5\text{K}$.

Characterization

X-ray diffraction spectra were collected on a Phillips diffractometer using Cu K α radiation, ($\lambda = 0.1505945 \text{ nm}$). Powder samples were ground to a particle size of less than 40 μm . Solid polymer-clay

monoliths were typically 14 mm by 14 mm with a 2 mm thickness.

The thermogravimetric analysis, TGA, was done on a Perkin-Elmer 7 Series TGA. Four runs of each sample type were typically run, the results averaged and the uncertainties calculated using standard methods. The samples were heated from 30 °C to 600 °C at a heating rate of 10 °C/ minute in a nitrogen atmosphere. For the differential TGA plots (Figure 9) the uncertainty in maximum of the mass loss rate ($d(m/m_0)/dT$ (°C⁻¹)), in the normalized mass loss rate versus temperature plots, was found to be $\pm 20 \%$ (± 1 standard deviation). The uncertainty in the temperature at the maximum, in the normalized mass loss rate versus temperature plots, was found to be $\pm 2 \%$ (± 1 standard deviation).

TGA-FTIR was performed on a TA Instruments (Model TGA-951) TGA coupled to a FTIR gas analyzer manufactured by Nicolet Inc. (Model 7-SX). Samples (5 mg - 10 mg) were first flushed with nitrogen at 100 cm³/minute for 30 minutes and then heated at 10 °C/minute from room temperature (25 °C) to 1000 °C under nitrogen. Evolved gases from the sample were swept through a heated (250 °C) capillary transfer line to a gas analysis cell and then to the spectrometer sample compartment by nitrogen purge gas. FTIR spectra were recorded once every 6 s at resolution of 8 cm⁻¹.

For the transmission electron microscopy (TEM), the char was broken into small pieces, embedded in an epoxy resin (Epofix), and cured overnight at room temperature. Ultra-thin sections were prepared with a 45° diamond knife at room temperature using a DuPont-Sorvall 6000 ultramicrotome. Thin sections (nominally 50 nm-70 nm) were floated onto water and mounted on 200-mesh carbon-coated copper grids. Bright-field TEM images were obtained with a Philips 400T microscope operating at 120 kV, utilizing low-dose techniques.

BACKGROUND

The polymer-clay nanocomposites contain montmorillonite clay that has had the sodium ions removed by ion-exchange with various alkyl ammonium salts. This modification renders the usually hydrophilic clay organophilic. A molecular representation of the layered structure of sodium montmorillonite is shown in Figure 1.

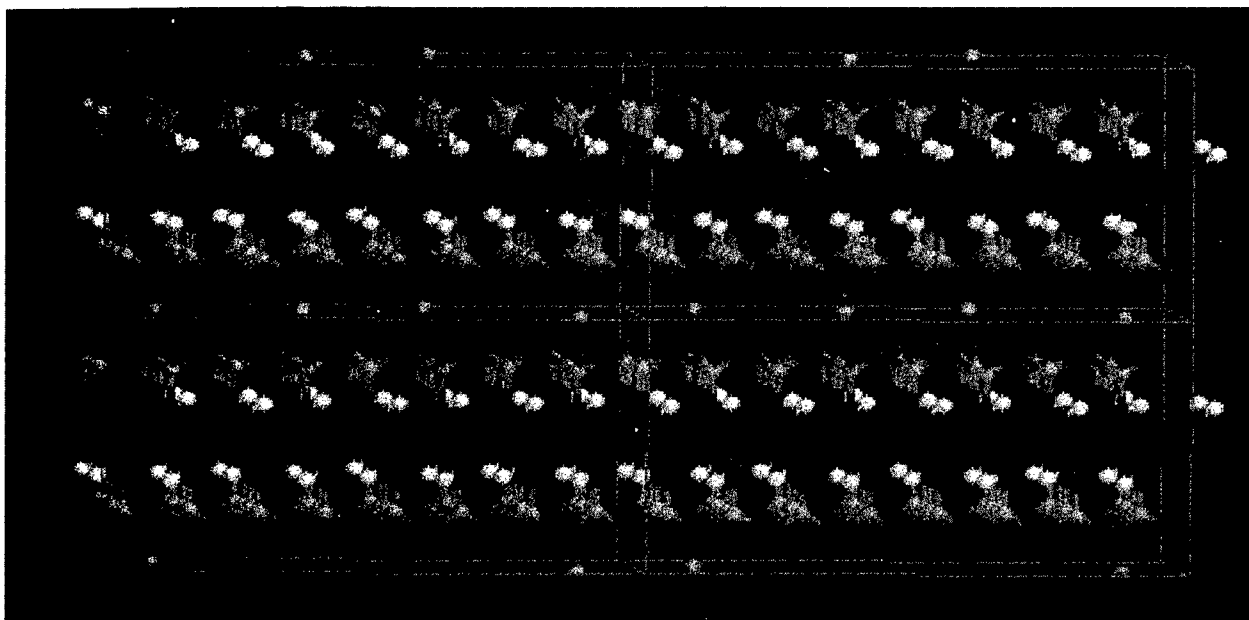
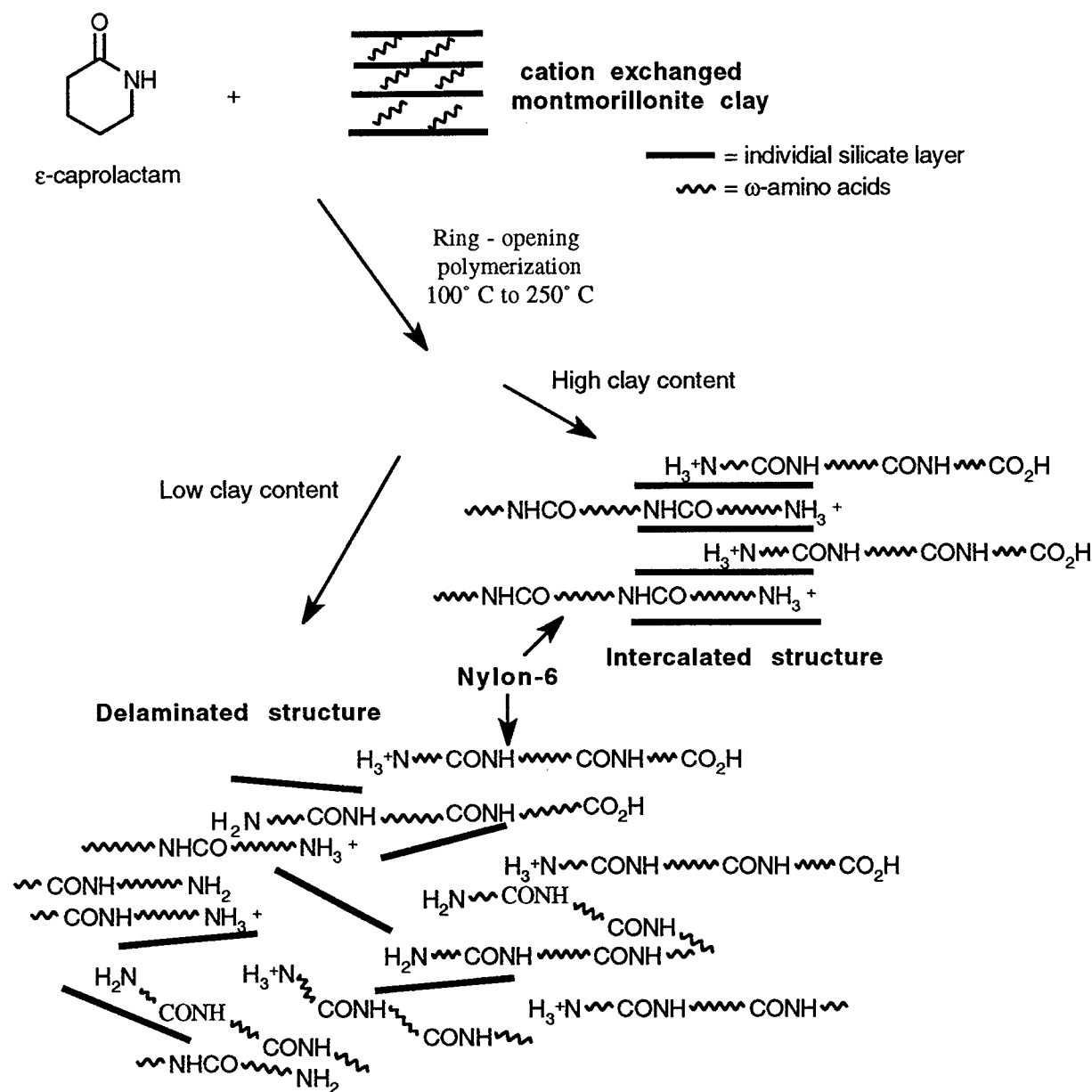


Figure 1. Molecular representation of sodium montmorillonite, showing two aluminosilicate layers with the Na⁺ cations in the interlayer gap or gallery (1.14 nm spacing between layers).

The nylon-6 clay nanocomposites are synthesized by ring-opening polymerization of ϵ -caprolactam in the presence of cation exchanged montmorillonite clay.⁹ This process creates a polymer layered silicate nanocomposite with either a *delaminated* structure or an *intercalated* structure (see Scheme 1), depending on the clay content. The *intercalated* structure, which forms when the mass

fraction of clay is greater than 20 %, is characterized by a well ordered multilayer with spacing between the silicate layers (gallery spacing) of only a few nanometers. The *delaminated* structure, which forms when the mass fraction of clay is less than 20 %, contains the silicate layers individually dispersed in the polymer matrix. The *delaminated* structure is less ordered and the gallery spacing is greater, 10 nm to 100 nm.



Scheme 1. Diagram of the process used to prepare polymer layered silicate nanocomposites with either a *delaminated* structure or an *intercalated* structure.

FLAMMABILITY STUDIES

Nylon-6 clay nanocomposite

To evaluate the feasibility of controlling polymer flammability via a nanocomposite approach, we examined the flammability properties, using the Cone calorimeter, of nylon-6 clay nanocomposites and compared them to

those for pure nylon-6.⁵ The Cone calorimeter data, shown in Figure 2, indicates that the peak heat release rate (HRR), an important parameter for predicting fire hazard¹⁰, is reduced by 63 % in a nylon-6 clay-nanocomposite containing a clay mass fraction of only 5 %. These samples were exposed to a heat flux of 35 kW/m².

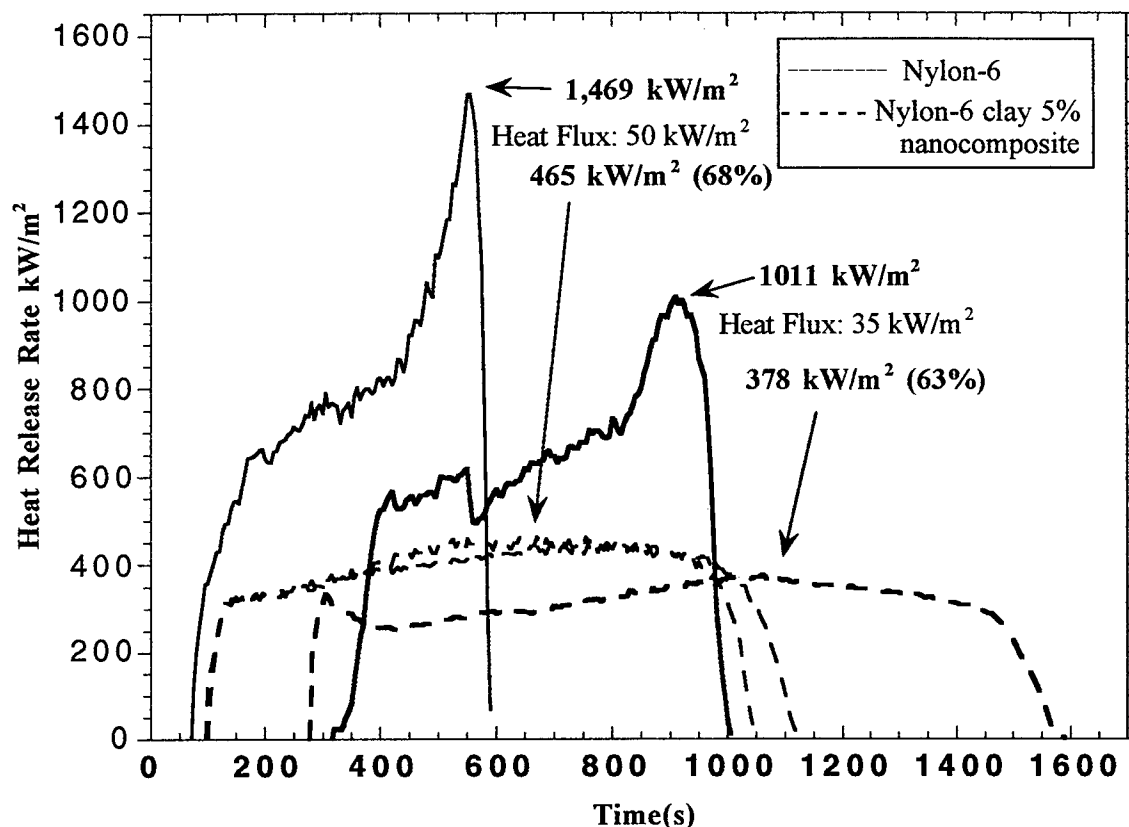


Figure 2. Rate of heat release versus time plot for nylon-6 clay-nanocomposite (5 mass %) and pure nylon-6. The data for the 35 kW/m² and 50 kW/m² flux exposures are shown. Two experiments at the 50 kW/m² flux exposure are included to show the typical reproducibility. The nanocomposite has a 63 % lower HRR at 35 kW/m² and a 68 % lower HRR at 50 kW/m².

This reduction in HRR is comparable to that found for commercial flame retarded (FR) polymers, but at a lower mass fraction of "additive" than is typical (see Table 1). This system maintains effectiveness even at higher heat fluxes. The peak HRR is reduced by 68 % when the samples are exposed to a heat flux of 50 kW/m². From the Cone calorimeter data the nanocomposites were found to

have the same heat of combustion as the pure nylon-6. Furthermore, the nanocomposites did not increase the rate of carbon monoxide or soot (measured by the specific extinction area, SEA) formation during the combustion, as some flame retardants do.^{11,12} Figure 3 shows the mass loss rate data for nylon-6, and nylon-6 clay-nanocomposite (5 mass %).

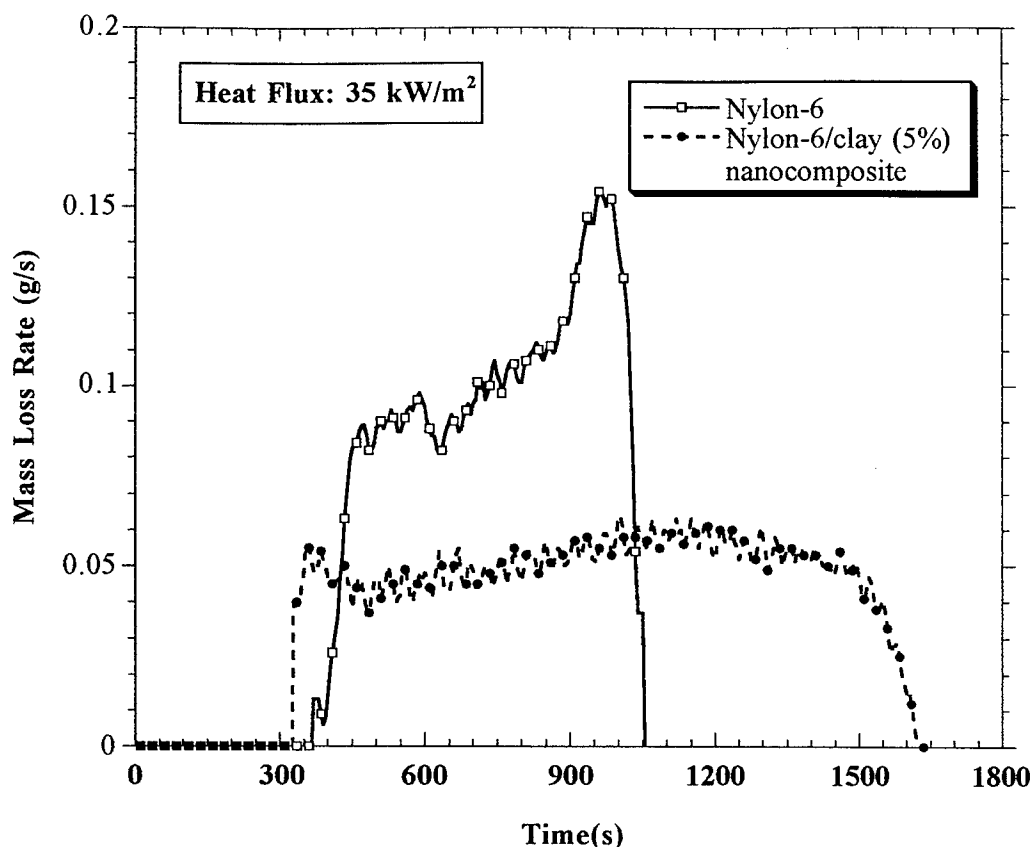


Figure 3. The mass loss rate data for nylon-6, and nylon-6 clay-nanocomposite (5 %).

The two curves closely resemble the HRR curves, indicating that the reduction in HRR for the nanocomposites is primarily due to the reduced mass loss rate and the resulting lower fuel feed rate to the gas phase. This data indicates that the nano-dispersed clay modifies the condensed phase and not the gas phase processes of the polymer during the combustion.

We did not find the same behavior when we studied the milligram scale thermal properties of these materials. We found that the nylon-6 nanocomposite had the same thermal decomposition behavior when the thermal stability was probed using thermogravimetric analysis combined with Fourier transform infrared spectroscopy, TGA-FTIR. The peak of the derivative of the mass loss versus time curves were both at $460\text{ }^{\circ}\text{C} \pm 10\text{ }^{\circ}\text{C}$. The FTIR data for both samples were identical and corresponded to the spectrum for ϵ -caprolactam with traces of CO and CO₂. The TGA-residue yields were 0.3 mass % (± 0.1 mass %) for nylon-6 and 5.5 mass % (± 1.0 mass %) for the nanocomposite. After accounting for the amount of clay present (5 mass %) in the nanocomposite, these carbonaceous residue yields are essentially the same. This was somewhat surprising since

other studies of the thermal reactions in layered organic-clay intercalates, at $400\text{ }^{\circ}\text{C}$, reported formation of carbonaceous-clay residues and other condensation and crosslinking type reaction products.¹³ These data indicate that the mechanism of flame retardancy is not via retention of a large fraction of carbonaceous char in the condensed phase.

Visual observations of the combustion experiments, in the Cone calorimeter, reveals different behavior for the nylon-6 clay-nanocomposites, compared to the pure nylon-6. A thin char layer forms, on the top of all the samples, in the first few minutes of exposure, prior to ignition. In the case of pure nylon-6, this char layer fractures into small pieces early in the combustion. The char does not fracture with the nylon-6 clay-nanocomposites. This tougher char layer survives and grows throughout the combustion, yielding a rigid multicellular char-brick with somewhat larger dimensions as compared to the original sample.

We proposed that the delaminated hybrid structure collapses as the nylon-6 decomposes.⁵ This forms a reinforced char layer which acts as an insulator and a mass transport barrier, slowing the escape of the volatile

products (e.g. ϵ -caprolactam) generated as the nylon-6 decomposes. Indeed, transmission electron microscopy (TEM) of a section of the char-residue from the combustion of the nylon-6 clay-nanocomposite, shown in Figure 4, reveals a multilayered-silicate structure. X-ray diffraction, XRD, shown in Figure 5, and TEM give an interlayer spacing of 1.3 nm ($2\theta = 6.9^\circ$). XRD also shows a peak for the 0.33 nm spacing between layers in graphitic-carbon ($2\theta = 26.7^\circ$). The carbon presumably occupies the interlayer space between the silicate layers. The nanocomposite structure of the char appears to

enhance the performance of the char, just as the nanocomposite structure enhances the performance of the nylon-6. Since these materials have excellent barrier properties, an additional effect, due to the low permeability of liquids and gases through the nylon-6 nanocomposite itself, may also be responsible for the slow the transport of volatile fuel to the gas phase.¹⁴ Recent molecular dynamics simulations of the thermal degradation of nano-confined polypropylene support this type of mechanistic hypothesis.¹⁵

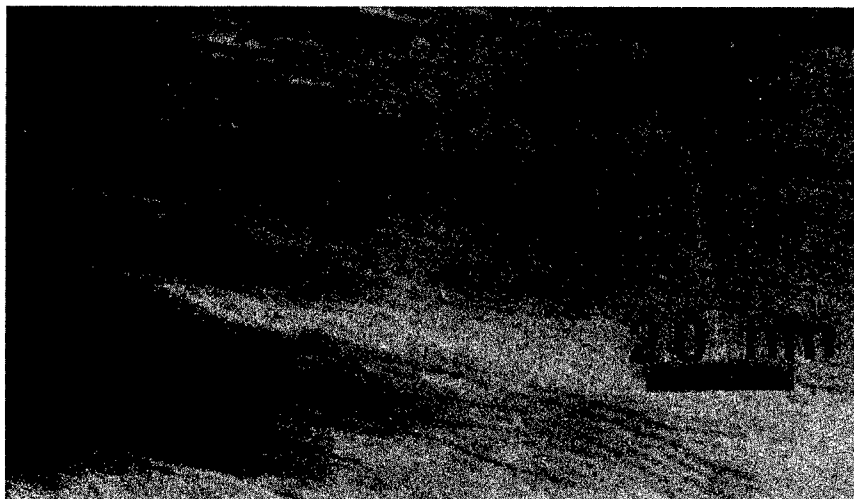


Figure 4. TEM of a section of the combustion char from the nylon-6 clay-nanocomposite (5 %) showing the silicate (1 nm thick, dark bands) multilayered structure. This layer may act as an insulator and a mass transport barrier.

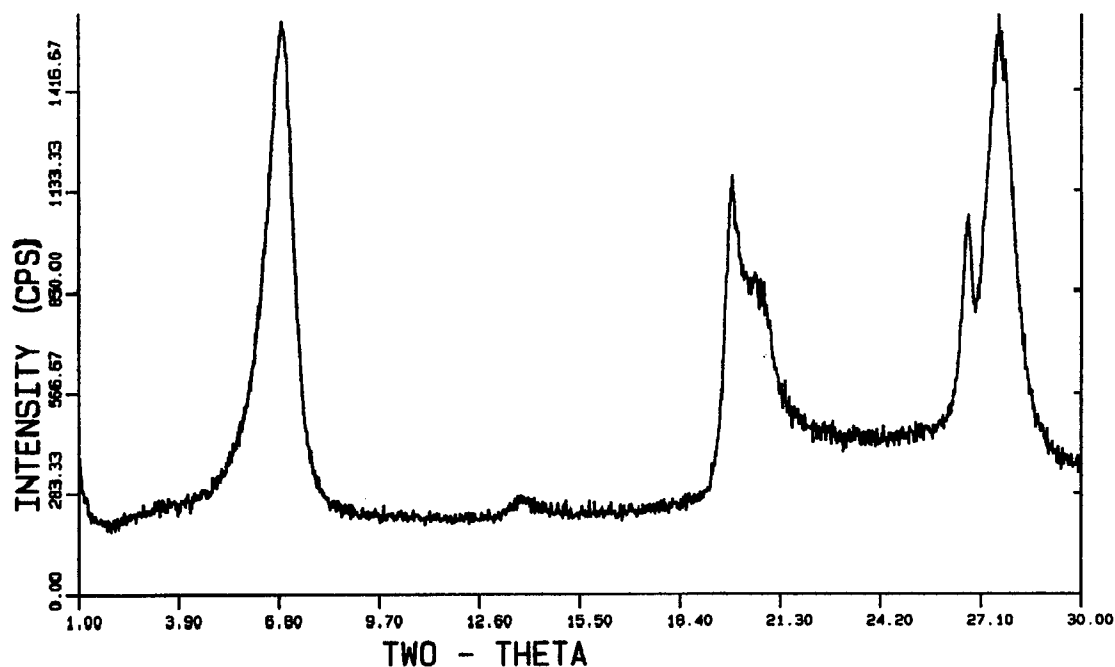


Figure 5. X-ray diffraction patten of the char residue from combustion of nylon-6-clay nanocomposite in the Cone calorimeter. This gives an interlayer spacing for the clay in the char residue of 1.3 nm ($2\theta = 6.9^\circ$).

RADIATIVE GASIFICATION

Nylon-6 clay nanocomposite

Figure 6 shows the gasification apparatus. The gasification apparatus allows pyrolysis, in a nitrogen atmosphere, of samples identical to those used in the Cone calorimeter.

Figure 7 shows the mass loss rate curves for a set of experiments carried out in the gasification apparatus, aimed at comparing the pyrolysis behavior of the nanocomposite to that for pure nylon-6. The slope of the mass loss curve for the nanocomposite significantly differs from that for the pure nylon-6 at ~ 180 seconds. The digitized video images, shown in Figure 8, of the pyrolysis experiments, reveal that the nanocomposite (center column) begins to char at the edges of the sample at 120 seconds. The thermocouple on the bottom of the sample shows that the temperature, at 240 seconds, is $\sim 50^\circ\text{C}$ to 75°C lower under the nanocomposite sample than under the pure nylon-6 sample. These images also show that the formation of a char layer on the top of the nanocomposite sample (center column) occurs at the same time, 180 seconds, that the mass loss rate of the sample slows. Presumably it is this char layer that is responsible for both the lower back-side temperature and the lower mass loss rate for the nylon-6 nanocomposite.

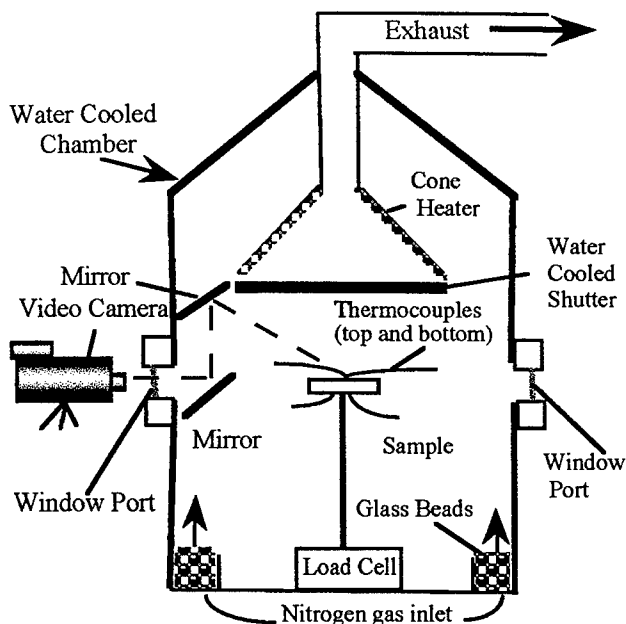


Figure 6. A schematic of the radiative gasification apparatus (1 m diameter, 2 m height). The gasification apparatus allows pyrolysis, in a nitrogen atmosphere, of samples identical to those used in the Cone calorimeter.

Figure 8 also shows the effect of oxygen on the charring process for the nylon-6 nanocomposite. The images in the column on the right are of the pyrolysis of the nylon-6 nanocomposite in a nitrogen - oxygen atmosphere with an oxygen volume fraction of 7.5 %. It appears that the presence of oxygen causes the charring process to occur earlier in the pyrolysis. Even at 60 seconds the entire sample is darkened and at 120 seconds most of the surface is charred.

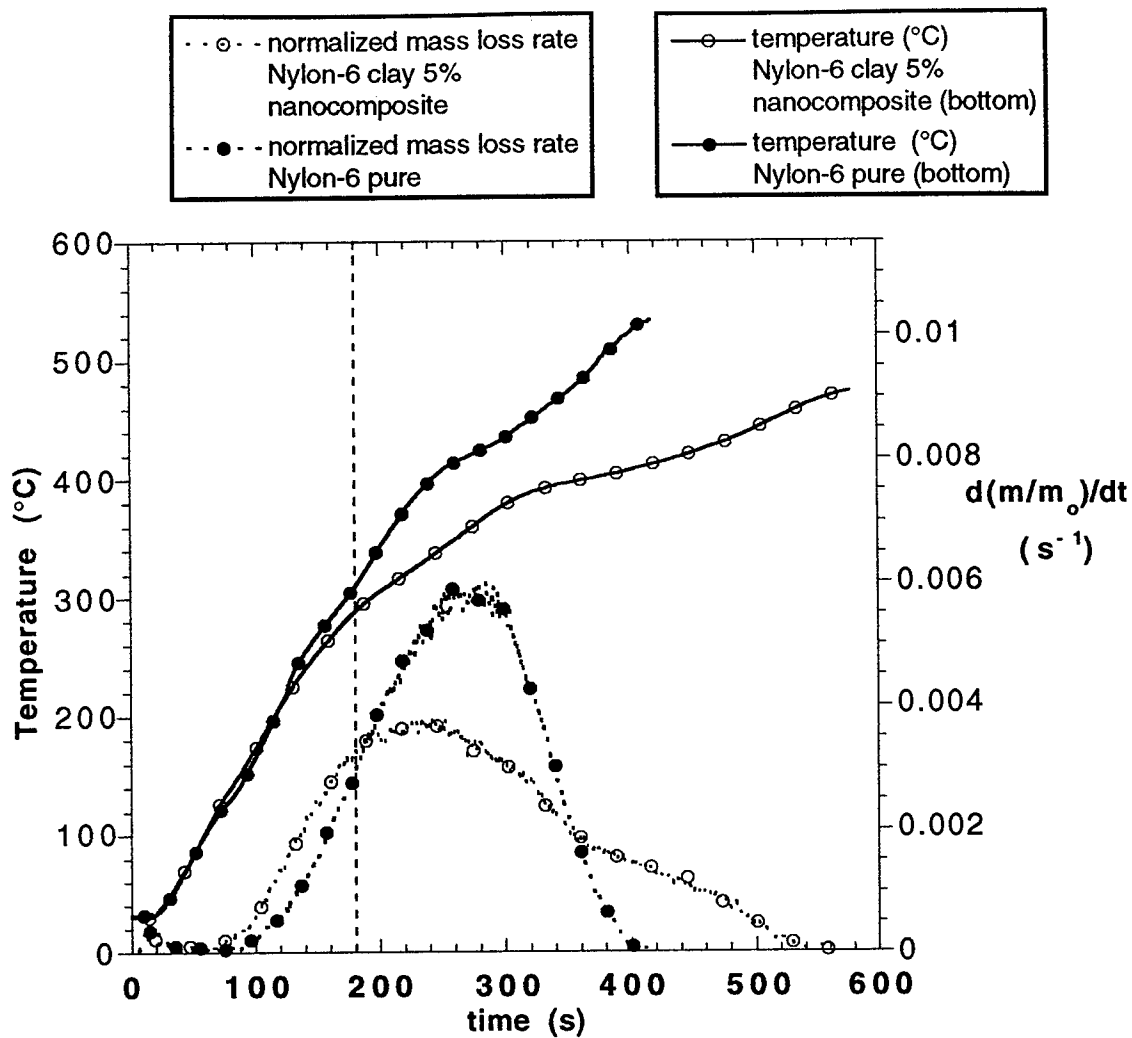


Figure 7. Normalized Mass loss rate and temperature versus time plots for the gasification experiments for nylon-6 and nylon-6 clay (5%) nanocomposite with N_2 atmosphere. All samples were exposed to a flux of 40 kW/m^2 in a N_2 atmosphere. The mass loss rate curves begin to differ at 180 seconds when the surface of the nanocomposite sample is partially covered by char.

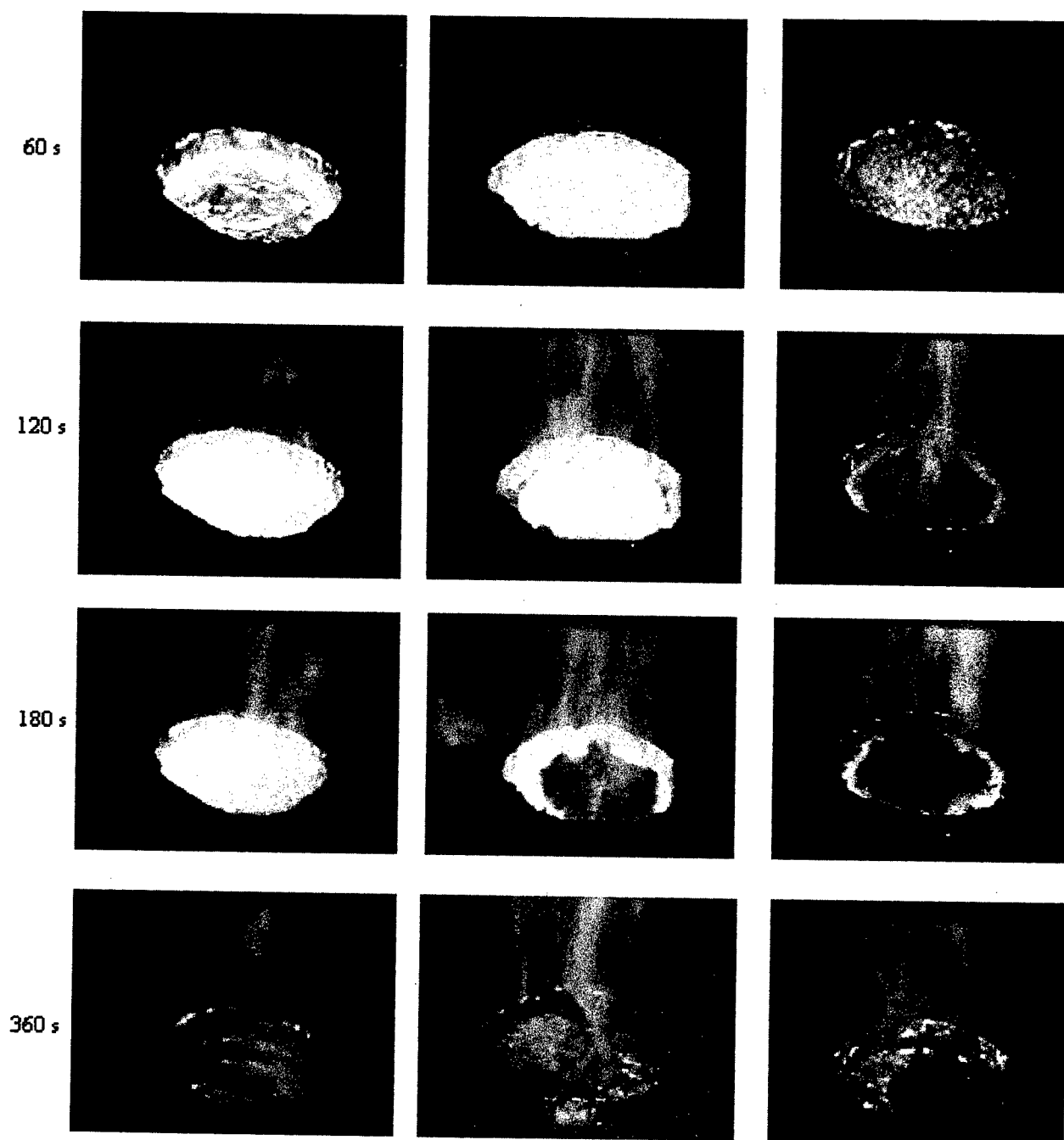


Figure 8. Images from radiative gasification, at various times, of nylon-6 with N₂ atmosphere (left), nylon-6 clay (5%) nanocomposite with N₂ atmosphere (center) and nylon-6 clay (5%) nanocomposite in a N₂/O₂ atmosphere containing a volume fraction of 7.5 % O₂ (right). All samples were exposed to a flux of 40 kW/m².

This is similar to the pre-ignition charring, mentioned above, for the nanocomposite in the Cone experiment. However the mass loss rate for the nylon-6 nanocomposite is not significantly different in the oxygenated pyrolysis atmosphere. The residue yields are also the same (5.0 mass % \pm 0.5 mass %) within the experimental uncertainty. Comparison of the mass loss data from the Cone calorimeter experiment (Figure 3) to the mass loss data from the gasification experiment (Figure 7), shows that the nanocomposite has a lower mass loss rate in the Cone than in the gasification apparatus. In the Cone calorimeter, the mass loss rate for the nanocomposite, is 62 % lower than the mass loss rate for nylon-6. In the gasification apparatus, the mass loss rate for the nanocomposite, is only 35 % lower than the mass loss rate for nylon-6. Some of this difference is due to the fact that in the Cone a sample with a lower HRR experiences a reduced heat feed back ($\sim 10 \text{ kW/m}^2$) from the flame and hence is exposed to a lower net flux. This further reduces the HRR and the mass loss rate. This does not occur in the gasification experiment. Each sample is exposed to the same flux throughout the pyrolysis. Some of this effect may be due to the effect of oxygen on the mechanism of flame retardancy for the nanocomposite. Another difference was also observed for the nanocomposites between the Cone results and the gasification results. Although the residue yields for both experiments are the same (~ 5.5 mass %), the volume of the residue from the Cone sample is several times greater than that from the gasification sample. Recall that above we mentioned the formation of a rigid multicellular char-brick with the same or somewhat larger dimensions as the original sample. We have observed similar differences between Cone data and gasification data in another system, the results of which were published previously. In this case the reduction in mass loss rate, due to the presence of silica-additives, in the gasification experiment was only half of that observed in the Cone experiment. However, in this system the residue yield was 15 mass % in the Cone and only 9 mass % in the gasification apparatus.¹⁶

Further study of the possible role of oxygen in the mechanism of flame retardancy for the nanocomposite is underway.

VINYL POLYMER NANOCOMPOSITES FLAMMABILITY

Many other polymers have also been prepared as polymer-clay nanocomposites.¹⁷ For the purpose of investigating the general effectiveness of this new approach to flame retarding polymers we have examined the flammability of polymer-clay nanocomposites prepared from polystyrene, PS, and polypropylene-graft-maleic anhydride, PP-g-MA. Like the nylon-6 nanocomposites these polymer-clay nanocomposites are prepared using organic-modified montmorillonite clay. In contrast to the nylon system, these nanocomposites were prepared by the melt blending process.¹⁷ In this process the appropriately modified (compatibilized) montmorillonite clay and the polymer are combined in the melt to form the nanocomposite.

PS-clay nanocomposite

As described in the experimental section the PS-clay nanocomposite (3 %) has an *intercalated* structure (see Scheme 1). The intergallery spacing, by XRD analysis, is 3.1 nm ($2\theta = 2.7^\circ$). The data in Table 1 shows that the peak HRR for the *intercalated* PS-clay nanocomposite is half of that for pure PS or for the *immiscible* PS-clay mixture. Comparison of this Cone data with that for PS flame retarded using decabromodiphenyl oxide, DBDPO, and antimony trioxide, Sb_2O_3 , (Table 1) shows that the nanocomposite results in a similar reduction in the peak HRR for PS, but without as much of an increase in the soot (measured by the specific extinction area, SEA) or CO yields.

This result was surprising since, the *intercalated* form of the nanocomposite, at such a low clay concentration is essentially a blend, with *intercalated*-PS-clay domains dispersed in pure PS. However the thermal stability of this system is also seen in the TGA behavior shown in Figure 9. The TGA of the *intercalated*-PS-clay nanocomposite reveals almost a 50 °C increase in the peak for the derivative of the TG plot (DTG) as compared to the peak of the DTG for the *immiscible* PS-clay mixture.

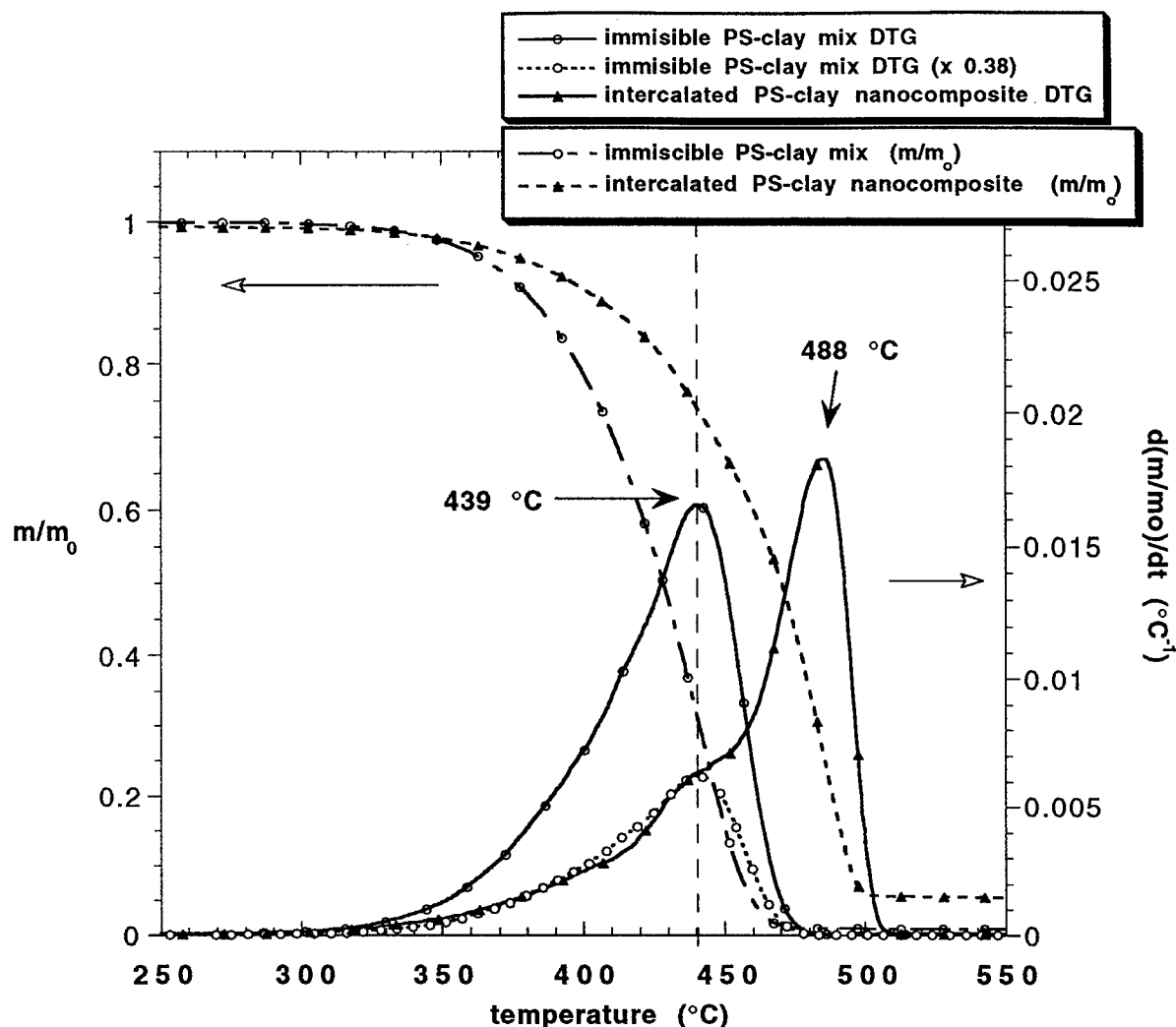


Figure 9. Normalized TGA plots and DTG plots for *immiscible* PS-clay (3 %) mixture and *intercalated* PS-clay (3 %) nanocomposite. The *intercalated*-PS clay is clearly has greater thermal stability than the *immiscible* PS-clay mixture.

This is in contract to the nylon-6 clay nanocomposite which showed no change in the peak DTG.⁵ Also apparent from the DTG data is the presence of two decomposition peaks for the *intercalated*-PS-clay nanocomposite. The first, at 440 °C, coincides with the DTG peak for the *immiscible* PS-clay mixture, the second at 488 °C, is most likely from the decomposition of the *intercalated*-PS. Studies, published previously, of the thermal decomposition behavior of several polymer-clay nanocomposite also showed that the *intercalated* form had the highest stability, even greater stability than the *delaminated* nanocomposite.^{18, 19}

We determined that the ratio of the area under the DTG curves for these two decomposition processes is 1.0 to

1.5. This indicates that the presence of a mass fraction of only 3 % clay in the *intercalated*-PS nanocomposite increases the thermal stability of 60 % of the PS. This ratio was determined using the DTG curve for the *immiscible* PS-clay decomposition to approximate the decomposition contained in the shoulder of the *intercalated*-PS-clay DTG curve. We find that multiplication by the appropriate factor (0.38) gives a ratio of the area under the DTG curves for these two decomposition processes, *immiscible* and *intercalated* respectively, of 1.0 to 1.5. This is in agreement with studies on other polymer-clay nanocomposites where the mass fraction of polymer directly effected by the presence of the clay was found to be ~ 60 %.²⁰

Table 1. Cone Calorimeter Data

Sample (structure)	sample mass (g)	Residue Yield (%) ± 0.5	Peak HRR ($\Delta\%$) (kW/m ²)	Mean HRR ($\Delta\%$) (kW/m ²)	Mean H _c (MJ/kg)	Total Heat Released (MJ/m ²)	Mean Specific Ext. Area (m ² /kg)	Mean CO yield (kg/kg)
Nylon-6	53	1.0	1,011	603	27	413	197	0.01
Nylon-6 clay- nanocomposite 2% <i>delaminated</i>	54	3.0	686 (32%)	390 (35%)	27	406	271	0.01
Nylon-6 clay- nanocomposite 5% <i>delaminated</i>	55	5.7	378 (63%)	304 (50%)	27	397	296	0.02
PS		0	1,118	703	29	102	1,464	0.09
PS clay- mix 3% <i>immiscible</i>	19	3.2	1,080	715	29	96	1,836	0.09
PS clay- nanocomposite 3% <i>intercalated</i>	19	3.7	567 (48%)	444 (38%)	27	89	1,727	0.08
PS w/ DBDPO/Sb ₂ O ₃ 30%	15	2.6	491 (56%)	318 (54%)	11	38	2,577	0.14
PP-g-MA	23	0	2,028	861	38	219	756	0.04
PP-g-MA clay nanocomposite 5% <i>intercalated</i>	21	8.0	922 (54%)	651 (24%)	37	179	994	0.05

H_c : Heat of combustion

PP-g-MA-clay-nanocomposite

The Cone data for the PP-g-MA-clay-nanocomposite (clay mass fraction of 5 %) prepared by melt blending PP-g-MA with bis(dimethyl)bis(tallow)ammonium-exchanged montmorillonite, is also shown in Table 1. In this case the melt blending yielded a nanocomposite with the *intercalated* structure (see Scheme 1). The intergallery spacing, by XRD analysis, is 3.6 nm ($2\theta = 2.4^\circ$). The data in Table 1 shows that the peak HRR for the *intercalated* PP-g-MA-clay nanocomposite is half of that for pure PP-g-MA.

SUMMARY

The Cone data in Table 1 shows that the FR performance of the PS-clay nanocomposite and the PP-g-MA-clay nanocomposite is very similar to that for the nylon-6 clay nanocomposite. The Cone data also shows that the FR mechanism for the PS-clay nanocomposite and the PP-g-MA-clay nanocomposite is very similar to that for the nylon-6 clay nanocomposite. As with nylon-6, the heat of combustion, and rates of soot and CO formation are unchanged, within the experimental uncertainty, by the

presence of the clay in the PS and PP nanocomposites. Furthermore, the residue yields from combustion, for all the polymer, are not high enough to account for the reduced flammability due to retention of carbon in the condensed phase. A condensed phase mechanism where a reinforced char layer forms, which acts as an insulator and a mass transport barrier, slowing the escape of the volatile decomposition products generated as the polymer decomposes appears to be one likely explanation for the excellent FR performance of the clay-nanocomposites.

ACKNOWLEDGMENTS

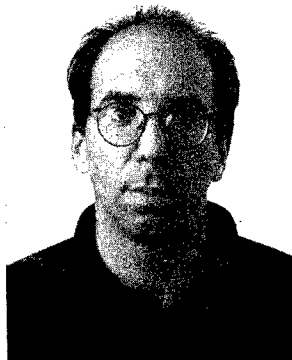
The authors (J.G. and T. K.) would like to thank the Federal Aviation Administration for partial funding of this work, through Interagency Agreement DTFA0003-92-Z-0018. We would also like to thank Mr. Michael Smith for Cone Calorimeter analysis, Lori Brassel for TGA analysis, Dr. Catheryn Jackson and Dr. Henri Chanzy for TEM analysis of the char samples, Dr. Marc Nyden for the montmorillonite structure. We would also like to express our gratitude to Dow chemical Co. for PS samples (STYRON 6127), Ube America Inc. for nylon-6

clay nanocomposite samples and Southern Clay Products for the organic-modified clays, Cloisite 15A and 3A.

REFERENCES

† Guest Researcher at NIST from the Russian Academy of Sciences, Moscow, Russia.

1. G. L. Nelson, *Fire and Polymers II*, ACS Symposium Series 599 (ed. G. L. Nelson) American Chemical Society, Washington, DC pp. 1-28 (1995).
2. S. Levchik, G. Camino, L. Costa, and G. Levchik, *Fire and Materials*, **19**, 1 (1995).
3. A. Hochberg, Proceedings of the Fall FRCA Meeting, Naples, FL., 159 (1996).
4. Y. Kojima, A. Usuki, M. Kawasumi, A. Okada, Y. Fukushima, T. Kurauchi, and O. Kamigaito, *J. Mater. Res.* **8**, 1185 (1993).
5. J. W. Gilman, T. Kashiwagi, J. D. Lichtenhan, *SAMPE Journal*, **33**, no. 4, 40 (1997).
6. V. Babrauskas, R. Peacock, *Fire Safety Journal*, **18**, 255 (1992).
7. V. Babrauskas, *Fire and Materials*, **19**, 243 (1995).
8. Certain commercial equipment, instruments, materials, services or companies are identified in this paper in order to specify adequately the experimental procedure. This in no way implies endorsement or recommendation by NIST.
9. A. Usuki, Y. Kojima, M. Kawasumi, A. Okada, Y. Fukushima, T. Kurauchi, and O. Kamigaito, *J. Mater. Res.* **8**, 1179 (1993).
10. V. Babrauskas, R. Peacock, *Fire Safety Journal*, **18**, 255 (1992).
11. A. Grand, *SAMPE Journal*, **33**, no. 4, 47 (1997).
12. R. Harris, Jr., V. Babrauskas, B. C. Levin and M. Paabo, NISTR 4649, 1991.
13. J. M. Thomas, "Intercalation Chemistry", Academic Press, Inc., London, 1982, Chapter 3, p. 55.
14. E. Giannelis, and P. Messersmith, *J. Polym. Sci. A: Polym. Chem.*, **33**, 1047 (1995).
15. M. Nyden, J. W. Gilman, *Computational and Theoretical Polymer Science*, in press, 1998.
16. J. Gilman, S. Ritchie, T. Kashiwagi, and S. Lomakin, *Fire and Materials*, **21**, p. 23 (1997).
17. E. Giannelis, *Adv. Mater.* **8**, 29 (1996).
18. J. Lee, T. Takekoshi and E. Gannelis, *Mat. Res. Soc. Symp. Proc.* vol 457, p. 513, (1997).
19. J. Lee and E. Giannelis, *Polymer Preprints*, vol. 38, p. 688, (1997).
20. S. Burnside, Ph. D. Thesis, Cornell University, 1997.



Jeff Gilman, Ph. D.
NIST
Polymer Building -224, Rm B258
Gaithersburg, MD 20899-0001
Phone 301-975-6573
FAX 301-975-4052

Jeffrey W. Gilman was born in Rochester, NY, the son of a college chemistry professor. He obtained his BA in chemistry from Ithaca College in 1980 and his Ph. D. in organic chemistry from the University of California, Irvine in 1986. Dr. Gilman worked from 1987 to 1992 at the Phillips laboratory at Edwards Air Force Base where he led the propulsion materials group. He has worked as a Research Polymer Chemist in the Materials Fire Research Group at the National Institute of Standards and Technology since 1994. His research at NIST focuses on mechanistic studies of new flame retardants for polymers, using the Cone calorimeter and solid state NMR techniques.

Comparison of Fire Behavior of Copper and Fiber Optic Cables in Large and Full Scale Fire Test Facilities

J. Thomas Chapin, Ph.D.
Lucent Technologies
Norcross, GA 30071

Loren Caudill
DuPont
Wilmington, DE 19880

James R. Hoover
DuPont
Wilmington, DE 19880

ABSTRACT

This paper presents data on the fire behavior of various copper and fiber optic local area network (LAN) cables in large and full-scale fire test facilities. This investigation was prompted by concerns over the hazard of fire and smoke associated with the installation of lower fire performance cable installed in hidden cavities and void (plenum) spaces in buildings. The fire test methods were chosen to simulate full scale installation conditions. The methods compare the cables from the standpoint of temperature, flame spread, smoke density, smoke release rate and oxygen consumption. The tests indicate that cables constructed of jacket, insulation and/or buffer materials with high heats of combustion have correspondingly higher temperatures, flame spread and oxygen consumption. While comparable smoke release rates were observed for the cables, the increased flame spread and higher overall temperatures appears much more significant from an overall fire hazard standpoint than smoke opacity alone.

INTRODUCTION

Worldwide, ceiling and floor voids in commercial buildings are increasingly being used for utilities and ventilation. This design approach helps maximize flexibility in meeting tenant requirements. Many new and refurbished buildings use cavity voids, typically called

plenums, when they are used for handling air, to contain communications and power cables, plumbing, fire detection and suppression systems and similar mechanical and electrical services. Installing services in voids provides convenient access, easy alterations, lower construction costs and HVAC energy conservation.

Unfortunately, the uncontrolled installation of combustibles in concealed spaces is an important concern because of the potential for undetected spread of fire and smoke throughout the building. A number of large, devastating fires have recently occurred in multi-story buildings involving combustibles in concealed spaces.¹ In Europe, the proliferation of local area networks (LANs) in buildings can result in heavy concentrations of low-fire-performance communications cables in concealed spaces and communications rooms. In the US, plenum spaces are intended for non-combustible or limited-combustible products.² These areas have been the subject of extensive investigations over the past 20 years.^{3 4 5}

The distinction between "low" and "high" performance cables can be made either by comparing properties of cable materials (combustion energy, oxygen index, heat release and smoke release rates, etc.) or by burning completed cable in large scale fire tests (which are described below) and comparing flame spread and smoke opacity behavior.

If concealed void spaces contain combustibles they are potential sites for the undetected generation and movement of fire and smoke. Historically, this has meant that products exposed in the void areas have been required to be either (a) fire partitioned, or be (b) very low in fuel-load and combustibility, or be (c) protected by either fire resistant coverings or fire extinguishment systems. In the past, these options worked quite well. However, with the growing use of voids for cabling, new fire-path and fire-load problems are emerging. LANs are growing at 25%/year in many regions and LAN cabling systems are being replaced every 2 to 3 years as personal computers (PC's) become faster and more powerful. Most often cables are not removed on re-cabling. As a result, many voids are becoming filled with multiple generations of data communications cables with low or unknown aggregate fire performance.

CABLE FIRE TESTS

There are a number of small and large scale fire test methods cited in US and international customer specifications and tender documents to assess communications cable flame spread and smoke behavior. The comparison of US and IEC fire test methods by relative severity is displayed in Figure 1. At the bottom of the list are two single cable, low energy burner tests (IEC 332-1 and UL 1581 VW-1). Next, there are several vertical ladder tests (IEC 332-3C, UL 1581 and UL 1685). UL 1685 is the UL 1581 method with peak smoke release rate and total smoke requirements added. At the high end of the list are the UL 1666 Riser and UL 910 Plenum fire test methods. Details of the tests and pass/fail criteria are described in detail in the Experimental section.

More recently, a full scale fire test for concealed spaces was developed at BRE/FRS (Building Research Establishment - Fire Research Station) at their fire test facility in Cardington, UK.⁶ The test rig and subsequent fire test programs were designed to support the development of new performance data for hazard assessments,

international fire test protocols and fire safety engineering.

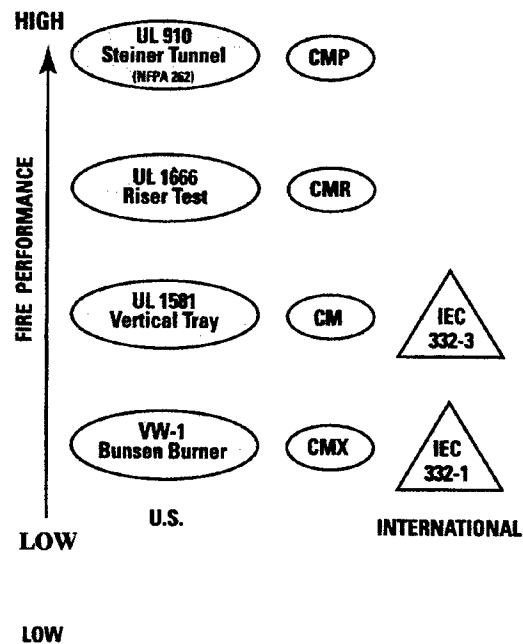


Figure 1
Hierarchy of Communications Cable Fire Tests

OBJECTIVES

This paper evaluates the fire performance of a series commercial copper and fiber optic (LAN) data communications cables in the UL 910 (or Steiner Tunnel (NFPA 262-1990)⁷ test method and the full-scale fire test facility at BRE/FRS, Cardington, UK. The cables were selected to provide a wide range of fire performance, based on their advertised fire rating (meeting either UL or IEC fire test methods).

EXPERIMENTAL

Communications Cable Products Tested

A total of 6 copper and fiber optic cables, obtained commercially were selected for this study; four were copper and two were fiber optic cables. The copper cables were composed of 4-pair, 24 gauge, unshielded twisted pair (UTP) constructions. The fiber optic cables consisted of

12 buffered fibers surrounded by aramid yarn and an outer thermoplastic jacket. The buffered fiber consists of an outer thermoplastic layer over a nominal 250 micron, dual acrylate coated optical fiber. The buffered fiber has a nominal OD of 900 microns (35 mils). The cable identities and fire performance rating are described in Table 1. All cables are composed of thermoplastic materials and are typically installed in horizontal concealed spaces to connect PCs to LANs.

Table 1

Communications Cable Products and Fire Rating

Cable ID	Media	Fire Rating
K	Copper	IEC 332-1
B	Copper	UL 1581, CMX
J	Copper	IEC 332-3C
O	Fiber	IEC 332-3C
F	Copper	UL 910, CMP
M	Fiber	UL 910, OFNP

Large and Full Scale Fire Tests

UL 910 Steiner Tunnel Test

The most severe intermediate-scale horizontal tray fire test in the US is UL 910 (NFPA 262-1990, *Test for Fire and Smoke Characteristics of Wires and Cables* which is a modification of the 7.6m (meter) Steiner Tunnel used for construction products.⁸ In this method, an array of cables 0.3m wide and 7.6m long is strung beneath the ceiling on a ladder extending for the length of the tunnel. A diffusion gas burner flame of 90kW (nominal) engulfs up to 1.5m of the cable at the far upstream end. Ventilation is supplied from the burner end at a linear flow rate of 73m per minute. A photograph of the UL 910 facility at Underwriter's Laboratories in Northbrook, Ill., is found in Figure 2.

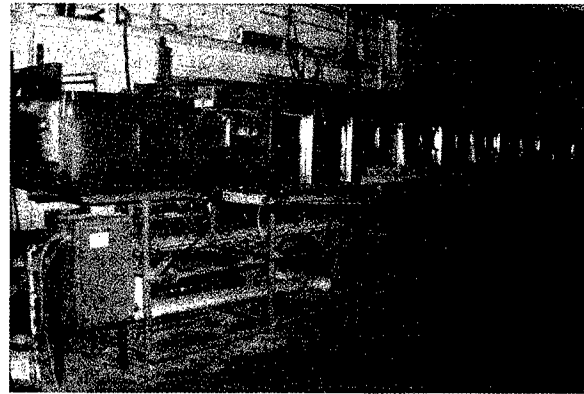


Figure 2

UL 910 Facility at Underwriter's Laboratories, Northbrook, IL

Cables for plenum installation in the US must pass the UL 910 test and are required to spread flame no more than 1.5m past the burner flame tip and produce a peak smoke optical density no greater than 0.5 and an average smoke optical density no greater than 0.15 in the exhaust duct. Additional measurements of heat release and smoke release rates were made on the cables. While these measurements are not required, they allow further comparison of cable performance and provide data for fire safety engineering calculations.

Full Scale Horizontal Cavity Fire Test

The full scale fire tests were carried out at the Fire Research Station, Building Research Establishment (BRE/FRS) in Cardington, UK. The fire facility consisted of a burn-room - ceiling-void re-burnable structure with a nominal 1-megawatt wood crib source-fire. In ongoing investigations, fire scenarios, ventilation conditions, and LAN cable designs and configurations have been varied. The full-scale test rig was a 7.4m x 5.7m x 4m high concrete block burn-room/ceiling-void re-burnable structure with a 2-hour fire rated suspended ceiling. The ceiling forms an above-ceiling concealed space 1 meter deep (see Figure 3, Figure 5 and Figure 6).

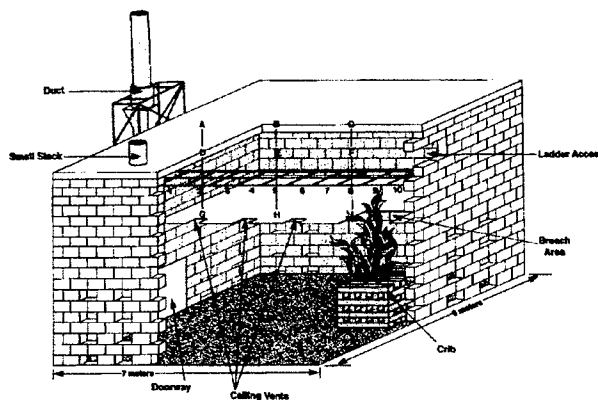


Figure 3
BRE/FRS Full Scale Fire Test Facility



Figure 4
Photo of BRE/FRS Fire Test

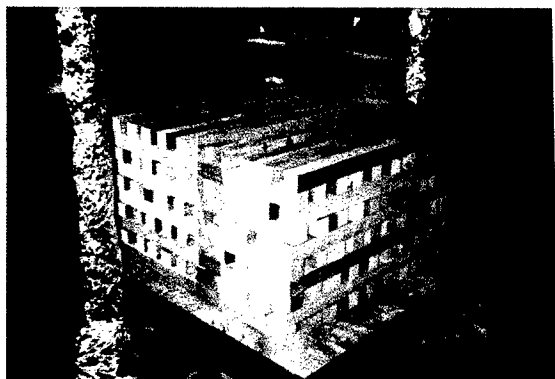


Figure 5
BRE/FRS Wood Crib Fire Source

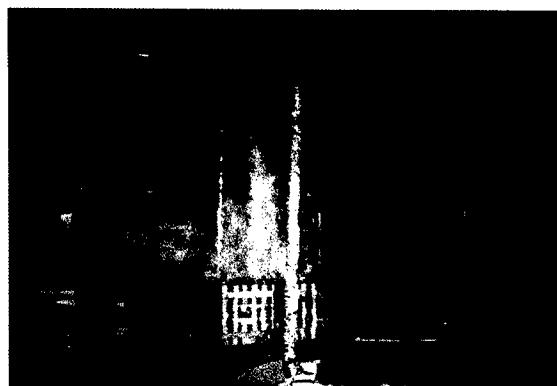


Figure 6
Wood Crib After Ignition

The source fire was created with a nominal 150kg. crib of kiln-dried pinus sylvestris with 20% moisture content. This fuel was stored in conditioning rooms until used. One hundred sticks, 60mm x 60mm x 1m, were stacked 10 per row in 10 rows to generate a nominal 1-megawatt fire over 30 minutes. The 1-megawatt intensity was chosen to simulate a fire in an open-plan office workstation. Recent National Institute of Science and Technology research indicates such workstation fire energies can typically range from 2 to 6 megawatts.⁹

The wood crib calibrations in the BRE/FRS full-scale calorimeter showed very linear mass loss after about 8 minutes from ignition. However, the energy output ramped up sharply until about 10 minutes into the burn and then plateaued until about 20 minutes. The energy output then ramped up again from 20 minutes until about 30 minutes.

The air extraction system was capable of 4.5m³/sec. The hot gas and smoke from the crib fire entered the cavity void through a breach (hole) in the suspended ceiling directly over the crib and were then extracted through vents at the far end of the plenum. Cables were supported on a steel ladder 7.2m long by 0.38m wide. The ladder was located midway between the suspended ceiling and the structural ceiling of the test rig.

Thermocouples (TCs) arrayed vertically in the burn room provided data for mapping

temperature profiles. Other thermocouples arrayed horizontally and vertically in the void space provided data for mapping both temperature profiles and flame spread Figure 3. The baseline performance of the source fire and test apparatus without cable combustibles was determined by operating the system with an insulated board on the ladder in place of cable.

RESULTS

Characterization of Cable Materials - FTIR Spectroscopy

Each cable material (jacket, insulation or buffer material) was subjected to Fourier Transform

Infrared Analysis (FTIR), heat of combustion and % ash content to characterize the materials involved in the fire tests. Reflectance FTIR spectroscopy is well suited to rapidly identify the base polymer and some flame retardant additives found in thermoplastic materials used in wire and cable manufacture. By employing thin film (approximately 10 mils) "reference" materials, unknown samples can be compared to materials of known composition. FTIR spectra were obtained in the range of 4000 to 650 cm^{-1} on compression molded samples of cable materials. Comparison of multiple absorbance bands allows for functional group analysis. The FTIR data is found in Table 2

Table 2 FTIR Analysis of Cable Materials

Cable	Media	Fire Rating	Jacket	Insulation/Buffer
K	Copper	IEC 332-1	EVA/ATH	HDPE
B	Copper	UL 1581, CMX	PVC/ATH	HDPE
J	Copper	IEC 332-3C	EVA/Mg(OH) ₂	HDPE
O	Fiber	IEC 332-3C	LSPVC	LSPVC
F	Copper	UL 910, CMP	LSPVC	FEP
M	Fiber	UL 910, OFNP	EVA/ATH	EVA/ATH

The polymer abbreviations are as follows: PVC - plasticized polyvinyl chloride, LSPVC - PVC compound modified to evolve low levels of smoke on combustion, FEP - fluorinated ethylene propylene, EVA - ethylene vinyl acetate copolymer, PP - polypropylene, HDPE - high density polyethylene, Mg(OH)₂ - magnesium hydroxide, ATH - alumina trihydrate (Al₂O₃ 3H₂O).

Cables J, K and O are marketed as LSZH (for Low Smoke Zero Halogen) products as the jacket and insulation or buffer materials are free of halogens. The flame retardant property of these cables is characterized by the presence of hydrates of aluminum or magnesium oxide. Flame retardancy is achieved by the retardation of flame through the endothermic evolution of water from the burning material. Evolution of water arises from the decomposition of metal hydrate at elevated temperatures (well above extrusion temperatures). Once the water is exhausted from the cable materials, the residue

will burn almost as vigorously as typical non-flame retarded materials; i.e., polypropylene, polyethylene or copolymers with vinyl acetate. The copious amounts of hydrogen and carbon in these samples serve as fuel for the combustion process.

In contrast, the halogenated materials (PVC, FEP) are intrinsically flame retarded due to the generation of Cl[•] and F[•] (radicals). Quenching is accomplished by the halogenated free radicals reacting with hydrogen and hydroxyl radicals in the flame.

With regards to smoke evolution, there is not a direct correlation between smoke opacity and halogen content (as is implied, but not substantiated with LSZH materials). Often smoke arises from PVC compounds due the high concentration of aromatic plasticizers (phthalates and trimellitates) which are employed to improve properties such as flexibility and toughness. It is well known that most fluorinated materials (FEP,

PVDF and their copolymers) exhibit little smoke on combustion; this is also true of low smoke PVC compounds which have been modified with metal complexes, solid plasticizers and char forming ingredients to reduce smoke evolution.

Ash Content and Combustion Energy of Cable Materials

Samples of cable materials were analyzed using the Oxygen Bomb Calorimetry Method per ASTM D2015 or ISO 1716¹⁰. The gross heat of combustion (calorific potential) and % ash content were obtained. The data is found in Table 3 and Table 4.

Table 3
Gross Heat of Combustion, H_c , for Cable Materials

Cable	Jacket H_c kJ/kg.	Insulation/Buffer H_c kJ/kg.
K 332-1	16242	46493
B CMX	19628	46493
J 332-3C	16033	46493
O 332-3	15284	18814
F CMP	14977	4856
M OFNP	14977	15112

Table 4
Ash Content of Cable Materials

Cable	Jacket %Ash Content	Insulation/Buffer % Ash Content
-------	---------------------	---------------------------------

K 332-1	60	0
B CMX	10	0
J 332-3C	25	0
O 332-3	42	40
F CMP	23	0
M OFNP	26	28

Note that the LSZH jacket materials found in cables J, K and O have high ash content which is associated with the presence of ATH or $Mg(OH)_2$ metal hydrates.

UL 910 Fire Test Results

The six copper and fiber optic cables were subjected to the UL 910 test and the results are found in Table 5 and Table 6. The data represents an average of two or three runs for each cable. Table 5 contains combustion data: time to ignition, flame spread, peak heat release rate and total heat released. The data for total heat released and peak heat release rate are corrected for the burner output.

Table 5
UL 910 Steiner Tunnel Flame Spread and Heat Release Results

Cable	Ignition, sec.	Flame Spread, ft	Total Heat Released, MJ	Peak Heat Release Rate, kW
K 332-1	25	19.5	117.5	407.7
B CMX	11	19.5	99.9	159.3
J 332-3C	34	19.5	249.4	464.6
O 332-3	30	19.5	125.5	357.3
F CMP	7	1.3	17.8	28.3
M OFNP	10	2.5	20.0	52.3

Table 6 contains data on the smoke behavior for each cable: peak OD, average OD, total smoke release rate and total smoke released.

Table 6
UL 910 Steiner Tunnel Smoke Optical Density and Release Rate Results

Cable	Peak OD	Average OD	Total Smoke Release Rate, m2/s	Total Smoke Released, m2
K 332-1	0.70	0.08	0.60	73.7
B CMX	2.0	0.84	1.86	668.5
J 332-3C	0.28	0.05	0.24	62.5
O 332-3	0.43	0.06	0.5	70.8
F CMP	0.30	0.09	0.17	62.3
M OFNP	0.25	0.07	0.4	61.8

BRE/FRS Full Scale Test Results

Cable B (CMX) and LSZH Cables (J, K and O) released comparatively large amounts of heat when burned in the full scale test. These cables burned the full length of the plenum space and developed large fireballs on the ladder and large pool fires on the suspended ceiling. The LSZH smoke density was approximately the same as Cable F (CMP) or Cable M (OFNP), but notably lower than Cable B (CMX).

An array of thermocouples were attached along the length of the plenum ladder to measure the temperature increase during the fire test (see the diagram in Figure 3). Thermocouple (TC) 10 is before the ceiling breach, TC 9 is in the breach areas and TC8 through TC 1 are equally spaced to the end of the ladder (7m). A plot of the maximum temperatures at each TC point are shown in Figure 7.

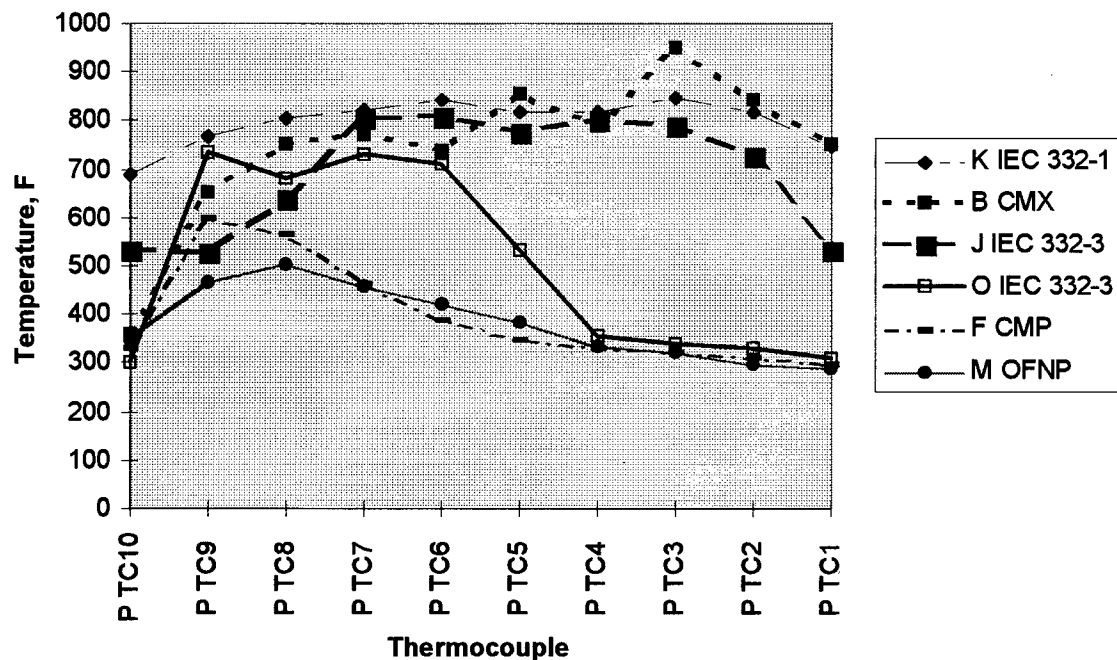


Figure 7 Maximum Thermocouple Temperatures Along the Plenum Ladder for Test Cables

Figure 8 is a photograph illustrating the fire performance of Cable K (LSZH). Figure 9 shows no flame spread with Cable F (CMP) under similar conditions.

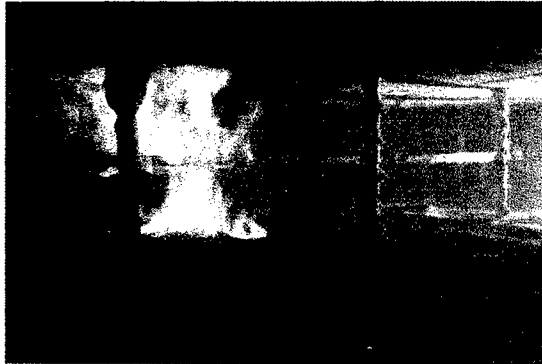


Figure 8
Flame Spread Behavior of Cable K in the
BRE/FRS Full Scale Test

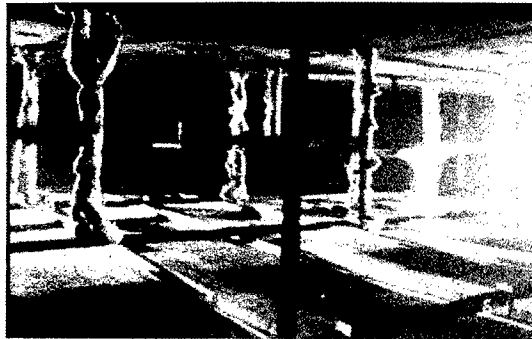


Figure 9
Flame Spread Behavior of Cable F in the
BRE/FRS Full Scale Test

Downstream peak temperatures along the entire length of the ladder could exceed 800°C when exposed LSZH cables burned. Cable B (CMX) downstream peak temperatures averaged slightly under 775°C. Recent British Steel Technical fire tests at BRE/FRS indicate that temperatures exceeding 800°C can cause structural steel beams to severely deform. This is illustrated in Figure 10.

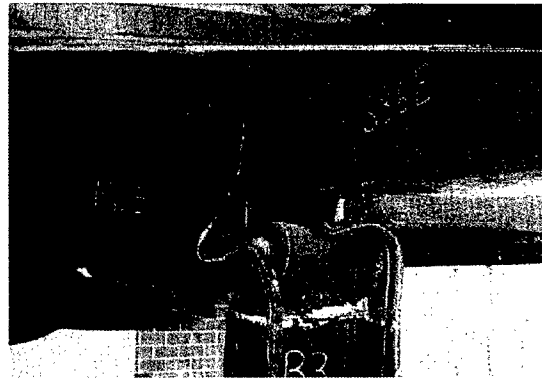


Figure 10
Steel Beam Deformation after Flame Exposure¹¹

Cable F (CMP) downstream peak temperatures are less than about 350°C. Baseline downstream peak temperatures with no combustibles in the plenum void averaged slightly under 325°C in calibration tests.

With regards to smoke opacity, maximum optical densities are shown in. Note that Cable B (CMX) is substantially higher in peak smoke than any of the other cables tested. The peak smoke values for the other cables (LSZH and halogenated) cables are comparable.

Cable	Peak Smoke OD
K 332-1	0.34
B CMX	>2.00
J 332-3C	0.19
O 332-3	0.31
F CMP	0.24
M OFNP	0.23

Table 7 Peak Smoke and Optical Density Values

DISCUSSION

In the BRE/FRS full scale test facility, the LSZH Cables J, K and O ignited readily and burned the full length of the ceiling void (plenum)

configuration. A large fire-ball developed on the horizontal cable ladder and a pool of fire formed on the suspended ceiling beneath the cable ladder in the plenum space. Ceiling tiles often fell out during tests.

Under the same test conditions, high-fire-performance LAN cables that pass NFPA 262 (Steiner Tunnel) test criteria showed no sign of flame spread and generated little smoke. These cables are designated CMP in North America, Canada, Mexico and Asia. CMP materials produced no explosions in small-scale tests.

Steiner Tunnel facilities are now being installed in Europe by BRE/FRS and by the LPC (Loss Prevention Council) to help companies develop higher fire performance cables intended for use in horizontal concealed spaces.

CONCLUSIONS

1. The fire performance of the CMP cable (F) was comparable to the OFNP cable (M) in the BRE/FRS full-scale and UL 910 Steiner tunnel test.
2. The flame spread, heat release and smoke opacity results for CMP cable (F) were significantly lower than results for exposed LSZH and CMX cable.
3. For first-generation LSZH cables, the high temperatures, high heat release rates, flame spread, fire-balls, pool fires and tube furnace explosions were unexpected considering their extensive use in concealed spaces in commercial buildings.

FUTURE WORK These and other cables are being evaluated with variations in source fires, ventilation, installation configuration, fuel loads, fire loads and fire scenarios. Data for concealed space fire modeling is also being developed.

ACKNOWLEDGEMENTS A special thanks is due to the following people who have provided valuable professional advice over the course of this work: A. Fine, TC Tan, J.L. Hardiman, S. Kaufman and of G. Miller Lucent Technologies, L. Przybyla, P. Gandhi, T. Ebert, W. Metes, and R. Backstrom of UL, Northbrook, Ill., USA

A. Parnell and G. Butcher of Firecheck Consultants, Tonbridge, Kent, UK, P. Fardell, S. Rogers, R. Colwell and W. Mallows of BRE/FRS, UK M. K. James, M. Cardona, J. Walnock and D. Benson of DuPont, Wilmington, DE, USA



J. Thomas Chapin is a Member of Technical Staff in the Chemistry, Environment and Safety Group at Lucent Technologies, Bell Laboratories in Norcross, Georgia. He is responsible for fire technology research and materials development for copper and fiber optic cables. He joined AT&T Bell Laboratories in 1980 after working at the Upjohn Company for three years. He received his B.S. in Chemistry and Ph.D. in Polymer Science from the Institute of Materials Science at the University of Connecticut. Since 1980 he worked in the areas of outside plant materials failure phenomena, optical fiber coating development and fiber optic cable development. He has been awarded 11 patents and has 15 publications.

REFERENCES

- ¹ These fires included the Dusseldorf Airport in April, '96, the Paris Credit Lyonnais Bank in May '96, the New York Rockefeller Center in October '96, the Hong Kong Golden Mile, Garly Building in November '96 and the Bangkok President Tower (36-story office complex) in February, '97, among many others.

² National Electrical Manufacturers Association, 1987, "Registration Categories of the National Electrical Manufacturers Association for Compliance with the New York State Uniform Fire Prevention and Building Code", R. Anderson, P. Kopf, pub., Arthur D. Little, Inc.

³ S. Kaufman and M. Yocum, "Behavior of Fire-Resistant Communications Cables in Large-Scale Fires", *Plastics and Rubber: Materials and Applications*, November, 1979, 149.

⁴ L. Przybyla, E. Coffey, S. Kaufman, M. Yocum, J. Reed, D. Allen, "Low-Smoke and Flame Spread Cables", *The 28th International Wire and Cable Symposium Proceedings*, Cherry Hill, N.J., USA, 1979.

⁵ L. Przybyla, E. J. Coffey, S. Kaufman, M. Yocum, J. Reed and D. Allen, "Low Smoke and Flame Spread Cables", *Journal of Fire and Flammability* 12, 177 (1987).

⁶ J. R. Hoover, L. M. Caudill, J. T. Chapin and F. Clarke, "Full-Scale Fire Research on Concealed Space Communications Cable", *Interflam '96*, Seventh International Fire Science and Engineering Conference, 26-28 March 1996, conference proceedings pp 295.

⁷ "Test for Fire and Smoke Characteristics of Wires and Cables", NFPA 262-1990, National Fire Protection Association, Quincy, Mass., USA, 1990.

⁸ "Standard Test for Surface Burning Characteristics of Materials", ASTM E84-87, ASTM, Philadelphia, Pa, USA, 1987.

⁹ D. Madrzykowski, "Office Work Station Heat Release Rate Study: Full Scale vs. Bench Scale", *Interflam '96*, Seventh International Fire Science and Engineering Conference, 26-28 March 1996, conference proceedings pp 47.

¹⁰ ISO - International Organization for Standardization Method 1716, First Edition, 1973-12-01.

¹¹ J. Hoover, L. M. Caudill, J. T. Chapin, "Results of Full-Scale Fire Tests on Communications Cables Used in Concealed-Space Applications" Presented at the BICSI Conference, Orlando, Fla., 1997.

Study of the SZ-slotted rod type optical cable with the 4-fiber ribbons for aerial applications

**Naoki Okada, Masayoshi Yamanaka, Yoshiyasu Sato,
Hirohito Watanabe, Osamu Koyasu, Matsuhiko Miyamoto**

Fujikura.Ltd.

**Telecommunication cable department, Opt-electronics laboratory
1440, Mutsuzaki, Sakura-shi, Chiba, Japan**

ABSTRACT

The newly designed aerial optical cables have been developed. The cable structure has excellent mid span access performance on the aerial environment, therefore the access networks can be constructed efficiently and economically.

The advanced contents of this new cable are as follows. Firstly, the 4-fiber ribbons are inserted into the slots of a SZ-slotted rod in order to get the easy mid span access operations. The SZ-slotted rod cables with the mono-fibers or the 2-fiber ribbons had been already reported. However, in the case of adapting the 4-fiber ribbons to the SZ-slotted rod, the special technique must be needed. Secondly, the new self-supporting aerial cable structure is adapted. This newly developed self-supporting aerial cable has not only the excellent transmission characteristics but also the aerodynamic characteristics, the installing performance and the easy mid span access operation. In this paper, the designing method and the characteristics of the newly developed cables are reported.

INTRODUCTION

In recent years, the optical access networks are under construction to achieve the FTTH networks in the future. In order to construct this network economically, the following contents are most important from the view point of the design of the cable structures.

1) The aerial networks are general configuration to get the economical networks for distributed subscribers in Japan. Therefore, the self-supporting aerial cable is the suitable structure from the view point of the easy installation.

2) The mid span access is the efficiency method to construct the distributed networks. If the any optical fibers can be picked out from the cable at the any points, the construction of the networks may be easily.

From the above mentioned, it is very important to design the optical cable structure to get the easy mid span access operation on the aerial environments. Therefore, the SZ-slotted rod type optical fiber cables with 4-fiber ribbons and the new aerial self-supporting cable structure have been introduced.

CABLE DESIGN

The advanced contents of this work are the SZ-slotted rod optical cable with 4-fiber ribbons and the new aerial self-supporting cable structure.

The SZ-slotted type optical cable with 4-fiber ribbons

The SZ-slotted type optical cable structure with 4-fiber ribbons is shown in Fig.1. The keys to design the SZ-slotted type optical cable with 4-fiber ribbons are as follows. The cable structure should be designed considering the cable characteristics and the mid span access operation.

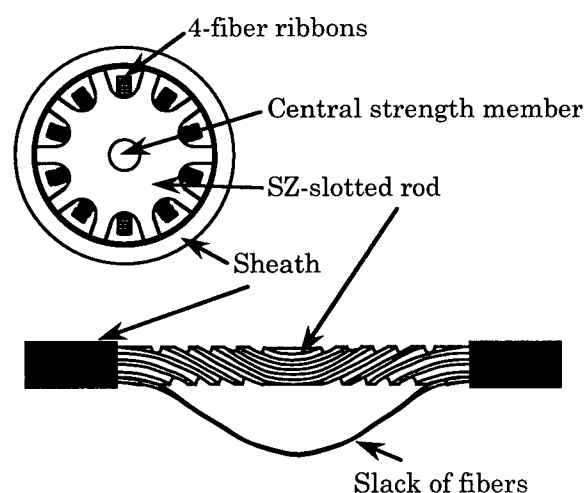


Fig.1 Structure of the SZ-slotted type optical cable with 4-fiber ribbons

1) To design the cable structure from the view point of the cable characteristics

In the case of designing the SZ stranded optical cables, the fiber strain in the bent cable is most considerable factor. The structural parameters of a SZ-slotted rod are defined in Fig.2. Especially, the SZ reverse lay angle is important to reduce the fiber strain. The best angle had been calculated theoretically,

however, the experimental approach has not been reported, yet[1,2]. We investigated the optimum SZ reverse lay angle experimentally, using the SZ-slotted rod structure with the 4-fiber ribbons. The results of theoretical and experimental approach to investigate the optimum SZ reverse lay angle are show in Fig.3-1 and Fig.3-2. Fig.3-1 shows the relationship between SZ reverse lay angle and the calculated fiber strain in the bent cable. It is verified that the optimum value is about 275 degree. In practice, we investigated the relation between the characteristic of the cable and reverse lay angle of slots on SZ-slotted rod, and show the results as Fig.3-2. The transmission losses and the fiber strain in bent cable were measured by B-OTDR(Brillouin Optical Time-Domain Reflectometry) at 70 degrees centigrade. From the results in Fig.3-2, it is confirmed that an optimum value of a reverse lay angle is about 275 degree centigrade.

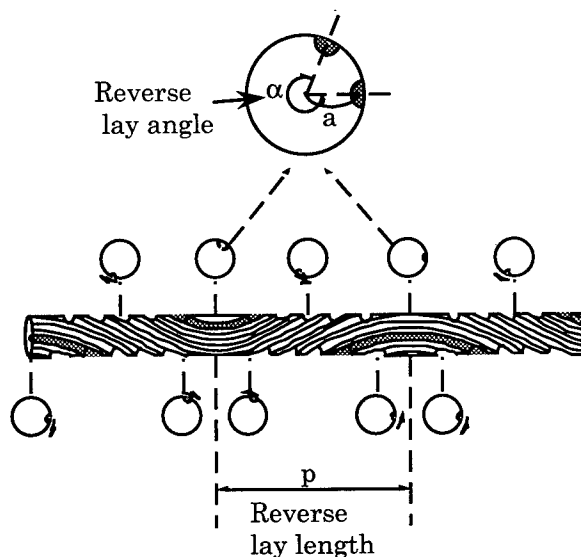


Fig.2 Structural parameters of a SZ-slotted rod

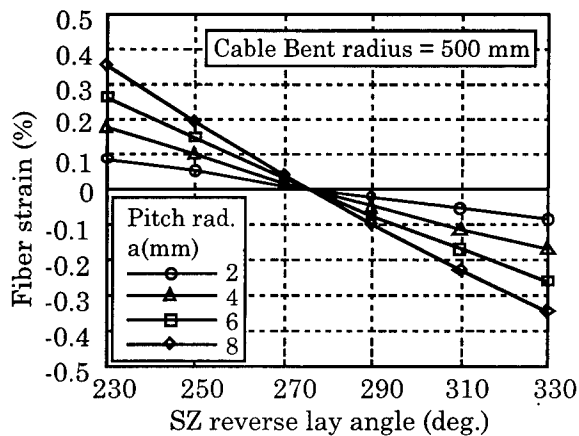


Fig.3-1 Theoretical investigation of the SZ reverse lay length

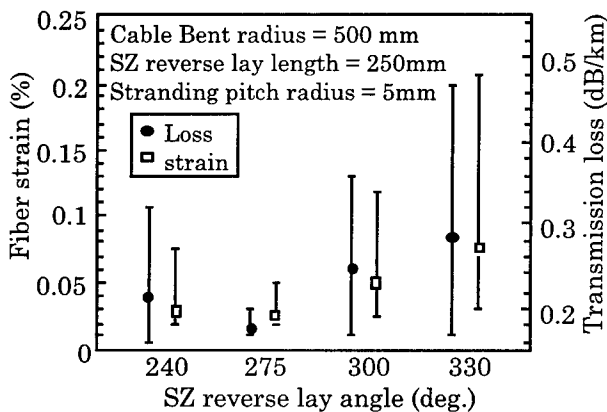


Fig.3-2 Experimental investigation of the SZ reverse lay length

Moreover, in order to get the good transmission characteristics, the stacked 4-fiber ribbons configuration in the SZ slot should be considered in the short SZ lay length. The 4-fiber ribbons should be stranded to the SZ-slotted rod so as to prevent the unexpected force to the fibers. The best stranding method to get the good cable characteristics is as follows; the 4-fiber ribbons should be stacked and back-twisted to prevent the twisting force. Especially, the back-twisting method is new manufacturing technique compared with the ordinary method used for the helical slotted rod structures as shown in Fig.4.

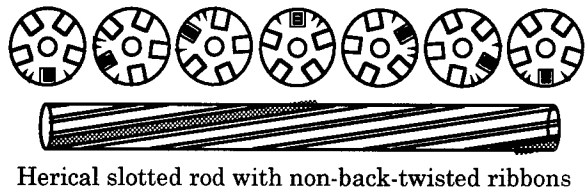
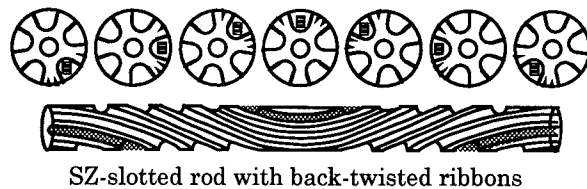


Fig.4 Condition of the stacked ribbons in a slot

2) To design the cable structure from the view point of the mid span access

For easy mid span access operation, the SZ-slotted rod should be designed to get the enough slack of the fibers at the branching points. The larger slack of the fibers make easier mid span access operation. The structural parameters of the SZ-slotted rod are as follows; the pitch diameter, the SZ reverse lay length, and the SZ reverse lay angle. On the other hand, these parameters influence the cable characteristics. Therefore, the slack of the fibers and the bending radius of the fiber in the cable are analyzed theoretically.

The fibers are picked out from the installed cable at the mid span point as shown in Fig.5. The amount of fiber slack is calculated considering the stranding pitch and pitch diameter. The results are shown in Fig.6. While, the bending radius of the fiber in the cable is calculated as shown in Fig.7. As results of Fig.6, the slack of the fiber becomes larger, as the stranding pitch designed shorter and the pitch radius designed larger. The amount of the fiber slack should be designed as large as possible. The least amount of the slack is about 20 mm for easy mid span access operations which are the selection and the identification of the fibers. However, a large

amount of slack causes the small curvature radius of the stranded fibers. Therefore, to get good cable characteristics may be difficult. As results, the suitable area of these parameters can be estimated. On the basis above analysis, the maximum fiber count in a cable can be got up to 200 fiber in 18.5mm diameter. In the case of the thin cable, the short SZ reverse lay length up to 125mm is successfully achieved in order to get the large fiber slack at the branching point.

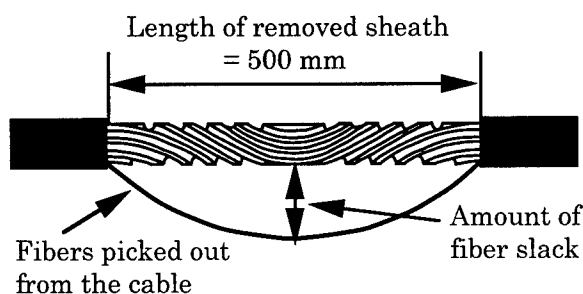


Fig.5 Fiber slack at the mid span access point

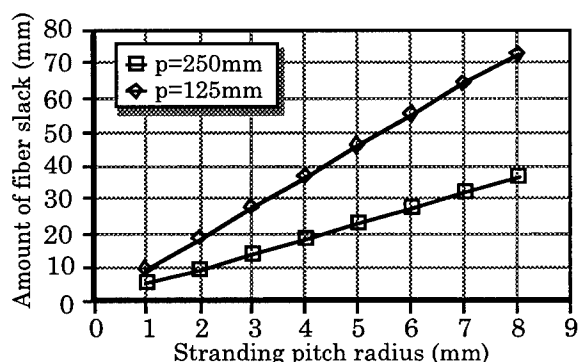


Fig.6 Stranding pitch and diameter dependence of the fiber slack

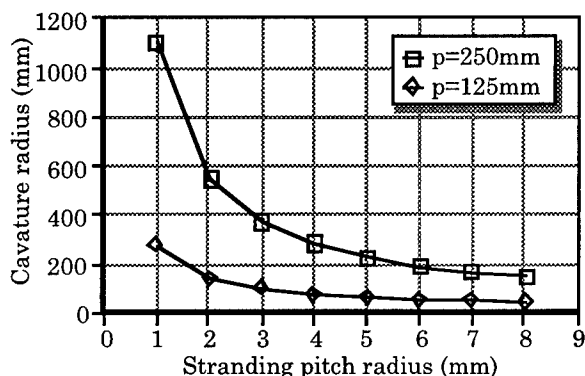


Fig.7 Stranding pitch and diameter dependence of the cavature radius in the cable

New aerial self-supporting cable structure

The structure of the new aerial self-supporting cable is designed considering the aerial environment, the aerodynamic characteristics, the installing operation, the mid span access operation and the economical manufacturing process.

Fig.8 shows the new aerial self-supporting cable. This aerial cable is consisted from the two parts which are the optical cable and the messenger wire. The structure has the excess length of the optical cable part compared with the messenger wire part like as the ordinary pre-hanger cables used for the aerial application in Japan. And then, the cable structure is designed to be manufactured in single process. The excess cable length as against the messenger wire is about 0.2~0.3%. This means that the fiber and the cable core are stress free at the severe aerial environment. Moreover, it is confirmed experimentally that the space between the cable and the messenger wire are effective to prevent the galloping phenomenon and to achieve the easy mid span access operation.

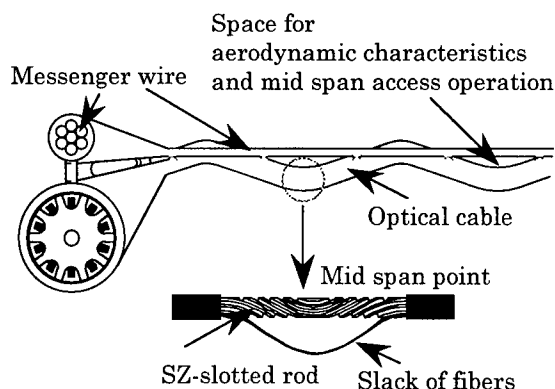


Fig.8 New aerial self-supporting cable structure

CABLE CHARACTERISTICS

In order to investigate the cable characteristics, the 200-fiber SZ-slotted rod cable with 4-fiber ribbons which have new aerial self-supporting structure is manufactured in laboratory. And then, the experimental cable is tested assuming severe aerial conditions.

Transmission characteristics

The excellent transmission loss and the stable thermal characteristics in 200-fiber cable are shown in Fig.9 and Fig.10 respectively. The excellent transmission characteristics are confirmed in large temperature range, from -30 to 70 degree centigrade.

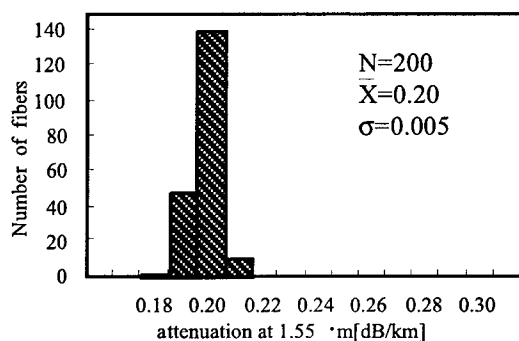


Fig.9 The histogram of the transmission loss in 200-fiber cable

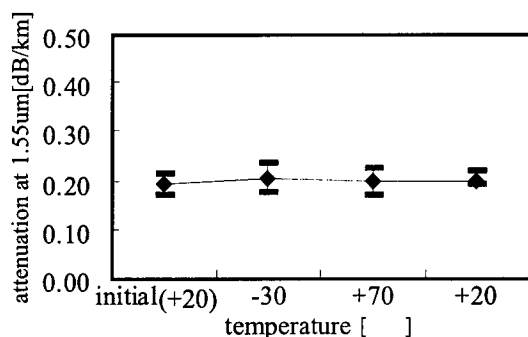


Fig.10 The results of heat cycle test

Tensile characteristics

The aerial self-supporting cables are exposed

to the strong wind and the large temperature change. Under these severe condition, the tension will be up to about 10kN. Therefore the tensile test at high tension is performed. The result shows in Fig.11. It is verified that the fiber stress free is achieved up to about 11kN tensile load.

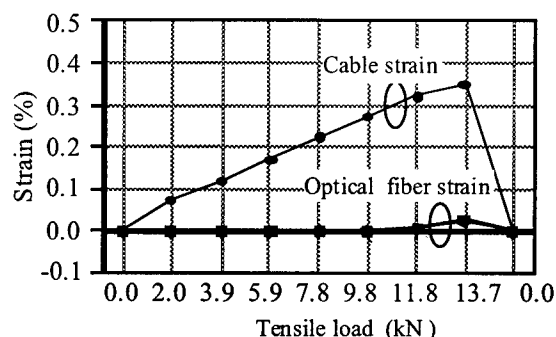
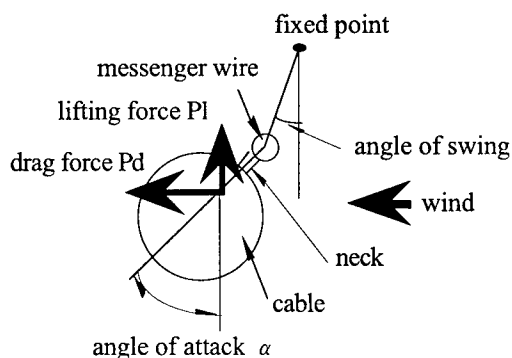


Fig.11 The results of tensile test

Aerodynamic characteristics

The galloping of the cable should be also taken into account for designing the aerial cable structure[3]. The information about galloping of the cable will be obtained by means of analyzing the forces acting on cross section of the cable in the wind tunnel test. The lifting force P_l , the drag force P_d and angle of wind attack α are shown in Fig.12. The aerodynamic coefficients C_l and C_d are obtained by measuring P_l and P_d . The several cables provided for the wind tunnel test and the dependence of the lifting force coefficient C_l on the angle of wind attack are indicated in Fig.13. These results show that the lifting force (which is the cause of the galloping) of the new aerial cable is small compared with that of the conventional cables.



**Fig.12 Aerodynamic forces
under the wind condition**

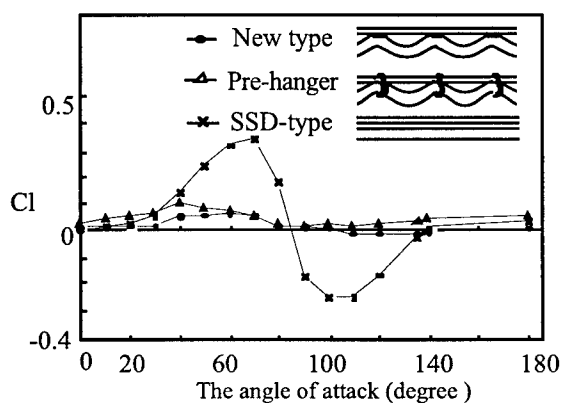


Fig.13 Aerodynamic characteristics

Mechanical test

The mechanical tests consist of installation test, cable twist, cable cyclic flexing, compressive strength and impact test. The method of the tests are based on IEC794-1. The results of these tests showed good performance.

CONCLUSION

A new aerial cables in which SZ-slotted rod including 4-fiber ribbons have been designed, manufactured, and tested. As results, it has been verified that this newly developed self-supporting aerial cables have not only the excellent transmission characteristics but also the aerodynamic characteristics considering the galloping phenomenon, the easy installing

performance and mid span access operation. This cable structure is suitable for the aerial application to adapt the distributed subscribers.

REFERENCES

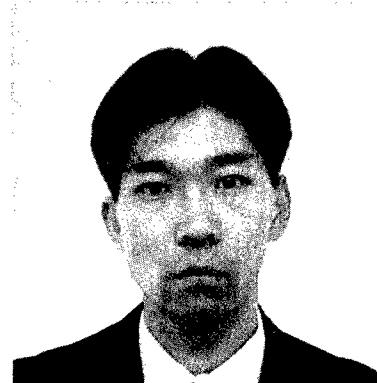
- [1] T S Swiecick et al., " Unit core cable structures for optical communication systems", Wire Industry, Sep.1979.
- [2] N. Okada et al., "Design of the SZ-slotted rod type optical fiber cables" A Prcos of IEICE'97.
- [3] Y. Sugawara, "Design of the Messenger Wire of a Self-Supporting Optical Fiber Cable", Trans IEICE 1982/1 Vol.J65-B No.1

AUTHORS



Naoki Okada

Naoki Okada was born in 1964. He joined Fujikura Ltd. after his graduation from Chiba University with a B.E. degree in 1986 and has been engaged in research and development of optical fiber cables. He is now an engineer in the Telecommunication Cable Department and a member of the IEICE of Japan.



Yoshiyasu Sato

Yoshiyasu Sato was born in 1969. He joined Fujikura Ltd. after his graduation from Tokyo Institute of Technology University with a M.E. degree in 1995 and has been engaged in research and development of optical fiber cables. He is now an engineer in the Telecommunication Cable Department and a member of the IEICE of Japan.



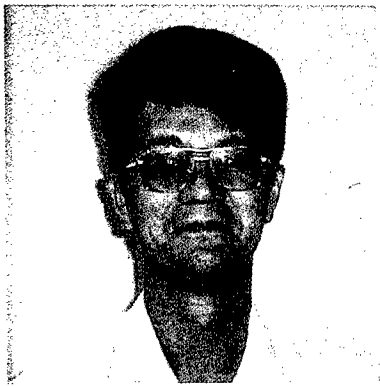
Masayoshi Yamanaka

Masayoshi Yamanaka was born in 1966. He joined Fujikura Ltd. after his graduation from Tohoku University with a M.E. degree in 1992 and has been engaged in research and development of optical fiber cables. He is now an engineer in the Telecommunication Cable Department and a member of the IEICE of Japan.



Hirohito Watanabe

Hirohito Watanabe was born in 1971. He joined Fujikura Ltd. after his graduation from Yokohama National University with a M.E. degree in 1996 and has been engaged in research and development of optical fiber cables. He is now an engineer in the Telecommunication Cable Department and a member of the IEICE of Japan.



Osamu Koyasu

Osamu Koyasu was born in 1953. He joined Fujikura Ltd. after his graduation from Kisarazu Technical College in 1973 and has been engaged in research and development of transmission cables. He is now an engineer in the Telecommunication Cable Department and a member of the IEICE of Japan.



Matsuhiko Miyamoto

Matsuhiko Miyamoto was born in 1953. He graduated from Nagoya Institute of Technology with a B.E. degree of electrical engineering. He joined Fujikura Ltd. after his graduation from Tokyo Institute of Technology with a M.S. degree in 1978 and has been engaged in research and development of optical fiber and optical fiber cables. He is now a manager of the Telecommunication Cable Department and a member of IEICE in Japan.

Development of stacked ribbon SZ- slotted rod cable

D. Iwakura, I. Kobayashi, M. Hara, R. Takaoka, E. Konda, Y. Kamikura

<OPTO-TECHNOLOGY LABORATORY>

THE FURUKAWA ELECTRIC CO., LTD.

6 YAWATA KAIGAN-DORI, ICHIHARA-SHI, CHIBA , JAPAN

ABSTRACT

In conjunction with the deployment of optical fibers in access networks to realize the FTTH (fiber-to-the-home), there is a considerable demand for optical fiber cables from low to high fiber count, with an easy mid span branch. In order to comply with such demands, we have developed a new type of SZ-slotted rod cable with stacked ribbons. In the first half of this paper, we present the calculation method of the fiber strain in the SZ slot and this leads to a basic design theory of the new structure cable.

In the second half of the paper, we present the test results of the prototype cables containing 4-fiber ribbons and 8-fiber ribbons and show that these cables are most fitted for both aerial and underground cable from low to high fiber count.

1. INTRODUCTION

In order to realize the FTTH, a cable structure which facilitates easy mid-span branch is in increasing demand. SZ-slotted rod cable has superior mid span branching characteristics because of the easy fiber access by simply removing the cable sheath.1)

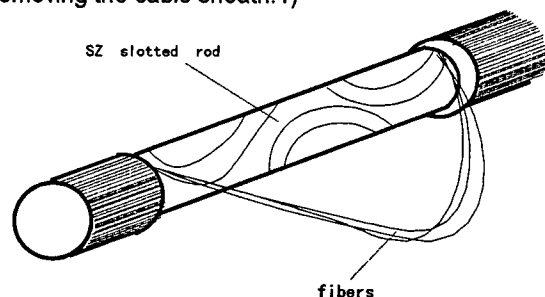


fig.1 SZ slotted rod cable

SZ-slotted rod cables containing either single-fibers or 2-fiber ribbons have already been put to practical use. However, these types of cables cannot accommodate large number of fibers in small diameter as needed for the FTTH. For this reason, we developed a stacked ribbon SZ-slotted rod cable that holds the stacks of multi-fiber ribbons within the SZ-slots. It has been believed that this type of cable structure is difficult to adopt because it gives excessive strain to the fiber by the edgewise bend at the reverse points. We developed a new design concept which can relax the edgewise bend, and realized a cable from low to high fiber count suited for aerial and under ground usage with good mid-span branching performance.

2. METHOD OF RIBBON ACCOMMODATION

2.1 Conventional stacked ribbon slotted rod cables

As illustrated in Fig. 2, the conventional cable design that contains a stack of plural ribbons within a slot holds the ribbon stack in such a way that the flat surface of the ribbon stack is parallel to the bottom surface of the slot. However, in this case, the edgewise bend occurring at the reverse points as shown in Fig. 2 gives excessive strain to the fibers especially at both ends of each ribbon. Therefore this cable design has not been practically used.

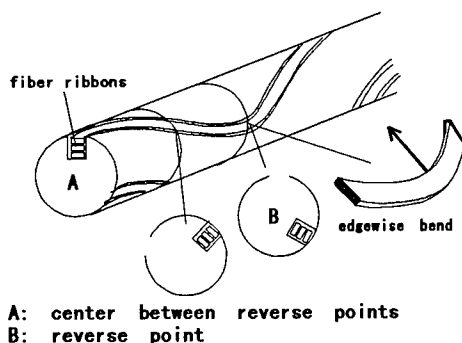


Fig. 2 Conventional cable design

2.2 Newly developed stacked ribbon SZ-slotted rod cable

The structure of the newly developed stacked ribbon SZ-slotted rod cable is illustrated in Fig. 3. At the center between reverse points, the stacked ribbons are accommodated in the slot with each ribbon parallel to the bottom of the slot. However, at the reverse point, the stacked ribbons are accommodated so that their sides face the bottom of the slot. With this arrangement, the ribbons are bent in the thickness direction both at the center between reverse points and at the reverse points. Thus the strain caused by the edgewise bend at the reverse points (which was a problem with the conventional design) is relaxed. The superiority of this newly developed accommodation method is discussed in more detail in the following sections.

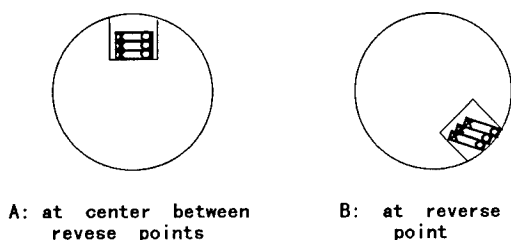


Fig. 3 New cable design

3. SLOTTED ROD DESIGN

3-1. A model for numerical calculation

We made a model of the ribbon position in a SZ slot (i.e., the angle between the ribbon surface and the slot bottom) over the length from the center between reverse points to a reverse point and, then using the model, we calculated the strain on the fiber at both ends of the ribbon. First we explain the way we modeled the ribbon position in the slot. It is well known that, when stacking several layers of fiber ribbons in the conventional helical slot (a

helical slot can be regarded as an SZ slot having an infinitely large turning angle), placing the flat surface of the ribbons parallel to the bottom of the slot is advantageous in terms of the strain of the fiber. Thus we made a model in which the flat surface of the ribbon stack is parallel to the bottom of the slot at the center between the reverse points and is slant at an angle κ (the angle between the fiber surface and the slot bottom) at the reverse points (Fig. 4). The angle ξ which is the angle between the ribbon surface and the slot bottom at phase angle θ is given by Equation (1)

$$\xi = f(\kappa, \theta) \quad (1)$$

where

$$f(\kappa, \theta) = \kappa \frac{(\theta - c)}{(\frac{\phi}{2} - c)} \cdot \Phi(\theta - c)$$

$$\Phi(\theta - c) = 0 \quad (\theta - c < 0)$$

$$\Phi(\theta - c) = 1 \quad (\theta - c \geq 0)$$

$$c = 0 \sim \frac{\phi}{2}$$

The model assumes that the locus of the center of the slot exactly matches the locus of the center of the ribbon.

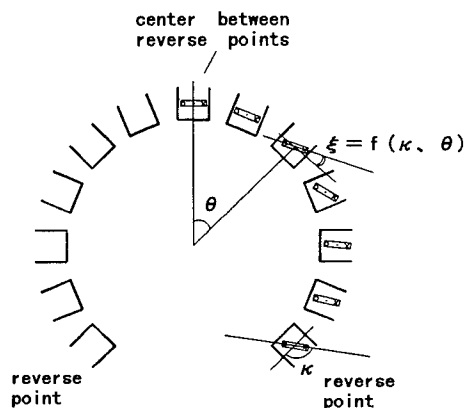


Fig. 4 Ribbon position model

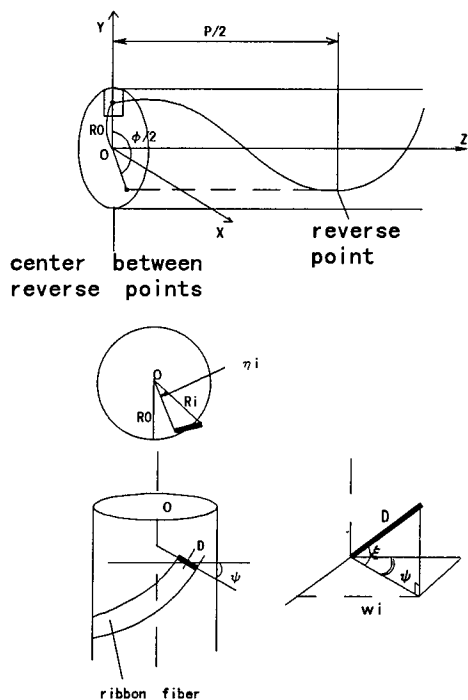


Fig. 5 Locus of slot center

3.2 Calculation method of strain

(1) Numerical modeling of locus

We numerically modeled the locus of the fibers at both ends of a ribbon and, calculated the fiber strain using the fiber ribbon accommodation model discussed in Section 3.1. Three types of strain – elongation, torsion (twisting), and bending – were calculated separately and then combined to give a total strain. The locus of the center of the slot (which corresponds to the locus of the ribbon center) for the SZ slot model shown in Fig. 5 (the model assumes that SZ locus is a sine curve when projected to a plane) is expressed by Equations (2) to (4).

$$x_0 = R_0 \cos \theta \quad (2)$$

$$y_0 = R_0 \sin \theta \quad (3)$$

$$z_0 = \left(\frac{P}{2}\right) + \left(\frac{P}{2\pi}\right) \sin^{-1} \left(\frac{2\theta}{\phi}\right) \quad (4)$$

The locus of the fiber 1 and the fiber 2 at both ends of a ribbon are respectively given by Equations (5) to (10).

$$x_1 = R_1 \cos(\theta + \eta_1) \quad (5)$$

$$y_1 = R_1 \sin(\theta + \eta_1) \quad (6)$$

$$z_1 = z_0 - D \cos \xi \sin \psi \quad (7)$$

$$x_2 = R_2 \cos(\theta - \eta_2) \quad (8)$$

$$y_2 = R_2 \sin(\theta - \eta_2) \quad (9)$$

$$z_2 = z_0 + D \cos \xi \sin \psi \quad (10)$$

$$R_i = \sqrt{(R_0 + D \sin \xi)^2 + (\omega_i)^2}$$

$$w_i = D \cos \xi \cdot \cos \psi$$

$$\eta_i = \tan^{-1} \left(\frac{w_i}{R_0 \pm D \sin \xi} \right)$$

$$\psi = \tan^{-1} \left[\frac{\phi \pi R_0}{P} \cos \left(\sin^{-1} \frac{2\theta}{\phi} \right) \right]$$

(2) Elongation strain

We calculated the elongation strain ε_E of the fibers at both ends of a ribbon by equation(11) when the ribbon is bend edgewise.

$$\varepsilon_{Ei} = \frac{ds_i(\theta, \kappa) - ds_0(\theta)}{ds_0} \quad (11)$$

where

$$ds_i^2 = (x_i(\theta + d\theta, \kappa) - x_i(\theta, \kappa))^2 + (y_i(\theta + d\theta, \kappa) - y_i(\theta, \kappa))^2 + (z_i(\theta + d\theta, \kappa) - z_i(\theta, \kappa))^2$$

(3) Torsion strain

Likewise, the strain from torsion acting on the fibers at both ends of a ribbon is calculated by Equation (12).

$$\varepsilon_{Ti} = \frac{K d_f}{2 \tau_i} \quad (12)$$

where

$$K = 1 - \frac{\xi(\theta, \kappa)}{\phi}$$

$$\left(\frac{1}{\tau_i}\right)^2 = \left(\frac{d\alpha_i}{ds_i}\right)^2 + \left(\frac{d\beta_i}{ds_i}\right)^2 + \left(\frac{d\gamma_i}{ds_i}\right)^2$$

$$\alpha_i = \rho_i \left(\frac{dy_i}{ds_i} \frac{d^2 z_i}{ds_i^2} - \frac{dz_i}{ds_i} \frac{d^2 y_i}{ds_i^2} \right)$$

$$\beta_i = \rho_i \left(\frac{dz_i}{ds_i} \frac{d^2 x_i}{ds_i^2} - \frac{dx_i}{ds_i} \frac{d^2 z_i}{ds_i^2} \right)$$

$$\gamma_i = \rho_i \left(\frac{dx_i}{ds_i} \frac{d^2 y_i}{ds_i^2} - \frac{dy_i}{ds_i} \frac{d^2 x_i}{ds_i^2} \right)$$

d_f = fiber diameter

$$\left(\frac{1}{\rho_i}\right)^2 = \left(\frac{d^2 x_i}{ds_i^2}\right)^2 + \left(\frac{d^2 y_i}{ds_i^2}\right)^2 + \left(\frac{d^2 z_i}{ds_i^2}\right)^2$$

(4) Bending strain

The strain of the fiber caused by bending is small in comparison to that by elongation or torsion. Equation (13) was used for the calculation.

$$\varepsilon_B = \frac{d_f}{2 \rho_i} \quad (13)$$

(5) Total strain

The total strain produced by elongation, torsion, and bending is given by Equation (14).⁽²⁾

$$\varepsilon_{tot} = \frac{1}{2} (\varepsilon_E + \varepsilon_B + ((\varepsilon_E + \varepsilon_B)^2 + (\frac{2G\varepsilon_T}{E})^2)^{1/2})$$

G : modulus of elasticity (14)

We then compared the total strain for different ribbon accommodation conditions or in other words for different values of κ .

3.3 Example of calculation

As an example, Fig. 6 depicts the calculated results for a case in which 4-fiber ribbons (width: 1.1 mm), are accommodated in SZ-slotted rod with reverse pitch of 250mm and also for a case in which 8-fiber ribbons (width: 2.2mm) are accommodated with reverse pitch of 500mm. For both cases, R_o is 6.0 mm and reverse angle is 270degrees.

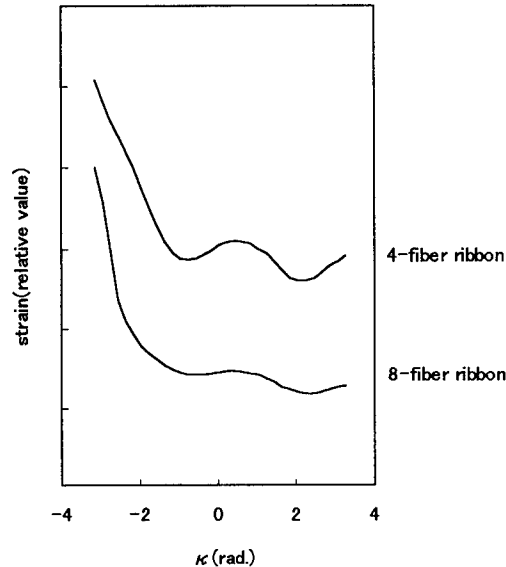


Fig. 6 Total strain for different κ

Fig. 6 indicates that as for the accommodation mode, there exist two low strain modes. One mode exists in the range of $\kappa = 1.7$ to 2.4 rad (Fig. 7) which we now call the Mode1, and the other, the Mode2, exists in the range of $\kappa = -0.5$ to -1.2 rad (Fig. 8).⁽³⁾

The results prove that the newly developed accommodation method, in which the fiber ribbons are stacked with their flat side parallel to the bottom of the slot at the center between the reverse points and with their sides facing the bottom of the slot at the reverse points, reduces the fiber strain.

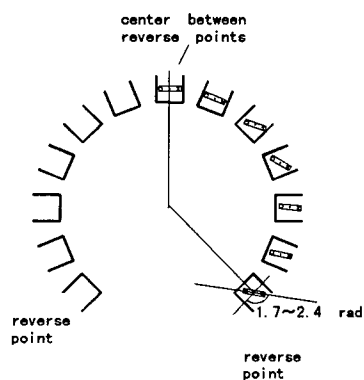


Fig. 7 The Mode 1

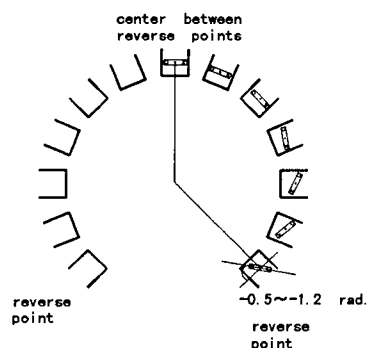


Fig. 8 The Mode 2

For 4-fiber ribbon, Fig. 9 shows the results of the strain calculations while varying R_o and keeping the reverse pitch constant at 250 mm. Fig. 10 shows the results of similar calculations while varying the reverse pitch and keeping R_o constant.

We note that, as R_o becomes larger and the reverse pitch becomes shorter, the low-strain mode shifts from the Mode 1 ($\kappa > 0$) to the Mode 2 ($\kappa < 0$). This shows that, the Mode1 is the most stable mode for the cable of relatively low strain design and the Mode2 is the most stable mode for the cable of high strain design. (Fig. 11).

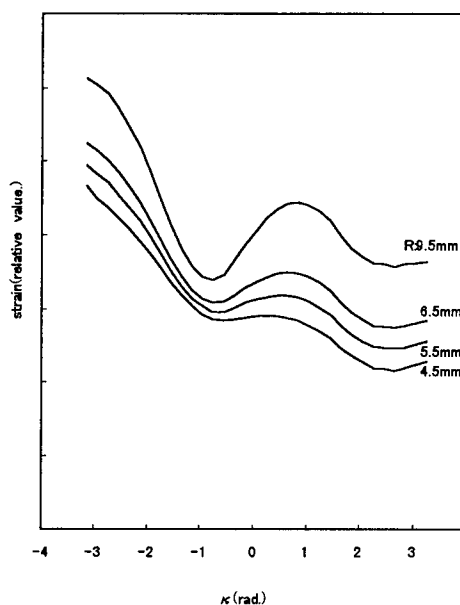


Fig. 9 Total strain for different R_o

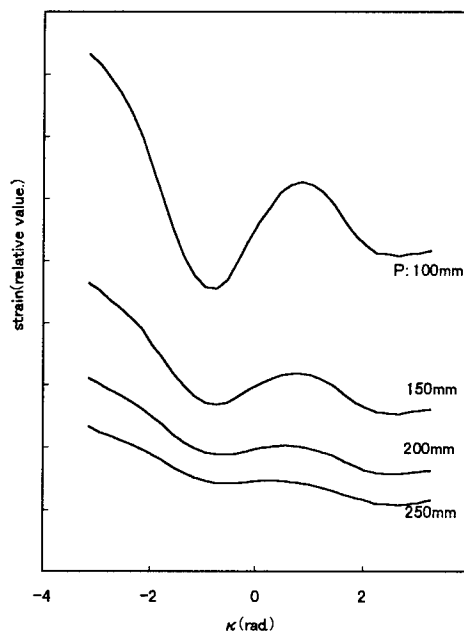


Fig. 10 Total strain for different reverse pitch

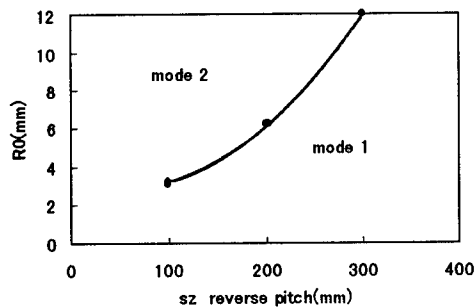


Fig. 11 Mode 1 and 2 regions

3.4 SZ slot design

The previous calculations showed that accommodating the ribbons in the Mode1 is ideal in terms of strain. Thus we designed the cross section of the slot to realize the Mode1 accommodation condition. To contain N fiber ribbons of thickness T and width W in a slot, the cross-section dimensions of the slot should be such that a circle of diameter D ($D = (W^2 + T^2N^2)^{1/2}$) can fit completely inside (Fig. 12).

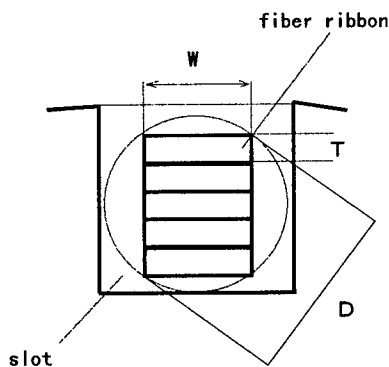


Fig. 12 Design of slot

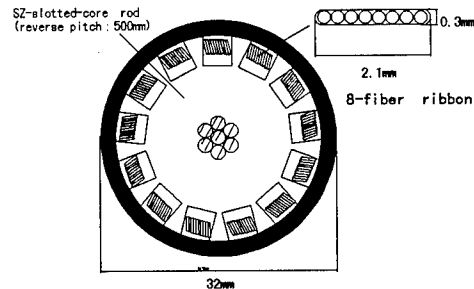
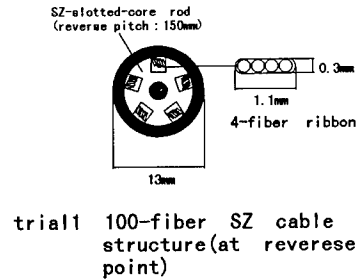
4. EVALUATION OF PROTOTYPE CABLES

4.1 Application for underground cables

We made two prototype cables based on the design theory of Section 3.2.

Trial1 utilizes 4-fiber ribbon; trial2, 8-fiber ribbon. The ribbons were stacked in the Mode 1 ($\kappa > 0$) accommodation condition. The structures of the prototype cables are illustrated in Figs. 13.

The transmission, temperature, and mechanical characteristics of the two prototype cables are presented in Table 1.



trial2 1000-fiber SZ cable structure(at reverse point)

Fig.13 Trial cables

table1 Test results of trial cables

Item	result	
	trial1 (4-fiber ribbon)	trial2 (8-fiber ribbon)
Attenuation	0.20dB/km	0.20dB/km
temperature cycle (-20°C~70°C)	<0.05dB/km	<0.05dB/km
Bending	<0.02dB at R:50mm	<0.02dB at R:200mm
Lateral force (2000N/100mm)	<0.02dB	<0.02dB
Tensile	<0.05dB at 0.2%	<0.05dB at 0.2%
Squeezing	<0.02dB	<0.02dB

The characteristics are all good and present no problems. These results demonstrate that the stacked ribbon SZ-slotted core design can provide cables with small diameter, high fiber density and good mid span brunching from low to high fiber count.

4.2 Application for aerial cables

4.2.1 Self-supporting cable structure with extra cable length

For FTTH service, aerial cables must have a structure that facilitates mid span branching.

It is generally known that aerial cables elongate by more than 0.2% under high temperatures and strong winds. Thereby, one important point in cable design is to ensure that no strain is imparted to the fibers under such conditions. Listed below are two plausible approaches.

- (1) Give the cable an extra length relative to the suspension member. (extra cable length type⁽⁴⁾, Fig. 14)
- (2) Give the fibers an extra length relative to the cable (extra fiber length type⁽⁵⁾, Fig. 15)

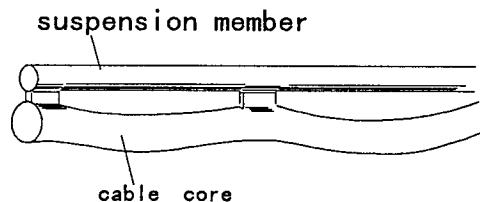


Fig. 14 Extra cable length design

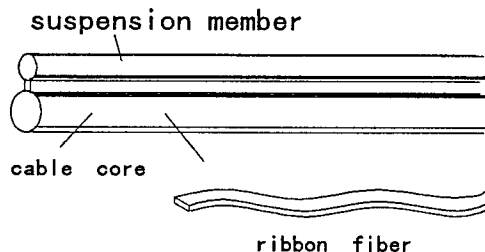


Fig. 15 Extra cable length design

With the newly designed stacked ribbon SZ-slotted core cable design, we developed aerial cables of these two types and confirmed their suitability for practical use. The slot design theory of Section 3.2 can also be applied to the design of the extra cable length type. However, as for the extra fiber length type, the design of Section 3.2 must be modified because the dimensions of the slot have to be increased to accommodate the extra length of the fiber.

4.2.2 The design of self-supporting cable structure with extra fiber length

The best accommodation condition in terms of strain for the stacked ribbon SZ-slotted core cable is the Mode 1 condition shown in Fig. 7. When extra length is given to the fiber ribbon in the Mode 1 condition, the resulting undulation of the ribbon is generally in the direction of the arrow in Fig. 16. This is because, as the width of the ribbon is made wider, the ribbon becomes progressively less prone to bend in the width direction and more likely to bend in the thickness direction.

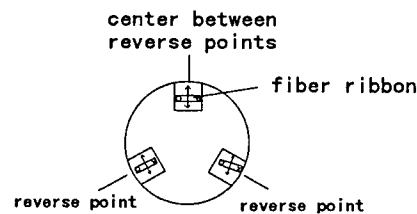


Fig. 16 Undulation direction

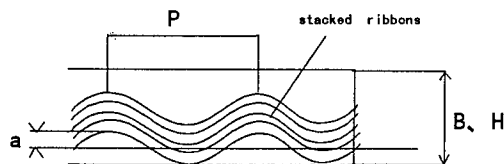


Fig. 17 Undulation model in slot

Fig. 17 depicts the model that we used to describe how a fiber ribbon with an extra length factor ν would undulate within a slot. In our model, we assumed that the curve of the ribbon undulation can be approximated with a sine curve.

We then determined the suitable dimensions for the slot by seeking a minimum amplitude a that satisfies the following conditions to realize low attenuation loss and long-term reliability of fiber.

(Conditions)

$$f(z) = a \sin\left(\frac{2\pi z}{p}\right)$$

$$v = \frac{\int_0^{2\pi} \sqrt{1 + (f'(z))^2} dz - p}{p}$$

$$R_{sin} = \frac{1}{a} \left(\frac{p}{2\pi} \right)^2 \geq 20\text{mm} \sim 30\text{mm}$$

$$\varepsilon_B = \frac{d_f}{2R_{sin}} \leq 0.001$$

Values satisfying Equations (15) and (16) below were taken as the dimensions of the slot (width B, depth H).

$$B \geq NT + 2a \quad (15)$$

$$H \geq NT + 2a \quad (16)$$

At the same time, as described earlier, it is also important that the dimensions of the slot be such that a circle of diameter D ($D = (W^2 + T^2 N^2)^{1/2}$) can fit completely inside.

4.2.3 Evaluation of the prototype cables

We next performed an evaluation of the aerial cable prototypes. We evaluated prototypes of three cable structures (fig.18 trial3,4,5) of the first type of aerial cable (self-supporting cable structure with extra cable length) and one cable structure (fig.18 trial6) of the second type (self-supporting cable structure with extra fiber length). Structures trial3,4 and 5, which contain 24, 100, and 200 fibers, respectively, were given an extra cable length of about 0.3% relative to the suspension member. Structure of trial6 was given an extra fiber length of about 0.2% relative to the suspension member. The tensile stress-strain characteristics of trial4 and 6 are shown in Figs. 19 and 20, respectively. Little fiber strain was observed under a cable elongation of 0.2% which is equivalent to that encountered under high temperatures and strong winds, thus demonstrating that the both types of cables benefit from the extra length.

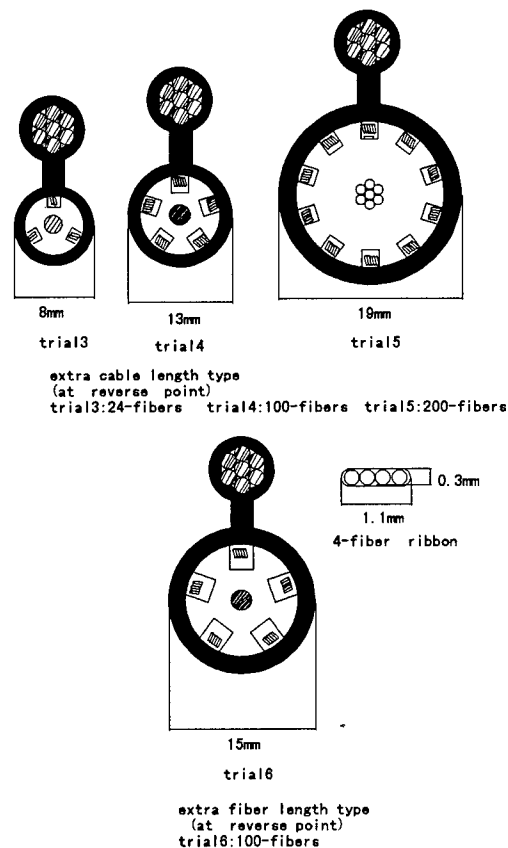


Fig.18 Trial cables

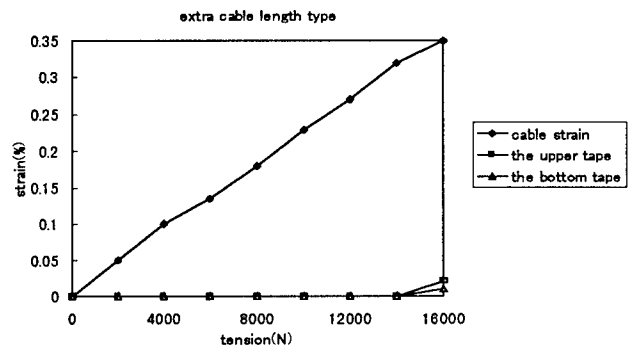


Fig.19 S-S curve (extra cable length)

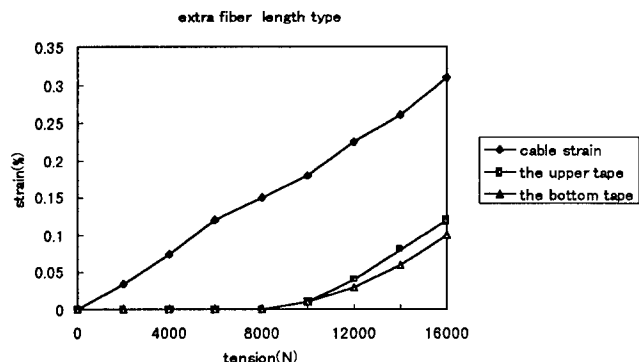


Fig.20 S-S curve (extra fiber length)

The transmission, temperature, and mechanical characteristics of the four prototypes are presented in Table 2.

Table 2 Test results of trial cables

Item	result			
	trial 3	trial 4	trial 5	trial 6
Attenuation	0.20dB/km			
temperature cycle (-20°C~70°C)	<0.05dB/km			
Bending	<0.02dB at R:50mm			
Lateral force (2000N/100mm)	<0.02dB			
Tensile	<0.02dB at 0.3%	<0.02dB at 0.3%	<0.02dB at 0.3%	<0.02dB at 0.2%
Squeezing	<0.02dB			

5. CONCLUSION

We have developed a stacked ribbon SZ-slotted core cable which facilitates the mid span branching and enables high fiber density.

The structure is such that, at the center between the reverse points, the stacked ribbons are accommodated within the slot so that the flat surface of the ribbons is parallel to the bottom surface of the slot and, at the reverse points, the sides of the ribbons face the bottom of the slot at an angle from 1.7 to 2.4 rad. We tested various prototype cables of this structure and found that all had good cable characteristics in both underground and aerial applications. We will continue to conduct the long-term reliability test of these cables.

REFERENCES

- (1) M. Okada, "Study on slotted-rod structure for midspan access," IEICE B940, 1996 (in Japanese).
- (2) S. Tomita, "Preliminary Research into Ultra High Density and High Count Optical Fiber Cables," IWCS, 1991.
- (3) D. Iwakura, "Studies on the relation between fiber strain and stacked fiber ribbon state in SZ-slotted rod cable," IEICE B-10-13, 1997 (in Japanese)
- (4) H. Iwata, "Design in self-supporting optical fiber cable using SZ-slotted rod," IEICE B-10-8, 1997 (in Japanese).
- (5) D. Iwakura, "Development of SZ-slotted core cable using extra-length optical fiber ribbons in SZ-slots," IEICE B-10-5, 1997 (in Japanese).

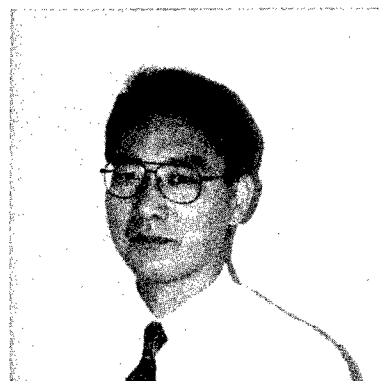
AUTHORS



Disuke Iwakura

The Furukawa Electric co.,Ltd.
6,Yawata Kaigandori Ichihara,Chiba
290,Japan

Daisuke Iwakura received his M.E.degree in Engineering from Electro-Communications University in 1993.He joined The Furukawa Electric co.,Ltd.in 1993 and has been engaged in research and development of optical fiber cables.He is now a research engineer of Opto-Technology Laboratory



Ichiro Kobayashi

The Furukawa Electric co.,Ltd
6,Yawata Kaigandori Ichihara,Chiba
290,Japan

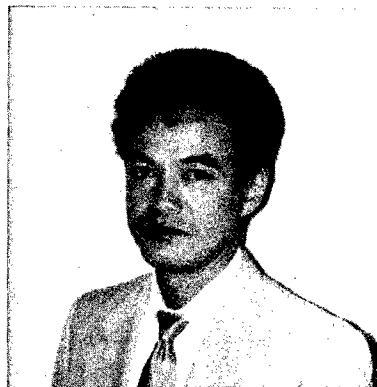
Ichiro Kobayashi received his B.E.degree in Pyhysics from Chuo university in 1986. He joined The Furukawa Electric Co.,LTD.in 1986 and has been engaged in the development of the optical fiber and cables. He is now a senior research engineer of Opto-Technology Laboratory. He is a member of the Institute of Electronics, Information and communication Engineers of Japan.



Masami Hara

The Furukawa Electric co.,Ltd.
6,Yawata Kaigandori Ichihara,Chiba
290,Japan

Masami Hara received his M.E.degree in Pysics from Osaka University in 1987.He joined The Furukawa Electric co.,Ltd.in 1987 and has been engaged in research and development of optical fiber cables.He is now a senior research engineer of Opto-Technology Laboratory.He is a member of the Institute of Electronics, Information and communication Engineers of Japan.



Eiji Konda

The Furukawa Electric co.,Ltd.
6,Yawata Kaigandori Ichihara,Chiba
290,Japan

Eiji Konda joined The Furukawa Electric co.,Ltd.in 1977 and has been engaged in research and development of materials and optical fiber cables.He is now an engineer of Opto-Technology Laboratory.



The Furukawa Electric co.,Ltd.
6,Yawata Kaigandori Ichihara,Chiba
290,Japan

Ryuji Takaoka received his M.E.degree in Mechanical Engineering from Keio University in 1996.He joined The Furukawa Electric co.,Ltd.in 1996 and has been engaged in research and development of optical fiber cables. He is now a research engineer of Opto-Technology Laboratory.



Yasuhiro Kamikura

The Furukawa Electric co.,Ltd.
6,Yawata Kaigandori Ichihara,Chiba
290,Japan

Yasuhiro Kamikura received his B.E.degree in Electronic Engineering from Tokyo University in 1975. He joined The Furukawa Electric co.,Ltd.in 1975 and has been engaged in the development of optical fiber and cables. He is now a general manager of Opto-Technology Laboratory. He is a member of the Institute of Electronics, Information and communication Engineers of Japan.

HIGH FIBER COUNT SLOTTED-CORE RIBBON CABLES: CHOOSING PROCESSING PARAMETERS FOR SUPERIOR PERFORMANCE

Ron O. Livingston
Christopher K. Eoll

Siecor Corporation
Hickory, North Carolina

ABSTRACT

In the manufacture of slotted-core ribbon cable, the back tensions applied to the ribbons during the stranding process are conventionally chosen so that the tensions on the ribbons inserted into any particular slot are graduated, with the bottom ribbon in the slot applied at the highest tension and the top ribbon applied at the lowest. A model describing certain aspects of the mechanical behavior of ribbons in a stack is presented along with experimental data to show that superior attenuation performance may be achieved by using graduated stranding tensions with the bottom ribbon in the slot applied with the lowest tension and the top ribbon applied with the highest.

I. INTRODUCTION

The emerging multimedia access network in Japan requires small diameter, ultra-high fiber count cables in the feeder segment of the optical access network. Deployment of high density slotted-core ribbon (SCR) optical fiber cables with up to 1000 fibers has recently proceeded in Japan. These cables are manufactured with standard OD optical fibers in thin 8-fiber ribbons which are stranded in the helical grooves of slotted rods. A cross-section of a 1000-fiber slotted-core ribbon cable with a full complement of fibers is shown in Figure 1 [1,2].

When a stack of ribbons is stranded in a slot of the slotted rod of an SCR cable, common sense would seem to dictate that, to keep the ribbons within the stack from becoming disorganized, the ribbon being laid on the bottom of the slot should be applied with the highest tension of all the ribbons in the stack; and each of the other ribbons in the stack should be applied at a tension that is lower than the application tension of the ribbon underneath it. One analogy might be a pile of rocks—for a stable pile, one would be

inclined to put the heaviest rock on the bottom of the pile and the lightest on the top.

Until recently, published literature (e.g. reference [3]) has recommended the use of the above sequence of ribbon stranding tensions. These are called "standard" ribbon tensions here, and they are depicted in Figure 2.

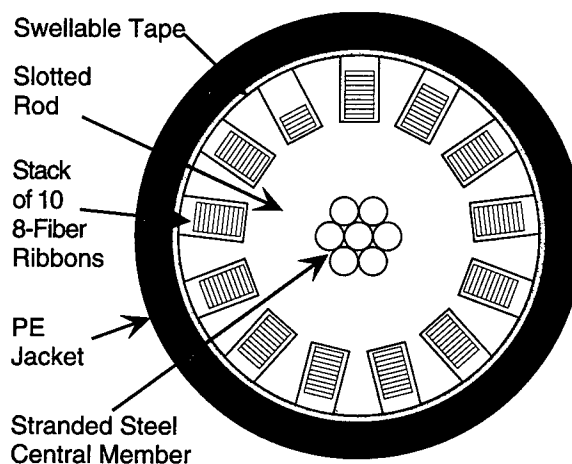


Figure 1: Cross-Section of 1000-Fiber
Slotted-Core Ribbon Cable

A model describing certain aspects of the mechanical behavior of ribbons in a stack in a helical slot in an SCR cable is presented in this paper. The model suggests that a stack stranded using the standard tensions is actually less stable than a stack stranded using a reversed sequence of ribbon stranding tensions, called "inverted" tensions here. In this case, the bottom ribbon in each stack is applied with the lowest tension of all the ribbons in the stack, and each remaining ribbon is applied at a higher tension than the application tension of the ribbon underlying it. This sequence is depicted in Figure 3.

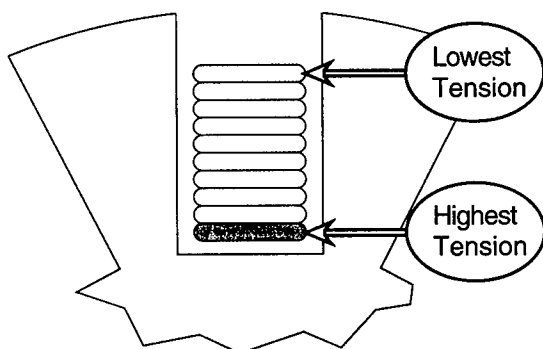


Figure 2: Standard Ribbon Tensions

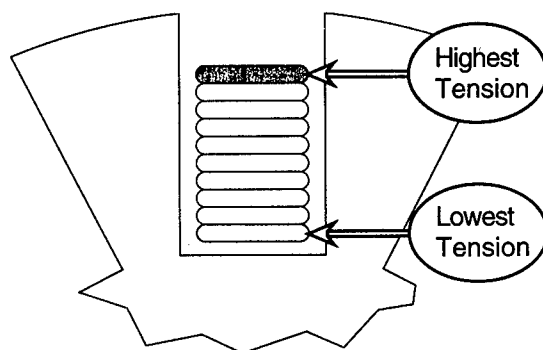


Figure 3: Inverted Ribbon Tensions

One might expect that attenuation values for SCR cables would reflect the stability or lack of stability of ribbon stacks. Attenuation data is presented for the particular case of 1000-fiber SCR cables. Overall, fibers in stacks with inverted tensions exhibit better attenuation performance than fibers in stacks with standard tensions.

II. MODELING RIBBON MOVEMENT

When a ribbon is stranded helically, each fiber in the ribbon is in a helical configuration. If P is the pitch of the helix of a representative fiber in the ribbon, and r is its radius, then the length, L , of the helical path over a pitch or lay length is given by the following formula, which is well-known in the cable industry:

$$L^2 = (2\pi r)^2 + P^2. \quad (1)$$

By taking differentials of both sides, noting that L and P are approximately equal when r is much smaller than P , and replacing the differentials with incremental quantities, one obtains

$$\frac{\Delta L}{L} \approx \left(\frac{2\pi}{P}\right)^2 \cdot r \Delta r + \frac{\Delta P}{P}. \quad (2)$$

In order to investigate the behavior of the ribbons in a stack in a cable which is cooling from high temperatures, one may assume that, at the highest temperatures, the stack is pressed tightly against the bottom of the slot and all the ribbons are under tensile strain. As the temperature drops, all the ribbon lengths eventually exceed the helical lengths they would exhibit if the stack remained sitting on the floor of the slot, so the stack moves radially outward. If the stack was stranded under standard tensions (Fig. 1) so that, at the highest temperatures, the ribbons are under tensions that decrease as one moves from the bottom to the top of the stack, one may use Eq. (2) to show that the ribbons lift off the stack one at a time as the temperature drops.

As the temperature begins to drop below the highest temperature, the strain in each ribbon first falls by the same amount ($\Delta L/L$) as the core strain falls ($\Delta P/P$); there is no tendency for any ribbon to move radially ($\Delta r=0$) as long as tension remains in each ribbon. Considering the top ribbon, for example, with the lowest stranding strain (ϵ_{top}) in the stack, when $\Delta P/P$ falls by an amount numerically equal to ϵ_{top} , i.e. $\Delta L/L = -\epsilon_{top}$, then the strain in the top ribbon vanishes. If one now uses Eq. (2) to describe the incremental changes starting from the point at which the strain in the ribbon first vanishes, the left hand side of the equation vanishes because the ribbon is no longer changing in length. Thus, the equation may be rewritten in the form

$$\frac{\Delta r}{r} \approx -\left(\frac{P}{2\pi r}\right)^2 \cdot \frac{\Delta P}{P}. \quad (3)$$

Because ΔP is negative as the rod continues to get shorter, the right-hand side of Eq. (3) is positive, and the ribbon moves incrementally away from the axis of the core. Finally, because the underlying ribbons were all stranded at higher tensions than the top ribbon, the top ribbon begins to move radially away from the stack before the tensions vanish in any of the ribbons below, whereby no radially outward movement on their part can occur. This process continues, with the ribbons lifting one at a time.

The stack may reform once all the ribbons have lifted, with the ribbons again all pressed tightly together and the stack "floating" above the bottom of its slot. In the meantime, however, the ribbons have been separated. Any mechanical

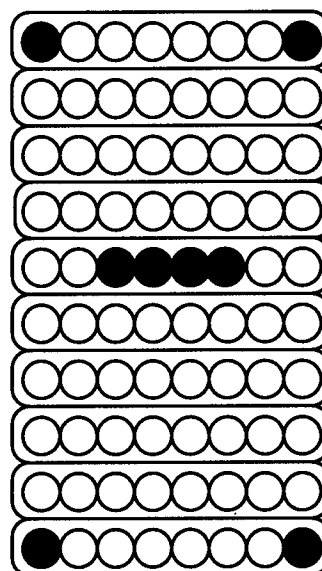
perturbation of the ribbons when inter-ribbon friction is unavailable to resist movement of the ribbons laterally may cause the stack to lose its integrity, no longer having a rectangular cross-section but having ribbons sticking out on one or both sides of the stack. Fibers that are sticking out are especially vulnerable to undesirable lateral forces which could cause excess attenuation.

Similar things may also happen when the tension on an SCR cable is released after the cable has been subject to a sufficient tensile force to stretch the core enough for the ribbon stack to be pulled tightly against the bottom of the slot with all ribbons under tension. When the ribbon tensions decrease from the bottom to the top of the stack, the ribbons will lift off the stack one at a time as the cable tension is reduced, and the stack again has the opportunity to become disorganized.

The potential problems predicted above do not arise if one uses inverted tensions (Fig. 3), with the bottom ribbon in a stack having the lowest tension and the top ribbon having the highest, where each ribbon in the stack has a lower tension than the tension of the ribbon immediately above it. With such an arrangement, each time a ribbon's tension vanishes during cable shrinkage—whether due to dropping temperatures or dropping cable tension—the ribbons above it still have positive tensions and will resist the attempt of the first-mentioned ribbon to move radially outward. Thus the ribbons in the stack stay pressed together, and mechanical perturbations cannot readily disrupt the integrity of the stack.

III. CABLE PERFORMANCE

Two experimental 1000-fiber SCR cables each contained stacks of ribbons with standard ribbon tensions and stacks of ribbons with inverted ribbon tensions. This setup was used to help eliminate differences due to varying cabling effects amongst the cables. Of the 80 fibers in the stack of ribbons in each slot, eight were measured for attenuation. Figure 4 shows the fibers that were measured. The corner fibers were chosen for measurement because they are especially susceptible to attenuation increases in such SCR cables. Fibers in the middle of the stack were chosen to ensure that no unanticipated attenuation increases occurred due to inverted ribbon tensions.



Filled circles indicate optical fibers measured

Figure 4: Stack of Ten, 8-Fiber Ribbons

After Manufacturing

Table 1 displays attenuation on the reel for both standard and inverted stranding tensions at 1310 nm and 1550 nm shortly after the cables were manufactured. Comparing the two stranding tensions at 1310 nm, one will find no significant difference when all measured fibers are considered together. Furthermore, at 1550 nm, analysis of the attenuation data for all measured fibers using the t distribution shows that there is no significant difference between inverted tensions and standard tensions after manufacturing at a 95% confidence level ($t = 1.90$, $dF = 190$, $p = 0.058$). However, further investigation of the data shows that the attenuation of the fibers in the bottom corners of the slots with inverted ribbon tensions is significantly better ($t = 2.06$, $dF = 94$, $p = 0.04$) than in the case of the standard ribbon tensions at a 95% confidence level. There is no significant difference between the middle fiber attenuations.

Most noteworthy at 1550 nm is that the variability of the attenuation in the ribbon stacks that contain standard tensions and in those that contain inverted tensions is considerably different. Considering all the fibers together, the mean attenuation for the stacks with inverted tensions is 0.21 dB/km with a standard deviation of 0.01 dB/km at 1550 nm. The stacks with standard tensions have a mean of 0.22 dB/km with a standard deviation of 0.03 dB/km.

Ribbon Tensions	Attenuation (dB/km) @ 1310 nm		Attenuation (dB/km) @ 1550 nm	
	Mean	Std. Dev.	Mean	Std. Dev.
Standard	0.35	0.01	0.22	0.03
Inverted	0.34	0.01	0.21	0.01

Table 1: After Manufacturing Attenuation for All Measured Fibers

Thermal Cycling

The experimental cables were subjected to the extreme temperatures (-30°C and +70°C) of thermal cycling three times. A 24 hour transition between temperatures and a 48 hour soak at each extreme temperature were used.

-30°C Attenuation. Considering all fibers at once at -30°C, the two tension sequences did not lead to significantly different attenuations at the low temperature extreme at a confidence level of 95%. However, attenuations for the bottom corner fibers alone were significantly better for the inverted ribbon tensions than for the standard ribbon tensions ($t = 4.57$, $dF = 118$, $p = 0.00$).

+70°C Attenuation. The inverted ribbon tension sequence performed significantly better

than the standard ribbon tension sequence for all fibers in this case ($t = 2.84$, $dF = 382$, $p = 0.005$). Again, the largest difference was found to be in the performance of the bottom corner fibers ($t = 4.33$, $dF = 94$, $p = 0.000$).

Focusing on all the measured fibers together, Table 2 and Figure 5 display thermal cycling results for both inverted ribbon tensions and standard ribbon tensions. At both -30°C and +70°C, the standard ribbon tensions had standard deviations that were, on the average, twice as large as those for the inverted ribbon tensions. See Figure 6.

Finally, Figure 7 presents thermal cycling data for all four corner fibers in all the ribbon stacks.

Attenuation (dB/km) @ 1550 nm	Standard Tensions		Inverted Tensions	
	Mean	Std. Dev	Mean	Std. Dev
1st -30°C	0.21	0.01	0.21	0.01
1st +70°C	0.24	0.07	0.23	0.04
2nd -30°C	0.21	0.02	0.21	0.01
2nd +70°C	0.23	0.07	0.21	0.03
3rd -30°C	0.21	0.02	0.21	0.01
3rd +70°C	0.23	0.06	0.22	0.01
Final 23°C	0.21	0.02	0.21	0.01

Table 2: Thermal Cycling Results for All Measured Fibers

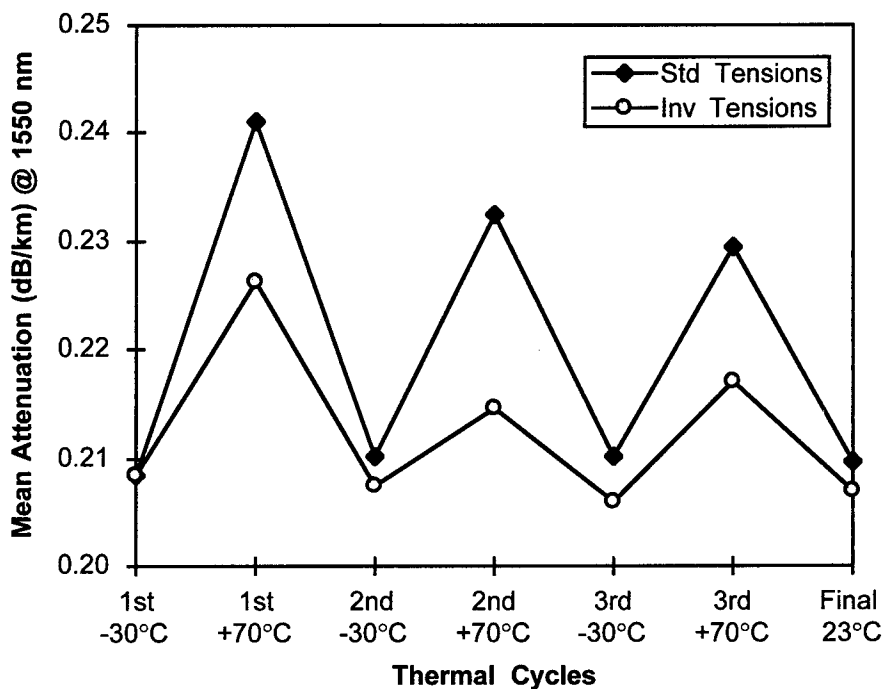


Figure 5: Mean Attenuations for Standard and Inverted Ribbon Tensions during Thermal Cycling

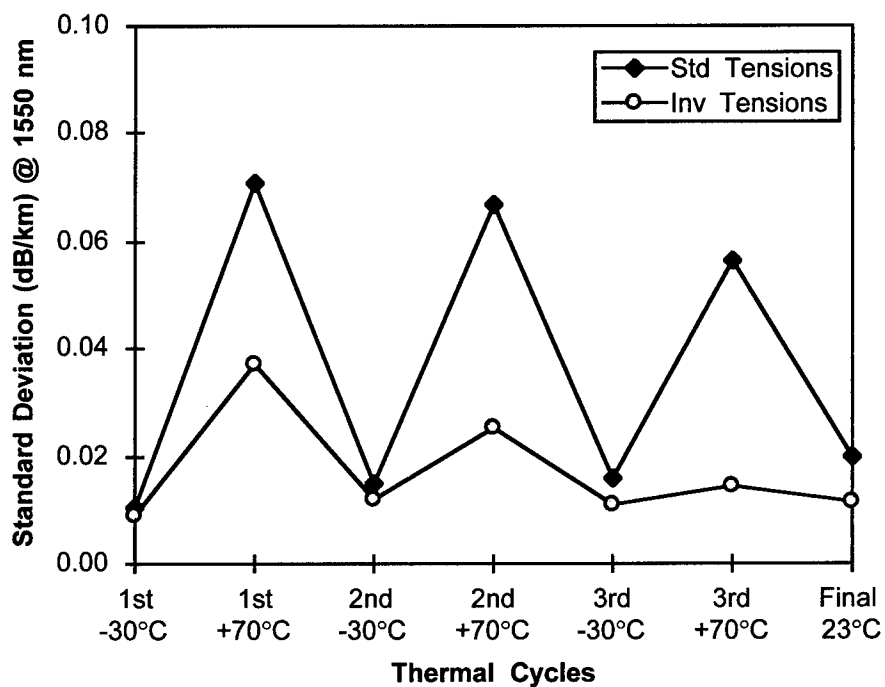


Figure 6: Standard Deviations of Attenuations for Standard and Inverted Ribbon Tensions during Thermal Cycling

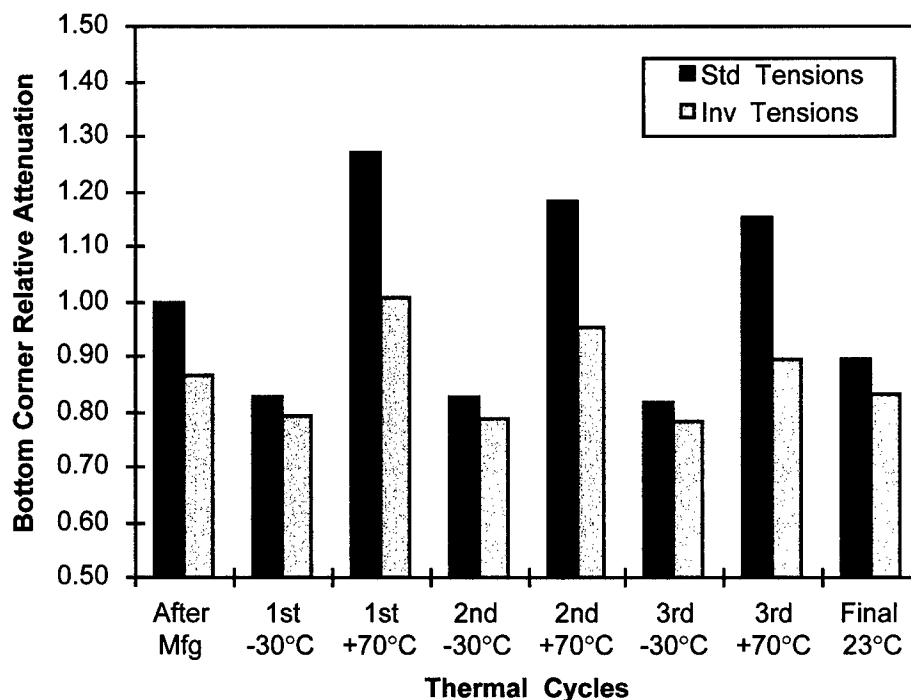


Figure 7: Mean Attenuations for Four Corner Fibers (referenced to the value for standard tensions after manufacturing)

Elongation Tests

Elongation testing was performed on cables with inverted and standard ribbon tensions. Attenuation change during this test was measured at 1550 nm. The cables were stretched to 0.15% and 0.25% and measured at each respective elongation, then measured again after releasing the tension on the cable. In this case, no significant difference in attenuation behavior was found between fibers in stacks with inverted stranding tensions and fibers in stacks with standard stranding tensions.

IV. CONCLUSIONS

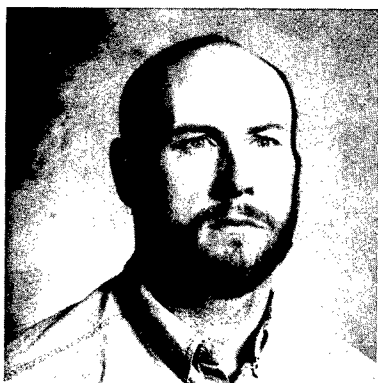
Superior and more stable attenuation performance may be achieved for slotted-core ribbon cables by using graduated stranding tensions with the bottom ribbon in each slot being applied with the lowest tension and the top ribbon being applied with the highest.

In particular, because the use of inverted tensions leads to narrower distributions of attenuation values, outliers that may cause a cable to

fail after manufacturing or after thermal cycling are less likely to occur.

References:

- [1] H. Iwata et al., *Pre-connectorized 1000-fiber Single Slotted Core Cable*, Proceedings of the 44th International Wire and Cable Symposium, pp. 627-634, 1995.
- [2] R. Wagman et al., *Component Optimization for Slotted Core Ribbon Cables Using 8-Fiber Ribbons*, Proceedings of the 44th International Wire and Cable Symposium, pp. 472-478, 1995.
- [3] K. Hogari et al., *Residual Strain Characteristics of Optical Fiber Ribbons Inserted Tightly into Slots*, Trans. IEICE, Vol. E 71, p. 688, 1988 (in English).



Ron O. Livingston was born in Loris, South Carolina, in 1968. He received his B.Sc. in Physics and Applied Mathematics from Presbyterian College in 1990. He has been employed at Siecor Corporation since 1992. At Siecor, he has worked with statistical analysis of high fiber count cables, database management and network design. He is currently employed as an Analytical and Systems Engineer in the Research, Development and Engineering Department.

The authors can be reached at the following address:

Siecor Corporation - RD
P. O. Box 489
Hickory, NC 28603-0489



Christopher K. Eoll was born in Thunder Bay, Ont., Canada in 1940. He received a B.Sc. in physics and an M.Sc. in theoretical physics from Queen's University in Kingston, Ontario, Canada in 1962 and 1964, respectively. In 1967, he was granted a Ph.D. in mathematical physics by the University of Toronto in Toronto, Ontario, Canada. Subsequently, he spent two years as a Postdoctoral Fellow at the University of Sussex in Brighton, England and the International Centre for Theoretical Physics in Trieste, Italy.

From 1969 to 1977, he was employed by Canada Wire & Cable Ltd., where his final position was Product Development Manager for the Communication Products Division. He joined Superior Cable Corporation in 1977 as Technical Director. At present, he holds the position of Scientist in the Research, Development & Engineering Department of Siecor Corporation. He has recently been focusing on various matters relating to optical cables, including aspects of design, materials, processing and light transmission.

BENDING SIMULATION OF A SLOTTED CORE CABLE

Ernst Opel, Andreas Stingl, Michael Schuebbe

SIEMENS AG, D-96465 Neustadt and D-81739 Munich, Germany

ABSTRACT

In high fiber count slotted core ribbon cables different changes in attenuation values, depending on the position in the ribbon stack were found. If macrobending can be excluded microbending effects can be studied.

Due to production parameters, material properties and design dimensions the microbending sensitivity can be described by glass, coating and surface parameters on the one hand. On the other hand the absolute amount of pressure on the fiber is of interest for the model.

A bending simulation of a test cable, by using finite element analysis (= FEA), was done to get the local pressure distribution between fiber ribbons and the slot wall.

In the case of microbending we use an average pressure value, along one pitch length, to calculate the attenuation loss.

Furthermore the bending radii and bending length were calculated via FEA to evaluate macrobending loss of the fiber during bending.

INTRODUCTION

The bending load causes a rotation of the ribbon stack and therefore an increase of pressure of the corner fibers against the slot wall, depending on the slot dimensions.

This pressure between ribbon stack and slot wall is of interest for our model. If a local pressure occurs, the ribbon stack is bent as well as the cable.

A model has been developed to predict the bending loss as a function of cable design, cable materials, surface quality and the bending load.

For the model some basic assumptions have to be made:

- Limited by the computer and the software we can only simulate a cable for one laylength in a reasonable time.
- We assume that the pressure distribution along one laylength is repeatable for the whole cable.
- The calculated pressure distribution has been averaged to simplify the model.

- As the PETERMANN [8] model involves the fiber symmetry (i.e. radial symmetry), it is a one dimensional model, strictly speaking only for bare single fibers. If a fiber ribbon is under consideration, we only consider the part of the edge fibers which show approximate radial symmetry.
- Due to the ribbon stiffness we expect only local contact areas between ribbons and slot wall, but for the model we use line contact behavior (= simplification)
- Ribbon to slot and ribbon to ribbon friction has been taken into account.
- The cable section, which has been simulated is a section from the middle of a very long cable (we don't observe cable end effects in this simulation).
- The surface quality of the slot wall has been measured by scanning the surface structure. With this data the surface roughness power spectrum has been calculated. By using a fit of this power spectrum we get the missing parameters for the calculation of C_{mech} (= mechanical parameter which is a function of glass, coating, surface properties and the wavelength of the propagating light).
- Regarding macrobending loss calculations only bend radii greater than 10 mm have been evaluated.

We are interested in the effects of changing the cable parameters, but we don't expect to get precise values, because of the aforesaid assumptions.

Now, we can optimize a cable design with theoretical parameter studies.

1. BASIC THEORY

1.1 Microbending

The fundamental theory is based on the work of PETERMANN [8-10], GLOGE [3], BALDAUF [1] and GRASSO [4].

The microbending loss with respect to the fundamental mode amplitude is given by Petermann

$$\Delta\alpha \equiv \frac{1}{4} \cdot (k \cdot n_1 \cdot \varpi_{02})^2 \cdot \Phi(\Omega) \quad (1)$$

$\Phi(\Omega)$ denotes the power spectrum of the fiber axis curvature distribution.

k is the free space wavenumber of the light (i.e. $2\pi/\lambda$ λ : wavelength of propagating light)

Ω is the coupling wavenumber

$$(i.e.: \Omega = \frac{1}{(\varpi_{01}^2 \cdot k \cdot n_1)}) \quad [8])$$

ϖ_{01}, ϖ_{02} are effective spotsize parameters that are defined [9] by equations

$$\begin{aligned} \varpi_{01} &= \varpi_0 + e^{(3.34-3.28 \cdot V)} \\ \varpi_{02} &= \varpi_0 - e^{(2.45-3.31 \cdot V)} \end{aligned} \quad (2a) \text{ and } (2b)$$

ϖ_0 is the Petermann spot radius that is approximated by equation

$$\varpi_0 = a \cdot \sqrt{\frac{2}{3} \cdot \frac{J_0(U)}{U \cdot J_1(U)} + \frac{1}{W^2} - \frac{1}{U^2}} \quad (3)$$

$J_{0,1}$ Besselfunctions
 U, V, W fiber parameters
 a core radius

The Petermann equation (1) describes the additional microbending loss of a bare fiber, i.e. a glass fiber without coating.

Taking buffer effects of primary and secondary coating into account the bending power-spectrum [1] extends to

$$\Phi(\Omega) \approx \frac{2 \cdot l_c^{\mu+0.5} \cdot (2 \cdot \mu - 1)^{0.5} \cdot \Gamma^{0.5}(\mu)}{\pi^{0.5} \cdot \Gamma^{0.5}(0.5) \cdot \left(\mu - \frac{1}{2}\right) \cdot \Omega^4 \cdot \left(1 + (l_c \cdot \Omega)^2\right)^\mu} \cdot \frac{\sigma \cdot p_0 \cdot \kappa_s^2}{H_f^2 \cdot H_0^{0.25 \cdot \mu - 0.125} \cdot D_0^{1.125 - 0.25 \cdot \mu}} \quad (4)$$

κ_s primary spring constant
 σ standard deviation of surface
 p_0 constant lateral pressure
 H_0 stiffness of the secondary coating
 H_f stiffness of the glass portion
 μ the distortion spectral coefficient
 l_c the distortion correlation length

In further calculations one more distortion parameter is inserted in equation (4), i.e. Ω_0 the central radian frequency [4]

To simplify the equation (1) a mechanical parameter $C_{mech}(\lambda, \sigma, \mu, \Omega, l_c, \dots)$ is used :

$$\Delta\alpha \equiv C_{mech} \cdot p_0 \quad (5)$$

The parameter C_{mech} must be determined.

Well known are all fiber properties like glass or coating parameters.

Unknown are all parameters describing distortion properties, like l_c , σ and μ .

To avoid a theoretical assumption of these parameters, i.e. a power spectrum estimation, the missing parameters in (4) are derived from the surface in contact with the fiber or ribbon. Therefore the surface is scanned and characterized by the parameters μ, σ, l_c and Ω_0 .

Therefore the C_{mech} -value we use is dependent on the surface under test.

1.2 Macro bending

If the local bend radii (calculated with the FEA) are smaller than 35mm, we assume that the additional attenuation is caused mainly by macrobending.

The idea is to calculate the attenuation data bit by bit over the simulated cable length by the macrobending formalism introduced by MARCUSE in 1976.

$$\alpha_{01} = \frac{10}{2 \cdot \ln 10} \sqrt{\frac{\pi}{a \cdot W^3 R}} \frac{U^2}{V^2 K_1^2(W)} e^{\left(\frac{2}{3} \left(\frac{W}{a}\right)^3 \frac{R}{\beta_s}\right)}$$

α_{01} macrobending loss of the fundamental mode fieldamplitude (LP₀₁).
 β propagation constant of the light wave.
 R curvature bending radii.
 U, V, W fiber parameters
 K Hankelfunction

2. SURFACE QUALITY OF THE SLOT WALL

2.1. Definition

The wall of a slotted core ribbon cable is called slot wall.

Due to the load (bending, tension, temperature) on a cable, the fiber or ribbon comes into contact with the slot wall. Thus the surface quality of the contact areas is of interest.

2.2 Measurement device

The power spectrum of the glass fiber axis-deformation is thought to be caused only by the surface roughness of the slot wall, and not by the coating roughness, because the roughness of the secondary coating outer surface is assumed to be negligible compared to the roughness of the slot wall.

To get the information about the surface roughness power spectrum the measurement-device as shown in Figure 1 was used.

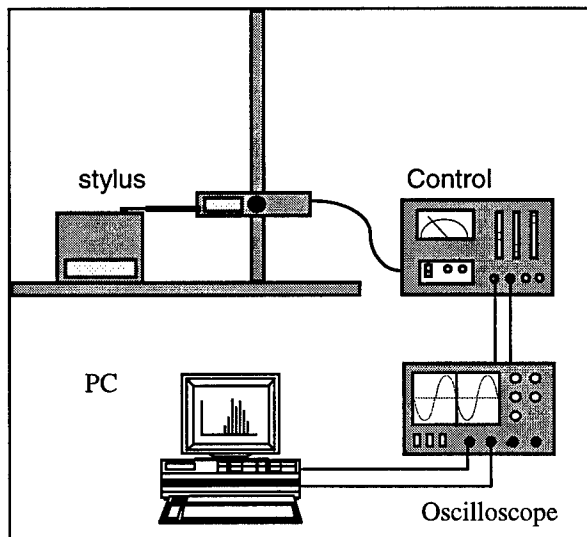


Fig. 1.: Measurement Device for the Surface Roughness

The measurement system consists of three main entities:

The surface scanner, the scanning control and the signal processing via Personal Computer.

The signal scanner is a 10 μ m stylus, that touches the surface only slightly.

It is guided over the surface and gives a one dimensional image of the scanning trace. A group of single traces may be concatenated to get a two dimensional image of the surface.

The sampling length is variable, up to 48 mm.

The control/measurement apparatus provides two scanning speeds of 0.1 mm/sec and 0.5 mm/sec.

Furthermore the device generates a voltage proportional to the signal's amplitude.

The output voltage is used to follow the trace of the stylus over the surface via oscilloscope.

This is necessary to control whether the scanning plane and the sampling plane are parallel, as the stylus is guided freely over the surface.

A nonparallel scanning process would cause error estimation of the power spectrum spatial frequency maximum.

Invalid low frequency components are generated by a nonparallel scanning process.

The measurement device has an amplitude-resolution of at least 0.1 μ m.

The spatial resolution of the scanning process is limited by the computer sampling speed and the Nyquist theorem.

The digitized signal trace is used for further calculations in the computer.

For our case, power-spectrum calculations via fast fourier transformation (FFT) algorithm were done.

As the surface irregularities are assumed to be statistical and the sampling length (i.e. 48 mm) is quite long, the measurement trace is assumed to be ergodic and therefore periodic.

As we are interested in the surface roughness power spectrum we take advantage of the fact that the surface autocorrelation function and the surface power spectrum represent a fourier- transform pair.

Therefore we first generate the autocorrelation function of the signal trace via a personal computer.

Next we calculate the amplitude spectrum of the autocorrelation function which represents the signal power spectrum.

In our measurement the scanning speed, sampling length, sampling frequency and number of samples were arranged to achieve a spatial resolution between 0.2 mm⁻¹ and 1 mm⁻¹.

2.3. Surface quality measurement results

2.3.1. Device calibration

The measurement system and the software were tested with good results on a calibration standard. This calibration standard is a glass plate with a periodic structure of wavelength 0.12 mm and amplitudes of 3.2 μm . The calculated power spectrum shows a distinct peak at the spatial frequency number 52.7 mm^{-1} .

2.3.2 Basic measurement

The surfaces under test showed rather irregular amplitudes as in Fig.2

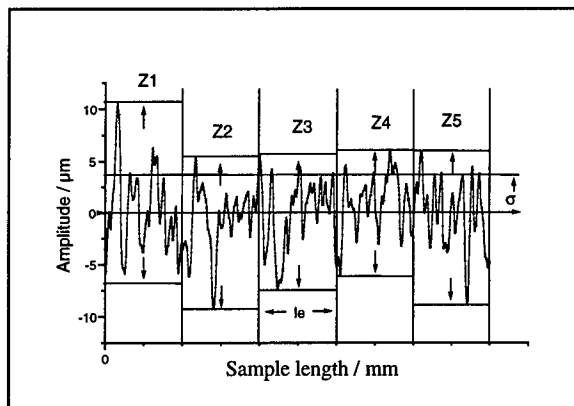


Fig. 2: Part of the Trace Signal

As mentioned above the whole signal trace is autocorrelated to generate the signal trace autocorrelation function.

In Figure 3 the autocorrelation function of crepe paper is displayed. The maximum peakvalue is normalized to one.

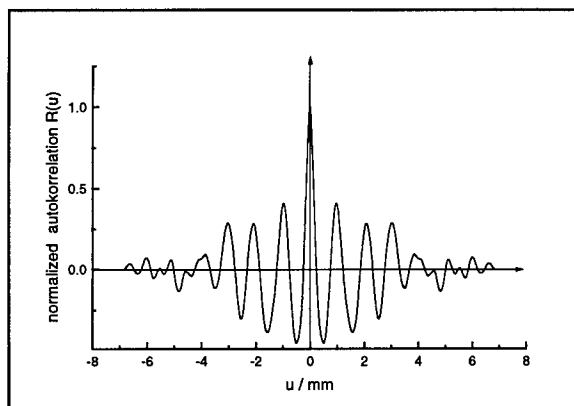


Fig. 3 Autocorrelation Function of Crepe Paper

Crepe paper was chosen, because it is wellknown, that crepepaper contains amplitudes in a spatial frequency range that cause high microbending attenuation values.

The autocorrelationfunction (acf) and the power spectrum represent a pair of fourier-transforms. Therefore we calculate the amplitude spectrum of the acf to get information about the spatial frequency power spectrum.

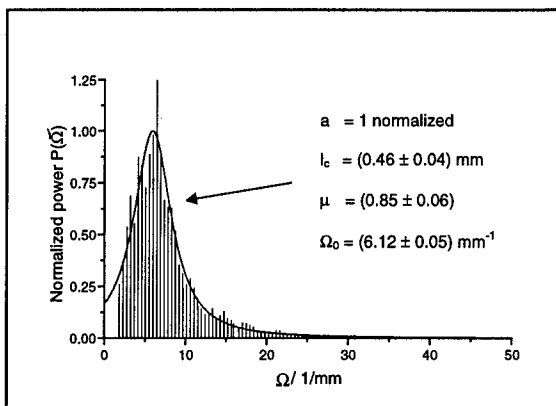


Fig.4 Surface- Power Spectrum of Crepe Paper

As proposed by G. GRASSO [4] the power-spectrum is fitted by a four parameter Lorentzian fitting curve.

$$P(\Omega) = \frac{a}{(1 + (l_c \cdot (\Omega - \Omega_0))^2)^\mu} \quad (7)$$

Using this function the missing parameters in equation 4 are derived. As the fitting function shows a distinct peak, a further parameter Ω_0 is to be inserted in equation 4.

The parameter ,a, is normalized to 1 as the height of the power spectrum is calculated by the average surface roughness σ .

a	μ	L_c	Ω_0
1	0.85	0.46 mm	6.12 mm^{-1}

Table 1: Surface Parameters for Crepe Paper

These parameters are inserted in equation 4 to predict spectral attenuation.

2.4 Validity check

To check the calculated attenuation data of equation 4 a simple winding experiment was performed. The fiber was wound under constant back tension onto a bobbin which was coated with the surface of interest. The constant pressure p_0 of the fiber on the surface is calculated by

$$p_0 = \frac{F_t}{R}$$

F_t : winding force
 R : bobbin radius

The microbending attenuation of the stressed fiber was measured with a spectral attenuation measurement device.

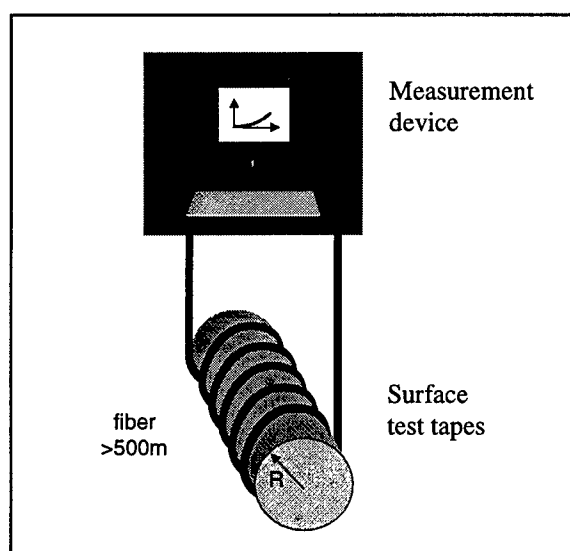


Fig. 5 Attenuation Measurement Device

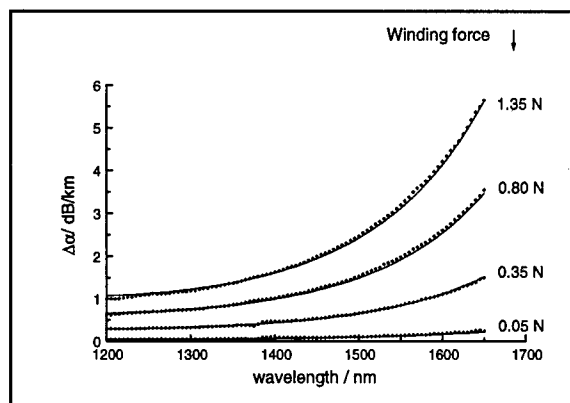


Fig.6 Validity Check: Calculated and Measured Spectral Attenuation of a Fiber

2.5 Surface quality of cable samples

Several cable samples and tapes have been scanned to derive the missing parameter C_{mech} .

Cable type	Relative C_{mech}
U- groove test cable	5
600 f SCR cable	3
PP buffer tube	1

Table 2: C_{mech} of a Standard Fiber normalized on a PP - Buffer Tube.

For a ribbon, a substitute a so – called up-coated fiber is under investigation for C_{mech} .

This procedure is adequate for corner fibers of the ribbon stack, where the significant pressure is concentrated.

3. FINITE ELEMENT ANALYSIS (FEA)

As mentioned above, the missing link in the microbending theory is the pressure on the ribbons, whereas in the macrobending theory the bending radii distribution is unknown. The possible contact partner of a ribbon can be the slot wall or another adjacent ribbon. An appropriate tool to calculate the contact pressure distributions and the bending radii is the FEA-method.

In an FEA analysis, contact, friction effects and large displacements are dealt with as non-linearities. Bending in this simulation is really a static process. For this reason the first simulation attempts were done with an implicit nonlinear FEA program using an iterative solution procedure. But because of the huge number of possible contacts this approach failed.

There is another class of FEA programs, which simulate the dynamic behavior of structures. To solve the following dynamic equation the central difference method, an explicit integration scheme [2] is used:

$$[M]\{\ddot{u}\} + [C]\{\dot{u}\} + [K]\{u\} = \{F\} \quad (8)$$

A disadvantage is, that due to numerical stability these programs require very small time steps. The critical time step dt_{crit} is calculated so that a sound wave will pass through the smallest element edge length during this time. This means that only small time intervals may be analyzed. But an advantage is, that the large number of contact entities may be handled without any problem.

So an explicit dynamic FEA program was used for the bending simulation of a SCR cable. Bending is achieved by rolling the cable onto a cylinder. Two limitations influence the simulation model:

- To be able to neglect centrifugal mass effects of the cable, the rotational velocity of the cylinder should not be too great.
- The critical time step will be limited by one ribbon dimension.

In order to get results in a reasonable computation time a relative coarse FEA mesh is used for the ribbons.

The FEA results give a lot of additional information. So the local bending radii of the ribbon edge fibers due to buckling or other instability effects may be calculated. In this

fashion it is possible to discuss macrobending due to local bending radii as well.

3.1 Parameters of the FEA model

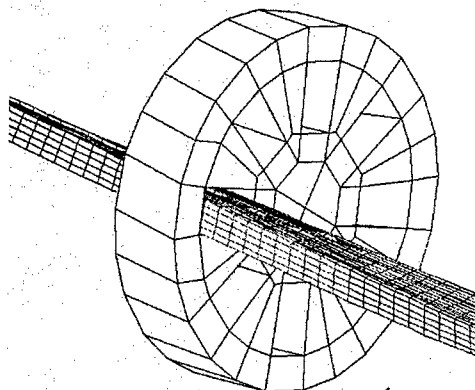


Fig. 7: FEA Model – Sample Crosssection

- The bending radius is 350 mm
- The laylength of the stack is 425 mm
- The cable diameter is 23.3 mm
- 8 fiber ribbons have been used
- A stack of max. 10 ribbons is in one cable slot, only one stack has been simulated.
- The static friction coefficient between two ribbons has been selected to be 0.6
- The static friction coefficient between ribbon and slot wall has been selected to be 0.3
- A back tension on a ribbon of 1.35 N has been used.

3.2 Cable model

3.2.1 First simulation step

In the first simulation step a laylength was brought into the cable part by linear drilling of each node cross section along the cable axis. The stiffness of the glass fiber stack elements and contact forces move the stack to a new position.

The second simulation step is then to eliminate the rotational velocity around the cable axis.

The third simulation step is to start the bending process. If contact occurs between the slot walls and the ribbons the bending of the cable induces bending effects into the ribbon.

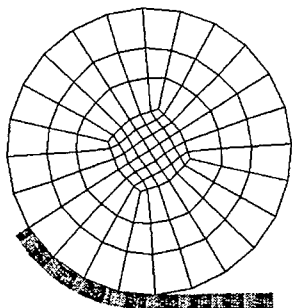


Fig. 8: Bending of the Cable

3.2.2 Precise model

The mentioned steps of 3.2.1 are conducted first for a coarse model. For each glass fiber ribbon a so called interface is defined. During the whole simulation process the displacement history is stored for all interface nodes.

After finishing the coarse model simulation the mentioned steps of 3.2.1 will be repeated for a refined precise model of only one ribbon using the appropriate interface displacement history of the coarse model.

3.3 Results

The ribbon positions in the slot changed due to the bending.

The results of the precise model are used to evaluate the pressure distribution on the ribbons due to wall contact.

Their final position is displayed as a function of the laylength. The local bending radii of the glass fibers along the cable axis are calculated using a circle fit of 3 successive nodes.

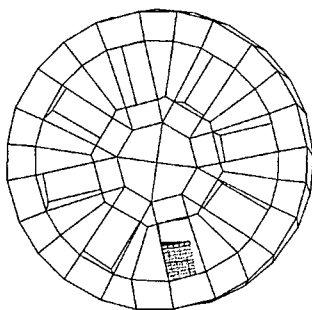


Fig. 9: Example of a Displaced Ribbon Stack

If an inner ribbon of the stack is under investigation, no significant pressure values on an edge fiber have been calculated.

If the top or bottom ribbon of the stack is under investigation a significant pressure distribution due to the cable design has been calculated.

4. VALIDITY CHECK

To check the calculated attenuation values a simple winding experiment was done.

To gain high accuracy, a cable length of 100 m was used. Furthermore the edge fibers of the ribbon stack were spliced in a ring to multiply the fiber length under test.

To avoid any torsional effects caused by winding the cable onto a bobbin, the spooling was started with the ring end of the cable, whereas the measurement end of the cable remained calm.

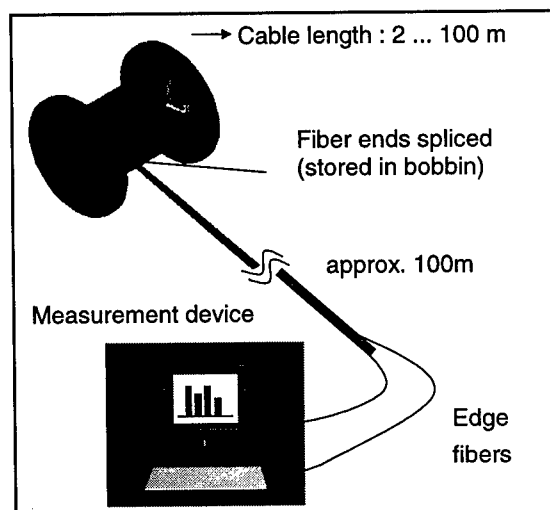


Fig. 10 Simple Winding Experiment.

The cable was wound on a bobbin with diameter of 70 cm.

The following table shows a an average value for all four corner fibers of one ribbon stack.

Measurement Value (dB/km)	Macro-bending Loss (dB/km)	Micro-bending Loss (dB/km)
0.055	0.09	0.015

Table 3: Comparison between Measurement and Theoretical Model Results at 1550 nm.

5. CONCLUSION

We can optimize a cable design with theoretical parameter studies.

From a FEA model we get the local bend radii and the local pressure distribution ("p") on the corner fibers of the ribbon stack. With well known fiber parameters specified by the fiber manufacturer and the measured surface parameters of the slot wall, we evaluate a mechanical parameter C_{mech} .

Now we can calculate microbending loss due to surface roughness by multiplying C_{mech} with p.

On the other hand, we can calculate the macrobending loss by summing up the influence of the local bend radii along one pitch length.

These macro - and microbending studies can be done for each cable design by using FEA simulations.

6. REFERENCES

- [1] J. Baldauf, N. Okada, M. Miyamoto:
Relationship of mechanical characteristics of dual coated single mode optical fibers and microbending losses
IEICE Trans. Commun., E 76-B (1993) pp. 352- 357
- [2] K.J Bathe:
Finite- Elemente Methoden
Springer- Verlag
Berlin Heidelberg New York 1990
pp. 547 – 610
- [3] D. Gloge:
Optical- fiber packaging and its influence on fiber straightness and loss
Bell System Technical Journal
(1975) pp. 245- 262
- [4] G. Grasso, F. Meli, E. Usai, F. Esposito:
Microbending loss in single mode optical fibres; IWCS 1988, Proceedings, pp. 722- 731
- [5] D. Marcuse:
Curvature loss formula for optical fiber fibers
Journal of optical Society of America,
66 (1976) pp. 216- 220

- [6] D. Marcuse:
Field deformation and loss caused by curvature of optical fibers
Journal of Optical Society of America,
66 (1976) pp. 311- 320
- [7] D. Marcuse:
Influence of curvature on the losses of doubly clad fibers
Applied Optics, 21(1982),
pp. 4208- 4213
- [8] K. Petermann
Theory of microbending loss in mono-mode- fibers with arbitrary refractive index profile
Archiv der elektrischen Übertragung (AEÜ) 30 (1976), pp. 337- 342
- [9] K. Petermann
Fundamental mode microbending loss in graded index and w- fibres
Optical and Quantum Electronics , 9 (1977), pp. 167- 175
- [10] K. Petermann
Upper and lower limits for the microbending loss in graded- index and w-fibres
Journal of Lightwave Technology
- [11] J.V. Wright
Microbending loss in monomode fibers
Electronic Letters 8th December 1983
Vol. 19 No. 25/26



Ernst A. Opel

SIEMENS AG, ÖN NKE K5
Austr. 101
D-96465 Neustadt bei Coburg
Germany

Ernst Opel is a development engineer in the field of communication cables. He was born in 1959 and received his Dipl.-Ing. (FH) in Feinwerktechnik from Georg-Simon-Ohm-FH in Nürnberg in 1987. He joined SIEMENS in 1988. Since 1989 he has been engaged in the development of high-density optical fiber cables. In 1994 he joined the cable measurements group where he is responsible for the development of theoretical models.



Michael Schuebbe

SIEMENS AG, ZT PP 5
Otto-Hahn- Ring 6
D-81 739 Munich
Germany

Michael Schuebbe is a technical consultant in the field of development methods. He was born in 1950 and received his Dipl. Ing. in Structural Engineering from the Technical University of Munich in 1976. He joined Siemens Corporate Technology in 1986. As a project manager he is responsible for highly sophisticated numerical simulations using Finite Element software.



Andreas H. Stingl

SIEMENS AG, ÖN NKE K5
Austr. 101
D-96465 Neustadt bei Coburg
Germany

Andreas Stingl is a doctoral candidate at the University Bayreuth. He was born in November 1970 and received his Dipl.- Phys in 1997 from the University of Bayreuth. He joined Siemens in 1996 as a co-op student. His activities are on the field of the theoretical cable model and cable simulation.

THE DEVELOPMENT OF RODENT PROTECTED ALL-DIELECTRIC OPTICAL CABLES

Hélio J. Durigan, Leonardo Silvério, Renato F. Cruz, Marcos A. B. Caetano

Furukawa Industrial S.A. Produtos Elétricos, Curitiba-PR, Brazil

ABSTRACT

This paper describes the process of optimizing the construction of rodent protected dielectric optical cables for use in telecommunication buried networks. The investigation into all-dielectric protection cable sheaths was initiated in response to specific customer's requests from Embratel and Telebrás - Brazil. Some of the Brazilian specifications define requirements for a fully dielectric protection sheath.

Experimental cables have been manufactured to assess the effect of a dielectric protection sheath on cable performance and manufacturability. Enhanced performance was achieved by selecting materials and processes conditions.

Laboratory tests results are presented showing both mechanical behavior and rodent protection performance.

company personnel and the electronic equipment³. Some of the Brazilian specifications define requirements for a fully dielectric protection sheath^{4,5}.

A wide range of dielectric sheath materials were submitted to rodent attack tests in previous trials^{1,2}. The tests results show that the following sheath cable designs might represent a sufficient protection against rodent attacks:

- glass yarns or tape reinforcement;
- polyamide outer sheath;
- GRP (pultruded glass reinforced plastic) armored layer.

To verify the practicality of these protection sheath cable designs when submitted to the Brazilian specifications requirements, four experimental cables have been manufactured to assess the effect of a fully dielectric protection sheath on cable performance and manufacturability.

INTRODUCTION

There is a growing demand for optical cables for use in long distance telecommunication networks in Brazil. These cables are subject to attack by rodents which are urban and native of the country¹. Such damage can lead to a total breakdown of the system.

Usually direct buried cables are preferably protected with a metallic armour. The introduction of metallic components into the cable subject it to lightning strikes or lightning induced potential that in turn constitutes a hazard to the users, operating telephone

CABLE DESIGN

All experimental cables present a loose-tube core design with a central strength member (GRP). The core sheath was manufactured by coextruding low density polyethylene (LDPE) with polyamide 12. The 0.4 mm thick Nylon 12 jacket serves as a protection against termites. The coextrusion creates a permanent bond between the polyethylene and the Nylon 12.

Some basic characteristics of four different experimental cables with fully dielectric rodent protection sheath are summarized in Table 1.

Table 1 - Cables Characteristics

Cable type	A	B	C	D
Number of fibers, max.	36	36	36	36
Inner sheath thickness (mm)	1.0	2.0	1.0	1.0
Rodent protection sheath thickness(mm)	2.0	1.5	1.3	1.6
Outer sheath thickness (mm)	1.8	2.0	3.0	1.8
Cable diameter (mm)	18	22.5	21	18
Cable weight (kg/km)	255	460	350	256
Minimum bend radius (mm)	108	136	126	108
Operating temperature range (°C)	-20 to +65	-20 to +65	-20 to +65	-20 to +65

Cable Protection Sheaths

The cross section of the Cable A is shown in Figure 1. This cable has been made to verify the performance and manufacturability in using a semi-aromatic polyamide as rodent protection layer. Due to its high hardness (80 to 85 Shore D), semi-aromatic polyamide is used as protection-layer for optical fiber cables against rodents attacks. This material was applied in the form of an inner layer under a high density polyethylene (HDPE) outer sheath.

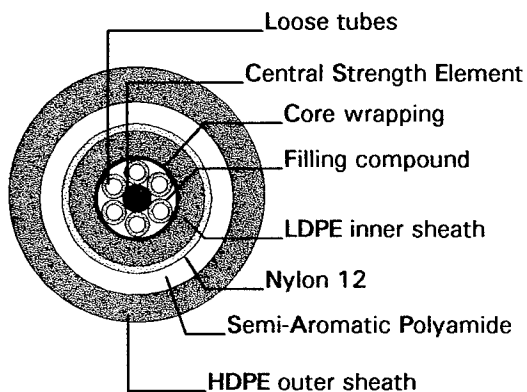


Fig. 1 - Cable "A" cross section

The cross section of the Cable B is shown in Figure 2. A reinforcing layer of fiberglass yarns with a minimum thickness of 1.5 mm was applied over the inner sheath of the cable. Due to the discomfort caused to the rodent while attacking this material, it might protect the cable¹.

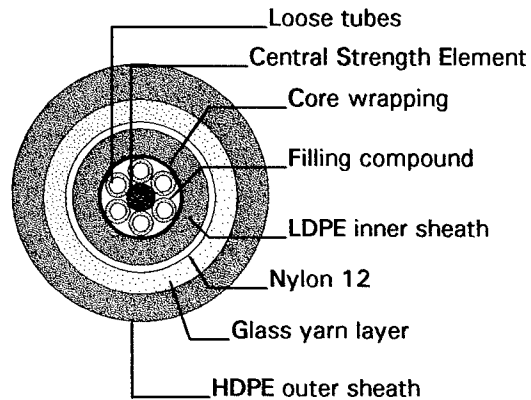


Fig. 2 - Cable "B" cross section

The cross section of the experimental Cable C is shown in Figure 3. A single helical layer of rounded GRP strength members was applied over the inner LDPE sheath. Each GRP has a 1.30mm diameter. The GRP armouring was covered with a high density polyethylene (HDPE) jacket.

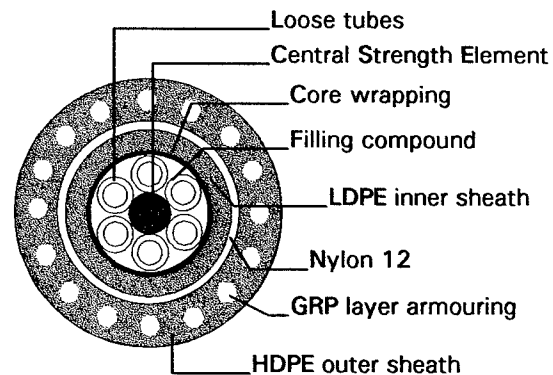


Fig. 3 - Cable "C" cross section

The cross section of the experimental Cable D is shown in Figure 4. The inner sheath was covered with two layers of E-glass woven tape with 1.5 mm and 0.18 mm nominal thick each.

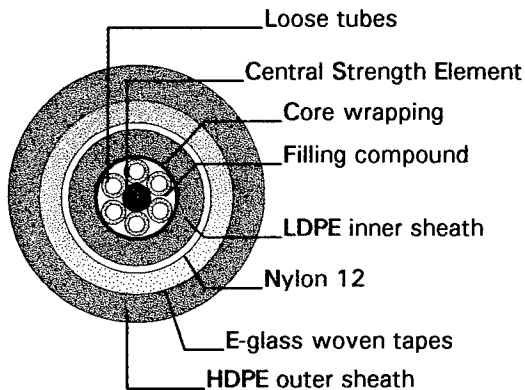


Fig. 4 - Cable "D" cross section

CABLE PRODUCTION

In order to develop the cable designs, several processes trials were performed on prototype cables. Processes trials results and recommendations for the production of these cables are presented.

Cable "A"

Sleeve (tubing) type tooling was used during semi-aromatic polyamide extrusion. The extrusion ran smoothly except for some lumps which occurred at the start of the process. A decreased die temperature seemed to cure the problem. A consistent thickness and good surface finish was obtained.

Cable "B"

The development of this cable was initiated in response to a specific customer request⁵. The requirements calls for a LDPE inner jacket with a

minimum thickness of 2.0 mm and a glass yarn sheath with a minimum thickness of 1.5mm.

Several material tests were performed using different types of glass yarns. The materials qualified were a glass yarn 44,000 dTex (non-impregnated) and a glass yarn 8,600 dTex (impregnated with an abrasion resistant coating).

Due to the requirement of a minimum thickness of 1.5 mm, a large quantity of glass yarn is necessary. The final rodent protection sheath thickness was obtained using 1,650,800 dTex of glass yarn.

Although in some cases the several layers of the glass yarns may result in a good barrier against rodent attack, it must be borne in mind that the mechanical characteristics of the cable could be prejudiced. In the first prototype cable, the glass yarn reinforcing layer was applied longitudinally in a sheathing line. Unfortunately, the glass yarn applied longitudinally turn the cable too stiff and hard to handle. During the mechanical tests of this prototype, it was noticed that all of the cable stresses were transmitted directly to the optical fibers causing high optical power losses.

Finally, it was clear that applying helically layers of glass yarn could result in a free movement of the optical fibers within the loose tube for a given range of elongation and compression, and therefore improve the mechanical performance. The problem was solved using a planetary strander machine, helically applying the glass yarns around the inner sheath and wrapping it with a polyester tape.

Cable "C"

The development of this cable was also initiated in response to a specific customer request⁴. The requirements calls for an armour layer composed by GRP strength members with a minimum diameter of 1.30 mm and separated from each other by a maximum distance of 1.30mm.

The minimum thickness for the HDPE outer sheath is 3.0 mm. This thickness is made up of the GRP armouring layer and the HDPE jacket.

Each GRP was previously upjacketed with HDPE to 2.6 mm outer diameter in order to guarantee a distance of 1.3 mm between them.

A single layer with seventeen GRP strength members was helically applied around the inner sheath and wrapped with a polyester tape. One advantage of wrapping the GRP layer is to avoid the possible adhesion of the upjacketed GRP to the HDPE jacket inner surface. Therefore, an improved bending cable performance was obtained.

Cable "D"

This cable was covered with two layers of E-glass woven tapes. The first layer (1600 g/m², 1.5 mm nominal thick) was applied longitudinally and the second layer (165 g/m², 0.18 mm nominal thick) was applied cross-wound to the cable axis. No practical problem occurred during this process.

RODENT PROTECTION PERFORMANCE

The rodent resistance of the four designed cables was verified during a three-day test conducted by the Rio de Janeiro Federal University (UFRJ) - Ecology Department, in accordance with Embratel and Telebrás standards.

The tests were carried out with *Trycomis apereoides* ("Punaré ") rodent, using captured animals of both sexes ranging from 200 to 300 mm in length and 250 to 400 g in weight. As described in reference 1, *Trycomis apereoides* rodents commonly attack the sample cable without stimulus. The animal's natural instinct is to gnaw the exposed cable.

For this test, a cable sample 20 ± 1 cm long was placed in a 50 x 40 x 40 cm cage with a rodent and food. Each cable evaluation involves 15 cable samples.

Each day the samples were visually inspected and a damage index recorded for each sample as follows:

- 0 = no damage
- 1 = outer sheath damaged, but not penetrated
- 2 = protection layer partially damaged
- 3 = protection layer penetrated, without damage to the core sheath
- 4 = core sheath damaged, but not penetrated
- 5 = core sheath penetrated, with damage to the optical fibers
- 6 = core destroyed
- 7 = cable severed (cable cut)

The customers' requirements define that out of the fifteen samples tested for a cable design, a maximum of three should have a damage index rating of 3 or above, just one sample could have a damage index of 4 and no sample should have a damage index of 5, 6 or 7.

Table 2 shows the results for 15 samples of each experimental cable.

Table 2 - Rodent attack damage results

Damage Index	Cables			
	A	B	C	D
0	7	6	8	4
1	0	3	2	2
2	1	5	5	6
3	1	1	0	1
4	3	0	0	0
5	3	0	0	2
6	0	0	0	0
7	0	0	0	0
Average	2.1	1	0.8	1.8
Maximum	5	3	2	5

The designed Cables B and C showed good results, which are in compliance with Telebrás and Embratel requirements. The Cable C with a GRP armouring gave the best result.

MECHANICAL AND ENVIRONMENTAL PERFORMANCE

The experimental cables B and C have been subjected to a variety of standard laboratory tests to verify that they can withstand mechanical forces and environmental aspects comparable to what could occur in the field.

Due to the results of the rodent resistance evaluation, experimental cables A and D were rejected and thus not mechanically and environmentally evaluated.

The standard tests were taken from Telebrás and Embratel specifications are summarized in Table 3. These tests are based on international standards (e.g. EIA-FOTP).

Table 3 - Mechanical and Environmental tests

Test	Request
Tensile loading	attenuation change ≤ 0.1 dB/km, fiber strain $\leq 0.2\%$ under load, fiber strain $\leq 0.05\%$ after load removed load = 1000 N
Impact	3 cycles, 500 mm drop, 4 kgf, any cracking in the sheath and in the optical fibers
Cyclic Flex	attenuation change ≤ 0.1 dB/km, 50 cycles, mandrel 20 X cable diameter
Bending	attenuation increase ≤ 0.1 dB/km, radius of 6 X cable diameter, 5 wraps
Low temperature bending	any cracking in the cable, radius of 12 X cable diameter, 2 wraps at -20°C , 24 hours
Compression	attenuation increase ≤ 0.1 dB/km, 5000 N / 100 mm
Twist	attenuation increase ≤ 0.1 dB/km, 10 cycles, $\pm 180^{\circ}$
Thermal cycle	attenuation increase ≤ 0.05 dB/km, 4 cycles from -20°C to $+65^{\circ}\text{C}$
Waterblock	no leakage, 3 meters long, 1 hour, 1 meter head

The laboratory measurements showed that B and C cables designs pass in all the requirements. Optical changes equal or less than 0.02 dB/km were measured during the bend, flex, twist, compression and thermal cycle testing. A fiber strain less than 0.025% under load and less than 0.01% after load removed were measured during the tensile load test.

The cables performance met or exceeded all requirements with no adverse mechanical or optical effect.

CONCLUSIONS

Assuming the damage caused by rodent attacks, a variety of rodent protected all-dielectric optical cables designs were evaluated.

All the tests performed showed that the rodent protected all-dielectric optical fiber cable characteristics are at least equal to the values used during cable design, provided that the cable manufacturability is feasible.

On the basis of the UFRJ test results, the conclusion must be that of the tested designs the GRP armouring layer is the best option for a fully dielectric rodent resistant cable.

Processing trials and performance test results indicate that a GRP armouring layer and a large quantity of glass yarn layer present an acceptable level of protection against rodent attacks. To reach good mechanical and optical characteristics all production processes must be selected very carefully.

The cables designs meet or exceed accepted customers requirements for rodent protection, mechanical and optical performance. The designed cables were tested according to Brazilian standards, and comply with Telebrás and Embratel requirements. The tests results showed that the proposed cables designs are well suited for a direct buried use.

These all-dielectric rodent protected cables have been successfully installed since their introduction almost a year ago. The cables designs are easy to handle and well suited for installation in directly buried conditions.

ACKNOWLEDGMENTS

The authors wish to acknowledge the support of many people and organizations. Many people in our own organization worked with us in the understanding and application of the various process parameters which effect the functionality of the all-dielectric rodent protected sheath.

We would like to thank Mr. Paulo Curado of the Telebrás - R&D Center and Mr. João Elias Filho and Mr. Marcílio E. Latini of the Embratel - Optical Systems Division who provided valuable information on rodent attacks on optical fiber cables. Thanks are also given to UFRJ for the rodent tests.

REFERENCES

[1] Curado, P. et al, " Study and Analyses of Rodent Attacks in Optical Fiber Cables", Proceedings of the 45th International Wire and Cable Symposium, 1996.

[2] Gaillard, P. et al, " Rodent Protected Dielectric Cables: Where is the Solution ?", Proceedings of the 44th International Wire and Cable Symposium, 1995.

[3] Olszewski, J.A. and Masterson, J.B, " Lightning Considerations in Optical Cables Design", Proceedings of the 35th International Wire and Cable Symposium, 1986.

[4] Embratel, Edital de Concorrência DTT-020/96, Seção 2 - Anexo B, 1996.

[5] Companhia Riograndense de Telecomunicações - CRT, Edital de Concorrência CEL CC 950745 - Seção 3, 1996.

AUTHORS



Hélio José Durigan
Furukawa Industrial S.A. Produtos Elétricos
Rua Hasdrubal Bellegrad, 820 - CIC
81450-140 Curitiba - PR - BRAZIL

HÉLIO José Durigan joined Furukawa Industrial S.A. in January 1982 after receiving his degree as an Electrical Engineer from Universidade Federal do Paraná (UFPR). Since then he has been involved in technical service and development of new products. He is currently General Technical Manager.



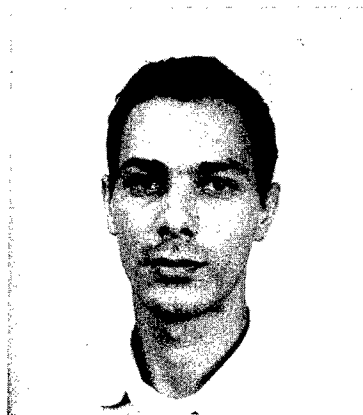
Leonardo Silvério
Furukawa Industrial S.A. Produtos Elétricos
Rua Hasdrubal Bellegrad, 820 - CIC
81450-140 Curitiba - PR - BRAZIL

LEONARDO Silvério joined Furukawa Industrial S/A in January 1984 after receiving his degree as an Electrical Engineer from CEFET. He has been involved in the optical fiber cables design and development. He is currently responsible for the Plant Engineering Management.



Renato Flávio Cruz
Furukawa Industrial S.A. Produtos Elétricos
Rua Hasdrubal Bellegrad, 820 - CIC
81450-140 Curitiba - PR - BRAZIL

RENATO Flávio Cruz received his Chemical Engineer degree from Universidade Federal do Paraná (UFPR) in 1988. He joined Furukawa Industrial S.A. in February 1989. Since then he has been involved in the development of materials for telecommunication cables. Now he is in charge of the Products and Processes Development Engineer Department.



Marcos Aurélio Barreto Caetano
Furukawa Industrial S.A. Produtos Elétricos
Rua Hasdrubal Bellegrad, 820 - CIC
81450-140 Curitiba - PR - BRAZIL

MARCOS Aurélio Barreto Caetano is a Product Development Engineer at Furukawa Industrial S/A. He received his Electrical Engineer degree from Universidade Federal de Santa Catarina (UFSC) in 1995. He joined Furukawa Industrial S.A. in January 1996.

EVOLVING TECHNOLOGIES OF OPTICAL INFRASTRUCTURE TO OPTIMIZE THE FTTH DEPLOYMENT SCENARIOS

D Boscher G Le Noane* I Hardy JC Bizeul JP Louboutin

France Telecom / CNET / DTD 22300 Lannion

*France Telecom / CNET / Caen

ABSTRACT

The point to point FTTH architecture is undeniably the best solution in terms of capacity , upgrading capability , safety and maintenance .The main task in hand is to transform the all copper networks into all fiber networks with the best way in economical terms

This paper describes three independent means to decrease the cost of the optical infrastructure .

- a) The multicore design with the geometrical and mechanical improvements .
- b) The high ultra light cables wich are very efficient for the overlay installation and micri civil works .
- c) The possibility of double full duplex with the point to point concept .

Finally an economical approach gives the gain of these technologies for the infrastructure cost

INTRODUCTION

The copper versus optics competition is nowadays conditioned by the service-cost duality . The question is whether these services encourage or discourage technology

The point to point FTTH architecture is technically the best solution , but alternative solutions , such as PON and FTTB are now being implemented and are prefered for medium distance links to ADSL technique . At the same time , the FTTH configuration is cost efficient for rural areas , where the ONU cannot be shared among several subscribers

The main task in hand is to transform the all copper networks into all fiber networks using overlay technique , taking into account several rates of deployment and evolving technologies .

In order to lower the costs of a passive optical infrastructure, it is necessary to reduce the cost of cabled fibres. It is also necessary to avoid new civil engineering, and to try and place the cables according to user's demand, therefore have high density cables.

The multicore design answers to both these requirements.

II MULTICORE DESIGN

The design was published in 1994. Since then it has gradually been evolved. Figure 1 shows the basic principle. The dimensions of the four unitary preforms produced are presented in Table 1. The core diameter to mechanic sheath diameter ratio is inferior to that of a traditional preform. (1/10 in comparison to 1/5.6). The technology used in producing the preform is FCVD. This enables the preforms to be produced straight away with exact dimensions, an excellent geometric accuracy and a cost effective technique.

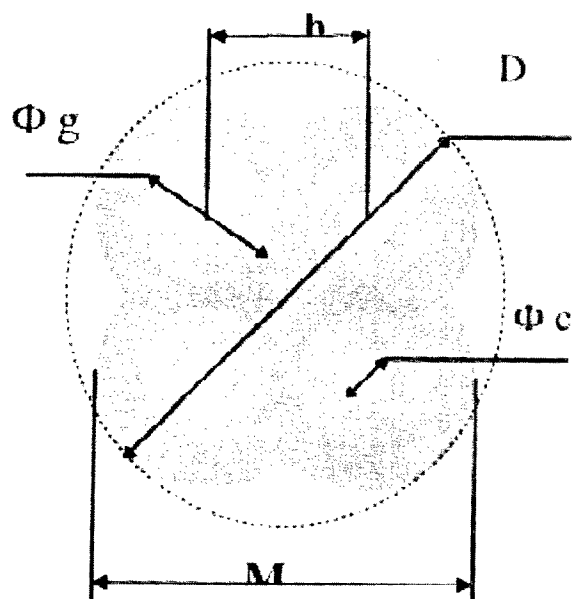


Fig 1

	PREFORM for 200 Kms of FIBER in mm	FIBER μm
optical cladding	12	28
core	4	7
h	13,4	51,78
M	32,4	125
D	38	146,45

Table 1

The preforms are then grinded to form two perpendicular planes. The preforms are assembled in order to form the shape then soldered together using the same HF furnace as was used in the production of the preforms. The soldering of two pigtails at the ends gives a preform which can be used immediately on a conventional fibre drawing tower, with drawing characteristics identical to those of a conventional fibre (see photo2)

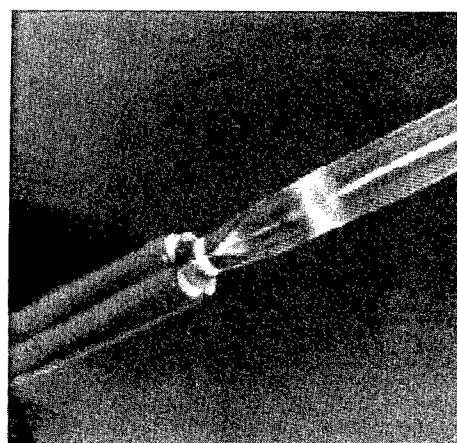


Photo 2

The fibre short side nominal dimension is 125μ , giving a silica diameter identical to that of a fibre. This dimension therefore gives a theoretical intercore surface of $51,78\mu$. The 4-core fibre is covered with a conventional 250μ thick coating. Photo 3 shows a fibre end.

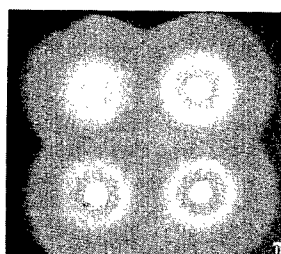


Photo 3

The optical characteristics obtained are those of a conventional fibre, and the mean values in the last 60 km are from 0.42 dB/km to 1.3μ and $0.3. \text{ dB /km}$ to 1.55μ with 45dB (de diaphotic) on 10 km. These values have not been optimised; publication (10) covering the 4-core concept using another production technique, has published better results in this domain.

The non-optimised optical characteristics are sufficient to be used in distribution networks. The two parameters to be improved are:

- The above-mentioned accuracy to be able to insure the conventional connections.

- The mechanical strength, in order to guarantee a good cabling, easy installation and good durability.

These two parameters, as well as the ease of production, will influence the choice of technology.

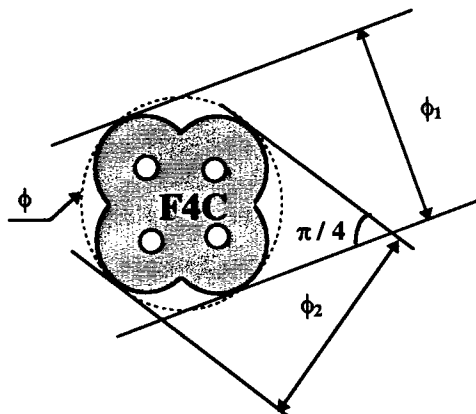
III GEOMETRICAL ACCURACY

The F4C is not circular, and its rotating position is not determined during the fibre drawing. It is essential to be able to characterise its geometry at any time.

A device was developed to make measurements along 3 axes at an angle of 45°.

Figure 4 illustrates the principle of this measurement, which allows the calculation of the F4C theoretical diameter at any time.

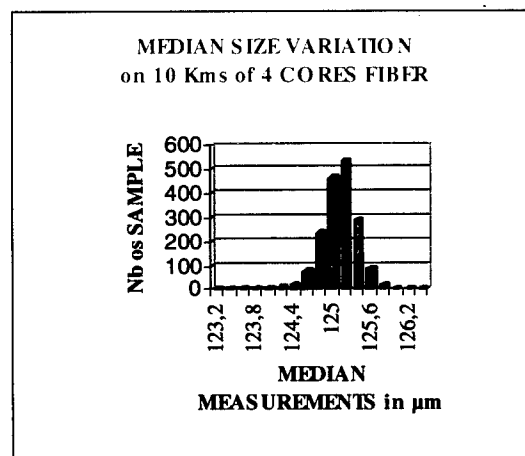
Two axes at 45° are sufficient, and the third axis allows the characterisation of the deformation with respect to the theoretical profile.



$$\phi = \phi_1 / \cos^2 [\text{Atg} (2.6131 (\phi_2 / \phi_1)^{1/2} - 2.4142)]$$

Fig 4

The calculated value is introduced into the PiD servo-control in the same way as for a conventional fibre. The histogram (5) illustrates the variation of the side dimension over 10km, showing a standard deviation of 0.27 μ , not much different from that of a conventional fibre. This element is of course fundamental for the quality and ease of connection.



Histogram 5

IV MECHANICAL STRENGTH

The monomode multicore design, (published 1986 (11), was not developed further due to a lack of reliability, regarding mechanical strength. The latter is essential and in addition the bottle technique presents drawbacks, namely the necessity to fill in the spaces during fibre drawing, and the assembly of different interfaces having different expansion co-efficients. The processing of these interfaces, and the residual stress field after fibre drawing are the key to success of the process.

Our technique avoids the above-mentioned drawbacks.

The level of the mechanical strength will therefore only depend on the quality of the preform before processing and of the soldering before fibre drawing.

Figure 6 shows the Weibull diagram of a F4C, in keeping with quality requirements:

Note the progress made between 1994 and 1997 with the achievement of an almost unimode Weibull diagram, with a minimum strength of 4GPa.

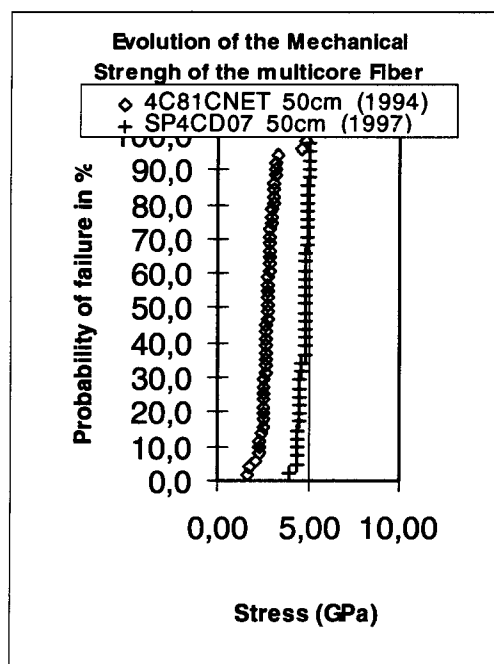


Fig6

V CROSS - TALK

This parameter is important for the transmission system quality. The F4C is to be applied to point-to-point distribution systems having a nominal distance of 10km. Hence the power budget is low (15 dB maximum) and a crosstalk of below 25 dB is sufficient (12). However, an understanding of the phenomenon is important.

The first publications gave the following theoretical formula for intercore coupling.

Because of the low coupling coefficient C in our structure, the slightest variation of optogeometric parameters should limit the crosstalk to a very low level - independently of the length.

The variation of crosstalk with distance, and the measured levels which show that the phenomena are very complex and in particular that the fibre bending plays an important role in the coupling rates.

In our experiment, a sufficient level was reached - 45 dB over 10 km, however, further investigations are being carried out in this field.

VI CABLE STRUCTURING

The F4C fibres have been cabled using ribbon and microsheat structures. No characteristic modifications occurred after the cabling. The ribbon structure presents no real advantages for the linking of the F4C fibres (angular indexing), hence we recently tested the latest developed microsheat structures.

These very conventional structures offer a 1152-core cable, with a diameter of 15.8mm, corresponding to 5.87 core/mm, i.e. four times than the best predictions (3).

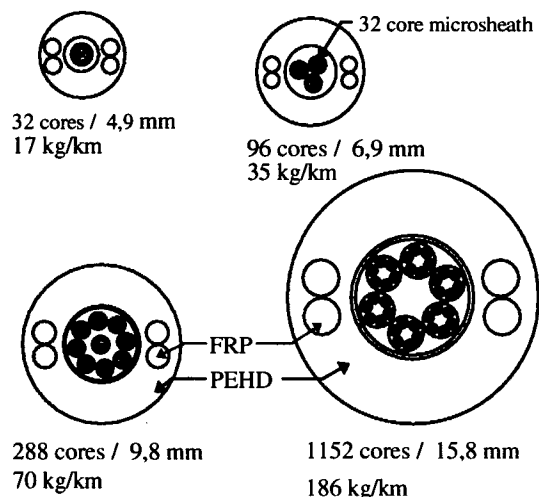


Fig 7

VII CONNECTING DEVICES

The square shape suits the linking in V or U grooves used for conventional monomode connection. The results depend on the geometric accuracy of the F4C technique. The results published (12/13) show that the splices, the connectors and the fan out can be produced using traditional techniques.

VIII MICRO CIVIL WORK

The traditional layout had to take into account physical constraints induced by the size and weight of copper cables. The techniques have not been optimised for smaller and lighter optical fibres which tolerate long lengths of cable. This has a strong economical impact on the costs of laying and linking cables. Some publications (14) show the interest of micro civil work. This concept is shown in the diagram below (figure 8):

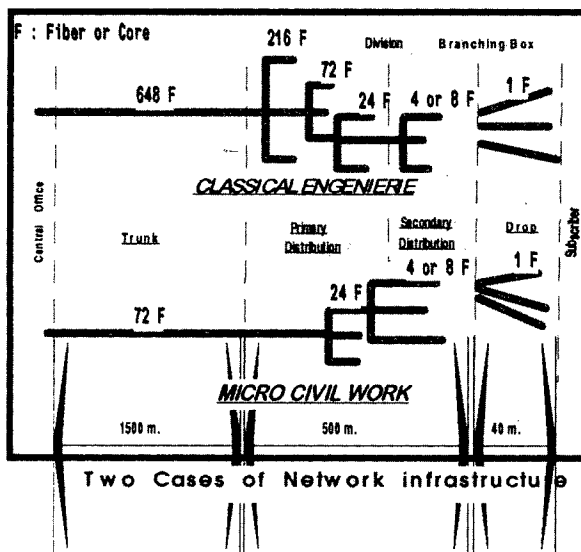


Fig 8

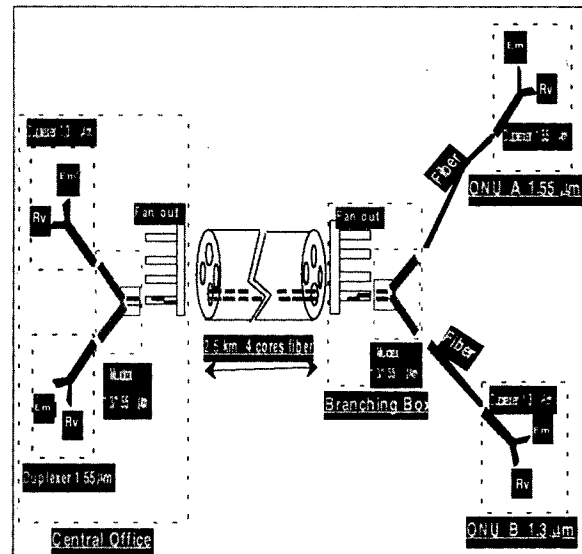
This technique in addition to its intrinsic economic interest, studied in the following paragraph, allows the overlay technique, which is essential to transform all-copper networks into all-optical networks.

IX Double Full Duplex Link

It has now been proven that the point-to-point FTTH concept allows the relaxation of optical characteristics in active and passive components (15). This concept was applied to an F4C predemonstrator as shown in the following diagram, (Figure 9):

It was proven in this way that an electronic transmission of 8 two-way frames at 155 Mb/s on a single 4-core fibre of 125 μ , is feasible.

This wavelength Division Multiplexing can be considered as an upgrade of a 50% cabled network. This allows the initial installation costs to be halved, allowing the rate of return to be considerably improved.



X Economic Interest

The evolution of these techniques is essentially concerned with economic interest.

1. Comparison of F4C with a conventional fibre

This study is based on the production of 210 km long preforms (\approx 80mm exterior to

700mm Length). Four stages are analysed, namely production of preform, manufacturing of the F4C, drawing and measurements.

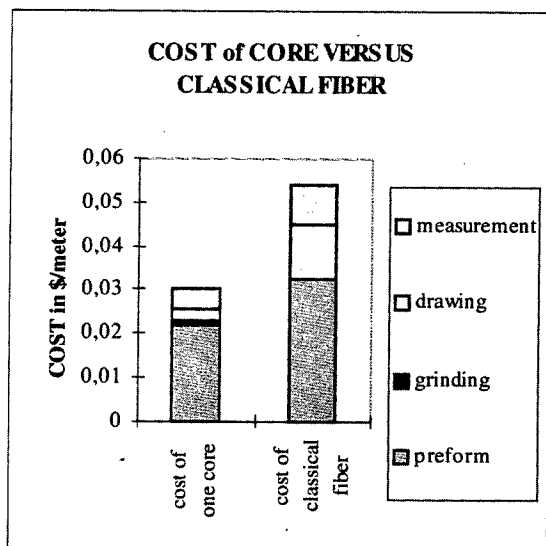


Fig 10

The graph shows a weak incidence of the preform manufacturing, as well as savings on fibre production and the F4C windings. However, we only saved 1.5 on the preforms. For the whole process, a ratio of 2 appears between the cost of the core and that of the fibre.

2. Cabling Costs

The cabling cost is the same for a 4-core fibre as for a conventional fibre. As far as a core is concerned we obtained additional savings:

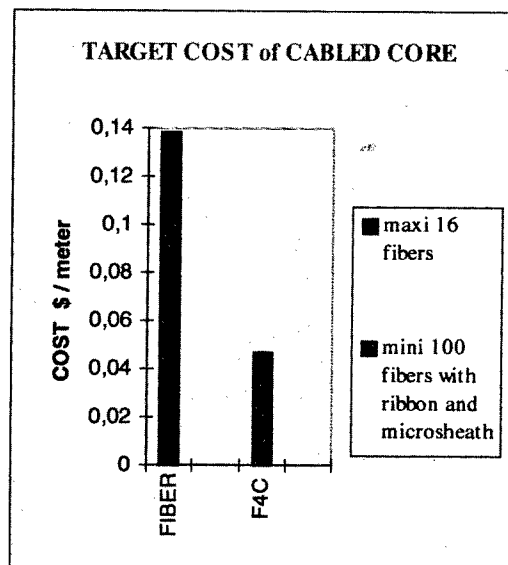


Fig 11

The upper part of the graph shows the minimum and maximum costs of a metre of cable as a function of capacity (16 to 100) and of the two tested cable structures (Ribbon and Microsheath). There is a ratio of 3 between the cost per metre of core-cable and that of a fibre cable.

3. Micro-civil engineering and Double Full Duplex

This graph shows the different elements of the passive optical infrastructure:

The cables with the drop-cable whose cost is fixed, independent of the technique chosen.

The layout

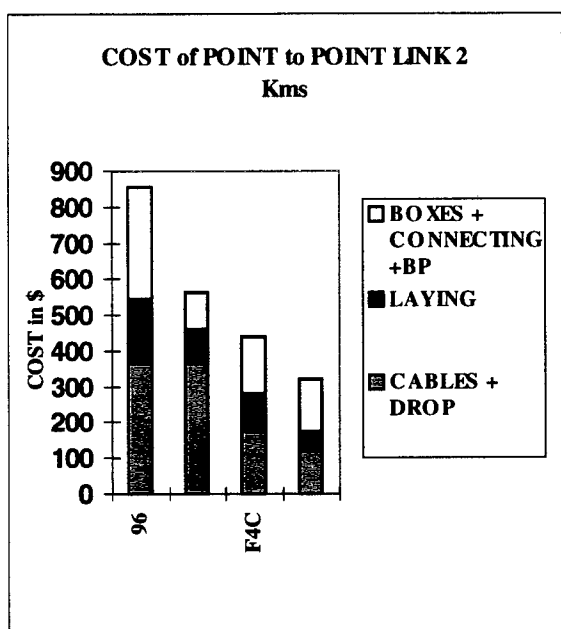


Fig 12

Note the impact of micro civil work on the layout and the splices. Also note the savings of only 37% on the double full duplex link, limited by the cost of muldexes and the fixed part of the drop cable.

Finally, note that the three new technologies have divided the final installation costs by 2.65. This offers a 2km long point-to-point link for about \$300 - the same as for copper pairs.

CONCLUSION

The intrinsic economical aspects of the fibre, the cable, as well as their miniaturization for applications to micro civil engineering and overlay techniques, are essential for the changeover from all-copper networks to all-optical networks. An unquestionable prospect for the third millennium.

We have improved the multicore fibre production technique, enabling the design to be industrialised in the near future.

The reduction of the intrinsic costs, regarding the savings induced by the new very fast

layout methods and double full duplex techniques, offers point-to-point optical fibre links for the same price as copper pair cables.

REFERENCES

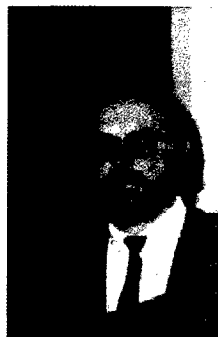
- 1) Design and performance of a high capacity compact modular ribbon cable comprising 24 fiber ribbons, KW Jackson, IWCS 96
- 2) Development of 3000 fiber cable using 16 fiber ribbons, H Iwata, IWCS 96
- 3) Design and performances of 3200 fiber hybrid SCR/U groove cable using 16 fiber ribbons, F.M Sears, IWCS 96
- 4) Development of 3000 fiber cable with 8 or 16 fiber ribbons, N. Okada, IWCS 96
- 5) Development of 3000 fiber multislotted core cable, M. Hara, IWCS 96
- 6) Optical fiber ribbon cable design for a wide range of application as the availability of FTTH is realized, F. Legros, IWCS 96
- 7) Manufacturing and field experimentation of microsheath cable for low cost subscriber loop, P. Jamet, IWCS 94
- 8) Ultra high density cables using a new concept of bunched multicore monomode fibers: a key for the future FTTH networks, G. Le Noane, IWCS 94
- 9) Preform manufacturing by FCVD using very large and precisely bored synthetic silica ingots, G. Le Noane, IWCS 93
- 10) Manufacturing and characterization of multicore fibers, JF. Bourhis, IWCS 97
- 11) Characterization of crosstalk of two cores single mode bunched fiber, A. Nishimura, ECOC 86 Barcelona
- 12) Splices and connectors for bunched multicore monomode fibers, H. Aoustin, IWCS 95
- 13) Distribution link components for point to point ultra low cost FTTH networks using bunched multicore monomode fiber design, D. Boscher, IOOC 95 Hong Kong
- 14) A new application of air pulled cable in microduct for local loop, P. Lesueur, IWCS 95
- 15) Feasibility of 155Mbits/s double full duplex link at 1.3 μ and 1.55 μ on bunched multicore monomode fiber, D. Boscher 8th OAN Atlanta

BIOGRAPHY



Daniel BOSCHER
FRANCE TELECOM
CNET/DTD/FCM
BP 40 22300 LANNION
FRANCE

Daniel BOSCHER born in 1951 received his engineering degree from the Ecole Nationale des Arts et Metiers and joined CNET in 1973. Working on circular waveguide until 1979, he then joined the optical fibers and cables Fiber, Cables and Measurement Department



Georges LE NOANE
FRANCE TELECOM
CNET/CAEN
14066 CAEN
FRANCE

Georges LE NOANE born in 1945 received his degree from the Ecole Nationale des Arts et Metiers and joined CNET in 1974. He began working on optical fiber connector technique, then switched to cables. From 1979 to 1993 he was responsible of optical fibers and cables department, then head of division 'fibers cables and interconnections'. He is now director of CNET / CAEN.



Jean Claude BIZEUL
FRANCE TELECOM
CNET/DTD/FCM
22300 LANNION
FRANCE

Jean Claude BIZEUL was born in 1948. In 1973 he joined the CNET in Lannion. He was engaged in research on fabrication and characterization of optical fibers. Since 1988 he is involved in optical fiber and cable measurement group with special interests on transmission and geometrical single mode fiber features. He represents France Telecom in CCITT especially on optical transmission study group.



Jean Pierre LOUBOUTIN
FRANCE TELECOM
CNET / DTD / FCM
22300 LANNION
FRANCE

Jean Pierre LOUBOUTIN was born in 1954. Doctor in solid physics, he joined CNET in 1982. He is now head of group 'Cables in Distribution'



Isabelle HARDY
FRANCE TELECOM
CNET / DTD / FCM
22300 LANNION
FRANCE

Isabelle HARDY received her engineer diploma from INSA of Rennes in 1981 and her Ingenieur Docteur diploma from University of Toulouse in 1984. She is in charge of studies on new preform fabrication processes in department of Fibers Cables and Measurement

CATV Video Distribution System: From Trials to Operation with FTTH

Naoyuki ATOBE, Hiroshige OGURA, and *Tsuneto HINOHARA

**NTT Service Marketing and Support Headquarters
Nishi-shinjyuku, Shinjyuku-ku, Tokyo, Japan
*NTT Long-Distance Communications Sector
Otemachi, Chiyoda-ku, Tokyo, Japan**

Abstract

In recent years there have been major developments in computer network technology and in related applications and software. Customers are becoming attracted to even more advanced communication services, such as high-speed computer communication, multimedia communication, and video transmission.

In this environment, NTT implemented trials in the use of CATV video transmission from July 1995 to March 1997. It provided CATV video transmission, VOD, and ISDN service using an optical fiber network that reached all households. These trials were evaluated with a view to starting a practical FTTH system. Based on the results of these trials, an advanced CATV video distribution system using FTTH began operation in July 1997.

1. Introduction

Over the last 10 years, NTT has been systematically proceeded with network development to enable practical use of fiber to the home (FTTH) technology in order that the increasingly sophisticated and diversified needs of its customers may be met. The integration of the increasingly large access network to a fiber network is a major factor in enabling a common platform to be built so

that advanced services such as video and computer communication can be provided economically in the future.

As an immediate response to customers requiring high-speed and broadband communication, NTT developed optical fiber to the office (FTTO) and fiber to the zone (FTTZ) networks. However, a network where new, attractive services and applications can be applied is now required if any real expansion in multimedia services for the 21st century is to be realized. For this reason, over the past two years, field trials have been implemented in three areas around Tokyo using FTTH technology. Through the provision of a more economical approach and the establishment of an operation system, NTT has been able to anticipate the future of FTTH technology. In July this year, in Yokohama City, an operational CATV video distribution system was introduced using FTTH technology.

This paper will overview the trial, explaining the distinctive features of the main system and the results of the trial.

2. Utilization Tests of CATV Video Transmission

2.1) Overview of Trial

This trial was called the "Utilization Tests of CATV Video Transmission." It aimed to create convenient interactive communication

These tests involve approximately 300 subscribers in each of the Yokosuka, Urayasu, and Tachigawa areas around Tokyo (approximately 900 households, about 2,700 people).

To make both systems more economical, a Wavelength Division Multiplex (WDM) was used and video type (broadband) services and communication type (narrowband) services were multiplexed. The network topology was based on a point-to-multipoint passive optical network (PON). All optical

- (1) As the current optical fiber testing system use a point-to-point fiber topology, the point-to-multipoint fiber topology can not be adopted.
- (2) In the implementation of these optical media tests, test pulses have to be inserted after branching using an optical splitter.
- (3) If the optical splitters were installed in the field, this would complicate operation and management of the optical fiber and the splitters (branch locations, branch numbers etc.). This could not be managed in the current optical fiber facilities operation system.
- (4) Because the ratio of telephone demand to video demand is not 1:1, installation of the optical splitters in NTT's central building enables improved video equipment accommodating capability.

Figure 1 and shows the equipment configuration for the FDM-PON system and Table 1 shows its main specifications.



Table.1 Outline of FDM-PON System

Items	
Services	VOD, D-CATV, ISDN (BRI)
Fiber Topology	Passive Double Star
Modulation Format	AM, FM, QAM16 (Video)
Transmission-rate & Transmission Bandwidth	28.8Mbps (Comm.) 70MHz~2.4GHz (Video)
Wavelengths	1.3 μ m (Comm.) & 1.5 μ m (Video)
Fiber	Single-mode Fiber (1.3 μ m zero-dispersion)
Optical Loss	23 dB
Maximum Length	7 km

The communication system consisting of the Narrowband Subscriber Line Terminal (N-SLT) and a Narrowband Optical Network Unit (N-ONU) provides BRI service by the Time Compression Multiplexing - Passive Optical Network (TCM-PON) using a 1.3 μ m wavelength. The N-SLT allocated 4 B (64 kbps) channels to one ONU. That is, it allocated 2 B for communication channels, 1 B for a control D channel, and 1 B for a maintenance and testing channel. The N-ONU serves one ISDN circuit (2 B + D) for each subscriber. It uses 1 B in the communication channel and controls the VOD server through dialing.

In this system, upstream Time Division Multiple Access (TDMA) and downstream Time Division Multiplexing (TDM), as used in satellite communication, were used to identify communication partners. Security is maintained through encoding where, in the downstream direction, the same downstream signal is sent to eight N-ONU in broadcast transmission after having been subject to time division multiplexing.

The video system comprises a FDM-MUX, Video Subscriber Line Terminal (V-SLT), Video Optical Network Unit (V-ONU), and Channel Selection Unit (CSU). A wavelength of 1.5 μ m is used. Direct optical amplification technology and optical fiber dispersion compensation technology, which inhibits deterioration of picture quality, have enabled the economical provision of high quality service.

In this system, all channels can be transmitted to a subscriber's home. Therefore, the provision of transmission that uses the same channel frequency

arrangement as used in current broadcasts enables subscribers to view video on both ground wave channels and BS broadcast channels without a special tuner, merely by connecting to an existing BS television. Figure 2 shows the frequency arrangement.

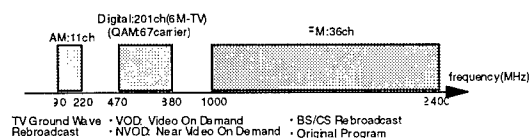


Fig.2 Frequency Allocation

The video system was designed so that the overall signal quality on CATV video channels would be equivalent to that required for Level 4 in the Prime Evaluation Standards. The CNR for the AM signal was set at 48 dB or more, the CNR for the FM signal at 52 dB or more. On the other hand, with regard to the digital VOD channels, the system was designed to have a signal error rate of 10^{-11} and the CNR for each QAM carrier was set at 27 dB or more.

b) ATM-PON system

In the ATM-PON system, WDM transmission uses a 1.3 μ m optical wavelength for upstream signals and a 1.5 μ m optical wavelength for downstream signals. The upstream and downstream bit rates are 156 Mbps.

Figure 3 shows the equipment configuration for the ATM-PON system and Table 2 shows its main specifications.

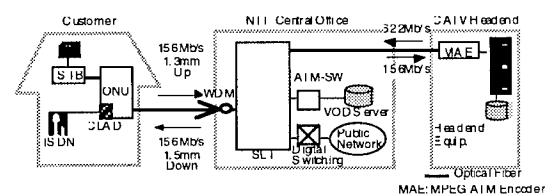


Fig.3 ATM-PON System Configuration

Table.2 Outline of ATM-PON System

Items	
Services	VOD,D-CATV,ISDN (BRI)
Fiber Topology	Passive Double Star
Modulation Format	155.52Mb/s (NRZ)
Line-rate & Transmission Bandwidth	SLT-ONU(average): 6.6Mb/s (up) & 7.36Mb/s (down)
Wavelengths	1.3mm (up) & 1.5mm (down)
Fiber	Single-mode Fiber (1.3mm zero-dispersion)
Optical Loss	25 dB
Maximum Length	7 km

An ISDN service is provided for communication. A cell formation was designed to enable the requirements of transmission delay to be satisfied. As communication services increase cell formation delays, the system adopts a partial filling technology in which only part of the cell payload is filled. In this way, NTT was able to guarantee that the total delay in the ATM-PON system would be the 1 ms or less as required for telephone services. Figure 4 indicates the transmission frame.

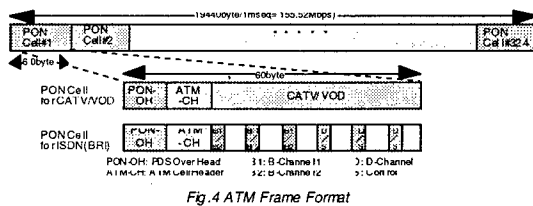


Fig. 4 ATM Frame Format

In the video system, between the HE and ATM-SLT transmitted via ATM circuits at 600 Mbps using a newly developed MPEG ATM encoder (MAE) for tens of CATV program channels. Only CATV channels requested by the subscriber were sent from the ATM-SLT to the ONU. Using the 156 Mbps PON system, this enabled transmission at approximately 2 channels to each subscriber.

2.3) VOD System

Another distinctive feature of this trial is in the VOD system that enables the provision of a high-quality video-on-demand service. In the VOD system, video and audio signals are encoded using MPEG-2 and MPEG-1 audio respectively, to achieve a 6 Mbps stream.

The maximum capacity of the video server is approximately 200 hours and this enables them to provide a service to 100 subscribers simultaneously. By using different server systems at three trial sites, the trials was able to evaluate the human-machine interfaces and the service and verify the compatibility of the network architecture and servers.

2.4) VOD Service

This trial was implemented jointly by NTT and the contents provider. This enabled provision in full digital format of programs and services such as films, news programs, community information, animation, timetables, karaoke, video games, and travel guides.

a) Overall evaluation

In this trial, the on demand nature of the VOD service was recognized by many of the monitors as something that "can be used at a convenient time." The appeal of the VOD service as an application that enables use of multimedia in the home was clear.

Approximately 50% of the users said that they were satisfied with the trial service, with 80% of users praising the picture and sound quality. We thus confirmed that it is possible to transmit high quality pictures using optic fiber communication.

Over 80% of the households indicated that they intended to use the commercial service, depending on the service conditions. This led us to the conclusion that VOD can be a commercially viable application as long as a wide variety of appealing material can be provided cheaply. However, this would also require a revolution in the system that deals with material distribution, including for example, in the processing of copyright.

b) Service use

Males were more likely to use the VOD service than females, particularly males aged between 30 and 40. There was an increase in the number of users when new services were introduced or when material was updated.

There was also a slight increase in usage on Saturdays when compared to weekdays. There was also a tendency for more use in the evenings and nights than in the daytime.

For reference, the types of users in Tachikawa City are shown in Figure 5 and the use by content is shown in Figures 6 and 7.

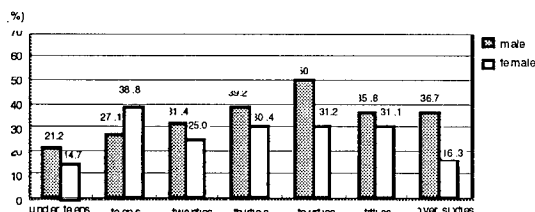


Fig.5 Types of Users

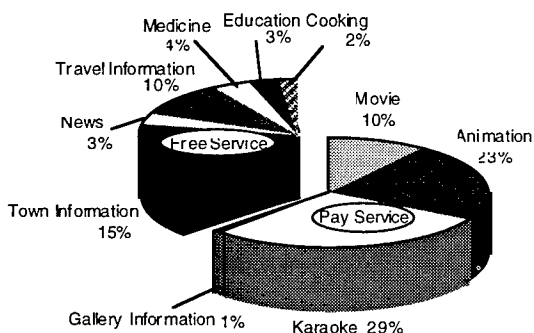


Fig.6 Number of Access

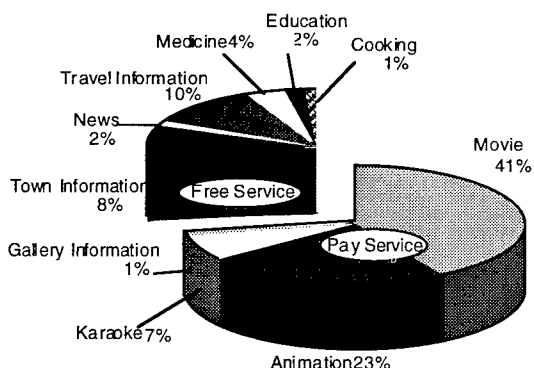


Fig.7 Server Holding Time

c) Evaluation of service by monitors

Approximately 50% of users said that they were satisfied with the service, with approximately 80% giving high praise to

picture and sound quality. The content, quantity and price of material provided was evaluated by users in comparison to existing services. Users wanted the type of variety of films found in video rental shops and also wanted the variety of new songs on karaoke channels as would be found in karaoke boxes.

Approximately 80% of the monitor households indicated an intention to use a commercial VOD service provided the material and fees were acceptable. We were thus able to confirm the level of the latent need for this service.

3. Results and Future Outlook

Through this trial, CATV operators were, based on the evaluations provided by monitors, able to confirm the appeal and acceptability of material provided in the VOD service. Such evaluations clarified the problems that must be addressed if a commercial service is to be introduced.

NTT, in turn, was able to establish technology for constructing and managing optical fibers with a view to using them in FTTH technology, and was also able to establish technology such as PON and picture encoding and compression (MPEG2) for constructing economical optical access networks.

NTT began operation of a CATV video distribution system in July this year based on the results of this trial.

This is the world's first FTTH oriented system and it provides potential for CATV operators to provide new services.

3.1) Comparison of Trial System and Advanced System

Because the current quality of CATV had to be transmitted the same performance as HFC in this system, it is based on the FDM-PON system used in the trial in Tachikawa City. The differences between the system used in

the Tachikawa trial and the advanced system are shown Table 3.

Table.3 Comparison CATV Test System And This System

		Test system	CATV video distribution system
Platform		TCM-PDS (1.3 μ m, 30Mbit/s)	TCM-PDS (1.3 μ m, 50Mbit/s)
		192B (1B = 64kbit/s)	256B
CATV	Mode	FDM (1.5 μ m)	FDM (1.5 μ m)
	Modulation	AM and FM	AM
	Signal frequency	70 ~ 2400MHz	70 ~ 770MHz
VOD	Encoding	MPEG2	MPEG2
	Modulation	16QAM (201 ch)	64QAM (120 ch)
	Control	ISDN	POTS, ISDN
Number of splitter branch		8branch Max.	32branch Max.

a) Communications system

To increase the number of subscribers that can be accommodated in the N-SLT, this system used the following technology. The transmission speed between OSU to N-ONU has been improved to 50 Mbps, the maximum capacity of current complementary metal-oxide semiconductors (C-MOS) technology. The number of B channels (B = 64 kbps) that can be allocated in one OSU has also been changed from 192 to 256. The enable N-ONU accommodation of one optical subscriber unit was increased four times (8 to 32) from trial system. Thus the efficiency of the system has been greatly enhanced.

In the trial, only one type of N-ONU which provided the service interface of 1 ISDN BRI was provided. To make new system more economical, new type of N-ONU have been developed for use in the multiple-home in addition to the single-home type. The single-home type has maximum 8B capacity and the multiple-home type has maximum 48B capacity. These provide the service interface of POTS and ISDN BRI.

b) Video system

Bandwidth of 2.4 GHz bands or lower can be used, but here we limited the bandwidth to those of 770 MHz or less, that is bandwidth

used for current Japanese CATV. Also, in anticipation of picture quality standards and because of improvements in the differences between optical sending and receiving levels, this system increased the number of branches in optical splitters to 16, thus increasing the number of subscribers that can be accommodated. This system changed the modulation mode for digital channels from 16 QAM to 64 QAM. This enables provision of 40-channel AM television service and a 120-channel digital service that uses MPEG2 conversion.

c) Operation system

To enable compatibility with existing communication operation systems, NTT developed a "New Optical Operation System" that supports service provisioning, surveillance of SLT and ONU, and fault repair.

In the FTTH system, a number of services are provided simultaneously and new services will be added in the future. Therefore the optical access network must be managed in a way that is not dependent on the services offered. Thus, the New Optical Operation System has a functions that enable only path layers to be monitored and tested without awareness of the services provided.

In addition to, this system adopt the Q3 interface, an international standard.

d) Optical fibers

The structure and configuration of network components was designed to enable the access network to be economically converted to an optical network. At the same time we were thus able to reduce the cost of components themselves and reduce their installation costs. Also, in the network configuration, non-reducing star topology were used to reduce connection/splicing losses that occur when the number of connection points increase.

Some of the main products developed were the ultra-high-density 1,000 underground optic fiber cable (cable diameter: reduced from 40 mm to 30 mm), the

aerial SZ slot cable that enables simple dropping, the simple small fusion splicer (size: 80% smaller than previous model, weight: reduced from 16 kg to 3 kg) that simplifies connections in users' houses, and the mechanical splicer (size: 4 mm x 4 mm x 40 mm, connection loss: 0.4 dB or less) that simply connects optic fibers with few cores.

4. Conclusion

The test was completed at the end of March 1997. Both transmission systems had attained stable operation status, and the video quality of the VOD system is generally good. The contents providers were also satisfied that the video quality is sufficient for commercialization.

Because of the satisfactory test results, NTT developed new type CATV video distribution system on the basis of the FDM-PON system. Actual operation of this system

began in July this year in Yokohama City, Kanagawa Prefecture.

This is the world's first real FTTH system and, as such, has attracted a great deal of interest from within Japan and overseas.

In the future, we will comprehensively examine the FTTH system so that it can be provided more economically.

References

- (1) T. Kanada and N. Terada, "ATM-PDS-Based Broadband Fiber Access System," NTT R&D, 12(VOL.44), 1995, PP.1157-1162
- (2) K. Harikae, K. Yoshimura, N. Miki and H. Yoshinaga, "Optical Access Systems for Narrowband Communication and Video Distribution," NTT R&D, 12(VOL.44), 1995, PP.1163-1170.
- (3) I. Sakakibara and Y. Motohashi, "Trial of CATV, VOD and ISDN Services over FTTH," IEEE, 1996.



Naoyuki ATOBE

NTT
Service Marketing
and Support Headquarters
Shinjyuku-ku, Tokyo,
163-14, Japan
atobe@mod.hqs.ntt.co.jp

Naoyuki Atobe is a senior manager of NTT Service Marketing and Support Headquarters. He was born in 1957 and received B.E. degrees in electronic engineering from Kyushu University in 1979.

He joined NTT in 1979. He worked in research and development on optical cable system and optical access system. Since 1997 he has been engaged in planning multimedia services.

Mr. Atobe is a member of IEICE of Japan.



Tsuneto HINOHARA

NTT
Long-Distance
Communications Sector
Chiyoda-ku, Tokyo, Japan
t.hinohara@hqt.
longdist.ntt.co.jp

Tsuneto Hinohara is a senior manager of NTT Long-Distance Communications Sector. He was born in 1952 and received B.E. and M.E. degrees in electronic engineering from Keio University in 1975 and 1977, respectively.

He joined NTT in 1977. Since 1997 he has been engaged in making global communication strategy and planning communication network.



Hiroshige OGURA

NTT
Service Marketing
and Support Headquarters
Shinjyuku-ku, Tokyo,
163-14, Japan
ogura@mod.hqs.ntt.co.jp

Hiroshige Ogura is a chief of NTT Service Marketing and Support Headquarters. He was born in 1966 and received B.E. degrees in mathematics from Meiji University in 1989.

He joined NTT in 1989. Since 1996 he has been engaged in planning multimedia services.

AN ECONOMICAL AND PRACTICAL OPTICAL FIBER DISTRIBUTION SYSTEM FOR RESIDENTIAL PREMISES

Shin-ichi FURUKAWA, Kazuo HOGARI*, Masao TERASAWA, Mitsuo KAMA**,
Izumi SANKAWA, Norio KASHIMA, Kanemitsu TOMIYAMA, Hiroshi ISHIKAWA,
Tetsuya HOSHIJIMA and Katsutoshi TSUCHIDE

NTT Access Network Systems Laboratories

* NTT R&D Management Department, ** NTT Technology Department
Tokai-mura, Naka-gun, Ibaraki-ken JAPAN

ABSTRACT

We have developed an economical and practical optical fiber distribution system for residential premises designed to provide subscribers with current narrow-band services and future broad-band services via fiber. The system consists of various types of new optical fiber cable, closures, optical outlet boxes and a field-installable single-connector which are inexpensive and offer easy handling. The total cost including both the above hardware and its installation is dramatically reduced by this system.

INTRODUCTION

Broad-band optical access networks are expected to be capable of providing high-bit rate digital and broad-band analog services to subscribers and have been actively investigated. 1-4 A way to reduce the cost of the last hundred meters in an optical access network is currently one of the most important issues in terms of realizing fiber to the home (FTTH) and thus providing customers with such multimedia services economically. 5

Optical fiber cables assembled using 0.9 mm diameter tight-buffer fibers or optical cords about 2.5 mm in diameter have already been used to distribute optical fiber to residential premises including apartment houses. 6,7 Although these cables are strong and have stable transmission and mechanical characteristics, they are large, heavy and generally expensive. Closures accommodating fibers and splices are also large, complex and expensive. Therefore, new low-cost optical cables and closures with good characteristics are urgently required if we are to realize FTTH.

We have recently developed an enhanced optical fiber distribution system for residential premises which consists of various types of new optical cables such as a new drop cable, a new cluster-type drop cable, a new indoor cable and a new termination cable, new closures, a new outside cabinet and a field-installable single-fiber connector. The structural design and material of these components have been investigated taking two problems into consideration: cost and installation workability. We decided to use 0.25 mm diameter mono-coated fiber in these cables in order to minimize the hardware costs. We have fabricated these cables, newly designed closures and cabinets and an easily installable connector and examined their performance and workability. We confirmed their stable characteristics, good workability and reduced cost.

OPTICAL FIBER DISTRIBUTION SYSTEM CONFIGURATION FOR RESIDENTIAL PREMISES

Figure 1 shows the configuration for optical fiber distribution to and inside residential premises using our newly developed system.

In existing optical access network systems, one or two fibers are connected to an optical network unit (ONU) inside a residence. 1-4 So, one or two optical fibers are introduced into each residence through aerial drops or underground cables from an access point installed aerially or underground. They then reach the ONU via indoor and termination cables. An optical outlet box is installed in the house to accommodate fusion or mechanical splices and fibers between the indoor and termination cables. A cabinet is installed on the outside wall of the house to

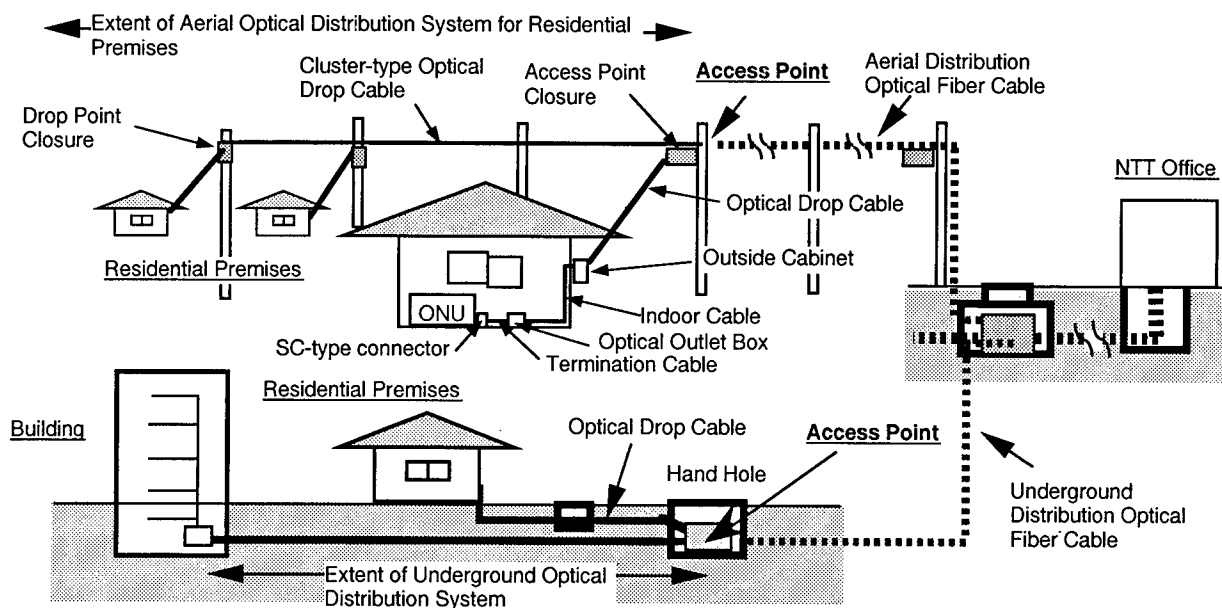


Fig. 1 Optical fiber distribution for residential premises

Table 1 Optical cable requirements

Item	Fiber Number	Essential Conditions	Mechanical Conditions	Environmental Conditions
Optical Drop Cable	One or Two	Low cost and superior handling and reliability	Tension: 700 N (Aerial), 800 N (Underground) Bending radius: 30 mm, Lateral force: 1200 N /25 mm	Temperature: -30 ~ 70°C, Humidity: < 95%
Optical Indoor Cable			Tension: 200 N Bending radius: 30 mm, Lateral force: 1200 N /25 mm,	Temperature: -20 ~ 50°C, Humidity: < 95%

accommodate joints and fibers between the drop and indoor cables. The outlet box and outside cabinet are not needed when the drop cable can be installed on the premises. An access point closure accommodates many fusion or mechanical splices, fiber ribbons contained in an aerial distribution cable, fan-out fibers changing from a four-fiber ribbon to single-fibers and mono-coated fibers contained in the drop cable.

Fewer access points are installed for optical distribution to residential premises than with a metallic system. This is because optical system penetration will initially be low in the access networks and the optical fiber in the four-fiber ribbon, which is distributed up to the access point, must be used as efficiently as possible. This increases the distance between the access point and the premises and means that there must be several installations between a number

of poles or hand holes during construction. So, we have developed a new cluster-type optical drop cable containing mono-coated fiber.

The requirements for the drop and indoor cables are summarized in Table 1. They are generally required to be inexpensive and good in terms of handling and reliability. They are also expected to be stable when exposed to severe mechanical force and harsh environments. An experiment involving the installation of a practical duct using the indoor and termination cables revealed that the maximum applied tension was less than 200 N. So, the allowable tensile strength can be reduced from 400 N to 200 N. 8

OPTICAL FIBER CABLE DESIGN AND CHARACTERISTICS

Optical fiber

Single-mode (SM) fiber with the specification ITU G. 652 is the most commonly used for residential premises. Its mode field diameter (MFD) tends to decrease i.e. its central value changes in the 8.6 to 9.5 μm range. 9 In some cases, we have to bend a fiber with a small radius in the outlet box used for metallic wire distribution on residential premises. We chose SM fiber with a central MFD value of 9.2 μm and an allowable 0.5 dB loss increase when bent with a radius of 20 mm and 20 turns. Figure 2 shows the MFD and cut-off wavelength area for SM fiber to be used solely on residential premises.

As mentioned above, mono-coated fiber with a diameter of 25 mm is used because of its low cost, small size and de facto standards. Loss

increase is a well-known problem with 0.25 mm diameter fiber which arises when it is handled with a small radius in a closure. We have solved this problem by developing a new accommodation tray for the closure.

Optical drop cable

The structures of aerial drop cables containing one fiber are shown in Fig. 3. (a) is the conventional structure and (b) is the new structure. The optical fiber insertion part of the new cable has a steel wire located on either side of the 0.25 mm diameter mono-coated fiber for reinforcement. It is combined with a self supporting wire part by a polyvinyl chloride (PVC) sheath. This is achieved in one cable manufacturing process. By contrast, the insertion part in the conventional structure is wound around a self-supporting wire part. This cable needs three manufacturing processes. The new design is much cheaper because of the reduced size, simple unified structure and single manufacturing process. The sectional area of the new cable is 34 % that of conventional cable.

There is a notch between the two parts which allows them to be separated easily when the drop cable is fixed between a pole and a residence. Moreover, there is also a notch on either side of the optical fiber insertion part to enable the mono-coated fiber to be removed easily. The insertion part has the same structure as indoor cable. So, by using the optical fiber insertion part separated from the self-supporting wire part, it is possible to install the cable on residential premises without the need for a fiber joint.

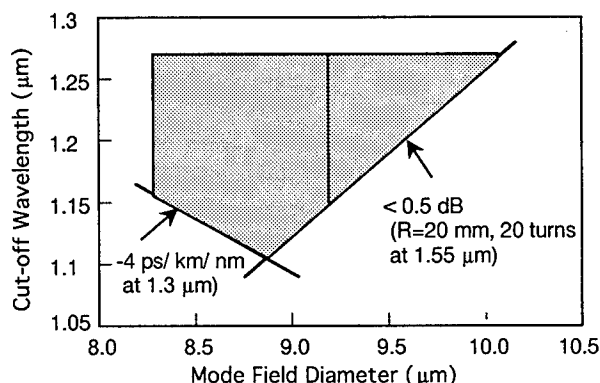


Fig. 2 SM fiber parameters for residential premises distribution

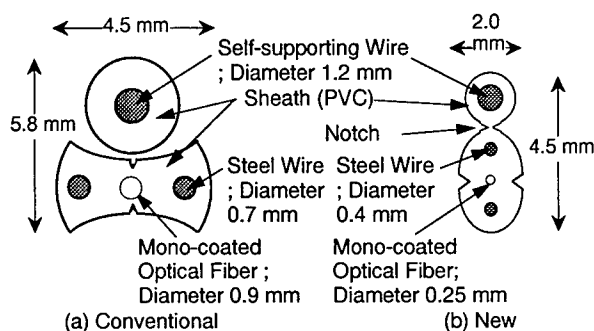


Fig. 3 Aerial optical drop cable structures containing one mono-coated optical fiber

We fabricated this optical drop cable, and its transmission and mechanical characteristics are shown in Table 2. We found that these characteristics were almost the same as those of conventional drop cable. We also confirmed that the optical fiber insertion part could be easily separated from the self-supporting wire part with a nipper, and the mono-coated fiber was easily removed using the notch.

Table 2 Optical losses and loss changes of the new drop cables due to mechanical force

Item		Aerial		Underground	
		Drop Cable	Cluster-type Drop Cable	Drop Cable	Cluster-type Drop Cable
Optical loss	$\lambda = 1.3 \text{ }\mu\text{m}$	0.33~0.36 dB/km			
	$\lambda = 1.55 \text{ }\mu\text{m}$	0.20~0.22 dB/km			
Test Condition and Loss Change at 1.55 μm	Tension	700 N/50 m	2000 N/50 m	800 N/50m	
		< 0.01 dB	< 0.02 dB	<0.03 dB	<0.01 dB
	Lateral Force	1200 N/ 25 mm	1000 N/ 100 mm	1200 N/ 25 mm	1000 N/ 100 mm
		< 0.03 dB	< 0.01 dB	<0.03 dB	<0.01 dB
	Bending	Radius: 30 mm	Radius: 70 mm	Radius: 30 mm	Radius: 75 mm
		< 0.01 dB	< 0.03 dB	< 0.02 dB	< 0.01 dB
	Heat Cycle	-30℃~70℃		-30℃~70℃	
		< 0.04 dB/km	< 0.03 dB/km	< 0.02 dB/km	< 0.05 dB/km
	Vibration	Frequency: 3.5 Hz, Amplitude: 10 mm (Length: 70 m)			
		< 0.04 dB	< 0.03 dB		
Squeezing	Tension: 2000 N, R250 mm (Length: 50 m)		Tension: 800 N, R 300 mm (Length: 50 m)		
	< 0.01 dB		< 0.01 dB	< 0.01 dB	

The estimated cable cost is about 60 % lower than that of conventional cable.

The structure of an underground optical drop cable containing two 0.25 mm diameter mono-coated fibers is shown in Fig. 4. This cable has a 0.7 mm diameter steel wire located on either side of the fibers as a strength member and for reinforcement during installation in a duct. We confirmed that the manufactured cable had good characteristics as shown in Table 2.

Cluster-type optical drop cable

The aerial cluster-type optical drop cable structure is shown in Fig. 5. The cable is composed of optical indoor cable, which is described below, and a strength member. Eight optical indoor cables are simply wound around the strength member. There are also other cable structures in which two or four indoor cables are used. These cables have a non-sheath structure to reduce the cost. Namely, the advantages of this cable are its ease of manufacture, small size and the simplicity with which the indoor cable can be accessed when connecting it with a drop cable.

We fabricated this cluster-type optical drop cable, which was 12 mm diameter and weighed 0.15 kg/m, with eight optical indoor cables. The transmission and mechanical characteristics of the cable are also shown in Table 2. The optical loss change was very small and the cable had stable characteristics.

The underground cluster-type drop cable has a similar structure to the aerial cable. The diameter is 13 mm since underground drop cables are wound around a strength member. The optical loss change during mechanical tests was negligible and the cable had stable characteristics as shown in Table 2.

Indoor cable, under-carpet cable and termination cable

Figure 6 shows the structures of an optical indoor cable, an optical under-carpet cable and an optical termination cable. These cables have a 0.4 mm diameter steel wire located on either side of the 0.25 mm diameter fiber for reinforcement. The cable dimensions can be reduced and the cable flexibility can be improved. This is because we can use smaller steel wires than those of conventional cable. Moreover, a new 1.5 mm diameter optical cord is used in the termination cable. Again, there is a notch on both sides of the cable to allow the mono-coated fiber or optical cord to be removed easily. The advantages of these cables are their ease of manufacture, small size and the fact that the mono-coated fiber or optical cord can be removed easily.

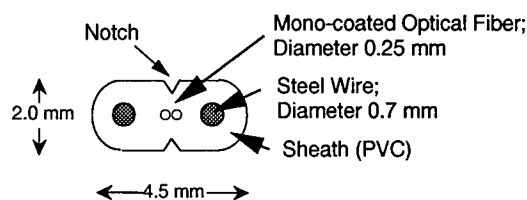


Fig. 4 Underground drop cable structure containing two mono-coated optical fibers

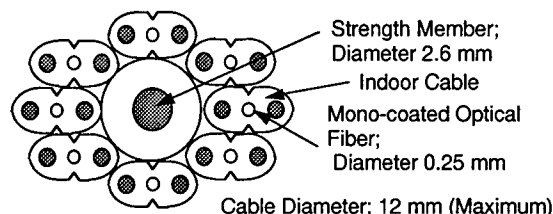


Fig. 5 Cluster-type drop cable structure with 8 indoor cables wound around a strength member

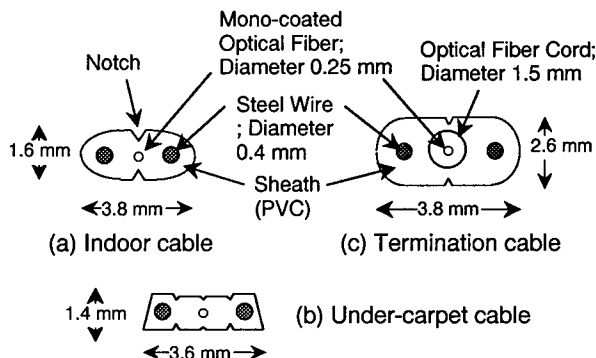


Fig. 6 Indoor, under-carpet and termination cable structures

Table 3 Optical losses and loss changes of the indoor cables due to mechanical force

Item	Test Conditions	Indoor Cable	Under-carpet Cable	Termination Cable
Optical loss	$\lambda=1.31 \mu\text{m}$	0.33 ~ 0.36 dB/km		
	$\lambda=1.55 \mu\text{m}$	0.19 ~ 0.22 dB/km		
Tension ^{*1}	200 N / 50 m	< 0.01 dB	< 0.01 dB	< 0.02 dB
Lateral Force ^{*1}	1200 N / 25 mm	< 0.02 dB	< 0.03 dB	< 0.02 dB
Bending ^{*1}	Radius; 30 mm	< 0.01 dB	< 0.01 dB	< 0.01 dB
Heat Cycle ^{*1}	- 30 °C ~ 70 °C	< 0.02 dB/km	< 0.02 dB/km	< 0.03 dB/km

(*1) Measurement wavelength: $\lambda=1.55 \mu\text{m}$

The optical indoor cable, under-carpet cable and termination cable were all fabricated. The cross-sectional areas of these cables are less than 50% those of conventional ones. Table 3 shows the transmission and mechanical

characteristics of these cables. We confirmed that these cables had suitable characteristics for internal distribution on residential premises.

In our experiment, there was no loss increase in the indoor cable when staples were used for its internal distribution. The staple is shown in Fig. 7. This is inexpensive, made of plastic and has a space suitable for the indoor cable. It can be installed with a nail in about a minute and it holds the indoor cable securely. This means that the cost of indoor cable installation can be reduced by using this staple for the internal distribution.

CLOSURE, CABINET DESIGN AND CHARACTERISTICS

Splice and accommodation of mono-coated fibers

We have recently developed a compact mass-fusion splicer and a small mechanical splice for the efficient construction of aerial distribution cable systems. 10 They can be used for joining 0.25 mm diameter mono-coated fibers. Table 4 summarizes the splice loss, return loss, and working time measured with this new machine and tool. 10 It also provides the sizes of the reinforcement and the machine and tool. These reinforcements, a fiber cutter and a UV coating remover can be commonly used for joining four-fiber ribbons to reduce the cost.

Fibers are accommodated with a minimum radius of 30 mm taking two items into consideration; optical loss increase and fiber reliability.

Aerial access point closure

An aerial access point closure has many functions such as housing the termination or branch point of an aerial distribution cable, the

Table 4 Fusion and mechanical splices for mono-coated optical fiber

Item	Fusion Splice	Mechanical Splice
Loss (Average value) @1.31 μ m	0.07 dB	0.13 dB
Return Loss @ 1.31 μ m	> 60 dB	> 40 dB
Working Time	~ 6 min.	~ 3 min.
Size of Reinforcement	ϕ 4 mm x 40 mm	4 x 4 x 40 mm
Machine / Tool	< 15 x 15 x 15 cm, < 3 kg Battery operation	< 20 x 13 x 5 cm, < 1 kg No power supply

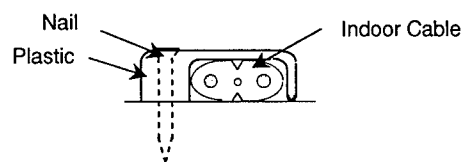


Fig. 7 Staple for indoor cable

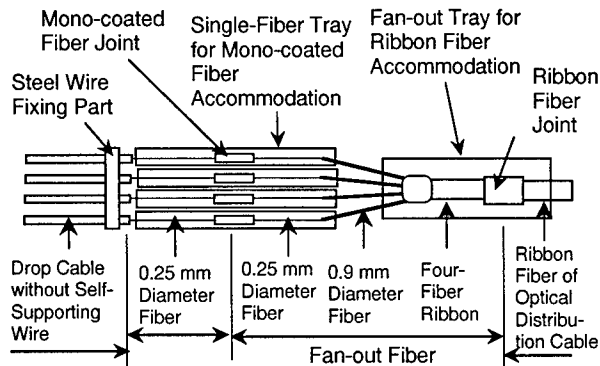


Fig. 8 Fiber joints and their accommodation in an access point closure

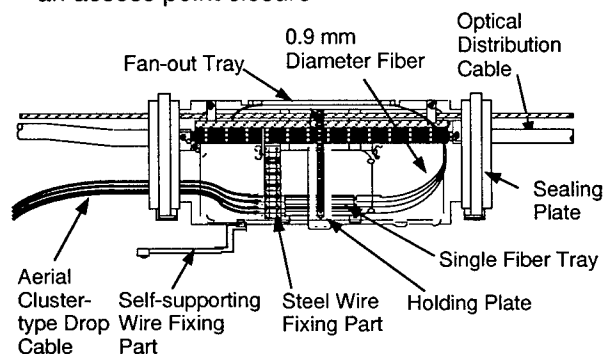


Fig. 9 Aerial access point closure structure

termination of drop cables and the accommodation of fiber joints between four-fiber ribbon and 0.25 mm diameter mono-coated fibers. The fiber joints and their accommodation in the closure is shown in Fig. 8. The actual closure structure is shown in Fig. 9. There are two fiber joints; one is for 0.25 mm diameter fibers, the other is for four-fiber ribbon. To achieve these joints, we have developed the simple fan-out fiber shown in Fig. 10. We also developed a single-fiber tray for the individual accommodation of a 0.25 mm diameter fiber joint. This is because we want to avoid the possibility of touching a live fiber during fiber dropping or fiber splicing and avoid causing any loss change in a live fiber. Moreover, we prepared a separate fan-out tray to contain four-fiber ribbon joints and their accompanying fibers in order to make it easy to extract a desired fiber ribbon from the distribution cable and accommodate it.

The drop cables with steel wires can be introduced into the closure and then fixed in position near the single-fiber tray because of their good flexibility. As a result, the exposed length of 0.25 mm diameter fiber is kept as short as possible in the closure, and the loss change which may be caused by touching the 0.25 mm diameter fiber can be suppressed.

The four single fibers of the fan-out fiber have a two-layer coating structure and 0.9 mm diameters. Their outer coatings can be removed to reveal 0.25 mm diameter mono-coated fibers. This means they can be easily spliced to the 0.25 mm diameter fiber of the drop cable. Fiber handling between the single-fiber tray and the fan-out tray can also be facilitated by using this 0.9 mm fiber. The ribbon of the fan-out fiber is conventional fiber ribbon, so we can splice it to the fiber ribbon of the distribution cable easily. The closure is 620 mm long, 150 mm wide and 200 mm high.

We examined the fiber handling characteristics with the fabricated closure and measured the loss changes in a fiber near the fiber being handled at wavelengths of 1.31 μm and 1.55 μm . The results are shown in Table 5. Frequency in the table shows the number of loss increases which occurred in ten experiments. A small loss increase was measured with a very low frequency. When mono-coated fiber was fixed to a single-fiber tray using a sponge rubber, the loss increases was less than 0.1 dB with a frequency of 20 % at 1.55 μm . Fiber ribbon extraction caused a maximum loss increase of 0.3 dB with a frequency of 30 %. However, these loss increases are very small and present no problems in terms of transmission characteristics.

11

The sealing plate for the introduced portions of distribution or drop cable was made of flexible plastic. A simple cable holding structure was formed easily by using this sealing plate. To reduce the cost, the number of parts was reduced and some were used for more than one purpose such as the connecting or branching closure. As a result, the cost was reduced to about 50 % that of a conventional closure and the labor required for construction was also estimated to be about half.

Aerial drop point closure

We have developed a drop point closure to accommodate splices and their fibers between a cluster-type drop cable and a drop cable on a pole. Its structure is shown in Fig. 11. It has four individual fiber organizers to accommodate fiber splices and fibers. This also prevents any loss increase as a result of handling a neighboring fiber. This simple structure and small size make its cost sufficiently low.

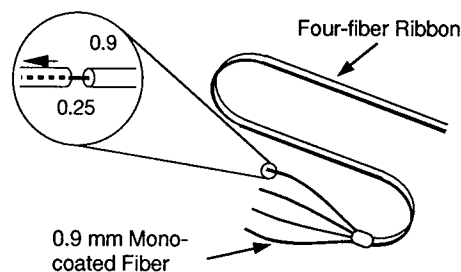


Fig. 10 Fan-out fiber structure

Table 5 Loss changes during fiber handling at the aerial closure for access points

(Ten experiments, Measurement Wavelength: Upper; 1.31 μm , Lower; 1.55 μm)

Item	Frequency	Max. Loss Change
1. Extraction of fiber ribbon from cable or tray	0/10	< 0.01 dB
	3/10	0.3 dB
2. Accommodation of fan-out fiber in fan-out tray	0/10	< 0.01 dB
	0/10	< 0.01 dB
3. Installation or movement of single-fiber tray	0/10	< 0.01 dB
	0/10	< 0.01 dB
4. Installation or removal of drop cable	0/10	< 0.01 dB
	0/10	< 0.01 dB
5. Fixing of mono-coated fiber to a single-fiber tray	1/10	0.03 dB
	2/10	0.1 dB
6. Mono-coated fiber joining and accommodation	0/10	< 0.01 dB
	0/10	< 0.01 dB

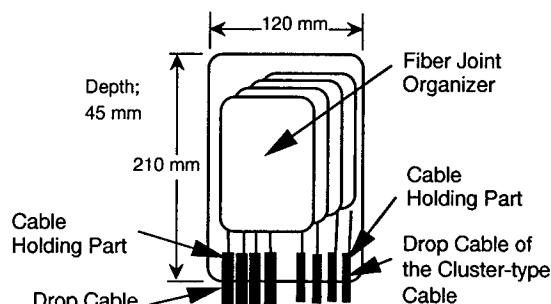


Fig. 11 Drop point closure structure

Outdoor cabinet and optical outlet

The outdoor cabinet structure is shown in Fig. 12. It is installed on the outside wall of residential premises and it accommodates the fiber joints between drop and indoor cables. It may also function as the demarcation line between the customer and the network operator. It can therefore contain two SC-type connectors and four fiber splices in this small body. We have introduced a new cable holding part which does not require the cable sheath to be removed, thus providing low cost and quick installation.

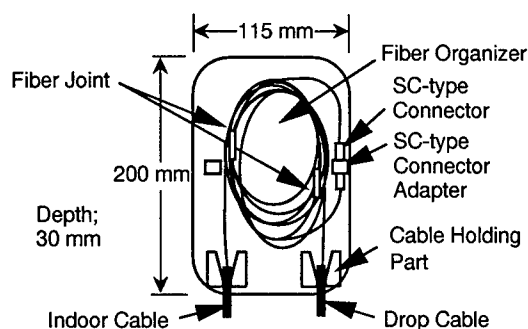


Fig. 12 Outside cabinet structure with a demarcation function

In addition, an optical outlet has been prepared which can accommodate a fiber joint between indoor and termination cables. It can hold two cables and accommodate two fusion or mechanical splices. The size is as small as 120 x 115 x 16 mm.

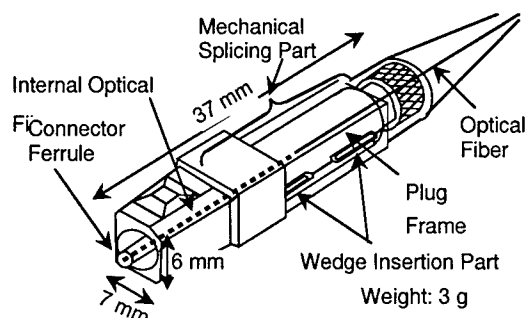
FIELD-INSTALLABLE SINGLE-FIBER CONNECTOR

We have developed a field-installable single-fiber connector which is compatible with an SC-type connector and which can be assembled quickly on residential premises.

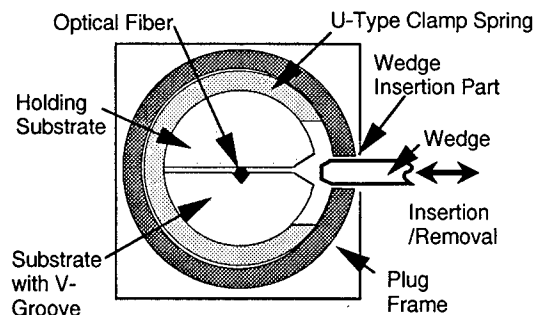
Quick connection using a field-installable connector

The field-installable connector plug structure is shown in Fig. 13(a). It is composed of a connector ferrule and a mechanical splicing part. The optical fiber is housed internally between the connector ferrule endface and the middle of the mechanical splicing part and the endface is polished at the factory beforehand. When the connector is assembled on residential premises, a fiber is joined to the internal fiber in the mechanical splicing part by operating a wedge. This connector is compatible with the SC-type optical fiber connector since it has the same interface dimensions. Moreover, the fiber connection region of the mechanical splice has index matching material to reduce the Fresnel reflection.

A cross-section of the mechanical splicing part is shown in Fig. 13(b). The connecting optical fiber is clamped mechanically between the substrate with the V-groove and the holding substrate using a U-type clamp spring. When we assemble the connector, the wedge is inserted into the mechanical splicing part from



(a) Connector plug structure



(b) Cross-section of mechanical splicing part

Fig. 13 Field-installable single-fiber connector structure

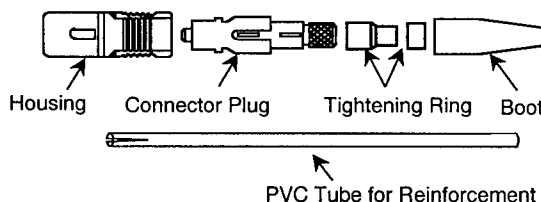


Fig. 14 Components of a field-installable single-fiber connector for an optical fiber cord

outside, then the clamp is neutralized and the fiber can be inserted along the V-groove and joined to the internal fiber. After the fibers have been joined, the wedge is removed. Figure 14 shows all the components of a field-installable connector for an optical cord. A Kevlar cord must be fixed to the connector plug with a tightening ring. A PVC tube for reinforcement covers the fiber and Kevlar near the connector plug and its end is fixed to the plug using another tightening ring. Therefore, this connector can be assembled very easily and quickly on residential premises. This is because no adhesive hardening or connector endface polishing processes are needed with this connector. When the connector is assembled using 0.25 mm diameter mono-coated fiber, the

fiber must be inserted into a reinforcement pipe in advance to reduce any unexpected loss change during fiber handling.

We fabricated this field-installable connector and examined its ease of use and its optical and mechanical characteristics. The average assembly time was less than 9 min. for the optical cord and less than only 3 min. for 0.25 mm mono-coated fiber because no cord reinforcement was necessary. The average tensile strength was higher than 70 N for the optical cord and higher than 5.2 N for the 0.25 mm diameter mono-coated fiber. The optical and mechanical characteristics are shown in Table 6. The average insertion loss was less than 0.23 dB. We also found that this connector has stable characteristics during severe mechanical tests.

CONCLUSION

We have recently developed various types of new optical cables, new closures, new cabinets and a field-installable connector in order to distribute a fiber from an aerial or underground access point to a home economically and practically. The main results are summarized below.

(1) Very small and lightweight drop cables and indoor cables have been developed, which employ 0.25 mm diameter mono-coated fiber. Their cost can be reduced to less than 50 % that of conventional cable.

(2) A compact closure for access or drop points has been developed, which can handle 0.25 mm diameter mono-coated fiber with ease and without loss increase. The cost reduction is estimated to be about 50 % for both the closure itself and for the labor required in its construction.

(3) A field-installable single-fiber connector has been developed. It is compatible with an SC-type connector and can be assembled with an optical cord or 0.25 mm diameter mono-coated fiber in several minutes with low loss.

We can now construct fiber to the home economically and practically using this newly developed optical fiber distribution system, which included cables, closures, cabinets and fiber joining technologies. In fact, the new system has been used to provide a video distribution test service using FTTH in Totsuka, Kanagawa since July, 1997.

ACKNOWLEDGEMENT

The authors wish to thank T. Yabuta, A. Hirooka and S. Sugiyura for their support and encouragement.

Table 6 Field-installable SC-type connector characteristics for an optical cord

Item		Test Conditions	Result
Average Loss		Room temperature	0.23 dB
Return Loss			≥ 41.0 dB
Loss Change	Tension	Tension: 50 N Loading time: 1 Min.	≤ 0.15 dB
	Heat Cycle	Temperature:-25 ℃~70 ℃ Number of cycles: 10	≤ 0.16 dB
	Heat and Humidity Cycle	Temperature:-25 ℃~70 ℃ Humidity: 95 %RH, 65 ℃	≤ 0.02 dB

Measurement wavelength: 1.31 μ m

REFERENCES

- [1] G. Le Noane, et al., "Towards FTTH networks based on new passive, active devices and installation techniques", NOC'96, pp.274-277, 1996
- [2] U. Ferrero, "Broadband optical access network: cooperative work among European PONs", ECOC'96, WeB.1.1, pp. 3.3-3.10, 1996
- [3] G. V. Plas et al., "Demonstration of an ATM-based passive optical network in the FTTH trial on Bermuda", ICC, 1995
- [4] K. Suto et al., "Home use trial of regional PC communication network system constructed on FTTH", 8th International Workshop on Optical/hybrid Access Networks, Session III 3.4 Atlanta, 1997
- [5] Takasugi, et al., "An economical optical fiber cable network design for the initial stage of FTTH", *ibid*, p.19, Atlanta, 1997
- [6] F. Nihei, et al., "Optical Subscriber Cable Technologies in Japan", *Journal of Lightwave Technology*, LT-5, 6, pp.809-821, 1987.
- [7] V. Abadia, et al., "Communication cables for fibre in the loop", *Proceeding of the 44th IWCS*, pp.569-573, 1995
- [8] S. Kukita, et al., "Design and Performance of Optical Drop and Indoor Cables", *Review of the Electrical Communication Laboratories*, 32, 4, pp. 636-645, 1984.
- [9] IEC SC86A/WG1, No.25 (20 Feb., 1997)
- [10] M. Takaya et al., "Design and development of optical fiber jointing techniques for efficient construction of aerial distribution cable systems", 46th IWCS, 1997
- [11] S. Tomita, et al., "Optical Loss Variation due to Fiber Handling at the Jointing Point on the Subscriber Loop", *Trans. IEICE Japan*, J74-B-1, 2, pp.144-150, 1991 (in Japanese).
- [12] K. Hogari, et al., "Field-installable single fibre connector", *Electron. Lett.*, 33,12, pp.1072-1073, June, 1997



Shin-ichi FURUKAWA
NTT Access Network
Systems Laboratories
Tokai-mura, Naka-gun
Ibaraki-ken, 319-11
Japan

Shin-ichi Furukawa received B.E. and Dr. Eng. degrees in electrical engineering from Kyushu University in 1974 and 1987, respectively. He joined the NTT Ibaraki Electrical Communication Laboratory in 1974, where he engaged in the research and development of submarine cables and joints, optical fiber measurement techniques and remote test and surveillance systems. Since March 1995, he has been engaged in the research and development of optical fiber cable systems for customer premises. He is presently a Senior Research Engineer, Supervisor of NTT Access Network Systems Laboratories. Dr. Furukawa is a member of the IEEE and IEICE of Japan.



Kazuo HOGARI
NTT R&D Management
Department
Nishi-shinjuku
Shinjuku-ku
Tokyo, 163-19
Japan

Kazuo Hogari received the B.E. degree in electrical engineering from Ibaraki University, Ibaraki, Japan, in 1981, and the Dr. Eng. degree from Waseda University, Tokyo, Japan, in 1994. He joined the NTT Electrical Communications Laboratories, Ibaraki, Japan, in 1981, where has been engaged in research and development of optical fiber cables and optical components. He is now Associate Manager of NTT R&D Management Department.

Dr. Hogari is a member of the IEEE and the IEICE of Japan. He received the most outstanding technical paper of 43rd IWCS in 1994.



Masao TERASAWA
NTT Access Network
Systems Laboratories
Hanabatake, Tsukuba-shi
Ibaraki-ken, 305
Japan

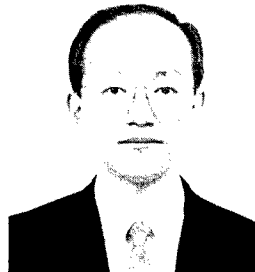
Masao Terasawa graduated Nagano technical college in March, 1972. He joined NTT in 1972, where he engaged in the design and maintenance of outside

plant in Shinetsu branch mainly. Since March 1992, he has joined the NTT Telecommunication Field Systems R&D Center, he has been engaged in the research and development of the laying technology of the high-density optical fiber cable and the institution technology of optical wiring products in the premises. He is presently a Senior Research Engineer, Supervisor of NTT Access Network Systems Laboratories.



Mitsuo KAMA
NTT Technology
Department
Nishi-shinjuku
Shinjuku-ku
Tokyo, 163-19
Japan

Mitsuo Kama received the B.E. degree in electrical engineering from Tokyo Metropolitan University, Japan, in 1984. He joined NTT in 1984. He has been engaged in developmental work on outside plant technology for the optical-fiber cable system. He is now manager of Technology Department of NTT head office. He is a member of the institute of Electronics, Information and Communication Engineers of Japan.



Izumi SANKAWA
NTT Access Network
Systems Laboratories
Nakase, Mihama-ku
Chiba-ken, 261
Japan

Izumi Sankawa received the B.E. and Dr. Eng. degrees in electrical engineering from Waseda University, Tokyo, Japan, in 1979 and 1991, respectively.

He joined the Ibaraki Electrical Communication Laboratories, NTT, Ibaraki, Japan, in 1979. He has been engaged in research on optical fiber splicing, testing techniques, and cabling techniques for high temperature superconductors. Since 1989, he has been engaged in research and development of optical fiber measurement and surveillance systems. He is presently Senior Research Engineer, Supervisor of NTT Access Network Systems Laboratories, Makuhashi, Japan. Dr. Sankawa is a member of the IEICE of Japan, the Japan Society of Applied Physics, and the Japan Society of Physics.



Norio KASHIMA
NTT Access Network
Systems Laboratories
Tokai-mura, Naka-gun
Ibaraki-ken, 319-11
Japan

Norio Kashima received B.E. and M.E. degrees from Yokohama National University, Japan, in 1973 and 1975, respectively and a Ph. D. degree from the Tokyo Institute of Technology, Japan, in 1984. He joined NTT in 1975. He has been engaged in research and development of optical fiber design, optical fiber cable, fusion splicing, optical connectors, optical transmission systems, and access network operation systems. He is a senior member of the IEEE and a member of the IEICE of Japan. He received the Young Engineer Award from the IEICE of Japan in 1982. He is the author of the books entitled "Optical Transmission for the Subscriber Loop" and "Passive Optical Components for Optical Fiber Transmission", which were published by Artech House Publishers (Boston, London) in 1993 and 1995, respectively.



Kanemitsu TOMIYAMA
NTT Access Network
Systems Laboratories
Tokai-mura, Naka-gun
Ibaraki-ken, 319-11
Japan

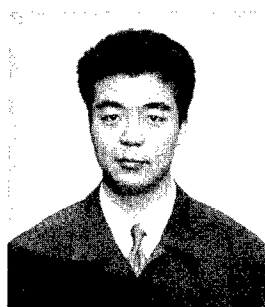
Kanemitsu Tomiyama graduated Oita technical college, Japan, in March, 1981. He joined NTT in 1981, where he engaged in the maintenance and install of outside plant and telecommunication equipment. Since 1994, he has been engaged in the research and development of subscriber optical fiber cables. He is presently a Research Engineer of NTT Access Network Systems Laboratories.



Hiroshi ISHIKAWA
NTT Access Network
Systems Laboratories
Hanabatake
Tsukuba-shi
Ibaraki-ken, 305
Japan

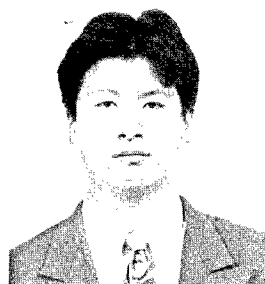
Hiroshi Ishikawa graduated Iwate graduate school in March 1989. He joined NTT in 1989. Since March 1993, he has joined NTT Telecommunication Field Systems R&D Center. He has been engaged in

the development of constructing method of optical cable wiring system in customer's building. He is presently an Engineer of NTT Access Network Systems Laboratories.



Tetsuya HOSHIJIMA
NTT Technology and
Development Support
Center
Nakase, Mihama-ku
Chiba-ken, 261
Japan

Tetsuya Hoshijima received the B.E. degrees in electrical engineering from Hiroshima University in 1986. He joined NTT in 1986. He has been engaged in developing the closure of optical fiber cable for subscriber line. He is presently engaged in planning technology transfer promotion. He is now Engineer of NTT Technology and Development Support Center. He is a member of the Institute of Electronics, Information and Communication Engineers of Japan.



Katsutoshi TSUCHIDE
NTT Access Network
Systems Laboratories
Tokai-mura, Naka-gun
Ibaraki-ken, 319-11
Japan

Katsutoshi Tsuchide graduated Miki high school, Hyogo, Japan, in March 1986. He joined NTT in 1986. He engaged in the design, construction and maintenance of outside plants. Since 1995, he has been engaged in the research and development of the field-installable connecting technology in the NTT Access Network Systems Laboratories.

DEVELOPMENT OF OPTICAL WIRING SYSTEM FOR AERIAL AND PREMISES DISTRIBUTION NETWORKS

Sadaaki Koshio, Shinji Kato and Hidenori Fukumoto

NTT Access Network Systems Laboratories
Nippon Telegraph and Telephone Corporation
1-6 mihamma, chiba 261 Japan

ABSTRACT

Previously, NTT (Nippon Telegraph and Telephone Corp.) had been progressing towards a switch-over to optical infrastructure that extended up to the metropolitan feeder points, but in view of the trend in demand for multimedia communication services and the aging of the existing metallic-cable facilities, policy was revised to include a planned expansion of the optical network into the cabling system beyond those feeder points. In addition to developing the new optical access systems and the FTTH system required to put this policy concretely underway, NTT has also conducted a major reworking of the specifications for its traditional aerial distribution optical fiber cables, user distribution optical fiber cables, and fiber jointing, etc. As a result, overall costs were reduced. The new components are now being put into use.

INTRODUCTION

NTT predicts that the Internet-communication, video-transfer and other multimedia services for which demand had been increasing so rapidly of late will soon show demand increases at a rate still steeper yet, and so the company is hard at work on a variety of projects to respond to this. In the services arena, NTT began to provide low-cost OCN (Open Computer Network) service last April, making Internet communication

even easier. Similarly, in the field of CATV (cable television), NTT began providing carriers with communications lines (from CATV centers to user residences) in July; and these are just two of the multimedia-type services that the company is now beginning to provide for practical use.

On the facilities side, on the other hand, NTT has developed systems—such as the π System[1] and FTTH system—based on optical PDS (Passive Double Star) technology, in order to make it possible to provide these services, POTS, and other services at low cost. Furthermore, to reduce costs below those of the optical-fiber cables and other systems used in the past, the company has conducted a ground-up reconsideration of system specifications. More specifically, since installation costs represent a large proportion of the total in Japan, thought was devoted to improving "instalability," and specifications were revised so that the *total* cost (components + installation) of the system would be minimized.

This paper describes NTT's concept of optical access network and the role of the new optical access network itself, as well as outline of the newly-developed components[2] that are used in it.

CONCEPT FOR THE CONSTRUCTION OF OPTICAL ACCESS NETWORK

First let us consider the medium for the provision of a group of a high-speed, broadband service—namely: multimedia

communication. With the metallic-wire facilities comprising the larger portion of the current access network, limits on transfer speed, quality problems, and other issues make the provision of such services difficult. Thus, it is indispensable to construct an access network that employs optical fiber, which is far superior in terms of speed and quality. However, at the current time, the demand for multimedia service is extremely low, not having expanded beyond the point where it is scattered over a few metropolitan centers. Given this, the only way to accommodate the demand at present is to use individual leased lines. With this method, a situation arises in which optical-fiber facilities are installed on the same routes as existing metallic facilities, thus rendering operations more complex, and as a result greatly increasing maintenance costs. For this reason, the most economical method is thought to be to construct the optical access network while progressively "winding up" the existing metallic facilities. In order to do this, the most important task is to develop a system that allows almost all of the services (such as POTS and narrow-band ISDN) that are currently provided using metallic facilities to be provided using optical ones as well. Moreover, since the target is currently-existing services, it must be possible to hold the costs of providing those services down to their metallic-system levels, even when they are switched over to the optical system.

The problem is that currently available optical fibers and other optical components are still priced expensively. Therefore, until now it has been necessary to multiplex multiple circuits together, in order to share fibers, and thus reduce per-circuit costs. For this reason, NTT began its development on optical systems with high levels of circuit multiplexing, and has progressively been expanding the extent to which these systems are adopted into the access network. The most representative of these efforts has been the CT-RT system, which multiplexes 100-500 circuits, and has been used to gradually begin the construction of the new access network (starting in metropolitan areas), by installing it inside volume-users' buildings, and at feeder points in feeder distribution area. Progress is being made in using this CT-RT technology to "opticalize" the feeder distribution network that spans feeder points in the major cities in Japan (Fig. 1). As of fiscal 1995, the switch to optical systems within NTT had already begun (albeit only to somewhat less than 13%), and the plan is to work towards ratios of 20% by 2000, and a full 100% by the year 2010 (Fig. 2). However, since the multiplexing level is high in the CT-RT system, it cannot be used in the distribution section that are beyond the feeder points, and as a result, metallic cables must still be used.

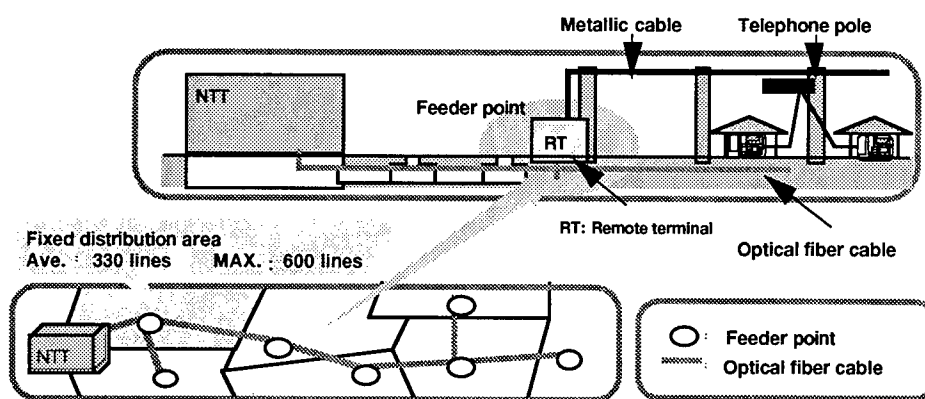


Fig.1 Outline of current optical access

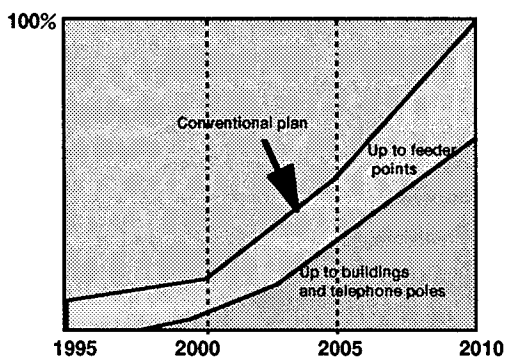


Fig.2 NTT's deployment plan

In order to respond in a timely way to future demand for high-speed, broad-band services, it is necessary to do everything possible to make the "opticalized" system extend as close as possible to the users' locations of final use. In other words, the progressive switch-over to optical must be made in the aerial distribution section just as it is in the underground feeder section. With this in mind, NTT has developed a new optical access system that can be applied inexpensively to such distribution sections as well, which takes the form of an extremely compact set of components that employ a level of multiplexing that has been reduced to 10 circuits. We have named this the π System, and will begin adopting it into the network in 1998. The π System helps us progress with the switch-over of the access network to optical, and will even enable a smooth transition to FTTH, when future demand for high-speed, broad-band services requires it.

As a future development of this system, we are now also actively underway on the creation of a new network structure technology—the loop distribution network (Fig. 3)[3]—that will permit us to reduce costs even further. Moreover, since we have succeeded in reducing the costs of the optical fiber cables themselves and of the other components used in these systems, the π system has become the most cost-effective means of providing multimedia communication services.

In the future, we intend to expand the π system to cover the entire nation, and by progressing with a planned and continuous introduction of it into the network, we expect that not only will we be able to make the switch-over to an optical infrastructure possible, but that we may also succeed in producing a synergistic effect that will enable on-the-spot provision of new services at low cost, and thereby contribute to the expansion of multimedia communication.

THE NEW OPTICAL ACCESS SYSTEM (π SYSTEM)

The cost of establishing FTTH is higher than that for metallic cable (Fig. 4)[4]. To handle this problem, we of course devoted consideration to the costs of optical cable parts and to simplification of installation procedures, but we also worked out a new concept for an optical access system, and succeeded in the related development effort.

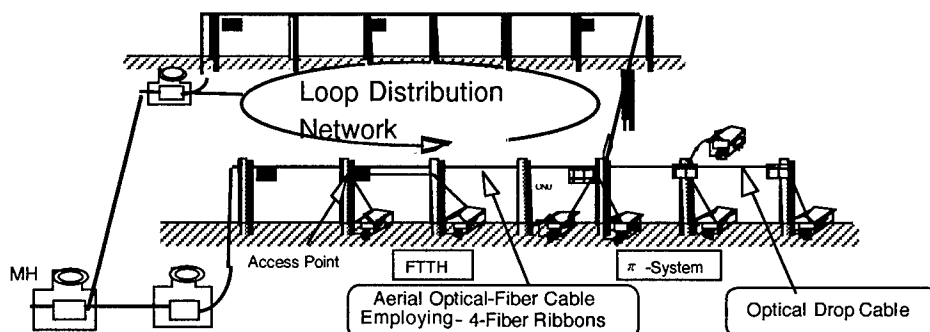


Fig.3 Schematic Overview of New Optical-Fiber Cable Network

The form that this system takes is as follows: the optical fiber network is constructed to extend to a pole in the immediate vicinity of the point of end use, where an ONU (Fig. 5) is installed, thus allowing the provision of telephone (POTS) and other existing services.

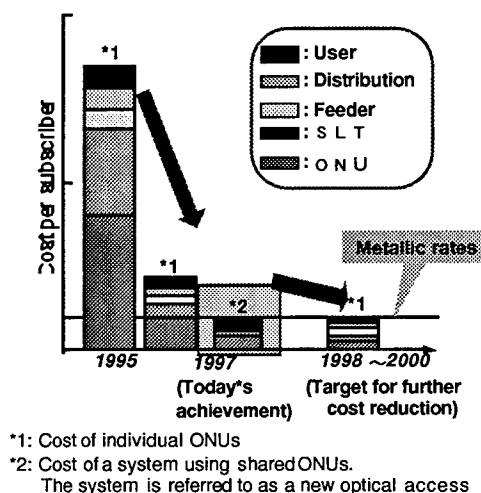


Fig.4 FTTH cost reduction

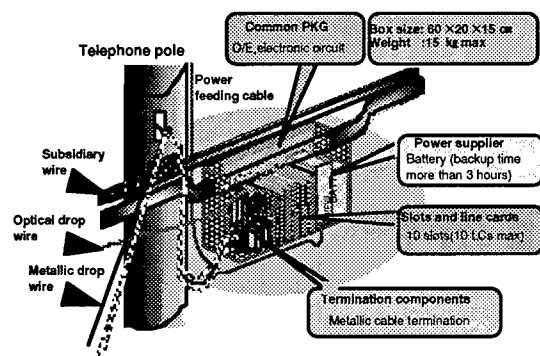


Fig.5 Scheme view of ONU

The advantage of this structure is that a single optical fiber carries multiple (about ten) circuits multiplexed together, so that even with the extremely high cost of optical fiber systems, the per-user cost is reduced all the way to the level of previous metallic cable systems. Furthermore, the existing aged/deteriorated metallic cables can be replaced, thereby reducing cross-line leakage (interference) and earthing—faults specific to metallic systems. As a result, total

running costs are also reduced.

Also, the new system means that demands for high-speed and broad-band service arise, they can be handled speedily. Until now, NTT has had to deal with the scattered requests for such service by newly installing the required number of fiber-optical cables from the nearest feeder points to the users' homes or offices. With the π System, however, since the infrastructure in aerial access network can be quickly and widely replaced with optical components, such scattered demand can be met immediately.

Since demand for high-speed, broad-band service is currently so low, we believe that the π System will be the most efficient means to provide it. Further in the future, though, as demand for such services increases along with the requirements of the services themselves, the π system will reach its limits. At that point, FTTH service will have become cost-effective, and a transition will be made from the π thereto. Since the compatibility of the two systems is excellent, however, that transition will be possible to make smoothly and at low cost.

NEWLY-DEVELOPED COMPONENTS FOR OPTICAL ACCESS NETWORKS

NTT has developed optical cables and related components that can be applied in the π System, while giving consideration to the eventual arrival of FTTH, as well. These parts have produced great reductions in costs from those of their predecessors. Their adoption for commercial use was begun in December of 1996, and they are being employed in a CATV business in the Totsuka region of Kanagawa prefecture.

Simplified descriptions of certain of these newly-developed components are given in the sections below.

SM-TYPE OPTICAL FIBER SS CABLES

SM-type optical-fiber SS cables[5] are used in the distribution section. This system is subject to much more frequent connection procedures than are the cables of the feeder

section, since its cabling is often split (branched) and brought into buildings, etc. With previous cables, it was difficult to obtain the extra length (slack) in the optical fibers that was needed for splitting and making connections. The reason for this problem was that the slots used to hold the optical-fiber ribbons were of a structure that twisted in a single direction, making it hard to remove the ribbons therefrom. It was felt that this was an issue that required resolution if a low-cost optical fiber access network was to be constructed.

The SM-type optical-fiber SS cables that were developed to solve this problem employ an "SZ slot-structure" cable specification that makes it easy to pull out optical-fiber ribbons simply by removing the outer jacket of the cable itself. This specification states that the direction in which the ribbon-holding slots twist must be reversed at fixed intervals along the cable. Because of this, the optical-fiber ribbons have a certain amount of slack, as shown in Fig. 6. This technology has resulted in a drastic simplification of the procedures for branching and connection.

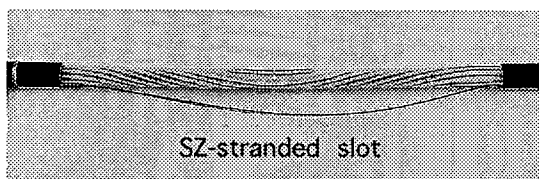


Fig.6 Aerial Optical-Fiber Cable

OPTICAL CLOSURES

Optical closures are box-like containers that protect the points at which optical fibers are joined. In traditional closures, it took significant time to apply water-leakage prevention to the end surfaces where the cables were inserted, so there was a strong desire for a system with improved ease-of-handling. In the new optical closures, an end-surface seal of jell material is used, making water blocking easy to apply, and thereby greatly reducing the cost of installation.

In addition, there is a great deal of

attention being paid to the compatibility of optical closures and other outdoors-installation components with the environment, and to their aesthetics. For this reason, in consultation with experts, decisions were made to revise the color of the housing from to silver from the previous black, and to give it a rounded shape (Fig. 7).

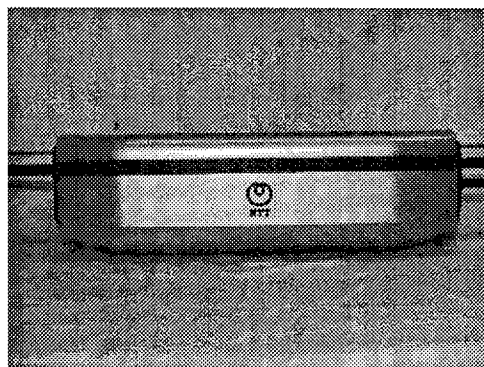


Fig.7 Aerial Closure

MECHANICAL SPLICE

Traditionally, tools such as fusion splicer and MT connectors have been used to connect optical fibers, but their requirements for sources of electrical power and/or of heat, and their use of adhesives, meant that the pre-processing and post-processing requirements took significant amounts of time. With these connection methods, since a connection was made between all of the cores in two optical fiber ribbons at the same time, the per-core cost was not viewed as being extremely high. In systems such as the π System and FTTH, however, single fiber connections need to be made very frequently, so if traditional connection methods with their pre- and post-processing requirements were used, connection costs would seem to account for an extremely large proportions of the cost of the system as a whole. Therefore, a simpler connection method was an absolute necessity.

The method that eliminates this problem is the mechanical splice (Fig. 8). The mechanical splice takes the form of two plates pressed together by a spring. By inserting

the optical fibers into cracks made in both ends of such "sandwiches" by inserting wedges, and assuring that the fiber ends meet, it is possible to make mechanical connections between the fibers by simply removing the wedges so that the fibers are then locked in place. Furthermore, since this connection method requires no source of power or heat, nor any adhesives, it can be used with the simplest of tools, and thus makes low cost single fiber connections possible.

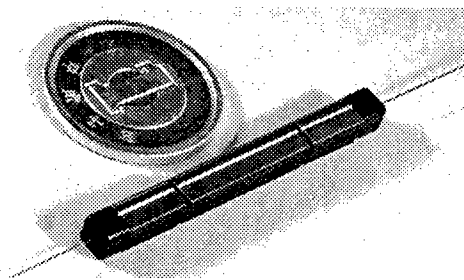


Fig.8 Mechanical Splice

CONCLUSION

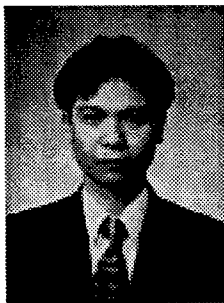
In order to implement multimedia services such as high-speed, broad-band data communications and video transfer at low cost, it is necessary to create the optical access network both economically and efficiently. To do this NTT has developed a new optical access system (the π System) that can handle current service demands and that will also be able to make the transition to future FTTH systems at low cost. It is planned to put this system into commercial service in 1998. We have also succeeded in developing low cost optical fiber cables and connection equipment with an emphasis on ease of installation and maintenance, and these components have already been adopted by a commercial service provider—a CATV business in the Totsuka region of Kanagawa prefecture, where service began in July 1997.

ACKNOWLEDGMENTS

We would like to thank Mr. Sugiura, Senior Manager of the NTT Access Network Systems Laboratories, as well as the numerous others who provided guidance throughout the entire development effort.

REFERENCES

- [1] K.Ikeda, M.Tsubokawa, K.Harikaie and H.Kitajima "Deployment of New Optical Access Systems" 8th International Workshop on Optical / Hybrid Access Networks Conference Proceedings, March. 1997
- [2] A.Hirooka et al. NTT Tecnorojy Journal, Vol 9, No.4, pp.25-29, Apr.1997
- [3] H.Takasugi, T.Horikoshi, and O.Kawata "An Economical Optical Fiber Cable Network Design for the Initial Stage of FTTH" 8th International Workshop on Optical / Hybrid Access Networks Conference Proceedings, March. 1997
- [4] Y.Bessyo et al. NTT Tecnorojy Journal, Vol 9, No.4, pp.9-13, Apr.1997
- [5] H.Iwata, M.Okada, S.Tomita, N.Kashima, T.Hoshijima, M.Kama and K.Nishizawa, "Design of Aerial Fiber Cable System Suitable for Easy Branching" "46th IWCS Proceedings, 1996 (to be published)



Sadaaki Koshio
NTT
Access Network
Systems Laboratories
Mihama-Ku, Chiba
261, JAPAN
mail address:
koshio.sadaaki@nsc.
cae.ntt.co.jp

Sadaaki Koshio graduated Osaka City University in 1995. He joined NTT in 1995. Since 1995 he has been engaged in development of fiber optic cables and components. He is an Engineer of NTT Access Network Systems Laboratories, and responsible for development of fiber optic cables.



Shinji Kato
NTT
Access Network
Systems Laboratories
Mihama-Ku, Chiba
261, JAPAN
mail address:
kato.shinji@nsc.cae.
ntt.co.jp

Shinji Kato graduated Ehime University in 1992. He joined NTT in 1992. Since 1997 he has been engaged in development of fiber optic cables and components. He is an Engineer of NTT Access Network Systems Laboratories, and responsible for development of optical cabinets.



Hidenori Fukumoto
NTT
Access Network
Systems Laboratories
Mihama-Ku, Chiba
261, JAPAN
mail address:
fukumoto.hidenori@
nsc-host.nsc.cae.ntt.jp

Hidenori Fukumoto graduated Kagoshima University in 1982. After joining NTT in 1982. Since 1996 he has been engaged in development of fiber optic cables and components. He is a Senior Engineer of NTT Access Network Systems Laboratories, and responsible for development of fiber optic cables and components for optical access network.

OPTICAL FIBER DISTRIBUTION SYSTEM IN CENTRAL OFFICES FOR THE FTTH ERA

Masao Tachikura, Yoshitaka Enomoto, Shigenori Uruno, Hajime Takemoto,
Nobuo Tomita and Hidetoshi Takasugi

NTT Access Network Systems Laboratories
Tokai-mura, Naka-gun, Ibaraki-ken, Japan

ABSTRACT

This paper describes a new concept for an optical fiber distribution system to be used in central offices in the FTTH era. To avoid cable congestion, an intermediate fiber termination frame (IFTM) is introduced between fiber termination modules (FTM) and optical transmission systems. This makes it possible to lay optical cables containing a large number of fibers from an IFTM to FTMs and to transmission system frames in advance of service demands. We describe FTM and IFTM prototypes, and several types of thin optical fiber cord designed to increase the fiber-density in the cables and frames. A separable cord ribbon has the potential to play an important role in the system. We have also developed a database application system to manage this fiber distribution system.

1. INTRODUCTION

In the FTTH era, NTT expects that it will be

common for several tens of thousands of optical fibers to be terminated in a central office. Since fiber wiring in NTT central offices has mainly consisted of 2- or 4-fiber cables, cable congestion under the floor will become a serious problem in the future if the fiber distribution system remains unchanged. The fiber wiring of concern here is that between the fiber termination modules (FTM) [1] and subscriber line terminals (SLT) of optical transmission systems. The FTM is a kind of main distribution frame for optical fibers.

To avoid cable congestion, the number of optical cables should be decreased by using high fiber-count cables. We have developed a new concept for an optical fiber distribution system which enables the number of optical cables to be decreased. This new distribution system employs an intermediate fiber termination frame (IFTM) between FTMs and SLTs.

The current FTM[1] can hold a maximum of two thousand fiber terminations. It would also be beneficial for the FTM to have a larger fiber-terminating capacity in terms of saving central office floor space. This requires that the optical

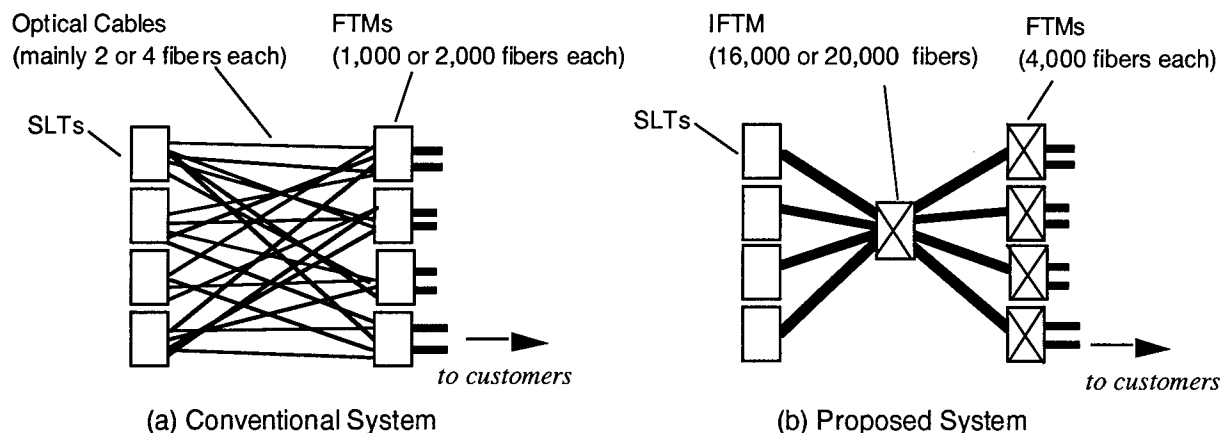


Fig.1 Improvement in central office cable distribution

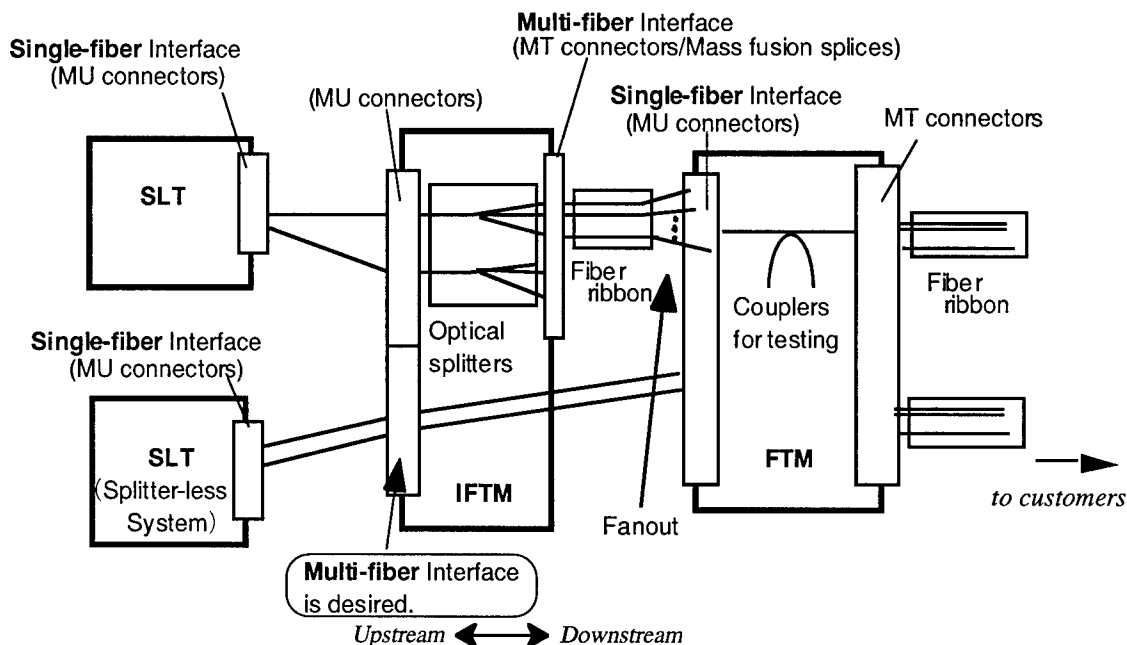


Fig. 2 Fiber distribution in central office

cords in FTMs be much thinner than the currently-used 1.7 mm-diam. cord[2]. Since the optical cables used in NTT central offices contain optical cords, the diameter of these cords must also decreased to provide high fiber-density cables.

In this paper, we describe a new concept for the optical fiber distribution system, prototypes of FTMs and IFTMs to be used in the system, and several types of thin optical cord with which to produce high fiber-density cables and realize practical operation at the distribution frames.

2. FIBER DISTRIBUTION SYSTEM IN CENTRAL OFFICE

The new distribution system we have designed is shown in Fig. 1 alongside the conventional system. The intermediate fiber termination module (IFTM) is newly introduced here between the fiber termination modules (FTM) and subscriber line terminals (SLT) of optical transmission systems. This makes it possible to lay optical cables containing a large number of fibers from an IFTM to FTMs and to SLT frames in advance of service demands. This can radically reduce the number of cables between frames.

Since fibers must be distributed from an IFTM to several FTMs, the fiber capacity of the former must be much larger than that of the latter. Accordingly, the unit of cross-connection in the IFTM should be a fiber ribbon rather than a fiber. Since connectors in FTMs and SLTs are normally single-fiber type, there is a mismatch to be overcome.

Figure 2 is a schematic of the fiber distribution. Optical splitters which are now utilized for several transmission systems are installed in the IFTM. In this case, the upstream-side terminals of the IFTM can be mono-fiber connectors. This will not result in a lack of space because there are considerably fewer fibers on this side than on the downstream side. The fiber ribbon from the downstream side of IFTM must be fanout to single fibers at the FTM. This requires a simple and cost-effective fanout method. If possible, the fanout should be applied at the SLTs and then fiber connection can be realized in fiber ribbon units at the IFTM. The multi-fiber connection at IFTM will be indispensable if splitter-less systems are popularized in the future.

3. FIBER DISTRIBUTION FRAMES (FTM and IFTM)

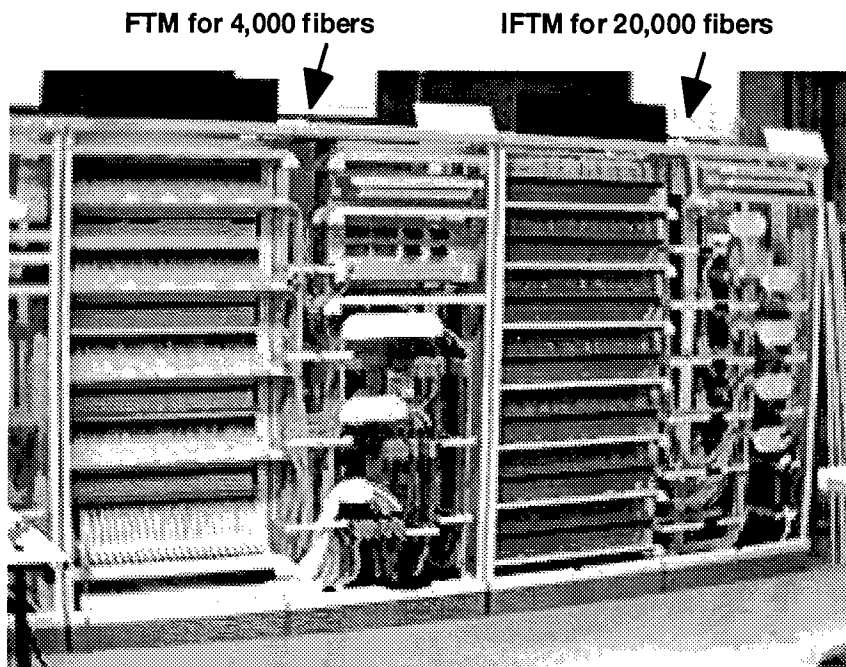


Fig. 3 Fiber distribution frames (FTM, IFTM)

To save space in central offices, we have already made a prototype of an FTM which can accommodate 4,000 fibers[3]. Because an IFTM has to operate as a fiber distribution hub, its fiber-terminating capacity needs to be several times larger than that of the FTM. We have also made a prototype IFTM for 20,000 fibers which is the same size as the FTM. Figure 3 shows a photograph of the FTM and the IFTM. They are both 1.6 m(W) x 0.6 m(D) x 1.8 m(H) in size.

The FTM is composed of 5 jumper plate shelves which have 50 optical modules. Each module has 16 ports for MU-type connectors[4] for the optical cords from the IFTM. The module is called an optical branch module, because it contains a 16-channel optical coupler for an OTDR testing system and has 6 ports for 8MT type connectors (2 for outside cables and 4 for the testing system)[5]. The testing system is called AURORA (automatic optical fiber operations support system)[1][3][6], and fiber selectors for the system have also been installed in the FTM. Optical cords 1.0 mm in diameter are used in the FTM. We also made another type of optical branch module which has MT connector ports to enable easy connection with an IFTM. Since this requires the fiber ribbon

jumper at the FTM, its applicability is restricted at this time.

The IFTM is composed of 7 jumper plate shelves which can accommodate 50 optical splitter modules. The optical splitter module have 8 ports for 8MT connectors to connect with a FTM, and 2 ports of 4MT connector in the upstream side to connect with a SLT. The MT connector ports were included on the expectation that fanout in the cable or multi-fiber connectors at SLT will be practical in the future. Since MU connectors are suitable for upstream side ports at this time, we are also designing another IFTM prototype which can accommodate about 16,000 fibers on the downstream side.

4. OPTICAL FIBER CORDS FOR HIGH DENSITY CABLES

Optical cables in the proposed distribution system should contain a large number of fibers. To realize high fiber-density, optical cords contained in the cables must be much thinner than the currently-used 1.7-mm. diam cords. When cord diameter is reduced, the possibility of a radical decrease in flexural rigidity is more serious than any decrease in tensile strength.

Insufficient flexural rigidity can lead to sudden bending loss as the result of rough handling. Several prototype cords which we have developed are shown in Figs. 4 to 7.

Loose-type 1.0-mm cord

Figure 4 shows the cross-sectional structure of the latest 1-mm diam. cord[7]. It has a loose-type structure, so the buffered fiber can slide inside the cord sheath. By using polyamide (i.e., Nylon) for the cord sheath, instead of conventional PVC, the cord has been improved by four times in terms of its flexural rigidity compared with the one we reported previously[8]. MU connectors fit this type of cord.

Tight-type 0.9-mm cord

Figure 5 shows the structure of a tight-type 0.9 mm-diam. cord which is designed for cost reduction. Glass fiber yarn was used for the tension member instead of conventional aramid yarn. The outer coat is UV-cured resin and this has partially penetrated the inner glass fiber yarn. Since this cord has a simple tight-type structure, a simplified connector should be employed with this type of cord.

Tight-type 0.25-mm cord

The 0.25 mm-diam. cord[7] in Fig. 6 has a state-of-the-art structure which provides sufficient flexural rigidity despite its extremely small cross-section. A buffered fiber with a diameter of 150 μm and 12 surrounding steel wires 45 μm in diameter are formed into a solid bundle with UV-cured resin. We chose steel wires as tension members in order to achieve the highest flexural rigidity in this extremely small cross-section.

Separable 8-cord ribbon

By bundling 0.25 mm-diam. cord in Fig. 6, we can produce a cord ribbon which is almost the same size as currently used fiber ribbons. But the ribbon will not be practical because it is not easy to remove the tension members.

Figure 7 shows a steel-wire-reinforced cord with an improved structure for use in ribbons to be employed for multi-fiber splicing and with multi-fiber connectors. Two steel wires are positioned on one side of the rectangular cross-section of the cord. The reduced number of steel wires and the conventional 0.25-mm diameter of the buffered fiber are of great benefit as regards decreasing the production cost.

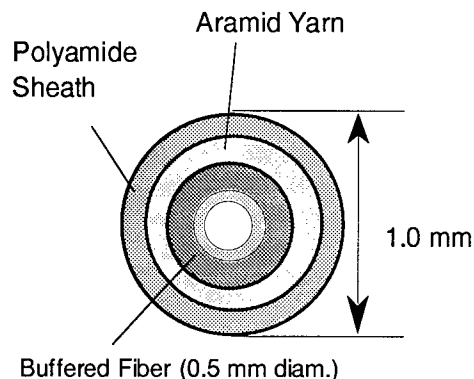


Fig. 4 Loose-type 1.0 mm cord

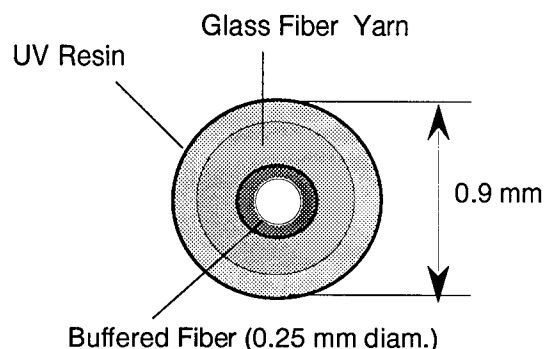


Fig.5 Tight-type 0.9 mm cord

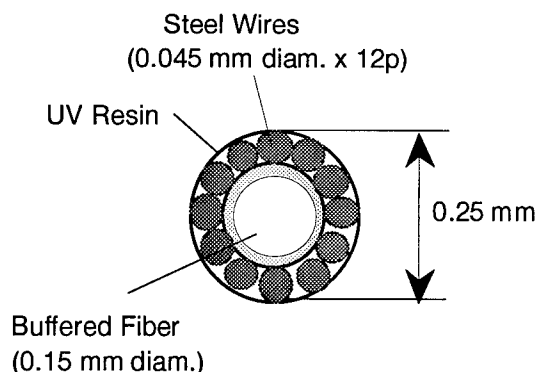


Fig. 6 Tight-type 0.25 mm cord

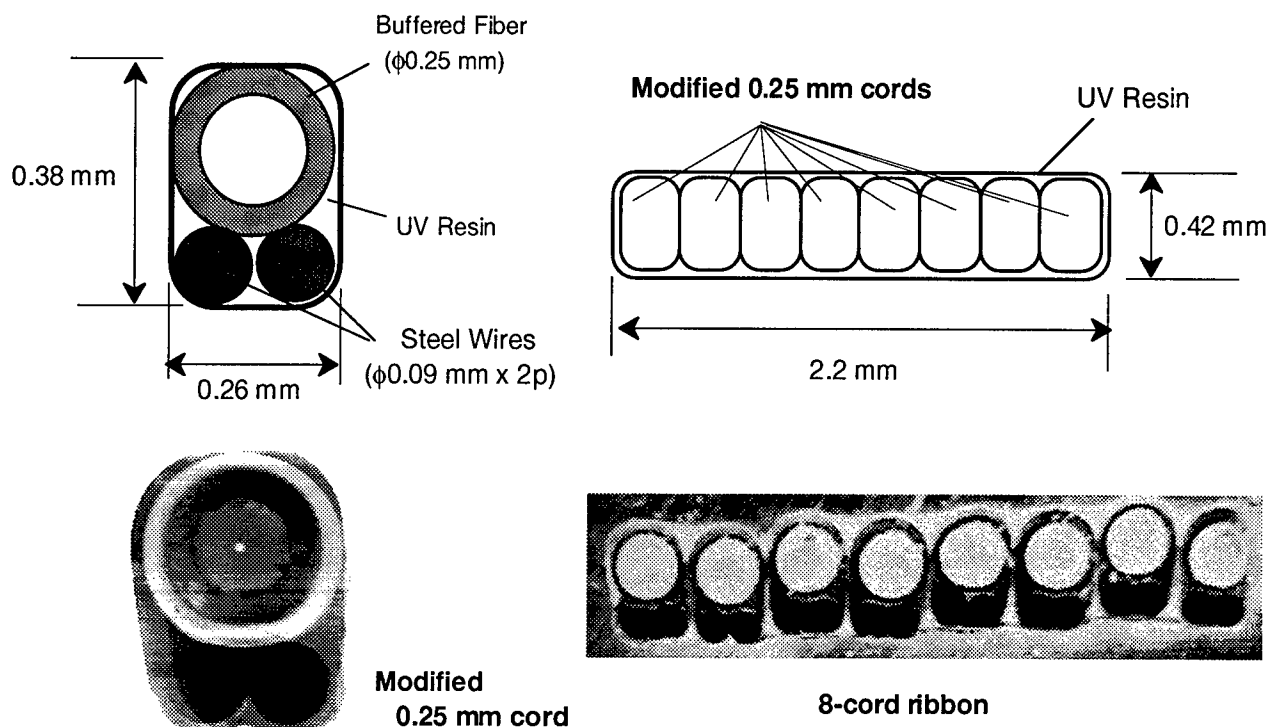


Fig.7 Separable 8-cord ribbon

A diagram and a photograph of an 8-cord ribbon produced by bundling the cords is also shown in Fig.7. Although the fiber pitch in the cord ribbon is about 0.01 mm larger than that in normal fiber ribbons, this slight difference does not affect splicing or connector assembly procedures. Since all the steel wires are aligned on one side, they can be easily removed by a one-time procedure of fiber cutting and wire

peeling. This cord ribbon can also be easily separated to single fiber cords by tearing it from one end.

Performance of the prototype cords described above is shown in Table 1. The flexural rigidities given in the table were evaluated by the 2-point bend technique[7]. Although there are some differences in performance, we believe that all

Table 1 Performance of prototype cords

cord	φ1.0 mm cord	φ0.9 mm cord	φ0.25 mm cord	Modified φ0.25 mm cord	Separable 8-cord ribbon
Flexural rigidity	4.4 kgf·mm ²	4.2 kgf·mm ²	1.7 kgf·mm ²	0.8 kgf·mm ²	13.7 kgf·mm ²
Fiber elongation at 7kgf tension	0.76 %	1.22 %	1.66 %	1.90 %	0.35 %
Temperature cycle test (-10 ~ +40 °C)	0.04 dB/km	0.04 dB/km	0.22 dB/km	< 0.02 dB/km	< 0.02 dB/km
Crush test @1550 nm (50 kgf on 100 mm)	0.02 dB	0.14 dB	0.18 dB	0.02 dB	0.01 dB
Bending loss @1550 nm (10 turns at φ30 mm)	0.09 dB/turn	0.09 dB/turn	0.01 dB/turn	0.07 dB/turn	0.06 dB/turn
Transmission loss @1550 nm	0.20 dB/km	0.23 dB/km	0.66 dB/km	0.20 dB/km	0.20 dB/km
@1310 nm	0.32 dB/km	0.37 dB/km	0.62 dB/km	0.33 dB/km	0.36 dB/km

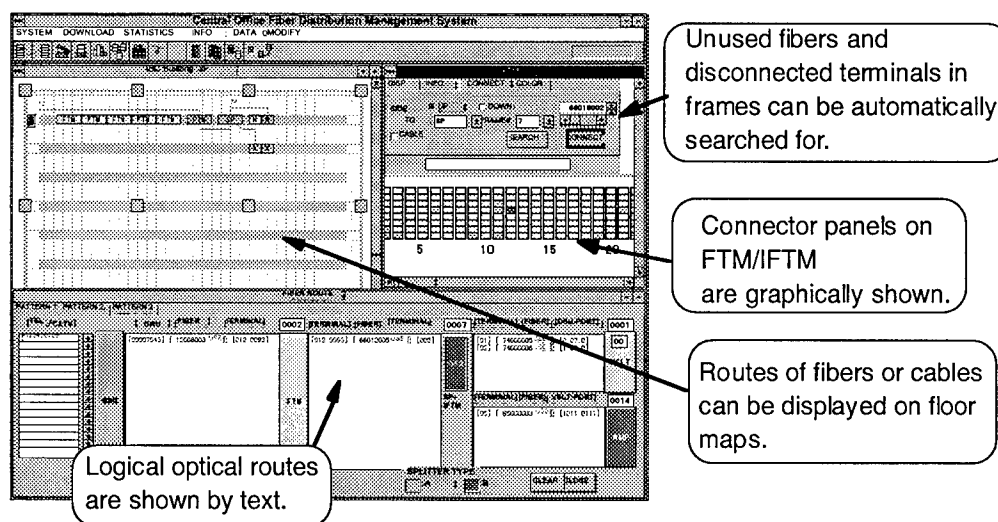


Fig.8 Display sample on management system

of the cords are also within the allowable range.

We also expect that the easy fanout function of the cord ribbon will play an important role in the new fiber distribution system, because the current single-fiber interface at FTMs and SLTs can be matched with the multi-fiber interface of IFTM only by using the cord ribbons. Nevertheless, several points must yet be considered including the choice of suitable connectors, the mechanical reliability of the bent portion and the resistance of the coating to rubbing.

5. FIBER DISTRIBUTION MANAGEMENT SYSTEM

In order to employ the new distribution system, which requires cables containing many fibers to be laid in advance of service demands, data on unused fibers in cables must be systematically managed.

For this reason, we have developed a database application system for a personal computer to manage the fiber distribution system proposed here. In this PC-based system, object-oriented data management has been achieved with a normal relational database. This makes it possible to manage complex optical lines which incorporate such optical components as optical splitters.

This system has been developed with a visual programming tool, and provides a multi-window

graphical user interface (GUI) and keyboard-less operation. A display sample is shown in Fig. 8. By using this system, we can easily search for unused fibers in previously laid cables and disconnected terminals in fiber distribution frames. This system also has the potential to control automated FTMs[9].

6. CONCLUSION

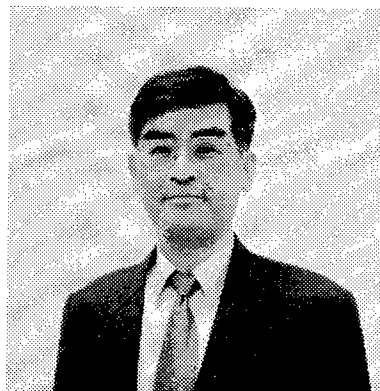
We have described a new concept for an optical fiber distribution system in central offices. To avoid cable congestion, an intermediate fiber termination frame (IFTM) is introduced between fiber termination modules (FTM) and optical transmission systems. This makes it possible to lay optical cables containing a large number of fibers from an IFTM to FTMs and SLTs in advance of service demands.

We have made prototypes of an FTM for 4,000 fibers and an IFTM for 20,000 fibers to be employed in the distribution system. To increase fiber-density in cables and frames, we also made several types of thin optical fiber cord; a 1-mm diam. loose cord, a 0.9-mm diam. tight cord, a 0.25-mm diam. tight cord, and a separable 8-cord ribbon. The separable cord ribbon has the potential to overcome the mismatch between the fiber connection interfaces of the IFTM and FTM, and the IFTM and SLT. In addition, we have developed a database application system to manage the fiber distribution system.

REFERENCES

- [1] T. Ebihara, N. Nakao and M. Kuroiwa, "Novel automatic remote fiber line testing system and new fiber termination module for expanding local subscriber loops", Proc. ECOC'96, Vol.3, pp.39-42, 1996.
- [2] T. Ebihara, R. Nagano and Y. Sakuyama, "Commercialization of intra-office cable using thinner jacketed optical fiber cord", Proc. of National Convention of IEICE Japan, B-950, Sept. 1996. (in Japanese)
- [3] Y. Enomoto, N. Tomita, T. Ibayashi, R. Honda, A. Takagi and N. Nakao, "High-density fiber termination module (FTM) for AURORA", Technical Digest of 2nd Optoelectronics & Communications Conf.(OECC), pp.536-537, 1997.
- [4] S. Iwano, R. Nagase, K. Kanayama, E. Sugita, K. Yasuda and Y. Ando, "Compact and self-retentive multi-ferrule optical backpanel connector" IEEE J. Lightwave Technol. Vol.10, No.10, pp.1356-1362, 1992.
- [5] T. Satake, P. W. Blubaugh, J. Midkiff and T. Akikawa, "US Connec spreads MT connector into North American markets", NTT Review, Vol.5, No.4, pp.82-89, 1993.
- [6] N. Tomita, H. Takasugi, N. Atobe, I. Nakamura, F. Takaesu and S. Takashima, "Design and performance of a novel automatic fiber line testing system with OTDR for optical subscriber loops", IEEE J. Lightwave Technol., Vol. 12, No. 5, pp.717-726, 1994.
- [7] M. Tachikura, H. Takemoto and N. Tomita, "Miniature optical fiber cords with high flexural rigidity", Technical Digest of 2nd Optoelectronics & Communications Conf.(OECC), pp.526-527, 1997.
- [8] M. Sato, M. Tachikura, N. Tomita and S. Iwano, "A 1-mm ϕ miniature optical fiber cord adaptable for MU-type connectors", Proc. of 45th IWCS, pp.374-380, 1996.
- [9] Y. Nishida, F. Ohira, T. Kanai, N. Tamaru, T. Shoji, J. Yamaguchi and H. Kimura, "Main-distributing frame using a fiber-handling method in optical access networks", Technical Digest of OFC'95, pp.57-58, 1995.

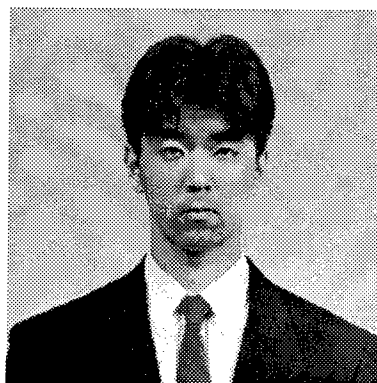
Authors



Masao Tachikura

NTT Access Network Systems Laboratories, Tokaimura, Naka-gun, Ibaraki-ken, 319-11 Japan

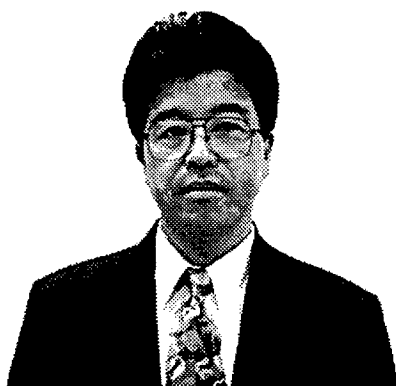
Masao Tachikura is a Senior Research Engineer at NTT Access Network Systems Laboratories. Since he joined NTT Electrical Communication Laboratories in 1976, he has been engaged in research on fiber splicing and connecting techniques, on the mechanical reliability of optical fibers, and on fiber switching techniques. He is currently engaged in the research and development of optical cords and a management system for a central office fiber distribution system.



Yoshitaka Enomoto

NTT Access Network Systems Laboratories, Tokaimura, Naka-gun, Ibaraki-ken, 319-11 Japan

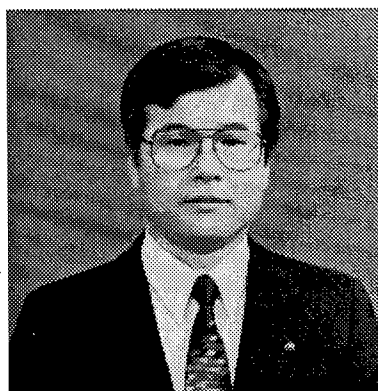
Yoshitaka Enomoto joined NTT Telecommunication Field Systems R & D Center Ibaraki, Japan in 1992. He is engaged in the research and development of an optical fiber line testing system and optical components for the central offices of access network systems.



Shigenori Uruno

NTT Access Network Systems Laboratories, Tokaimura, Naka-gun, Ibaraki-ken, 319-11 Japan

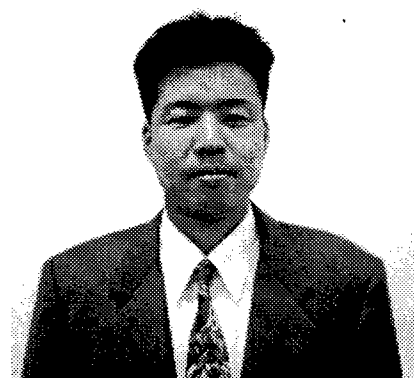
Shigenori Uruno is a Research Engineer at NTT Access Network Systems Laboratories. Since he joined NTT Electrical Communication Laboratories in 1969, he has been engaged in research on cable jointing, fluoride fiber transmission, the remote control of fiber switches, and in the development on a management system for a central office fiber distribution system.



Nobuo Tomita

NTT Access Network Systems Laboratories, Tokaimura, Naka-gun, Ibaraki-ken, 319-11 Japan

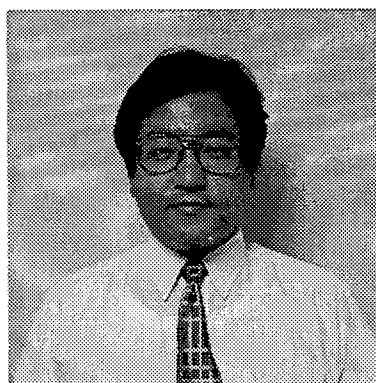
Nobuo Tomita is an Executive Research Engineer at NTT Access Network Systems Laboratories. In 1974, he joined NTT Ibaraki Electrical Communication Laboratory, Ibaraki, Japan, where he was engaged in research on broadband and digital subscriber loops and the development of optical fiber cable components. Since 1987, he has been engaged in the research and development of operation and maintenance systems for optical trunk and subscriber lines.



Hajime Takemoto

NTT Access Network Systems Laboratories, Tokaimura, Naka-gun, Ibaraki-ken, 319-11 Japan

Hajime Takemoto joined NTT in 1983, and was engaged in the planning of outside plant maintenance, and development & installation guidance of New Outside Plant Management System. Since he transferred to NTT Access Network Systems Laboratories in 1996, he has been engaged in the development of optical cords and of a central office fiber distribution management system.



Hidetoshi Takasugi

NTT Access Network Systems Laboratories, Tsukuba-shi, Ibaraki-ken, 305 Japan

Hidetoshi Takasugi is a Senior Engineer at NTT Access Network Systems Laboratories. In 1987, he joined NTT and engaged in the development of optical fiber cable components. Recently, he has been working on the system design for the fiber distribution of access networks.

COMPOSITE DRY CORE SERVICE CABLE FOR THE LOCAL LOOP NETWORK

William E. Beasley*, Tsuneo Yamazaki**, Stephen R. Stokes*, Mikio Kobayashi**

*Sumitomo Electric Lightwave Corp., Research Triangle Park, North Carolina

**Tsushin Kogyo Electric Wire & Cable Co., Ltd., Kawagoe-shi, Saitama-ken, Japan

ABSTRACT

A composite optical fiber and copper pair cable has been developed for drop cable applications in the local loop portion of the network. Dry water absorbing technologies, flame retardant materials, and a self-supporting design have yielded excellent cable performance in the laboratory against industry standards. Results of field evaluation anticipates reduced labor and cost savings with the deployment of the composite service cable over dual gel-filled cables.

INTRODUCTION

Background

Over the past several years, costs of field electronics have been driven down, making Fiber to the Curb (FTTC) and Fiber to the Home (FTTH) network solutions economically feasible. With the availability of field and customer premises mounted Optical Network Units (ONU), designed for bringing digital services to small clusters of homes, new cabling solutions specifically tailored for the last leg of the distribution plant are now needed.

Current commercially available optical fiber cables for the outside plant (OSP) network encompass a wide range of styles, fiber counts, and sheath constructions. Most optical cables were originally designed for the trunk portion of the network spanning between central offices (CO) of local exchange carriers (LEC) or between repeater stations for long distance carriers. These cables are traditionally medium fiber counts (24 to 72 fibers), are of loose tube design and are either pulled into ducts or aerially lashed.

As demands for greater reliability and bandwidth increased, LEC's spread fiber into the feeder portion of the network. These cables are typically of the same design as trunk cables since the feeder portions of the network are branch extensions of the trunk network.

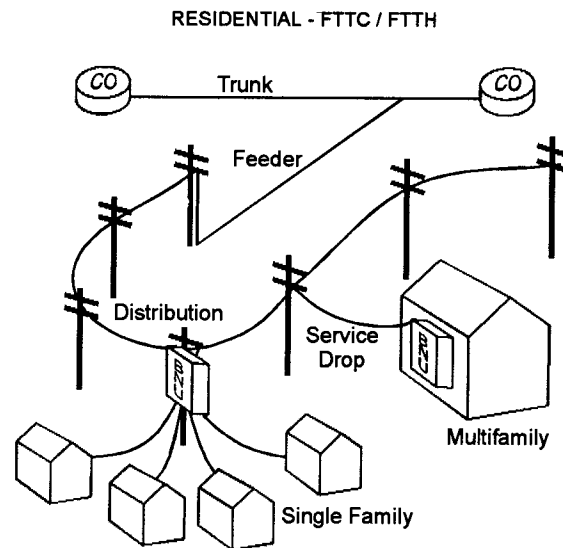


Figure 1. Typical deployment of optical cable in the OSP network.

The distribution plant brought new requirements to the cable manufacturers. High fiber counts and more craft friendly designs drove the US industry towards central tube - ribbon style cables. These cables offer rapid midspan entry, improved splicing productivity with mass splicing and compact high fiber count designs. All these characteristics are necessary for rapid, cost effective deployment in the local loop where many cable access and splice points are anticipated.

In today's distribution plant, Fiber in the Loop (FITL) projects are being rapidly deployed by many Regional Bell Operating Companies (RBOC) using primarily pole and ground mounted ONU's.^{1,2} These electronics filled cabinets are being directly connected to high count distribution cables within the ONU or are being fed by small fiber count drop cables. For pole and ground mounted ONU's, the drop cable design is simple: standard small fiber count cables made with OSP cable materials that can be strand lashed or direct buried.

It has been suggested that in the case of feeding urban multifamily dwellings or multiple tenant office buildings, a pole mounted ONU would present a large number of drops, both copper and coaxial, spanning between the pole and the building.³ Premises mounting of the ONU on the exterior of the building would eliminate the unsightly array of drop cables. Instead, a single aerial service cable can run between the strand mounted distribution cable and the customer's ONU.

Field Requirements

For the aerial service cable, a composite fiber and copper pair cable construction is ideal, since the LEC's must provide electricity to the ONU's for powering the electronics in addition to providing fiber for the communications. This eliminates the need to install dual cables from the strand mounted distribution cables to the ONU.³ Termination of both fiber and copper within a common closure is allowed by the National Electrical Code, section 770-52, as long as the powering voltages are below 600V and the functions of the electrical and optical circuits are associated.⁴

Second, since the distribution plant for the dense urban housing is typically aerial, a self-supporting aerial drop cable is desired. This saves the costly step of first installing a strand wire, then lashing of the drop cable. A maximum self-supporting span up to 50 m was targeted.

For aerial cable attachment to a customer premises, the RBOC's require that the service cable be flame retardant. This reduces the possibility of fire spreading from a pole to a customer's building.

As an added measure of security, shielding was requested to prevent the effect of electromagnetic interference (EMI) on the ONU's electronics.

CABLE DESIGN

Sumitomo with Tsushin Kogyo have developed a small, lightweight service drop cable that meets all of these requirements and at the same time includes the industry's newly popular dry water blocking technology.

Cable Core

Three 22 AWG copper pairs are stranded together with a standard gel-filled polymer loose tube housing two Single-Mode optical fibers. 22 AWG wire was chosen based on the powering requirements set forth by the ONU supplier. Voltages are maintained below communication grade levels so as to not require a voltage rating on the cable. Three pairs were chosen to provide ample capacity for a range of ONU mounting distances and for future equipment upgrades. Two fibers were included; one as active, the second as back-up.

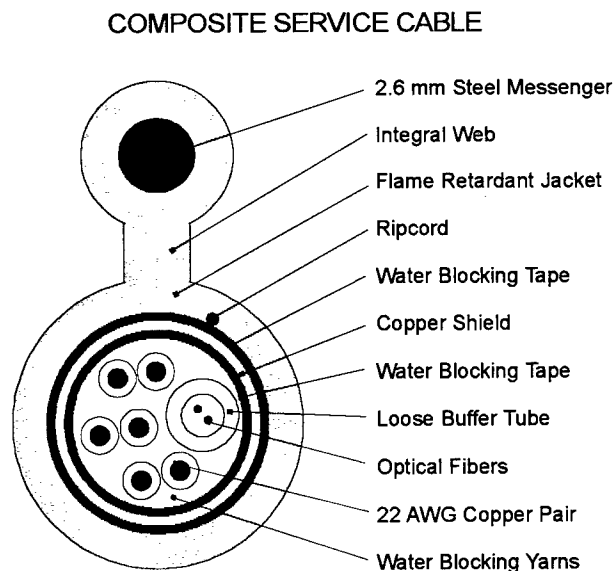


Figure 2. Cross sectional view of Figure-8 Style Composite Service Cable.

For protection against water migration down the cable core, Sumitomo wanted to take advantage of the cleanliness and quick entry benefits found with new dry water absorbing materials over traditional gel based materials. A combination of dry water absorbing yarns and tapes were used in the drop cable. Use of polyacrylic acid and other superabsorbent polymer impregnated materials

within a loose tube style cable has been recently well documented.^{5,6,7} The reliability of these materials has also undergone much evaluation and has proven itself through field application over the past several years.^{8,9}

A thin copper tape was stranded around the cable core as protection against induced noise along the copper pairs. An additional dry water absorbing tape layer protects the region between the shield and the outer jacket from water intrusion.

Sheath Construction

To meet the maximum 50 m span lengths requested by the customer, additional load bearing strength elements are necessary to support the composite cable core. A figure-8 style construction, as opposed to a circular cable, is chosen for ease of installation at the customer premises and for compatibility with current installation techniques used by the customer.

A 2.6 mm diameter high strength galvanized steel messenger is used for compatibility with existing field termination and support hardware for service drop cables.

Table 1. Composite Service Cable Specifications.

PROPERTY	VALUE
Fiber Type	Single-Mode
# of Fibers	2
Copper Pair Type	22 AWG, PIC
# of Pairs	3
Messenger	2.6 mm Steel
EMI Protection	Copper Shield
Jacket	FRPE
Cable Dimensions	9.0 x 16.5 mm

Both the steel messenger and cable core are co-extruded with a flame retardant polyethylene (FRPE) material, to meet the burn requirements as required by Bellcore & the RBOC's. FRPE was chosen over Polyvinyl Chloride (PVC) for its halogen-free properties and improved weatherability.

Cable Processing

The optical performance of the Single-Mode optical fibers were measured at each processing step during the manufacture of the cable. No significant change in attenuation was observed at either 1310 or 1550 nm at any step.

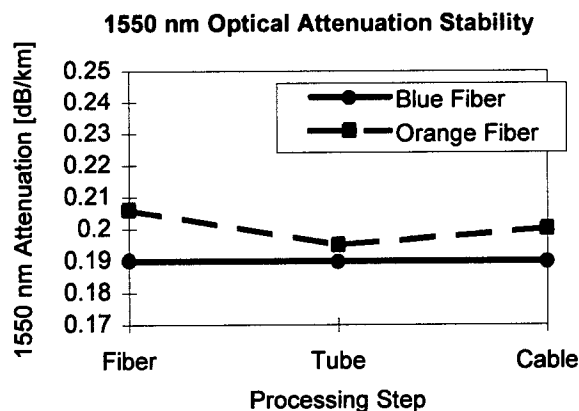


Figure 3. Attenuation stability during processing.

Sag & Tension Calculations

Summation of the independent loads acting on an aerial cable such as wind, ice, temperature change and the weight of the cable, produces a loading resultant which can be used to predict the catenary behavior of the suspended composite drop cable.

Based on the maximum allowed long-term service loads of the cable and clearance regulations as specified in the National Electrical Safety Code (NESC), Section 250,¹⁰ the installation conditions were calculated. Shown below is the minimum allowed sag at installation versus span length for each of the regional loading conditions as specified in the NESC.

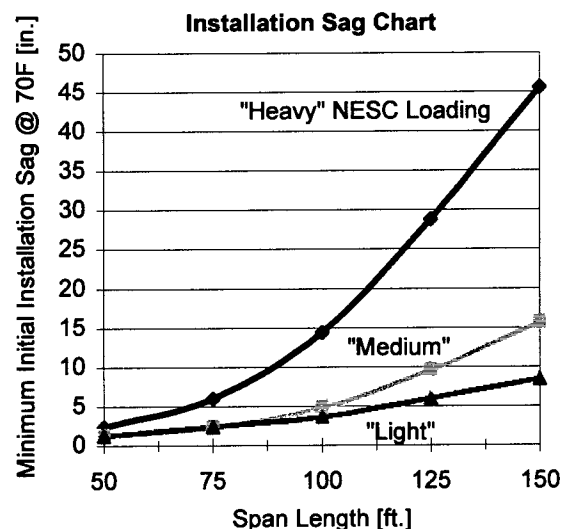


Figure 4. Installation conditions for the composite drop cable.

LABORATORY TESTING

The performance of this cable has been proven in the laboratory through rigorous testing against industry specifications such as Bellcore's GR-20¹¹, TR-122¹², GR-2879¹³ and TR-843¹⁴. Due to the unique design of this cable, applicable tests were applied from each specification. In several instances, modifications were made to the test to better suit the cable's intended use in the field.

Standard Bellcore Tests

For each of the standard specification tests performed, appropriate EIA/TIA fiber optic test procedures as defined under EIA/TIA-RS-455¹⁵ were used. No permanent mechanical damage was imparted on the cable sheath or any of its components from any of the tests.

Table 2. Cable Specification Test Summary: Mechanical

Test	Conditions / Requirement	Result
Hot & Cold Bend	3 in. Mandrel @ -30°C & +60°C	Pass No Jacket Cracks
Impact	Impact Energy: 4.5 N·m, 25 cycles	Exceeded Spec Impact Energy: 16N·m
Compression	Plain Sheath: 220 N/cm	Exceeded Spec Comp. load: 440 N/cm
Twist	≤ 2 m Length, Rotation of ± 180°, 10 Cycles	Exceeded Spec 1 m Length, ± 360°
Cyclic Flexing	Bend Diameter ≤ 20 x Cable Diameter, ± 90°, 25 Cycles	Exceeded Spec 13 x Cable Diameter
Tensile Strength	Maximum Service Load = 700 lbs.	Pass $\epsilon_{\text{cable}} \leq 0.30\%$ $\epsilon_{\text{fiber}} \leq 0.05\%$

Table 3. Cable Specification Test Summary: Environmental

Test	Conditions / Requirement	Result
Temperature Cycling	-40°C to +70°C, Two Cycles	Pass Avg. $\Delta\alpha_{1.55} \leq 0.01$ dB/km
Cable Aging	+85°C, 168 hr. -40°C to +70°C, Two Cycles	Pass Avg. $\Delta\alpha_{1.55} \leq 0.03$ dB/km
Jacket Shrinkage	Terminated cable, -40°C to +70°C, Two Cycles, +85°C, 168 hr., -40°C to +70°C, Two Cycles	Pass
Water Penetration	Unaged: 1m, 24 hr., Aged: 1m, 1 hr.	Pass
Flammability	UL 1581, VW-1 Test	Pass

Electrical Properties

The properties of the copper twisted pairs were evaluated under adverse conditions as might possibly be encountered in the field. A 50 m length of the composite service cable was subjected to a 10 cm sheath breach. Both the outer jacket and copper foil shield were completely removed. A 1 meter head of water was imparted to the exposed section of cable core for a 4 week period at 23°C. Insulation resistance, conductor resistance, capacitance and dielectric strength measurements were made at specific intervals during the test to evaluate the effects of a water exposed core on the electrical performance of the drop cable.

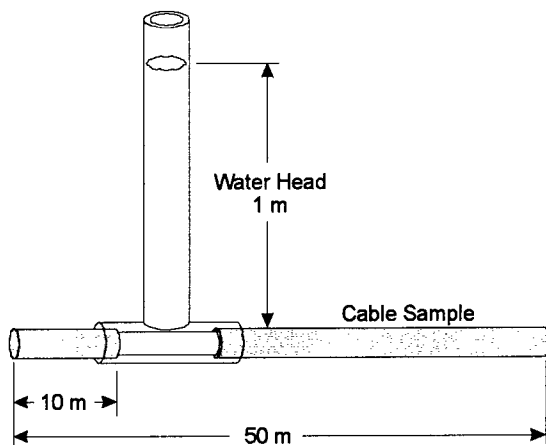


Figure 5. Test configuration for the water penetration / electrical properties measurement.

The performance of each copper pair was stable during the duration of the test. No significant change was observed in any of the properties measured and all values remained well above the Bellcore limits as defined in TR-122. Shown below are average results for all three copper pairs. Note that since measurements were made on a 50 m test length, the variations shown below are magnified by 20 times to present results per km. Therefore, the variations seen are mostly within the measurement accuracy of the test equipment. All values shown are the average of all three copper pairs.

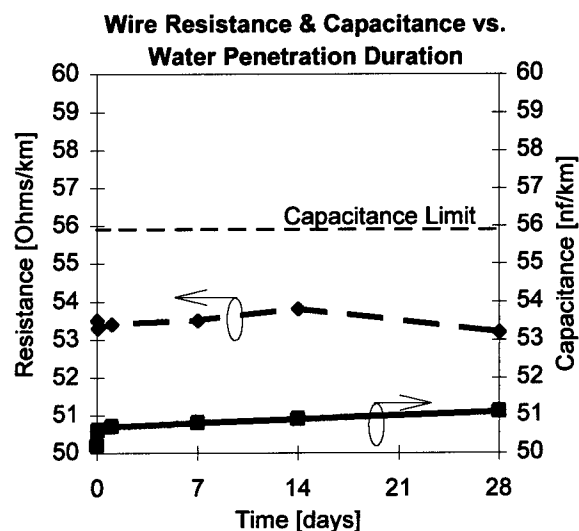
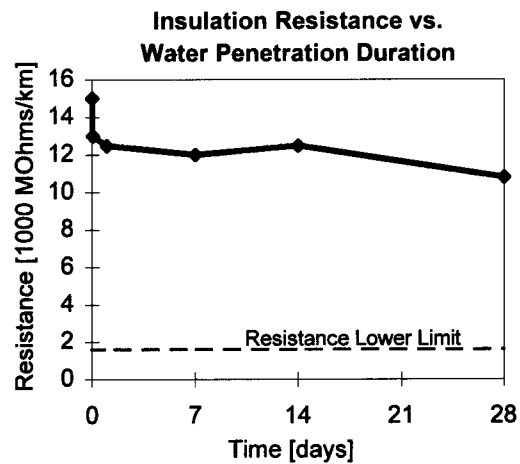


Figure 6. Electrical properties of copper pairs during water penetration test.

The dielectric strength measurements were made at 350 VAC for 1 minute duration. The dielectric strength between the copper wires of all the pairs passed this voltage level without breakdown during the entire test of 4 weeks.

Suspension Clamp Retention

The compatibility of the attachment hardware with the new composite cable was verified through clamp retention force testing on an Instron test bench in the laboratory. Two different sized clamps from the same manufacturer with different acceptable wire diameter ranges were evaluated. Both clamps were tested because the 2.6 mm (0.102 in.) wire of the drop cable falls close to each clamp's acceptable diameter range.

Clamp	Maximum Test Load	Failure Mechanism
A	1200 lbs.	Clamp Material Yield
B	1400 lbs.	None

Both clamps held up to and beyond the 700 lbs. long-term cable service tensile rating. At these high tensile loads, which exceed the rated loads of the attachment hardware, several millimeters of strain was measured. Subsequent analysis of the tested samples revealed deformation of the clamp's bail as it straightened out around the test fixture bolt.

Tensile Test

For the composite service cable, the Long Tensile & Bend test is not representative of how it will be installed nor the forces the cable will experience during its service lifetime. Tensile forces will be directly imparted to the suspension clamps and born by the messenger wire. Also, the suspended cable will not experience any tight bending while under service tensile loads.

The diagram illustrates the experimental setup for measuring the mechanical properties of a cable. It shows a horizontal arrangement of components. On the left, a 'Messenger Suspension Clamp' is attached to a 'Messenger Cable'. The cable extends to the right, where it is 'wrapped around a fixed mandrel' (labeled 'Messenger only Wrapped Around Fixed Mandrel'). After the mandrel, the cable passes through a 'Pistoning Measurement' section. Below the cable, a 'Fiber Strain Measurement' device is connected to the 'Exposed Cable Core'. A force vector T is shown at the right end of the cable, indicating tension.

The tensile load applied to the cable was incrementally increased to 700 lbs and then reduced back to approximately no load. Two subsequent cycles were performed to confirm the fiber strain measurement and to observe any possible pistoning of the core at the cable ends. Cable and fiber strain measurements were made at each load increment.

No movement of the cable core was observed at either end of the cable sample during the load cycling, therefore, pistoning is not anticipated in the field.

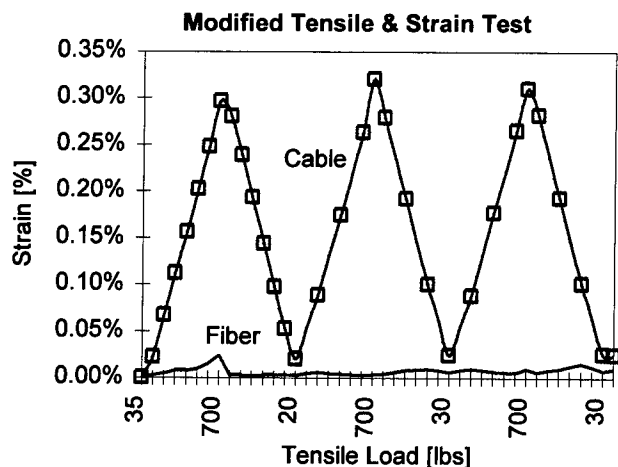


Figure 9. Cable and fiber strain results from the Tensile test.

FIELD EVALUATION

The composite service drop cable was installed in a test bed in the field to obtain handling and performance comments from the customer. Several distinctive observations were made.

Cable installation is easily achieved using standard field practices. Web slitting is accomplished using standard commercially available slitting tools. The jacket easily and cleanly stripped from the cable's messenger for messenger wire hardware attachment.

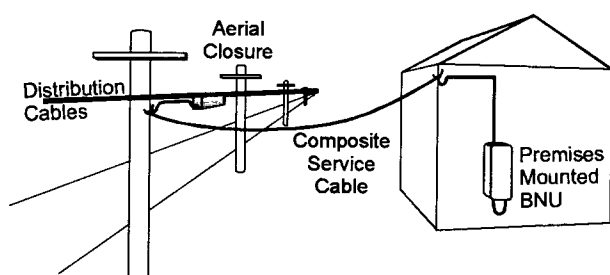


Figure 10. Intended application of the composite service cable in the FITL network.

The total cable preparation time was minimized with one common cable core, as opposed to separate copper and fiber cables. Also, the dry water blocking technology is anticipated to significantly contribute to the labor savings in the field.¹⁶

The cable core was easily mounted in an ONU housing and within an aerial splice closure using standard hardware and practices. Both housings provided a splice tray which the single, fiber filled, buffer tube was easily routed to for fiber splicing.

The copper pairs were connected to the copper distribution cable on the strand and terminated in a power connector provided within the ONU with no issues.

CONCLUSION

A new composite fiber and copper pair cable has been developed utilizing dry water blocking technologies. Flame retardant properties and a self-supporting figure-8 style construction makes this cable ideal for service drop applications.

The service cable passes applicable Bellcore and field requirements. Modified tensile, water penetration and attachment hardware tests helped predict field performance. The cable is fully compatible with standard field hardware and installation techniques.

Labor and cost savings with field deployment are expected with the single, dry core composite drop cable over dual gel-filled cables.

Future applications of a similar drop cable design minus the self-supporting messenger and with standard OSP cable materials are anticipated for direct buried and lashed aerial drop applications.

ACKNOWLEDGEMENTS

The authors would like to thank Greg Karl of Nynex for his support with the development of this cable.

REFERENCES

1. "Next Level Begins Nynex SDV Buildout," *Fiber Optic News*, ed. C.D. Chaffee, pg. 8, June 16, 1997.
2. L.K. Vanston, R.L. Hodges, "All-fiber Telecommunications Networks are Expected in the Local Loop by 2015," *Lightwave*, pp. 53-54, May 1997.
3. Personal Communications with Greg Karl at Nynex, 1997.
4. *1993 National Electrical Code Handbook*, Ed. M.W. Earley, National Fire Protection Association, 1993.
5. R.G. Gravely, S.R. Stokes, "An Improved Loose Tube Cable with Dry Water Blocking Elements," *National Fiber Optic Engineers Conference*, pp 367-375, 1995.
6. A.G. Bringuier, C.E. Clyburn, "Development of a Loose Tube Cable with Non-flooded Core for Outdoor Plant Environment," *National Fiber Optic Engineers Conference*, pp 376-386, 1995.
7. J.W. Thornton, S.M. Chastain, S.D. Motz, "Materials, Development, and Field Trials of a Dry Core Cable," *National Fiber Optic Engineers Conference*, pp 359-370, 1996.
8. H. Sawano, Y. Sato, M. Miyamoto, "The Reliability of Water Proof Optical Cable with a Plastic Sheath and Water Swellable Materials," *International Wire & Cable Symposium*, pp 333-340, 1991.
9. A.G. Bringuier, C.E. Clyburn, "Reliability of Dry Waterblocking Materials," *International Wire & Cable Symposium*, pp 779-787, 1996.
10. C2-1993, *1993 National Electrical Safety Code*, The Institute of Electrical and Electronics Engineers, Inc., 1992.
11. GR-20-CORE, *Generic Requirements for Optical Fiber and Fiber Optic Cable*, Issue 1, Bellcore, 1994.
12. TR-NWT-000122, *Generic Requirements for Multiple Pair Aerial Service Wire*, Issue 1, Bellcore, 1993.
13. GR-2879-CORE, *Generic Requirements for Hybrid Coaxial / Twisted Pair Aerial Drop Cable*, Issue 1, Bellcore, 1995.
14. TR-TSY-000843, *Generic Requirements for Optical and Optical / Metallic Buried Service Cable*, Issue 1, Bellcore, 1989.
15. EIA/TIA-RS-455-A, *Standard Test Procedure for Fiber Optic Fibers, Cables, Transducers, Sensors, Connecting and Terminating Devices, and other Fiber Optic Components*, Telecommunications Industry Association, 1991.
16. W.E. Beasley, S.R. Stokes, G. Karl, "Delivering Fiber to the Node- A New Composite Service Cable," *National Fiber Optic Engineers Conference*, 1997.



William E. Beasley

Sumitomo Electric
Lightwave Corp.
78 Alexander Drive
Research Triangle Park,
NC, 27709

William Beasley is a 1990 graduate of Duke University where he received a B.S.E. in Mechanical Engineering and a B.A. in Mathematics. He joined Sumitomo Electric Lightwave Corp. in 1990 as a Product Design Engineer supervising the Fiber Optic Cable Testing Laboratories. William is now a Senior Applications Engineer in the optical cable section. He is involved in coordinating Sumitomo's optical fiber cable development projects and accompanying accessories for broadband markets.



Tsuneo Yamazaki

Tsushin Kogyo Electric
Wire & Cable Co., Ltd.
Tsukiji MK Bld. 11-26,
2-Chome, Tsukiji,
Chuoku, Tokyo 104,
Japan

Tsuneo Yamazaki received a B.E. degree in Electrical Engineering from Toyo University in 1977 and joined Tsushin Kogyo Electric Wire & Cable Co., Ltd. He has been engaged in the development of product engineering of optical cable and connectors. He is now Manager of the Fiber Optics Development Section.



Stephen R. Stokes

Sumitomo Electric
Lightwave Corp.
78 Alexander Drive
Research Triangle Park,
NC, 27709

Stephen Stokes obtained a B.S. degree in Electrical Engineering from Virginia Polytechnic Institute and State University in 1988. He was employed by ITT Electro Optical Products Division and subsequently, Alcatel Cable Systems from 1980 to 1990 in the development of fiber optic measurement systems. From 1990 to 1991, Steve was employed by Galileo Electro-Optics Corporation as a Design Engineer in the development of light guide and imagescope products. He has been engaged in the research and development of fiber optic cables since joining Sumitomo Electric Lightwave Corp. in 1991. Steve is currently Manager of Product Design Engineering.



Mikio Kobayashi

Tsushin Kogyo Electric
Wire & Cable Co., Ltd.
Tsukiji MK Bld. 11-26,
2-Chome, Tsukiji,
Chuoku, Tokyo 104,
Japan

Mikio Kobayashi received a B.E. degree in Chemical Engineering from Toyo University in 1969 and joined Tsushin Kogyo Electric Wire & Cable Co., Ltd. He has been engaged in design and development of product engineering of communication cable. He is now Manager of Communication Cable Engineering Department.

Reliability of fiber ribbon in UV exposure environment

Tomoyuki Hattori, Atsushi Suzuki, Megumi Ban and Yasuo Matsuda

Sumitomo Electric Industries, Ltd. Yokohama, Japan

ABSTRACT

UV degradation behavior of fiber ribbon has been investigated. In an environment of UV exposure, it is found that the critical performance of fiber ribbon is the discernibility of each fiber after separation, and that almost no degradation was observed in transmission and mechanical properties after outdoor exposure for a year. It is confirmed that the partial removal of color layer could be accelerated by Xenon exposure test and that the acceleration factor for color removal is almost the same as that for the degradation of mechanical property. It is also found that the rate of deterioration of the coating layer in fiber ribbon is slower than that in film. In order to estimate the durability of fiber ribbon against a sunburning environment, the Xenon acceleration test is presumed to be suitable for fiber ribbon.

1. INTRODUCTION

While optical fiber networks are widely constructed in the world today, opportunities for their exposure to harsh environments have also increased. Aerial cable or drop cable are especially vulnerable to damage by direct sunlight or unforeseeable events. Generally the weatherability of UV curable resin, which is currently used for coating materials of optical fiber, has lower durability than cable sheath materials because additives to shield UV light, such as carbon black, cannot be applied to UV curable resin. The degradation process

of UV cured resin, especially polyurethane resin, has been widely investigated.¹ Although several studies on UV resistance for fiber coatings and coated fibers also have been made,^{2,3} they have focused on only one aspect of coating's properties or coated fibers. The evaluation program at our laboratories has been advancing studies on the weatherability of coated fibers and fiber ribbons including the clarification of the effect of each degradation factor such as heat,⁴ humidity and UV light. The purpose of this paper is to clarify a critical property of fiber ribbon in a UV exposed environment and to estimate the lifetime against UV degradation.

2. EXPERIMENTAL PROCEDURE

2-1 Sample

Model UV curable coating materials have been prepared for this investigation. Aromatic polyurethane acrylates based on ether backbone were used for the primary coating and ribbon matrix. For the aging test, coating films were drawn on a clean glass plate using a film applicator. The films were cured by a metal halide lamp in an atmosphere of nitrogen at $100\text{mJ}/\text{cm}^2$. The thickness of the test film is about $130\mu\text{m}$.

Two kinds of fiber ribbons with different ribbon matrix layer thicknesses were prepared, designated as ribbons A and B. The thickness of ribbon A is $310\mu\text{m}$ and that of ribbon B is $380\mu\text{m}$. Each ribbon contains four color-coded fibers. The optical glass fiber is a normal single-mode type with a diameter of $125\mu\text{m}$. Uncolored fiber

was also exposed to an outdoor environment to evaluate the primary coating layer.

2-2 Exposure Test

The Atlas Ci35A Xenon Exposure System was used for the accelerated test. Black panel temperature was 65°C, and irradiance was 45W/m². Test specimen were not wetted. The relative humidity in the test enclosure was maintained constant at about 40%. For the outdoor exposure test, a house with a transparent plastic roof in Yokohama, Japan was used to prevent direct contact of water to investigate the UV resistance only. The relative humidity in the house could rise up to 99%RH on a rainy day. The outdoor exposure test has been started in January, 1996.

2-3 Evaluation Method

Modulus and elongation

Tensile modulus was measured with a standard method at 1mm/min tensile speed using a 25 mm gauge length. For the evaluation of the ribbon matrix layer, test specimens were removed from the fiber ribbon with a razor blade. To evaluate the in-situ modulus of the primary coating layer, the Push-In Modulus Test⁵ was applied. Elongation was measured only for film specimens at 50 mm/min tensile speed using a 25 mm gauge length.

MEK extraction test

The amount of uncrosslinked components in coating materials was evaluated by gel fraction. About 0.15 g of the coating material was weighed and extracted for 16 hours with Methyl Ethyl Ketone (MEK) at 60°C. The gel fraction percentages (%GF) were calculated by the following equation:

$$\%GF = \frac{\text{weight (after extraction)}}{\text{weight (before extraction)}} \times 100$$

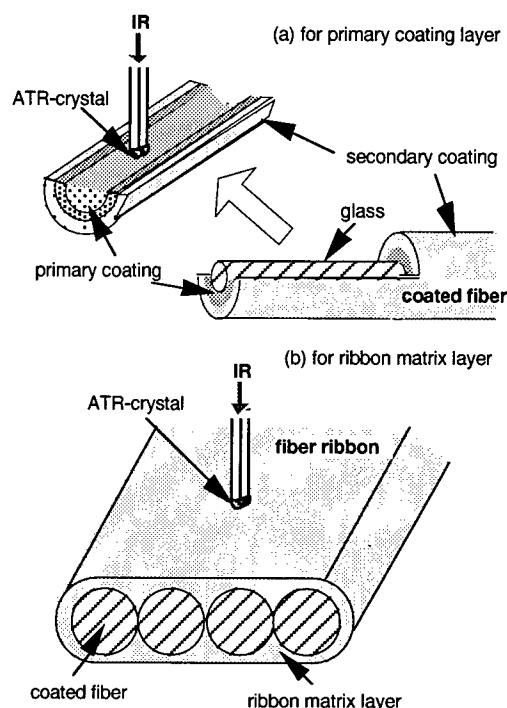


Figure 1 Scheme of μ -ATR-FT-IR method for the evaluation of coating layer

Chemical structure of coatings

IR spectra were used to evaluate the change in the chemical structure of the coating layers with the Attenuated Total Reflection (ATR) microscopy (model IR-PRAN produced by Spectra-Tech) as illustrated in Figure 1.

Transmission loss

The fiber ribbon of 700 m length was wound on a reel whose diameter was 310 mm. Before and after the exposure test, the transmission loss of the wound fiber ribbon was measured with OTDR at a wavelength of 1.55 μ m at 20°C and -40°C.

Strippability

Strippability was evaluated by two methods. One is the cleanliness after removal of the coating layers by hand with a commercial stripping tool (Hot Jacket Remover JR-4A produced by Sumitomo Electric). The test fiber ribbon was pulled out after holding firmly for 5 seconds. The other method is the force required to remove the coating using a tensile tester with the same

stripping tool. The test fiber ribbon was mounted in the sample holder of the stripper. Then the stripper was set to the tensile tester. After 30 seconds, strip force was measured at a rate of 10 mm/min with the stripped length of 30mm.

Flexibility

Flexibility of the fiber ribbon was evaluated by the following method. The test fiber ribbon was inserted between parallel face plates connected with a computer controlled motorized translation stage. Maximum bending strain was calculated by the following equation where d is the faceplate separation, and t is the thickness of the fiber ribbon.

$$\varepsilon = 1.198 \times \frac{t}{d - t}$$

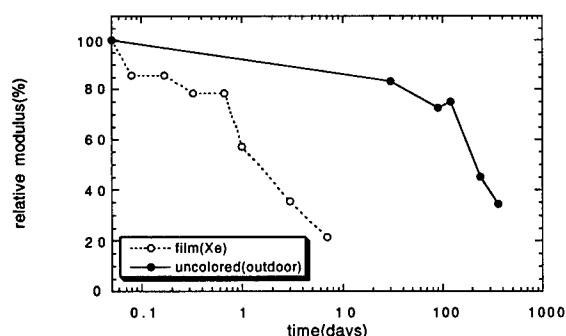


Figure 2 Change in modulus of primary coating after UV exposure

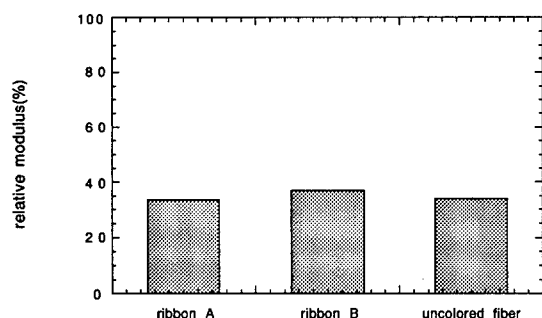


Figure 3 Comparison of modulus decrease of primary coating after outdoor exposure for a year

3. RESULTS

3-1 Mechanical properties of coating materials

The modulus of primary coating material decreased after UV exposure as shown in Figure 2. It is supposed that the main chain scission of polymer leads to the modulus decrease. A comparison of modulus change in the primary coating layer after outdoor exposure is summarized in Figure 3. It is surprising that no shielding effect of the ribbon matrix and coloring layer was observed. The mechanism is now under investigation in detail. For the ribbon matrix, the modulus increased after UV exposure, and elongation decreased in the film test as indicated in Figure 4. The modulus of the ribbon matrix in the film test was found to increase faster than that in the fiber ribbon test. The comparison of the modulus and gel fraction change for the ribbon matrix layer is shown in Figure 5. The decrease of gel fraction can be explained by the generation of low molecular weight

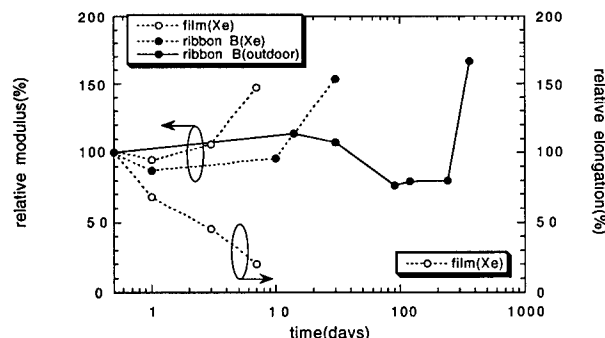


Figure 4 Change in modulus of ribbon matrix after UV exposure

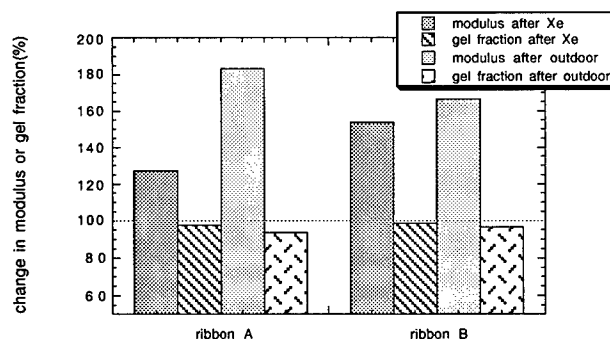


Figure 5 Change in modulus and gel fraction of ribbon matrix layer after Xenon exposure for 30 days and outdoor exposure for a year

components through UV degradation. Therefore the increase of modulus is thought to be caused by the radical recombination generated by the UV degradation process, rather than by the curing reaction. The large thickness of the ribbon matrix layer seems to slightly improve UV resistance.

3-2 Chemical structure

IR spectra of the primary coating layer after UV exposure are shown in Figure 6. The main feature of the IR spectra is that the absorption peak of the carbonyl group grew in width and height. This change indicates the main chain scission of the polymer network by photo-oxidation. Comparing the IR spectra after Xenon with outdoor exposure, the same chemical reaction seems to occur. Same trend was observed for the IR spectra of the ribbon matrix layer after UV exposure.

3-3 Performance of ribbon fiber

Transmission loss change after outdoor exposure for a year is shown in Figure 7. Both ribbons showed stable transmission loss at 25°C and -40°C. The changes in the modulus of the primary coating layer and ribbon matrix have no effect on the transmission loss of fiber ribbons after outdoor exposure.

Figure 8 indicates the strip force change of ribbon fibers. Although the strip force of 380 μ m thickness ribbon fiber is larger than that of 310 μ m thickness ribbon fiber,

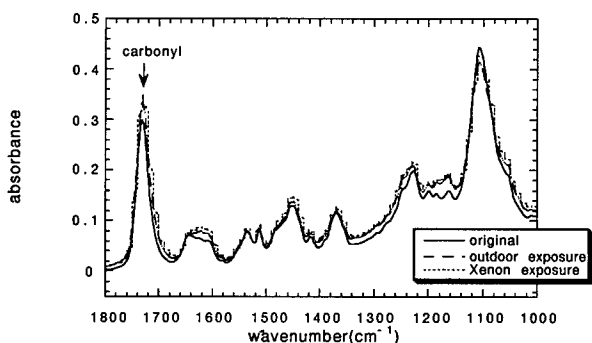


Figure 6 Change in IR spectrum after UV exposure for primary coating layer

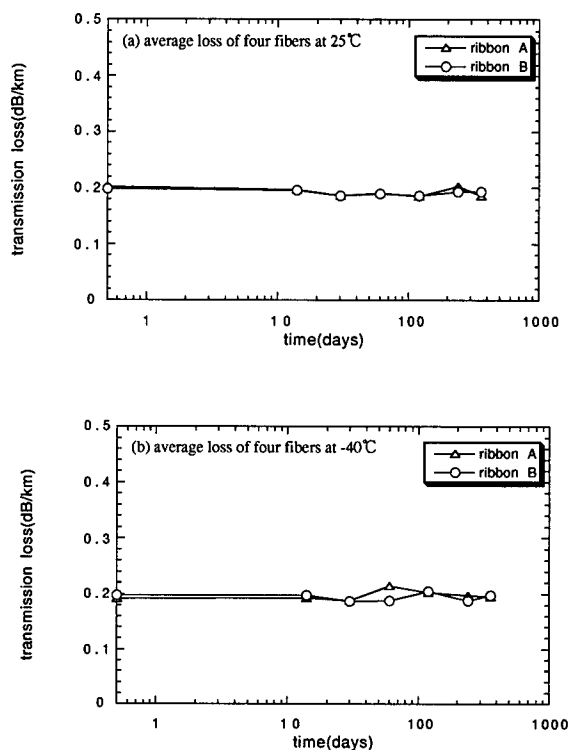


Figure 7 Transmission loss change of fiber ribbon after outdoor exposure

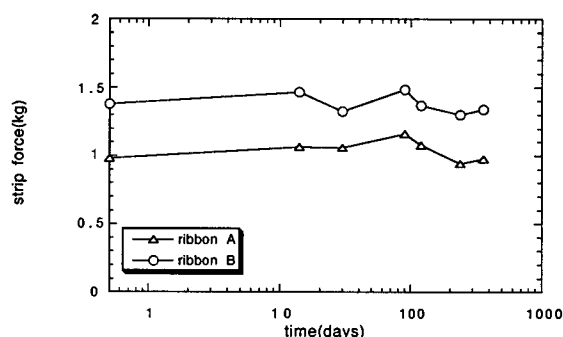


Figure 8 Strip force change of fiber ribbon after outdoor exposure

little change in strip force was observed for both fiber ribbons after UV exposure.

Other performances of ribbon fiber after outdoor exposure for a year is summarized in Table 1. Both fiber ribbons maintained good strippability. In terms of flexibility, both ribbons could be bent up to more than 20% strain (the distance between two faceplates was about 2mm), which is the upper limit of strain because of the break of glass fiber. The discernibility of each color code in fiber ribbon did not deteriorate after outdoor

exposure for a year, and each fiber could be separated from the ribbon matrix individually. The only problem in this severe environment test was the partial removal of the color layer from each fiber after separation. The partial removal of the color layer had occurred after 240 days exposure for both ribbons. In the Xenon acceleration test, the coloring removal was observed after 30 days exposure.

Table 1 Performance of fiber ribbons after outdoor exposure for a year

item	ribbon A (310 μ m thickness)	ribbon B (380 μ m thickness)
transmission loss	good	good
strippability	good	good
flexibility	>about 20%	>about 20%
separability	good	good
discernibility <i>before separation</i>	good	good
<i>after separation</i>	partial removal of color layer	partial removal of color layer

4. DISCUSSION

UV degradation reaction of urethane acrylate has been widely investigated. In the case of aromatic polyurethane, radical-induced reactions play a significant part in photodegradation.¹ This process leads to the deterioration of urethane group. Figure 9 shows the relationship between the retention of the urethane segment and the modulus of the primary coating for thermal⁴ and UV light aging. Although the chemical reactions are different between thermal and UV degradation, it may be safe to assume that the degree of the decomposition in the urethane segment dominates the change in mechanical properties of the primary coating.

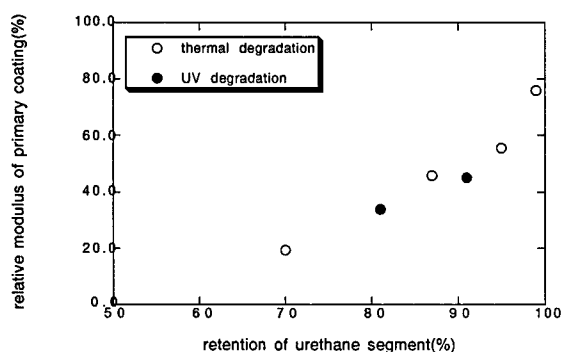


Figure 9 Relationship between retention of urethane segment and modulus of primary coating for thermal and UV degradation

Though the modulus of the ribbon matrix also changed as well after the outdoor exposure test, both changes proved to cause no degradation in the temperature dependence of transmission loss. In addition these changes in modulus are expected to have a good effect on optical characteristics under lateral force.^{6,7} It is well known that UV degradation of urethane acrylate coating causes the growth of hydrogen generation because of the hydrogen abstraction by the auto-oxidation of the polyether segment.^{2,8} If the UV exposure environment for fiber ribbon generates by accident after cable installation, however, the cable sheath or the closure will be broken. Therefore the generated hydrogen will disappear immediately and will not affect the transmission characteristic of the fiber ribbon.

Judging from the IR spectrum after Xenon and outdoor exposure, it seems reasonable to suppose that the Xenon exposure test could be available for the accelerated outdoor exposure test. Table 2 summarizes the acceleration factor for each property of the ribbon matrix. There is little difference in the acceleration factor of the Xenon exposure test between thin-coated ribbon and thick-coated ribbon. It is confirmed that partial removal of the color layer could be accelerated by the Xenon exposure test. It must be noted that the acceleration factor for color removal is almost the same as that for the degradation of mechanical property. The mechanism of the color layer removal is considered to be due to the increase of adhesion between the color layer and ribbon

matrix and the deterioration of the color layer. Concerning the evaluation of the coating film, the rate of deterioration of coating layer in the fiber ribbon is slower than that in film. Much still remains to be studied about this phenomena. In considering the validity of acceleration, the acceleration factor of the Xenon exposure test in film to the outdoor exposure test in fiber ribbon is estimated to be 45 times.

In this study, only UV light has been considered. In actual circumstances, however, fiber ribbon will be subjected to sunlight and rain. Further investigation about the effect of humidity has been progressing for studies on weatherability of fiber ribbon.

Table 2 Acceleration factor of Xenon test compared with outdoor exposure for ribbon matrix

item	ribbon A (310 μ m thickness)	ribbon B (380 μ m thickness)
modulus	10	11
gel fraction	9	7
color removal	8	8

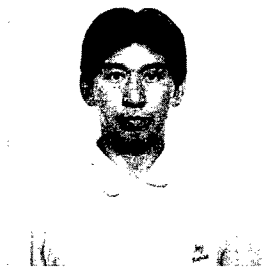
5. CONCLUSION

UV degradation behavior of fiber ribbons were investigated. In a UV exposed environment, the modulus of the primary coating layer decreased and the modulus of the ribbon matrix increased. There is little difference in the degradation behaviors between the 310 μ m thick ribbon and the 380 μ m thick ribbon. The critical performance of fiber ribbon is found to be the discernibility of each fiber after separation, and that almost no degradation was observed in the transmission and mechanical properties after outdoor exposure for a year. The Xenon acceleration test can be available for the estimation of durability of fiber ribbon. The same acceleration factor was obtained for both mechanical and chemical proper-

ties. It is also found that the rate of deterioration of the coating layer in fiber ribbon is slower than that in film.

REFERENCES

- [1] C. Decker, K. Mousa, and T. Bendaikha, "Photodegradation of UV-Cured Coatings II. Polyurethane-Acrylate Networks", J. Polym. Sci., **29**, 739 (1991)
- [2] T. Hosoya and Y. Matsuda, "UV resistance properties of UV-cured resin coated optical fiber", Proc. of 40th IWCS, 149 (1991)
- [3] K. Shiraishi, H. Nakamura, M. Ito and T. Shiono, "Study on ultraviolet degradation characteristics of optical fiber ribbons", Proc. of 45th IWCS, 537 (1996)
- [4] A. Suzuki, M. Ban, T. Hattori, N. Akasaka and Y. Matsuda, "Thermal stability of coated fiber", Proc. of 45th IWCS, 471 (1996)
- [5] K. Oishi, N. Akasaka, T. Hattori, T. Kakuta, and Y. Matsuda, "Push-In Modulus Test for primary coating of dual-coated fiber", Proc. of 43rd. IWCS, 552 (1994)
- [6] N. Akasaka, W. Katsurashima, N. Nonaka, T. Hattori, and Y. Matsuda, "Design and qualification of optical fiber coating for ribbon fiber", Proc. of 41st. IWCS, 428 (1992)
- [7] T. Kakuta, K. Oishi, N. H. Hongo, and Y. Matsuda, "A study of 16-fiber ribbon for ultra high density optical fiber cable", Proc. of 43rd. IWCS, 423 (1994)
- [8] K. Ohashi, K. Nakai, S. Kitayama, and T. Kawaguchi, "Mechanism of hydrogen Evolution and stabilization of UV-cured urethane acrylate resin for coating of optical fiber", Polym. Deg. and Stab., **22**, 223 (1988)

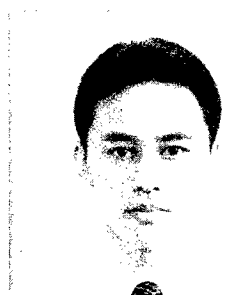


Tomoyuki Hattori

Sumitomo Electric Industries, Ltd.

1, Taya-cho, Sakae-ku Yokohama, JAPAN

Tomoyuki Hattori received his M.E. degree in Chemistry from Kyoto University in 1987. He joined Sumitomo Electric Industries, Ltd. in 1987, and has been engaged in the research and development of optical fiber and cables. He is a member of the Transmission Media Department in Yokohama Research Laboratories and a member of the Institute of Electronics and Communication Engineers of Japan.



Atsushi Suzuki

Sumitomo Electric Industries, Ltd.

1, Taya-cho, Sakae-ku Yokohama, JAPAN

Atsushi Suzuki received his M.E. degree in chemical engineering from Nagoya University in 1994. He joined Sumitomo Electric Industries, Ltd. in 1994 and has been engaged in the research and development of optical fiber and cable. He is a member of the Transmission Media Department in Yokohama Research Laboratories

Megumi Ban

Sumitomo Electric Industries, Ltd.

1, Taya-cho, Sakae-ku Yokohama, JAPAN

Megumi Ban received her M.E. degree in Applied Chemistry from Sophia University in 1992. She joined Sumitomo Electric Industries, Ltd. in 1992, and has been engaged in the research of polymeric materials. She is a member of the Analytical Characterization Center in Yokohama, the Society of Polymer Science of Japan, the Japan Society for Analytical Chemistry,

and the Chemical Society of Japan.



Yasuo Matsuda

Sumitomo Electric Industries, Ltd.

1, Taya-cho, Sakae-ku Yokohama, JAPAN

Yasuo Matsuda received his M.E. degree in Chemistry from Tokyo University in 1978. He joined Sumitomo Electric Industries, Ltd. in 1978, and has been engaged in the research and development of optical fiber and cables. He is a chief research associate of the Transmission Media Department in Yokohama Research Laboratories.

MECHANICAL RELIABILITY PREDICTIONS: AN ATTEMPT AT MEASURING THE INITIAL STRENGTH OF DRAW-ABRADED OPTICAL FIBER USING HIGH STRESSING RATES

P. T. Garvey, T. A. Hanson, M. G. Estep, G. S. Glaesemann

Corning Incorporated, Corning, New York

ABSTRACT

The strength of draw-abraded optical fiber was found to level off at stressing rates in the range of 200,000 kpsi/s (1400 GPa/s). Non-power law curvature at high speeds can be explained with a two-region power law crack velocity model. Modeling of this data enables one to incorporate complex stress/time events into lifetime predictions.

INTRODUCTION

Mechanical reliability predictions for optical fiber are based on knowledge of the initial strength and strength degradation over time from this initial value due to subcritical crack growth. The initial strength or inert strength is the strength in the absence of fatigue or subcritical crack growth. The modeling of strength degradation from this initial value is often thought of in terms of short and long-term loading events such as proof testing and in-service life, respectively. There is considerable data on the long-term fatigue of optical fiber, but significant work remains on initial strength measurements and strength degradation during short-term loading events like proof testing and fiber processing. The purpose of this paper is to report on a recent attempt at measuring the initial strength of flaws near the proof stress level and their growth during short-term loading events.

BACKGROUND

An excellent summary of initial strength measurement techniques and results up to 1995 was published by Kurkjian et al.¹ These authors concluded that measurements at liquid nitrogen temperatures have inherent difficulties and high speed testing methods need further development. Testing in vacuum is noted as a simple and direct method of measuring the

initial strength. Since this publication there have been two notable publications on initial strength measurements, both using the high-speed test method.

Gouronnec and Ev Anno² reportedly achieved stressing rates as high as 1000 GPa/s on as-drawn fiber. An example of their data shown in typical dynamic fatigue fashion is shown in Figure 1.

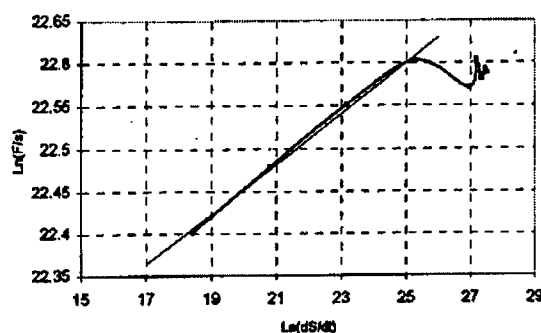


Figure 1. Strength versus stressing rate data on as-drawn fiber from reference 2.

They measured the initial strength of as-drawn fibers to be in the 6 to 7 GPa range which is similar to that measured in tension by Svensson et al.³ It has already been shown that these strengths are lower than one would expect for as-drawn fiber.⁴ In addition, the shape of the dynamic fatigue curves at the highest rates in Figure 1 show the strength to decrease at successively higher rates. It is not clear if this is the behavior of the fiber or the test technique. Whereas the results in Figure 1 are for as-drawn fiber, the interest here is the behavior of flaws near the proof stress level. It is these flaws that are affected by proof testing and in-service stresses.

The other study consisted of high speed tensile testing of draw-abraded fiber.⁴ Loading rates on the order of those experienced by fiber during proof testing were achieved. Of particular interest was the non-linear dynamic fatigue behavior at the higher loading rates. This is shown in Figure 2.

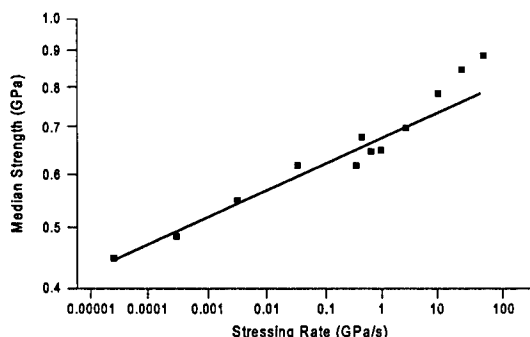


Figure 2. Dynamic fatigue plot showing curvature at high stressing rates from data in reference 4.

Evidence of reaching the initial strength level was not observed; namely, a leveling off of the strength at the highest rates. Here we seek to extend this work to see if new high-speed test methods can shorten test times enough to avoid the effects of fatigue.

EXPERIMENTATION

Draw-abraded fiber was used in this study because it is identical to standard fiber in composition and manufacturing process while providing a high density of flaws near the proof stress level. The fiber used in this study was a standard single-mode silica-clad fiber coated with CPC6 coating.

High speed testing was used in this attempt at measuring the initial strength for three reasons. First, the data obtained in successively faster stressing rates allows one to "fill in" strength values between those obtained at usual test speeds and the highest speeds. This allows observation and modeling of flaw growth behavior at speeds found during proof testing and fiber handling. Second, testing at high speeds allows one to maintain the same test environment for all tests. This reduces the possibility of other

phenomenon affecting the measured strength as is the case for testing at low temperatures.^{1,6} Some have hypothesized that the environment plays a role in the establishment of the initial strength,⁴ however, this remains to be proven.¹ Third, there have been many new developments in the area of high speed testing that hold promise for reaching and detecting the initial strength of optical fiber.

In this study three loading techniques were used to generate strength values over nearly eight decades of stressing rates. For the slower speed tests, 0.005 to 100 kpsi/s (3×10^{-5} to 0.7 GPa/s), a conventional universal testing machine^a was adapted with eight load cells and corresponding capstans. Thus, instead of the usual single fiber testing method, eight fibers could be tested in tension simultaneously. This greatly decreases the overall experimental time at the slower rates. A belt slide apparatus similar to that described in reference 3 was used to generate stressing rates ranging from 150 to 7000 kpsi/s (1 to 50 GPa/s). For the highest load rates, a pneumatic piston^b was fitted with a gas reservoir at the inlet to provide a ready volume of air for the piston chamber. Nitrogen pressure levels ranging from 40 to 95 psi (280 to 665 kPa) were used to achieve stressing rates ranging from 53,000 to 2.2×10^5 kpsi/s (365 to 1530 GPa/s).

A gauge length of 0.5 m was used for all tests. A small amount of slack in the fiber gauge length was introduced at the higher loading rates to allow the test device to reach its maximum speed before fiber loading.

Of primary importance to high speed testing is the mass of the fiber attachment system and the method of data acquisition. All tests on the belt slide and air piston were performed with two load cells in place, a conventional lightweight strain gauge load cell^c and a piezoelectric load cell.⁶ The

^a Instron Corp., Canton, MA.

^b Airmatic-Allied, Inc.

^c Interface, Inc., Scottsdale, AZ.

piezoelectric load cell was chosen such that drift and resonant frequency problems were minimized for the range of failure times used in this study.

Fiber was attached to both load cells by carefully taping the fiber to a nylon screw that was threaded directly into the load cell. The total weight of the screw and tape was approximately 1 gram. Fiber pullout from the tape was not an issue since the maximum loads were sufficiently low with the abraded fiber.

The data acquisition rate for the strain gauge load cell at the highest speeds was 40,000 HZ. At the highest loading rate the failure times were on the order of 10^{-3} seconds; and therefore, the number of data points using this load cell were considerable. The signal from the piezoelectric load cell, on the other hand, was monitored at 5×10^6 HZ using a digital oscilloscope. This yielded several thousand data points per test at the highest speed. Figure 3 shows a typical loading curve for both load cells operating at the fastest loading rate.

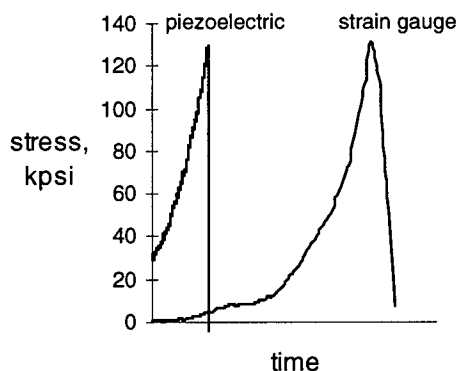


Figure 3. Loading curves for both load cell types at the fastest loading rate.

The curvature shown in Figure 3 is typical for strength test optical fiber; and therefore, the stressing rate was taken from the last 20% of the loading region. The temperature and humidity were maintained at 22°C and 50%,

respectively. A minimum of 15 specimens per loading rate were tested. Only failures in the gauge length were accepted. All Weibull slopes, m , were in the 10 to 20 range.

RESULTS AND DISCUSSION

The strength versus stressing rate is plotted in typical dynamic fatigue fashion in Figure 4. In Figure 4 only the middle two or three data points are shown for each stressing rate.

At the lower rates a typical n value in the low 20s is found. As the stressing rates increase the local slope decreases somewhat before increasing significantly at the higher rates. The last two rates have nearly the same strength values.

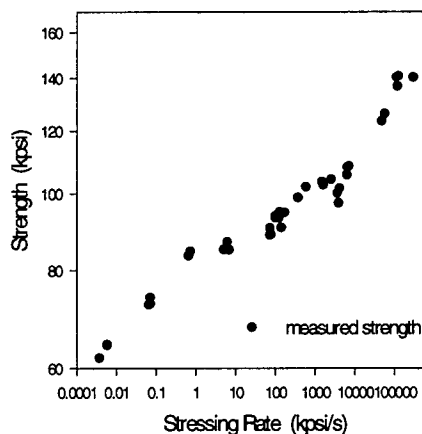


Figure 4. Middle strength values for a wide range of stressing rates in an ambient environment using draw-abraded fiber.

There are two possible explanations for the same strength values at the two fastest loading rates. Either the limit of the load detection system has been reached or strengths very close to initial strength values have been achieved. The failure times at these rates are well within the capability of the piezoelectric load cell and with the low mass attachment it is believed that the measurements are accurate.

Comparing the strengths at the highest rate to those at a typical loading rate of 6 kpsi/s (0.04 GPa/s) reveals approximately 40%

⁸ Kistler Instrument Corp., Amherst, NY.

strength degradation from the initial strength. This is in the range of what has been found for tests in liquid nitrogen environments. Note that in this comparison one must take into account the dependence of strength at low temperatures.^{1,5}

The curvature in the dynamic fatigue plot is expected. A model for such behavior has been proposed where region II type crack growth is incorporated into the basic power law crack growth model. This was first suggested by Fuller et al.⁷ for proof test events and recently was used to model optical fiber strength data obtained at high speeds.⁸ The basic model is shown in Figure 5 below in terms of crack velocity, V , and stress intensity factor, K_I .

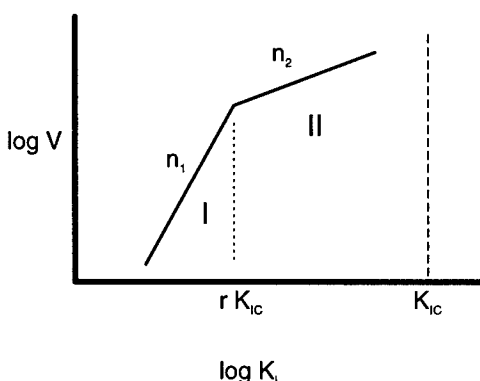


Figure 5. Schematic of the two region power law crack velocity model.

The basic mathematical form of the two region power law model is,

$$\frac{da}{dt} = V_c r^{(n_2 - n_1)} \left(\frac{K_I}{K_{IC}} \right) \text{ for } K_I \leq r K_{IC} \quad (1a)$$

$$\frac{da}{dt} = V_c \left(\frac{K_I}{K_{IC}} \right) \text{ for } K_I > r K_{IC} \quad (1b)$$

A more detailed description this model is given in reference 8. The data in Figure 4 were analyzed using this model and the results are shown in Figure 6.

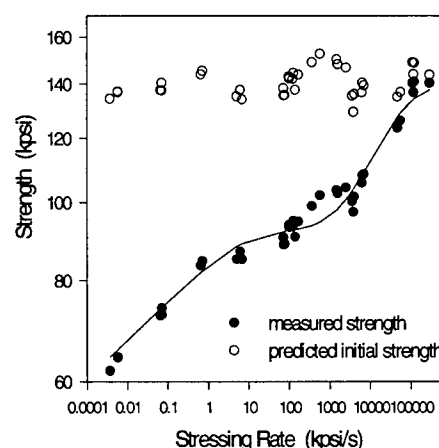


Figure 6. Predicted initial strengths and measured strengths using the two-region power law model from reference 7. the predicted measured strength using this model is shown as a line.

The open circles in Figure 6 represent the predicted initial strength for each measured strength value. The line in this figure is the predicted measured strength using the same model. There is good agreement between the predicted measured strength and the measured values with this model. This suggests that the curvature in the data can be explained using existing crack growth models.

The fact that the measured strength can be modeled over a wide range of stressing rates allows one to model a variety of fiber processing events. For example, proof testers and many coloring machines often operate at speeds well into the non-linear region of the data in Figure 4. The loading rates and dwell times on these machines can be more accurately modeled than in the past. Furthermore, this data allows one to model successive stressing events with greater accuracy.

SUMMARY

Strength testing over eight decades in stressing rates was performed on draw-abraded silica-clad fiber. A maximum stressing rate of 220,000 kpsi/s was

achieved by using an air piston. The strength leveled off approximately at a level 60% above typical testing values. The curvature in the dynamic fatigue plot was modeled using a two-region power law model. Such data combined with a proper model can be used to model multiple stress events.

ACKNOWLEDGEMENTS

The authors are grateful to D. Clark and D. Walter for experimental assistance.

REFERENCES

1. C.R. Kurkjian, D. Biswas and H.H. Yuce, "Intrinsic Strength of Lightguide Fibers," Proc. SPIE, **2611**, 56-63 (1995).
2. A. Gouronnec and N. Ev Anno, "High Speed Axial Strength Setup for the Measurement of the "B" Value," Proc. 45th IWCS, 906-913 (1996).
3. T. Svensson, "High Strain-Rate Testing of Optical Fibers," Proc. 37th IWCS, 217 (1988).
4. W. Griffioen, T. Svensson, and B. Friderich, "Optical Fiber Inert Strength and B-Value," Proc. 43rd IWCS, 750-758 (1994).
5. G.S. Glaesemann, "High Speed Strength Testing of Optical Fibers," Proc. SPIE, **2611**, 38-44 (1995).
6. G.S. Glaesemann, and J.D. Helfinstine, "Measuring the Inert Strength of Large Flaws in Optical Fibers," Proc. SPIE, **2074**, 95-107 (1993).
7. E.R. Fuller Jr., S.M. Wiederhorn, J.E. Ritter, Jr., and P.B. Oats, "Proof Testing of Ceramics, Part 2: Theory," J. Mater. Sci, **15**, 2282-2295 (1980).
8. T.A. Hanson and G.S. Glaesemann, "Incorporating Multi-Region Crack Growth into Mechanical Reliability Predictions for Optical Fiber," J. Mater. Sci, to be published.



Patrick T. Garvey
MP-RO-1
Corning
Incorporated
Corning, NY 14831

Patrick T. Garvey is a senior applications engineer for the Telecommunications

Products Division. He is responsible for providing technical support to optical fiber cable and end-user customers. Garvey joined Corning in 1992 as an environmental/mechanical engineer for the Telecommunications Products Division. He assumed his current responsibilities in 1994. Prior to joining Corning, Garvey was an engineer for General Electric Company - Knolls Atomic Power Laboratory. He holds a bachelor's degree in chemical engineering from Clarkson University and a master's degree in mechanical engineering from Union College.



Matthew G. Estep
MP-RO-1
Corning
Incorporated
Corning, NY 14831

As a senior market development engineer, Matthew G. Estep is responsible for providing engineering support

to select cable customers, and monitors changing customer requirements in evolving markets. He also manages the current technical issues surrounding mechanical reliability of optical fiber.

Estep joined Corning in 1986 working in the Advanced Fiber Products Group manufacturing specialty fibers. He then moved to the OEG Strength Lab in 1990 as a development engineer. Estep holds a bachelor of science degree in ceramic engineering from Alfred University.



Thomas A. Hanson
MP-R3-3
Corning
Incorporated
Corning, NY 14831

Thomas A. Hanson is the standards engineering manager and an engineering associate in the

Telecommunications Products Division. He is responsible for coordinating standards activities. Hanson joined Corning as a statistical engineer in 1977. He held several positions in manufacturing in the areas of quality assurance and process and product engineering. He holds a bachelor's degree in mathematics from the University of Iowa and received a master's degree in statistics from Iowa State University. Hanson is a member of the Society of Photo-Optical Instrumentation Engineers and the Telecommunications Industry Association.



G. Scott Glaesemann
SP-DV-01-8
Corning
Incorporated
Corning, NY
14831

Scott Glaesemann is a senior

development engineer responsible for the optical fiber mechanical testing laboratory at Corning's Sullivan Park technology center and has been employed by Corning for 11 years. He received his master's degree and Ph.D. in mechanical engineering from the University of Massachusetts and a B.S. in mechanical engineering from North Dakota State University.

A CONSIDERATION OF THE EFFECT OF AGEING ON THE MECHANICAL RELIABILITY OF SILICA LIGHTGUIDES BY THE USE OF STRENGTH-PROBABILITY-TIME GRAPHS

Darran R. Cairns, Stephen N. Kukureka

The University of Birmingham, School of Metallurgy & Materials, Birmingham, UK

Rosamund C. Neat

Pirelli Cables Ltd., Harlow, Essex, UK

Andrew Marshall

Pirelli Cables Ltd., Bishopstoke, Hampshire, UK

ABSTRACT

The mechanical reliability of silica lightguides is essential for maintaining the integrity of communication networks. The strength of silica is reduced in the presence of water. Two mechanisms of strength reduction have been reported in the literature: ageing and stress corrosion. In this paper strength-probability-time (SPT) graphs are used as a tool to consider the effect of ageing and stress corrosion on lightguide strength. SPT graphs for fibre aged at 85°C for 48, 128 and 238 hours are presented. These ageing times represent data obtained before, near to and after the ageing knee. Delayed fracture data were also obtained after pre-ageing in distilled water for 48, 128 and 238 hours. Predictions represented by the SPT graphs were seen to agree reasonably well with the measured delayed fracture data; the agreement after the knee raises questions about the relationship between ageing and stress corrosion. Further consideration of this relationship is suggested.

INTRODUCTION

Silica lightguides are now used extensively in communication networks. One single mode lightguide is capable of carrying

several thousand bits of information per second¹. The combination of a high data transfer rate and their widespread use ensures that the mechanical reliability of lightguides is crucial.

A method for estimating the lifetime of silica lightguides is extremely desirable. Models reported in the literature often neglect the degradation of strength due to ageing and the change in stress corrosion susceptibility with loading time, both of which have been widely reported²⁻⁴. The purpose of this paper is to consider the relative magnitudes of ageing and stress corrosion with regard to strength degradation and to examine the use of strength-probability-time graphs as a design tool.

Silica lightguides are extremely strong with tensile strengths in ambient conditions of the order of 6 GPa. The strength of silica lightguides can be described by a statistical distribution - the Weibull distribution is often used⁵. Fibre strength is also dependent upon the rate at which it is measured⁶. This dependence on strain rate (or stress rate) is due to stress corrosion.

The sub-critical crack growth model is widely used to estimate time-to-failure of lightguides. The model is based on two relationships².

The first of these is Irwin's equation⁷:

$$K_I = \sigma Y \sqrt{c} \quad (1)$$

where K_I is the stress intensity factor, Y is a shape parameter, c the flaw size and σ the applied stress. The assumptions made in applying Irwin's equation are that flaws in the fibre are atomically sharp; residual stresses are neglected and that the flaw strength is dependent on the size of the largest flaw. This model has been applied to a great number of problems in brittle fracture and is well supported in the literature⁸.

The second relationship concerns the time dependence of strength. The model is based on fatigue laws proposed by Charles⁹. Charles and more recently Wiederhorn¹⁰ have proposed both exponential and power law relationships to relate crack velocity to stress intensity factor. It is difficult to differentiate between these models with the range of experimental data available to date.

A power law relationship results in presenting a simpler mathematical problem than would be the case with an exponential relationship. It is therefore not surprising that a power law model is most often assumed. A common form of the power law expression is:

$$\dot{c} = AK_I^n \quad (2)$$

where \dot{c} is the crack-growth rate, A is a constant of proportionality and n the stress corrosion susceptibility parameter.

By combining these two relationships it is possible to derive an expression for a time-to-failure model¹¹. The most common form used is as follows:

$$t_f = \frac{2}{AY^2(n-2)\sigma^n} \left(\frac{S_i}{K_{IC}} \right)^{n-2} = B\sigma^{-n} \quad (3)$$

where S_i is the strength measured in an inert environment. Estimating B and n from accelerated tests leads to an estimate of the maximum service stress, σ , for an acceptable time-to-failure.

Concern has been expressed by a number of authors about the difficulty of finding physical significance for the B -value^{2,4}. Also of concern is the difficulty of measuring the B -value directly. In addition the sub-critical crack-growth model fails to take into account the zero-stress ageing and fatigue knees.

This study has used an alternative approach based on strength-probability-time (SPT) graphs. The two relationships on which the sub-critical crack-growth model is based are retained but, however, measurement of the B -value is not required. The SPT method also allows for predictions based on dynamic tests and experimental results from static tests to be compared. By considering ageing conditions in order to investigate the effects of ageing on lifetime predictions.

SPT graphs have previously been reported for a number of engineering ceramics^{8, 12-13} and have also been proposed as a design tool in deciding proof-test levels^{8,12}. SPT graphs show the predicted failure probability of the component as a function of applied load for a series of failure times. Their construction is described below.

AGEING

The reduction of lightguide strength in the absence of an applied stress has been reported in the literature¹⁴. A recent paper by Kurkjian, Yuce and Matthewson¹⁵ suggests that this reduction of strength is temperature dependent and can be described by an Arrhenius relationship. A 40-50% reduction in fibre strength is predicted to occur in distilled water at 25°C over a 25 year period. This strength reduction is certainly significant. Perhaps more significant is the strong dependence upon ageing temperature; at 40°C a similar reduction in strength could occur after 2-3 years. The effect of ageing on time-to-failure predictions cannot therefore be neglected.

In this study silica lightguides have been aged at 85°C in distilled water for a range of times. Prior to ageing, the fibres were pre-soaked in distilled water for 3 days under ambient conditions (25±2°C). This was to ensure that the fibres were in equilibrium

with the water before ageing began. After ageing, the fibres were allowed to cool in air and were then soaked in distilled water under ambient conditions for a further 3 days. A minimum of 20 samples were then tested, by 2-point bending, in distilled water at a strain rate of 1.667×10^{-3} (10% per minute). The data are shown in figure 1. A pronounced knee is visible after approximately 3.5 days (85 hours). In order to consider the effect of ageing on reliability, the strain-rate dependence of strength was measured after 48, 128 and 238 hours. The measured data were used to draw a series of SPT graphs. Delayed fracture tests were also performed to assess the applicability of the technique. The resulting graphs are discussed in the following section.

STRENGTH-PROBABILITY-TIME GRAPHS

An SPT graph is a plot of cumulative survival probability against failure strength for a series of times-to-failure. The theory of SPT graphs follows from Irwin's equation and the power law approximation of crack growth. Combining these relationships we have:

$$\tau \sigma^n = d \quad (4)$$

where τ is the time-to-failure for a sample under an applied load σ , d is a constant and n is the stress-corrosion susceptibility parameter. This relationship forms the basis of SPT graphs. The time-to-failure for a sample under an applied load can be calculated from:

$$\tau_c = \frac{\tau^*}{n+1} \quad (5)$$

where τ_c is the time to failure under an applied load and τ^* the time to failure at the experimental strain rate. The steps to constructing an SPT graph are as follows:

1. Measure failure strength and time-to-failure at a number of strain rates
2. Estimate values for the mean failure stress at each strain rate

3. Calculate the stress corrosion susceptibility parameter n from the slope of log strain rate versus log mean failure stress
4. Choose an anchor point (e.g. the mean of the largest data set)
5. Calculate the equivalent time-to-failure under an applied load for the anchor point using equation 5
6. Estimate a value for d by inserting the equivalent time-to-failure into equation 4
7. Estimate the Weibull modulus m , for the data set containing the anchor point
8. Choose a number of times-to-failure (e.g. 10,100,1000 seconds etc.)
9. Use equation 4 to calculate the mean applied load for this series of failure times
10. Construct failure lines for the chosen times-to-failure using the calculated means and the Weibull modulus

The SPT method depends upon an experimental constant d . This dependence on d is similar to the dependence on B of the slow crack growth models. Thus the technique of SPT graphs is an alternative to the existing time-to-failure models and is based on similar physical assumptions.

However, rather than introduce new parameters to existing lifetime models to fit the experimental data, we have made time-to-failure predictions using a simple method and compared experimental data to these SPT graphs.

SPT graphs are generated from dynamic measurements which facilitate prediction of the static behavior at long times. These long times are otherwise inaccessible experimentally.

Results

This technique has been used successfully to compare reliability predictions for various ageing times with delayed fracture tests of aged fibre.

In this study we measured failure strength at three ageing times. At each ageing time failure strength was measured at three strain

rates. These measurements were used to calculate values of n for each ageing time.

The dynamic n -values calculated are all close to 20 (18.9, 20.3 and 22). These are consistent with the n -values measured dynamically that have been reported in the literature¹⁶. The measured strength as a function of strain rate for fibre aged for 48 hours is shown in figure 2.

The anchor point was taken as that corresponding to a survival probability of 50% at a strain rate of 10% per minute. An SPT graph for fibre aged for 48 hours using this anchor point is shown in figure 3.

Delayed fracture tests were performed on aged samples by measuring time-to-failure in bending under a constant applied load. These experiments were performed in distilled water.

Because time and stress are related by $\tau\sigma^n$ is equal to a constant, then data can be transformed from one time-to-failure under an applied load to a corresponding time-to-failure at a different applied load. This principle has been applied to transform experimental time-to-failure data at a constant applied load to the distribution of failure strengths at 10 seconds.

These delayed fracture data are compared with the SPT predictions in figure 3. The delayed fracture data can be seen to lie slightly to the left of the appropriate failure line and the weakest failure data deviate significantly.

A comparison of delayed fracture data with SPT graphs for ageing times of 128 and 238 hours exhibits similar behavior. Delayed fracture data for the three ageing times, transformed to 10 seconds and compared with the corresponding lines from the SPT graphs are shown in figure 4.

Discussion

In this study we have considered dynamic fatigue by the use of SPT graphs and compared the resulting predictions with delayed fracture data. By considering static and dynamic behaviour as a function of ageing time it is hoped that further insight

into the relationship between ageing and fatigue may be gained.

In the literature, plots of stress against ageing time in an aggressive environment exhibit a knee. Graphs of load against time-to-failure (static fatigue) under similar conditions also exhibit a knee. These knees are reported as occurring at similar times³. This suggests that the two phenomena can be attributed to the same mechanism.

Typical reported values of n are 20 before the knee and 7 after the knee. This would suggest that the extent of stress corrosion increases after the knee. The reduction in n -value could be due to the increased surface roughness which is evident after the knee¹⁷.

A comparison of delayed fracture data (experimental) with SPT graphs (prediction) suggests a similar agreement before and after the ageing knee. The n -values measured by two-point bending in this study are close to 20. Although desirable, this is a somewhat surprising result. One might have expected that the dynamic n -value would not change. However one would have expected that the static n -value would have changed after the ageing knee. We may have expected the delayed fracture data to be characterised by an n -value of around 7. This would result in poor correlation between experiment and prediction. A change in the agreement between experiment and prediction was not observed.

It has been suggested that¹⁷ an increase in surface roughness at the ageing knee can be correlated with a change in the stress-corrosion susceptibility parameter. This increase in roughness could be indicative of a change in stress corrosion susceptibility parameter. If this were the case one might expect that an n -value of 7 would more accurately describe the data.

Delayed fracture data for fibre aged for 238 hours (i.e. after the ageing knee) are compared to the corresponding SPT graph using an n -value of 7 in figure 6. The correlation between experimental and predictions is much weaker than for an n -value of 20 (see fig.4).

It should be noted that the delayed fracture data in this study were measured in distilled water at ambient conditions. To our knowledge no fatigue knee has been reported for fibre under these conditions.

It has also been suggested that measurements of strength as a function of ageing time at high temperatures can be extrapolated to lower temperatures¹⁵. If this is the case fibre aged at 85°C, as in our study, should be equivalent to fibre aged at room temperature for a longer period of time.

This suggest that further work is of interest in considering the relationship between the ageing and stress-corrosion knees.

CONCLUSIONS

1. SPT graphs are a simple method for comparing graphically failure predictions with experimental data (delayed fracture).
2. The correlation between prediction and experiments are reasonable for data before and after the ageing knee.
3. SPT graphs generated using value of 20 for the stress corrosion susceptibility parameter after the ageing knee exhibited greater correlation with delayed fracture than those generated using $n=7$.
4. The use of SPT graphs facilitated a comparison between stress corrosion susceptibility parameter and ageing data.
5. Further work to consider the relationship between ageing and stress-corrosion knees would be of great interest

ACKNOWLEDGEMENTS

We would like to thank Pirelli Cables Ltd. for their support of this project.

REFERENCES

1. Senior J.M., "Optical Fibre Communications Principles and Practice" (2nd Ed), Prentice Hall (1992)
2. Matthewson M.J., "Models for Fibre reliability", SPIE **1973**, 128 (1993)
3. Kurkjian C.R., Inniss D., "Understanding Mechanical Properties of Lightguides: a Commentary", Opt. Eng., **30**, 691 (1991)
4. Ostojic P., "Stress Enhanced Environmental Corrosion and Lifetime Prediction Modelling in Silica Optical Fibres", J. Mat. Sci., **30**, 3011 (1995)
5. Olsankey R., Maurer R.D., "Tensile Strength and Fatigue of Optical Fibres", J.Appl. Phys. **47**, 4497 (1976)
6. Kalish D., Tariyal B.K., "Static and Dynamic Fatigue of a Polymer-Coated Fused Silica Optical Fibre", J. Am. Ceram. Soc., **61**, 518 (1978)
7. Irwin G.R., "Structural Aspects of Brittle Fracture", Applied Mechanics Research, **3**, 65-81 (1964)
8. Knott J.F., "Structural integrity Assessment Methods, With Particular Reference to High Duty Materials", Eng. Failure. Anal., **1**, 119 (1995)
9. Charles R.J., "Static Fatigue of Glass II", J.Appl. Phys. **29**, 1549 (1958)
10. Wiederhorn S.M., "A Chemical Interpretation of Static Fatigue", J.Am.Ceram.Soc., **55**, 81 (1972)
11. Griffieon W., Svennson T., Friderich B., "Optical Fiber Inert Strength and B-Value" Proc. IWCS **43**, 750 (1994)
12. Davidge R.W., McLaren J.R., Tappin G., "Strength-Probability-Time (SPT) relationships in ceramics", J. Mat. Sci., **8**, 1699 (1973)
13. Davidge R.W., "Engineering Performance Prediction for Ceramics", Mat. Sci. and Eng. **2**, 902 (1986)
14. Matthewson M.J., Kurkjian C.R., "Environmental Effects on the Static Fatigue of Silica Optical Fibre", J. Am. Ceram. Soc., **71**, 177 (1988)

15. Kurkjian C.R., Yuce H.H., Matthewson M.J., "Room Temperature Strength Degradation of Optical Fibres", SPIE 2611, 34 (1996)
16. Kurkjian C.R., Simpkins P.G., Inniss D., "Strength Degradation and Coatings of Silica Lightguides", J. Am. Ceram. Soc., 76, 1106 (1993)
17. Matthewson M.J., Yuce H.H., "Kinetics of Degradation During Fatigue and Ageing of Fused Silica Optical Fibre", SPIE 2290, 204 (1994)

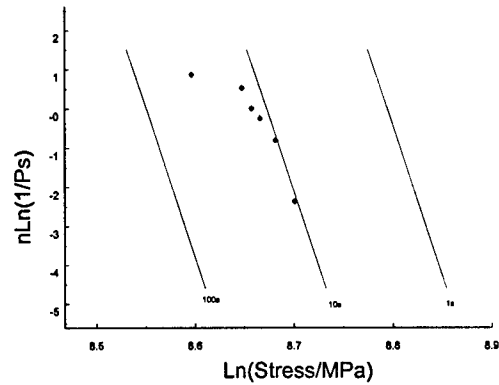


Figure 3 SPT graph for fibre aged at 85°C for 48 hours

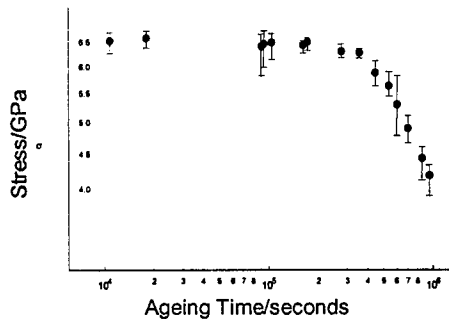


Figure 1 Failure stress versus ageing time for fibre aged at 85°C in distilled water.

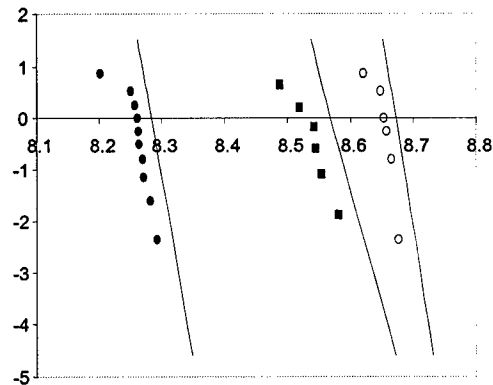


Figure 4 Ten second time-to-failure lines from SPT graphs at 48, 128 and 238 hours with delayed fracture data plotted

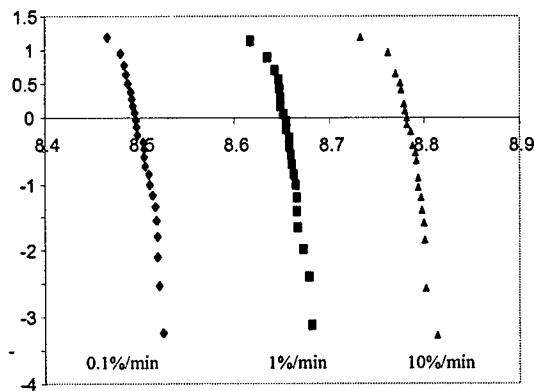


Figure 2 Cumulative Survival Probability (Weibull Scale) versus failure stress for strain rates of 0.1%, 1% and 10% per minute

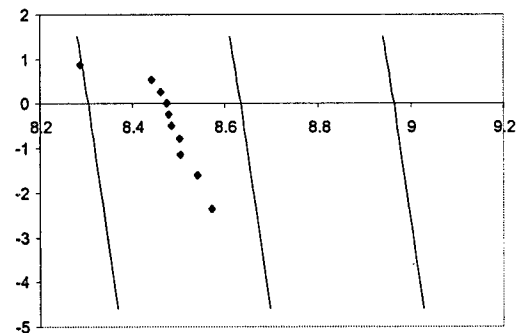


Figure 5 SPT graph for fibre aged for 238 hours. The n-value has been adjusted to 7.

BIOGRAPHIES

Darran R Cairns graduated with a BSc in Physics from the University of Birmingham in 1995. He joined the School of Metallurgy and Materials of the University of Birmingham as a graduate student in 1995. He is now working towards a PhD with a thesis on the mechanical reliability of optical fibres.

Stephen N Kukureka has a BSc in Physics from Bristol University and a PhD in Materials Science from Cambridge University. He joined the faculty of the University of Birmingham in 1990 in Metallurgy and Materials and is now director of undergraduate studies. Current research interests include the reliability of materials in telecommunications and the tribology of polymers and composites

Dr. Andrew Marshall

Engineering Manager, Optical Fibre Manufacturing Unit, Fibre Products, Pirelli Cables, Bishopstoke, Hampshire, UK

Rosamund Neat

Product Manager, Optical Fibre Unit, Fibre Products, Pirelli Cables, Harlow, Essex, UK

AN APPRAISAL OF MECHANICAL RELIABILITY PREDICTIONS FOR OPTICAL FIBERS BASED ON BREAK RATES

Aditi Paul and G. Scott Glaesemann

Corning Incorporated, Corning, New York

ABSTRACT

This paper examines the use of proof test break rates in estimating lifetime for optical fiber. The statistical basis for models that rely on break rate data is reviewed. The key assumption of the initial strength distribution following the form of Weibull distribution is examined. To test this assumption, the break rate is compared with the strength distribution after proof testing of many kilometers of fiber. Little correlation was found implying that fiber break rate is a poor predictor of the frequency of surviving flaws. This is attributed to the existence of multi-modal flaw populations in the region of proof testing. Alternate approaches that do not necessitate the use of break rate data are, therefore, found to be more appropriate in predicting mechanical fiber reliability.

INTRODUCTION

It is well known that optical fiber strength distributions are multi-modal. For example, Figure 1 shows a schematic of a typical measured strength distribution with the various regions identified. Note that even region 3 in Figure 1 has been shown to have multiple flaw populations.¹ What has received less attention is the nature of fiber strength distributions below the proof stress level. The strength distribution of these flaws are of considerable importance due to the fact that some mechanical reliability models use the failure probability at the proof stress level, i.e., break rate, in making long-term reliability predictions.^{2,3,4}

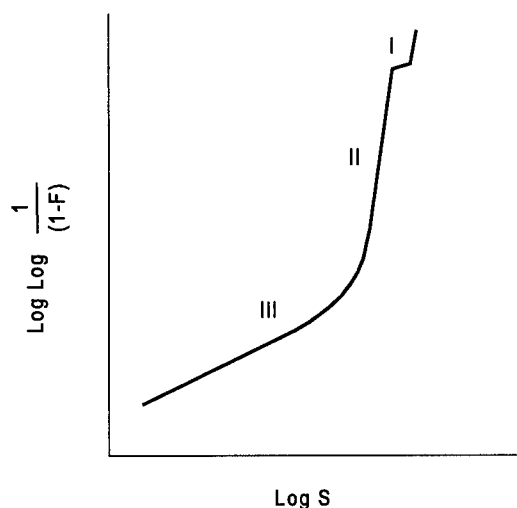


Figure 1. Schematic showing the various regions of a typical 20 meter gauge length optical fiber strength distribution.

The purpose of this research is to explore this region of the fiber strength distribution and to discuss the findings in light of the commonly assumed statistical behavior of the flaw population; namely, that flaws failing proof testing come from the same population as those surviving proof testing.

BACKGROUND

A methodology for incorporating the effect of proof testing on the strength distribution of brittle material has evolved over the years beginning with the work of Evans and Weiderhorn.⁵ One begins with the basic statistical expression of the cumulative failure probability, F , of a given length of fiber with strength S ,

$$F = 1 - \exp[-N(S)] \quad (1)$$

where $N(S)$ is the cumulative number of flaws per unit length with strength less than S . It usually is assumed for optical fiber that the initial pre-proof strength distribution follows the Weibull distribution,⁶

$$N(S) = \left(\frac{S_i}{S_o} \right)^m \quad (2)$$

where S_i is the initial strength, m and S_o are the Weibull slope and scaling parameters, respectively, for a given unit length. Therefore, the initial pre-proof test strength distribution of fiber is expressed as,

$$F = 1 - \exp \left[- \left(\frac{S_i}{S_o} \right)^m \right] \quad (3)$$

Using Eq. (3), Figure 2 shows an initial strength distribution of fiber before proof testing as a solid line.⁷

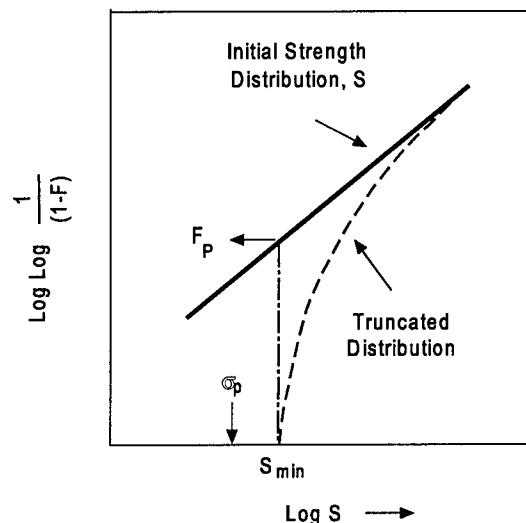


Figure 2. A Weibull strength distribution and the truncation effect of proof testing.⁷

Proof testing of fiber is incorporated through the accepted expression where the post-proof test failure probability, F_f , is expressed in terms of the initial failure probability, F_i , and the probability of failure during proof testing, F_p ,⁵

$$F_f = \frac{F_i - F_p}{1 - F_p} \quad (4a)$$

or

$$\ln \left(\frac{1}{1 - F_f} \right) = \ln \left(\frac{1}{1 - F_i} \right) - \ln \left(\frac{1}{1 - F_p} \right) \quad (4b)$$

This is a general expression for obtaining the post-proof test failure probability for any distribution. The post proof test failure probability, F_f , for an initial strength distribution, F_i , that is Weibull is obtained simply by substituting Eq. (3) into Eq. (4),

$$\ln \left(\frac{1}{1 - F_f} \right) = \left(\frac{S_i}{S_o} \right)^m - \ln \left(\frac{1}{1 - F_p} \right) \quad (5a)$$

or

$$F_f = 1 - \exp \left(- \left[\left(\frac{S_i}{S_o} \right)^m - \ln \left(\frac{1}{1 - F_p} \right) \right] \right) \quad (5b)$$

The predicted truncation of an initial Weibull strength distribution as a result of proof testing is shown in Figure 2 as a dashed line.

Proof testing is the process by which flaws below a particular level S_{\min} are eliminated by applying a proof stress, σ_p . The probability of a given length failing at S_{\min} during proof testing is taken from Eqs. (2) and (3) where $F_i = F_p$,

$$\ln \left(\frac{1}{1 - F_p} \right) = N_p = \left(\frac{S_{\min}}{S_o} \right)^m \quad (6)$$

where $S_i = S_{\min}$ is the initial strength at the proof stress. $\ln(1 - F_p)^{-1} = N_p$ is the cumulative number of flaws failing below S_{\min} or simply the break rate for a given length of fiber. The break rate is estimated by counting the number of breaks over a length of processed fiber.

Substituting Eq.(6) into Eq.(5) gives the post-proof test failure probability, F_f , in terms of

the initial strength distribution and the break rate, N_p ,

$$F_f = 1 - \exp \left(- \left[\left(\frac{S_i}{S_o} \right)^m - N_p \right] \right) \quad (7)$$

It is important to note that by assuming the initial strength distribution to be Weibull the flaws that contribute to break rate, those less than S_{\min} , are from the same initial population as those surviving proof testing, $> S_{\min}$. This can be seen in Eq.(6) as well as in Figure 2. If the overall failure probability of the initial strength distribution increases, both the break rate and the overall failure probability of the flaws surviving proof testing increase. This point is illustrated in Figure 3 where two initial strength distributions with the same Weibull slope, m , but different scaling parameters, S_o , are proof tested at the same stress level. The break rate and the post-proof test failure probability increase with a shift to the left in the initial strength distribution.

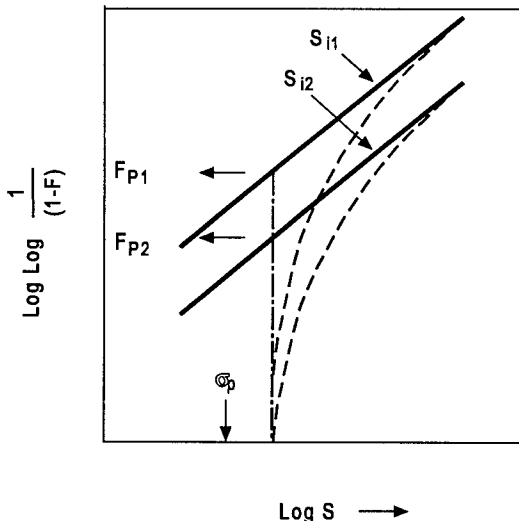


Figure 3. How the initial strength distribution affects the break rate and the post-proof test failure probability.

This is reflected in existing fiber failure probability models based on break rate and can be shown more clearly by substituting Eq.(6) into Eq.(7) and rearranging to give,

$$F_f = 1 - \exp \left(- N_p \left[\left(\frac{S_i}{S_{\min}} \right)^m - 1 \right] \right) \quad (8)$$

In practical terms, it follows from Eq. (8) that the fiber with the higher break rate has a poorer post-proof test strength distribution. Furthermore, it is thought that by monitoring the break rate the risk of field failures can be determined for that fiber. Again, this is predicted on the assumption that the initial strength distribution is Weibull.

In this paper we examine the basic underlying assumption that the initial strength distribution follows the Weibull distribution and, therefore, that the break rate is a measure of optical fiber reliability.

POST-PROOF TEST STRENGTH DISTRIBUTION AND BREAK RATE DATA

In the previous section it was shown that the number of flaws failing proof testing should correlate with the number surviving assuming the initial pre-proof test strength follows a Weibull distribution. An attempt was made at examining this correlation by comparing the proof test break rate of fibers from individual preforms and the number of flaws surviving the proof test event.

Fiber was generated from 34 preforms manufactured over an 18 month time period. The break rate was estimated by counting the number of flaws that fail during proof testing at 0.69 GPa (100 kpsi) and dividing by the length proof tested. To characterize the post-proof test strength distribution a minimum of 30 kilometers from each preform was strength tested on a continuous fiber strength testing apparatus to 2.45 GPa (350 kpsi). This apparatus has been described in detail elsewhere.⁸ Its operation consists of stressing sequential 20 meter sections of a given reel of fiber to a pre-determined stress level, such as 2.45 GPa. In this way all the flaws below this stress level are loaded to failure and those surviving are accounted for statistically.

The post-proof failure probability, F_f , was taken from the 1.4 GPa (200 kpsi) strength level on the post-proof Weibull distributions from each fiber. That is to say, the proof test survivors used to represent the post-proof test strength distribution were obtained by simply counting the number of flaws that failed at or below 1.4 GPa (200 kpsi) during post-proof strength testing and dividing that value by the number of kilometers tested for that fiber. The stress level of 1.4 GPa (200 kpsi) was chosen to avoid the interference of other Weibull modes known to exist above this strength level.

RESULTS AND DISCUSSION

Figure 4 is a plot of the 0.7 GPa proof test break rate versus the frequency of flaws below 1.4 GPa after proof testing. Each data point in Figure 4 represents data from a single preform. Note that the proof test break rate has been normalized for proprietary reasons.

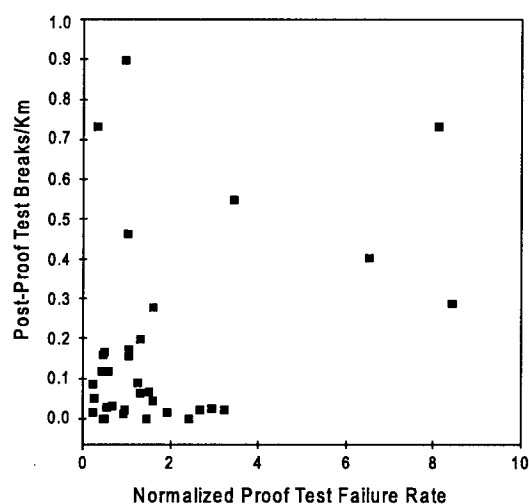


Figure 4. comparison of break rate from proof testing at 0.7 GPa and the frequency of flaws below 1.4 GPa from the post-proof strength distribution.

There is little correlation between the proof test break rate and the frequency of flaws surviving proof testing suggesting that break rate is not a good predictor of the post-proof strength distribution.

It is believed that the lack of correlation observed in Figure 4 is due simply to multiple flaw populations in the region of the strength distribution affected by the proof test. It is quite common for brittle materials to exhibit multi-modal strength distributions. For example, optical fiber is shown in Figure 1 to have several distinct strength distribution regions above the proof stress level. Such regions in the strength distribution also can exist below the proof stress level.

Assuming the initial strength to be a single Weibull distribution when in fact it is multi-modal can cause reliability models based on break rate to either overestimate or underestimate the post-proof test failure probability. Figure 5 shows three distributions, two of which are bi-modal in the region of the proof test stress and one is the usual uni-modal shape.

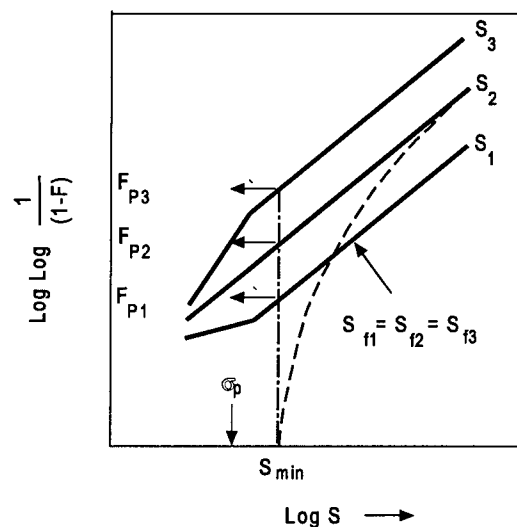


Figure 5. The effect of a multi-modal initial strength distributions on break rate and the post-proof test strength distribution.

With an initial strength distribution S_{i1} there exists a large population of flaws with strengths less than the proof stress level. For optical fiber, these flaws usually result from mechanical abrasion to the fiber surface before the coating is applied, surface contamination, or internal contamination during preform manufacturing. In this case

the flaw population above the proof stress level is shown to be the same as that for the uni-modal distribution, S_{i2} . When proof testing fiber with distribution S_{i1} the break rate will be higher than that for S_{i2} , however, the post-proof strength distributions will be the same. Thus, the break rate would predict a poorer post-proof strength distribution than what actually exists after proof testing.

In the case of distribution S_{i3} the situation is reversed from that of S_{i1} . Here the manufacturing process has provided fewer flaw sources that contribute to breaks during proof testing and so the break rate is lowered. However, flaws above the proof stress level are, again, from the same population as the uni-modal distribution and so the post-proof test distribution is identical to that of the uni-modal distribution.

One can see that the effect of multi-modal strength distributions in the range of the proof test stress is to frustrate the convenient assumption of an initial strength distribution that is Weibull.

The question remains, how can one improve the confidence in post-proof test failure probability predictions? The temptation is to assume a conservative break rate, N_p , in Eq. (8). However, one risks the situation where a process consistently produces a particular multi-modal strength distribution. This is especially true in the case where the process produces a distribution similar to S_{i1} in Figure 5. Here one could grossly overestimate the post-proof test failure probability. Basing the reliability model on an actual measured fiber strength distribution, though time consuming, would be the best method for improving confidence in failure probability predictions. However, from the data in Figure 4 one observes some variability here as well. This is mitigated by choosing an overall distribution for modeling purposes that passes through the middle of the data. Where there is wide variability in the post-proof test strength distribution from fiber to fiber, one would choose a more

conservative estimate of the overall distribution for modeling purposes.

SUMMARY

Mechanical reliability models employing the fiber break rate as a convenient measure of post-proof test fiber reliability have an implicit assumption that the failure probability of fiber lengths surviving proof testing can be measured by the break rate. Extensive data comparing the post-proof strength to the break rate show a lack of correlation. It is shown that initial strength distributions that are multi-modal in nature give rise to such behavior. Knowledge of the actual post-proof test strength distribution is the best means of reducing uncertainty in fiber failure probability predictions.

ACKNOWLEDGMENTS

The authors thank T. Hanson, S. Edens, J. Hunter, R. Trapp, E. Hodge, and D. Smith for their helpful insights and technical support.

REFERENCES

1. G. S. Glaesemann, "Optical Fiber Failure Probability Predictions from Long-Length Strength Distributions," pp.819-825 in proceedings of the 40th International Wire & Cable Symposium, St. Louis, Mo., 1991.
2. E.R. Fuller, Jr., S.M. Wiederhorn, J.E. Ritter, Jr., P.B. Oats, "Proof Testing of Ceramics, Part 2 Theory," J. Mater. Sci., 15, 2282-2295 (1980).
3. Y. Mitsunaga, Y. Katsuyama, H. Kobayashi, and Y. Ishida, "Failure Prediction for Long-Length Optical Fiber Based on Proof Testing," J. Appl. Phys. 53 (7), 4847-4853 (1982).
4. J.G. Titchmarsh, "Failure Rate as the True Parameter of Optical Fibre Reliability," pp. 441-416 in proceedings of the 41st International Wire & Cable Symposium, Reno, Nevada, 1992.
5. A.G. Evans, and S.M. Wiederhorn, "Proof Testing of Ceramic Materials - an Analytical Basis for Failure Prediction.
6. W. Weibull, "Statistical Distribution Function of Wide Applicability," J. Appl. Mech., 18 (3) 293-297 (1951).

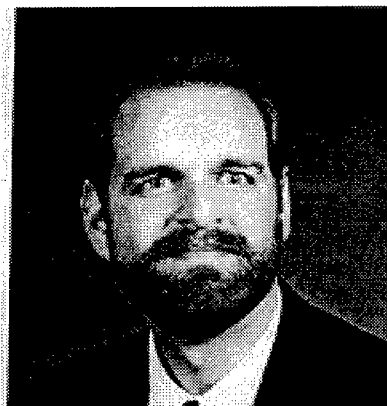
7. A.G. Evans and E.R. Fuller, "Proof Testing - The Effects of Slow Crack Growth," Mat. Sci. and Eng., 19, 69-77 (1975).
8. G.S. Glaesemann and D.J. Walter, "Method for Obtaining Long-Length Strength

Distributions for Reliability Prediction," Opt. Eng., 30 (6) 746-748 (1991).



Aditi Paul
MP-RO-1
Corning Incorporated
Corning, NY 14831

Aditi Paul is a Product Engineer in Corning's Telecommunications Products Division. She has worked on strength and mechanical reliability issues at Corning and on issues relating to coating reliability. Aditi joined Corning in 1996 after having gained work experience at Bellcore's Morristown NJ strength lab in 1995. She has a masters degree in physical chemistry from the Indian Institute of Technology, Kharagpur and another Masters degree from Alfred University, New York where her research involved spectroscopic studies of zeolites and calcium phosphate glass-ceramics.



G. Scott Glaesemann
SP-DV-01-8
Corning Incorporated
Corning, NY 14831

Scott Glaesemann is a senior development engineer responsible for the optical fiber mechanical testing laboratory at Corning's Sullivan Park technology center and has been employed by Corning for 11 years. He received his master's degree and Ph.D. in mechanical engineering from the University of Massachusetts and a B.S. in mechanical engineering from North Dakota State University.

Kinetics Models for Fatigue of High-Strength Fused Silica Optical Fiber

J. L. Armstrong,¹ M. J. Matthewson,¹ C. R. Kurkjian,² and C. Y. Chou¹

¹Rutgers University, Piscataway, New Jersey

²Bell Communications Research, Morristown, New Jersey

ABSTRACT

The strength and dynamic fatigue behavior of fused silica fiber has been measured as a function of the ambient humidity, both when the fiber is bare and polymer coated. The use of bare fiber is important since it makes it possible to separate the effects of fatigue and mass transport through the coating. The results for coated fiber verify earlier work that suggests that the degradation reaction is approximately second order with respect to humidity in the range of 20-95% RH; the bare fiber shows similar trends. A purpose-designed computer program is used to simultaneously analyze the effects of loading rate and humidity in a self-consistent manner. The results are consistent with a simple chemical kinetics model in which the degradation rate shows an exponential dependence on stress. In contrast, careful dynamic fatigue experiments have been found to empirically show better agreement with a power law kinetics model.

INTRODUCTION

Even though there have been many studies of the strength and fatigue behavior of fused silica fiber, no self-consistent detailed model has emerged for the degradation kinetics, which relates the crack growth rate to the applied stress intensity. A power-law model has been widely used for making reliability predictions even though it is not based on any physical model and even though it predicts longer lifetimes than other, more physically reasonable models.^{1,2} Additionally, the effect of such

environmental parameters as temperature, humidity, or pH, are usually either ignored (by assuming that the proof testing, strength testing and service environments are all the same) or are incorporated in an empirical fashion.

The commonly used power law model for lifetime predictions is mathematically simple to manipulate, but is empirical and has no physical basis. Environmental effects, such as temperature, cannot be incorporated in a self consistent manner.³ The power law, designated model 1 here, may be expressed in the form:

$$\frac{dc}{dt} = A_1 \left(\frac{K_I}{K_{IC}} \right)^{n_1}, \quad \text{Model 1 (1)}$$

where n_1 is the stress corrosion parameter, K_I is the stress intensity factor, K_{IC} is the critical stress intensity factor, and A_1 is a scaling parameter. n_1 is usually assumed to be a material constant which represents the sensitivity of fatigue to stress and A_1 depends on the environment. If we assume a simple chemical kinetics model for fatigue where the reaction rate between water and silica determines the crack growth rate, A_1 may be expressed as

$$A_1 = \nu f(a_{H_2O}) \exp\left(-\frac{Q}{RT}\right), \quad (2)$$

i.e. the reaction kinetics are thermally activated with an activation energy, Q , and has some functional dependence on the water activity, $f(a_{H_2O})$; and ν is a frequency factor. In this model the activation energy, Q , is assumed to be stress independent even though there is evidence to the contrary.⁴ a_{H_2O} is the

thermodynamic activity of the water. For water vapor at moderate pressure, a_{H_2O} is equal to the partial pressure of water vapor, p_{H_2O} . At a given temperature, p_{H_2O} is proportional to the relative humidity

$$RH = \frac{p_{H_2O}}{p_{H_2O}^{sat}} \quad (3)$$

The reaction between water and silica is not in the vapor phase, but assuming that the water at the crack tip is in equilibrium with the vapor (a good approximation since the fibers are strong meaning that very little water is consumed by the growth of such small cracks), Eq. (2) then reduces to the form:

$$A_1 = v_1 f_1(RH) \exp\left(-\frac{Q}{RT}\right) \quad (4)$$

The more physically reasonable chemical kinetics model proposed by Wiederhorn,⁵ assumes that the stress at the crack tip modifies the activation energy of the chemical reaction via an activation volume. This leads to a kinetics model (designated model 2) of the form:

$$\frac{dc}{dt} = A_2 \exp\left(n_2 \frac{K_I}{K_{IC}}\right), \quad \text{Model 2} \quad (5)$$

$$\text{where } A_2 = v_2 f_2(RH) \exp\left(-\frac{Q_0}{RT}\right), \quad (6)$$

and where Q_0 is the activation energy under zero applied stress. In this model the activation energy is linearly dependent on K_I (i.e. it treats stress as if it were a negative hydrostatic pressure).

A third model (designated model 3), based on an analysis due to Lawn⁶, assumes that the strain energy density at the crack tip modifies the activation energy as a contribution to the chemical potential. After some simplification, this leads to a quadratic dependence of the activation energy on the stress and hence

$$\frac{dc}{dt} = A_3 \exp\left(n_3 \left(\frac{K_I}{K_{IC}}\right)^2\right), \quad \text{Model 3} \quad (7)$$

$$\text{where } A_3 = v_3 f_3(RH) \exp\left(-\frac{Q_0}{RT}\right) \quad (8)$$

Lifetime extrapolations are sensitive to the assumed form of the kinetics model.^{3,2} Determination of the kinetics model by measurement of both static and dynamic fatigue over a broad range of failure times tends to favor the power law, model 1.³ An alternative way of assessing models is to examine the environmental dependencies. The above three models all assume that the stress dependence is contained in the n_i , ($i=1..3$), while the environmental dependence is contained in the A_i , and explicitly depends on the humidity by the functions $f_i(RH)$. In this paper we examine the kinetics models by measuring the strength and dynamic fatigue at various humidities to determine which model is most consistent with the data; i.e. shows the least dependence of n_i on humidity. Further, we will use the results to determine the reaction order, m , defined by

$$f_i(RH) = RH^m \quad (9)$$

While the humidity dependence of strength of fiber has been studied elsewhere,^{4,7,8} none of these studies interpreted their results in terms of kinetics models. The data are generally sparse and only consider polymer coated fiber. Since the presence of the coating may perturb the kinetics, we will present results not only for coated but also for bare fiber.

The derivation of fatigue equations combines with the crack growth kinetics equation (1), the concept of sharp, well-defined cracks, as embodied by the Griffith equation:

$$K_I = \sigma_a Y c^{1/2} \quad (10)$$

However, pristine fiber does not contain such cracks.⁹ The fatigue equations are very much more dependent on the kinetics equation (1) because of its stronger dependence on stress. Therefore, even though the micromechanical details of the weakening process described by equation (10) are probably not accurate, use of the standard fatigue equations gives a good description of the degradation kinetics

EXPERIMENTAL PROCEDURE

The specimens used in this study were 125 μm diameter fused silica coated fiber with a UV-curable polyurethane-acrylate, giving an overall diameter of 250 μm . The fiber strength was measured at five different faceplate velocities (1, 10, 100, 1000, 5000 $\mu\text{m/s}$) using a two-point bending apparatus.¹⁰ The strength was measured in different humidities by allowing the coated fiber to equilibrate overnight in the appropriate environment, which ranged from 20 to 95% RH at $25 \pm 0.1^\circ\text{C}$. Bare specimens were prepared by stripping the coating in $\sim 200^\circ\text{C}$ concentrated sulfuric acid. Stripping in this way does not degrade the strength of the fiber provided sufficient care is taken.¹¹ Bare fibers were tested immediately after immersion in the humid environment since it was found that no equilibration time was necessary. Since only one bare specimen can be broken at a time, ten samples were measured at each speed. Twenty samples were measured at each speed for the coated specimens.

The strength data were fitted to each of the kinetics models and the fatigue parameters, A_i and n_i , were determined by utilizing a computer program. Probably the main reason the power law (Eq. 1) is used so widely is that it is comparatively simple to extract analytic expressions for fatigue behavior under simple loading conditions. In contrast, the exponential forms (Eq. 5 and 7) are not analytically integrable for dynamic fatigue (constant rate of loading). Fitting to experimental data was therefore achieved using a purpose-written computer program to perform the integration and parameter fitting. A key feature of the program that distinguishes it from earlier work¹ is that it performs careful statistical analysis in order to estimate the confidence limits on the fit parameters together with their cross correlations. Throughout this work, reasonable

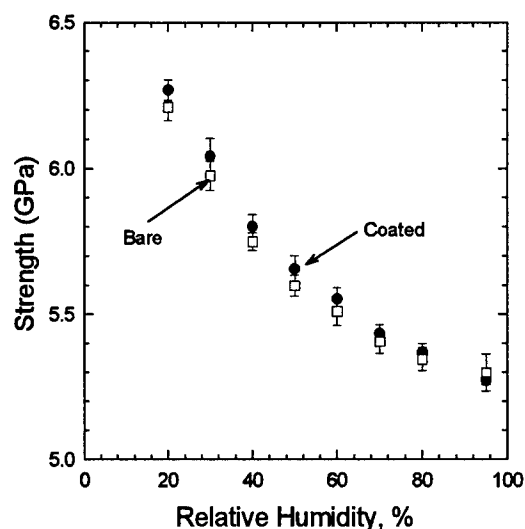


Figure 1: The strength of both the bare and coated fibers as a function of relative humidity, calculated for a faceplate velocity of 75 $\mu\text{m/s}$.

values for key parameters were assumed: $K_{IC} = 0.75 \text{ MPa}\cdot\text{m}^{1/2}$, $Y = 1.16$, and $\sigma_i = 12 \text{ GPa}$. The n_i values are sensibly independent of these parameters; the A_i values are not independent but, while their magnitudes do depend on the values chosen, the trends observed with humidity do not change. Therefore all of the conclusions drawn from this work are independent of these values. All error bars presented here represent a 95% confidence interval.

RESULTS AND DISCUSSION

Figure 1 shows the strength of coated and bare fibers as a function of relative humidity. These data were interpolated from all five faceplate speeds to a speed of 75 $\mu\text{m/s}$. This effectively considers all of the data to give a smaller error bar than would be obtained from the data at a single speed.¹² The coated and bare fibers show similar trends. The relationship between the strength and humidity is nonlinear, both on this graph and on a semi-log plot.

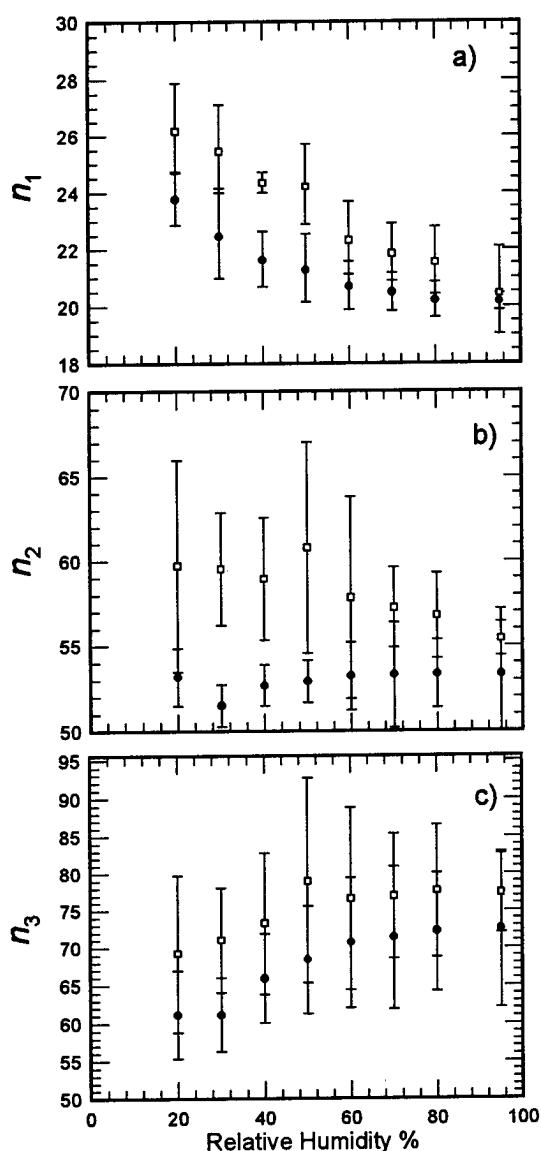


Figure 2: Fatigue parameter, n_i , for each model vs. relative humidity for (●) coated fiber and (□) bare fiber.

The fatigue parameters, n_i and $\log A_i$, found by fitting model 1 to the humidity data, are shown in Figures 2(a) and 3(a) and (d). The value of n_1 shows a systematic decrease with humidity for both bare and coated fibers, while the value of A_i is roughly constant; as described above this violates a common assumption of model 1, that the humidity should be solely contained in A_1 . This represents an internal inconsistency with the power law model if it is to be considered as anything other than purely empirical. Earlier

work also showed similar trends in n_1 . (e.g. ref.4). These trends in n_1 are modest compared with the size of the error bars. However, this is deceptive since the trends in the raw data are clear. The error bars are large because the values of A_i and n_i are strongly correlated. Since the models all assume that n_i are constant, we found values for A_i assuming fixed values for n_i which is calculated from a weighted average of the values in Figure 2. This is a weak constraint since it uses an underlying assumption of the models. The result of the constraint is that the error bars on A_i are substantially smaller and more closely represent the obvious trends in the raw data. However, Figures 3(a) and (d) show that the value of A_1 found by constraining n_1 (triangles) show different trends compared to the unconstrained values (squares). This again shows that model 1 does not give a consistent description of the data.

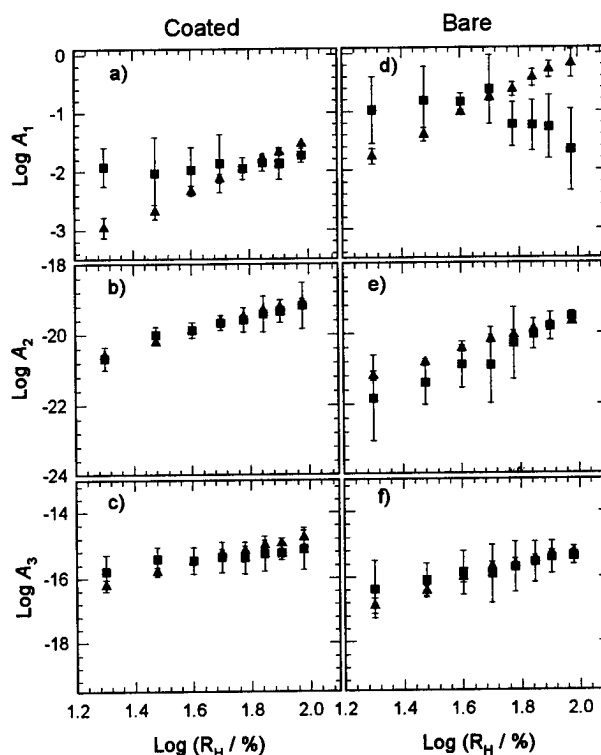


Figure 3: $\log A_i$ vs. \log (Relative Humidity) using (■) unconstrained and (▲) constrained values of n_i . (a) to (c) are for coated fibers, and (d) to (f) are for bare fibers

Table I: Reaction orders calculated for each model using (u) unconstrained and (c) constrained values for the n_i 's

	Coated		Bare	
	u	c	u	c
Model 1	0.40 ± 0.28	2.16 ± 0.12	-1.17 ± 0.87	2.48 ± 0.15
Model 2	1.98 ± 0.40	2.31 ± 0.14	3.68 ± 0.27	2.18 ± 0.26
Model 3	0.75 ± 0.29	2.12 ± 0.22	1.51 ± 0.17	2.29 ± 0.34

Figures 2 and 3 also show the fit parameters for models 2 and 3. Model 2 shows the least dependence of n_i on humidity. The constrained and unconstrained values of A_2 show essentially identical behavior. Model 3 shows some discrepancy between constrained and unconstrained A_3 values, though not as severe as for model 1.

The reaction order, m , in Eq. 9, can be determined by the slopes of the data in Figure 3, and results are shown in Table I. Values are given for fits to A_i for both the constrained and unconstrained values of n_i . Clearly the values for model 2 are more reliable since the constrained and unconstrained values are the same. Here all models give similar values for the constrained data, but substantially different values for the unconstrained data. These clearly show that calculations of a reaction order from strength data must be performed with care. The results may be dependent upon which kinetics model is assumed. We show here that the reaction order is roughly independent of the kinetics model assumed only if a constant value of n_i is assumed, even if it is observed to vary with the environment.

From Table I, the reaction order for coated fiber is around two. This value is in agreement with Duncan *et al.*⁴ who analyzed their data assuming a power law. An approximate second order was also found for E-glass fibers.¹³ A 2.5 order was obtained from direct measurements of slow crack growth rates.¹⁴ The simplest interpretation of a second order reaction is that two water molecules take part in the rate

determining step. The actual reaction mechanism, while not known, is likely to be much more complex.

Up until this point, each model has been discussed in terms of how well it incorporates the dependence on the test environment. It is also important to examine how well each model fits the dynamic fatigue data, irrespective of the environmental conditions. Figure 4 shows the residual sum of squares for each model as a function of relative humidity; the model that fits the best will have the smallest residual sum of squares. From Figure 4, it is clear that model 3 gives by far the worst fit. The residual sum of squares for models 1 and 2 give similar degrees

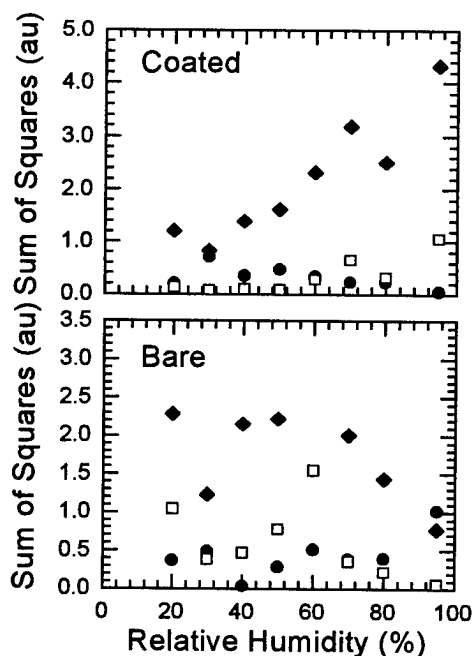


Figure 4: Residual sum of squares vs. relative humidity • Model 1 □ Model 2 ♦ Model 3

of fit. These results are consistent with earlier, more extensive experiments³, which also showed a poor fit for model 3 but a considerably better fit for model 1.

Reliability predictions usually avoid considering the values of K_{IC} and Y by using the so-called B parameter:

$$B = \frac{2K_{IC}^2}{AY^2(n-2)}, \quad (11)$$

which separates fatigue effects and the inert strength. The value of B is a subject of discussion since its value is sensitive to the assumed inert strength, σ_i . However assuming $\sigma_i = 12$ GPa, we found B , calculated from the unconstrained values of A_1 , is in the range of $(2.5 - 4.4) \times 10^{-6}$ GPa².s for the coated data and $(0.16 - 2.08) \times 10^{-6}$ GPa².s for the bare. If the value of n_1 is constrained, B ranges from 1.55×10^{-6} to 4.07×10^{-5} GPa².s for the coated data and 5.82×10^{-8} to 2.23×10^{-6} GPa².s for the bare over the humidity range 95 to 20% respectively.

The above three models were also fitted to data for polyimide, silicone, and double buffer acrylate coated fibers and similar trends and results were found for the reaction order.

CONCLUSIONS

The results show that fatigue data must be analyzed carefully in order to extract valid values for parameters such as the apparent reaction order with humidity. In particular, the values obtained may depend as much on the kinetics model assumed as anything else. We outline a protocol for calculating the reaction order independently of the kinetics model. The strength degradation kinetics of both coated and bare fiber are approximately second order in humidity.

While in earlier work the power law was found to give the best fit to fatigue data, we show here that the power law gives a poor and inconsistent description of the humidity dependence. The

simple exponential model, $\sim \exp(K_1)$, gives the best description of the humidity data and a moderately good fit to fatigue data. The quadratic exponential, $\sim \exp(K_1^2)$, gives a poor fit to fatigue data. Based on this and earlier results, the simple exponential model gives the best description of the overall behavior. It should be noted that lifetimes predicted by extrapolating are significantly shorter when using the exponential than the commonly used power law.

In general, coated and bare fibers give similar results. The polymer coatings studied here have a negligible effect on the kinetics. This may not be the case for other coatings. Therefore it is always useful to compare coated and bare data to distinguish if there is a coating effect.

ACKNOWLEDGEMENT

We would like to thank Bell Communications Research - Morristown, N. J. for their financial support of this research.

REFERENCES

1. K. Jakus, J. E. Ritter, Jr. and J. M. Sullivan, "Dependency of fatigue predictions on the form of the crack velocity equation," *J. Am. Ceram. Soc.*, **64** [6] 372-374 1981.
2. G. M. Bubel and M. J. Matthewson, "Optical fiber reliability implications of uncertainty in the fatigue crack growth model," *Optical Eng.*, **30** [6] 737-745 1991.
3. M. J. Matthewson, "Fiber lifetime predictions," *Proc. Soc. Photo-Opt. Instrum. Eng.*, **1580** 130-141 1991.
4. W. J. Duncan, P. W. France and S. P. Craig, "The effect of environment on the strength of optical fiber" in "Strength of inorganic glass," ed. C.R. Kurkjian, 309-328 Plenum Press, New York, 1985.
5. S. M. Wiederhorn and L. H. Bolz, "Stress corrosion and static fatigue of glass," *J. Am. Ceram. Soc.*, **53** [10] 543-549 1970.

6. B. R. Lawn, "An atomistic model of kinetic crack growth in brittle solids," *J. Mat. Sci.*, **10** 469-480 1975.

7. D. Kalish and B. K. Taryal, "Static and dynamic fatigue of a polymer-coated fused silica optical fiber," *J. Am. Ceram. Soc.*, **61** [11-12] 518-523 1978.

8. S. Sakaguchi and T. Kimura, "Influence of temperature and humidity on dynamic fatigue of optical fibers," *J. Am. Ceram. Soc.*, **64** [5] 259-262 1981.

9. C. R. Kurkjian, J. T. Krause and U. C. Paek, "Tensile strength characteristics of 'perfect' silica fibers," *J. de Phys.*, **43** [12] C9-585-586 1982.

10. M. J. Matthewson, C. R. Kurkjian and S. T. Gulati, "Strength measurement of optical fibers by bending," *J. Am. Ceram. Soc.*, **69** [11] 815-821 1986.

11. M. J. Matthewson, C. R. Kurkjian and J. R. Hamblin, "Acid stripping of fused silica optical fibers without strength degradation," *J. Lightwave Tech.* in press.

12. V. V. Rondinella and M. J. Matthewson, "Effect of loading mode and coating on dynamic fatigue of optical fiber in two-point bending," *J. Am. Ceram. Soc.*, **76** [1] 139-144 1993.

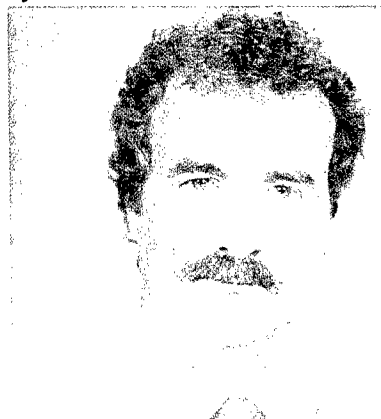
13. P. K. Gupta, "Effects on testing parameters on the tensile strengths of pristine E and S glass fibers" in "Strength of inorganic glass," ed. C.R. Kurkjian, 351-362 Plenum Press, New York, 1985.

14. M. Muraoka, K. Ebata and H. Abé, "Effect of humidity on small-crack growth in silica optical fibers," *J. Am. Ceram. Soc.*, **76** [6] 1545-1550 1993.



Janet L. Armstrong
Rutgers University
Dept. of Ceramic and Materials Eng.
Brett & Bowser Roads
Piscataway, New Jersey 08855-0909

Janet Armstrong received her BS and MS in Ceramic Engineering from Rutgers University in 1995 and 1997 respectively. She is currently pursuing her PhD in Ceramic Engineering at Rutgers University. Her thesis work consists of investigating the mechanical reliability of optical materials. She has been jointly working at Bellcore in Morristown, NJ and Rutgers University.



Dr. M. John Matthewson
Rutgers University
Dept. of Ceramic and Materials Eng.
Brett & Bowser Roads
Piscataway, New Jersey 08855-0909

John Matthewson received his BA in Theoretical Physics in 1975 from Cambridge University

where he was a Kitchener Scholar and a Prize Scholar. He obtained MA and PhD degrees in 1978, also from Cambridge University, for his work at the Cavendish Laboratory on contact mechanics and high speed fracture. He then continued his research in this area as concurrently the Goldsmiths Junior Research Fellow at Churchill College, Cambridge and as a Science Research Council Postdoctoral Fellow. After three years as a consultant in the Cambridge University Computing Service, in 1984 he moved to AT&T Bell Laboratories as a postdoctoral member of technical staff where he worked on optical fiber strength and fatigue. From 1986 to 1989 he was an Advisory Engineer at IBM Almaden Research Center, San Jose, where he worked on reliability of magnetic recording devices and various aspects of adhesion. He is now an Associate Professor in the Fiber Optic Materials Research Program at Rutgers University where his research group is concerned with strength and fatigue of optical materials in general and oxide and non-oxide fibers in particular.



Dr. Charles R. Kurkjian
Bell Communications Research
445 South Street
Morristown, New Jersey 07960-6438

Chuck Kurkjian is a member of the Fiber Media and Components Reliability Group at Bellcore in Morristown, N. J. He spent 35 years at Bell Labs involved in various aspects of glass and glass fiber research, and since joining Bellcore

in 1994 he has concentrated on issues of mechanical reliability of lightguide fiber, cable and optical components. He graduated from Rutgers University in 1952 and M.I.T. in 1955 with degrees in Ceramics.

Catherine Y. Chou
Rutgers University
Dept. of Ceramic and Materials Eng.
Brett & Bowser Roads
Piscataway, New Jersey 08855-0909

Catherine Chou is an undergraduate student who is current pursuing her degree in Applied Science at Rutgers University.

THE FATIGUE BEHAVIOR OF VICKERS INDENTATIONS IN FUSED SILICA OPTICAL FIBERS

Andrew T. Taylor, M. John Matthewson

Rutgers University, Dept. of Ceramic and Materials Eng., Piscataway, New Jersey

ABSTRACT

Catastrophic fatigue failure of optical fiber in the field is expected to occur at the occasional weak defects. The behavior of these defects is different from that of high strength pristine optical fiber, and therefore it is desirable to study them directly rather than by extrapolating from the behavior of the pristine material. Because the probability of encountering a weak defect is very low, alternative means of studying these defects have been developed. We have used Vickers diamond pyramid indentations to introduce controlled flaws under controlled environmental conditions into fused silica of three geometries: 1000 μm diameter flat fiber, 1000 μm diameter cylindrical fiber, and 2 mm thick sheet glass. The resulting crack morphologies were studied using optical microscopy and SEM. Implications of these results to fiber optic reliability will be discussed.

INTRODUCTION

The behavior of weak fiber has often been modeled by deliberately damaging fiber by abrasion, or other techniques (e.g. ref. 1). Such studies give little detail of the nature and behavior of the flaws responsible for failure. In this study we use Vickers indentation to introduce a single dominant flaw of a predetermined size, shape, and location. In this way, the flaw can be examined before, during and after exposure to corrosive environments.² This provides information about the possible behavior of real weak defects which have key

similarities, such as the presence of residual stress.

The Vickers indentation technique utilizes a diamond ground in the shape of a square based pyramid with an included angle of 136° between opposite faces. The indentation depth is about $1/7$ the length of the diagonal, i.e. the indents are shallow. The indentation diagonal length, $2a$, shown in Fig. 1, is used to measure the hardness, while the indentation radial crack length, $2c$, is a measure of the material toughness.

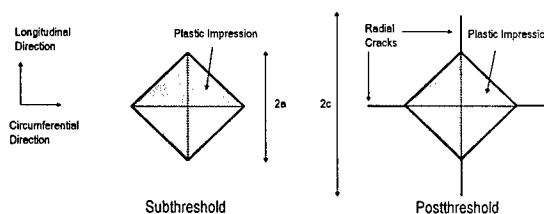


Fig. 1. Top view of indentation.

It is well established that a threshold load for radial crack formation exists. Low load indentations create crack-free plastic impressions and are termed "subthreshold" while higher load indentations with radial cracks are called "postthreshold".³ Radial crack "pop-in" may occur some time after indentation resulting in a subthreshold to postthreshold transition with a corresponding loss in strength due to an increase in the effective flaw size. The pop-in of these strength-controlling radial cracks occurs over a range of loads which depends on the indentation environment, duration of indentation contact, surrounding environment after indentation, and the length of time after

indentation. The pyramidal indenter causes plastic deformation in the glass which leaves a residual stress field upon unloading and acts as the driving force for radial crack pop-in. "Real" flaws, such as particles which adhere to the fiber surface during drawing, are likely to also have a residual stress field associated with them due to thermal expansion mismatch upon cooling. Abrasion damage will also have residual stress due to plastic deformation.

The purpose of this study is to examine the behavior of the Vickers indentation as a model flaw and to study the post-indentation pop-in behavior under various environmental conditions both during and after indentation.

EXPERIMENTAL PROCEDURE

All indentations were performed using a Leco M-400-G3 microhardness tester with loads ranging from 2 mN to 20 N (0.2 g-f to 2 kg-f). The peak indentation load was held for 10 s throughout. Indentations were performed inside an environmental chamber held at 100%, 50%, or ~0% humidity. Special experimental procedures were used in the case of the dry indentation experiments. Although not precisely measured, the lowest humidity was obtained using drierite in the chamber while flushing with dry N₂ gas, and finally, by blowing this gas directly onto the surface of the material at the indentation location. The amount of water in the N₂ gas was between 5-10 ppm. The chamber was equipped with an optical microscope for cursory evaluation after indentation. Samples were then placed in a vacuum desiccator while inside the chamber to avoid contact with environmental moisture during transport to either an optical microscope equipped with a camera or a scanning electron microscope.

Before indentation, the fiber specimens were stripped of their polymer coating by immersing in hot sulfuric acid (~200°C) for about 30 s followed by rinsing with water and acetone. This

stripping method does not degrade the strength of the fiber.⁴ 50 indentations were performed for each load on flat fused silica fiber. The evolution of the crack morphologies was studied with respect to aging time in 90°C pH 7 buffer solution.

Given the intricacy of the experimental techniques and the large numbers of specimens required for strength testing to obtain statistically significant results, several approaches have been used to speed data acquisition. While cylindrical fiber was used early in this work, we have also used flat fiber, which was fabricated by drawing from a preform whose sides have been ground flat and flame polished, as seen in Fig. 2. This fiber geometry has several advantages; indentations are much easier to produce on the flat surface since the Vickers indenter tip does not need to be accurately aligned with the apex of a curved surface. Furthermore, aligning the indenter tip with the fiber diameter is not necessary for flat fiber because the distance from the neutral axis during bending is the same across the flat. Also, when bent, the fiber automatically bends in the direction of minimum second moment of area, *i.e.*, the neutral axis is always parallel to the flats on the fiber. The indentation therefore automatically aligns on the surface of maximum tension. This obviates the need for careful azimuthal alignment of the indentation. However, there is a possibility that the residual stress fields of an indent on a flat fiber will be different from those on a cylindrical fiber due to the difference in geometry. Both specimen geometries have been found to give similar strength and fatigue results.^{5,6}

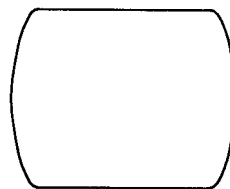


Fig. 2. Cross section of flat fiber.

A length of fiber was broken into 1000 specimens. Samples for any given experiment were then selected randomly from this batch in order to avoid any systematic variations along the fiber length. After stripping, each specimen was indented on the flat surface between two ink dots. The indentation diagonal, $2a$, and radial crack length, $2c$, (if present) were measured. The ink dots are used to identify the location of the indent during subsequent testing. For longer aging times an additional high load indent was applied at one end of the fiber to act as a marker for easy identification of the side of the fiber containing the indent of interest. This was necessary since the marker dots sometimes washed off after prolonged aging time in 90°C pH 7 buffer. Fibers were protected from contacting each other during aging by placing in a holder that keeps them separate. After aging, each fiber was rinsed with water and acetone to clean the surface and then re-examined under an optical microscope to observe if radial cracks had popped-in during aging. The fiber was then broken in a 4-point bend apparatus with the indent on the tensile side of the bend.^{7,8} Finally, fracture surfaces of the two fragments were evaluated and then preserved for future reference. An example of a fracture surface for an indented flat fiber is shown in Fig. 3.

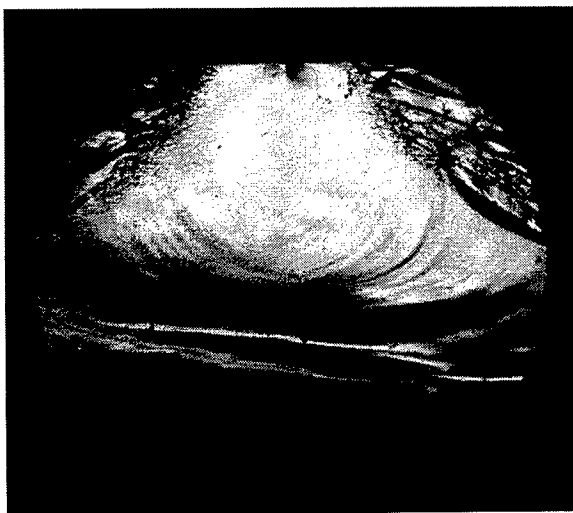


Fig. 3. Fracture surface of indented flat fiber.

RESULTS

The post indentation behavior for a 5 N load indentation performed while blowing 25°C dry N_2 onto the indent is drawn in Fig. 4. Upon unloading, a simple plastic impression is observed, as seen in Fig. 4a. If the dry N_2 is turned off, allowing some moisture to reach the indent, edge cracks appear at the indentation contact edge, as seen in Fig. 4b, and continue to grow over the next ~ 15 s, but do not reach the indentation corners, as seen in Fig. 4c. Much later (hours), radial cracks develop, as seen in Fig. 4d. These cracks emanate from near the corners and are therefore called secondary radial cracks.⁹ They are different from the primary radial cracks which emanate from the corners and extend to longer lengths.

In comparison, in a 100% humidity, 25°C, environment, a 5 N indentation results in edge cracks that are immediately apparent after unloading and extend along the whole contact edge all the way to the corners. Thus, a 5 N indentation in fused silica is typically referred to as postthreshold. The typical apparent threshold load is between 2 N and 3 N for fused silica.^{2,5} However, the severity of the radial crack pop-in is dependent on the environmental history during and after indentation. Indentation in a dry N_2 gas environment shows that apparent postthreshold indents are in fact subthreshold indents which have popped-in due to attack by ambient moisture for loads up to 20 N. Others have seen some similar results for inert conditions.¹⁰ Also, the dry N_2 gas enables the kinetics of crack pop-in to be slowed for microscopic observation. Edge cracks, whose existence was speculated in a fracture mechanics model for indentation behavior¹¹ have been observed to form after unloading at the indentation contact edge.

The comparison of indentations made in dry N_2 gas and humid environments give different crack morphologies. Even after the dry indent is

exposed to moisture, the cracks that develop are principally secondary radial. This means that there is not a single type of defect for a given indentation load.

An example of typical delayed radial crack pop-in behavior is shown in Figs. 5 and 6. Fig. 5 shows a 1000X optical micrograph of a 3 N indent performed in 50% humidity and 25°C. Some, but not all the edge cracks reached the indentation corners. This sample was then aged for 1 week in 90°C pH 7 buffer solution. The resulting radial cracks are shown in Fig. 6. All the radial cracks formed from the ends of the edge cracks, close to their initial position as shown in Fig. 5.

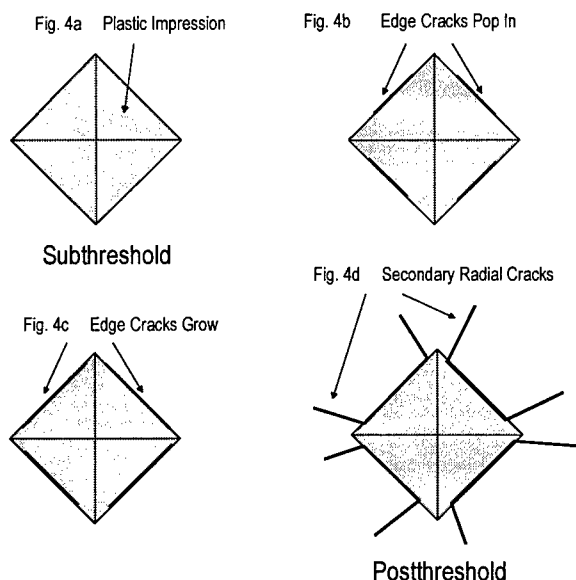


Fig. 4. Pop in sequence for dry N₂ indentation.

The radial crack pop-in behavior and the development of additional crack systems has been observed as a function of zero stress aging time in 90°C pH 7 buffer. 50 indentations for each load ranging from 5 mN to 3 N were placed on flat fused silica fiber. Each indentation was inspected after indentation, and after various aging times. The probability of radial crack pop-in as a function of aging time is shown in Fig. 7. The reported threshold load of 2 N to 3 N quickly produces radial cracks. However, at loads below

the threshold, radial cracks are seen to pop in, even at loads as low as 50 mN. The consequence of this behavior may be significant. It is possible under very aggressive conditions to induce pop-in at loads far from the threshold.

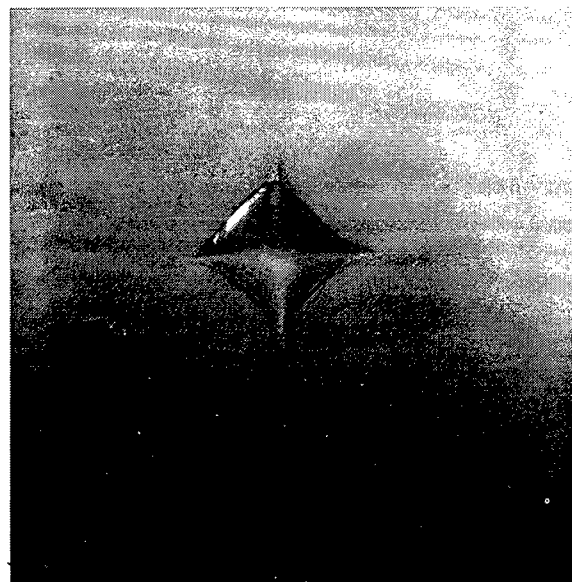


Fig. 5. 3 N indentation performed in 50% humidity on flat fused silica fiber (1000X).

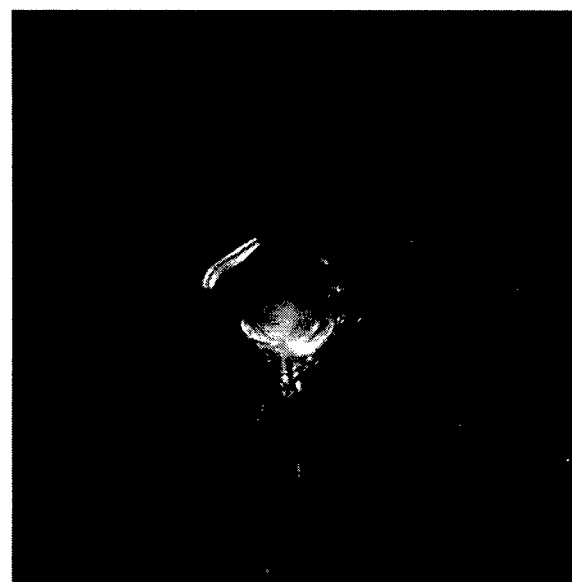


Fig. 6. Same 3 N indent after 1 week aging in 90°C pH 7 buffer environment (1000X).

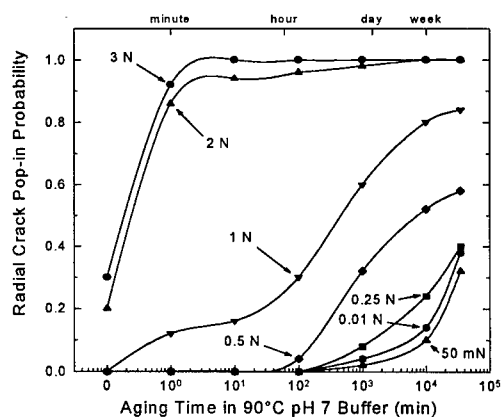


Fig. 7. Radial crack pop-in probability.

Except near the threshold, both subthreshold (low load) and post-threshold (high load) flaws show a strength increase with aging time.^{5,6} These results are similar to observations on abraded fiber.¹ Two possible mechanisms for this increase have been proposed: crack tip blunting and reduction of residual stresses. Both of these mechanisms have been observed in this work. Upon careful examination of Fig. 6, a lateral crack, the light circular region under the indentation, can be seen. Laterals cracks were observed to pop-in some time after radial cracks, and even on indentations which never exhibited radial cracking. It was observed that these lateral cracks grew slowly with aging time thereby reducing the residual stress field associated with the plastic deformation zone.¹² This explains "weak" fiber increasing in strength with zero stress aging. However, another possibility is crack tip blunting. Figs. 8 and 9 show 8000X SEM images of 0.25 N indentations, which have been aged for 4 weeks in 90°C pH 7 buffer solution, with and without radial crack pop in. Fig. 7 shows that the probability of pop-in is around 40% and these images show examples of both behaviors. The edge cracks are etched away this aggressive environment. Additionally, the radial cracks in Fig. 9 appear, at least on the surface, blunt. An SEM image of a 50 mN

indentation at 8000x is depicted in Fig. 10. Here, the edge cracks popped in at different locations below the contact edge on the surface resulting in regions which were more aggressively attacked, or etched, by the 90°C pH 7 buffer environment.

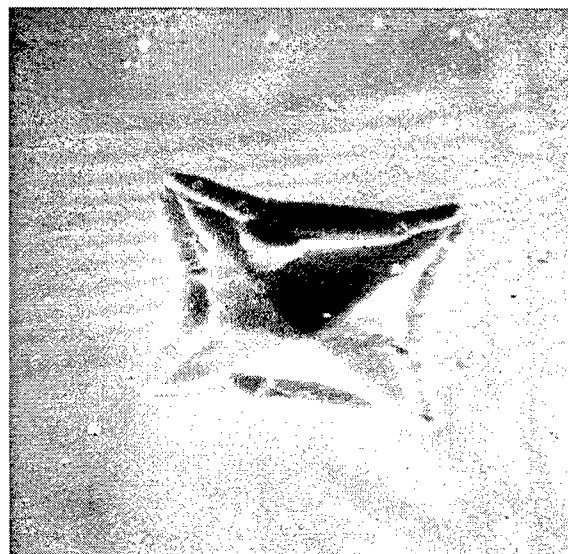


Fig. 8. SEM image of 25 mN indent aged 4 weeks in 90°C pH 7 buffer without radial cracks (8000X).

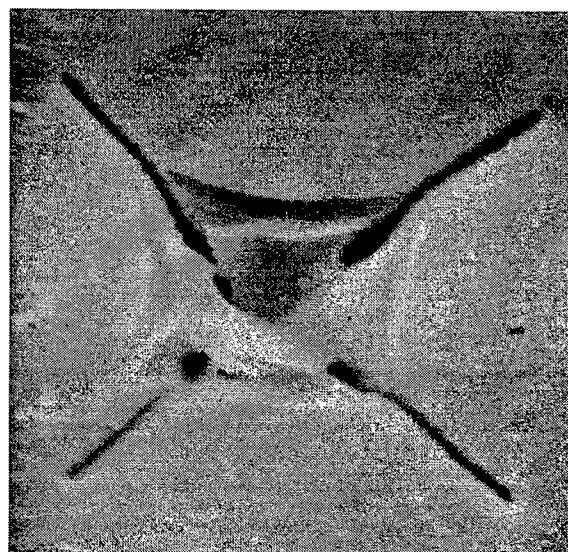


Fig. 9. SEM image of 25 mN indent aged 4 weeks in 90°C pH 7 buffer with radial cracks (8000X).



Fig. 10. SEM image of 50 mN indentation aged 4 weeks in 90°C pH 7 buffer (8000X).

DISCUSSION AND CONCLUSIONS

Contact damage on fused silica produces a complex system of cracks. The radial crack is the most important for reliability studies since it produces the greatest reduction in strength. This work shows that the initiation of radial cracks is controlled by edge cracks which form during or after indentation. The sequence of events leading to radial cracking is complex and is very sensitive to both the indentation environment and the post indentation conditions.

This work also provides direct evidence for the two possible mechanisms for strength recovery upon aging; namely residual stress relief and crack tip blunting. However, in the critical threshold region, radial crack formation, initiated by the mechanisms elucidated here, produces a discontinuous loss in strength with obvious practical implications.

The radial crack formation is sensitive to the boundary conditions of the indentation. The threshold load is slightly different for the three specimens geometries studied here. Also the indentation shape is important; a cube corner indenter initiates a 1 μm crack at loads as low as

0.02 mN.⁹ The indentation defects we study here are in the strength range of typical proof loads. That is, they may model the kind of behavior exhibited by real practical defects. Clearly, the complex behavior of an indentation defect is not described by the Griffith relation for a simple stress free crack which is the basis for most optical fiber reliability models.

ACKNOWLEDGEMENTS

We thank the AT&T foundation for an equipment grant used for this work. We also thank the Corning Foundation for there support with a Corning Foundation Fellowship.

REFERENCES

1. G. S. Glaesemann, "The mechanical reliability of large flaws in optical fiber and their role in reliability predictions," *Proc. 41st Int. Wire & Cable Symp.*, 698-704 1992.
2. B. Lin, M. J. Matthewson and G. J. Nelson, "Indentation experiments on silica optical fibers," *Proc. Soc. Photo-Opt. Instrum. Eng.*, **1366** 157-166 1990.
3. T. P. Dabbs, D. B. Marshall and B. R. Lawn, "Flaw generation by indentation in glass fibers," *J. Am. Ceram. Soc.*, **63** [3-4] C224-225 1980.
4. M. J. Matthewson, C. R. Kurkjian and J. R. Hamblin, "Acid stripping of fused silica optical fibers without strength degradation," *J. Lightwave Tech.* in press.
5. M. J. Matthewson, B. Lin and A. P. Stanzeski, "Modeling weak optical fiber by using Vickers indentation," *OFC'94 Tech. Digest*, **5** 245-246 1994.
6. B. Lin, M. J. Matthewson "Inert strength of sub-threshold and post-threshold Vickers indentations on fused silica fibres," *Phil. Mag.*, **74** 1235-1244 1996.
7. G. J. Nelson, M. J. Matthewson and B. Lin, "A novel four-point bend test for strength measurement of optical fibers and thin beams: Part I: bending analysis," *J. Lightwave Tech.*, **14** [4] 555-563 1996.

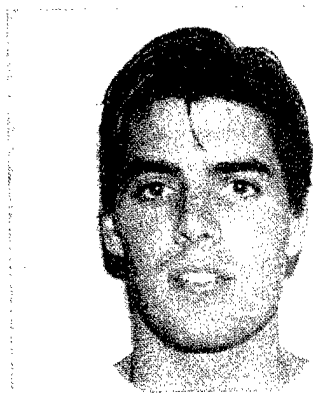
8. M. J. Matthewson and G. J. Nelson, "A novel four-point bend test for strength measurement of optical fibers and thin beams: Part II: statistical analysis," *J. Lightwave Tech.*, **14** [4] 564-571 1996.

9. G. M. Pharr, D. S. Harding and W. C. Oliver, "Measurement of fracture toughness in thin films and small volumes using nanoindentation methods" in "Mechanical properties and deformation behavior of materials having ultra-fine microstructures," ed. M. Nastasi, 449-461 Kluwer, 1993.

10. C. R. Kurkjian, G. W. Kammlott and M. M. Chaudhri, "Indentation behavior of soda-lime silica glass, fused silica, and single-crystal quartz at liquid nitrogen temperature," *J. Am. Ceram. Soc.*, **78** [3] 737-744 1995.

11. S. Lathabai, J. Rödel, T. P. Dabbs and B. R. Lawn, "Fracture mechanics model for subthreshold indentation flaws: Part I equilibrium fracture," *J. Mat. Sci.*, **26** 2157-2168 1991.

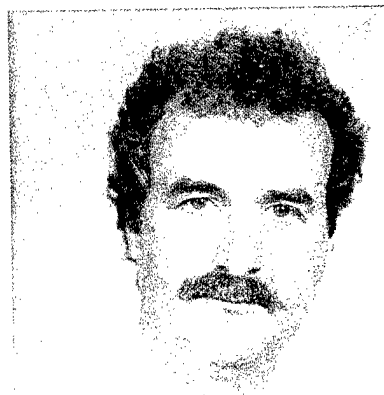
12. R. F. Cook and D. H. Roach, "The effect of lateral crack growth on the strength of contact flaws in brittle materials," *J. Mat. Res.*, **1** [4] 589-600 1986.



Andrew Thomas Taylor
Rutgers University
Depart. of Ceramic and Materials Eng.
Brett & Bowser Roads
Piscataway, New Jersey 08855-0909

Andrew Taylor received his BS and MS in Ceramic and Materials Engineering from Rutgers University in 1993 and 1995, respectively. He was awarded the Corning Foundation Fellowship at Rutgers University from 1995-1997. He is currently pursuing his PhD in the Fiber Optic

Materials Research Program at Rutgers University investigating the strength and reliability of optical fibers.



Dr. M. John Matthewson
Rutgers University
Depart. of Ceramic and Materials Eng.
Brett & Bowser Roads
Piscataway, New Jersey 08855-0909

John Matthewson received his BA in Theoretical Physics in 1975 from Cambridge University where he was a Kitchener Scholar and a Prize Scholar. He obtained MA and PhD degrees in 1978, also from Cambridge University, for his work at the Cavendish Laboratory on contact mechanics and high speed fracture. He then continued his research in this area as concurrently the Goldsmiths Junior Research Fellow at Churchill College, Cambridge and as a Science Research Council Postdoctoral Fellow. After three years as a consultant in the Cambridge University Computing Service, in 1984 he moved to AT&T Bell Laboratories as a postdoctoral member of technical staff where he worked on optical fiber strength and fatigue. From 1986 to 1989 he was an Advisory Engineer at IBM Almaden Research Center, San Jose, where he worked on reliability of magnetic recording devices and various aspects of adhesion. He is now an Associate Professor in the Fiber Optic Materials Research Program at Rutgers University where his research group is concerned with strength and fatigue of optical materials in general and oxide and non-oxide fibers in particular.

AUTHOR INDEX

Name	Page	Name	Page
ABADÍA, V.	573	COLLINS, M.	32
ANADA, T.	381	COPE, K. E.	132
ANDERSON, D. K.	642	COTTINO, E.	391, 675
AOUSTIN, H.	218	CRAWFORD, S. K.	151
ARAI, O.	12	CRUZ, R. F.	819
ARAKAWA, K.	650	DAMIANO, A.	675
ARIGA, Y.	74	DAVIDSON, F.	24
ARIKAWA, T.	57	DAVIES, M.	32, 348
ARMSTRONG, J. L.	902	DE WIN, P.	692
ASANO, K.	68	DEAS, J.	622
ASPELL, J.	86	DEFABRITIS, R. P.	274
ATKINS, R. M.	86	DURIGAN, H. J.	819
ATOBE, N.	834	ENOMOTO, Y.	493, 859
AU, T. W.	274	EOLL, C. K.	803
AZUMA, Y.	650	ESPINDOLA, R. P.	86
BACKMANN, M.	238	ESTEP, M. G.	883
BAN, M.	876	FACCHINI, M.	658
BASTIDE, C.	24, 198	FÄRLIN, R.	436
BEASLEY, W. E.	867	FELLAY, A.	658
BELANGER, M.	698	FOKINE, M.	82
BENZEL, D. J.	24	FOKINE, M. A.	64
BIZEUL, J. C.	826	FRENCH, M.	102, 107
BLANARIK, M.	452	FUJIWARA, Y.	547
BOITEL, M.	218	FUKUMOTO, H.	852
BONICEL, J. P.	24, 181	FURUKAWA, S.	842
BORICK, J. M.	86	GAO, Z.	122
BORKE, J. S.	146	GARVEY, P. T.	883
BOSCHER, D.	409, 826	GIANNELIS, E. P.	761
BOTTANELLI, M.	391	GILMAN, J. W.	761
BOUFFANT, O.	374	GIRBIG, R.	181
BOURHIS, J.-F.	584	GLAESEMANN, G. S.	883, 896
BOWMER, T. N.	426	GODARD, G.	218
BRINGUIER, A. G.	556	GOHDES, H.	97
BROWN, S. C.	727	GRAJEWSKI, F.	478
BULUSCHEK, B. E.	452	GRAVELY, III, R. G.	191
BURGETT, S. J.	642	GRIFFIOEN, W.	363
CADIER, B.	409	GUILLAS, P.	374
CAETANO, M. A. B.	819	HAGER, T. P.	556
CAIATA, M.	617	HAIGH, N. R.	622
CAIRNS, D. R.	889	HAILES, R.	205
CARTER, C. N.	622	HANSON, T. A.	883
CAUDILL, L.	775	HARA, M.	176, 793
CHANG, S.-T.	526	HARADA, H.	231
CHAPIN, J. T.	590, 775	HARDY, I.	826
CHARLES, Y.	306	HASSETT, S.	156
CHEN, C.-H.	526	HATTORI, T.	876
CHIN, K.-H.	506	HATTRICH, G. A.	138
CHOU, C. Y.	902	HAYES, T. M.	244
CHOU, S.-H.	462	HESS, D. C.	111
CLAESSON, Å.	82	HINOHARA, T.	834
COCCHINI, F.	617	HISHIKAWA, Y.	483
COCKRILL, K.	348	HOG, G.	181

Name	Page	Name	Page
HOGARI, K.	842	KOYASU, O.	17, 720, 785
HONGU, H.	483	KUCK, V. J.	86
HOOVER, J. R.	775	KUKUREKA, S. N.	889
HOPLAND, S.	316	KUNUGIYAMA, H.	212
HORWATT, S. W.	138	KUO, R.-S.	526
HOSHIJIMA, T.	4, 842	KURKJIAN, C. R.	902
HOSOI, F.	176	KUROSAWA, Y.	12
HOSOYA, H.	68	KUSAKARI, M.	17
HSIAO, C.-M.	462	KUTT, T.	298
HSU, H.-P.	462, 526	KUZE, Y.	632
HUANG, L.-J.	526	LAI, S.-W.	526
INNISS, D.	86	LANG, J.-L.	306
INOUE, M.	231	LATORRE, V.	573
ISHIBASHI, Y.	12	LAURENCY, P.	218
ISHIDA, H.	381	LAWRENCE, E. J.	111
ISHIDA, K.	368	LE COZIC, H.	374
ISHII, K.	12	LE NOANE, G.	826
ISHIKAWA, H.	42, 354, 842	LEE, L. Y.	744
ISHIZAKI, H.	602	LEE, Y. I.	609
IWAKURA, D.	166, 793	LENIR, V.	681
IWATA, H.	4	LIBERT, J.-F.	306, 326
IZUKURA, H.	166	LICHTENHAN, J. D.	761
JACKSON, K. W.	274, 289	LIN, H.-F.	462
JEON, Y. H.	539	LIN, J.-C.	462
JOLY, B.	218	LIN, W.-L.	526
JONES, P.	761	LIN, Y.-C.	462, 526
JUNG, C. H.	609	LISSILLOUR, M.	374
KAMA, M.	4, 842	LIVINGSTON, R. O.	803
KAMIKO, K.	51	LJUNG, M.-C.	736
KAMIKURA, Y.	166, 176, 793	LOCHKOVIC, G. A.	260
KANAI, K.	516	LOMAKIN, S.	761
KANG, H. J.	609	LOUBOUTIN, J. P.	826
KANG, S.-K.	506	LU, M.-S.	526
KASHIMA, N.	4, 500, 842	LUDL, A.	396
KASHIWAGI, T.	761	LYYTIKÄINEN, K. J.	468
KATAGIRI, T.	500	MACEY, R. D.	94
KATO, M.	381	MAGUIRE, S.	205
KATO, S.	852	MAHE, T.	218
KATO, T.	666	MAKIYAMA, A.	42
KATOH, M.	253	MANIAS, E.	761
KATSURASHIMA, W.	341, 354	MARSHALL, A.	889
KELLER, D. A.	24	MARTINSSON, H.-B.	126
KIM, C.-H.	506	MARX, M. F.	590
KIM, S. H.	539	MASUMITSU, S.	381
KIM, S.-H.	506	MATSUDA, Y.	876
KIPP, S. G.	568	MATSUNO, K.	650
KOBAYASHI, I.	166, 793	MATTHEWSON, M. J.	902, 910
KOBAYASHI, K.	368	MATUOKA, R.	166
KOBAYASHI, M.	867	MAZZOTTI, A.	617
KOHMOTO, K.	68	MCALPIN, T. B.	642
KOMIYA, Z.	418	MCMINN, J. R.	642
KONAKA, T.	443	MEILLEUR, R.	584
KONDA, E.	166, 793	MITA, K.	720
KONSTADINIDIS, K.	274	MITSUHASHI, K.	281
KOSHIO, S.	852	MIYAMOTO, M.	17, 368, 785

Name	Page	Name	Page
MOGI, A.....	17, 368	PERETTA, P.....	563
MONETTI, A.....	617	PFEILER, C.....	238
MOORJANI, S. K.....	260	PIFFARI, I.....	675
MORGAND, A.....	409	PLUMETTAZ, G.....	363
MORISHITA, Y.....	74	POZZI, F.....	563
MOSS, P. A.....	590	PRUDHON, D.....	102, 107
MURAI, S.....	443	RAGAN, R.....	86
MURAKAMI, K.....	212	REAU, A. C.....	409
MURATA, A.....	281	REGINI, A.....	675
MURPHY, M.....	32	RESLINGER, M.....	218
MUTA, K.....	74	RICHARD, J.-F.....	681
NAGASAWA, S.....	500	RICHTER, S.....	752
NAGASE, Y.....	488	ROBERT, P. A.....	658
NAITO, Y.....	418	RODRÍGUEZ, J. L.....	573
NAKAI, H.....	212	ROGESTEDT, L.....	126
NAKANO, T.....	225	ROWLAND, S. M.....	622
NAKATANI, Y.....	212	RUELLE, F.....	326
NARAOKA, S.....	51	RUELLO, Y.....	409
NASU, H.....	632	SAHLGREN, B.....	82
NEAT, R. C.....	889	SAIJO, M.....	74
NELSON, K. T.....	86	SAITO, T.....	42
NEMOTO, K.....	602	SAKABE, I.....	341
NEWTON, W. M.....	590	SAKAI, Y.....	720
NIKLÈS, M.....	658	SALINA, P.....	658
NILSSON, M.....	736	SANKAWA, I.....	842
NISHI, S.....	443	SANO, H.....	341, 354
NISHIZAWA, K.....	4	SANO, T.....	483
NITTA, M.....	521	SATO, Y.....	381, 785
NIXEY, J.....	348	SCHARF, J.....	698
NOUCHI, P.....	584	SCHIAFFO, A.....	617
NYGÅRD-SKALMAN, K.....	436, 736	SCHMIDT, R.....	752
O'BOW-HOVE, S.....	298	SCHUEBBE, M.....	810
OGURA, H.....	834	SCHÜRMANN, H.....	396
OHKAWA, Y.....	166	SEGUCHI, T.....	521
OHSAKO, T.....	602	SEKII, Y.....	166
OHTA, J.....	42	SEO, G. W.....	539
OHTA, M.....	720	SERRANDER, H.....	473
OKADA, N.....	785	SHIGEMATSU, T.....	225
OKADA, M.....	4	SHIMOJI, N.....	510
OKUDA, M.....	51	SHINODA, Y.....	632
OLOFSSON, H.....	473	SIDDIQUI, S.....	274
OMURA, H.....	253, 632, 666	SIGNORELLI, M.....	563
ONO, M.....	720	SILVINO DE ALMEIDA PRATA, H.....	530
OOHASHI, K.....	281, 368	SILVÉRIO, L.....	819
OPEL, E.....	810	SIMOFF, D. A.....	86
ORCEL, G.....	584	SOLLENBERGER, N. W.....	274
OSAKA, K.....	483	SPEIGHTS, R. J.....	260
PACZKOWSKI, M. A.....	86	STEPHENS, B. L.....	260
PARK, S. C.....	609	STIEB, W.....	478
PARRIS, D. R.....	122	STINGL, A.....	810
PARSONS, A.....	156	STOKES, S. R.....	867
PATEL, N. I.....	260	STRASSER, T. A.....	86
PAUL, A.....	896	STREIBERT, F.....	552
PEDRAZZANI, J. R.....	86	STUBBE, R.....	82
PELT, M.....	111, 692	STUDD, R.....	348
PENG, A.....	568	SUDO, Y.....	602

Name	Page	Name	Page
SUETSUGU, Y.	42	TSAI, K.	568
SUGI, K.	74	TSUCHIDE, K.	842
SUGIMOTO, M.	418	TU, Y.-K.	462, 526
SUGIYAMA, M.	521	TURNIPSEED, J. M.	274
SUTEHALL, R.	32, 348	UCHIDA, H.	418
SUZUKI, A.	876	UCHIDA, N.	493
SUZUKI, J.	457	UKACHI, T.	418
SUZUKI, O.	516	URATA, K.	212
TABADDOR, M.	289	URUNO, S.	859
TACHIKURA, M.	859	VERHAEGE, T.	198
TAKAOKA, R.	166, 793	VINCENT, A.	218
TAKASHIMA, S.	666	VIRIYAYUTHAKORN, M.	590
TAKASUGI, H.	859	WAGMAN, R.	156
TAKAYA, M.	500	WALLING, J.-H.	681, 698, 708
TAKAYANAGI, H.	483	WASSMUTH, A.	238
TAKEMOTO, H.	859	WATANABE, A.	12
TAKIZAWA, K.	57	WATANABE, H.	785
TAMAKI, Y.	57, 547	WATANABE, K.	17
TAMURA, H.	488	WATANABE, M.	42
TANAKA, S.	42, 341, 354	WATANABE, T.	516
TANAKA, T.	547	WILHELM, D.	534
TANI, T.	521	WILSON, C. G.	590
TARDY, A.	584	WORTHINGTON, P.	306, 326
TATAT, O.	181, 198	YAGI, T.	521
TAYLOR, A. T.	910	YAGUCHI, S.	457
TAYLOR, C. R.	274	YAMADA, Y.	493
TAZUMI, K.	720	YAMAGUCHI, S.	51
TERAOKA, T.	212	YAMAKAWA, J.	225, 510
TERASAWA, M.	842	YAMANAKA, M.	785
TERUI, H.	493	YAMAZAKI, H.	12
THORNTON, J. W.	191	YAMAZAKI, T.	867
THÉVENAZ, L.	658	YOKOSUKA, H.	57, 68, 547
TODA, S.	516	YOSHIDA, K.	650
TOMITA, N.	493, 859	YOSHIDA, M.	488
TOMITA, S.	4	YOSHIKAWA, K.	381
TOMIYAMA, K.	842	YOSHINUMA, M.	457
TOMIZU, D.	231	ZAMZOW, P. E.	396
TRAVIESO, R.	289	ZENIMURA, S.	381

46TH INTERNATIONAL WIRE AND CABLE SYMPOSIUM (IWCS) SYMPOSIUM COMMITTEE

IWCS STAFF

ELMER F. GODWIN

(President/Director)

GEF Associates
3A Buttonwood Drive
Shrewsbury, NJ 07702
Tel: (732) 389-0990 (Office)
Fax: (732) 389-0991 (Office)
E-mail: iwcs@monmouth.com

IRVING KOLODNY

(Director's Assistant)

31 Maple Run Drive
Jericho, NY 11753
Tel & Fax: (516) 932-0699

MICHAEL A. DELUCIA

(Director's Assistant)

1775 Crofton Parkway
Crofton, MD 21114
Tel & Fax: (410) 721-5588
E-mail: mdelucia@clark.net

PATRICIA HUDAK

(Administrative Assistant)

174 Main Street
Eatontown, NJ 07724
Tel: (732) 389-0990
Fax: (732) 389-0991
E-mail: iwcs@monmouth.com

1997 OFFICERS

JAMES R. LEECH

(Chairman)

Union Carbide Corp.
Weston Canal Center
PO Box 450
Somerset, NJ 08875-0450
Tel: (732) 271-7935
Fax: (732) 271-7949
E-mail: leechjr@ucarb.com

JOHN R. SICOTTE

(Vice-Chairman)

Corning Incorporated
35 W. Market St; MP-RO-02
Corning, NY 14831
Tel: (607) 974-4447
Fax: (607) 974-7041
E-mail: sicottejr@corning.com

XAVIER MANN

(Secretary)

Fitel Lucent Technologies
201 Adamson Industrial Blvd
Carrollton, GA 30117
Tel: (770) 838-5278
Fax: (770) 836-8820
E-mail: xmann@attmail.com

DR. HOWARD WICHANSKY

(Treasurer)

Cdr, US Army CECOM
ATTN: AMSEL-RD-ST-WL-AW
Fort Monmouth, NJ 07703-5203
Tel: (732) 427-4713
Fax: (732) 427-2150
E-Mail:
wichansk@doim6.monmouth.
army.mil

1997 COMMITTEE MEMBERS

NILS ARTLÖVE

Telia AB
123 86 Farsta
Sweden
Tel: +46-8-713-1212
Fax: +46-8-713-2926
E-mail: Nils.A.Artlove@telia.com

JAMES A. CABALLERO

Synergistics Industries (NJ) Inc.
10 Ruckle Avenue
Farmingdale, NJ 07727
Tel: (732) 938-5980
Fax: (732) 938-6035
E-mail:
caballerojim@worldnet.att.net

RUSSELL S. DANIELS

Millennium Petrochemicals Inc.
11500 Northlake Drive
PO Box 429550
Cincinnati, OH 45249
Tel: (513) 530-6500
Fax: (513) 530-6440
E-mail: danielsrus@aol.com

HIROTOSHI HONDO

The Furukawa Electric Co. Ltd.
Information & Electronics
Laboratory
5-1-9 Higashiyawata
Hiratsuka, Kamagawa, 254, Japan
Tel: +81-463-24-8450
Fax: +81-463-24-8491
E-mail:
hondo@ie.inf.furukawa.co.jp

DR. MAREK KAPÚSCÍŃSKI

NORDX/CDT
105, Marcel-Laurin Blvd
St-Laurent, Quebec
Canada H4N 2M3
Tel: (514) 639-2328
Fax: (514) 639-2468

INGE B. KOVACS

Consultant for Polychex Ltd
180 Durham Court
Hackettstown, NJ 07840
Tel: (908) 852-1610
Fax: (908) 852-1518
E-mail: ibkovacs@goes.com

DR. JOHN MELLIS

B67, Rm 115
British Telecom Laboratories
Martlesham Heath
Ipswich IP5 7RE
United Kingdom
Tel: +44-1473-642959
Fax: +44-1473-644142
Email: mellisj@boat.bt.com

FRED NARAYAN

Phelps Dodge International Corp.
2121 Ponce de Leon Blvd.
Coral Gables, FL 33134
Tel: (305) 447-4322
Fax: (305) 447-4321
Email: fnarayan@phelpsd.com

MICHEL ROUSSEAU

Alcatel Cable
30, rue P. Bergeovoy
BP 309
92111 Clichy Cedex
France
Tel: +33-1-4756-6900
Fax: +33-1-4756-6739

JOHN R. SACH

Pirelli Cables Corp. North America
700 Industrial Drive
Lexington, SC 29072
Tel: (803) 951-4020
Fax: (803) 957-8654

ADVISORY

DR. PETER R. BARK

Siecor Corporation
P.O. Box 489
489 Siecor Park
Hickory, NC 28603
Tel: (704) 323-6205
Fax: (704) 323-6264
E-mail: Peter_Bark@siecor.com

LEO CHATTLER

DCM Industries, Inc.
2930 Faber Street
Union City, CA 94587
Tel: (510) 429-9500
Fax: (510) 429-1250

DAVE FALLOWFIELD

TELUS Advanced Communications
10039 102 Avenue
Edmonton, Alberta
Canada T5J 0E5
Tel: (403) 944-4272
Fax: (403) 426-3868
E-mail: dave.fallowfield@telus.com

DIETER S. NORDMANN

(European Representative)

Alcatel Contracting
P.O. Box 260; Kabelkamp 20
D30179 Hannover, Germany
Tel: +49-511-676-2020
Fax: +49-511-676-3042
E-mail: Norddieter@aol.com

MANUEL R. SANTANA

Lucent Technologies
Bell Laboratories
2000 NE Expressway; Rm 1D32
Norcross, GA 30071
Tel: (770) 798-2754
Fax: (770) 798-4654
E-mail: msantana@lucent.com

CONSULTANTS

DR. REINER J. GERDES

TransTel Group Inc.
5555 Oakbrook Pkwy, Suite 110
Norcross, GA 30093
Tel: (770) 368-8343
Fax: (770) 368-8382
E-mail: rgerdes@transtelgroup.com

DR. RAYMOND E. JAEGER

SpecTran Corporation
50 Hall Road
Sturbridge, MA 01566
Tel: (508) 347-2261
Fax: (508) 347-8626

HANS A. MAYER

Olex Cables
(A Division of Pacific Dunlop Ltd.)
207 Sunshine Road
Tottenham, VIC 3012
Melbourne, Australia
Tel: +61-3-9294-3311
Fax: +61-3-9294-3340